Asymmetric Total Synthesis of (–)-Myrifabral A and B, Havellockate, and New Strategies for Acyclic Stereocontrol

Thesis by

Tyler James Fulton

In Partial Fulfillment of the Requirements for

the Degree of

Doctor of Philosophy

CALIFORNIA INSTITUTE OF TECHNOLOGY

Pasadena, California

2022

(Defended April 13, 2022)

Tyler James Fulton
ORCID: 0000-0002-9343-2456

In Loving Memory of Carol Valsechi

ACKNOWLEDGEMENTS

The research presented in this thesis would not be possible without the support, mentoring, and friendship of so many people. I have nothing but gratitude for the once in a lifetime opportunity to work with an advisor as caring, supportive, understanding, and human as Professor Brian Stoltz. Caltech is a truly special place to be, but Brian's lab is on another level entirely. The freedom Brian gives us fosters a unique environment of student-driven ideas and enables us to become independent scientists. Brian has given me every opportunity to succeed, and I am thankful for all his sage wisdom and council, especially during the pandemic. The first months of lockdown were incredibly isolating and challenging and I am immensely thankful for Brian's casual meetings and support during those dark days.

I would also like to extend my utmost appreciation to the members of my thesis committee. Professor Bob Grubbs was an incredibly supportive and generous thesis chair, freely offering his time and wisdom without a second thought. I will always cherish my interactions with Bob, especially our first conversation while hiking during my visit weekend at Caltech. Professor Sarah Reisman has been an incredibly supportive second mentor on the floor and recently became the chair of my committee. Sarah is an inspirational figure in organic chemistry and sharing the floor with her lab has provided a lot of additional support and knowledge. Professor Harry Gray was also an incredibly supportive committee member and I appreciate all the interactions I have had with Harry. Professor Max Robb joined my committee just weeks before my propositions exam and has been incredibly kind, insightful, and supportive. It has been a joy watching Max's lab grow and take shape during my time at Caltech.

I especially need to recognize my undergraduate advisors and mentors at Bucknell who supported my early studies and inspired me to go to graduate school. I am indebted to Prof. Mike Krout who allowed me to start research in his new lab as a first-year student. Mike's persistent support, insightful critiques, and high standards molded me into the scientist that I am today. Under Mike's direction I was able to pursue a joint B.S./M.S. degree and gain a significant amount of independence and skills in the lab. I am also thankful to Professors Tim Strein, Will Kerber, Karen Castle, Eric Tillman, Molly McGuire, Dabrina Dutcher, David Rovnyak, Rob Stockland, and Brian Williams for their exceptional teaching and mentorship during my time at Bucknell. I am beyond fortunate to have been a chemistry major at Bucknell with such a uniquely caring, thoughtful, and supportive faculty.

At Caltech, we are fortunate to be supported by such a dedicated support staff. Dr. Scott Virgil works tirelessly to help every single person that comes to the catalysis center, often causing him to lose track of time and leave late. Scott has provided invaluable insight and support at every stage of my graduate studies, and I can't thank him enough. Scott's other half, Silva, has been equally supportive and caring throughout my studies. Pandemics, NMR room floods, and high scorers on the FID probe can't stop Dr. David VanderVelde. Dave has an encyclopedic knowledge of all things NMR and was always happy to sit with me and talk through my NMR spectra. Dave's NMR digest is an often-underappreciated source of levity that never failed to give me a hearty chuckle during rough days in the lab. Dr. Mike Takase and Dr. Larry Henling are some of the most gifted and patient crystallographers. I've brought my fair share of mediocre crystals to Mike and Larry, yet

they always pulled out a structure for me. The moment of terror and subsequent peace of mind provided by Mike and Larry's crystal structure emails always made me feel alive.

I would also like to thank Dr. Mona Shahgholi for her mass spectrometry expertise and ability to turn around a hundred samples in a just few days. Beth Marshall has been an incredibly supportive and helpful administrative assistant. I don't think I could have successfully scheduled my propositions exam and thesis defense on such a tight timeline if not for Beth's persistence and dedicated support. I would also like to thank Joe Drew for his work in keeping things running and the Church freezer shuffle days that kept the pandemic days interesting. I am also thankful for Greg and Armando and everything they do behind the scenes to keep our lab stocked and supplied. Alison Ross and the rest of the graduate studies staff have kept things running smooth even in the face of a global pandemic.

The Stoltz group has been a cavalcade of characters that made graduate school open, collaborative, and fun. I'm incredibly fortunate to have a number of excellent project partners and friends. Dr. Eric Alexy invited me to join him in Pd-chemistry in my second year when I previously had no mentor in the lab. Through Eric, I learned a substantial amount about chemistry, how to set up and organize projects, and most importantly: how to save trips to the solvent system. I consider Eric one of my best friends and I am fortunate to have so many great memories thanks to his friendship. Alex Cusumano is a brilliant chemist that joined the lab in my third year. Alex has had an incredible impact on me and the group in bringing theoretical studies into the fold. Although most things he talks about go way over my head, his passion and conviction for theory and applications thereof are inspiring. Nick Hafeman is another of my best friends and has made the last two pandemic

years of graduate school some of the best. Nick and I have a lot of shared humor that has really kept me going during the most stressful times of graduate school. Nick is also a brilliant and skilled chemist and has a knack for total synthesis. Nick's persistence, hard "ruhsearch," and knowledge are inspirational. Abbvie is a lucky company for hiring Nick and I can't wait to see what he accomplishes in the future. Melinda Chan is a dedicated and hardworking chemist and I admire her conviction and determination in the face of so many challenging reactions on team Havellockate. I appreciate having had the opportunity to research (not work) with such a talented student during my last two years. Joel Monroy was an incredibly hard working, talented, and fun person to collaborate with. I am so thrilled that he has found a career in teaching that makes him happy.

I have also been fortunate to mentor two brilliant undergraduate students. Brenda Wu was brave enough to join me in the lab when I was barely a second-year graduate student. I am thankful for everything Brenda taught me about being a supportive mentor and for all her hard work, especially when my project ideas failed. I am happy to have stayed in contact with Brenda as she pursues her graduate studies at Stanford and I can't wait to see where she goes in life. Emily Du joined me in my third year and was incredibly fun to work with. Emily always surprised me with their knowledge of organic chemistry and ability to quickly assimilate new information in their research. Emily was courageous in eagerly undertaking two book chapters with me during the pandemic. I am delighted that Emily has joined the ongoing interrupted Tsuji projects to finish out their senior year.

Throughout my graduate studies, I have overlapped with many talented chemists. I would like to recognize Stoltz alumni Austin Wright, David Schuman, Steven Loskot, Beau Pritchett, Caleb Hethcox, Eric Welin, Gerit Pototschnig, and Carina Jette for their friendship

and intellectual discussions during my time in the Stoltz lab. I want to particularly highlight Chris Reimann, Fa Ngamnithiporn, Nick Hafeman, and Eric Alexy for being like a family to me. Some of my best memories are with this group and I can't imagine life without them. Going to Ernie's 5 days a week, dinner-time ping pong matches, and playing "Down the Clown" at Bowlero were peak graduate school fun. Although it was hard to convince Fa to go to Ernie's more than once a week, I am thankful she was there the day I was attacked by a praying mantis. I am also thankful to have overlapped with two talented and exceptionally funny visiting students, Álvaro Velasco-Rubio and Rémi Lavernhe.

I also want to acknowledge the talented class of G4's, Alexia Kim, Tyler "the back" Casselman, Zack Sercel, and Alex Cusumano for their leadership and dedication to the lab. I want to thank Alexia for interjecting some new tunes into our bay and for being a supportive lab mate. I can't say the same for Alex, his music was NSFS (not safe for Scott) and made Reiman's music look tame.

In my last two years 14(!) exceptional graduate students joined our lab. It has been a pleasure to watch these students acclimate and succeed at Caltech, despite the challenges of a pandemic and a pandemic of broken hoods. I want to acknowledge the G2's Elliot Hicks, Samir Rezgui, Kevin Gonzalez, and Farbod Moghadam for their friendship and fun times during my last two years. I am confident that the Stoltz lab is in great hands, and I look forward to seeing their achievements in the coming years.

Outside of lab, I was fortunate to have served as the residential associate (RA) of Venerable House for 2.5 years. Through this experience, I had the opportunity to mentor and learn from some of the brightest students in the world. The students of Caltech are truly a unique and fun bunch. I will fondly remember our tea times and various other events. I

would also like to extend my most sincere gratitude to my mentors as a RA: Felicia Hunt, Erica Crawford, Kenny Carter, and Vanessa Tejada.

Finally, I want to acknowledge my family for their unwavering support and love. Despite being across the country, my mom and dad have been incredibly supportive and understanding of the time commitments of graduate school. My gram, Carol Valsechi, was one of my biggest supporters and was always there to cheer me on. Every time we talked, she would start by asking "Did you make any new molecules?" I was heartbroken at her sudden and unexpected passing during my fifth year after being apart for all the pandemic, so I am happy to dedicate this thesis to her memory. Last, and certainly not least, I want to thank my partner Bernice Sanchez and her family for their support, especially during the stressful concluding months of my graduate studies. Bernice has been my rock and a constant source of support. I am thankful for everything she does and look forward to returning to our campfires at the beach this summer.

ABSTRACT

Research in the Stoltz group aims, generally, to develop novel technologies for the preparation of stereochemically rich molecules and, further, to apply these technologies in the context of complex natural product total synthesis. Chapter 1 of this thesis describes the strategic utilization of a Pd-catalyzed asymmetric allylic allylation and *N*-acyl iminium ion cyclization to accomplish short, enantioselective total syntheses of *Myrioneuron* alkaloids (–)-myrifabral A and (–)-myrifabral B. Chapter 2 describes the development of a Pd-catalyzed asymmetric allylic alkylation to generate acyclic α-quaternary carboxylic acid derivatives from geometrically defined fully substituted *N*-acyl indole-derived allyl enol carbonates. While ester-derived enol carbonates could be prepared with a high degree of enolate geometry control, they were ineffective in the asymmetric allylic alkylation reaction. Thus, *N*-acyl indole substrates served as excellent carboxylic ester equivalents. Chapter 3 discusses an unusual Pd-catalyzed decarboxylative α,β-dehydrogenation reaction of *N*-acyl indole-derived enol carbonates enabled by a novel, highly electron-deficient phosphinooxazoline ligand. Research presented in Chapter 4 delineates a globally diastereoconvergent approach to the Ireland–Claisen rearrangement for the synthesis of α-tetrasubstituted amino acids bearing vicinal tertiary stereogenic centers. Computational investigation of the diastereoconvergence in Ireland–Claisen rearrangement revealed key intramolecular interactions which enable the reaction to proceed in exceptional diastereoselectivity without the need for a selective enolization protocol. A diastereodivergent approach for the Ireland–Claisen rearrangement in acyclic systems to generate vicinal quaternary/tertiary and quaternary/quaternary stereogenic centers in good to high diastereoselectivity is also discussed. Enolate geometry control and substrate design

are critical for achieving high diastereoselectivity in these transformations. Finally, the applications of the cryoEM technique micro-electron diffraction (microED) to the structural elucidation of small organic and organometallic molecules are presented.

PUBLISHED CONTENT AND CONTRIBUTIONS

1. Fulton, T. J.; Chen, A. Y.; Bartberger, M. D.; Stoltz, B. M. "Enantioselective Total Synthesis of (–)-Myrifabral A and B." *Chem*. *Sci*. **2020**, *11*, 10802–10806. DOI: 10.1039/D0SC01141J.

   T. J. F. participated in synthetic planning, reaction optimization, experimental work, data analysis, and manuscript preparation.

2. Alexy, E. J.[‡]; Fulton, T. J.[‡]; Zhang, H.; Stoltz, B. M. "Palladium-Catalyzed Enantioselective Decarboxylative Allylic Alkylation of Fully Substituted *N*-Acyl Indole-Derived Enol Carbonates." *Chem*. *Sci*. **2019**, *10*, 5996–6000. DOI: 10.1039/C9SC01726G.

   T. J. F. participated in reaction optimization, experimental work, data analysis, and manuscript preparation.

3. Fulton, T. J.; Wu, B.; Alexy, E. J.; Zhang, H.; Stoltz, B. M. "Palladium-Catalyzed Dehydrogenation of Acyclic Ester Equivalents Promoted by a Novel Electron Deficient Phosphinooxazoline Ligand." *Tetrahedron* **2019**, *31*, 4104–4109. DOI: 10.1016/j.tet.2019.05.065.

   T. J. F. participated in reaction optimization, experimental work, data analysis, and manuscript preparation.

4. Fulton, T. J.[‡]; Cusumano, A. Q.[‡]; Alexy, E. J.; Du, Y. E.; Zhang, H.; Stoltz, B. M. "Global Diastereoconvergence in the Ireland–Claisen Rearrangement of Isomeric Enolates: Synthesis of Tetrasubstituted α-Amino Acids." *J*. *Am*. *Chem*. *Soc*. **2020**, *142*, 21938–21947. DOI: 10.1021/jacs.0c11480. (Highlighted in *Synfacts* **2021**, *17*, 349).

T. J. F. participated in reaction optimization, experimental work, data analysis, and manuscript preparation.

5. Jones, C. G.; Martynowycz, M. W.; Hattne, J.; Fulton, T. J.; Stoltz, B. M.; Rodríguez, J. A.; Nelson, H. M.; Gonen, T. "The CryoEM Method MicroED as a Powerful Tool for Small Molecule Structure Determination." *ACS Cent. Sci.* **2018**, *11*, 1587–1592.

   T. J. F. participated in experimental work, data analysis, and manuscript preparation.

6. Jones, C. G.; Asay, M.; Kim, L. J.; Kleinsasser, J. F.; Saha, A.; Fulton, T. J.; Berkly, K. R.; Cascio, D.; Malyutin, A. G.; Conley, M. P.; Stoltz, B. M.; Lavallo, V.; Rodríguez, J. A.; Nelson, H. M. "Characterization of Reactive Organometallic Species via MicroED." *ACS Cent. Sci.* **2019**, *5*, 1507–1513.

   T. J. F. participated in experimental work, data analysis, and manuscript preparation.

TABLE OF CONTENTS

LIST OF FIGURES

CHAPTER 1
Enantioselective Total Synthesis of (–)-Myrifabral A and B

APPENDIX 2
Spectra Relevant to Chapter 1

APPENDIX 4

X-Ray Crystallography Reports Relevant to Chapter 2

CHAPTER 3

Pd-Catalyzed Decarboxylative Dehydrogenation of Full Substituted N-Acyl Indole-Derived Enol Carbonates

APPENDIX 5

Spectra Relevant to Chapter 3

CHAPTER 4

Global Diastereoconvergence in the Ireland–Claisen Rearrangement of Isomeric Enolates: Synthesis of Tetrasubstituted α-Amino Acids

APPENDIX 6

Spectra Relevant to Chapter 4

LIST OF SCHEMES

CHAPTER 1
Enantioselective Total Synthesis of (–)-Myrifabral A and B

APPENDIX 1
Synthetic Summary to Chapter 1

CHAPTER 2
Pd-Catalyzed Asymmetric Decarboxylative Allylic Alkylation of Fully Substituted N-Acyl Indole-Derived Enol Carbonates

CHAPTER 3
Pd-Catalyzed Decarboxylative Dehydrogenation of Full Substituted N-Acyl Indole-Derived Enol Carbonates

CHAPTER 4

Global Diastereoconvergence in the Ireland–Claisen Rearrangement of Isomeric Enolates: Synthesis of Tetrasubstituted α-Amino Acids

APPENDIX 8

Diastereodivergent Ireland–Claisen Rearrangements of Isomeric Enolates

APPENDIX 9

The Total Synthesis of Havellockate

LIST OF TABLES

CHAPTER 1

Enantioselective Total Synthesis of (–)-Myrifabral A and B

CHAPTER 2

Pd-Catalyzed Asymmetric Decarboxylative Allylic Alkylation of Fully Substituted N-Acyl Indole-Derived Enol Carbonates

APPENDIX 4

X-Ray Crystallography Reports Relevant to Chapter 2

CHAPTER 3

Pd-Catalyzed Decarboxylative Dehydrogenation of Full Substituted N-Acyl Indole-Derived Enol Carbonates

CHAPTER 4

Global Diastereoconvergence in the Ireland–Claisen Rearrangement of Isomeric Enolates: Synthesis of Tetrasubstituted α-Amino Acids

APPENDIX 7

X-Ray Crystallography Reports Relevant to Chapter 4

APPENDIX 8

Diastereodivergent Ireland–Claisen Rearrangements of Isomeric Enolates

APPENDIX 13

Notebook Cross-Reference for New Compounds

LIST OF ABBREVIATIONS

$[\alpha]_D$	specific rotation at wavelength of sodium D line
ºC	degrees Celcius
Å	Ångstrom
app	apparent
aq	aqueous
Ar	aryl
atm	atmosphere
Bn	benzyl
Boc	*tert*-butyloxycarbonyl
bp	boiling point
br	broad
c	concentration for specific rotation measurements
calc'd	calculated
CBS	Corey–Bakshi–Shibata
cm^{-1}	wavenumber(s)
d	doublet
D	deuterium

dba	dibenzylideneacetone
DDQ	2,3-dichloro-5,6-dicyano-*p*-benzoquinone
DMAP	4-dimethylaminopyridine
DMF	dimethylformamide
DMS	dimethylsulfide
dr	diastereomeric ratio
EDC	*N*-(3-dimethylaminopropyl)-*N'*-ethylcarbodimide
ee	enantiomeric excess
EI+	electron impact
equiv	equivalent(s)
ESI	electrospray ionization
Et	ethyl
EtOAc	ethyl acetate
FAB	fast atom bombardment
g	gram(s)
GC	gas chromatography
h	hour(s)

HG-II	Hoveyda–Grubbs catalyst 2nd generation
HPLC	high-performance liquid chromatography
HRMS	high-resolution mass spectrometry
Hz	hertz
i-Bu	*iso*-butyl
IR	infrared (spectroscopy)
J	coupling constant
K	Kelvin (absolute temperature)
kcal	kilocalorie
KHMDS	potassium hexamethyldisilazide
L	liter; ligand
L*	chiral ligand
LDA	lithium diisopropylamide
m	multiplet, milli
m	meta
m/z	mass to charge ratio
Me	methyl

mg	milligram(s)
MHz	megahertz
min	minute(s)
MM	mixed method
mol	mole(s)
mp	melting point
n	nano
n-Bu	*n*-butyl
NBS	*N*-bromosuccimide
NMR	nuclear magnetic resonance
NPhth	phthalimide
Nu	nucleophile
o	ortho
p	para
Pd/C	palladium on carbon
Ph	phenyl
pH	hydrogen ion concentration in aqueous solution

PHOX	phosphinooxazoline
ppm	parts per million
Pr	propyl
q	quartet
R	generic for any atom or functional group
Ref.	reference
R_f	retention factor
s	singlet
sat.	saturated
SFC	supercritical fluid chromatography
t	triplet
t-Bu	*tert*-butyl
TBAF	tetrabutylammonium fluoride
TBS	*tert*-butyldimethylsilyl
TES	triethylsilyl
THF	tetrahydrofuran
TLC	thin-layer chromatography

TMS	trimethylsilyl
t_R	retention time
UV	ultraviolet
v/v	volume to volume
w/v	weight to volume
λ	wavelength
μ	micro

CHAPTER 1

Enantioselective Total Synthesis of (–)-Myrifabral A and B[†]

1.1 INTRODUCTION

The *Myrioneuron* alkaloids are a family of structurally diverse polycyclic (tri-, tetra-, penta-, hexa-, and decacyclic) alkaloids hypothesized to share a common biosynthetic origin from lysine (Figure 1.1.1).[1] The first *Myrioneuron* alkaloids from *Myrioneuron nutans* were reported in 2002, with altogether 10 structures reported to date.[2] Since 2013, many new alkaloids have been isolated from *Myrioneuron faberi*,[3] *Myrioneuron tonkinesis*,[4] and *Myrioneuron effusum*.[5] In addition to their interesting structural features, a number of these alkaloids possess a range of biological activities such as antimalarial properties, KB cell cytotoxicity, antimicrobial, and hepatitis C virus (HCV) replication inhibition.[1–5] Despite possessing promising biological properties and synthetically attractive motifs , relatively few of these alkaloids have been prepared by total synthesis efforts.[2d,e,f,6]

Figure 1.1.1 *Representative Myrioneuron alkaloids.*

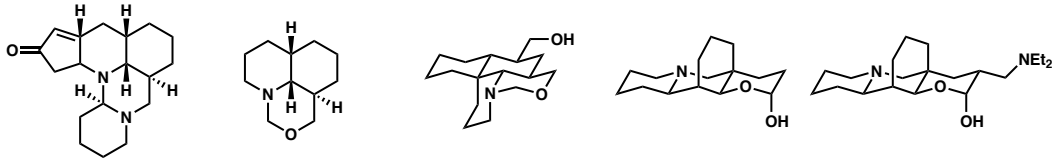

We became interested in (±)-myrifabral A (**4**) and (±)-myrifabral B (**5**) due to their unique cyclohexane-fused octahydroquinolizine skeletons, which contain four contiguous stereogenic

[†]This research was performed in collaboration with Anthony Y. Chen and Dr. Michael D. Bartberger. Portions of this chapter have been reproduced with permission from Fulton, T. J.; Chen, A. Y.; Bartberger, M. D.; Stoltz, B. M. *Chem. Sci*. **2020**, *11*, 10802–10806. © 2020 Royal Society of Chemistry.

centers including an all-carbon quaternary center embedded in the cyclohexane fusion. Interestingly, both **4** and **5** were isolated from *Myrioneuron faberi* as racemic mixtures of α- and β-hydroxy epimers. Even as racemates, these clusters display promising HCV replication inhibition (EC_{50} = 4.7 μM for (±)-α,β-OH-**4** and 2.2 μM for (±)-α,β-OH-**5**, respectively) with significantly reduced liver cell cytotoxicity compared to commercial pharmaceutical HCV drug telaprevir (EC_{50} = 0.09 μM).[3c] She *et al*. reported a rapid total synthesis of (±)-α,β-OH-**4** and 2 (±)-α,β-OH-**5**, however, prior to our publication, no asymmetric approaches were disclosed.[6c] To enable further studies of these alkaloids in enantioenriched form, we developed a short, catalytic enantioselective total synthesis of (–)-α,β-OH-**4** and (–)-α,β-OH-**5**.

1.2 RETROSYNTHETIC ANALYSIS

In devising our strategy, we targeted (–)-myrifabral A (**4**), which can be directly converted to (–)-myrifabral B (**5**), as reported by She (Scheme 1.2.1).[6c] Retrosynthetically, we envisioned (–)-myrifabral A (**4**) could be simplified to tricyclic lactam (**6**). Importantly, the versatile ketone, allyl, and lactam functional handles in tricyclic lactam **6** provide ample opportunity for future diversification of the natural product scaffold for medicinal chemistry efforts and potential derivative synthesis. We envisioned the critical C(6)–C(7) bond could arise by means of a diastereoselective *N*-acyl iminium ion cyclization of enantioenriched ketone **7**.[7] Finally, the C(10) all-carbon quaternary center could be forged in an enantioselective manner by means of asymmetric allylic alkylation of glutarimide **8**. In turn, glutarimide **8** could be prepared from β-ketoester **9**.

Scheme 1.2.1. *Retrosynthetic Analysis of (–)-Myrifabral A.*

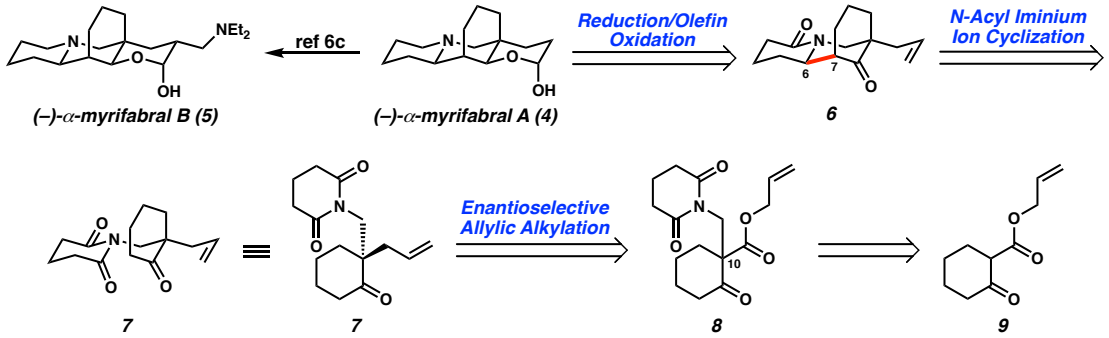

1.3 DEVELOPMENT OF A ONE-POT GLUTARIMIDE SYNTHESIS

Our synthetic efforts commenced with the preparation of glutarimide **8** (Scheme 1.3.1). Alkylation of β-ketoester **9** with sulfonylmethyl carbamate **10** in the presence of Cs_2CO_3 proceeded smoothly on a 30.0 g scale to afford α-aminoketone **11** in 95% yield.[8] Elaboration of the Boc-protected amine to glutarimide **8** proceeded via a three-step reaction sequence: 1) amine-deprotection via TFA mediated Boc removal, 2) mono-acylation of the amine with glutaric anhydride, and 3) glutarimide ring closure utilizing standard protocols. Unfortunately, this procedure proved untenable for material throughput, inspiring the development of a practical, one-pot procedure.

Scheme 1.3.1. *Initial Synthesis of Glutarimide **8**.*

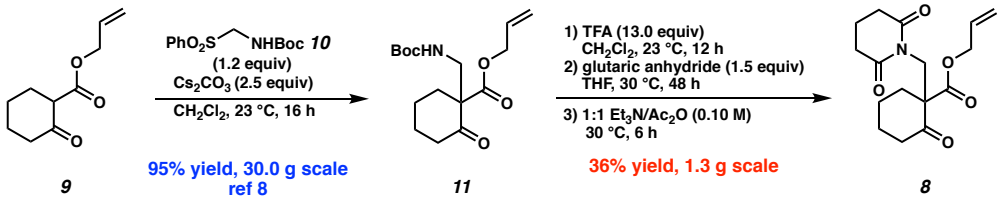

Trifluoroacetic acid-mediated amine deprotection and double condensation in refluxing DMF provided glutarimide **8** in 60% yield (Table 1.3.1, entry 1). Utilizing 1,4-dioxane as a solvent instead of DMF improved the yield of glutarimide **8** to 70% (entry 2).

Stoichiometric boric acid enabled the transformation in excellent yield in xylenes at 140 °C (entry 3). While aryl boronic acids[9] and boric acid[10] have been demonstrated as effective catalysts for amidation of carboxylic acids with amines, we were surprised to observe commensurate Boc removal, amidation, and glutarimide cyclization in a single reaction pot. Control experiments revealed the reaction only proceeds with the complete set of reagents (entries 4–6). Furthermore, Boc protected α-aminoketone **11** was stable to xylenes at reflux for 120 h (entry 7). Catalytic boric acid (10 mol %) with 2 equivalents of glutaric anhydride (**12**) performed equally well as our best conditions (entry 8). Glutaric anhydride (**12**) was replaced with glutaric acid (**13**) without loss of reactivity (entry 9). Rendering the transformation homogeneous by utilizing $PhB(OH)_2$ as a soluble boronic acid reduced the reaction time (entry 10), however, this benefit was tempered in larger scale reactions (entry 11). Finally, electron-poor 4-CF_3-$PhB(OH)_2$ enabled the one-pot transformation to proceed at a faster rate in identical yield (entry 12).

Table 1.3.1. *Glutarimide Synthesis Reaction Optimization.*[a]

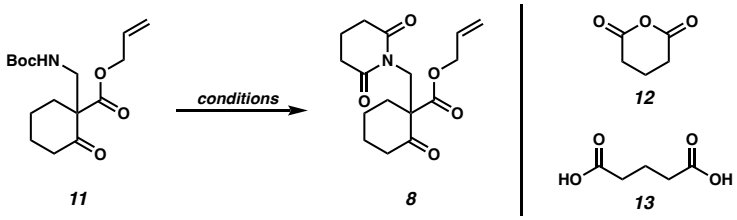

entry	conditions	isolated yield (%)
1	3:1 DMF/TFA, *12* (4.0 equiv), reflux, 48 h	60
2	3:1 1,4-dioxane/TFA, *12* (4.0 equiv), reflux, 48 h	70
3	$B(OH)_3$ (3.0 equiv), *12* (4.0 equiv), xylenes, Dean–Stark, reflux, 36 h	90–95
4	$B(OH)_3$ (3.0 equiv), *12* (4.0 equiv), xylenes, Dean–Stark, reflux, 36 h	>95% *11*
5	*12* (4.0 equiv), xylenes, Dean–Stark, reflux, 72 h	>95% *11*
6	*13* (4.0 equiv), xylenes, Dean–Stark, reflux, 72 h	>95% *11*
7	xylenes, Dean–Stark, reflux, 120 h	>95% *11*
8	$B(OH)_3$ (10 mol %), *12* (2.0 equiv), xylenes, Dean–Stark, reflux, 36 h	90–95
9	$B(OH)_3$ (10 mol %), *13* (2.0 equiv), xylenes, Dean–Stark, reflux, 36 h	90–95
10	$PhB(OH)_2$ (10 mol %), *13* (2.0 equiv), xylenes, Dean–Stark, reflux, 24 h	90–95
11[b]	$PhB(OH)_2$ (10 mol %), *13* (2.0 equiv), xylenes, Dean–Stark, reflux, 24 h	90–95
12[b]	4-CF_3-$PhB(OH)_2$ (10 mol %), *13* (2.0 equiv), xylenes, Dean–Stark, reflux, 24 h	90–95

[a] Reaction performed on a 0.16 mmol scale unless otherwise noted. [b] Reaction performed on a 0.80 mmol scale.

1.4 TOTAL SYNTHESIS OF (–)-MYRIFABRAL A AND B

With optimized conditions for the one-pot glutarimide synthesis in hand, α-aminoketone **11** was converted to glutarimide **8** on a 15.0 g scale in 85% yield (Scheme 1.4.1). Palladium-catalyzed decarboxylative asymmetric allylic alkylation of glutarimide **8** with *(S)*-$(CF_3)_3$-*t*-BuPHOX (**L1**) as the chiral ligand established the C(10) all-carbon quaternary center, affording ketone **7** in 94% yield and 88% ee. The absolute configuration of the all-carbon quaternary was determined as *(S)* via vibrational circular dichroism (VCD) analysis. To affect the key *N*-acyl iminium ion cyclization, the ketone was first protected as ethyl vinyl ether **14**. Mono-reduction of the glutarimide with $LiEt_3BH$ formed intermediate *N*-acyl hemiaminal **15** which underwent *N*-acyl iminium ion cyclization upon treatment with

BF_3•OEt_2 to provide tricyclic lactam **6** as a single diastereomer in 81% yield over three steps. Completion of the synthesis required reduction of the lactam and ketone and elaboration of the terminal olefin to an aldehyde. To this end, a one-pot procedure was developed wherein the ketone was first reduced by L-Selectride with exceptional diastereoselection (>19:1). Following the reduction of the ketone, addition of $LiAlH_4$ and heating to reflux afforded complete reduction of the lactam to the corresponding tertiary amine. A modified Fieser work up then provided desired amino alcohol 16 in 97% yield.

Scheme 1.4.1. *Enantioselective Synthesis of the Tricyclic Core.*

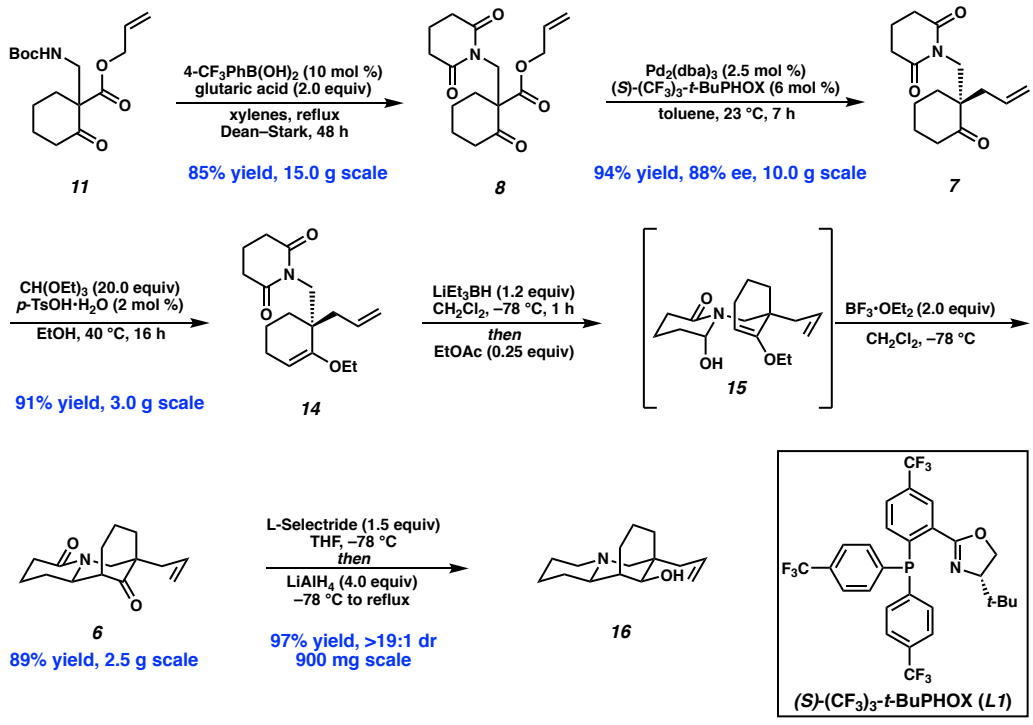

Initially, we found the terminal olefin recalcitrant to both direct and two-step oxidations to the aldehyde due to challenges with olefin isomerization and undesired or poor reactivity. To our delight, olefin cross metathesis using Hoveyda–Grubbs II catalyst of amino alcohol 16 with vinyl boronic acid pinacol ester (17) as an aldehyde surrogate smoothly afforded metathesis product 18 (Scheme 1.4.2). Elaboration of the vinyl boronate was then

affected by deprotection and oxidation of the boronic acid, with in situ lactolization providing (–)-myrifabral A in 50% yield. Adaptation of She's conditions for the synthesis of (±)-myrifabral B then provided access to (–)-myrifabral B in 70% yield.[6c] In our hands both (–)-myrifabral B, and (–)-myrifabral A were isolated as oils, whereas racemates of these compounds are isolated as solids amenable to crystallization for X-Ray crystallography.[3c,6c] The absolute stereochemistry of the natural products was therefore determined via VCD analysis (vide supra). Spectroscopic data obtained were in excellent agreement with the natural compound (see section 1.6.4).

Scheme 1.4.2 *Completion of the Synthesis of (–)-Myrifabral A and B.*

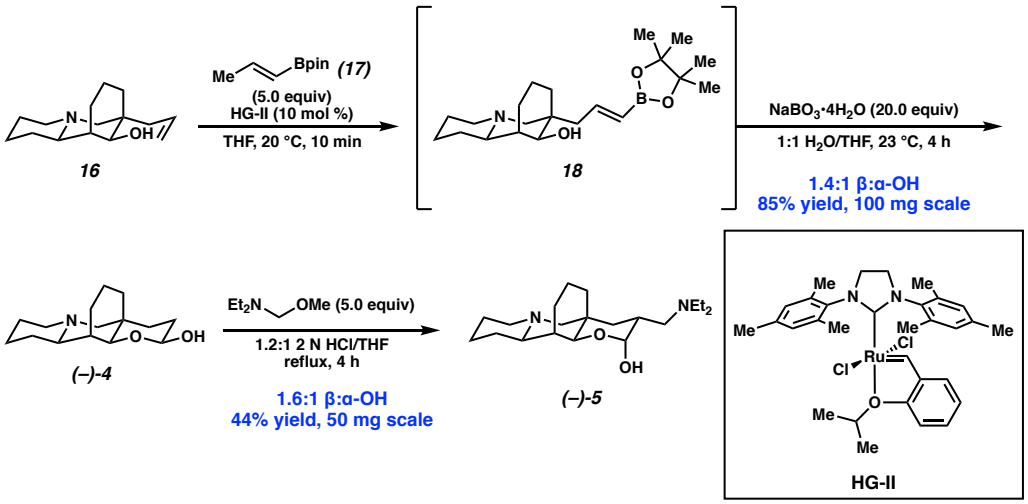

1.5 CONCLUSION

We have described the first enantioselective total synthesis of (–)-myrifabral A and B. Critical to the success of this strategy was the development of a direct and high yielding one-pot conversion of a Boc-protected amine (**11**) to the glutarimide (**8**). Palladium catalyzed decarboxylative asymmetric allylic alkylation provided the C(10) all-carbon quaternary center in 88% ee, setting the stage for ketone protection, glutarimide reduction, and an exclusively diastereoselective *N*-acyl iminium ion

cyclization. Following ketone and lactam reduction, cross metathesis with vinyl boronic acid pinacol boronate and subsequent boronic acid deprotection and oxidation afforded (–)-myrifabral A. Utilizing previously reported conditions, (–)-myrifabral A was converted to (–)-myrifabral B. This marks the first catalyst-controlled asymmetric synthesis of myrifabral A and B, enabling future biological study of individual enantiomeric series.

1.6 EXPERIMENTAL SECTION

1.6.1 MATERIALS AND METHODS

Unless otherwise stated, reactions were performed in flame-dried glassware under an argon or nitrogen atmosphere using dry, deoxygenated solvents. Solvents were dried by passage through an activated alumina column under argon.[11] Reaction progress was monitored by thin-layer chromatography (TLC) or Agilent 1290 UHPLC-MS. TLC was performed using E. Merck silica gel 60 F254 precoated glass plates (0.25 mm) and visualized by UV fluorescence quenching, *p*-anisaldehyde, or $KMnO_4$ staining. Silicycle Silia*Flash*® P60 Academic Silica gel (particle size 40–63 μm) was used for flash chromatography. ^{1}H NMR spectra were recorded on Varian Inova 500 MHz and Oxford 600 MHz spectrometers and are reported relative to residual $CHCl_3$ (δ = 7.26 ppm) or TMS (δ = 0.00 ppm). ^{13}C NMR spectra were recorded on a Bruker 400 MHz spectrometer (100 MHz) and are reported relative to $CHCl_3$ (δ = 77.16 ppm), C_6D_6 (δ = 128.06 ppm). Data for ^{1}H NMR are reported as follows: chemical shift (δ ppm) (multiplicity, coupling constant (Hz), integration). Multiplicities are reported as follows: s = singlet, d = doublet, t = triplet, q = quartet, p = pentet, sept = septuplet, m = multiplet, br s = broad singlet, br d = broad doublet. Data for ^{13}C NMR are reported in terms of chemical shifts (δ ppm). IR spectra

were obtained by use of a Perkin Elmer Spectrum BXII spectrometer or Nicolet 6700 FTIR spectrometer using thin films deposited on NaCl plates and reported in frequency of absorption (cm^{-1}). Optical rotations were measured with a Jasco P-2000 polarimeter operating on the sodium D-line (589 nm), using a 100 mm path-length cell. High resolution mass spectra (HRMS) were obtained from Agilent 6200 Series TOF with an Agilent G1978A Multimode source in electrospray ionization (ESI+), atmospheric pressure chemical ionization (APCI+), or mixed ionization mode (MM: ESI-APCI+). Reagents were purchased from commercial sources and used as received unless otherwise stated.

1.6.2 EXPERIMENTAL PROCEDURES

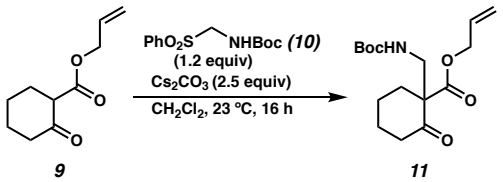

α-aminomethyl β-keto ester 11

Compound **11** was prepared as previously described by Stoltz et al.[2] To a stirred solution of β-keto ester **9** (20.0 g, 120.3 mmol, 1.0 equiv) in CH_2Cl_2 (600 mL) was added sulfonylmethyl carbamate **10** (39.2 g, 144.4 mmol, 1.2 equiv) in one portion at ambient temperature. After stirring for 5 min, Cs_2CO_3 (98.0 g, 300 mmol, 2.5 equiv) was added in one portion. The resulting white suspension was stirred vigorously at 20 ºC. After 16 h, full consumption of starting material was determined by TLC analysis. Saturated aqueous ammonium chloride (300 mL) was added slowly, and the biphasic mixture was stirred at ambient temperature for 40 min and extracted with CH_2Cl_2 (3 x 100 mL). The combined organic layers were dried over Na_2SO_4, filtered, and concentrated to a viscous, colorless oil. Flash column chromatography (SiO_2, 10% EtOAc in hexanes) afforded α-aminomethyl

β-keto ester **11** as an amorphous white solid (35.61 g, 114.36 mmol, 95% yield); ^{1}H NMR (500 MHz, $CDCl_3$) δ 5.91 (ddt, *J* = 17.2, 10.4, 5.9, 1H), 5.33 (dq, *J* = 17.2, 1.4, 1H), 5.25 (dd, *J* = 10.4, 1.4 Hz, 1H), 5.17 (t, *J* = 5.7 Hz, 1H), 4.63 (d, *J* = 5.8 Hz, 1H), 3.55 (dd, *J* = 13.9, 7.7 Hz, 1H), 3.41 (dd, *J* = 13.9, 5.7 Hz, 1H), 2.63–2.34 (m, 3H), 2.07–1.94 (m, 1H), 1.87–1.75 (m, 1H), 1.74 – 1.53 (m, 4H), 1.41 (s, 9 H);^{13}C NMR (100 MHz, $CDCl_3$) δ 208.9, 170.9, 155.9, 131.6, 119.2, 79.4, 66.3, 62.4, 44.3, 40.8, 33.8, 28.4, 27.2, 22.1; IR (Neat Film, NaCl) 3460, 2936, 2869, 1712, 1501, 1451, 1391, 1366, 1315, 1225, 1202, 1170, 1140, 1099, 931, 856 cm^{-1}; HRMS (MM:ESI-APCI+) *m/z* calc'd for $C_{16}H_{26}NO_5$ $[M+H]^+$: 312.1805, found 312.1805.

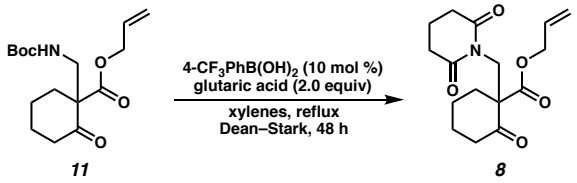

Glutarimide 8

A flame-dried 2 L round bottom flask equipped with a Dean–Stark trap, a reflux condenser and a stirring bar was charged with **11** (15.00 g, 48.17 mmol, 1.0 equiv), glutaric acid (12.73 g, 96.35 mmol, 2.0 equiv), 4-$CF_3PhB(OH)_2$ (915.3 mg, 4.82 mmol, 10 mol %), and xylenes (960 mL). The resulting suspension was heated to reflux in a heating mantle with vigorous stirring. After 48 h, the light orange reaction solution was cooled to 20 ºC and concentrated to provide a crude orange oil. The crude oil was purified by column chromatography (2 → 5% EtOAc in CH_2Cl_2) to afford an off-white semisolid which was further purified by column chromatography (SiO_2, 20→ 40% EtOAc in hexanes) to provide **8** as an amorphous white solid (12.62 g, 41.05 mmol, 85% yield); ^{1}H NMR (500 MHz, $CDCl_3$) δ 5.94 (dddd, *J* = 17.3, 10.4, 6.1, 5.6 Hz, 1H), 5.33 (dd, *J* = 17.3, 1.5 Hz, 1H), 5.25

(dd, J = 10.4, 1.5 Hz, 1H), 4.66 (ddt, J = 13.1, 6.1, 1.2 Hz, 1H), 4.53 (ddt, J = 13.1, 5.6, 1.2 Hz, 1H), 4.32 (ABq, $\Delta\delta_{AB}$ = 0.05, J_{AB} = 14.1 Hz, 2H), 2.64 (t, J = 6.5 Hz, 4H), 2.48–2.36 (m, 2H), 2.30–2.24 (m, 1H), 2.03–1.97 (m, 1H), 1.94 (p, J = 6.6 Hz, 2H), 1.77–1.70 (m, 1H), 1.67–1.49 (m, 3H); ^{13}C NMR (100 MHz, $CDCl_3$) δ 206.0, 172.8, 169.8, 131.5, 118.6, 66.4, 59.6, 41.9, 40.9, 34.0, 32.8, 27.1, 22.2, 16.7; IR (Neat Film, NaCl) 2942, 1711, 1681, 1426, 1379, 1334, 1265, 1204, 1122, 1098, 1057, 1020 cm^{-1}; HRMS (MM:ESI-APCI+) *m/z* calc'd for $C_{16}H_{22}NO_5$ $[M+H]^+$: 308.1492, found 308.1504.

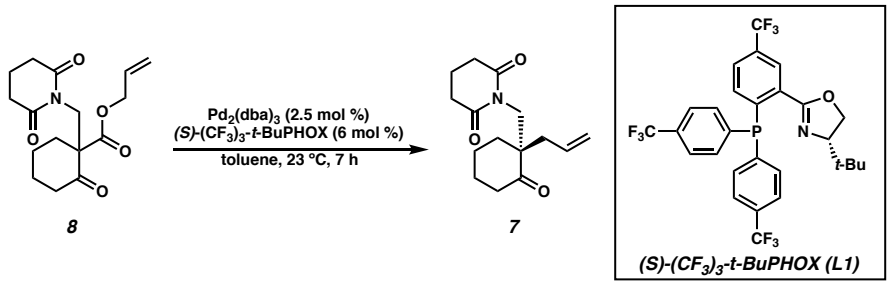

Ketone 7

An oven-dried 1 L round bottom flask was charged with $Pd_2(dba)_3$ (819.6 mg, 0.895 mmol, 2.75 mol %), (*S*)-$(CF_3)_3$-*t*-BuPHOX (1.1548 g, 1.95 mmol, 6.0 mol %), and a magnetic stirring bar in a N_2-filled glovebox. The flask was then charged with toluene (650 mL) and stirred at 24 ºC for 40 min, generating a dark orange/red solution. The preformed catalyst solution was then cannulated into a solution of **8** (10.0 g, 32.54 mmol, 1.0 equiv) dissolved in toluene (325 mL) in a 2 L flame-dried round bottom flask. The resulting dark green solution was stirred at 24 ºC. Full consumption of the starting material was achieved after 7 h, as determined by TLC analysis (25% EtOAc in hexanes). The crude reaction mixture was concentrated and directly purified by column chromatography (SiO_2, 10 → 40% EtOAc in hexanes) to yield glutarimide **7** as an off white semi-solid (8.06 g, 30.6 mmol, 94% yield); 88% ee, $[\alpha]_D^{25}$ +32.9 (*c* 1.0, $CHCl_3$); ^{1}H NMR (500 MHz, C_6D_6) δ 5.67

(dddd, J = 16.7, 10.3, 8.4, 5.9 Hz, 1H), 5.04–4.94 (m, 2H), 4.12 (ABq, $\Delta\delta_{AB}$ = 0.22, J_{AB} = 13.7 Hz, 2H), 2.90 (ddd, J = 15.6, 12.4, 6.2 Hz, 1H), 2.63 (t, J = 6.4 Hz, 4H), 2.38 (ddt, J = 14.2, 5.8, 1.3 Hz, 1H), 2.32 (dt, J = 15.8, 4.4 Hz, 1H), 2.01–1.87 (m, 4H), 1.83–1.68 (m, 4H), 1.64–1.53 (m, 1H); ^{13}C NMR (100 MHz, $CDCl_3$) δ 213.2, 173.2, 134.7, 118.2, 51.8, 44.2, 39.6, 38.7, 35.3, 33.1, 26.1, 21.2, 16.8; IR (Neat Film, NaCl) 3072, 2937, 2864, 1727, 1701, 1679, 1638, 1430, 1380, 1340, 1319, 1243, 1173, 1120, 1056, 1008, 914, 868, 803 cm^{-1}; HRMS (MM:ESI-APCI+) *m/z* calc'd for $C_{15}H_{22}NO_3$ $[M+H]^+$: 264.1594, found 264.1591; SFC Conditions: 35% IPA, 3.5 mL/min, Chiralpak AD-H column, λ = 210 nm, t_R (min): major = 1.28, minor = 1.68.

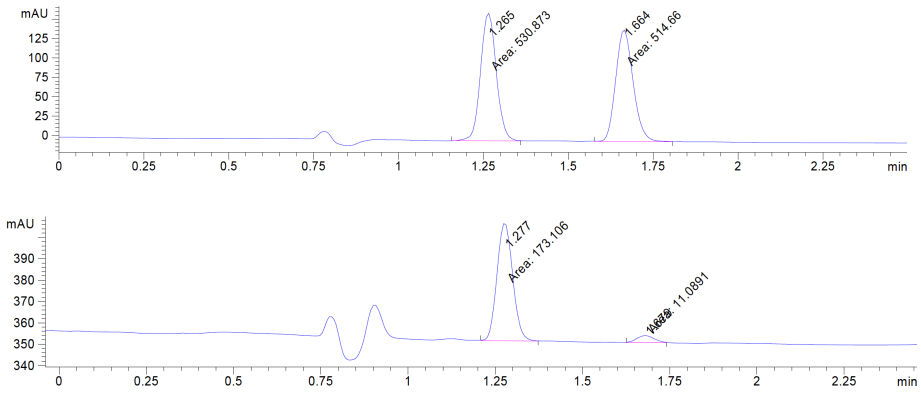

Peak #	RetTime [min]	Type	Width [min]	Area [mAU*s]	Height [mAU]	Area %
1	1.277	MM	0.0520	173.10646	55.52397	93.9797
2	1.679	MM	0.0568	11.08910	3.25302	6.0203

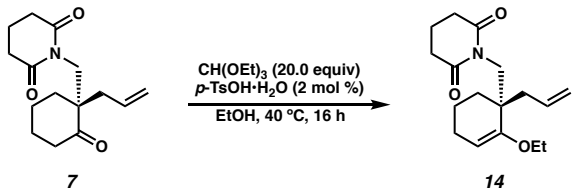

7 *14*

Ethyl vinyl ether 14

A flame-dried 250 mL round bottom flask was charged with **7** (3.00 g, 11.4 mmol, 1.0 equiv), EtOH (114 mL), *p*-TsOH•H_2O (43.4 mg, 0.228 mmol, 0.02 equiv), and $CH(OEt)_3$ (38.0 mL, 228 mmol, 20.0 equiv). The resulting clear, colorless solution was heated in a 40 ºC heating block for 16 h, after which time complete conversion was observed by TLC analysis (40% EtOAc in hexanes). The reaction mixture was concentrated under reduced pressure and the resulting colorless oil was dissolved in EtOAc (50 mL) and poured into a separatory funnel containing saturated aqueous $NaHCO_3$ (50 mL). The layers were separated, and the aqueous layer was extracted with EtOAc (2 x 100 mL). The combined organics were washed with brine (25 mL), dried over Na_2SO_4, filtered, and concentrated. Flash column chromatography (SiO_2, 30% EtOAc in hexanes) provided **14** as a colorless oil (3.0326 g, 10.41 mmol, 91% yield); $[\alpha]_D^{25}$ –72.6 (*c* 1.0, $CHCl_3$); ^{1}H NMR (500 MHz, C_6D_6) δ 5.90 (dddd, J = 17.3, 10.0, 9.2, 5.3 Hz, 1H), 5.18–5.01 (m, 2H), 4.66–4.54 (m, 1H), 4.35 (ABq, $\Delta\delta_{AB}$ = 0.23, J_{AB} = 13.1 Hz, 2H), 3.55–3.31 (m, 2H), 2.95 (ddt, J = 13.4, 5.1, 1.3 Hz, 1H), 2.14–1.81 (m, 8H), 1.77–1.64 (m, 1H), 1.64–1.50 (m, 2H), 1.10 (t, J = 7.0 Hz, 3H), 1.06 – 0.91 (m, 2H); ^{13}C NMR (100 MHz, C_6D_6) δ 172.2, 156.5, 136.4, 117.1, 96.6, 61.8, 45.1, 42.7, 41.4, 33.2, 31.8, 24.5, 19.5, 16.8, 14.8; IR (Neat Film, NaCl) 3393, 3071, 2974, 2935, 2876, 2839, 1730, 1682, 1430, 1359, 1341, 1275, 1240, 1220, 1176, 1158, 1138, 1113, 1057, 1046, 1002, 930, 912, 879, 846, 816, 787, 745, 698

cm^{-1}; HRMS (MM:ESI-APCI+) *m/z* calc'd for $C_{17}H_{26}NO_3$ $[M+H]^+$: 292.1907, found 292.1910.

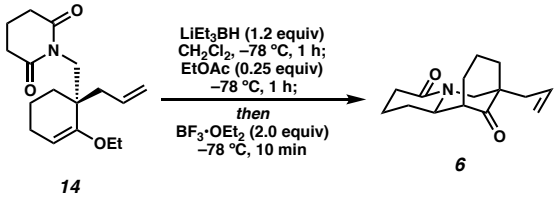

Tricyclic lactam 6

A flame-dried 250 mL round bottom flask was charged with **14** (2.50 g, 8.58 mmol, 1.0 equiv) and CH_2Cl_2 (86 mL). The resulting clear, colorless solution was cooled in a –78 ºC bath. After 15 min, $LiEt_3BH$ in (9.44 mL, 1.0 M in THF, 9.44 mmol, 1.1 equiv) was added dropwise over 5 min. After 30 min, an additional portion of $LiEt_3BH$ (360 µL, 0.360 mmol, 0.042 equiv) was added. After 10 min, an additional portion of $LiEt_3BH$ (300 µL, 0.300 mmol, 0.035 equiv) was added. After stirring for 10 min, the reaction was complete by TLC analysis (40% EtOAc in hexanes). EtOAc (210 µL, 2.15 mmol, 0.25 equiv) was added and the reaction was allowed to stir at –78 ºC. After 1 h, BF_3•OEt_2 (2.11 mL, 17.2 mmol, 2.0 equiv) was added dropwise over 5 min. After 15 min, the reaction was complete by LC/MS analysis. The reaction mixture was quenched with H_2O (60 mL), warmed to 20 ºC, and transferred to a separatory funnel with CH_2Cl_2 (10 mL). The layers were separated and the aqueous was extracted with CH_2Cl_2 (3 x 25 mL). The combined organics were dried over Na_2SO_4, filtered, and concentrated to afford a pale-yellow oil. Purification by column chromatography (SiO_2, 25% acetone in hexanes) yielded **6** as a white semi-solid (1.8841 g, 7.62 mmol, 89% yield); $[\alpha]_D^{25}$ –22.6 (*c* 1.0, $CHCl_3$); ^{1}H NMR (400 MHz, C_6D_6) δ 5.91 (ddt, *J* = 17.4, 10.2, 7.5 Hz, 1H), 5.06–4.93 (m, 3H), 2.97 (dtd, *J* = 10.6, 5.5, 2.8 Hz, 1H), 2.49 (dd, *J* = 13.7, 2.4 Hz, 1H), 2.29 (ddt, *J* = 17.1, 4.8, 2.6 Hz, 1H), 2.18 (dq, *J* = 7.4, 1.3

Hz, 2H), 1.93 (dq, J = 4.9, 2.7 Hz, 1H), 1.91–1.72 (m, 4H), 1.48–1.30 (m, 2H), 1.25 – 1.15 (m, 1H), 1.15–1.05 (m, 1H), 1.04 – 0.95 (m, 2H), 0.94–0.85 (m, 1H); ^{13}C NMR (100 MHz, C_6D_6) δ 213.8, 168.5, 134.1, 118.3, 59.9, 52.8, 51.6, 49.1, 39.6, 39.2, 33.3, 28.9, 26.7, 20.5, 19.7; IR (Neat Film, NaCl) 3074, 2937, 2870, 1716, 1644, 1460, 1440, 1416, 1346, 1264, 1235, 1166, 1120, 1064, 994, 958, 916 cm^{-1}; HRMS (MM:ESI-APCI+) *m/z* calc'd for $C_{15}H_{21}NO_2$ [M+H]$^+$: 248.1645, found 248.1653.

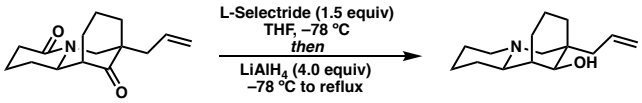

6 *16*

Amino alcohol 16

A two-necked 250 mL round bottom flask equipped with a reflux condenser, septum, and stir bar was charged with **6** (905 mg, 3.66 mmol, 1.0 equiv) and THF (73 mL). A flame-dried 25 mL conical flask under N_2 was charged with L-Selectride (5.90 mL, 1.0 M in THF, 5.90 mmol, 1.6 equiv). Both flasks were cooled to –78 ºC for 30 min, after which time the L-Selectride solution was slowly transferred to the flask containing **6** via syringe over 20 min via positive pressure cannulation, resulting in the formation of an opaque white reaction mixture. After 30 min, the septum was exchanged for an oven-dried glass stopper and $LiAlH_4$ (555.6 mg, 14.6 mmol, 4.0 equiv) was added in a single portion to the reaction mixture. The reaction was then removed from the cooling bath and allowed to reach 20 ºC, after which time the flask was immersed in a 75 ºC oil bath. After refluxing for 9 h, complete conversion to **16** was observed by LC/MS and TLC analysis. The reaction mixture was diluted with Et_2O (50 mL) and cooled in an ice/water bath. After 10 min, the reaction was slowly quenched with dropwise addition of H_2O (800 μL) over 10 min, followed by the addition of aqueous NaOH (4.0 mL of a 2.5 M solution), and H_2O_2 (4.0

mL of a 30% solution). The resulting gray suspension was then stirred vigorously for 30 min before being filtered through a pad of celite (5 x 5 cm), washing with EtOAc (3 x 75 mL). The filtrate was then transferred to a separatory funnel and washed with H_2O (60 mL) and brine (60 mL). The combined aqueous layers were extracted with EtOAc (3 x 80 mL). The combined organics were then dried over Na_2SO_4, filtered, and concentrated to a pale yellow oil. Purification by column chromatography (SiO_2, 25% EtOAc in hexanes with 1% Et_3N) afforded **16** as a colorless, viscous oil which slowly turns red with exposure to air (833.1 mg, 3.54 mmol, 97% yield); $[\alpha]_D^{25}$ –13.4 (*c* 1.0, $CHCl_3$); ^{1}H NMR (500 MHz, C_6D_6) δ 5.83 (dddd, *J* = 15.1, 11.2, 8.3, 7.6 Hz, 1H), 5.04 (app t, *J* = 1.2 Hz, 1H), 5.02–4.99 (m, 1H), 3.25 (m, 1H), 2.78–2.60 (m, 2H), 2.55 (d, *J* = 11.3 Hz, 1H), 2.08–1.74 (m, 6H), 1.68–1.37 (m, 9H), 1.32–1.03 (m, 3H); ^{13}C NMR (100 MHz, C_6D_6) δ 134.8, 116.8, 75.4, 65.5, 65.4, 56.4, 43.3, 41.8, 37.8, 30.5, 30.0, 26.1, 24.7, 20.9, 20.0; IR (Neat Film, NaCl) 3404 (br), 3072, 2931, 2856, 2797, 2759, 1638, 1463, 1442, 1375, 1336, 1271, 1223, 1198, 1182, 1124, 1106, 1044, 995, 958, 947, 912, 844, 813, 768, 714, 678, 635 cm^{-1}; HRMS (MM:ESI-APCI+) *m/z* calc'd for $C_{15}H_{26}NO$ $[M+H]^+$: 236.2009, found 236.2012.

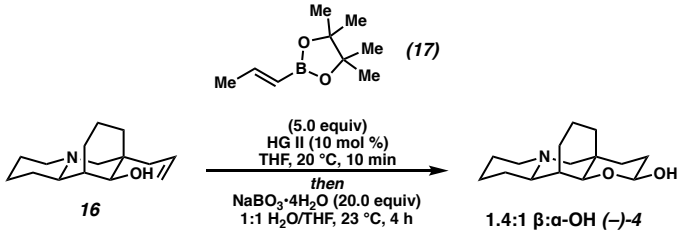

(–)-α,β-myrifabral A (4)

In a nitrogen-filled glovebox, an oven-dried 25 mL round bottom flask was charged with amino alcohol **16** (100.0 mg, 0.424 mmol, 1.0 equiv), pinacol boronate **17** (356.2 mg, 2.12 mmol, 5.0 equiv), and a Teflon-coated stir bar. The flask was sealed with a septum,

removed from the glovebox, and placed under an atmosphere of nitrogen. To the flask was added THF (2.2 mL) to provide a clear, colorless solution. Hoveyda–Grubbs II catalyst (26.6 mg, 0.0424 mmol, 10 mol %) was then added rapidly in a single portion, and the flask was subjected to vacuum until the green solution began to bubble. The dark green reaction was allowed to stir for 10 min under a static vacuum, at which point the flask was backfilled with nitrogen and an aliquot was analyzed by LC/MS, indicating full conversion of amino alcohol **16** to the putative cross metathesis product. *Note: Typically, the reaction solution rapidly turns dark brown/black when the flask is backfilled with nitrogen*. The metathesis catalyst was quenched with the addition of ethyl vinyl ether (40 μL) at 20 °C. After stirring for 30 min at 20 °C, deionized water (2.2 mL) and $NaBO_3$•$4H_2O$ (1.30 g, 8.48 mmol, 20.0 equiv) were added and the resulting black, biphasic suspension was stirred rapidly at 20 °C. After 4 h, full conversion of the intermediate cross metathesis product was observed by LC/MS analysis. The reaction mixture was poured into a separatory funnel with EtOAc (5 mL) and H_2O (10 mL). The layers were separated and the aqueous layer was extracted 3 x 5 mL EtOAc. The combined organics were dried over Na_2SO_4, filtered, and concentrated to yield a dark brown oil. Purification by column chromatography (SiO_2, 0→50% EtOAc in hexanes with 2% Et_3N) yielded (–)-myrifabral A (**4**) as a 1.4:1 mixture of β:α-OH epimers as a viscous yellow oil (90.1 mg, 0.358 mmol, 85% yield). Note: racemic samples of this compound are isolated as a colorless solid, in accordance with previous reports.[3,4] Due to the complicated overlap of β- and α-OH epimers of (–)-4, the ^{1}H NMR spectral data are reported with raw integration values; $[\alpha]_D^{25}$ –41.4 (*c* 1.0, $CHCl_3$); ^{1}H NMR (600 MHz, Pyridine-d_5) δ 8.36 (s, 1.00), 7.70 (s, 0.72), 5.68 (d, *J* = 3.7 Hz, 0.82), 5.10 (d, *J* = 9.6 Hz, 1.19), 4.19 (d, *J* = 3.4 Hz, 0.89), 3.21 (d, *J* = 3.6

Hz, 1.17), 2.80–2.64 (m, 4.30), 2.54 (t, J = 10.7 Hz, 2.16), 2.30–2.19 (m, 2.22), 2.10 – 1.88 (m, 7.28), 1.88 – 1.80 (m, 2.19), 1.78–1.72 (d, J = 11.9 Hz, 3.43), 1.68–1.59 (m, 8.86), 1.57–1.40 (m, 8.86), 1.27 – 1.05 (m, 10.40); ^{13}C NMR (100 MHz, Pyridine-d_5) δ 98.3, 92.3, 80.7, 72.5, 69.6, 69.1, 66.8, 66.4, 57.2, 57.2, 40.4, 40.2, 34.4, 33.1, 32.6, 30.7, 30.7, 30.6, 29.6, 29.6, 28.7, 27.5, 26.9, 26.9, 25.5, 25.5, 21.4, 21.3, 21.3, 21.2; IR (Neat Film, NaCl) 3381 (br), 3054, 2933, 2851, 2796, 2756, 2728, 2253, 1714, 1562, 1549, 1540, 1462, 1456, 1444, 1396, 1374, 1336, 1298, 1277, 1243, 1209, 1189, 1124, 1106, 1077, 1057, 1009, 998, 961, 949, 928, 917, 902, 886, 870, 856, 840, 826, 762, 739, 704, 673 cm^{-1}, HRMS (MM:ESI-APCI+) *m/z* calc'd for $C_{15}H_{26}NO_2$ $[M+H]^+$: 252.1958, found 252.1960.

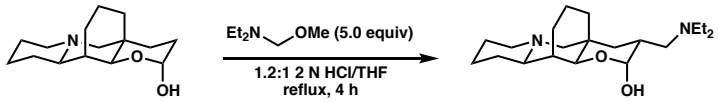

(–)-4, 1.4:1 α:β-OH 1.6:1 α:β-OH *(–)-5*

(–)-α,β-myrifabral B (**5**)

The following procedure was adapted from Song's total synthesis of (±)-myrifabral B.[4] To a one dram vial with a stir bar was added (–)-**4** (50.0 mg, 0.199 mmol, 1.0 equiv), THF (220 μL), 2 N aqueous HCl (250 μL), and *N*-ethyl-*N*-(methoxymethyl)ethanamine (117.2 mg, 0.995 mmol, 5.0 equiv) to provide a colorless, biphasic reaction mixture. The vial was sealed with a Teflon-lined cap and heated in a vial well at 80 °C with rapid stirring. After 4 h, the reaction was complete by LC/MS analysis. The vial was cooled to 20 °C, then the biphasic reaction mixture was poured into a separatory funnel with EtOAc (5 mL), and saturated aqueous $NaHCO_3$ (10 mL). The layers were separated, and the aqueous layer was extracted with EtOAc (3 x 5 mL). The combined organics were dried over Na_2SO_4, filtered, and concentrated to a brown/yellow oil. Purification by column chromatography (SiO_2, 20→60% EtOAc in hexanes with 2% Et_3N) yielded (–)-myrifabral B (**5**) as a 1.6:1

mixture of β:α-OH epimers as a viscous yellow oil (29.5 mg, 0.0877 mmol, 44% yield). Note: racemic samples of this compound are isolated as a colorless solid, in accordance with previous reports.[3,4] Due to the complicated overlap of β and α-OH epimers of (–)-5, the ^{1}H NMR spectral data are reported with raw integration values; $[\alpha]_D^{25}$ –37.5 (*c* 1.0, $CHCl_3$); ^{1}H NMR (600 MHz, Pyridine-d_5) δ 5.72 (d, *J* = 3.0 Hz, 1.00), 4.82 (d, *J* = 8.2 Hz, 1.67), 4.22 (d, *J* = 3.4 Hz, 1.01), 4.22 (d, *J* = 3.4 Hz, 1.40), 2.83–2.74 (m, 2.40), 2.73–2.68 (m, 3.86), 2.66 (dd, *J* = 12.7, 7.9 Hz, 1.75), 2.60 (dd, *J* = 10.9, 7.2 Hz, 2.92), 2.57–2.47 (m, 7.18), 2.45–2.33 (m, 6.41), 2.28 (tdd, *J* = 13.1, 6.6, 2.4 Hz, 1.64), 2.21 (dd, *J* = 12.8, 6.1 Hz, 1.61), 2.15–2.01 (m, 4.23), 2.01–1.93 (m, 4.26), 1.83–1.78 (m, 3.00), 1.73–1.60 (m, 9.07), 1.58–1.43 (m, 11.78), 1.39 (dd, *J* = 13.3, 4.4 Hz, 1.56), 1.34–1.28 (m, 3.61), 1.25 (dt, *J* = 13.0, 3.1 Hz, 2.86), 1.21 – 1.09 (m, 3.00), 1.02 (t, *J* = 7.1 Hz, 5.89), 0.99 (t, *J* = 7.1 Hz, 8.22), 0.85 (t, *J* = 12.9 Hz, 1.39); ^{13}C NMR (100 MHz, Pyridine-d_5) δ 103.1, 94.2, 80.4, 72.6, 69.8, 69.0, 66.9, 66.4, 57.2, 57.2, 57.1, 56.8, 48.5, 48.0, 40.1, 40.0, 39.1, 37.3, 35.2, 35.2, 33.8, 33.8, 30.7, 30.7, 30.5, 29.8, 26.9, 26.8, 25.5, 25.4, 21.6, 21.4, 21.3, 21.3, 12.9, 12.4; IR (Neat Film, NaCl) 3076 (br), 2966, 2933, 2851, 2801, 2757, 2728, 2251, 1722, 1692, 1557, 1462, 1444, 1375, 1346, 1297, 1276, 1267, 1243, 1205, 1196, 1178, 1144, 1124, 1104, 1089, 1076, 1059, 1037, 967, 918, 904, 885, 813, 860, 833, 753, 715, 666, 616 cm^{-1}, HRMS (FAB+) *m/z* calc'd for $C_{20}H_{37}N_2O_2$ $[M+H]^+$: 337.2855, found 337.2857.

1.6.3 ABSOLUTE STEREOCHEMISTRY DETERMINATION OF KETONE 7

1.6.3.1 VIBRATIONAL CIRCULAR DICHROISM

Solutions of compounds **7** and ***ent*-7** (69 mg/mL) were each prepared in $CDCl_3$ and loaded into a front-loading SL-4 cell (International Crystal Laboratories) possessing BaF_2

windows and 100 μm path length. Infrared (IR) and VCD spectra were individually acquired on a BioTools ChiralIR-2X VCD spectrometer as sets of 24 one-hour blocks (24 blocks, 3120 scans per block) at 4 cm^{-1} resolution in dual PEM mode. A 15-minute acquisition of neat (–)-α-pinene control (separate 75 μm BaF_2 cell) yielded a VCD spectrum in agreement with literature spectra and those previously acquired on the same instrument. IR and VCD spectra were background-corrected using a 30-minute block IR acquisition of the empty instrument chamber under gentle N_2 purge, and were solvent corrected using a 12-hour (12 blocks, 3120 scans per block) IR/VCD acquisition of $CDCl_3$ in the same 100 μm BaF_2 cell as used for **7** and ***ent*-7**. The reported spectra represent the result of block averaging.

The arbitrarily chosen (*R*)-enantiomer of compound **7** was subjected to an initial exhaustive stochastic molecular mechanics-based conformational search (MMFF94 force field, 0.06 Å geometric RMSD cutoff, and 30 kcal/mol energy window) as implemented in MOE 2019.0102 (Chemical Computing Group, Montreal, CA). All conformers retained the *(R)*-configuration and were subjected to geometry optimization, harmonic frequency calculation, and VCD rotational strength evaluation using density functional theory. Initial quantum mechanical calculations utilized the B3LYP functional, small 6-31G* basis, and IEFPCM model (chloroform solvent) as an initial filter. This was followed by subsequent treatment using the B3PW91 functional, cc-pVTZ basis, and implicit IEFPCM chloroform solvation model on all IEFPCM-B3LYP/6-31G* conformers below 5 kcal/mol, reusing the exact Hessian of the latter to facilitate optimization at the higher level of theory. All calculations were performed with the *Gaussian 16* program system (Rev. C.01; Frisch *et al*., Gaussian, Inc., Wallingford, CT). Resultant IEFPCM-B3PW91/cc-pVTZ harmonic

frequencies were scaled by 0.98. All structurally unique conformers possessing all positive Hessian eigenvalues were Boltzmann weighted by relative free energy at 298.15 K. The predicted IR and VCD frequencies and intensities of the retained conformers were convolved using Lorentzian line shapes (γ = 4 cm^{-1}) and summed using the respective Boltzmann weights to yield the final predicted IR and VCD spectra. The predicted VCD spectrum of the *(S)* enantiomer was generated by inversion of sign. From the outstanding agreement between the theoretical and measured IR and VCD spectra across the entire useful range of the spectrum (900–1500 cm^{-1}; regions **A**–**J** below) along with support of this assignment using the directly predicted versus measured optical rotations (see Method 2) the absolute configurations of species **7** and ***ent*-7** were established as *(R)* and *(S)*, respectively.

Figure 1.6.3.1 *Experimental (left) and Theoretical (right) VCD and IR of* ***7*** *and* ***ent-7***

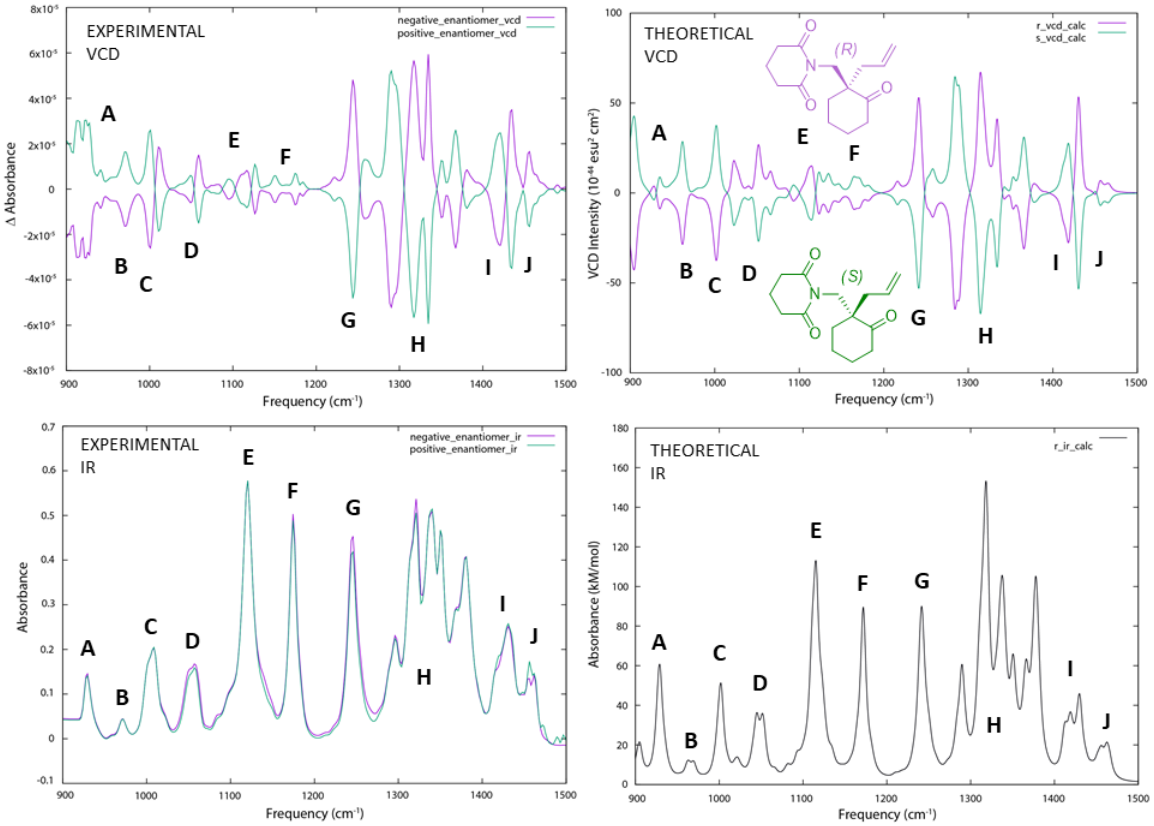

1.6.3.2 OPTICAL ROTATION

The ensemble of unique IEFPCM-B3PW91/cc-pVTZ conformers of ***(R)*****-7** generated in Method 1 above were subjected to optical rotation calculation at 589.0 nm using the B3LYP hybrid density functional, the large and diffuse 6-311++G(2df,2pd) basis set, and the IEFPCM implicit chloroform solvent model. The computed IEFPCM-B3LYP/6-311++G(2df,2pd) optical rotations (weighted by IEFPCM-B3PW91/cc-pVTZ free energies at 298.15 K) along with those resulting from alternatively weighting by either the IEFPCM-B3PW91/cc-pVTZ total energies or IEFPCM-B3LYP/6-311++G(2df,2pd)//IEFPCM-B3PW91/cc-pVTZ total energies are reported in (a)–(b) below. From comparison of the theoretically calculated and measured optical rotations (for

which reasonably good agreement in magnitude was found to exist) the respective VCD-based AC assignments of *(R)* and *(S)* for **7** and ***ent*-7** were further supported by those from the separate OR-based methodology.

(a) 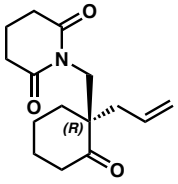

Predicted optical rotation, weighted by IEFPCM-B3PW91/cc-pVTZ free energies: **–47.5°**

Predicted optical rotations, weighted by IEFPCM-B3PW91/cc-pVTZ total energies: **–45.5°**

Predicted optical rotations, weighted by IEFPCM-B3LYP/6-311++G(2df,2pd)//IEFPCM-B3PW91/cc-pVTZ total energies: **–45.8°**

∴

(b) 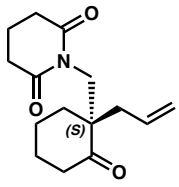

Predicted optical rotation, weighted by IEFPCM-B3PW91/cc-pVTZ free energies: **+47.5°**

Predicted optical rotations, weighted by IEFPCM-B3PW91/cc-pVTZ total energies: **+45.5°**

Predicted optical rotations, weighted by IEFPCM-B3LYP/6-311++G(2df,2pd)//IEFPCM-B3PW91/cc-pVTZ total energies: **+45.8°**

Measured optical rotation: ($CHCl_3$ solvent, 25 °C, c = 10.0 mg/mL, 10 cm pathlength, 88% ee)

7: + 32.9, ***ent*-7: –28.**

1.6.4 COMPARISON OF NATURAL AND SYNTETIC MYRIFABRALS

Figure 1.6.4.1 *Natural (top) and Synthetic (bottom) ^{1}H NMR of Myrifabral A, 600 MHz, Pyridine-d_5*

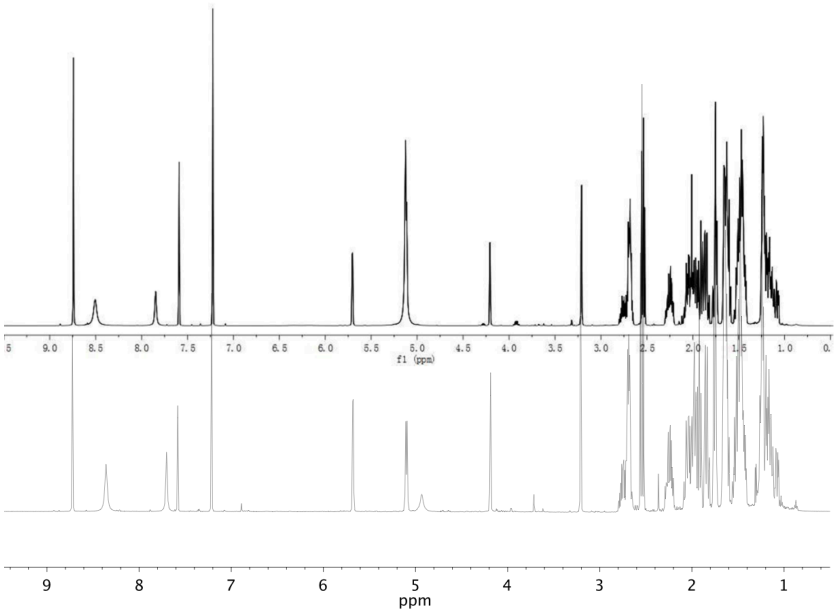

Figure 1.6.4.2 *Natural (top) and Synthetic (bottom) ^{13}C NMR of Myrifabral A, 100 MHz, Pyridine-d_5*

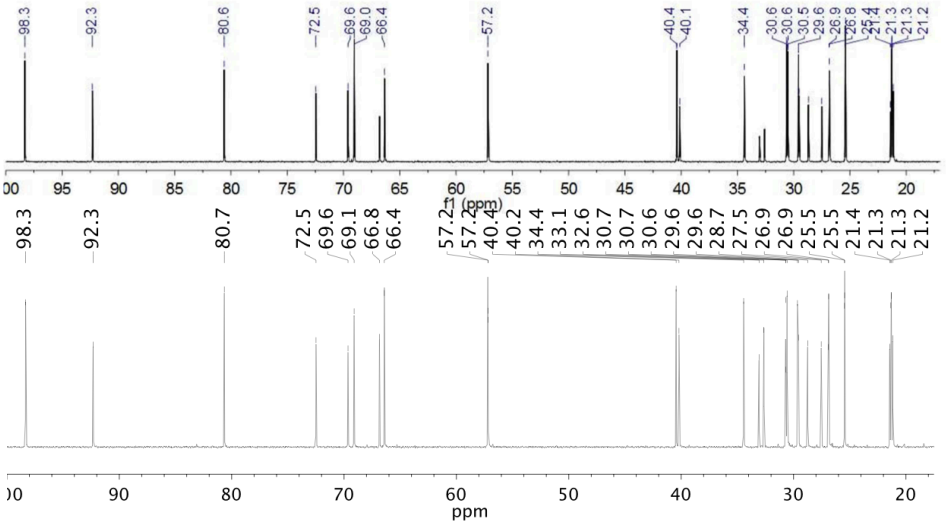

Figure 1.6.4.3 *Natural (top) and Synthetic (bottom) ^{1}H NMR of Myrifabral B, 600 MHz, Pyridine-d_5*

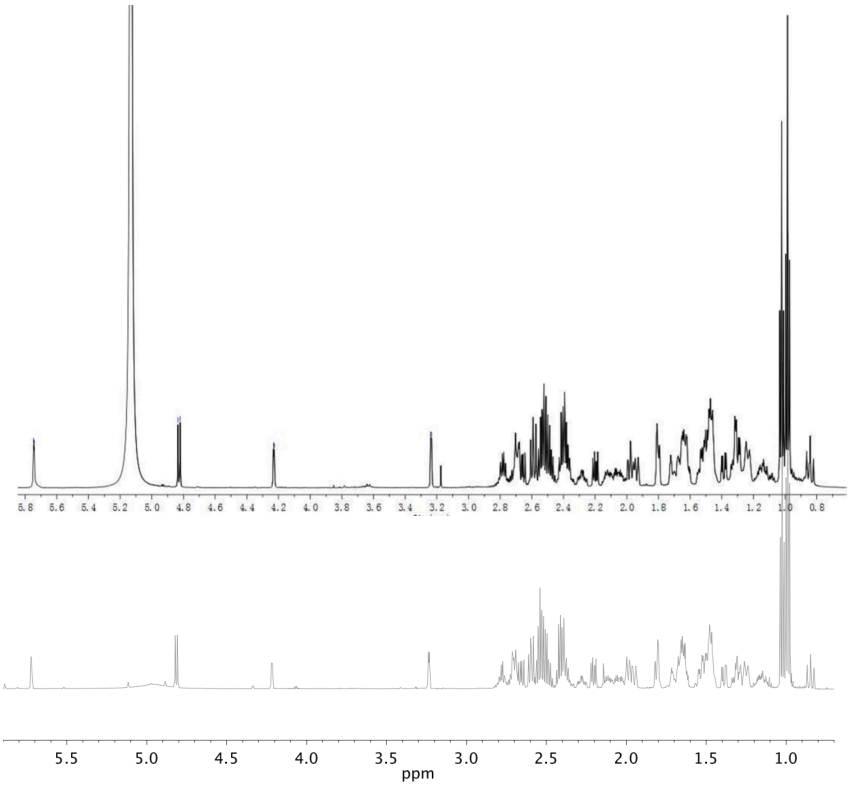

Figure 1.6.4.4 *Natural (top) and Synthetic (bottom) ^{13}C NMR of Myrifabral B, 100 MHz, Pyridine-d_5*

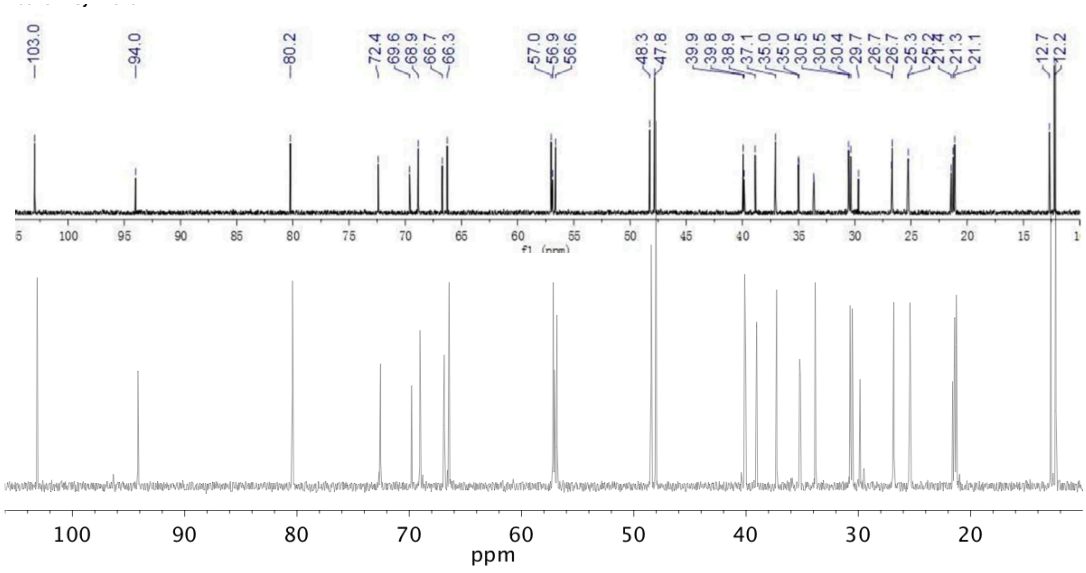

1.7 REFERENCES AND NOTES

(1) For a review see: E. Gravel, E. Poupon, Biosynthesis and biomimetic synthesis of alkaloids isolated from plants of the Nitraria and Myrioneuron genera: an unusual lysine-based metabolism. *Nat*. *Prod*. *Rep*. **2010**, *27*, 32–56.

(2) (a) V.C. Pham, A. Jossang, T. Sévenet, V. H. Nguyen, B. Bodo, Absolute configuration of Myrobotinol, New Fused-Hexacyclic Alkaloid Skeleton from *Myrionueron nutans*. *J. Org*. *Chem*. **2007**, *72*, 9826–9829. (b) V.C. Pham, A. Jossang, T. Sévenet, V. H. Nguyen, B. Bodo, Myrioneurinol: a novel alkaloid skeleton from *Myrioneuron nutans*. *Tetrahedron* **2007**, *63*, 11244–11249. (c) V. C. Pham, A. Jossang, T. Sévenet, V. H. Nguyen, B. Bodo, Novel Alkaloids from *Myrioneuron nutans*. *Eur*. *J*. *Org*. *Chem*. **2009**, *74*, 1412–1416. (d) V. C. Pham, A. Jossang, A. Chiaroni, T. Sévenet, B. Bodo, Asymmetric synthesis of myrioxazines A and B, novel alkaloids of *Myrioneuron nutans*. *Tetrahedron Lett*. **2002**, *43*, 7565–7568. (e) V. C. Pham, A. Jossang, A. Chiaroni, T. Sévenet, V. H. Nguyen, B. Bodo, Solution and Crystal Conformations of Myrionine, a new 8β-Alkyl-*cis*-decahydroquinoline of *Myrioneuron nutans*. *Org*. *Lett*. **2007**, *9*, 3531–3534. (f) V. C. Pham, A. Jossang, P. Grellier, T. Sévenet, V. H. Nguyen, B. Bodo, Structure and Total Synthesis of (–)-Myrionidine and (–)-Schoberine, Antimalarial Alkaloids from *Myrioneuron nutans*. *J*. *Org*. *Chem*. **2008**, *73*, 7565–7573.

(3) (a) S.-D. Huang, Y. Zhang, M.-M. Cao, Y.-T. Di, G.-H. Tang, Z.-G. Peng, J.-D. Jiang, H.-P. He, X.-J. Hao, Myriberine A, a New Alkaloid with an Unprecedented Heteropentacyclic Skeleton from *Myrioneuron faberi*. *Org*. *Lett*. **2013**, *15*, 590–

593. (b) M.-M. Cao, S.-D. Huang, Y.-T. Di, C.-M. Yuan, G.-Y. Zuo, Y.-C. Gu, Y. Zhang, X.-J. Hao, Myrifabine, the First Dimeric *Myrioneuron* Alkaloid from *Myrioneuron faberi*. *Org*. *Lett*. **2014**, *16*, 528–531. (c) M.-M. Cao, Y. Zhang, X.-H. Li, Z.-G. Peng, J.-D. Jiang, Y.-C. Gu, Y.-T. Di, X.-N. Li, D.-Z. Chen, C.-F. Xia, H.-P. He, S.-L. Li, X.-J. Hao, Cyclohexane-Fused Octahydroquinolizine Alkaloids from *Myrioneuron faberi* with Activity against Hepatitis C Virus. *J*. *Org*. *Chem*. **2014**, *79*, 7945–7950. (d) M.-M. Cao, Y. Zhang, S.-D. Huang, Y.-T. Di, Z.-G. Peng, J.-D. Jiang, C.-M. Yuan, D.-Z. Chen, S.-L. Li, H.-P. He, X.-J. Hao, Alkaloids with Different Carbon Units from *Myrioneuron faberi*. *J*. *Nat*. *Prod*. **2015**, *78*, 2609–2616. (e) M.-M. Cao, Y. Zhang, Z.-G. Peng, J.-D. Jiang, Y.-J. Gao, X.-J. Hao, Schoberine B, an alkaloid with an unprecedented straight C_5 side chain, and myriberine B from *Myrioneuron faberi*. *RSC Adv*. **2016**, *6*, 10180–10184. (f) M.-M. Cao, Y. Zhang, S.-D. Huang, Z.-G. Peng, J.-D. Jiang, X.-J. Hao, Three new alkaloids from *Myrioneuron faberi*. *Tetrahedron Lett*. **2016**, *57*, 4021–4023. (g) M.-M. Cao, J.-H. Zhang, Y. Zhang, Z.-G. Peng, J.-D. Jiang, X.-J. Hao, New findings of cyclohexane-fused octahydroquinolizine alkaloids from *Myrioneuron faberi*. *Tetrahedron Lett*. **2016**, *57*, 5632–5635.

(4) X.-H. Li, Y. Zhang, J.-H. Zhang, X.-N. Li, M.-M. Cao, Y.-T. Di, Z.-G. Peng, J.-D. Jiang, X.-J. Hao, Myritonines A–C, Alkaloids from *Myrioneuron tonkinesis* Based on a Novel Hexacyclic Skeleton. *J*. *Nat*. *Prod*. **2016**, *79*, 1203–1207.

(5) Z. -H. Zhang, J.-J. Guo, Y. -X. Yuan, Y.-H. Fu, Y. C. Gu, Y. Zhang, D. -Z. Chen, S.-L. Li, Y.-T. Di, X.-J. Hao, Four new tetracyclic alkaloids with cis-

decahydroquinoline motif from *Myrioneuron effusum*. *Fitoterapia* **2016**, *112*, 217–221.

(6) (a) A. J. Nocket, S. M. Weinreb, Total Synthesis of the Tetracyclic Antimalarial Alkaloid (±)-Myrioneurinol. *Angew*. *Chem*. *Int*. *Ed*. **2014**, *53*, 14162–14165. (b) A. J. Nocket, Y. Feng, S. M. Weinreb, Construction of the *Myrioneuron* Alkaloids: A Total Synthesis of (±)-Myrioneurinol. *J. Org*. *Chem*. **2015**, *80*, 1116–1129. (c) D. Song, Z. Wang, R. Mei, W. Zhang, D. Ma, D. Xu, X. Xie, X. She, Short and Scalable Total Synthesis of Myrioneuron Alkaloids (±)-α,β-Myrifabral A and B. *Org*. *Lett*. **2016**, *18*, 669–671.

(7) A. Plas, F. Marchand, A. Eschalier, Y. Troin, P. Chalard, Stereoselective Synthesis and In Vivo Evaluation of the Analgesic Activity of Polysubstituted Bispidines *Eur*. *J. Org*. *Chem*. **2012**, 6070–6079.

(8) Y. Numajiri, B. P. Pritchett, K. Chiyoda, B.M. Stoltz, Enantioselective Synthesis of α-Quaternary Mannich Adducts by Palladium-Catalyzed Allylic Alkylation: Total Synthesis of (+)-Sibirinine. *J. Am*. *Chem*. *Soc*. **2015**, *137*, 1040–1043.

(9) K. Ishihara, S. Ohara, H. Yamamoto, 3,4,5-Trifluorobenzeneboronic Acid as an Extremely Active Amidation Catalyst *J. Org. Chem.* **1996**, *61*, 4196–4197. (b) K. Ishihara, S. Kondo, H. Yamamoto, 3,5-Bis(perfluorodecyl)phenylboronic Acid as an Easily Recyclable Direct Amide Condensation Catalyst *Synlett* **2001**, *9*, 1371–1374. (c) K. Ishihara, S. Ohara, H. Yamamoto, (3,4,5-trifluorophenyl)boronic

Acid-catalyzed Amide Formation from Carboxylic Acids and Amines: *N*-benzyl-4-phenylbutyramide. *Org. Synth.* 2004, *X*, 80–86.

(10) P. Tang, H. Krause, Boric Acid Catalyzed Amide Formation from Carboxylic Acids and Amines: *N*-benzyl-4-phenylbutyramide. *Org*. *Synth*. **2005**, *81*, 262–272.

(11) A. M. Pangborn, M. A. Giardello, R. H. Grubbs, R. K. Rosen, F. J. Timmers, *Organometallics* **1996**, *15*, 1518–1520.

APPENDIX 1

Synthetic Summary for Chapter 1:

Enantioselective Total Synthesis of (–)-Myrifabral A and B

Scheme A1.1 *Enantioselective Total Synthesis of (–)-Myrifabral A and B*

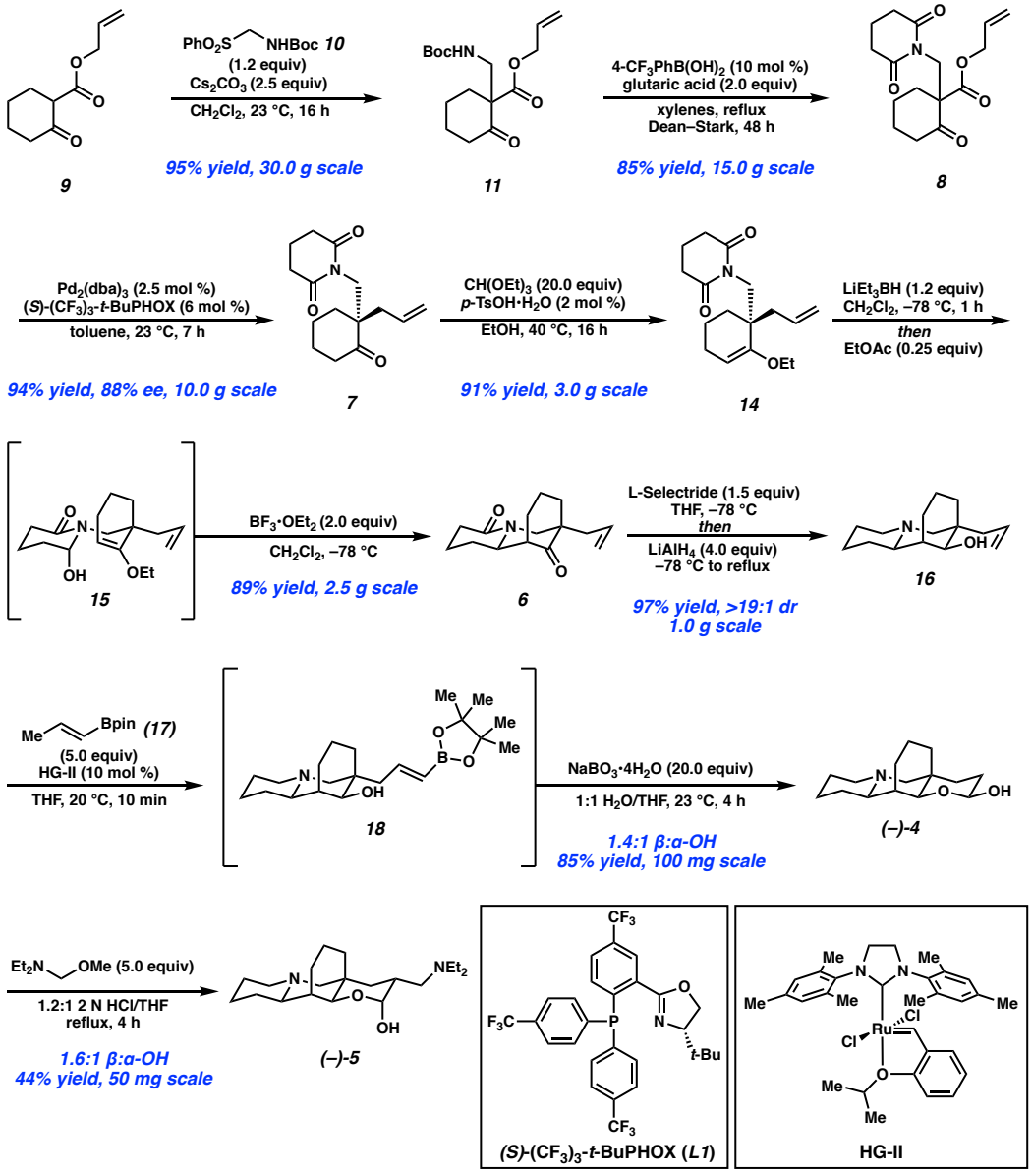

APPENDIX 2

Spectra Relevant to Chapter 1:

Enantioselective Total Synthesis of (–)-Myrifabral A and B

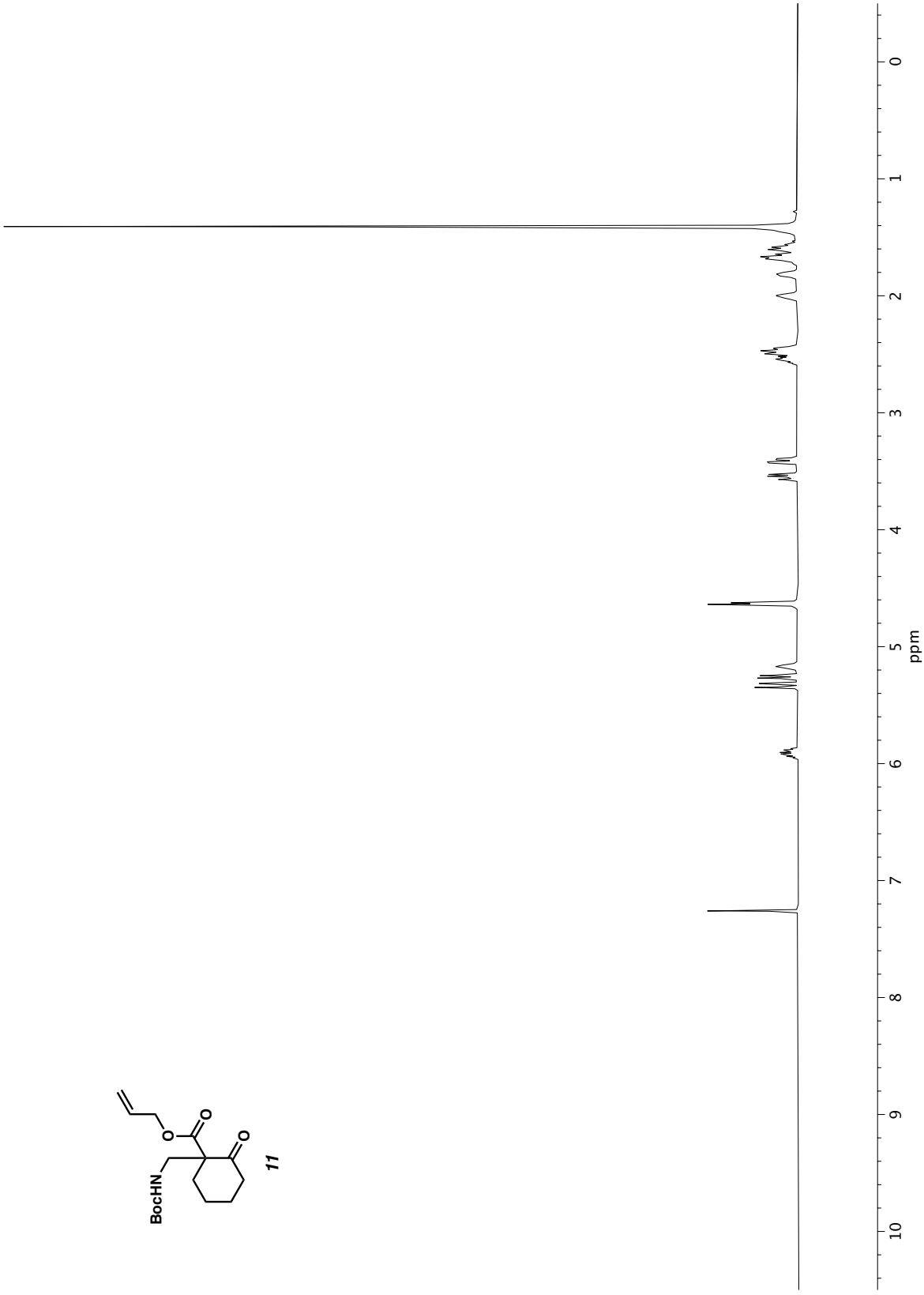

Figure A2.1 *^1H NMR (500 MHz, $CDCl_3$) of compound **11**.*

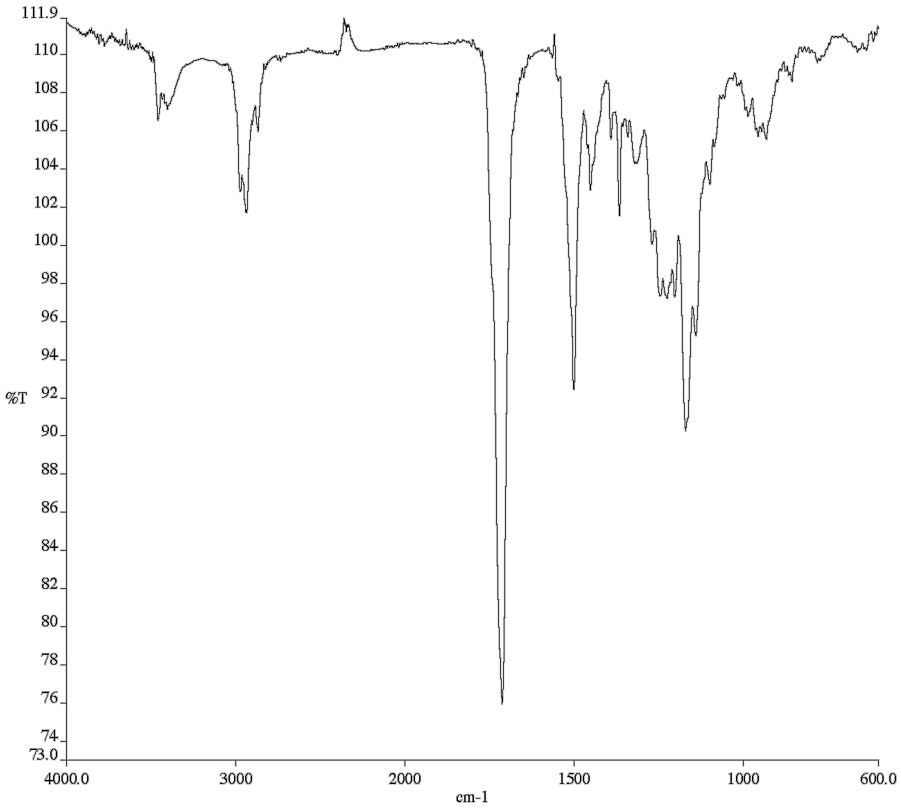

Figure A2.2 *Infrared spectrum (Thin Film, NaCl) of compound* ***11****.*

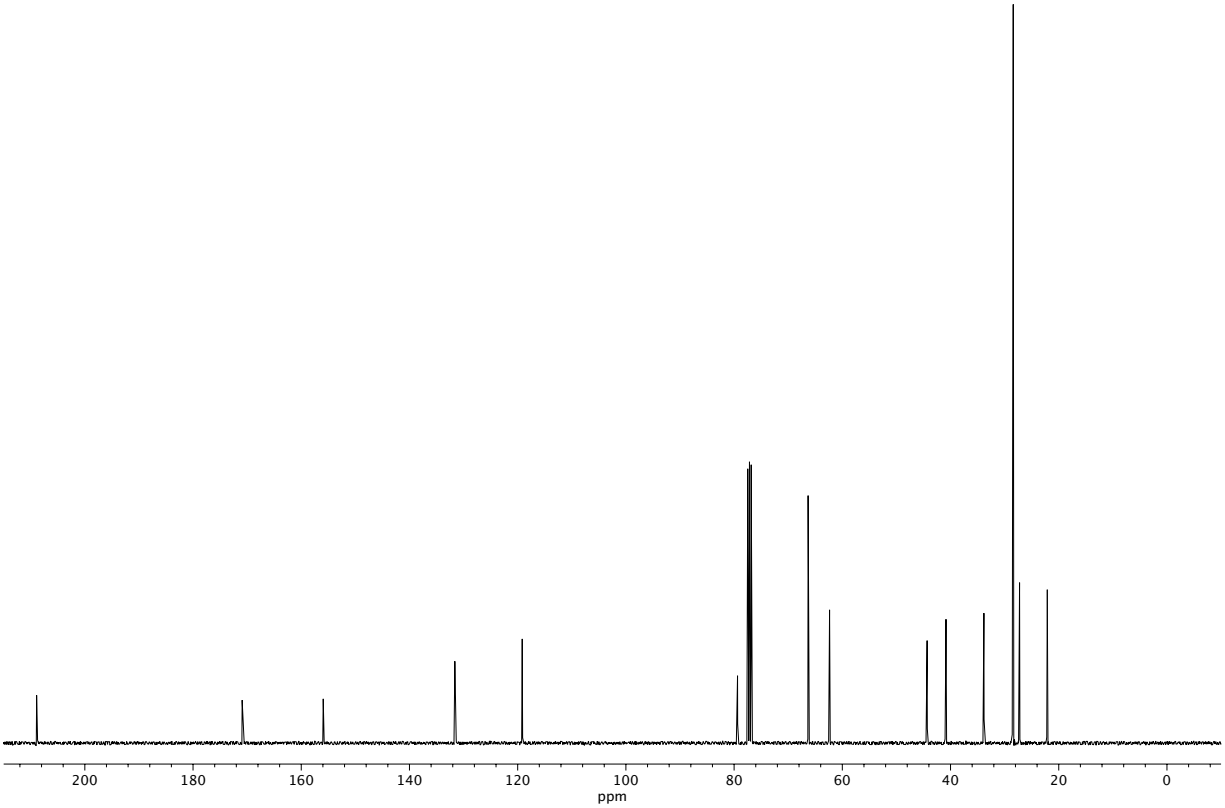

Figure A2.3 *^{13}C NMR (100 MHz, $CDCl_3$) of compound* ***11****.*

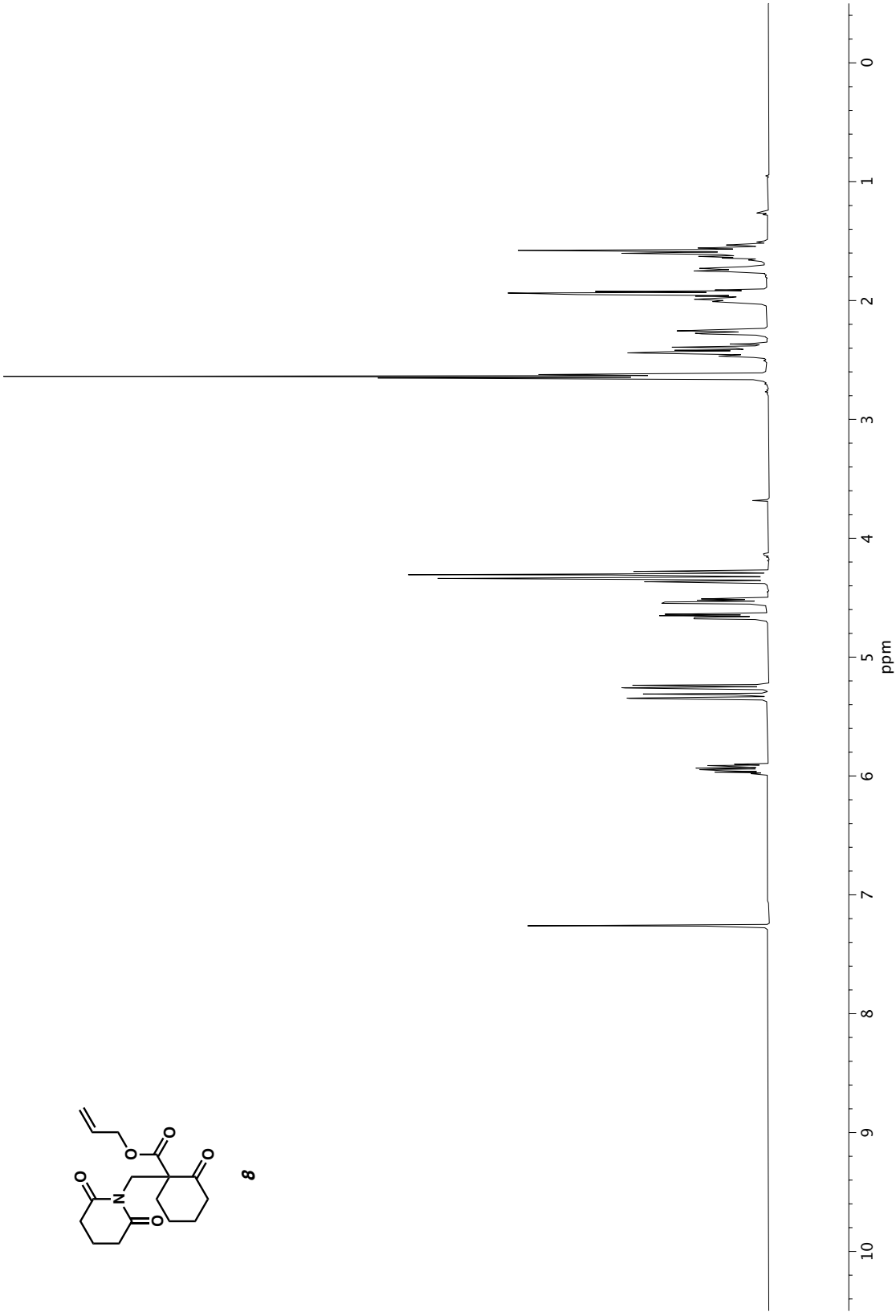

Figure A2.4 *^1H NMR (500 MHz, $CDCl_3$) of compound **8**.*

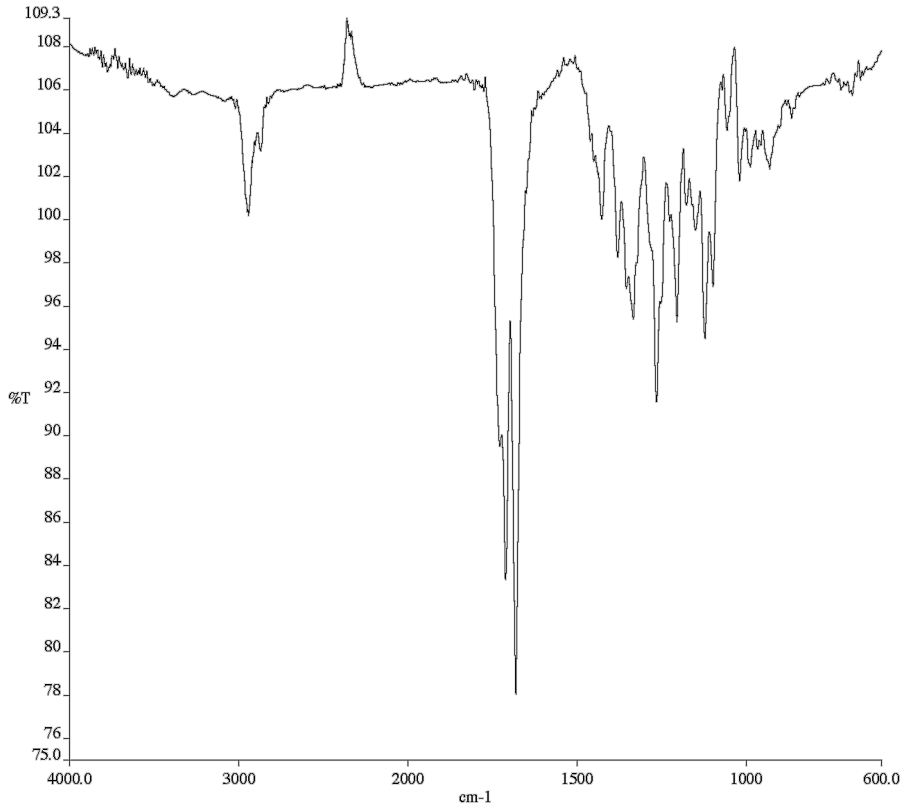

Figure A2.5 *Infrared spectrum (Thin Film, NaCl) of compound* ***8****.*

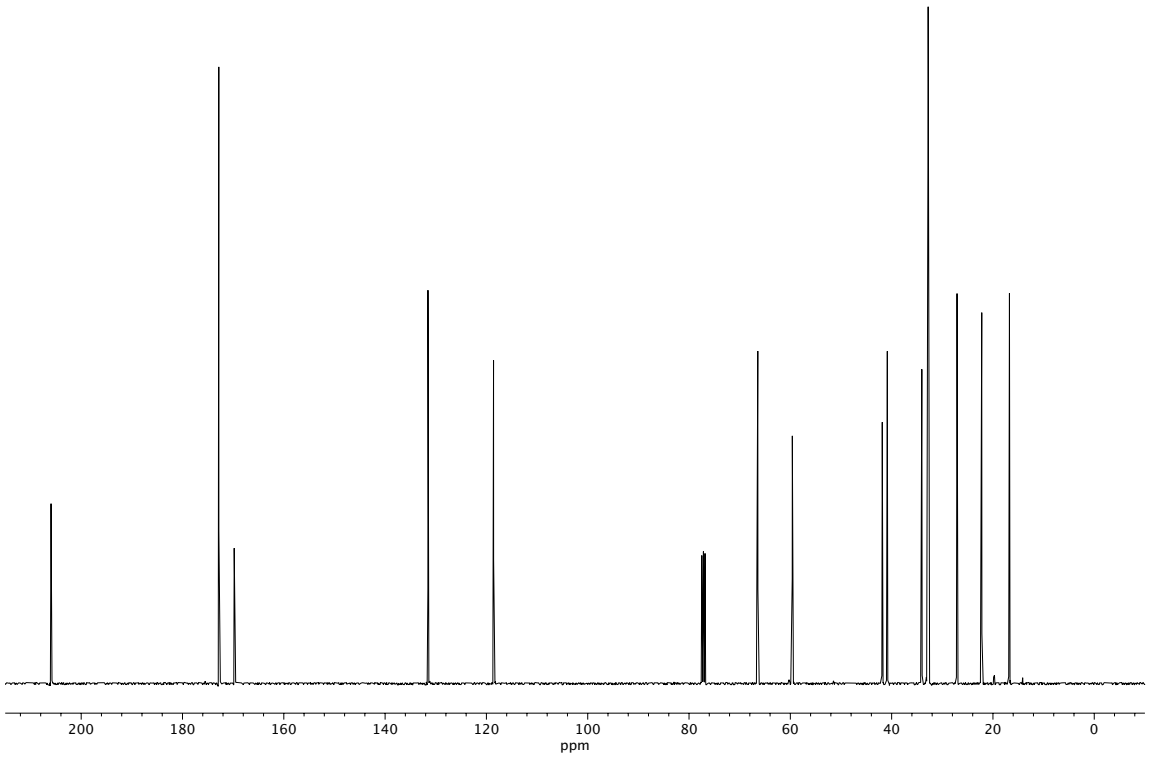

Figure A2.6 *^{13}C NMR (100 MHz, $CDCl_3$) of compound* ***8****.*

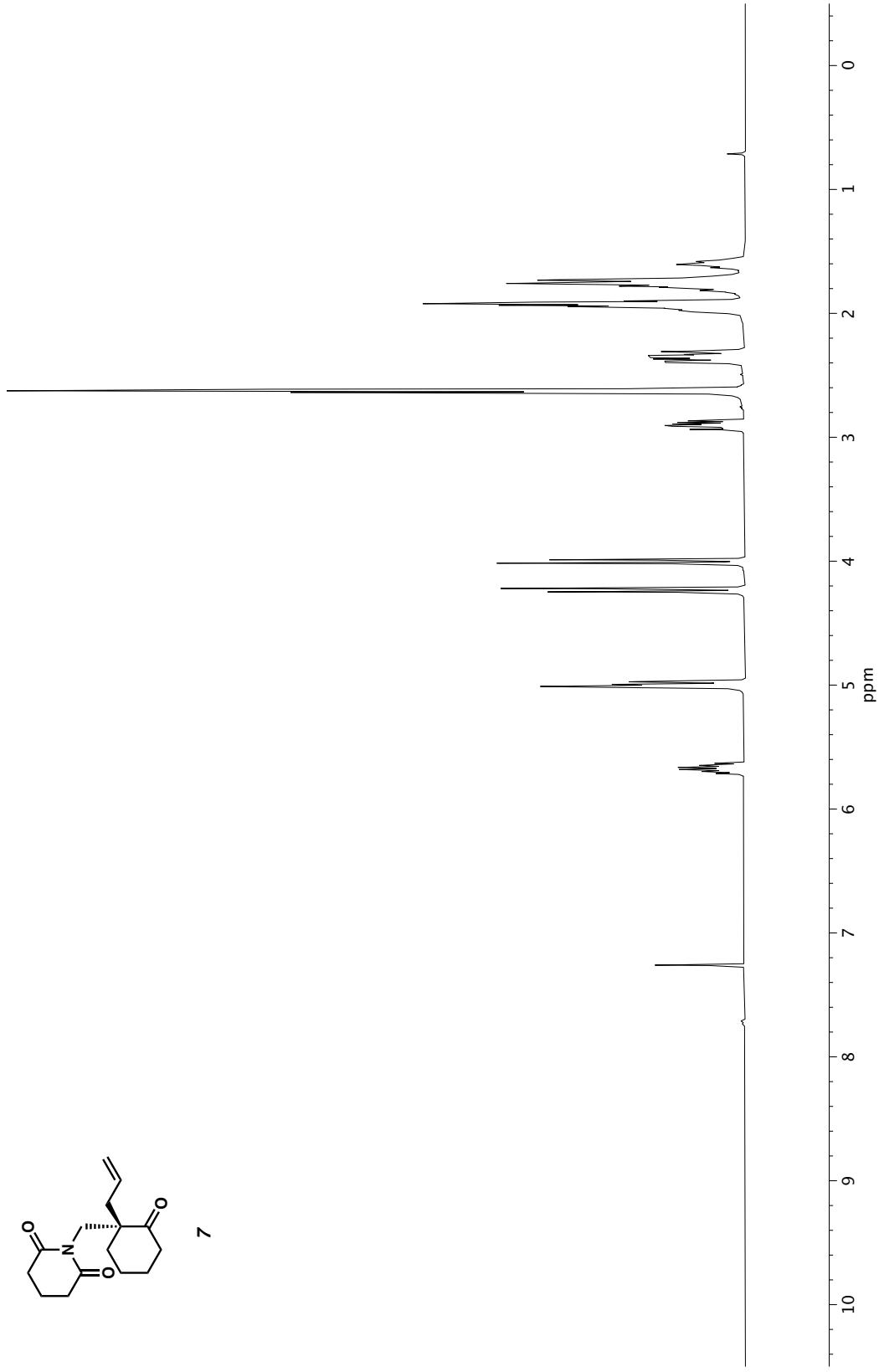

Figure A2.7 *^{1}H NMR (500 MHz, $CDCl_3$) of compound 7.*

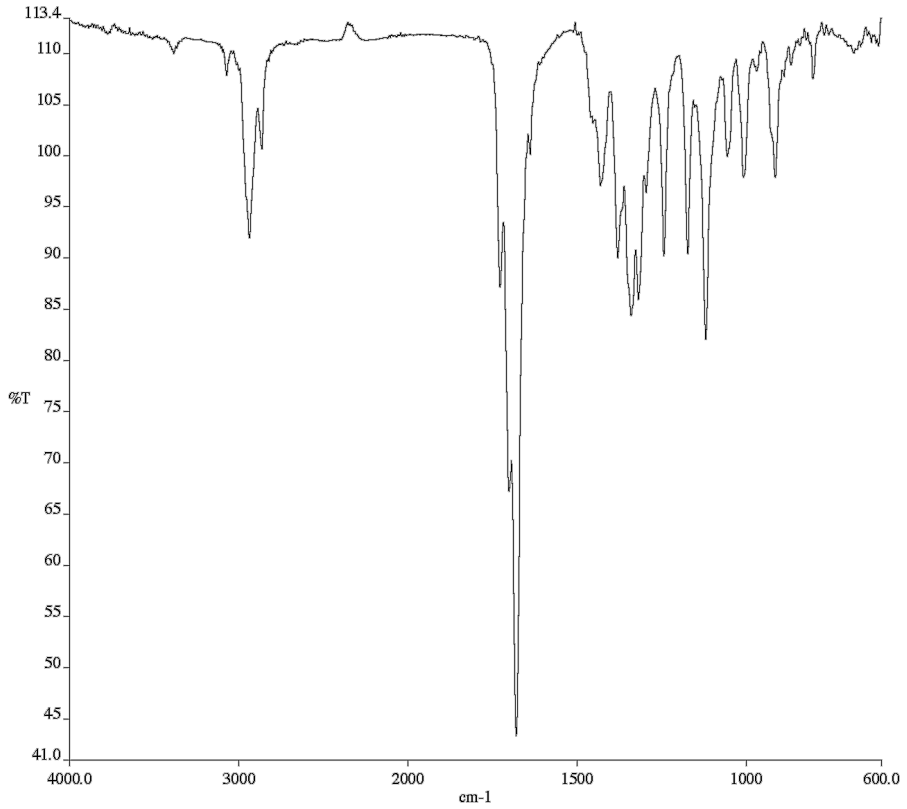

Figure A2.8 *Infrared spectrum (Thin Film, NaCl) of compound **7**.*

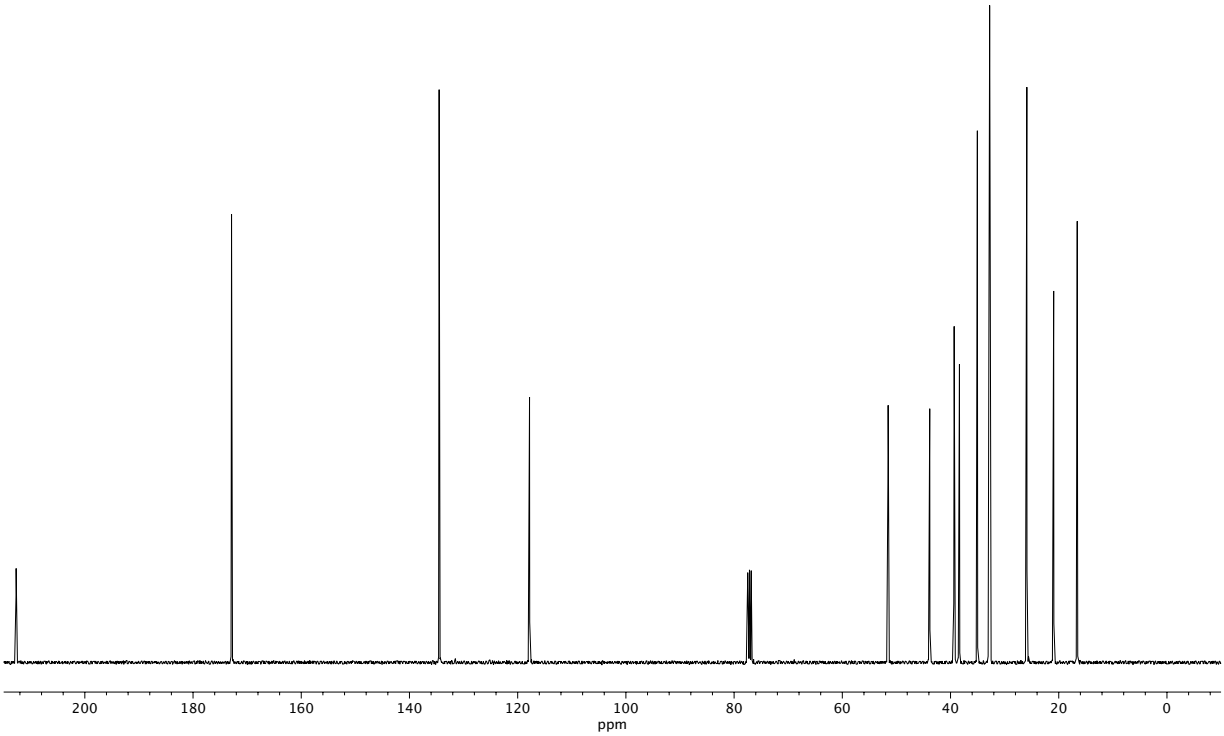

Figure A2.9 *^{13}C NMR (100 MHz, $CDCl_3$) of compound **7**.*

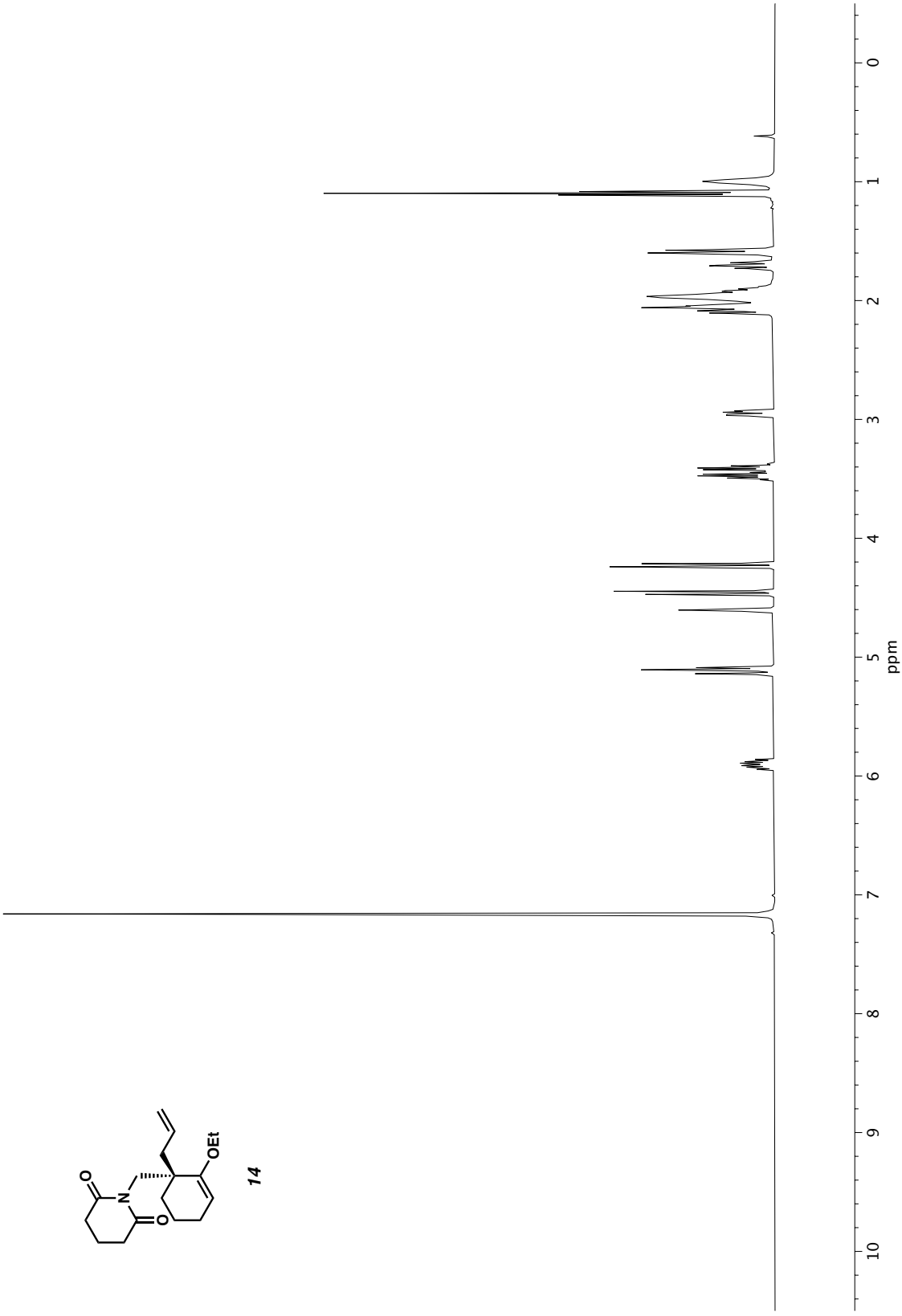

Figure A2.10 *^{1}H NMR (500 MHz, C_6D_6) of compound **14**.*

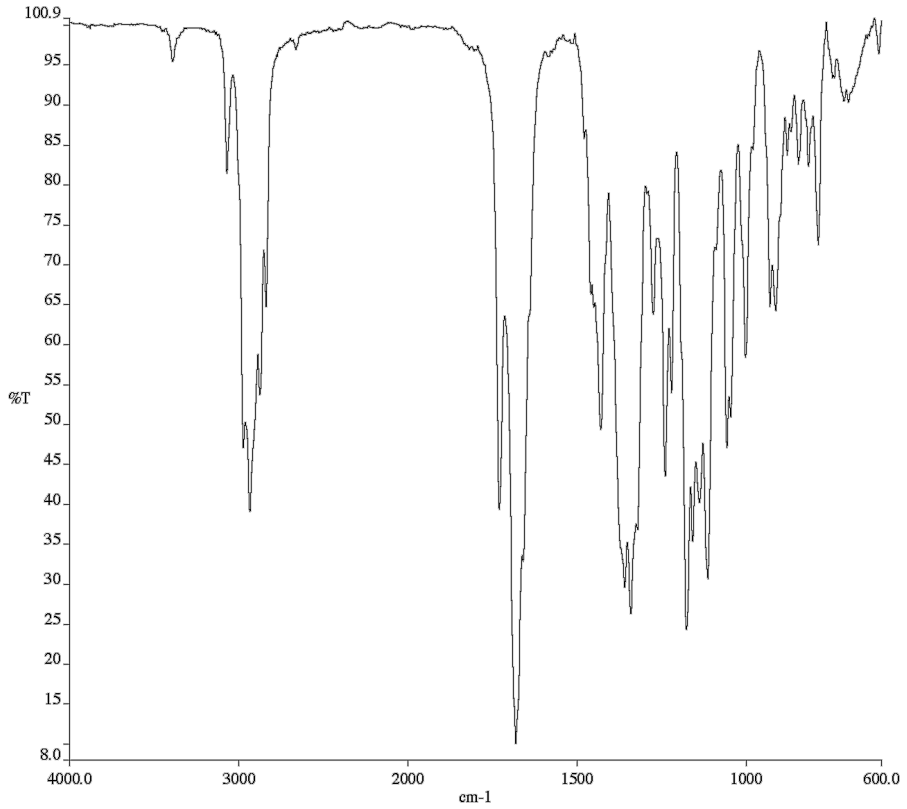

Figure A2.11 *Infrared spectrum (Thin Film, NaCl) of compound* ***14****.*

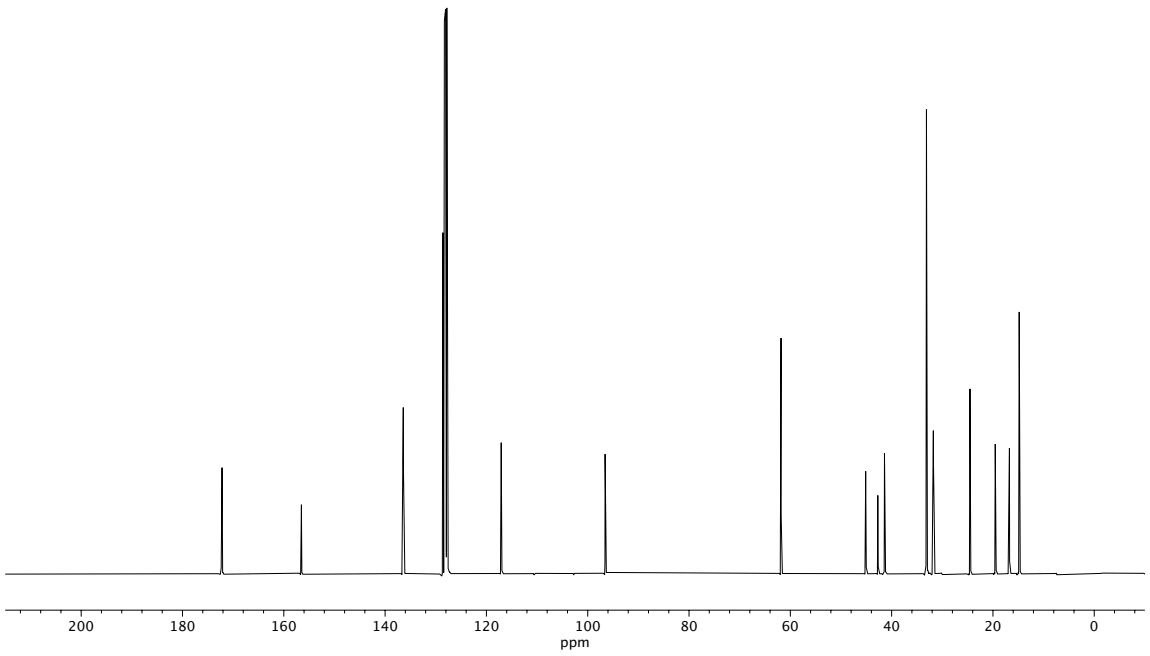

Figure A2.12 *^{13}C NMR (100 MHz, C_6D_6) of compound* ***14****.*

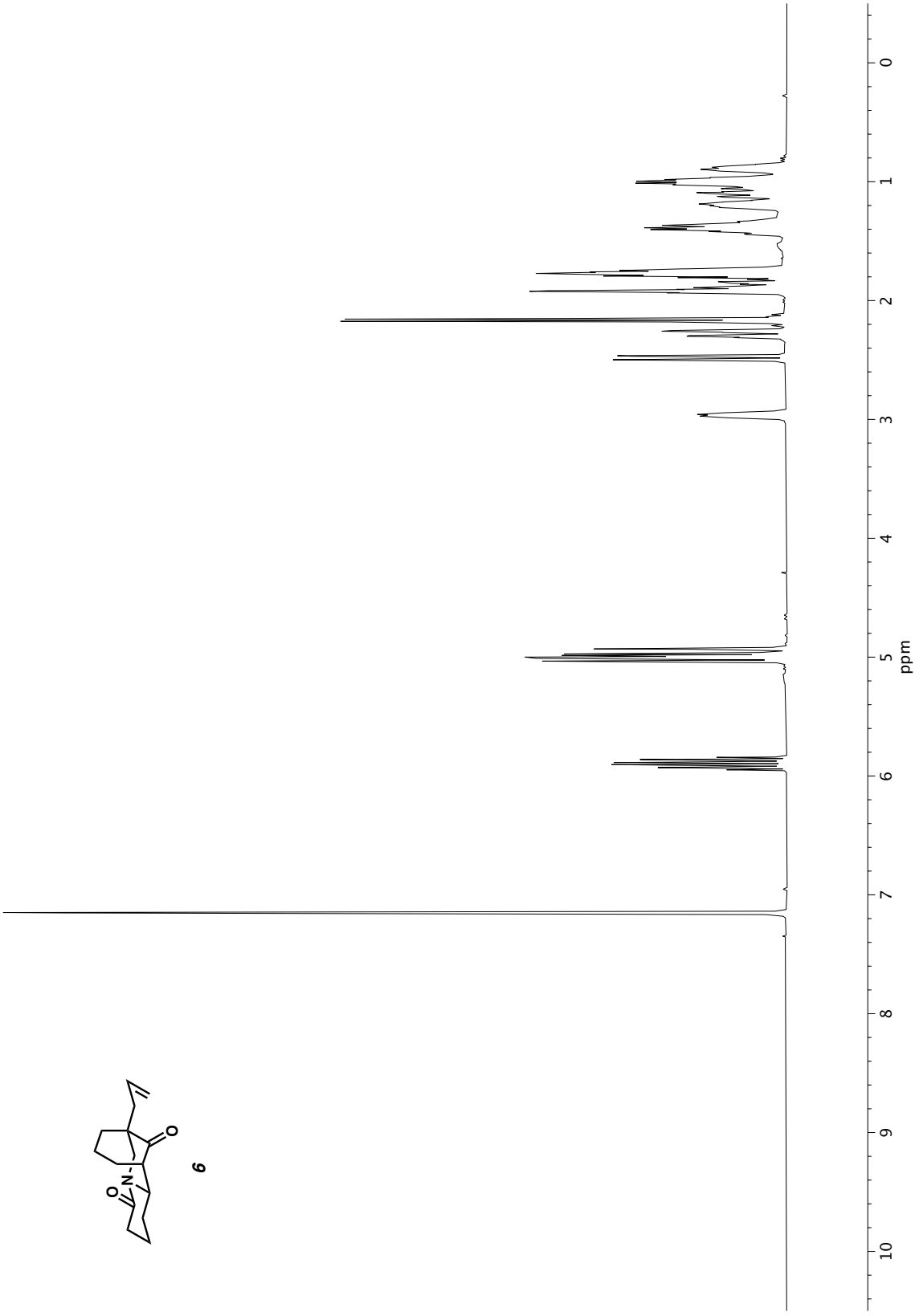

Figure A2.13 *^1H NMR (600 MHz, C_6D_6) of compound* ***6***.

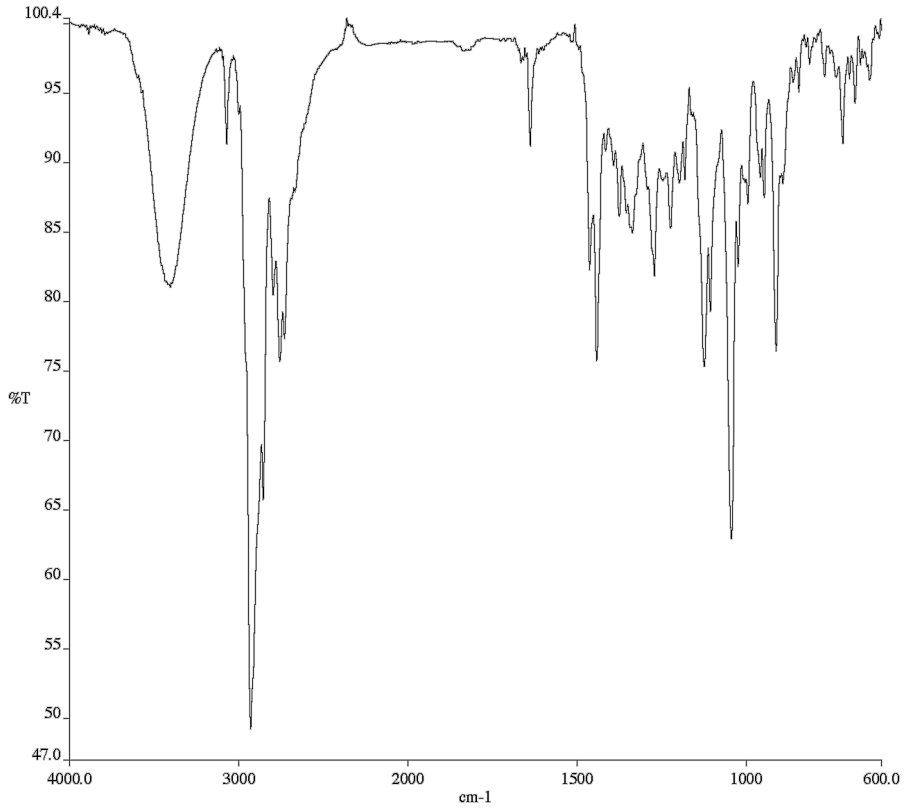

Figure A2.14 *Infrared spectrum (Thin Film, NaCl) of compound* ***6****.*

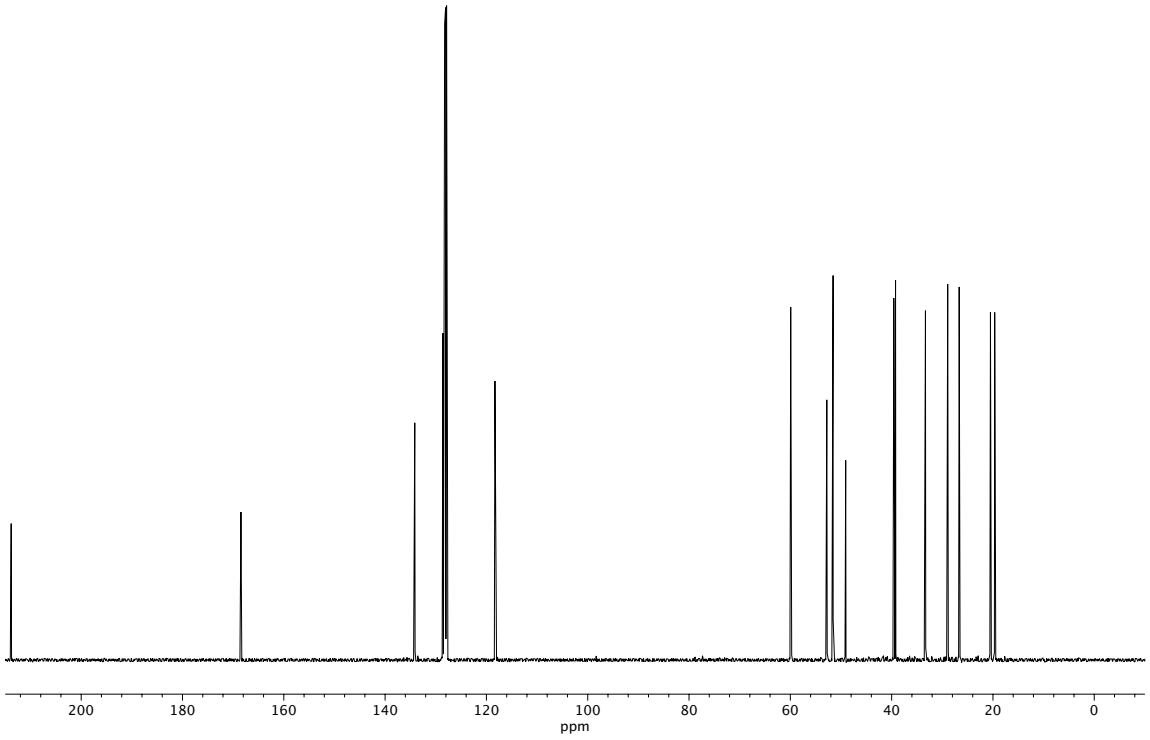

Figure A2.15 *^{13}C NMR (100 MHz, C_6D_6) of compound* ***6****.*

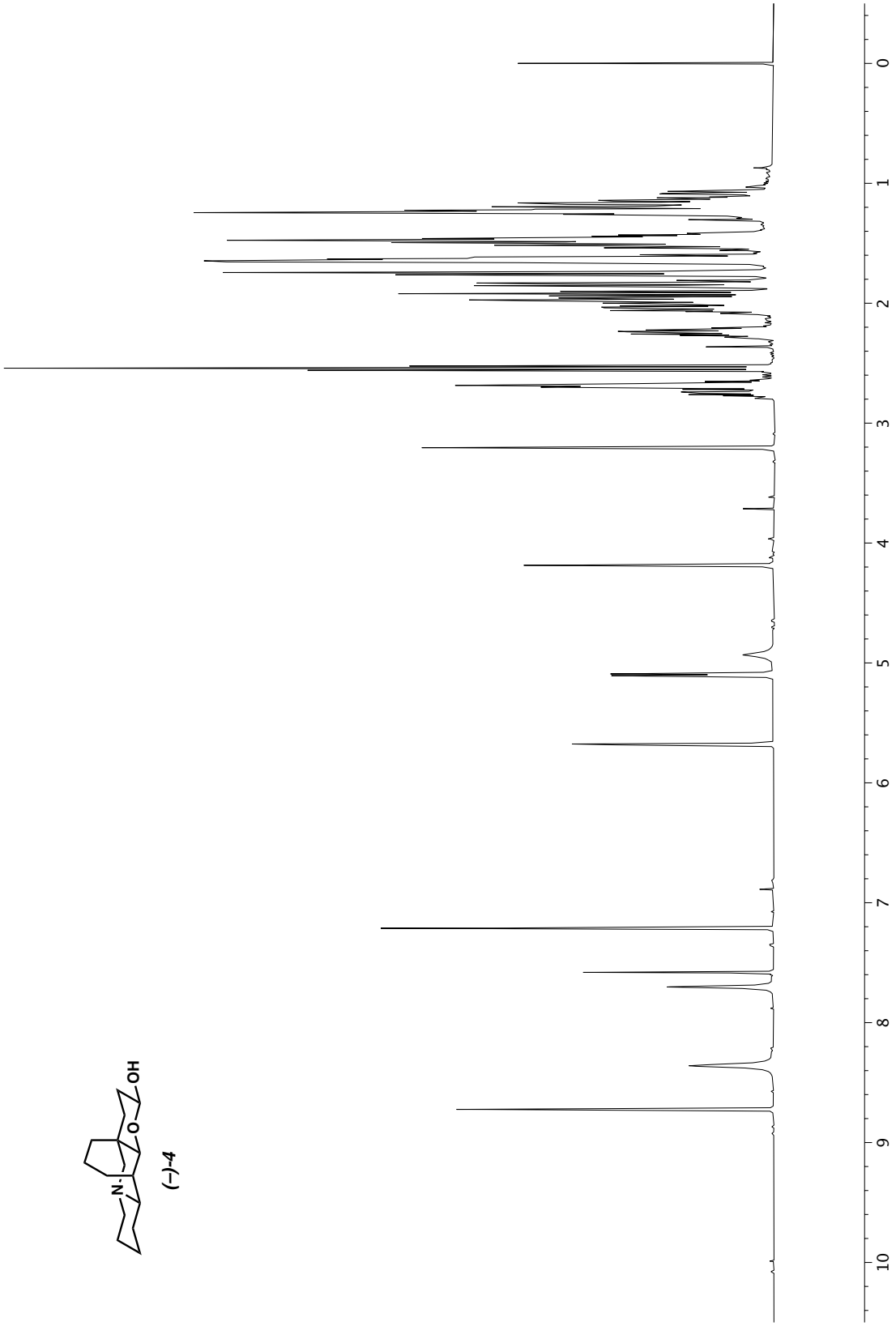

Figure A2.16 *^{1}H NMR (600 MHz, pyridine-d_5) of compound* ***(–)-4****.*

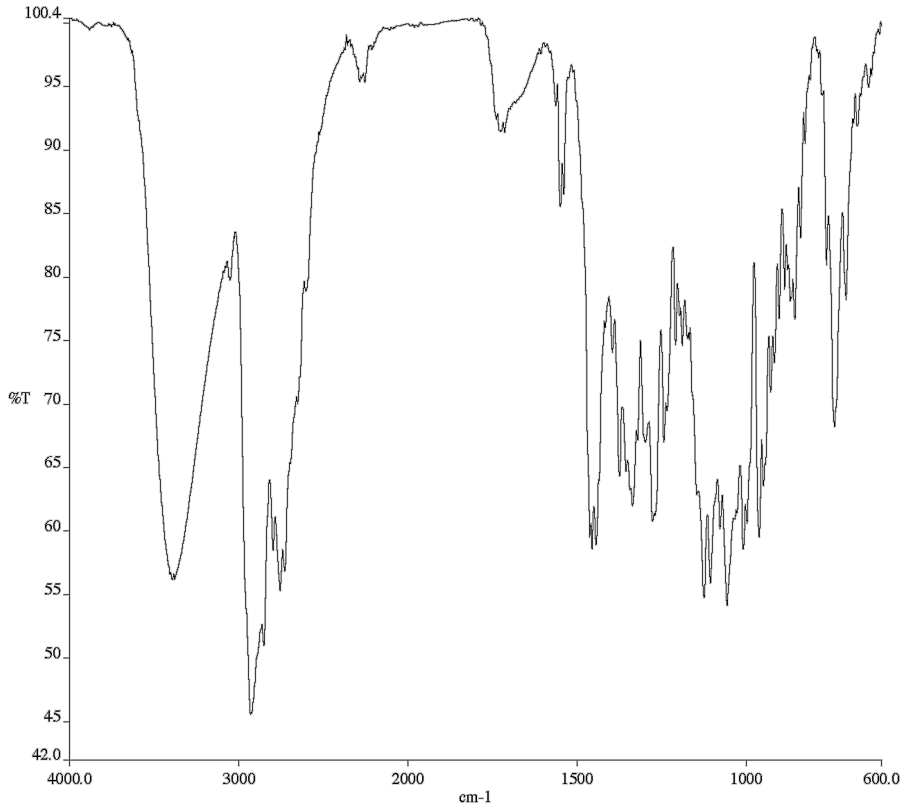

Figure A2.17 *Infrared spectrum (Thin Film, NaCl) of compound* ***(–)-4****.*

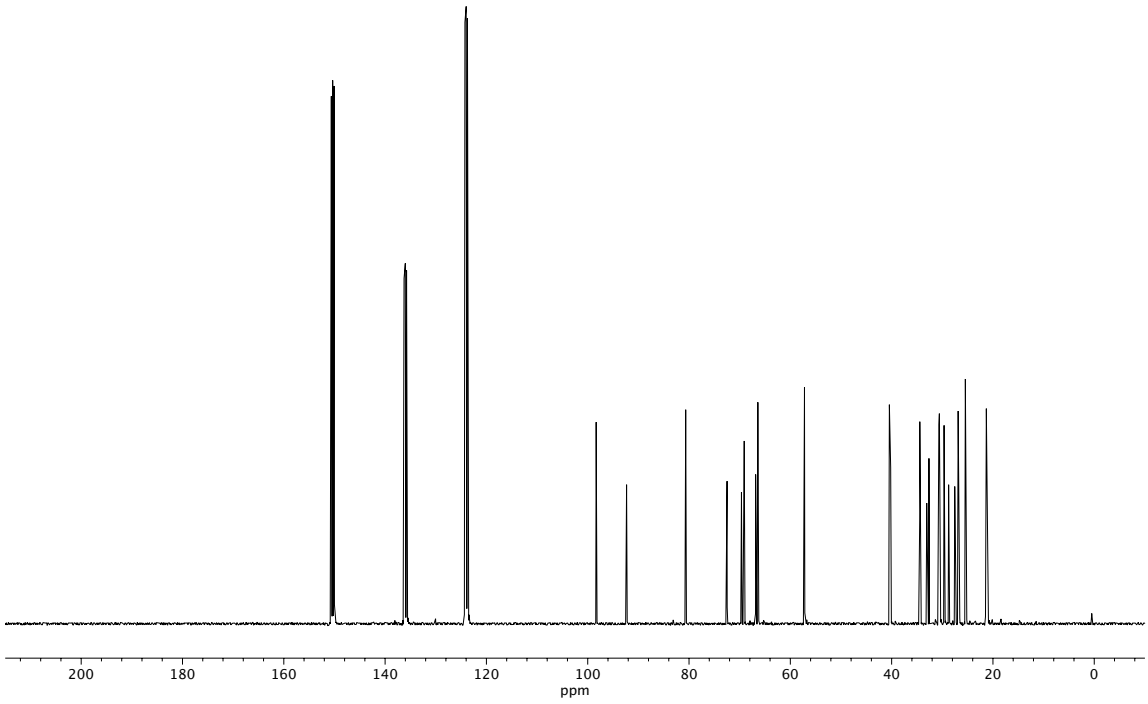

Figure A2.18 *^{13}C NMR (100 MHz, pyridine-d_5) of compound* ***(–)-4****.*

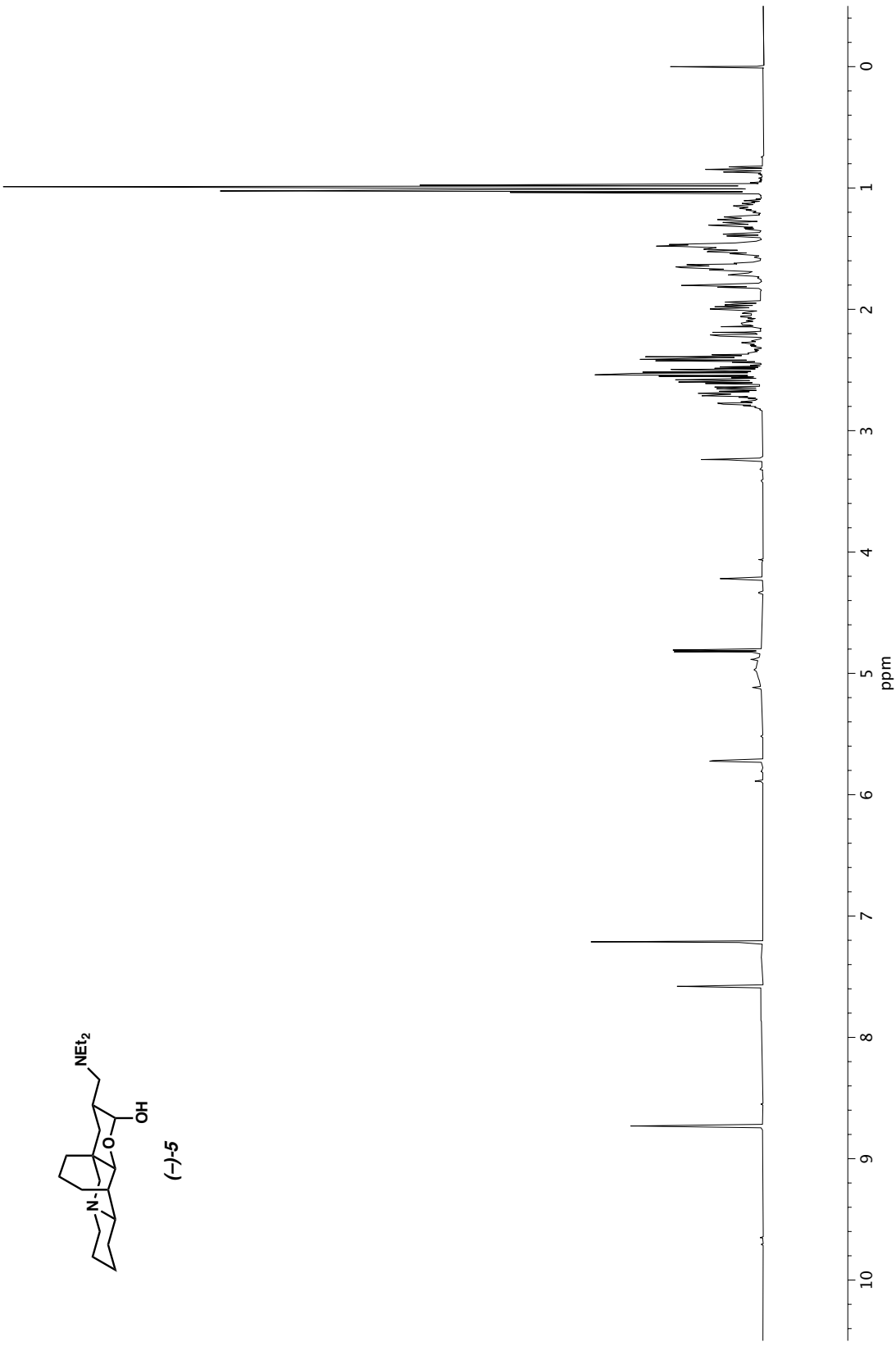

Figure A2.19 *^{1}H NMR (500 MHz, pyridine-d_5) of compound* ***(–)-5***.

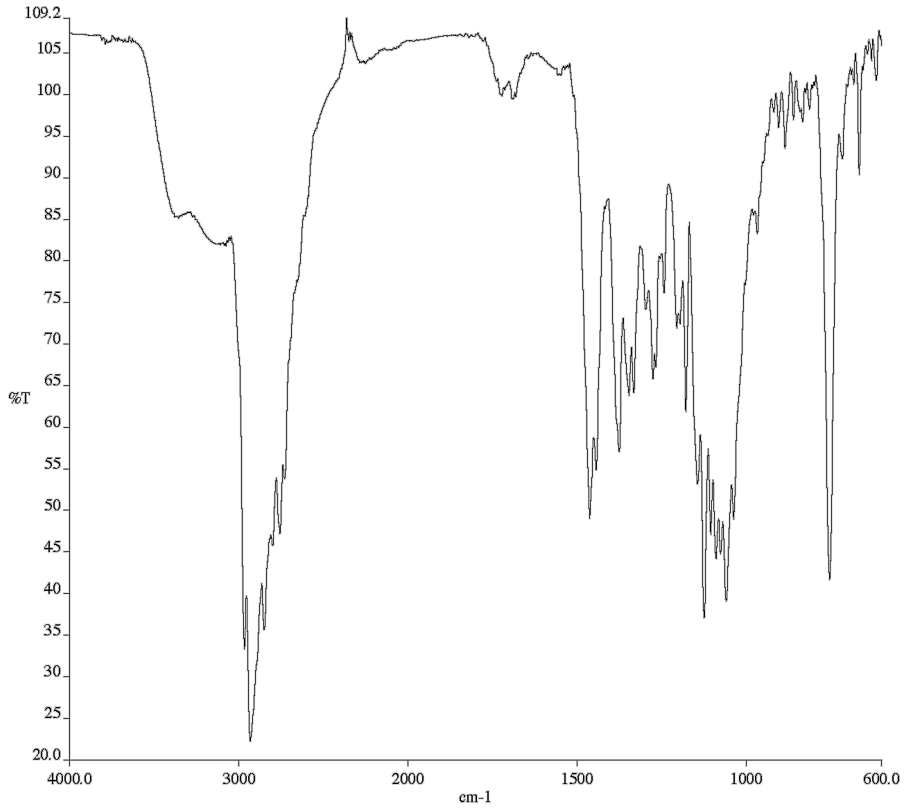

Figure A2.20 *Infrared spectrum (Thin Film, NaCl) of compound* ***(–)-5****.*

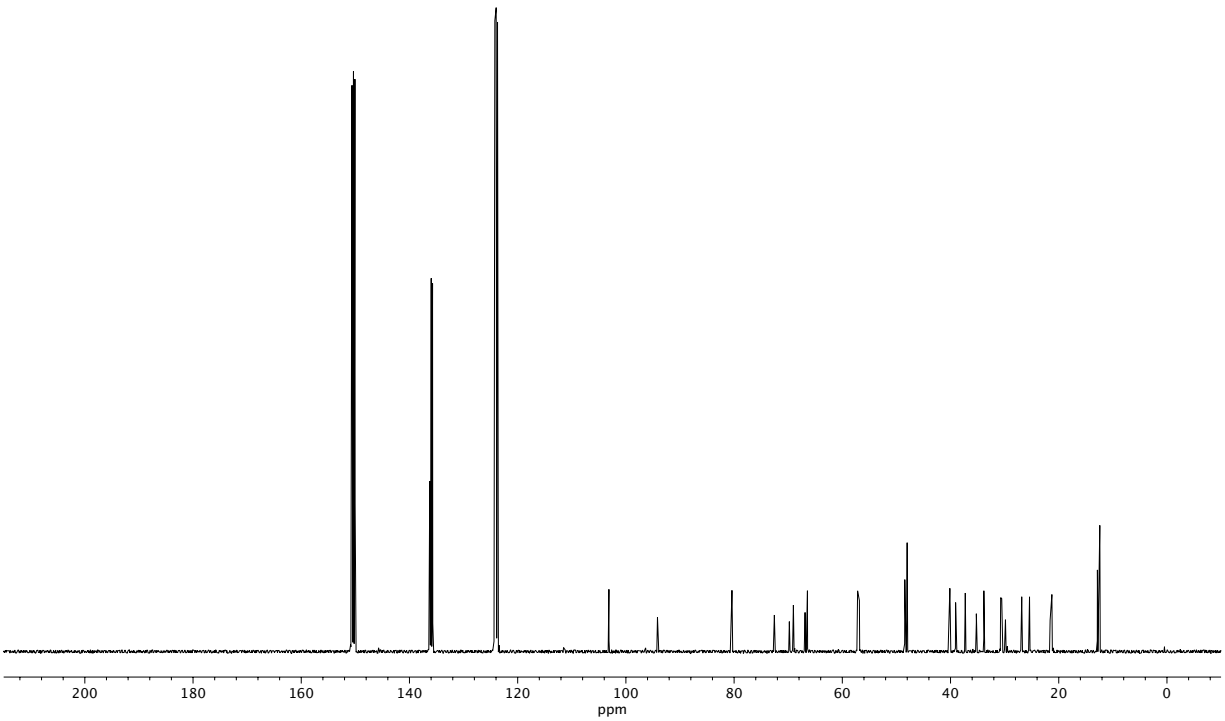

Figure A2.21 *^{13}C NMR (100 MHz, pyridine-d_5) of compound* ***(–)-5****.*

CHAPTER 2

Pd-Catalyzed Asymmetric Decarboxylative Allylic Alkylation of Fully Substituted N-Acyl Indole-Derived Enol Carbonates †

2.1 INTRODUCTION

The catalytic, enantioselective synthesis of all-carbon quaternary stereogenic centers has become an important area of research owing to the prominence of such structural motifs in natural products and their potential utility in medicinal applications.[1] Numerous strategies have been developed for the synthesis of all-carbon quaternary stereogenic centers in cyclic systems.[1,2] In contrast, approaches to the synthesis of all-carbon quaternary stereogenic in acyclic systems are limited in scope. This is ostensibly due to the requirement for stereodefined tetrasubstituted olefins or enolates typically necessary for high levels of enantioinduction.[3] Our group has previously reported the utility of Pd-catalyzed decarboxylative allylic alkylation for preparing acyclic α-quaternary stereogenic aryl amides and ketones in high ee from the corresponding fully substituted acyclic allyl enol carbonates.[4] In the case of acyclic aryl ketones (Figure 2.1.1A), the enol carbonates could be prepared with excellent control of enolate geometry utilizing conditions developed by Zhang and

Gosselin (Figure 2.1.2),[5] however, this was found to be inconsequential on the stereochemical outcome of the reaction. Specifically, the same enantiomer of product was obtained in identical enantiomeric excess regardless of the ratio of starting enolate geometric isomers.[4b] This result runs contrary to reports in the literature highlighting the central importance of controlling enolate geometry in acyclic Pd-catalyzed allylic alkylation.[4a,6]

To expand the scope of this transformation, we sought to evaluate ester enolates as possible substrates, enabling access to synthetically versatile α-quaternary carboxylic acid derivatives. The Trost group has previously reported the enantioselective Pd-catalyzed allylic alkylation of two different ester enolate equivalents: 2-acylimidazoles[7a] and *N*-acyl oxazolidinones[7b] (Figure 2.1.1B). Both reports are limited to the synthesis of tertiary stereogenic centers from trisubstituted enolate nucleophiles, highlighting the difficulty of forming acyclic quaternary stereogenic centers via fully substituted enolates. Unique strategies have emerged to circumvent the challenges of fully substituted enolate preparation. For example, Shimizu and Kanai reported a dual boron-Pd catalytic system which enables access to α-quaternary carboxylic acids through a symmetrical, chiral carboxylic acid dianion (Figure 2.1.1C).[8] Additionally, both Rh-[9] and Ir-catalyzed[10] allylic alkylation have been utilized in the synthesis of acyclic all-carbon quaternary stereogenic centers. The limited methodologies available for the synthesis of acyclic α-quaternary carboxylic acid derivatives therefore warrant additional methods to access these challenging motifs. Toward this end, we investigated the synthesis of stereodefined acyclic ester enolates, or enolate

equivalents, and their application in enantioselective decarboxylative Pd-catalyzed allylic alkylation (Figure 2.1.1D).

Figure 2.1.1 *Pd-Catalyzed Enantioselective Allylic Alkylation of Acyclic Substrates.*

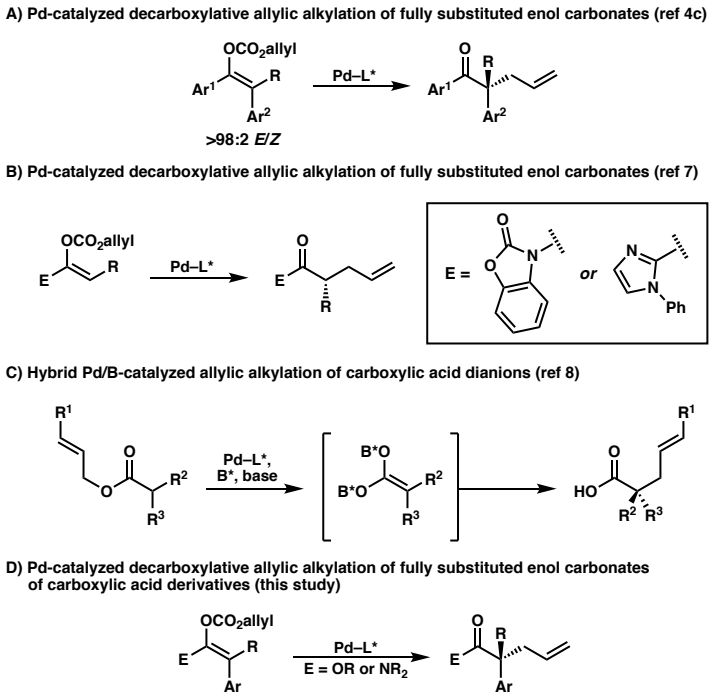

Figure 2.1.2 *Selective Enolization of Fully Substituted Acyclic Ketones.*

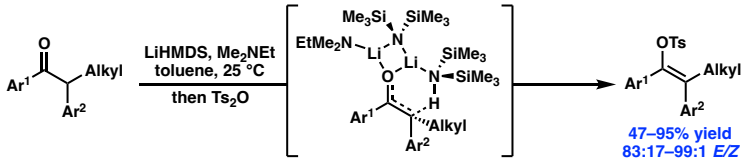

2.2 SELECTIVE ENOLIZATION AND Pd-CATALYZED ALLYIC ALKYLATION OF ACYCLIC ESTERS

This study began with the investigation of the stereoselective enolization of sterically varied α-alkyl,α-aryl-substituted esters. We were intrigued to find that treatment with

LiHMDS and Me_2NEt at 25 ºC and enolate *O*-acylation with allyl chloroformate provided the desired ester-derived enol carbonates in high *E*/*Z*-selectivity, albeit in moderate yield (Scheme 2.1.1). This selectivity was encouraging, given that all previous examples of enolization with this protocol had been performed on aryl ketones.[5] Our excitement was quickly tempered, however, as the ester-derived allyl enol carbonates were poor substrates for our standard[4b] Pd-catalyzed decarboxylative allylic alkylation conditions (Table 2.2.1). Despite optimization efforts, the best result obtained was utilizing the ethyl ester-derived substrate which provided the allylic alkylation product in 43% yield as a racemate with *(S)*-$(CF_3)_3$-*t*-BuPHOX (**L1**) (entries 2 and 3). Both phenyl ester-derived (entry 1) and *t*-Bu ester-derived (entries 4 and 5) substrates provided only trace quantities of product.

Scheme 2.2.1 *Selective Enolization and O-Acylation of Acyclic Esters.*

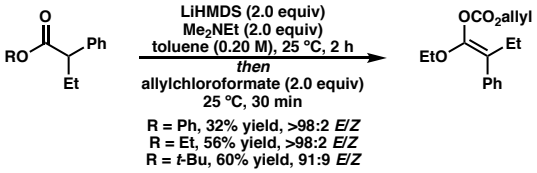

Table 2.2.1 *Ester-derived Enol Carbonates in the Pd-Catalyzed Allylic Alkylation.*[a]

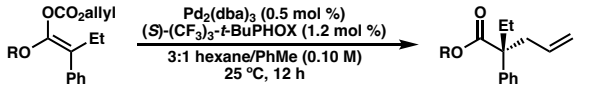

entry	R	*E*:*Z* ratio	temp (ºC)	time (h)	% conversion (yield)	% ee
1	Ph	>98:2	25	16	>95 (<10)	–
2	Et	>98:2	25–60	24–48	trace	–
3	Et	>98:2	70	48	>95 (43)	0
4	*t*-Bu	91:9	25	16	trace	–
5	*t*-Bu	91:9	80	48	partial (<10)	–

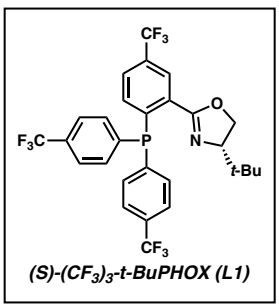

[a] Reactions were performed on a 0.100 mmol scale. Yields are isolated yields.

2.3 SELECTIVE ENOLIZATION AND Pd-CATALYZED ALLYIC ALKYLATION OF ACYCLIC ESTER EQUIVALENTS

To address this challenge, we turned to ester-enolate equivalents as an alternative to poorly reactive ester-derived enol carbonates. Based on literature precedent and our own recent studies of cyclic enolate derivatives,[6b,11] we investigated *N*-acyl-heterocycles as potential substrates. We were pleased to find that a variety of *N*-acyl heterocycles can be prepared in good to excellent *E*/*Z*-selectivity with the LiHMDS and Me_2NEt selective enolization protocol and provided promising reactivity in the subsequent Pd-catalyzed decarboxylative allylic alkylation under our standard conditions (Table 2.3.1). We found that the *N*-acyl pyrrole-derived enol carbonate affords the desired allylic alkylation product in a high 92% yield and a moderate 73% ee with electron-poor PHOX ligand **L1**, entry 1). The ee was improved to 83% by switching to a 3:1 methylcyclohexane/PhMe solvent system (entry 2), however, further experimentation led to no additional increase in selectivity for this substrate. By increasing the steric bulk on the pyrrole through the inclusion of an *ortho*-methyl group (entry 3), the high enolization selectivity is retained, however, the resultant alkylation product is obtained in only 65% ee. An *N*-methylimidazole-derived *C*-acyl substrate (entry 4) was unreactive under the alkylation conditions. Further increasing the steric bulk of the *N*-acyl group to a carbazole (entry 5) results in a drop in enolization selectivity and no reaction is observed in the allylic alkylation. The optimal substrate was determined to be an *N*-acyl indole (entry 6), which both undergoes highly selective enolization and selectively and affords the desired alkylation product in an excellent 95%

yield and 90% ee. After additional experimentation, we found that the use of a novel electron-defcient PHOX ligand *(S)*-Ty-PHOX (**L2**) provides the desired product in an improved 99% yield and 95% ee when a slightly modified 3:1 hexanes/toluene solvent mixture is used (entry 7). Notably, the reaction is performed using only 0.5 mol % $Pd_2(dba)_3$ with 1.2 mol % of ligand and is complete in 12 h at 25 ºC.

Table 2.3.1 *Optimization of the Acyclic Decarboxylative Allylic Alkylation.*[a]

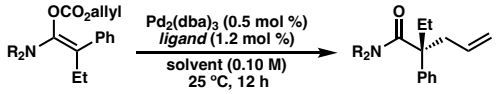

entry	R_2N–	ligand	solvent	% yield[b]	% ee[c]
1	 >98:2 *E/Z*	*L1*	3:1 hexanes/toluene	92	73
2	 >98:2 *E/Z*	*L1*	3:1 MeCy[d]/toluene	97	83
3	 >98:2 *E/Z*	*L1*	3:1 MeCy/toluene	not determined	65
4	 >98:2 *E/Z*	*L1*	3:1 MeCy/toluene	no reaction	–
5	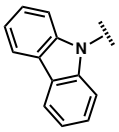 >98:2 *E/Z*	*L1*	3:1 MeCy/toluene	no reaction	–
6	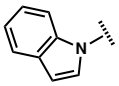 >98:2 *E/Z*	*L1*	3:1 MeCy/toluene	95	90
7	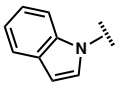 >98:2 *E/Z*	*L2*	3:1 hexanes/toluene	99	95

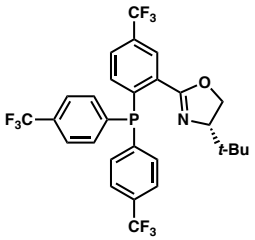

(S)-(CF_3)$_3$-t-BuPHOX (L1)

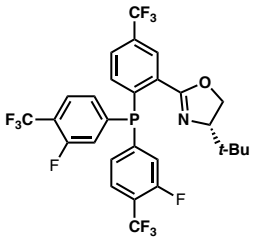

(S)-Ty-PHOX (L2)

[a] Reactions performed on a 0.100 mmol scale. [b] Yield of isolated product. [c] Determined by chiral SFC analysis. [d] MeCy = Methylcyclohexane.

2.4 IMPORTANCE OF ENOLATE GEOMETRY

With optimal reaction conditions identified, we sought to examine the impact of substrate enolate geometry. In our group's prior report on acyclic ketone enolates, the initial ratio of enolate geometries was found to be inconsequential to the reaction stereoselectivity.[4b] In contrast, the initial ratio of enolate geometries in acyclic *N*-acyl indole-derived enol carbonates has a significant impact on the stereoselectivity of the Pd-catalyzed allylic alkylation (Table 2.4.1). A 21:79 *E*/*Z* mixture of enol carbonates (**19a**) provides the alkylation product (**20a**) in a significantly diminished 66% ee with **L2** as the ligand, although the same enantiomer of product is the same as when a 98:2 *E*/*Z* mixture is used (entries 1 and 2). This result suggests that some degree of enolate geometry equilibration is occurring during the catalytic process, however, to a lesser extent than in the previously reported acyclic aryl ketone systems.

Table 2.4.1 *Importance of Enolate Geometry for Enantioselectivity.*

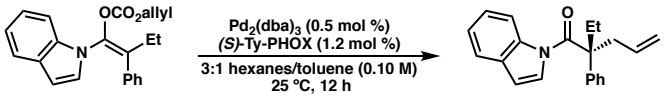

19a ***20a***

entry	*E*/*Z* ratio of 19a	% ee 20a
1	>98:2	95
2	21:79	66

2.5 SCOPE OF THE ASYMMETRIC ALLYLIC ALKYLATION

With optimized reaction conditions and the importance of enol carbonate geometry established, we examined the scope of this transformation for accessing various acyclic all-carbon quaternary stereogenic centers (Table 2.5.1). All enol carbonates were accessed in excellent *E*/*Z*-geometry control (>98:2, see Experimental Section 2.8.2.2 for details) and the corresponding allylic alkylation products were obtained in high yields. Products

bearing a longer α-alkyl chain such as *n*-pentyl (**20b**) or a branching *i*-Bu group (**20c**) were obtained in excellent 96% ee. Benzyl-substitution substrate **20d** was also well tolerated, albeit in a slightly dimished 90% ee. Substrate **20d** was crystallized and the absolute stereochemical configuration of *(S)* was determined by X-Ray crystallographic analysis, all other substrates' stereochemistry were assigned by analogy. The presence of electron-rich aryl groups resulted in a slight increase in enantioselectivity: both 4-methyl (**20e**) and 4-methoxy (**20f**) substrates were isolated in 98% ee while 3,5-dimethoxy (**20g**) was obtained in 95% ee. Notably, both methoxy-substituted aryl substrates **20f** and **20g** required longer reaction times of 24 h for full conversion of the enol carbonates. Substitution with weakly electron-withdrawing substituents[12] at the *para*-position were well tolerated in the case of 4-chloro (**20h**), 4-bromo (**20i**), and 4-fluoro (**20j**) substrates which were isolated in 94, 94, and 96% ee, respectively. On the other hand, substitution with a strongly electron-withdrawing 4-trifluoromethyl group (**20k**) led to a sharp drop in enantioselectivity to 72% ee, believed to result from the increased inductive stabilization of the enolate generated in situ.[2f] Substitution of the *N*-acyl indole was also well tolerated, with methyl-substituted substrate **20l** isolated in 98% ee and bromo-substituted substrate **20m** isolated in 92% ee. While *ortho*-substitution of the α-aryl substituent resulted in poor enolization geometry control and enantioselectivity in *N*-acyl indole-derived substrates, employing less sterically encumbered *N*-acyl 3-methyl pyrrole enabled 3-Me (**20n**) and 3-Br (**20o**) allylic alkylation products to be generated in moderate 89% and 80% ee, respectively. Notably, the use of a more electron-rich *N*-acyl pyrrole (i.e. 3-methyl pyrrole vs. pyrrole) provides a slight boost

in enantioselectivity analogous to *N*-acyl indole **20l** vs. *N*-acyl indole **20a** (95 vs. 98% ee).[13]

The broad scope of α-aryl substituted substrates tolerated in this transformation, as well as the related ketone allylic alkylation,[4b] is in stark contrast to previous examples of α-aryl substituted and weakly basic substrates which are poor substrates for the Pd-catalyzed enantioselective allylic alkylation with PHOX ligands.[2f] To rationalize this observation, as well as to explain the necessity for α-aryl substituents, we propose the α-aryl group is likely rotated out of plane with respect to the enolate and that the *N*-acyl group is planar and in conjugation with the enolate to avoid steric clashing between both aromatic groups (Figure 2.5.1). With the α-aryl group out of plane with the enolate, there may also be an attractive edge-to-face interaction with the *N*-acyl aromatic group. As a result of the out of plane α-aryl group, there is no significant resonance stabilization of the enolate and therefore high enantioselectivities can be achieved. Inductive stabilization through electron-withdrawing substituents (e.g. 4-trifluoromethyl, **20k**) may still impart lower levels of enantioselectivity.

Table 2.5.1 *Scope of the Enantioselective Allylic Alkylation.*[a]

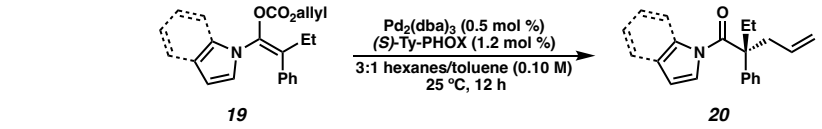

19 ***20***

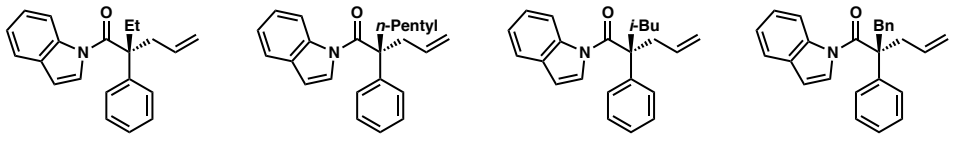

20a
99% yield, 95% ee

20b
99% yield, 96% ee

20c
99% yield, 96% ee

20d[b]
96% yield, 90% ee

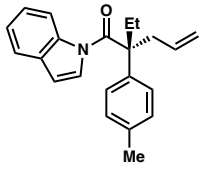

20e
99% yield, 98% ee

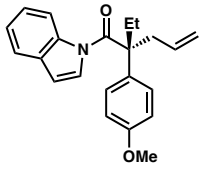

20f[c]
89% yield, 98% ee

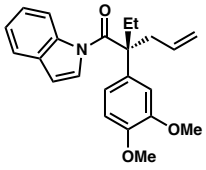

20g[c]
99% yield, 95% ee

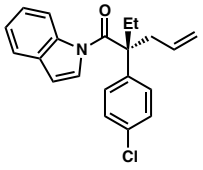

20h
99% yield, 94% ee

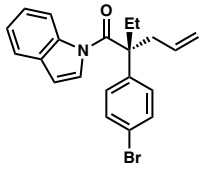

20i
98% yield, 94% ee

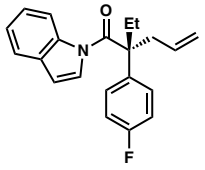

20j
97% yield, 96% ee

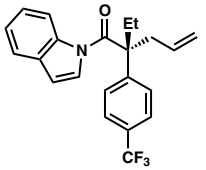

20k
98% yield, 72% ee

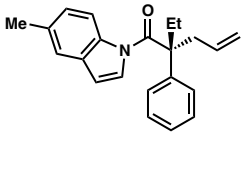

20l
99% yield, 98% ee

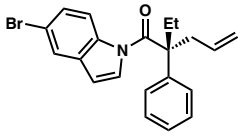

20m
97% yield, 92% ee

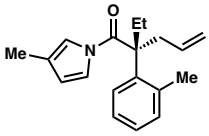

20n
99% yield, 89% ee

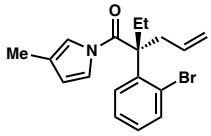

20o
87% yield, 80% ee

[a] All reactions performed on a 0.200 mmol scale. Yields are of isolated products. % ee was determined by chiral SFC analysis. [b] Absolute stereochemistry was determined by X-Ray crystallography, all other products assigned by analogy. [c] Reaction time of 24 h.

Figure 2.5.1 *Hypothesis for Tolerance of α-Aryl Substituents.*

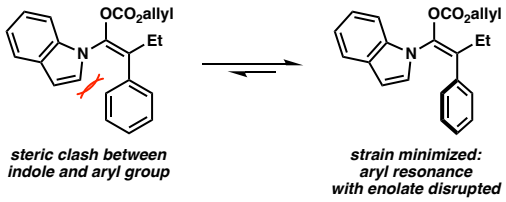

To further investigate our hypothesis, we prepared substrate **19p** bearing α-*N*-pyrrolo substitution and examined its reactivity under our optimized Pd-catalyzed allylic alkylation conditions (Scheme 2.5.1). We reasoned that α-*N*-pyrrolo substitution mimic an α-phenyl substituent in the same manner that an *N*-acyl indole mimics a phenyl ketone. This is indeed the case, with alkylation product **20p** isolated in an excellent 97% yield and 99% ee.

Scheme 2.5.1 *Investigation of an α-N-pyrrole Substituted N-Acyl Indole Substrate.*

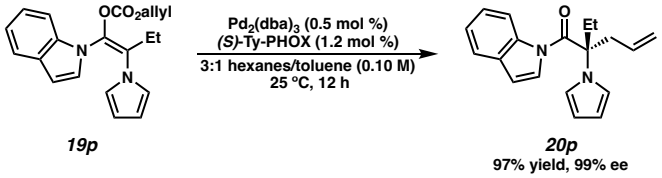

2.6 DERIVATIZATION OF *N*-ACYL INDOLE PRODUCTS

To highlight the utility of the enantioenriched α-quaternary *N*-acyl indole products, we examined product derivatizations (Scheme 2.6.1). Cleavage of allylic alkylation product **20a** with KOTMS affords carboxylic acid **21** which can be isolated in 99% yield following a chromatography-free acid/base extraction procedure. Ethyl ester **22** was prepared in 75% yield following treatment of *N*-acyl indole **20a** with KOEt. Reduction of the *N*-acyl indole with $LiAlH_4$ generates β-quaternary alcohol **23** in 84% yield. The olefin of product **20a** is also a valuable synthetic handle, demonstrated by Wacker oxidation to

1,4-dicarbonyl **24** in 95% yield as a 5:1 mixture of ketone/aldehyde. Surprisingly, *N*-acyl indole allylic alkylation product **20a** was recalcitrant to react with MeMgBr as well as direct Weinreb amide-forming reaction conditions, even at elevated temperatures, suggesting the potential to employ this moiety as a robust and orthogonal carboxylic acid masking group (Scheme 2.6.2).

Scheme 2.6.1 *Derivatization of N-Acyl Indole Allylic Alkylation Product* ***20a****.*

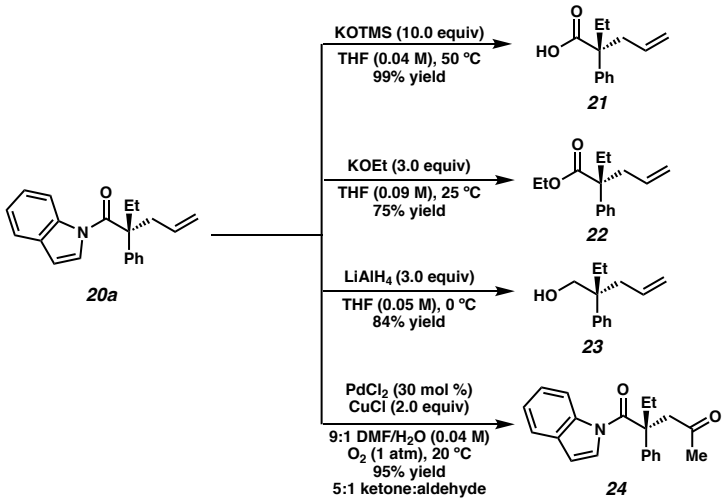

Scheme 2.6.2 *Failed Derivatizations of N-Acyl Indole Allylic Alkylation Product* ***20a****.*

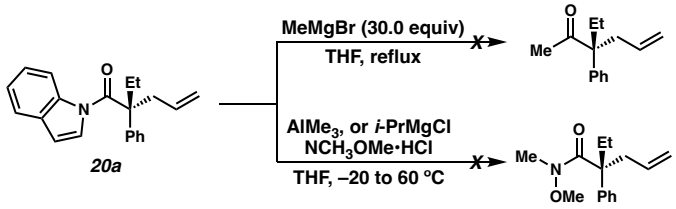

2.7 CONCLUSION

This study delineates the first example of a Pd-catalyzed allylic alkylation of *N*-acyl indole-derived enol carbonates to provide access to acyclic all-carbon quaternary stereogenic centers in high yield and ee. While ester-derived enol carbonates could be generated with excellent geometrical isomer selectivity, these substrates we poorly reactive

under standard Pd-catalyzed allylic alkylation conditions, necessitating the utilization of *N*-acyl indoles and pyrroles as ester-enolate equivalents. The preparation of the *N*-acyl indole- and pyrrole-derived enol carbonates as single geometrical enolate isomers, as well as the utilization of new electron-deficient PHOX ligand *(S)*-Ty-PHOX (**L2**), were critical to obtaining the excellent enantioselectivities observed.

2.8 EXPERIMENTAL SECTION

2.8.1 MATERIALS AND METHODS

Unless otherwise noted, reactions were performed in flame-dried glassware under an Ar or N_2 atmosphere using dry, deoxygenated solvents. Solvents were dried by passage through an activated alumina column under Ar.[14] Reaction progress was monitored by thin-layer chromatography (TLC) or Agilent 1290 UHPLC-MS. TLC was performed using E. Merck silica gel 60 F254 precoated glass plates (0.25 mm) and visualized by UV fluorescence quenching, *p*-anisaldehyde, or KMnO4 staining. Silicycle Silia*Flash*® P60 Academic Silica gel (particle size 40–63 μm) was used for flash chromatography. ^{1}H NMR spectra were recorded on Varian Inova 500 MHz and Bruker 400 MHz spectrometers and are reported relative to residual $CHCl_3$ (δ 7.26 ppm) ^{13}C NMR spectra were recorded on a Varian Inova 500 MHz spectrometer (125 MHz) and Bruker 400 MHz spectrometers (100 MHz) and are reported relative to $CHCl_3$ (δ 77.16 ppm). Data for ^{1}H NMR are reported as follows: chemical shift (δ ppm) (multiplicity, coupling constant (Hz), integration). Multiplicities are reported as follows: s = singlet, d = doublet, t = triplet, q = quartet, p = pentent, sept = septuplet, m = multiplet, br s =broad singlet, br d = broad doublet, app = apparent. Data for ^{13}C NMR reported in terms of chemical shifts (δ ppm). IR spectra were

obtained by the use of a Perkin Elmer Spectrum BXII spectrometer or Nicolet 6700 FTIR spectrometer using thin films deposited on NaCl plates and reported in frequency of absorption (cm^{-1}). Optical rotations were measured with a Jasco P-2000 polarimeter operating on the sodium D-line (589 nm), using a 100 mm path-length cell and reported as $[\alpha]_D^T$ (concentration in 10 mg/1 mL, solvent). Analytical SFC was performed with a Mettler SFC supercritical CO_2 analytical chromatography system utilizing Chiralpak (AD-H, AS-H, or IC) or Chiracel (OD-H, OJ-H, or OB-H) columns (4.6 mm x 25 cm) obtained from Daicel Chemical Industries, Ltd. High resolution mass spectra (HRMS) were obtained from Agilent 6200 Series TOF with an Agilent G1978A Multimode source in electrospray ionization (ESI+), atmospheric pressure chemical ionization (APCI+), or mixed ionization more (MM: ESI-APCI+), or obtained from the Caltech mass spectrometry laboratory. Ligands were prepared by known methods.[15]

2.8.2 EXPERIMENTAL PROCEDURES

2.8.2.1 General Procedure for the Pd-Catalyzed Decarboxylative Allylic Alkylation Reactions

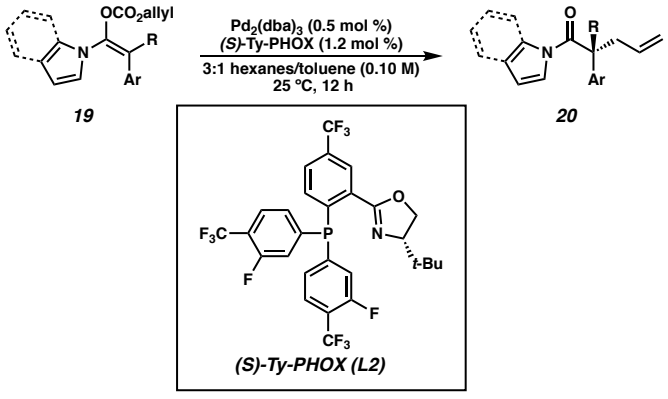

In a nitrogen-filled glovebox, a solution of $Pd_2(dba)_3$ (1.8 mg/mL) and **L2** (2.8 mg/mL) in toluene was stirred for 30 min at 25 ºC, then 0.5 mL of the resulting catalyst

solution was added to a one-dram vial containing the allyl enol carbonate substrate (0.200 mmol) dissolved in hexanes (1.5 mL). The vial was sealed with a Teflon-lined cap and electrical tape, removed from the glovebox, and stirred at 25 ºC for 12 h unless otherwise noted. The crude reaction mixture was concentrated then purified by silica gel flash chromatography to provide the desired alkylation product.

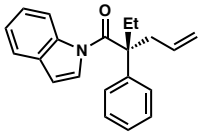

_(R)_-2-ethyl-1-(1_H_-indol-1-yl)-2-phenylpent-4-en-1-one (20a)

Purified by column chromatography (5% Et_2O in hexanes) to provide an amorphous white solid (64.8 mg, 99% yield); 95% ee, $[\alpha]_D^{25}$ –111.4 (*c* 1.0, $CHCl_3$); ^1H NMR (500 MHz, $CDCl_3$) δ 8.58 (dt, *J* = 8.3, 0.8 Hz, 1H), 7.48–7.44 (m, 1H), 7.39–7.32 (m, 3H), 7.32–7.22 (m, 4H), 6.84 (d, *J* = 3.9 Hz, 1H), 6.26 (d, *J* = 3.8 Hz, 1H), 5.45 (dddd, *J* = 16.6, 10.2, 8.5, 6.2 Hz, 1H), 5.03–4.92 (m, 2H), 2.99 (dd, *J* = 14.0, 8.5 Hz, 1H), 2.88 (dd, *J* = 14.0, 6.2 Hz, 1H), 2.25 (qd, *J* = 7.4, 1.5 Hz, 2H), 0.81 (t, *J* = 7.4 Hz, 3H); ^{13}C NMR (100 MHz, $CDCl_3$) δ 174.3, 143.0, 136.5, 133.0, 129.5, 129.2, 127.3, 126.5, 126.1, 125.1, 123.7, 120.6, 119.0, 117.2, 108.2, 56.8, 40.5, 28.0, 8.4.; IR (Neat Film, NaCl) 3154, 3071, 2974, 2880, 1694, 1643, 1600, 1584, 1538, 1495, 1471, 1463, 1446, 1380, 1303, 1206, 1225, 1149, 1077, 1019, 1000, 920, 891, 820, 767, 701 cm^{-1}; HRMS (MM:ESI-APCI+) *m/z* calc'd for $C_{21}H_{22}NO$ $[M+H]^+$: 304.1696, found 304.1691; SFC Conditions: 10% IPA, 2.5 mL/min, Chiralpak AD-H column, λ = 210 nm, t_R (min): minor = 6.41, major = 6.95.

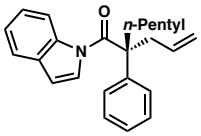

_(R)_-2-allyl-1-(1_H_-indol-1-yl)-2-phenylheptan-1-one (20b)

Purified by column chromatography (5% Et_2O in hexanes) to provide an amorphous white solid (68.4 mg, 99% yield); 96% ee; $[\alpha]_D^{25}$ –81.8 (*c* 1.0, $CHCl_3$); ^1H NMR (500 MHz, $CDCl_3$) δ 8.58 (dq, *J* = 8.4, 0.8 Hz, 1H), 7.46 (dt, *J* = 7.6, 1.1 Hz, 1H), 7.35 (ddt, *J* = 8.3, 5.3, 1.7 Hz, 3H), 7.30–7.22 (m, 4H), 6.85 (d, *J* = 3.9 Hz, 1H), 6.26 (dd, *J* = 3.8, 0.7 Hz, 1H), 5.44 (dddd, *J* = 16.6, 10.1, 8.5, 6.1 Hz, 1H), 5.03–4.90 (m, 2H), 3.00 (dd, *J* = 14.0, 8.6 Hz, 1H), 2.88 (dd, *J* = 14.0, 6.1 Hz, 1H), 2.25–2.11 (m, 2H), 1.35–1.24 (m, 1H), 1.21 (qd, *J* = 6.5, 6.0, 3.1 Hz, 4H), 1.10–0.98 (m, 1H), 0.81–0.75 (m, 3H); ^{13}C NMR (100 MHz, $CDCl_3$) δ 174.4, 143.2, 136.5, 133.2, 129.5, 129.2, 127.3, 126.4, 126.1, 125.1, 123.7, 120.6, 119.0, 117.3, 108.2, 56.4, 41.3, 35.0, 32.2, 23.4, 22.4, 14.0; IR (Neat Film, NaCl) 3071, 2954, 2928, 2859, 1696, 1449, 1304, 1204, 1078, 919, 750, 702 cm^{-1}; HRMS (MM:ESI-APCI+) *m/z* calc'd for $C_{24}H_{28}NO$ $[M+H]^+$: 346.2165, found 346.2156; SFC Conditions: 10% IPA, 2.5 mL/min, Chiralpak AD-H column, λ = 210 nm, t_R (min): minor = 4.87, major = 5.84.

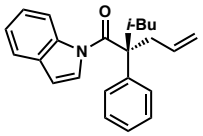

(*R*)-1-(1*H*-indol-1-yl)-2-isobutyl-2-phenylpent-4-en-1-one (20c)

Purified by column chromatography (5% Et_2O in hexanes) to provide an amorphous white solid (66.1 mg, 99% yield); 96% ee, $[\alpha]_D^{25}$ –109.1 (*c* 1.0, $CHCl_3$); ^1H NMR (500 MHz, $CDCl_3$) δ 8.62–8.52 (m, 1H), 7.49–7.43 (m, 1H), 7.39–7.32 (m, 3H), 7.30–7.21 (m, 4H), 6.87 (d, *J* = 3.8 Hz, 1H), 6.27 (d, *J* = 3.8 Hz, 1H), 5.42 (dddd, *J* = 16.5, 9.9, 8.7, 5.9 Hz, 1H), 5.04–4.89 (m, 2H), 3.13–3.01 (m, 1H), 2.91 (ddd, *J* = 14.2, 5.9, 1.5 Hz, 1H), 2.26 (dd, *J* = 14.1, 4.4 Hz, 1H), 2.10 (ddd, *J* = 14.1, 6.5, 1.1 Hz, 1H), 1.74 (ddt, *J* = 13.2, 11.0, 6.5 Hz, 1H), 0.84 (d, *J* = 6.6 Hz, 3H), 0.62 (d, *J* = 6.6 Hz, 3H); ^{13}C NMR (100 MHz, $CDCl_3$) δ 174.8, 143.3, 136.5, 133.3, 129.6, 129.2, 127.3, 126.4, 126.1, 125.2, 123.8, 120.6, 119.2, 117.3, 108.2, 56.1, 43.5, 42.2, 25.2, 24.1, 23.5; IR (Neat Film, NaCl) 3164, 3071, 3026, 2957, 2868, 1693, 1639, 1600, 1584, 1537, 1472, 1449, 1306, 1222, 1206, 1149, 1079, 919, 890, 767, 750, 702 cm^{-1}; HRMS (MM:ESI-APCI+) *m/z* calc'd for $C_{23}H_{26}NO$ $[M+H]^+$: 332.2009, found 332.1998; SFC Conditions: 10% IPA, 2.5 mL/min, Chiralpak AD-H column, λ = 210 nm, t_R (min): minor = 4.86, major = 5.20.

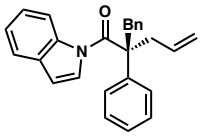

***(S)*-2-benzyl-1-(1*H*-indol-1-yl)-2-phenylpent-4-en-1-one (20d)**

Purified by column chromatography (5% Et_2O in hexanes) to provide an amorphous white solid (70.5 mg, 96% yield); 90% ee, $[\alpha]_D^{25}$ +50.9 (*c* 1.0, $CHCl_3$); ^1H NMR (500 MHz, $CDCl_3$) δ 8.54–8.50 (m, 1H), 7.48 (dt, *J* = 7.8, 1.0 Hz, 1H), 7.38–7.29 (m, 4H), 7.29–7.23 (m, 1H), 7.18– 7.11 (m, 3H), 7.06 (dd, *J* = 8.2, 6.9 Hz, 2H), 6.92 (d, *J* = 3.8 Hz, 1H), 6.60 (dd, *J* = 7.6, 1.5 Hz, 2H), 6.32 (d, *J* = 3.9 Hz, 1H), 5.82–5.69 (m, 1H), 5.11–5.05 (m, 1H), 5.00–4.93 (m, 1H), 3.56 (d, *J* = 13.5 Hz, 1H), 3.42 (d, *J* = 13.5 Hz, 1H), 2.89 (d, *J* = 7.1 Hz, 2H); ^{13}C NMR (100 MHz, $CDCl_3$) δ 173.7, 142.4, 136.6, 136.3, 132.8, 130.8, 129.5, 129.1, 127.8, 127.6, 126.8, 126.7, 126.0, 125.2, 123.8, 120.6, 119.8, 117.3, 108.5, 57.8, 42.4, 39.0; IR (Neat Film, NaCl) 3062, 3028, 2926, 1694, 1601, 1584, 1537, 1495, 1449, 1328, 1305, 1203, 1078, 1019, 894, 751, 720, 702 cm^{-1}; HRMS ((MM:ESI-APCI+) *m/z* calc'd for $C_{26}H_{24}NO$ $[M+H]^+$: 366.1852, found 366.1855; SFC Conditions: 10% IPA, 2.5 mL/min, Chiralpak AD-H column, λ = 235 nm, t_R (min): minor = 17.49, major = 18.37.

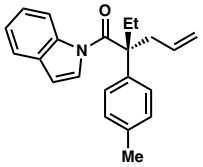

(*R*)-2-ethyl-1-(1*H*-indol-1-yl)-2-(*p*-tolyl)pent-4-en-1-one (20e)

Purified by column chromatography (5% Et_2O in hexanes) to provide a colorless oil (62.9 mg, 99% yield); 98% ee, $[\alpha]_D^{25}$ –112.1 (*c* 1.0, $CHCl_3$); ^1H NMR (500 MHz, $CDCl_3$) δ 8.57 (dq, *J* = 8.4, 1.0 Hz, 1H), 7.46 (d, *J* = 7.6 Hz, 1H), 7.35 (ddt, *J* = 8.4, 7.1, 1.3 Hz, 1H), 7.26–7.21 (m, 1H), 7.15 (d, *J* = 1.0 Hz, 4H), 6.88 (dd, *J* = 3.9, 1.2 Hz, 1H), 6.27 (d, *J* = 3.8 Hz, 1H), 5.44 (dddd, *J* = 17.6, 10.9, 9.3, 6.6 Hz, 1H), 5.03–4.91 (m, 2H), 3.00– 2.81 (m, 2H), 2.35 (s, 3H), 2.22 (q, *J* = 7.4 Hz, 2H), 0.80 (td, *J* = 7.4, 1.2 Hz, 3H); ^{13}C NMR (100 MHz, $CDCl_3$) δ 174.5, 139.9, 137.0, 136.5, 133.2, 129.9, 129.5, 126.3, 126.3, 125.0, 123.7, 120.5, 118.9, 117.2, 108.1, 56.4, 40.5, 28.0, 21.2, 8.4; IR (Neat Film, NaCl) 2973, 1695, 1640, 1585, 1537, 1514, 1472, 1450, 1380, 1321, 1304, 1224, 1206, 1105, 1077, 1020, 918, 893, 813, 768, 750 cm^{-1}; HRMS (MM:ESI-APCI+) *m/z* calc'd for $C_{22}H_{24}NO$ $[M+H]^+$: 318.1852, found 318.1848; SFC Conditions: 15% IPA, 2.5 mL/min, Chiralpak AD-H column, λ = 210 nm, t_R (min): minor = 4.21, major = 4.75.

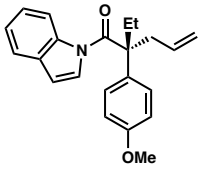

***(R)*-2-ethyl-1-(1*H*-indol-1-yl)-2-(4-methoxyphenyl)pent-4-en-1-one (20f)**

Purified by column chromatography (10% Et_2O in hexanes) to provide an amorphous white solid (59.2mg, 89% yield); 98% ee, $[\alpha]_D^{25}$ –112.1 (*c* 1.0, $CHCl_3$); ^1H NMR (500 MHz, $CDCl_3$) δ 8.58 (dq, *J* = 8.3, 0.8 Hz, 1H), 7.47 (ddd, *J* = 7.7, 1.4, 0.7 Hz, 1H), 7.35 (ddd, *J* = 8.3, 7.1, 1.3 Hz, 1H), 7.30–7.21 (m, 1H), 7.21–7.15 (m, 2H), 6.93–6.85 (m, 3H), 6.28 (dd, *J* = 3.9, 0.7 Hz, 1H), 5.45 (dddd, *J* = 16.6, 10.2, 8.5, 6.1 Hz, 1H), 5.04– 4.90 (m, 2H), 3.81 (s, 3H), 2.96 (dd, *J* = 13.9, 8.5 Hz, 1H), 2.85 (dd, *J* = 14.0, 6.1 Hz, 1H), 2.21(q, *J* = 7.4Hz, 2H),0.80(t, *J* = 7.4Hz, 3H); ^{13}C NMR (100 MHz, $CDCl_3$) δ 174.6, 158.6, 136.5, 134.9, 133.2, 129.5, 127.5, 126.3, 125.1, 123.7, 120.5, 118.9, 117.2, 114.5, 108.1, 56.1, 55.3, 40.5, 28.1, 8.4; IR (Neat Film, NaCl) 3163, 3073, 2973, 2837, 1694, 1640, 1609, 153, 1538, 1514, 1450, 1380, 1304, 1250, 1206, 1184, 1076, 1034, 919, 890, 819, 768, 750 cm^{-1}; HRMS (MM:ESI-APCI+) *m/z* calc'd for $C_{22}H_{24}NO_2$ $[M+H]^+$: 334.1802 found 334.1816; SFC Conditions: 15% IPA, 2.5 mL/min, Chiralpak AD-H column, λ = 210 nm, t_R (min): minor = 5.09, major = 5.73.

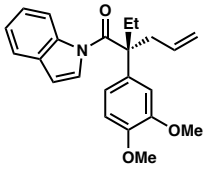

_(R)_-2-(3,4-dimethoxyphenyl)-2-ethyl-1-(1_H_-indol-1-yl)pent-4-en-1-one (20g)

Purified by column chromatography (20% Et_2O in hexanes) to provide an amorphous white solid (72.6 mg, 99% yield); 95% ee, $[\alpha]_D^{25}$ –112.1 (*c* 1.0, $CHCl_3$); ^1H NMR (500 MHz, $CDCl_3$) δ 8.61 (dt, *J* = 8.3, 0.9 Hz, 1H), 7.53 (dt, *J* = 7.7, 1.0 Hz, 1H), 7.40 (ddd, *J* = 8.2, 7.2, 1.3 Hz, 1H), 7.33–7.28 (m, 1H), 6.98 (d, *J* = 3.8 Hz, 1H), 6.96–6.87 (m, 2H), 6.78 (d, *J* = 1.7 Hz, 1H), 6.34 (dt, *J* = 3.8, 0.8 Hz, 1H), 5.56–5.43 (m, 1H), 5.09–4.97 (m, 2H), 3.95 (s, 3H), 3.86 (s, 3H), 3.01 (dd, *J* = 14.0, 8.5 Hz, 1H), 2.91 (dd, *J* = 14.0, 6.2 Hz, 1H), 2.26 (q, *J* = 7.5 Hz, 2H), 0.91–0.78 (m, 3H); ^{13}C NMR (100 MHz, $CDCl_3$) 174.5, 149.5, 148.1, 136.4, 135.3, 133.1, 129.5, 126.1, 125.0, 123.7, 120.5, 118.9, 118.5, 117.0, 111.3, 109.6, 108.1, 56.3, 56.0, 55.9, 40.4, 28.0, 8.3; IR (Neat Film, NaCl) 3072, 2967, 2835, 1694, 1640, 1587, 1518, 1449, 1412, 1306, 1260, 1206, 1150, 1077, 1027, 917, 893, 803, 768, 751 cm^{-1}; HRMS (MM:ESI-APCI+) *m/z* calc'd for $C_{23}H_{26}NO_3$ $[M+H]^+$: 364.1907 found 364.1892; SFC Conditions: 15% IPA, 2.5 mL/min, Chiralpak AD-H column, λ = 210 nm, t_R (min): minor = 4.14, major = 4.92.

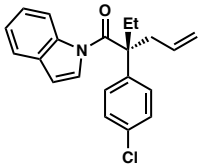

_(R)_-2-(4-chlorophenyl)-2-ethyl-1-(1_H_-indol-1-yl)pent-4-en-1-one (20h)

Purified by column chromatography (5% Et_2O in hexanes) to provide a colorless oil (68.2 mg, 99% yield); 94% ee, $[\alpha]_D^{25}$ –103.2 (*c* 1.0, $CHCl_3$); ^{1}H NMR (500 MHz, $CDCl_3$) δ 8.57 (d, *J* = 8.3 Hz, 1H), 7.48 (d, *J* = 7.7 Hz, 1H), 7.39–7.32 (m, 3H), 7.30–7.23 (m, 1H), 7.23–7.18 (m, 2H), 6.81 (dd, *J* = 3.9, 0.8 Hz, 1H), 6.31 (dd, *J* = 3.9, 0.7 Hz, 1H), 5.48– 5.38 (m, 1H), 5.05–4.92 (m, 2H), 2.97 (ddt, *J* = 14.1, 8.4, 0.9 Hz, 1H), 2.84 (ddt, *J* = 13.9, 6.1, 1.3 Hz, 1H), 2.23 (q, *J* = 7.4 Hz, 2H), 0.82 (t, *J* = 7.4 Hz, 3H); ^{13}C NMR (100 MHz, $CDCl_3$) δ 173.7, 141.6, 136.5, 133.3, 132.6, 129.5, 129.4, 127.9, 125.8, 125.3, 123.9, 120.7, 119.4, 117.2, 108.6, 56.5, 40.6, 28.1, 8.4; IR (Neat Film, NaCl) 3074, 2974, 2880, 1695, 1639, 1539, 1493, 1450, 1304, 1224, 1206, 1150, 1097, 1077, 1014, 920, 890, 815, 768, 752 cm^{-1}; HRMS (MM:ESI-APCI+) *m/z* calc'd for $C_{21}H_{21}ClNO$ $[M+H]^+$: 338.1306 found 338.1291; SFC Conditions: 15% IPA, 2.5 mL/min, Chiralpak AD-H column, λ = 210 nm, t_R (min): minor = 4.31, major = 4.78.

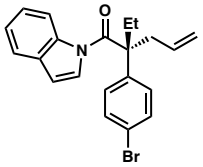

_(R)_-2-(4-bromophenyl)-2-ethyl-1-(1_H_-indol-1-yl)pent-4-en-1-one (20i)

Purified by column chromatography (5% Et_2O in hexanes) to provide a white foam (75.2 mg, 98% yield); 94% ee, $[\alpha]_D^{25}$ –83.1 (*c* 1.0, $CHCl_3$); ^1H NMR (500 MHz, $CDCl_3$) δ 8.45 (d, *J* = 9.6 Hz, 1H), 7.59 (d, *J* = 2.0 Hz, 1H), 7.44 (dd, *J* = 8.9, 2.0 Hz, 1H), 7.37 (dd, *J* = 8.1, 6.8 Hz, 2H), 7.33–7.26 (m, 1H), 7.29–7.23 (m, 2H), 6.84 (d, *J* = 3.8 Hz, 1H), 6.20 (dd, *J* = 3.9, 0.7 Hz, 1H), 5.44 (dddd, *J* = 16.6, 10.0, 8.5, 6.1 Hz, 1H), 5.05–4.89 (m, 2H), 3.02–2.91 (m, 1H), 2.87 (dd, *J* = 14.1, 6.2 Hz, 1H), 2.33–2.14 (m, 2H), 0.80 (t, *J* = 7.4 Hz, 3H); ^{13}C NMR (100 MHz, $CDCl_3$) δ 174.3, 142.7, 135.2, 132.8, 131.3, 129.3, 127.9, 127.5, 127.2, 126.4, 123.2, 119.2, 118.5, 117.0, 107.3, 56.8, 40.3, 28.0, 8.3; IR (Neat Film, NaCl) 3162, 3065, 2974, 2879, 1698, 1639, 1598, 1574, 1534, 1496, 1443, 1364, 1304, 1266, 1218, 1199, 1080, 1032, 1000, 947, 920, 887, 822, 811, 762, 734, 718, 702 cm^{-1}; HRMS (MM:ESI-APCI+) *m/z* calc'd for $C_{21}H_{21}BrNO$ $[M+H]^+$: 382.0801 found 382.0785; SFC Conditions: 15% IPA, 2.5 mL/min, Chiralpak AD-H column, λ = 210 nm, t_R (min): minor = 6.60, major = 7.38.

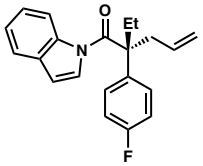

(*R*)-2-ethyl-2-(4-fluorophenyl)-1-(1*H*-indol-1-yl)pent-4-en-1-one (20j)

Purified by column chromatography (5% Et_2O in hexanes) to provide an amorphous white solid (62.1 mg, 97% yield); 96% ee, $[\alpha]_D^{25}$ –83.1 (*c* 1.0, $CHCl_3$); ^1H NMR (500 MHz, $CDCl_3$) δ 8.57 (d, *J* = 8.4 Hz, 1H), 7.46 (d, *J* = 7.7 Hz, 1H), 7.35 (t, *J* = 7.8 Hz, 1H), 7.27–7.19 (m, 3H), 7.05 (t, *J* = 8.5 Hz, 2H), 6.81 (d, *J* = 3.9 Hz, 1H), 6.29 (d, *J* = 3.8 Hz, 1H), 5.42 (dtd, *J* = 16.8, 9.0, 6.3 Hz, 1H), 5.02–4.89 (m, 2H), 2.95 (dd, *J* = 14.0, 8.4 Hz, 1H), 2.83 (dd, *J* = 14.0, 6.2 Hz, 1H), 2.21 (q, *J* = 7.4 Hz, 2H), 0.79 (t, *J* = 7.4 Hz, 3H); ^{19}F NMR (282 MHz, CDCl3) δ –114.82 (tt, *J* = 9.1, 4.7 Hz); ^{13}C NMR (100 MHz, $CDCl_3$) δ 174.0, 162.0 (d, *J*C–F = 246.9 Hz), 138.9 (d, *J*C–F = 3.4 Hz), 136.5, 132.8, 129.5, 128.10 (d, *J*C–F = 7.9 Hz), 125.9, 125.2, 123.9, 120.7, 119.3, 117.3, 116.1 (d, *J*C–F = 21.4 Hz), 108.4, 56.3, 40.7, 28.2, 8.4; IR (Neat Film, NaCl) 3073, 2973, 1694, 1602, 1539, 1510, 1450, 1305, 1226, 1206, 1164, 1102, 1077, 1016, 920, 890, 822, 810, 768, 751 cm^{-1}; HRMS (MM:ESI-APCI+) *m/z* calc'd for $C_{21}H_{21}FNO$ $[M+H]^+$: 322.1602 found 322.1607; SFC Conditions: 10% IPA, 2.5 mL/min, Chiralpak AD-H column, λ = 210 nm, t_R (min): minor = 4.57, major = 5.07.

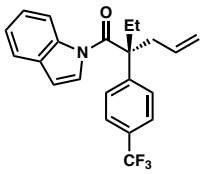

_(R)_-2-ethyl-1-(1_H_-indol-1-yl)-2-(4-(trifluoromethyl)phenyl)pent-4-en-1-one (20k)

Purified by column chromatography (5% Et_2O in hexanes) to provide an amorphous white solid (73.0 mg, 98% yield); 70% ee, $[\alpha]_D^{25}$ –75.6 (*c* 1.0, $CHCl_3$); ^1H NMR (500 MHz, $CDCl_3$) δ 8.58 (dt, *J* = 8.3, 0.8 Hz, 1H), 7.63 (d, *J* = 8.2 Hz, 2H), 7.48 (dd, *J* = 7.7, 1.1 Hz, 1H), 7.42–7.35 (m, 3H), 7.29–7.24 (m, 1H), 6.73 (d, *J* = 3.9 Hz, 1H), 6.31 (d, *J* = 3.9 Hz, 1H), 5.42 (dddd, *J* = 16.6, 10.2, 8.4, 6.2 Hz, 1H), 5.06–4.92 (m, 2H), 3.01 (dd, *J* = 14.0, 8.4 Hz, 1H), 2.88 (dd, *J* = 14.1, 6.3 Hz, 1H), 2.28 (qd, *J* = 7.3, 2.2 Hz, 2H), 0.83 (t, *J* = 7.4 Hz, 3H); ^{19}F NMR (376 MHz, $CDCl_3$) δ –62.67; ^{13}C NMR (100 MHz, $CDCl_3$) δ 173.3, 147.2 (overlapping), 136.5, 132.3, 129.6 (q, $J_{C–F}$ = 32.7 Hz), 129.5, 127.0, 126.1 (q, $J_{C–F}$ = 3.8 Hz), 125.5, 125.4, 124.1, 124.1 (q, $J_{C–F}$ = 272.2 Hz), 120.7, 119.7, 117.3, 108.8, 56.9, 40.6, 28.1, 8.4. IR (Neat Film, NaCl) 3076, 2977, 2882, 1697, 1618, 1549, 1450, 1412, 1328, 1307, 1225, 1207, 1169, 1126, 1070, 1017, 922, 890, 843, 819, 768, 751 cm^{-1}; HRMS (MM:ESI-APCI+) *m/z* calc'd for $C_{22}H_{21}F_3NO$ $[M+H]^+$: 372.1570 found 372.1555; SFC Conditions: 5% IPA, 2.5 mL/min, Chiralpak AD-H column, λ = 210 nm, t_R (min): minor = 4.48, major = 4.97.

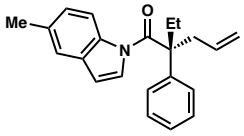

***(R)*-2-ethyl-1-(5-methyl-1*H*-indol-1-yl)-2-phenylpent-4-en-1-one (20l)**

Purified by column chromatography (5% Et_2O in hexanes) to provide a colorless oil (63.4 mg, 99% yield); 98% ee, $[\alpha]_D^{25}$ –111.7 (*c* 1.0, $CHCl_3$); ^1H NMR (500 MHz, $CDCl_3$) δ 8.45 (d, *J* = 8.5 Hz, 1H), 7.37–7.32 (m, 2H), 7.31–7.23 (m, 4H), 7.18 (dd, *J* = 8.5, 1.7 Hz, 1H), 6.80 (d, *J* = 3.9 Hz, 1H), 6.19 (d, *J* = 3.8 Hz, 1H), 5.44 (dddd, *J* = 16.7, 10.3, 8.5, 6.2 Hz, 1H), 5.02–4.93 (m, 2H), 2.98 (dd, *J* = 14.0, 8.5 Hz, 1H), 2.90–2.83 (m, 1H), 2.43 (s, 3H), 2.24 (qd, *J* = 7.4, 1.5 Hz, 2H), 0.80 (t, *J* = 7.4 Hz, 3H); ^{13}C NMR (100 MHz, $CDCl_3$) δ 174.1, 143.1, 134.7, 133.3, 133.1, 129.8, 129.1, 127.3, 126.5, 126.4, 126.1, 120.5, 118.9, 116.9, 108.0, 56.7, 40.5, 28.0, 21.4, 8.4; IR (Neat Film, NaCl) 3024, 2974, 2879, 1694, 1640, 1542, 1494, 1466, 1365, 1305, 1245, 1207, 1142, 1079, 1000, 919, 889, 830, 810, 766, 734, 716, 702 cm^{-1}; HRMS (MM:ESI-APCI+) *m/z* calc'd for $C_{22}H_{24}NO$ $[M+H]^+$: 318.1852 found 318.1846; SFC Conditions: 15% IPA, 2.5 mL/min, Chiralpak AD-H column, λ = 210 nm, t_R (min): minor = 5.21, major = 5.92.

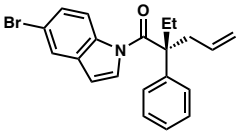

***(R)*-1-(5-bromo-1*H*-indol-1-yl)-2-ethyl-2-phenylpent-4-en-1-one (20m)**

Purified by column chromatography (5% Et_2O in hexanes) to provide an amorphous white foam (74.0 mg, 97% yield); 92% ee, $[\alpha]_D^{25}$ –112.5 (*c* 1.0, $CHCl_3$); ^1H NMR (500 MHz, $CDCl_3$) δ 8.57 (dq, *J* = 8.4, 0.9 Hz, 1H), 7.51–7.45 (m, 3H), 7.36 (ddd, *J* = 8.4, 7.2, 1.3 Hz, 1H), 7.28–7.24 (m, 1H), 7.17–7.11 (m, 2H), 6.81 (d, *J* = 3.9 Hz, 1H), 6.31 (dd, *J* = 3.9, 0.8 Hz, 1H), 5.43 (dddd, *J* = 16.6, 10.1, 8.4, 6.2 Hz, 1H), 5.03–4.92 (m, 2H), 2.96 (ddt, *J* = 14.0, 8.4, 1.0 Hz, 1H), 2.86–2.80 (m, 1H), 2.22 (q, *J* = 7.4 Hz, 2H), 0.81 (t, *J* = 7.5 Hz, 3H); ^{13}C NMR (100 MHz, $CDCl_3$) δ 173.6, 142.1, 136.5, 132.6, 132.3, 129.5, 128.2, 125.8, 125.3, 123.9, 121.4, 120.7, 119.4, 117.2, 108.6, 56.5, 40.5, 28.0, 8.4; IR (Neat Film, NaCl) 3073, 2974, 1694, 1586, 1537, 1492, 1450, 1305, 1224, 1206, 1149, 1076, 1010, 920, 890, 814, 768, 752 cm^{-1}; HRMS (MM:ESI-APCI+) *m/z* calc'd for $C_{21}H_{21}BrNO$ $[M+H]^+$: 382.0801 found 382.0811; SFC Conditions: 15% IPA, 2.5 mL/min, Chiralpak AD-H column, λ = 210 nm, t_R (min): minor = 5.28, major = 5.91.

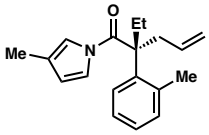

_(R)_-2-ethyl-1-(3-methyl-1_H_-pyrrol-1-yl)-2-(_o_-tolyl)pent-4-en-1-one (20n)

Purified by column chromatography (5% Et_2O in hexanes) to provide a colorless oil (56.1 mg, 99% yield); 89% ee, $[\alpha]_D^{25}$ –87.4 (*c* 1.0, $CHCl_3$); Note: Rotameric species were observed for this compound, thus the ^1H NMR spectrum was recorded at elevated temperature (50 ºC): ^1H NMR (400 MHz, $CDCl_3$, 50 ºC) δ 7.37 (dt, *J* = 8.0, 1.5 Hz, 1H), 7.30–7.21 (m, 1H), 7.18 (tt, *J* = 7.2, 1.4 Hz, 1H), 7.08 (d, *J* = 7.5 Hz, 1H), 6.77 (d, *J* = 10.9 Hz, 2H), 5.84 (dt, *J* = 3.2, 1.5 Hz, 1H), 5.39 (s, 1H), 5.05–4.90 (m, 2H), 2.90 (d, *J* = 7.3 Hz, 2H), 2.26 (dd, *J* = 13.1, 6.6 Hz, 1H), 2.14 (d, *J* = 11.3 Hz, 2H), 2.13 (s, 2H), 1.91 (d, *J* = 1.3 Hz, 3H), 0.77 (s, 3H); Note: Rotameric species were observed for this compound, thus the ^{13}C NMR spectrum contains broad peaks: ^{13}C NMR (100 MHz, $CDCl_3$) δ 173.5, 140.8, 136.8, 133.3, 132.7, 127.3, 126.4, 126.1, 122.5, 120.4, 118.8, 117.4, 114.4, 54.6, 37.8, 28.0, 20.3, 12.0, 8.4; IR (Neat Film, NaCl) 3143, 3073, 2976, 2880, 1699, 1639, 1490, 1459, 1490, 1459, 1389, 1337, 1309, 1199, 1134, 1080, 1068,990, 918, 893, 827, 773, 740 cm^{-1}; HRMS (MM:ESI-APCI+) *m/z* calc'd for $C_{19}H_{24}NO$ $[M+H]^+$: 282.1852 found 282.1843; SFC Conditions: 3% IPA, 2.5 mL/min, Chiralcel OD-H column, λ = 210 nm, t_R (min): minor = 4.99, major = 5.37.

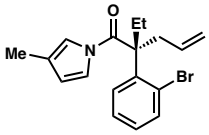

_(R)_-2-(2-bromophenyl)-2-ethyl-1-(3-methyl-1_H_-pyrrol-1-yl)pent-4-en-1-one (20o)

Purified by column chromatography (5% Et_2O in hexanes) to provide an amorphous white solid (60.1 mg, 87% yield); 80% ee, $[\alpha]_D^{25}$ –80.9 (*c* 1.0, $CHCl_3$); Note: Rotameric species were observed for this compound, thus the ^1H NMR spectrum was recorded at elevated temperature (50 ºC): ^1H NMR (400 MHz, $CDCl_3$, 50 ºC) δ 7.55 (dt, *J* = 8.0, 1.4 Hz, 1H), 7.45 (dd, *J* = 8.0, 1.8 Hz, 1H), 7.43–7.36 (m, 1H), 7.16 (td, *J* = 7.5, 1.6 Hz, 1H), 6.74 (d, *J* = 9.1 Hz, 2H), 5.86 (dd, *J* = 3.4, 1.7 Hz, 1H), 5.46–5.24 (m, 1H), 5.04–4.92 (m, 2H), 3.14 (dd, *J* = 14.4, 6.3 Hz, 1H), 3.01–2.85 (m, 1H), 2.46–2.33 (m, 1H), 2.19–2.05 (m, 1H), 1.92 (s, 3H), 0.80 (s, 3H); Note: Rotameric species were observed for this compound, thus the ^{13}C NMR spectrum contains broad peaks: ^{13}C NMR (100 MHz, $CDCl_3$) δ 171.5, 141.8, 135.3, 132.9, 129.0, 128.5, 127.8, 124.2, 122.5, 120.2, 119.1, 117.4, 114.4, 55.8, 36.5, 28.0, 12.1, 8.8; IR (Neat Film, NaCl) 2977, 1704, 1485, 1470, 1390, 1309, 1201, 1134, 1068, 1025, 919, 828, 769, 741 cm^{-1}; HRMS (MM:ESI-APCI+) *m/z* calc'd for $C_{18}H_{21}BrNO$ $[M+H]^+$: 346.0801 found 346.0790; SFC Conditions: 3% IPA, 2.5 mL/min, Chiralpak OD-H column, λ = 210 nm, t_R (min): minor = 9.10, major = 9.72.

2.8.2.2 General Procedure for the Selective Enolization and Acylation

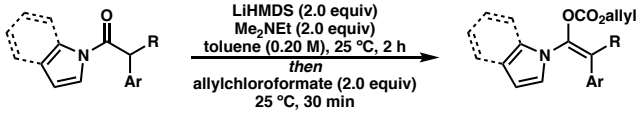

In a N_2-filled glovebox an oven-dried 25-mL round bottom flask equipped with a Teflon-coated magnetic stir bar was charged with LiHMDS (335 mg, 2.00 mmol, 2.0 equiv), sealed with a rubber septum, removed from the glovebox, and placed under a N_2 atmosphere. To the flask was then added toluene (3.0 mL) and *N*,*N*-dimethylethylamine (213 μL, 2.00 mmol, 2.0 equiv). The resulting clear, pale-yellow solution was stirred at 25 ºC for 5 min, after which time a solution of *N*-acyl indole (1.00 mmol, 1.0 equiv) in toluene (2.0 mL) was added dropwise over 5 min. The resulting pale-yellow solution was stirred at 25 ºC for 2 h. The flask was then immersed in a 25 ºC water bath and allyl chloroformate (217 μL, 2.00 mmol, 2.0 equiv) was added dropwise over 1 min, causing a the reaction to become white and heterogeneous. The reaction was continued until no starting material remained by TLC (typically less than 30 min). The reaction mixture was diluted with 5 mL Et_2O and quenched with 5 mL H_2O. The layers were separated, and the aqueous layer was extracted 2 x 5 mL Et_2O. The combined organic layers were dried over Na_2SO_4, filtered, and concentrated. The crude product was purified by silica gel flash chromatography to afford the desired enol carbonate. The *E*/*Z* ratio of enol carbonates was determined by ^1H NMR and is >95:5 unless stated otherwise.

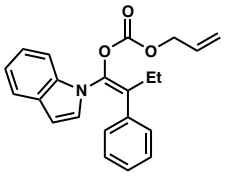

_(E)_-1-(1_H_-indol-1-yl)-2-phenylbut-1-en-1-yl allyl carbonate (19a)

Purified by column chromatography (5% Et_2O in hexanes) to provide the desired product as a colorless oil (2.08 g, 75% yield); ^{1}H NMR (500 MHz, $CDCl_3$) δ 7.55–7.43 (m, 2H), 7.24–7.18 (m, 1H), 7.15–7.06 (m, 4H), 7.02–6.94 (m, 2H), 6.89 (d, *J* = 3.3 Hz, 1H), 6.35 (dd, *J* = 0.9, 3.4 Hz, 1H), 5.88 (ddt, *J* = 5.8, 10.4, 17.1 Hz, 1H), 5.37–5.23 (m, 2H), 4.61 (dt, *J* = 1.4, 5.8 Hz, 2H), 2.68 (q, *J* = 7.5 Hz, 2H), 1.09 (t, *J* = 7.5 Hz, 3H); ^{13}C NMR (100 MHz, $CDCl_3$) δ 52.7, 136.2, 135.0, 130.8, 130.2, 129.0, 128.4, 128.2, 127.5, 127.5, 122.6, 120.7, 119.4, 111.2, 103.9, 69.3, 24.9, 12.6; IR (Neat Film, NaCl) 3056, 2974, 1766, 1682, 1519, 1456, 1333, 1259, 1238, 1209, 1143, 1119, 1094, 1042, 968, 946, 913, 765, 743, 699 cm^{-1}; HRMS (MM:ESI-APCI+) *m/z* calc'd for $C_{22}H_{22}NO_3$ $[M+H]^+$: 348.1594, found 348.1588.

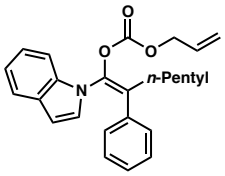

(*E*)-1-(1*H*-indol-1-yl)-2-phenylhept-1-en-1-yl allyl carbonate (19b)

Purified by column chromatography (5% Et_2O in hexanes) to provide the desired product as a colorless oil (337.6 mg, 87% yield); ^{1}H NMR (500 MHz, $CDCl_3$) δ 7.51–7.45 (m, 2H), 7.23–7.16 (m, 1H), 7.14–7.05 (m, 4H), 6.98–6.91 (m, 2H), 6.89–6.84 (m, 1H), 6.36– 6.30 (m, 1H), 5.94–5.81 (m, 1H), 5.36–5.22 (m, 2H), 4.60 (dq, *J* = 5.8, 1.4 Hz, 2H), 2.70–2.60 (m, 2H), 1.49–1.26 (m, 6H), 0.89 (td, *J* = 7.1, 1.6 Hz, 3H); ^{13}C NMR (100 MHz, $CDCl_3$) δ 152.7, 136.4, 136.3, 135.4, 130.9, 129.1, 129.0, 128.4, 128.2, 127.5, 127.5, 122.6, 120.7, 120.7, 119.4, 111.2, 103.9, 69.3, 31.5, 31.4, 27.3, 22.4, 14.1; IR (Neat Film, NaCl) 3055, 2956, 2929, 2860, 2363, 2340, 1765, 1684, 1457, 1332, 1242, 1211, 1142, 1118, 948, 764, 742, 699 cm^{-1}; HRMS (MM:ESI-APCI+) *m/z* calc'd for $C_{25}H_{28}NO_3$ $[M+H]^+$: 390.2064, found 390.2078.

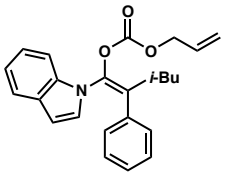

(*E*)-1-(1*H*-indol-1-yl)-4-methyl-2-phenylpent-1-en-1-yl allyl carbonate (19c)

Purified by column chromatography (5% EtO in hexanes) to provide the desired product as a white solid (327.6 mg, 87% yield); ^{1}H NMR (500 MHz, $CDCl_3$) δ 7.50 (ddd, *J* = 7.4, 5.8, 1.0 Hz, 2H), 7.21 (ddd, *J* = 8.3, 7.1, 1.1 Hz, 1H), 7.15–7.08 (m, 4H), 6.99–6.91 (m, 2H), 6.84 (d, *J* = 3.3 Hz, 1H), 6.33 (d, *J* = 3.3 Hz, 1H), 5.88 (ddt, *J* = 17.3, 10.5, 5.8 Hz, 1H), 5.32 (dq, *J* = 17.1, 1.5 Hz, 1H), 5.26 (dq, *J* = 10.3, 1.3 Hz, 1H), 4.60 (dt, *J* = 5.8, 1.4 Hz, 2H), 2.56 (d, *J* = 7.3 Hz, 2H), 1.62 (hept, *J* = 6.8 Hz, 1H), 1.00 (d, *J* = 6.6 Hz, 6H); ^{13}C NMR (100 MHz, $CDCl_3$) δ 152.6, 136.5, 136.3, 136.1, 130.9, 129.2, 128.4, 128.2, 128.0, 127.5, 127.4, 122.6, 120.7, 120.7, 119.4, 111.2, 103.8, 69.3, 40.2, 26.5, 22.4; IR (Neat Film, NaCl) 3057, 3031, 2957, 2869, 1766, 1682, 1519, 1456, 1331, 1246, 1331, 1246, 1209, 1144, 1118, 1046, 960, 767, 743, 699 cm^{-1}; HRMS (MM:ESI-APCI+) *m/z* calc'd for $C_{25}H_{26}NO_3$ $[M+H]^+$: 376.1907, found 376.1902.

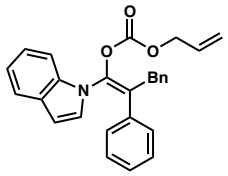

_(E)_-1-(1_H_-indol-1-yl)-2,3-diphenylprop-1-en-1-yl allyl carbonate (19d)

Purified by column chromatography (5% Et_2O in hexanes) to provide the desired product as a yellow oil (377.6 mg, 92% yield); ^{1}H NMR (500 MHz, $CDCl_3$) δ 7.58–7.49 (m, 2H), 7.34–7.25 (m, 4H), 7.26–7.18 (m, 2H), 7.14 (tt, *J* = 7.1, 0.9 Hz, 1H), 7.07–6.99 (m, 3H), 6.95 (m, 1H), 6.94–6.87 (m, 2H), 6.39 (dt, *J* = 3.4, 0.8 Hz, 1H), 5.91–5.79 (m, 1H), 5.35–5.22 (m, 2H), 4.58 (dt, *J* = 5.9, 1.3 Hz, 2H), 4.03 (s, 2H); ^{13}C NMR (100 MHz, $CDCl_3$) δ 152.4, 138.0, 136.5, 136.1, 136.1, 130.7, 128.9, 128.8, 128.5, 128.4, 128.1, 127.7, 127.5, 126.6, 126.4, 122.7, 120.9, 120.8, 119.4, 111.3, 104.2, 69.4, 37.7; IR (Neat Film, NaCl) 3059, 3028, 1766, 1678, 1602, 1519, 1495, 1456, 1384, 1364, 1333, 1243, 1214, 1142, 1117, 967, 945 cm^{-1}; HRMS (MM:ESI-APCI+) *m/z* calc'd for $C_{27}H_{24}NO_3$ $[M+H]^+$: 410.1751, found 410.1749.

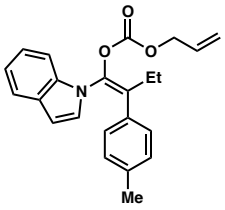

_(E)_-1-(1_H_-indol-1-yl)-2-(_p_-tolyl)but-1-en-1-yl allyl carbonate (19e)

Purified by column chromatography (6% Et_2O in hexanes) to provide the desired product as a yellow oil (268.7 mg, 74% yield); ^{1}H NMR (500 MHz, $CDCl_3$) δ 7.54–7.42 (m, 2H), 7.19 (ddd, *J* = 8.3, 7.1, 1.2 Hz, 1H), 7.10 (ddd, *J* = 8.0, 7.1, 1.0 Hz, 1H), 6.92–6.80 (m, 5H), 6.35 (dd, *J* = 3.3, 0.9 Hz, 1H), 5.87 (ddt, *J* = 17.2, 10.5, 5.8 Hz, 1H), 5.41–5.18 (m, 2H), 4.59 (dt, *J* = 5.8, 1.4 Hz, 2H), 2.64 (q, *J* = 7.5 Hz, 2H), 2.19 (s, 3H), 1.07 (t, *J* = 7.5 Hz, 3H); ^{13}C NMR (100 MHz, $CDCl_3$) δ 152.8, 137.2, 136.3, 134.8, 133.2, 130.9, 130.3, 129.2, 129.0, 128.5, 127.5, 122.6, 120.8, 120.7, 119.6, 111.4, 103.8, 69.4, 25.0, 21.2, 12.7; IR (Neat Film, NaCl) 1764, 1457, 1333, 1258, 1238, 1209, 1143, 1120, 945, 818, 743 cm^{-1}; HRMS (MM:ESI-APCI+) *m/z* calc'd for $C_{23}H_{24}NO_3$ $[M+H]^+$: 362.1751, found 362.1741.

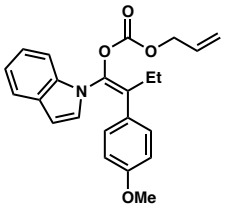

_(E)_-1-(1_H_-indol-1-yl)-2-(4-methoxyphenyl)but-1-en-1-yl allyl carbonate (19f)

Purified by column chromatography (10% Et_2O in hexanes) to provide the desired product as a yellow oil (245.6 mg, 65% yield); ^{1}H NMR (500 MHz, $CDCl_3$) δ 7.51 (ddd, *J* = 7.8, 1.2, 0.8 Hz, 1H), 7.45 (dq, *J* = 8.2, 0.9 Hz, 1H), 7.19 (ddd, *J* = 8.2, 7.1, 1.2 Hz, 1H), 7.10 (ddd, *J* = 8.0, 7.1, 1.0 Hz, 1H), 6.92–6.82 (m, 3H), 6.67– 6.57 (m, 2H), 6.36 (dd, *J* = 3.3, 0.9 Hz, 1H), 5.87 (ddt, *J* = 17.2, 10.4, 5.8 Hz, 1H), 5.37–5.19 (m, 2H), 4.59 (d, *J* = 5.8 Hz, 2H), 3.68 (s, 3H), 2.63 (q, *J* = 7.5 Hz, 2H), 1.07 (t, *J* = 7.5 Hz, 3H); ^{13}C NMR (100 MHz, $CDCl_3$) δ 158.9, 152.9, 136.3, 134.6, 131.0, 129.9, 129.2, 128.8, 128.5, 128.3, 122.7, 120.8, 120.8, 119.6, 113.7, 111.4, 103.9, 69.5, 55.2, 25.0, 12.8; IR (Neat Film, NaCl) 1764, 1609, 1513, 1456, 1293, 1247, 1209, 1142, 1121, 1038, 831, 744 cm^{-1}; HRMS (MM:ESI-APCI+) *m/z* calc'd for $C_{23}H_{24}NO_4$ $[M+H]^+$: 378.1700, found 378.1690.

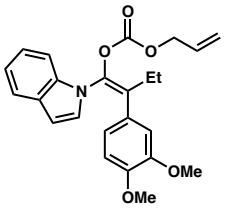

_(E)_-allyl (2-(3,4-dimethoxyphenyl)-1-(1_H_-indol-1-yl)but-1-en-1-yl) carbonate (19g)

Purified by column chromatography (20% Et_2O in hexanes) to provide the desired product as a colorless oil (262.1 mg, 64% yield); ^{1}H NMR (500 MHz, $CDCl_3$) δ 7.54– 7.48 (m, 2H), 7.21 (ddd, *J* = 1.3, 7.1, 8.3 Hz, 1H), 7.11 (td, *J* = 1.1, 7.5 Hz, 1H), 6.92 (t, *J* = 2.2 Hz, 1H), 6.71 (dt, *J* = 1.9, 8.3 Hz, 1H), 6.66 (d, *J* = 8.4 Hz, 1H), 6.38 (dt, *J* = 1.2, 3.5 Hz, 1H), 6.17 (t, *J* = 1.8 Hz, 1H), 5.89 (ddt, *J* = 5.8, 10.3, 17.1 Hz, 1H), 5.41–5.19 (m, 2H), 4.62 (dt, *J* = 1.4, 5.8 Hz, 2H), 3.77 (s, 3H), 3.23 (s, 3H), 2.68 (qd, *J* = 2.4, 7.6 Hz, 2H), 1.12 (td, *J* = 2.2, 7.5 Hz, 3H); ^{13}C NMR (100 MHz, $CDCl_3$) δ 152.9, 148.4, 148.3, 136.6, 134.5, 130.9, 130.6, 129.2, 128.4, 128.4, 122.7, 120.8, 120.8, 119.7, 119.6, 111.1, 110.7, 110.6, 104.0, 69.4, 55.7, 55.2, 24.7, 12.9; IR (Neat Film, NaCl) 1763, 1518, 1456, 1262, 1242, 1208, 1139, 1116, 1026, 946, 766, 744 cm^{-1}; HRMS (MM:ESI- APCI+) *m/z* calc'd for $C_{24}H_{26}NO_5$ [M+H]+: 408.1805, found 408.1817.

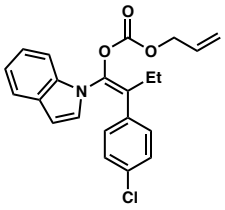

_(E)_-allyl (2-(4-chlorophenyl)-1-(1_H_-indol-1-yl)but-1-en-1-yl) carbonate (19h)

Purified by column chromatography (8% Et_2O in hexanes) to provide the desired product as a light yellow oil (356.3 mg, 93% yield); ^{1}H NMR (500 MHz, $CDCl_3$) δ 7.53–7.48 (m, 1H), 7.43 (dq, *J* = 0.9, 8.2 Hz, 1H), 7.19 (ddd, *J* = 1.2, 7.1, 8.2 Hz, 1H), 7.11 (ddd, *J* = 1.0, 7.1, 8.0 Hz, 1H), 7.09–7.03 (m, 2H), 6.92–6.82 (m, 3H), 6.37 (dd, *J* = 0.9, 3.4 Hz, 1H), 5.86 (ddt, *J* = 5.8, 10.5, 17.2 Hz, 1H), 5.36–5.23 (m, 2H), 4.59 (dt, *J* = 1.3, 5.8 Hz, 2H), 2.64 (q, *J* = 7.5 Hz, 2H), 1.06 (t, *J* = 7.5 Hz, 3H); ^{13}C NMR (100 MHz, $CDCl_3$) δ 152.6, 136.2, 135.4, 134.8, 133.4, 130.8, 129.2, 129.0, 128.9, 128.6, 128.5, 122.9, 121.0, 120.9, 119.8, 111.2, 104.4, 69.6, 24.9, 12.7; IR (Neat Film, NaCl) 1765, 1679, 1456, 1333, 1256, 1238, 1209, 1144, 1120, 1096, 945, 827, 743 cm^{-1}; HRMS (MM:ESI- APCI+) *m/z* calc'd for $C_{22}H_{21}ClNO_3$ $[M+H]^+$: 382.1204, found 382.1201.

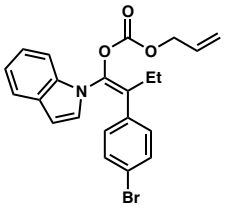

_(E)_-allyl (2-(4-bromophenyl)-1-(1_H_-indol-1-yl)but-1-en-1-yl) carbonate (19i)

Purified by column chromatography (5% Et_2O in hexanes) to provide the desired product as an amorphous white solid (341.0 mg, 80% yield); ^{1}H NMR (400 MHz, $CDCl_3$) δ 7.53–7.49 (m, 1H), 7.43 (dd, *J* = 8.2, 0.9 Hz, 1H), 7.24–7.17 (m, 3H), 7.14–7.09 (m, 1H), 6.86 (d, *J* = 3.4 Hz, 1H), 6.86–6.78 (m, 2H), 6.37 (d, *J* = 3.1 Hz, 1H), 5.86 (ddt, *J* = 17.3, 10.4, 5.8 Hz, 1H), 5.36–5.23 (m, 2H), 4.59 (dt, *J* = 5.8, 1.4 Hz, 2H), 2.64 (q, *J* = 7.5 Hz, 2H), 1.06 (t, *J* = 7.5 Hz, 3H); ^{13}C NMR (100 MHz, $CDCl_3$) 152.6, 136.1, 135.3, 135.2, 131.5, 130.8, 129.3, 129.2, 128.8, 128.5, 122.8, 121.6, 121.0, 120.9, 119.7, 111.2, 104.4, 69.5, 24.8, 12.7; IR (Neat Film, NaCl) 3053, 3032, 2974, 2937, 2876, 2248, 1899, 1766, 1681, 1588, 1519, 1488, 1455, 1385, 1364, 1333, 1238, 1209, 1144, 1120, 945, 824, 766, 743 cm^{-1}; HRMS (MM:ESI-APCI+) *m/z* calc'd for $C_{22}H_{21}BrNO_3$ $[M+H]^+$: 426.0699, found 426.0696.

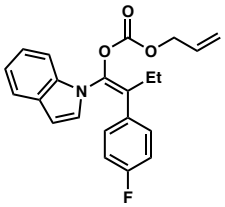

***(E)*-allyl (2-(4-fluorophenyl)-1-(1*H*-indol-1-yl)but-1-en-1-yl) carbonate (19j)**

Purified by column chromatography (5% Et_2O in hexanes) to provide the desired product as a colorless oil (312.6 mg, 86% yield); ^{1}H NMR (500 MHz, $CDCl_3$) 7.47 (dd, J = 37.4, 8.0 Hz, 2H), 7.15 (dt, J = 41.2, 7.4 Hz, 2H), 6.97–6.86 (m, 3H), 6.82–6.74 (m, 2H), 6.38 (d, J = 3.3 Hz, 1H), 5.88 (ddt, J = 16.7, 11.2, 5.8 Hz, 1H), 5.36–5.24 (m, 2H), 4.65– 4.55 (m, 2H), 2.66 (q, J = 7.5 Hz, 2H), 1.08 (t, J = 7.5 Hz, 3H); ^{19}F NMR (282 MHz, CDCl3) δ –114.05 – –114.17 (m); ^{13}C NMR (100 MHz, $CDCl_3$) δ 162.0 (d, J = 247.1 Hz), 152.7, 136.2, 135.2, 132.1 (d, $J_{C–F}$= 4.0 Hz), 130.8, 129.4, 129.3 (d, $J_{C–F}$ = 8.2 Hz), 128.8, 128.4, 122.7, 120.9, 120.8, 119.6, 115.3 (d, $J_{C–F}$ = 21.6 Hz), 111.2, 104.2, 69.5, 25.0, 12.6; IR (Neat Film, NaCl) 2974, 1766, 1681, 1604, 1510, 1456, 1333, 1238, 1208, 1144, 1119, 945, 835, 765, 743 cm^{-1}; HRMS (MM:ESI-APCI+) *m/z* calc'd for $C_{22}H_{21}FNO_3$ $[M+H]^+$: 366.1500, found 366.1502.

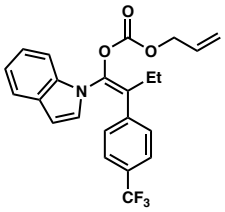

(*E*)-1-(1*H*-indol-1-yl)-2-(4-(trifluoromethyl)phenyl)but-1-en-1-yl allyl carbonate (19k)

Purified by column chromatography (5% Et_2O in hexanes) to provide the desired product as a white solid (375.1 mg, 90% yield); ^{1}H NMR (500 MHz, $CDCl_3$) 7.54 (dt, J = 1.0, 7.8 Hz, 1H), 7.49 (dq, J = 1.0, 8.2 Hz, 1H), 7.41–7.34 (m, 2H), 7.28–7.21 (m, 1H), 7.19– 7.08 (m, 3H), 6.87 (d, J = 3.3 Hz, 1H), 6.40 (dd, J = 0.9, 3.4 Hz, 1H), 5.89 (ddt, J = 5.9, 10.5, 17.2 Hz, 1H), 5.38–5.25 (m, 2H), 4.63 (dt, J = 1.4, 5.8 Hz, 2H), 2.72 (q, J = 7.5 Hz, 2H), 1.11 (t, J = 7.5 Hz, 3H); ^{19}F NMR (282 MHz, $CDCl_3$) δ –62.73; ^{13}C NMR (100 MHz, $CDCl_3$) δ 152.6, 140.2, 136.2, 136.0, 130.8, 129.5 (q, $J_{C–F}$ = 32.5 Hz), 129.0, 128.8, 128.5, 128.1, 125.4 (q, $J_{C–F}$ = 272 Hz), 125.4–125.2 (m), 123.0, 121.1, 121.0, 119.8, 111.2, 104.6, 69.7, 24.9, 12.6; IR (Neat Film, NaCl) 1766, 1681, 1617, 1456, 1325, 1260, 1239, 1211, 1167, 1123, 1067, 946, 834, 744 cm^{-1}; HRMS (MM:ESI-APCI+) *m/z* calc'd for $C_{23}H_{21}F_3NO_3$ $[M+H]^+$: 416.1468, found 416.1456.

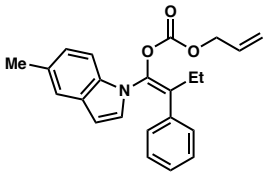

(*E*)-allyl (1-(5-methyl-1*H*-indol-1-yl)-2-phenylbut-1-en-1-yl) carbonate (19l)

Purified by column chromatography (hexanes → 5% Et_2O in hexanes) to provide the desired product as a yellow oil (336.3 mg, 93% yield); ^{1}H NMR (500 MHz, $CDCl_3$) δ 7.36 (d, *J* = 8.3 Hz, 1H), 7.30–7.28 (m, 1H), 7.12–7.08 (m, 3H), 7.02 (d, *J* = 8.3 Hz, 1H), 6.97 (dd, *J* = 6.4, 2.9 Hz, 2H), 6.83 (d, *J* = 3.3 Hz, 1H), 6.30–6.18 (m, 1H), 5.94–5.82 (m, 1H), 5.37–5.24 (m, 2H), 4.63–4.55 (m, 2H), 2.67 (q, *J* = 7.5 Hz, 2H), 2.42 (s, 3H), 1.09 (t, *J* = 7.5 Hz, 3H); ^{13}C NMR (100 MHz, $CDCl_3$) δ 152.7, 136.3, 135.3, 134.6, 130.9, 130.0, 129.8, 129.1, 128.7, 128.3, 127.7, 127.5, 124.2, 120.6 119.5, 111.0, 103.6, 69.4, 25.0, 21.5, 12.7; IR (Neat Film, NaCl) 3023, 2974, 2875, 1766, 1682, 1470, 1377, 1330, 1260, 1230, 1209, 1163, 1125, 1095, 1042, 967, 946, 843, 796, 763, 718, 699 cm^{-1}; HRMS (MM:ESI-APCI+) *m/z* calc'd for $C_{23}H_{24}NO_3$ $[M+H]^+$: 362.1751, found 362.1751.

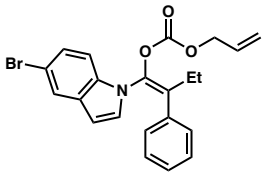

(*E*)-allyl (1-(5-bromo-1*H*-indol-1-yl)-2-phenylbut-1-en-1-yl) carbonate (19m)

Purified by column chromatography (5% Et_2O in hexanes) to provide the desired product as an amorphous white solid (352.3 mg, 83% yield); ^{1}H NMR (500 MHz, $CDCl_3$) δ 7.60 (d, *J* = 1.9 Hz, 1H), 7.29 (d, *J* = 8.6 Hz, 1H), 7.24 (dd, *J* = 8.6, 1.9 Hz, 1H), 7.12–7.08 (m, 3H), 6.94 (dd, *J* = 6.7, 3.0 Hz, 2H), 6.91 (d, *J* = 3.4 Hz, 1H), 6.29 (d, *J* = 3.3 Hz, 1H), 5.92–5.82 (m, 1H), 5.36–5.24 (m, 2H), 4.61 (dt, *J* = 5.8, 1.4 Hz, 2H), 2.66 (q, *J* = 7.5 Hz, 2H), 1.07 (t, *J* = 7.5 Hz, 3H); 152.7, 136.0, 134.9, 134.5, 131.0, 130.8, 130.2, 130.1, 128.4, 127.8, 127.5, 125.5, 123.3, 119.8, 114.1, 112.8, 103.5, 69.6, 25.0, 12.6; IR (Neat Film, NaCl) 2973, 2934, 2873, 1764, 1679, 1452, 1375, 1236, 1208, 1128, 945, 758, 698 cm^{-1}; ^{13}C NMR (100 MHz, $CDCl_3$) δ HRMS (MM:ESI-APCI+) *m/z* calc'd for $C_{22}H_{21}BrNO_3$ $[M+H]^+$: 426.0699, found 426.0696.

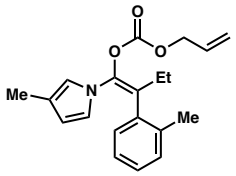

(*E*)-allyl (1-(3-methyl-1*H*-pyrrol-1-yl)-2-(*o*-tolyl)but-1-en-1-yl) carbonate (19n)

Purified by column chromatography (2.5% Et_2O in hexanes) to provide the desired product as a colorless oil (533.2 mg, 75% yield); Note: compound darkens in color overtime under Ar at –20 ºC. ^{1}H NMR (500 MHz, $CDCl_3$) δ 7.17–7.07 (m, 4H), 6.34 (dd, *J* = 2.9, 2.2 Hz, 1H), 6.29 (ddd, *J* = 2.2, 1.7, 1.0 Hz, 1H), 5.95 (ddt, *J* = 17.2, 10.4, 5.8 Hz, 1H), 5.76 (ddd, *J* = 2.9, 1.7, 0.5 Hz, 1H), 5.44–5.28 (m, 2H), 4.70 (dq, *J* = 5.8, 1.4 Hz, 2H), 2.44 (dq, *J* = 14.9, 7.3 Hz, 2H), 2.11 (d, *J* = 0.5 Hz, 3H), 1.91 (d, *J* = 1.0 Hz, 3H), 0.96 (t, *J* = 7.5 Hz, 3H); ^{13}C NMR (100 MHz, $CDCl_3$) δ 152.9, 136.5, 136.3, 136.3, 131.0, 130.2, 129.2, 127.5, 125.7, 122.8, 121.2, 119.6, 119.6, 118.2, 110.9, 69.5, 25.7, 19.4, 11.9, 11.8; IR (Neat Film, NaCl) 3061, 3019, 2972, 2936, 2874, 1769, 1688, 1487, 1456, 1350, 1258, 1234, 1185, 1139, 1118, 1070, 1047, 1022, 995, 958, 946, 915, 837, 761, 729, 694 cm^{-1}; HRMS (MM:ESI-APCI+) *m/z* calc'd for $C_{20}H_{24}NO_3$ [M+H]+: 326.1751, found 326.1733.

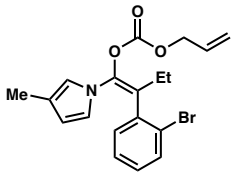

(*E*)-allyl (2-(2-bromophenyl)-1-(3-methyl-1*H*-pyrrol-1-yl)but-1-en-1-yl) carbonate (19o)

Purified by column chromatography (3% Et_2O in hexanes) to provide the desired product as a colorless oil (410 mg, 70% yield) Note: compound darkens in color overtime under Ar at –20 ºC. ^{1}H NMR (500 MHz, $CDCl_3$) δ 7.53 (dd, *J* = 8.0, 1.2 Hz, 1H), 7.18 (td, *J* = 7.5, 1.3 Hz, 1H), 7.13–7.03 (m, 2H), 6.50 (dd, *J* = 2.8, 2.2 Hz, 1H), 6.40 (m, 1H), 5.95 (ddt, *J* = 17.2, 10.5, 5.8 Hz, 1H), 5.77 (dd, *J* = 3.0, 1.7 Hz, 1H), 5.43–5.27 (m, 2H), 4.70 (dt, *J* = 5.8, 1.3 Hz, 2H), 2.51 (ddq, *J* = 36.7, 14.5, 7.3 Hz, 2H), 1.92 (d, *J* = 1.0 Hz, 3H), 0.98 (t, *J* = 7.5 Hz, 3H); ^{13}C NMR (100 MHz, $CDCl_3$) δ 152.5, 137.7, 137.4, 132.9, 131.0, 130.9, 129.1, 127.3, 125.0, 123.7, 121.4, 119.8, 119.6, 118.6, 111.0, 69.6, 24.5, 11.9, 11.8; IR (Neat Film, NaCl) 2972, 2936, 1770, 1692, 1488, 1470, 1392, 1364, 1350, 1292, 1251, 1231, 1187, 1133, 1070, 1024, 959, 947, 758 cm^{-1}; HRMS (MM:ESI- APCI+) *m/z* calc'd for $C_{19}H_{21}BrNO_3$ $[M+H]^+$: 390.0699, found 390.0688.

2.8.2.3 Preparation of *N*-Acyl Substrates

General Procedure 1

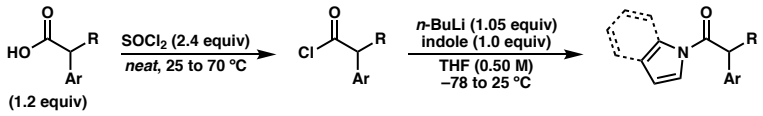

To an oven-dried scintillation vial containing the α-aryl carboxylic acid (1.2 equiv) was added $SOCl_2$ (2.4 equiv) and the resulting mixture was stirred at 25 ºC for 20 min then heated to 70 ºC for 2 h (Note: effluent gas is bubbled through a glass tube packed with powdered NaOH). The reaction was then concentrated in vacuo to afford the crude acid chloride which was used in the next step without purification.

A flame-dried flask containing the *N*-H heterocycle (1.0 equiv) in THF (0.50 M) was cooled to 0 ºC in an ice bath and *n*-BuLi (1.05 equiv) was added dropwise. The mixture was stirred at 0 ºC for 15 min then cooled to –78 ºC in a dry-ice/acetone bath. The crude acid chloride was dissolved in a small amount of THF and added rapidly to the deprotonated indole. The reaction mixture was allowed to warm to 25 ºC after which it was quenched with water and transferred to a separatory funnel with Et_2O. The layers were separated, and the aqueous layer was exacted with Et_2O. The combined organic layers were dried over Na_2SO_4, filtered, and concentrated. The *N*-acyl indole was then purified by silica gel flash chromatography.

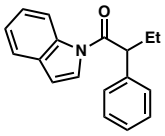

1-(1*H*-indol-1-yl)-2-phenylbutan-1-one (25)

Prepared on a 2.00 mmol scale and purified by column chromatography (3% Et_2O in hexanes) to provide the desired product as a white solid (428.2 mg, 81% yield); ^{1}H NMR (500 MHz, $CDCl_3$) δ 8.54 (d, *J* = 8.3, 1H), 7.51–7.42 (m, 2H), 7.38–7.13 (m, 7H), 6.48 (d, *J* = 3.8 Hz, 1H), 4.10 (t, *J* = 7.2 Hz, 1H), 2.35–2.18 (m, 1H), 1.89 (dt, *J* = 13.7, 7.2 Hz, 1H), 0.93 (t, *J* = 7.4 Hz, 3H); ^{13}C NMR (100 MHz, $CDCl_3$) δ 171.9, 139.1, 136.0, 130.3, 129.1, 127.7, 127.5, 125.2, 124.9, 123.8, 120.8, 117.0, 109.1, 53.7, 27.9, 12.3; IR (Neat Film, NaCl) 3063, 2967, 2943, 2874, 1704, 1602, 1584, 1539, 1472, 1451, 1384, 1355, 1328, 1304, 1222, 1208, 1181, 1154, 1082, 1017, 903, 880, 825, 807, 766, 749, 700 cm^{-1}; HRMS (MM:ESI-APCI+) *m/z* calc'd for $C_{18}H_{18}NO$ $[M+H]^+$: 264.1383, found 264.1377.

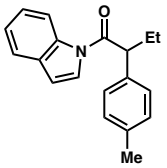

1-(1*H*-indol-1-yl)-2-(*p*-tolyl)butan-1-one (26)

Prepared on a 4.30 mmol scale and purified by column chromatography (3% Et_2O in hexanes) to provide the desired product as a yellow oil (901.0 mg, 76% yield); ^{1}H NMR (500 MHz, $CDCl_3$) δ 8.57 (dd, *J* = 8.4, 0.9 Hz, 1H), 7.53–7.46 (m, 2H), 7.35 (ddd, *J* = 8.5, 7.3, 1.3 Hz, 1H), 7.27–7.22 (m, 3H), 7.16–7.09 (m, 2H), 6.52 (dd, *J* = 3.8, 0.8 Hz, 1H), 4.11 (t, *J* = 7.2 Hz, 1H), 2.36–2.21 (m, 4H), 1.91 (dp, *J* = 13.7, 7.4 Hz, 1H), 0.97 (t, *J* = 7.4 Hz, 3H); ^{13}C NMR (100 MHz, $CDCl_3$) δ 172.0, 137.0, 136.1, 136.0, 130.3, 129.8, 127.5, 125.0, 124.9, 123.7, 120.7, 116.9, 108.9, 53.3, 27.8, 21.0, 12.2; IR (Neat Film, NaCl) 3051, 3024, 2966, 2931, 2874, 1704, 1584, 1539, 1514, 1472, 1451, 1384, 1355, 1325, 1304, 1223, 1208, 1187, 1155, 1084, 904, 808, 785, 767, 751, 715 cm^{-1}; HRMS (MM:ESI-APCI+) *m/z* calc'd for $C_{19}H_{20}NO$ $[M+H]^+$: 278.1539, found 278.1531.

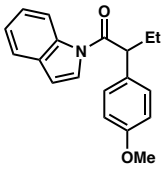

1-(1*H*-indol-1-yl)-2-(4-methoxyphenyl)butan-1-one (27)

Prepared on a 5.00 mmol scale and purified by column chromatography (3% Et_2O in hexanes) to provide the desired product as a yellow oil containing minor impurities (1.2439 g, 85% yield); ^{1}H NMR (500 MHz, $CDCl_3$) δ 8.56 (dq, *J* = 8.3, 0.9 Hz, 1H), 7.53–7.48 (m, 2H), 7.35 (ddd, *J* = 8.4, 7.2, 1.3 Hz, 1H), 7.30–7.22 (m, 3H), 6.89–6.82 (m, 2H), 6.53 (dd, *J* = 3.8, 0.7 Hz, 1H), 4.10 (t, *J* = 7.3 Hz, 1H), 3.76 (s, 3H), 2.37–2.20 (m, 1H), 1.90 (m, 1H), 0.97 (t, *J* = 7.3 Hz, 3H); ^{13}C NMR (100 MHz, $CDCl_3$) δ 172.2, 158.9, 135.9, 131.1, 130.3, 128.7, 125.1, 124.9, 123.7, 120.7, 116.9, 114.4, 108.9, 55.1, 52.8, 27.8, 12.2; IR (Neat Film, NaCl) 2964, 2933, 1702, 1610, 1540, 1511, 1450, 1384, 1354, 1324, 1302, 1252, 1222, 1207, 1179, 1154, 1033, 904, 820, 788, 766, 752 cm^{-1}; HRMS (MM:ESI-APCI+) *m/z* calc'd for $C_{19}H_{20}NO_2$ $[M+H]^+$: 294.1489, found 294.1494.

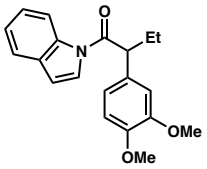

2-(3,4-dimethoxyphenyl)-1-(1*H*-indol-1-yl)butan-1-one (28)

Prepared on a 4.20 mmol scale and purified by column chromatography (20 → 30% Et_2O in hexanes) to provide the desired product as a yellow oil (838.3 mg, 62% yield); ^{1}H NMR (500 MHz, $CDCl_3$) δ 8.56 (dq, *J* = 8.3, 0.9 Hz, 1H), 7.54–7.49 (m, 2H), 7.35 (ddd, *J* = 8.4, 7.2, 1.3 Hz, 1H), 7.29–7.22 (m, 1H), 6.92–6.85 (m, 2H), 6.81 (d, *J* = 8.1 Hz, 1H), 6.54 (dd, *J* = 3.8, 0.8 Hz, 1H), 4.08 (t, *J* = 7.3 Hz, 1H), 3.86 (s, 3H), 3.84 (s, 3H), 2.28 (dt, *J* = 13.7, 7.3 Hz, 1H), 1.92 (dt, *J* = 13.8, 7.3 Hz, 1H), 0.97 (t, *J* = 7.3 Hz, 3H); ^{13}C NMR (100 MHz, $CDCl_3$) δ 172.1, 149.5, 148.4, 136.0, 131.6, 130.3, 125.2, 124.9, 123.8, 120.8, 120.2, 116.9, 111.5, 110.3, 109.1, 56.0, 55.9, 53.4, 27.9, 12.3; IR (Neat Film, NaCl) 2964, 2934, 1699, 1591, 1516, 1451, 1355, 1326, 1302, 1262, 1242, 1206, 1152, 1027, 790, 766, 752 cm^{-1}; HRMS (MM:ESI-APCI+) *m/z* calc'd for $C_{20}H_{22}NO_3$ $[M+H]^+$: 324.1594, found 324.1588.

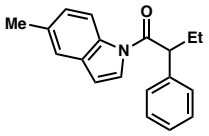

1-(5-methyl-1*H*-indol-1-yl)-2-phenylbutan-1-one (29)

Prepared on a 2.50 mmol scale and purified by column chromatography (5% Et_2O in hexanes) to provide the desired product as a cream-colored solid (567.3 mg, 82% yield); ^{1}H NMR (500 MHz, $CDCl_3$) δ 8.43 (d, *J* = 8.4 Hz, 1H), 7.45 (d, *J* = 3.7 Hz, 1H), 7.38–7.27 (m, 5H), 7.28–7.20 (m, 1H), 7.17 (d, *J* = 8.4 Hz, 1H), 6.45 (d, *J* = 3.7 Hz, 1H), 4.14 (t, *J* = 7.2 Hz, 1H), 2.43 (s, 3H), 2.31 (dtd, *J* = 14.7, 7.3, 1.0 Hz, 1H), 1.99–1.89 (m, 1H), 0.99 (td, *J* = 7.4, 0.9 Hz, 3H); ^{13}C NMR (100 MHz, $CDCl_3$) δ 171.7, 139.3, 134.2, 133.4, 130.6, 129.2, 127.8, 127.5, 126.5, 124.9, 120.7, 116.6, 109.0, 53.7, 27.9, 21.5, 12.4; IR (Neat Film, NaCl) 3027, 2967, 2931, 2874, 1703, 1582, 1541, 1468, 1382, 1328, 1304, 1208, 1182, 1089, 903, 833, 823, 811, 740, 700 cm^{-1}; HRMS (MM:ESI-APCI+) *m/z* calc'd for $C_{19}H_{20}NO$ $[M+H]^+$: 278.1539, found 278.1534.

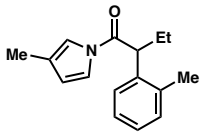

1-(3-methyl-1*H*-pyrrol-1-yl)-2-(*o*-tolyl)butan-1-one (30)

Prepared on a 4.20 mmol scale and purified by column chromatography (5% Et_2O in hexanes) to provide the desired product as a light yellow oil (539.3 mg, 54% yield); Note: compound darkens in color overtime under Ar at –20 ºC; ^{1}H NMR (500 MHz, $CDCl_3$) δ 7.27–6.92 (m, 6H), 6.03 (dd, *J* = 3.3, 1.6 Hz, 1H), 4.24 (dd, *J* = 8.5, 5.7 Hz, 1H), 2.47 (s, 3H), 2.20 (ddq, *J* = 14.5, 8.5, 7.3 Hz, 1H), 2.00 (d, *J* = 1.2 Hz, 3H), 1.84–1.64 (m, 1H), 0.98 (t, *J* = 7.4 Hz, 3H); ^{13}C NMR (100 MHz, $CDCl_3$) δ 170.9, 137.9, 134.6, 131.0, 127.3, 127.0, 126.8, 123.8, 119.3, 116.5, 115.4, 48.5, 27.4, 19.8, 12.7, 12.1; IR (Neat Film, NaCl) 3021, 2964, 2928, 2874, 1708, 1488, 1459, 1396, 1355, 1327, 1306, 1192, 1171, 1082, 1066, 952, 905, 834, 820, 780, 756, 730 cm^{-1}; HRMS (MM:ESI- APCI+) *m/z* calc'd for $C_{16}H_{20}NO$ $[M+H]^+$: 242.1539, found 242.1532.

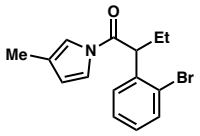

2-(2-bromophenyl)-1-(3-methyl-1*H*-pyrrol-1-yl)butan-1-one (31)

Prepared on a 7.00 mmol scale and purified by column chromatography (3% Et_2O in hexanes) to provide the desired product as a yellow oil (1.56 g, 72% yield) Note: Note: compound darkens in color overtime under Ar at –20 ºC; ^{1}H NMR (500 MHz, $CDCl_3$) δ 7.59 (dd, *J* = 8.0, 1.3 Hz, 1H), 7.36 (dd, *J* = 7.8, 1.7 Hz, 1H), 7.28–7.22 (m, 2H), 7.11 (ddd, *J* = 8.0, 7.3, 1.7 Hz, 2H), 6.07 (dd, *J* = 3.3, 1.6 Hz, 1H), 4.62 (dd, *J* = 8.2, 6.1 Hz, 1H), 2.16 (ddq, *J* = 13.7, 8.2, 7.3 Hz, 1H), 2.03 (d, *J* = 1.2 Hz, 3H), 1.83 (dqd, *J* = 13.6, 7.4, 6.2 Hz, 1H), 1.00 (t, *J* = 7.3 Hz, 3H); ^{13}C NMR (100 MHz, $CDCl_3$) δ 170.2, 138.7, 133.2, 129.0, 128.4, 128.4, 124.1, 124.1, 119.5, 116.6, 115.7, 50.7, 27.6, 12.3, 12.1; IR (Neat Film, NaCl) 2967, 2930, 2875, 1709, 1489, 1471, 1440, 1398, 1356, 1328, 1306, 1200, 1180, 1067, 1020, 908, 830, 810, 749 cm^{-1}; HRMS (MM:ESI-APCI+) *m/z* calc'd for $C_{15}H_{17}BrNO$ $[M+H]^+$: 306.0488, found 306.0477.

General Procedure 2

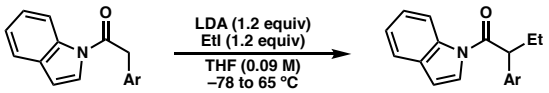

A flame-dried round bottom flask was charged with *i*-Pr_2NH (367 µL, 2.60 mmol, 1.3 equiv) and THF (18.0 mL). The solution was then cooled in a 0 ºC ice bath for 10 min and a 2.40 M solution of *n*-BuLi (996 µL, 2.40 mmol, 1.2 equiv) was added dropwise. After stirring for 15 min, the solution was cooled in a –78 ºC acetone/dry ice bath for 15 min, after which time a solution of acyl indole (498.6 mg, 2.00 mmol, 1.0 equiv) in THF (4.0 mL) was added dropwise over 5 min. After stirring at –78 ºC for 1 h, neat ethyl iodide (193 µL, 2.40 mmol, 1.2 equiv) was then added dropwise. The reaction mixture was allowed to slowly warm to 20 ºC, and then heated to 65 ºC and stirred for 16 h, after which time the reaction was quenched with the slow addition of 10 mL H_2O. The mixture was then transferred to a separatory funnel and the layers were separated. The aqueous layer was extracted 3 x 10 mL Et_2O and the combined organics were dried over Na_2SO_4, filtered, and concentrated. The desired *N*-acyl indole was isolated by silica gel flash chromatography.

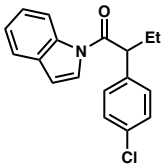

2-(4-chlorophenyl)-1-(1*H*-indol-1-yl)butan-1-one (32)

Purified by column chromatography (5% Et_2O in hexanes) to provide the desired product as a light yellow oil (373.8 mg, 63% yield); ^{1}H NMR (500 MHz, $CDCl_3$) δ 8.54 (dd, *J* = 8.4, 0.9 Hz, 1H), 7.52 (dt, *J* = 7.7, 1.1 Hz, 1H), 7.44 (d, *J* = 3.8 Hz, 1H), 7.36 (ddd, *J* = 8.4, 7.2, 1.3 Hz, 1H), 7.30 (s, 4H), 7.28–7.24 (m, 1H), 6.56 (dd, *J* = 3.9, 0.8 Hz, 1H), 4.13 (t, *J* = 7.3 Hz, 1H), 2.29 (dt, *J* = 13.8, 7.3 Hz, 1H), 2.03–1.76 (m, 1H), 0.97 (t, *J* = 7.4 Hz, 3H); ^{13}C NMR (100 MHz, $CDCl_3$) δ 171.5, 137.6, 136.0, 133.5, 130.4, 129.4, 129.2, 125.4, 124.6, 124.0, 120.9, 117.0, 109.5, 53.1, 27.9, 12.3; IR (Neat Film, NaCl) 2967, 2361, 1700, 1540, 1491, 1451, 1384, 1354, 1328, 1302, 1221, 1207, 1094, 1015, 904, 814, 794, 752 cm^{-1}; HRMS (MM:ESI-APCI+) *m/z* calc'd for $C_{18}H_{17}ClNO$ $[M+H]^+$: 298.0993, found 298.0984.

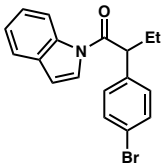

2-(4-bromophenyl)-1-(1*H*-indol-1-yl)butan-1-one (33)

Purified by column chromatography (5% Et_2O in hexanes) to provide the desired product as a white solid (451.0 mg, 66% yield); ^{1}H NMR (500 MHz, $CDCl_3$) δ 8.54 (d, *J* = 8.3 Hz, 1H), 7.52 (d, *J* = 7.7 Hz, 1H), 7.48–7.41 (m, 3H), 7.38–7.32 (m, 1H), 7.30–7.20 (m, 3H), 6.56 (d, *J* = 3.8 Hz, 1H), 4.12 (t, *J* = 7.2 Hz, 1H), 2.29 (dp, *J* = 14.6, 7.3 Hz, 1H), 1.92 (dp, *J* = 14.6, 7.3 Hz, 1H), 0.98 (t, *J* = 7.3 Hz, 3H); ^{13}C NMR (100 MHz, $CDCl_3$) δ 171.5, 138.1, 136.0, 132.3, 130.4, 129.6, 125.4, 124.6, 124.0, 121.6, 120.9, 117.0, 109.5, 53.2, 27.9, 12.3; IR (Neat Film, NaCl) 3052, 2967, 2931, 2874, 1703, 1486, 1451, 1383, 1354, 1327, 1301, 1207, 1154, 1074, 1011, 904, 880, 812, 792, 755, 751, 713 cm^{-1}; HRMS (MM:ESI-APCI+) *m/z* calc'd for $C_{18}H_{17}BrNO$ $[M+H]^+$: 342.0488, found 342.0497.

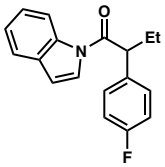

2-(4-fluorophenyl)-1-(1*H*-indol-1-yl)butan-1-one (34)

Purified by column chromatography (5% Et_2O in hexanes) to provide the desired product as a white solid (360.4 mg, 64% yield); ^{1}H NMR (500 MHz, $CDCl_3$) δ 8.55 (d, J = 8.3 Hz, 1H), 7.52 (dd, J = 7.7, 1.0 Hz, 1H), 7.46 (d, J = 3.8 Hz, 1H), 7.39– 7.29 (m, 3H), 7.30–7.22 (m, 1H), 7.07–6.97 (m, 2H), 6.56 (dd, J = 3.8, 0.6 Hz, 1H), 4.15 (t, J = 7.3 Hz, 1H), 2.30 (dt, J = 13.8, 7.3 Hz, 1H), 1.92 (dq, J = 14.1, 7.3 Hz, 1H), 0.98 (t, J = 7.3 Hz, 3H); ^{19}F NMR (282 MHz, $CDCl_3$) δ –114.9 (tt, J = 8.5, 5.2 Hz); ^{13}C NMR (100 MHz, $CDCl_3$) δ 171.8, 162.1 (d, $J_{C–F}$ = 246.2 Hz), 136.0, 134.8 (d, $J_{C–F}$ = 3.3 Hz), 130.3, 129.4 (d, $J_{C–F}$ = 8.0 Hz), 125.3, 124.7, 123.9, 120.9, 117.0, 116.0 (d, $J_{C–F}$ = 21.5 Hz), 109.3, 52.8, 27.9, 12.2; IR (Neat Film, NaCl) 3074, 2967, 2934, 2873, 1702, 1603, 1508, 1450, 1384, 1354, 1327, 1301, 1222, 1207, 1158, 818, 792, 752, 714 cm^{-1}; HRMS (MM:ESI-APCI+) *m/z* calc'd for $C_{18}H_{17}FNO$ $[M+H]^+$: 282.1289, found 282.1286.

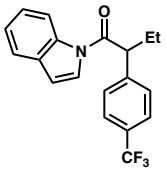

1-(1*H*-indol-1-yl)-2-(4-(trifluoromethyl)phenyl)butan-1-one (35)

Purified by column chromatography (6% Et_2O in hexanes) to provide the desired product as a white solid (190.8 mg, 58% yield); ^{1}H NMR (500 MHz, $CDCl_3$) δ 8.55 (dd, J = 8.3, 0.9 Hz, 1H), 7.62–7.58 (m, 2H), 7.55– 7.48 (m, 3H), 7.44 (d, J = 3.9 Hz, 1H), 7.37 (ddd, J = 8.5, 7.2, 1.3 Hz, 1H), 7.30–7.25 (m, 1H), 6.57 (dd, J = 3.8, 0.7 Hz, 1H), 4.23 (t, J = 7.3 Hz, 1H), 2.41–2.26 (m, 1H), 1.95 (dt, J = 13.8, 7.3 Hz, 1H), 0.99 (t, J = 7.4 Hz, 3H); ^{19}F NMR (282 MHz, $CDCl_3$) δ –62.6; ^{13}C NMR (100 MHz, $CDCl_3$) δ 171.2, 143.0 (d, $J_{C–F}$ = 1.5 Hz), 136.0, 130.4, 129.9 (q, $J_{C–F}$ = 32.6 Hz), 128.3, 126.1 (q, $J_{C–F}$ = 3.8 Hz), 125.5, 125.4 (q, $J_{C–F}$ = 272.4 Hz), 124.5, 124.1, 121.0, 117.0, 109.7, 53.5, 28.0, 12.3; IR (Neat Film, NaCl) 1702, 1451, 1384, 1354, 1324, 1304, 1208, 1166, 1123, 1068, 1068, 1018, 831, 800, 766, 752 cm^{-1}; HRMS (MM:ESI-APCI+) *m/z* calc'd for $C_{19}H_{17}F_3NO$ $[M+H]^+$: 332.1257, found 332.1248.

General Procedure 3

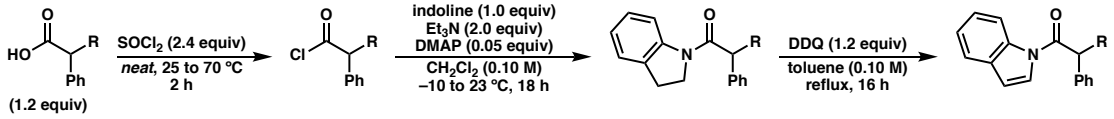

To an oven-dried flask containing α-aryl carboxylic acid (5.0 mmol, 1.0 equiv) was added $SOCl_2$ neat (620 μL, 8.50 mmol, 1.7 equiv) and the resulting mixture stirred at 25 °C for 20 min then 70 °C for 2 h (note: effluent gas flow is bubbled through a glass tube packed with powdered NaOH). The reaction was then concentrated in vacuo to afford the crude acid chloride, which was used in the next step without further purification. A separate flame-dried flask containing freshly distilled indoline (4.20 mmol, 1.0 equiv), Et_3N (1.17 mL, 8.40 mmol, 2.0 equiv), and DMAP (25.7 mg, 0.21 mmol, 0.05 equiv) in CH_2Cl_2 (42 mL) was cooled to –10 °C in an acetone/ice bath and the crude acid chloride (5.0 mmol, 1.2 equiv) dissolved in CH_2Cl_2 (21 mL) was added dropwise via cannula transfer. The mixture was stirred at –10 °C for 15 min then warmed to 23 ºC and stirred for 18 h. The reaction mixture was quenched with saturated $NaHCO_3$ (20 mL) and transferred to a separatory funnel. The layers were separated, and the aqueous layer was extracted twice with CH_2Cl_2 (20 mL). The combined organics were washed with brine (10 mL), dried over Na_2SO_4, filtered, and concentrated to afford the crude amide which was used in the next step without further purification.

The crude amide prepared above was transferred to a round bottom flask affixed with a reflux condenser. Dry toluene (42 mL) and DDQ (2,3-Dichloro-5,6-dicyano-1,4-benzoquinone) (1.14 g, 5.0 mmol, 1.2 equiv) were then added and the resulting dark red reaction solution was heated to reflux for 16 h. The crude reaction mixture was then filtered

through a pad of celite with toluene, concentrated, and purified via flash column chromatography to afford the desired acyl indole.

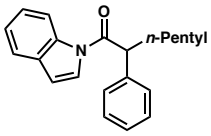

1-(1*H*-indol-1-yl)-2-phenylheptan-1-one (36)

Prepared according to General Procedure 3 and purified by column chromatography (5% Et_2O in hexanes) to provide the desired product as a colorless oil (319.5 mg, 25% yield); ^{1}H NMR (500 MHz, $CDCl_3$) δ 8.58 (dq, *J* = 8.4, 0.9 Hz, 1H), 7.54–7.48 (m, 2H), 7.39–7.30 (m, 5H), 7.30–7.21 (m, 2H), 6.54 (dd, *J* = 3.8, 0.8 Hz, 1H), 4.25 (t, *J* = 7.2 Hz, 1H), 2.34–2.25 (m, 1H), 1.90 (tdd, *J* = 12.9, 8.5, 5.7 Hz, 1H), 1.46–1.25 (m, 6H), 0.91–0.84 (m, 3H); ^{13}C NMR (100 MHz, $CDCl_3$) δ 172.0, 139.4, 136.0, 130.3, 129.2, 127.7, 127.5, 125.2, 124.8, 123.8, 120.7, 117.0, 109.1, 52.1, 34.7, 31.8, 27.4, 22.6, 14.1; IR (Neat Film, NaCl) 3063, 3029, 2954, 2928, 2858, 1704, 1602, 1584, 1539, 1451, 1384, 1353, 1311, 1207, 1154, 1102, 941, 919, 880, 766, 749, 700 cm^{-1}; HRMS (MM:ESI-APCI+) *m/z* calc'd for $C_{21}H_{24}NO$ $[M+H]^+$: 306.1846, found 306.1846.

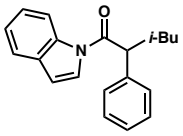

1-(1*H*-indol-1-yl)-4-methyl-2-phenylpentan-1-one (37)

Prepared according to General Procedure 3 and purified by column chromatography (5% Et_2O in hexanes) to provide the desired product as a colorless oil (1.2177 g, 99% yield); ^{1}H NMR (500 MHz, $CDCl_3$) δ (d, *J* = 8.3 Hz, 1H), 7.54 (d, *J* = 3.8 Hz, 1H), 7.52–7.50 (m, 1H), 7.39–7.29 (m, 5H), 7.27–7.22 (m, 2H), 6.55 (dd, *J* = 3.8, 0.7 Hz, 1H), 4.37 (t, *J* = 7.3 Hz, 1H), 2.22 (dt, *J* = 13.6 Hz, 7.4 Hz, 1H), 1.79 (dt, *J* = 13.7, 6.9 Hz, 1H), 1.61 (dp, *J* = 13.5, 6.8 Hz, 1H), 0.97 (dd, *J* = 27.5, 6.6 Hz, 6H); ^{13}C NMR (100 MHz, $CDCl_3$) δ 172.0, 139.5, 136.1, 130.4, 129.3, 127.8, 127.5, 125.3, 124.8, 123.9, 120.9, 117.1, 109.3, 49.8, 43.8, 25.9, 22.9, 22.7; IR (Neat Film, NaCl) 3386, 3154, 3063, 3029, 2956, 2868, 1703, 1602, 1585 1538, 1493, 1471, 1451, 1385, 1344, 1332, 1308, 1295, 1222, 1207, 1103, 1084, 1018, 943, 886, 766, 748, 670 cm^{-1}; HRMS (MM:ESI-APCI+) *m/z* calc'd for $C_{20}H_{22}NO$ $[M+H]^+$: 292.1696, found 292.1696.

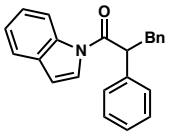

1-(1*H*-indol-1-yl)-2,3-diphenylpropan-1-one (38)

Prepared according to General Procedure 3 and purified by column chromatography (5% Et_2O in hexanes) to provide the desired product as a white solid (830.7 mg, 61% yield); ^1H NMR (500 MHz, $CDCl_3$) δ 8.56 (dd, *J* = 8.3, 0.9 Hz, 1H), 7.48 (dt, *J* = 7.5, 0.9 Hz, 1H), 7.39 (d, *J* = 3.8 Hz, 1H), 7.34 (ddd, *J* = 8.4, 7.2, 1.3 Hz, 1H), 7.32 – 7.27 (m, 4H), 7.26 – 7.10 (m, 7H), 6.48 (dd, *J* = 3.9, 0.7 Hz, 1H), 4.51 (t, *J* = 7.2 Hz, 1H), 3.67 (dd, *J* = 13.7, 7.6 Hz, 1H), 3.14 (dd, *J* = 13.8, 6.9 Hz, 1H); ^{13}C NMR (100 MHz, $CDCl_3$) δ 171.2, 139.1, 138.7, 136.0, 130.3, 129.3, 129.2, 128.5, 127.8, 127.7, 126.6, 125.3, 124.8, 123.9, 120.8, 117.0, 109.3, 54.4, 40.8; IR (Neat Film, NaCl) 3155, 3062, 3029, 2927, 1950, 1805, 1698, 1601, 1585, 1539, 1495, 1472, 1453, 1385, 1354, 1319, 1300, 1221, 1207, 1108, 1074, 911, 898, 766, 749, 699 cm^{-1}; HRMS (MM:ESI-APCI+) *m/z* calc'd for $C_{23}H_{20}NO$ $[M+H]^+$: 326.1539, found 326.1536.

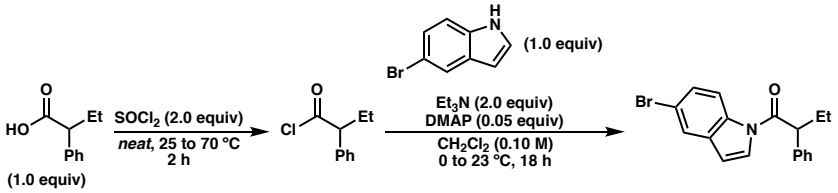

1-(5-bromo-1*H*-indol-1-yl)-2-phenylbutan-1-one (39)

To a flame-dried conical flask containing 2-phenyl butanoic acid (492.6 mg, 3.00 mmol, 1.0 equiv) was added $SOCl_2$ neat (6.00 mmol, 440 μL, 2.0 equiv) and the resulting mixture stirred at 25 °C for 20 min and then 70 °C for 2 h (note: effluent gas flow is bubbled through a glass tube packed with powdered NaOH). The reaction was then concentrated in vacuo to afford the crude acid chloride, which was used in the next step without further purification. To a flame-dried 25 mL round bottom flask was added 5-bromoindole (588.1 mg, 3.00 mmol, 1.0 equiv), DMAP (36.7 mg, 0.30 mmol, 0.10 equiv), CH_2Cl_2 (5.0 mL), and Et_3N (627 μL, 4.50 mmol, 1.5 equiv). The resulting clear, colorless solution was then cooled in a 0 ºC ice bath for 10 min before a solution of the above crude acid chloride in CH_2Cl_2 (3.0 mL) was added dropwise via cannula. The resulting bright yellow solution was stirred at 23 ºC for 18 h then concentrated under reduced pressure. The crude yellow oil was then dissolved in Et_2O (10 mL), transferred to a separatory funnel, and washed with H_2O (20 mL). The aqueous layer was then extracted with Et_2O (3 x 10 mL). The combined organics were then washed with brine (10 mL), dried over Na_2SO_4, filtered, and concentrated under reduced pressure to afford an orange oil which was purified by column chromatography (3% Et_2O in hexanes) to provide the desired product as an off white solid with minor impurities (654.3 mg, 64% yield); ^{1}H NMR (500 MHz, $CDCl_3$) δ 8.44 (d, J = 8.8 Hz, 1H), 7.63 (d, J = 1.9 Hz, 1H), 7.49 (d, J = 3.8 Hz, 1H), 7.44 (dd, J = 8.8, 2.0 Hz,

1H), 7.38–7.30 (m, 4H), 7.30–7.22 (m, 1H), 6.46 (d, J = 3.8 Hz, 1H), 4.12 (t, J = 7.2 Hz, 1H), 2.30 (dt, J = 14.1, 7.3 Hz, 1H), 1.95 (dt, J = 14.1, 7.01 Hz, 1H), 0.98 (t, J = 7.3, 3H); ^{13}C NMR (100 MHz, $CDCl_3$) δ 171.8, 138.8, 134.6, 132.0, 129.2, 127.9, 127.7, 127.6, 125.9, 123.4, 118.3, 117.0, 108.2, 53.7, 27.8, 12.3; IR (Neat Film, NaCl) 3063, 3028, 2967, 2932, 2874, 1704, 1575, 1534, 1444, 1377, 1325, 1304, 1217, 1199, 1181, 1088, 896, 826, 810, 699 cm^{-1}; HRMS (MM:ESI-APCI+) *m/z* calc'd for $C_{18}H_{17}BrNO$ $[M+H]^+$: 342.0488, found 342.0478.

2.8.2.4 Derivatization of Alkylation Products

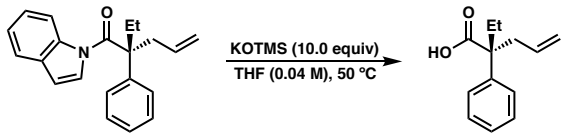

(*R*)-2-ethyl-1-(1*H*-indol-1-yl)-2-phenylpent-4-en-1-one (21)

To a flame-dried round bottom flask containing a stirred suspension of KOTMS (162 mg, 1.26 mmol) in THF (1.5 mL) was added a solution of *N*-acyl indole **20a** (38.2 mg, 0.126 mmol) in THF (1.5 mL). The resulting mixture was placed in a 50 ºC oil bath and stirred for 16 h. The crude reaction was diluted with Et_2O and 5 M NaOH, and the layers separated. The aqueous layer was washed with Et_2O and acidified with 4 M HCl to pH 1. The aqueous layer was extracted with Et_2O three times and the combined organic layers washed with water, dried over $MgSO_4$, and concentrated to a light yellow solid (25.6 mg, 99% yield), $[\alpha]_D^{25}$ –30.9 (*c* 1.0, $CHCl_3$); ^{1}H NMR (300 MHz, $CDCl_3$) δ 7.45–7.17 (m, 5H), 5.54 (dddd, *J* = 17.0, 10.1, 7.6, 6.8 Hz, 1H), 5.16–4.96 (m, 2H), 2.81 (qdt, *J* = 14.1, 6.8, 1.2 Hz, 2H), 2.22–1.90 (m, 2H), 0.81 (t, *J* = 7.4 Hz, 3H); ^{1}3C NMR (100 MHz, $CDCl_3$) δ 181.9, 141.5, 133.5, 128.5, 127.1, 126.8, 118.5, 54.0, 38.4, 26.9, 8.5; IR (Neat Film, NaCl) 3064, 2975, 1699, 1498, 1447, 1401, 1252, 918, 698 cm^{-1}; HRMS (MM:ESI-APCI+) *m/z* calc'd for $C_{13}H_{17}O_2$ $[M+H]^+$: 205.1223, found 205.1213.

ethyl *(R)*-2-ethyl-2-phenylpent-4-enoate (22)

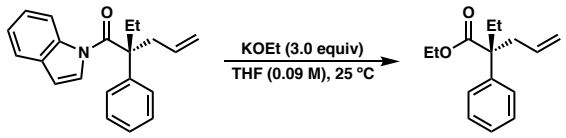

To a flame-dried round bottom flask containing a stirred solution of KOEt (32.2 mg, 0.383 mmol) in THF (1.5 mL) was added a solution of acyl indole **20a** (38.7 mg, 0.128 mmol) and the resulting mixture stirred at 25 °C for 15 h. The crude reaction was diluted with Et_2O and quenched with saturated NH_4Cl, and the layers separated. The aqueous layer was extracted with Et_2O and the combined organic fractions dried over Na_2SO_4 and concentrated. The crude product was purified by silica gel flash chromatography (5% Et_2O in hexanes) to provide the desired product as a colorless oil (22.3 mg, 75% yield), $[\alpha]D^{25}$ –4.7 (*c* 1.0, $CHCl_3$); ^1H NMR (400 MHz, $CDCl_3$) δ 7.33–7.07 (m, 5H), 5.46 (dddd, *J* = 16.9, 10.1, 7.8, 6.7 Hz, 1H), 5.07–4.87 (m, 2H), 4.08 (q, *J* = 7.1 Hz, 2H), 2.87–2.58 (m, 2H), 2.13–1.87 (m, 2H), 1.12 (t, *J* = 7.1 Hz, 3H), 0.71 (t, *J* = 7.4 Hz, 3H); ^{13}C NMR (100 MHz, $CDCl_3$) δ 175.6, 142.4, 133.8, 128.3, 126.7, 126.6, 118.2, 60.8, 54.1, 38.7, 27.1, 14.2, 8.5; IR (Neat Film, NaCl) 2976, 2360, 1728, 1220, 1135, 1030, 916, 700 cm^{-1}; HRMS (MM:ESI-APCI+) *m/z* calc'd for $C_{15}H_{21}O_2$ $[M+H]^+$: 233.1536, found 233.1531.

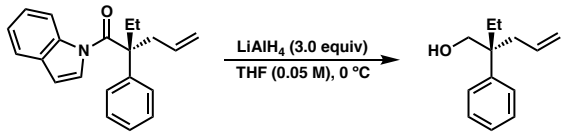

***(R)*-2-ethyl-2-phenylpent-4-en-1-ol (23)**

To a flame-dried round bottom flask was added acyl indole **20a** (32.6 mg, 0.107 mmol, 1.0 equiv) and THF (2.1 mL). The resulting solution was cooled to 0 ºC for 5 min and then a 1.0 M solution of $LiAlH_4$ (320 mL, 0.320 mmol, 3.0 equiv) was added dropwise. The resulting solution was stirred at 0 ºC for 5 min, then diluted with Et_2O (2.1 mL) and quenched with the addition of H_2O (12 μL) followed by 15% w/v $NaOH/H_2O$ (12 μL), and an additional portion of H_2O (36 μL). The resulting gray suspension was warmed to 20 ºC and stirred vigorously for 15 min. $MgSO_4$ (50 mg) was added and the resulting suspension was stirred for 15 min and filtered through a plug of celite with Et_2O. The crude product was purified by silica gel flash chromatography (10% Et_2O in hexanes) to provide the desired product as a colorless oil (17.2 mg, 84% yield); $[\alpha]D^{25}$ +12.9 (*c* 0.65, $CHCl_3$); ^1H NMR (500 MHz, $CDCl_3$) δ 7.38–7.31 (m, 4H), 7.23 (td, *J* = 6.4, 2.3 Hz, 1H), 5.70 (ddt, *J* = 17.3, 10.1, 7.3 Hz, 1H), 5.18–5.01 (m, 2H), 3.82–3.70 (m, 2H), 2.55 (ddd, *J* = 61.6, 13.9, 7.2 Hz, 2H), 1.73 (q, *J* = 7.4 Hz, 2H), 1.34 (s, 1H), 0.74 (t, *J* = 7.4 Hz, 3H); ^{13}C NMR (100 MHz, $CDCl_3$) δ 143.9, 134.9, 128.6, 127.0, 126.3, 117.8, 67.9, 46.3, 38.6, 27.5, 8.0; IR (Neat Film, NaCl) 3399 (br), 3060, 3024, 3004, 2966, 2934, 2880, 2361, 1638, 1497, 1459, 1456, 1379, 1045, 1001, 914, 760, 699 cm^{-1}; HRMS (MM:ESI- APCI+) *m/z* calc'd for $C_{13}H_{22}NO$ $[M+NH_4]+$: 208.1696, found 208.1692.

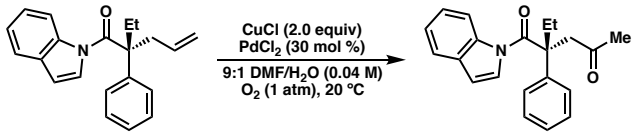

***(R)*-2-ethyl-1-(1*H*-indol-1-yl)-2-phenylpentane-1,4-dione (24)**

To a round bottom flask containing acyl indole **20a** (33.1 mg, 0.109 mmol, 1.0 equiv) dissolved in 2.5 mL of 9:1 DMF/H_2O was added $PdCl_2$ (5.8 mg, 0.033 mmol, 0.30 equiv) and CuCl (21.6 mg, 0.218 mmol, 2.0 equiv). The flask was then quickly evacuated and backfilled three times with a balloon of O_2, and then stirred at 20 ºC under a balloon of O_2 for 48 h. The crude reaction was then diluted with EtOAc (2 mL) followed by brine (2 mL). The layers were separated, and the aqueous layer was extracted with EtOAc (5 mL) twice. The combined organic layers were dried over Na_2SO_4, filtered, and concentrated. The crude product was purified by silica gel flash chromatography (10% Et2O in hexanes) to afford the desired product as a white foam in a 5:1 ketone/aldehyde ratio (33.2 mg, 0.104 mmol, 95% yield); $[\alpha]D^{25}$ –194.5 (*c* 0.58, $CHCl_3$); ^{1}H NMR (400 MHz, $CDCl_3$) δ 8.48 (d, *J* = 8.4 Hz, 1H), 7.37 (d, *J* = 7.7 Hz, 1H), 7.31–7.23 (m , 5H), 7.23– 7.12 (m, 2H), 6.70 (d, *J* = 3.9 Hz, 1H), 6.18 (d, *J* = 3.8 Hz, 1H), 3.26 (d, *J* = 15.4 Hz, 1H), 3.14 (d, *J* = 15.5 Hz, 1H), 2.64 (dq, *J* = 14.9, 7.5 Hz, 1H), 2.32–2.15 (m, 1H), 1.68 (s, 3H), 0.78 (t, *J* = 7.4 Hz, 3H); ^{13}C NMR (100 MHz, $CDCl_3$) δ 207.1, 173.5, 142.1, 136.5, 129.3, 127.7, 126.5, 125.7, 125.2, 123.8, 120.5, 117.1, 108.4, 108.4, 55.8, 48.5, 32.1, 27.5, 8.9; IR (Neat Film, NaCl) 3163, 3056, 3056, 2972, 1721, 1697, 1537, 1450, 1308, 1206, 1076, 882, 768, 752, 702 cm^{-1}; HRMS (MM:ESI-APCI+) *m/z* calc'd for $C_{21}H_{22}NO2$ $[M+H]^+$: 320.1645, found 320.1630.

2.8.2.5 Synthesis of *(S)*-Ty-PHOX

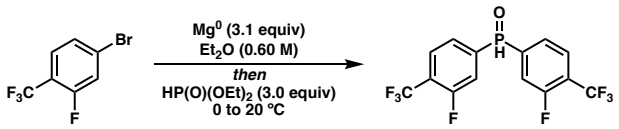

bis(3-fluoro-4-(trifluoromethyl)phenyl)phosphine oxide (40)

According to the procedure of Stoltz[15]; A flame-dried 50 mL round bottomed flask was charged with magnesium turnings (804.7 mg, 33.1 mmol, 3.1 equiv) and Et_2O (17.8 mL). The mixture was cooled to 0 ºC and 4-bromo-2-fluoro-1-(trifluoromethyl)benzene (4.52 mL, 32.0 mmol, 3.0 equiv) was added dropwise over 15 min during which the reaction mixture turned from colorless to brown to black. A reflux condenser was then attached to the flask, and the mixture was warmed to 30 ºC in a water bath and stirred for 1 h. The resulting black solution was then canula transferred to a second 50 mL flame-dried round bottom flask to remove residual magnesium turnings. The resulting solution was then cooled to 0 ºC and neat diethyl phosphite (1.38 mL, 10.7 mmol, 1.0 equiv) was added dropwise over 10 min. The black reaction mixture was then allowed to warm to 20 ºC over 1 h and stirred for 24 h. The reaction mixture was then cooled to 0 ºC and 2.0 N HCl (20 mL) was added dropwise with vigorous stirring, leading to the precipitation of a brown solid. The mixture was then allowed to warm to 20 ºC and extracted with EtOAc (3 x 10 mL). The combined organic layers were then washed with brine (10 mL), dried over Na2SO4, filtered, and concentrated to an orange oil. Purification by silica gel chromatography (30% EtOAc in hexanes to 60% EtOAc in hexanes) provided the desired product as a yellow solid (2.6803 g, 7.72 mmol, 72% yield); ^{1}H NMR (400 MHz, $CDCl_3$) δ 8.78 (s, 1H), 7.80 (td, *J* = 7.2, 3.2 Hz, 2H), 7.59 (ddd, *J* = 19.8, 13.7, 8.6 Hz, 4H); ^{19}F

NMR (282 MHz, $CDCl_3$) δ –62.02 (d, J = 12.7 Hz), –110.40 – –110.63 (m); ^{31}P NMR (162 MHz, $CDCl_3$) δ 14.77; ^{13}C NMR (100 MHz, $CDCl_3$) δ 159.9 (dd, J = 262.9, 17.6 Hz), 137.2 (dd, J = 98.7, 6.0 Hz), 128.7 (dq, J = 14.0, 4.4 Hz), 126.3 (dd, J = 11.1, 4.4 Hz), 123.7–122.4 (m), 121.8 (q, J = 273.2 Hz), 119.2 (dd, J = 22.0, 12.5 Hz); IR (Neat Film, NaCl) 3040, 2368, 1622, 1576, 1498, 1409, 1323, 1239, 1178, 1134, 1043, 951, 901, 833, 696, 632 cm^{-1}; HRMS (MM:ESI-APCI+) *m/z* calc'd for $C_{14}H_8F_8OP$ $[M+H]^+$: 375.0180, found 375.0172.

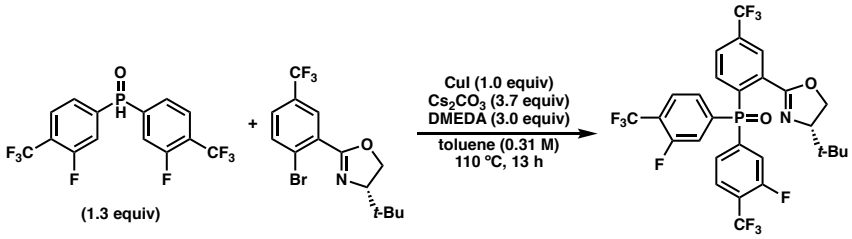

***(S)*-(2-(4-(*tert*-butyl)-4,5-dihydrooxazol-2-yl)-4-(trifluoromethyl)phenyl)bis(3-fluoro-4-(trifluoromethyl)phenyl)phosphine oxide (41)**

To a flame-dried 100 mL two-necked round bottom flask equipped with a reflux condenser and glass stopper was added phosphine oxide **40** (2.4321 g, 6.50 mmol, 1.3 equiv), CuI (952.3 mg, 5.00 mmol, 1.0 equiv), and toluene (11.4 mL) followed by *N*,*N*'-dimethylethylenediamine (1.61 mL, 15.0 mmol, 3.0 equiv). The resulting green solution was stirred at 20 ºC for 20 min after which time oxazoline (1.75 g, 5.00 mmol, 1.0 equiv), Cs_2CO_3 (6.03 g, 18.5 mmol, 3.7 equiv), and toluene (4.9 mL) were added. The flask was then immersed in a 110 ºC oil bath and the reaction suspension gradually turned blue and then orange. After 13 h, the reaction was cooled to 20 ºC and the orange reaction mixture was loaded directly onto a silica gel column (hexanes to 25% EtOAc in hexanes) to provide a white foam (841.9 mg, 26% yield); $[\alpha]D^{25}$ –47.5 (*c* 1.0, $CHCl_3$); ^{1}H NMR (500 MHz, $CDCl_3$) δ 8.24 (dd, *J* = 3.9, 1.8 Hz, 1H), 8.13–8.01 (m, 1H), 7.91–7.87 (m, 1H), 7.80–7.60 (m, 4H), 7.50–7.39 (m, 2H), 4.03 – 3.93 (m, 2H), 3.42 (dd, *J* = 10.2, 9.4 Hz, 1H), 0.72 (s, 9H); ^{31}P NMR (121 MHz, $CDCl_3$) δ 26.10; ^{19}F NMR (282 MHz, $CDCl_3$) δ – 61.90 (dd, *J* = 15.3, 12.6 Hz), –63.48, –111.76 – –112.14 (m); ^{13}C NMR (100 MHz, $CDCl_3$) δ 160.8 (d, *J* = 17.3 Hz), 160.4 (d, *J* = 2.1 Hz), 158.2 (d, *J* = 17.3 Hz), 140.7 (d, *J* = 5.7 Hz), 139.8 – 139.2 (m), 138.4 (d, *J* = 6.1 Hz), 136.2 (d, *J* = 10.3 Hz), 135.8 – 134.4 (m), 134.0, 133.0, 132.8 (d, *J* = 6.6 Hz), 127.7 (ddt, *J* = 20.1, 9.0, 4.2 Hz), 126.8 (dd, *J* = 9.5, 4.2 Hz), 124.4,

123.4, 122.4 – 121.3 (m), 120.9 – 120.3 (m), 119.9 (dd, J = 22.1, 11.1 Hz), 69.3, 33.6, 25.8s; IR (Neat Film, NaCl) 2963, 2907, 2873, 1664, 1621, 1574, 1497, 1479, 1664, 1621, 1574, 1497, 1479, 1407, 1322, 1235, 1178, 1136, 1178, 1083, 1042, 964, 915, 833, 720, 699, 629 cm^{-1}; HRMS (MM:ESI-APCI+) *m/z* calc'd for $C_{28}H_{22}F_{11}NO_2P$ $[M+H]^+$: 644.1207, found 644.1184.

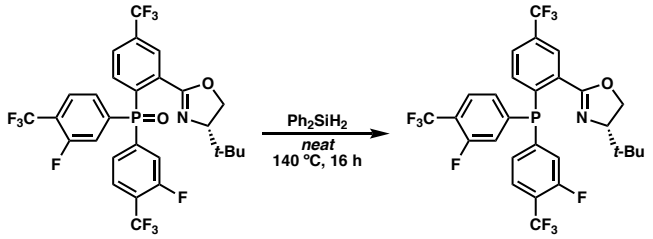

***(S)*-2-(2-(bis(3-fluoro-4-(trifluoromethyl)phenyl)phosphaneyl)-5-(trifluoromethyl)phenyl)-4-(*tert*-butyl)-4,5-dihydrooxazole (*L2,* Ty-PHOX)**

To an oven-dried 25 mL Schlenk tube was added phosphine oxide **41** and Ph_2SiH_2 (1.49 mL, 8.05 mmol, 7.0 equiv). The Schlenk tube was then sealed and heated in a 140 ºC oil bath behind a blast shield. After 16 h, the reaction was cooled to 20 ºC and slowly opened to a nitrogen atmosphere. The colorless reaction mixture was then loaded directly onto a silica gel column (hexanes to 25% CH_2Cl_2 in hexanes) to provide a white foam (610 mg, 85% yield); $[\alpha]D^{25}$ –12.5 (*c* 1.0, $CHCl_3$); ^{1}H NMR (500 MHz, $CDCl_3$) δ 8.31–8.25 (m, 1H), 7.67–7.54 (m, 3H), 7.10 (dt, *J* = 19.3, 7.4 Hz, 2H), 7.03–6.95 (m, 3H), 4.33 (dd, *J* = 10.1, 8.7 Hz, 1H), 4.16 (t, *J* = 8.6 Hz, 1H), 3.99 (dd, *J* = 10.1, 8.5 Hz, 1H), 0.74 (s, 9H); ^{19}F NMR (282 Hz, $CDCl_3$) δ –61.51 (dd, *J* = 21.1, 12.4 Hz), –63.10, –113.31 – –113.52 (m), –113.57 – –113.78 (m); ^{31}P NMR (121 MHz, CDCl3) δ –7.38; ^{13}C NMR (100 MHz, $CDCl_3$) δ 161.05 – 160.82 (m), 160.49 (d, *J* = 4.0 Hz), 158.46 – 158.25 (m), 145.63 (t, *J* = 4.2 Hz), 145.46 (d, *J* = 5.6 Hz), 140.49 (d, *J* = 28.6 Hz), 134.94, 134.74 – 134.58 (m), 134.47 – 134.20 (m), 132.38 (d, *J* = 20.4 Hz), 131.64 (q, *J* = 33.3 Hz), 129.24 (ddd, *J* = 34.0, 22.2, 3.7 Hz), 128.00 – 127.58 (m), 127.33 (dq, *J* = 12.2, 4.1 Hz), 126.65 (p, *J* = 3.4 Hz), 126.43, 124.79, 123.73, 122.44 – 120.79 (m), 119.75 – 118.09 (m), 68.83, 33.59, 25.60; IR (Neat Film, NaCl) 3071, 2960, 2871, 2138, 1655, 1617, 1570, 1491, 1430, 1403,

1323, 1176, 1133, 1083, 1042, 967, 830, 735, 714, 698, 684, 624 cm^{-1}; HRMS (MM:ESI-APCI+) *m/z* calc'd for $C_{28}H_{22}F_{11}NOP$ $[M+H]^+$: 628.1258, found 628.1271.

2.8.3 DETERMINATION OF ENANTIOMERIC EXCESS

Table 2.8.3.1 *Determination of Enantiomeric Excess of Asymmetric Allylic Alkylation Products*

entry	compound	assay conditions	t_R of major isomer (min)	t_R of minor isomer (min)	% ee
1	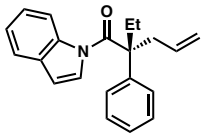 ***20a***	SFC Chiralpak AD-H 10% *i*-PrOH isocratic, 2.5 mL/min	6.95	6.41	91
2	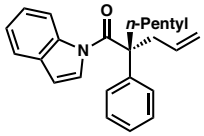 ***20b***	SFC Chiralpak AD-H 10% *i*-PrOH isocratic, 2.5 mL/min	5.84	4.87	96
3	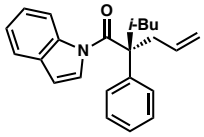 ***20c***	SFC Chiralpak AD-H 10% *i*-PrOH isocratic, 2.5 mL/min	5.20	4.86	96
4	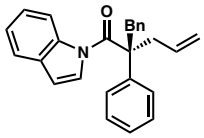 ***20d***	SFC Chiralpak AD-H 10% *i*-PrOH isocratic, 2.5 mL/min	18.37	17.49	96
5	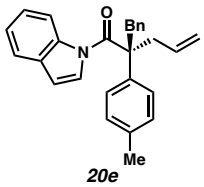 ***20e***	SFC Chiralpak AD-H 10% *i*-PrOH isocratic, 2.5 mL/min	18.37	17.49	96

entry	compound	assay conditions	t_R of major isomer (min)	t_R of minor isomer (min)	% ee
6	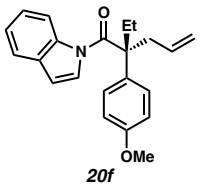 ***20f***	SFC Chiralpak AD-H 15% *i*-PrOH isocratic, 2.5 mL/min	5.73	5.09	98
7	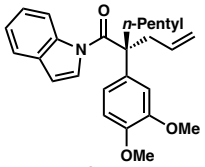 ***20g***	SFC Chiralpak AD-H 15% *i*-PrOH isocratic, 2.5 mL/min	4.92	4.14	95
8	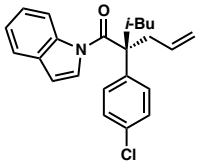 ***20h***	SFC Chiralpak AD-H 15% *i*-PrOH isocratic, 2.5 mL/min	4.78	4.31	94
9	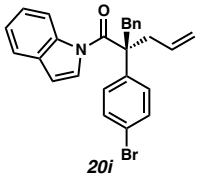 ***20i***	SFC Chiralpak AD-H 15% *i*-PrOH isocratic, 2.5 mL/min	7.38	6.60	94
10	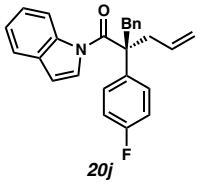 ***20j***	SFC Chiralpak AD-H 10% *i*-PrOH isocratic, 2.5 mL/min	5.07	4.57	96
11	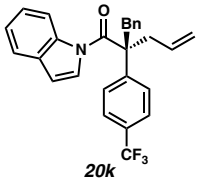 ***20k***	SFC Chiralpak AD-H 5% *i*-PrOH isocratic, 2.5 mL/min	4.97	4.48	70
12	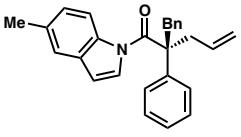 ***20l***	SFC Chiralpak AD-H 15% *i*-PrOH isocratic, 2.5 mL/min	5.92	5.21	98
13	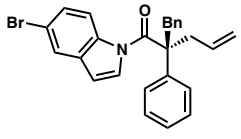 ***20m***	SFC Chiralpak AD-H 15% *i*-PrOH isocratic, 2.5 mL/min	5.91	5.28	92

entry	compound	assay conditions	t_R of major isomer (min)	t_R of minor isomer (min)	% ee
14	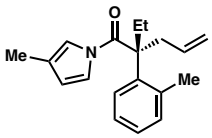 *20n*	SFC Chiralpak OD-H 3% *i*-PrOH isocratic, 2.5 mL/min	5.37	4.99	89
15	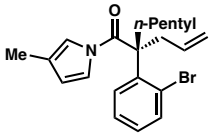 *20o*	SFC Chiralpak OD-H 3% *i*-PrOH isocratic, 2.5 mL/min	9.72	9.10	80

2.9 REFERENCES AND NOTES

(1) Liu, Y.; Han, S. J.; Liu, W. B.; Stoltz, B. M. Catalytic Enantioselective Construction of Quaternary Stereocenters: Assembly of Key Building Blocks for the Synthesis of Biologically Active Molecules. *Acc*. *Chem*. *Res*. **2015**, *48*, 740–751.

(2) (a) Martin, S. F. Methodology for the construction of quaternary carbon centers. *Tetrahedron* **1980**, *36*, 419–460. (b) Corey, E. J.; Guzman-Perez, A. The Catalytic Enantioselective Construction of Molecules with Quaternary Carbon Stereocenters. *Angew*. *Chem*. *Int*. *Ed*. **1998**, *37*, 388–401. (c) Douglas, C. J.; Overman, L. E. Catalytic asymmetric synthesis of all-carbon quaternary stereocenters. *Proc*. *Nat*. *Acad*. *Sci*. *U*. *S*. *A*. **2004**, *101*, 5363–5367. (d) Marek, I.; Sklute, G. Creation of quaternary stereocenters in carbonyl allylation reactions. *Chem*. *Commun*. **2007**, 1683–1691. (e) Trost, B. M.; Jiang, C. Catalytic Enantioselective Construction of All-Carbon Quaternary Stereocenters. *Synthesis* **2006**, 369–396. (f) Behenna, D.

C.; Mohr, J. T.; Sherden, N. H. Marinescu, S. C.; Harned, A. M.; Tani, K.; Seto, M.; Ma, S.; Novák, Z.; Krout, M. R.; McFadden, R. M.; Roizen, J. L.; Enquist, J. A.; White, D. E.; Levin, S. R.; Petrova, K. V.; Iwashita, A.; Virgil, S. C.; Stoltz, B. M. Enantioselective Dercarboxylative Alkylation Reaction: Catalyst Development, Substrate Scope, and Mechanistic Studies. *Chem*. *– Eur*. *J*. **2011**, *17*, 14199–14223. (g) Trost, B. M.; Xu, J.; Schmidt, T. Palladium-Catalyzed Decarboxylative Asymmetric Allylic Alkylation of Enol Carbonates. *J*. *Am*. *Chem*. *Soc*. **2009**, *131*, 18343–18357.

(3) (a) Feng, J.; Holmes, M.; Krische, M. J. Acyclic Quaternary Carbon Stereocenters via Enantioselective Transition Metal Catalysis. *Chem*. *Rev*. **2017**, *117*, 12564–12580. (b) Das, J. P.; Marek, I. Enantioselective synthesis of all-carbon quaternary stereogenic centers in acyclic systems. *Chem*. *Commun*. **2011**, *47*, 4593–4623. (c) Minko, Y.; Marek, I. Stereodefined acyclic trisubstituted metal enolates towards the asymmetric formation of quaternary carbon stereocentres. *Chem*. *Commun*. **2014**, *50*, 12597–12611. (d) Marek, I.; Minko, Y.; Pasco, M.; Mejuch, T.; Gilboa, N.; Chechik, H.; Das, J. P. All-Carbon Quaternary Stereogenic Centers in Acyclic Systems through the Creation of Several C–C Bonds per Chemical Step. *J*. *Am*. *Chem*. *Soc*. **2014**, *136*, 2682–2694. (e) Mei, T.-S.; Patel, H.; Sigman, M. S. Enantioselective construction of remote quaternary stereocentres. *Nature* **2014**, *508*, 340–344. (f) Zhang, K.; Peng, Q.; Hou, X.-L.; Wu, Y.-D. Highly

Enantioselective Palladium-Catalyzed Alkylation of Acyclic Amides. *Angew*. *Chem*. *Int*. *Ed*. **2008**, *47*, 1741–1744.

(4) (a) Starkov, P.; Moore, J. T.; Duquette, D. C.; Stoltz, B. M.; Marek, I. Enantioselective Construction of Acyclic Quaternary Carbon Stereocenters: Palladium-Catalyzed Decarboxylative Allylic Alkylation of Fully Substituted Amide Enolates. *J*. *Am*. *Chem*. *Soc*. **2017**, *139*, 9615–9620. (b) Alexy, E. J.; Zhang, H.; Stoltz, B. M. Catalytic Enantioselective Synthesis of Acyclic Quaternary Centers: Palladium-Catalyzed Decarboxylative Allylic Alkylation of Fully Substituted Acyclic Enol Carbonates. *J*. *Am*. *Chem*. *Soc*. **2018**, *140*. 10109–10112.

(5) (a) Li, B. X.; Le, D. N.; Mack, K. A.; McClory, A.; Lim, N.-K.; Cravillion, T.; Savage, S.; Han, C.; Collum, D. B.; Zhang, H.; Gosselin, F. Highly Stereoselective Sythesis of Tetrasubstituted Acyclic All-Carbon Olefins via Enol Tosylation and Suzuki–Miyaura Coupling. *J*. *Am*. *Chem*. *Soc*. **2017**, *139*, 10777–10783. (b) Mack, K. A.; McClory, A.; Zhang, H.; Gosselin, F.; Collum, D. B. Lithium Hexamethyldisilazide-Mediated Enolization of Highly Substituted Aryl Ketones: Structural and Mechanistic Basis of the *E*/*Z* Selectivities. *J*. *Am*. *Chem*. *Soc*. **2017**, *139*, 12182–12189.

(6) (a) Trost, B. M.; Xu, J.; Schmidt, T. Palladium-Catalyzed Decarboxylative Asymmetric Allylic Alkylation of Enol Carbonates. *J*. *Am*. *Chem*. *Soc*. **2009**, *131*, 18343–18357. (b) Ariyarathna, Y.; Tunge, J. A. Decarboxylative allylations of ester enolate equivalents. *Org*. *Biomol*. *Chem*. **2014**, *12*, 8386–8389.

(7) (a) Trost, B. M.; Lehr, K.; Michaelis, D. J.; Xu, J.; Buckl, A. K. Palladium-Catalyzed Asymmetric Allylic Alkylation of 2-Acylimidazoles as Ester Enolate Equivalents. *J*. *Am*. *Chem*. *Soc*. **2010**, *132*, 8915–8917. (b) Trost, B. M.; Michaelis, D. J.; Charpentier, J.; Xu, J. Palladium-Catalyzed Allylic Alkylation of Carboxylic Acid Derivatives: *N*-Acyloxazolinones as Ester Enolate Equivalents. *Angew*. *Chem*. *Int*. *Ed*. **2012**, *51*, 204–208.

(8) Fujita, T.; Yamamoto, T.; Morita, Y.; Chen, H.; Shimizu, Y.; Kanai, M. Chemo- and Enantioselective Pd/B Hybrid Catalysis for the Construction of Acyclic Quaternary Carbons: Migratory Allylation of *O*-Allyl Esters to α-*C*-Allyl Carboxylic Acids. *J*. *Am*. *Chem*. *Soc*. **2018**, *140*, 5899–5903.

(9) (a) Turnbull, B. W. H.; Evans, P. A. Enantioselective Rhodium-Catalyzed Allylic Substitution with a Nitrile Anion: Construction of Acyclic Quaternary Carbon Stereogenic Centers. *J*. *Am*. *Chem*. *Soc*. **2015**, *137*, 6156–6159. (b) Wright, T. B.; Evans, P. A. Enantioselective Rhodium-Catalyzed Allylic Alkylation of Prochiral α,α-Disubstituted Aldehyde Enolates for the Construction of Acyclic Quaternary Stereogenic Centers. *J*. *Am*. *Chem*. *Soc*. **2016**, *138*, 15303–15306. for stereoretentive examples, see: (c) Evans, P. A.; Oliver, S.; Chae, J. *J*. *Am*. *Chem*. *Soc*. Rhodium-Catalyzed Allylic Substitution with an Acyl Anion Equivalent: Stereospecific Construction of Acyclic Quaternary Carbon Stereogenic Centers. **2012**, *134*, 19314–19317. (d) Evans, P. A.; Oliver, S. Regio- and Enantiospecific Rhodium-Catalyzed Allylic Substitution with an Acyl Anion Equivalent. *Org*. *Lett*.

2013, *15*, 5626–5629. (e) Turnbull, B. W. H.; Oliver, S.; Evans, P. A. Stereospecific Rhodium-Catalyzed Allylic Substitution with Alkenyl Cyanohydrin Pronucleophiles: Construction of Acyclic Quaternary Substituted α,β-Unsaturated Ketones. *J. Am. Chem. Soc.* **2015**, *137*, 15374–15377.

(10) (b) Liu, W. -B. Reeves, C. M.; Stoltz, B. M. Enantio-, Diastereo-, and Regioselective Iridium-Catalyzed Asymmetric Allylic Alkylation of Acyclic β-Ketoesters. *J. Am. Chem. Soc.* **2013**, *135*, 17298–17301. (b) Shockley, S.; Hethcox, J. C.; Stoltz, B. M. Enantioselective Synthesis of Acyclic α-Quaternary Carboxylic Acid Derivatives through Iridium-Catalyzed Allylic Alkylation. *Angew. Chem. Int. Ed.* **2017**, *56*, 11545–11548. (c) Hethcox, J. C.; Shockley, S.; Stoltz, B. M. Enantioselective Synthesis of Vicinal All-Carbon Quaternary Centers via Iridium-Catalyzed Allylic Alkylation. *Angew. Chem. Int. Ed.* **2018**, *57*, 8664–8667.

(11) (a) Pritchett, B. P.; Donckele, E. J.; Stoltz, B. M. Enantioselective Catalysis Coupled with Stereodivergent Cyclization Strategies Enables Rapid Syntheses of (+)-Limaspermidine and Kopsihainanine A. *Angew. Chem. Int. Ed.* **2017**, *56*, 12624–12627. (b) Pritchett, B. P.; Kikuchi, J.; Numajiri, Y.; Stoltz, B. M. Enantioselective Pd-Catalyzed Allylic Alkylation Reactions of Dihydropyrido[1,2-*a*]indolone Substrates: Efficient Syntheses of (–)-Goniomitine, (+)-Aspidospermidine, and (–)-Quebrachamine. *Angew. Chem. Int. Ed.* **2016**, *55*, 13529–13532.

(12) Hammett, L. P. The Effect of Structure upon the Reactions of Organic Compounds. Benzene Derivatives. *J. Am. Chem. Soc*. **1937**, *59*, 96–103.

(13) The *N*-acyl pyrrole substrate provides the *o*-Me product in 80% ee.

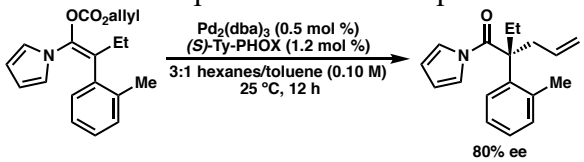

(14) Pangborn, A. B.; Giardello, M. A.; Grubbs, R. H.; Rosen, R. K.; Timmers, F. J. Safe and Convenient Procedure for Solvent Purification. *Organometallics* **1996**, *15*, 1518–1520.

(15) McDougal, N. T.; Streuff, J.; Mukherjee, H.; Virgil, S. C.; Stoltz, B. M. Rapid synthesis of an electron-deficient *t*-BuPHOX ligand: cross-coupling of aryl bromides with secondary phosphine oxides. *Tetrahedron Lett*. **2010**, *51*, 5550–5554.

APPENDIX 3

Spectra Relevant to Chapter 2:

Pd-Catalyzed Asymmetric Decarboxylative Allylic Alkylation of Fully Substituted N-Acyl Indole-Derived Enol Carbonates

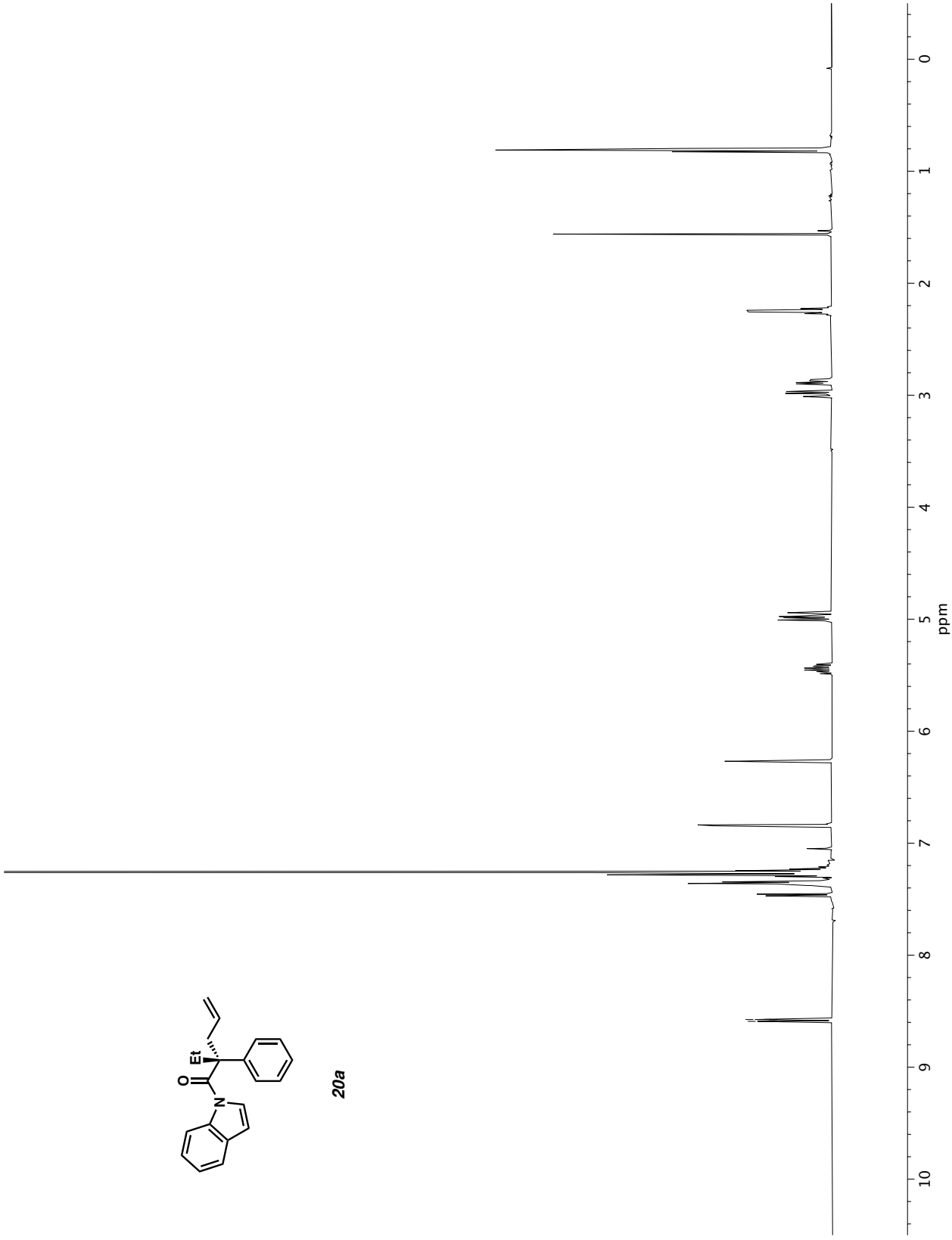

Figure A3.1 *^1H NMR (500 MHz, $CDCl_3$) of compound* ***20a****.*

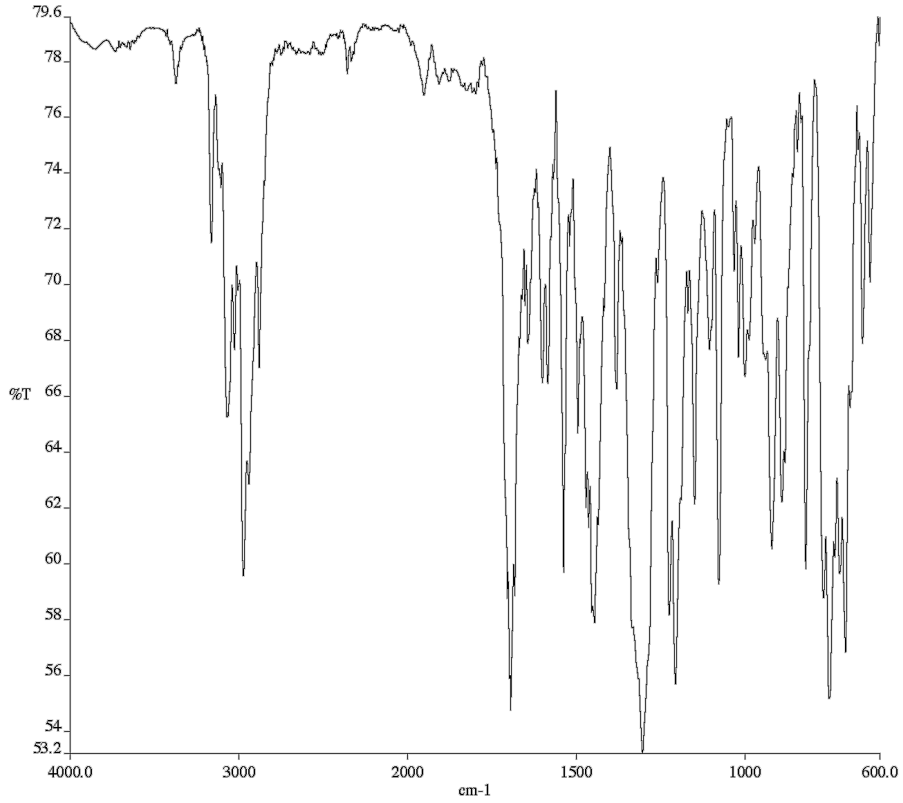

Figure A3.2 *Infrared spectrum (Thin Film, NaCl) of compound* ***20a****.*

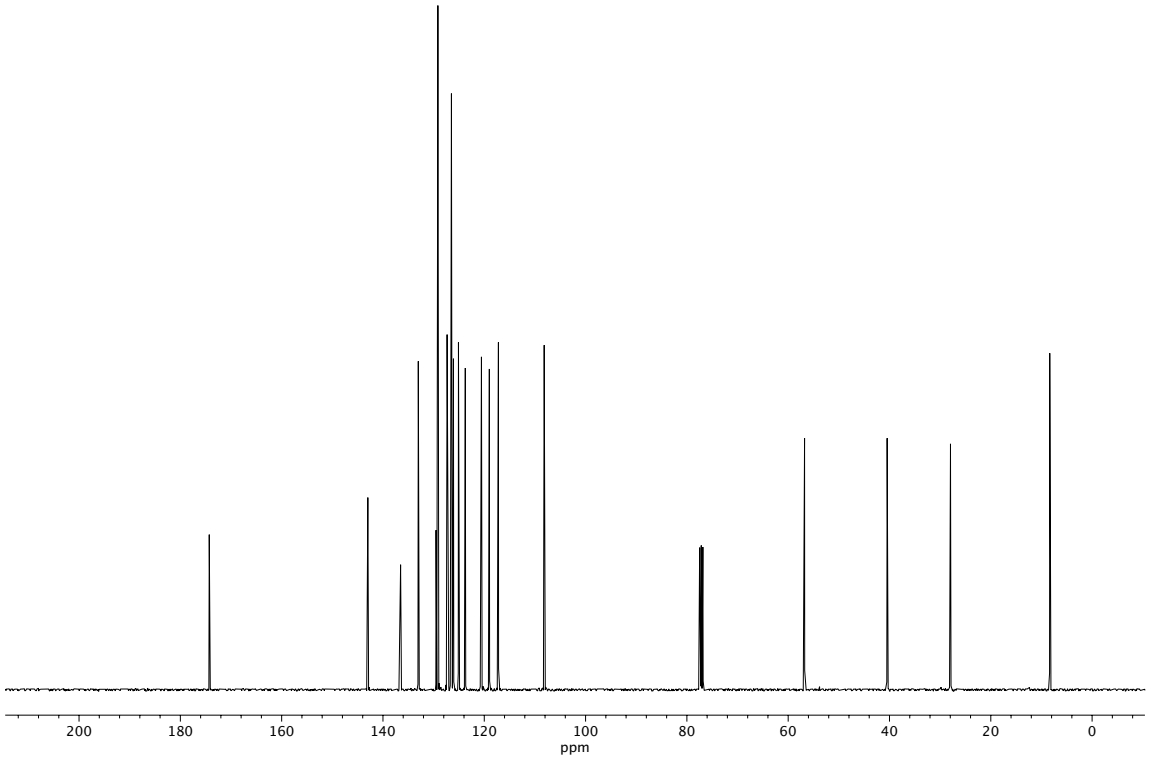

Figure A3.3 *^{13}C NMR (100 MHz, $CDCl_3$) of compound* ***20a****.*

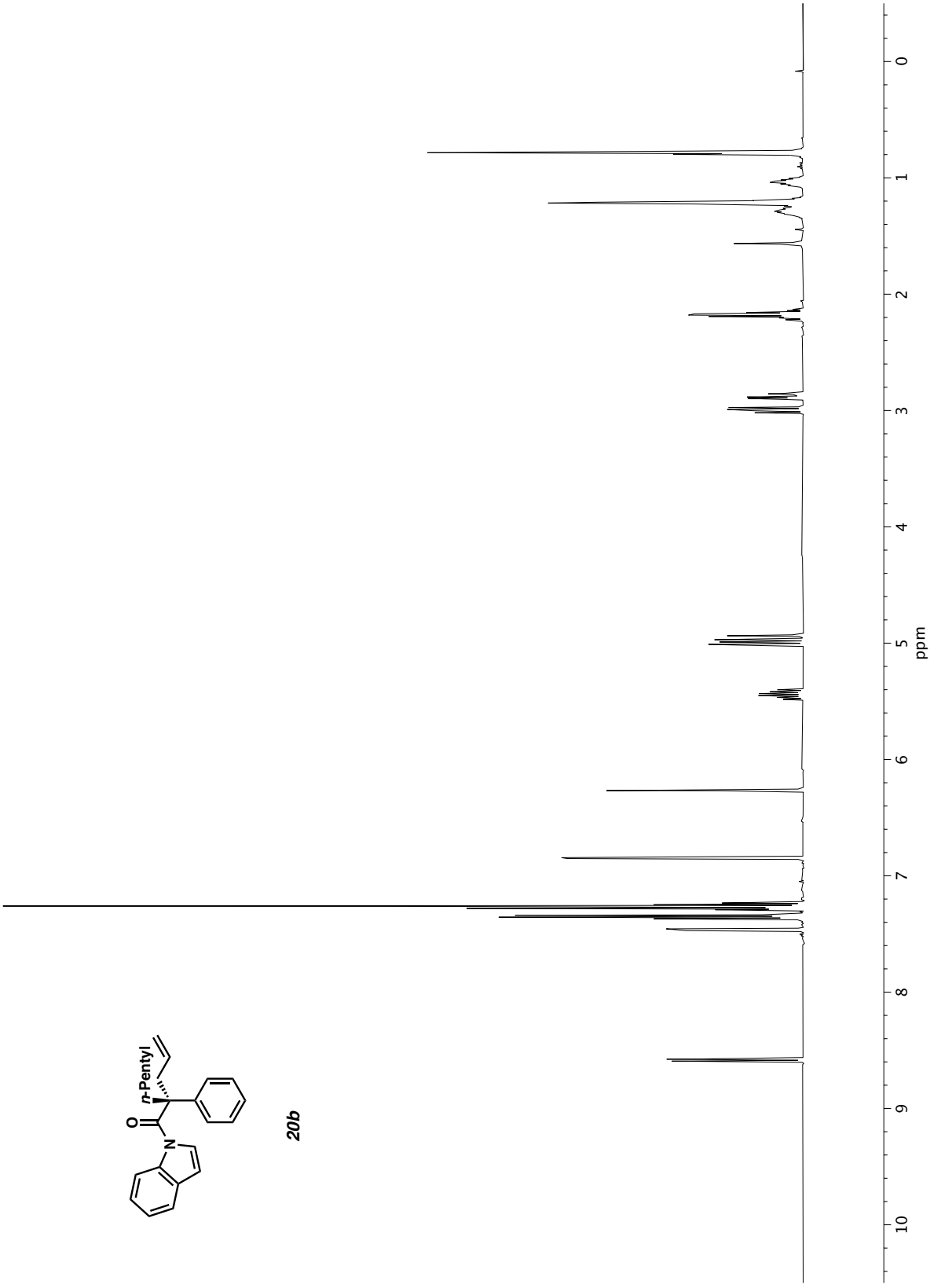

Figure A3.4 *^1H NMR (500 MHz, $CDCl_3$) of compound* ***20b****.*

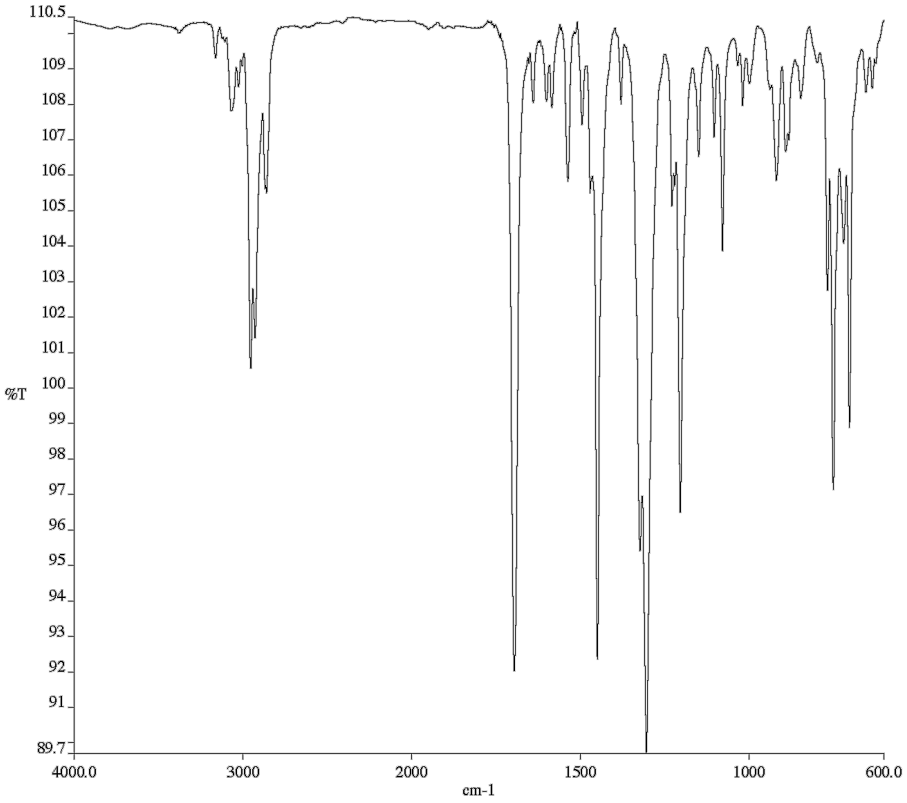

Figure A3.5 *Infrared spectrum (Thin Film, NaCl) of compound* ***20b****.*

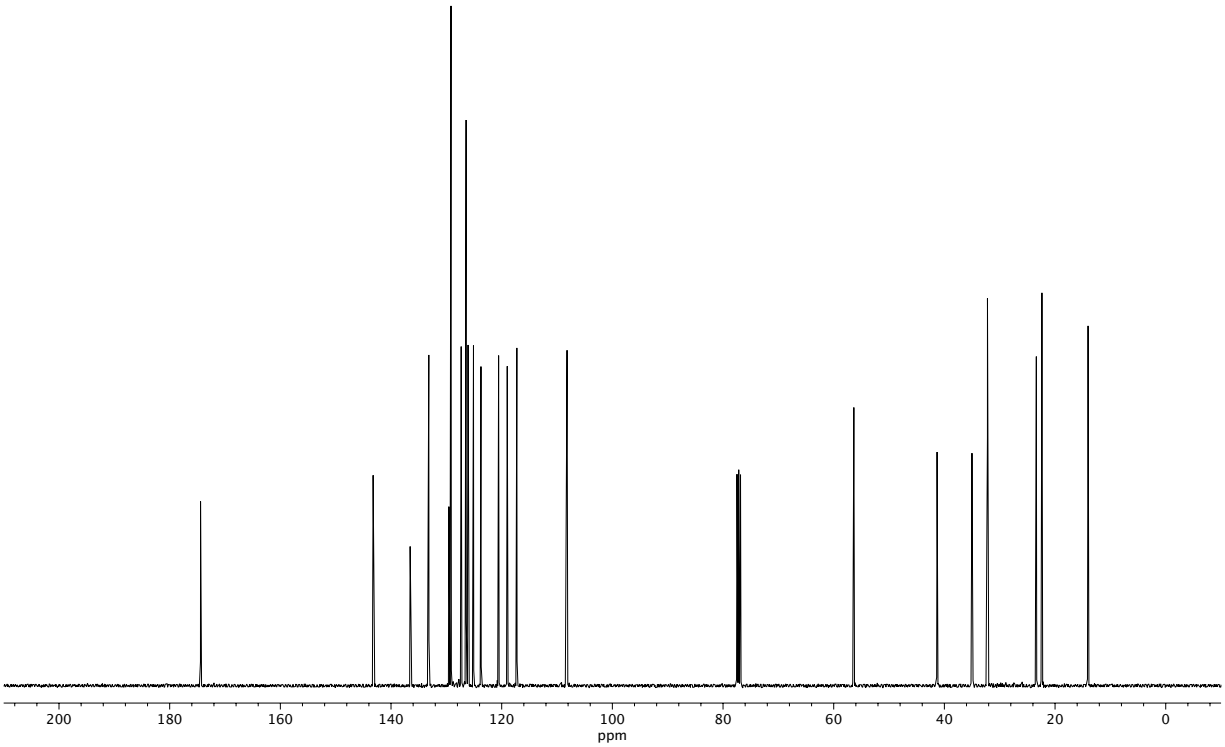

Figure A3.6 *^{13}C NMR (100 MHz, $CDCl_3$) of compound* ***20b****.*

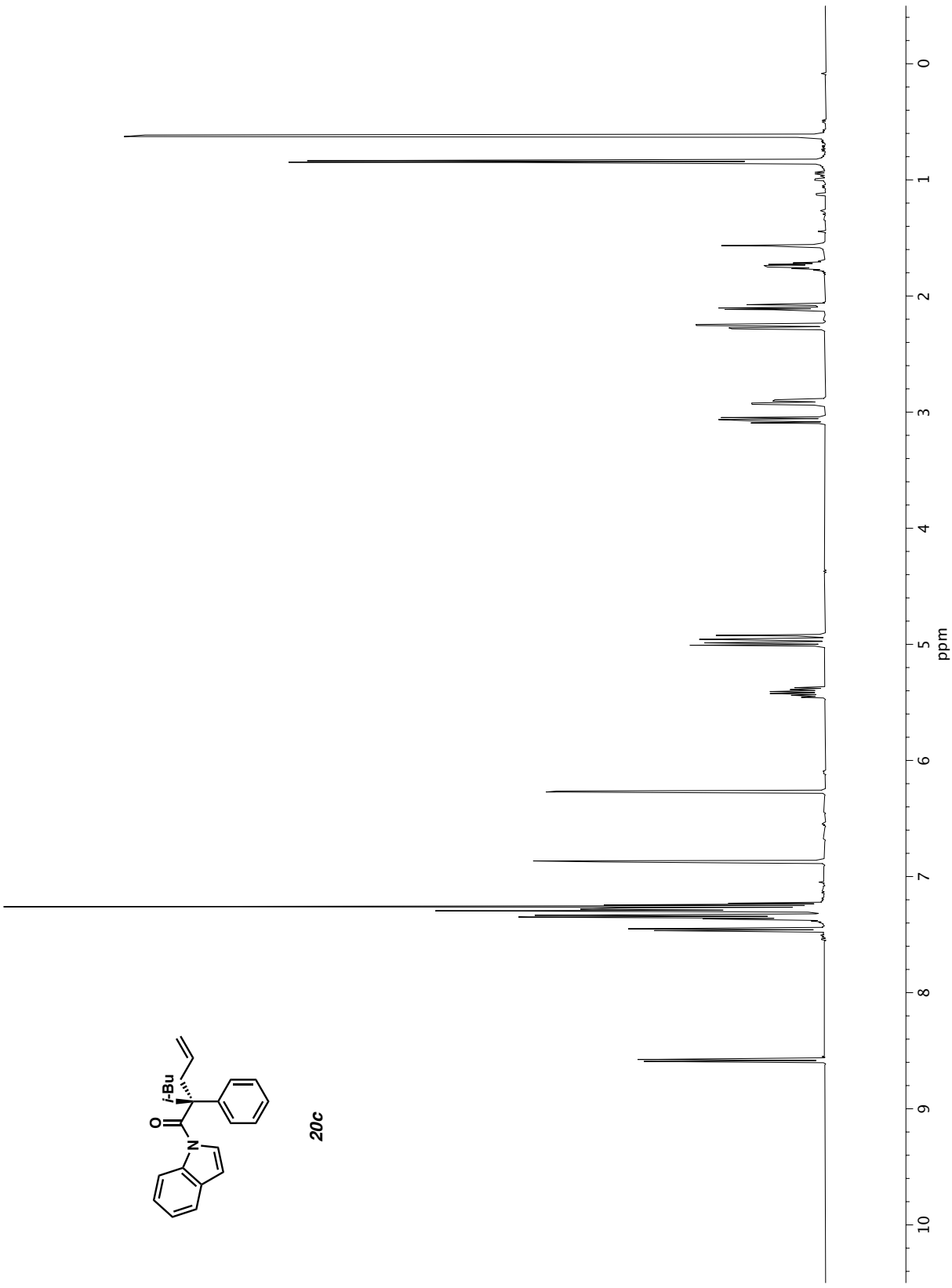

Figure A3.7 *^1H NMR (500 MHz, $CDCl_3$) of compound* ***20c****.*

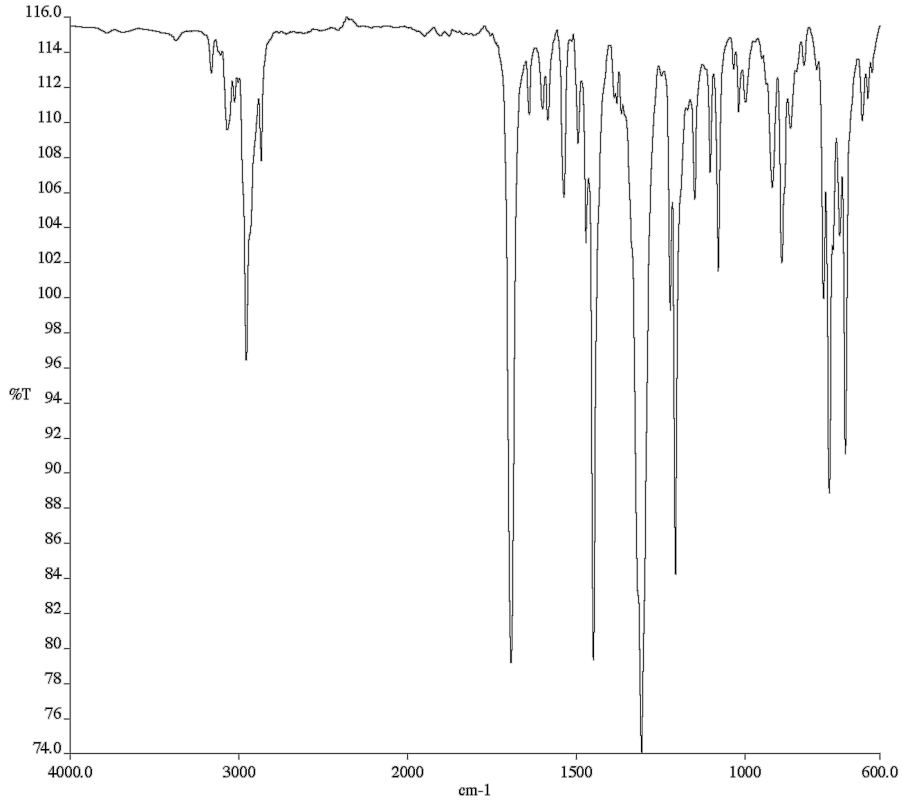

Figure A3.8 *Infrared spectrum (Thin Film, NaCl) of compound* ***20c****.*

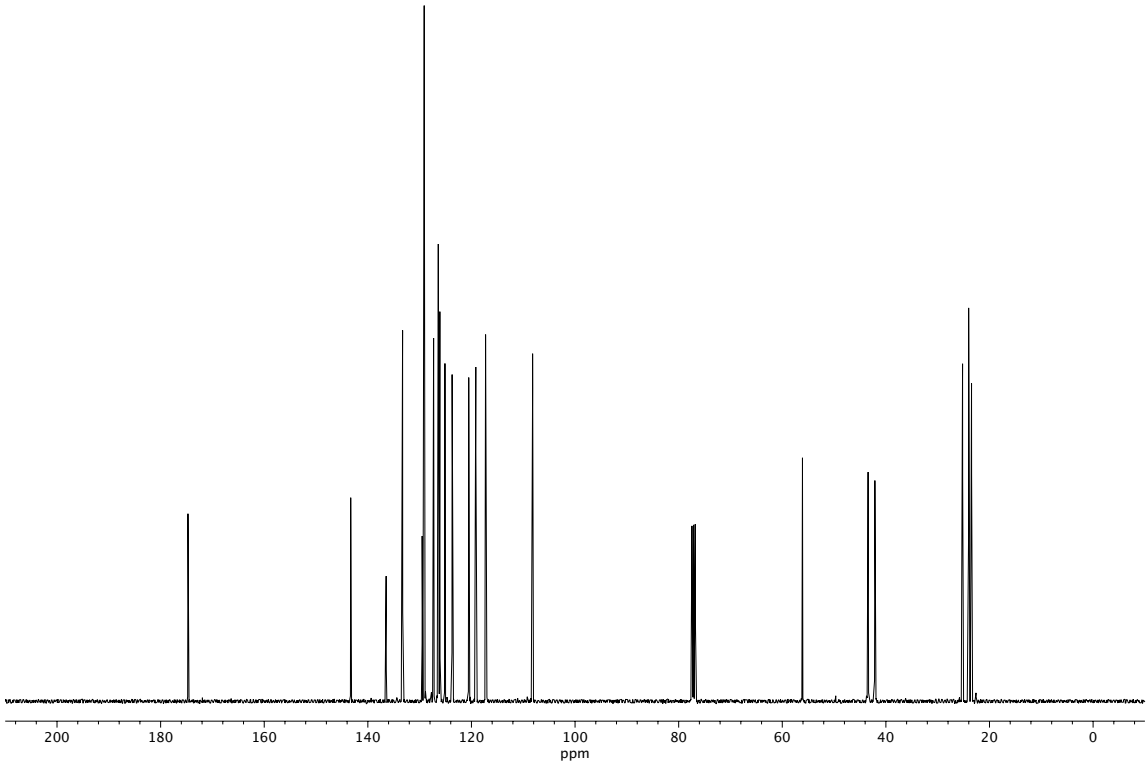

Figure A3.9 *^{13}C NMR (100 MHz, $CDCl_3$) of compound* ***20c****.*

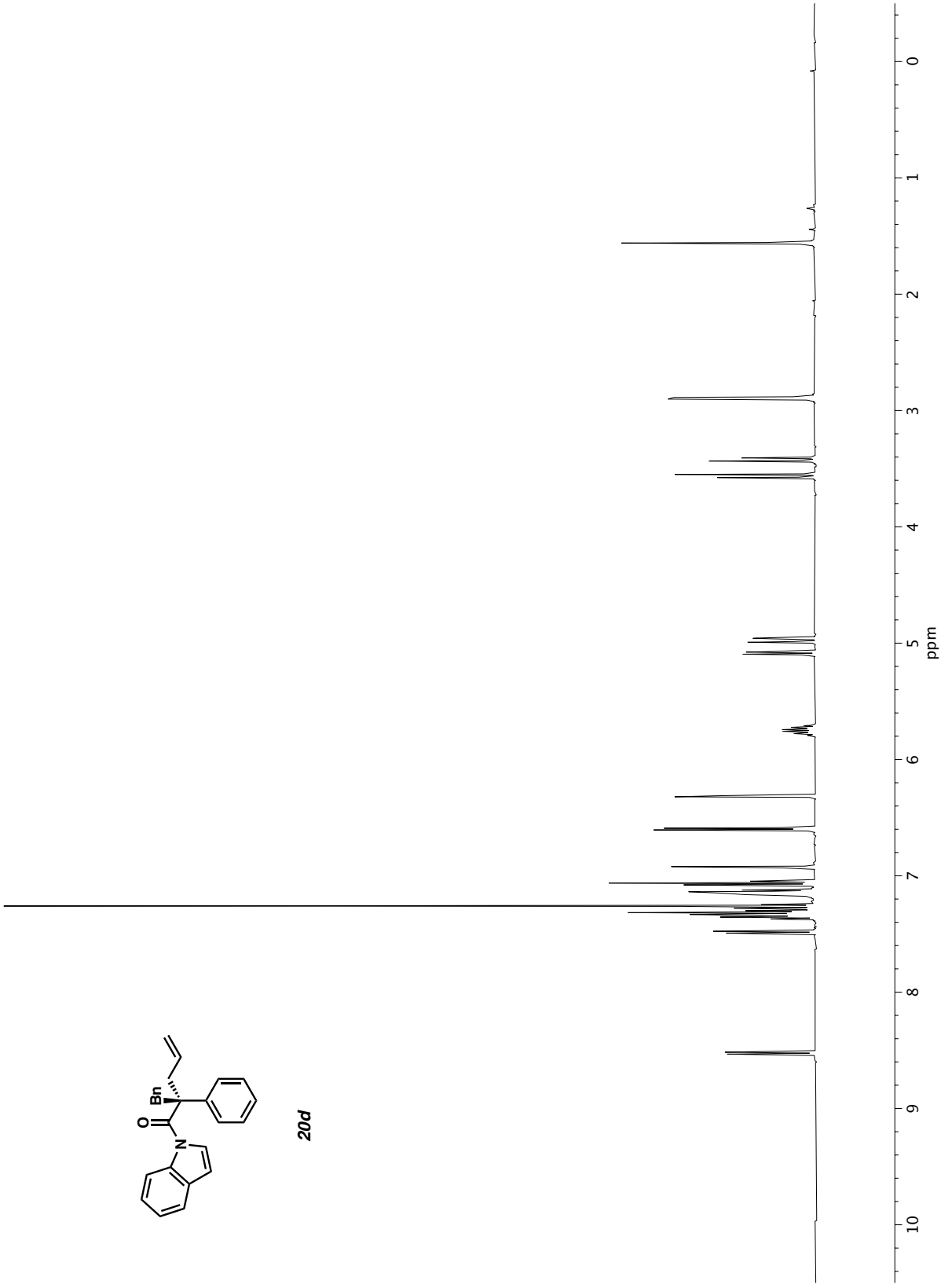

Figure A3.10 *^{1}H NMR (500 MHz, $CDCl_3$) of compound* ***20d****.*

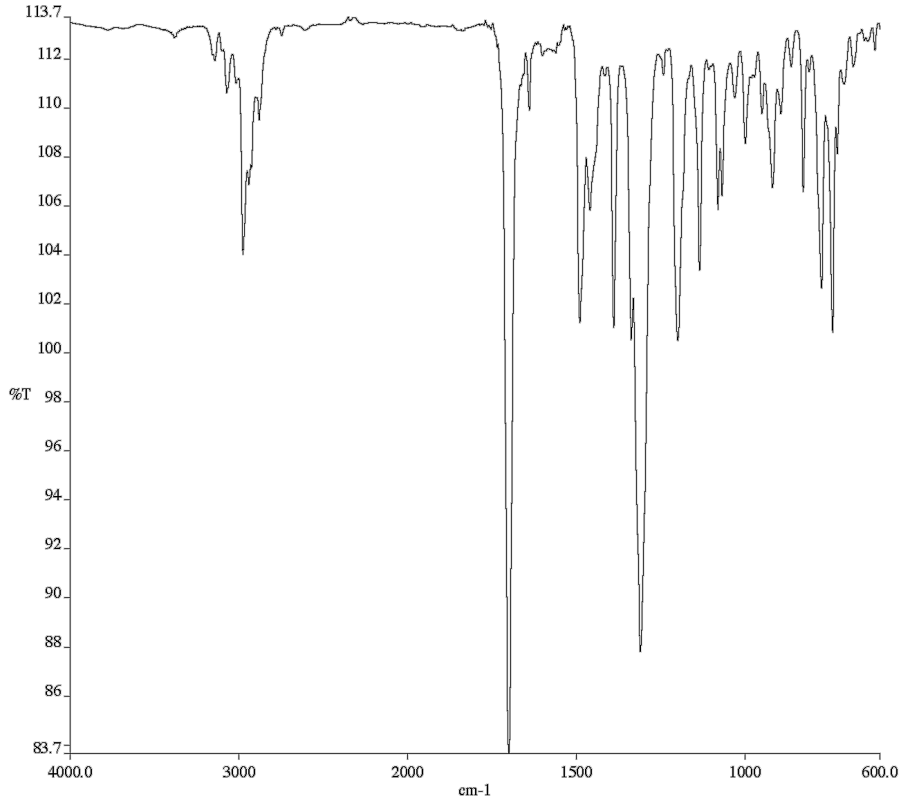

Figure A3.11 *Infrared spectrum (Thin Film, NaCl) of compound* ***20d****.*

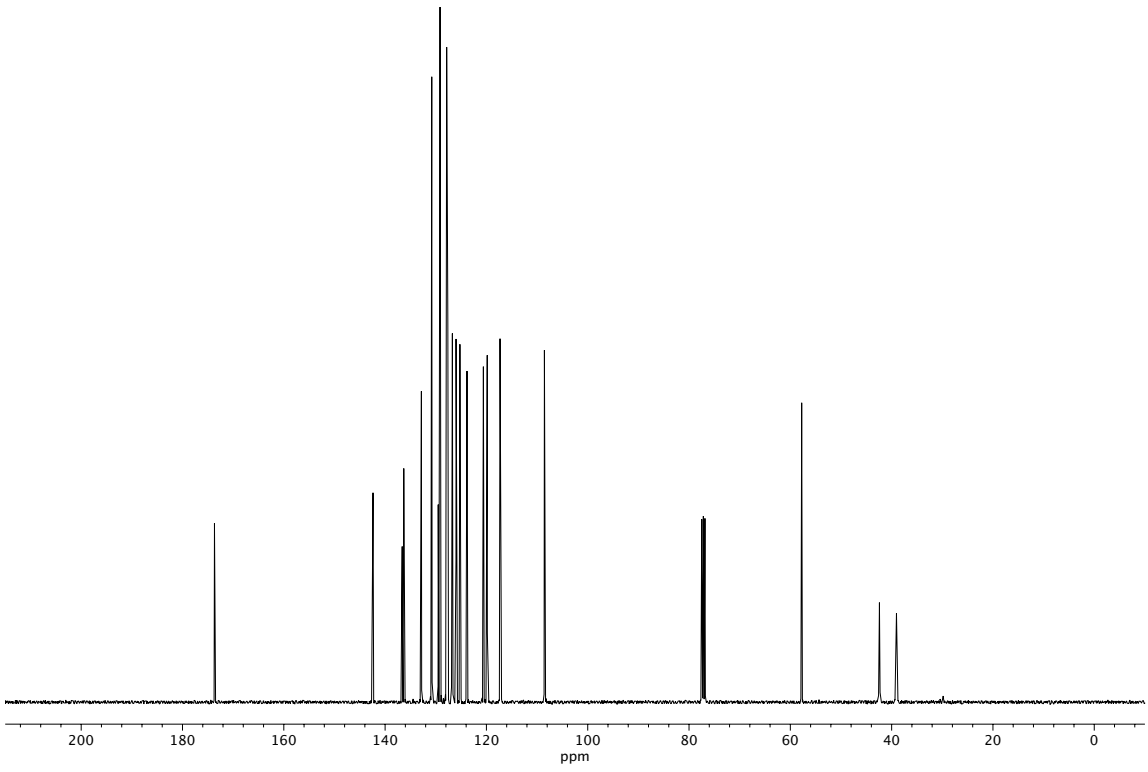

Figure A3.12 *^{13}C NMR (100 MHz, $CDCl_3$) of compound* ***20d****.*

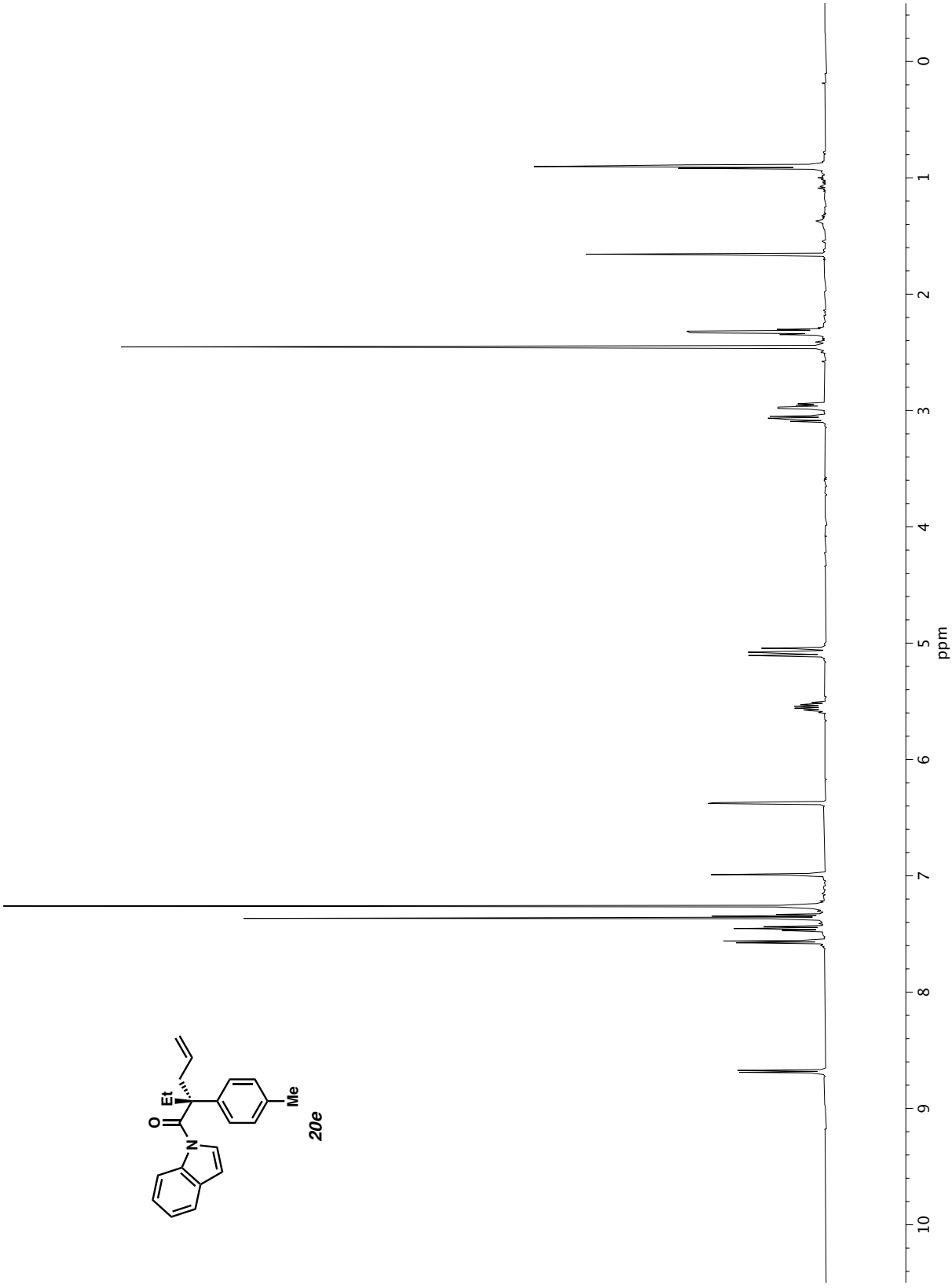

Figure A3.13 *^1H NMR (500 MHz, $CDCl_3$) of compound* ***20e****.*

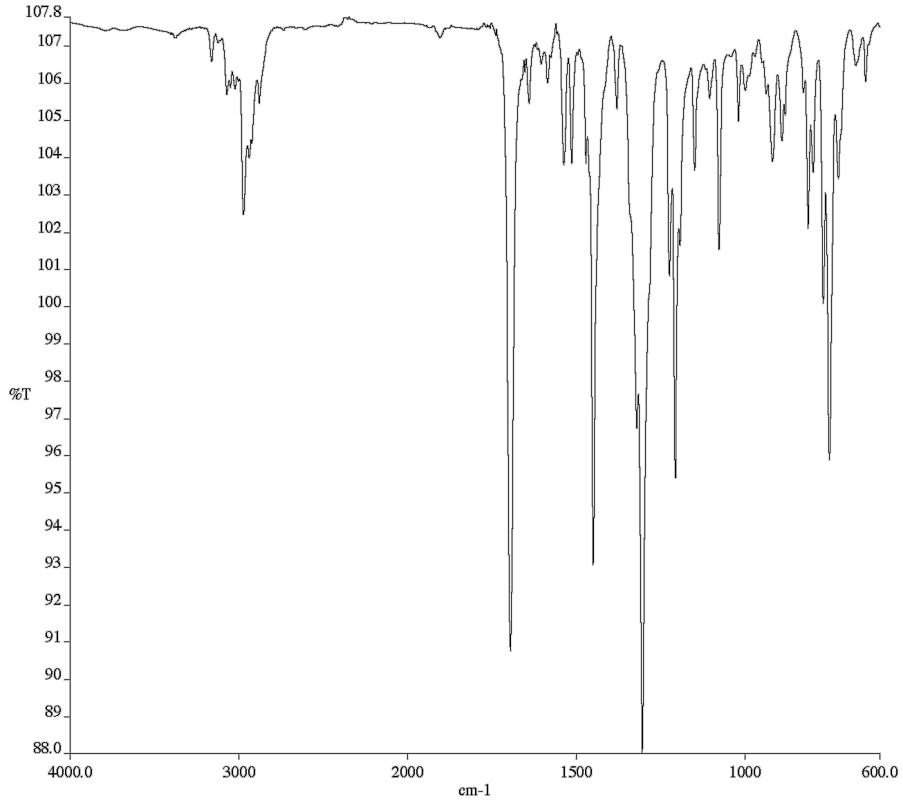

Figure A3.14 *Infrared spectrum (Thin Film, NaCl) of compound* ***20e****.*

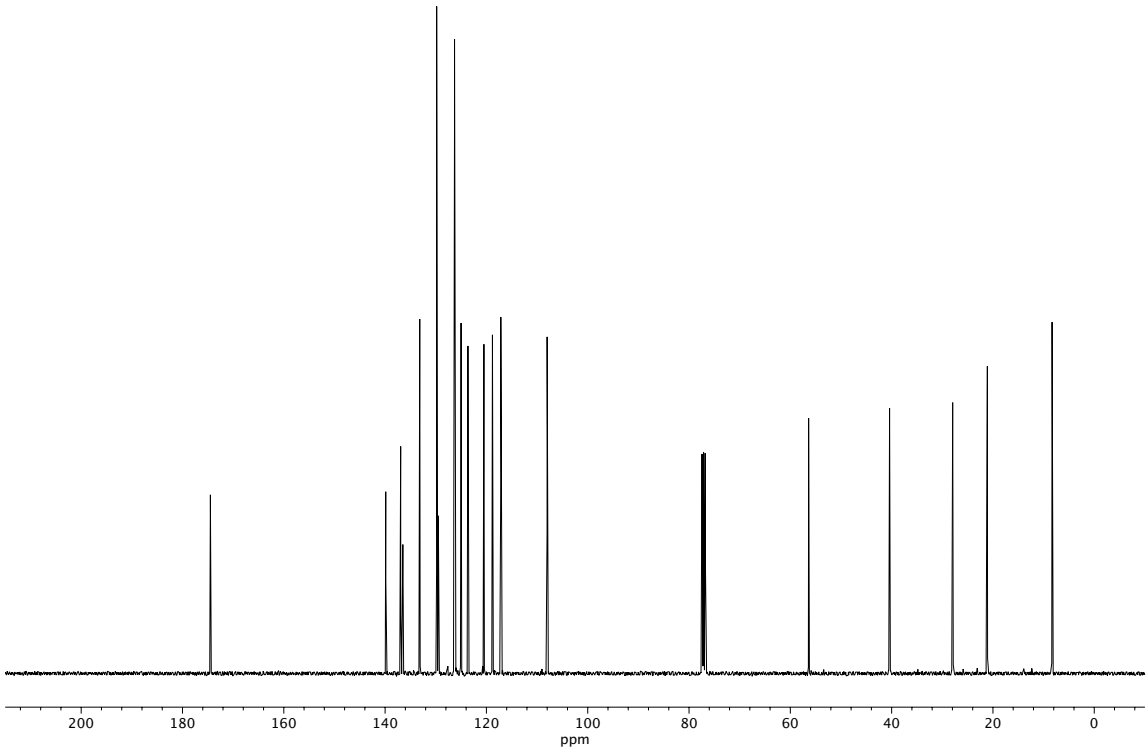

Figure A3.15 *^{13}C NMR (100 MHz, $CDCl_3$) of compound* ***20e****.*

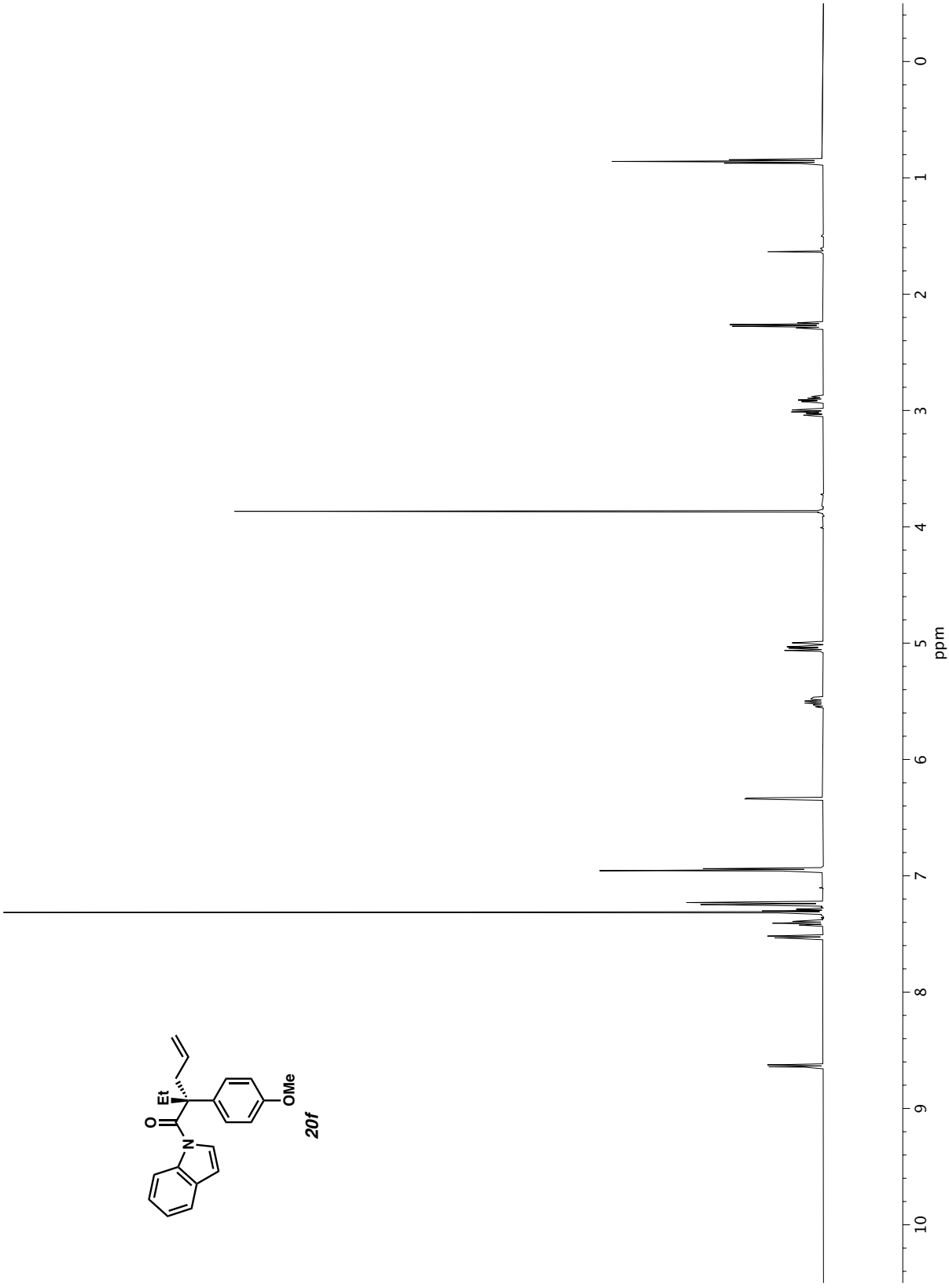

Figure A3.16 *^{1}H NMR (500 MHz, $CDCl_3$) of compound* ***20f****.*

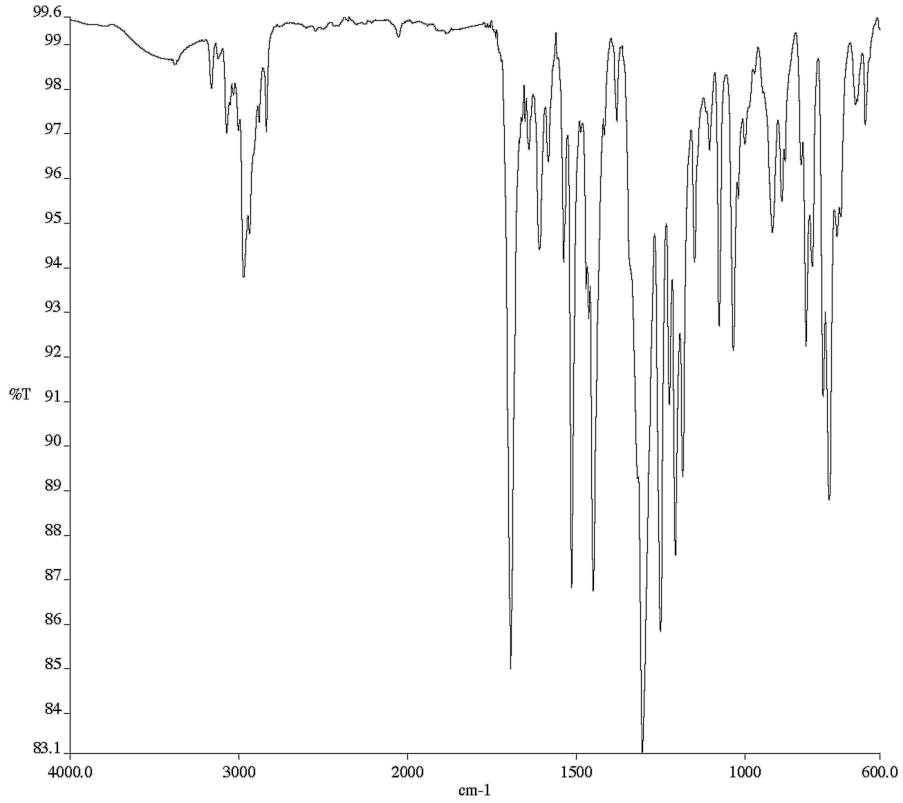

Figure A3.17 *Infrared spectrum (Thin Film, NaCl) of compound* ***20f****.*

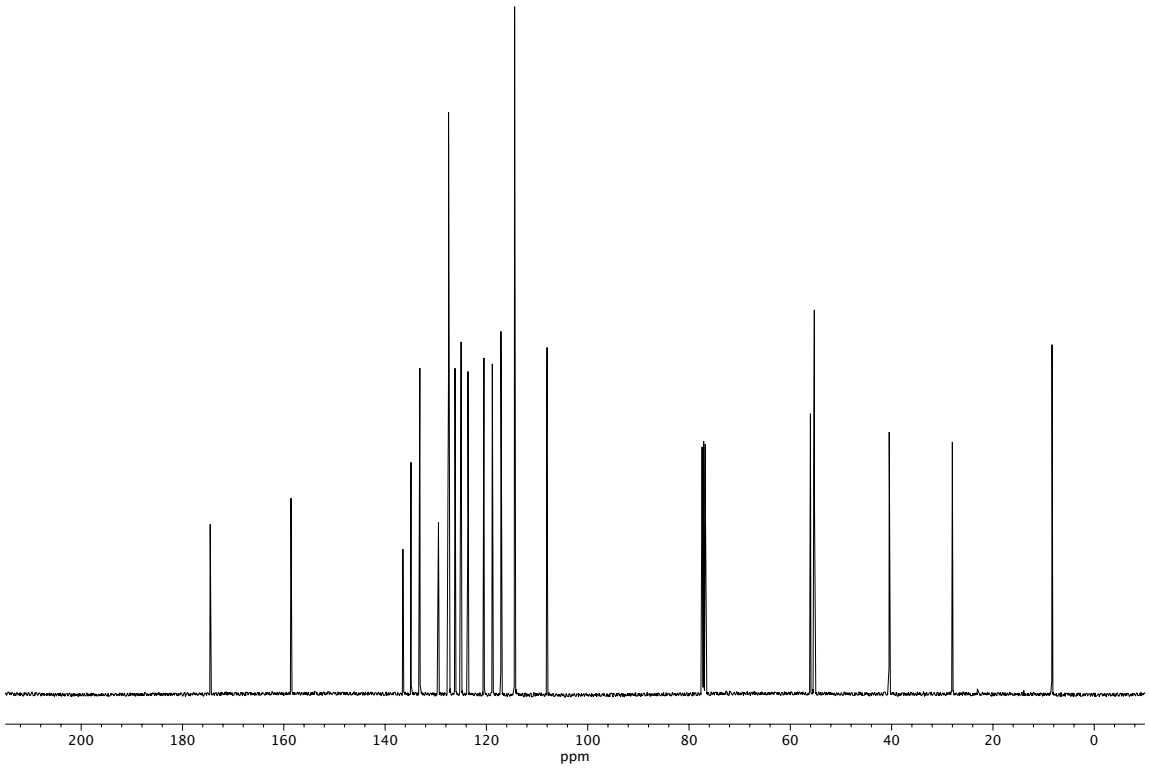

Figure A3.18 *^{13}C NMR (100 MHz, $CDCl_3$) of compound* ***20f****.*

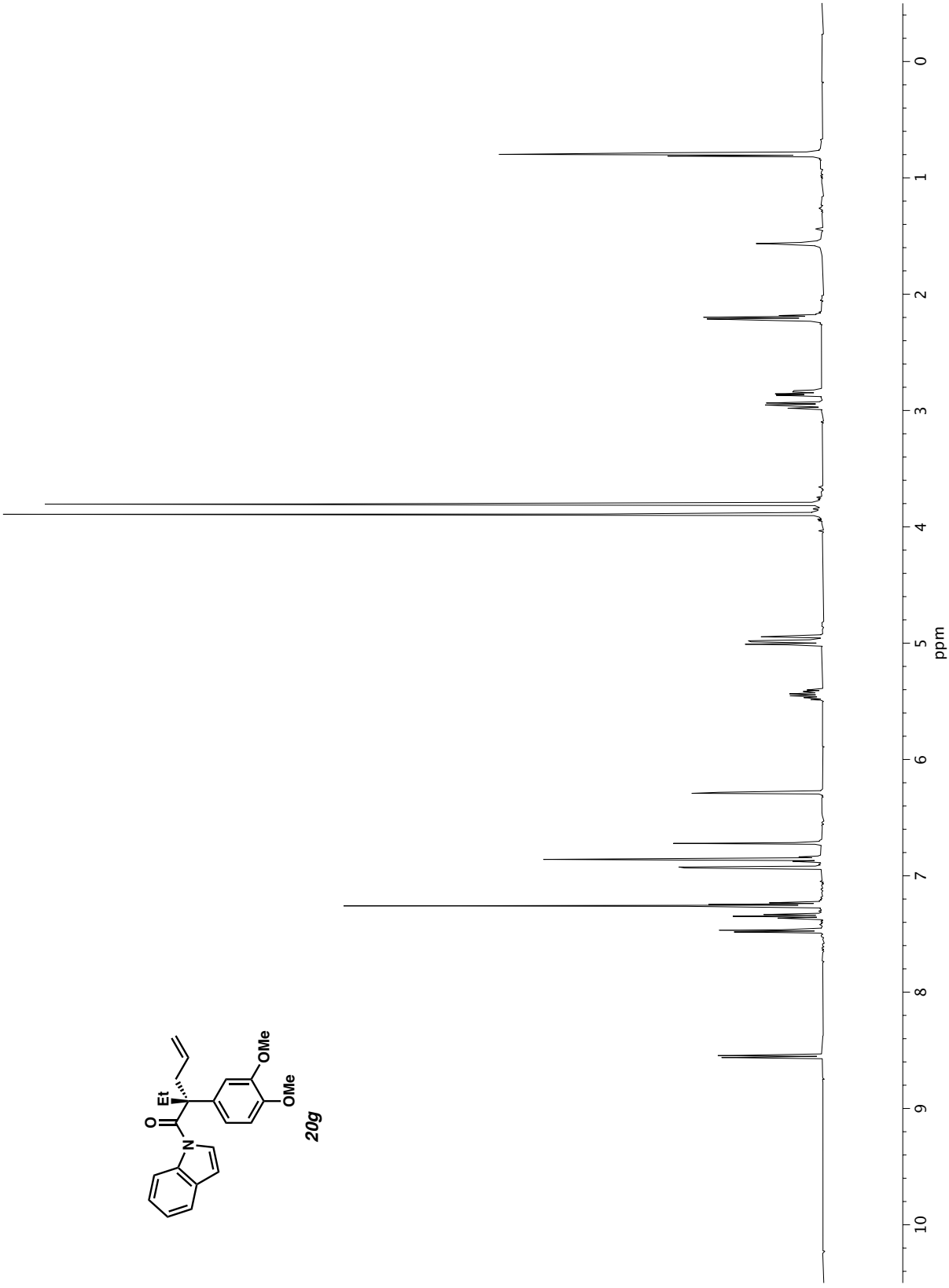

Figure A3.19 *^1H NMR (500 MHz, $CDCl_3$) of compound* ***20g****.*

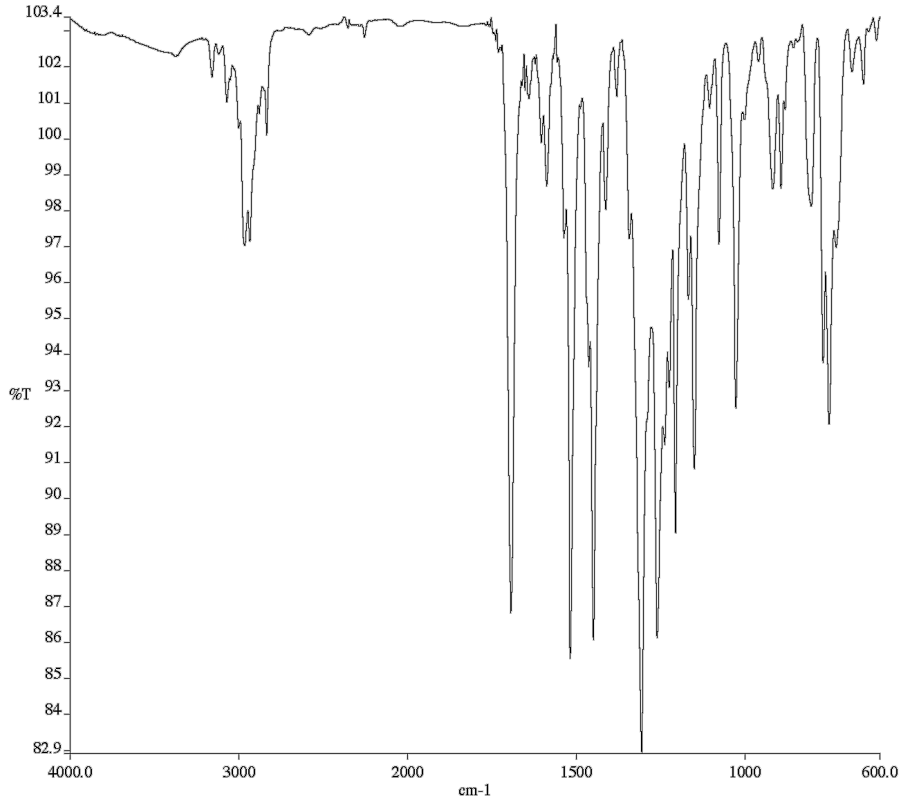

Figure A3.20 *Infrared spectrum (Thin Film, NaCl) of compound* ***20g****.*

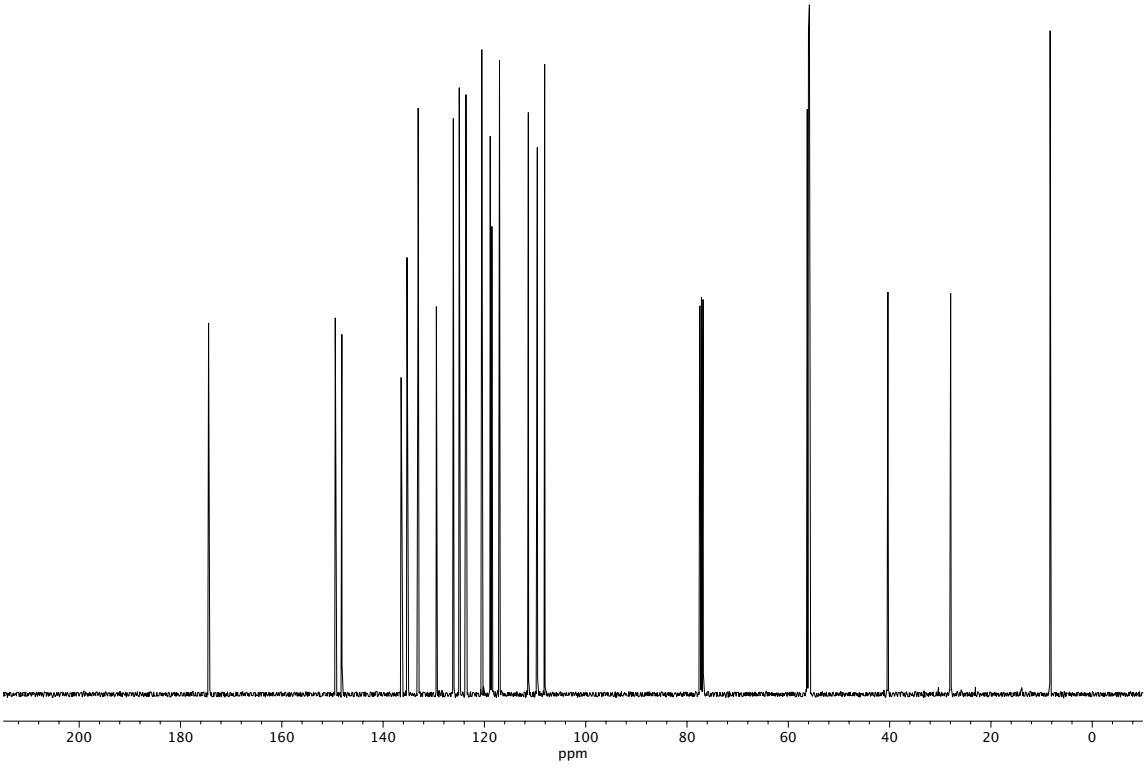

Figure A3.21 *^{13}C NMR (100 MHz, $CDCl_3$) of compound* ***20g****.*

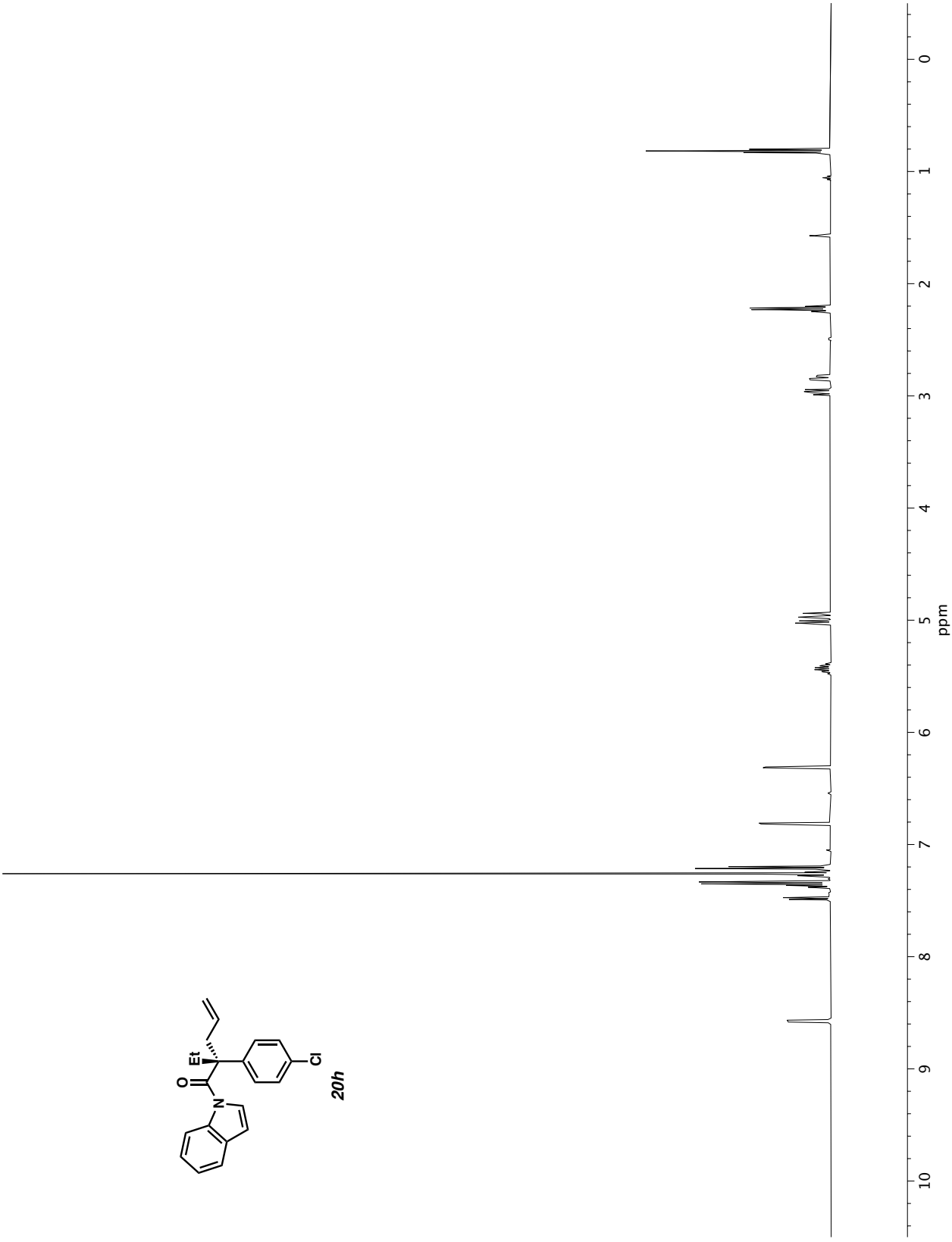

Figure A3.22 *^1H NMR (500 MHz, $CDCl_3$) of compound* ***20h****.*

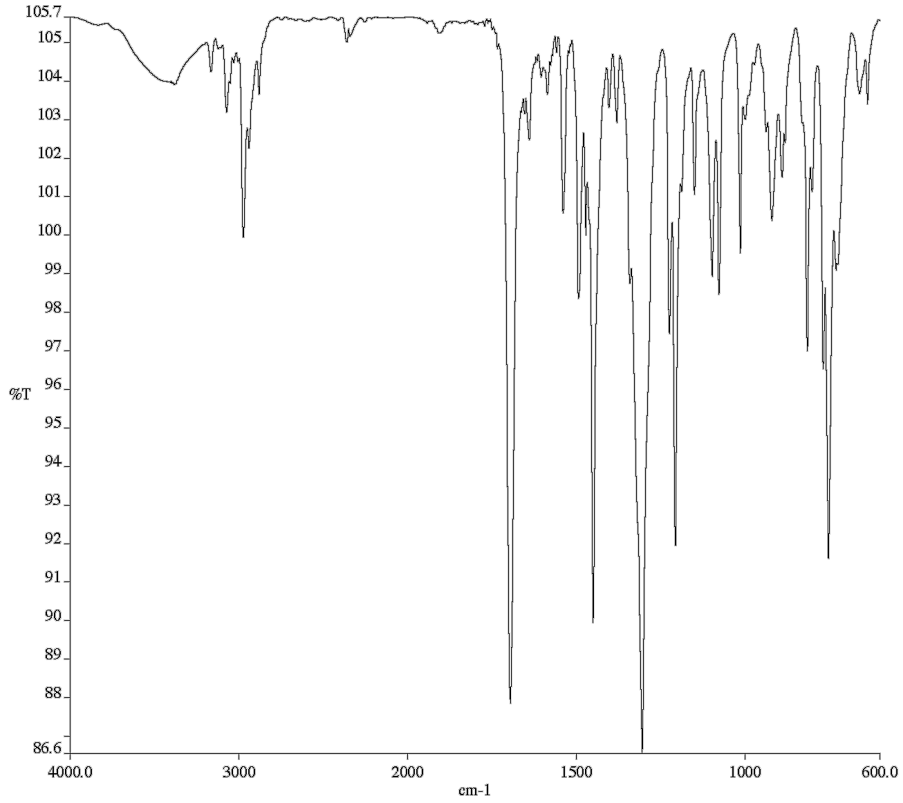

Figure A3.23 *Infrared spectrum (Thin Film, NaCl) of compound* ***20h****.*

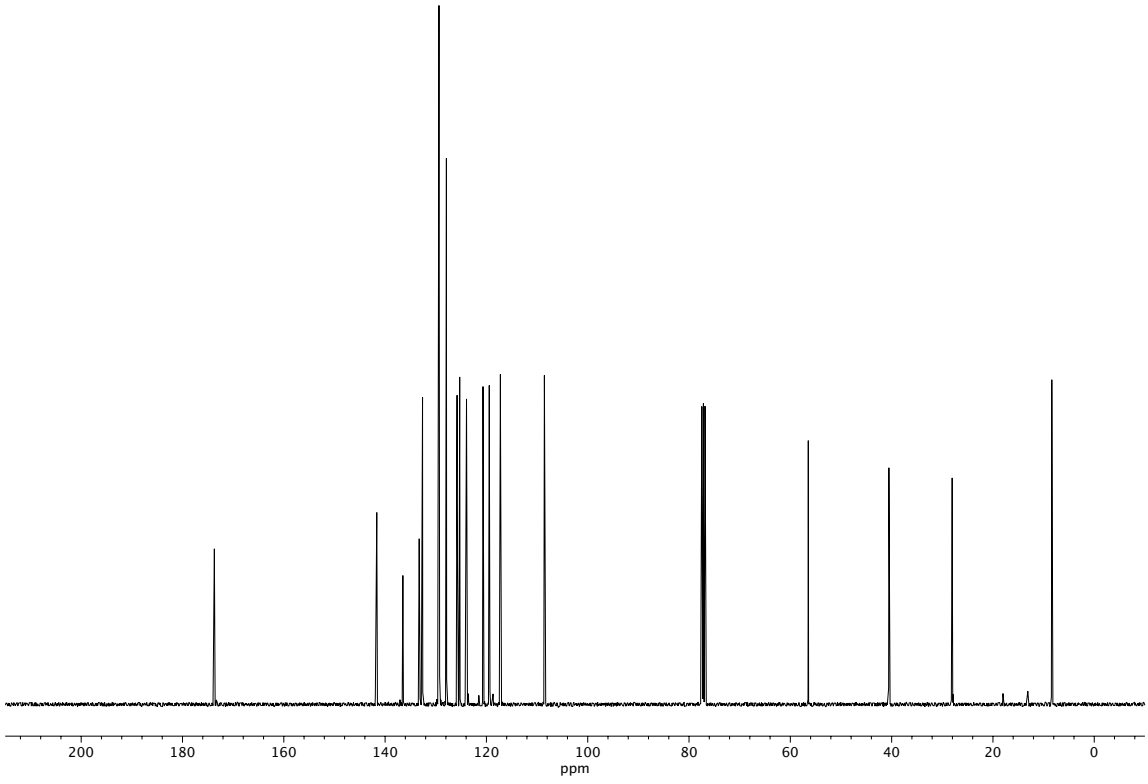

Figure A3.24 *^{13}C NMR (100 MHz, $CDCl_3$) of compound* ***20h****.*

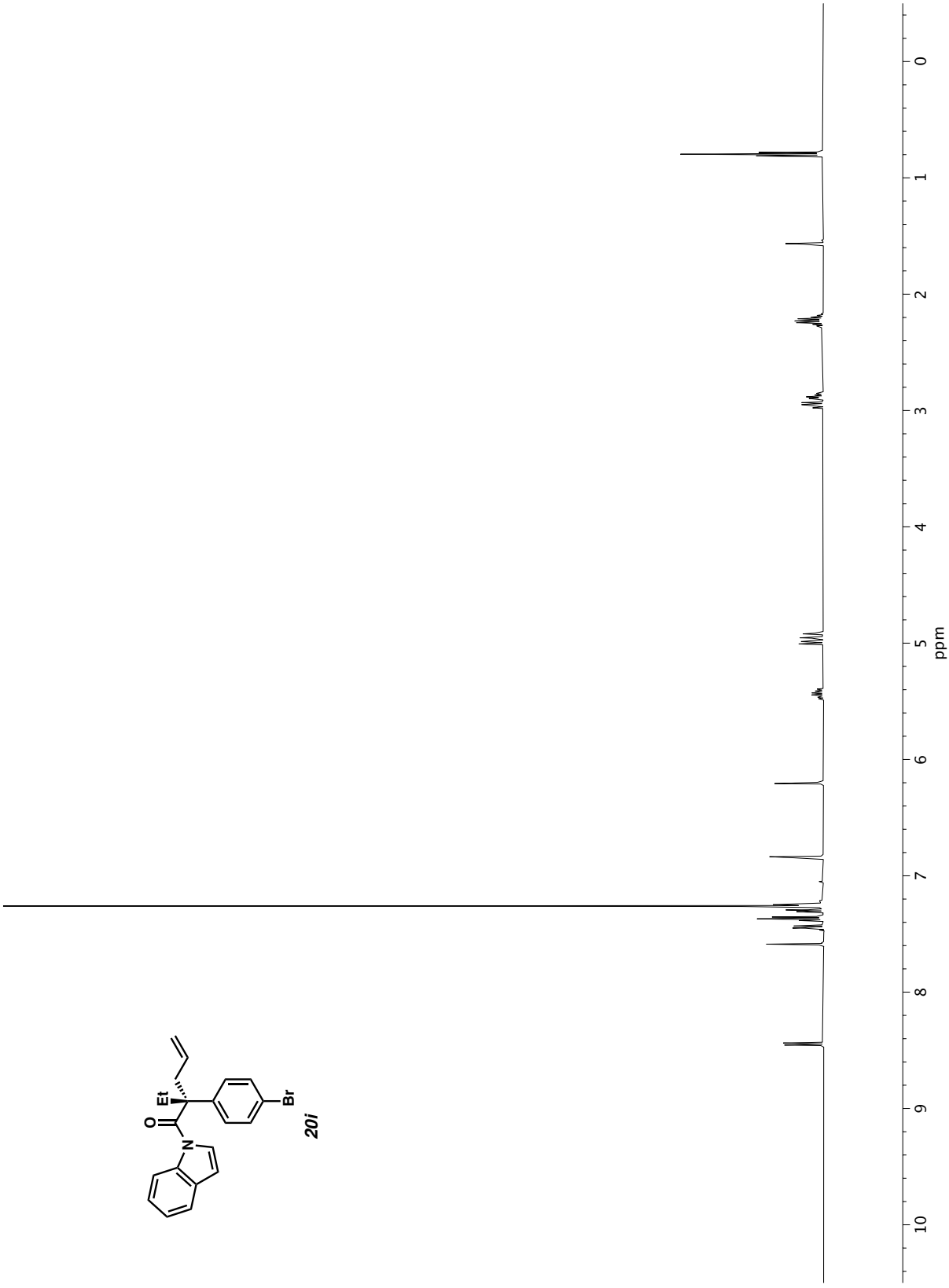

***Figure A3.25** ^1H NMR (500 MHz, $CDCl_3$) of compound **20i**.*

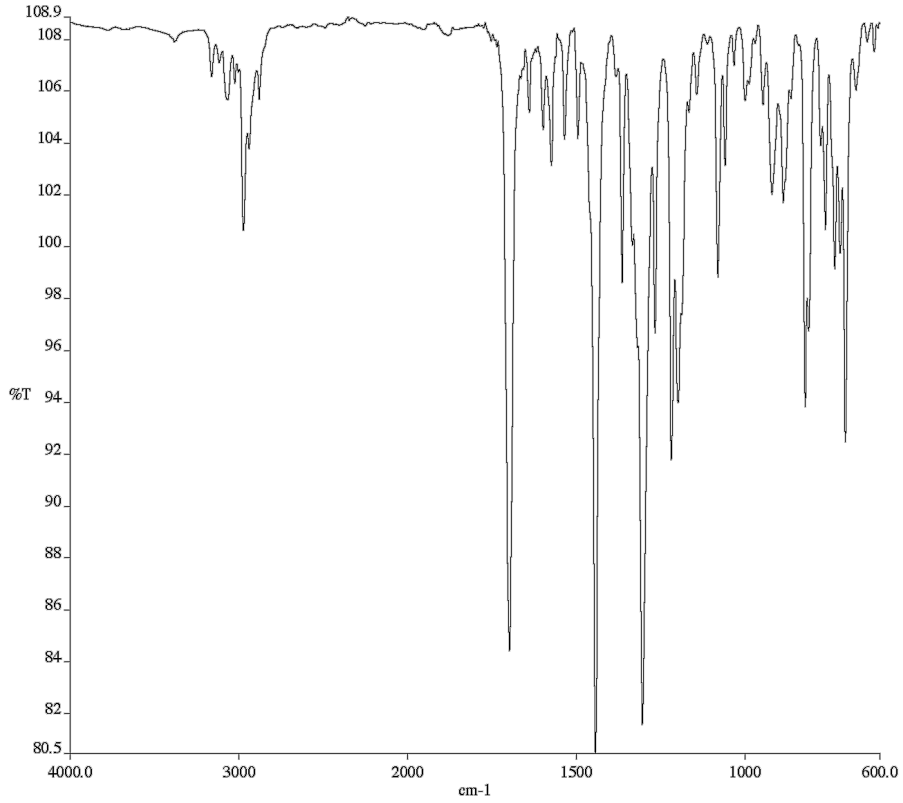

Figure A3.26 *Infrared spectrum (Thin Film, NaCl) of compound* ***20i****.*

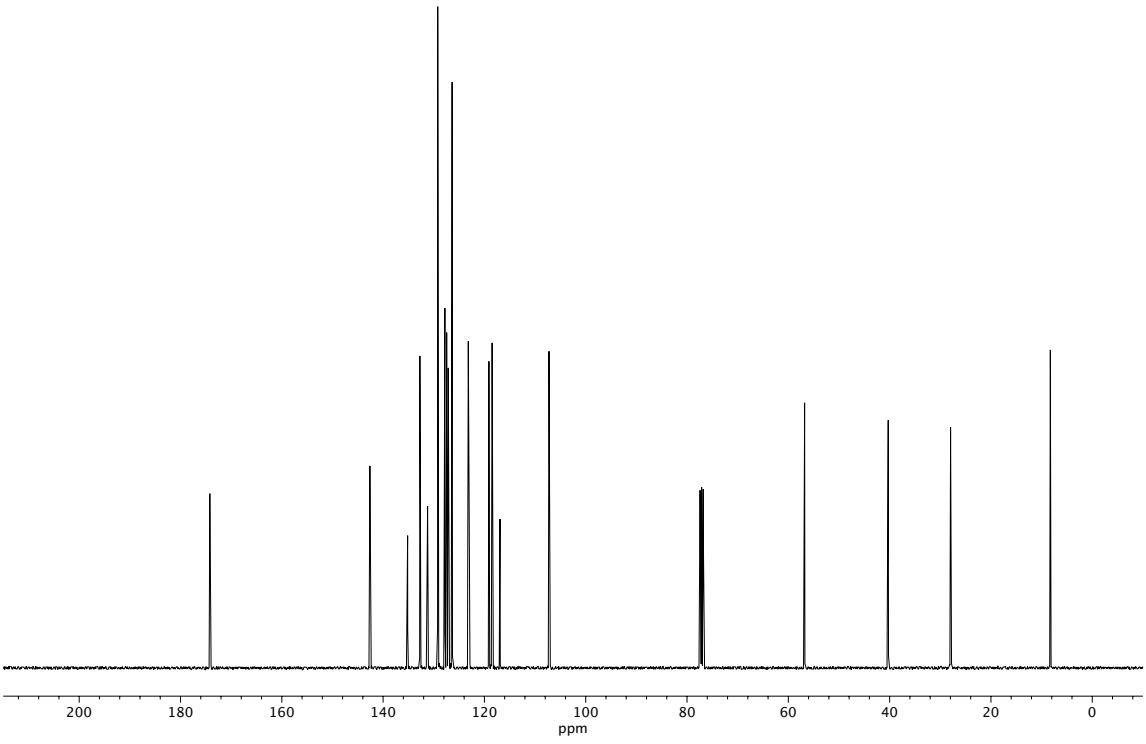

Figure A3.27 *^{13}C NMR (100 MHz, $CDCl_3$) of compound* ***20i****.*

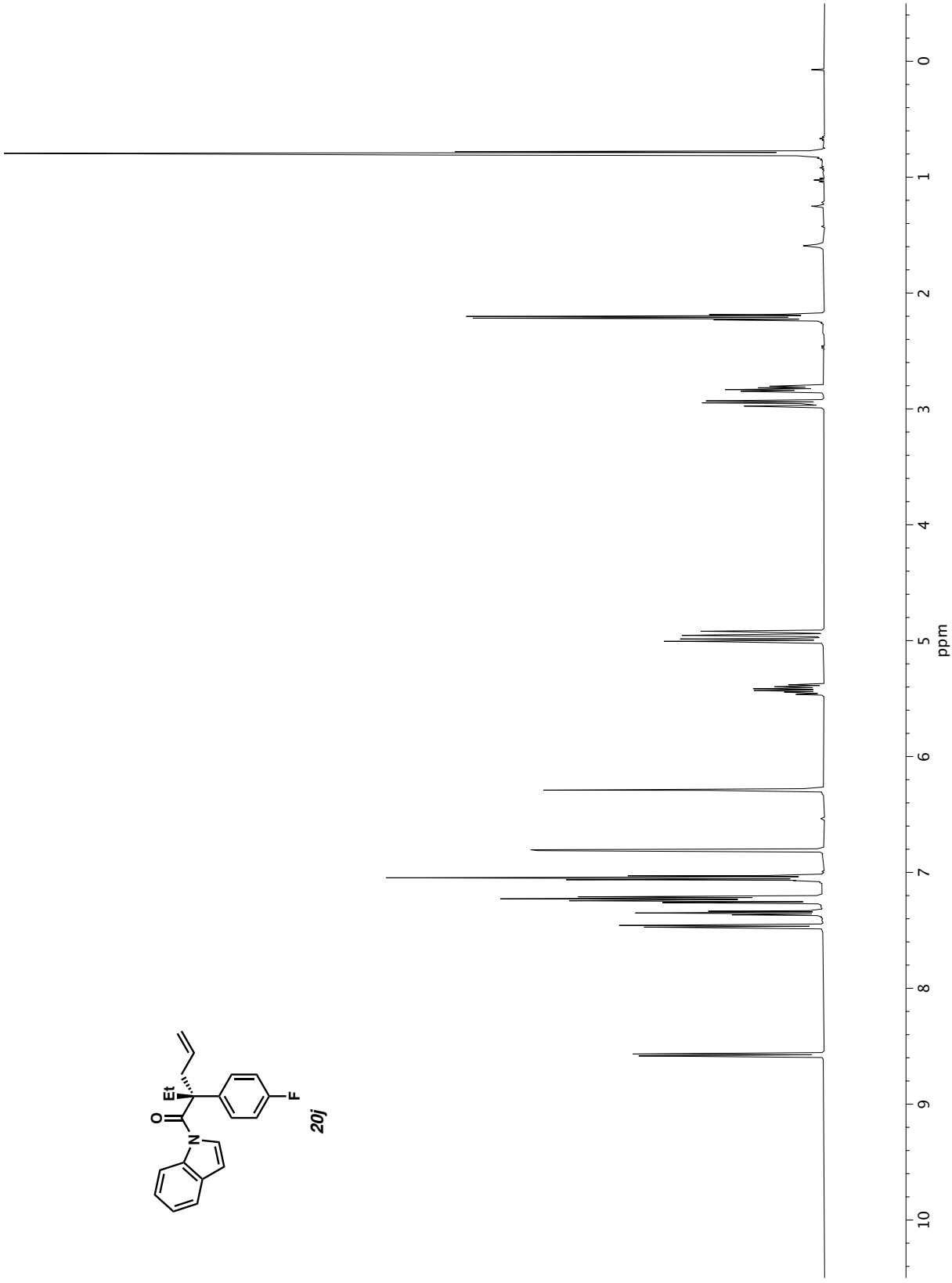

Figure A3.28 *^1H NMR (500 MHz, $CDCl_3$) of compound* ***20j****.*

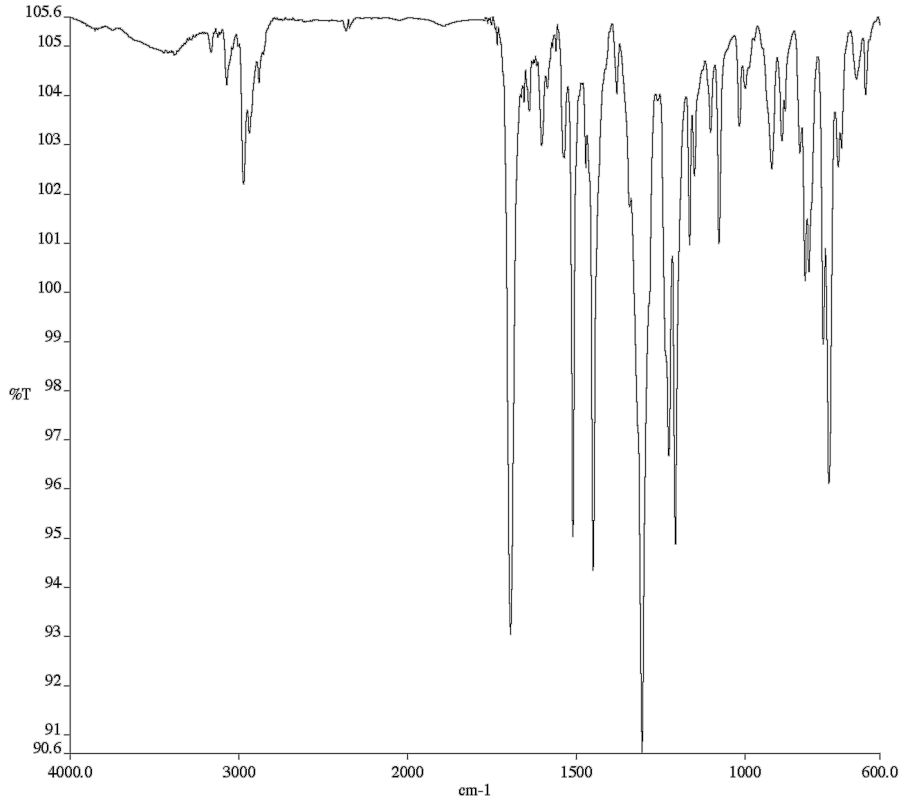

Figure A3.29 *Infrared spectrum (Thin Film, NaCl) of compound* ***20j****.*

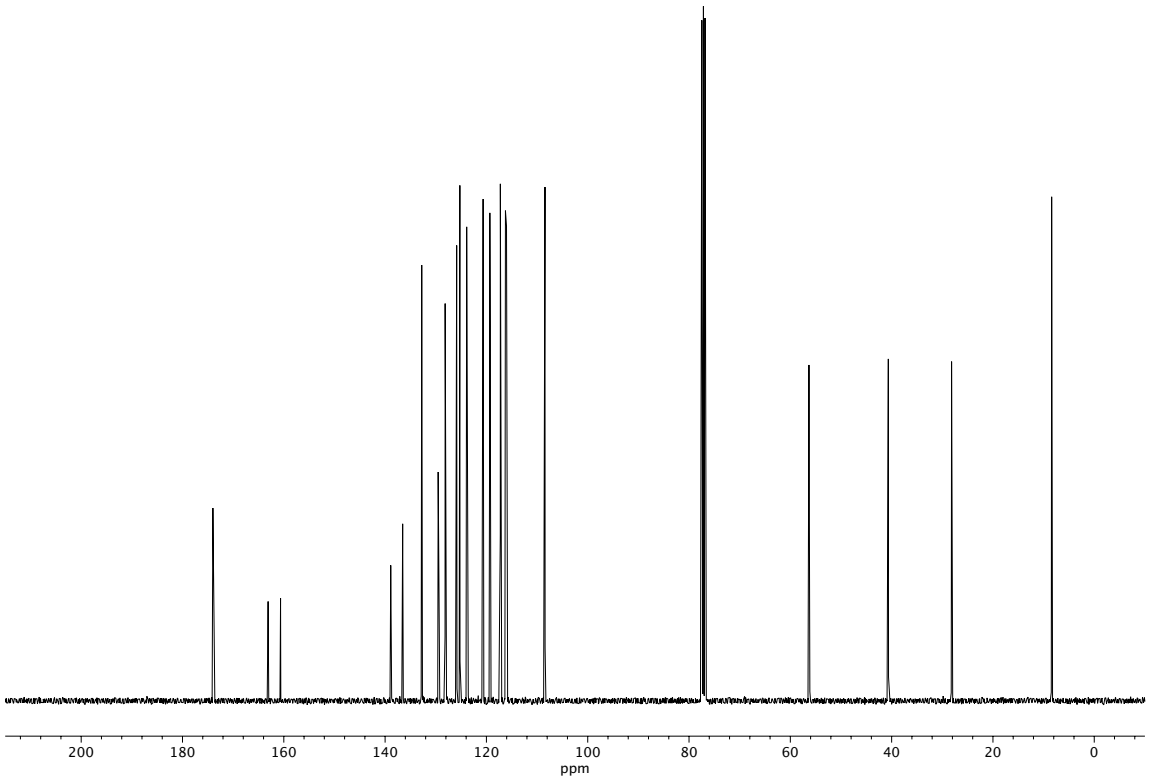

Figure A3.30 *^{13}C NMR (100 MHz, $CDCl_3$) of compound* ***20j****.*

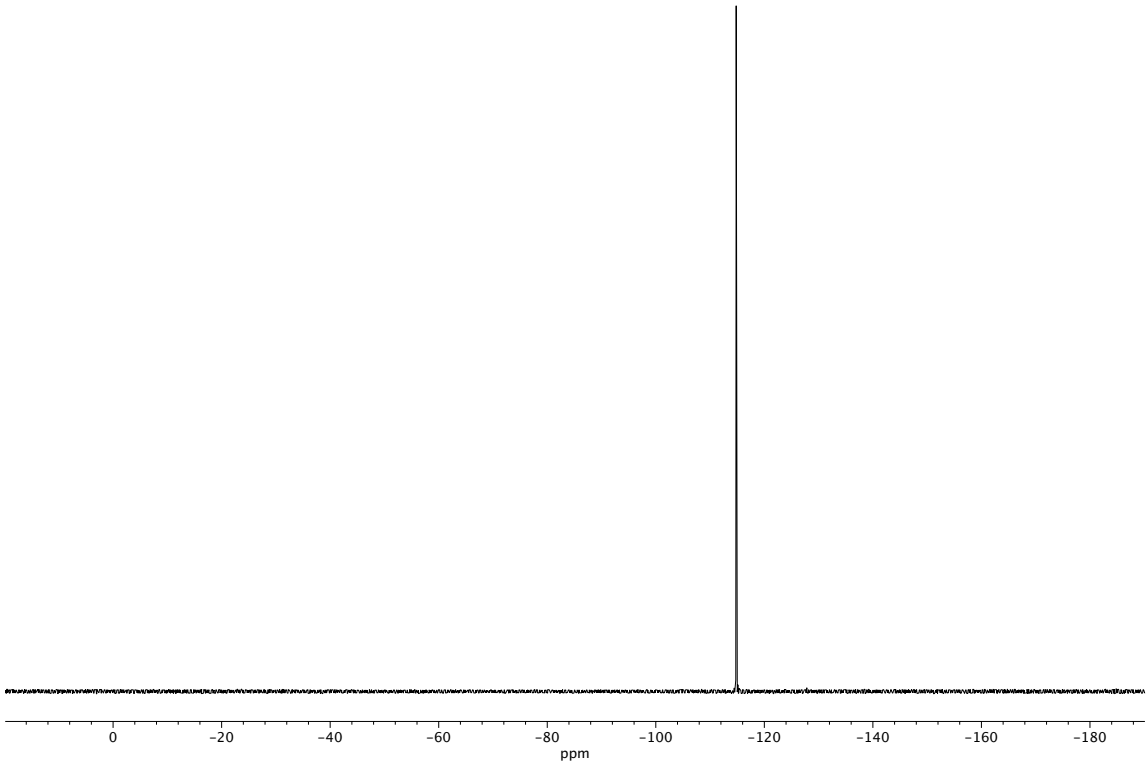

Figure A3.31 *^{19}F NMR (282 MHz, $CDCl_3$) of compound* ***20j****.*

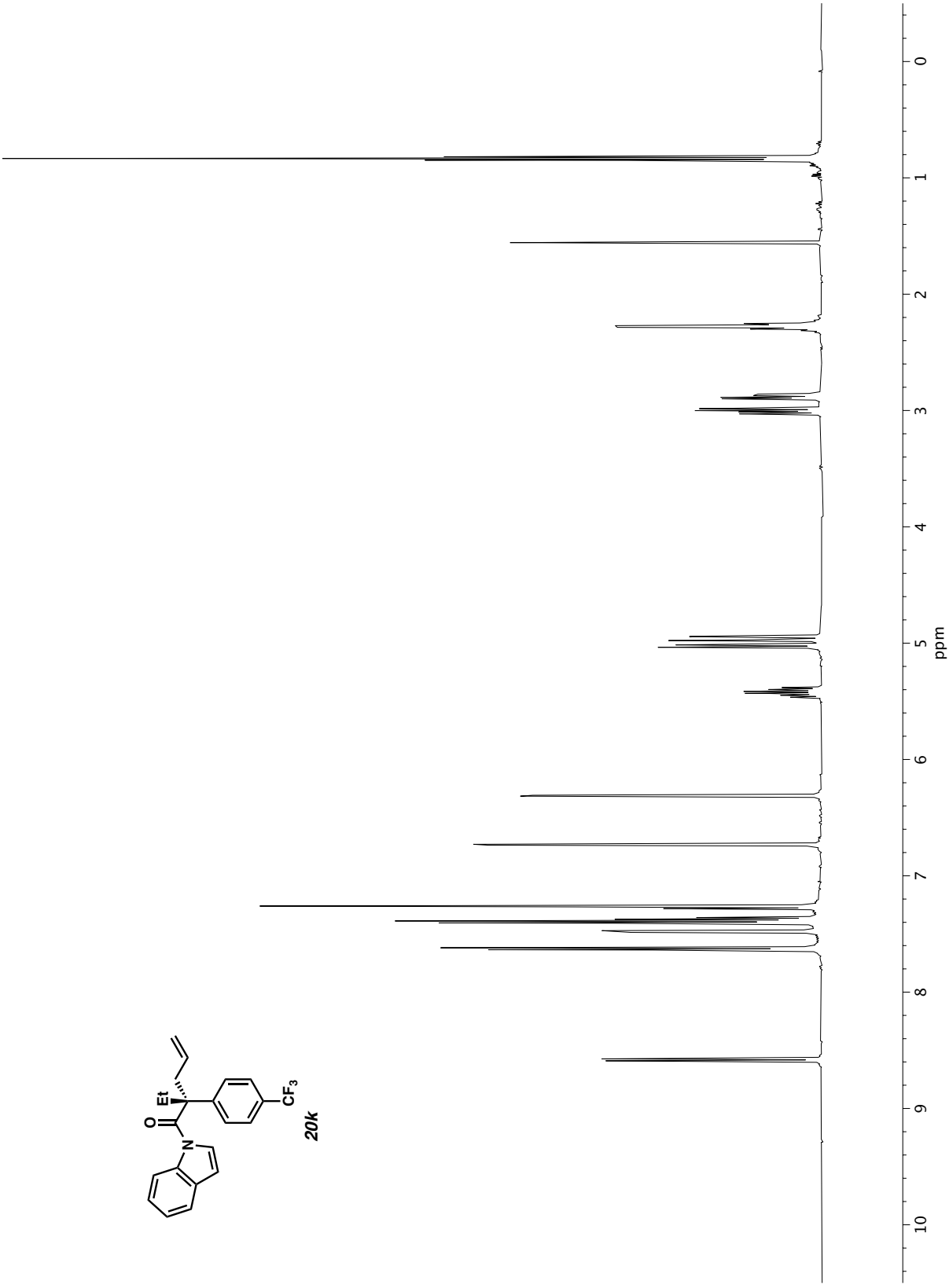

***Figure A3.32** ^{1}H NMR (500 MHz, $CDCl_3$) of compound **20k**.*

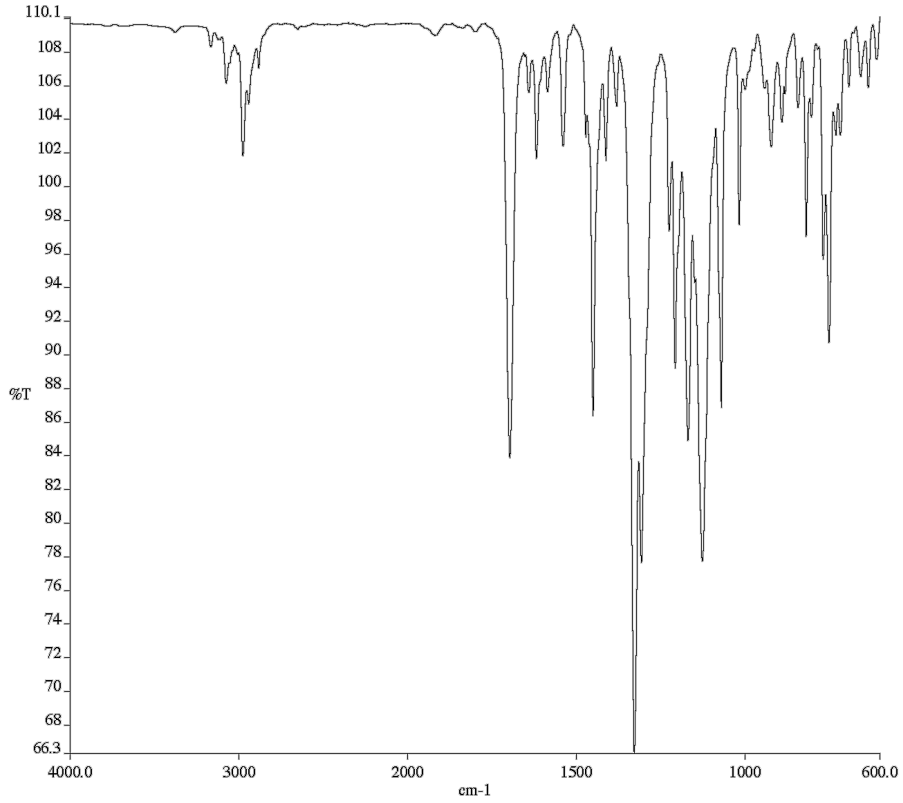

Figure A3.33 *Infrared spectrum (Thin Film, NaCl) of compound* ***20k****.*

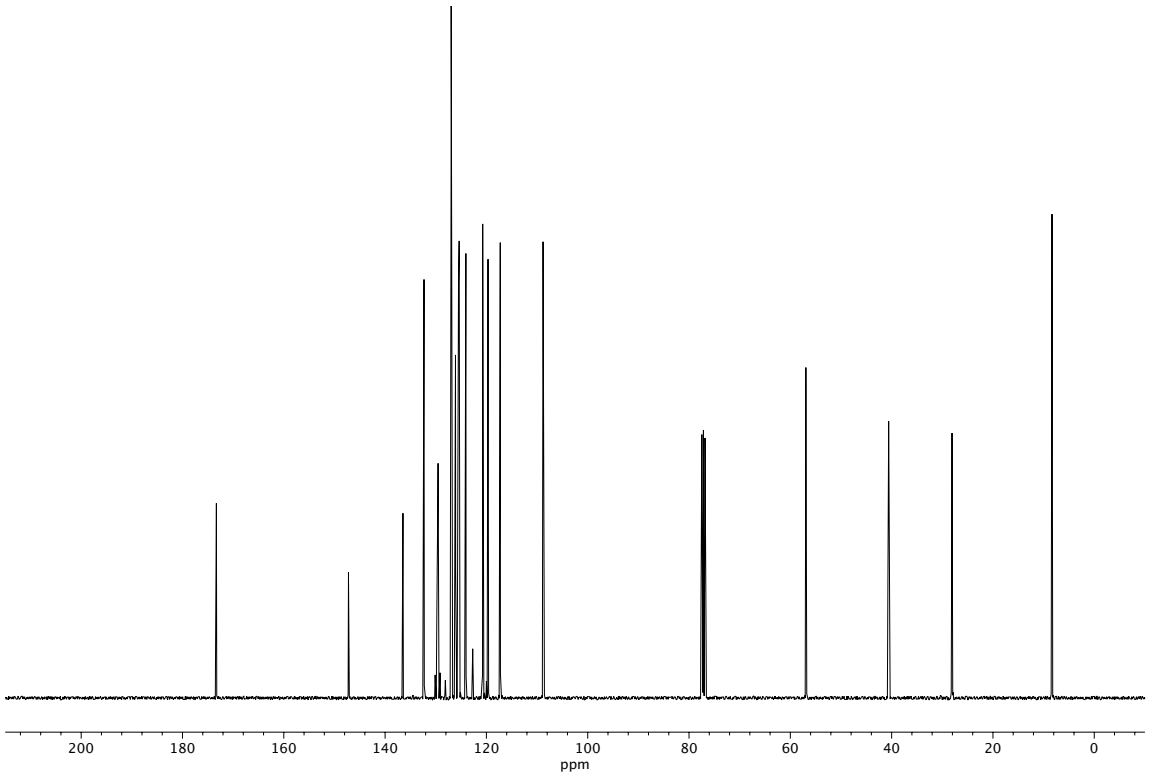

Figure A3.34 *^{13}C NMR (100 MHz, $CDCl_3$) of compound* ***20k****.*

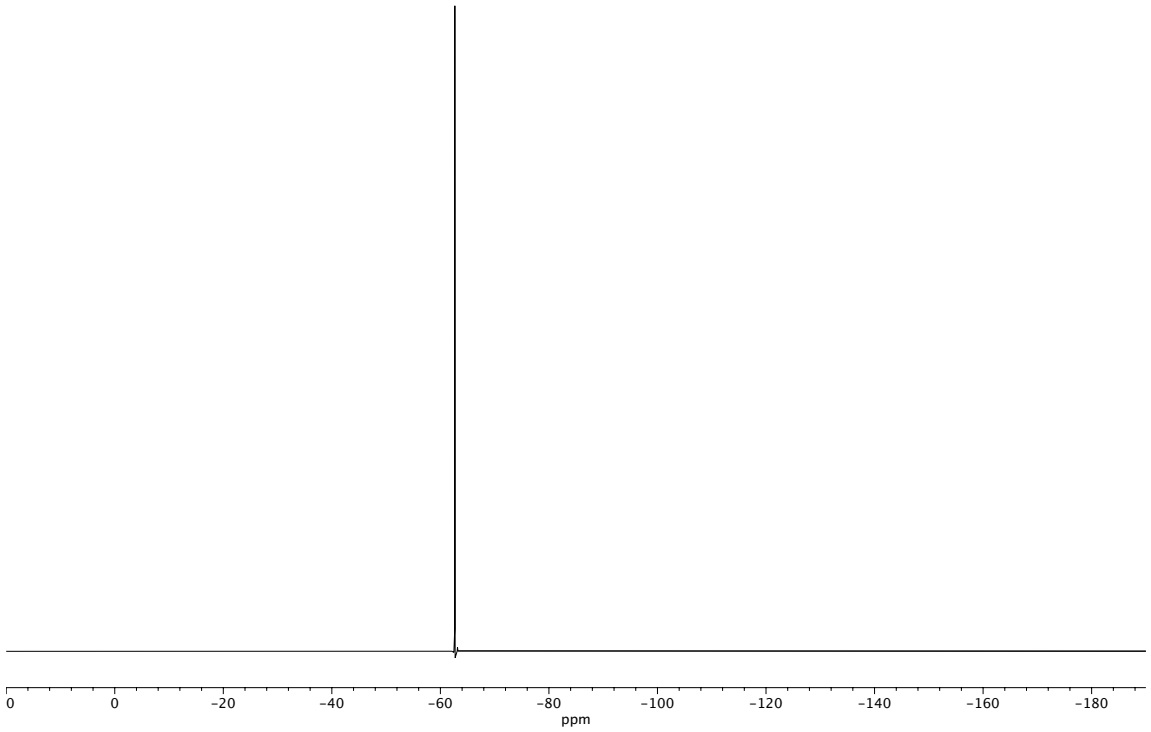

Figure A3.35 *^{19}F NMR (376 MHz, $CDCl_3$) of compound* ***20k****.*

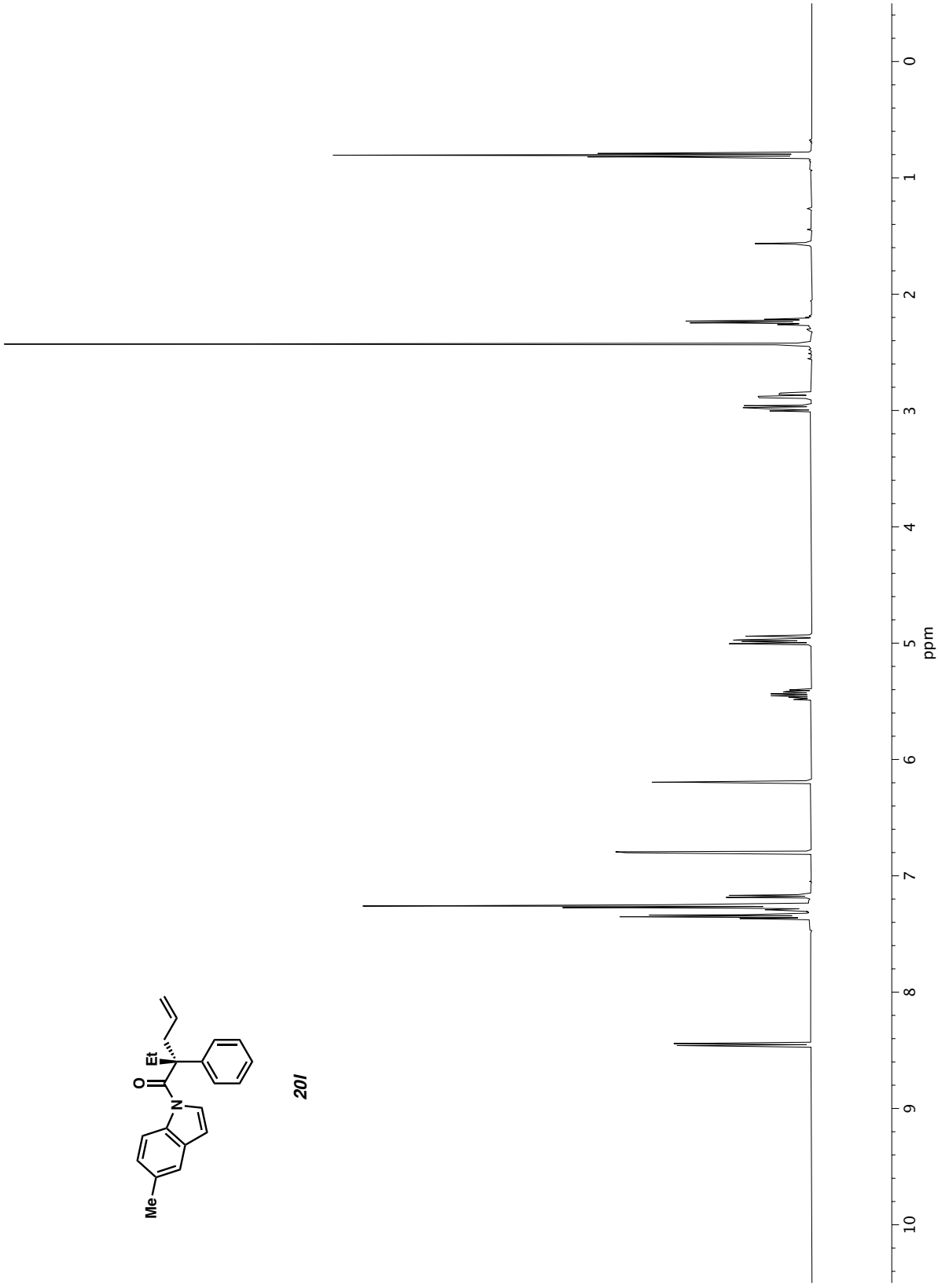

Figure A3.36 *^1H NMR (500 MHz, $CDCl_3$) of compound* ***20l****.*

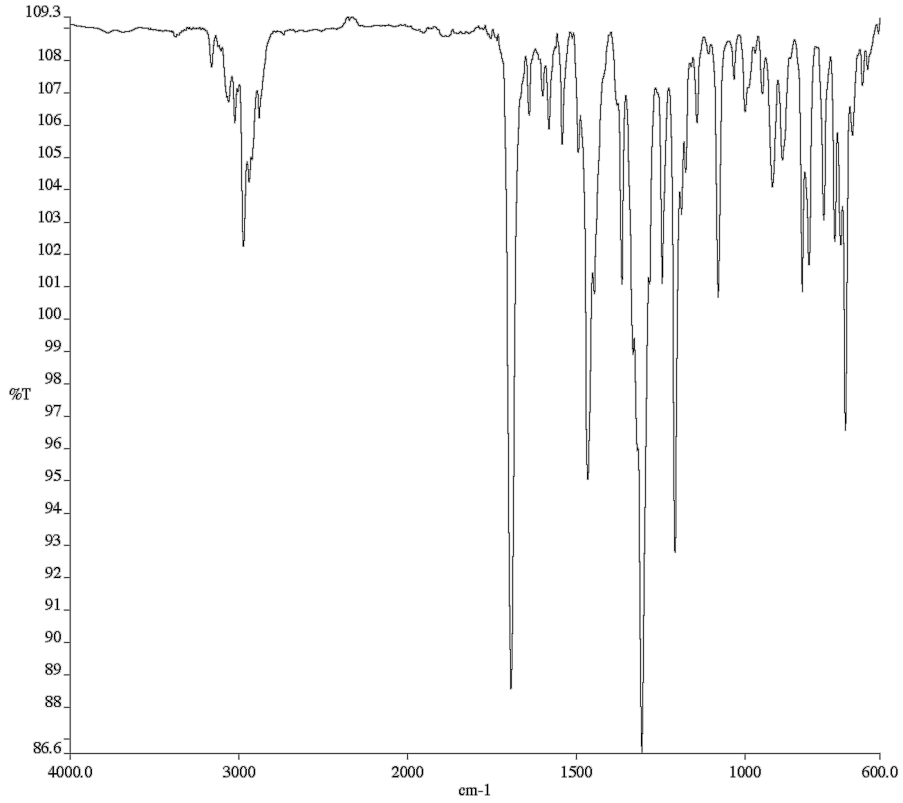

Figure A3.37 *Infrared spectrum (Thin Film, NaCl) of compound* ***20l****.*

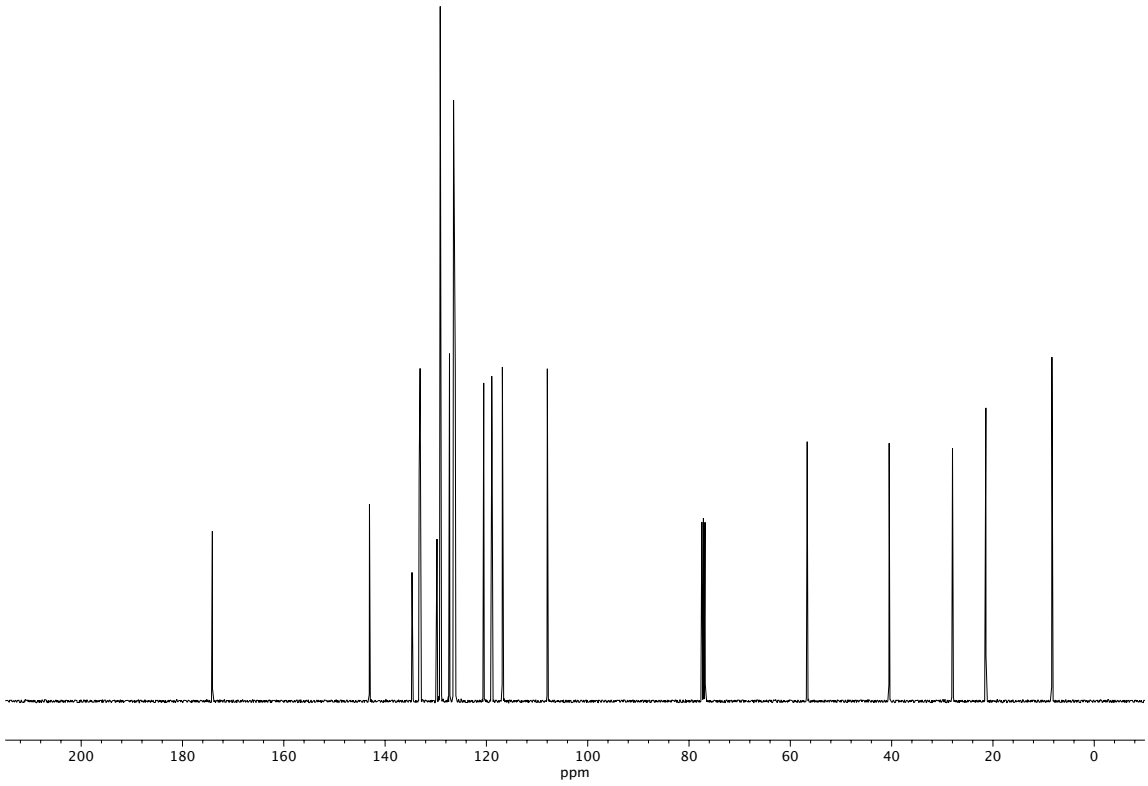

Figure A3.38 *^{13}C NMR (100 MHz, $CDCl_3$) of compound* ***20l****.*

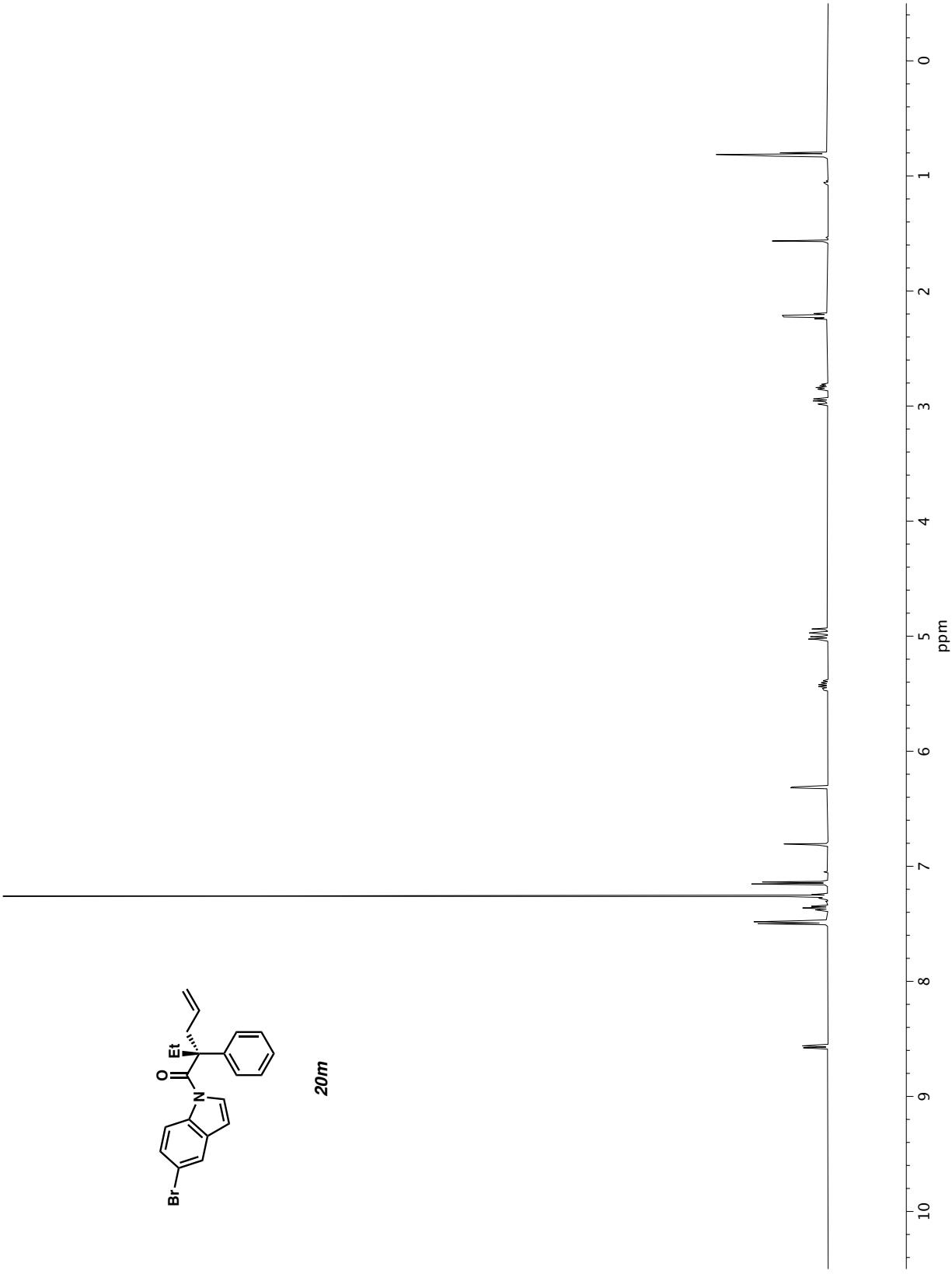

Figure A3.39 *^1H NMR (500 MHz, $CDCl_3$) of compound* ***20m***.

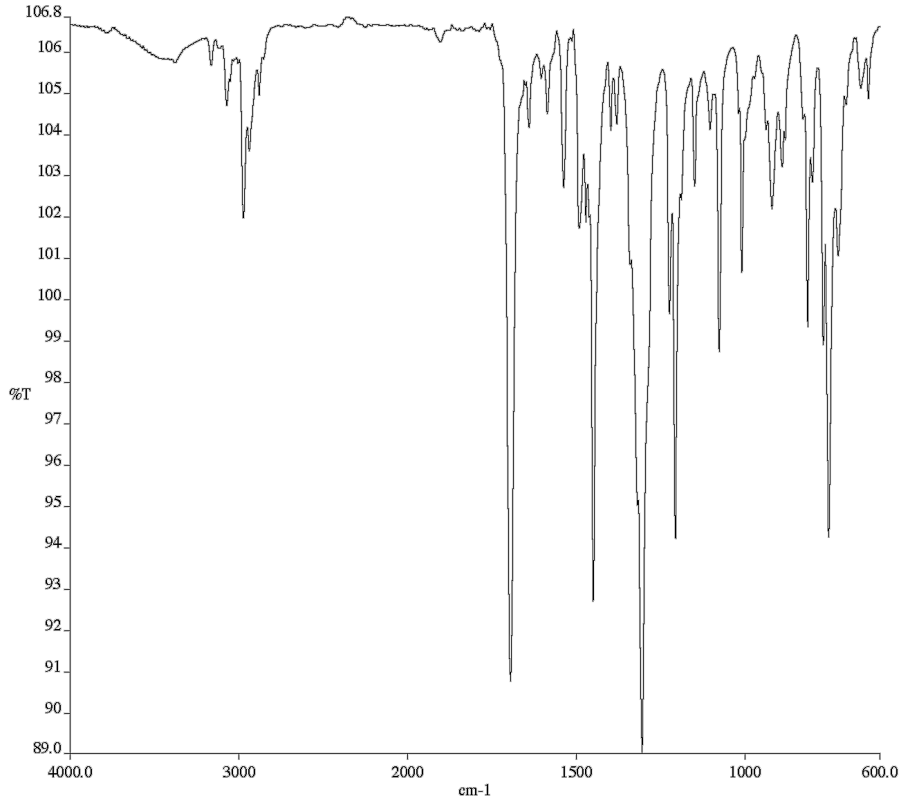

Figure A3.40 *Infrared spectrum (Thin Film, NaCl) of compound* ***20m****.*

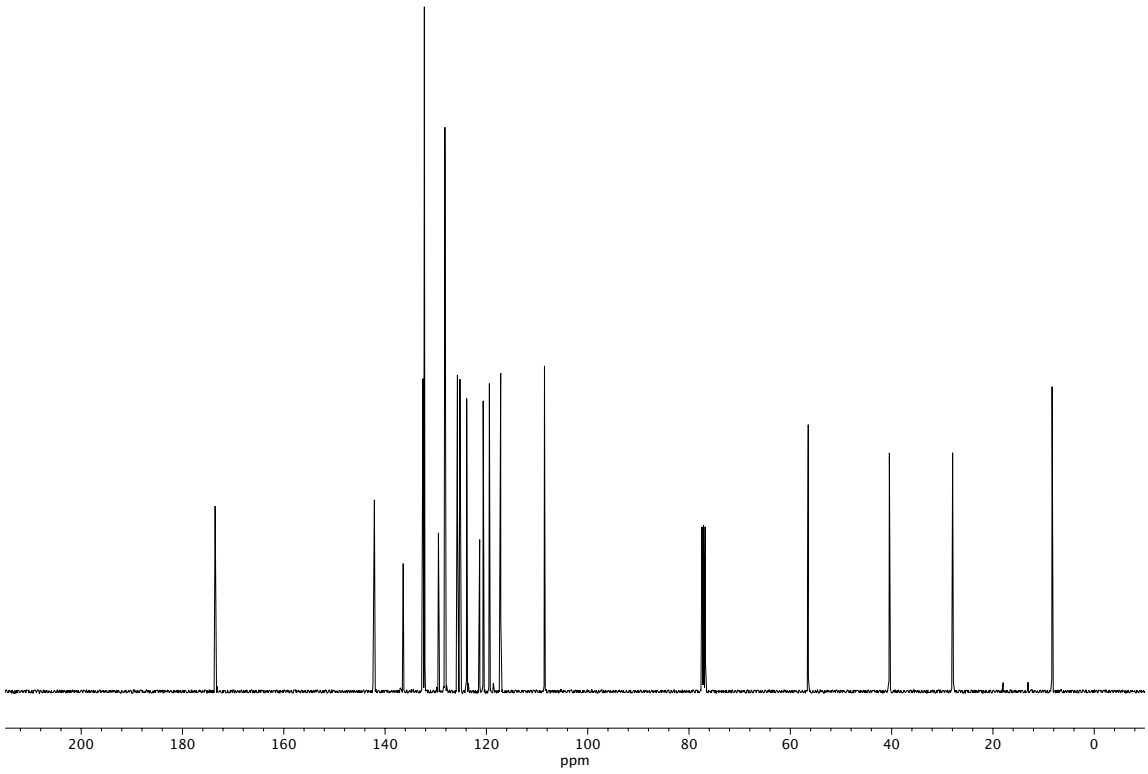

Figure A3.41 *^{13}C NMR (100 MHz, $CDCl_3$) of compound* ***20m****.*

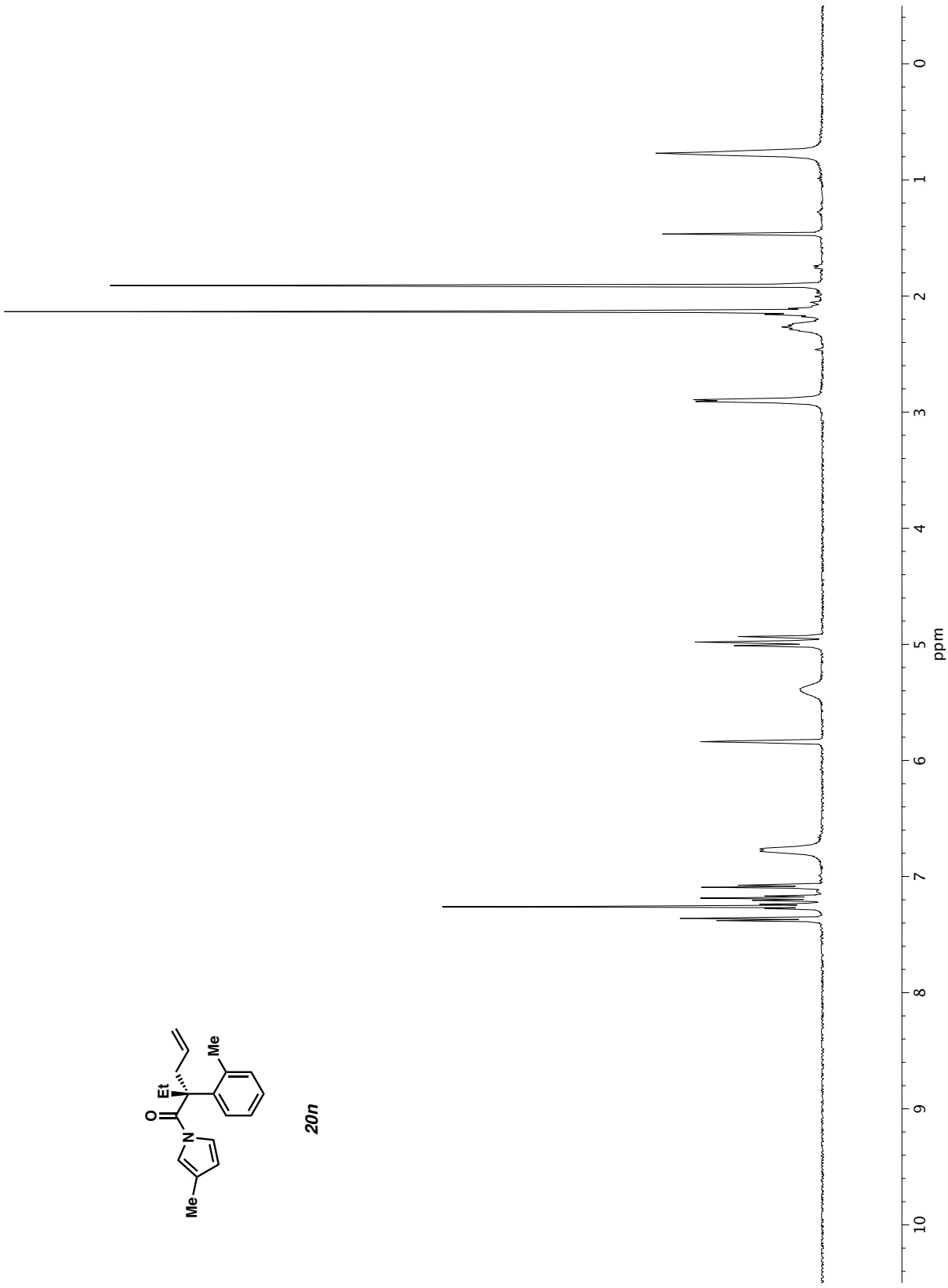

Figure A3.42 *^{1}H NMR (400 MHz, $CDCl_3$) of compound* ***20n*** *at 50 °C.*

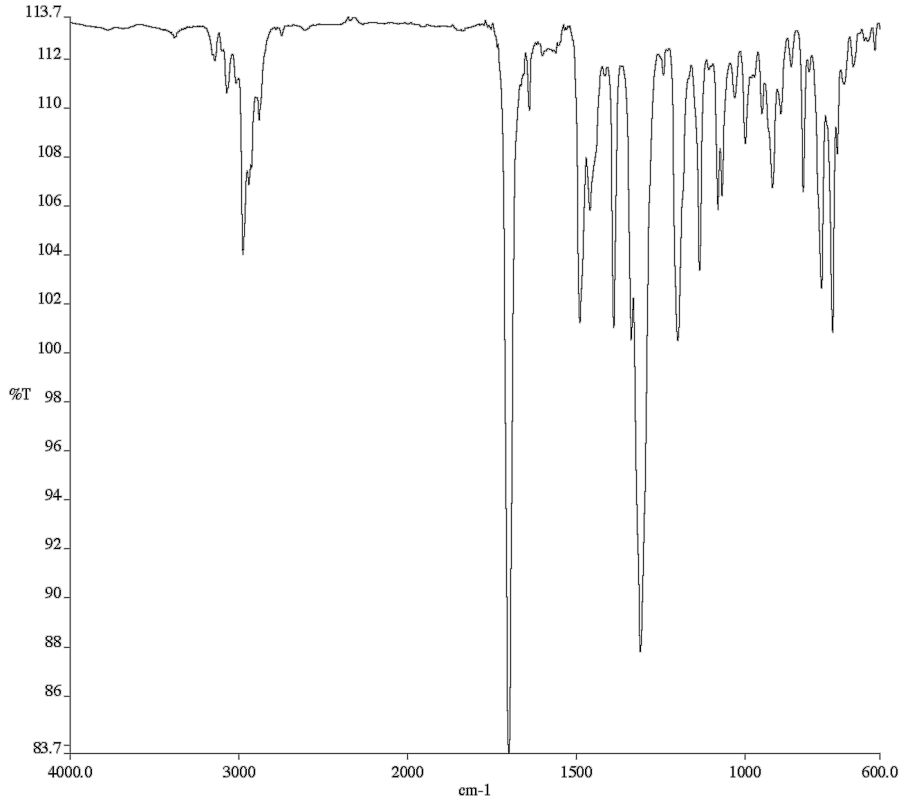

Figure A3.43 *Infrared spectrum (Thin Film, NaCl) of compound* ***20n****.*

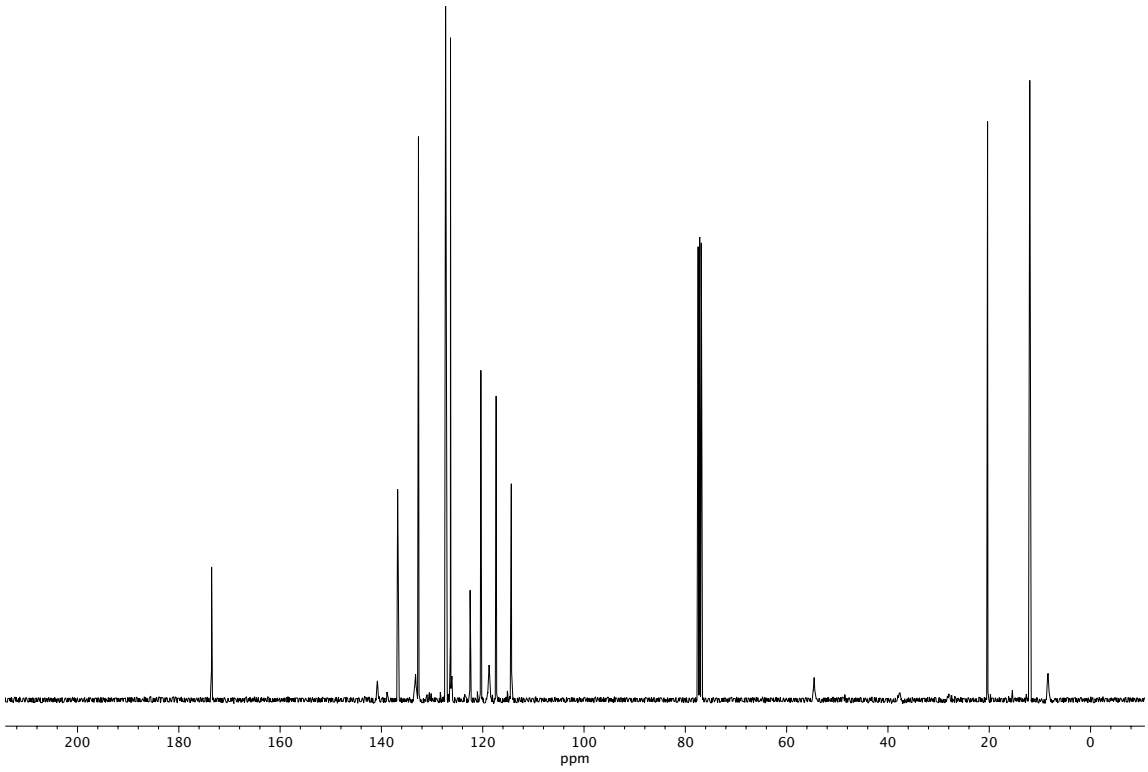

Figure A3.44 *^{13}C NMR (100 MHz, $CDCl_3$) of compound* ***20n****.*

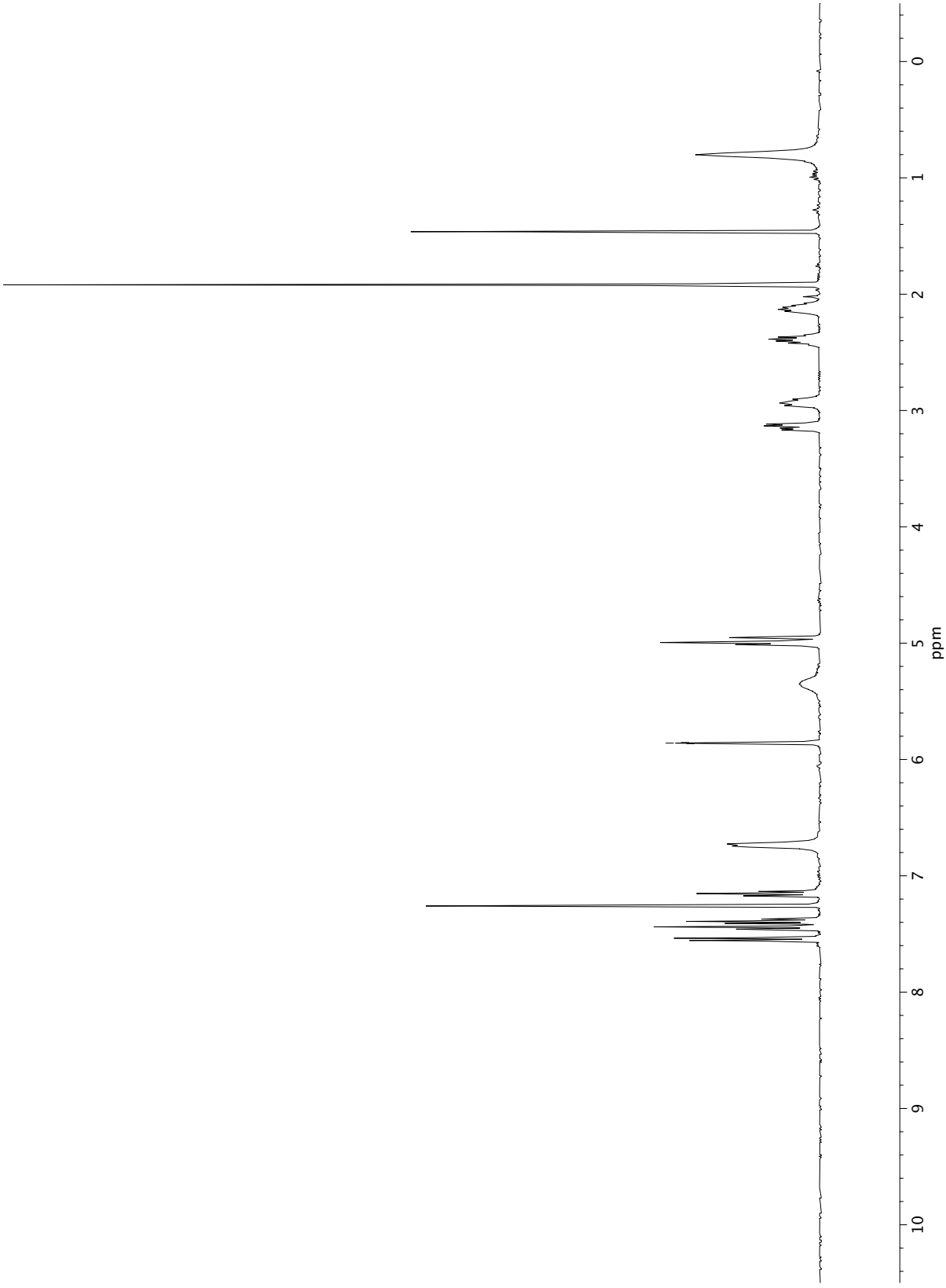

Figure A3.45 *^{1}H NMR (400 MHz, $CDCl_3$) of compound* ***20o*** *at 50 °C.*

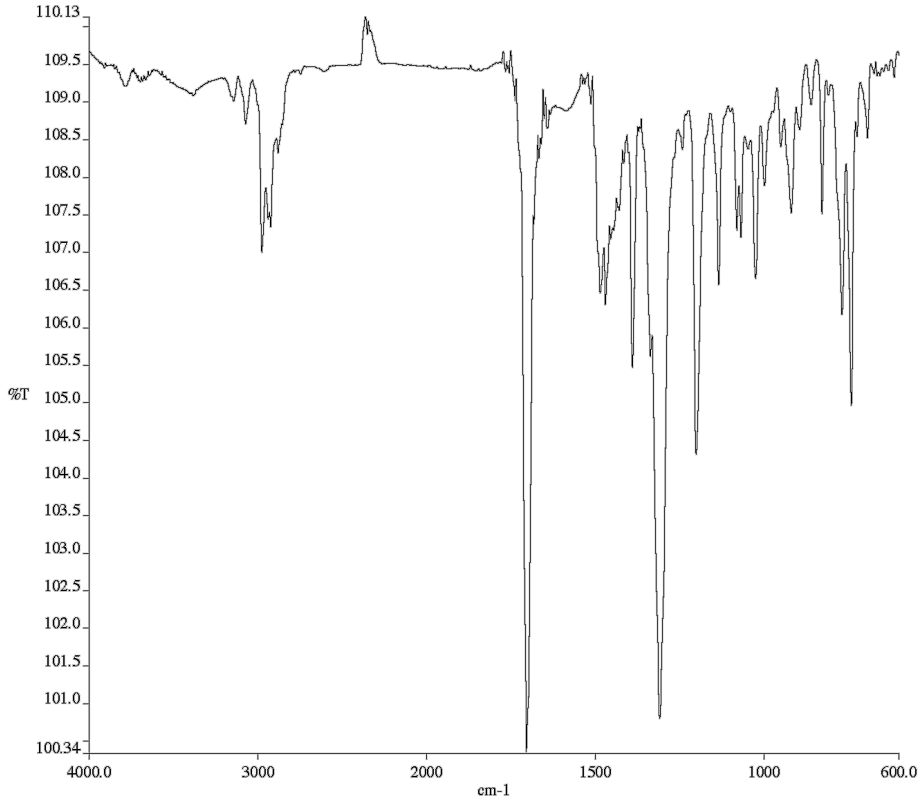

Figure A3.46 *Infrared spectrum (Thin Film, NaCl) of compound* ***20o****.*

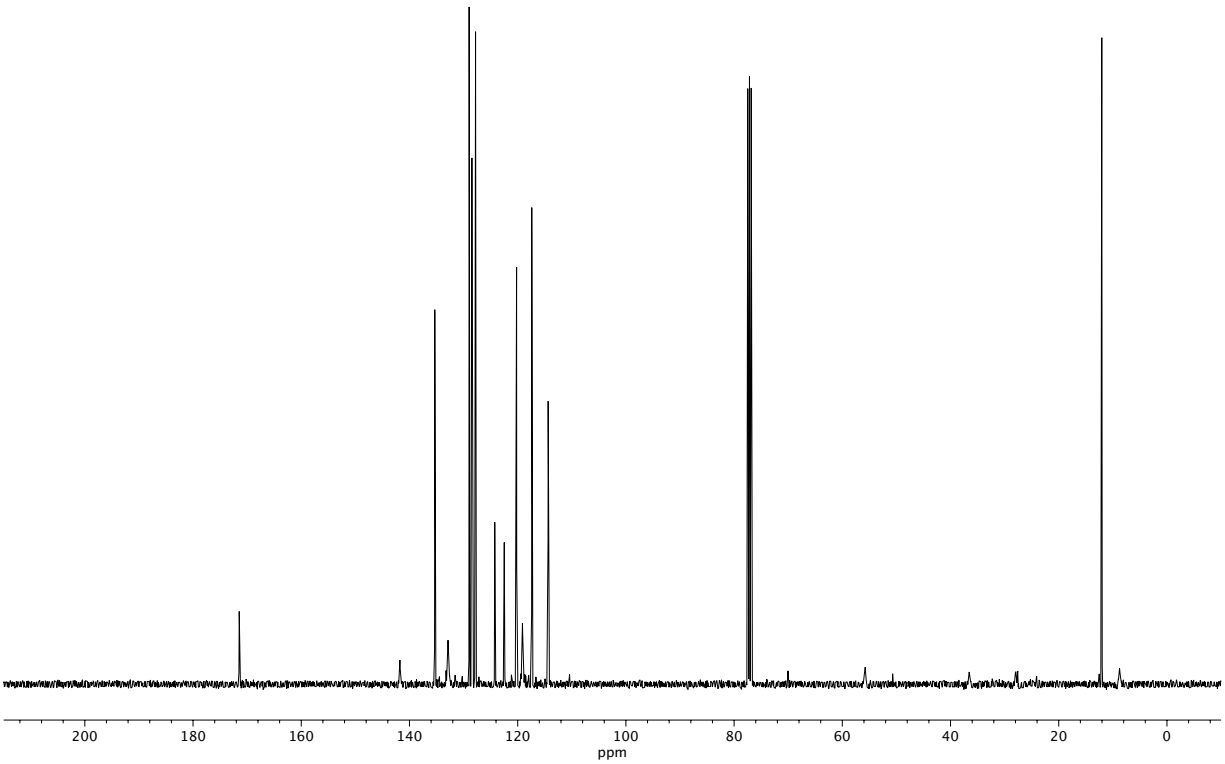

Figure A3.47 *^{13}C NMR (100 MHz, $CDCl_3$) of compound* ***20o****.*

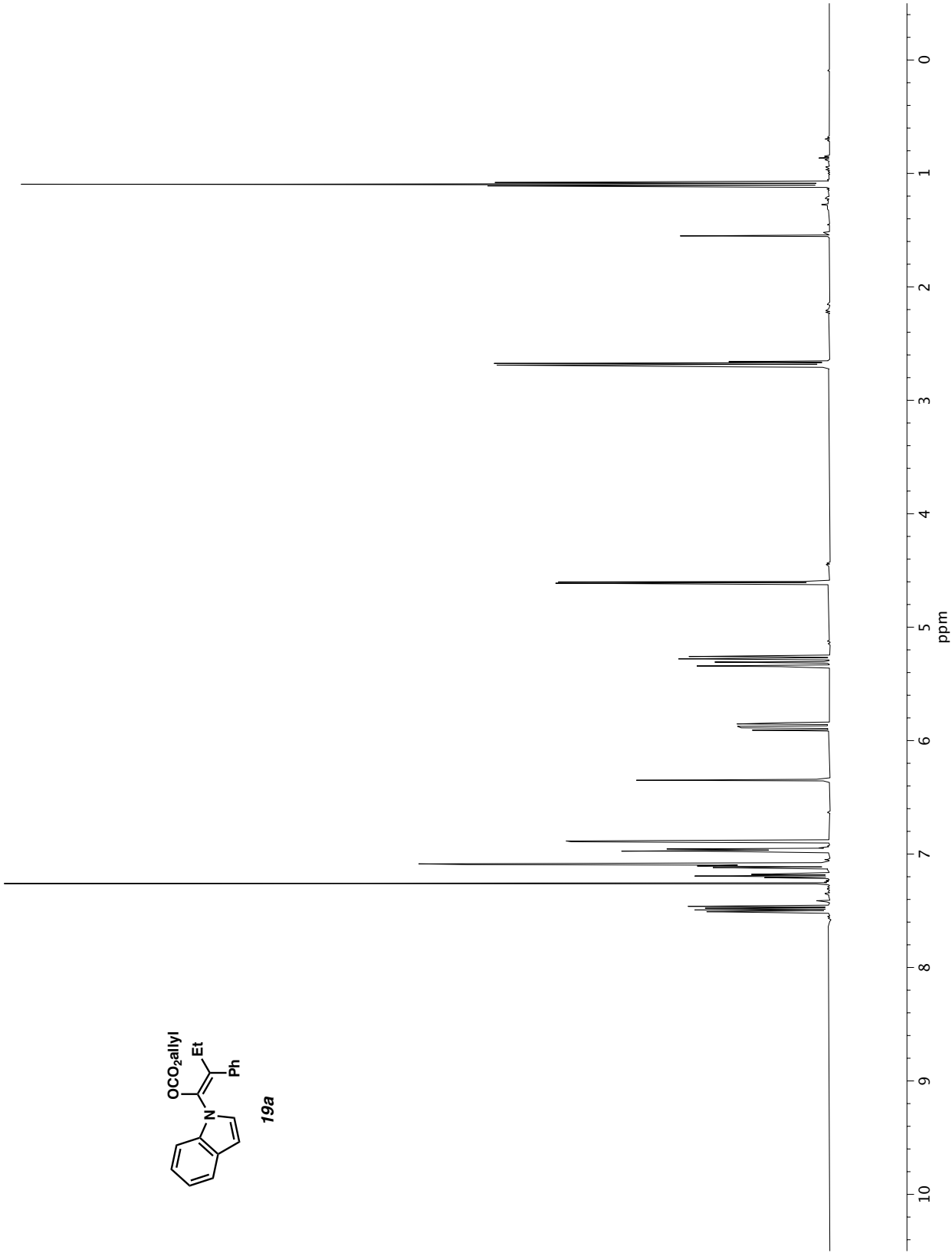

Figure A3.48 *^1H NMR (500 MHz, $CDCl_3$) of compound* ***19a***.

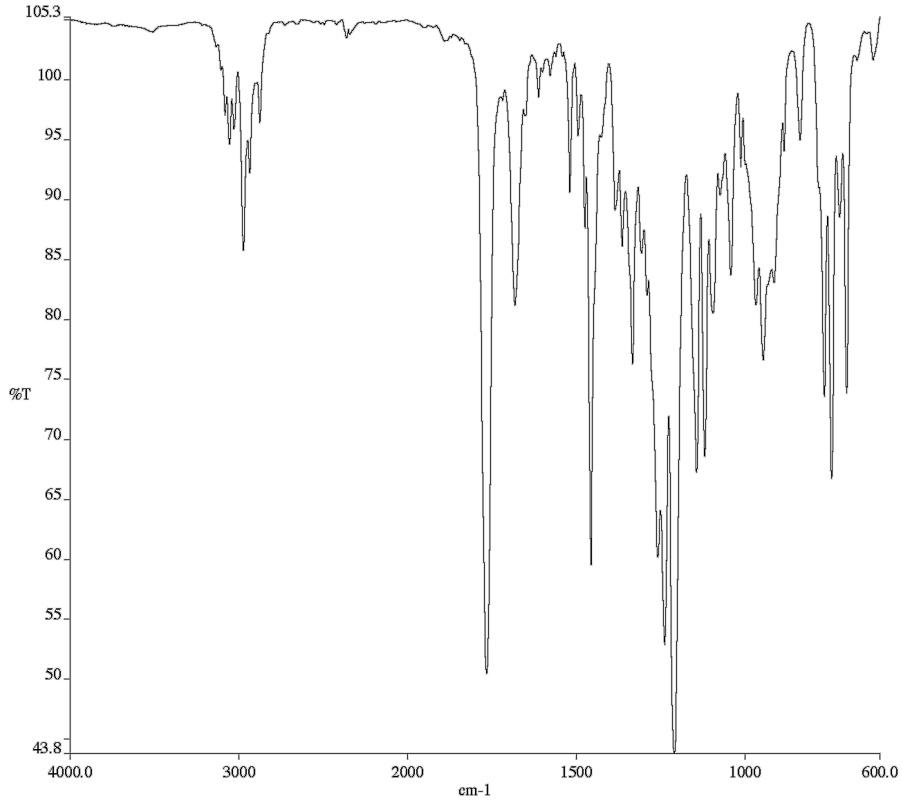

Figure A3.49 *Infrared spectrum (Thin Film, NaCl) of compound* ***19a****.*

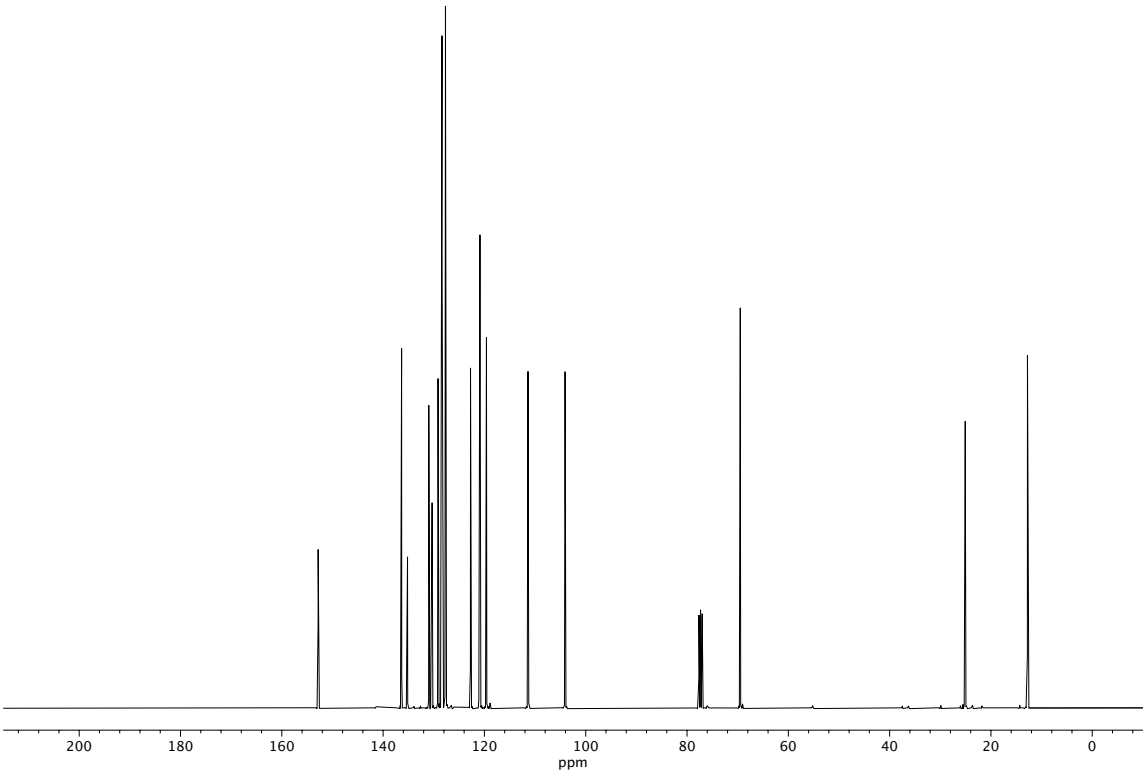

Figure A3.50 *^{13}C NMR (100 MHz, $CDCl_3$) of compound* ***19a****.*

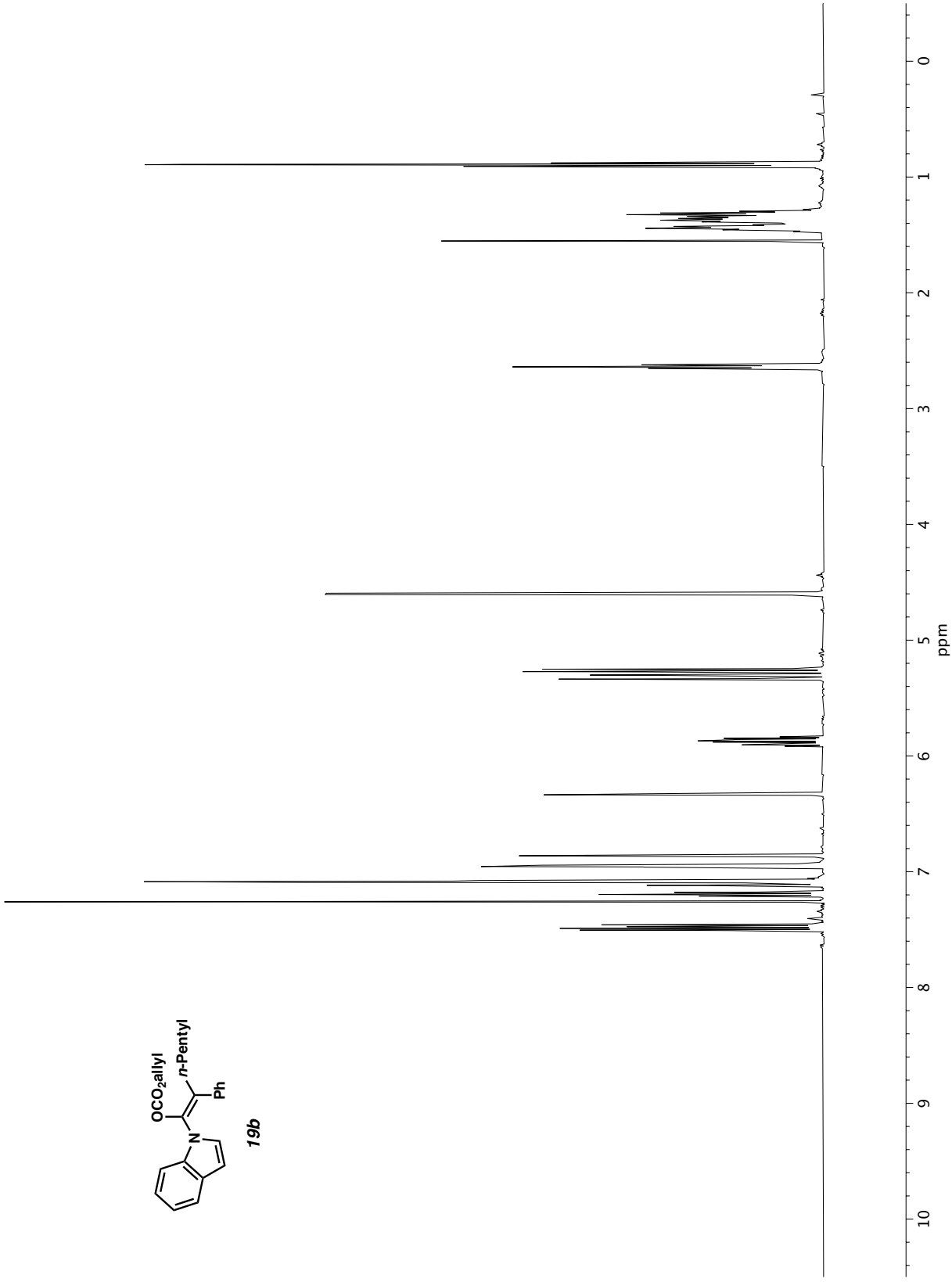

Figure A3.51 *^1H NMR (500 MHz, $CDCl_3$) of compound **19b**.*

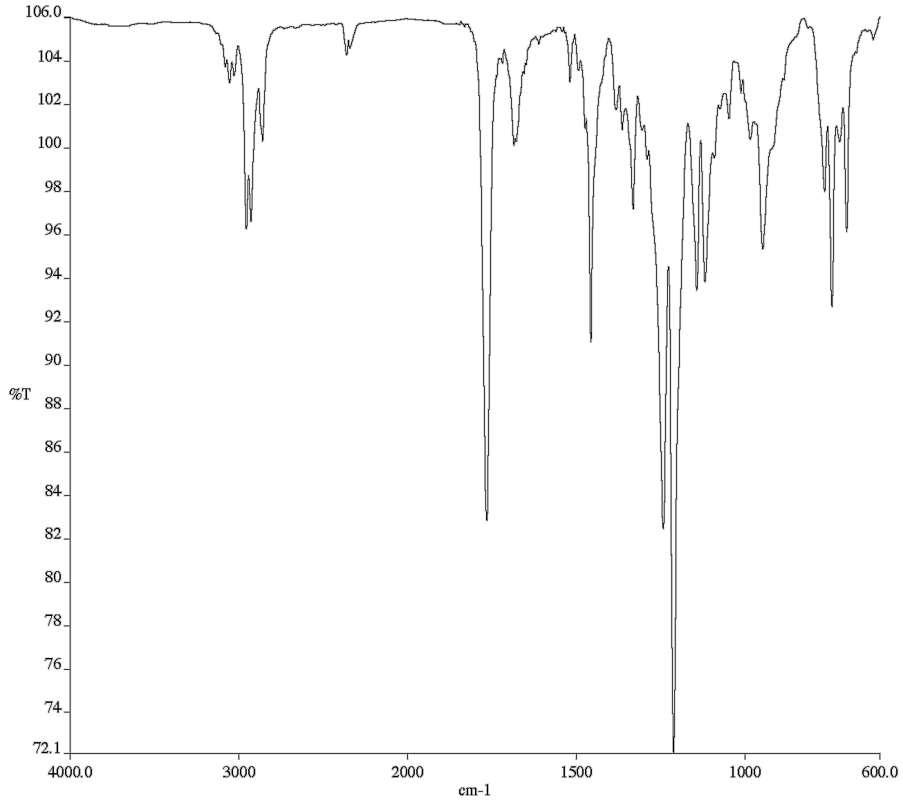

Figure A3.52 *Infrared spectrum (Thin Film, NaCl) of compound* ***19b****.*

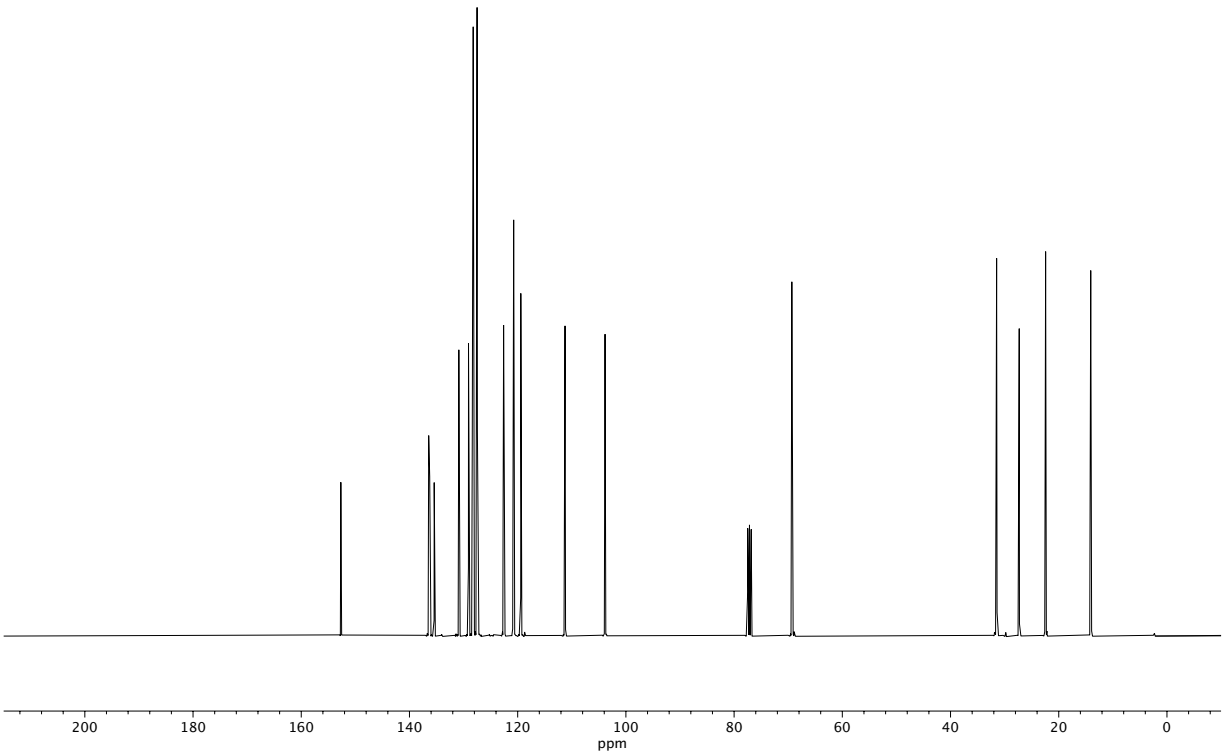

Figure A3.53 *^{13}C NMR (100 MHz, $CDCl_3$) of compound* ***19b****.*

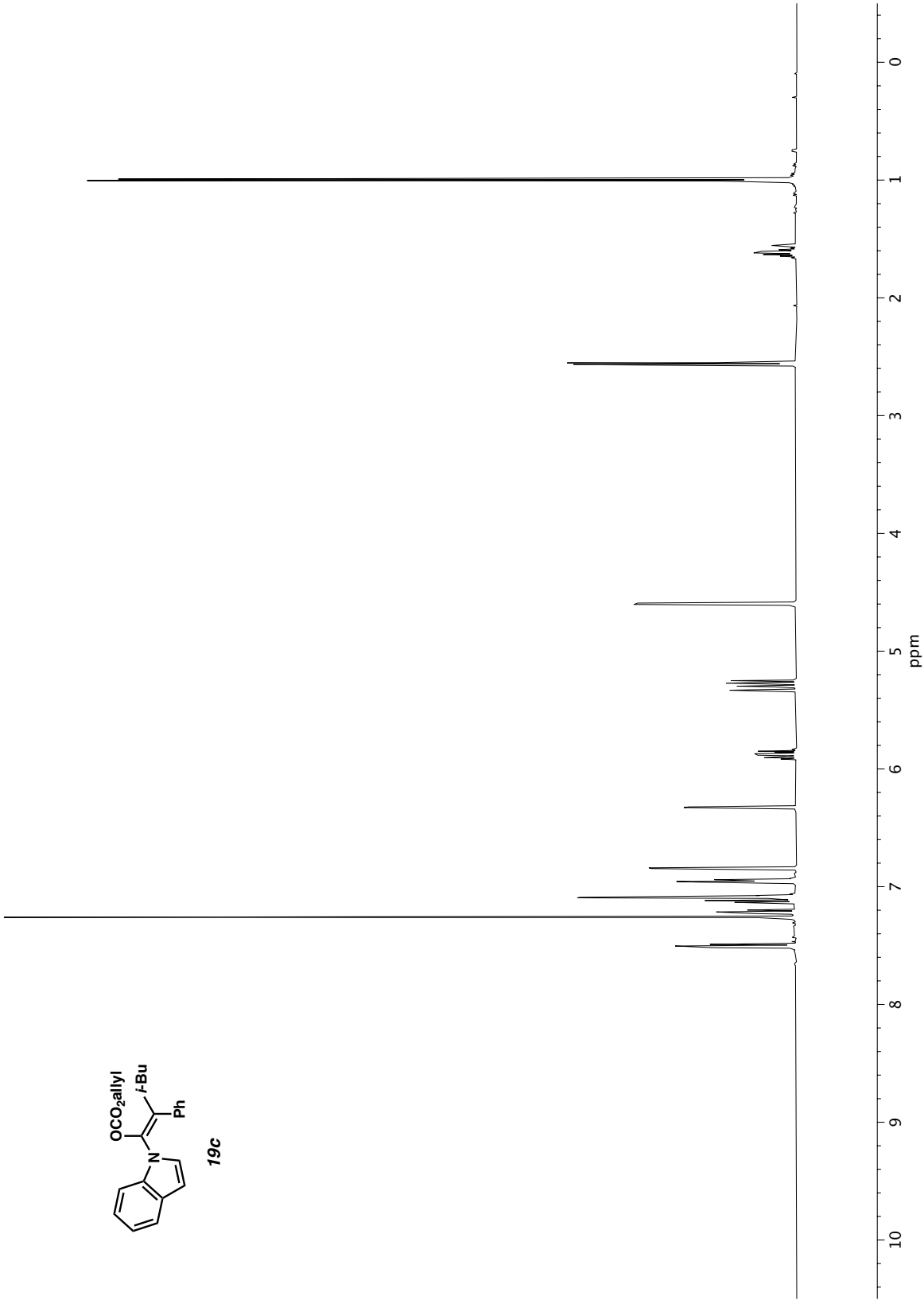

Figure A3.54 *^{1}H NMR (500 MHz, $CDCl_3$) of compound* ***19c****.*

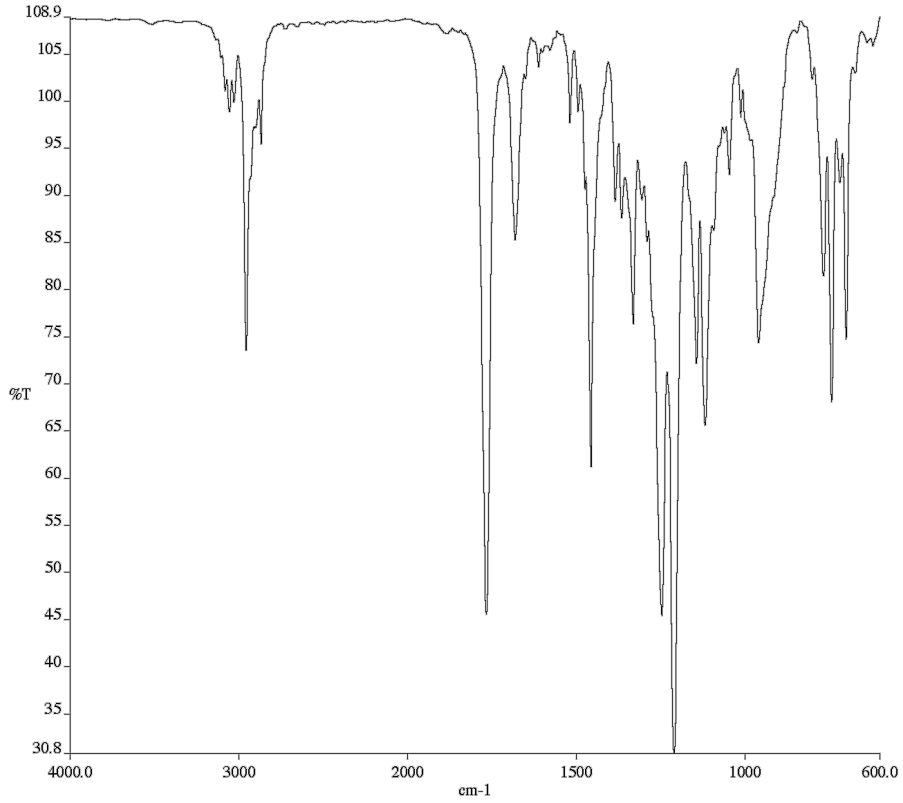

Figure A3.55 *Infrared spectrum (Thin Film, NaCl) of compound* ***19c****.*

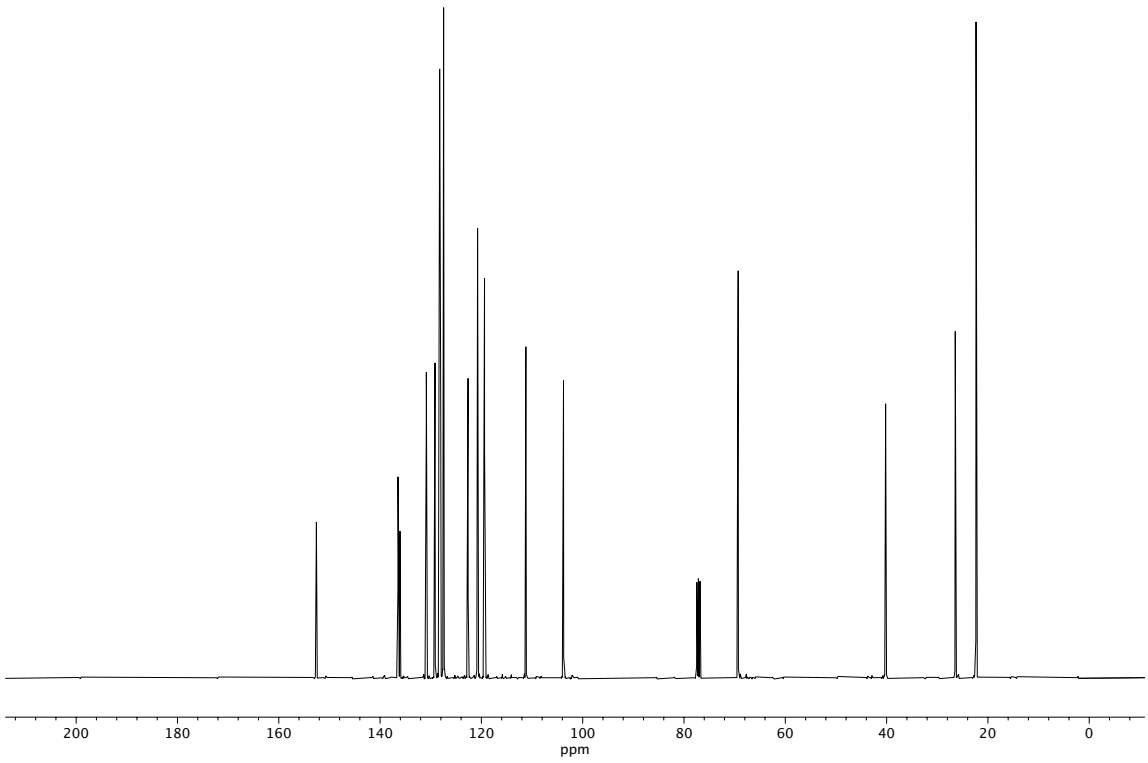

Figure A3.56 *^{13}C NMR (100 MHz, $CDCl_3$) of compound* ***19c****.*

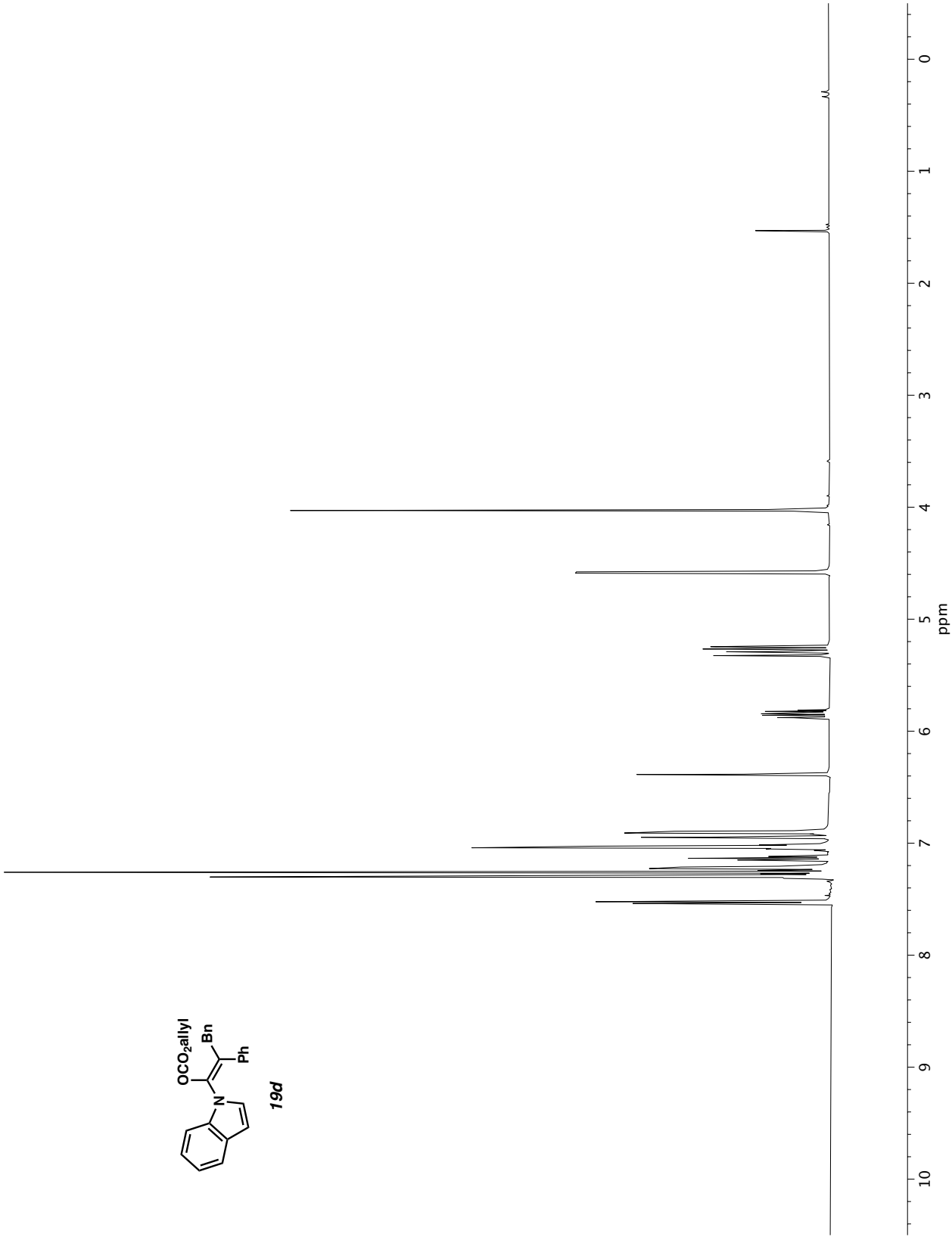

Figure A3.57 *^1H NMR (500 MHz, $CDCl_3$) of compound* ***19d****.*

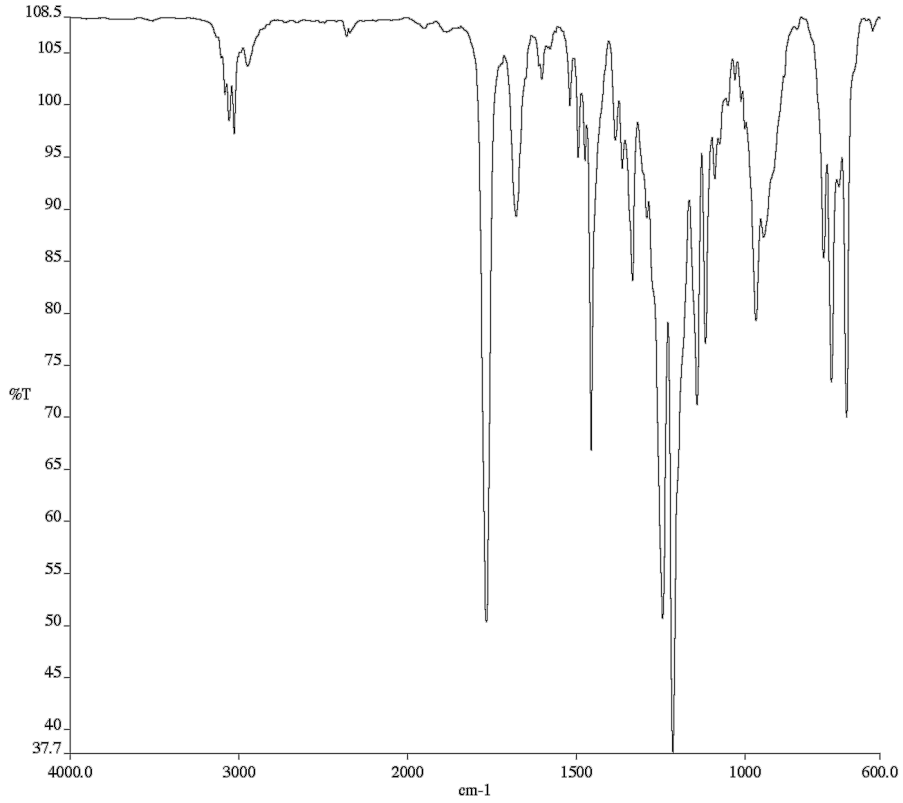

Figure A3.58 *Infrared spectrum (Thin Film, NaCl) of compound* ***19d****.*

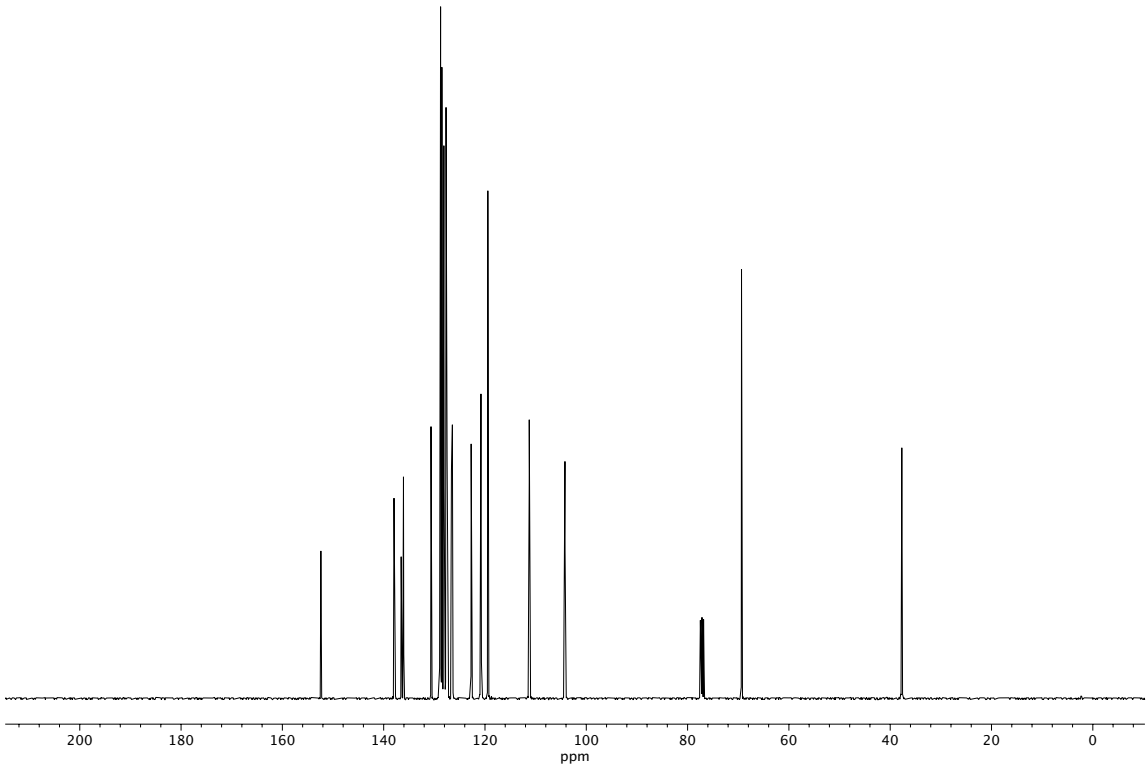

Figure A3.59 *^{13}C NMR (100 MHz, $CDCl_3$) of compound* ***19d****.*

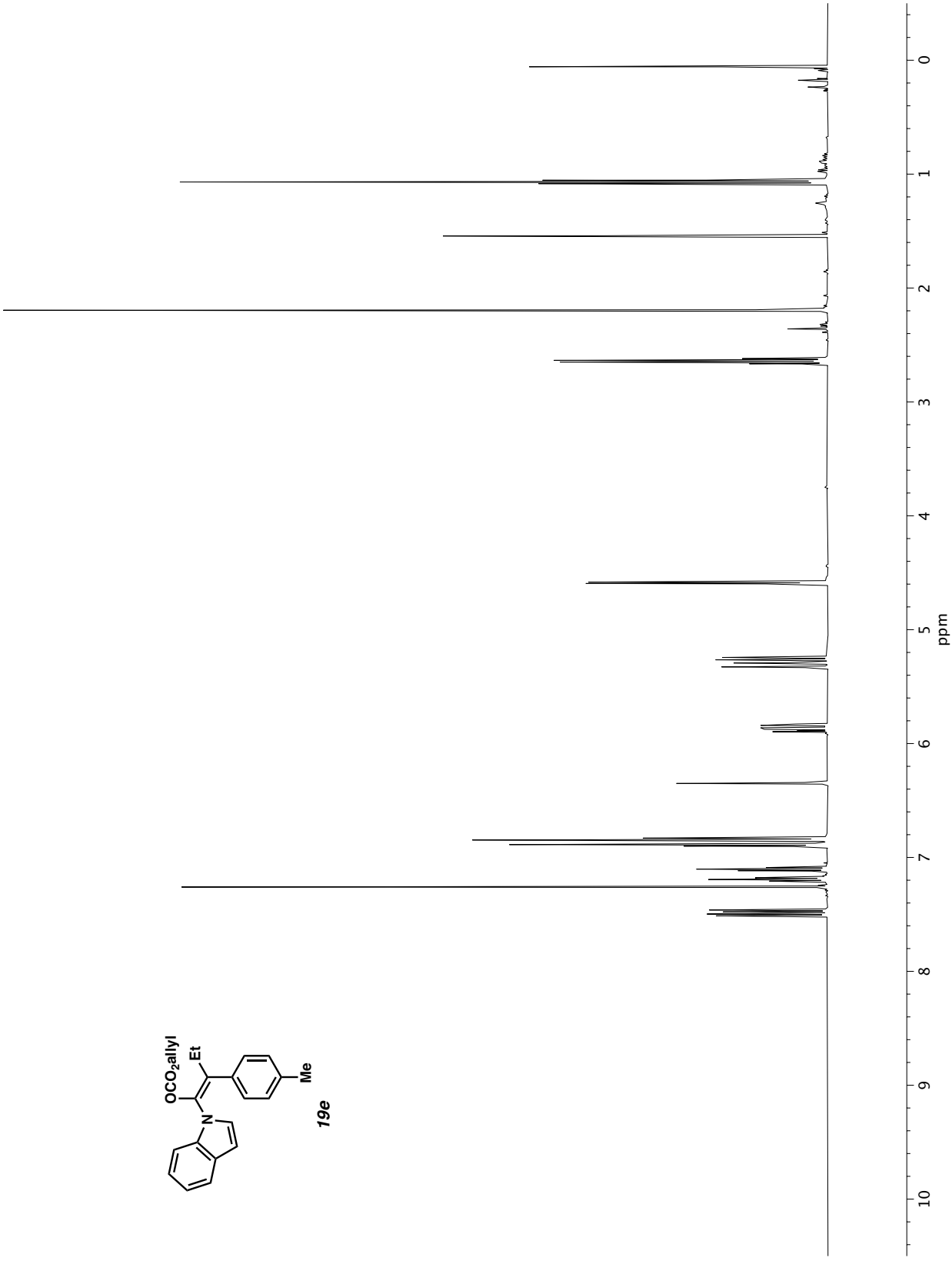

Figure A3.60 *^1H NMR (500 MHz, $CDCl_3$) of compound* ***19e****.*

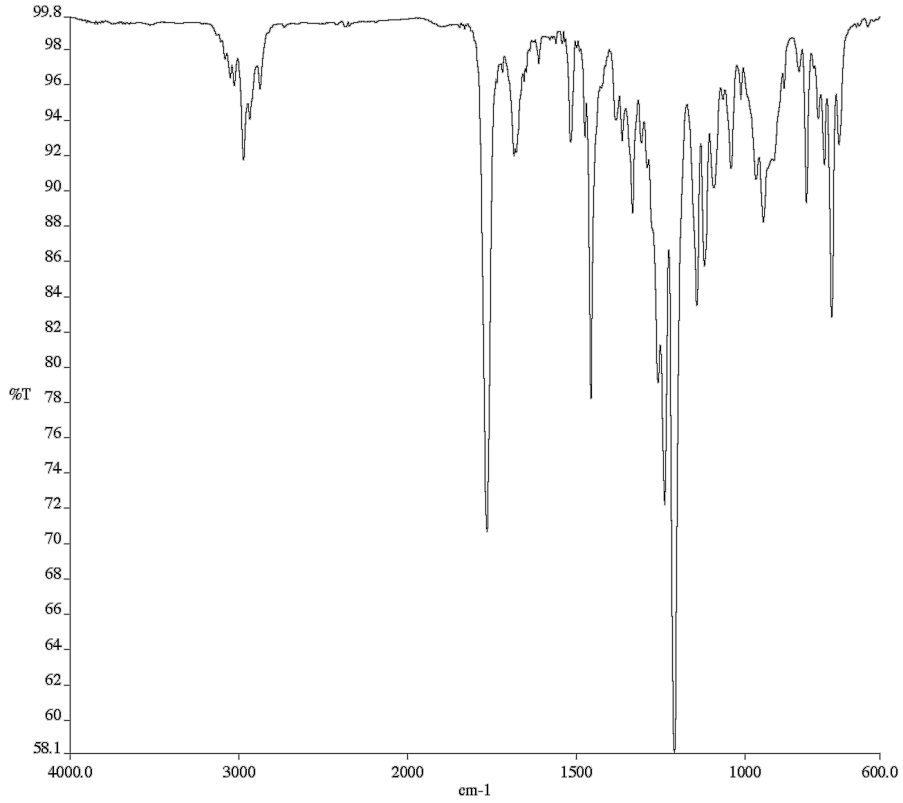

Figure A3.61 *Infrared spectrum (Thin Film, NaCl) of compound* ***19e****.*

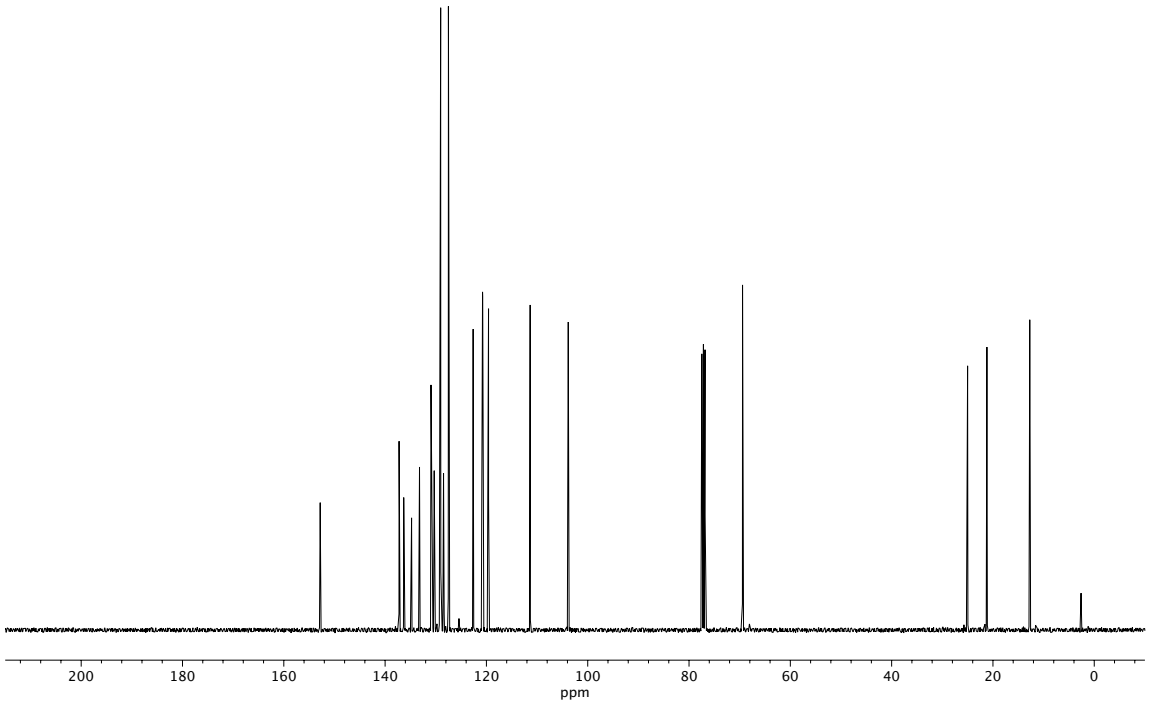

Figure A3.62 *^{13}C NMR (100 MHz, $CDCl_3$) of compound* ***19e****.*

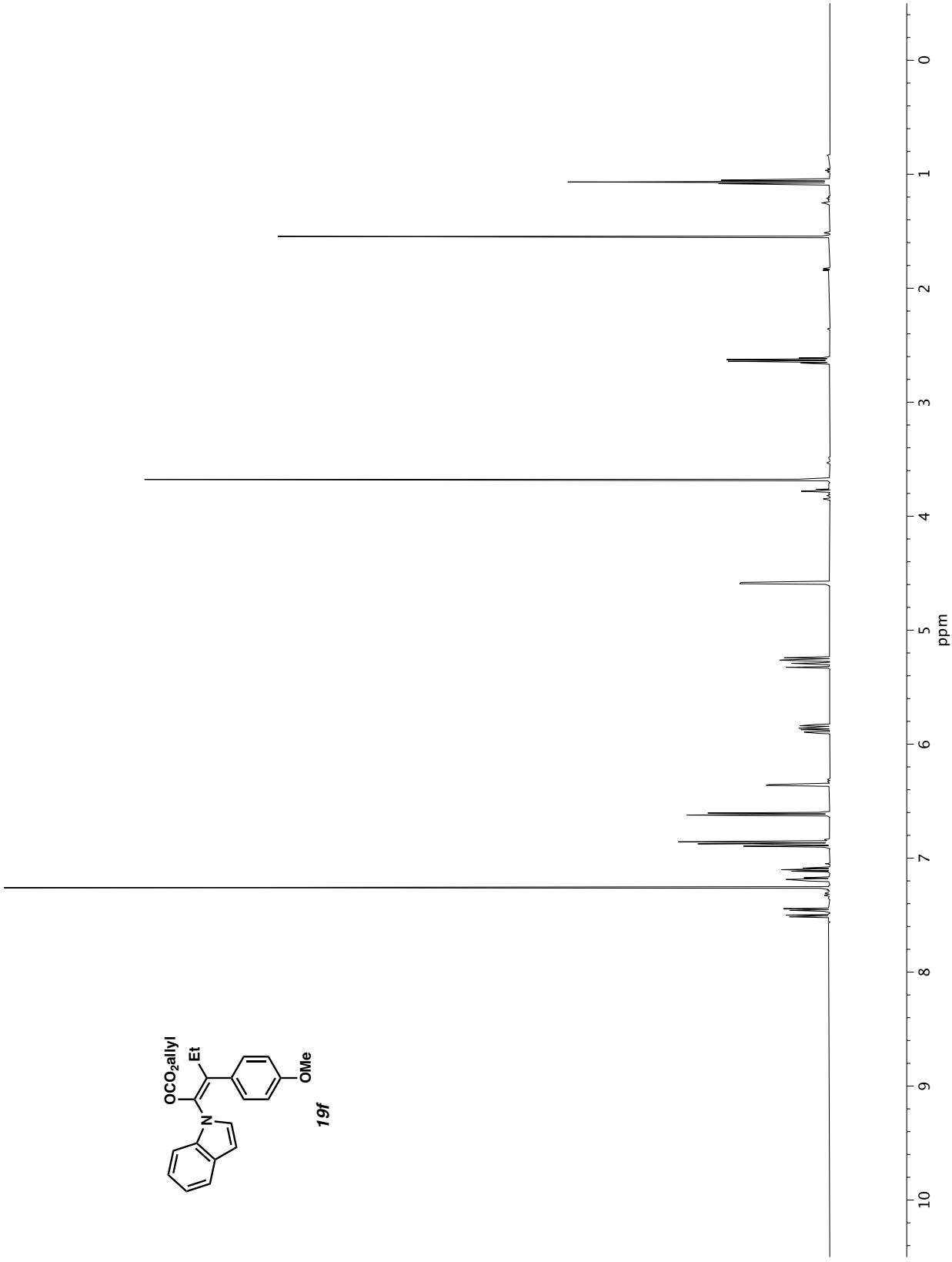

Figure A3.63 *^{1}H NMR (500 MHz, $CDCl_3$) of compound **19f**.*

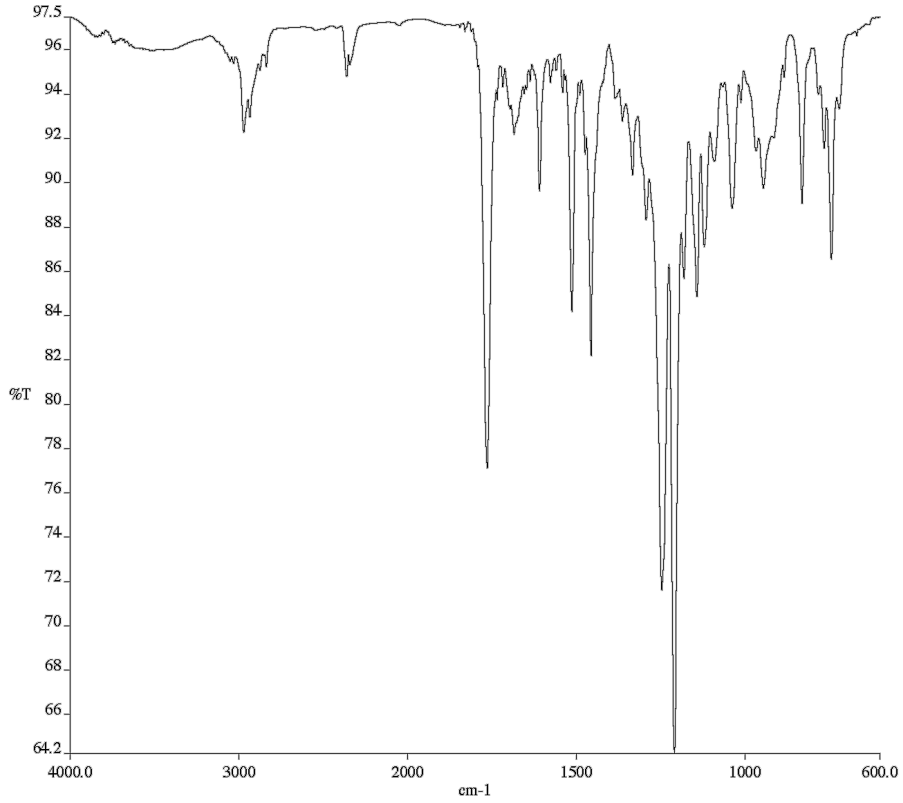

Figure A3.64 *Infrared spectrum (Thin Film, NaCl) of compound* ***19f****.*

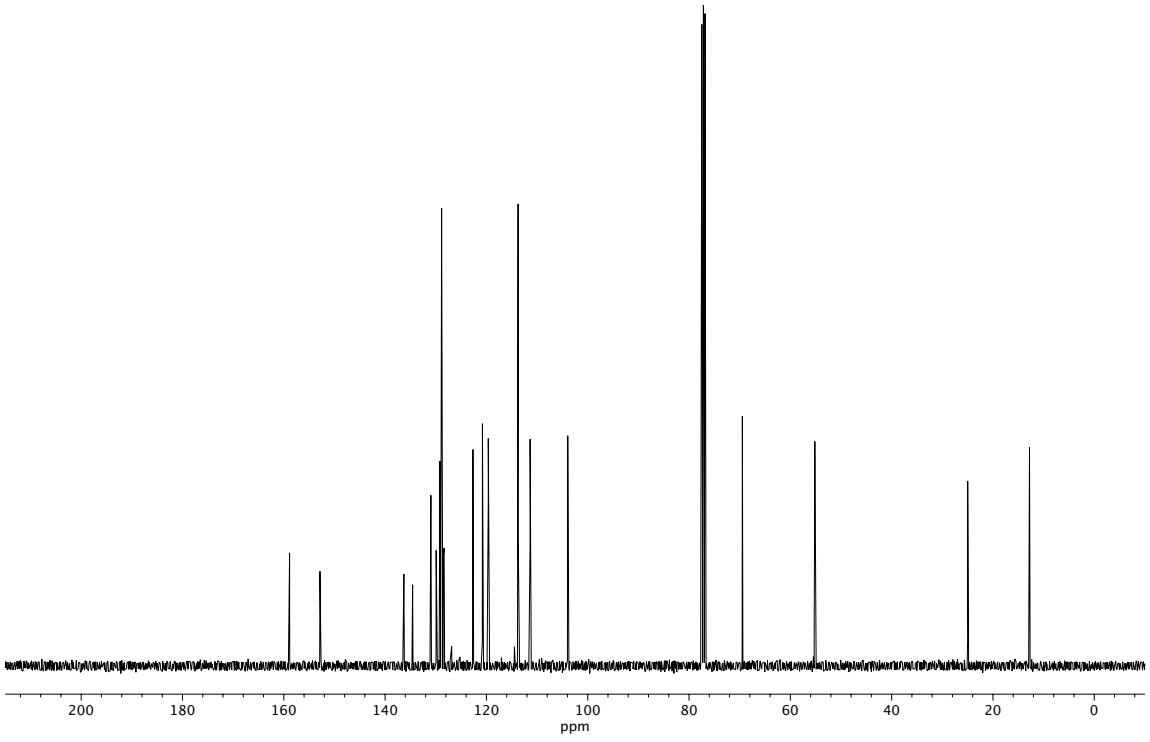

Figure A3.65 *^{13}C NMR (100 MHz, $CDCl_3$) of compound* ***19f****.*

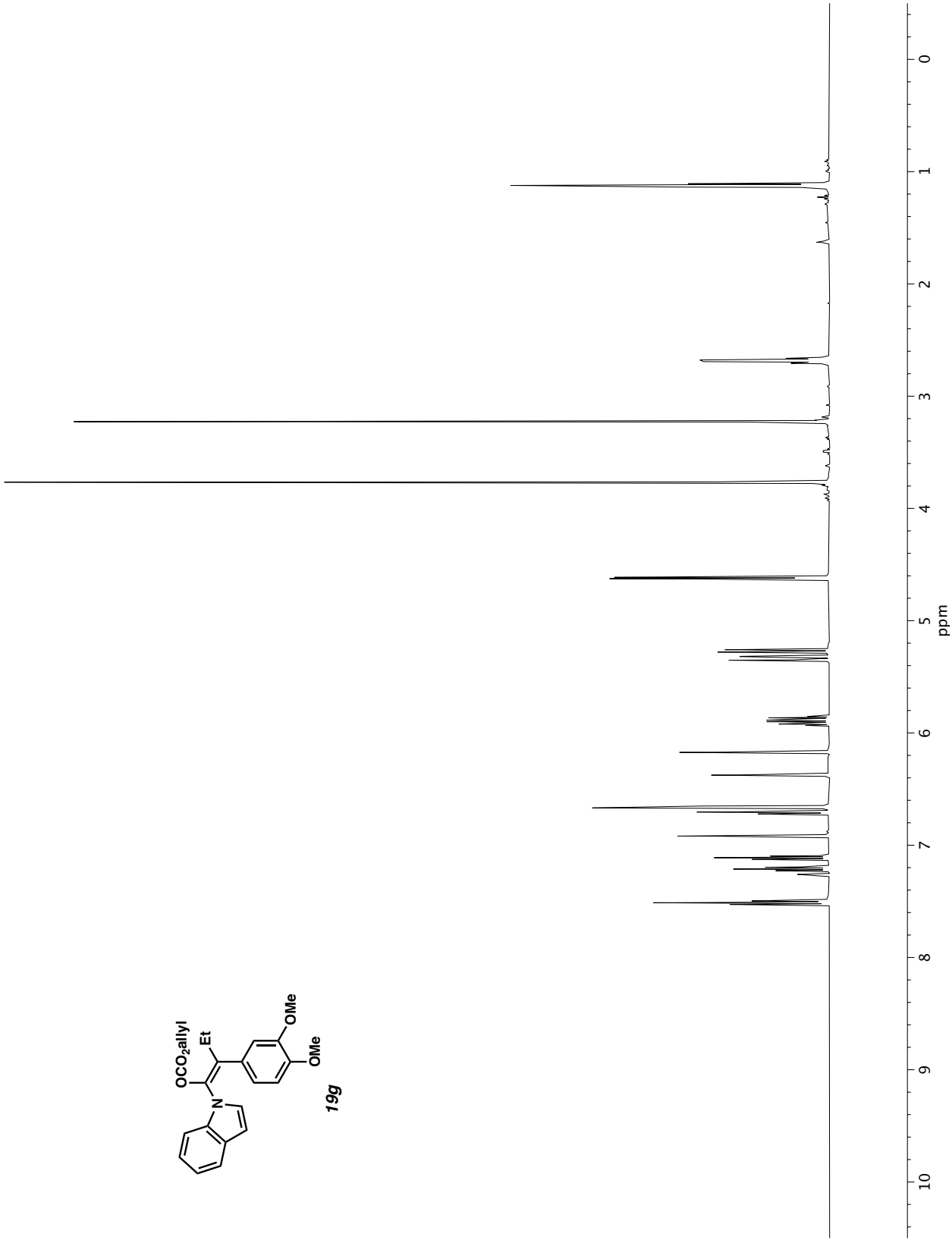

Figure A3.66 *^1H NMR (500 MHz, $CDCl_3$) of compound **19g**.*

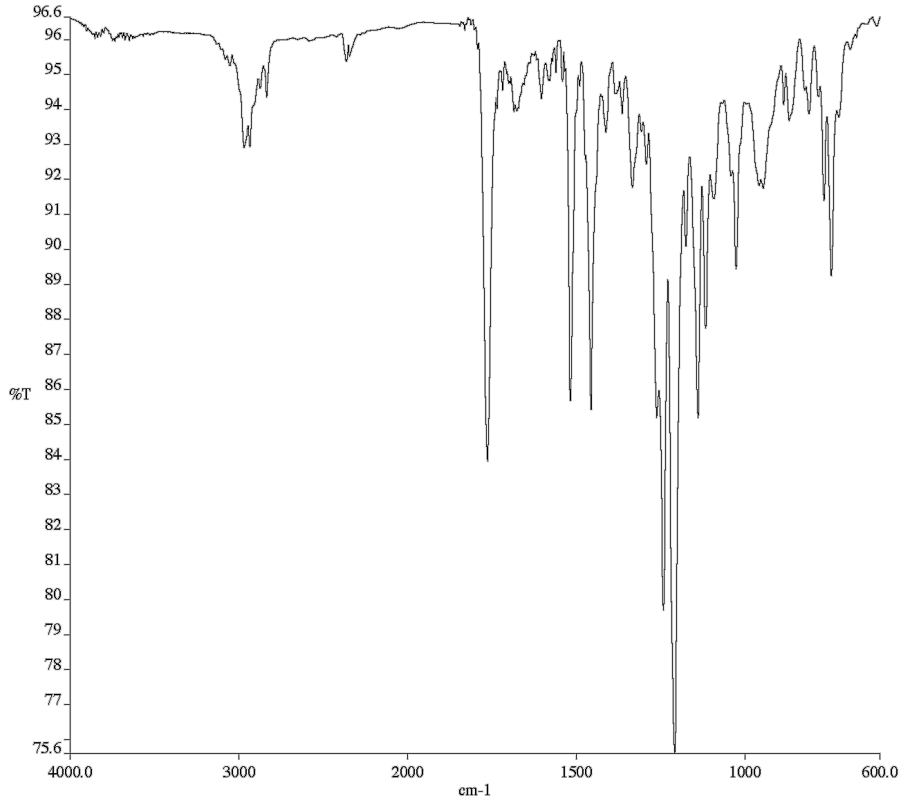

Figure A3.67 *Infrared spectrum (Thin Film, NaCl) of compound* ***19g****.*

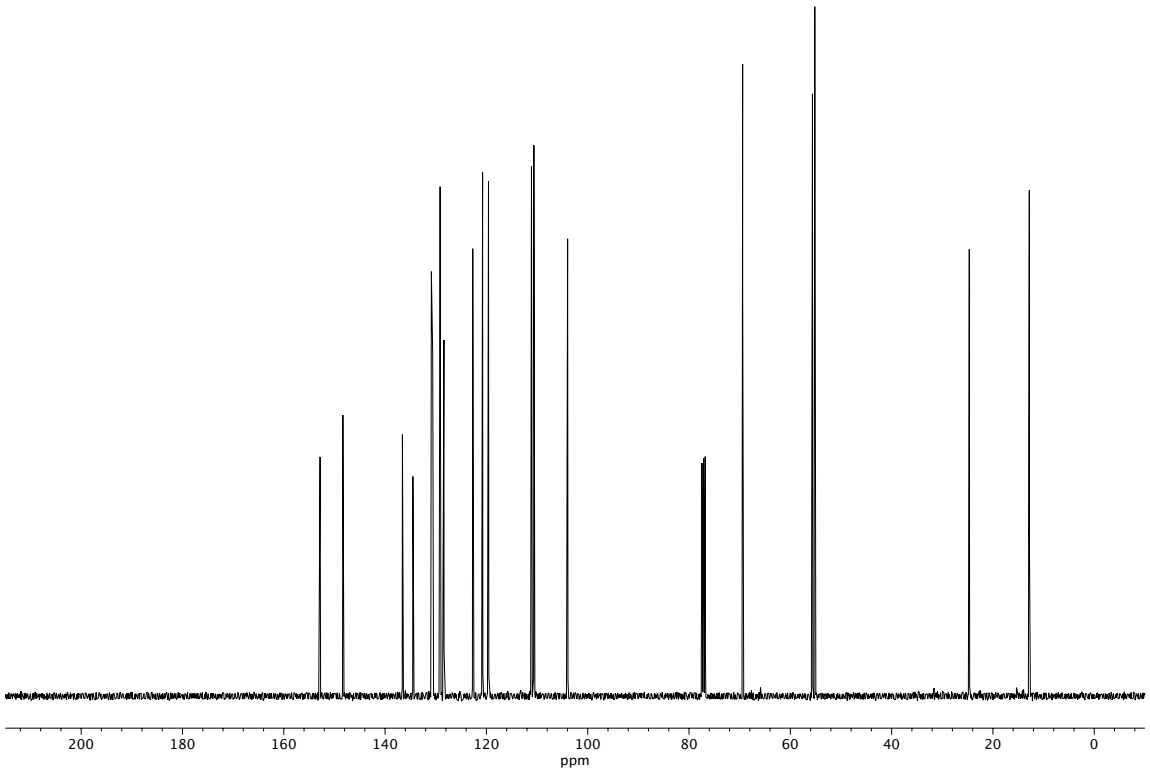

Figure A3.68 *^{13}C NMR (100 MHz, $CDCl_3$) of compound* ***19g****.*

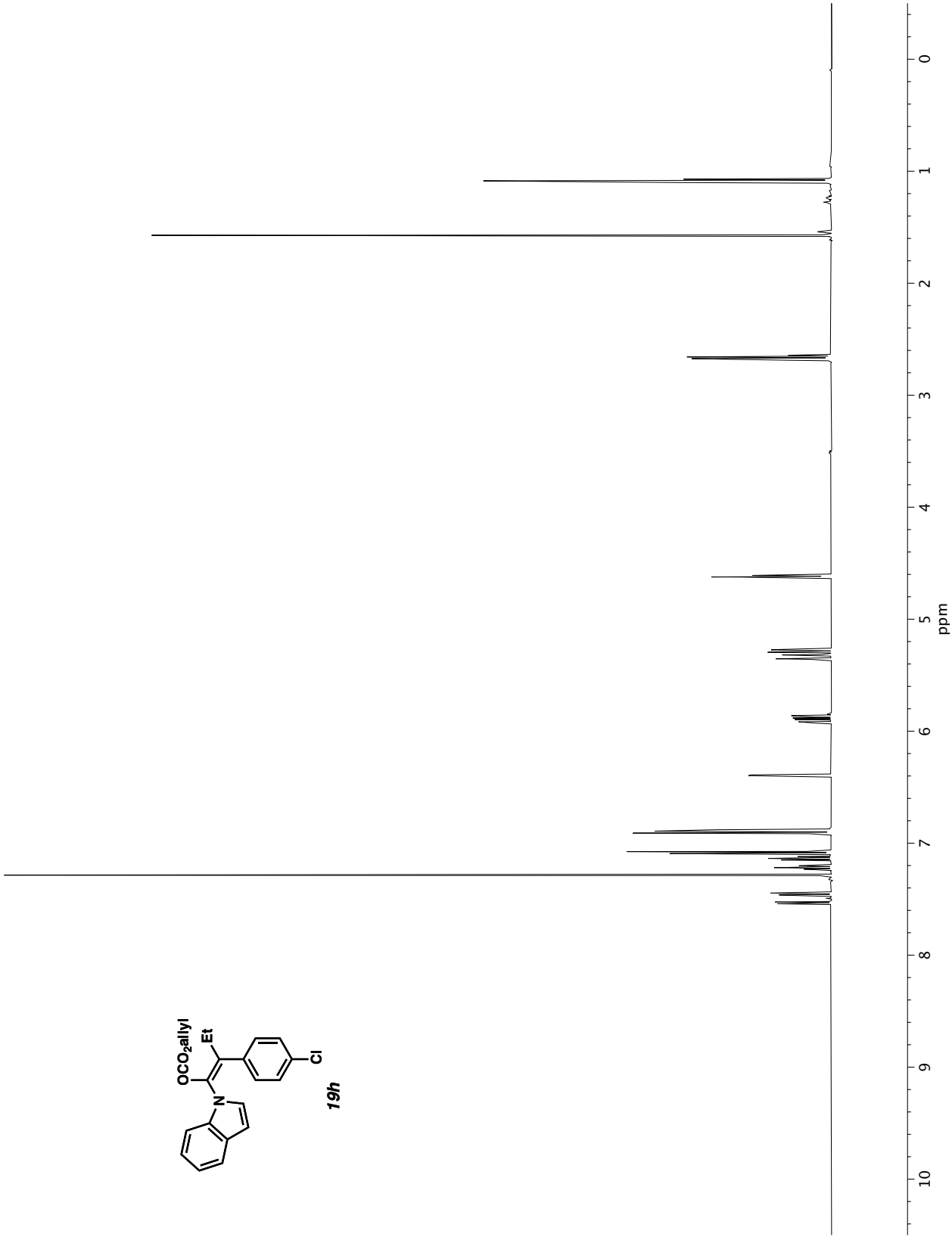

Figure A3.69 *^1H NMR (500 MHz, $CDCl_3$) of compound* ***19h***.

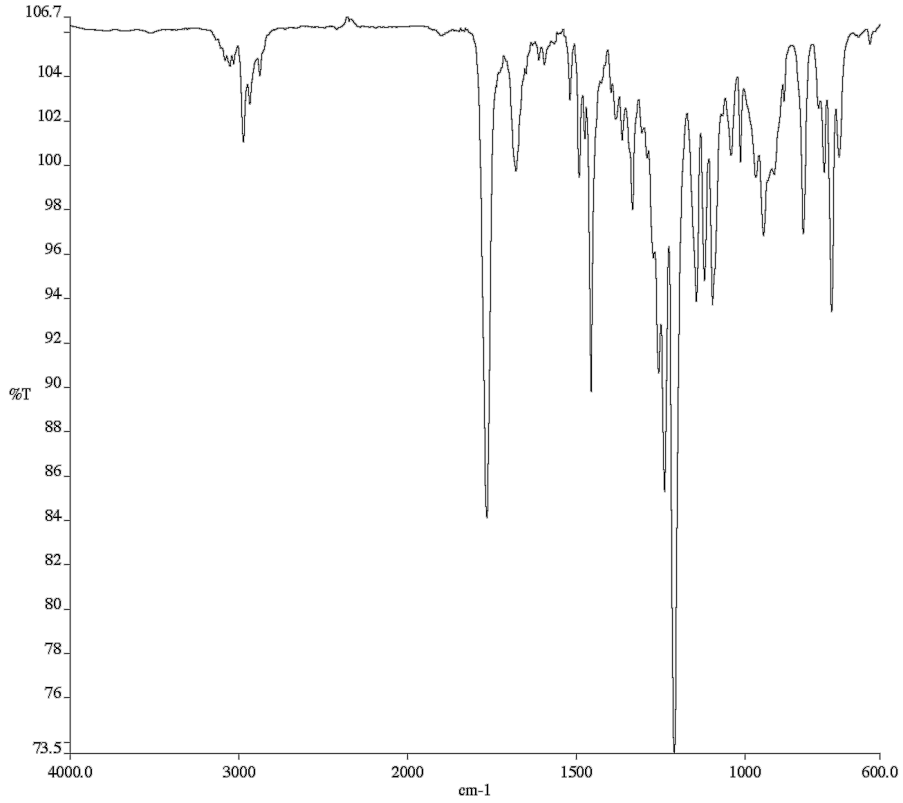

Figure A3.70 *Infrared spectrum (Thin Film, NaCl) of compound* ***19h****.*

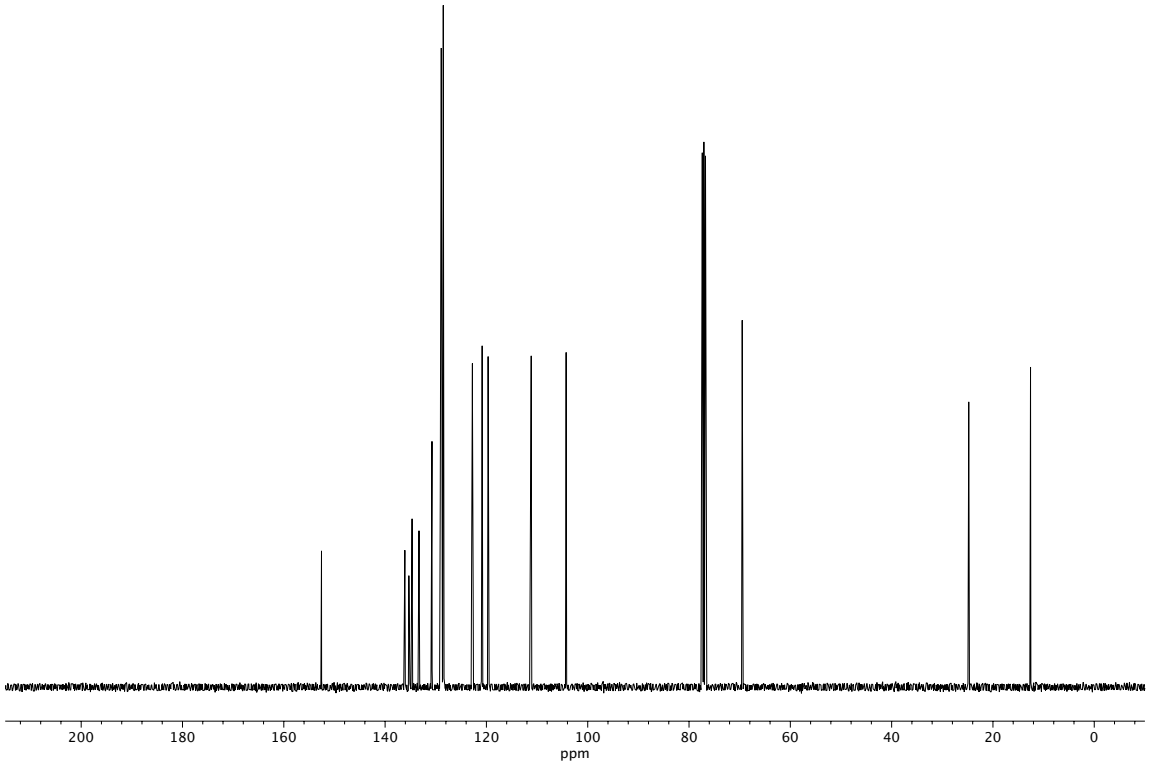

Figure A3.71 *^{13}C NMR (100 MHz, $CDCl_3$) of compound* ***19h****.*

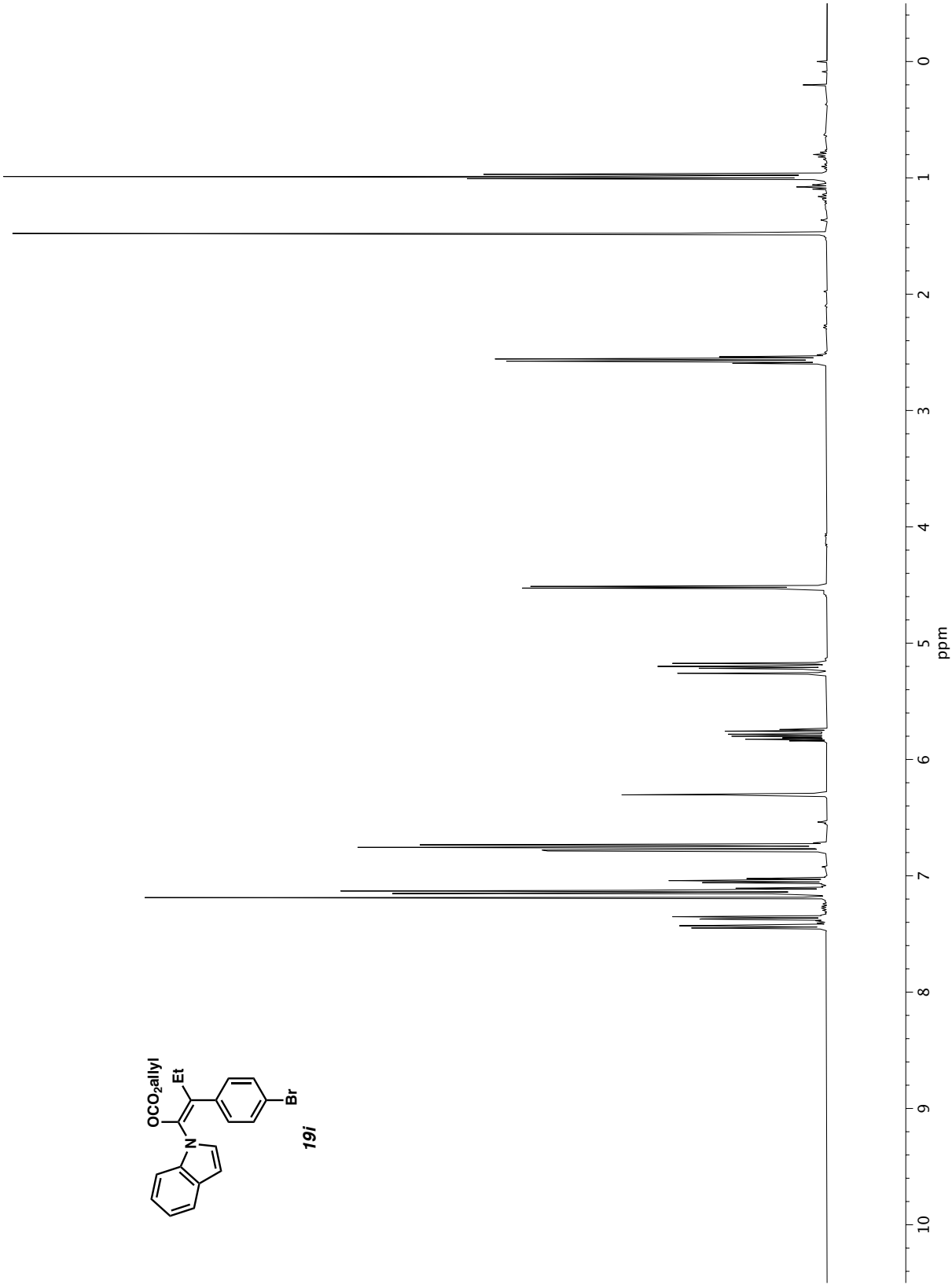

***Figure A3.72** ^1H NMR (500 MHz, $CDCl_3$) of compound **19i**.*

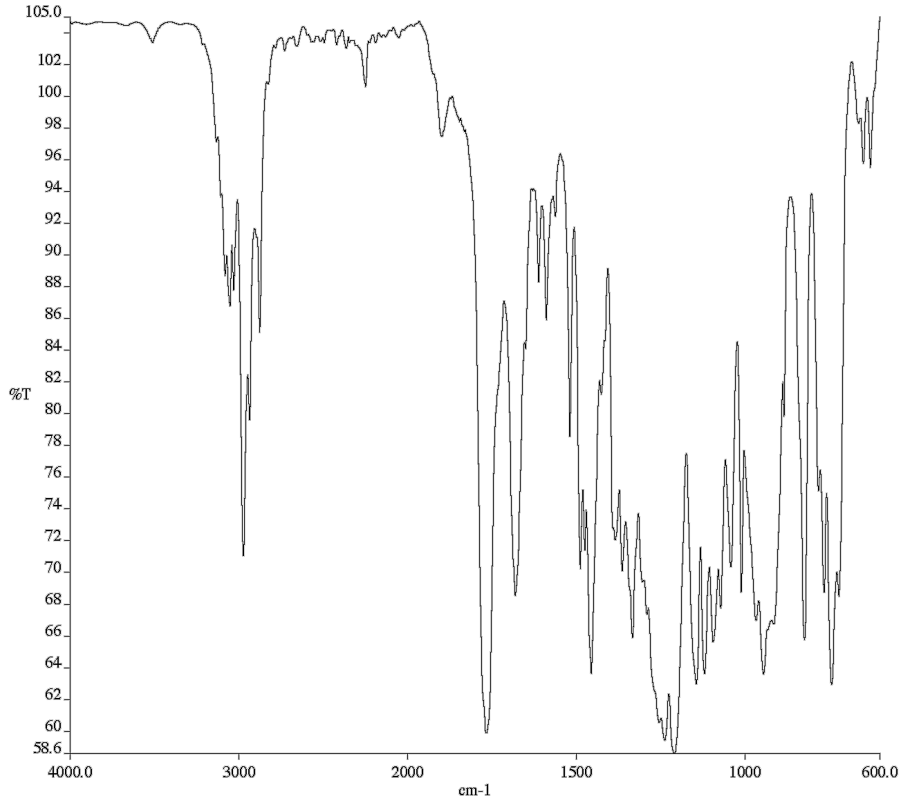

Figure A3.73 *Infrared spectrum (Thin Film, NaCl) of compound* ***19i****.*

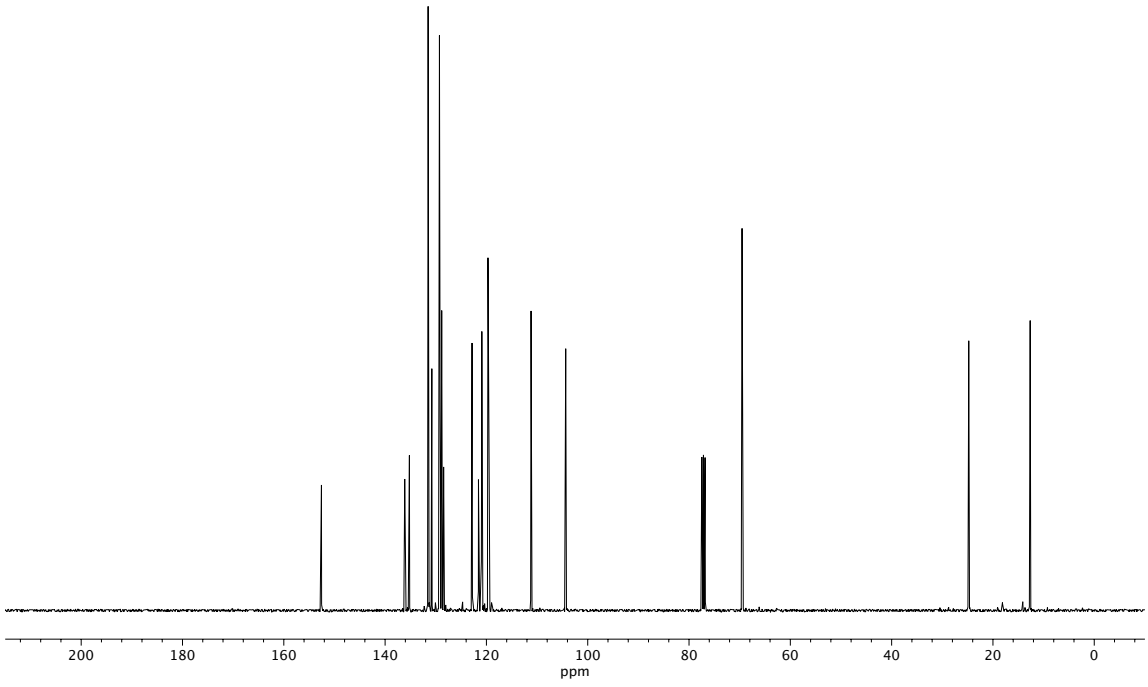

Figure A3.74 *^{13}C NMR (100 MHz, $CDCl_3$) of compound* ***19i****.*

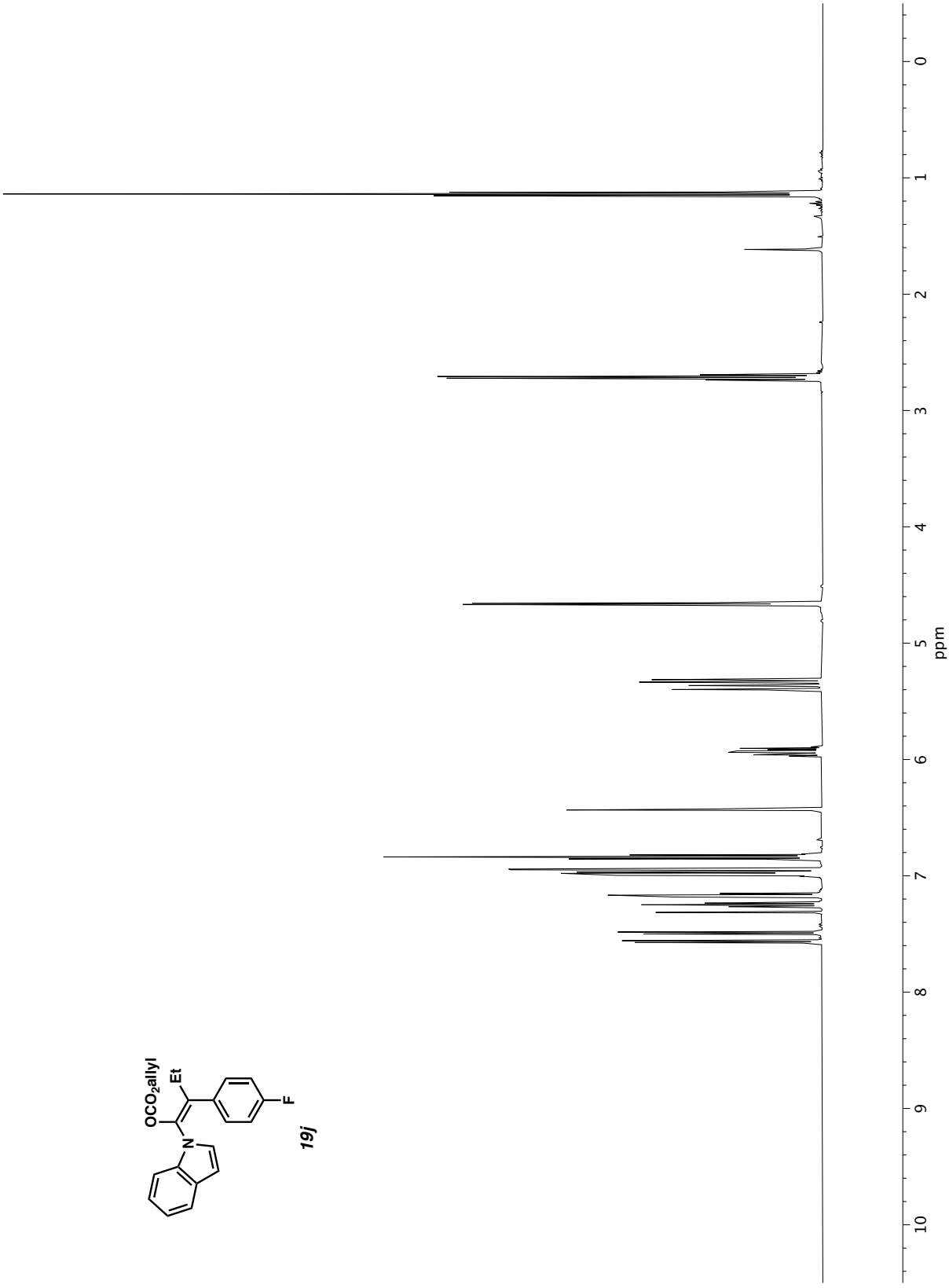

***Figure A3.75** ^1H NMR (500 MHz, $CDCl_3$) of compound **19j**.*

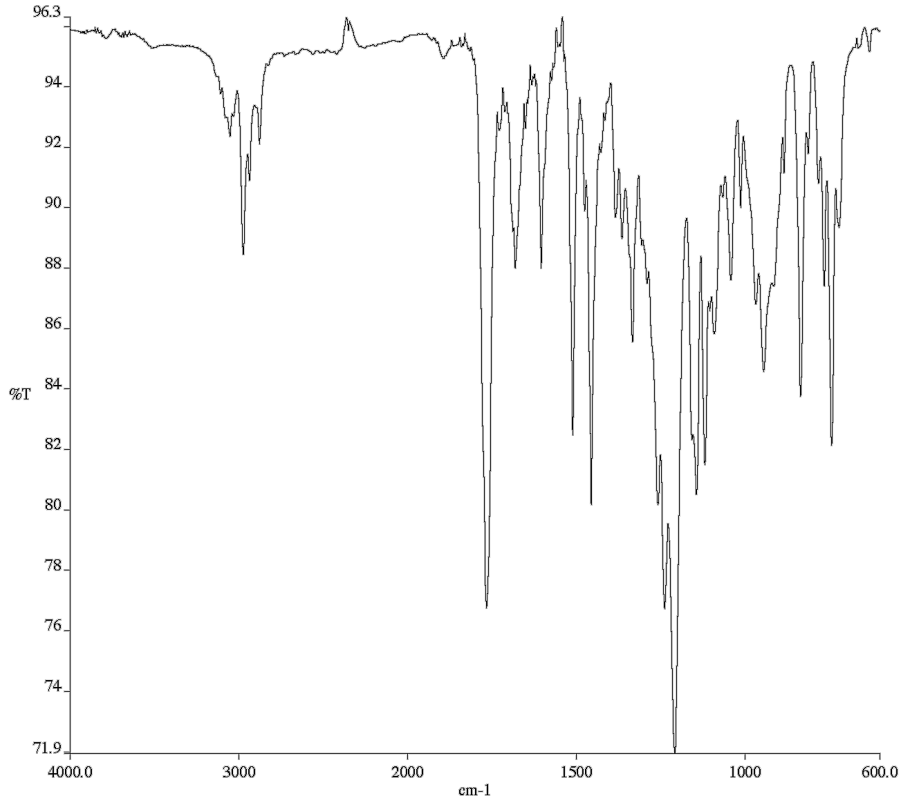

Figure A3.76 *Infrared spectrum (Thin Film, NaCl) of compound* ***19j****.*

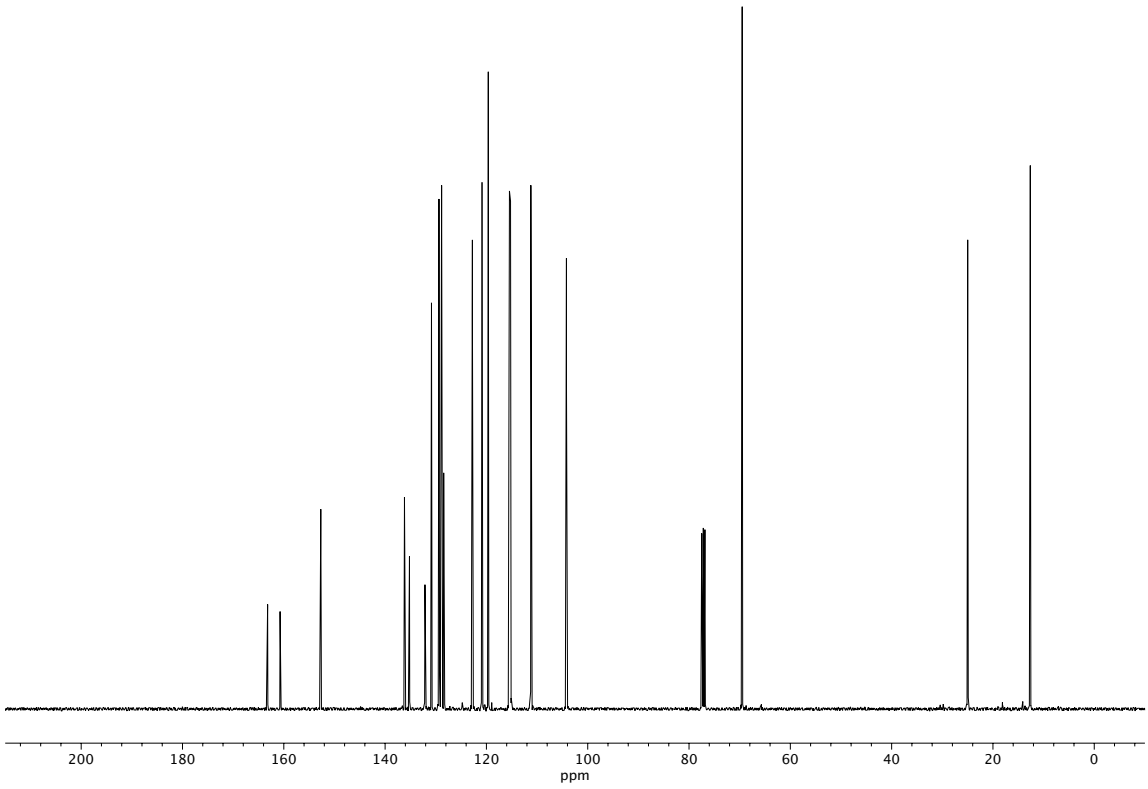

Figure A3.77 *^{13}C NMR (100 MHz, $CDCl_3$) of compound* ***19j****.*

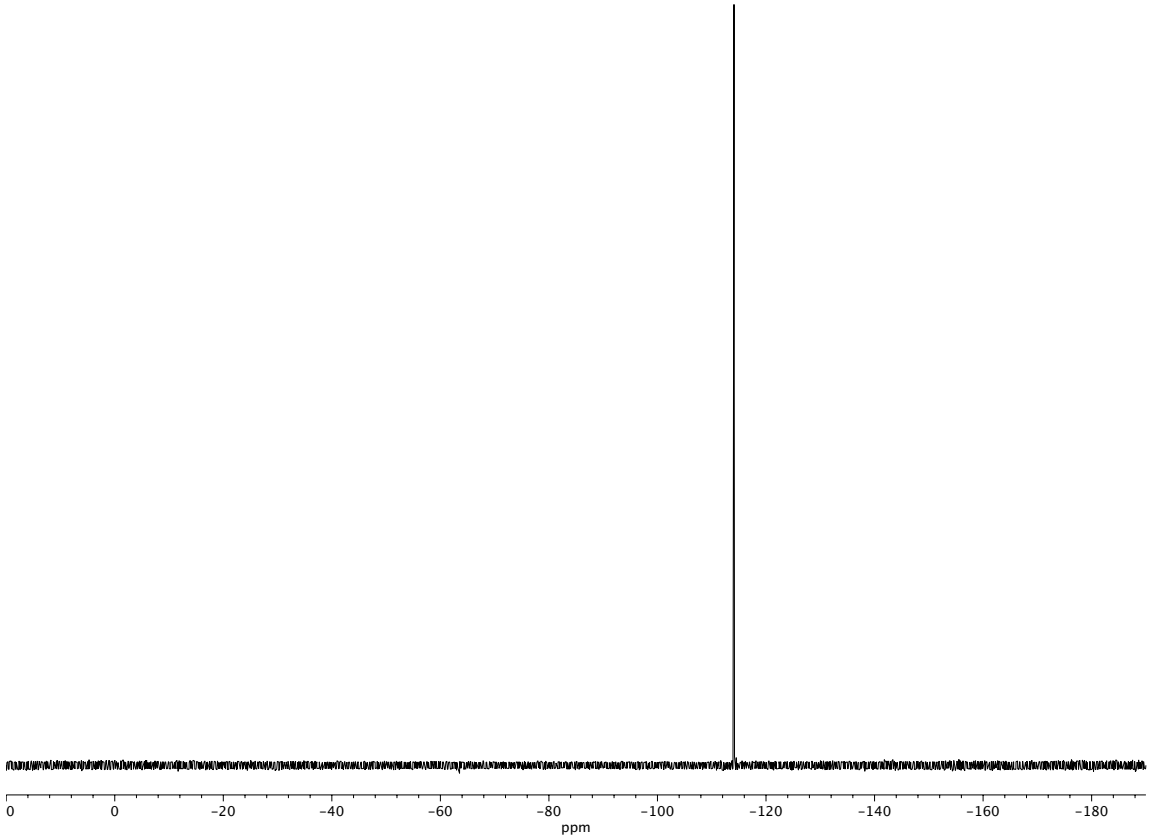

Figure A3.78 *^{19}F NMR (282 MHz, $CDCl_3$) of compound* ***19j****.*

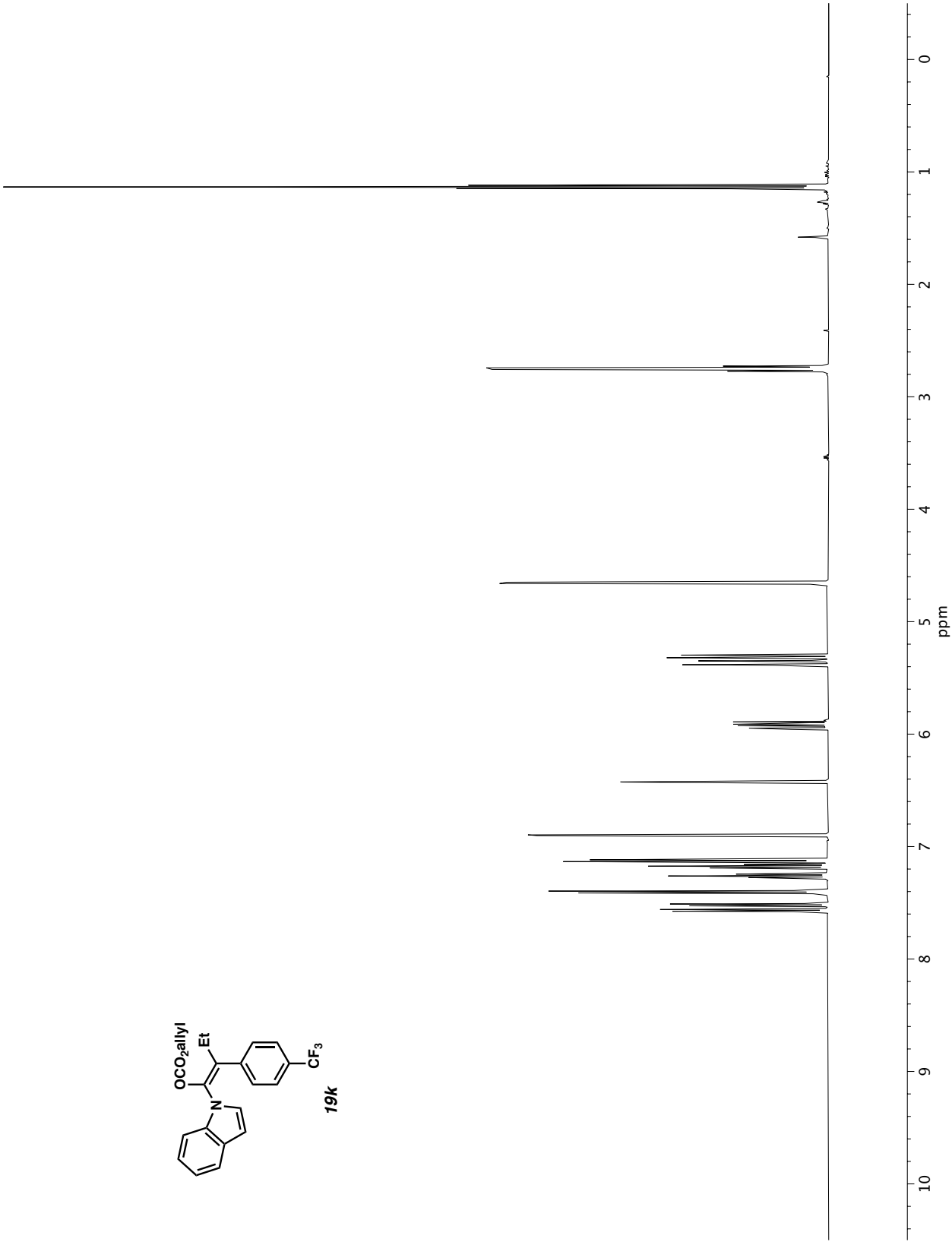

Figure A3.79 *^1H NMR (500 MHz, $CDCl_3$) of compound* ***19k****.*

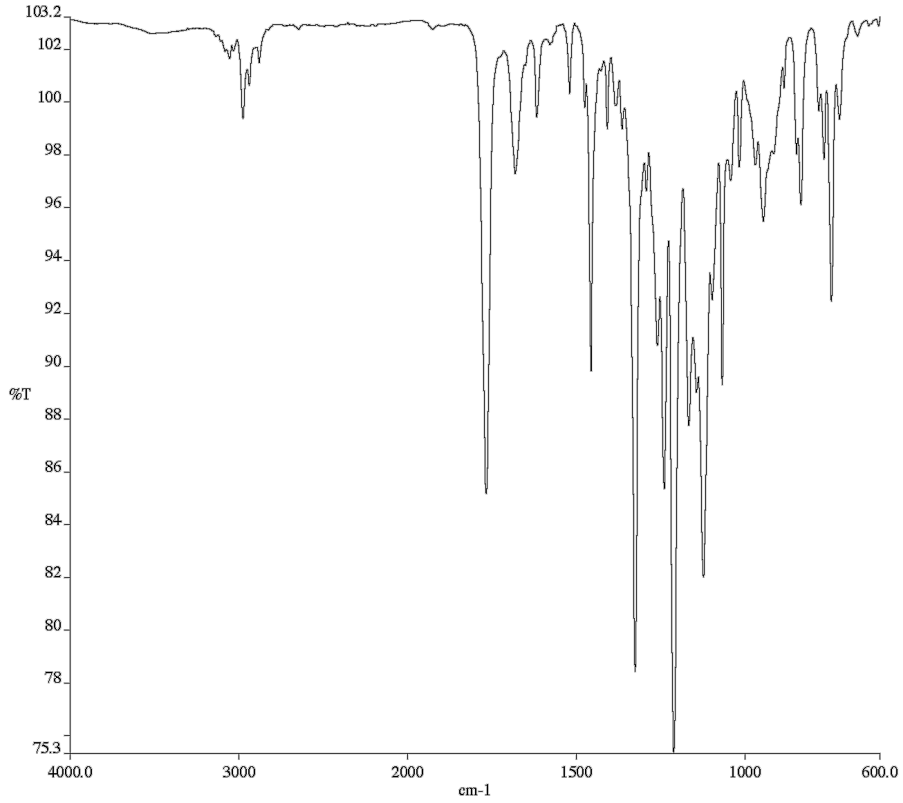

Figure A3.80 *Infrared spectrum (Thin Film, NaCl) of compound* ***19k****.*

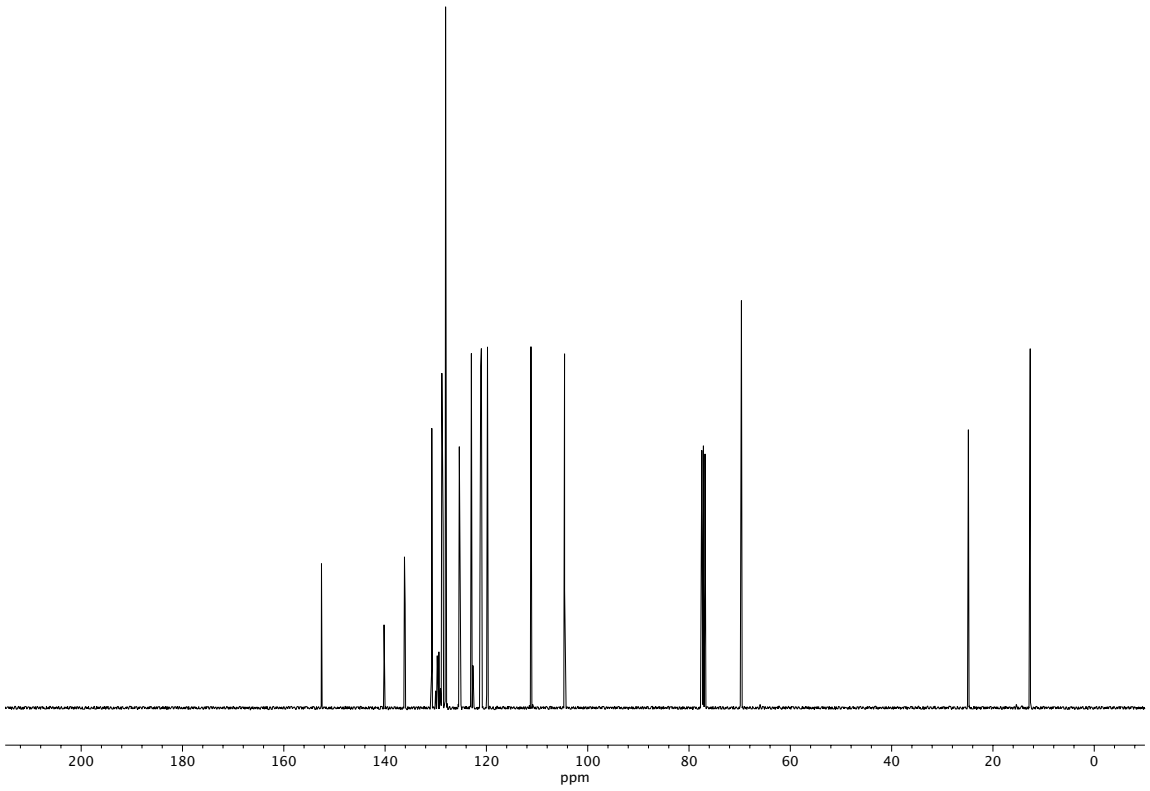

Figure A3.81 *^{13}C NMR (100 MHz, $CDCl_3$) of compound* ***19k****.*

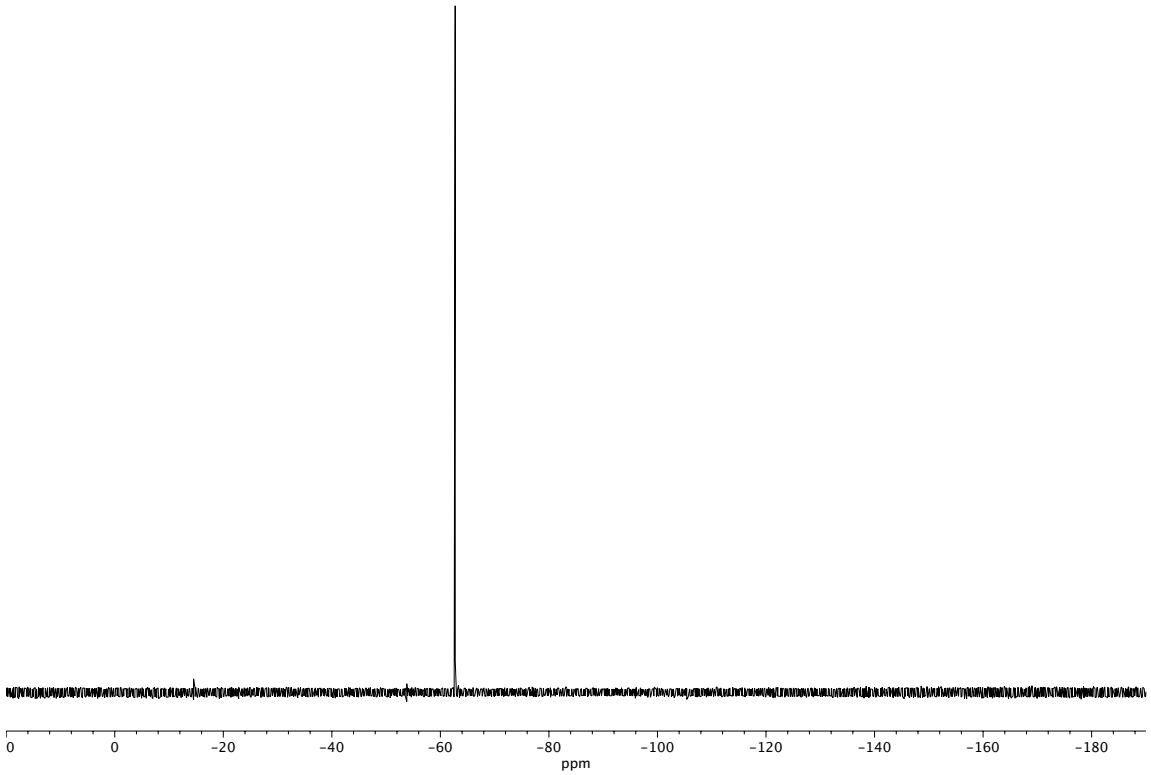

Figure A3.82 *^{19}F NMR (282 MHz, $CDCl_3$) of compound* ***19k***.

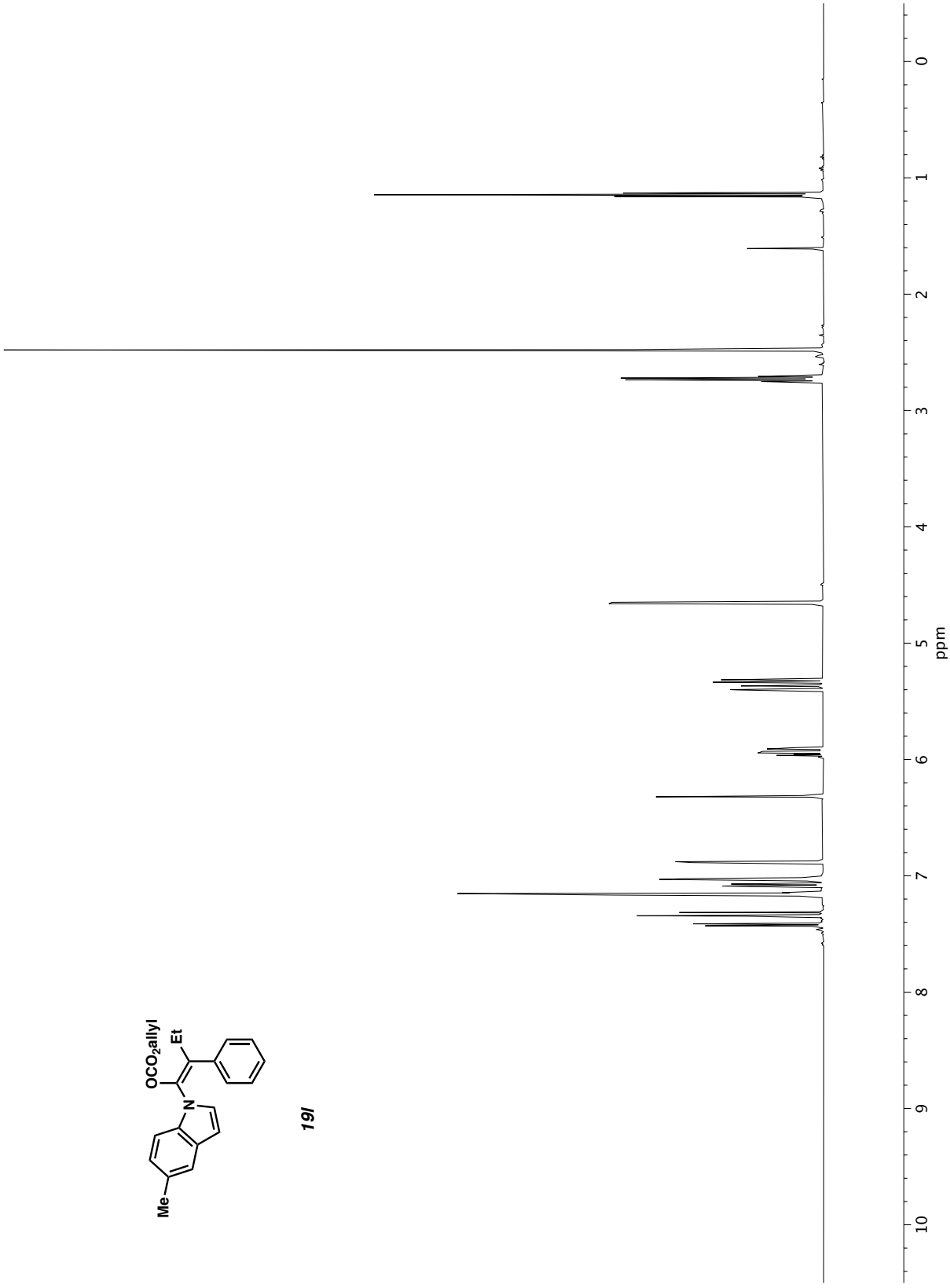

Figure A3.83 *^{1}H NMR (500 MHz, $CDCl_3$) of compound* ***19l****.*

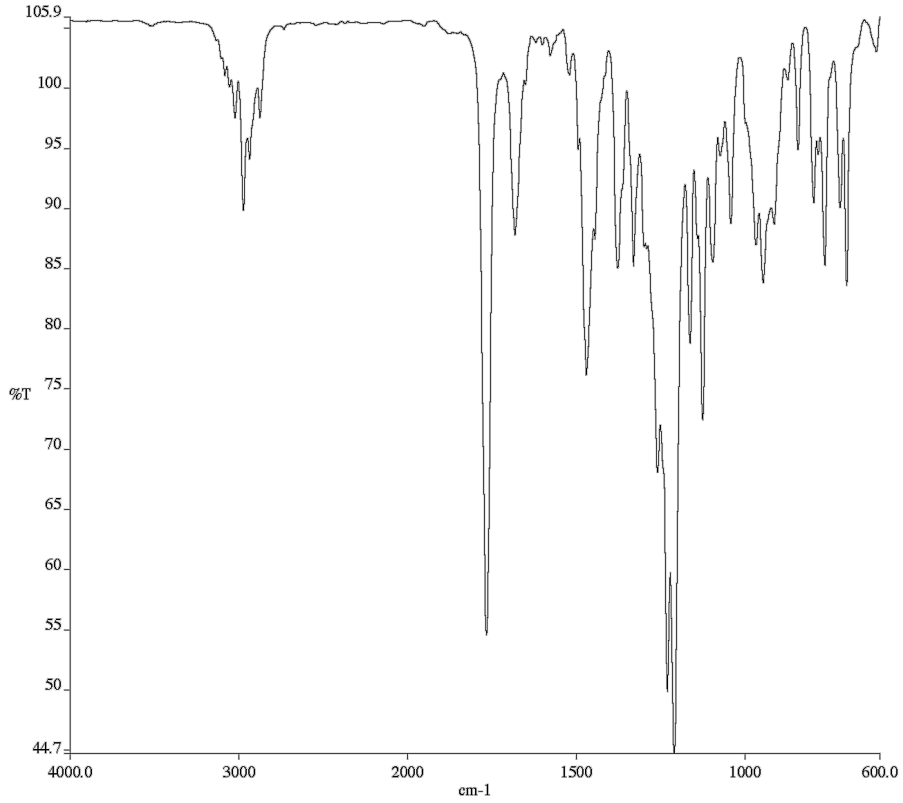

Figure A3.84 *Infrared spectrum (Thin Film, NaCl) of compound* ***19l****.*

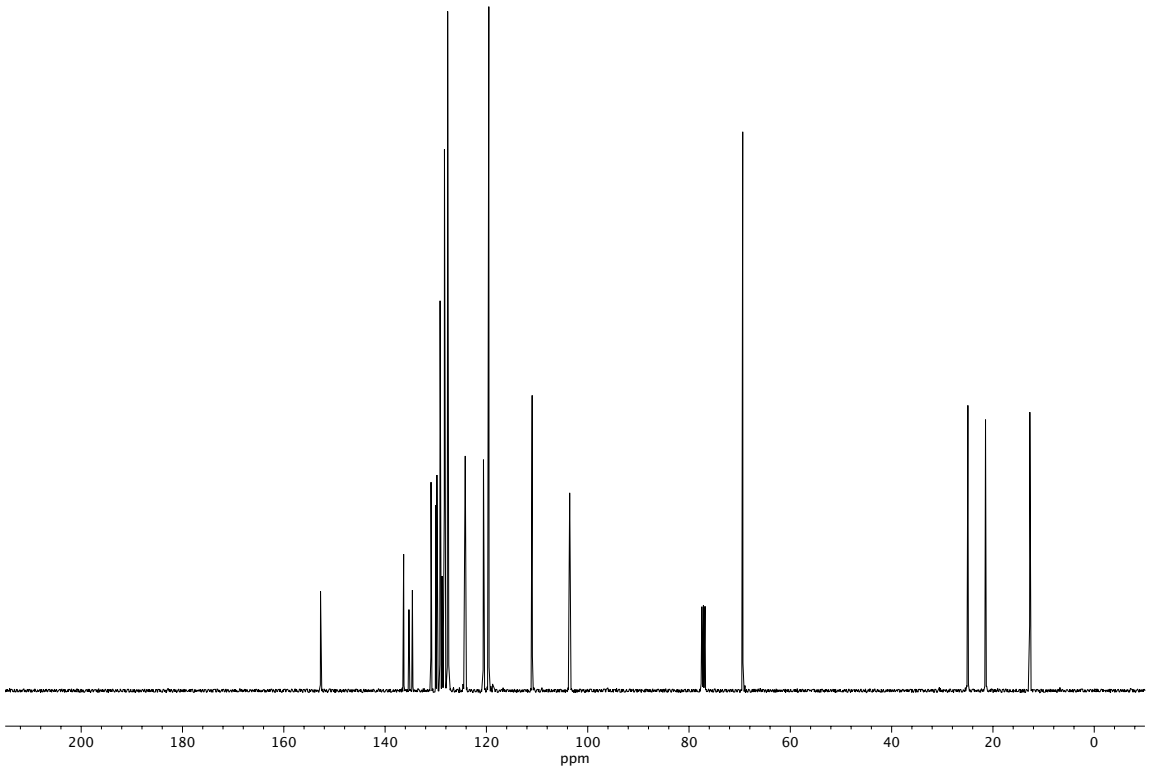

Figure A3.85 *^{13}C NMR (100 MHz, $CDCl_3$) of compound* ***19l****.*

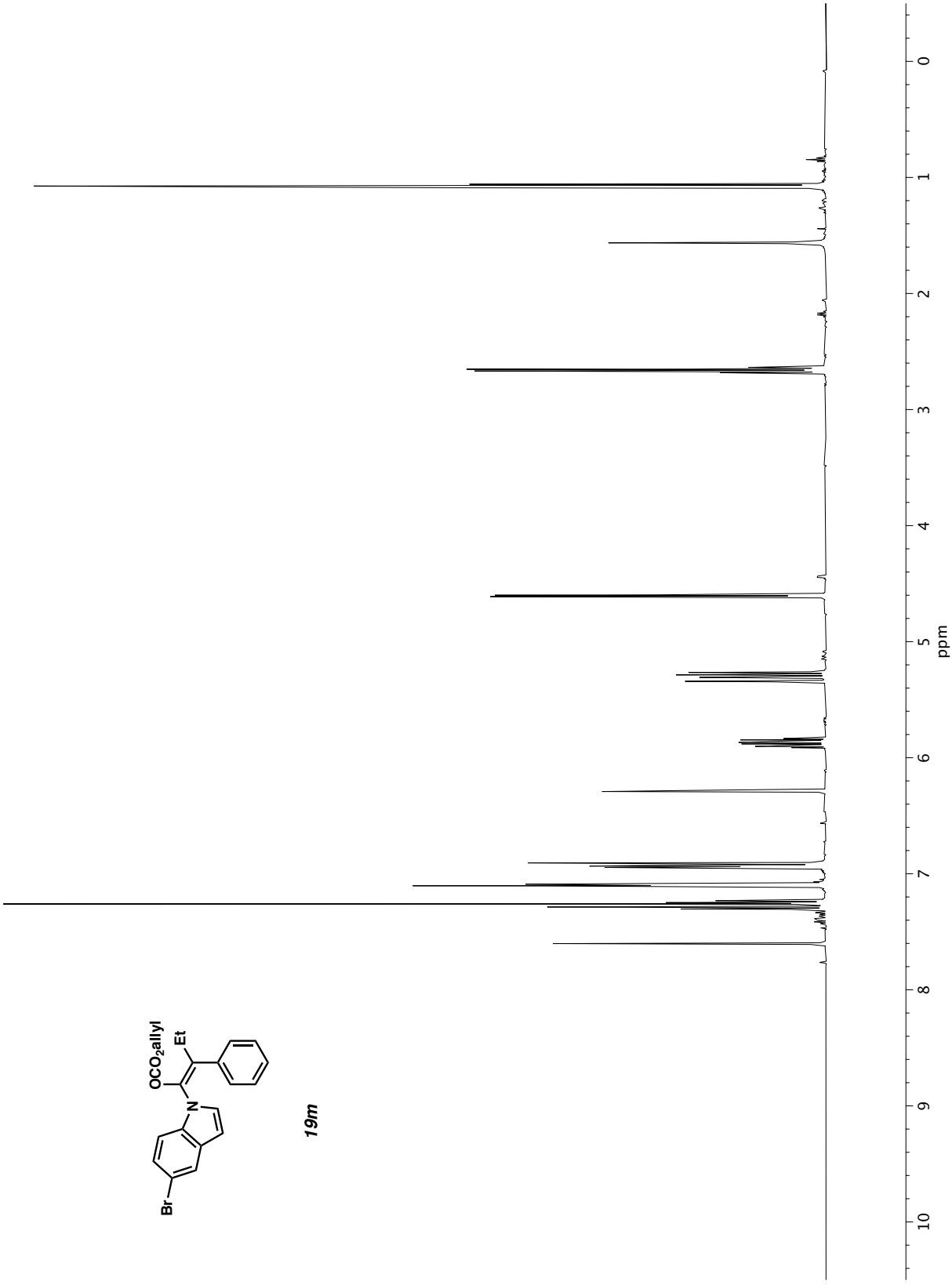

Figure A3.86 *^{1}H NMR (500 MHz, $CDCl_3$) of compound* ***19m****.*

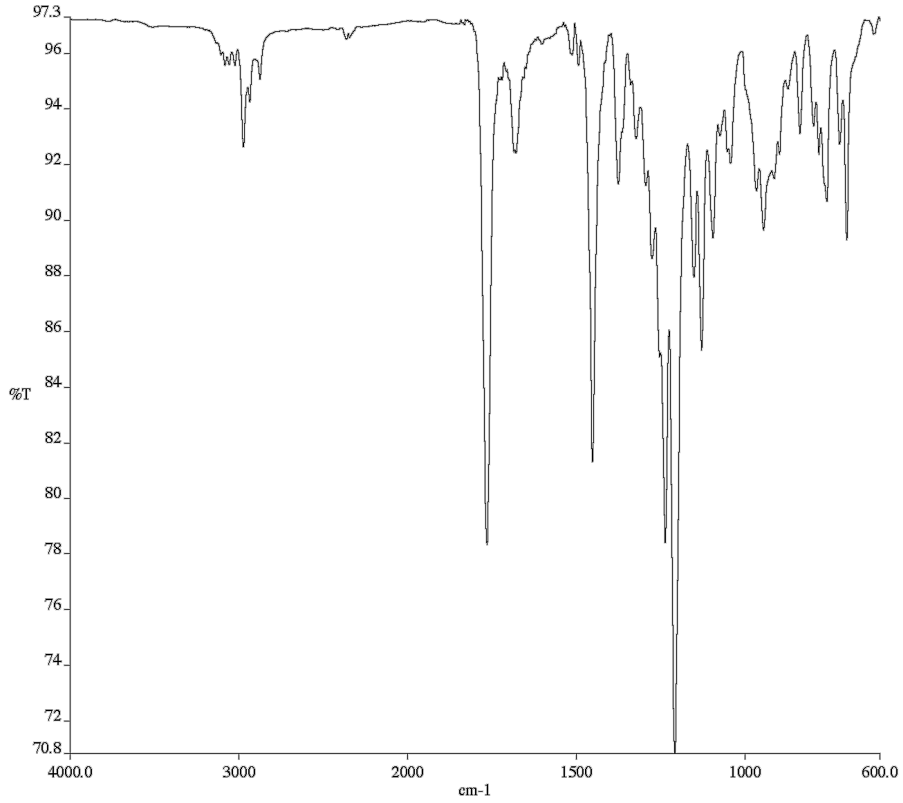

Figure A3.87 *Infrared spectrum (Thin Film, NaCl) of compound* ***19m****.*

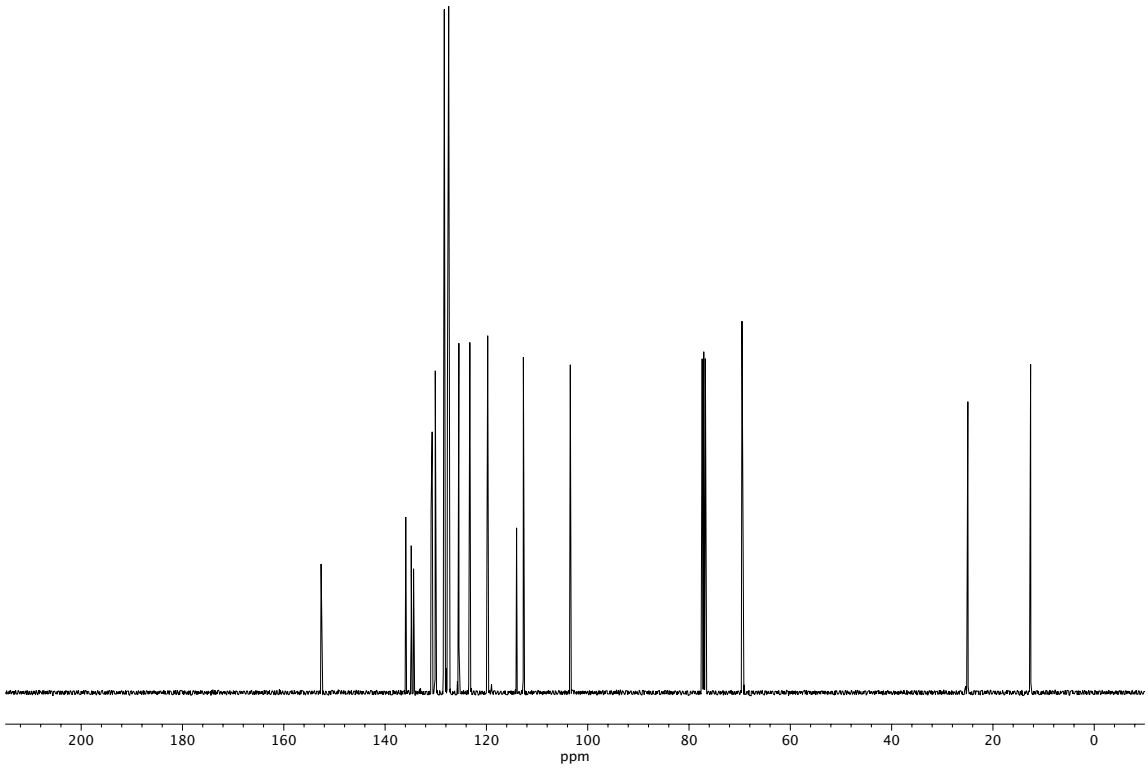

Figure A3.88 *^{13}C NMR (100 MHz, $CDCl_3$) of compound* ***19m****.*

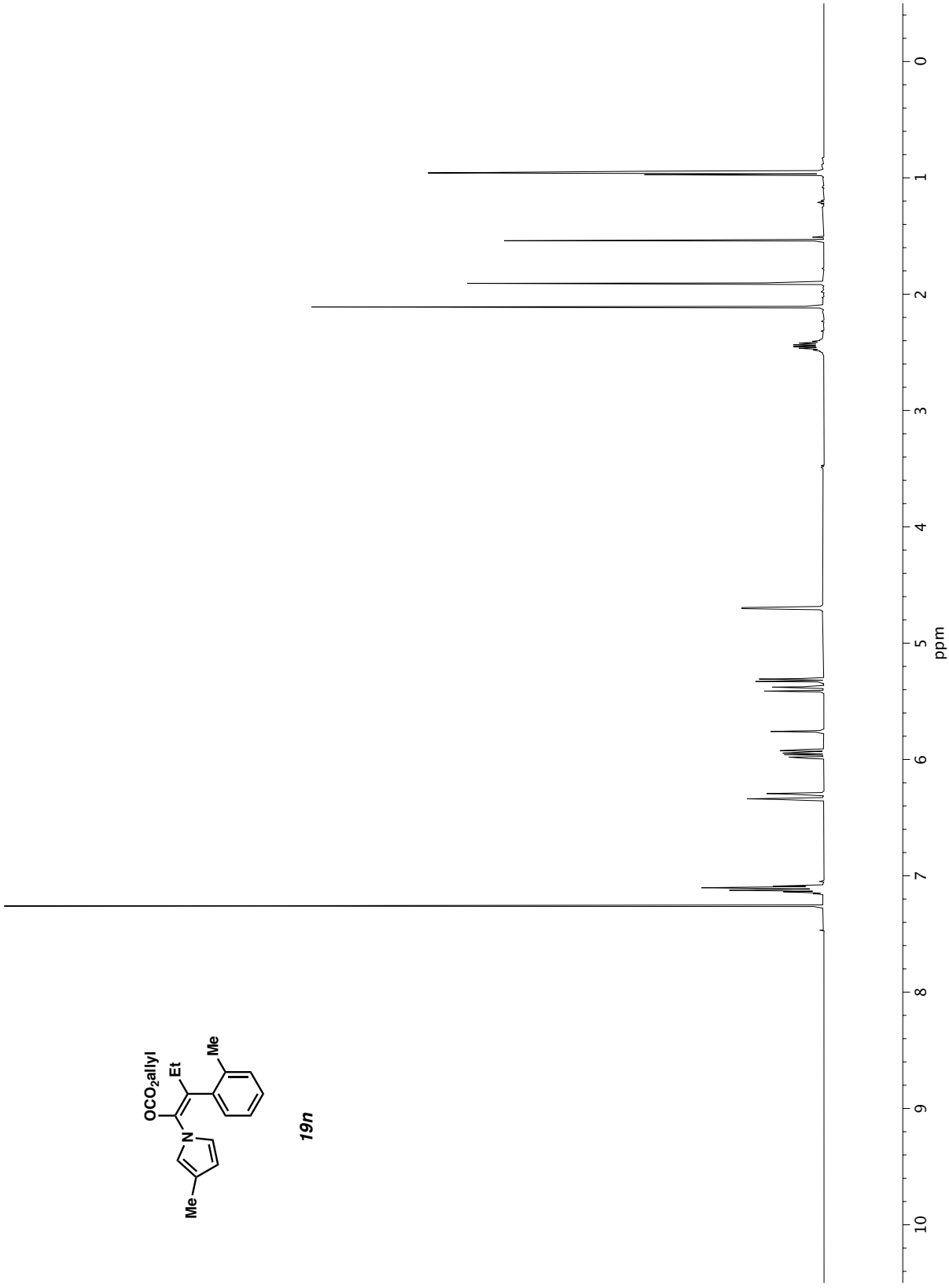

Figure A3.89 *^1H NMR (500 MHz, $CDCl_3$) of compound* ***19n***.

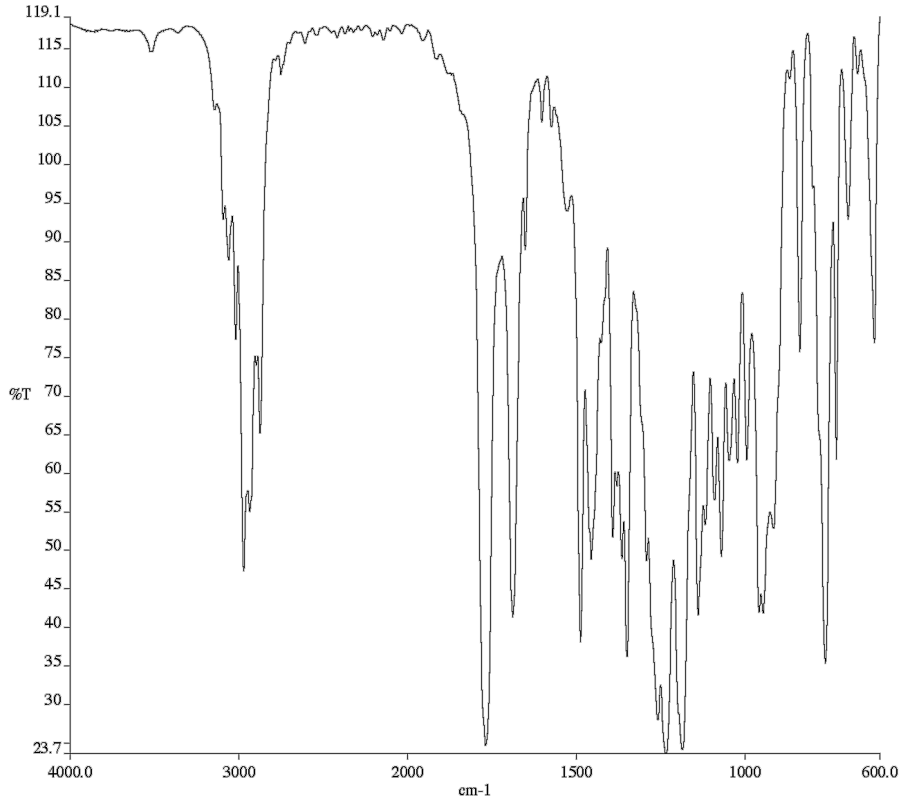

Figure A3.90 *Infrared spectrum (Thin Film, NaCl) of compound* ***19n****.*

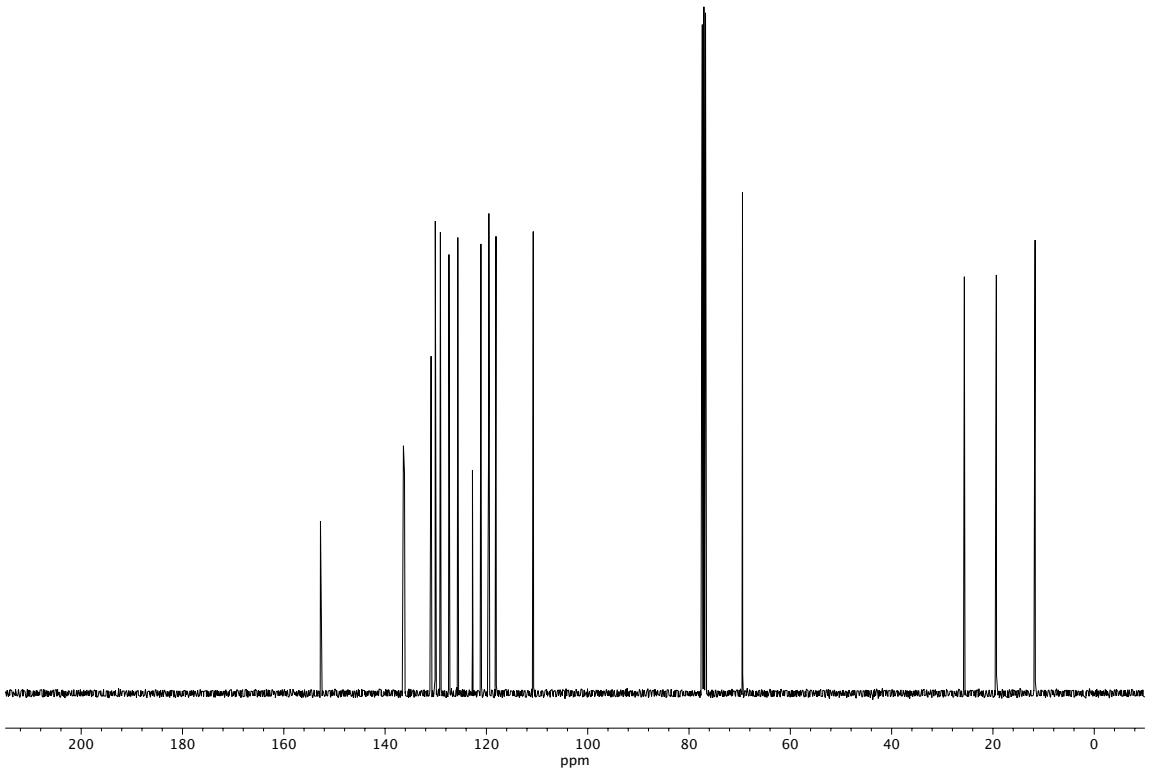

Figure A3.91 *^{13}C NMR (100 MHz, $CDCl_3$) of compound* ***19n****.*

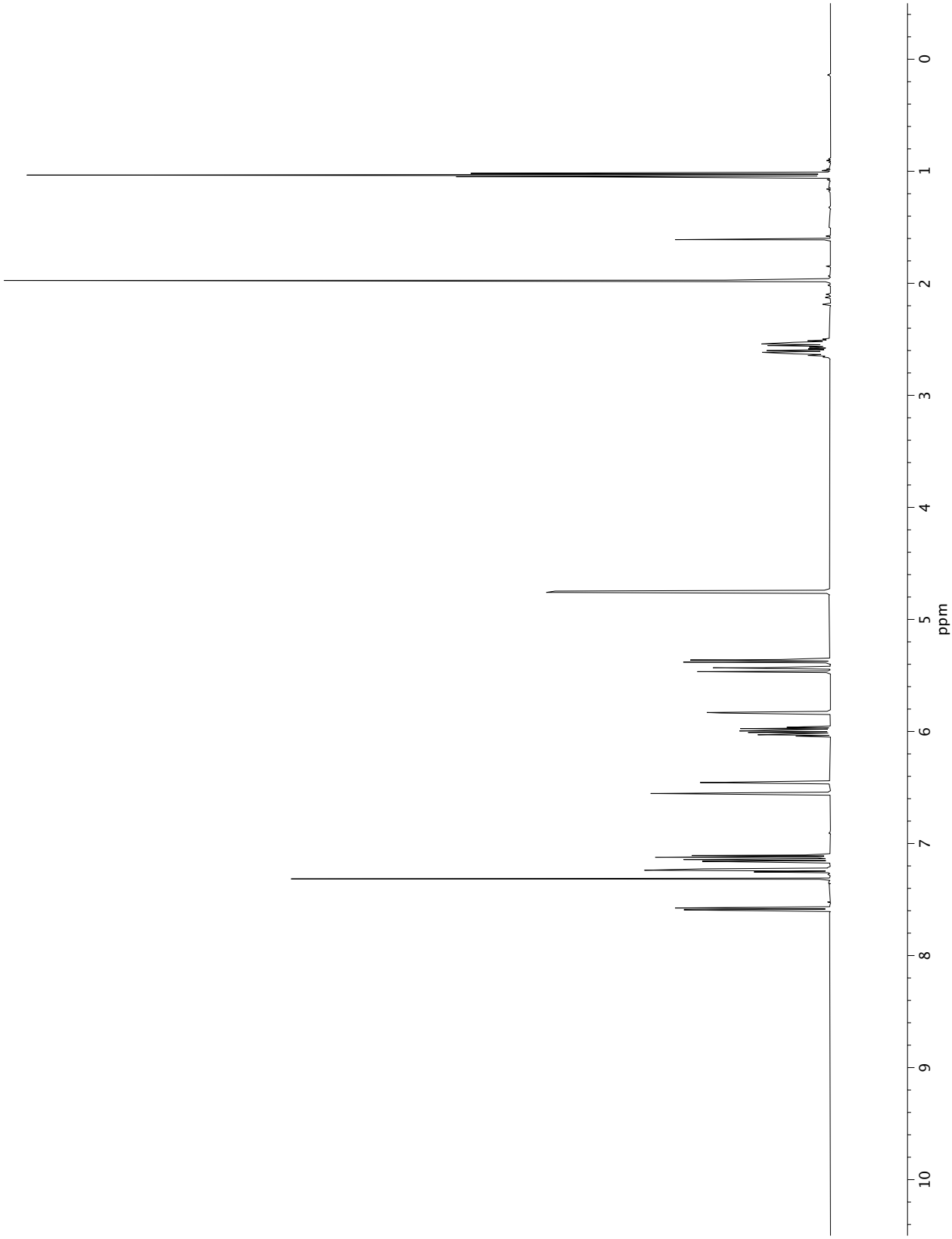

Figure A3.92 *^{1}H NMR (500 MHz, $CDCl_3$) of compound **19o**.*

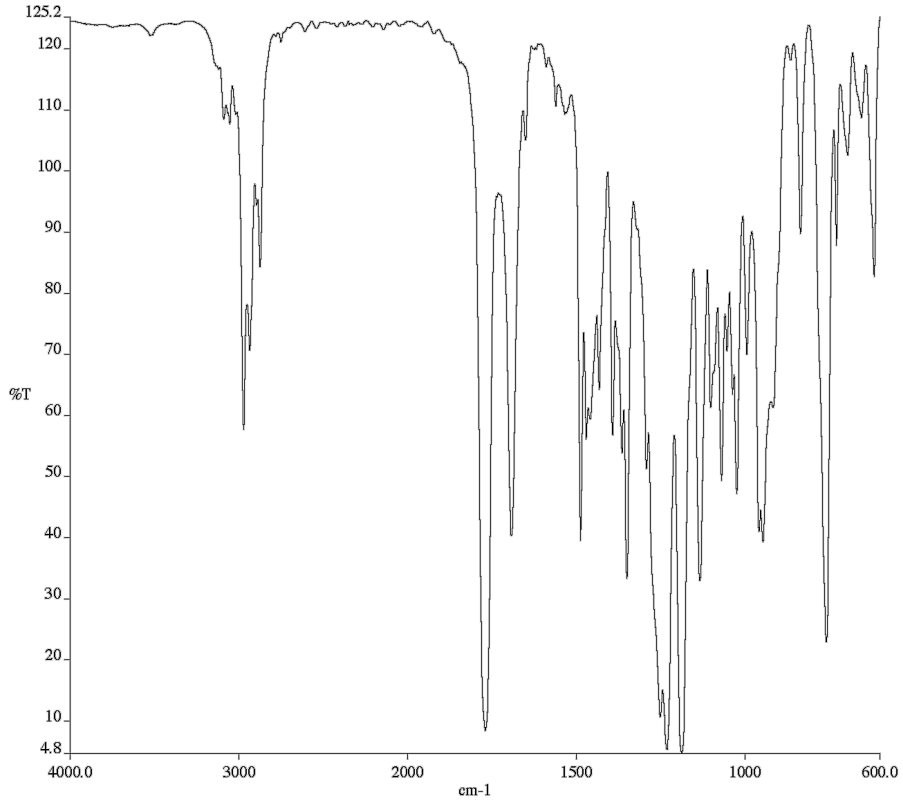

Figure A3.93 *Infrared spectrum (Thin Film, NaCl) of compound* ***19o****.*

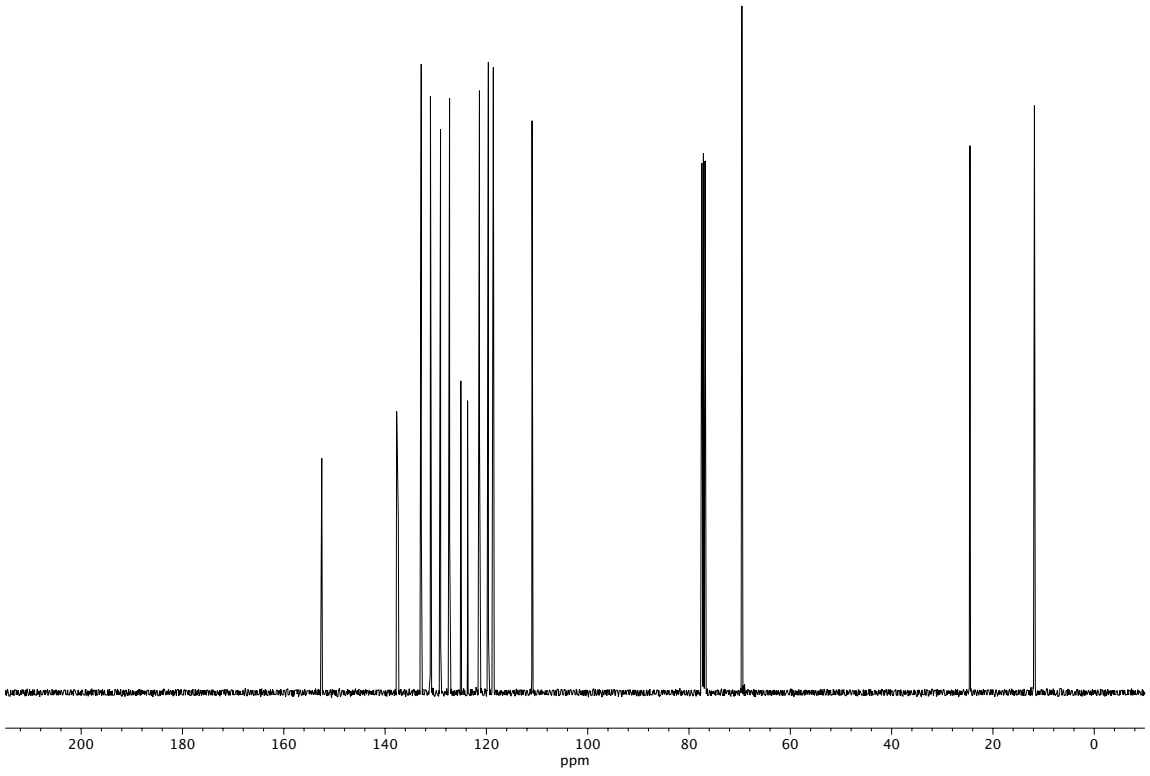

Figure A3.94 *^{13}C NMR (100 MHz, $CDCl_3$) of compound* ***19o****.*

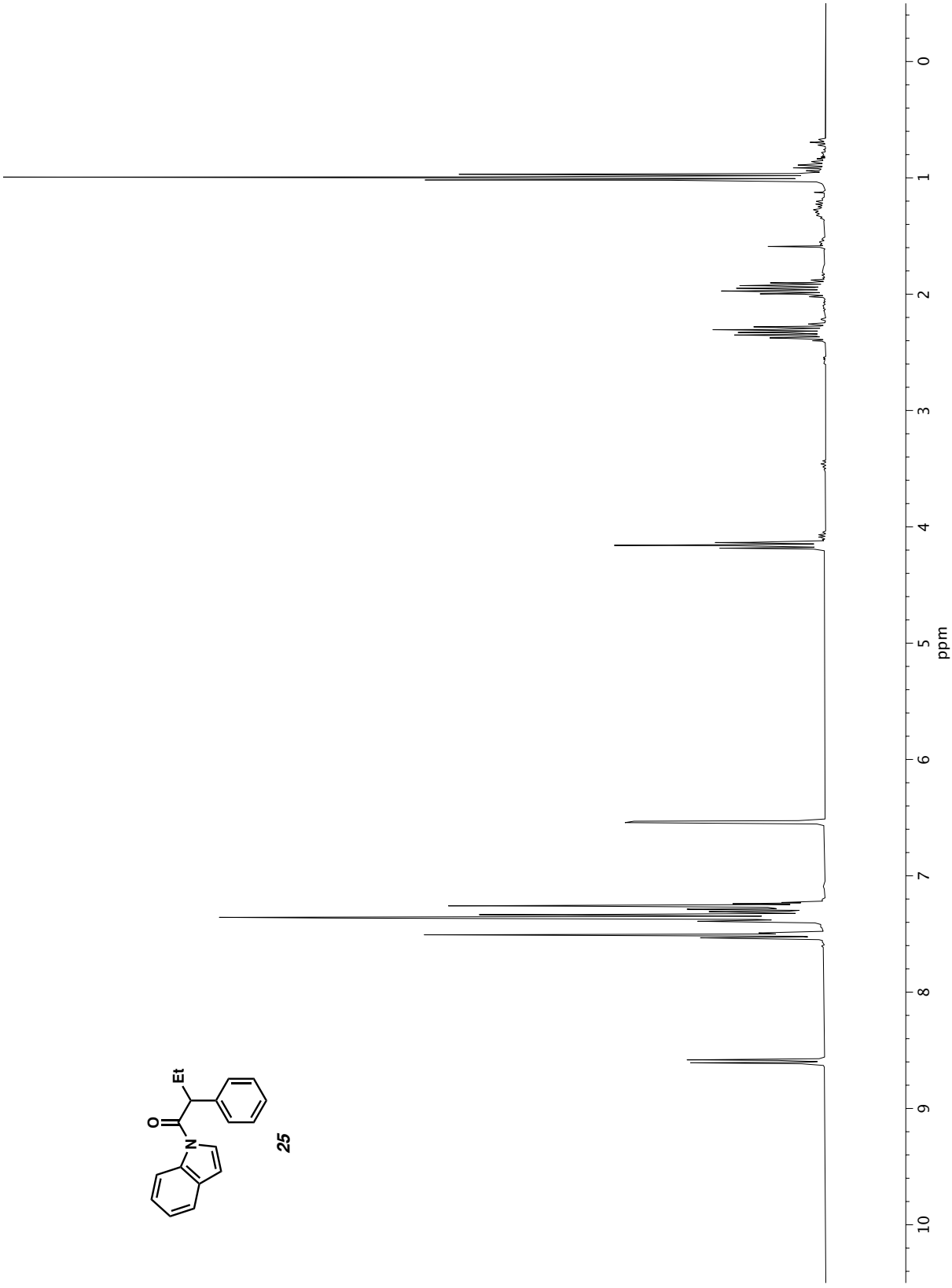

Figure A3.95 *^{1}H NMR (500 MHz, $CDCl_3$) of compound **25**.*

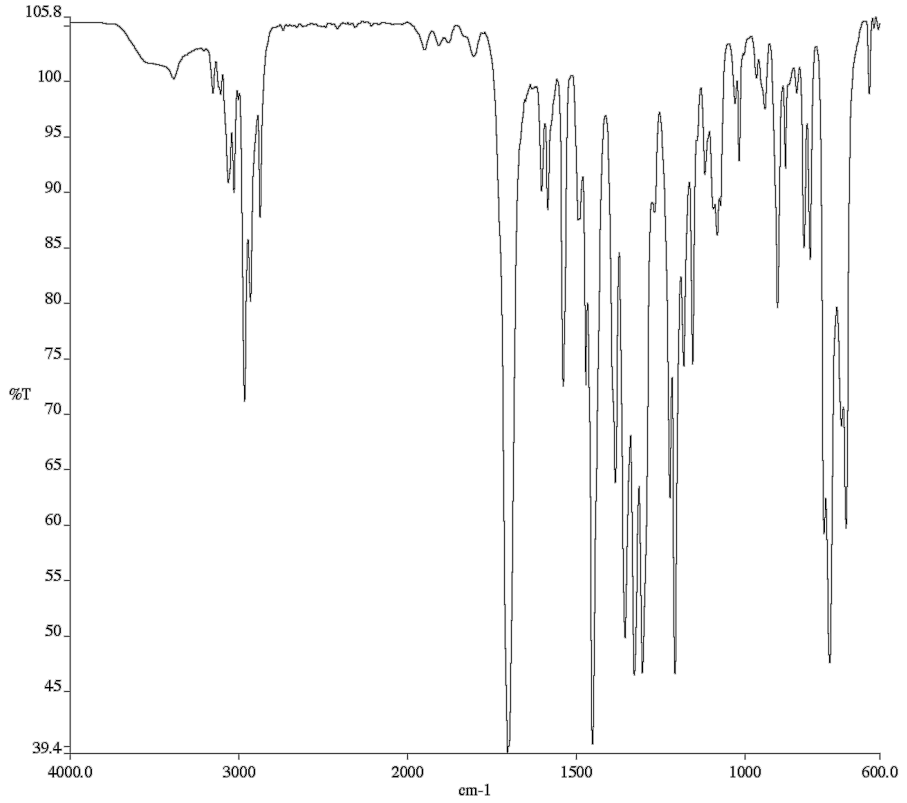

Figure A3.96 *Infrared spectrum (Thin Film, NaCl) of compound* ***25****.*

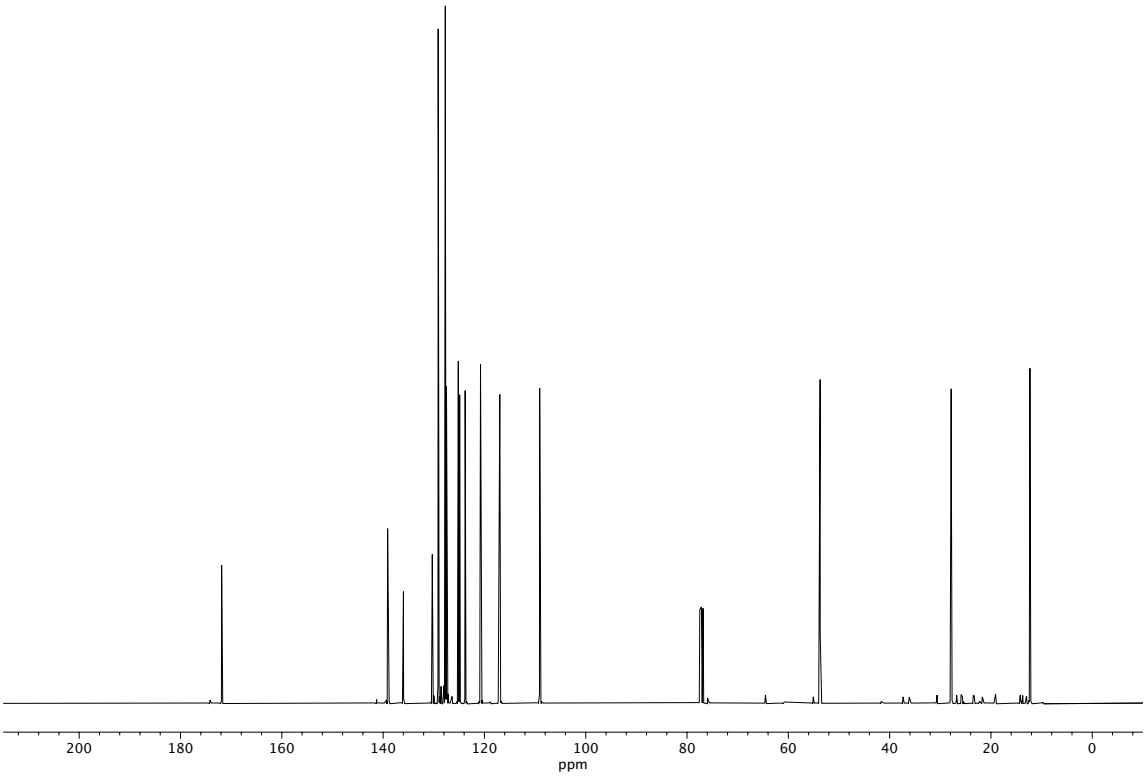

Figure A3.97 *^{13}C NMR (100 MHz, $CDCl_3$) of compound* ***25****.*

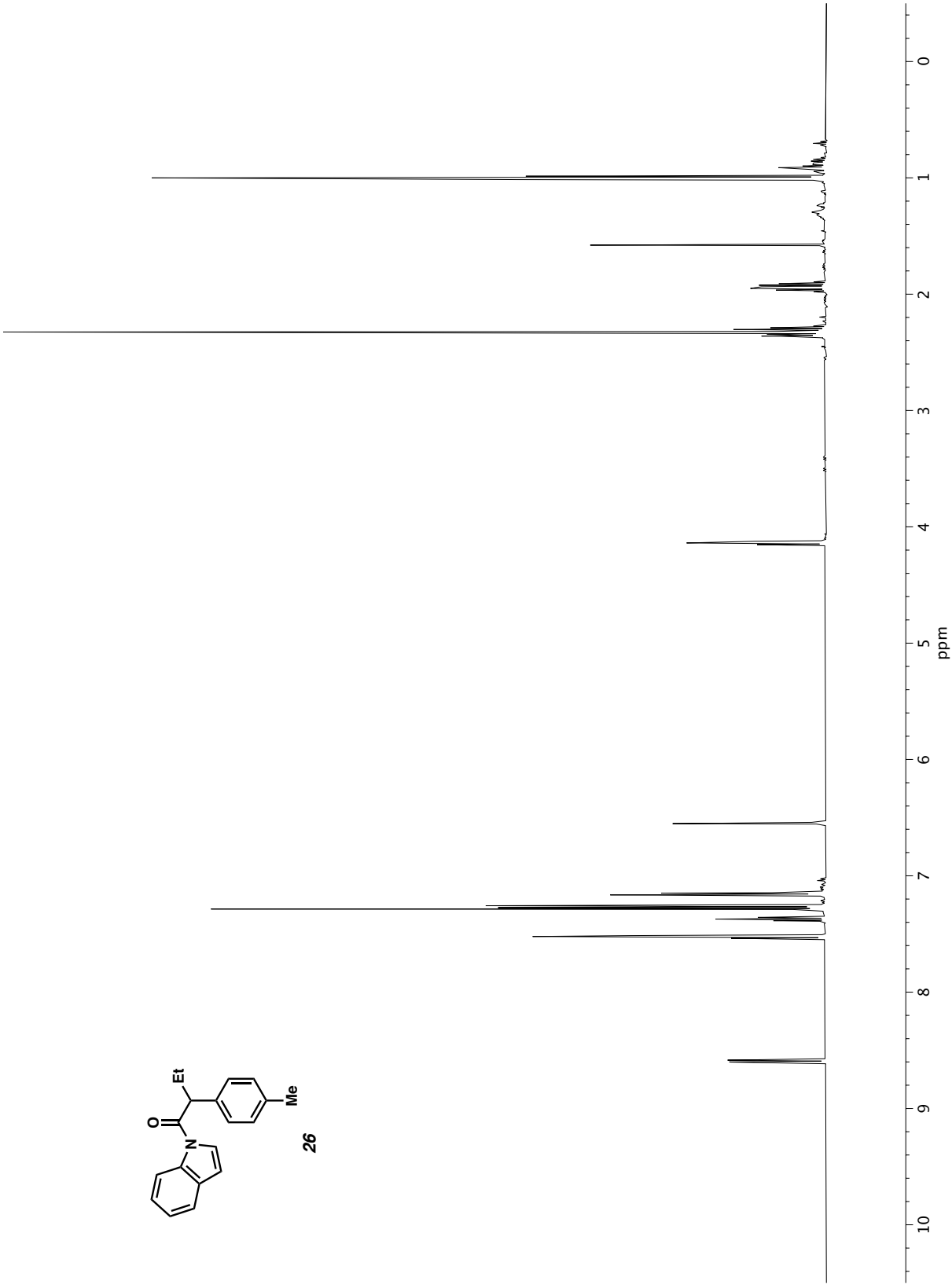

Figure A3.98 *^{1}H NMR (500 MHz, $CDCl_3$) of compound **26**.*

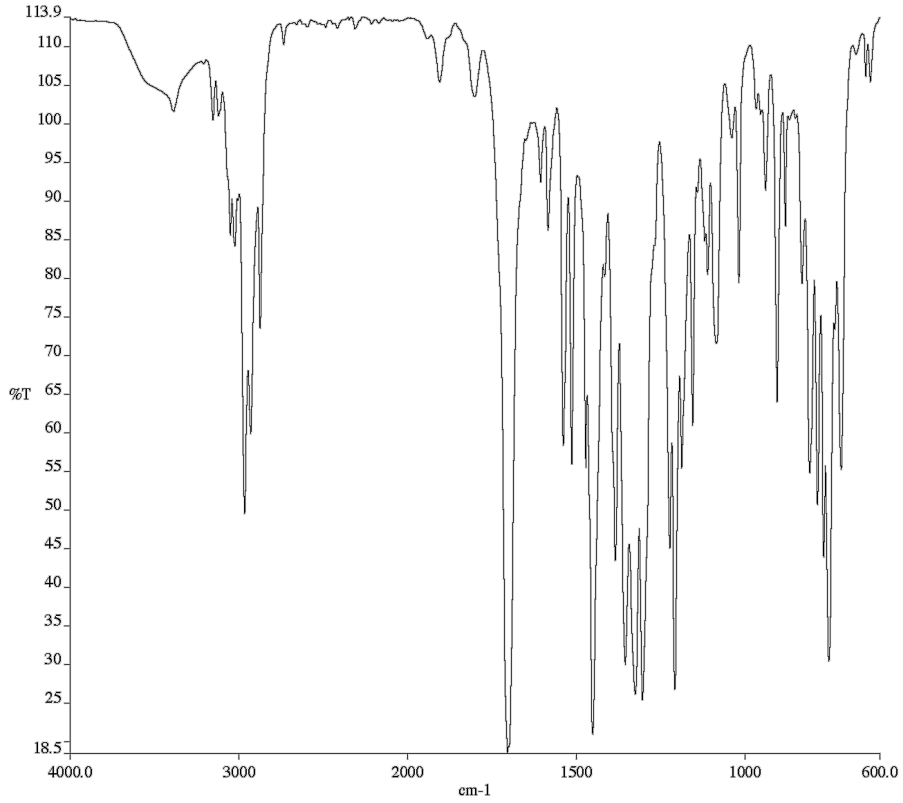

Figure A3.99 *Infrared spectrum (Thin Film, NaCl) of compound* ***26****.*

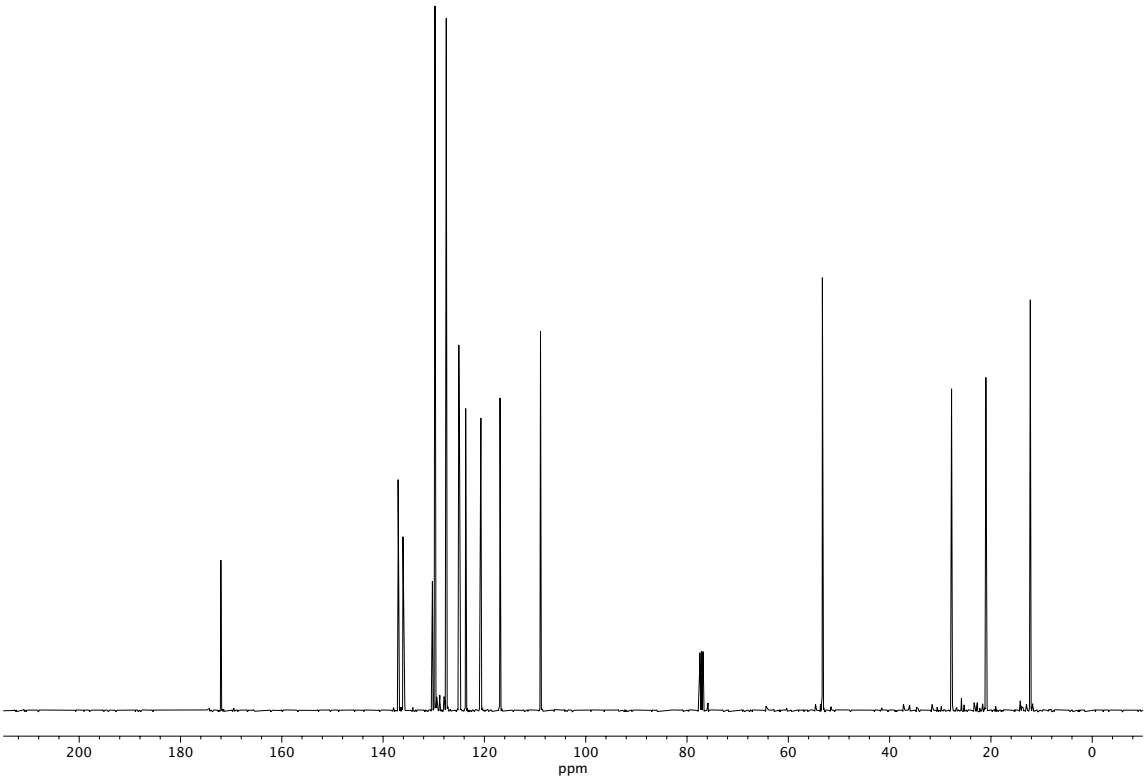

Figure A3.100 *^{13}C NMR (100 MHz, $CDCl_3$) of compound* ***26****.*

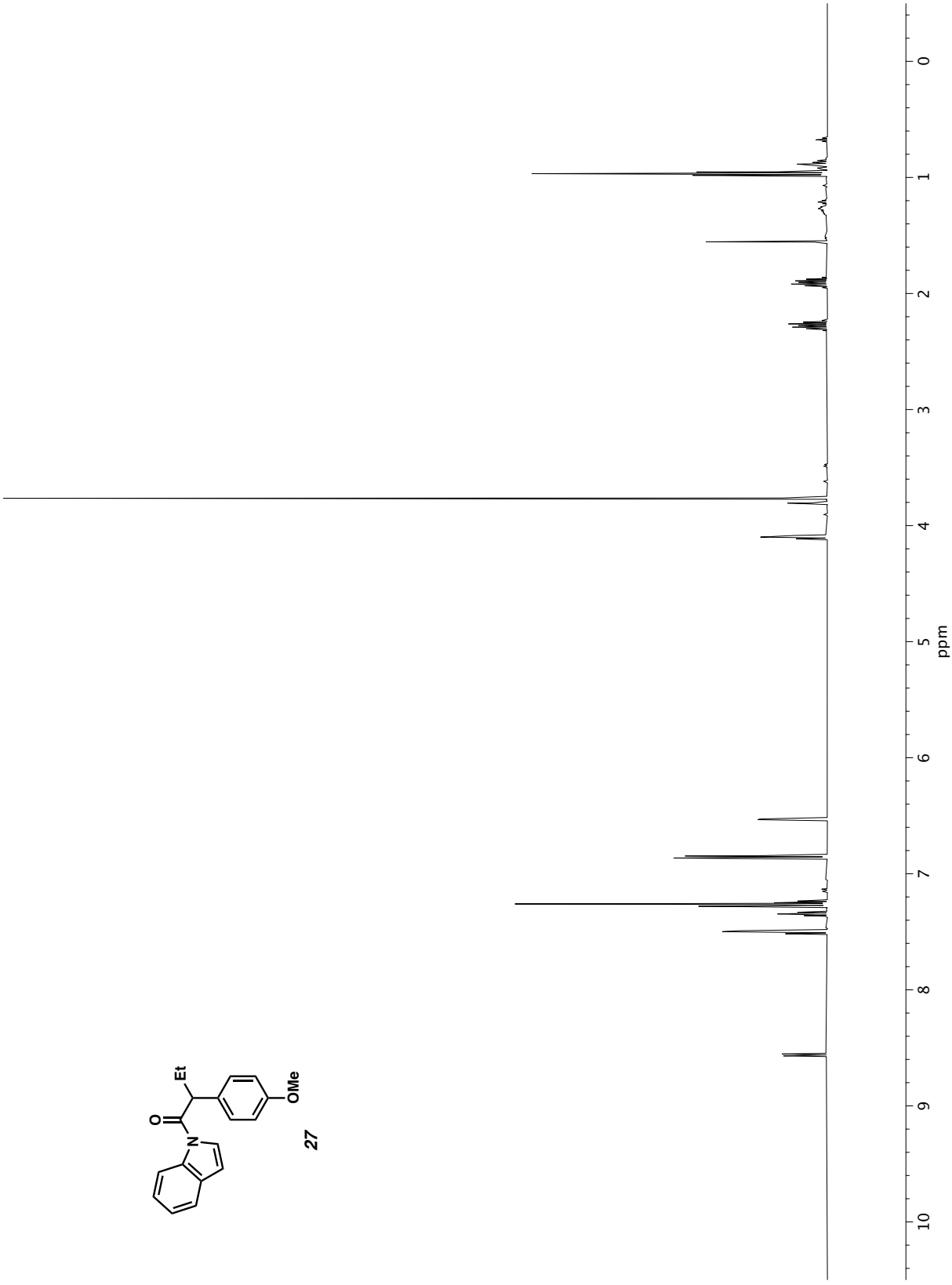

Figure A3.101 *^{1}H NMR (500 MHz, $CDCl_3$) of compound **27**.*

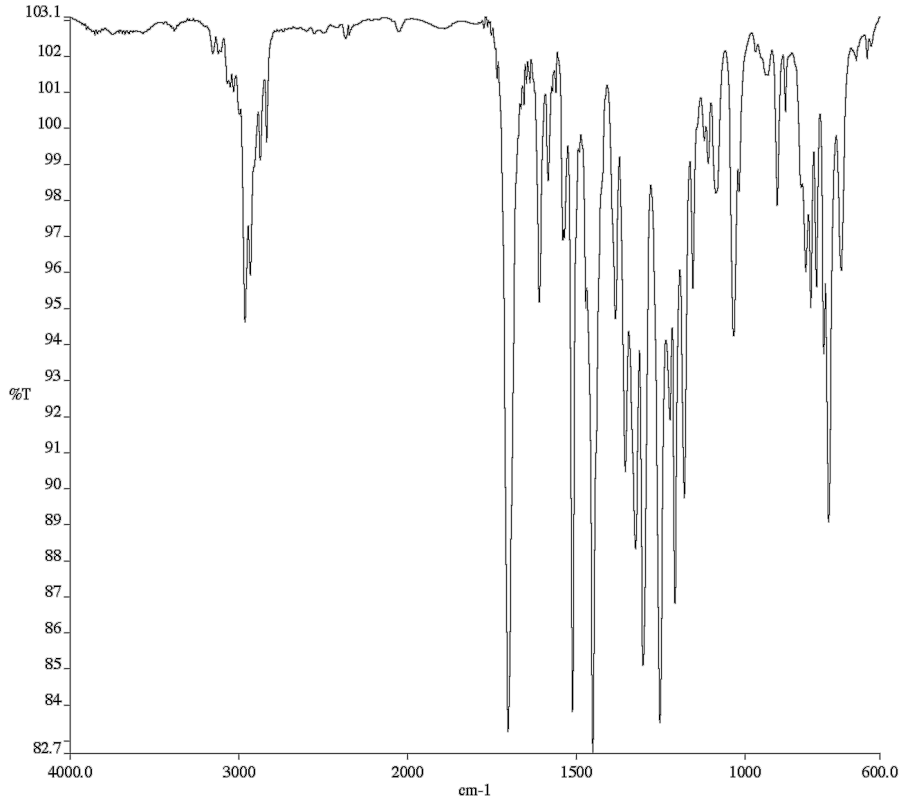

Figure A3.102 *Infrared spectrum (Thin Film, NaCl) of compound **27**.*

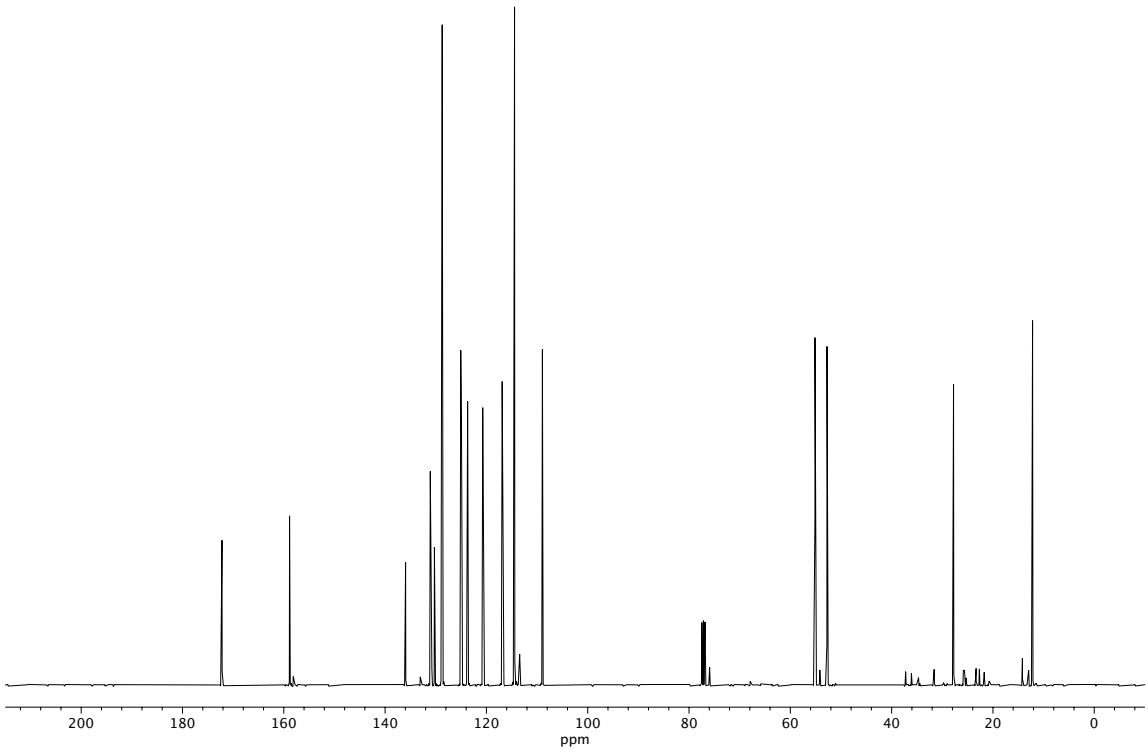

Figure A3.103 *^{13}C NMR (100 MHz, $CDCl_3$) of compound **27**.*

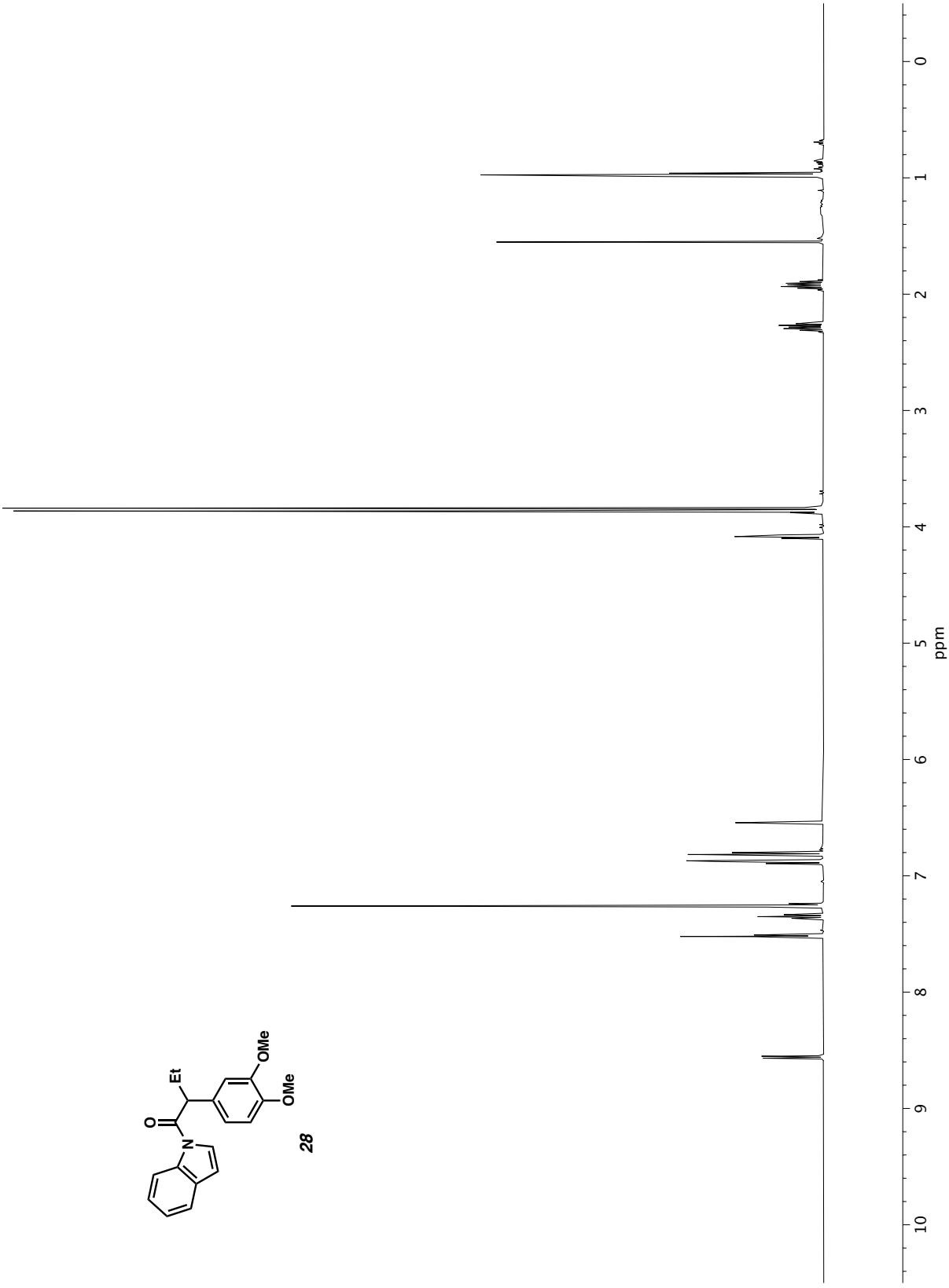

Figure A3.104 *^{1}H NMR (500 MHz, $CDCl_3$) of compound **28**.*

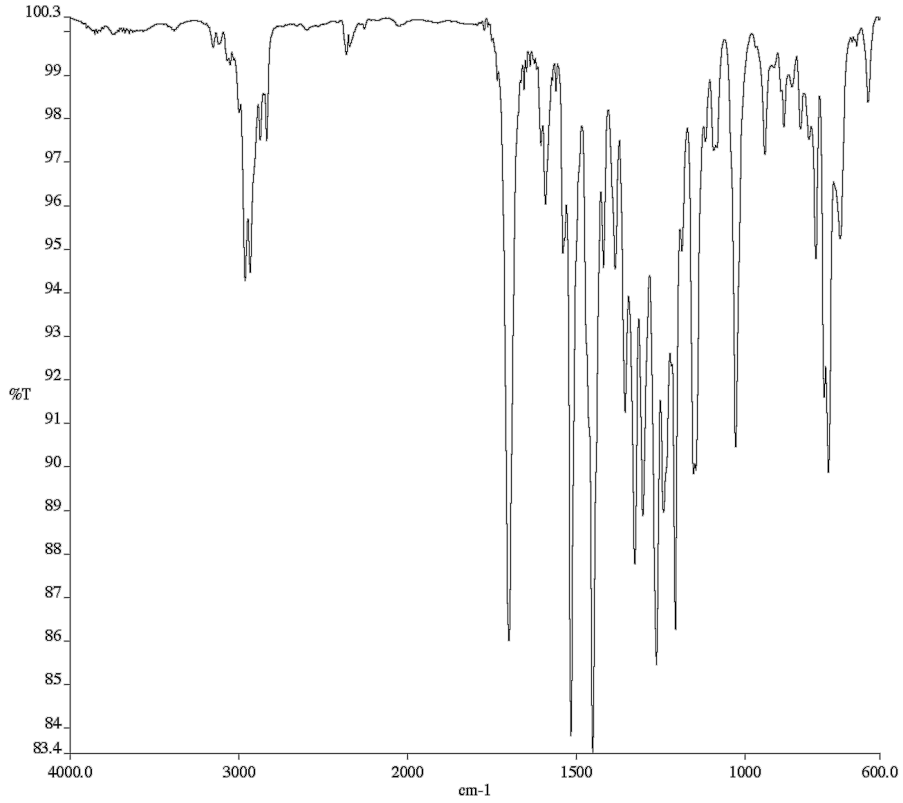

Figure A3.105 *Infrared spectrum (Thin Film, NaCl) of compound* ***28****.*

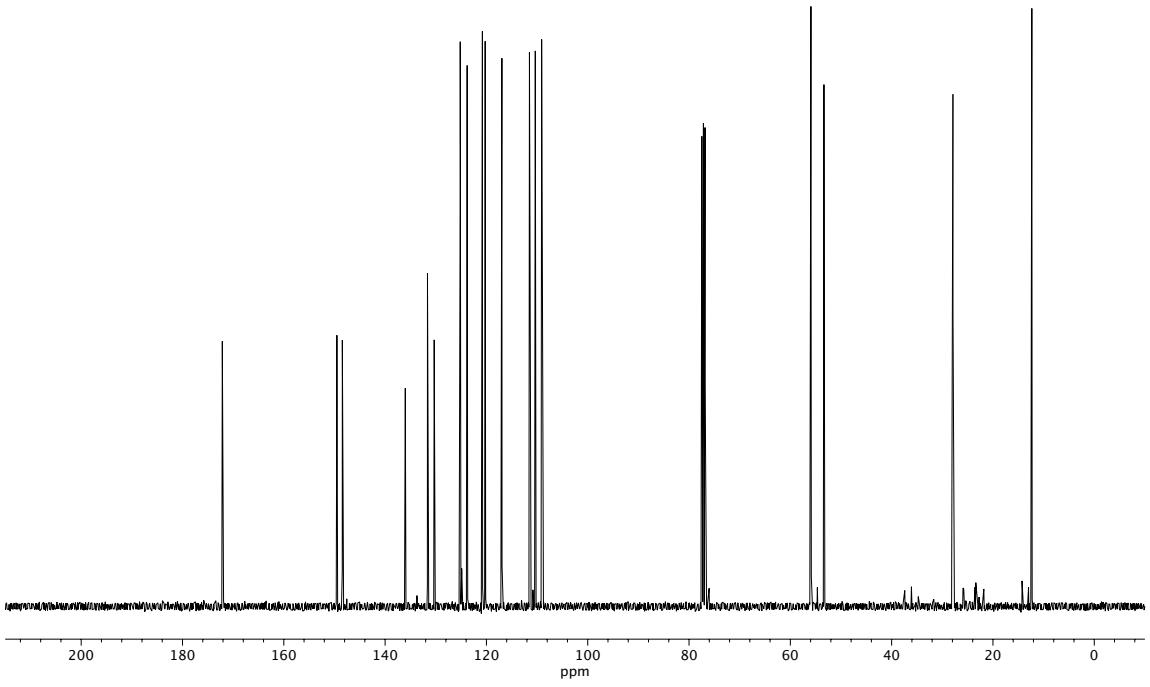

Figure A3.106 *^{13}C NMR (100 MHz, $CDCl_3$) of compound* ***28****.*

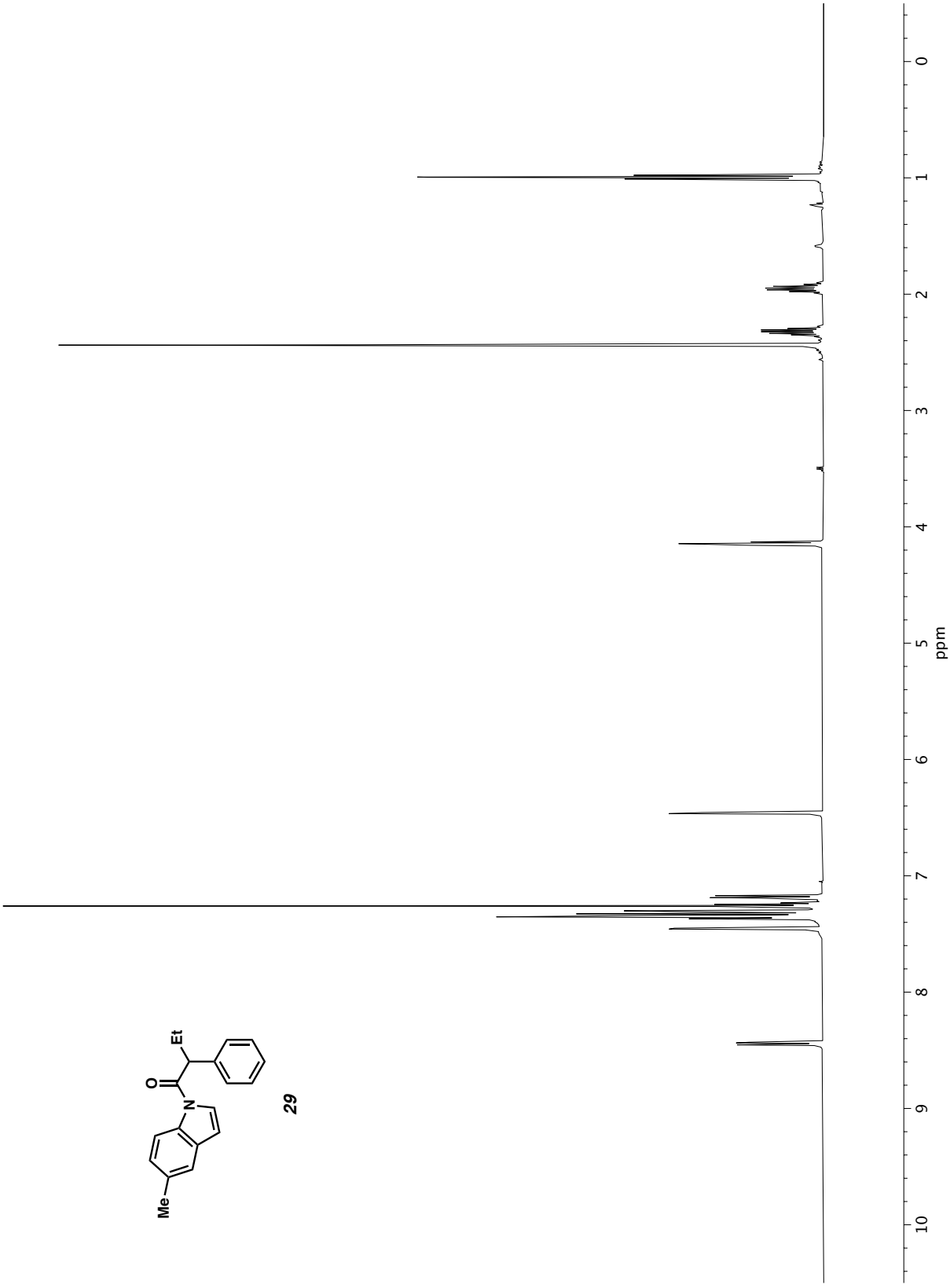

Figure A3.107 *^{1}H NMR (500 MHz, $CDCl_3$) of compound **29**.*

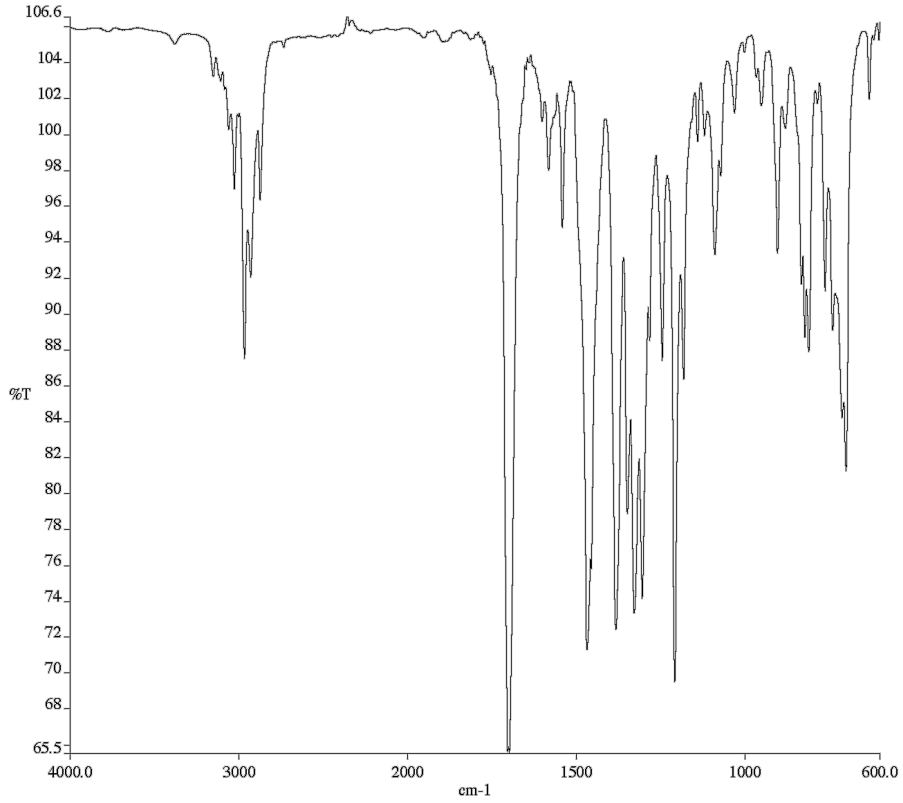

Figure A3.108 *Infrared spectrum (Thin Film, NaCl) of compound* ***29****.*

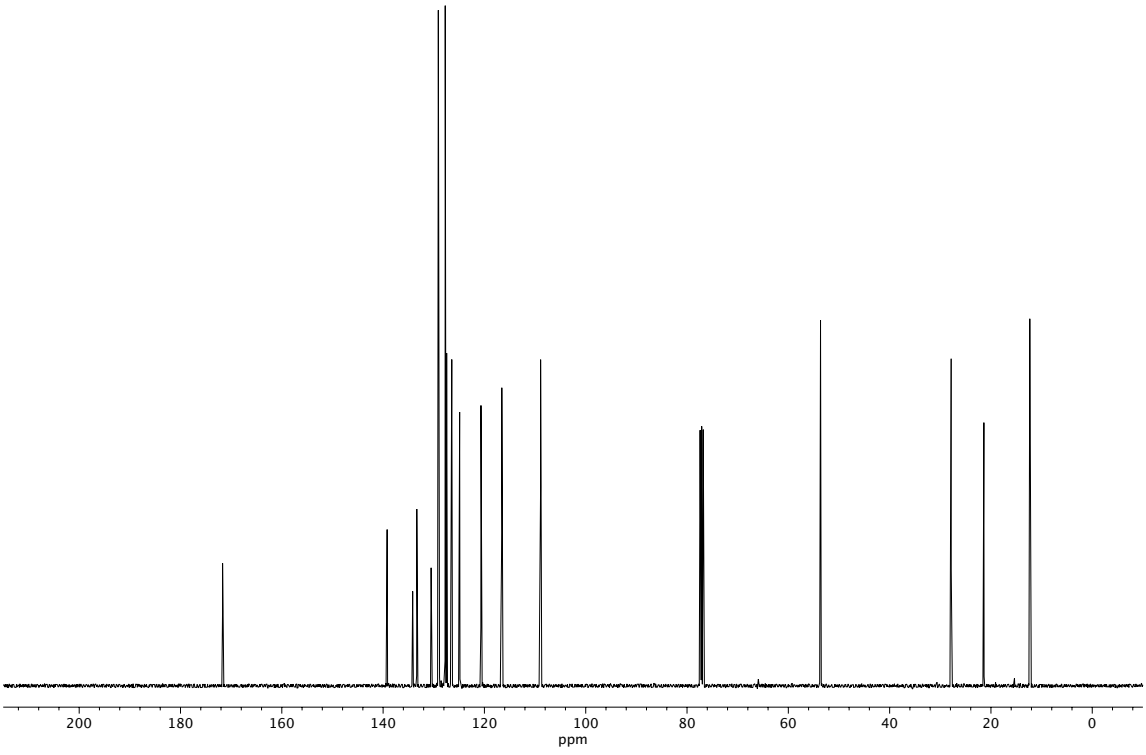

Figure A3.109 *^{13}C NMR (100 MHz, $CDCl_3$) of compound* ***29****.*

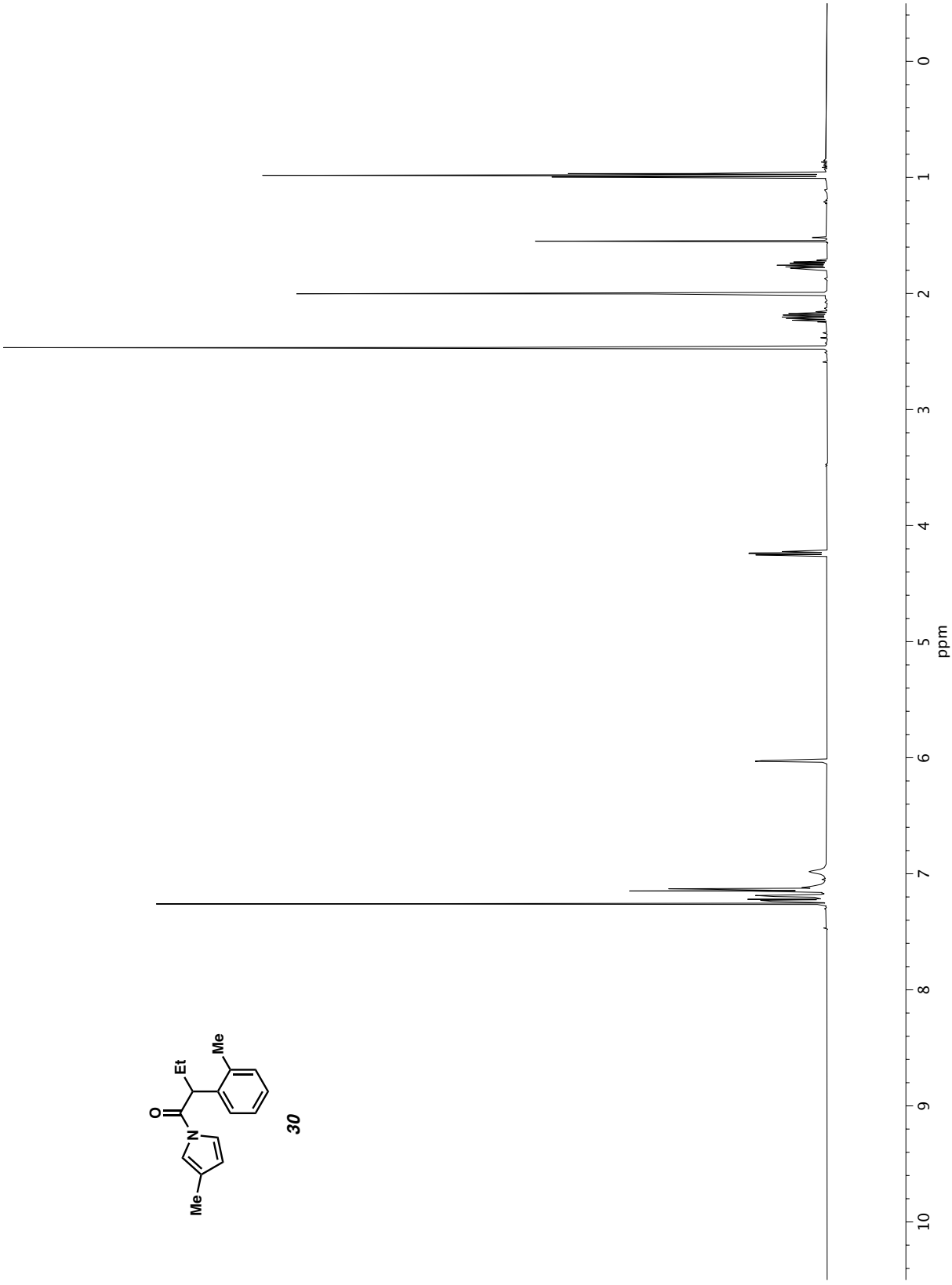

Figure A3.110 *^1H NMR (500 MHz, $CDCl_3$) of compound **30***

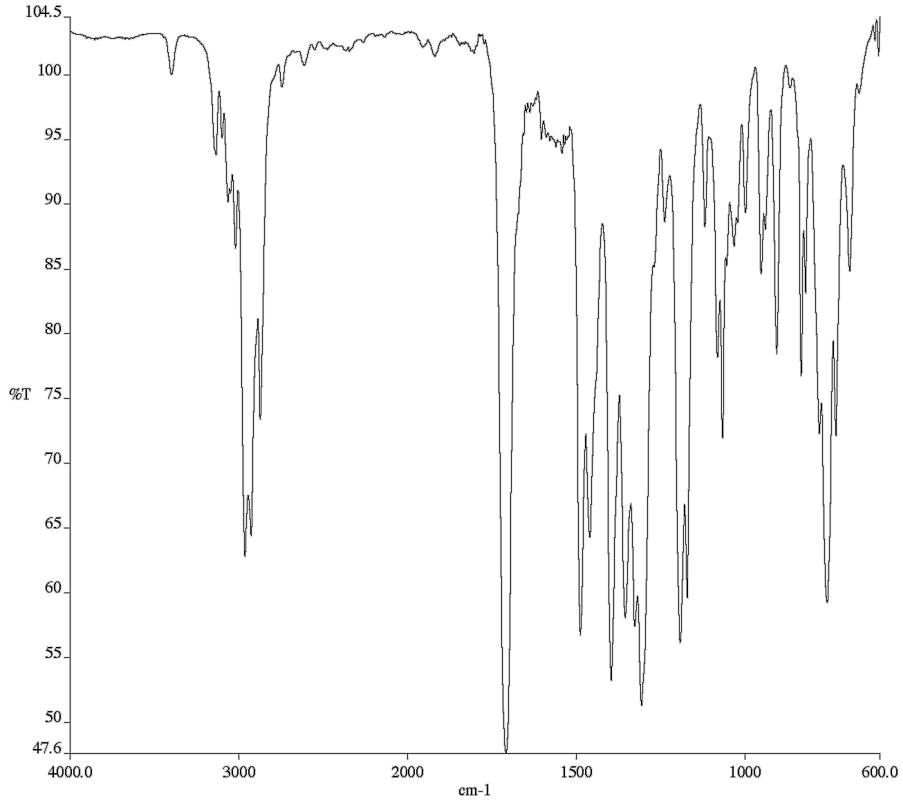

Figure A3.111 *Infrared spectrum (Thin Film, NaCl) of compound* ***30****.*

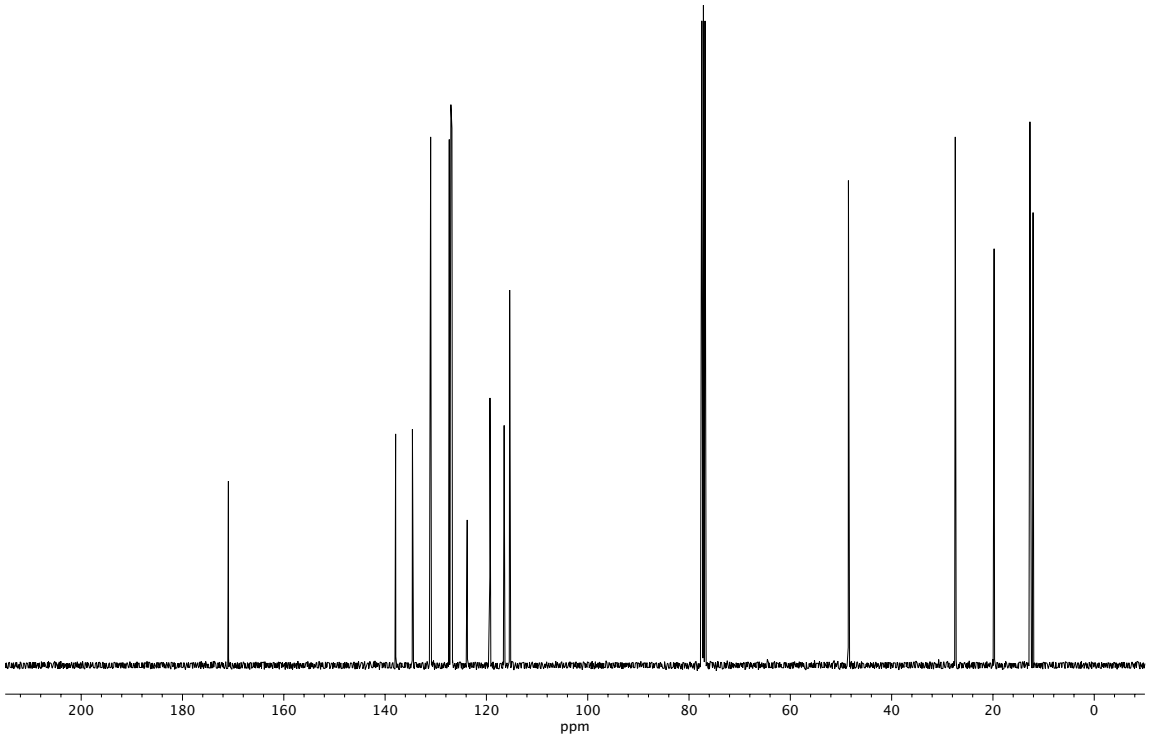

Figure A3.112 *^{13}C NMR (100 MHz, $CDCl_3$) of compound* ***30****.*

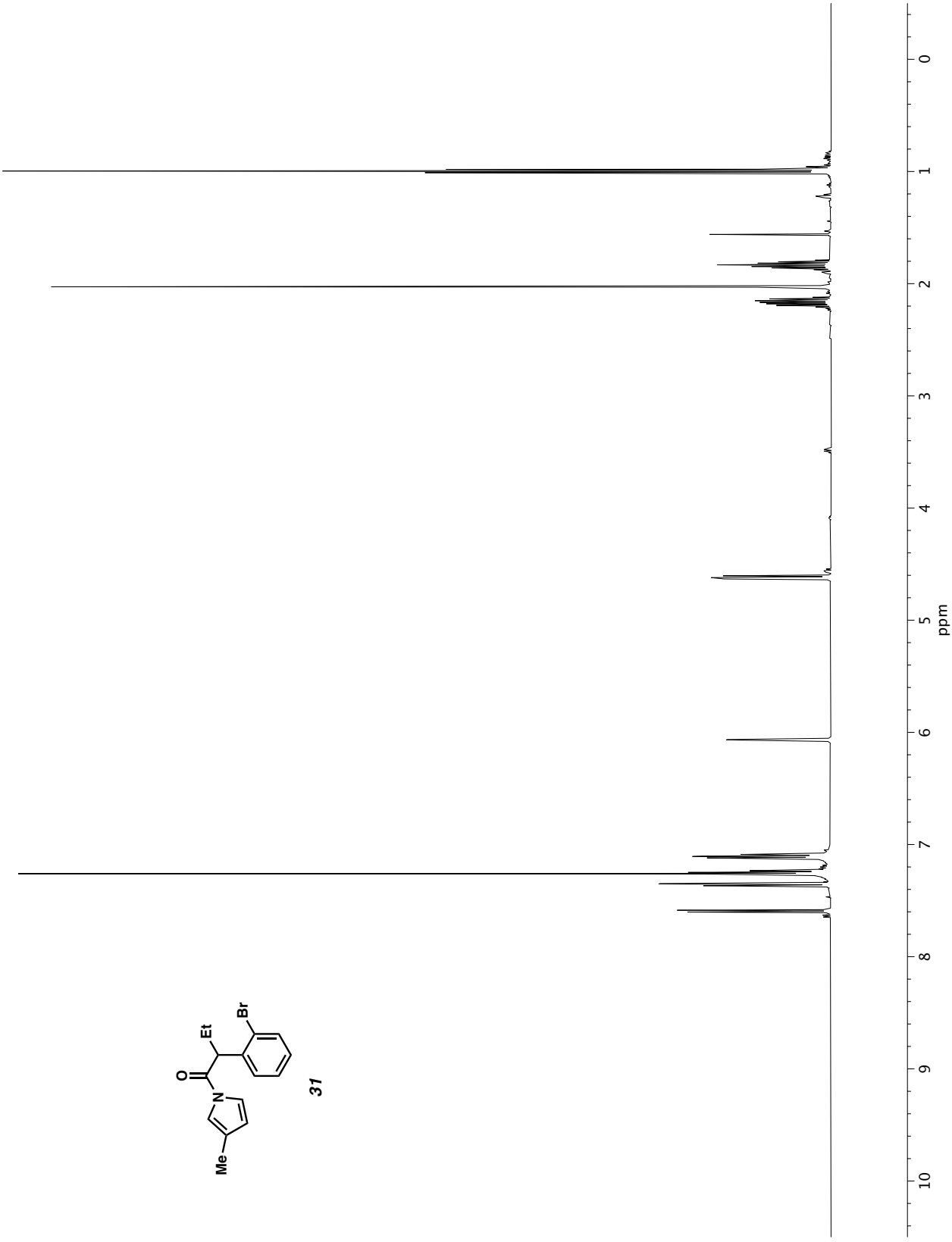

Figure A3.113 *^{1}H NMR (500 MHz, $CDCl_3$) of compound **31**.*

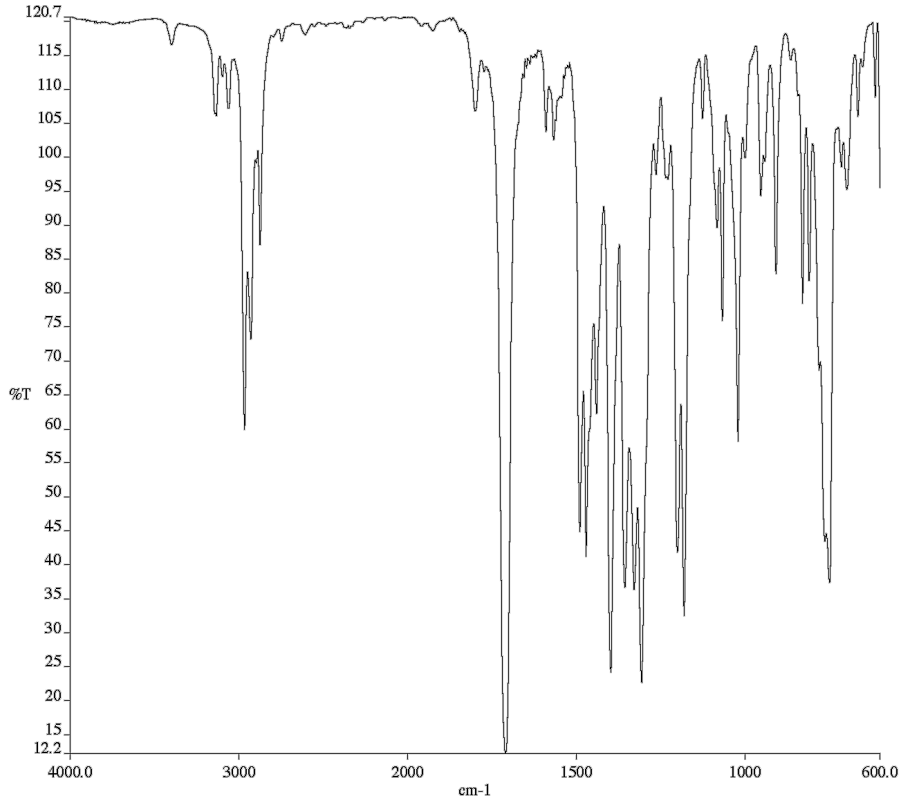

Figure A3.114 *Infrared spectrum (Thin Film, NaCl) of compound* ***31****.*

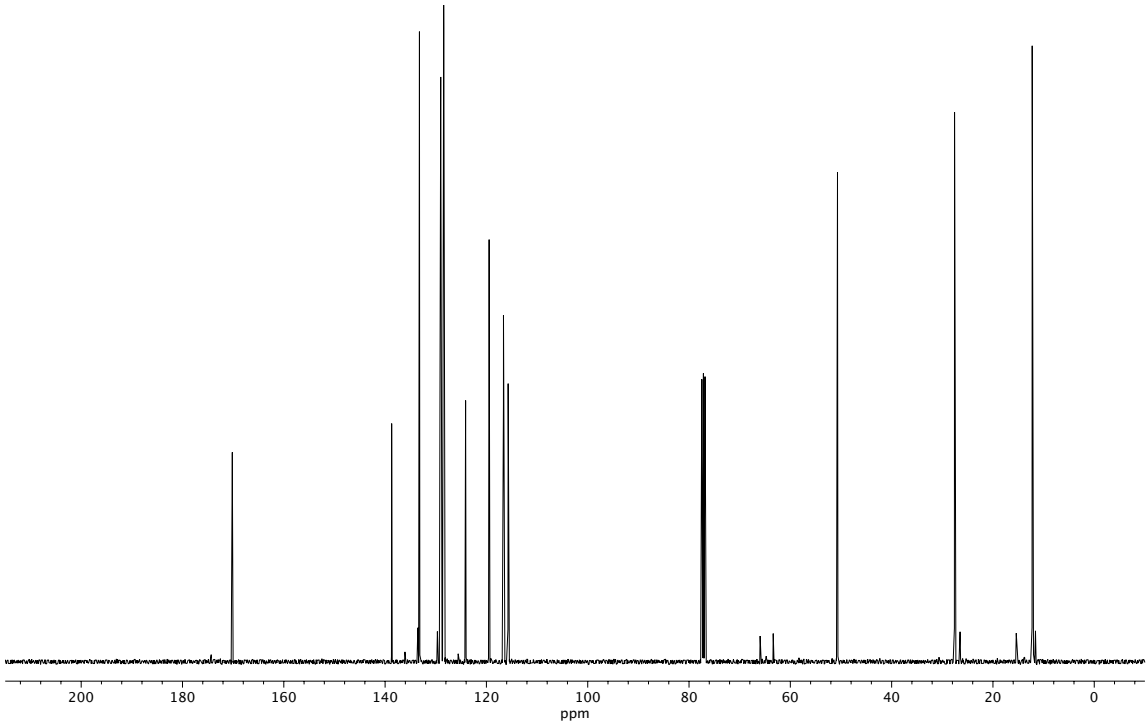

Figure A3.115 *^{13}C NMR (100 MHz, $CDCl_3$) of compound* ***31****.*

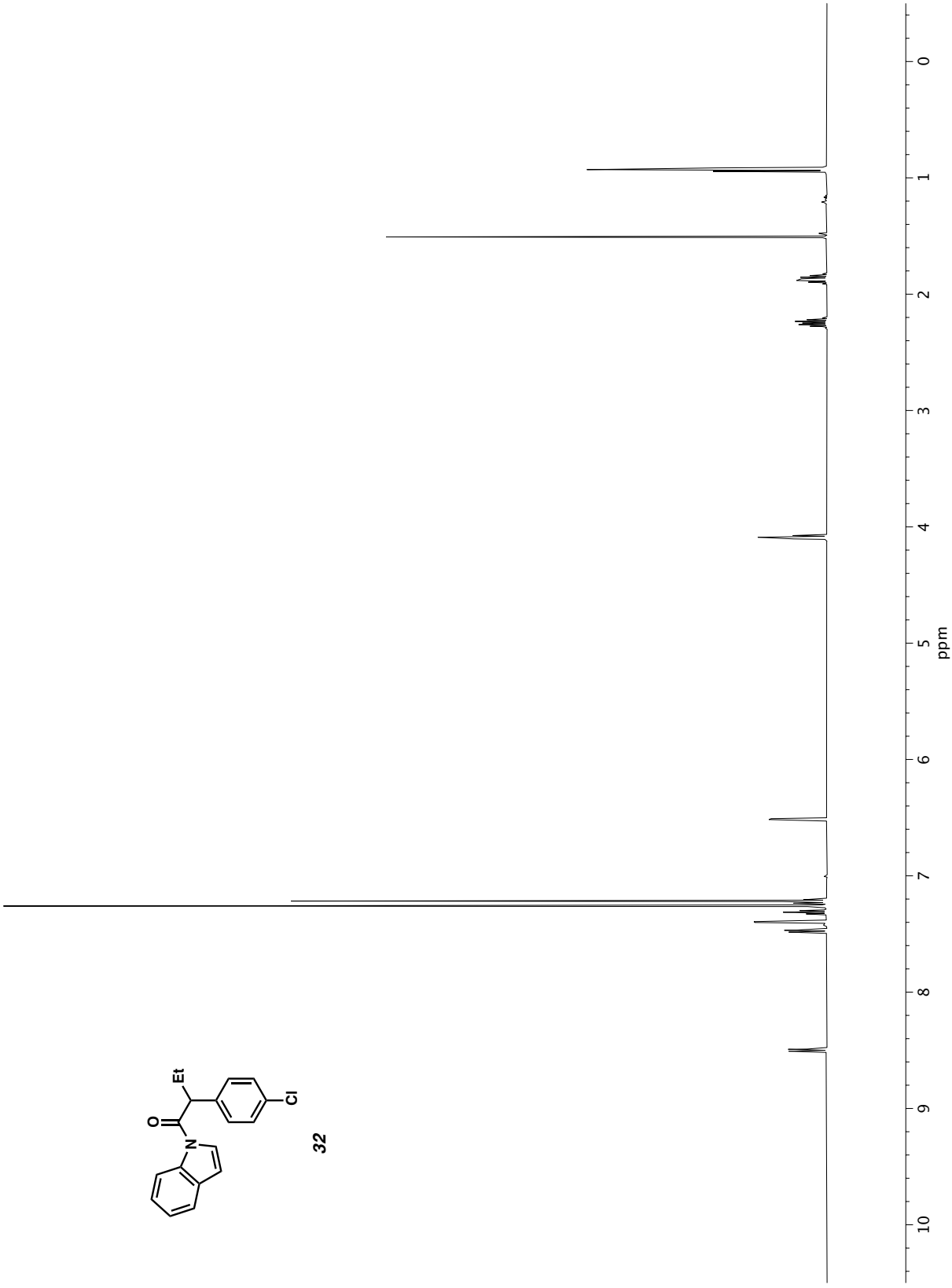

Figure A3.116 *^{1}H NMR (500 MHz, $CDCl_3$) of compound **32**.*

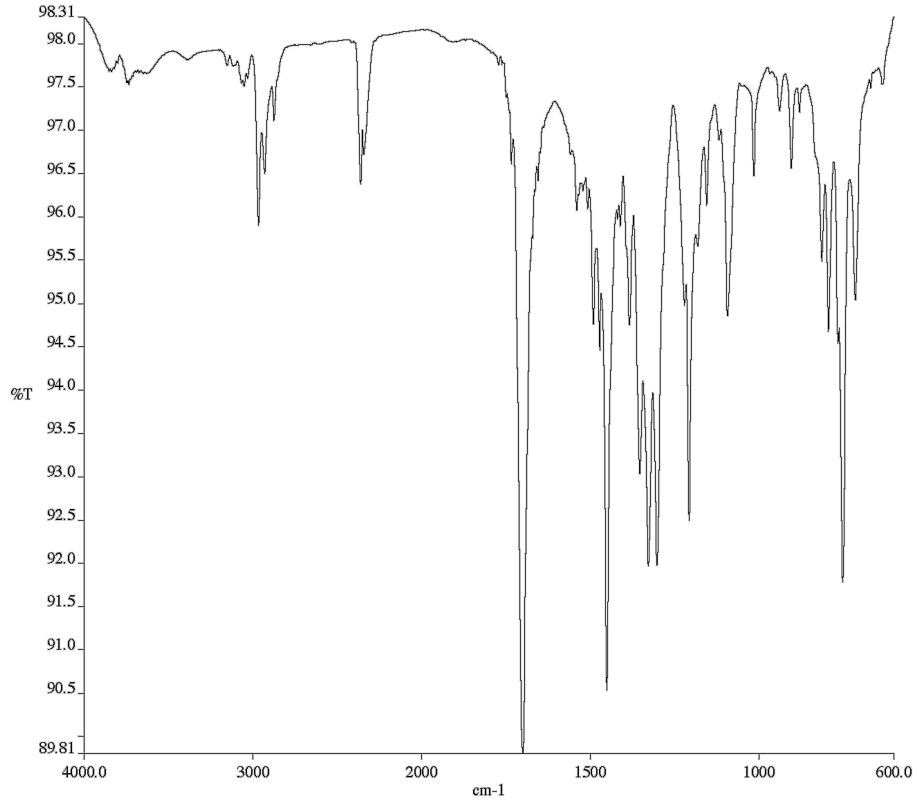

Figure A3.117 *Infrared spectrum (Thin Film, NaCl) of compound* ***32****.*

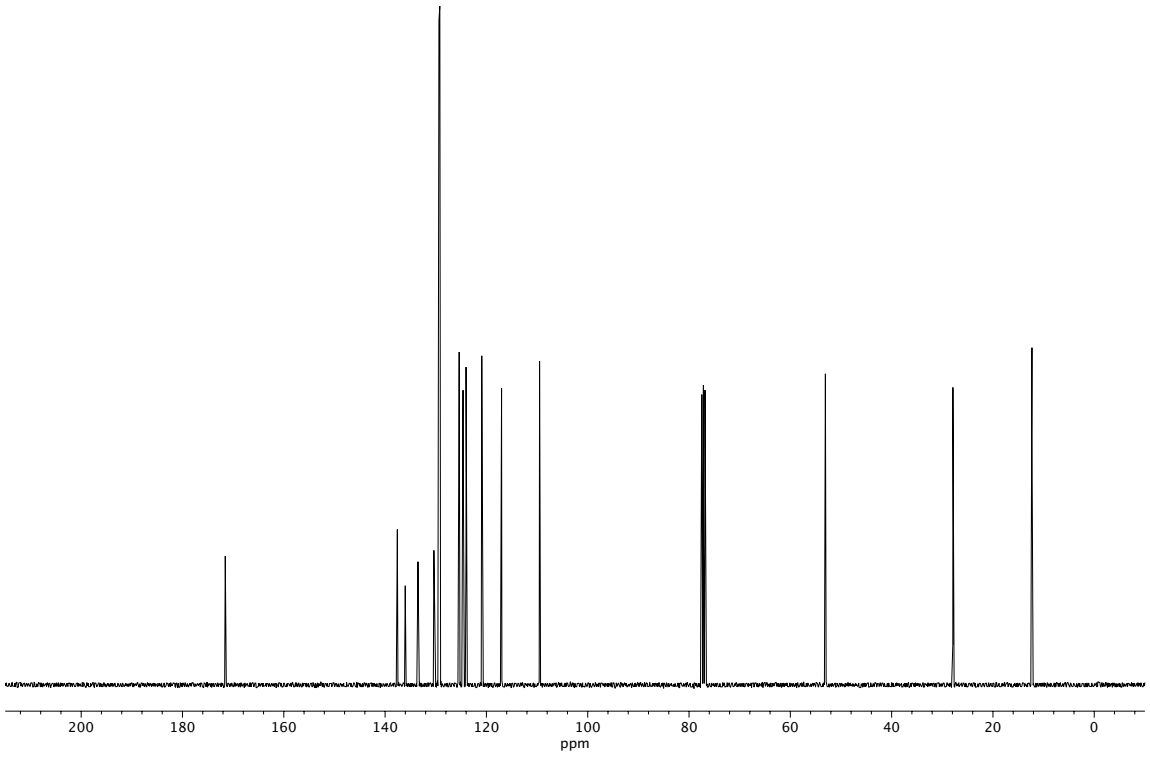

Figure A3.118 *^{13}C NMR (100 MHz, $CDCl_3$) of compound* ***32****.*

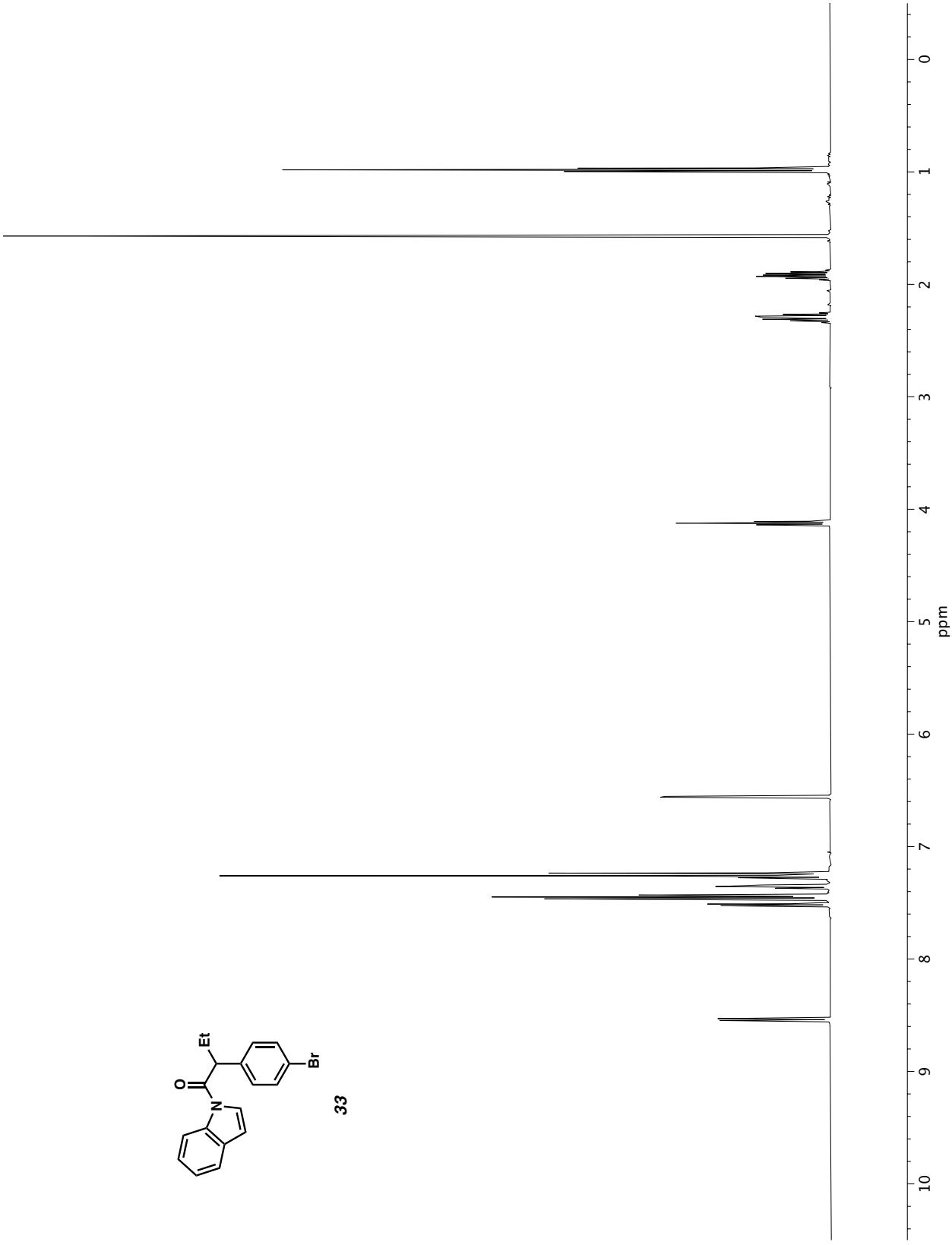

Figure A3.119 *^{1}H NMR (500 MHz, $CDCl_3$) of compound **33**.*

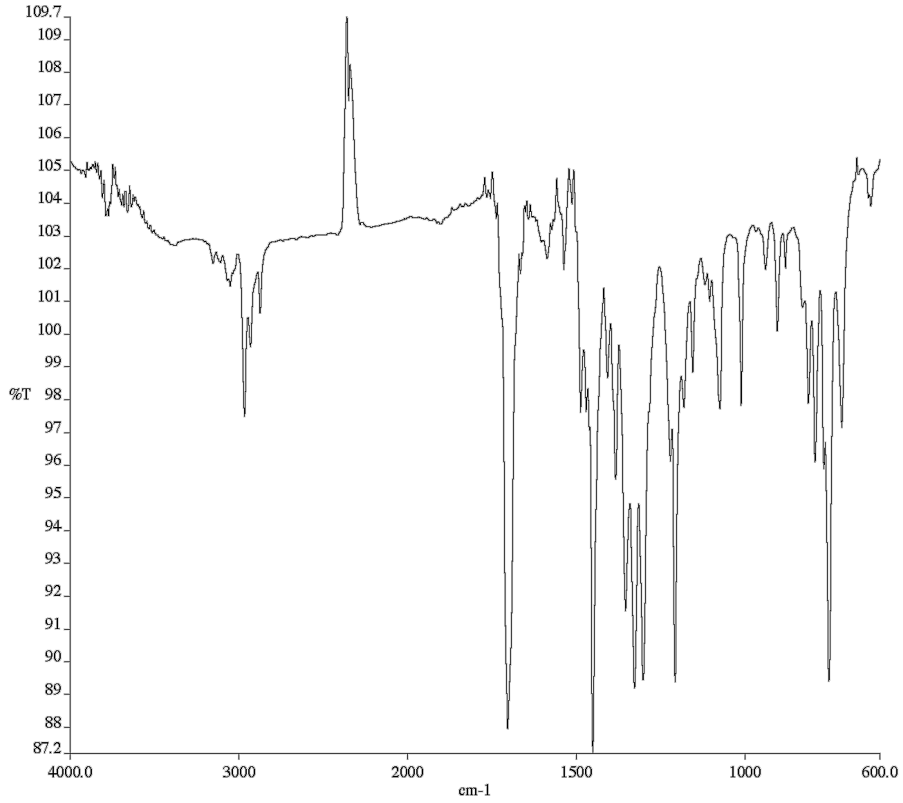

Figure A3.120 *Infrared spectrum (Thin Film, NaCl) of compound* ***33****.*

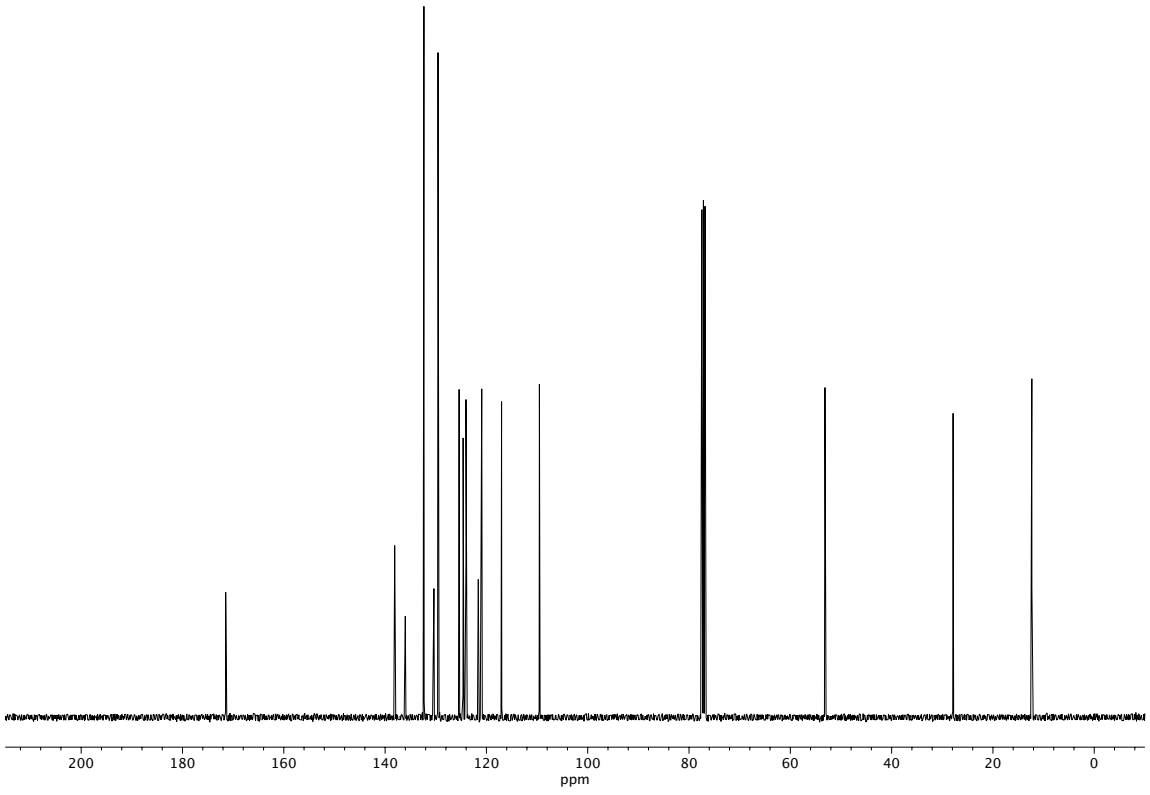

Figure A3.121 *^{13}C NMR (100 MHz, $CDCl_3$) of compound* ***33****.*

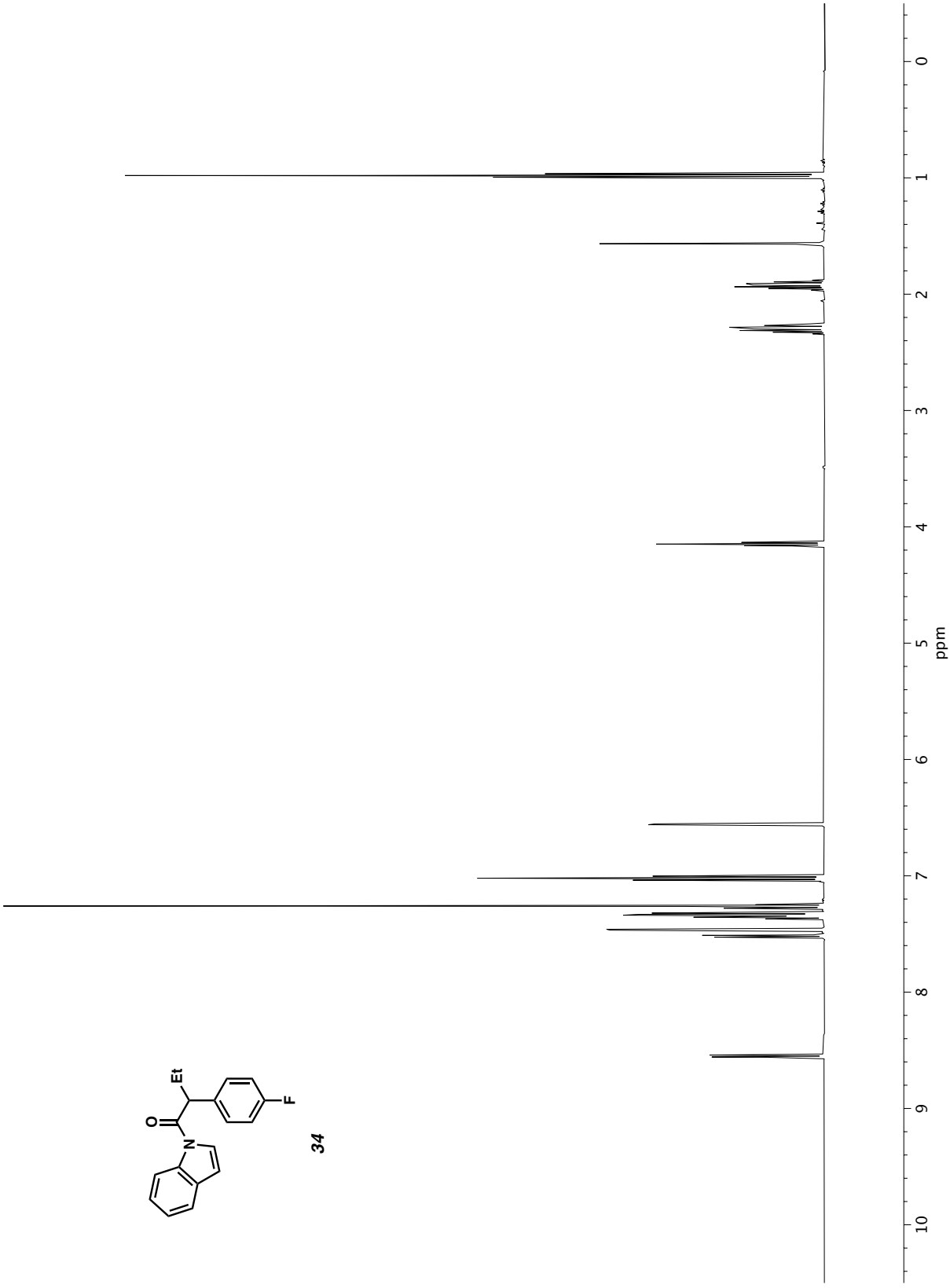

Figure A3.122 *^{1}H NMR (500 MHz, $CDCl_3$) of compound **34**.*

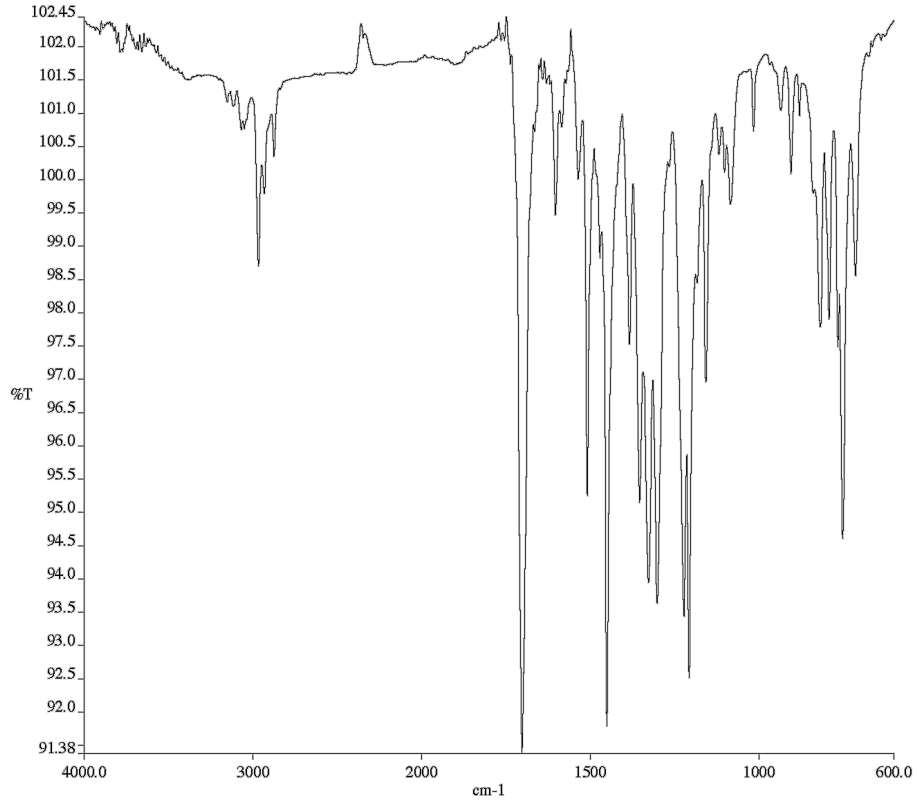

Figure A3.123 *Infrared spectrum (Thin Film, NaCl) of compound* ***34****.*

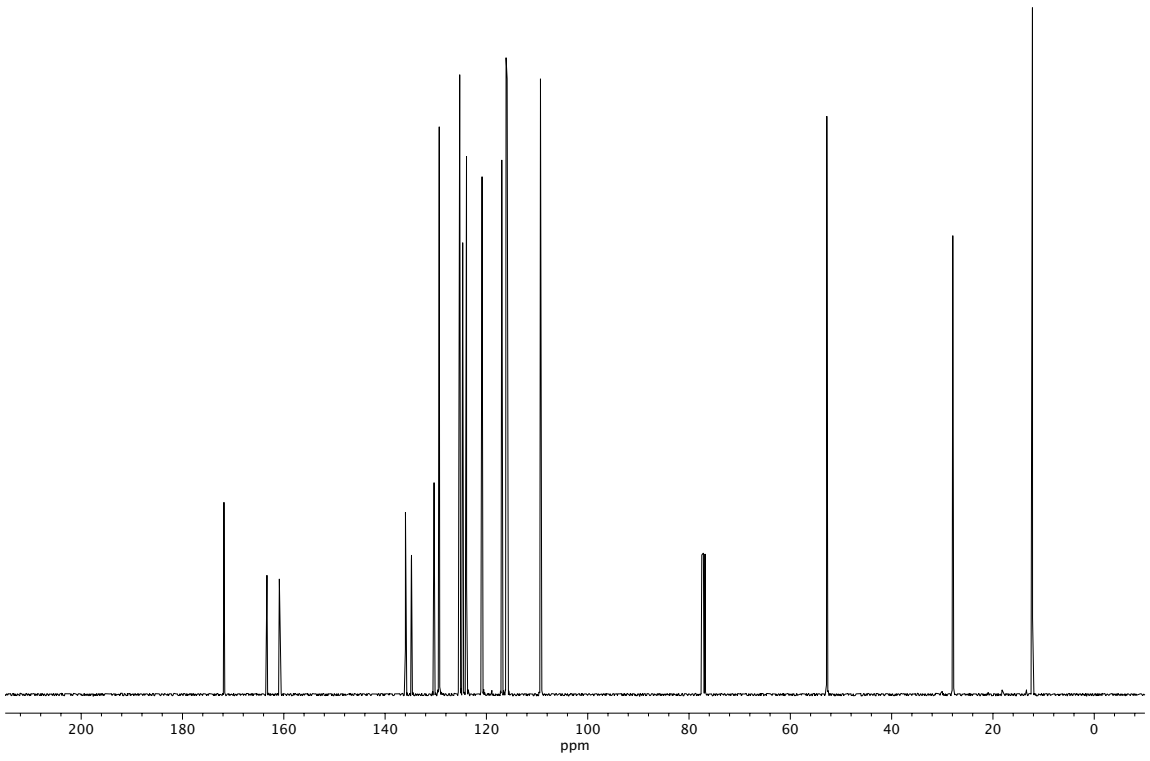

Figure A3.124 *^{13}C NMR (100 MHz, $CDCl_3$) of compound* ***34****.*

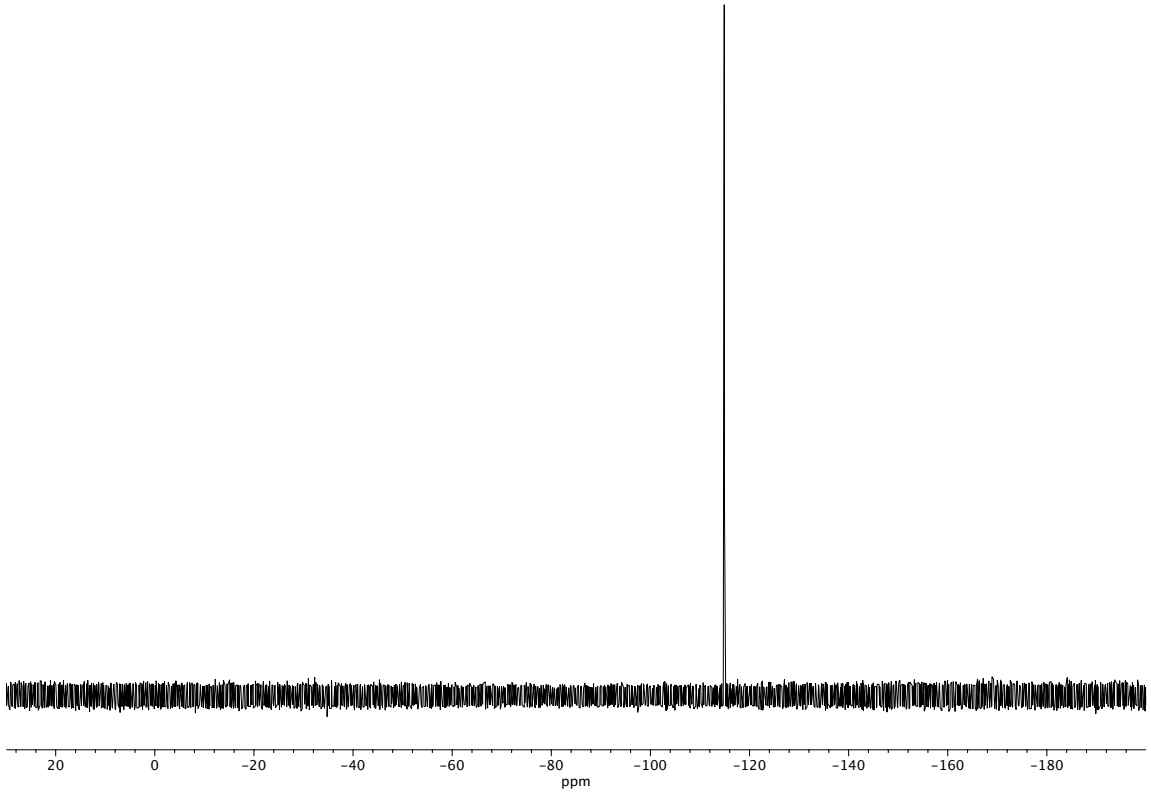

Figure A3.125 *^{19}F NMR (282 MHz, $CDCl_3$) of compound **34**.*

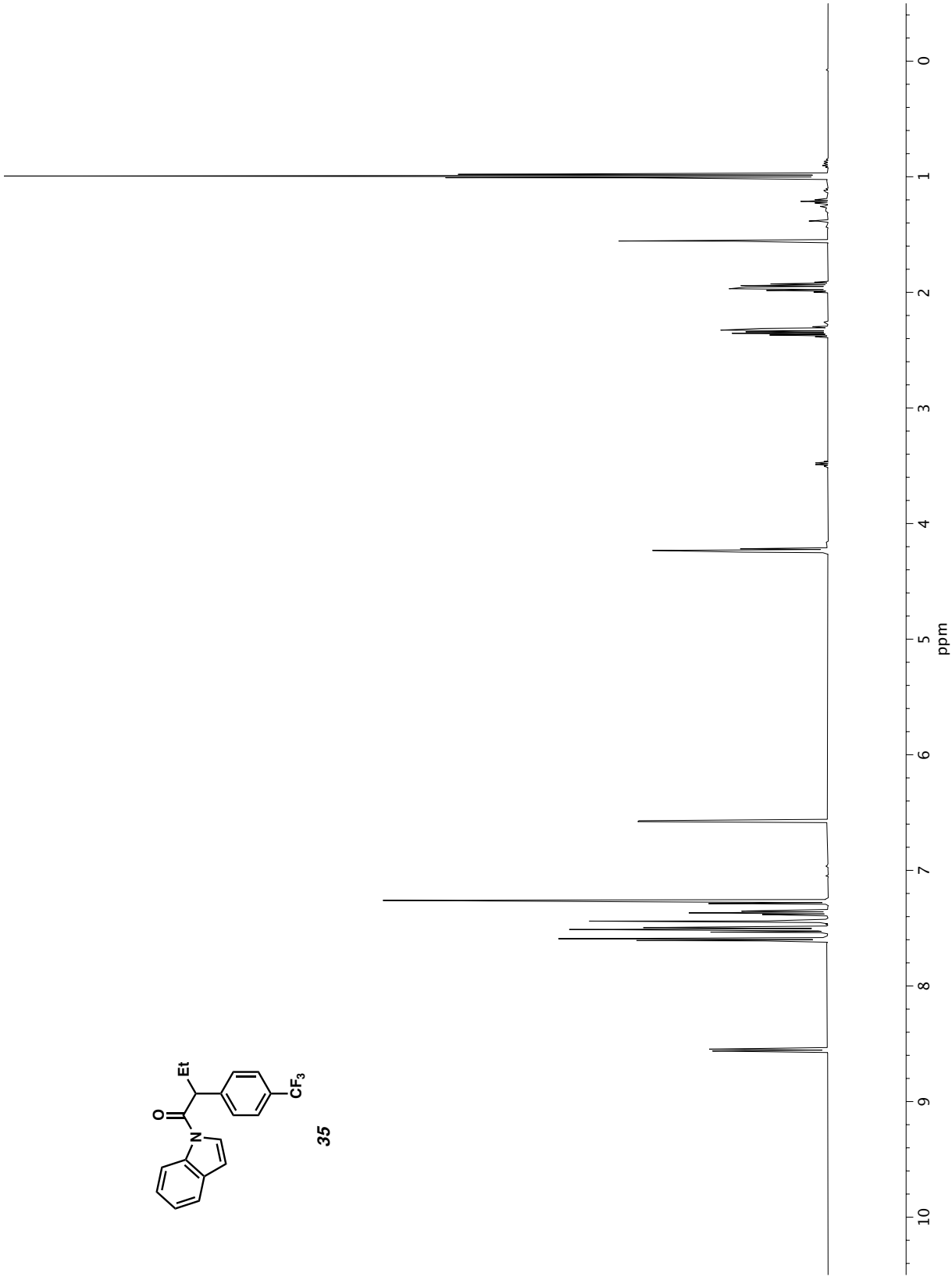

Figure A3.126 *^{1}H NMR (500 MHz, $CDCl_3$) of compound* ***35***.

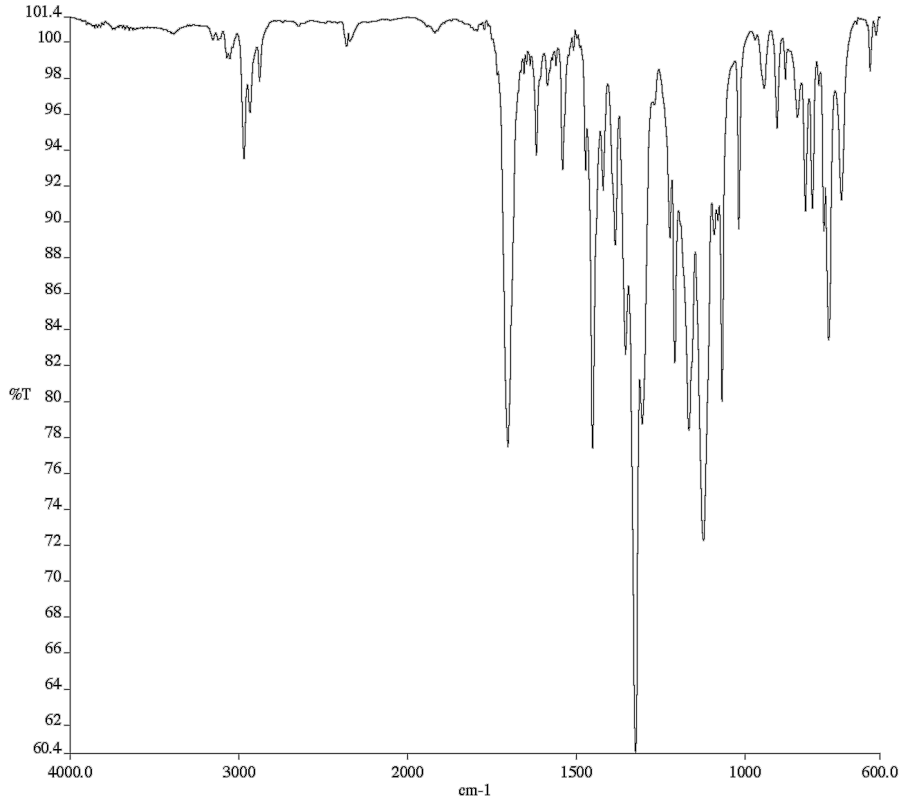

Figure A3.127 *Infrared spectrum (Thin Film, NaCl) of compound* ***35****.*

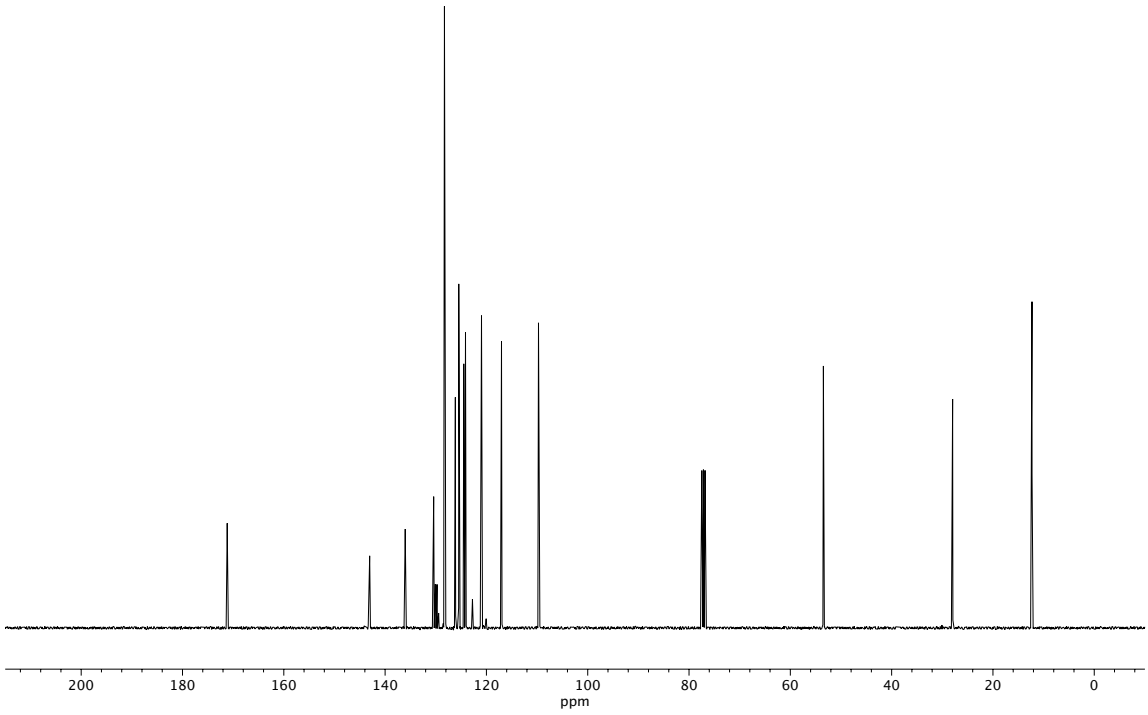

Figure A3.128 *^{13}C NMR (100 MHz, $CDCl_3$) of compound* ***35****.*

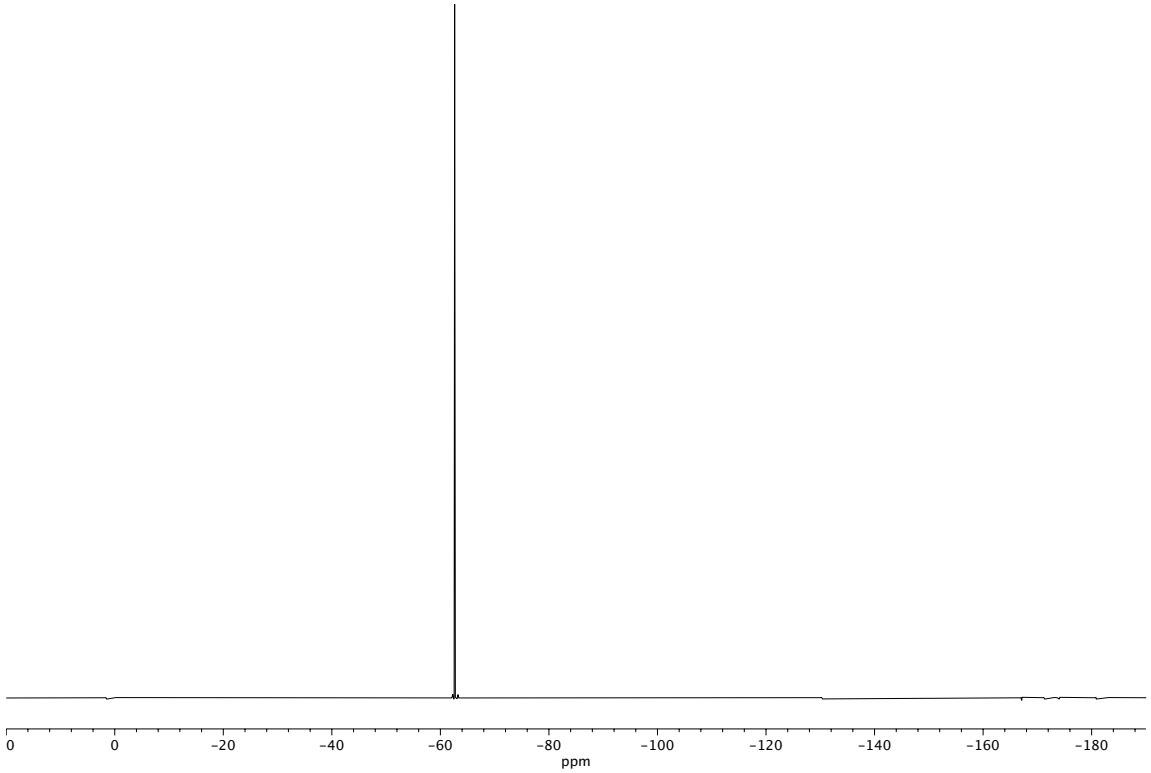

Figure A3.129 *^{19}F NMR (282 MHz, $CDCl_3$) of compound **35**.*

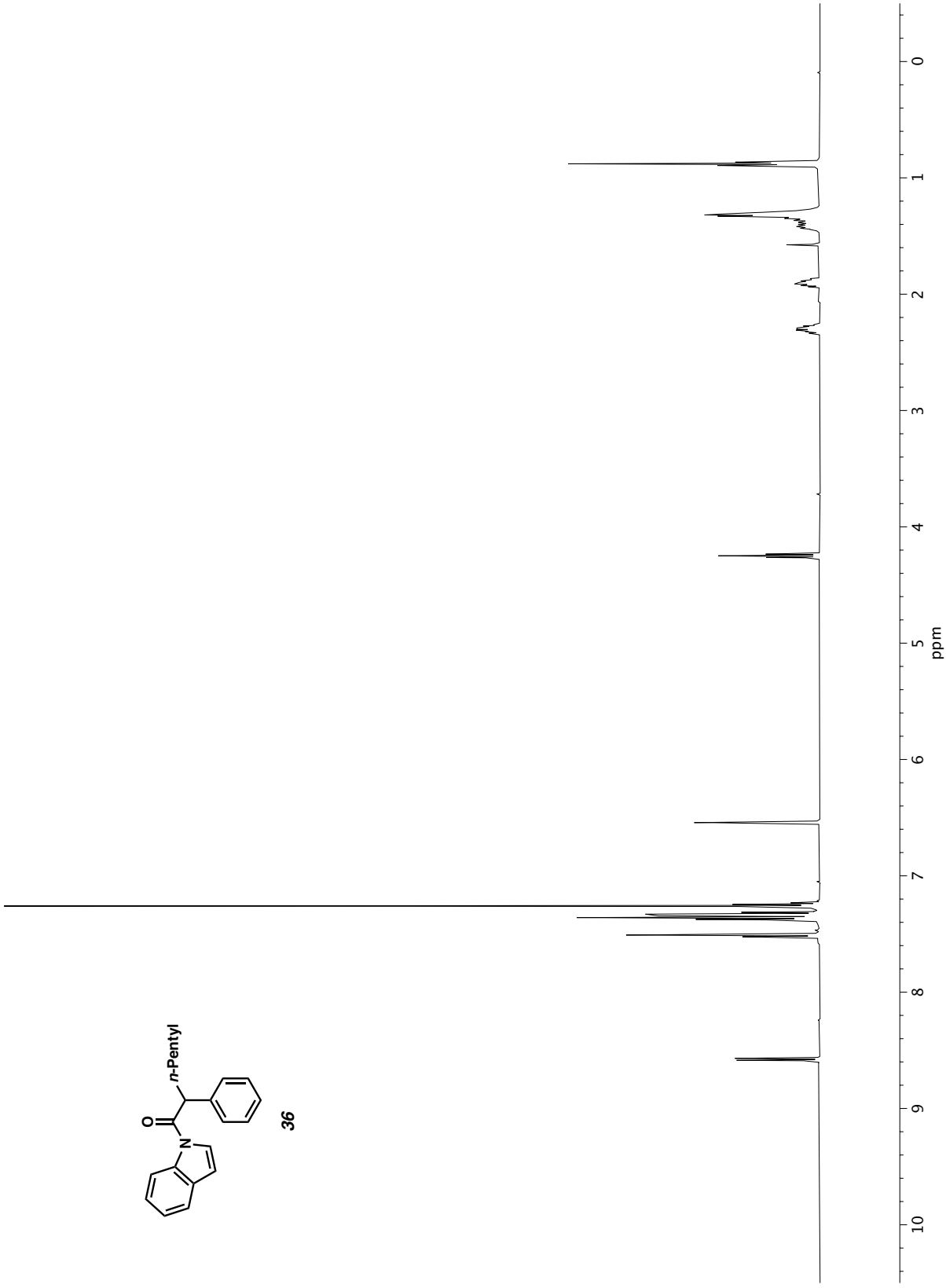

Figure A3.130 *^{1}H NMR (500 MHz, $CDCl_3$) of compound **36**.*

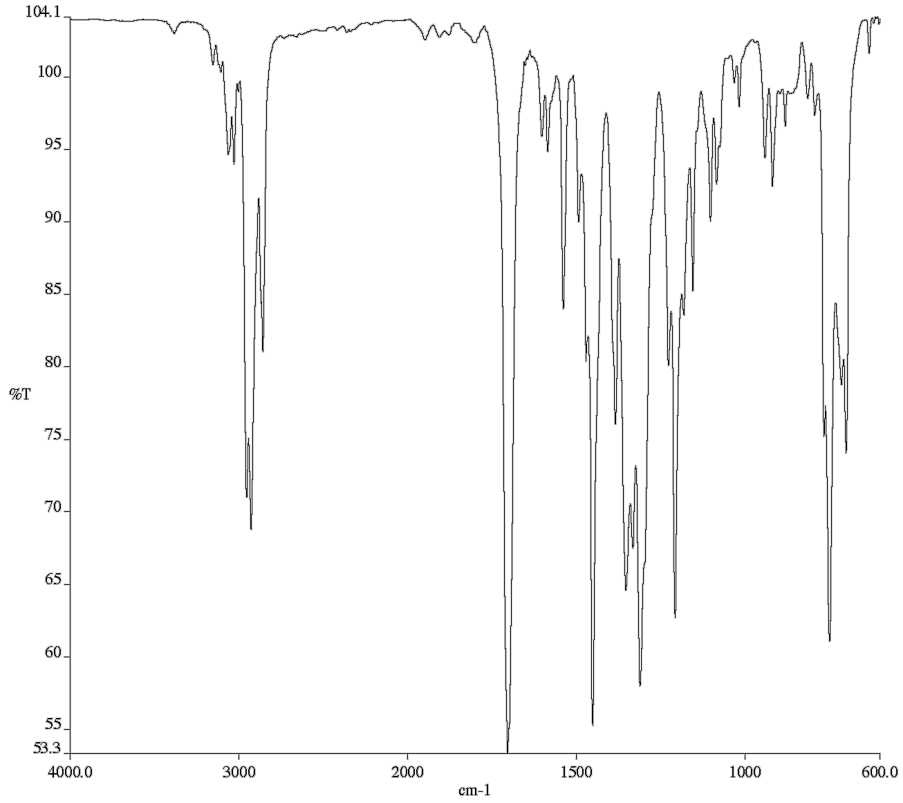

Figure A3.131 *Infrared spectrum (Thin Film, NaCl) of compound* ***36****.*

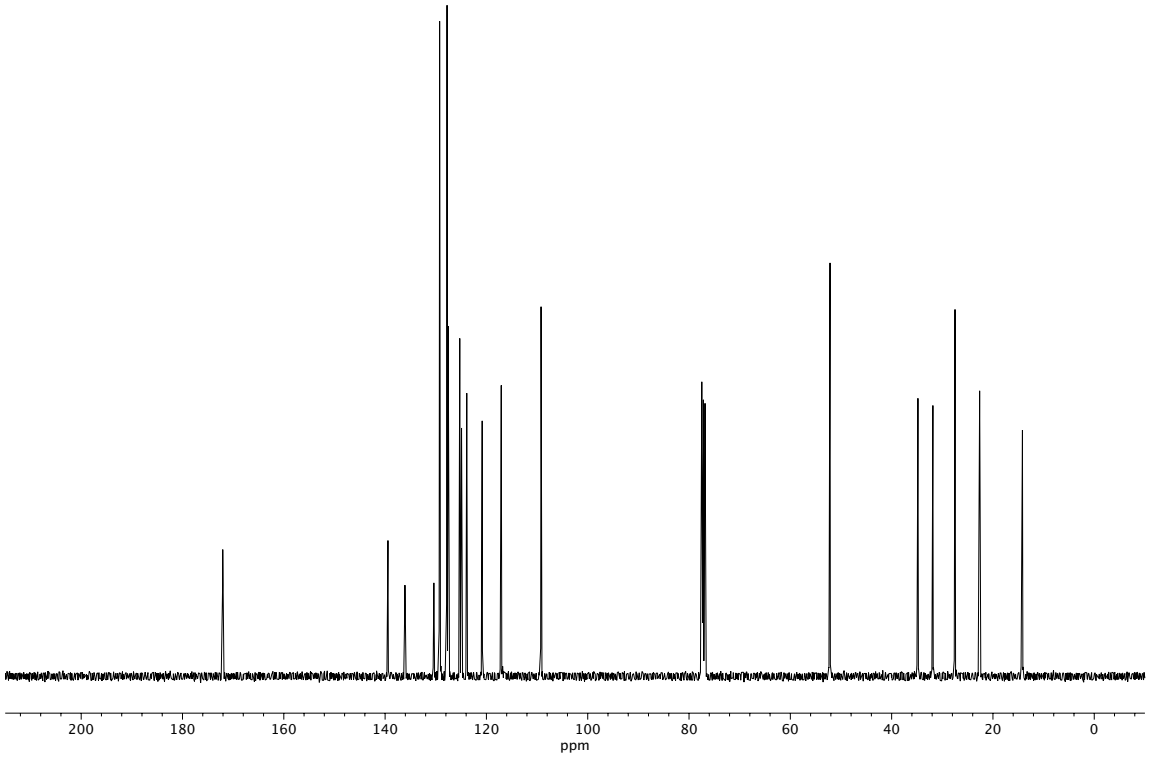

Figure A3.132 *^{13}C NMR (100 MHz, $CDCl_3$) of compound* ***38****.*

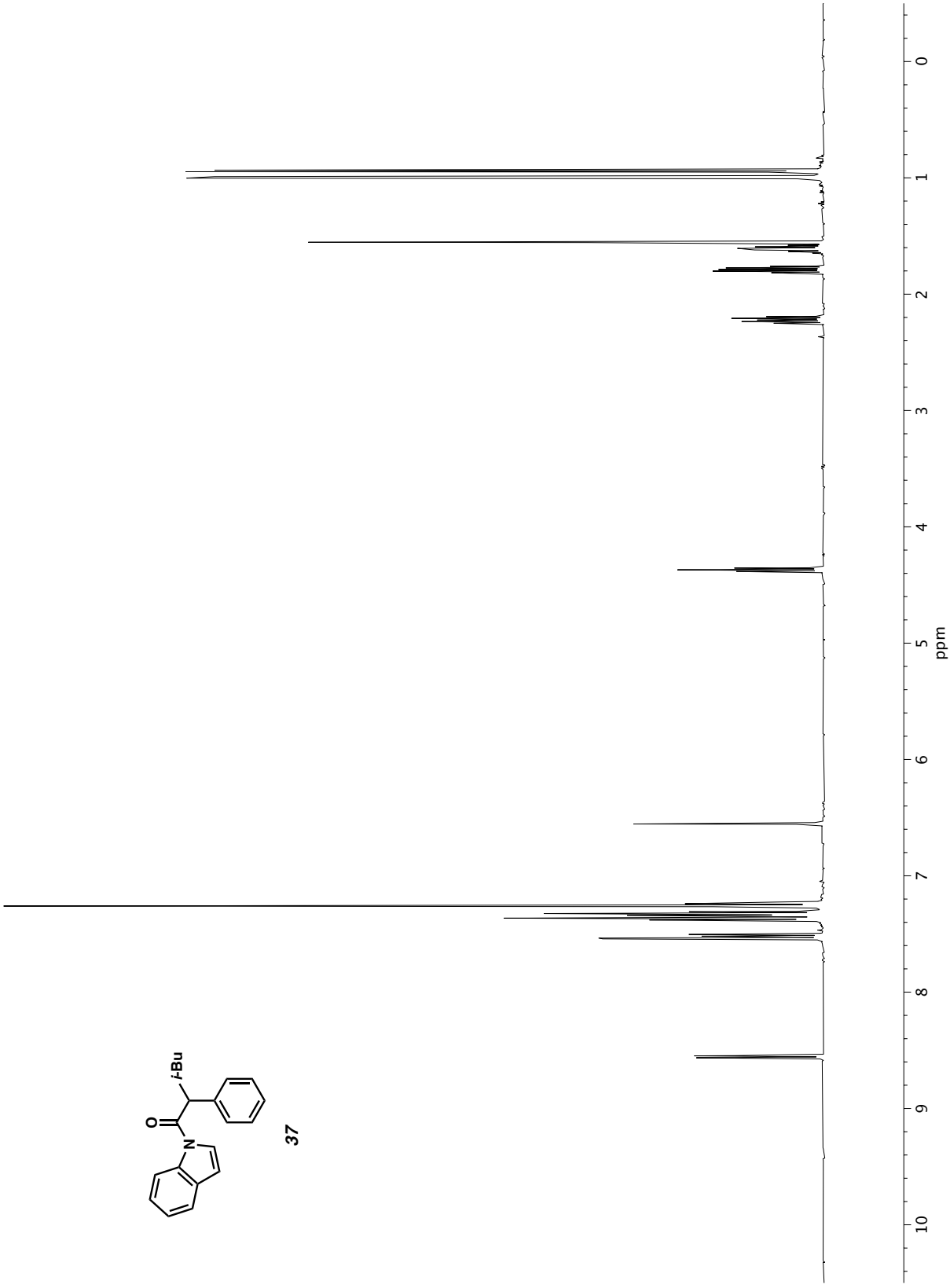

Figure A3.133 *^{1}H NMR (500 MHz, $CDCl_3$) of compound **37**.*

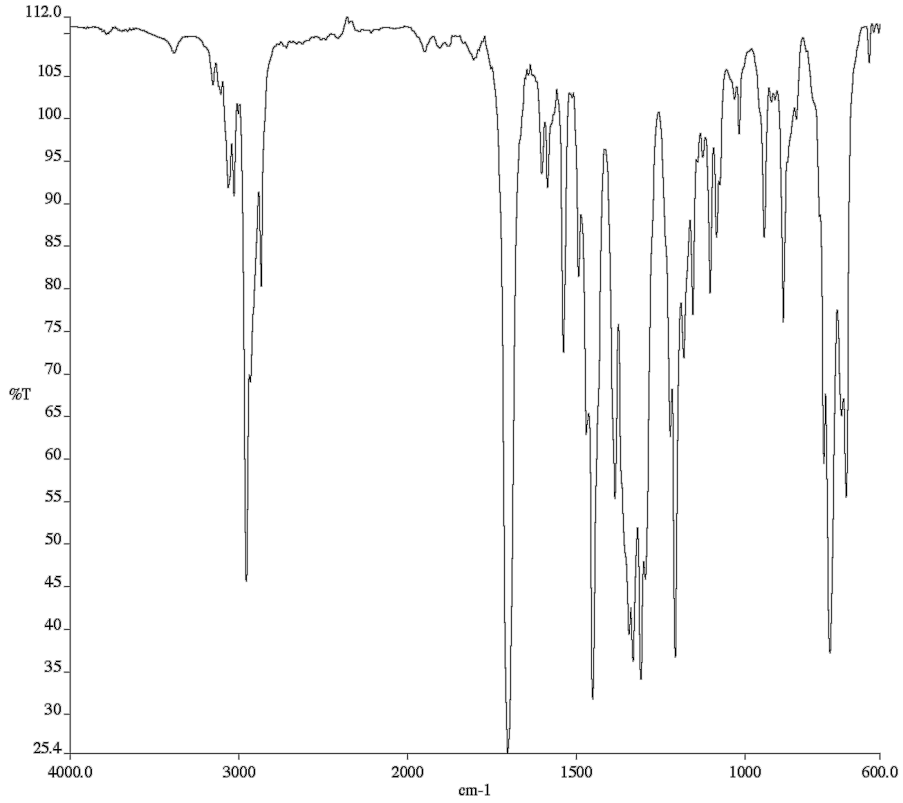

Figure A3.134 *Infrared spectrum (Thin Film, NaCl) of compound **37**.*

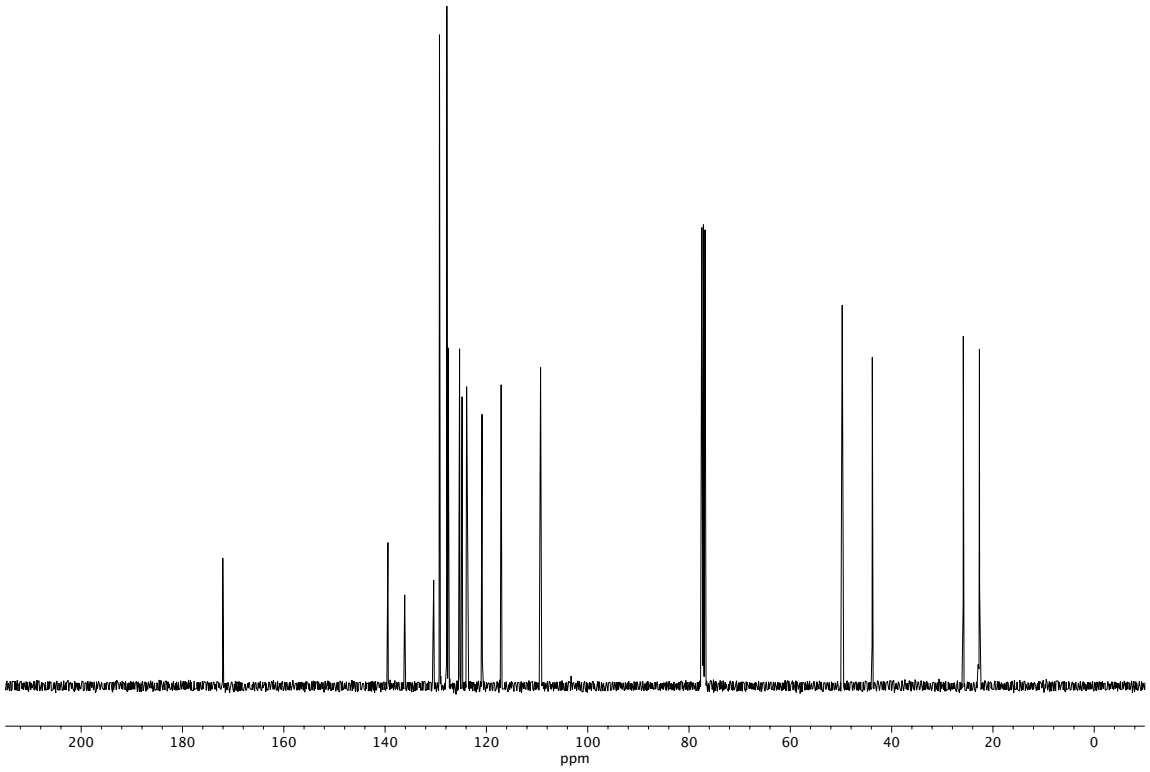

Figure A3.135 *^{13}C NMR (100 MHz, $CDCl_3$) of compound **37**.*

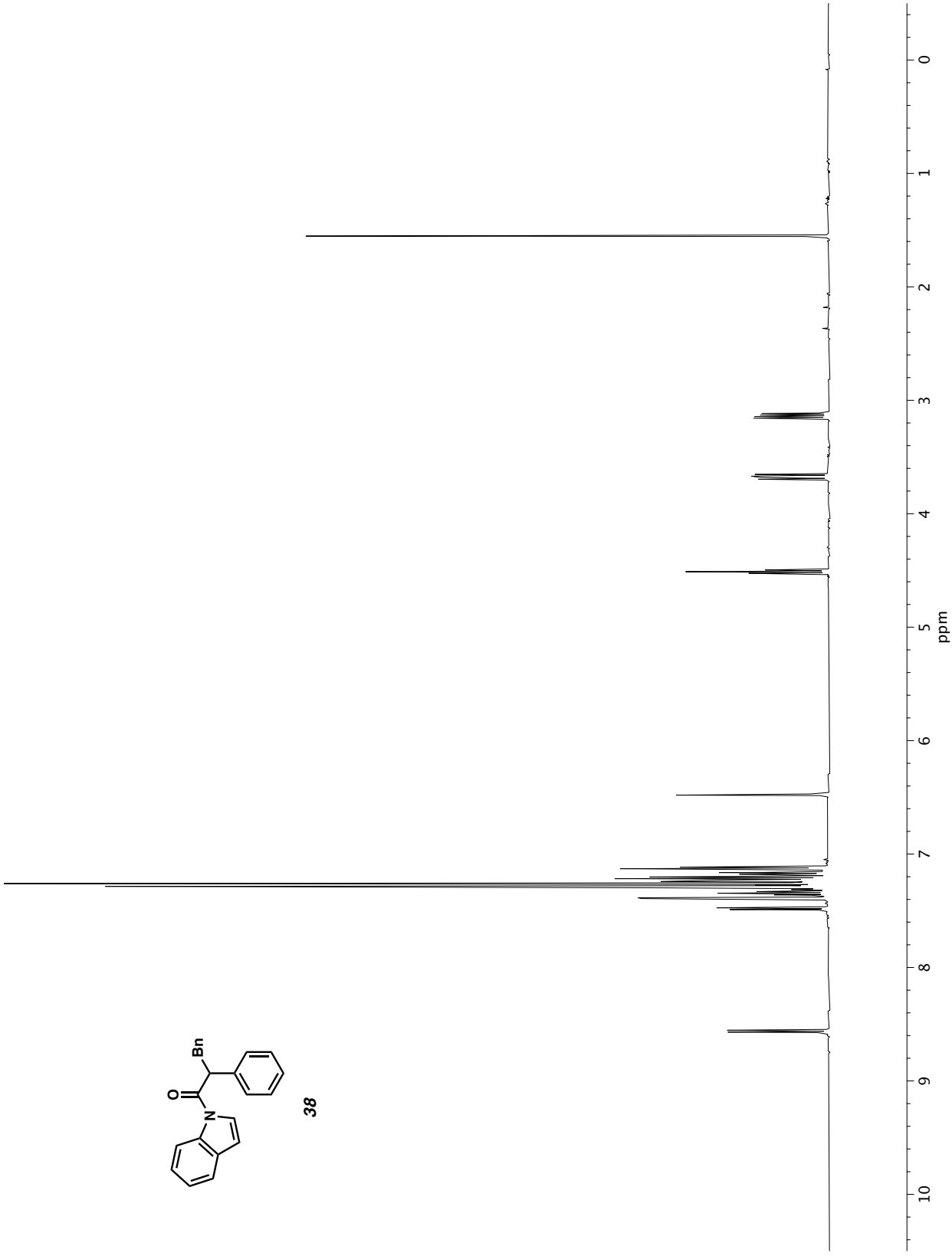

Figure A3.136 *^{1}H NMR (500 MHz, $CDCl_3$) of compound **38**.*

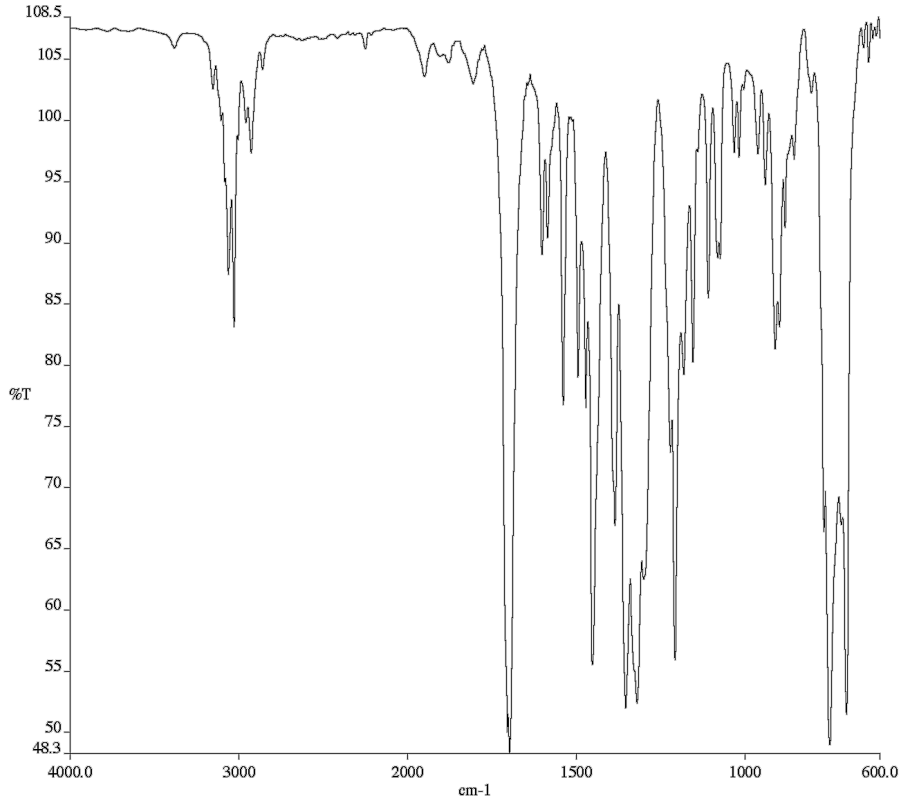

Figure A3.137 *Infrared spectrum (Thin Film, NaCl) of compound* ***38****.*

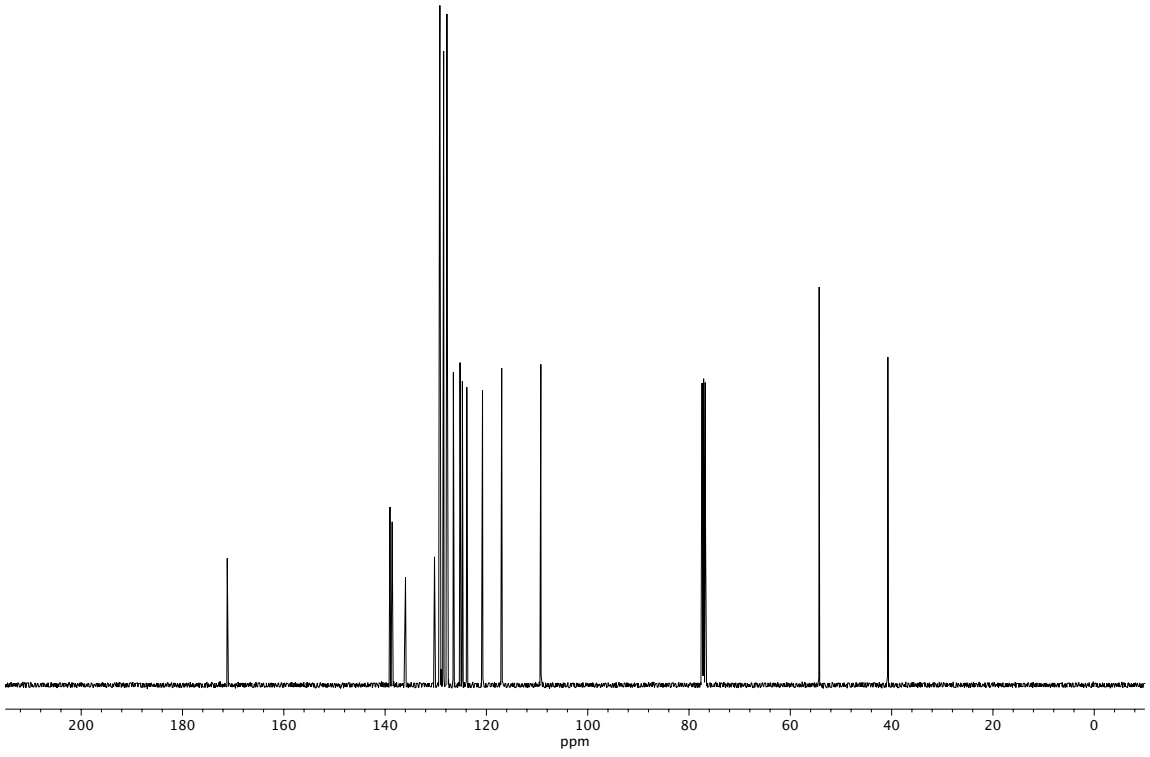

Figure A3.138 *^{13}C NMR (100 MHz, $CDCl_3$) of compound* ***38****.*

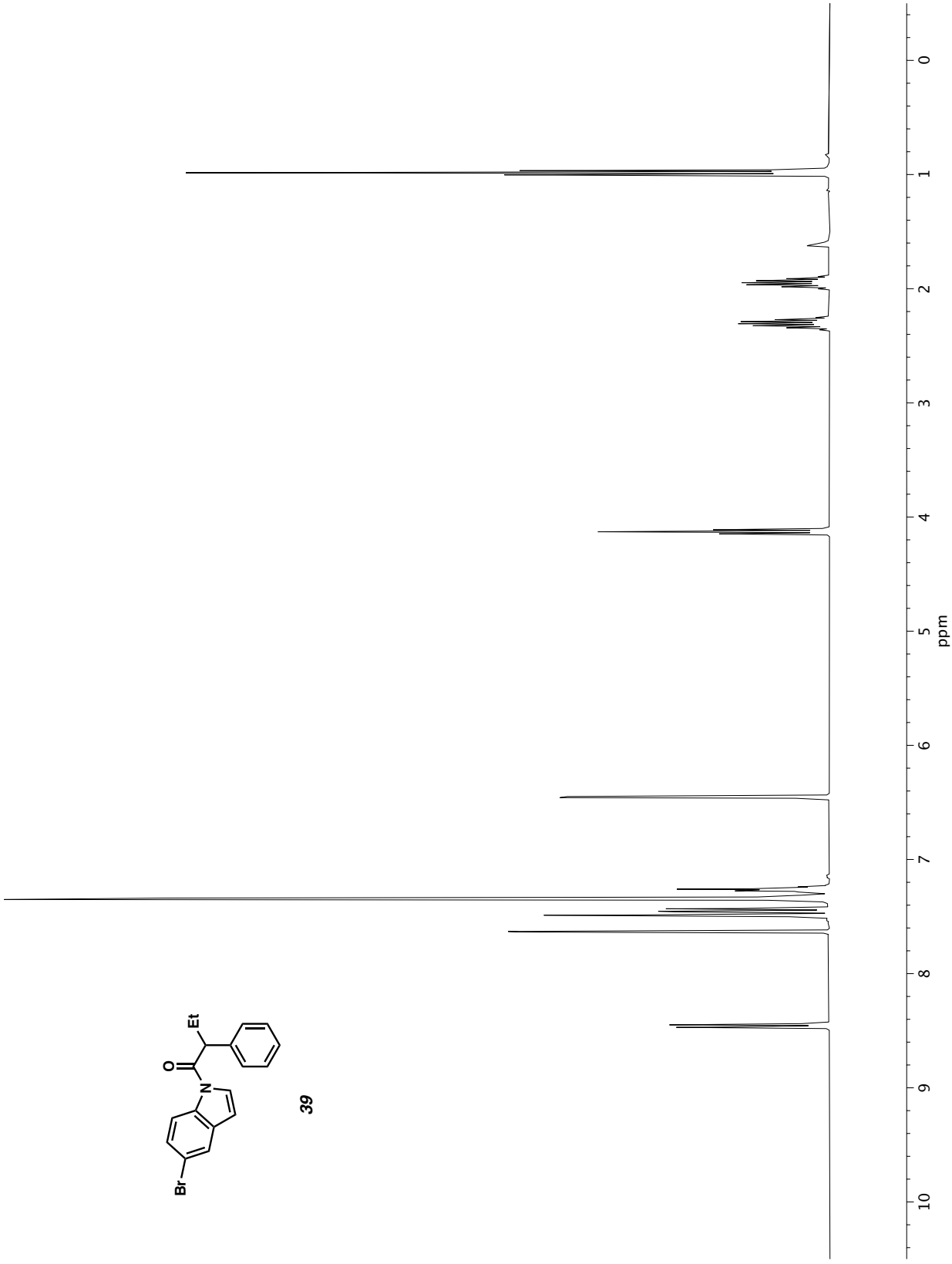

Figure A3.139 *^{1}H NMR (500 MHz, $CDCl_3$) of compound **39**.*

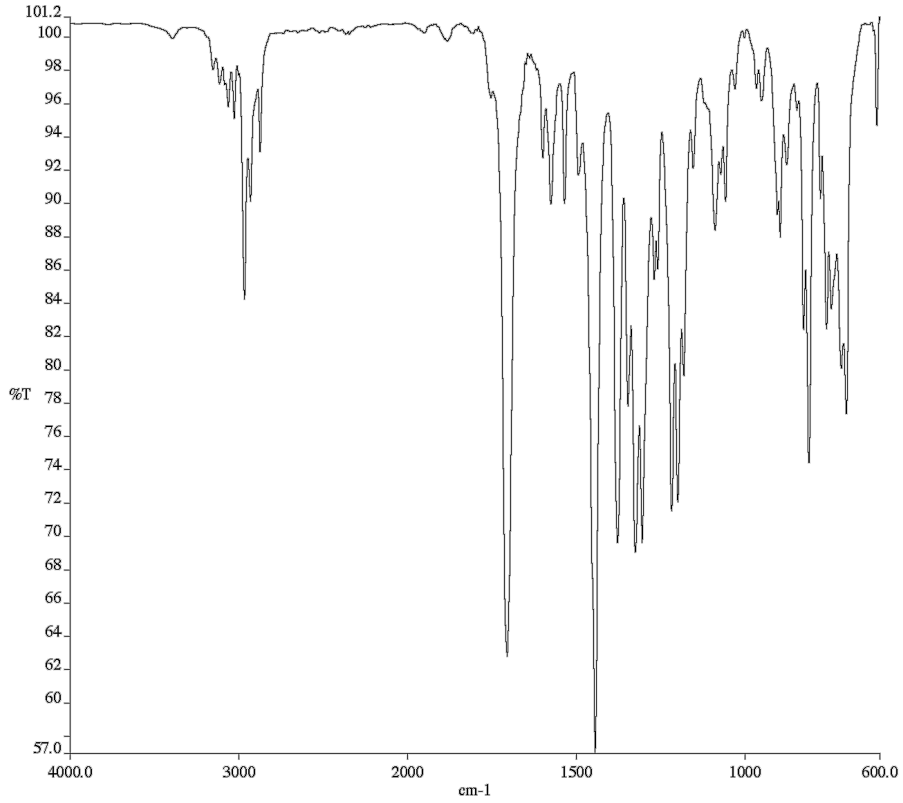

Figure A3.140 *Infrared spectrum (Thin Film, NaCl) of compound* ***39****.*

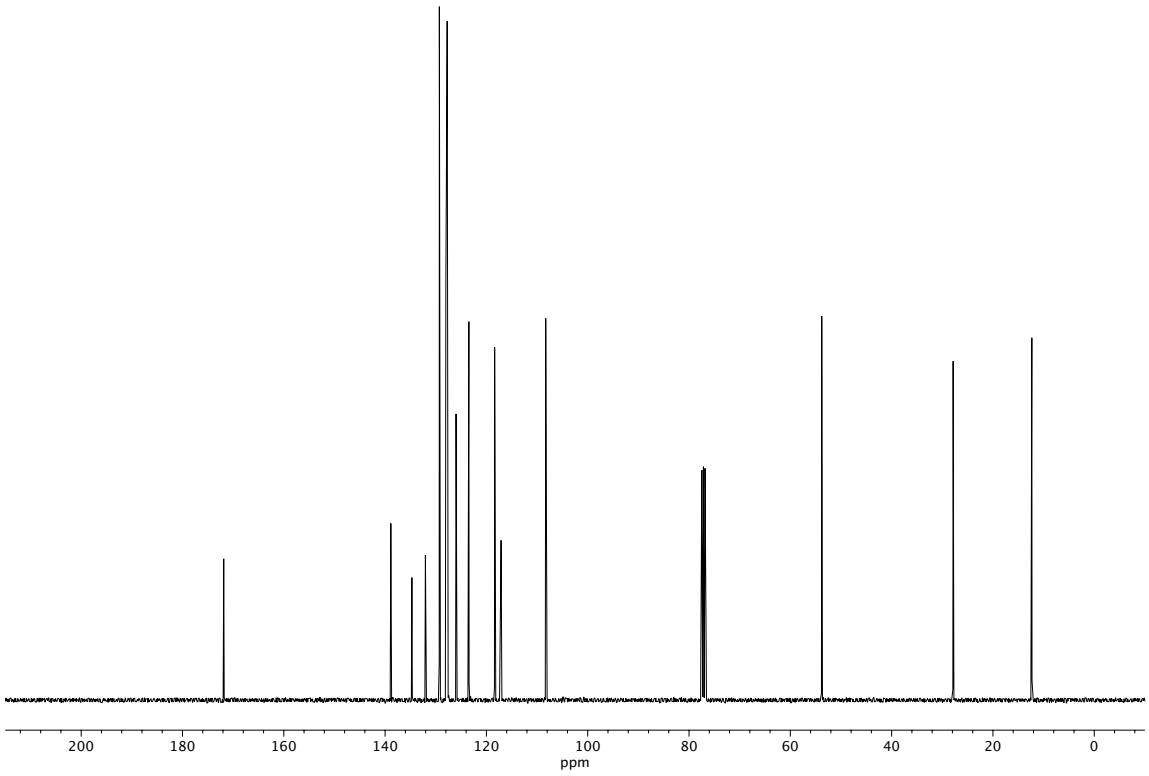

Figure A3.141 *^{13}C NMR (100 MHz, $CDCl_3$) of compound* ***39****.*

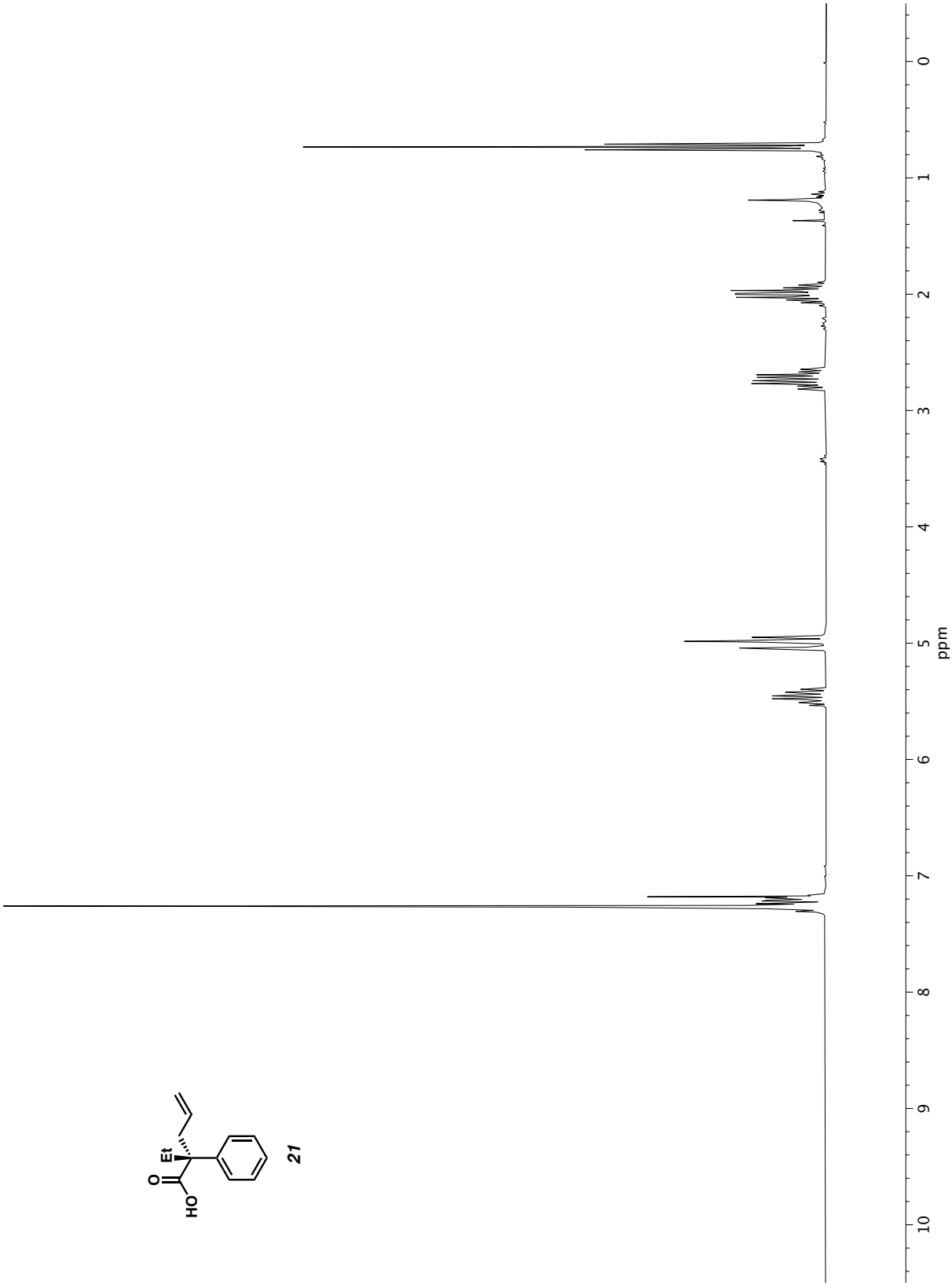

Figure A3.142 *^{1}H NMR (300 MHz, $CDCl_3$) of compound **21**.*

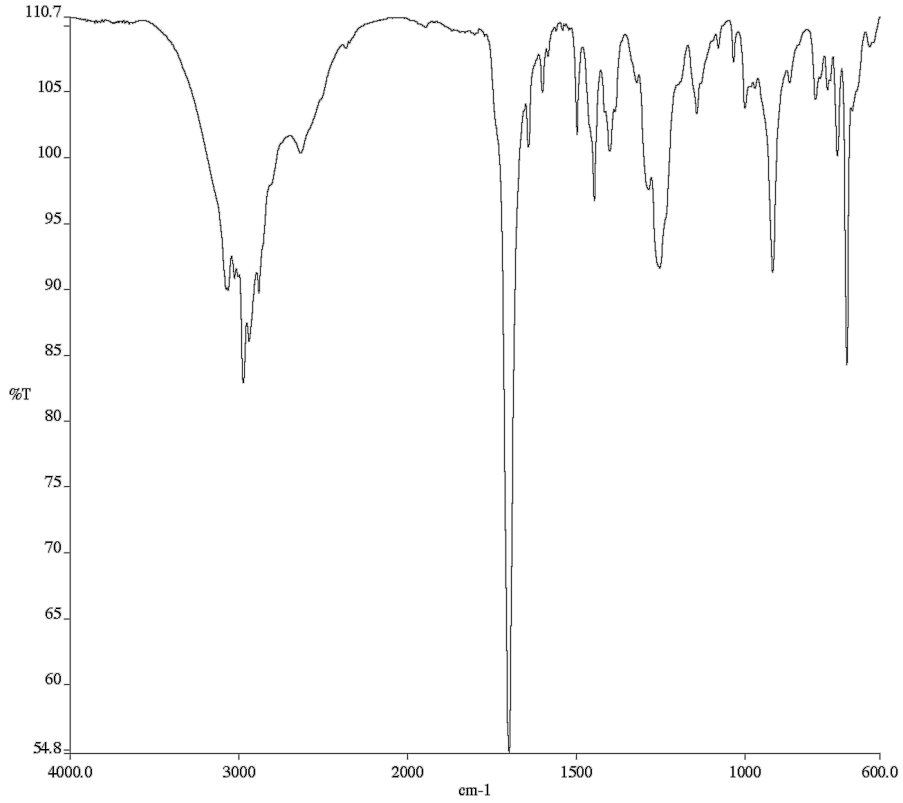

Figure A3.143 *Infrared spectrum (Thin Film, NaCl) of compound **21**.*

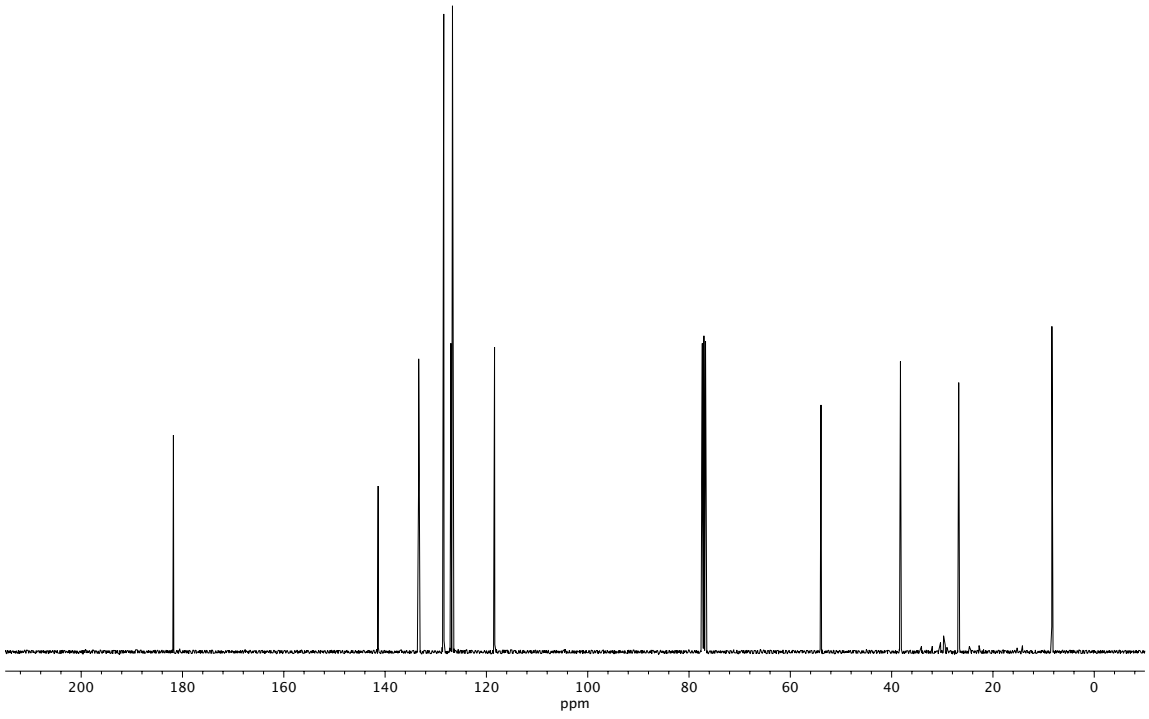

Figure A3.144 *^{13}C NMR (100 MHz, $CDCl_3$) of compound **21**.*

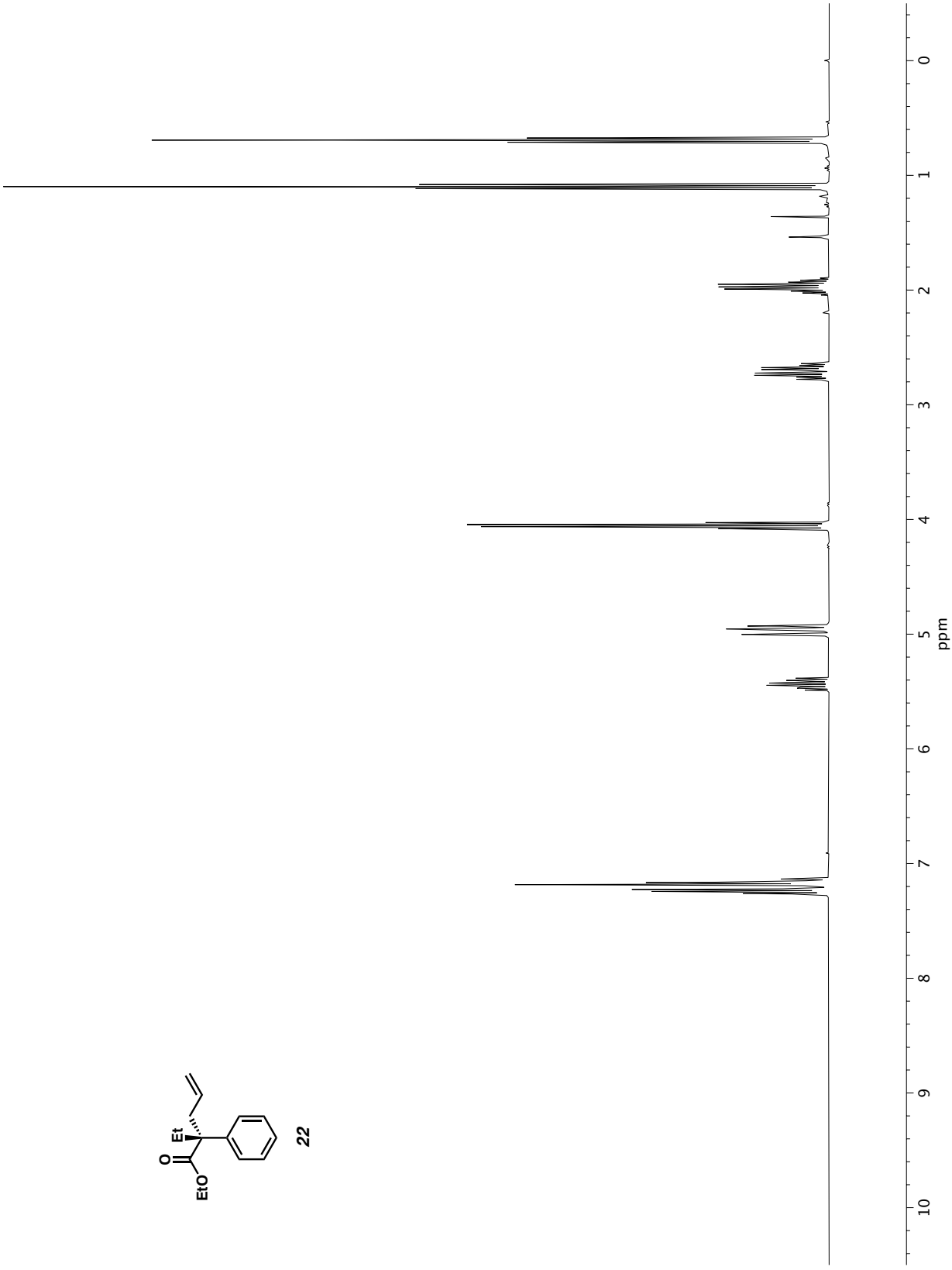

Figure A3.145 *^{1}H NMR (400 MHz, $CDCl_3$) of compound **22**.*

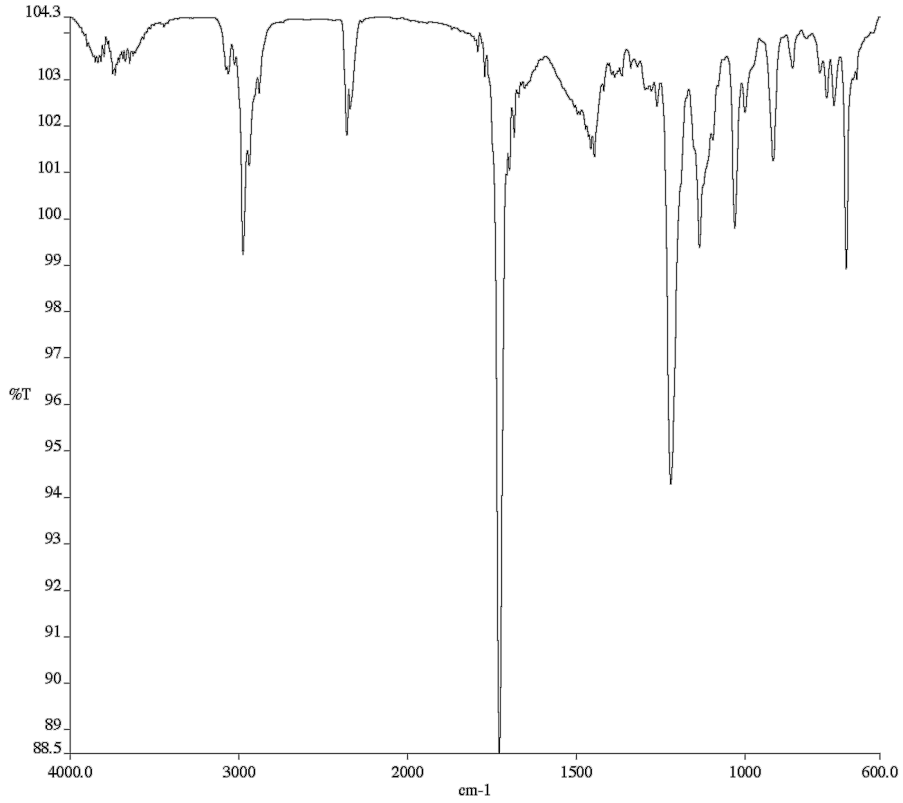

Figure A3.146 *Infrared spectrum (Thin Film, NaCl) of compound* ***22****.*

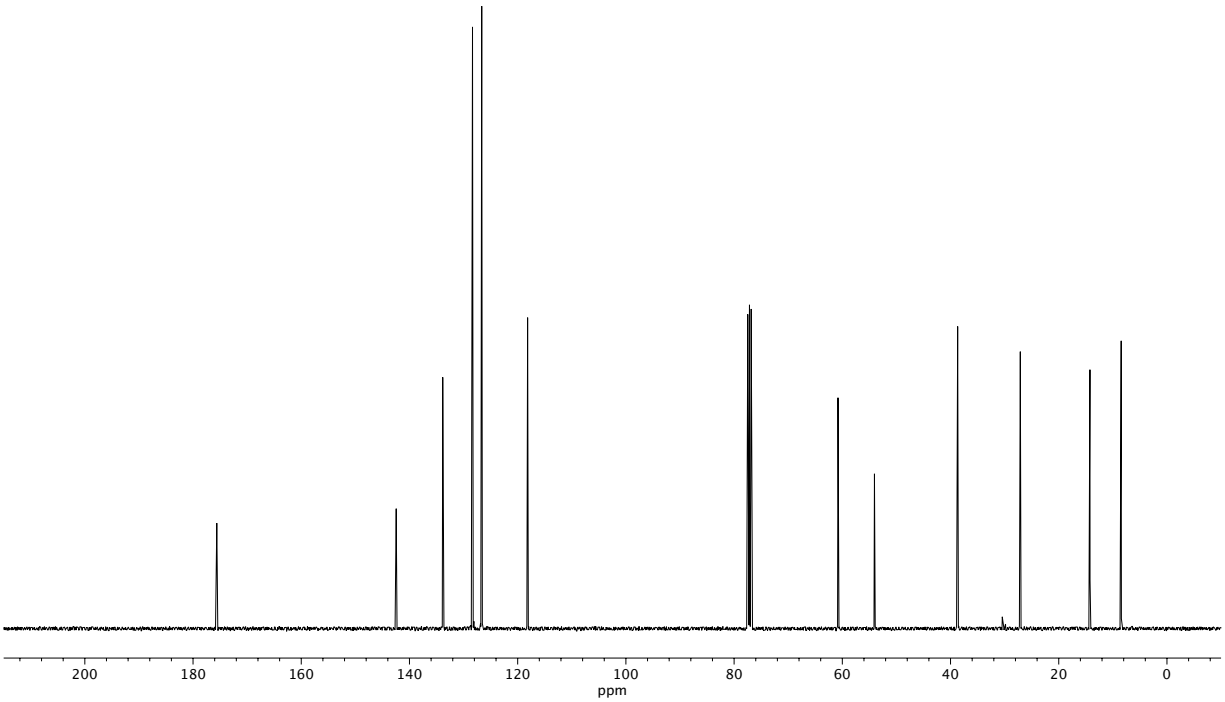

Figure A3.147 *^{13}C NMR (100 MHz, $CDCl_3$) of compound* ***22****.*

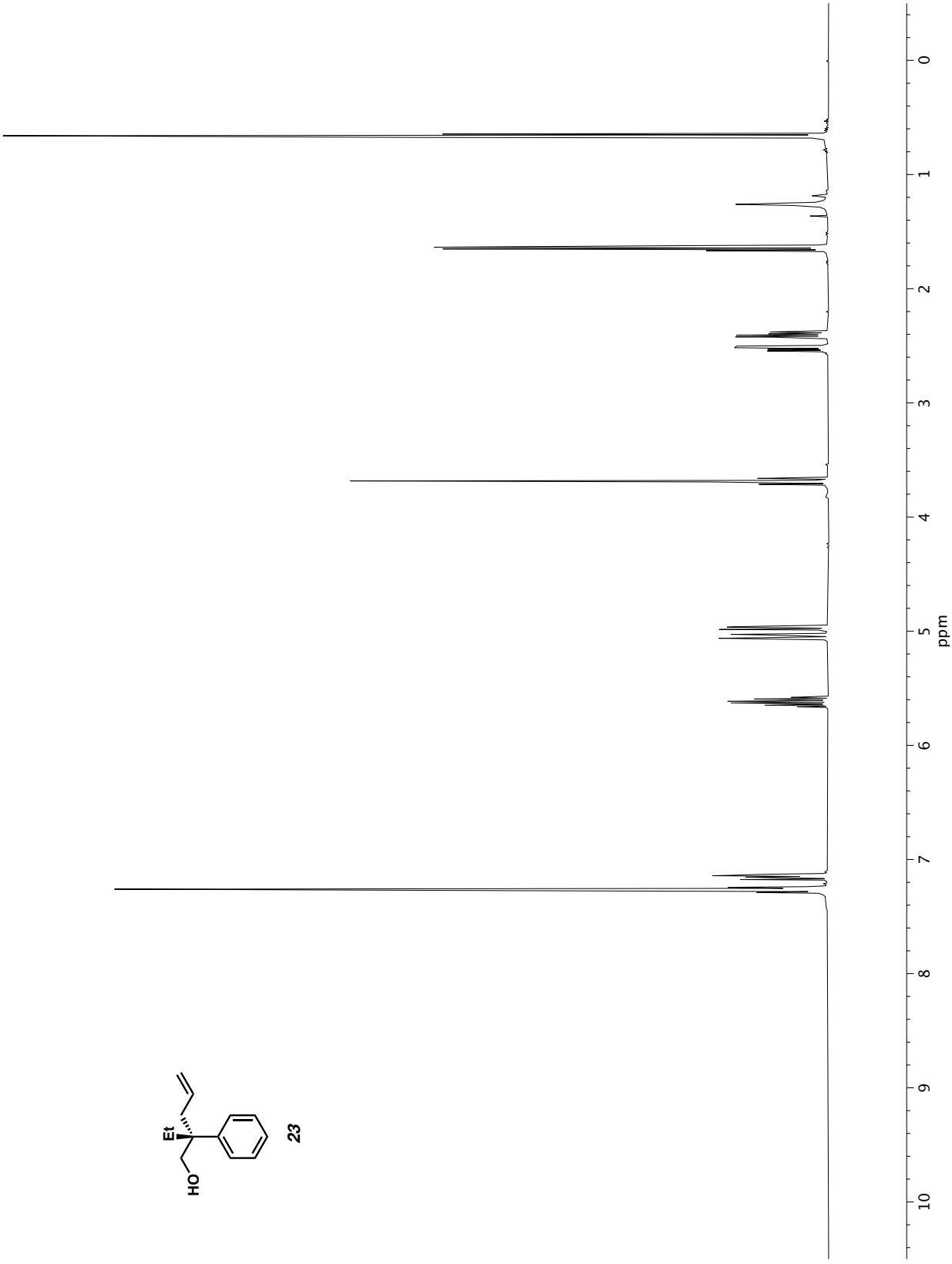

Figure A3.148 *^1H NMR (500 MHz, $CDCl_3$) of compound **23**.*

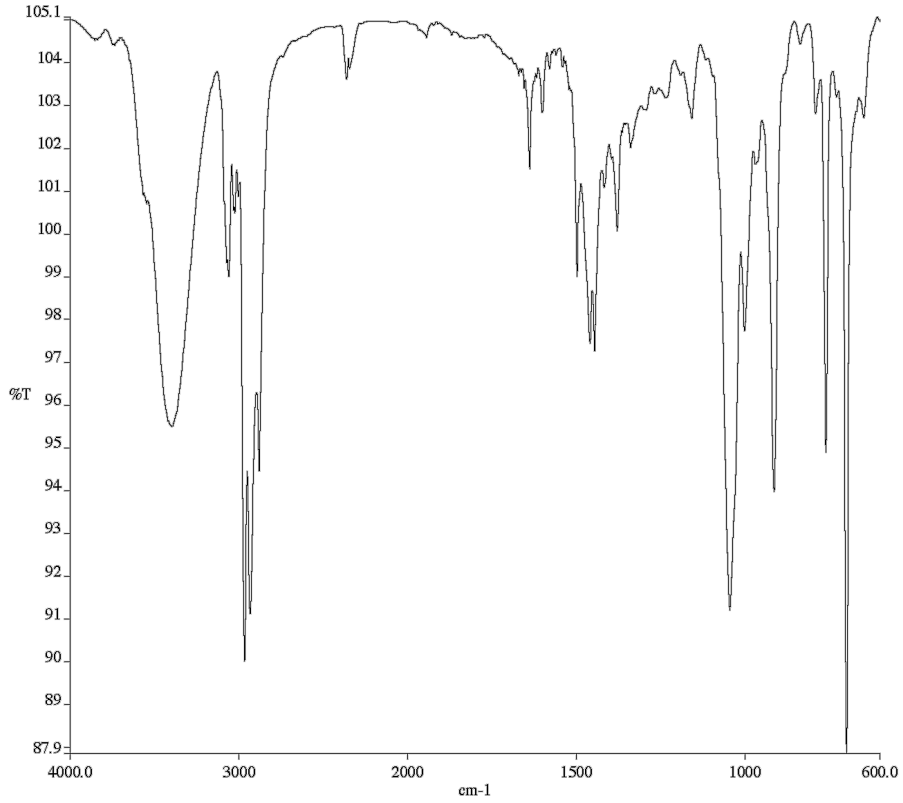

Figure A3.149 *Infrared spectrum (Thin Film, NaCl) of compound* ***23****.*

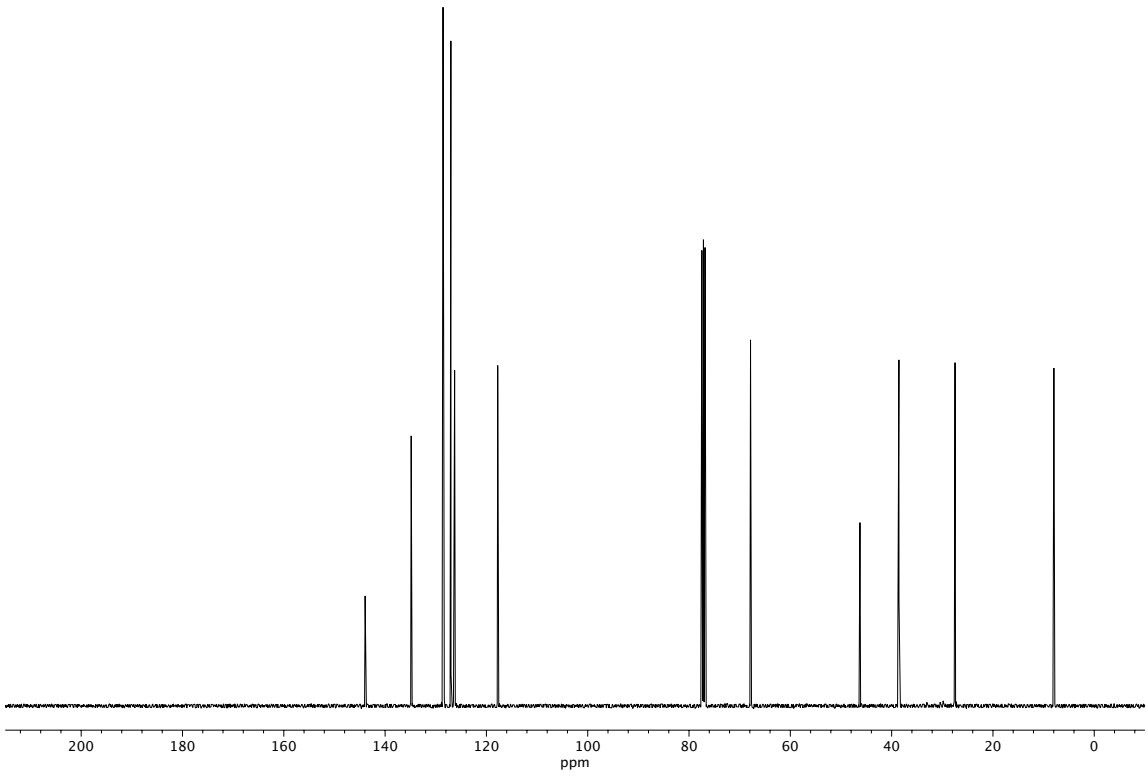

Figure A3.150 *^{13}C NMR (100 MHz, $CDCl_3$) of compound* ***23****.*

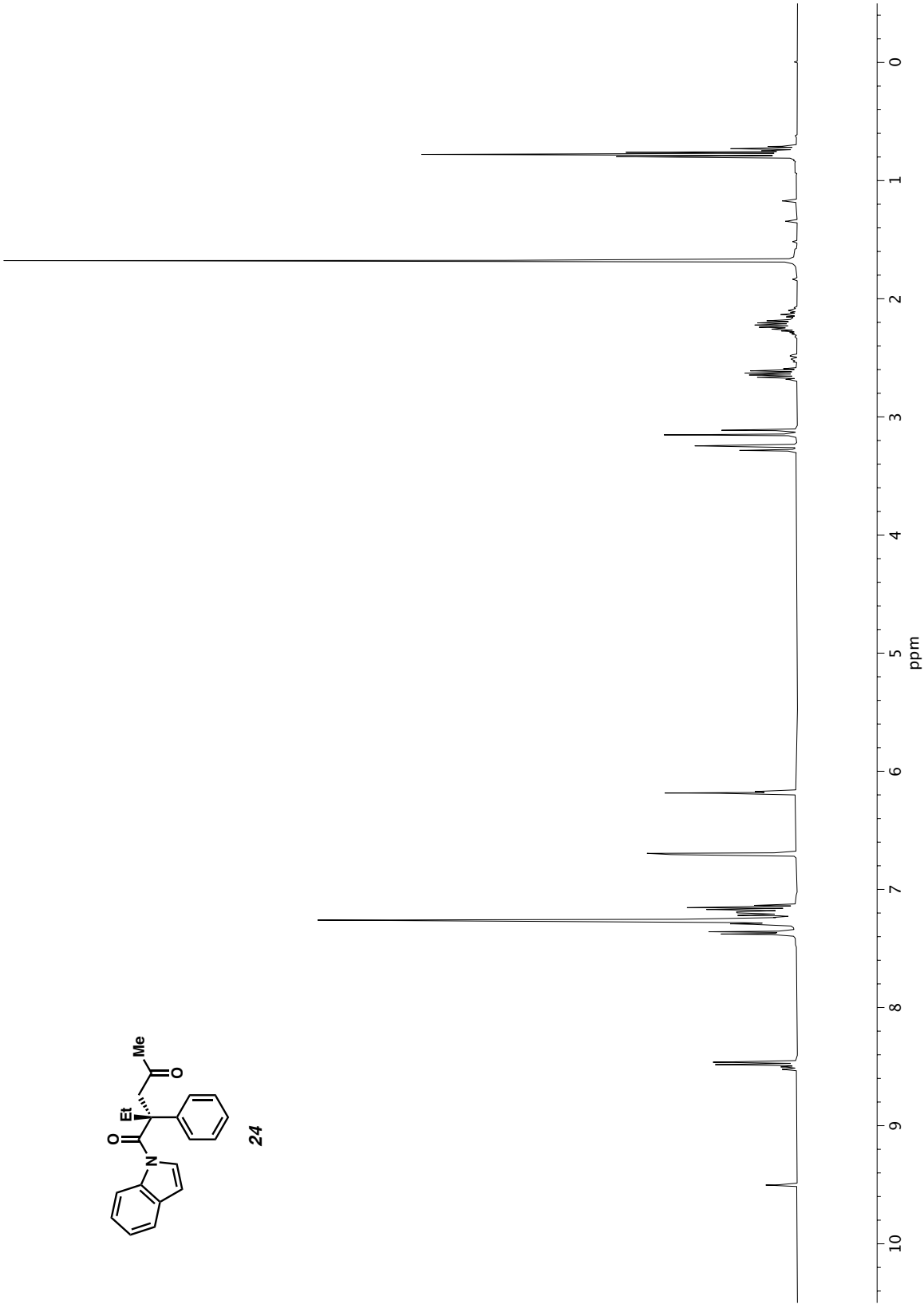

Figure A3.151 *^{1}H NMR (400 MHz, $CDCl_3$) of compound **24**.*

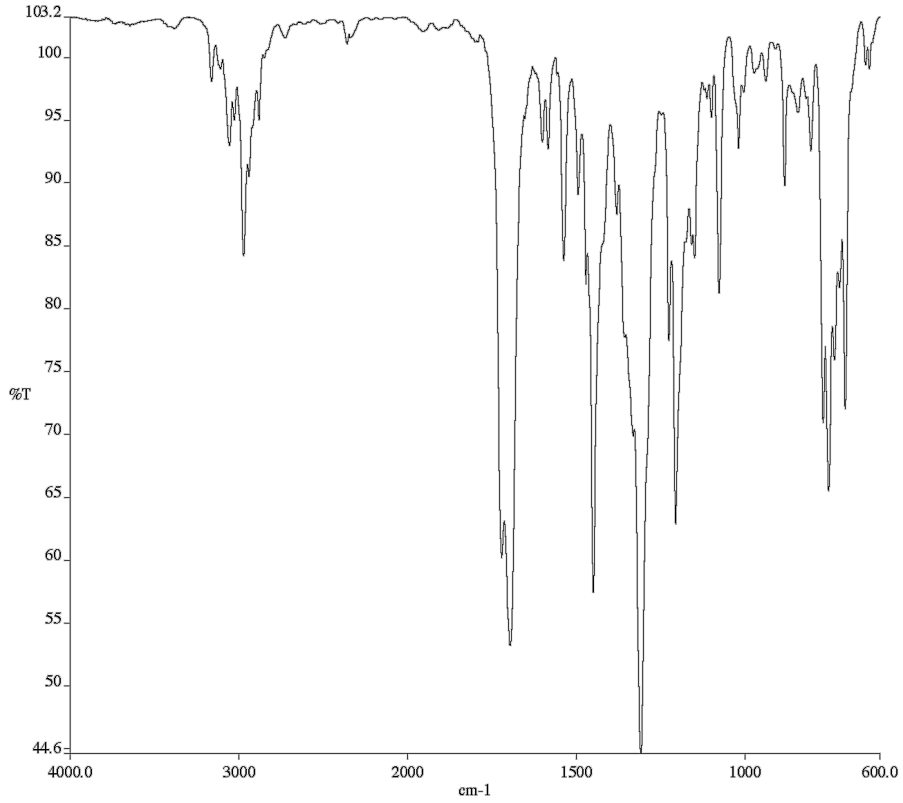

Figure A3.152 *Infrared spectrum (Thin Film, NaCl) of compound **24**.*

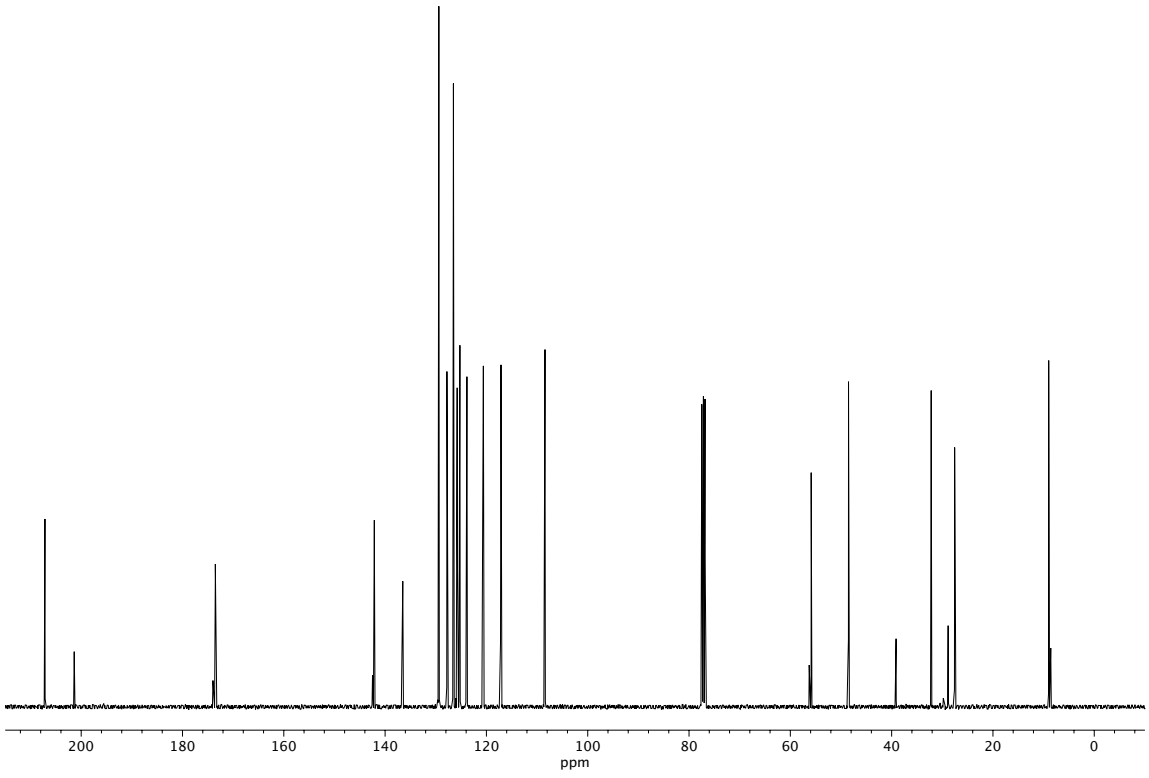

Figure A3.153 *^{13}C NMR (100 MHz, $CDCl_3$) of compound **24**.*

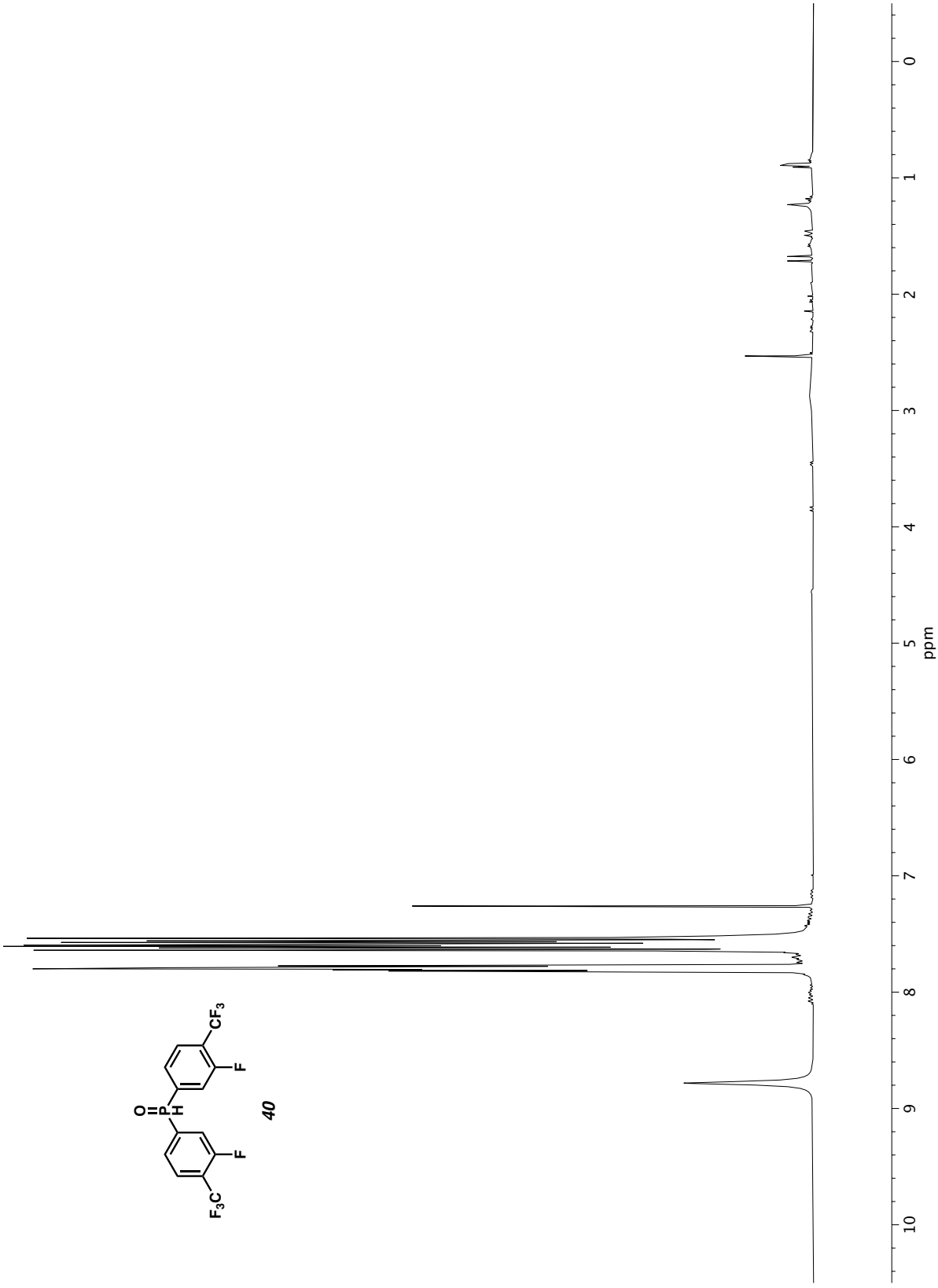

Figure A3.154 *^{1}H NMR (400 MHz, $CDCl_3$) of compound **40**.*

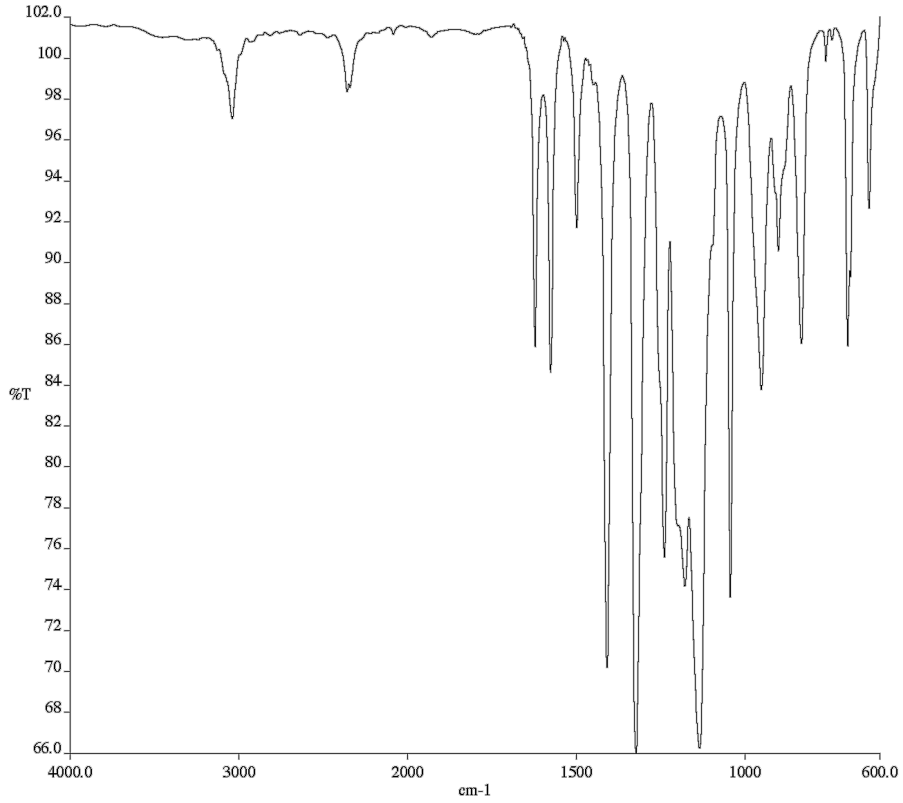

Figure A3.155 *Infrared spectrum (Thin Film, NaCl) of compound* ***40****.*

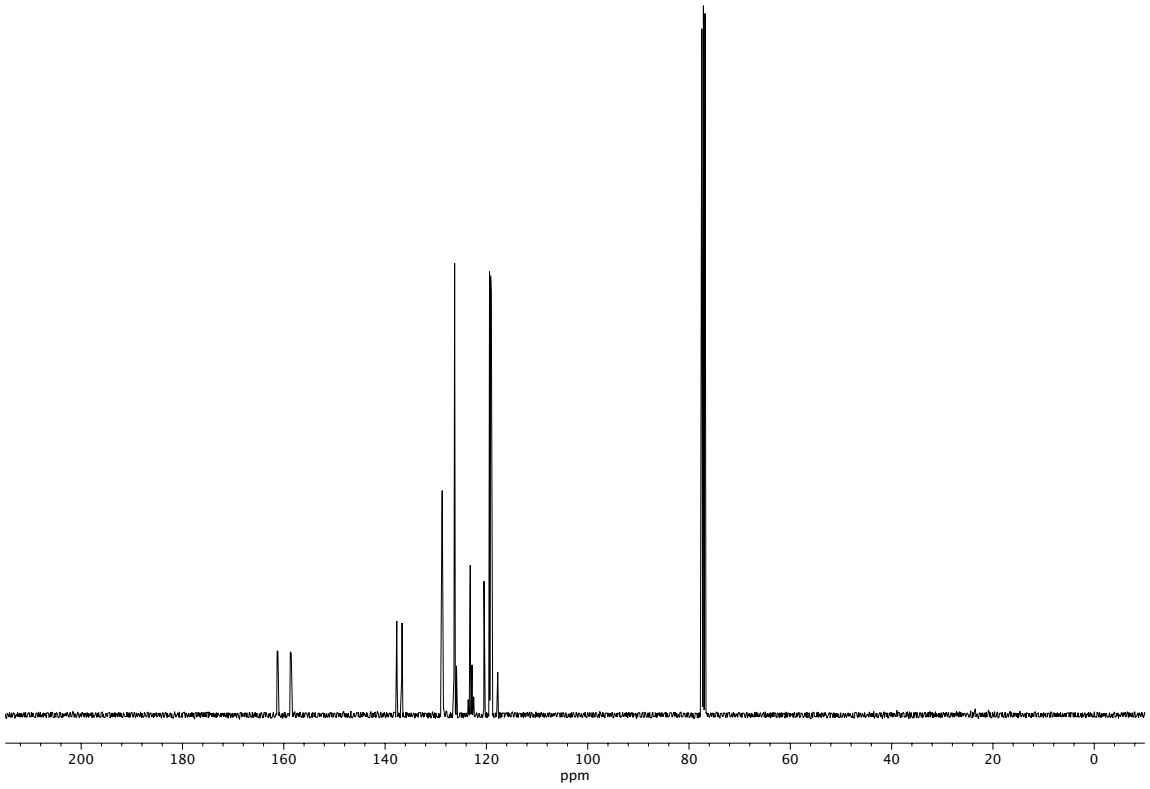

Figure A3.156 *^{13}C NMR (100 MHz, $CDCl_3$) of compound* ***40****.*

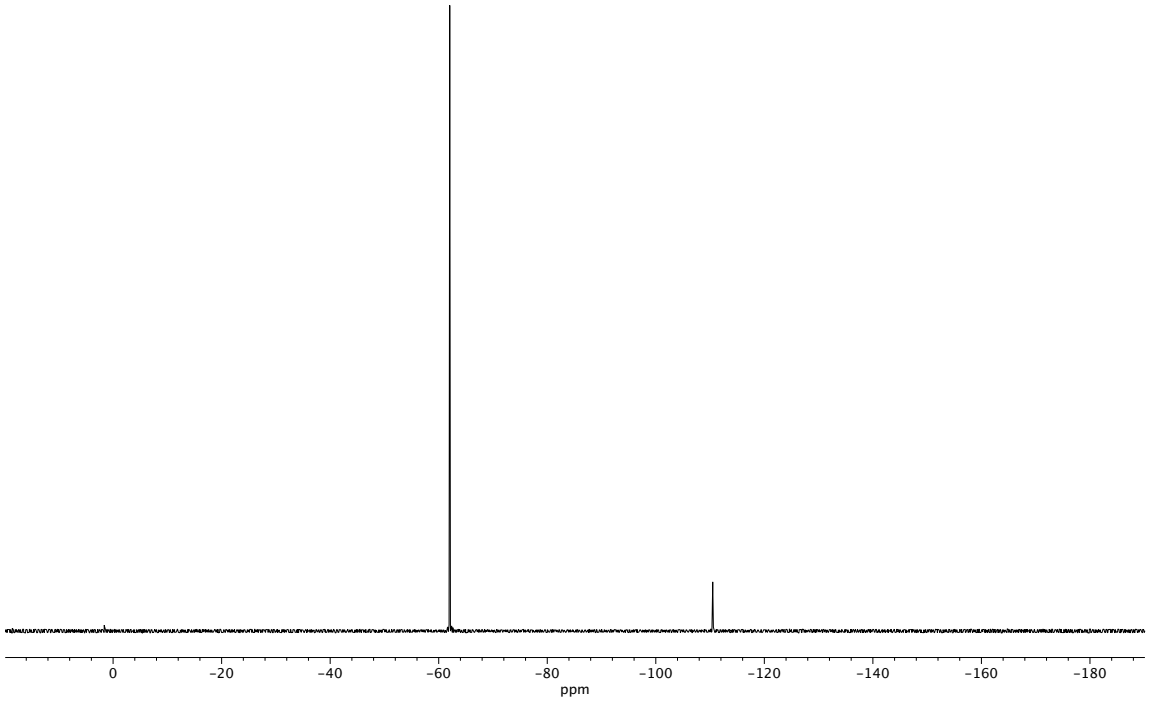

Figure A3.157 *^{19}F NMR (282 MHz, $CDCl_3$) of compound **40**.*

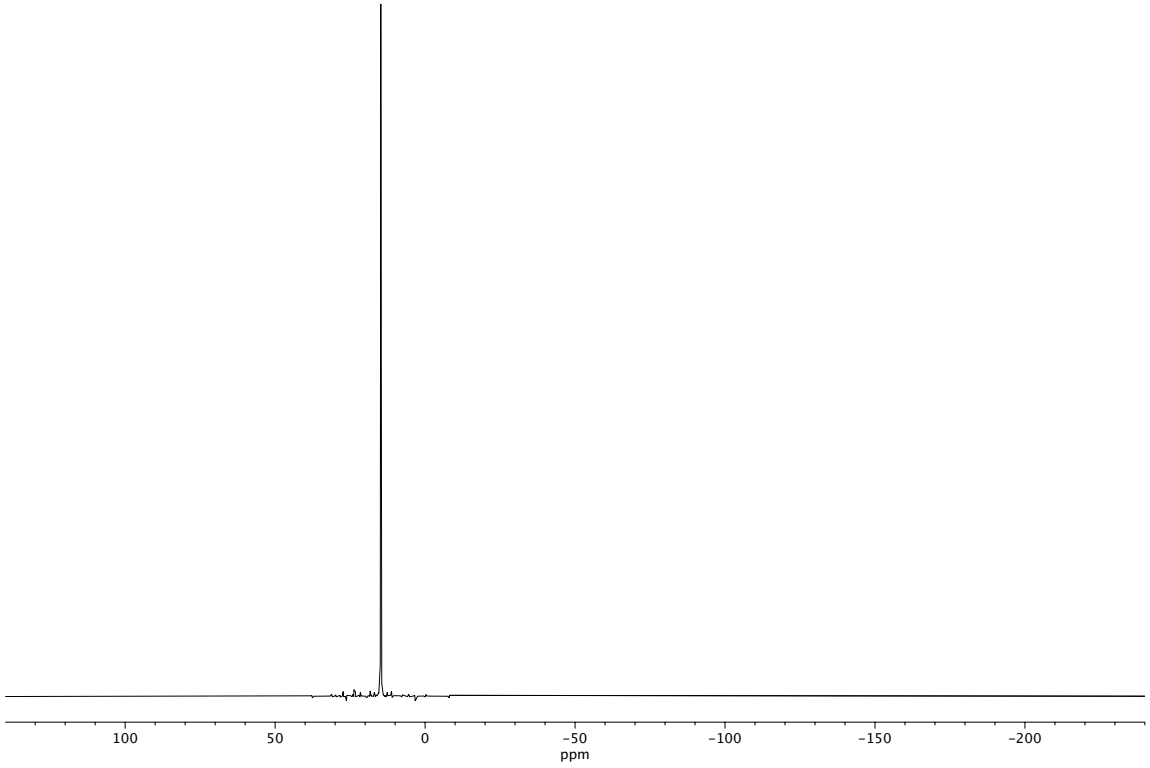

Figure A3.158 *^{31}P NMR (162 MHz, $CDCl_3$) of compound **40**.*

Figure A3.159 *^{1}H NMR (500 MHz, $CDCl_3$) of compound **41**.*

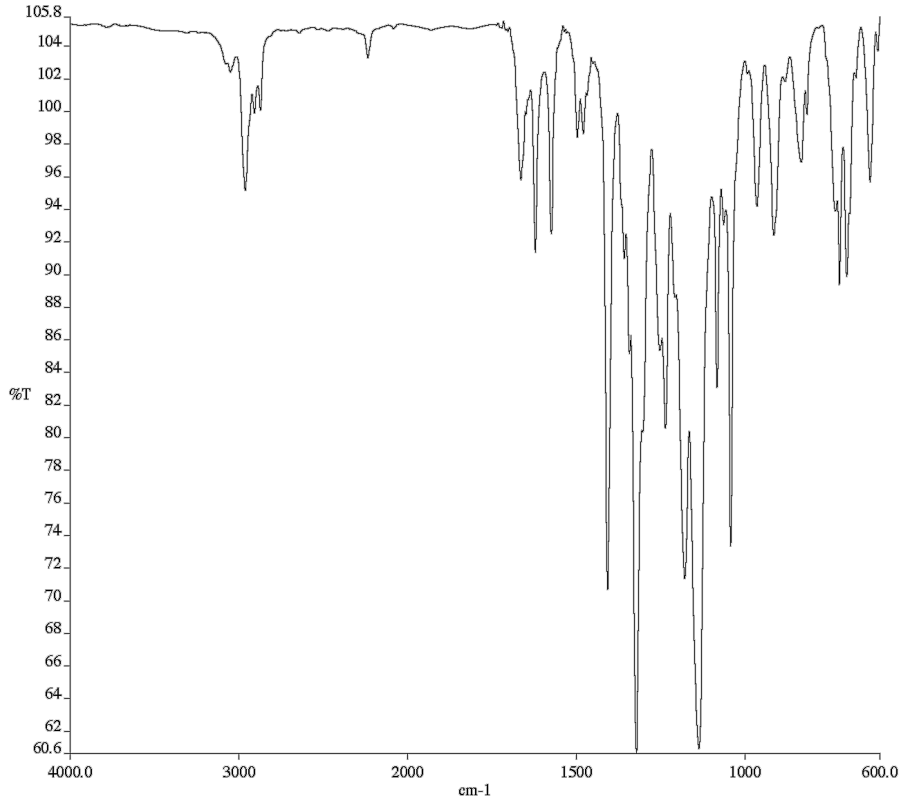

Figure A3.160 *Infrared spectrum (Thin Film, NaCl) of compound **41**.*

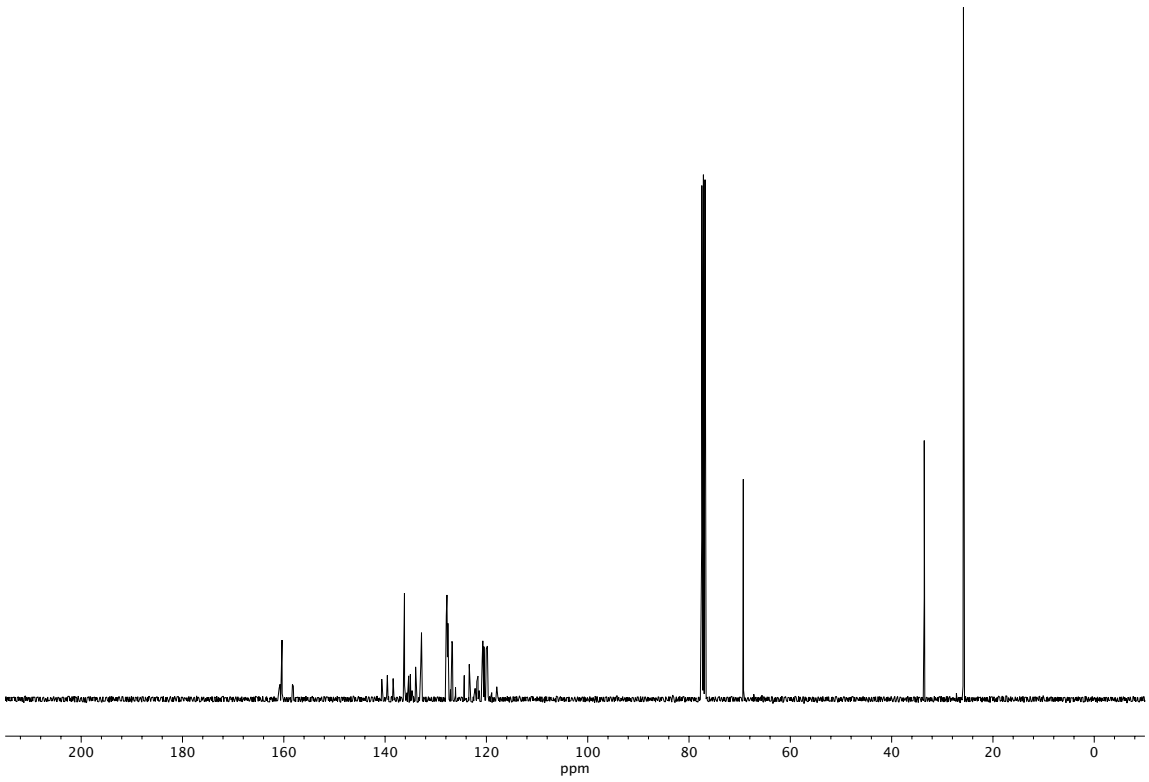

Figure A3.161 *^{13}C NMR (100 MHz, $CDCl_3$) of compound **41**.*

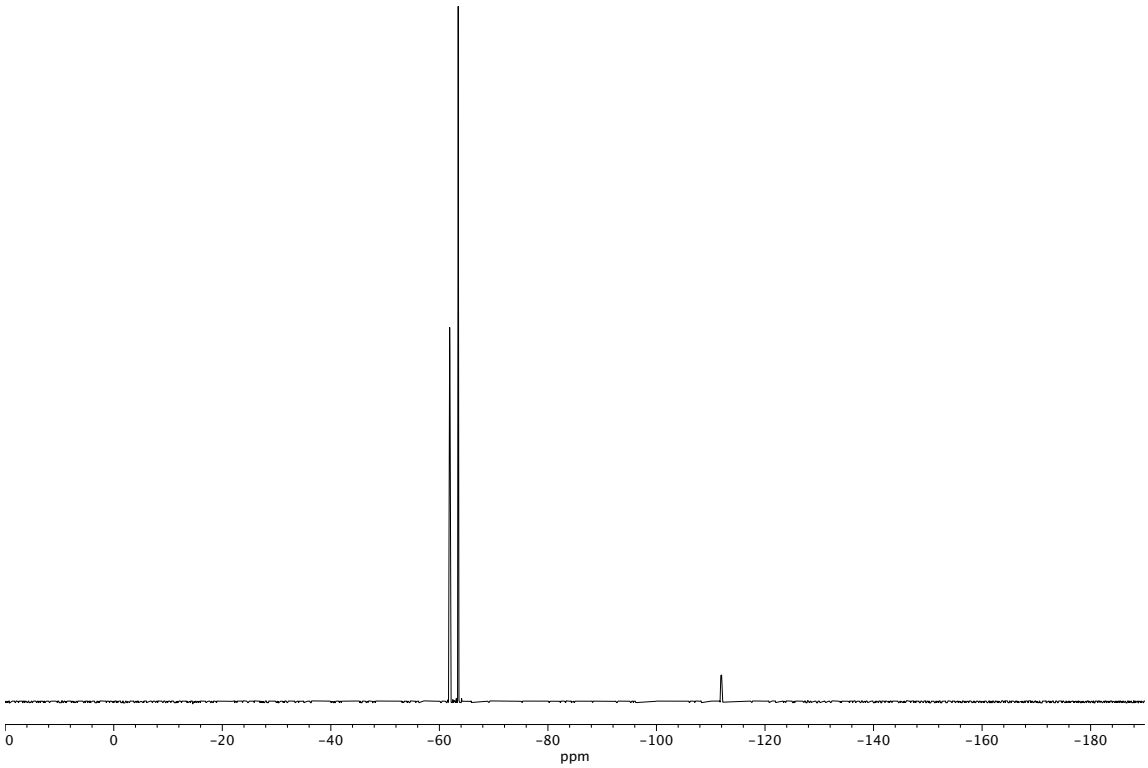

Figure A3.162 *^{19}F NMR (282 MHz, $CDCl_3$) of compound **41**.*

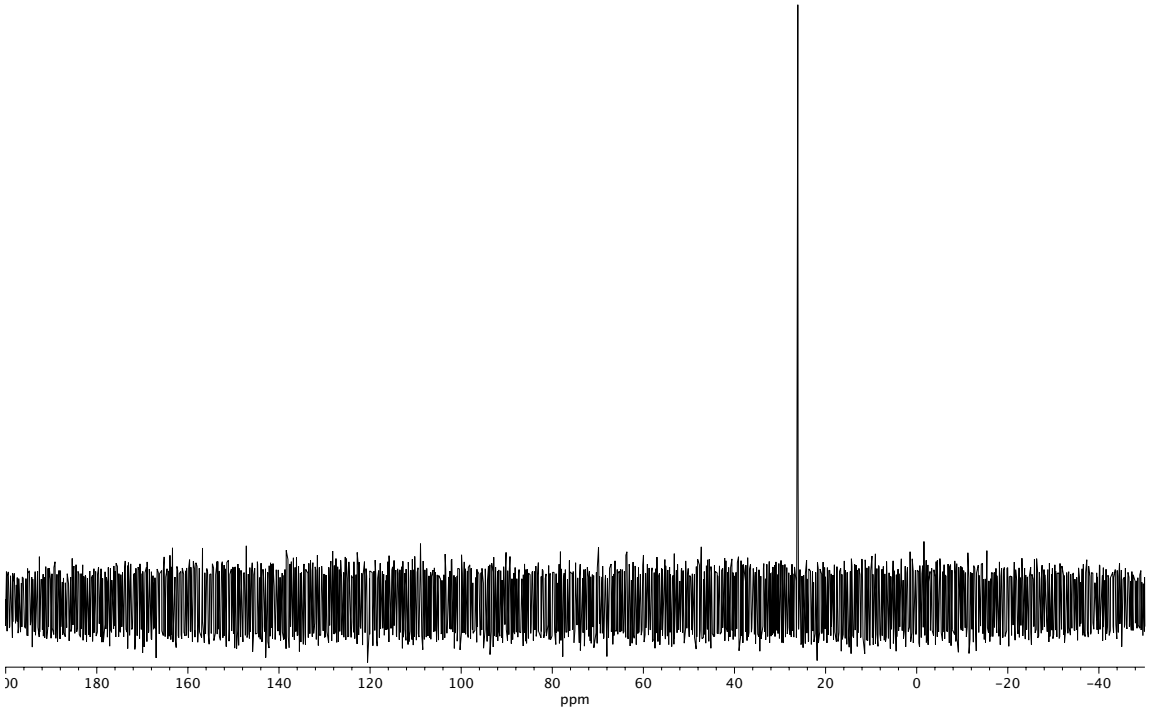

Figure A3.163 *^{31}P NMR (162 MHz, $CDCl_3$) of compound **41**.*

Figure A3.164 *^{1}H NMR (500 MHz, $CDCl_3$) of compound* ***L2****.*

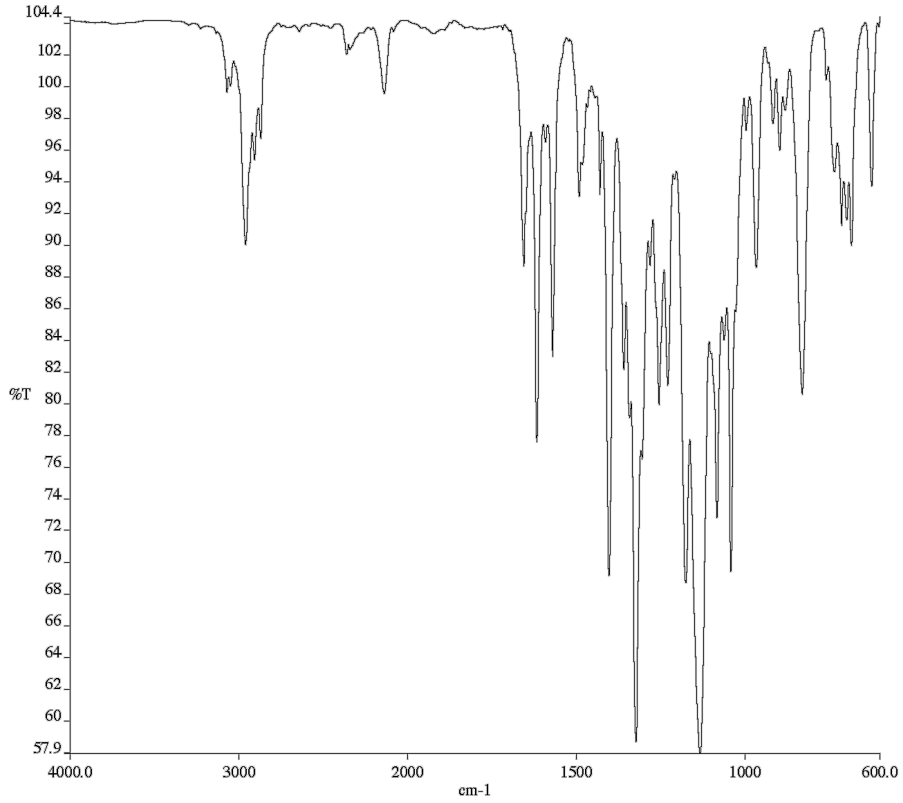

Figure A3.165 *Infrared spectrum (Thin Film, NaCl) of compound* ***L2****.*

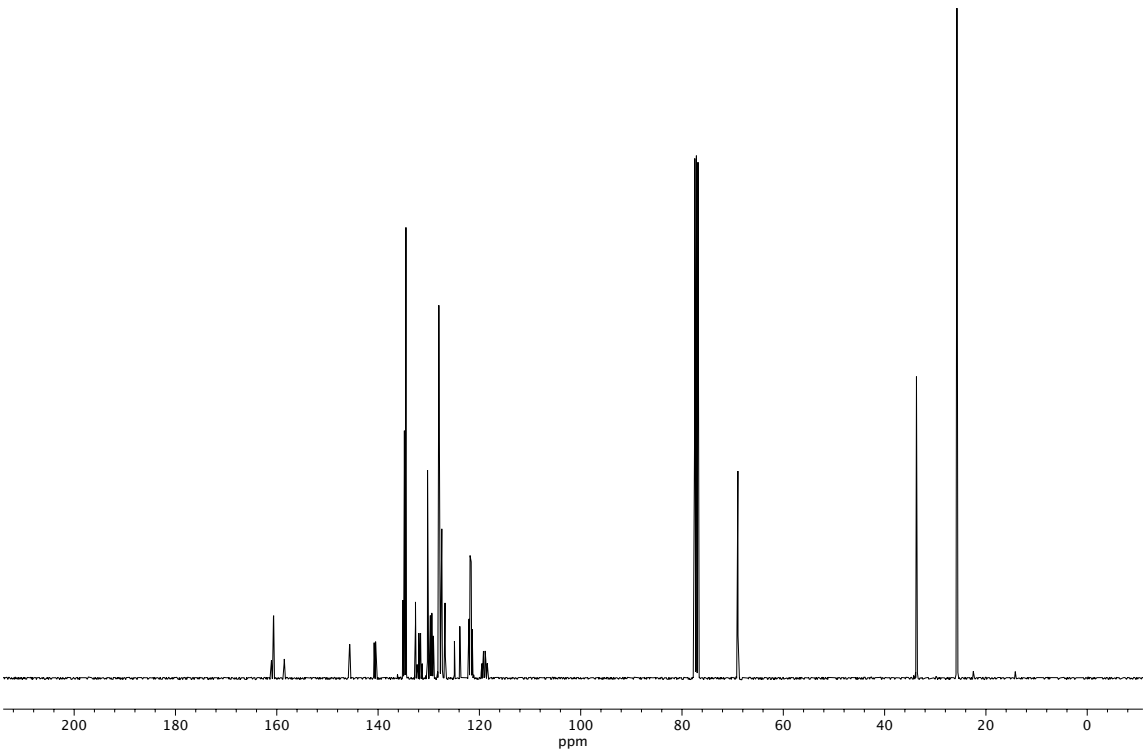

Figure A3.166 *^{13}C NMR (100 MHz, $CDCl_3$) of compound* ***L2****.*

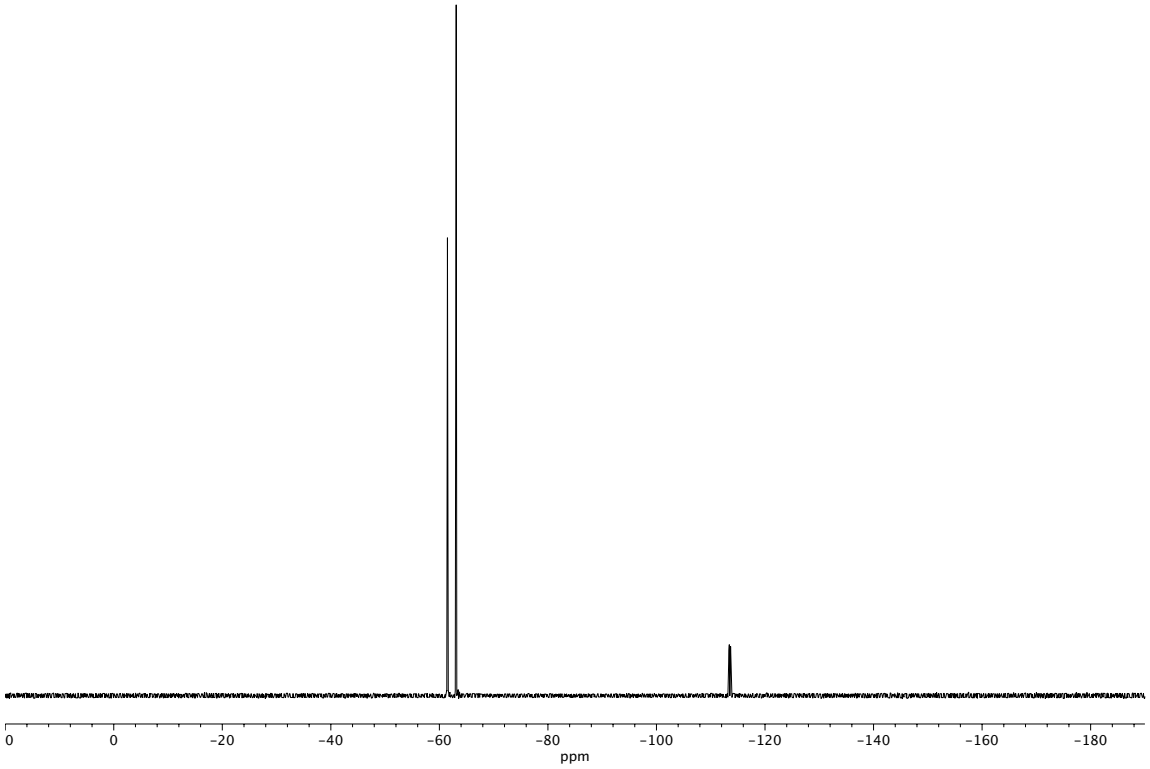

Figure A3.167 *^{19}F NMR (282 MHz, $CDCl_3$) of compound* ***L2****.*

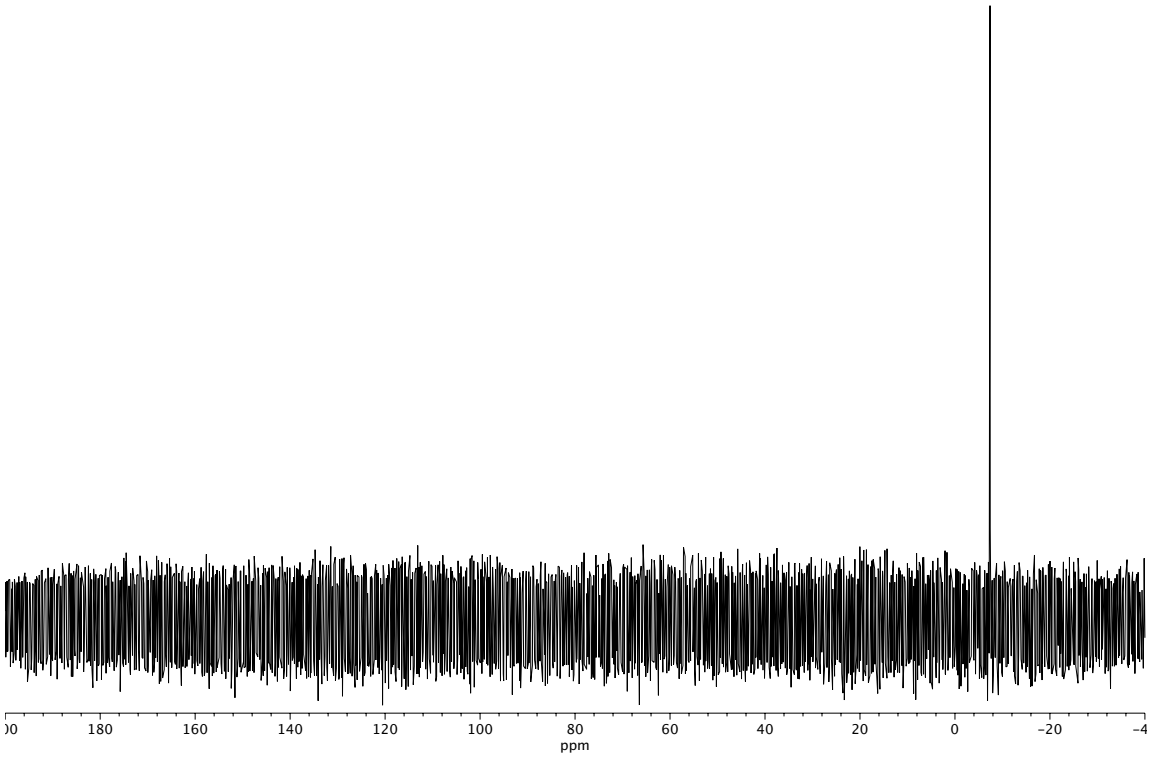

Figure A3.168 *^{31}P NMR (162 MHz, $CDCl_3$) of compound* ***L2****.*

APPENDIX 4

X-Ray Crystallography Reports Relevant to Chapter 2:

Pd-Catalyzed Asymmetric Decarboxylative Allylic Alkylation of Fully Substituted N-Acyl Indole-Derived Enol Carbonates

A4.1 GENERAL EXPERIMENTAL

X-Ray crystallographic analysis was obtained from the Caltech X-Ray Crystallography Facility using a Bruker D8 Venture Kappa Duo Photon 100 CMOS Diffractometer.

A4.2 X-RAY CRYSTAL STRUCTURE ANALYSIS OF ALLYLATION PRODUCT 20d (V18448)

An X-ray quality crystal of allylation product **20d** (compound V18448) was grown by slow evaporation of a solution in chloroform (approx. 30 mg/600 μL). Low-temperature diffraction data (ϕ-and ω-scans) were collected on a Bruker AXS D8 VENTURE KAPPA diffractometer coupled to a PHOTON II CPAD detector with Cu K_α radiation (λ = 1.54178 Å) from an IμS micro-source for the structure of compound V18448. The structure was solved by direct methods using SHELXS[1] and refined against F^2 on all data by full-matrix least squares with SHELXL-2017[2] using established refinement techniques.[3] All non-hydrogen atoms were refined anisotropically. All hydrogen atoms were included into the model at geometrically calculated positions and refined using a riding model. The isotropic

displacement parameters of all hydrogen atoms were fixed to 1.2 times the *U* value of the atoms they are linked to (1.5 times for methyl groups). Compound V18448 crystallizes in the monoclinic space group $P2_1$ with one molecule in the asymmetric unit.

Figure A4.2.1 *X-Ray Coordinate of Allylation Product* ***20d***

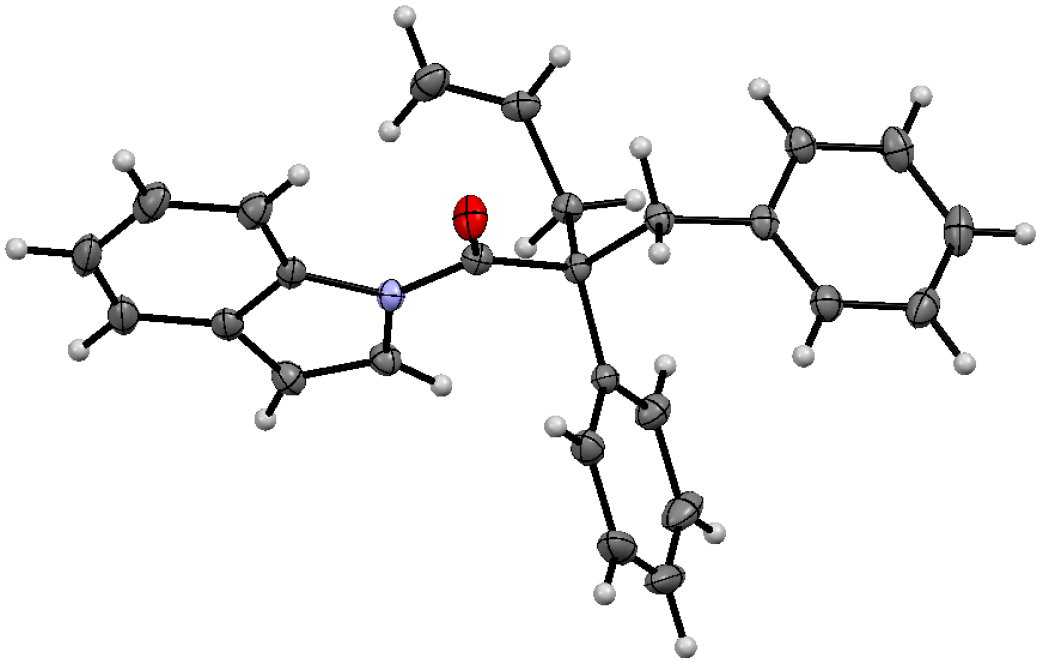

Table A4.2.1 *Crystal Data and Structure Refinement for* ***20d*** *(V18448)*

Identification code	v18448	
Empirical formula	C26 H23 N O	
Formula weight	365.45	
Temperature	100(2) K	
Wavelength	1.54178 Å	
Crystal system	Monoclinic	
Space group	$P2_1$	
Unit cell dimensions	a = 11.2225(10) Å	a= 90°.
	b = 6.4382(6) Å	b= 99.6595(18)°.
	c = 14.0893(13) Å	g = 90°.
Volume	1003.56(16) $Å^3$	
Z	2	
Density (calculated)	1.209 Mg/m^3	

Absorption coefficient	0.564 mm^{-1}
F(000)	388
Crystal size	0.500 x 0.500 x 0.300 mm^3
Theta range for data collection	3.182 to 80.104°.
Index ranges	-14<=h<=14, -7<=k<=7, -17<=l<=17
Reflections collected	34321
Independent reflections	4134 [R(int) = 0.0282]
Completeness to theta = 67.679°	99.0 %
Absorption correction	Semi-empirical from equivalents
Max. and min. transmission	1.0000 and 0.8766
Refinement method	Full-matrix least-squares on F^2
Data / restraints / parameters	4134 / 1 / 253
Goodness-of-fit on F^2	1.038
Final R indices [I>2sigma(I)]	R1 = 0.0265, wR2 = 0.0681
R indices (all data)	R1 = 0.0265, wR2 = 0.0682
Absolute structure parameter	0.05(4)
Extinction coefficient	n/a
Largest diff. peak and hole	0.201 and -0.133 $e.Å^{-3}$

Table A4.2.2 *Atomic coordinates (x 10^4) and equivalent isotropic displacement parameters ($Å^2$x 10^3) for* ***20d*** *(V18448). U(eq) is defined as one third of the trace of the orthogonalized U^{ij} tensor.*

	x	y	z	U(eq)
O(1)	5786(1)	1813(2)	7273(1)	26(1)
C(1)	5783(1)	3638(2)	7476(1)	17(1)
C(2)	4688(1)	5066(2)	7141(1)	15(1)
C(11)	4200(1)	5966(2)	8006(1)	17(1)
C(12)	4150(1)	4711(3)	8806(1)	24(1)
C(13)	3652(2)	5458(3)	9579(1)	35(1)
C(14)	3193(2)	7449(3)	9561(1)	37(1)
C(15)	3241(2)	8701(3)	8777(1)	34(1)
C(16)	3742(1)	7973(2)	8000(1)	24(1)
C(3)	3683(1)	3670(2)	6559(1)	18(1)
C(21)	2520(1)	4803(2)	6183(1)	18(1)
C(22)	1602(1)	4907(3)	6737(1)	24(1)
C(23)	530(1)	5950(3)	6403(1)	29(1)
C(24)	351(1)	6888(3)	5504(1)	30(1)
C(25)	1252(1)	6781(3)	4941(1)	27(1)
C(26)	2327(1)	5746(2)	5278(1)	21(1)
C(4)	5090(1)	6761(2)	6474(1)	17(1)
C(5)	5781(1)	5882(2)	5740(1)	22(1)
C(6)	6953(2)	6153(3)	5768(1)	29(1)
N(1)	6826(1)	4548(2)	7998(1)	17(1)
C(31)	6936(1)	6510(2)	8438(1)	20(1)
C(32)	8087(1)	6829(3)	8874(1)	23(1)
C(33)	8774(1)	5024(2)	8712(1)	21(1)
C(34)	9996(1)	4507(3)	8984(1)	27(1)
C(35)	10389(1)	2616(3)	8694(1)	31(1)
C(36)	9598(1)	1254(3)	8132(1)	31(1)
C(37)	8379(1)	1719(3)	7857(1)	24(1)
C(38)	7982(1)	3609(2)	8164(1)	18(1)

Table A4.2.3 *Bond lengths [Å] and angles [°] for* ***20d*** *(V18448).*

O(1)-C(1)	1.2093(19)
C(1)-N(1)	1.4021(17)
C(1)-C(2)	1.5434(18)
C(2)-C(11)	1.5317(17)
C(2)-C(4)	1.5553(17)
C(2)-C(3)	1.5630(18)
C(11)-C(16)	1.390(2)
C(11)-C(12)	1.3950(19)
C(12)-C(13)	1.391(2)
C(12)-H(12)	0.9500
C(13)-C(14)	1.380(3)
C(13)-H(13)	0.9500
C(14)-C(15)	1.375(3)
C(14)-H(14)	0.9500
C(15)-C(16)	1.393(2)
C(15)-H(15)	0.9500
C(16)-H(16)	0.9500
C(3)-C(21)	1.5111(18)
C(3)-H(3A)	0.9900
C(3)-H(3B)	0.9900
C(21)-C(22)	1.3949(19)
C(21)-C(26)	1.3967(19)
C(22)-C(23)	1.388(2)
C(22)-H(22)	0.9500
C(23)-C(24)	1.387(2)
C(23)-H(23)	0.9500
C(24)-C(25)	1.388(2)
C(24)-H(24)	0.9500
C(25)-C(26)	1.390(2)
C(25)-H(25)	0.9500
C(26)-H(26)	0.9500
C(4)-C(5)	1.5041(18)
C(4)-H(4A)	0.9900
C(4)-H(4B)	0.9900

C(5)-C(6)	1.320(2)
C(5)-H(5)	0.9500
C(6)-H(6A)	0.9500
C(6)-H(6B)	0.9500
N(1)-C(31)	1.4035(18)
N(1)-C(38)	1.4145(17)
C(31)-C(32)	1.3505(19)
C(31)-H(31)	0.9500
C(32)-C(33)	1.433(2)
C(32)-H(32)	0.9500
C(33)-C(34)	1.4006(19)
C(33)-C(38)	1.410(2)
C(34)-C(35)	1.380(3)
C(34)-H(34)	0.9500
C(35)-C(36)	1.395(3)
C(35)-H(35)	0.9500
C(36)-C(37)	1.391(2)
C(36)-H(36)	0.9500
C(37)-C(38)	1.390(2)
C(37)-H(37)	0.9500

O(1)-C(1)-N(1)	119.69(12)
O(1)-C(1)-C(2)	122.66(12)
N(1)-C(1)-C(2)	117.58(12)
C(11)-C(2)-C(1)	110.77(10)
C(11)-C(2)-C(4)	113.19(11)
C(1)-C(2)-C(4)	107.86(10)
C(11)-C(2)-C(3)	108.16(10)
C(1)-C(2)-C(3)	106.58(11)
C(4)-C(2)-C(3)	110.09(10)
C(16)-C(11)-C(12)	118.57(13)
C(16)-C(11)-C(2)	121.87(12)
C(12)-C(11)-C(2)	119.46(13)
C(13)-C(12)-C(11)	120.54(16)
C(13)-C(12)-H(12)	119.7
C(11)-C(12)-H(12)	119.7

C(14)-C(13)-C(12)	120.31(16)
C(14)-C(13)-H(13)	119.8
C(12)-C(13)-H(13)	119.8
C(15)-C(14)-C(13)	119.60(15)
C(15)-C(14)-H(14)	120.2
C(13)-C(14)-H(14)	120.2
C(14)-C(15)-C(16)	120.62(17)
C(14)-C(15)-H(15)	119.7
C(16)-C(15)-H(15)	119.7
C(11)-C(16)-C(15)	120.36(15)
C(11)-C(16)-H(16)	119.8
C(15)-C(16)-H(16)	119.8
C(21)-C(3)-C(2)	114.28(11)
C(21)-C(3)-H(3A)	108.7
C(2)-C(3)-H(3A)	108.7
C(21)-C(3)-H(3B)	108.7
C(2)-C(3)-H(3B)	108.7
H(3A)-C(3)-H(3B)	107.6
C(22)-C(21)-C(26)	118.29(13)
C(22)-C(21)-C(3)	120.20(12)
C(26)-C(21)-C(3)	121.50(12)
C(23)-C(22)-C(21)	120.85(14)
C(23)-C(22)-H(22)	119.6
C(21)-C(22)-H(22)	119.6
C(24)-C(23)-C(22)	120.35(14)
C(24)-C(23)-H(23)	119.8
C(22)-C(23)-H(23)	119.8
C(23)-C(24)-C(25)	119.44(14)
C(23)-C(24)-H(24)	120.3
C(25)-C(24)-H(24)	120.3
C(24)-C(25)-C(26)	120.22(14)
C(24)-C(25)-H(25)	119.9
C(26)-C(25)-H(25)	119.9
C(25)-C(26)-C(21)	120.85(13)
C(25)-C(26)-H(26)	119.6
C(21)-C(26)-H(26)	119.6

C(5)-C(4)-C(2)	112.72(12)
C(5)-C(4)-H(4A)	109.0
C(2)-C(4)-H(4A)	109.0
C(5)-C(4)-H(4B)	109.0
C(2)-C(4)-H(4B)	109.0
H(4A)-C(4)-H(4B)	107.8
C(6)-C(5)-C(4)	123.74(14)
C(6)-C(5)-H(5)	118.1
C(4)-C(5)-H(5)	118.1
C(5)-C(6)-H(6A)	120.0
C(5)-C(6)-H(6B)	120.0
H(6A)-C(6)-H(6B)	120.0
C(1)-N(1)-C(31)	127.69(12)
C(1)-N(1)-C(38)	124.72(12)
C(31)-N(1)-C(38)	107.59(11)
C(32)-C(31)-N(1)	110.11(13)
C(32)-C(31)-H(31)	124.9
N(1)-C(31)-H(31)	124.9
C(31)-C(32)-C(33)	107.67(13)
C(31)-C(32)-H(32)	126.2
C(33)-C(32)-H(32)	126.2
C(34)-C(33)-C(38)	119.61(15)
C(34)-C(33)-C(32)	132.62(15)
C(38)-C(33)-C(32)	107.76(12)
C(35)-C(34)-C(33)	118.44(15)
C(35)-C(34)-H(34)	120.8
C(33)-C(34)-H(34)	120.8
C(34)-C(35)-C(36)	121.20(14)
C(34)-C(35)-H(35)	119.4
C(36)-C(35)-H(35)	119.4
C(37)-C(36)-C(35)	121.68(16)
C(37)-C(36)-H(36)	119.2
C(35)-C(36)-H(36)	119.2
C(38)-C(37)-C(36)	116.98(15)
C(38)-C(37)-H(37)	121.5
C(36)-C(37)-H(37)	121.5

C(37)-C(38)-C(33)	122.06(13)
C(37)-C(38)-N(1)	131.03(13)
C(33)-C(38)-N(1)	106.87(12)

Table A4.2.4 *Anisotropic displacement parameters ($Å^2 x\ 10^3$) for V18448. The anisotropic displacement factor exponent takes the form: $-2p^2[\ h^2\ a^{*2}U^{11} + ... + 2\ h\ k\ a^*\ b^*\ U^{12}]$*

	U^{11}	U^{22}	U^{33}	U^{23}	U^{13}	U^{12}
O(1)	23(1)	15(1)	39(1)	-3(1)	-1(1)	2(1)
C(1)	18(1)	16(1)	18(1)	1(1)	3(1)	-1(1)
C(2)	16(1)	14(1)	16(1)	0(1)	2(1)	1(1)
C(11)	14(1)	20(1)	16(1)	-2(1)	2(1)	-3(1)
C(12)	21(1)	31(1)	21(1)	4(1)	3(1)	-2(1)
C(13)	27(1)	59(1)	19(1)	1(1)	6(1)	-9(1)
C(14)	26(1)	60(1)	27(1)	-19(1)	13(1)	-9(1)
C(15)	28(1)	34(1)	43(1)	-17(1)	15(1)	-2(1)
C(16)	24(1)	23(1)	28(1)	-4(1)	8(1)	0(1)
C(3)	18(1)	17(1)	20(1)	-1(1)	1(1)	-1(1)
C(21)	16(1)	15(1)	22(1)	-2(1)	1(1)	-2(1)
C(22)	20(1)	28(1)	24(1)	-2(1)	2(1)	-5(1)
C(23)	18(1)	32(1)	37(1)	-7(1)	7(1)	-2(1)
C(24)	17(1)	25(1)	46(1)	-1(1)	-2(1)	2(1)
C(25)	23(1)	23(1)	32(1)	6(1)	-3(1)	-2(1)
C(26)	18(1)	22(1)	24(1)	0(1)	1(1)	-3(1)
C(4)	18(1)	16(1)	17(1)	2(1)	3(1)	0(1)
C(5)	28(1)	22(1)	19(1)	1(1)	7(1)	0(1)
C(6)	30(1)	33(1)	28(1)	8(1)	13(1)	7(1)
N(1)	16(1)	15(1)	19(1)	1(1)	2(1)	1(1)
C(31)	20(1)	18(1)	20(1)	-2(1)	1(1)	0(1)
C(32)	22(1)	24(1)	21(1)	-1(1)	0(1)	-3(1)
C(33)	19(1)	27(1)	17(1)	4(1)	3(1)	-2(1)
C(34)	17(1)	40(1)	24(1)	6(1)	1(1)	0(1)
C(35)	17(1)	44(1)	31(1)	10(1)	5(1)	7(1)
C(36)	26(1)	33(1)	34(1)	7(1)	10(1)	11(1)
C(37)	23(1)	24(1)	27(1)	3(1)	6(1)	4(1)
C(38)	15(1)	22(1)	17(1)	6(1)	4(1)	1(1)

Table A4.2.5 *Hydrogen coordinates (x 10^4) and isotropic displacement parameters (Å^{2}x 10^3) for* ***20d*** *(V18448).*

_____	x	y	z	U(eq)
H(12)	4458	3335	8822	29
H(13)	3627	4594	10122	42
H(14)	2846	7953	10087	45
H(15)	2929	10074	8765	41
H(16)	3771	8853	7463	29
H(3A)	3999	3053	6008	22
H(3B)	3503	2516	6978	22
H(22)	1710	4257	7351	29
H(23)	-83	6021	6792	34
H(24)	-384	7599	5275	36
H(25)	1134	7416	4324	32
H(26)	2939	5680	4887	26
H(4A)	4365	7493	6137	20
H(4B)	5602	7793	6874	20
H(5)	5351	5085	5227	27
H(6A)	7407	6943	6273	35
H(6B)	7341	5559	5284	35
H(31)	6293	7474	8431	24
H(32)	8389	8032	9225	27
H(34)	10541	5436	9358	33
H(35)	11213	2235	8880	37
H(36)	9901	-24	7933	37
H(37)	7842	786	7476	29

A4.3 REFERENCES AND NOTES

(1) Sheldrick, G. M. Phase annealing in *SHELX*-90: direct methods for larger structures. *Acta Cryst.* **1990**, A46, 467–473.

(2) Sheldrick, G. M. Crystal structure refinement with *SHELXL*. *Acta Cryst.* **2015**, C71, 3–8.

(3) Müller, P. Practical suggestions for better crystal structures. *Crystallography Reviews* **2009**, *15*, 57–83.

CHAPTER 3

Pd-Catalyzed Decarboxylative Dehydrogenation of Fully Substituted N-acyl Indole-Derived Enol Carbonates [†]

3.1 INTRODUCTION

Our lab has recently become interested in developing palladium-catalyzed asymmetric allylic alkylation reactions of acyclic stereodefined fully substituted enol carbonates to generate acyclic quaternary stereogenic centers. In our initial efforts, we reported the application of a highly *E*-selective enolization[1] of acyclic α-aryl ketones to generate stereodefined, fully substituted acyclic ketone enol carbonates which were employed in a highly enantioselective Pd-catalyzed allylic alkylation to generate all carbon quaternary centers.[2] We then extended this methodology to the synthesis of acyclic α-quaternary carboxylic acid derivatives with *N*-acyl indole-derived enol carbonates as ester enolate equivalents (Scheme 3.1.1).[3] During the optimization of this transformation, we determined that electron-poor PHOX ligand *(S)*-Ty-PHOX (**L2**) (Scheme 3.1.1.B) provided enhanced enantioselectivity compared with our standard *(S)*-$(CF_3)_3$-*t*-BuPHOX ligand (**L3**) (Scheme 3.1.1A). Seeking to further enhance the enantioselectivity of this reaction, we also examined electron-poor PHOX ligand *(S)*-F_{13}-*t*-BuPHOX (**L3**). We were surprised to find that, while the desired allylic allylation product **20a** was generated in 94%

[†]This research was performed in collaboration with Eric J. Alexy and Brenda Wu. Portions of this chapter have been reproduced with permission from Fulton, T. J.; Wu, B.; Alexy, E. J.; Zhang, H.; Stoltz, B.M. *Tetrahedron* **2019**, *75*, 4104–4109. © 2019 Elsevier Ltd.

ee, an unexpected α,β-dehydrogenation product (**42a**) was isolated in 15% yield (Scheme 3.1.1C). Interestingly, dehydrogenation product **42a** was favored as the major product in 79% yield when a starting mixture of 71:29 mixture of *Z*/*E*-enol carbonate **19a** was used (Scheme 3.1.1D).

This unusual change in reactivity with *(S)-F_{13}-t*-BuPHOX (**L3**) prompted further investigation, especially given the limited methods available to access synthetically valuable α,β-unsaturated carboxylic acid derivatives such as **42a**. Numerous distinct strategies have been developed to access α,β-unsaturated carbonyl and carboxylic acid motifs including selenium,[4] sulfur,[5] hypervalent iodine,[6] and quinone[7] based transformations, as well as palladium catalyzed dehydrogenations.[8] One-step allyl-palladium catalyzed dehydrogenations have recently been developed by Newhouse, with pioneering studies from Tsuji,[9] as an effective method to generate α,β-unsaturated carbonyls,[10] carboxylic acids,[11] and carboxylic acid derivatives.[12] There are, however, limited examples employing acyclic systems bearing α-substitution, especially in high *E*/*Z*-selectivity. Moreover, to the best of our knowledge, this is the first example of an electron deficient PHOX ligand promoting dehydrogenation reactivity with an allyl-palladium species. This new reactivity is complementary to the available methodology for the generation of α,β-unsaturated compounds.

Scheme 3.1.1 *Discovery of a Ligand-Controlled α,β-Dehydrogenation.*

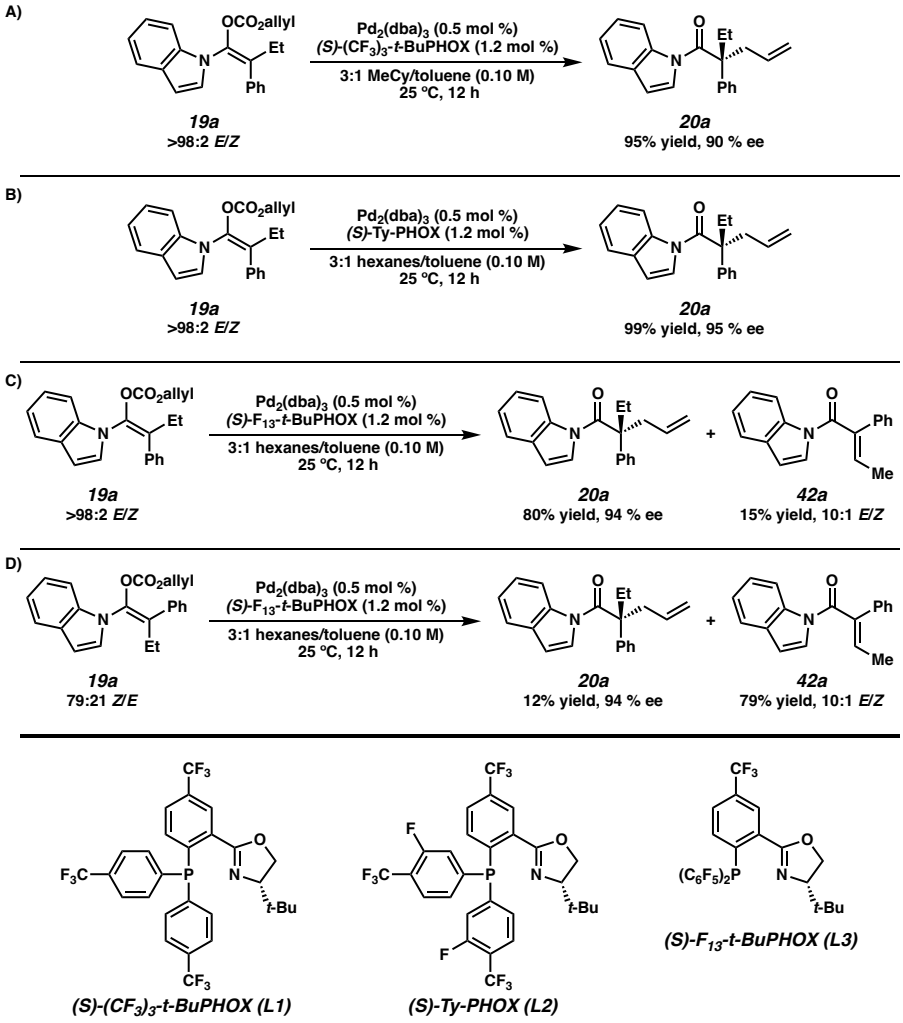

3.2 INVESTIGATION OF THE α,β-DEHYDROGENATION PROCESS

While *E*-selective enolization[1] and *O*-acylation provides reliable access to **20a** with >98:2 *E*/*Z*-selectivity, there are no reported methods for achieving comparable *Z*-selectivity (Scheme 3.2.1). Thus, enolization of *N*-acyl indole **25** with KHMDS in THF provided moderate *Z*-selectivity to enable our studies. Initially, we were interested in developing an achiral ligand to perform this transformation, however, we were surprised to find that analogous *F_{13}-glyPHOX* ligand (**L4**) did not catalyze this transformation, even

at elevated temperatures (Scheme 3.2.2). It should also be noted that utilizing *(R)*-**L3** in this transformation with a 75:25 *Z*/*E* mixture of **19a** provides identical yield and selectivity compared with *(S)*-**L3**.

Scheme 3.2.1 *E- and Z-Selective Enolizations of N-Acyl Indole **25**.*

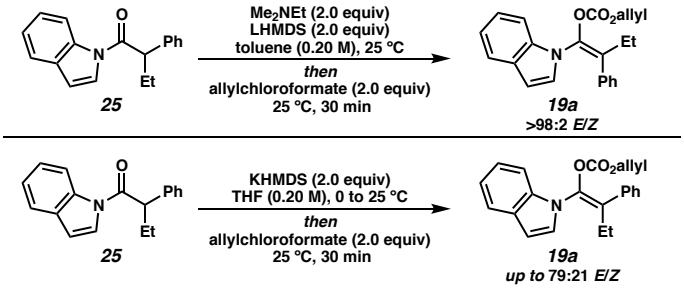

Scheme 3.2.2 *Investigation of an Achiral PHOX Ligand.*

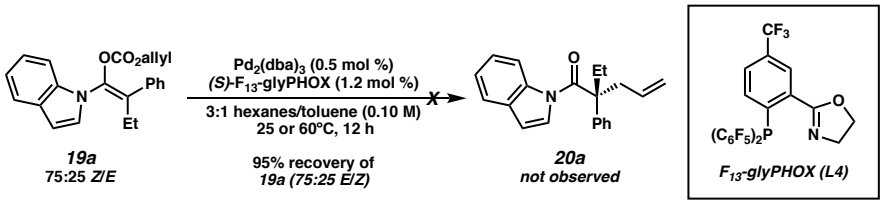

Subsequent studies aimed to identify conditions which could affect dehydrogenation from both enol carbonate geometries. Other solvents commonly employed in Pd-catalyzed dehydrogenation reactions were examined but provided no improvement over the 3:1 hexanes/toluene solvent system (Table 2, entries 1–6). When toluene or MTBE were used as solvents, full conversion of **19a** is observed, albeit with lower selectivity for dehydrogenation product **42a** over alkylation product **2** compared with 3:1 hexanes/toluene (entries 2 and 3). In THF, the reaction slows and 65% of the 75:25 *Z*/*E*-enol carbonate mixture was recovered after 24 h (entry 4). Polar, aprotic solvents such as DMF and MeCN utilized in the allyl-palladium catalyzed dehydrogenation by Tsuji[9]

lead to no conversion with high recovery of the enol carbonate in identical *Z*/*E*-enrichment (entries 5 and 6). Newhouse and co-workers demonstrated $ZnCl_2$ can affect transmetallation to generate a zinc enolate which exhibits attenuated nucleophilicity and disfavors enolate allylation in allyl-palladium catalyzed dehydrogenation reactions.[10–12] In our reaction, incorporation of stoichiometric $ZnCl_2$ impeded both allylation and dehydrogenation reactions with 92% recovery of the enol carbonate mixture (entry 7). Heating the reaction with $ZnCl_2$ additive to 60 ºC also failed to promote any appreciable level of conversion (entry 8). Importantly, when $ZnCl_2$ is used as an additive with a >98:2 *E*/*Z* mixture of enol carbonates, trace conversion to the allylation product is observed, albeit only after prolonged heating (>24 h) at 60 ºC (entry 9). This result further exemplifies the importance of enolate geometry in this transformation. We also examined *N*-acyl indole derived enol carbonate **19a** under Tsuji's original decarboxylative dehydrogenation conditions and found no dehydrogenation occurred (Scheme 3.2.3).[9a] Instead, a mixture of decarboxylative allylation, protonation and recovered enol carbonate **19a** were obtained.

Table 3.2.1 *Investigation of Reaction Parameters.*[a]

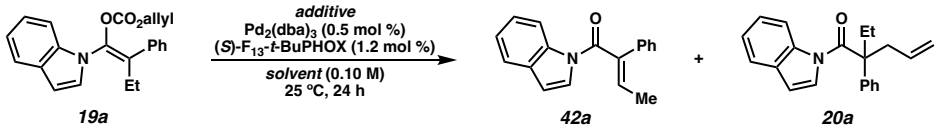

entry	*E*/*Z* ratio of *19a*	solvent	ligand	additive	result
1	25:75	3:1 hexanes/toluene	L3	none	80% yield *42a* (10:1 *E*/*Z*), 18% yield *20a*
2	25:75	toluene	L3	none	70% yield *42a* (10:1 *E*/*Z*), 26% yield *20a*
3	25:75	MTBE	L3	none	71% yield *42a* (10:1 *E*/*Z*), 28% yield *20a*
4[b]	25:75	THF	L3	none	65% recovery of *19a* (75:25 *Z*/*E*)
5	25:75	DMF	L3	none	94% recovery of *19a* (75:25 *Z*/*E*)
6	25:75	MeCN	L3	none	92% recovery of *19a* (75:25 *Z*/*E*)
7	25:75	3:1 hexanes/toluene	L3	$ZnCl_2$ (6.0 equiv)	92% recovery of *19a* (75:25 *Z*/*E*)
8[c]	25:75	3:1 hexanes/toluene	L3	$ZnCl_2$ (6.0 equiv)	94% recovery of *19a* (75:25 *Z*/*E*)
9[c]	>98:2	3:1 hexanes/toluene	L3	$ZnCl_2$ (6.0 equiv)	94% recovery of *19a* (75:25 *Z*/*E*)

[a] All reactions performed on a 0.200 mmol scale. All yields are of isolated products. E/Z ratios were determined by ^{1}H NMR integration. [b] Reaction did not go to completion. [c] Reaction performed at 60 °C.

Scheme 3.2.3 *Examination of Tsuji's Decarboxylative Dehydrogenation.*

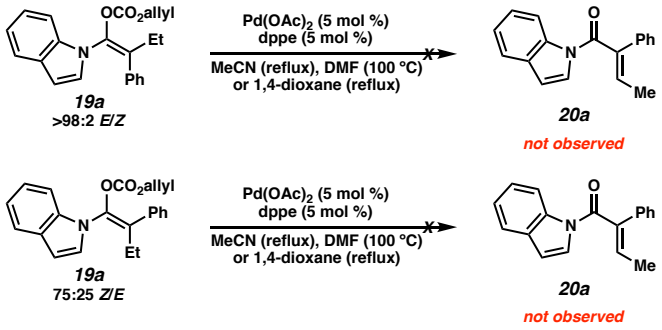

3.3 SCOPE OF THE α,β-DEHYDROGENATION PROCESS

Bereft of reaction conditions favoring dehydogenation for both enolate geometries, we examined the reaction scope with pure *Z*-enol carbonates to simplify reaction analysis and product purification. A variety of *N*-acyl indoles were enolized using *Z*-selective conditions (vide supra) and trapped as the corresponding allyl enol carbonates. The geometrically pure *Z*-enol carbonates could be isolated by preparative chromatography and subjected to our standard reaction conditions (Table 3.2.1). Pleasingly, a range of alkyl and aryl group substitutions were well tolerated under the reaction conditions and α,β-

unsaturated products were obtained in high yield and excellent *E*-selectivity. With pure *Z*-enol carbonate **1**, product **42a** was obtained in >99% yield with 10:1 *E*/*Z*-selectivity. Unsubstituted compound **42b** was obtained in 84% yield despite the increased potential to undergo competitive intermolecular conjugate addition during the reaction. Longer alkyl chains were well tolerated with *n*-butyl product **42c** isolated in 97% yield with 15:1 *E*/*Z*-selectivity. Sterically encumbered *i*-propyl product **42d** was also well tolerated with >98:2 *E*- selectivity, albeit in a diminished 77% yield. Product **42e** bearing 1,2- diphenyl substitution could be obtained in 75% yield and 6:1 *E*/*Z*-selectivity. A variety of aryl groups were also compatible with the dehydrogenation reaction. Notably, *ortho*-substituted product **42f** was obtained in an excellent 91% yield with 10:1 *E*/*Z*-selectivity. Electron-rich 4-methoxy phenyl product **42g** was isolated in an excellent 94% yield with 18:1 *E*/*Z*-selectivity. Finally, products with electron poor 4-fluoro (**42h**) and 4-chloro (**42i**) aryl groups were also obtained in high yields (89% and 79% yield, respectively) and excellent *E*-selectivity (12:1 and 8:1 *E*/*Z*, respectively).

Table 3.3.1 *Scope of the Catalytic Decarboxylative Dehydrogenation.*[a]

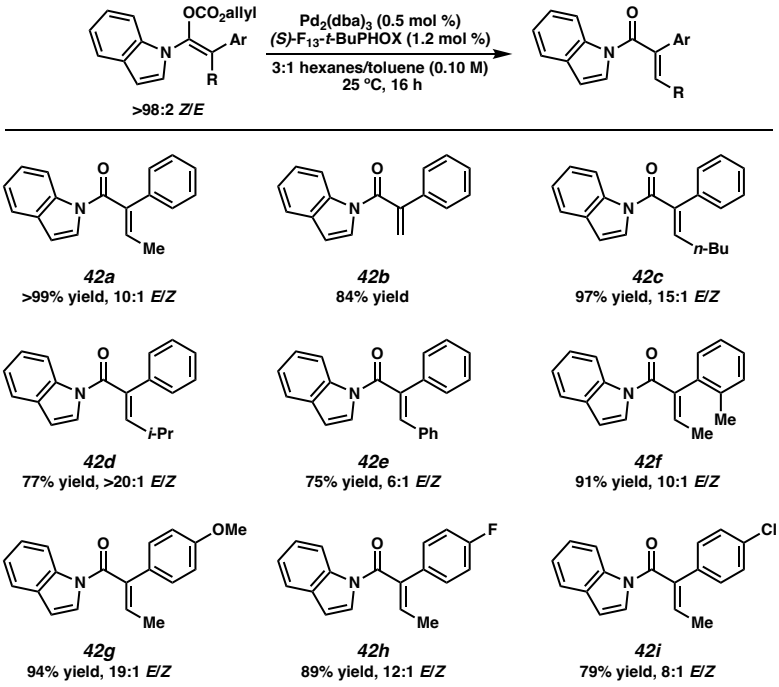

[a] All reactions performed on a 0.200 mmol scale. Yields of isolated products. Product *E/Z* ratios were measured by ^{1}H NMR integration.

While we were pleased with the scope of α,β-unsaturated *N*-acyl indoles afforded by the Pd-catalyzed decarboxylative dehydrogenation, we ultimately desired to extend this methodology toward accessing a broader range of α,β-unsaturated carbonyl compounds. In these initial efforts, we determined this reaction was unsuccessful with other substrates commonly utilized in Pd-catalyzed asymmetric decarboxylative allylic alkylation in our laboratory (Figure 3.3.1). Cyclic allyl enol carbonate **4** and β-ketoesters **5**–**7** failed to convert to either allylation or dehydrogenation products with these reaction conditions. Even with the analogous acyclic phenyl ketone derived allyl enol carbonate **8** (75:25 *Z*/*E*) no conversion was observed. Future efforts will be directed toward investigation of the dehydrogenation reaction with substrate classes unsuccessful in this unique system toward

a more general transformation and understanding the nature of the ligand promoted dehydrogenation.

Figure 3.3.1 *Unsuccessful Substrates for the Catalytic Decarboxylative Dehydrogenation.*

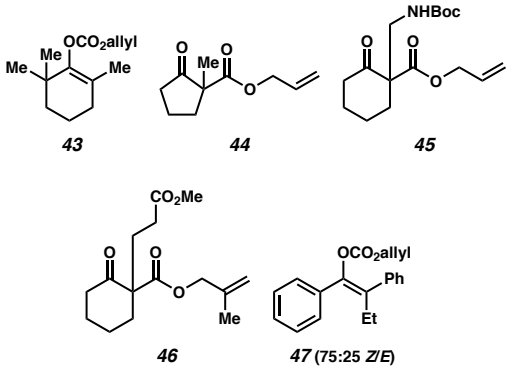

We posit a plausible catalytic cycle for this transformation can proceed as shown in Figure 3.3.2 wherein the allyl group of the enol carbonate ultimately serves as a hydride acceptor. A ligated Pd^0 species can undergo oxidative addition to allyl enol carbonate **19a**, generating palladium carboxylate **48**. Subsequent decarboxylation can form allyl palladium complex **49** and enolate **50** which can form carbon-bound palladium enolate **51**. At this stage, β-hydride elimination can occur to furnish product **42a** and palladium hydride **52**. Finally, reductive elimination of **13** regenerates the Pd^0 species and generates propene as a by-product.

Figure 3.3.2 *Plausible Catalytic Cycle.*

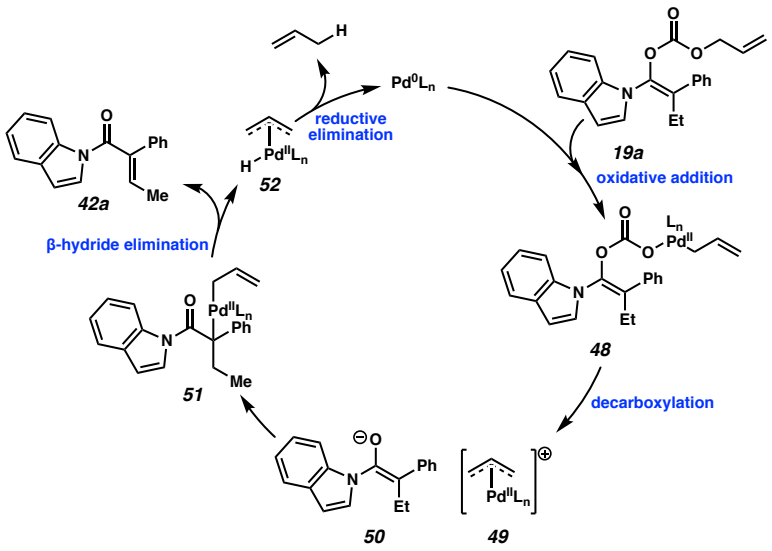

3.4 CONCLUSION

In summary, we have developed the allyl-palladium catalyzed decarboxylative dehydrogenation reaction of fully substituted *N*-acyl indole derived allyl enol carbonates promoted by a newly developed electron deficient PHOX ligand. The reaction was general with respect to *N*-acyl indole derived allyl enol carbonates and occurs only with F_{13}-*t*-BuPHOX (**L3**) ligand. Other substrate classes typically utilized in decarboxylative allylic alkylation in our laboratory were unreactive under these conditions. Future efforts will be directed toward probing the nature of this unusual resolution of enolate geometries and expand this methodology into a more general transformation for α,β-dehydrogenation. Ultimately, this methodology provides new precedent for ligand-controlled selectivity of dehydrogenation over allylic alkylation with allyl-palladium catalysis.

3.5 EXPERIMENTAL SECTION

3.5.1 MATERIALS AND METHODS

Unless otherwise noted, reactions were performed in flame-dried glassware under an Ar or N_2 atmosphere using dry, deoxygenated solvents. Solvents were dried by passage through an activated alumina column under Ar.[13] Reaction progress was monitored by thin-layer chromatography (TLC) or Agilent 1290 UHPLC-MS. TLC was performed using E. Merck silica gel 60 F254 precoated glass plates (0.25 mm) and visualized by UV fluorescence quenching, *p*-anisaldehyde, or KMnO4 staining. Silicycle Silia*Flash*® P60 Academic Silica gel (particle size 40–63 μm) was used for flash chromatography. ^{1}H NMR spectra were recorded on Varian Inova 500 MHz and Bruker 400 MHz spectrometers and are reported relative to residual $CHCl_3$ (δ 7.26 ppm) ^{13}C NMR spectra were recorded on a Varian Inova 500 MHz spectrometer (125 MHz) and Bruker 400 MHz spectrometers (100 MHz) and are reported relative to $CHCl_3$ (δ 77.16 ppm). Data for ^{1}H NMR are reported as follows: chemical shift (δ ppm) (multiplicity, coupling constant (Hz), integration). Multiplicities are reported as follows: s = singlet, d = doublet, t = triplet, q = quartet, p = pentent, sept = septuplet, m = multiplet, br s =broad singlet, br d = broad doublet, app = apparent. Data for ^{13}C NMR reported in terms of chemical shifts (δ ppm). IR spectra were obtained by the use of a Perkin Elmer Spectrum BXII spectrometer or Nicolet 6700 FTIR spectrometer using thin films deposited on NaCl plates and reported in frequency of absorption (cm^{-1}). Optical rotations were measured with a Jasco P-2000 polarimeter operating on the sodium D-line (589 nm), using a 100 mm path-length cell and reported as $[\alpha]_D^T$ (concentration in 10 mg/1 mL, solvent). Analytical SFC was performed with a Mettler

SFC supercritical CO_2 analytical chromatography system utilizing Chiralpak (AD-H, AS-H, or IC) or Chiracel (OD-H, OJ-H, or OB-H) columns (4.6 mm x 25 cm) obtained from Daicel Chemical Industries, Ltd. High resolution mass spectra (HRMS) were obtained from Agilent 6200 Series TOF with an Agilent G1978A Multimode source in electrospray ionization (ESI+), atmospheric pressure chemical ionization (APCI+), or mixed ionization more (MM: ESI-APCI+), or obtained from the Caltech mass spectrometry laboratory.

3.5.2 EXPERIMENTAL PROCEDURES

3.5.2.1 General Procedure for the Pd-Catalyzed Decarboxylative Dehydrogenation Reactions

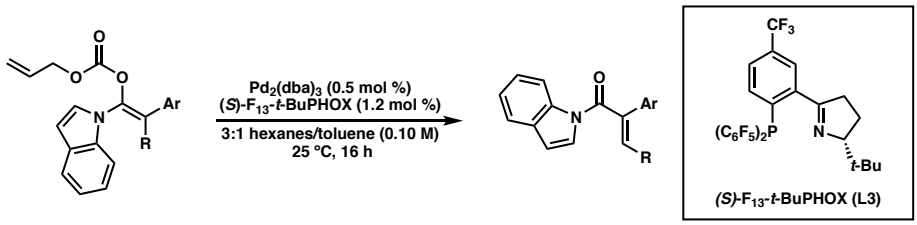

In a nitrogen-filled glovebox, a solution of $Pd_2(dba)_3$ (1.8 mg/mL) and (*S*)-F_{13}-*t*-BuPHOX (2.8 mg/mL) in toluene was stirred for 30 min at 25 °C, then 0.5 mL of the resulting catalyst solution was added to a one dram vial containing allyl enol carbonate substrate (0.2 mmol) dissolved in hexanes (1.5 mL). The vial was sealed with a Teflon-lined cap, removed from the glovebox, and stirred at 25 °C for 16 h unless noted otherwise. The crude reaction mixture was concentrated then purified by silica gel flash chromatography to provide the desired dehydrogenation product.

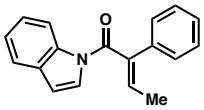

(*E*)-1-(1*H*-indol-1-yl)-2-phenylbut-2-en-1-one (42a)

Purified by column chromatography (5% Et_2O in hexanes) to provide a colorless oil (52.1 mg, 0.199 mmol, >99% yield, 10:1 *E*/*Z*); ^{1}H NMR (400 MHz, $CDCl_3$) δ 8.47 (dq, *J* = 8.3, 0.9 Hz, 1H), 7.54 (dq, *J* = 7.6, 0.8 Hz, 1H), 7.43–7.27 (m, 8H), 6.50 (dd, *J* = 3.8, 0.7 Hz, 1H), 6.46 (q, *J* = 7.2 Hz, 1H), 1.99 (d, *J* = 7.1 Hz, 3H); ^{13}C NMR (100 MHz, $CDCl_3$) δ 169.2, 138.0, 136.0, 134.9, 134.6, 130.8, 129.1, 128.8, 128.2, 127.2, 125.6, 125.0, 123.9, 120.9, 116.7, 108.5, 15.3; IR (Neat Film, NaCl) 3054, 2918, 2854, 1682, 1585, 1535, 1495, 1472, 1451, 1385, 1359, 1331, 1240, 1204, 1158, 1144, 1079, 1016, 946, 881, 815, 752, 703 cm^{-1}; HRMS (MM:ESI-APCI+) *m/z* calc'd for $C_{18}H_{16}NO$ $[M+H]^+$: 262.1226, found 262.1222.

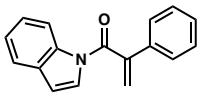

1-(1*H*-indol-1-yl)-2-phenylprop-2-en-1-one (42b)

Purified by column chromatography (5% Et_2O in hexanes) to provide a colorless oil (41.4 mg, 0.167 mmol, 84% yield);^{1}H NMR (400 MHz, $CDCl_3$) δ 8.57–8.54 (m, 1H), 7.57 (dt, *J* = 7.7, 1.0 Hz, 1H), 7.51–7.45 (m, 2H), 7.43–7.28 (m, 6H), 6.54 (d, *J* = 3.7 Hz, 1H), 6.08 (s, 1H), 5.70 (s, 1H); ^{13}C NMR (100 MHz, $CDCl_3$) δ 168.7, 144.5, 135.7, 135.4, 131.0, 129.2, 129.2, 127.1, 126.2, 125.3, 124.3, 121.0, 118.6, 116.8, 109.3; IR (Neat Film, NaCl) 3055, 2926, 1692, 1535, 1496, 1471, 1450, 1378, 1348, 1293, 1205, 1156, 1072, 1016, 931, 880, 752, 696 cm^{-1}; HRMS (MM:ESI-APCI+) *m/z* calc'd for $C_{17}H_{14}NO$ $[M+H]^+$: 248.1070, found 248.1063.

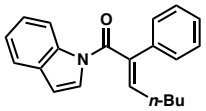

(*E*)-1-(1*H*-indol-1-yl)-2-phenylhept-2-en-1-one (42c)

Purified by column chromatography (3% Et_2O in hexanes) to provide a colorless oil (58.9 mg, 0.194 mmol, 97% yield, 14:1 *E*/*Z*); ^{1}H NMR (400 MHz, $CDCl_3$) δ 8.47 (d, *J* = 8.3 Hz, 1H), 7.54 (dd, *J* = 7.5, 0.9 Hz, 1H), 7.42 – 7.26 (m, 7H), 6.57–6.48 (m, 2H), 6.33 (t, *J* = 7.5 Hz, 1H), 2.36 (q, *J* = 7.5 Hz, 2H), 1.50 (tt, *J* = 8.2, 6.9 Hz, 2H), 1.37 (dq, *J* = 14.4, 7.2 Hz, 2H), 0.89 (t, *J* = 7.3 Hz, 3H); ^{13}C NMR (100 MHz, $CDCl_3$) δ 169.2, 140.2, 136.8, 136.0, 135.2, 130.8, 129.0, 128.8, 128.2, 127.2, 125.0, 123.9, 120.9, 116.7, 108.5, 31.5, 28.9, 22.6, 14.0; IR (Neat Film, NaCl) 3053, 2957, 2928, 2858, 1688, 1636, 1600, 1585, 1534, 1494, 1472, 1450, 1379, 1333, 1205, 1157, 1143, 1113, 1078, 1016, 938, 882, 816, 769, 752, 702 cm^{-1}; HRMS (MM:ESI-APCI+) *m/z* calc'd for $C_{21}H_{22}NO$ $[M+H]^+$: 304.1696, found 304.1688.

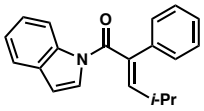

(*E*)-1-(1*H*-indol-1-yl)-4-methyl-2-phenylpent-2-en-1-one (42d)

Purified by column chromatography (3% Et_2O in hexanes) to provide a colorless oil (44.3 mg, 0.153 mmol, 77% yield, >20:1 *E*/*Z*); ^{1}H NMR (400 MHz, $CDCl_3$) δ 8.46 (dd, *J* = 8.3, 1.0 Hz, 1H), 7.55 (ddd, *J* = 7.7, 1.3, 0.7 Hz, 1H), 7.42–7.27 (m, 8H), 6.54 (d, *J* = 3.8 Hz, 1H), 6.10 (d, *J* = 10.5 Hz, 1H), 2.80 (dhept, *J* = 10.5, 6.6 Hz, 1H), 1.11 (d, *J* = 6.6 Hz, 6H); ^{13}C NMR (100 MHz, $CDCl_3$) δ 169.2, 146.6, 136.0, 135.3, 134.5, 130.9, 128.9, 128.8, 128.8, 127.2, 125.0, 123.9, 120.9, 116.7, 108.5, 28.3, 22.7; IR (Neat Film, NaCl) 3054, 2962, 2868, 1687, 1534, 1494, 1450, 1377, 1334, 1238, 1201, 1112, 1078, 1017, 882, 795, 769, 752, 698 cm^{-1}; HRMS (MM:ESI-APCI+) *m/z* calc'd for $C_{20}H_{20}NO$ $[M+H]^+$: 290.1539, found 290.1528.

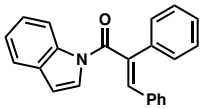

(*E*)-1-(1*H*-indol-1-yl)-2,3-diphenylprop-2-en-1-one (42e)

Purified by column chromatography (5% Et_2O in hexanes) to provide a colorless oil (48.3 mg, 0.149 mmol, 75% yield, 6:1 *E*/*Z*); ^{1}H NMR (400 MHz, $CDCl_3$) δ 8.67 (d, *J* = 8.2 Hz, 1H), 7.70 (dd, *J* = 11.3, 7.5 Hz, 2H), 7.65 (d, *J* = 3.8 Hz, 1H), 7.59–7.44 (m, 7H), 7.44–7.30 (m, 5H), 6.71 (d, *J* = 3.8 Hz, 1H); ^{13}C NMR (100 MHz, $CDCl_3$) δ 169.2, 136.4, 136.1, 135.3, 134.6, 130.9, 130.0, 129.3, 129.2, 128.9, 128.7, 128.5, 127.1, 126.0, 125.1, 124.1, 121.0, 116.8, 108.9.; IR (Neat Film, NaCl) 3053, 3026, 2923, 1684, 1535, 1492, 1472, 1450, 1381, 1333, 1235, 1206, 1155, 1141, 1112, 1077, 1016, 908, 882, 862, 753, 721, 694 cm^{-1}; HRMS (MM:ESI-APCI+) *m/z* calc'd for $C_{23}H_{18}NO$ $[M+H]^+$: 324.1383, found 324.1380.

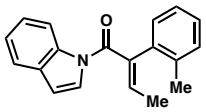

(*E*)-1-(1*H*-indol-1-yl)-2-(*o*-tolyl)but-2-en-1-one (42f)

Purified by column chromatography (3% Et_2O in hexanes) to provide a colorless oil (50.1 mg, 0.182 mmol, 91% yield, 12:1 *E*/*Z*); ^{1}H NMR (400 MHz, $CDCl_3$) δ 8.40 (d, *J* = 8.2 Hz, 1H), 7.46 (dd, *J* = 7.7, 1.1 Hz, 1H), 7.31–7.26 (m, 1H), 7.25 (d, *J* = 3.8 Hz, 1H), 7.22–7.16 (m, 3H), 7.12 (d, *J* = 7.9 Hz, 2H), 6.42 (d, *J* = 3.8 Hz, 1H), 6.35 (q, *J* = 7.2 Hz, 1H), 2.28 (s, 3H), 1.91 (d, *J* = 7.2 Hz, 3H); ^{13}C NMR (100 MHz, $CDCl_3$) δ 169.4, 138.0, 137.9, 135.9, 134.0, 131.9, 130.8, 129.7, 129.5, 128.9, 127.2, 125.5, 124.9, 123.9, 120.8, 116.7, 108.4, 21.4, 15.3; IR (Neat Film, NaCl) 3027, 2919, 2856, 1688, 1533, 1513, 1472, 1450, 1384, 1329, 1239, 1206, 1157, 1143, 1113, 1080, 1017, 946, 882, 828, 770, 753, 723 cm^{-1}; HRMS (MM:ESI-APCI+) *m/z* calc'd for $C_{19}H_{18}NO$ $[M+H]^+$: 276.1383, found 276.1375.

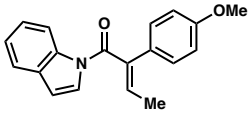

(*E*)-1-(1*H*-indol-1-yl)-2-(4-methoxyphenyl)but-2-en-1-one (42g)

Purified by column chromatography (8% Et_2O in hexanes) to provide a colorless oil (55.0 mg, 0.189 mmol, 94% yield, 19:1 *E*/*Z*); ^{1}H NMR (400 MHz, $CDCl_3$) δ 8.48 (d, *J* = 8.3 Hz, 1H), 7.54 (d, *J* = 7.7 Hz, 1H), 7.41–7.24 (m, 5H), 6.96–6.87 (m, 2H), 6.50 (d, *J* = 3.8 Hz, 1H), 6.40 (q, *J* = 7.1 Hz, 1H), 3.81 (s, 3H), 1.99 (d, *J* = 7.1 Hz, 3H).;^{13}C NMR (100 MHz, $CDCl_3$) δ 169.6, 159.4, 137.6, 135.9, 133.6, 130.8, 130.3, 127.3, 127.2, 124.9, 123.9, 120.8, 116.7, 114.2, 108.4, 55.4, 15.3; IR (Neat Film, NaCl) 2934, 2361, 1684, 1607, 1511, 1450, 1328, 1292, 1250, 1202, 1178, 1110, 1079, 1032, 948, 881, 838, 815, 770, 753 cm^{-1}; HRMS (MM:ESI-APCI+) *m/z* calc'd for $C_{19}H_{18}NO_2$ $[M+H]^+$: 292.1332, found 292.1340.

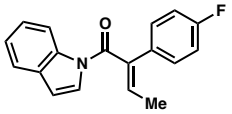

(*E*)-2-(4-fluorophenyl)-1-(1*H*-indol-1-yl)but-2-en-1-one (42h)

Purified by column chromatography (5% Et_2O in hexanes) to provide a colorless oil (49.8 mg, 0.178 mmol, 89% yield, 13:1 *E*/*Z*); ^{1}H NMR (400 MHz, $CDCl_3$) δ 8.45 (d, *J* = 8.2 Hz, 1H), 7.55 (dt, *J* = 7.7, 0.9 Hz, 1H), 7.40–7.32 (m, 4H), 7.32–7.26 (m, 1H), 7.13–7.06 (m, 2H), 6.53 (d, *J* = 3.8 Hz, 1H), 6.45 (q, *J* = 7.1 Hz, 1H), 1.96 (d, *J* = 7.1 Hz, 3H); ^{13}C NMR (100 MHz, $CDCl_3$) δ 169.0, 162.45 (d, $J_{C–F}$ = 248.2 Hz), 136.9, 135.9, 134.9, 130.9, 130.8, 127.0, 125.1, 124.0, 120.9, 116.6, 116.0, 115.7, 108.7, 15.2; ^{19}F NMR (282 MHz, $CDCl_3$) δ –113.18 (dtq, *J* = 10.8, 5.3, 2.3 Hz). IR (Neat Film, NaCl) 3051, 2917, 1685, 1602, 1534, 1509, 1472, 1450, 1385, 1331, 1224, 1202, 1160, 1101, 1080, 1016, 948, 881, 842, 786, 770, 754 cm^{-1}; HRMS (MM:ESI-APCI+) *m/z* calc'd for $C_{18}H_{15}FNO$ $[M+H]^+$: 280.1132, found 280.1137.

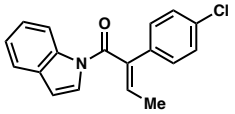

(*E*)-2-(4-chlorophenyl)-1-(1*H*-indol-1-yl)but-2-en-1-one (42i)

Purified by column chromatography (5% Et_2O in hexanes) to provide a colorless oil (46.7 mg, 0.158 mmol, 79% yield, 8:1 *E*/*Z*); ^{1}H NMR (400 MHz, $CDCl_3$) δ 8.45 (d, *J* = 8.1 Hz, 1H), 7.59–7.51 (m, 1H), 7.40–7.26 (m, 7H), 6.53 (d, *J* = 3.7 Hz, 1H), 6.46 (q, *J* = 7.2 Hz, 1H), 1.97 (d, *J* = 7.1 Hz, 3H); ^{13}C NMR (100 MHz, $CDCl_3$) δ 168.7, 136.9, 135.9, 135.3, 134.2, 133.2, 130.4, 129.2, 129.0, 127.0, 125.1, 124.1, 120.9, 116.6, 108.8, 15.3; IR (Neat Film, NaCl) 3051, 2916, 1688, 1534, 1491, 1472, 1451, 1384, 1330, 1204, 1143, 1089, 1016, 947, 881, 838, 802, 770, 754 cm^{-1}; HRMS (MM:ESI-APCI+) *m/z* calc'd for $C_{18}H_{15}ClNO$ $[M+H]^+$: 296.0837, found 296.0835.

3.5.2.2 General Procedure for the *Z*-Selective Enolization of *N*-Acyl Indole Substrates

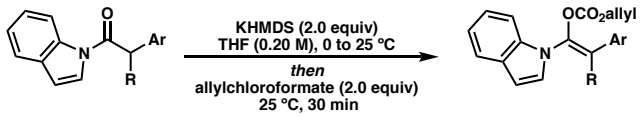

To a flame-dried flask was added KHMDS (2.0 equiv) followed by THF (0.20 M) and the resulting mixture stirred at 0 °C for 5 min. A solution of *N*-acyl indole (1.0 equiv) in THF (0.50 M) was then added dropwise, and the reaction stirred at 0 °C for 10 min then at 20 ºC for 3 h. The flask was then submerged in a room temperature water bath, and allyl chloroformate (2.0 equiv) was added neat, and the reaction continued until no starting material remained by TLC (typically less than 30 min). The crude reaction mixture was diluted with Et_2O (5 mL) and quenched with water. The layers were separated, and the aqueous layer was extracted with Et_2O (2 x 10 mL). The combined organic layers were dried over Na_2SO_4 and concentrated. The (*Z*)-enol carbonates were purified by preparative LC on a Teledyne Isco ACCQPrep HP125; column: C–18, 100 Å, 5 μm, ID 20 mm, gradient 50 to 100% MeCN/H_2O (0.25% AcOH).

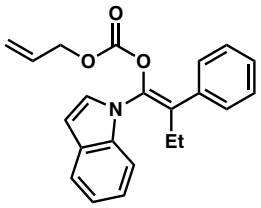

(*Z*)-1-(1*H*-indol-1-yl)-2-phenylbut-1-en-1-yl allyl carbonate (*(Z)*-19a)

Isolated as a viscous, colorless oil (168.2 mg, 0.484 mmol, 48% yield); ^{1}H NMR (400 MHz, $CDCl_3$) δ 7.63 (d, *J* = 0.9 Hz, 1H), 7.57–7.53 (m, 1H), 7.46–7.38 (m, 4H), 7.34 (dd, *J* = 8.5, 2.9 Hz, 2H), 7.31–7.27 (m, 1H), 7.19 (t, *J* = 7.5 Hz, 1H), 6.62 (d, *J* = 3.2 Hz, 1H), 5.68 (ddt, *J* = 17.1, 10.6, 5.6 Hz, 1H), 5.18–5.02 (m, 2H), 4.43 (dt, *J* = 5.6, 1.4 Hz, 2H), 2.20 (q, *J* = 7.5 Hz, 2H), 0.85 (t, *J* = 7.5 Hz, 3H); ^{13}C NMR (100 MHz, $CDCl_3$) δ 152.9, 136.7, 136.2, 133.7, 132.6, 130.8, 128.8, 128.5, 128.5, 128.1, 127.9, 122.9, 121.0, 118.8, 111.1, 104.0, 69.0, 25.4, 12.7; IR (Neat Film, NaCl) 3054, 2972, 2356, 1761, 1684, 1518, 1456, 1331, 1296, 1241, 1211, 1140, 1117, 1038, 961, 824, 765, 744, 702 cm^{-1}; HRMS (MM:ESI-APCI+) *m/z* calc'd for $C_{22}H_{22}NO_3$ $[M+H]^+$: 348.1594, found 348.1586.

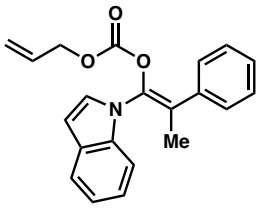

(*Z*)-1-(1*H*-indol-1-yl)-2-phenylprop-1-en-1-yl allyl carbonate (53)

Isolated as a viscous, colorless oil (145.4 mg, 0.436 mmol, 44% yield); ^{1}H NMR (400 MHz, $CDCl_3$) δ 7.65 (dt, *J* = 7.8, 0.8 Hz, 1H), 7.56–7.48 (m, 1H), 7.51–7.43 (m, 2H), 7.46–7.36 (m, 2H), 7.40–7.30 (m, 2H), 7.29 (ddd, *J* = 8.2, 7.0, 1.2 Hz, 1H), 7.24–7.15 (m, 1H), 6.64 (d, *J* = 3.1 Hz, 1H), 5.80–5.57 (m, 1H), 5.20–5.04 (m, 2H), 4.46 (dt, *J* = 5.6, 1.4 Hz, 2H), 1.88 (s, 3H); ^{13}C NMR (100 MHz, $CDCl_3$) δ 152.8, 137.8, 136.4, 134.1, 130.8, 128.6, 128.4, 128.2, 128.0, 127.7, 125.5, 122.9, 121.0, 121.0, 118.9, 111.3, 104.3, 69.1, 18.8; IR (Neat Film, NaCl) 3055, 1763, 1684, 1518, 1474, 1456, 1328, 1295, 1278, 1242, 1213, 1141, 1118, 1078, 1027, 950, 764, 744, 700 cm^{-1}; HRMS (MM:ESI-APCI+) *m/z* calc'd for $C_{21}H_{20}NO_3$ $[M+H]^+$: 334.1438, found 334.1447.

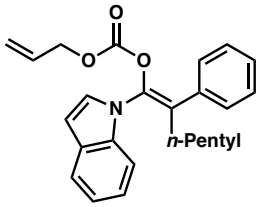

(*Z*)-1-(1H-indol-1-yl)-2-phenylhept-1-en-1-yl allyl carbonate (54)

Isolated as a viscous, colorless oil (152.7 mg, 0.436 mmol, 44% yield); ^{1}H NMR (400 MHz, $CDCl_3$) δ 7.64 (dt, *J* = 7.8, 0.7 Hz, 1H), 7.54 (dq, *J* = 8.1, 0.7 Hz, 1H), 7.40 (d, *J* = 3.5 Hz, 4H), 7.34 (p, *J* = 4.0 Hz, 2H), 7.30–7.25 (m, 1H), 7.19 (ddd, *J* = 8.0, 7.3, 1.1 Hz, 1H), 6.62 (d, *J* = 3.2 Hz, 1H), 5.68 (ddt, *J* = 17.2, 10.7, 5.6 Hz, 1H), 5.20–4.98 (m, 2H), 4.43 (dt, *J* = 5.6, 1.5 Hz, 2H), 2.26–2.08 (m, 2H), 1.21 (ddt, *J* = 12.6, 8.9, 4.6 Hz, 2H), 1.14–0.97 (m, 4H), 0.78–0.63 (m, 3H); ^{13}C NMR (100 MHz, $CDCl_3$) δ 152.9, 136.7, 136.5, 134.1, 131.5, 130.9, 129.0, 128.5, 128.5, 128.1, 127.9, 122.8, 121.0, 118.9, 111.2, 104.0, 69.0, 32.0, 31.3, 27.3, 22.3, 13.9; IR (Neat Film, NaCl) 3055, 2955, 2928, 1762, 1682, 1518, 1456, 1326, 1296, 1242, 1212, 1140, 1120, 988, 952, 765, 743, 718, 699 cm^{-1}; HRMS (MM:ESI-APCI+) *m/z* calc'd for $C_{25}H_{28}NO_3$ $[M+H]^+$: 390.2064, found 390.2060.

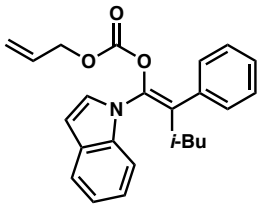

(*Z*)-1-(1*H*-indol-1-yl)-4-methyl-2-phenylpent-1-en-1-yl allyl carbonate (55)

Isolated as a viscous, colorless oil (137.2 mg, 0.365 mmol, 37% yield); ^{1}H NMR (400 MHz, $CDCl_3$) δ 7.64 (d, *J* = 7.8 Hz, 1H), 7.53 (d, *J* = 8.1 Hz, 1H), 7.45–7.38 (m, 4H), 7.38–7.31 (m, 2H), 7.31–7.26 (m, 1H), 7.19 (t, *J* = 7.5 Hz, 1H), 6.62 (d, *J* = 3.3 Hz, 1H), 5.78–5.47 (m, 1H), 5.18–4.97 (m, 2H), 4.42 (dt, *J* = 5.5, 1.3 Hz, 2H), 2.08 (d, *J* = 7.3 Hz, 2H), 1.42 (dh, *J* = 13.7, 6.8 Hz, 1H), 0.73 (d, *J* = 6.6 Hz, 6H); ^{13}C NMR (100 MHz, $CDCl_3$) δ 152.8, 135.9, 135.8, 135.7, 135.6, 130.9, 130.2, 129.7, 129.0, 128.9, 128.4, 127.6, 125.5, 122.5, 120.8, 120.7, 119.6, 111.4, 103.4, 69.5, 25.5, 19.7, 12.1; IR (Neat Film, NaCl) 3057, 3030, 2956, 1766, 1682, 1611, 1518, 1456, 1384, 1366, 1347, 1326, 1296, 1278, 1244, 1210, 1140, 1117, 1066, 971, 946, 888, 766, 743, 718, 700 cm^{-1}; HRMS (MM:ESI-APCI+) *m/z* calc'd for $C_{24}H_{26}NO_3$ $[M+H]^+$: 376.1907, found 376.1910.

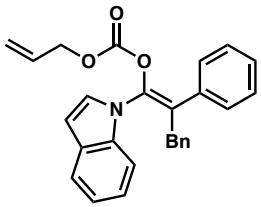

(*Z*)-1-(1*H*-indol-1-yl)-2,3-diphenylprop-1-en-1-yl allyl carbonate (56)

Isolated as a viscous, colorless oil (129.2 mg, 0.316 mmol, 32% yield); ^{1}H NMR (400 MHz, $CDCl_3$) δ 7.64 (dt, *J* = 7.8, 1.0 Hz, 1H), 7.63–7.55 (m, 1H), 7.38 (d, *J* = 3.4 Hz, 1H), 7.33–7.27 (m, 6H), 7.21 (ddd, *J* = 8.1, 7.1, 1.1 Hz, 1H), 7.16–7.08 (m, 3H), 6.95–6.87 (m, 2H), 6.67–6.53 (m, 1H), 5.68 (ddt, *J* = 17.3, 10.6, 5.6 Hz, 1H), 5.17–5.02 (m, 2H), 4.45 (dt, *J* = 5.6, 1.4 Hz, 2H), 3.55 (s, 2H); ^{13}C NMR (100 MHz, $CDCl_3$) δ 152.8, 137.6, 136.7, 136.2, 135.4, 130.8, 129.6, 128.8, 128.6, 128.4, 128.4, 128.0, 126.4, 123.0, 121.2, 121.1, 119.0, 111.2, 104.4, 69.1, 38.3; IR (Neat Film, NaCl) 3060, 3027, 1763, 1683, 1518, 1494, 1474, 1456, 1328, 1294, 1278, 1242, 1214, 1139, 1113, 1068, 987, 939, 766, 744, 712, 700 cm^{-1}; HRMS (MM:ESI-APCI+) *m/z* calc'd for $C_{27}H_{24}NO_3$ $[M+H]^+$: 410.1751, found 410.1732.

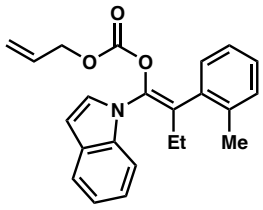

(*Z*)-1-(1H-indol-1-yl)-2-(o-tolyl)but-1-en-1-yl allyl carbonate (57)

Isolated as a viscous, colorless oil (117.4 mg, 0.324 mmol, 32% yield); ^{1}H NMR (400 MHz, $CDCl_3$) δ 7.56 (dq, *J* = 8.1, 0.7 Hz, 1H), 7.51–7.44 (m, 1H), 7.22 (ddd, *J* = 8.2, 7.0, 1.2 Hz, 1H), 7.14–7.08 (m, 1H), 7.08–6.97 (m, 4H), 6.85 (d, *J* = 3.3 Hz, 1H), 6.27 (d, *J* = 3.3 Hz, 1H), 5.90 (ddt, *J* = 17.3, 10.4, 5.8 Hz, 1H), 5.42–5.13 (m, 2H), 4.69–4.57 (m, 2H), 2.60 (ddt, *J* = 59.4, 13.8, 6.9 Hz, 2H), 2.17 (s, 3H), 1.09 (t, *J* = 7.5 Hz, 3H); ^{13}C NMR (100 MHz, $CDCl_3$) δ 152.8, 136.8, 136.5, 134.6, 131.1, 130.9, 129.1, 128.5, 128.5, 128.4, 128.2 (overlapping), 127.9, 122.8, 121.0, 118.8, 111.3, 104.0, 69.0, 40.8, 25.9, 22.3; IR (Neat Film, NaCl) 2934, 2361, 1684, 1607, 1511, 1450, 1328, 1292, 1250, 1202, 1178, 1110, 1079, 1032, 948, 881, 838, 815, 770, 753 cm^{-1}; HRMS (MM:ESI-APCI+) *m/z* calc'd for $C_{23}H_{24}NO_3$ $[M+H]^+$: 362.1751, found 362.1749.

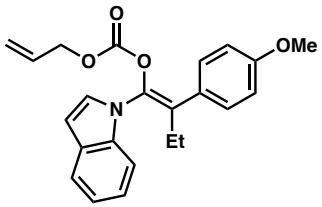

(*Z*)-1-(1*H*-indol-1-yl)-2-(4-methoxyphenyl)but-1-en-1-yl allyl carbonate (58)

Isolated as a viscous, colorless oil (168.6 mg, 0.447 mmol, 45% yield); ^{1}H NMR (400 MHz, $CDCl_3$) δ 7.63 (dt, *J* = 7.8, 1.0 Hz, 1H), 7.55–7.51 (m, 1H), 7.37–7.30 (m, 3H), 7.30–7.24 (m, 1H), 7.21–7.14 (m, 1H), 6.98–6.91 (m, 2H), 6.61 (dd, *J* = 3.3, 1.0 Hz, 1H), 5.82–5.57 (m, 1H), 5.21–5.02 (m, 2H), 4.45 (dt, *J* = 5.6, 1.4 Hz, 2H), 3.85 (s, 3H), 2.17 (q, *J* = 7.5 Hz, 2H), 0.84 (t, *J* = 7.5 Hz, 3H);^{13}C NMR (100 MHz, $CDCl_3$) δ 159.3, 152.9, 136.7, 133.5, 132.2, 130.9, 129.4, 128.9, 128.4, 128.3, 122.8, 121.0, 120.9, 118.9, 113.9, 111.2, 103.9, 69.0, 55.3, 25.4, 12.9; IR (Neat Film, NaCl) 2972, 1765, 1687, 1519, 1456, 1333, 1259, 1238, 1210, 1144, 1115, 1088, 1039, 969, 945, 763, 743 cm^{-1}; HRMS (MM:ESI-APCI+) *m/z* calc'd for $C_{23}H_{24}NO_4$ $[M+H]^+$: 378.1700, found 378.1713.

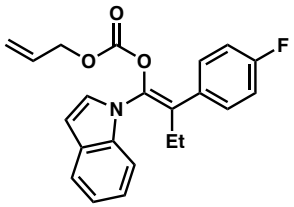

(*Z*)-allyl (2-(4-fluorophenyl)-1-(1*H*-indol-1-yl)but-1-en-1-yl) carbonate (59)

Isolated as a viscous, colorless oil (225.1 mg, 0.616 mmol, 31% yield); ^{1}H NMR (400 MHz, $CDCl_3$) δ 7.66 (dt, *J* = 7.8, 1.0 Hz, 1H), 7.55 (ddd, *J* = 8.2, 1.7, 0.6 Hz, 1H), 7.44–7.37 (m, 2H), 7.34 (d, *J* = 3.3 Hz, 1H), 7.33–7.29 (m, 1H), 7.22 (ddd, *J* = 8.0, 7.1, 1.1 Hz, 1H), 7.17–7.10 (m, 2H), 6.65 (dd, *J* = 3.2, 0.8 Hz, 1H), 5.72 (ddt, *J* = 17.2, 10.5, 5.7 Hz, 1H), 5.24–5.08 (m, 2H), 4.46 (dt, *J* = 5.7, 1.4 Hz, 2H), 2.21 (q, *J* = 7.5 Hz, 2H), 0.86 (t, *J* = 7.5 Hz, 3H); ^{13}C NMR (100 MHz, $CDCl_3$) δ 162.41 (d, $J_{C–F}$ = 246.9 Hz), 152.8, 136.7, 134.1, 132.1 (d, $J_{C–F}$ = 3.5 Hz), 131.6, 130.8, 130.0 (d, $J_{C–F}$ = 8.2 Hz), 128.7, 128.5, 122.9, 121.0, 119.1, 115.7, 115.5, 111.1, 104.2, 69.1, 25.5, 12.7**;**^{19}F NMR (282 MHz, $CDCl_3$) δ –113.98 – – 114.11 (m);.IR (Neat Film, NaCl) 3052, 2973, 1763, 1685, 1604, 1510, 1456, 1331, 1296, 1242, 1211, 1160, 1140, 1117, 1066, 1037, 1012, 960, 846, 767, 745 cm^{-1}; HRMS (MM:ESI-APCI+) *m/z* calc'd for $C_{22}H_{21}FNO_3$ $[M+H]^+$: 366.1500, found 366.1496.

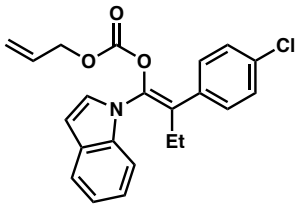

(*Z*)-allyl (2-(4-chlorophenyl)-1-(1*H*-indol-1-yl)but-1-en-1-yl) carbonate (60)

Isolated as a viscous, colorless oil (126.6 mg, 0.364 mmol, 36% yield); ^{1}H NMR (400 MHz, $CDCl_3$) δ 7.65 (dt, *J* = 7.8, 0.9 Hz, 1H), 7.57–7.50 (m, 1H), 7.43–7.34 (m, 4H), 7.32 (d, *J* = 3.3 Hz, 1H), 7.34–7.25 (m, 1H), 7.20 (td, *J* = 7.5, 7.1, 1.0 Hz, 1H), 6.64 (d, *J* = 3.2 Hz, 1H), 5.71 (ddt, *J* = 17.1, 10.5, 5.7 Hz, 1H), 5.21–5.08 (m, 2H), 4.45 (dt, *J* = 5.7, 1.5 Hz, 2H), 2.20 (q, *J* = 7.5 Hz, 2H), 0.85 (t, *J* = 7.5 Hz, 3H); ^{13}C NMR (100 MHz, $CDCl_3$) δ 152.7, 136.6, 134.7, 134.2, 133.9, 131.3, 130.7, 129.6, 128.8, 128.7, 128.5, 123.0, 121.1, 121.1, 119.2, 111.1, 104.3, 69.2, 25.3, 12.7; IR (Neat Film, NaCl) 2972, 1762, 1681, 1491, 1474, 1455, 1241, 1209, 1140, 1111, 1014, 960, 816, 765, 744 cm^{-1}; HRMS (MM:ESI-APCI+) *m/z* calc'd for $C_{22}H_{21}ClNO_3$ $[M+H]^+$: 382.1204, found 382.1189.

3.5.2.3 Ligand Synthesis

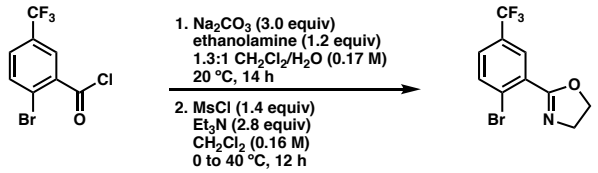

2-(2-bromo-5-(trifluoromethyl)phenyl)-4,5-dihydrooxazole (61)

To a 500 mL round bottomed flask charged with a magnetic stirring bar and ethanolamine (1.35 mL, 22.31 mmol, 1.20 equiv) was added CH_2Cl_2 (62 mL). To the mixture was added a solution of Na_2CO_3 (5.91 g, 55.77 mmol, 3.0 equiv) in water (46 mL). The biphasic mixture was vigorously stirred at 20 ºC. To the mixture was added 2-bromo-5-(trifluoromethyl)benzoyl chloride[14] (5.34 g, 18.59 mmol, 1.00 equiv) dropwise over 10 min. The reaction mixture was vigorously stirred at 20 ºC for 14 h. The layers were separated, and the aqueous layer was extracted with CH_2Cl_2 (4 x 50 mL). The combined organic layers were washed with brine (15 mL), dried over sodium sulfate, and concentrated to afford an amorphous white solid which was used in the next step without further purification.

To a 250 mL round bottomed flask charged with a stir bar and a reflux condenser was added the crude alcohol prepared above. To the flask was added CH_2Cl_2 (120 mL) and Et_3N (7.3 mL, 52.2 mmol, 2.8 equiv). The flask was cooled in a 0 ºC ice/water bath for 10 min, then MsCl (2.02 mL, 26.1 mmol, 1.4 equiv) was added dropwise over 2 min. The reaction was stirred at 0 ºC for 20 min then heated in an oil bath at 40 ºC for 8 h. The flask was then cooled to 20 ºC and the reaction mixture diluted with CH_2Cl_2 (50 mL) and transferred to a separatory funnel. The organic layer was washed with water (2 x 50 mL) and brine (50 mL), then dried over Na_2SO_4, filtered, and concentrated to an orange oil.

Purification by column chromatography (15 to 25% EtOAc/hexanes) provided the product as a colorless oil (3.1182 g, 10.6 mmol, 57% yield); ^{1}H NMR (400 MHz, $CDCl_3$) δ 8.01 (d, J = 2.3 Hz, 1H), 7.80 (d, J = 8.3 Hz, 1H), 7.53 (dd, J = 8.4, 2.2 Hz, 1H), 4.49 (t, J = 9.6 Hz, 2H), 4.15 (t, J = 9.6 Hz, 2H); ^{13}C NMR (100 MHz, $CDCl_3$) δ 162.7 (d, J = 3.7 Hz), 134.8, 130.5, 130.0 (q, $J_{C–F}$ = 35.3, 33.6 Hz), 128.3 (d, $J_{C–F}$ = 37.9 Hz), 126.0, 123.7 (q, $J_{C–F}$ = 272.4 Hz), 68.0, 55.6; ^{19}F NMR (282 MHz, $CDCl_3$) δ –62.93; IR (Neat Film, NaCl) 2977, 1652, 1609, 1580, 1474, 1426, 1403, 1337, 1312, 1263, 1242, 1173, 1133, 1077, 1027, 976, 947, 908, 831, 736, 712 cm^{-1}; HRMS (MM:ESI-APCI+) *m/z* calc'd for $C_{10}H_8BrF_3NO$ $[M+H]^+$: 293.9736, found 293.9740.

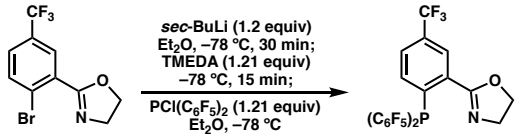

2-(2-(bis(perfluorophenyl)phosphaneyl)-5-(trifluoromethyl)phenyl)-4,5-dihydrooxazole (F_{13}-glyPHOX, L4)

To a 100 mL Schlenk tube charged with a stir bar was added **SI9** (320.5 mg, 1.09 mmol, 1.0 equiv) and Et_2O (22 mL). The resulting solution was cooled to –78 ºC in an acetone/dry ice bath for 30 min, then a 1.26 M solution of *sec*-BuLi in hexanes (1.04 mL, 1.31 mmol, 1.2 equiv) was added dropwise over 5 min. The resulting dark red solution was stirred for 30 min at –78 ºC, then TMEDA (200 μL, 1.32 mmol, 1.21 equiv) was added. After stirring for 15 min at –78 ºC, a solution of $PCl(C_6F_5)_2$[15] (530.0 mg, 1.32 mmol, 1.21 equiv) in Et_2O (11 mL) was added dropwise, resulting in an immediate color change to light red. After 1 h at –78 ºC, the reaction mixture was warmed to 0 ºC and quenched with water (10 mL). The mixture was transferred to a separatory funnel and diluted with 5 mL brine before being separated. The aqueous layer was then extracted with Et_2O (2 x 10 mL) and the combined organic layers dried over Na_2SO_4, filtered, and concentrated to yield a yellow oil. Purification by column chromatography (3% Et_2O/hexanes) provided F_{13}-glyPHOX as an amorphous white solid (128.7 mg, 0.222 mmol, 20% yield); ^{1}H NMR (400 MHz, $CDCl_3$) δ 8.24 (dd, J = 4.6, 1.9 Hz, 1H), 7.65 (dt, J = 8.4, 1.1 Hz, 1H), 7.36 (dd, J = 8.4, 3.1 Hz, 1H), 4.45 (t, J = 9.6 Hz, 2H), 3.96 (t, J = 9.5 Hz, 2H); ^{13}C NMR (100 MHz, $CDCl_3$) δ 162.7 (d, J = 5.7 Hz), 149.5–145.9 (m), 144.2–140.8 (m), 139.2–136.0 (m), 137.4 (d, J = 28.6 Hz), 133.1, 131.9 (q, J = 33.6 Hz), 131.6 (d, J = 21.7 Hz), 127.1 (d, J = 4.0 Hz), 126.4 (d, J = 4.1 Hz), 123.5 (q, J = 272.6 Hz), 111.5 – 109.3 (m), 68.2, 55.0; ^{19}F NMR (282 MHz,

$CDCl_3$) δ –62.09 – –65.06 (m), –128.89 – –130.15 (m), –149.89 (tt, *J* = 20.8, 3.8 Hz), –160.33 (tt, *J* = 20.8, 5.8 Hz); ^{31}P NMR (162 MHz, $CDCl_3$) δ –55.11 (p, *J* = 36.4 Hz); IR (Neat Film, NaCl) 1656, 1517, 1475, 1366, 1338, 1318, 1289, 1252, 1179, 1134, 1083, 1041, 977, 949 cm^{-1}; HRMS (MM:ESI-APCI+) *m/z* calc'd for $C_{22}H_8F_{13}NOP$ $[M+H]^+$: 580.0130, found 580.0138.

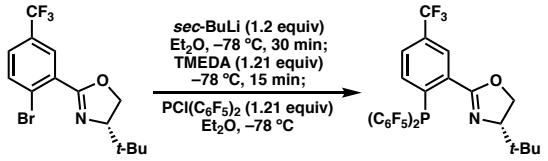

_(S)_-2-(2-(bis(perfluorophenyl)phosphaneyl)-5-(trifluoromethyl)phenyl)-4-(*tert*-butyl)-4,5-dihydrooxazole (_(S)_-F_{13}-glyPHOX, L3)

To a 100 mL Schlenk tube charged with a stir bar was added *(S)*-2-(2-bromo-5-(trifluoromethyl)phenyl)-4-(*tert*-butyl)-4,5-dihydrooxazole[16] (289.2 mg, 0.826 mmol, 1.0 equiv) and Et_2O (16.5 mL). The resulting solution was cooled to –78 ºC in an acetone/dry ice bath for 30 min, then a 1.26 M solution of *sec*-BuLi in hexanes (794 μL, 1.00 mmol, 1.2 equiv) was added dropwise over 5 min. The resulting dark red solution was stirred for 30 min at –78 ºC, then TMEDA (150 μL, 1.00 mmol, 1.2 equiv) was added. After stirring for 15 min at –78 ºC, a solution of $PCl(C_6F_5)_2$[15] (400.0 mg, 1.00 mmol, 1.2 equiv) in Et_2O (8.3 mL) was added dropwise, resulting in an immediate color change to light red. After 1 h at –78 ºC, the reaction mixture was warmed to 0 ºC and quenched with water (10 mL). The mixture was transferred to a separatory funnel and diluted with 5 mL brine before being separated. The aqueous layer was then extracted with Et_2O (2 x 10 mL) and the combined organic layers dried over Na_2SO_4, filtered, and concentrated to yield a yellow oil. Purification by column chromatography (10% CH_2Cl_2/hexanes); $[\alpha]_D^{25}$ –107.5 (*c* 1.0, $CHCl_3$); ^{1}H NMR (400 MHz, $CDCl_3$) δ 8.25 (dd, *J* = 4.6, 1.9 Hz, 1H), 7.68 – 7.60 (m, 1H), 7.31 (dd, *J* = 8.2, 3.0 Hz, 1H), 4.39 (dd, *J* = 10.2, 8.7 Hz, 1H), 4.22 (t, *J* = 8.7 Hz, 1H), 3.95 (dd, *J* = 10.1, 8.7 Hz, 1H), 0.77 (s, 9H); ^{13}C NMR (100 MHz, $CDCl_3$) δ 161.5 (d, *J* = 5.4 Hz), 149.5 – 145.5 (m), 144.5 – 140.2 (m), 139.7 – 135.4 (m), 137.3 (d, *J* = 28.9 Hz), 133.0, 132.5 – 131.3 (m), 131.9, 127.1 (q, *J* = 3.6 Hz), 126.4 (q, *J* = 4.1 Hz), 123.6 (q, *J* =

272.6 Hz), 111.95 – 110.41 (m), 69.44, 33.63, 25.63; ^{19}F NMR (282 MHz, $CDCl_3$) δ –61.9 – –64.6 (m), –127.5 – –132.1 (m), –150.3 (dtt, J = 213.8, 20.6, 3.8 Hz), –158.50 – –162.90 (m); ^{31}P NMR (162 MHz, $CDCl_3$) δ –55.79 (p, J = 38.0 Hz); IR (Neat Film, NaCl) 2962, 1654, 1517, 1473, 1362, 1327, 1306, 1287, 1179, 1135, 1085, 978, 834 cm^{-1}; HRMS (MM:ESI-APCI+) *m/z* calc'd for $C_{26}H_{16}F_{13}NOP$ $[M+H]^+$: 636.0756, found 636.0750.

3.6 REFERENCES AND NOTES

(1) (a) Li, B. X.; Le, D. N.; Mack, K. A.; McClory, A.; Lim, N.-K.; Cravillion, T.; Savage, S.; Han, C.; Collum, D. B.; Zhang, H.; Gosselin, F. Highly Stereoselective Sythesis of Tetrasubstituted Acyclic All-Carbon Olefins via Enol Tosylation and Suzuki–Miyaura Coupling. *J. Am. Chem. Soc.* **2017**, *139*, 10777–10783. (b) Mack, K. A.; McClory, A.; Zhang, H.; Gosselin, F.; Collum, D. B. Lithium Hexamethyldisilazide-Mediated Enolization of Highly Substituted Aryl Ketones: Structural and Mechanistic Basis of the *E*/*Z* Selectivities. *J. Am. Chem. Soc.* **2017**, *139*, 12182–12189.

(2) Alexy, E. J.; Zhang, H.; Stoltz, B. M. Catalytic Enantioselective Synthesis of Acyclic Quaternary Centers: Palladium-Catalyzed Decarboxylative Allylic Alkylation of Fully Substituted Acyclic Enol Carbonates. *J. Am. Chem. Soc.* **2018**, *140*. 10109–10112.

(3) Alexy, E. J.; Fulton, T. J.; Zhang, H.; Stoltz, B. M. Palladium-catalyzed enantioselective decarboxylative allylic alkylation of fully substituted *N*-acyl indole-derived enol carbonates. *Chem. Sci.* **2019**. *10*, 5996–6000.

(4) (a) Astin, S.; Newman, A. C. C.; Riley, H. L. Selenium dioxide, a new oxidizing agent. Part III. Its reaction with some alcohols and esters. *J. Chem. Soc., Res.* **1933**, 391–394. (b) Corey, E. J.; Schaefer, J. P. Studies on the Mechanism of Oxidation of Ketones by Selenium Dioxide (Part I). *J. Am. Chem. Soc.* **1960**, *82*, 917–929. (c) Sharpless, K. B.; Gordon, K. M. Selenium dioxide oxidation of ketones and aldehydes. Evidence for the intermediacy of β-Ketoselenic Acids. *J. Am. Chem.*

Soc. **1976**, *98*, 300–301.

(5) Mukaiyama, T.; Matsuo, J.-I.; Kitagawa, H. A New and One-Pot Synthesis of α,β-Unsaturated Ketones by Dehydrogenation of Various Ketones with *N*-*tert*-Butyl Phenylsulfinimidoyl Chloride. *Chem. Lett.* **2000**, *29*, 1250–1251.

(6) (a) Nicolaou, K. C.; Zhong, Y. L.; Baran, P. S. A New Method for the One-Step Synthesis of α,β-Unsaturated Carbonyl Systems from Saturated Alcohols and Carbonyl Compounds. *J. Am. Chem. Soc.* **2000**, *122*, 7596–7597. (b) Nicolaou, K. C.; Montagnon, T.; Baran, P. S.; Zhong, Y. L. *J. Am. Chem. Soc.* **2002**, *124*, 2245–2258. Iodine(V) Reagents in Organic Synthesis. Part 4. *o*-Iodoxybenzoic Acid as a Chemospecific Tool for Single Electron Transfer-Based Oxidation Processes. (c) Nicolaou, K. C.; Montagnon, T.; Baran, P. S. Modulation of Reactivity Profile of IBX by Ligand Complexation: Ambient Temperature Dehydrogenation of Aldehydes and Ketones to α,β-Unsaturated Carbonyl Compounds. *Angew. Chem. Int. Ed.* **2002**, *41*, 993–996.

(7) (a) Braude, E. A.; Brook, A. G.; Linstead, R. P. Hydrogen transfer. Part IV. The use of quinones of high potential as dehydrogenation reagents. *J. Chem. Soc., Res.* **1954**, 3569–3574. (b) Walker, D.; Hiebert, J. D. 2,3-Dichloro-5,6-Dicyanobenzoquinone and its Reactions. *Chem. Rev.* **1967**, *67*, 153–195.

(8) (a) Ito, Y.; Hirao, T.; Saegusa, T. Synthesis of α,β-unsaturated carbonyl compounds by palladium(II)-catalyzed dehydrosilylation of silyl enol ethers. *J. Org. Chem.* **1978**, *43*, 1011–1013. (b) Larock, R. C.; Hightower, T. R.; Kraus, G. A.; Hahn, P.; Zheng, D. A simple, effective, new, palladium-catalyzed conversion

of enol silanes to enones and enals. *Tetrahedron Lett.* **1995**, *36*, 2423–2426. (c) Shvo, Y.; Arisha, A. H. I. Regioselective Catalytic Dehydrogenation of Aldehydes and Ketones. *J. Org. Chem.* **1998**, *63*, 5640−5642. (d) Diao, T.; Stahl, S. S. Synthesis of Cyclic Enones via Direct Palladium-Catalyzed Aerobic Dehydrogenation of Ketones. *J. Am. Chem. Soc.* **2011**, *133*, 14566–14569. (e) Izawa, Y.; Pun, D.; Stahl, S. S. Palladium-cataalyzed aerobic dehydrogenation of substituted cyclohexanones to phenols. *Science* **2011**, *333*, 209–213. (f) Diao, T.;Wadzinski, T. J.; Stahl, S. S. Direct aerobic α,β-dehydrogenation of aldehydes and ketones with $Pd(TFA)_2$/4,5-diazafluorenone catalyst. *Chem. Sci.* **2012**, *3*, 887–891. (g) Gao, W.; He, Z.; Qian, Y.; Zhao, J. General palladium-catalyzed aerobic dehydrogenation to generate double bonds. *Chem. Sci.* **2012**, *3*, 883–886. (h) Diao, T.; Pun, D.; Stahl, S. S. Aerobic Dehydrogenation of Cyclohexanone to Cyclohexenone Catalyzed by $Pd(DMSO)_2(TFA)_2$: Evidence for Ligand-Controlled Chemoselectivity. *J. Am. Chem. Soc.* **2013**, *135*, 8205–8212. (i) Sakamoto, Y.; Amaya, T.; Suzuki, T.; Hirao, T. Palladium(II)-Catalyzed Dehydroboration via Generation of Boron Enolates. *Chem. - Eur. J.* **2016**, *22*, 18686−18689. (j) Chen, M.; Dong, G. Direct Catalytic Desaturation of Lactams Enabled by Soft Enolization. *J. Am. Chem. Soc.* **2017**, *139*, 7757−7760. (k) Muzart, J. One-Pot Syntheses of α,β-Unsaturated Carbonyl Compounds through Palladium-Mediated Dehydrogenation of Ketones, Aldehydes, Esters, Lactones, and Amides. *Eur. J. Org. Chem.* **2010**, 3779–3790.

(9) (a) Shimizu, I.; Tsuji, J. Palladium-catalyzed decarboxylation-dehydrogenation of

Allyl β-Keto Carboxylates and Allyl Enol Carbonates as a Novel Synthetic Method for α-Substituted α,β-Unsaturated Ketones. *J. Am. Chem. Soc.* **1982**, *104*, 5844–5846. (b) Shimizu, I.; Minami, I.; Tsuji, J. Palladium-catalyzed synthesis of α,β-unsaturated ketones via allyl enol carbonates. *Tetrahedron Lett.* **1983**, *24*, 1797–1800. (c) Minami, I.; Takahashi, K.; Shimizu, I.; Kimura, T.; Tsuji, J. New synthetic methods for α,β-unsaturated ketones, aldehydes, esters, and lactones by the palladium-catalyzed reactions of silyl enol ethers, ketene silyl acetals, and enol acetates with allyl carbonates. *Tetrahedron* **1986**, *42*, 2971–2977.

(10) (a) Chen, Y.; Huang, D.; Zhao, Y.; Newhouse, T. R. Allyl-Palladium-Catalyzed Ketone Dehydrogenation Enables Telescoping with Enone α,β-Vicinal Difunctionalization. *Angew. Chem., Int. Ed.* **2017**, *56*, 8258–8262. (b) Huang, D.; Zhao, Y.; Newhouse, T. R. Synthesis of Cyclic Enones by Allyl-Palladium-Catalyzed α,β-Dehydrogenation. *Org. Lett.* **2018**, *20*, 684–687.

(11) Zhao, Y.; Chen, Y.; Newhouse, T. R. Allyl-Palladium-Catalyzed α,β-Dehydrogenation of Carboxylic Acids via Enediolates. *Angew. Chem. Int. Ed.* **2017**, *56*, 13122–13125.

(12) (a) Chen, Y.; Romaire, J. P.; Newhouse, T. R. Palladium-Catalyzed α,β-Dehydrogenation of Esters and Nitriles. *J. Am. Chem. Soc.* **2015**, *137*, 5875–5878. (b) Chen, Y.; Turlik, A.; Newhouse, T. R. *J. Am. Chem. Soc.* **2016**, *138*, 1166–1169. Amide α,β-Dehydrogenation Using Allyl-Palladium Catalysis and a Hindered Monodentate Anilide. (c) Szewczyk, S. M.; Zhao, Y.; Sakai, H.; Dube,

P.; Newhouse, T. R. α,β-Dehydrogenation of esters with free OH and NH functionalities via allyl-palladium catalysis. *Tetrahedron* **2018**, *74*, 3293–3300.

(13) Pangborn, A. B.; Giardello, M. A.; Grubbs, R. H.; Rosen, R. K.; Timmers, F. J. Safe and Convenient Procedure for Solvent Purification. *Organometallics* **1996**, *15*, 1518–1520.

(14) Tani, K.; Behenna, D. C.; McFadden, R. M.; Stoltz, B. M. A Facile and Modular Synthesis of Phosphinoxazoline Ligands. *Org*. *Lett*. **2007**, *9*, 2529–2531.

(15) Mancino, G.; Ferguson, A. J.; Beeby, A.; Long, N. J.; Jones, T. S. Dramatic Increases in the Lifetime of the Er^{3+} Ion in a Molecular Complex Using a Perfluorinated Imidodiphosphinate Sensitizing Ligand. *J. Am*. *Chem*. *Soc*. **2005**, *127*, 524–525.

(16) McDougal, N. T.; Streuff, J.; Mukherjee, H.; Virgil, S. C.; Stoltz, B. M. Rapid synthesis of an electron-deficient *t*-BuPHOX ligand: cross-coupling of aryl bromides with secondary phosphine oxides. Tetrahedron *Lett.* **2010**, *51*, 5550–5554.

APPENDIX 5

Spectra Relevant to Chapter 3:

Pd-Catalyzed Decarboxylative Dehydrogenation of

Fully Substituted N-acyl Indole-derived Enol carbonates

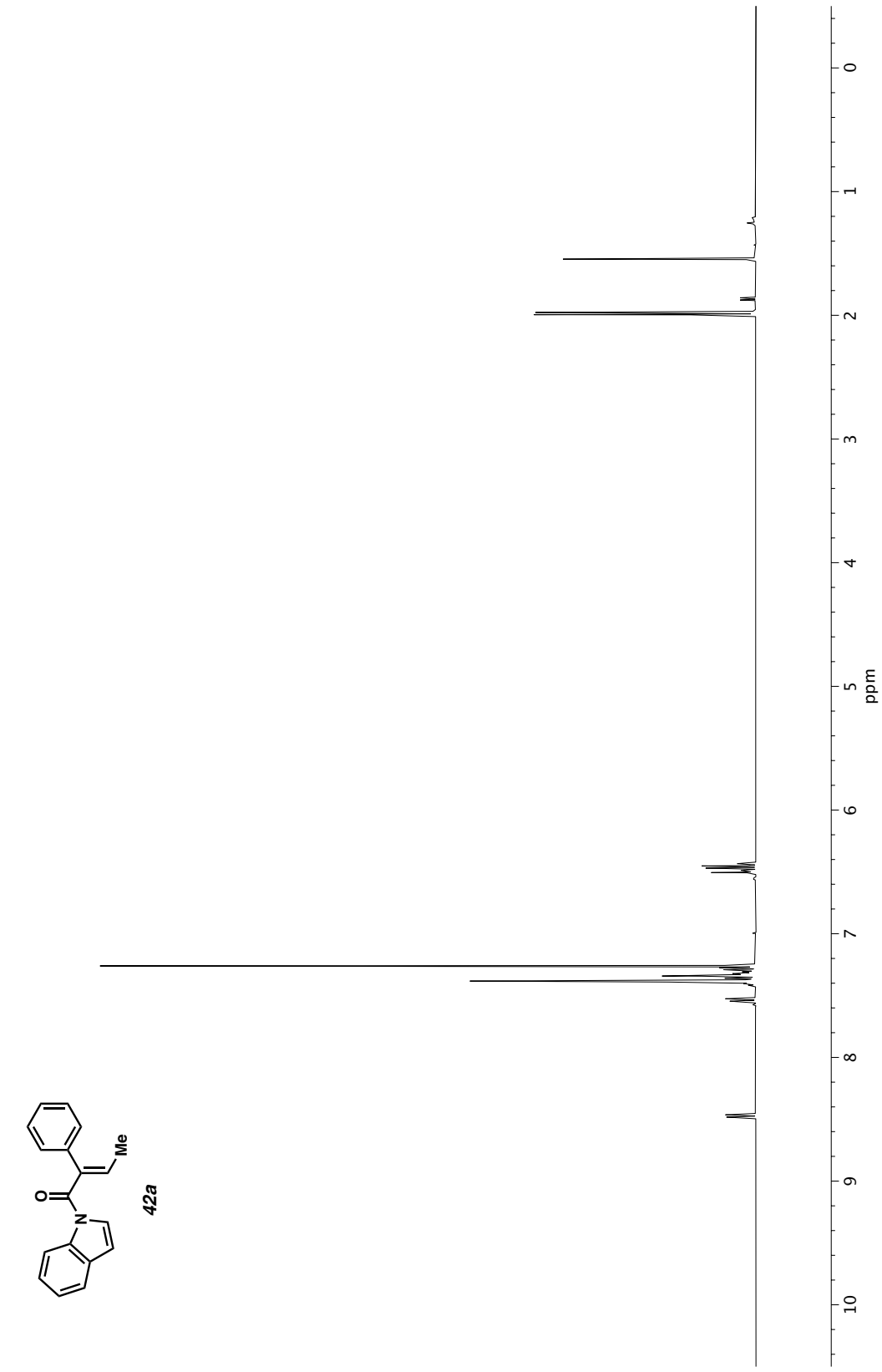

Figure A5.1 *^1H NMR (400 MHz, $CDCl_3$) of compound* ***42a****.*

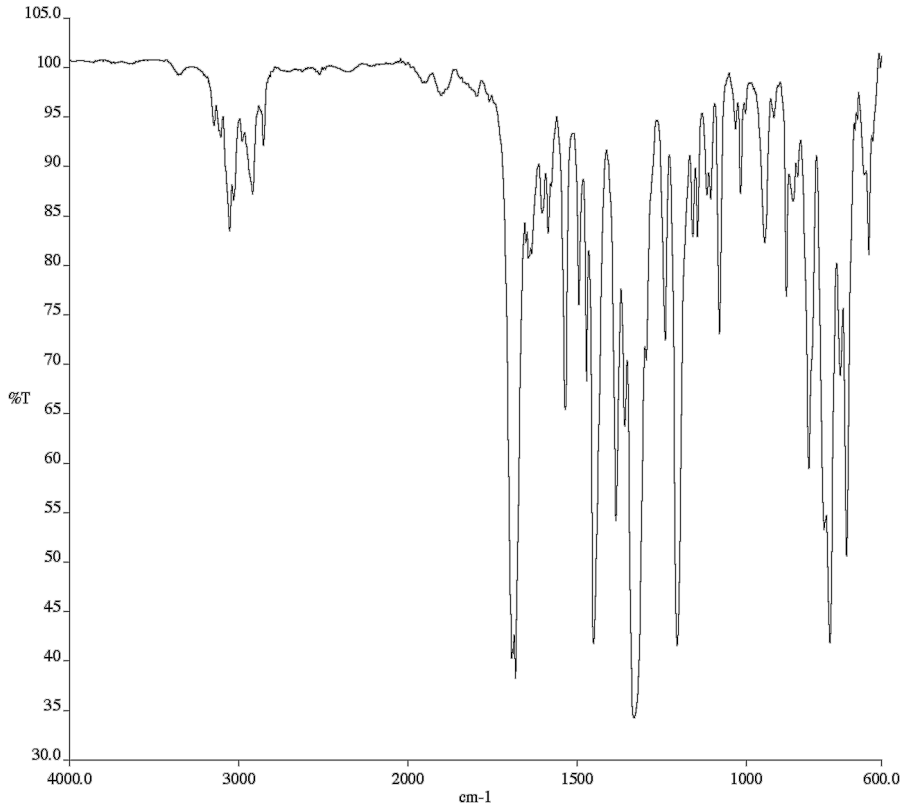

Figure A5.2 *Infrared spectrum (Thin Film, NaCl) of compound* ***42a****.*

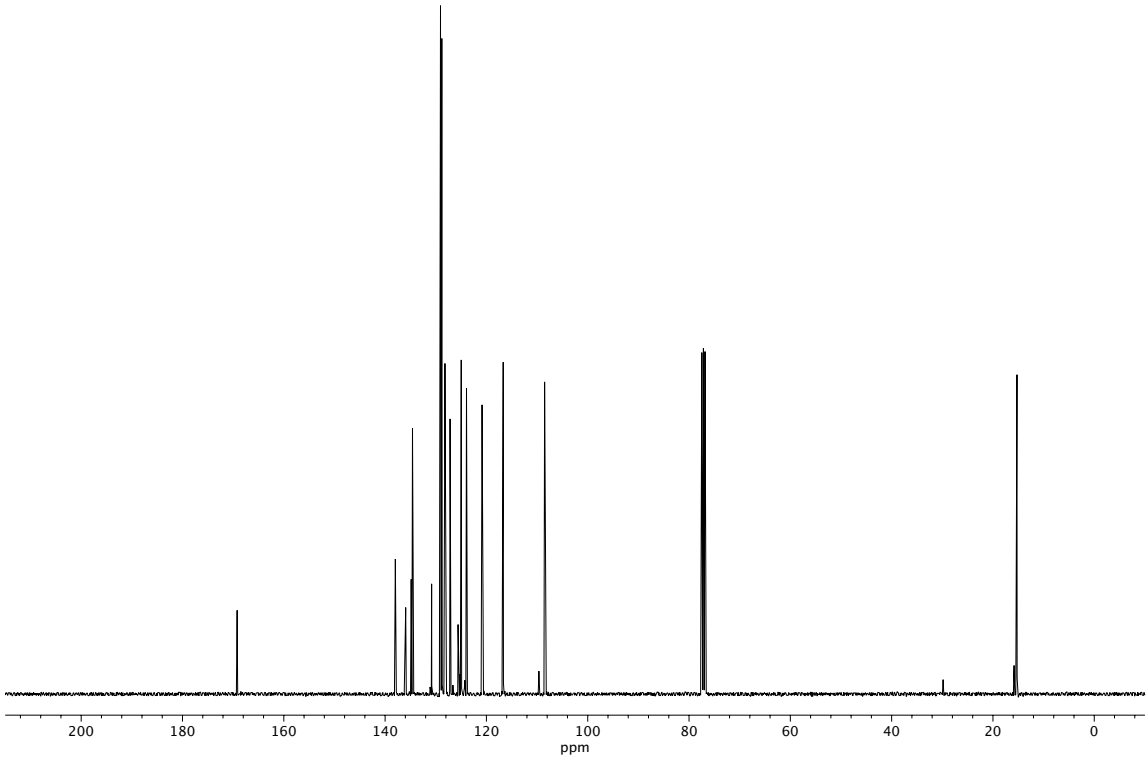

Figure A5.3 *^{13}C NMR (100 MHz, $CDCl_3$) of compound* ***42a****.*

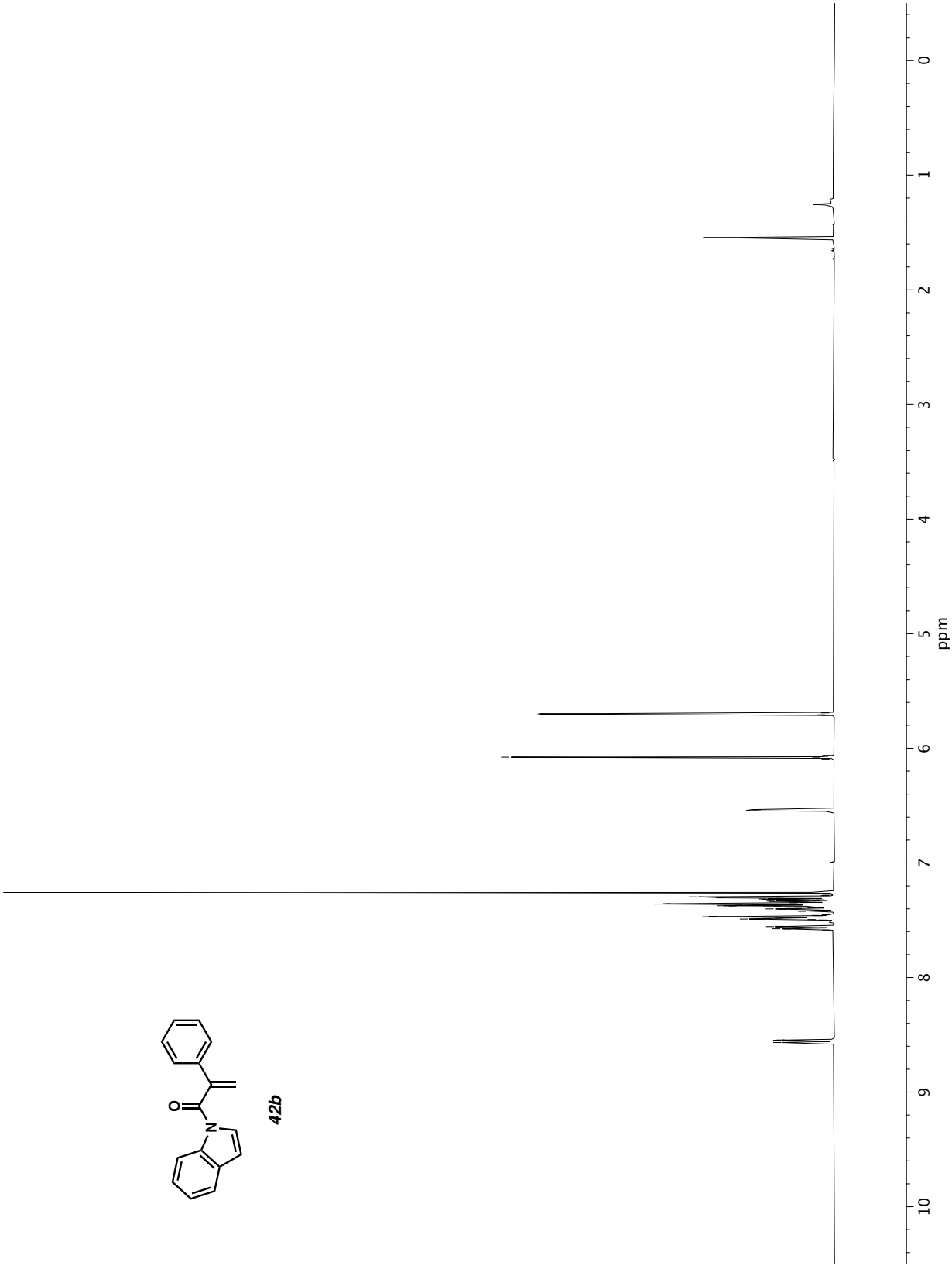

Figure A5.4 *^1H NMR (400 MHz, $CDCl_3$) of compound* ***42b****.*

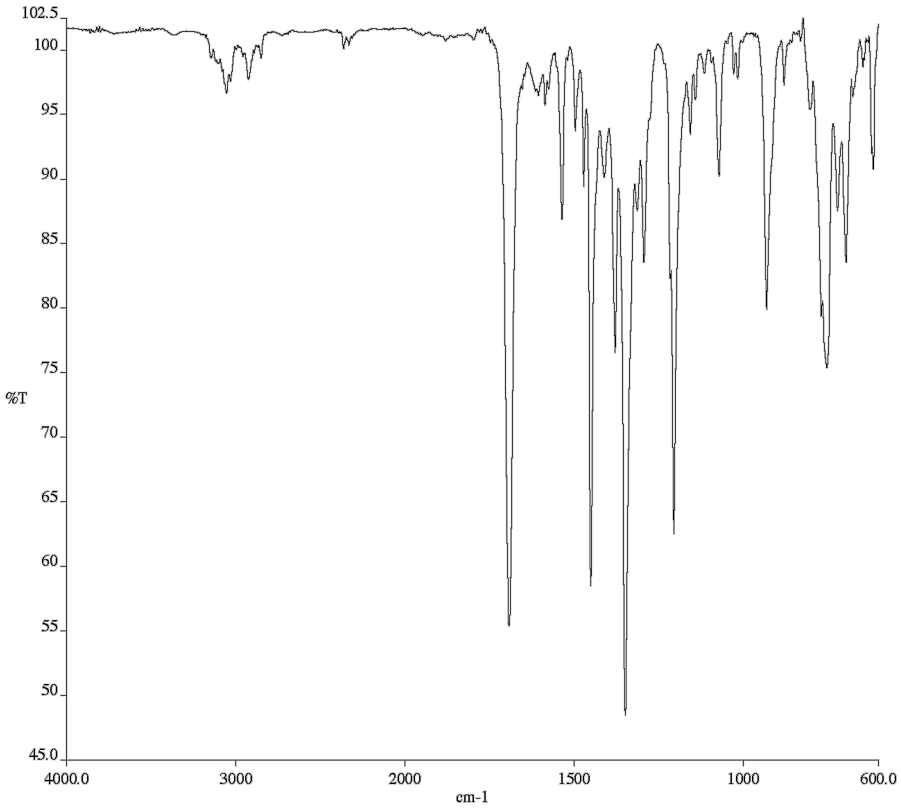

Figure A5.5 *Infrared spectrum (Thin Film, NaCl) of compound* ***42b****.*

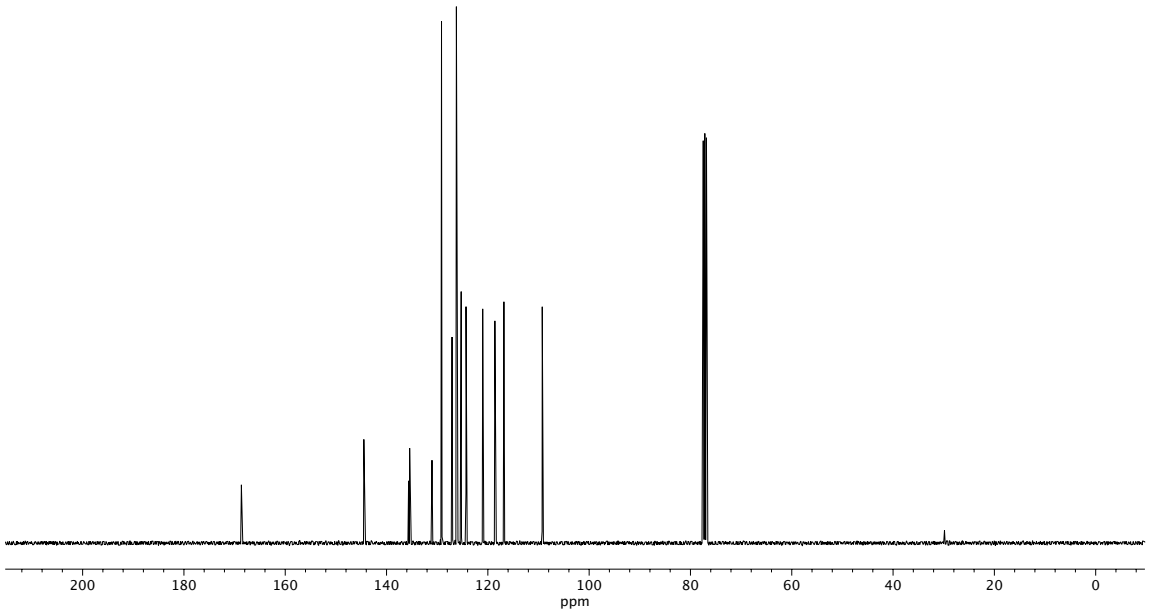

Figure A5.6 *^{13}C NMR (100 MHz, $CDCl_3$) of compound* ***42b****.*

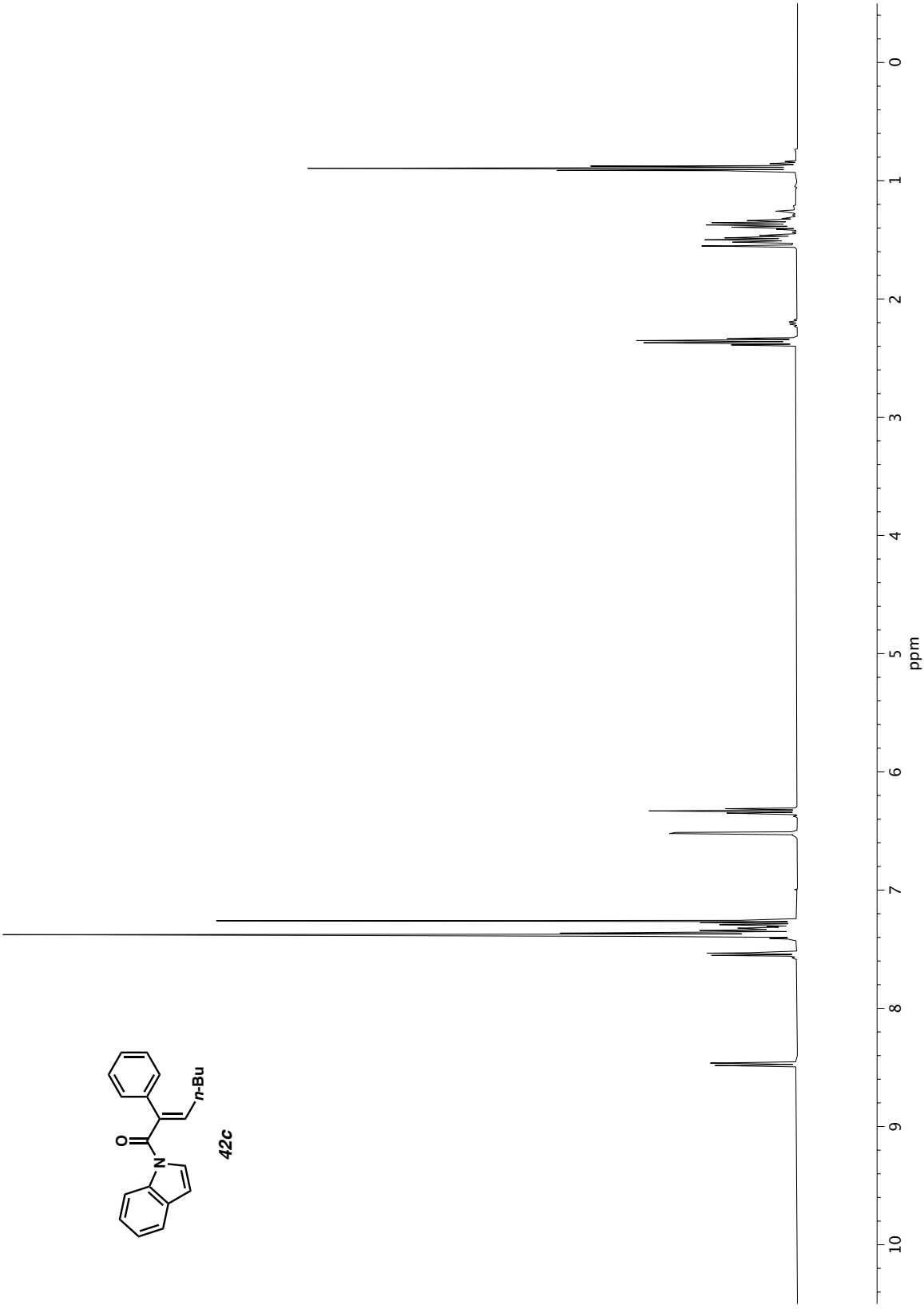

Figure A5.7 *^1H NMR (400 MHz, $CDCl_3$) of compound* ***42c****.*

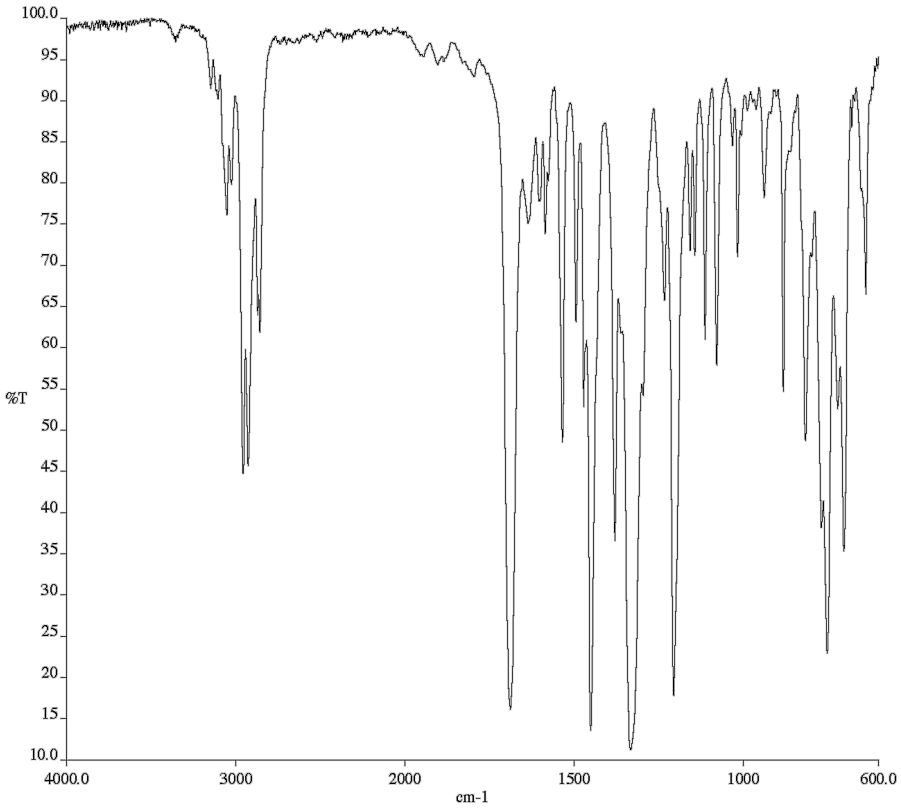

Figure A5.8 *Infrared spectrum (Thin Film, NaCl) of compound* ***42c****.*

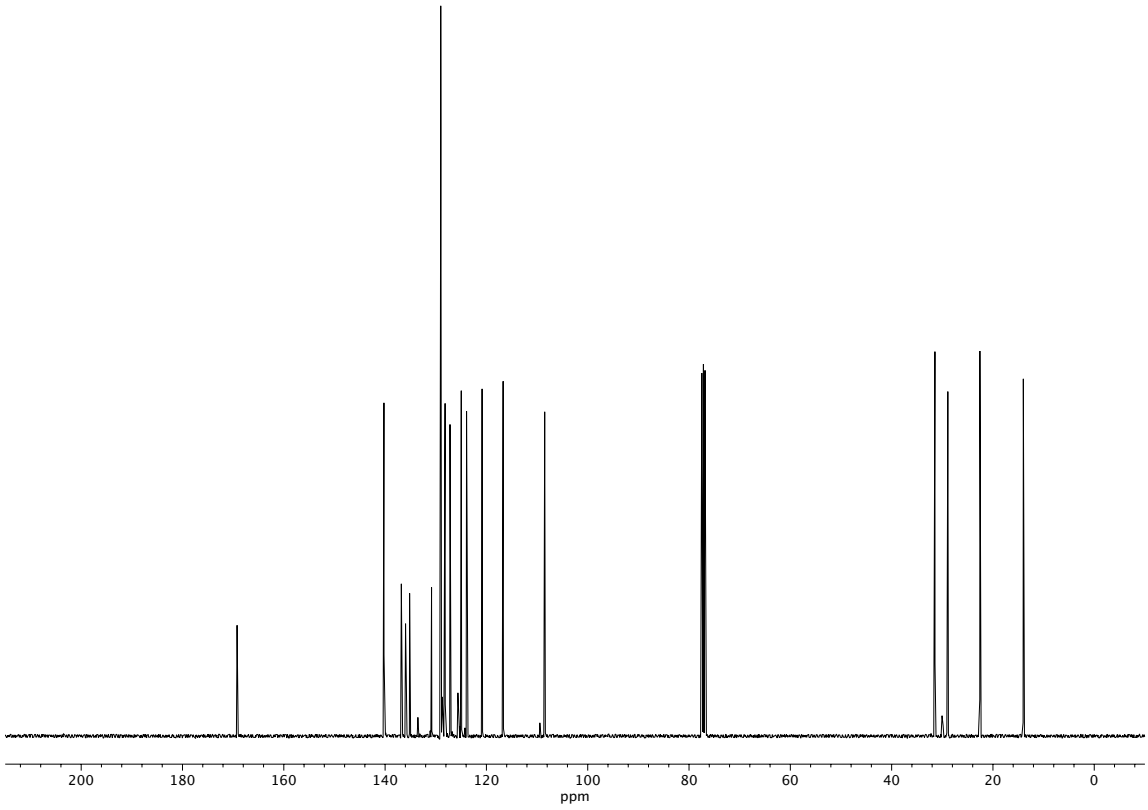

Figure A5.9 *^{13}C NMR (100 MHz, $CDCl_3$) of compound* ***42c****.*

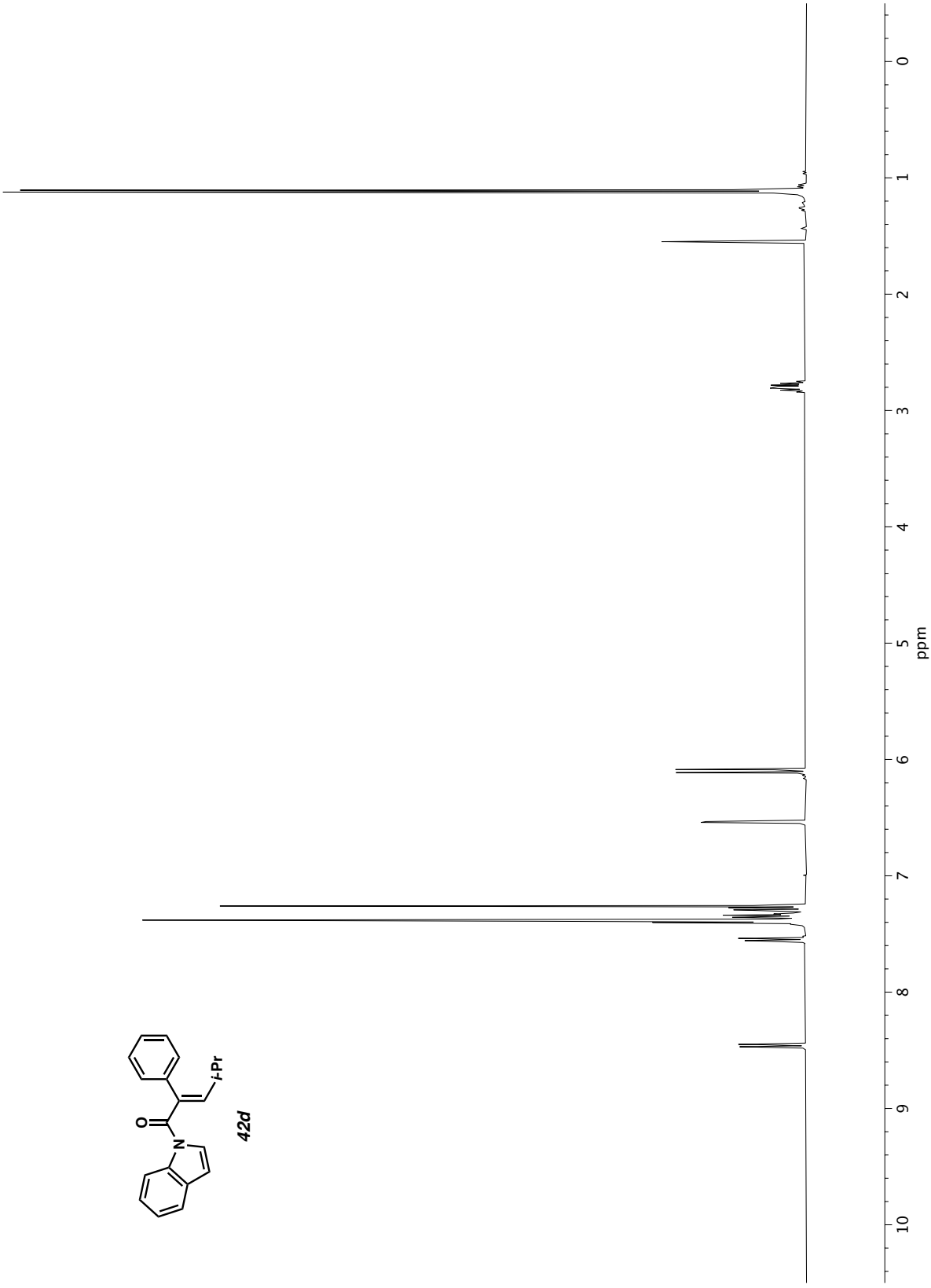

Figure A5.10 *^1H NMR (400 MHz, $CDCl_3$) of compound* ***42d****.*

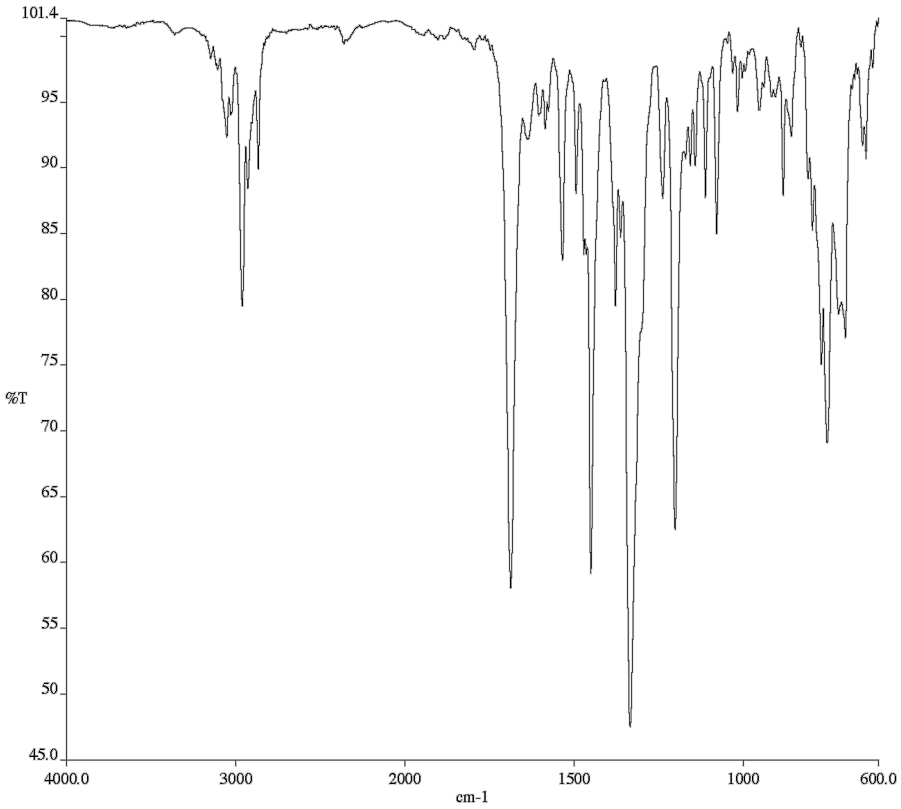

Figure A5.11 *Infrared spectrum (Thin Film, NaCl) of compound* ***42d****.*

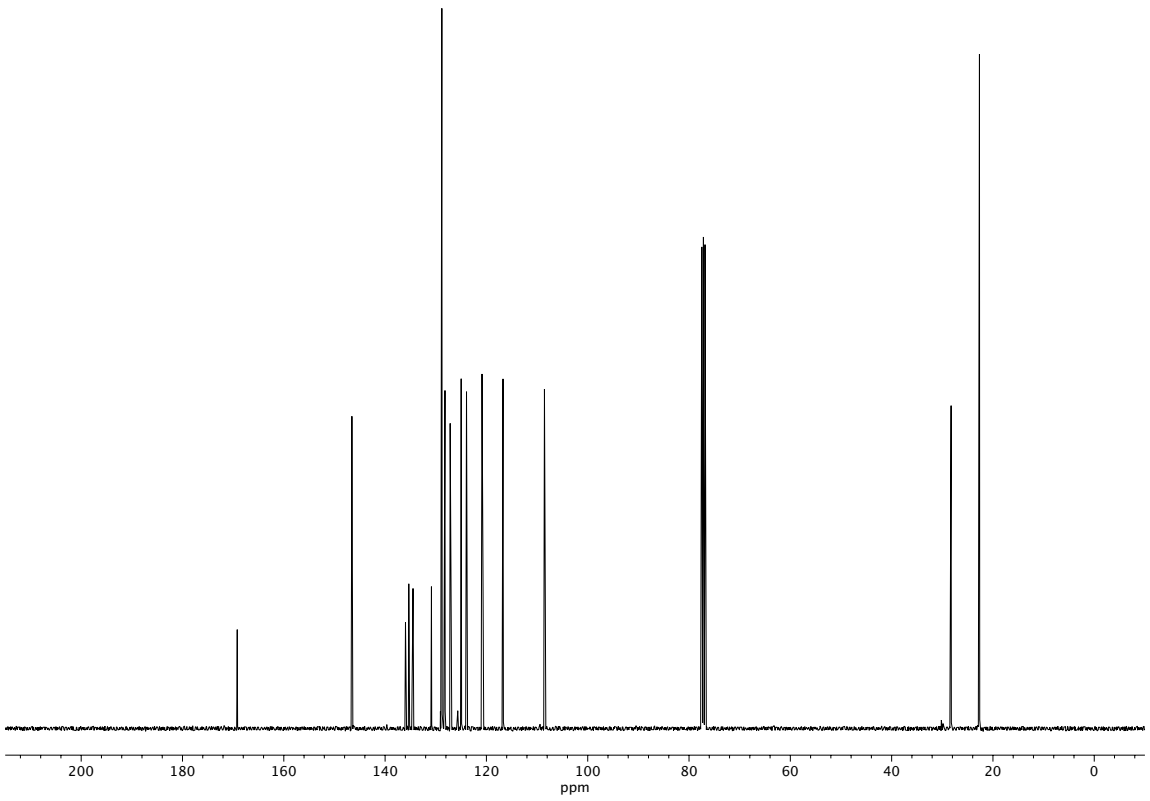

Figure A5.12 *^{13}C NMR (100 MHz, $CDCl_3$) of compound* ***42d****.*

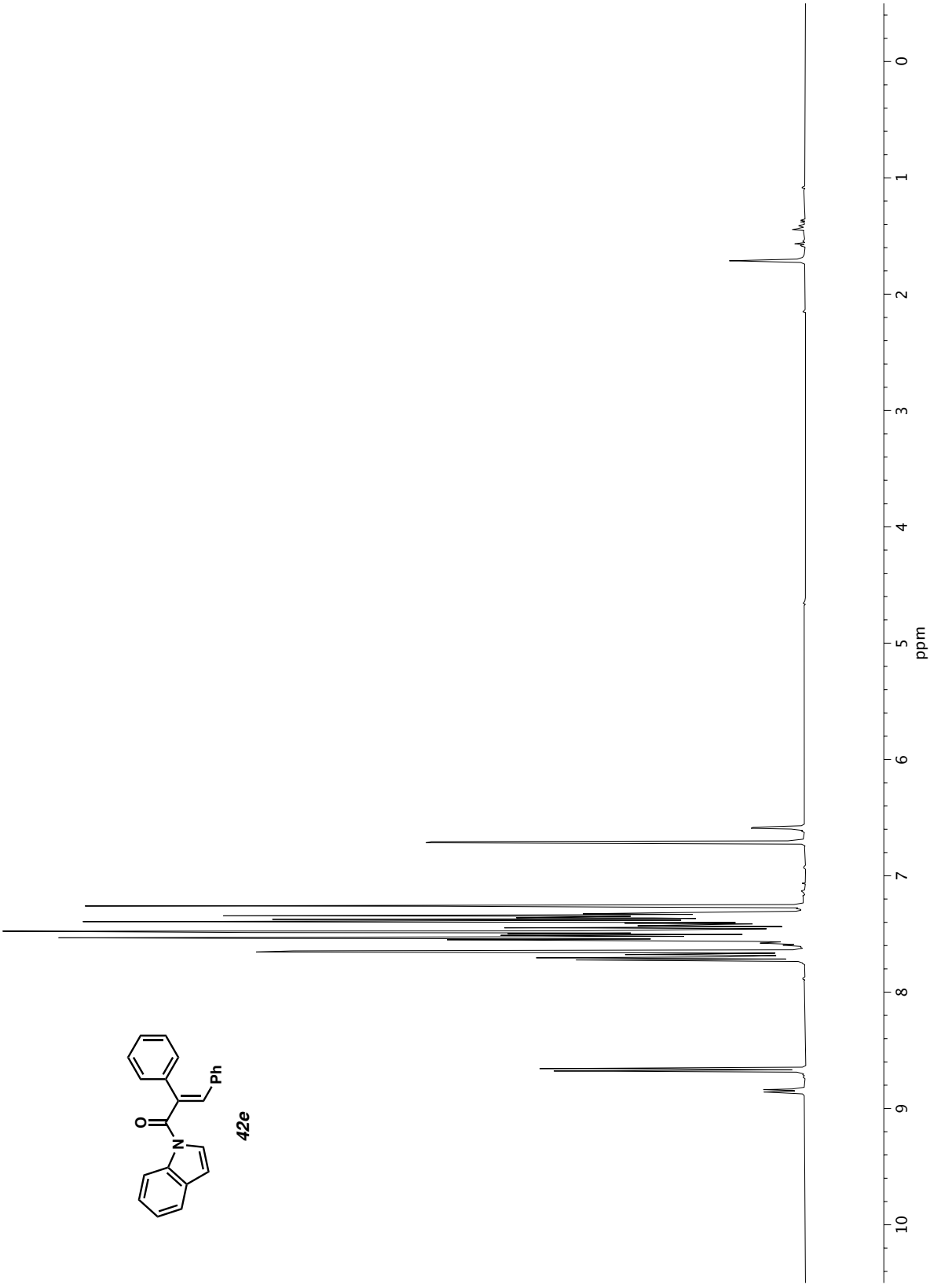

Figure A5.13 *^{1}H NMR (400 MHz, $CDCl_3$) of compound* ***42e****.*

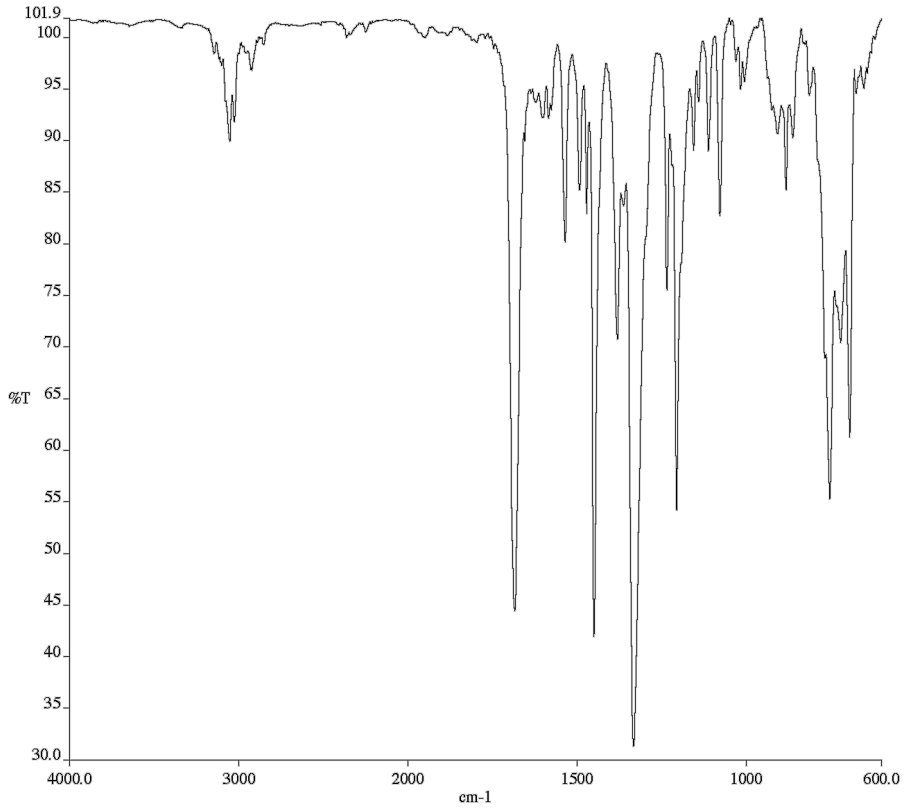

Figure A5.14 *Infrared spectrum (Thin Film, NaCl) of compound* ***42e****.*

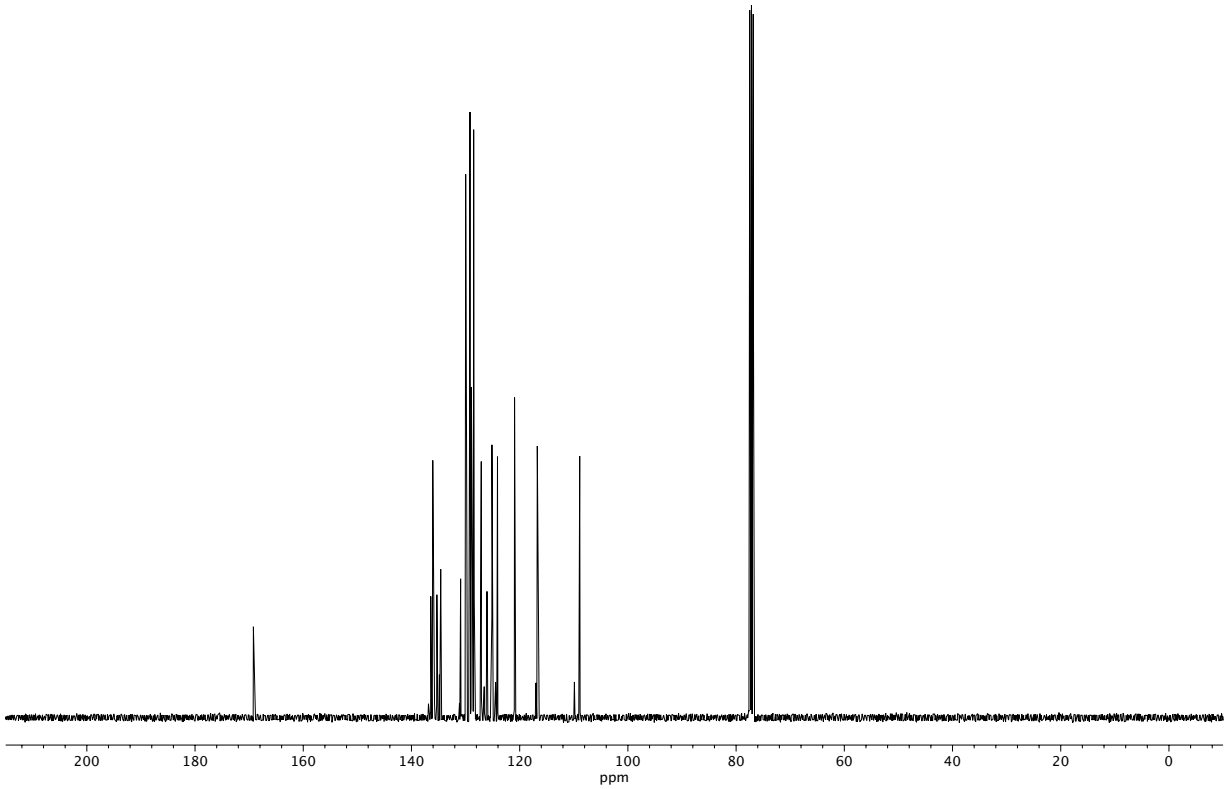

Figure A5.15 *^{13}C NMR (100 MHz, $CDCl_3$) of compound* ***42e****.*

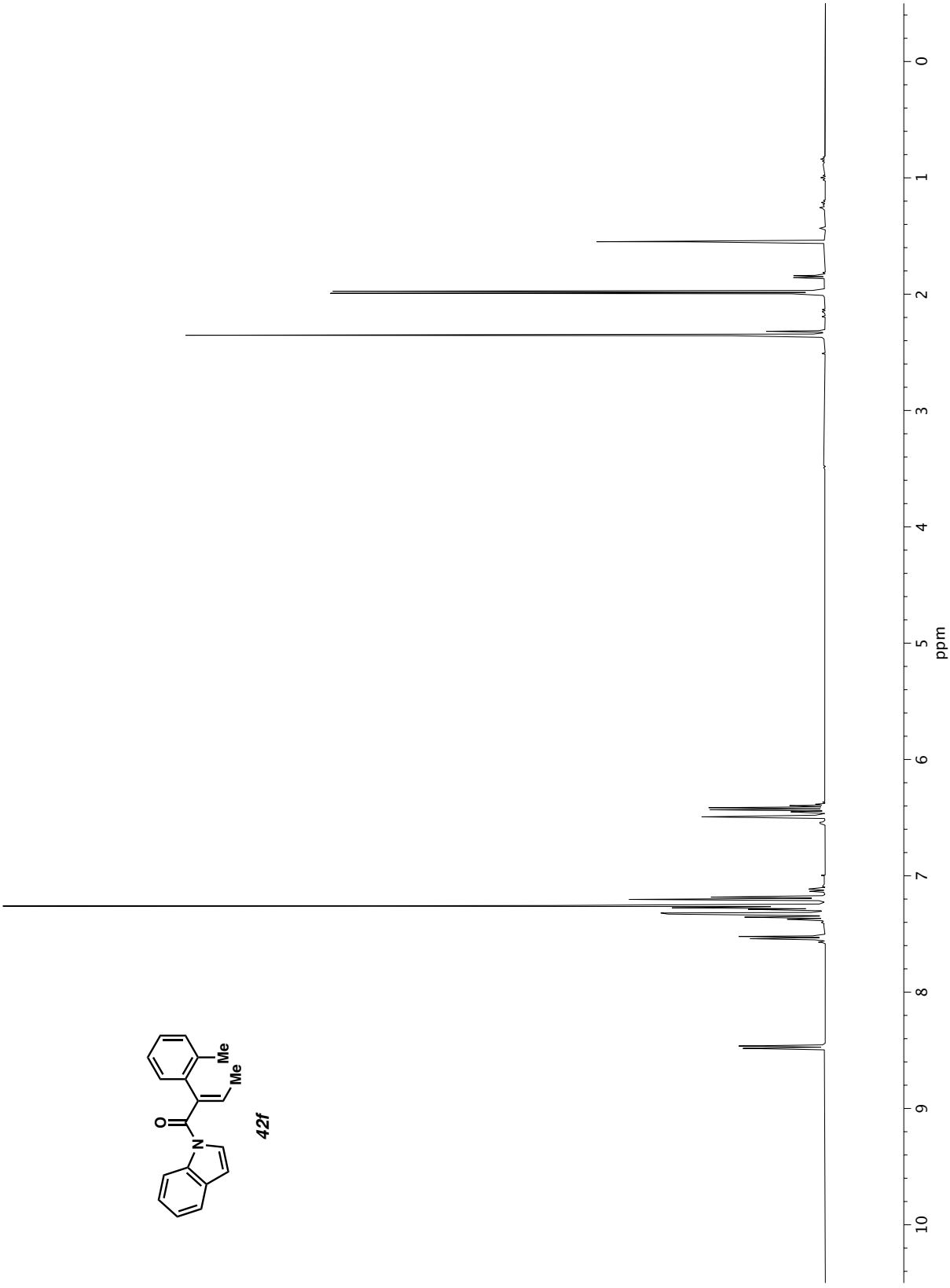

Figure A5.16 *^{1}H NMR (400 MHz, $CDCl_3$) of compound **42f**.*

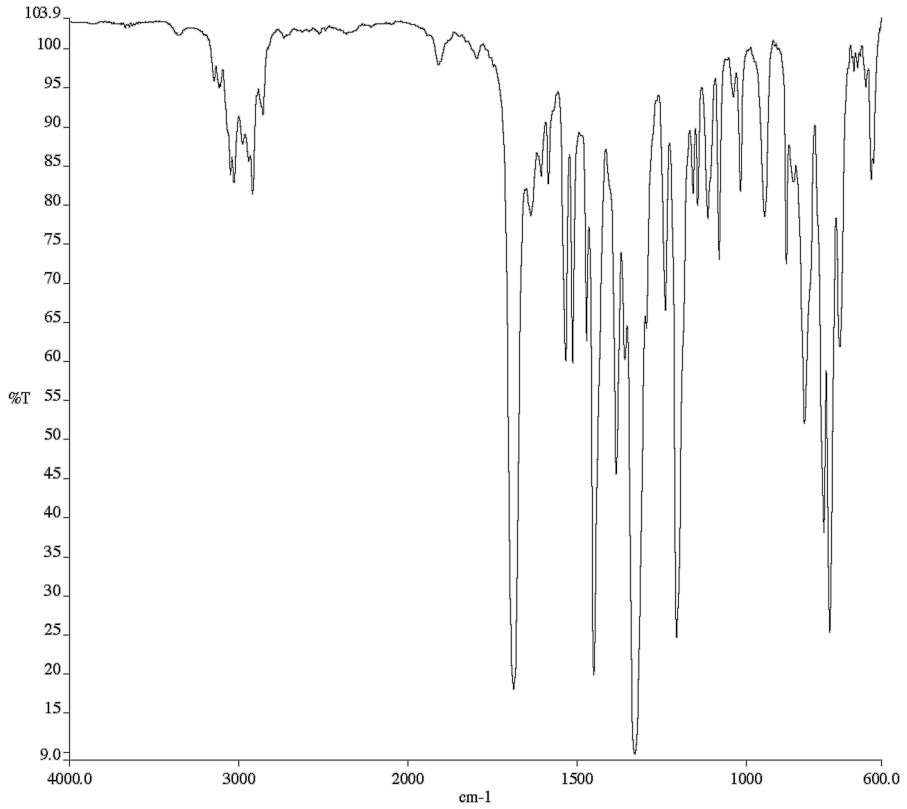

Figure A5.17 *Infrared spectrum (Thin Film, NaCl) of compound* ***42f****.*

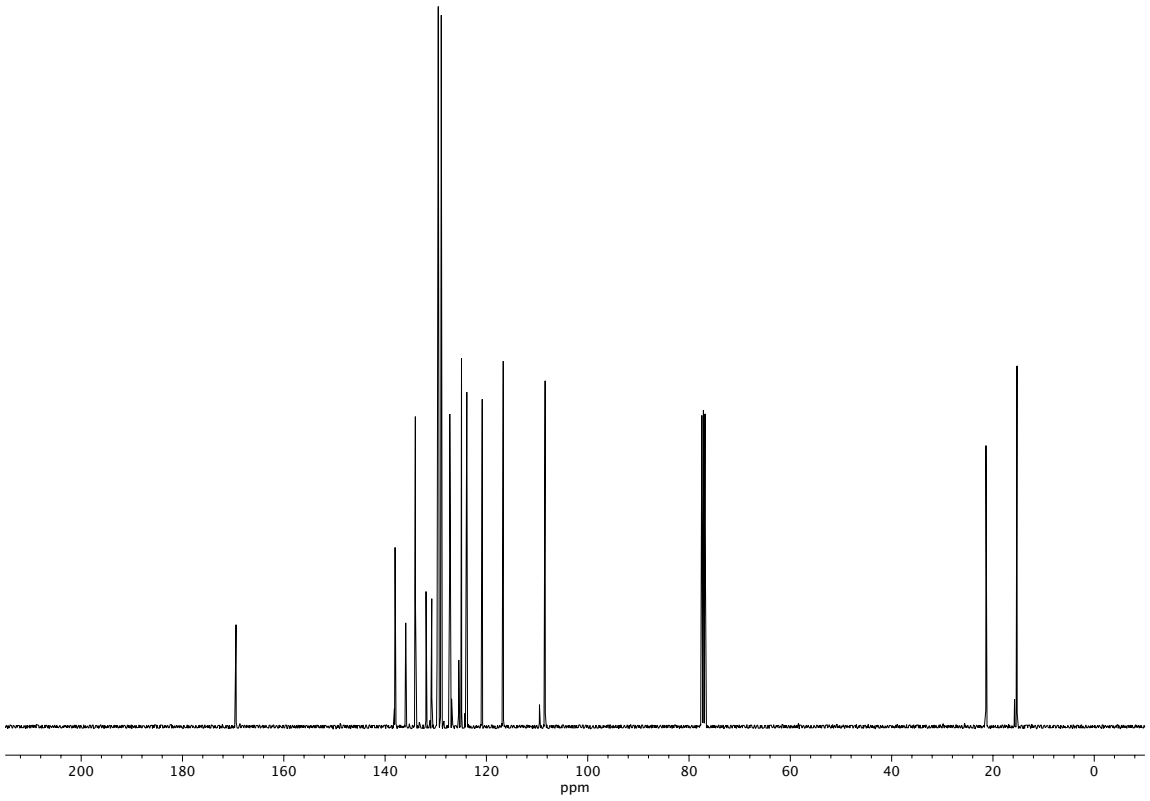

Figure A5.18 *^{13}C NMR (100 MHz, $CDCl_3$) of compound* ***42f****.*

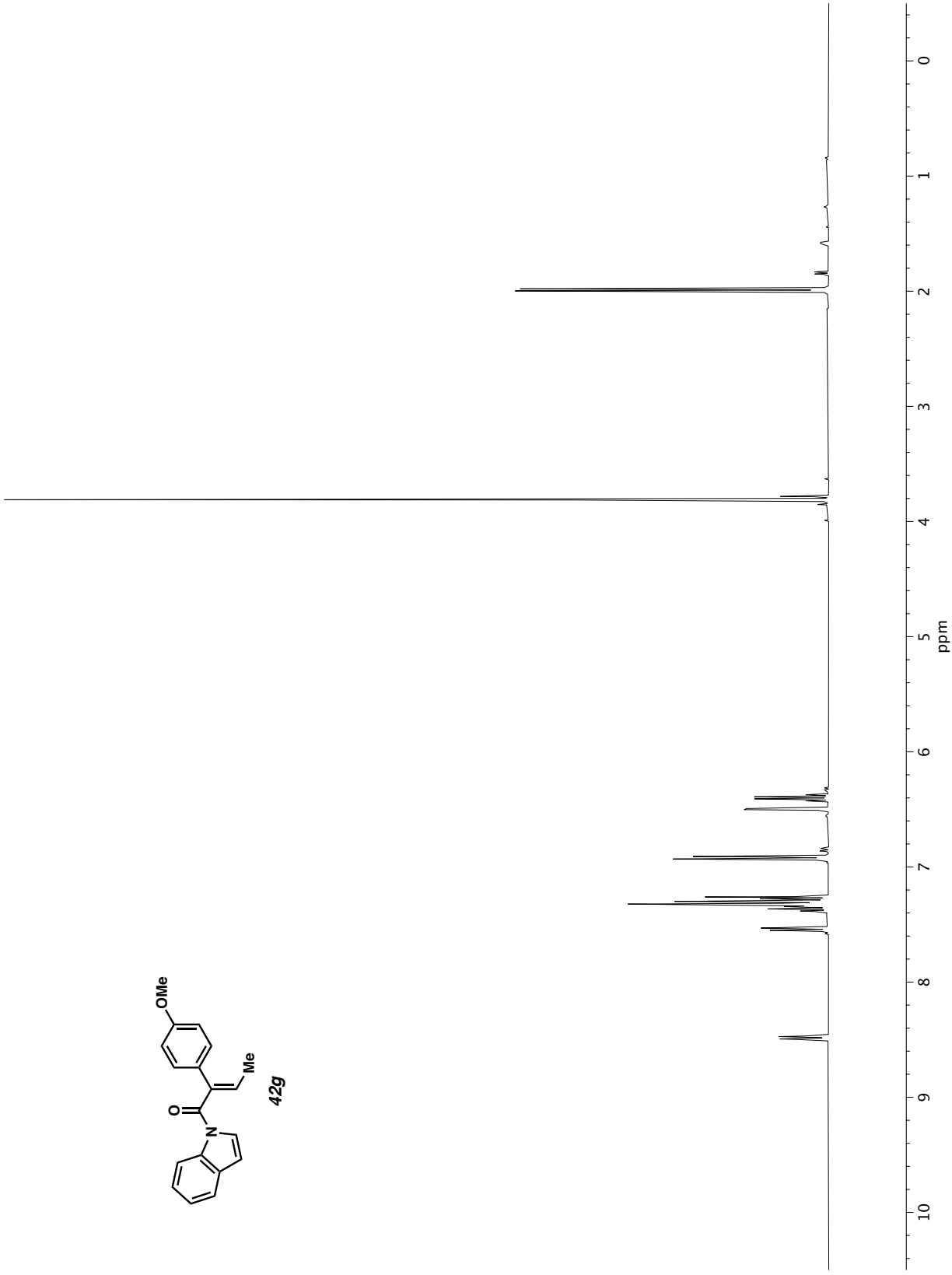

Figure A5.19 *^1H NMR (400 MHz, $CDCl_3$) of compound* ***42g***.

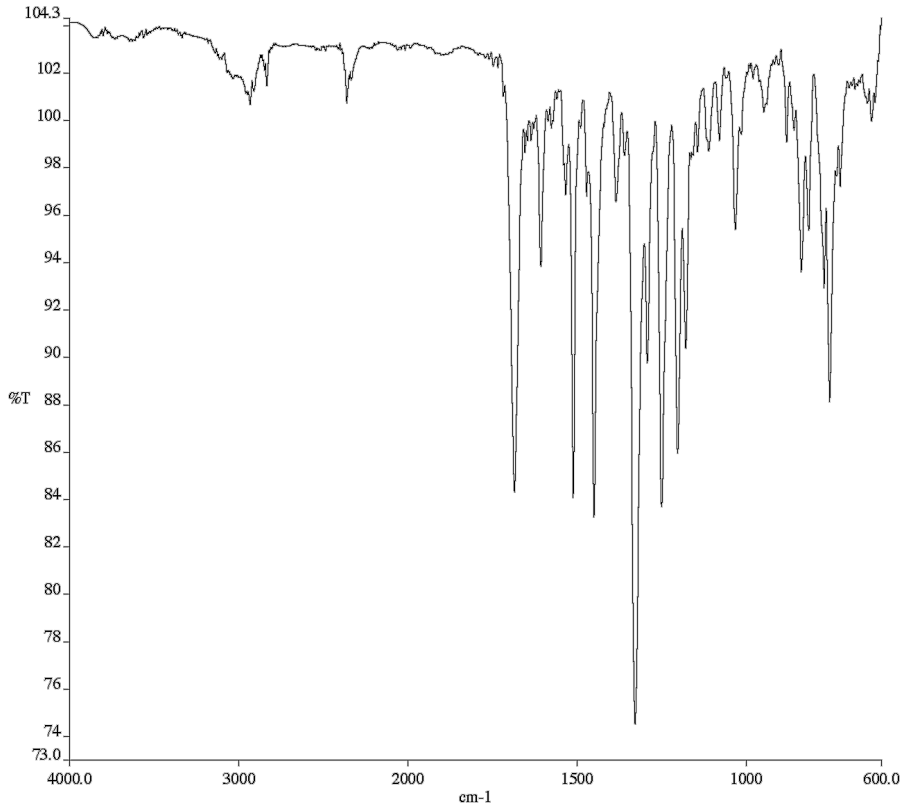

Figure A5.20 *Infrared spectrum (Thin Film, NaCl) of compound* ***42g****.*

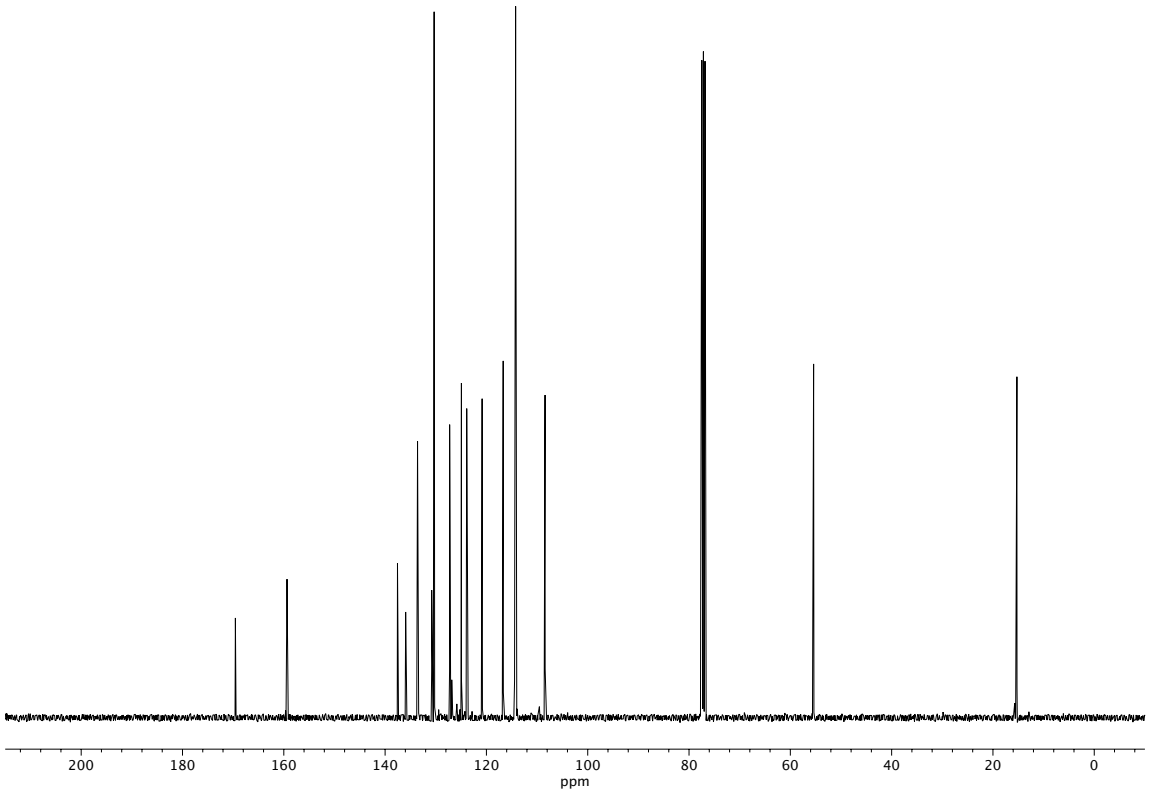

Figure A5.21 *^{13}C NMR (100 MHz, $CDCl_3$) of compound* ***42g****.*

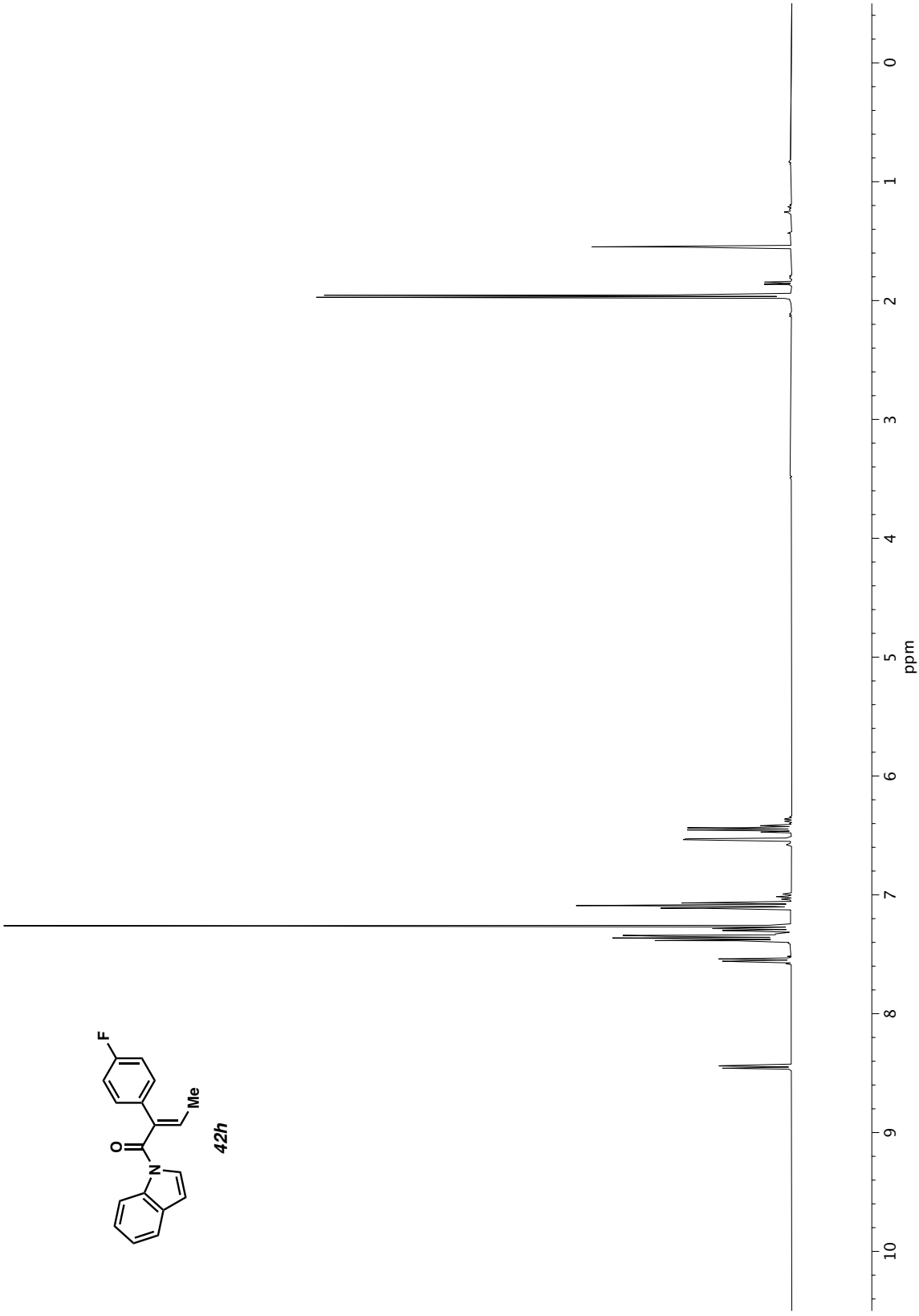

Figure A5.22 *^{1}H NMR (400 MHz, $CDCl_3$) of compound* ***42h****.*

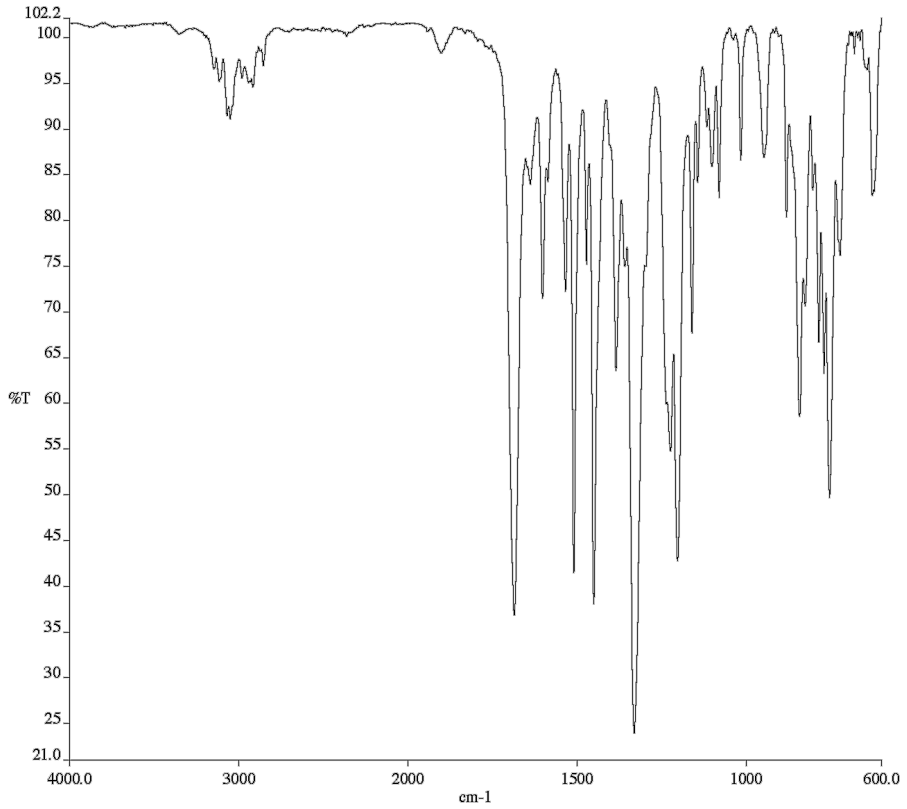

Figure A5.23 *Infrared spectrum (Thin Film, NaCl) of compound* ***42h****.*

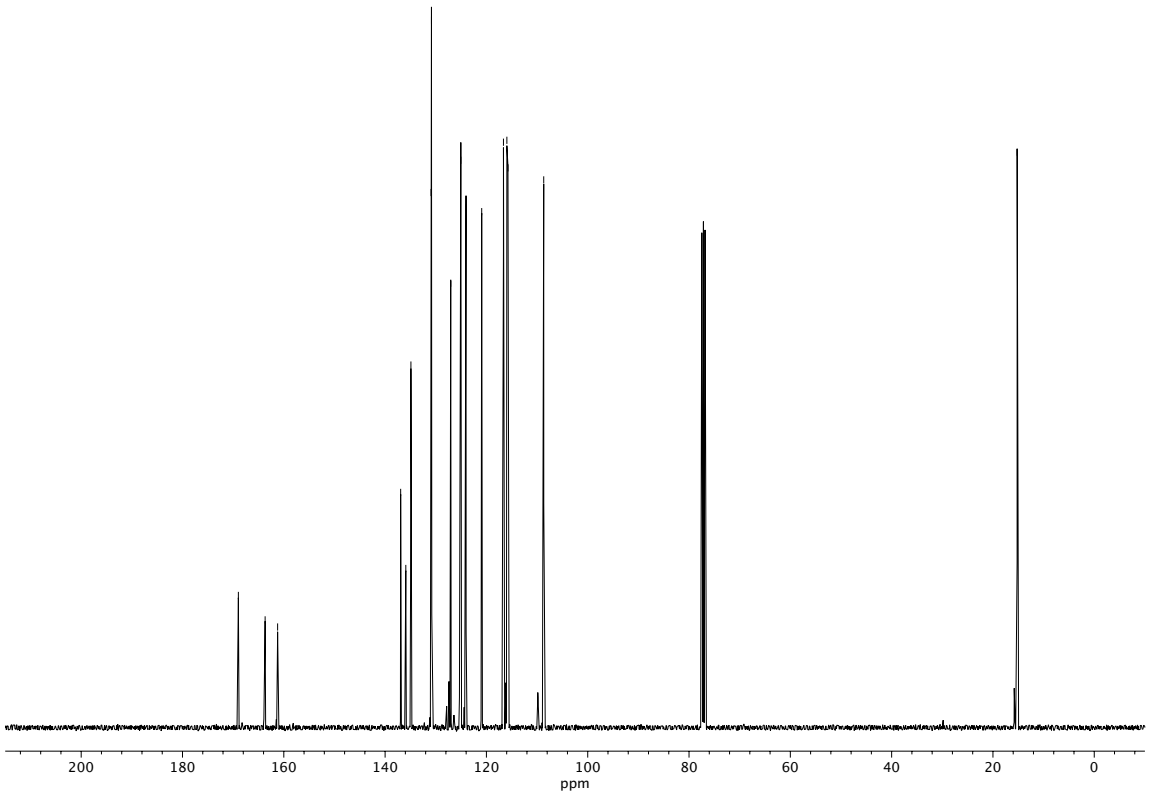

Figure A5.24 *^{13}C NMR (100 MHz, $CDCl_3$) of compound* ***42h****.*

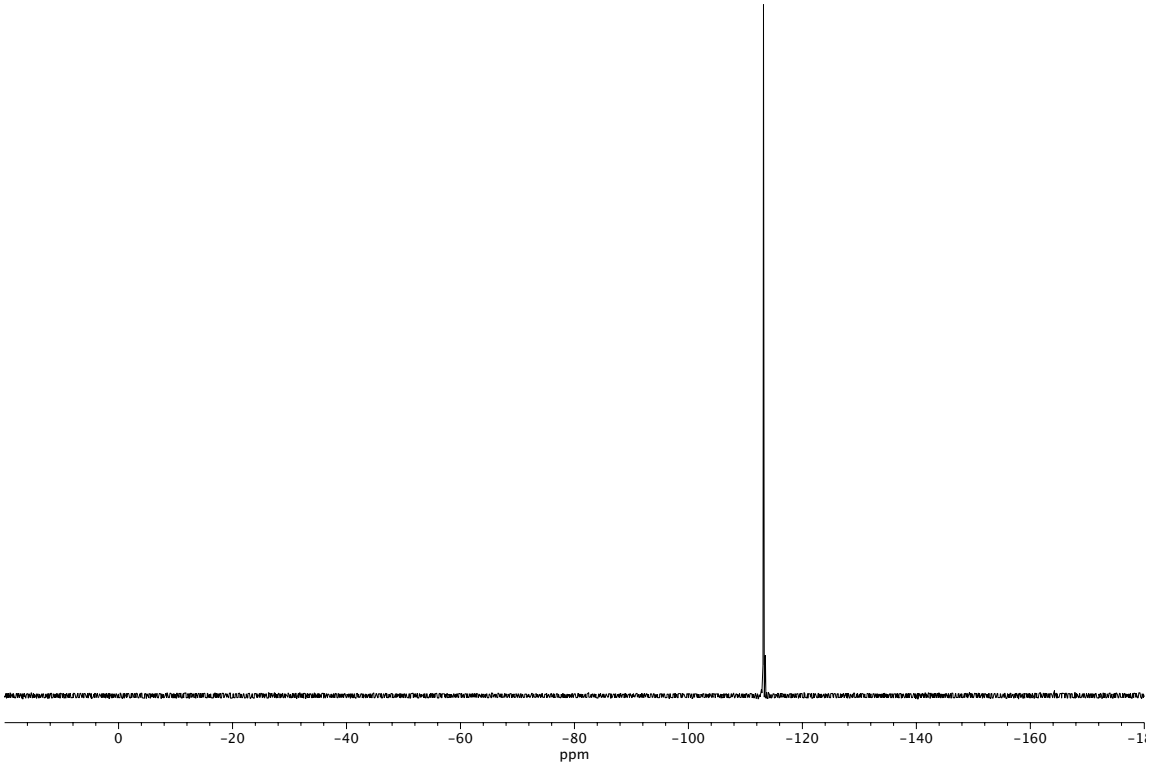

Figure A5.25 *^{19}F NMR (282 MHz, $CDCl_3$) of compound* ***42h.***

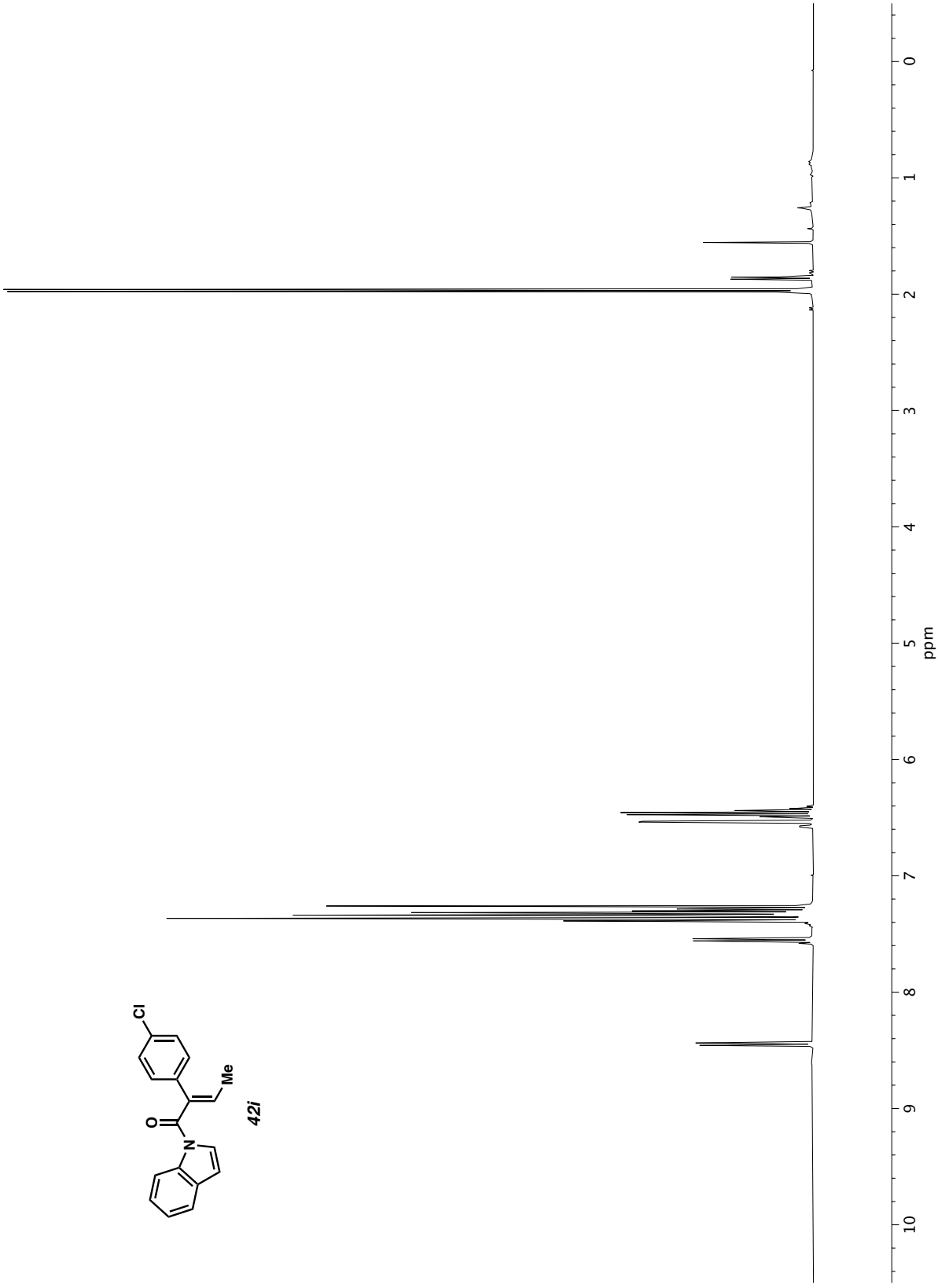

Figure A5.26 *^{1}H NMR (400 MHz, $CDCl_3$) of compound* ***42i****.*

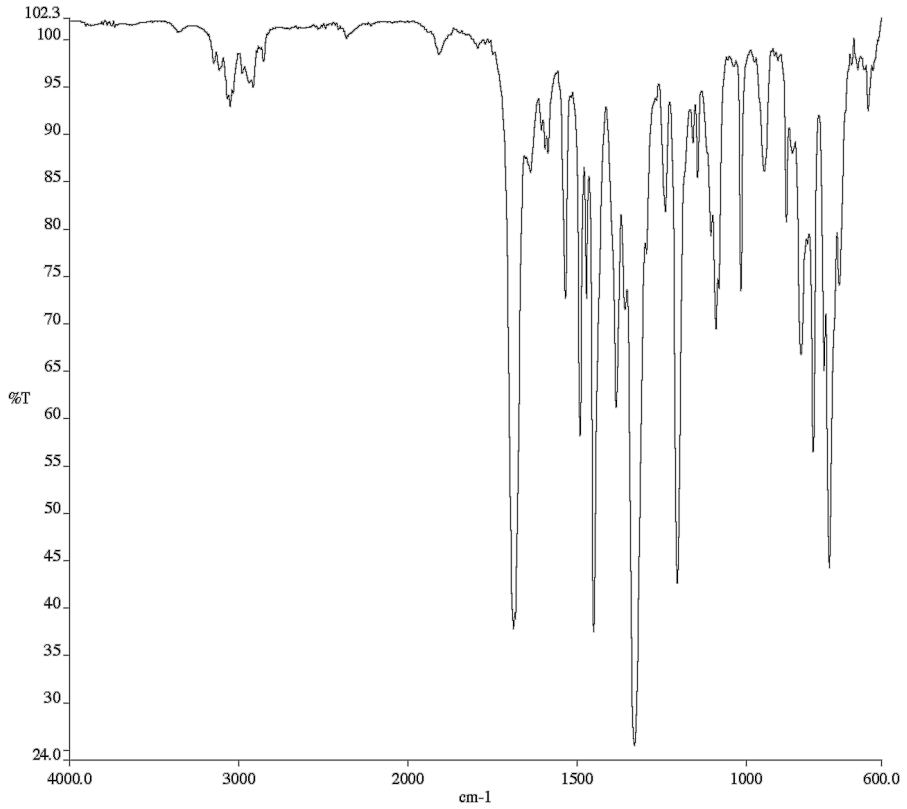

Figure A5.27 *Infrared spectrum (Thin Film, NaCl) of compound* ***42i****.*

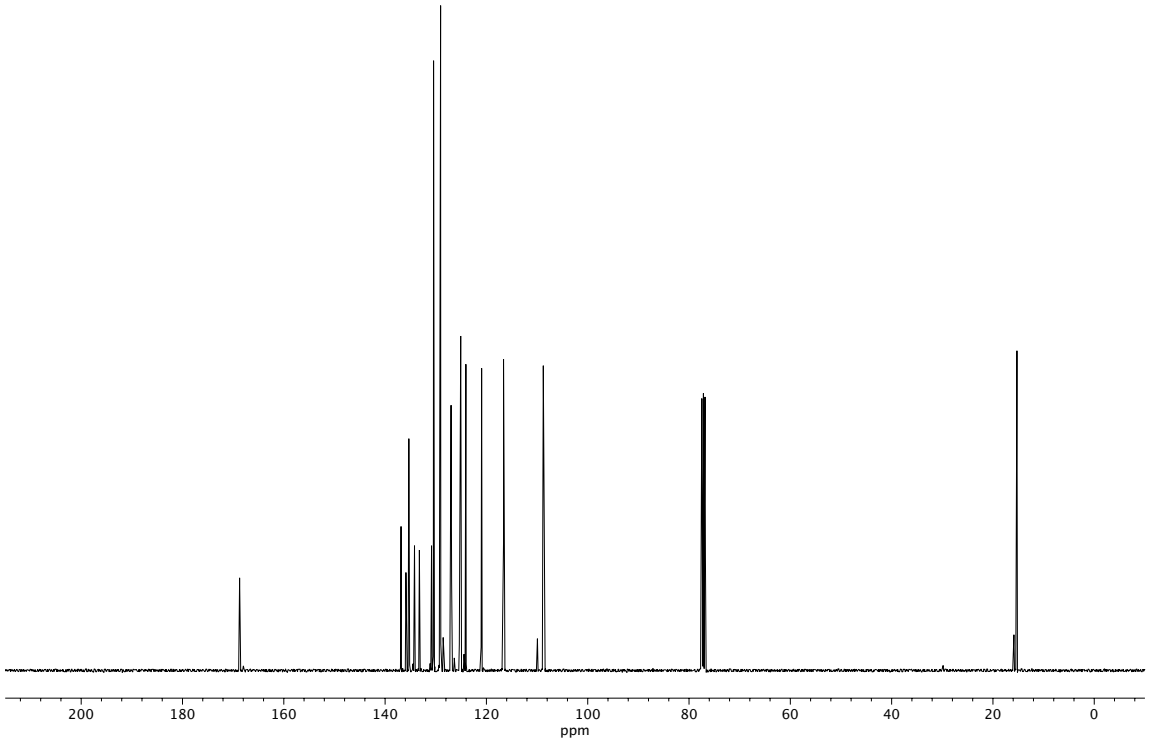

Figure A5.28 *^{13}C NMR (100 MHz, $CDCl_3$) of compound* ***42i****.*

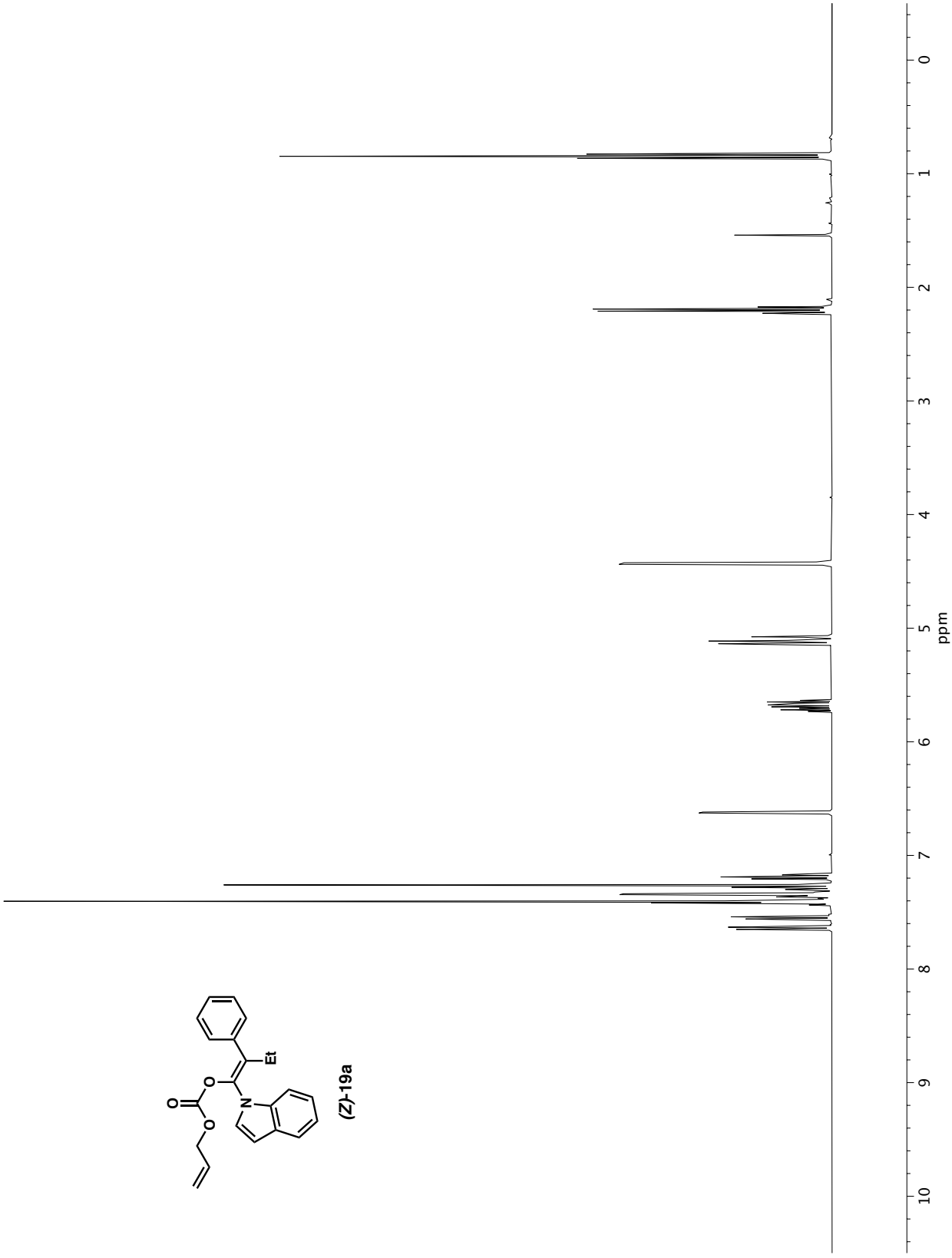

Figure A5.29 *^1H NMR (400 MHz, $CDCl_3$) of compound* ***(Z)-19a***.

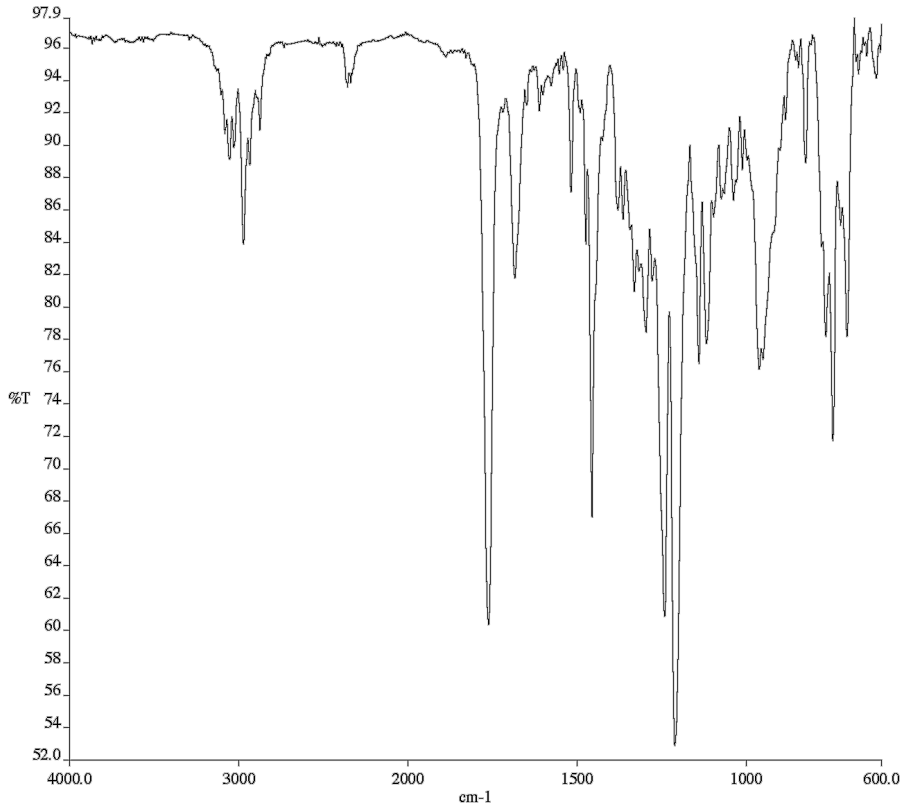

Figure A5.30 *Infrared spectrum (Thin Film, NaCl) of compound* ***(Z)-19a****.*

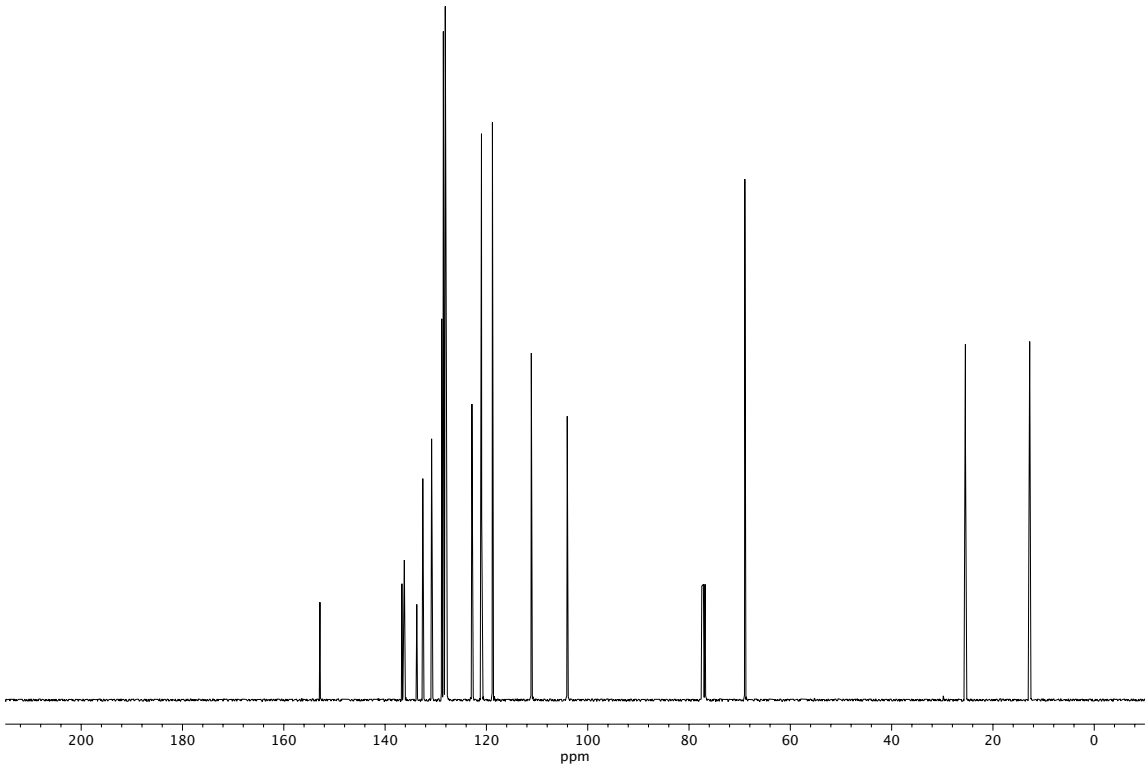

Figure A5.31 *^{13}C NMR (100 MHz, $CDCl_3$) of compound* ***(Z)-19a****.*

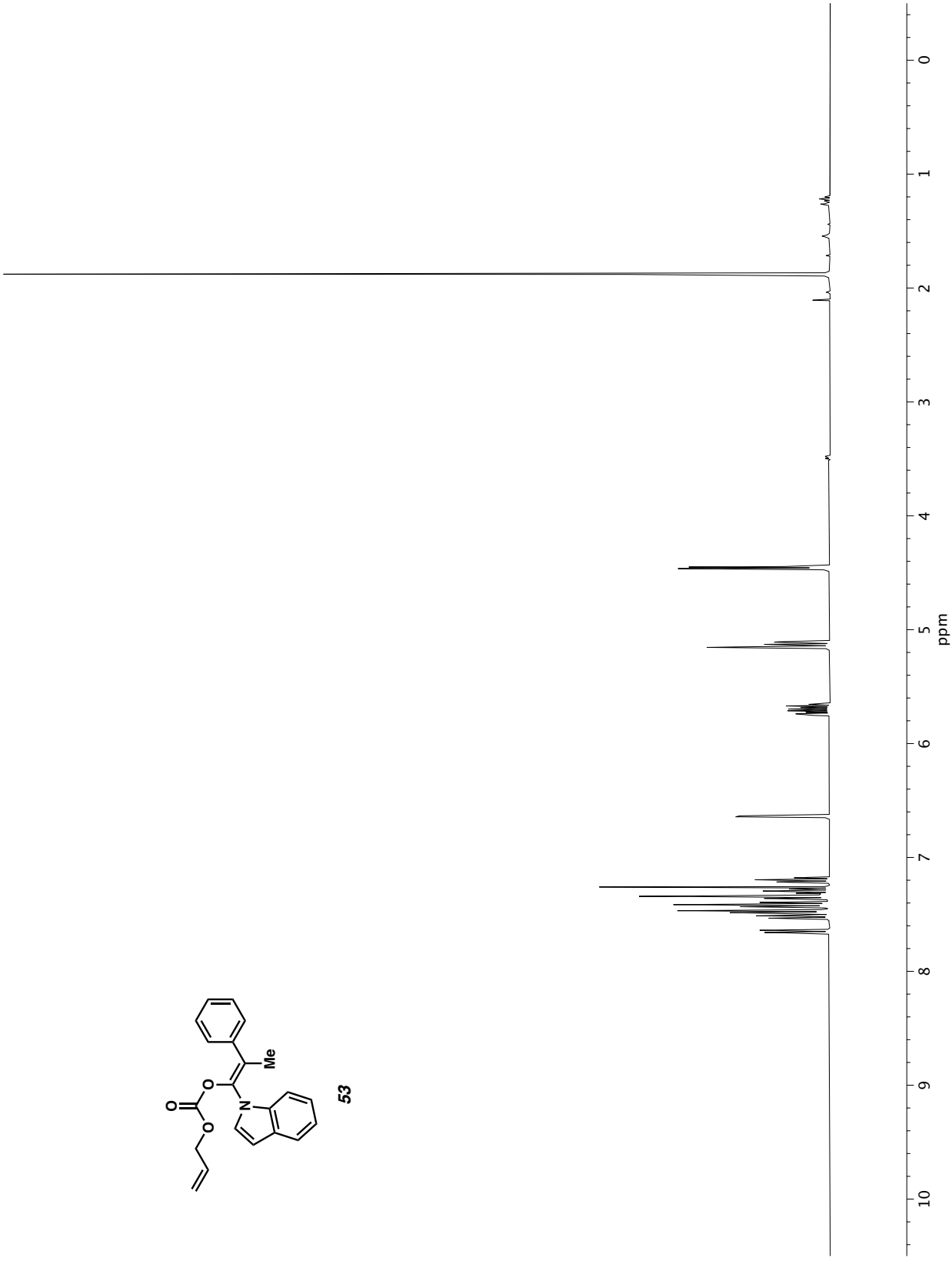

Figure A5.32 *^{1}H NMR (400 MHz, $CDCl_3$) of compound* ***53****.*

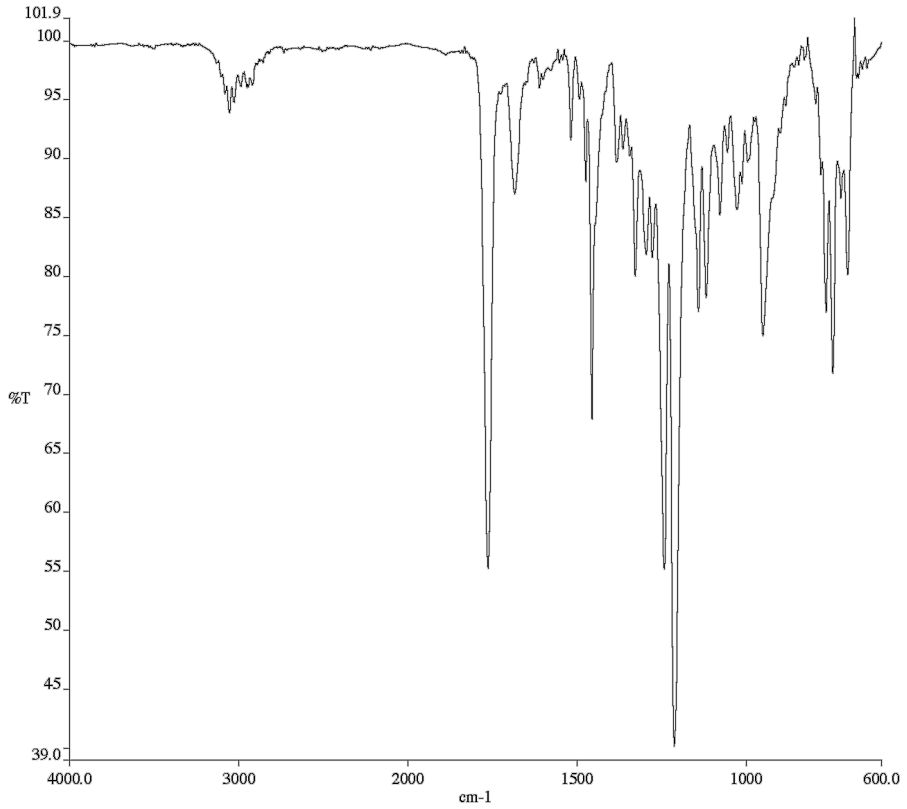

Figure A5.33 *Infrared spectrum (Thin Film, NaCl) of compound* ***53****.*

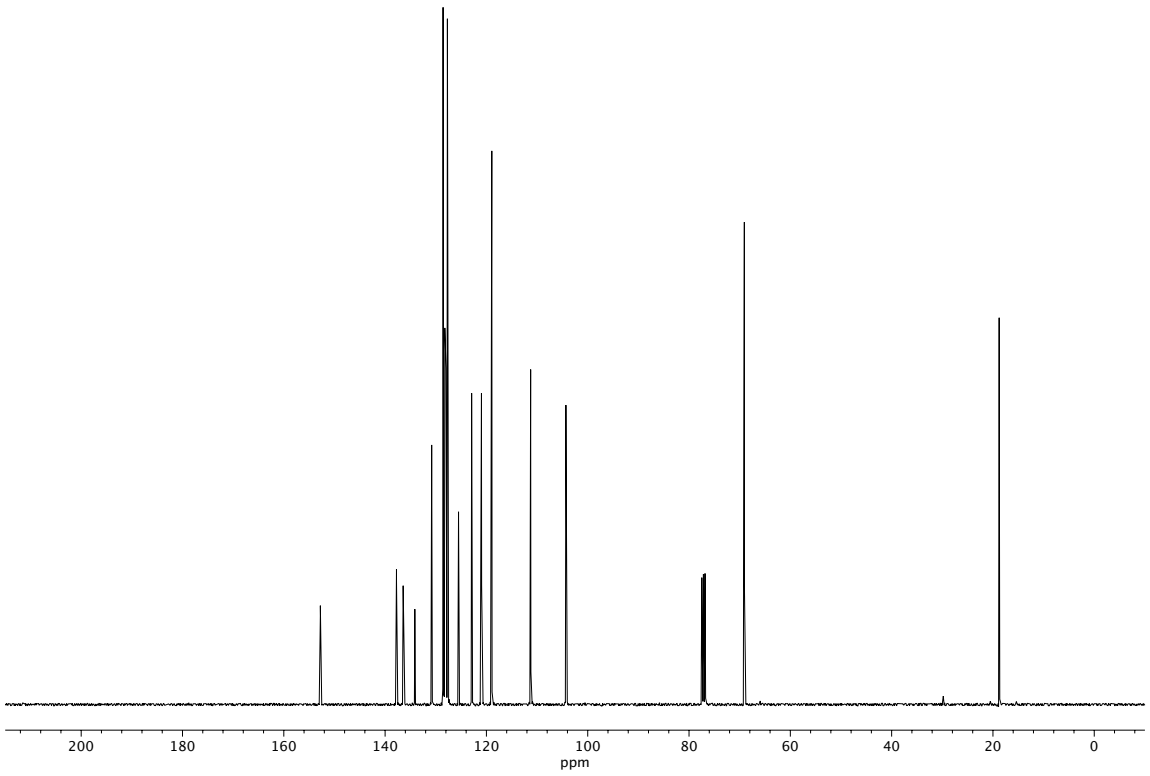

Figure A5.34 *^{13}C NMR (100 MHz, $CDCl_3$) of compound* ***53****.*

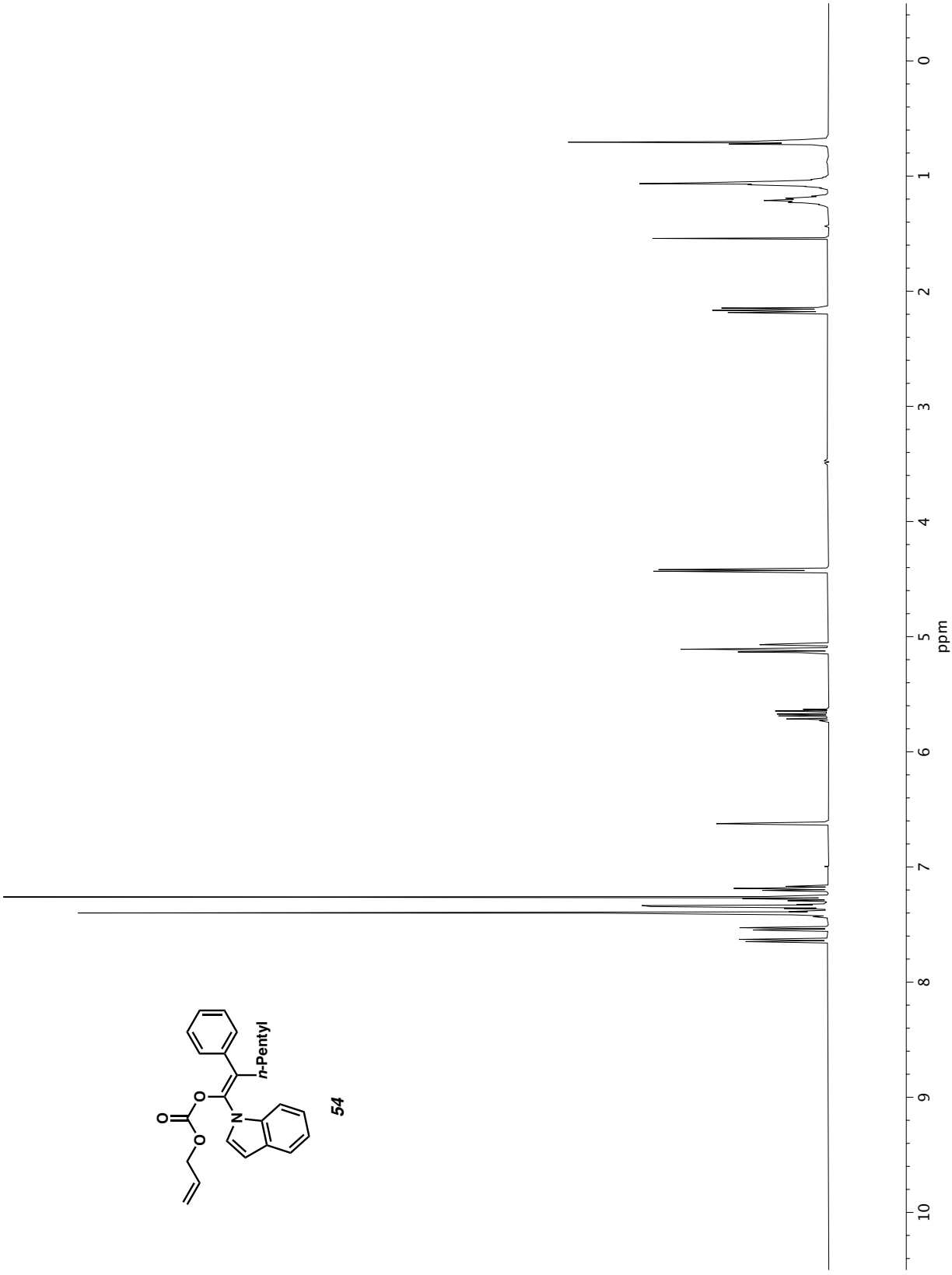

Figure A5.35 *^1H NMR (400 MHz, $CDCl_3$) of compound **54**.*

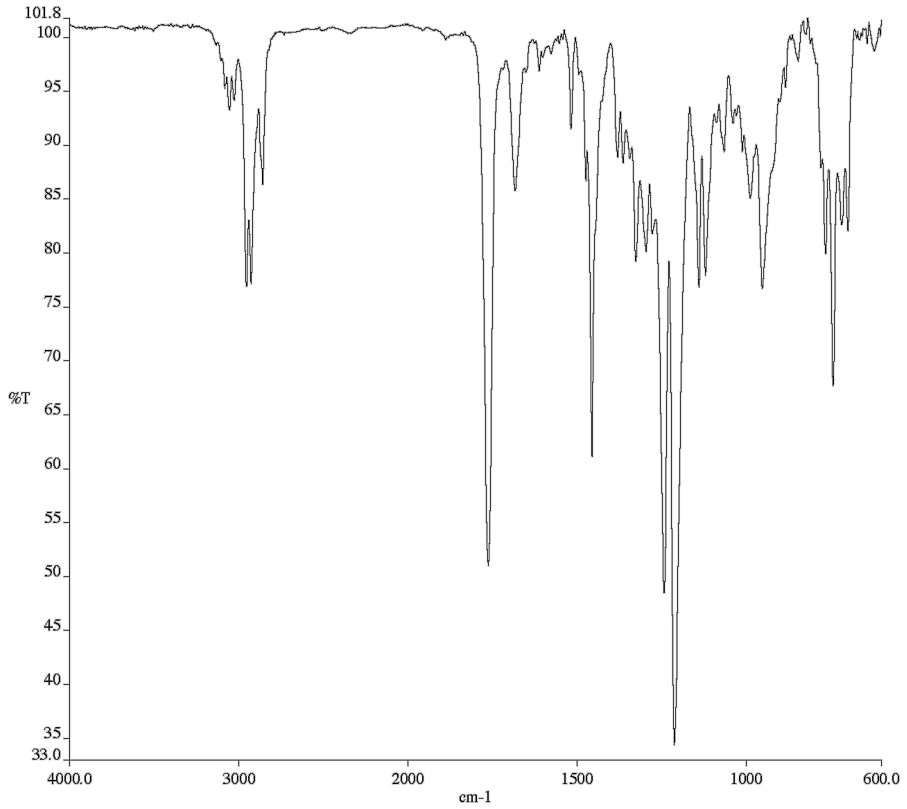

Figure A5.36 *Infrared spectrum (Thin Film, NaCl) of compound* ***54****.*

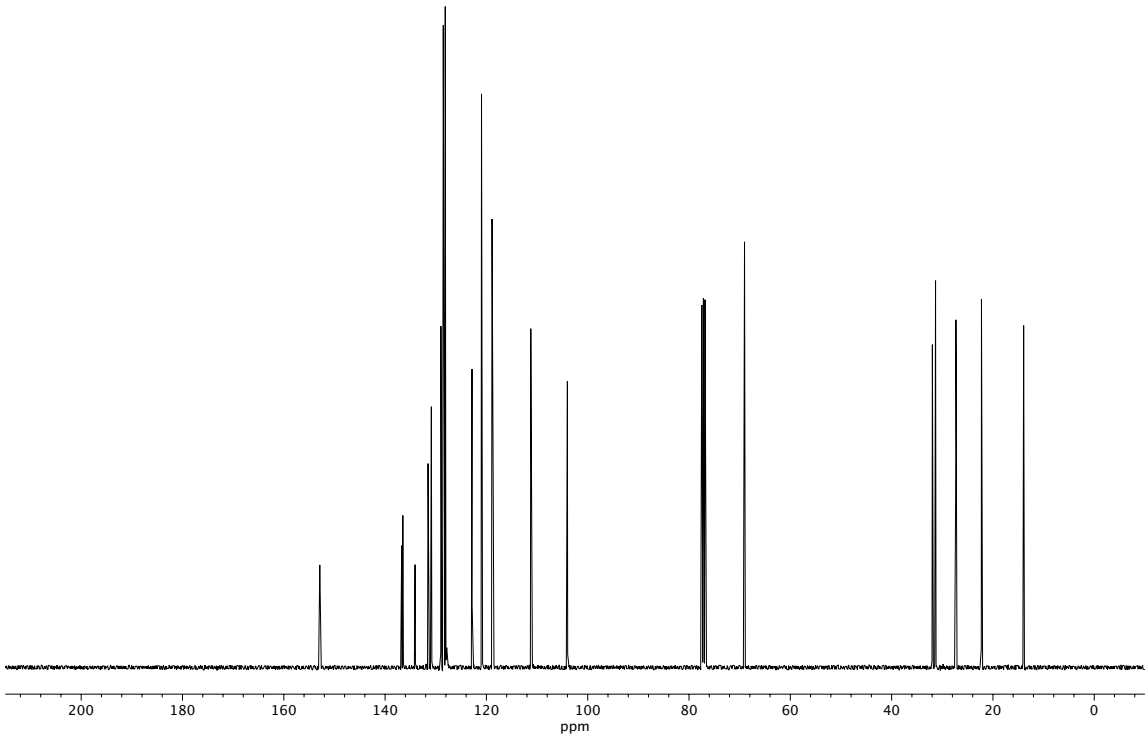

Figure A5.37 *^{13}C NMR (100 MHz, $CDCl_3$) of compound* ***54****.*

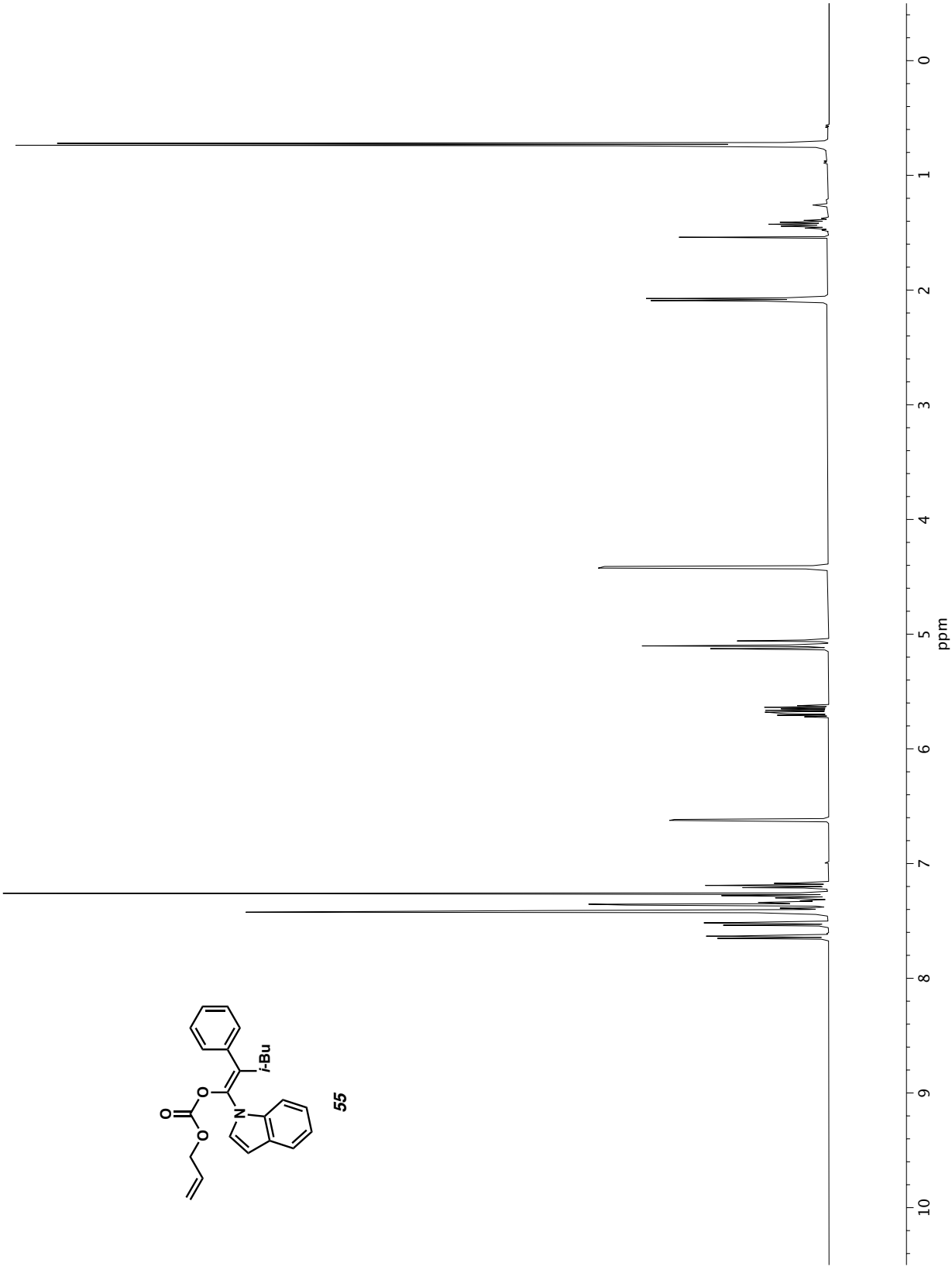

Figure A5.38 *^{1}H NMR (400 MHz, $CDCl_3$) of compound* ***55****.*

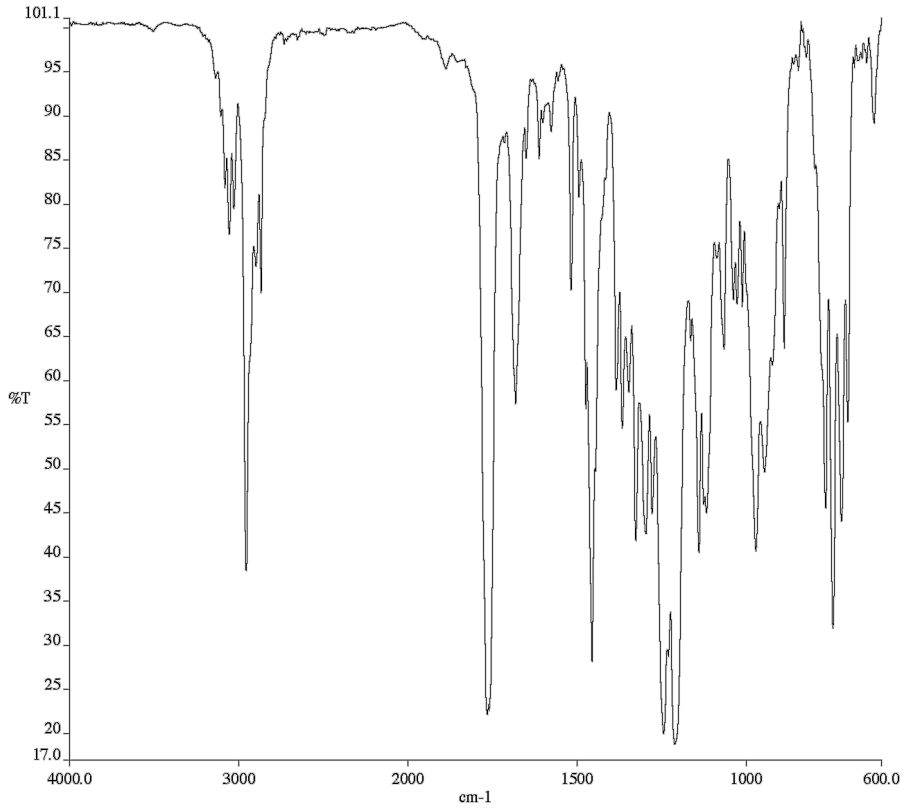

Figure A5.39 *Infrared spectrum (Thin Film, NaCl) of compound* ***55****.*

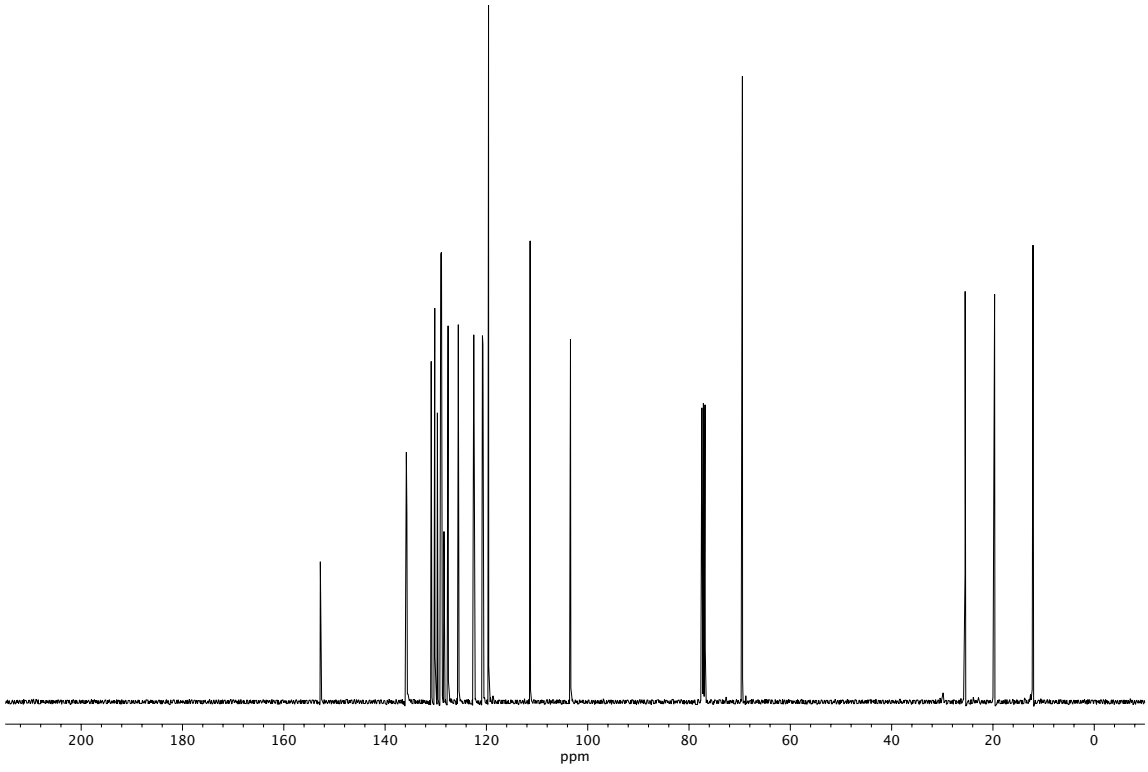

Figure A5.40 *^{13}C NMR (100 MHz, $CDCl_3$) of compound* ***55****.*

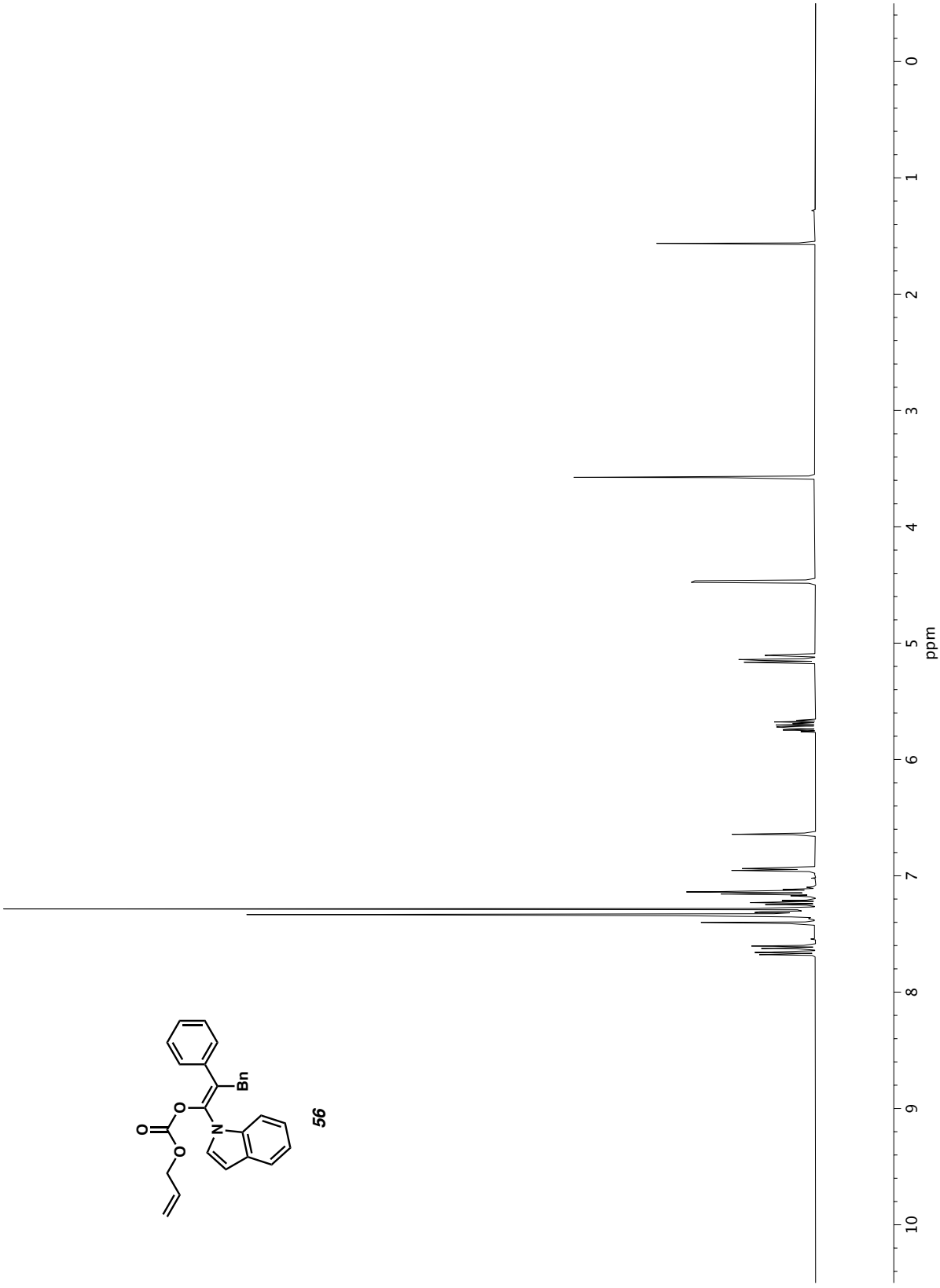

Figure A5.41 *^{1}H NMR (400 MHz, $CDCl_3$) of compound **56**.*

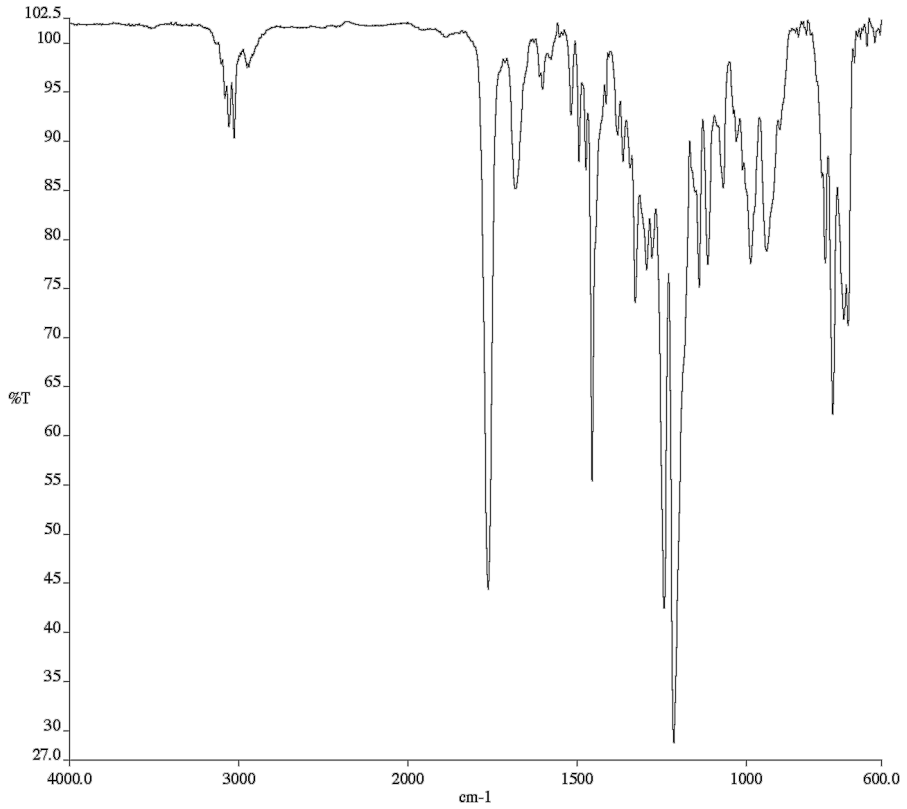

Figure A5.42 *Infrared spectrum (Thin Film, NaCl) of compound* ***56****.*

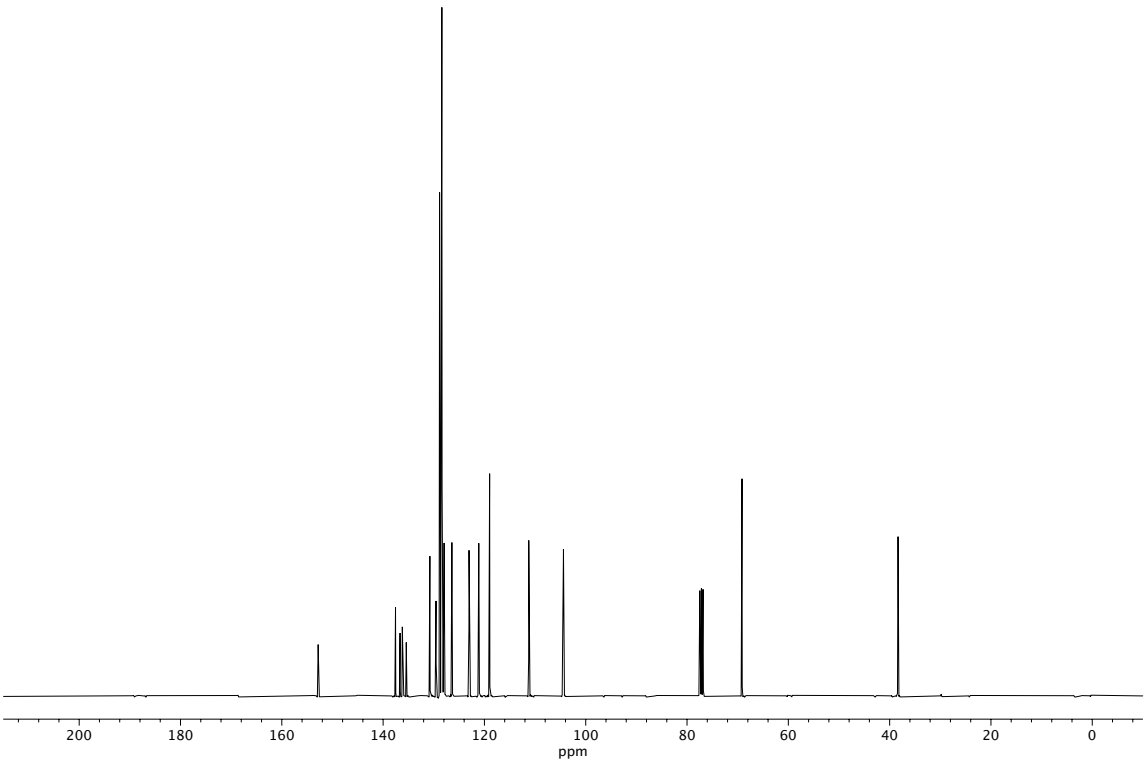

Figure A5.42 *^{13}C NMR (100 MHz, $CDCl_3$) of compound* ***56****.*

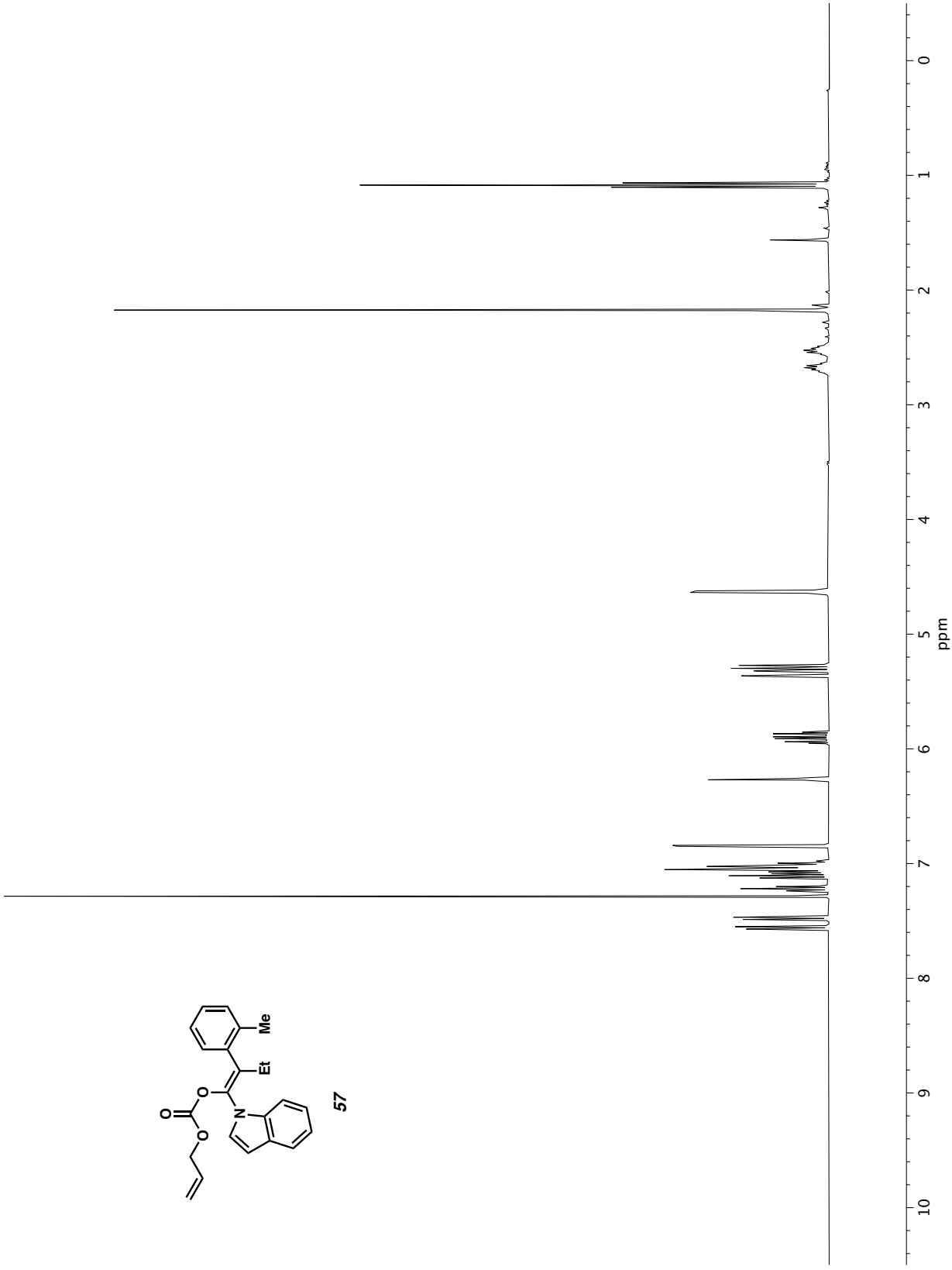

Figure A5.43 *^1H NMR (400 MHz, $CDCl_3$) of compound* ***57****.*

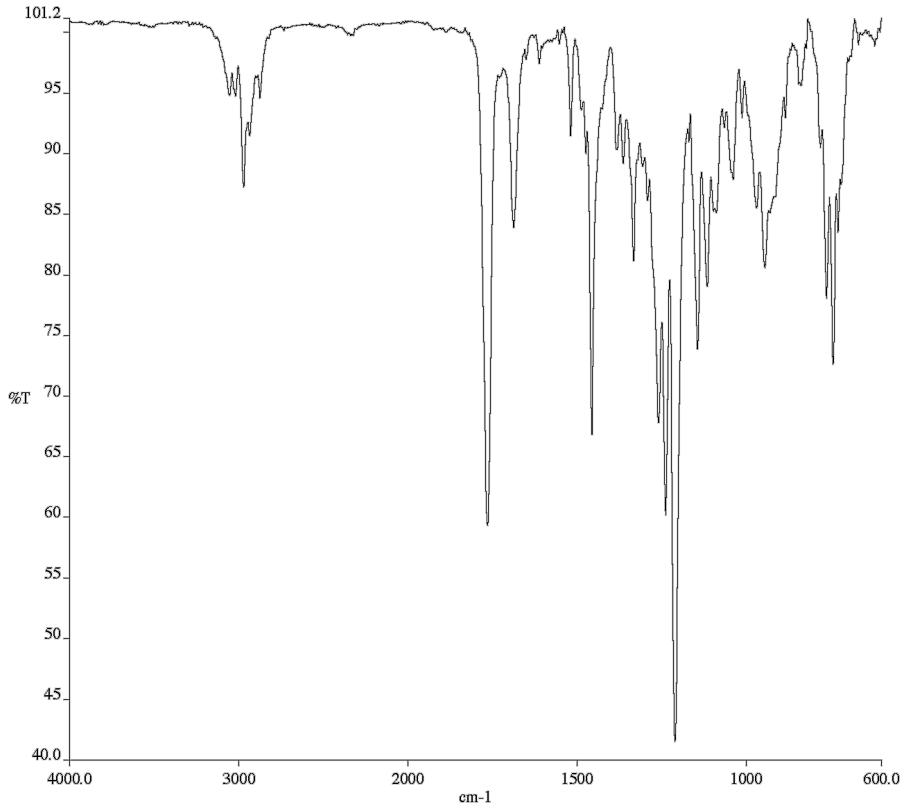

Figure A5.44 *Infrared spectrum (Thin Film, NaCl) of compound* ***57****.*

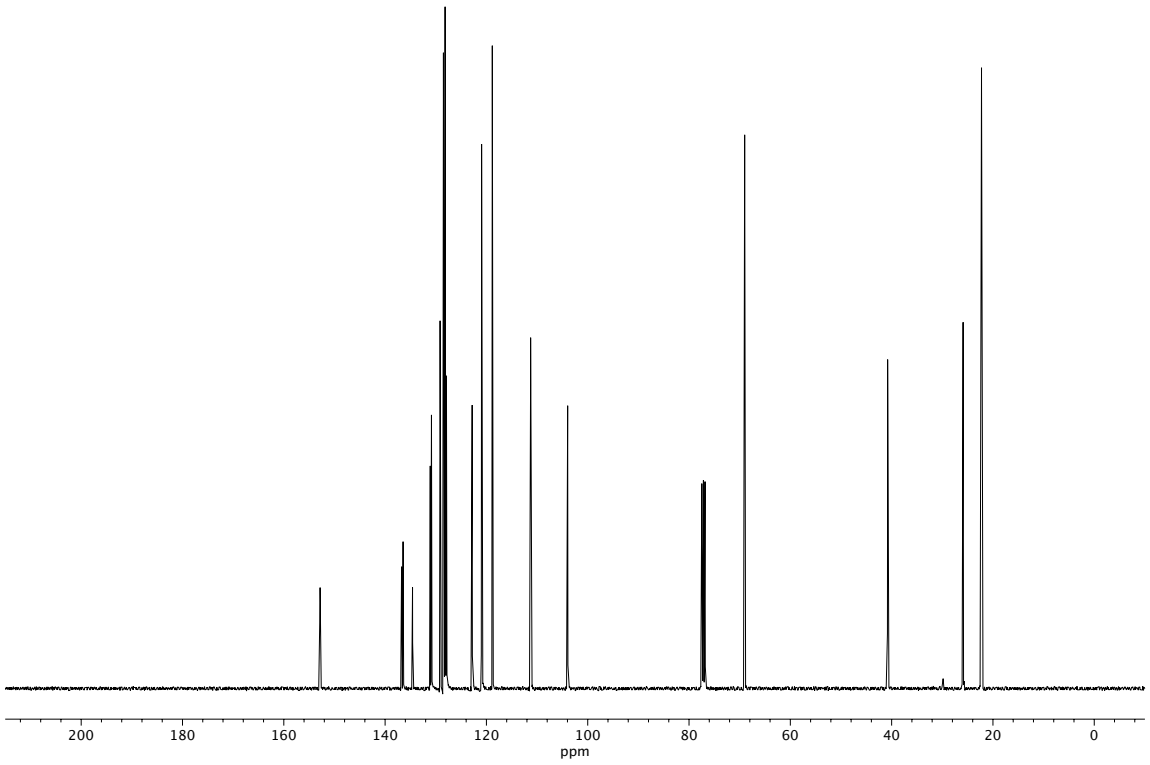

Figure A5.45 *^{13}C NMR (100 MHz, $CDCl_3$) of compound* ***57****.*

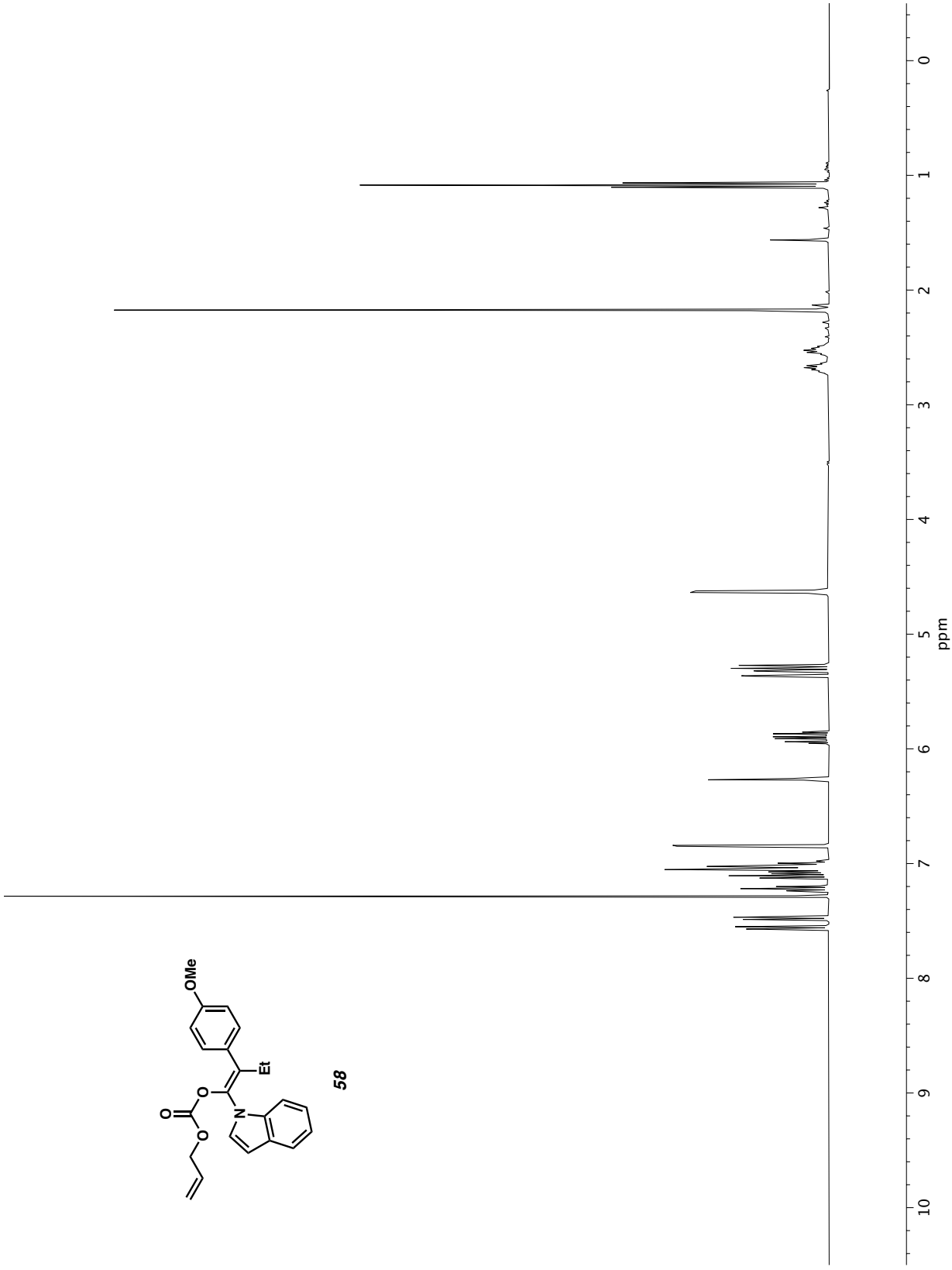

Figure A5.46 *^{1}H NMR (400 MHz, $CDCl_3$) of compound* ***58****.*

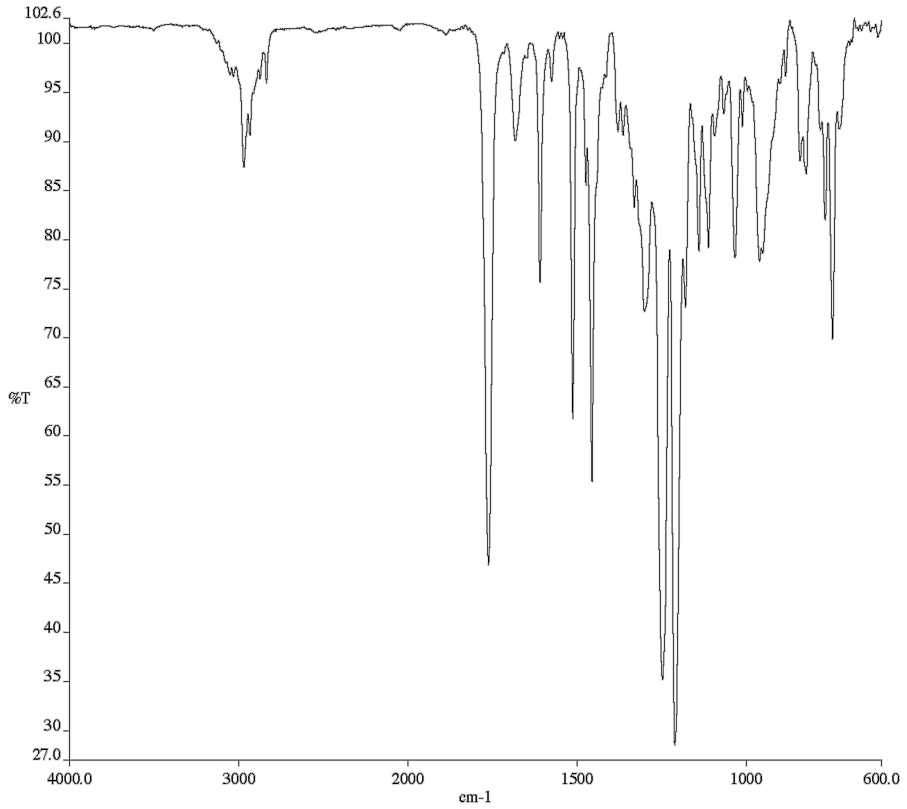

Figure A5.47 *Infrared spectrum (Thin Film, NaCl) of compound* ***58****.*

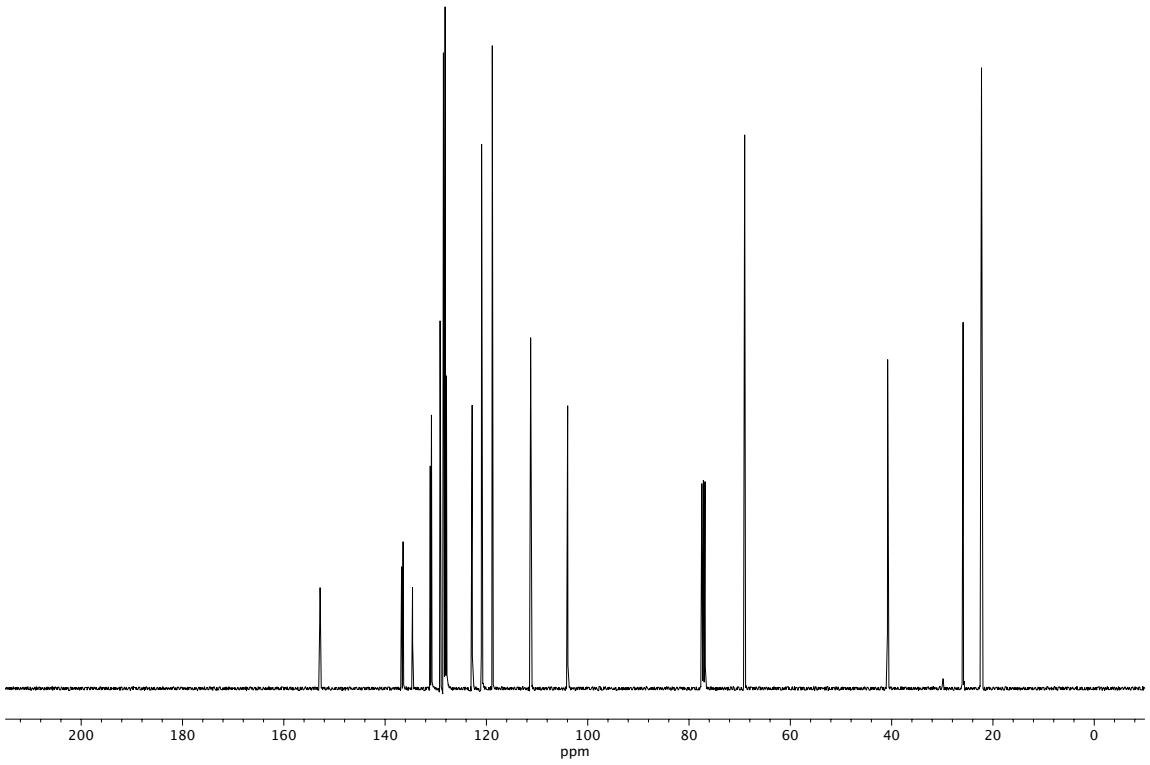

Figure A5.48 *^{13}C NMR (100 MHz, $CDCl_3$) of compound* ***58****.*

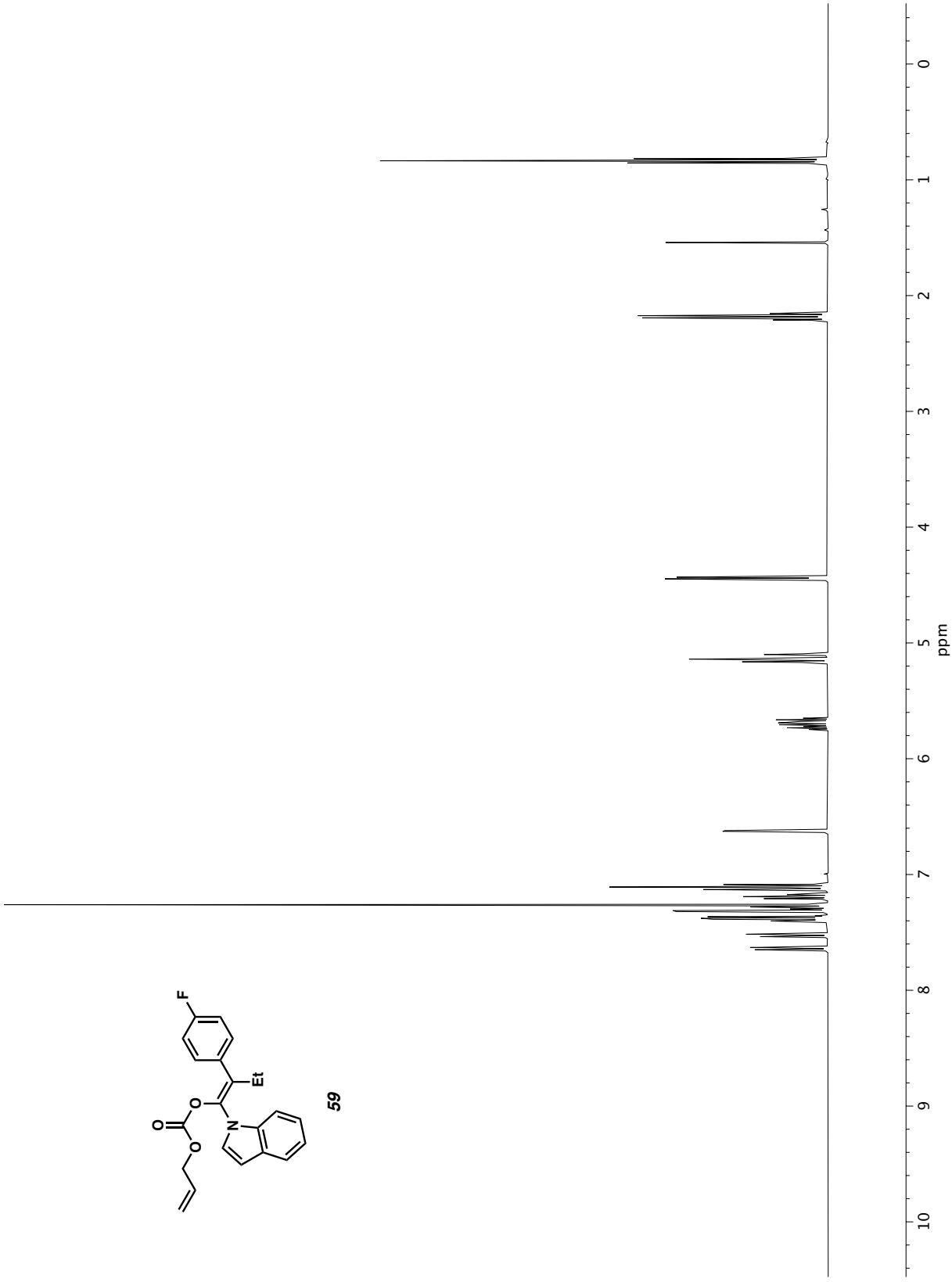

Figure A5.49 *^{1}H NMR (400 MHz, $CDCl_3$) of compound **59**.*

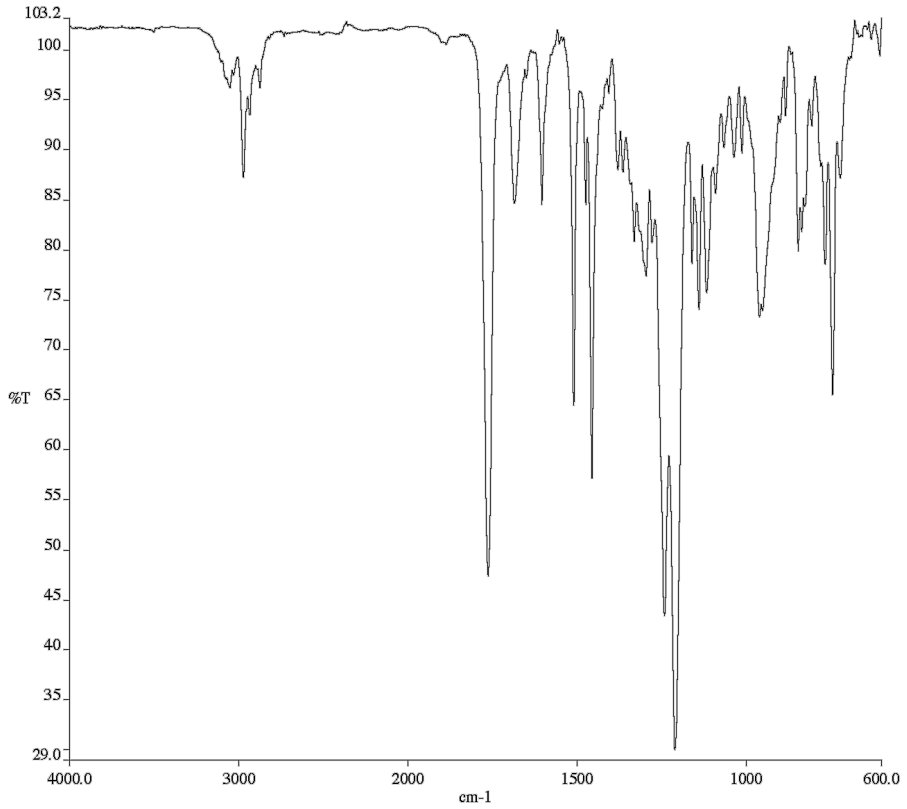

Figure A5.50 *Infrared spectrum (Thin Film, NaCl) of compound* ***59****.*

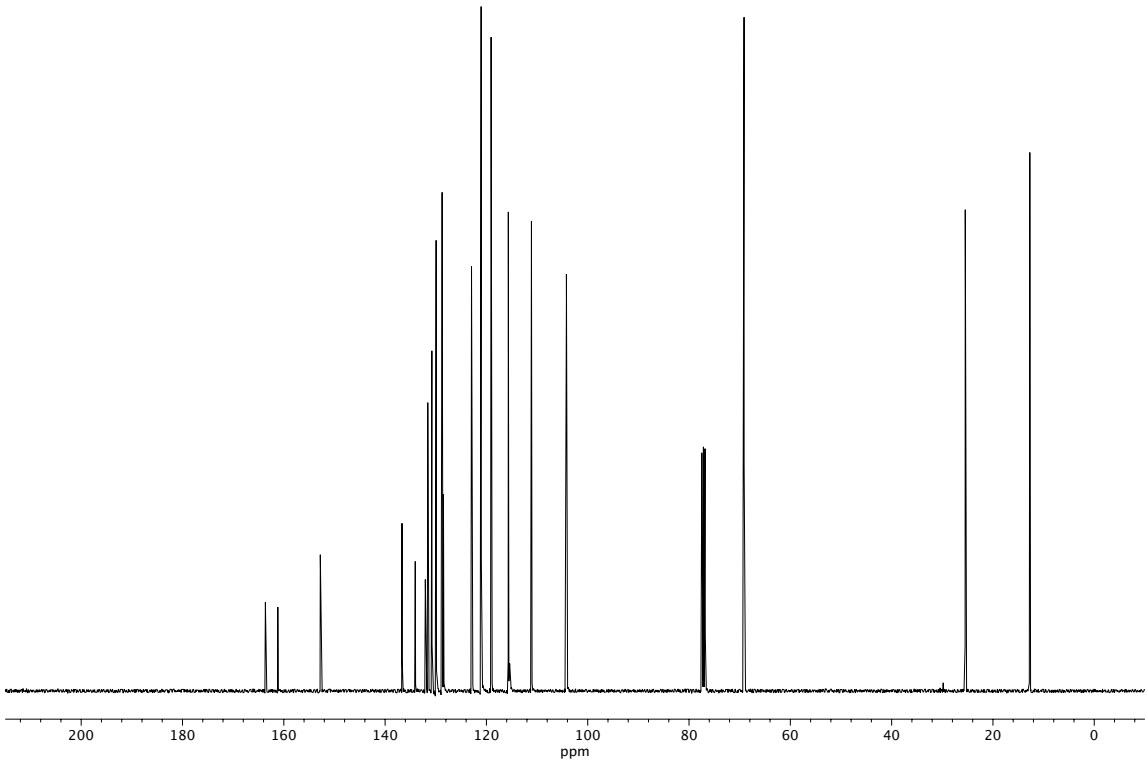

Figure A5.51 *^{13}C NMR (100 MHz, $CDCl_3$) of compound* ***59****.*

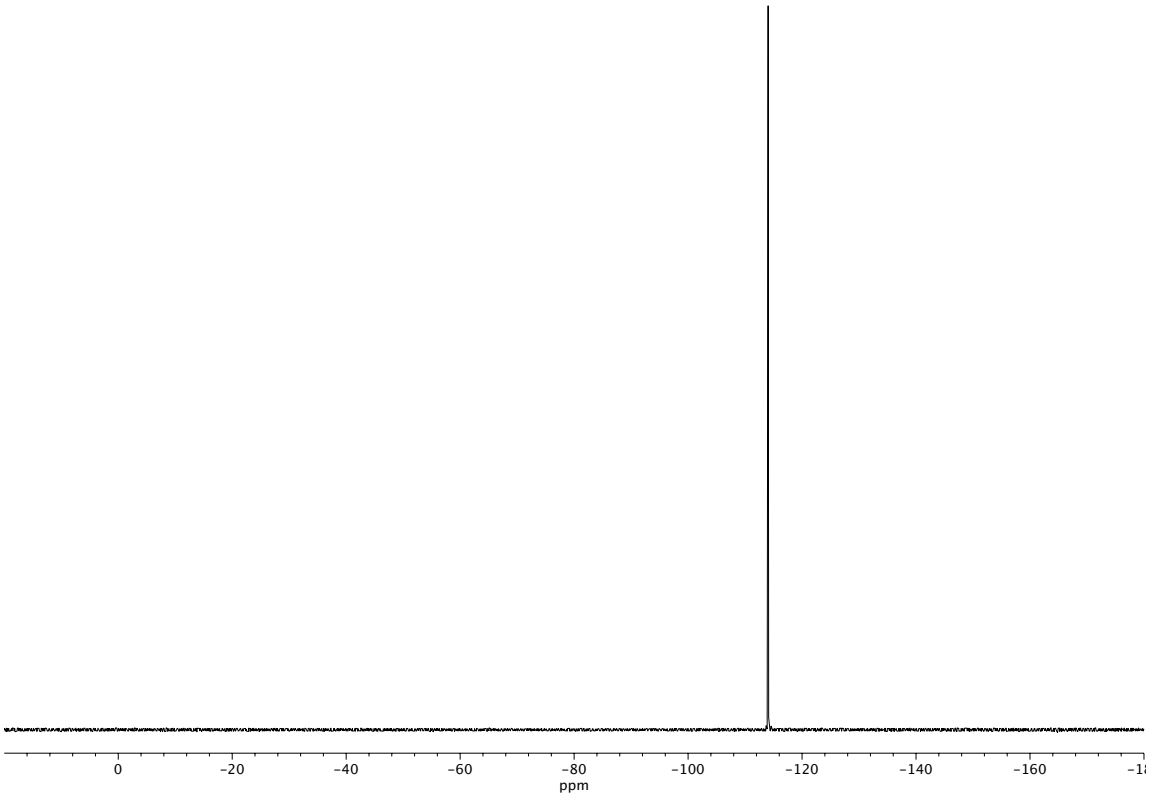

Figure A5.52 *^{19}F NMR (282 MHz, $CDCl_3$) of compound **59**.*

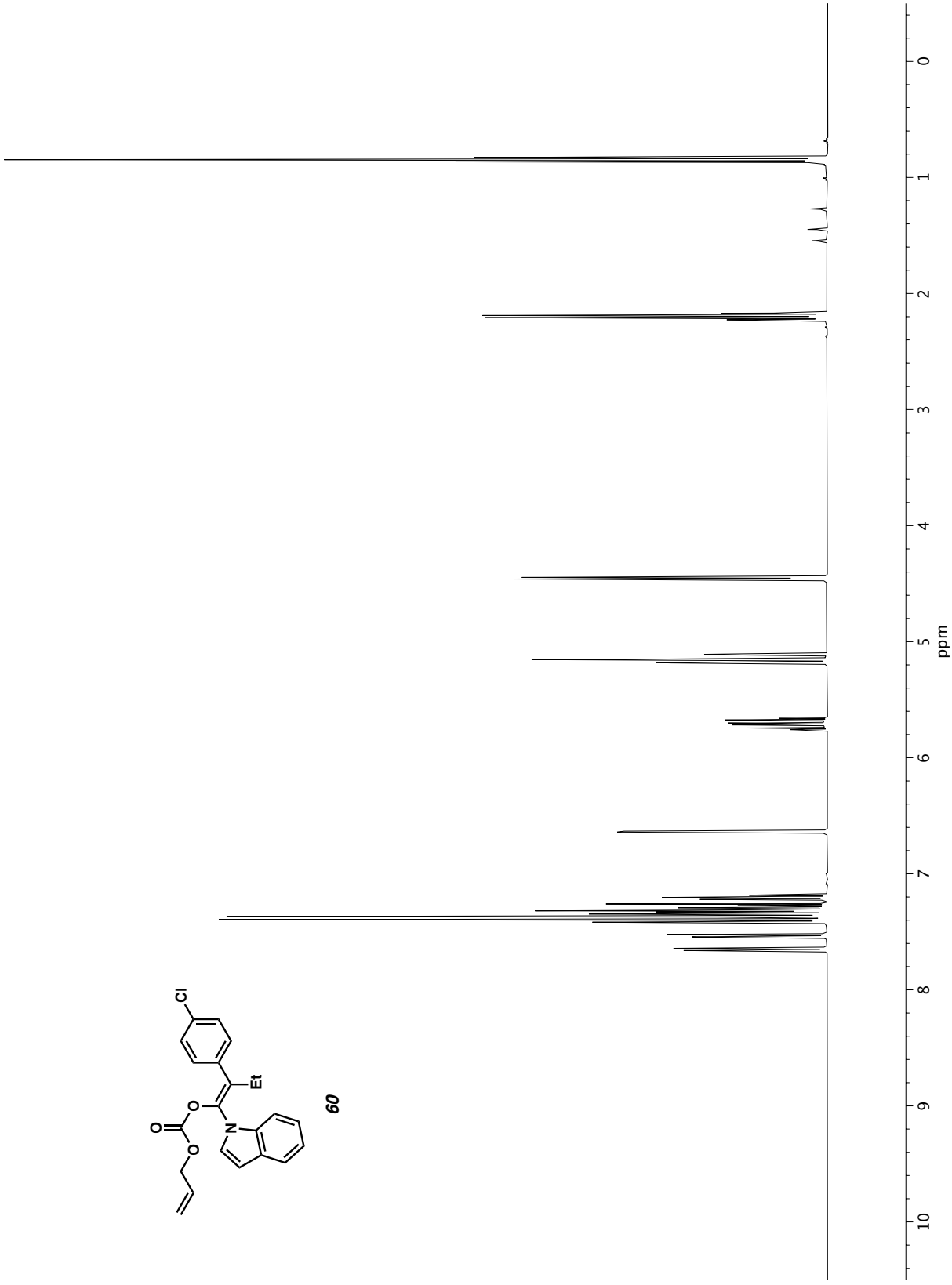

Figure A5.53 *^{1}H NMR (400 MHz, $CDCl_3$) of compound **60**.*

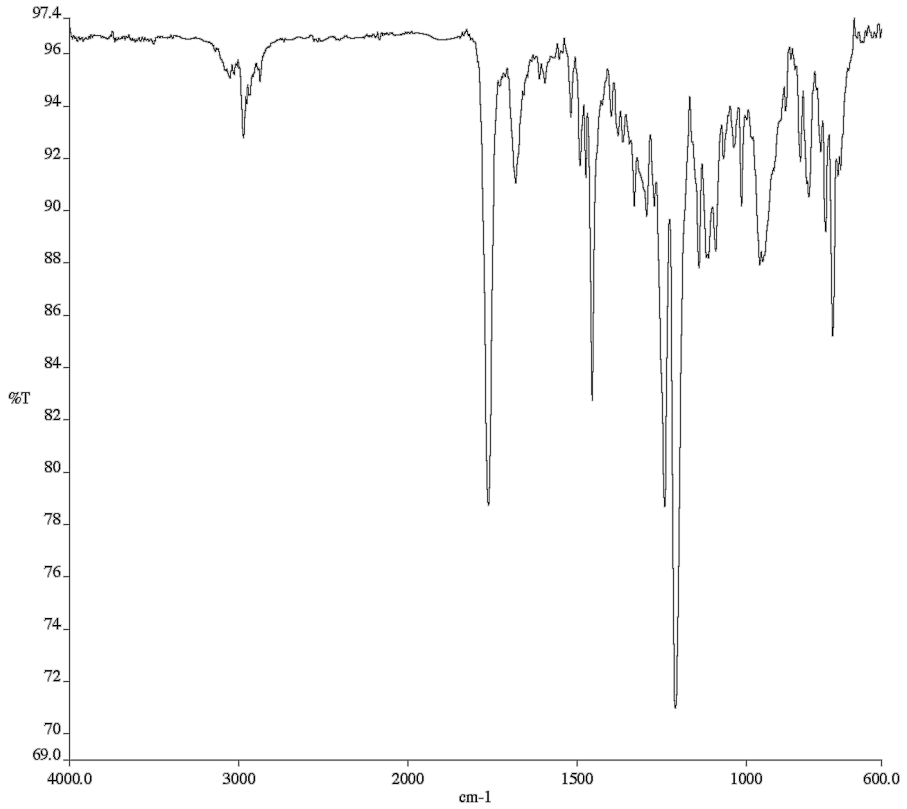

Figure A5.54 *Infrared spectrum (Thin Film, NaCl) of compound* ***60****.*

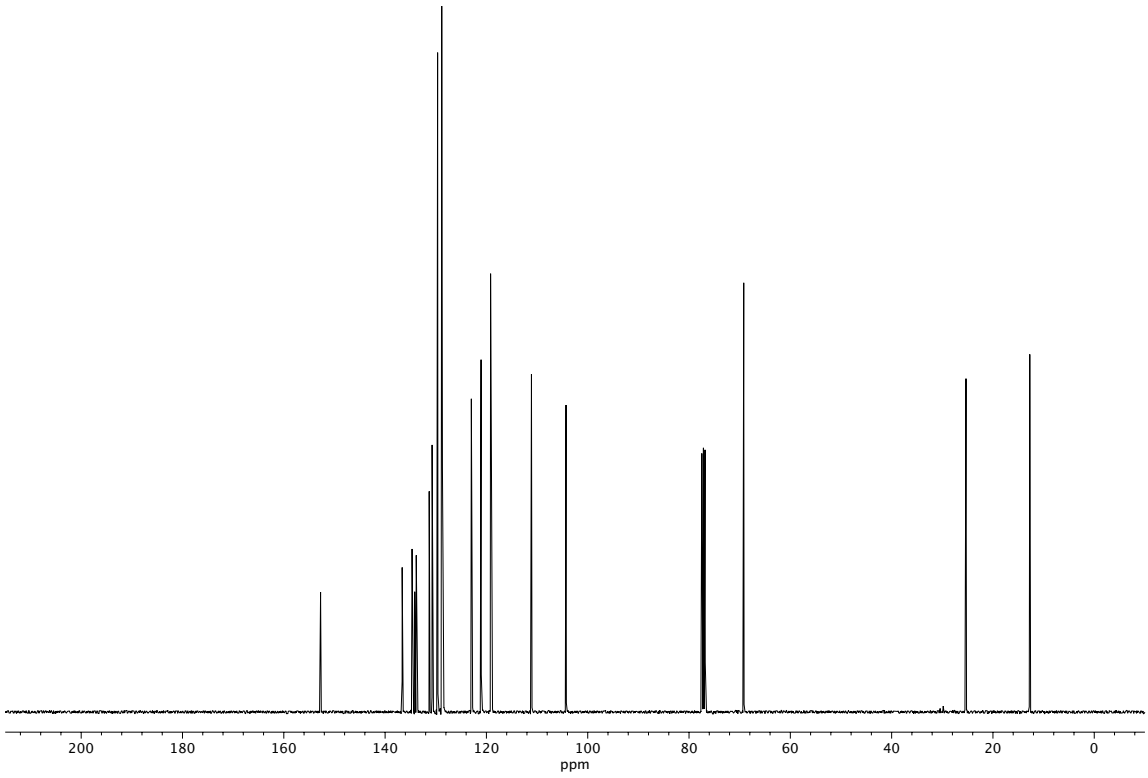

Figure A5.55 *^{13}C NMR (100 MHz, $CDCl_3$) of compound* ***60****.*

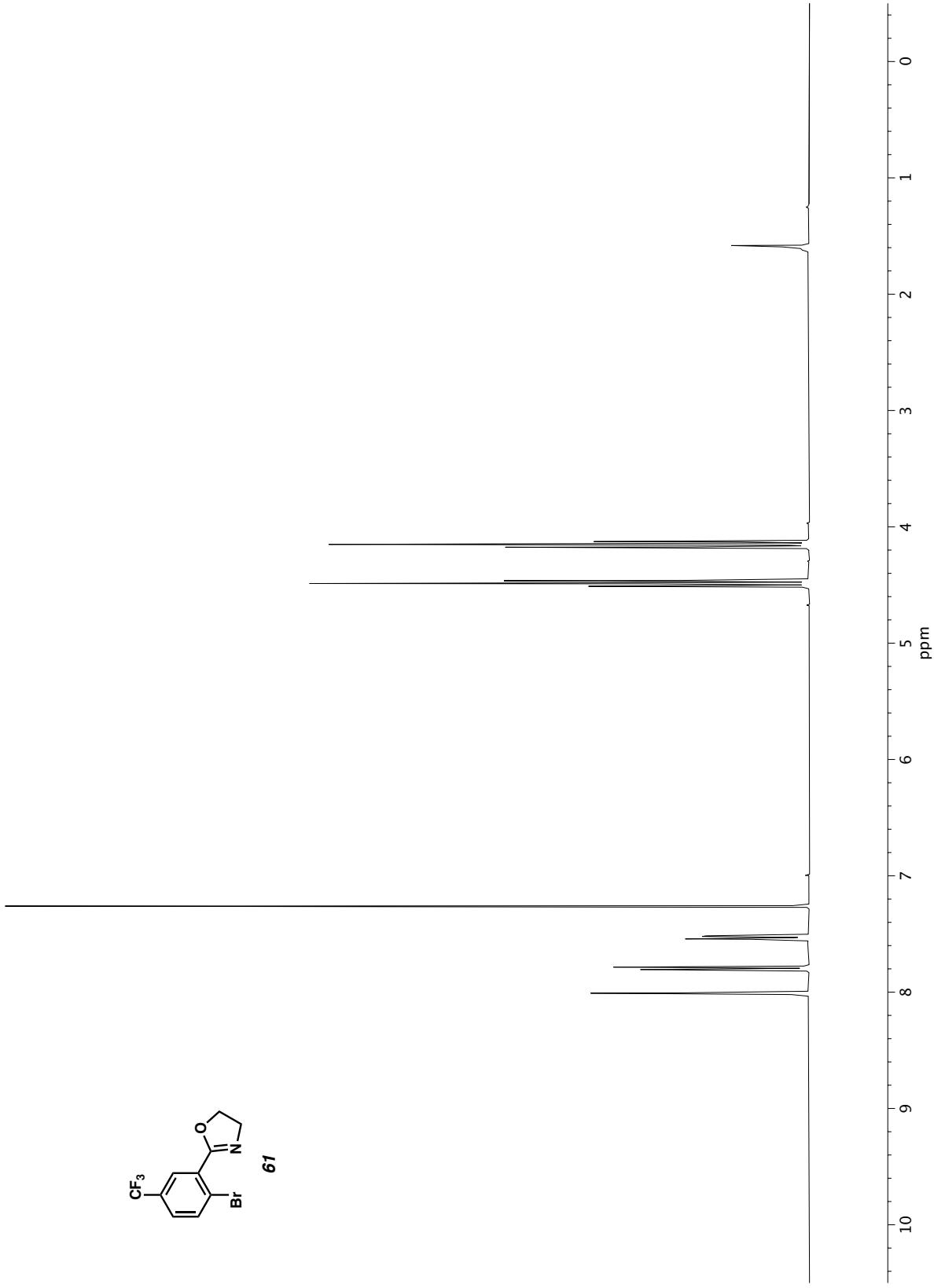

Figure A5.56 *^{1}H NMR (400 MHz, $CDCl_3$) of compound* ***61****.*

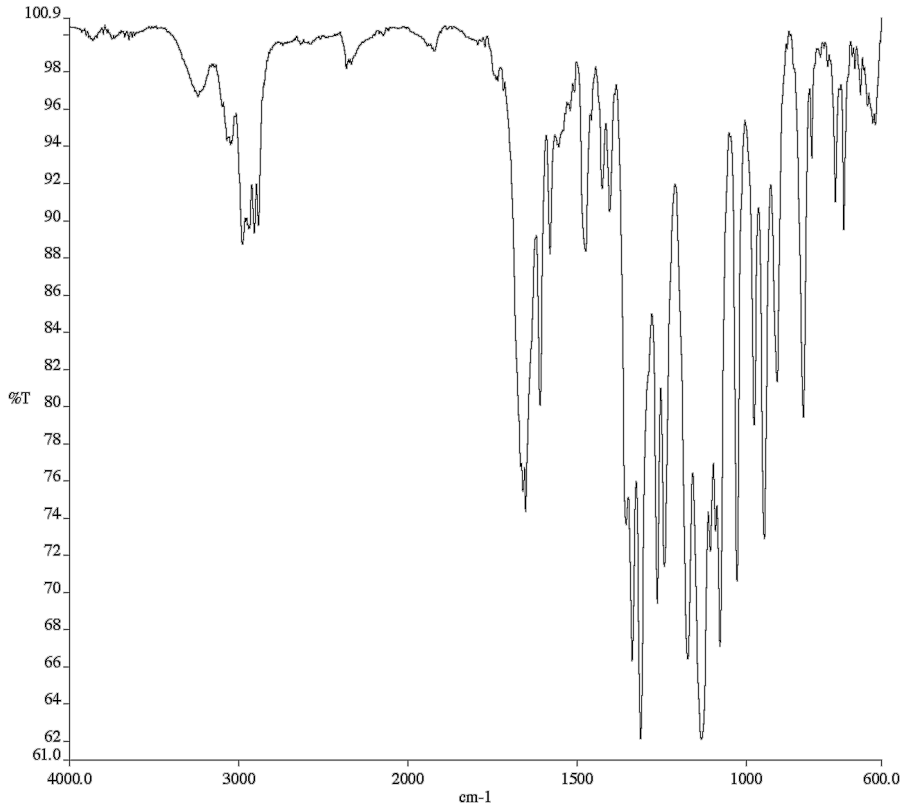

Figure A5.57 *Infrared spectrum (Thin Film, NaCl) of compound* ***61****.*

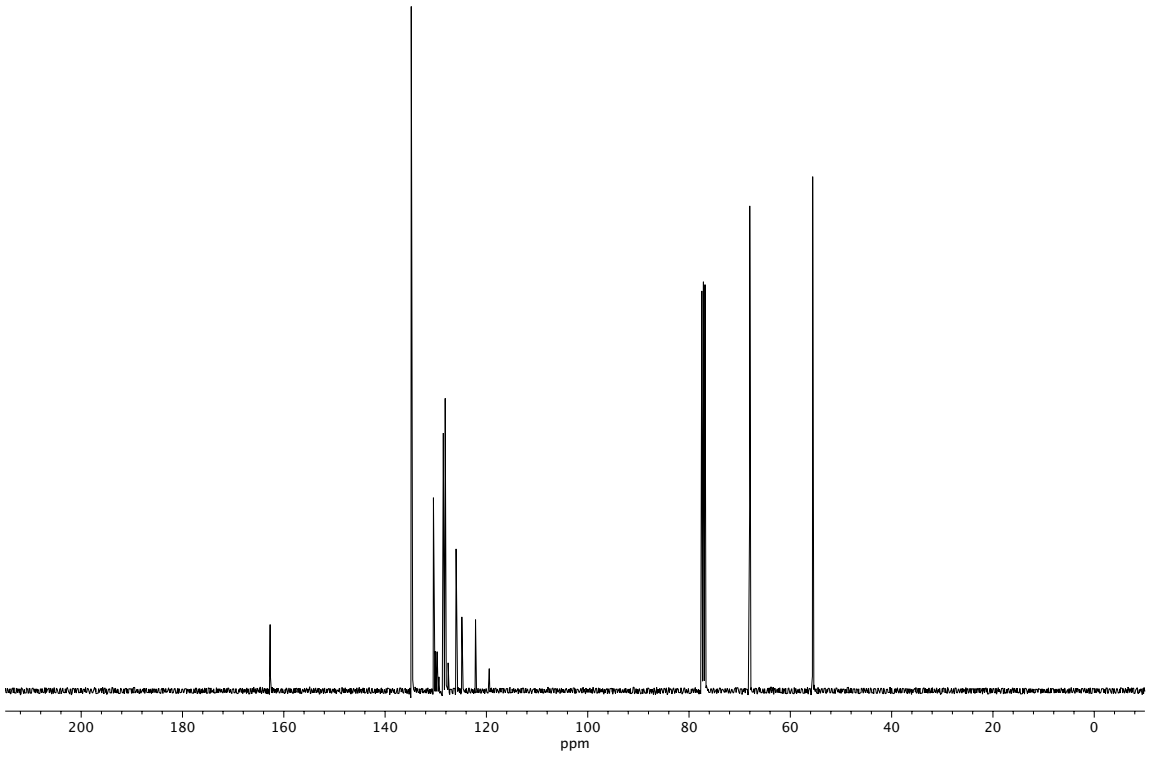

Figure A5.58 *^{13}C NMR (100 MHz, $CDCl_3$) of compound* ***61****.*

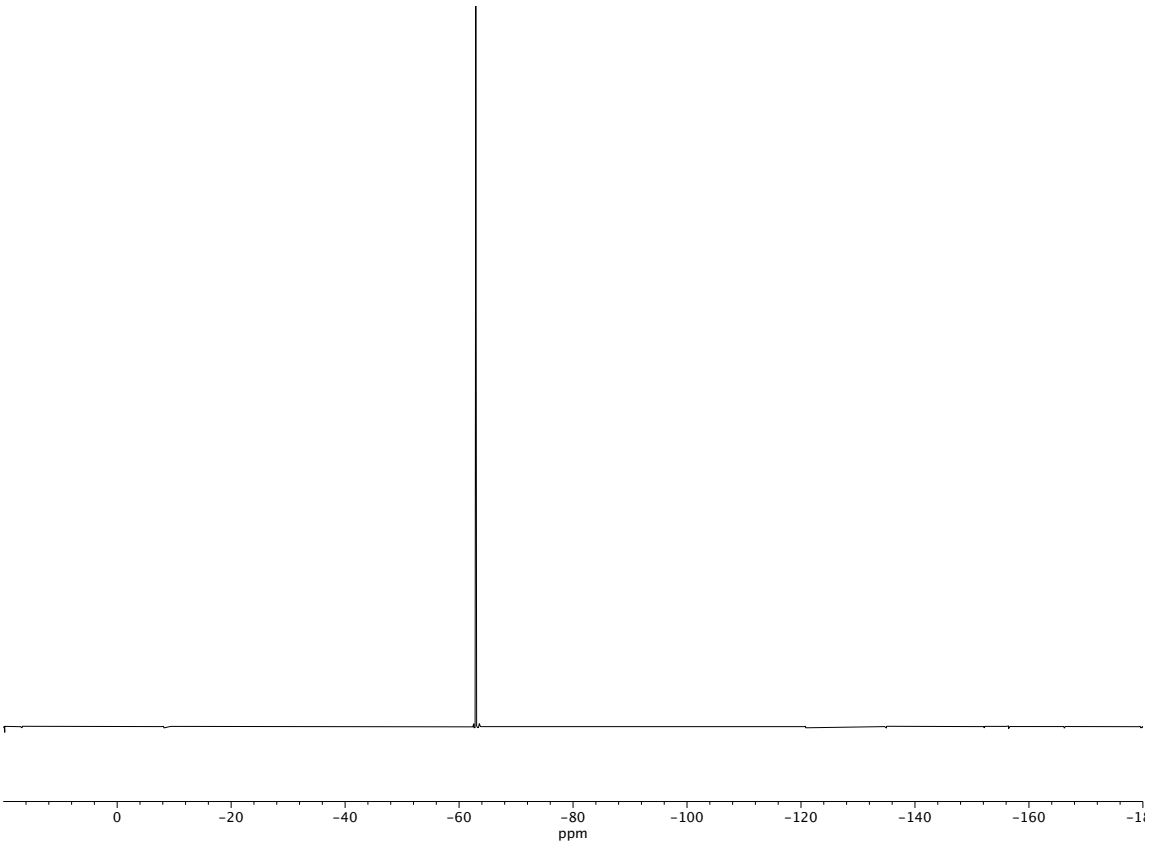

Figure A5.59 *^{19}F NMR (282 MHz, $CDCl_3$) of compound **61**.*

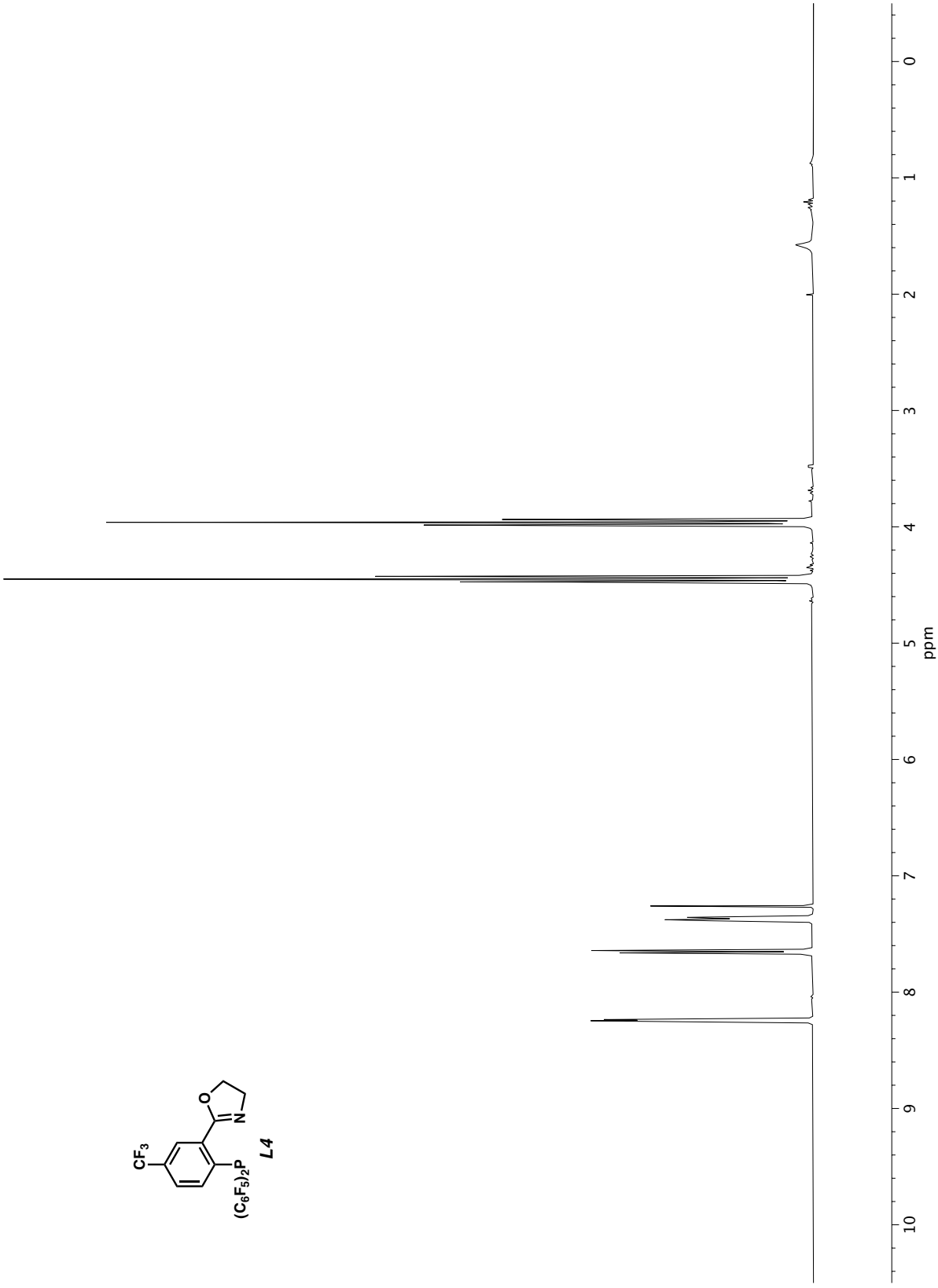

Figure A5.60 *^1H NMR (400 MHz, $CDCl_3$) of compound **L4**.*

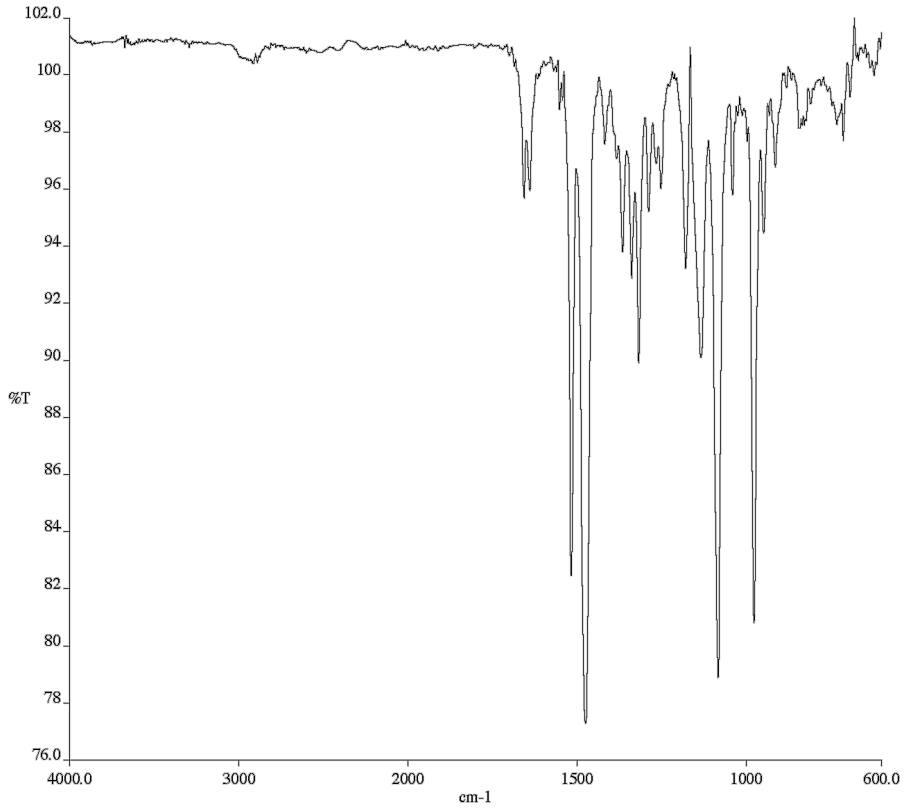

Figure A5.61 *Infrared spectrum (Thin Film, NaCl) of compound* ***L4****.*

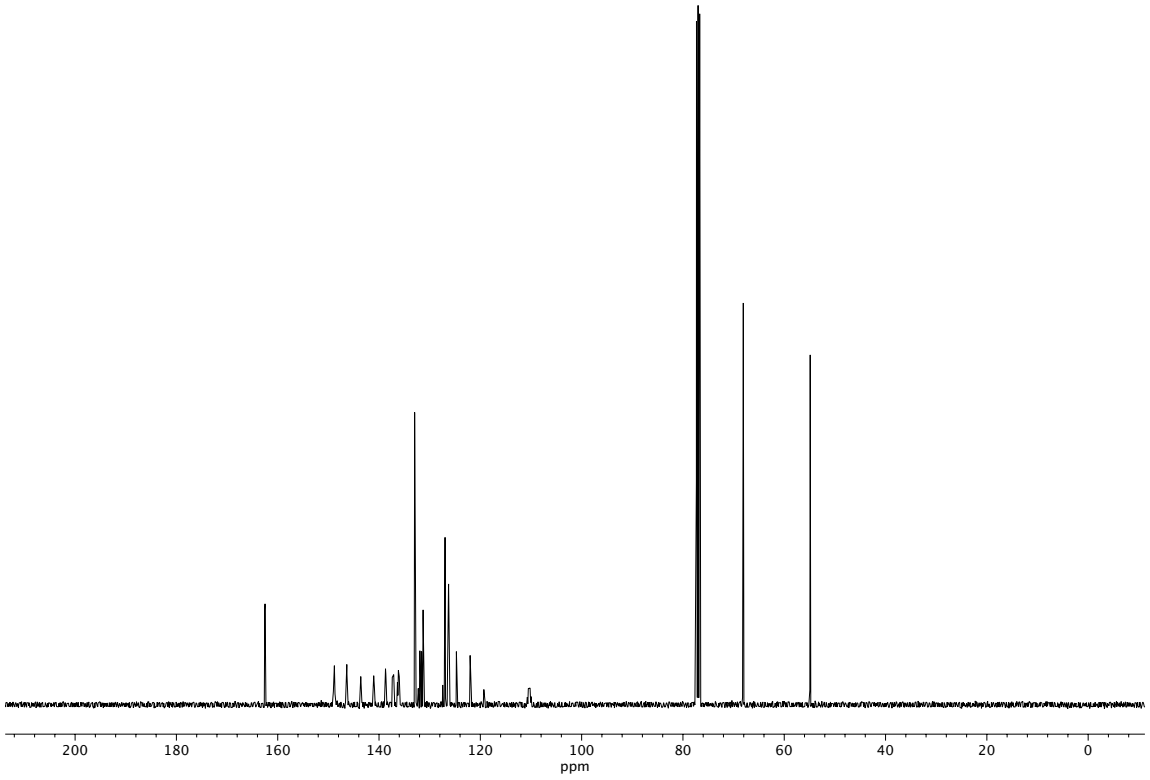

Figure A5.62 *^{13}C NMR (100 MHz, $CDCl_3$) of compound* ***L4****.*

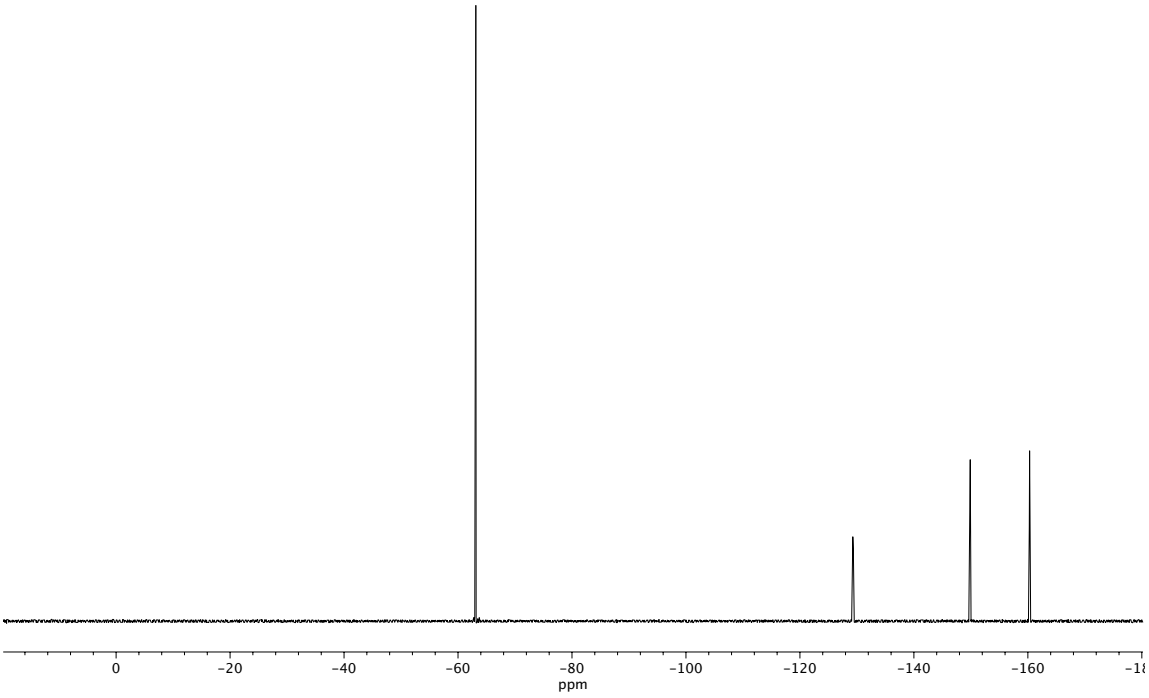

Figure A5.63 *^{19}F NMR (282 MHz, $CDCl_3$) of compound **L4**.*

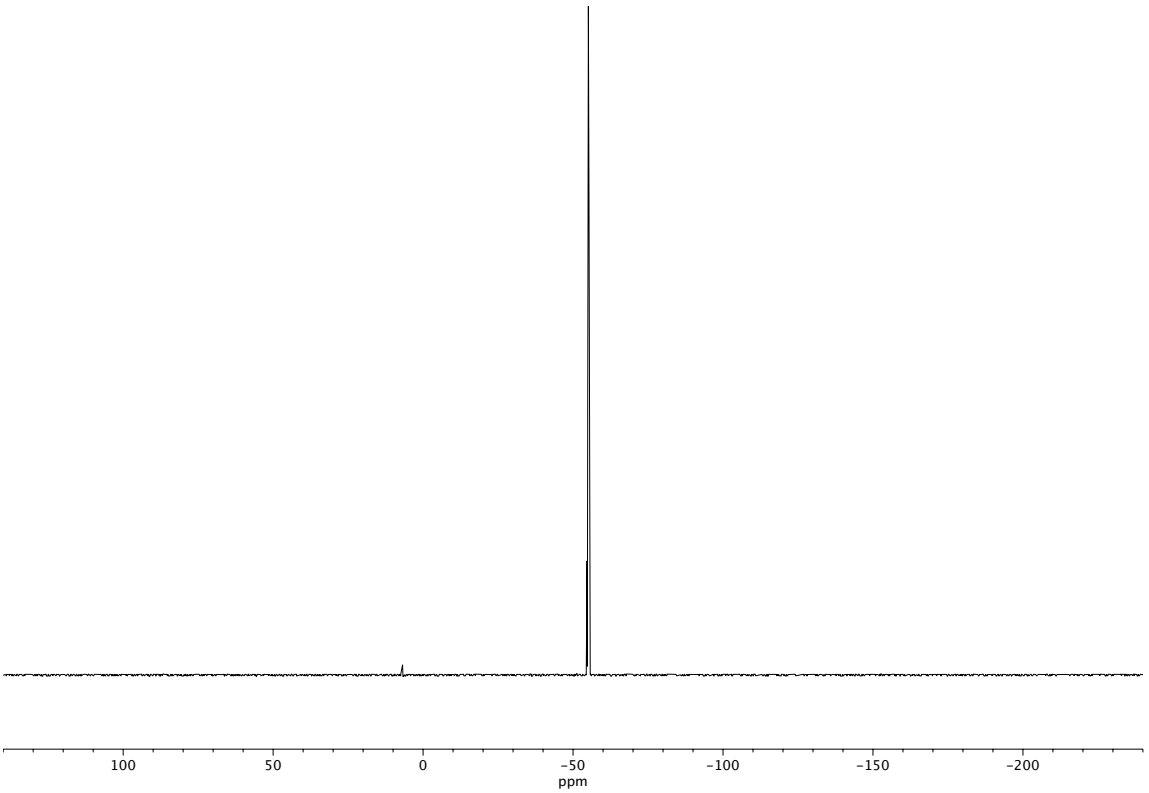

Figure A5.64 *^{31}P NMR (162 MHz, $CDCl_3$) of compound **L4**.*

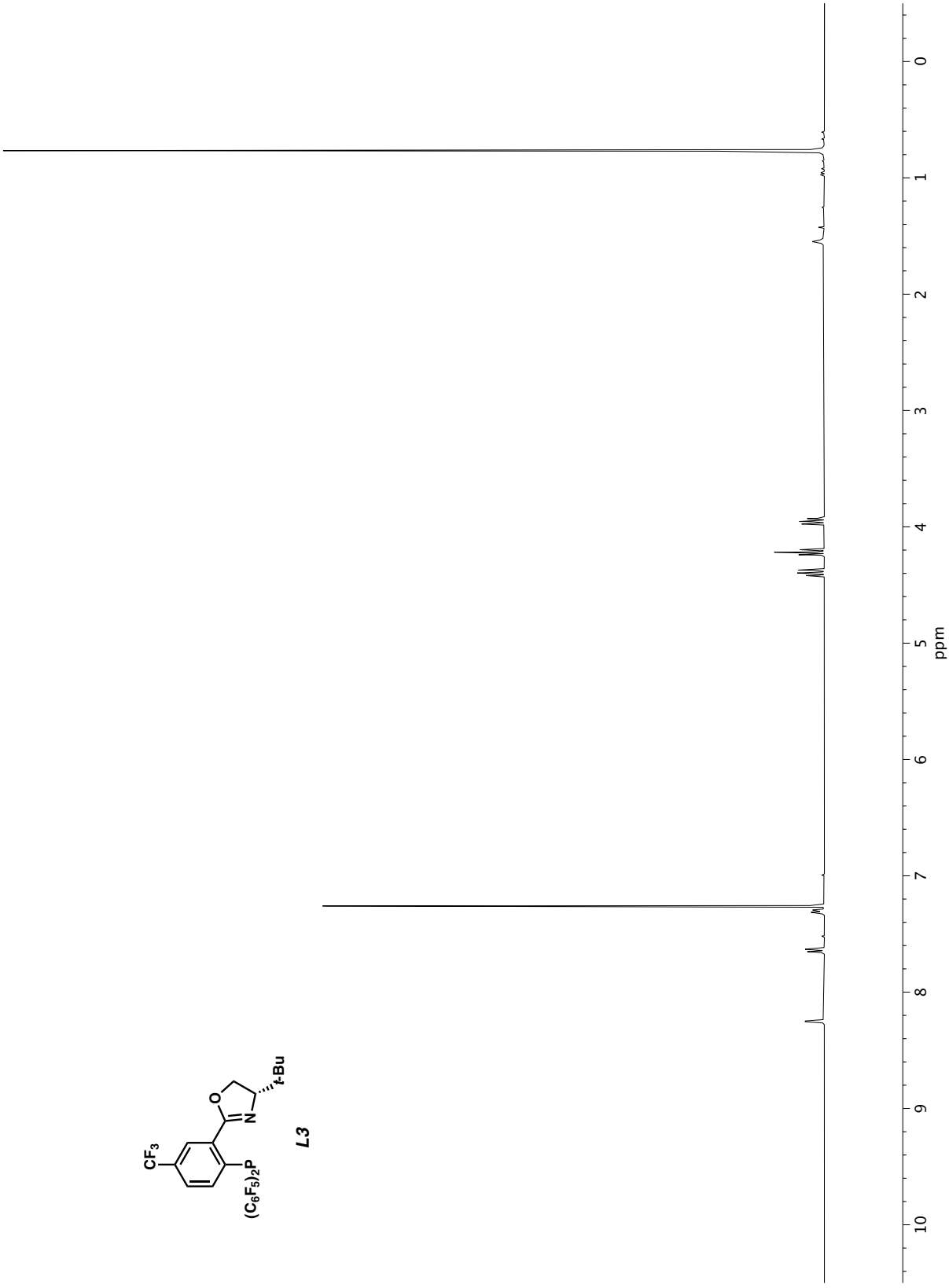

Figure A5.65 *^1H NMR (400 MHz, $CDCl_3$) of compound **L3**.*

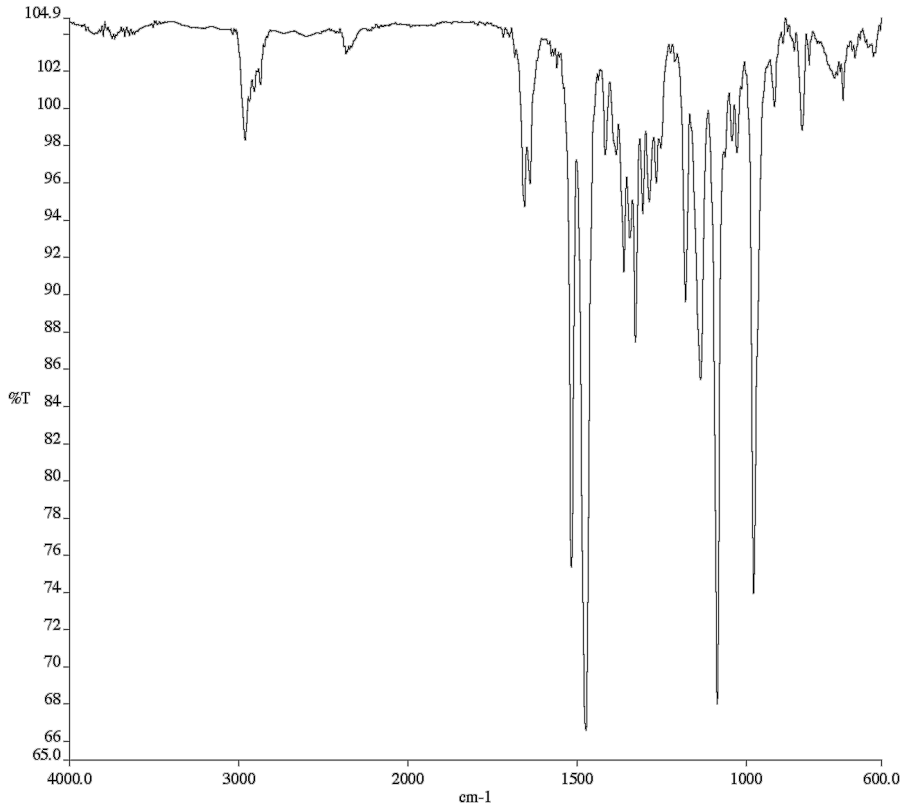

Figure A5.66 *Infrared spectrum (Thin Film, NaCl) of compound **L3**.*

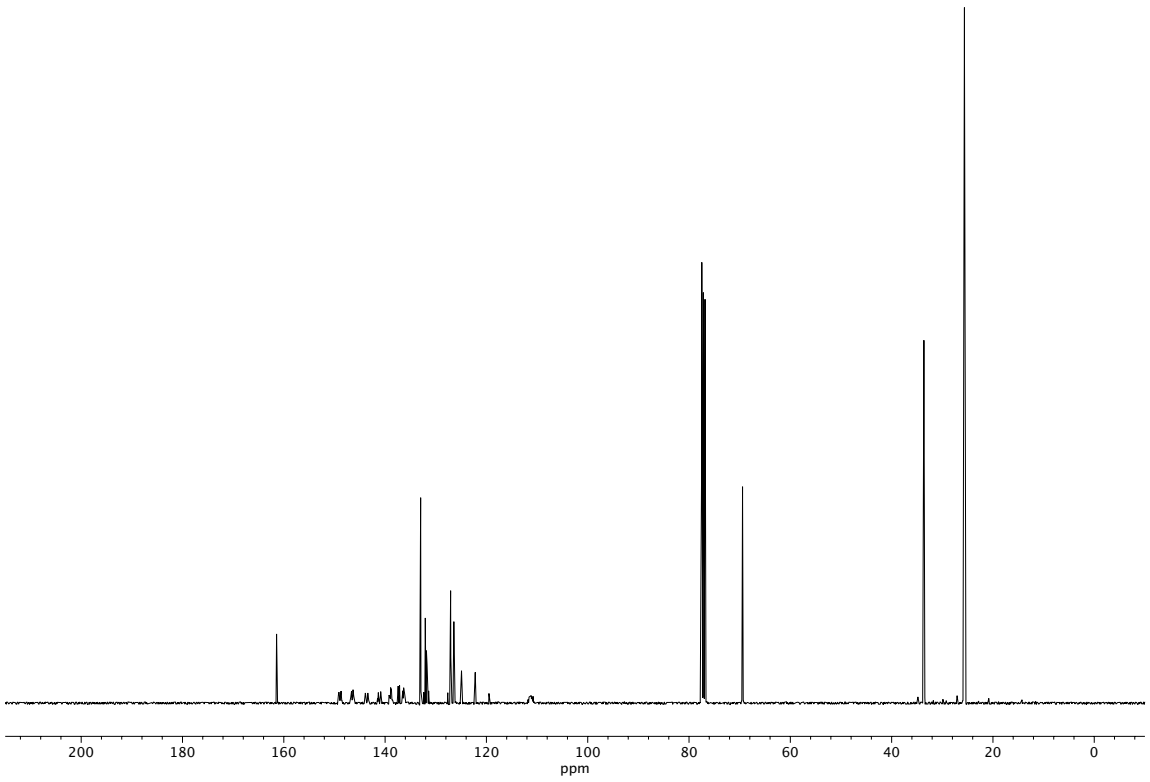

Figure A5.67 ^{13}C NMR (100 MHz, $CDCl_3$) of compound **L3**.

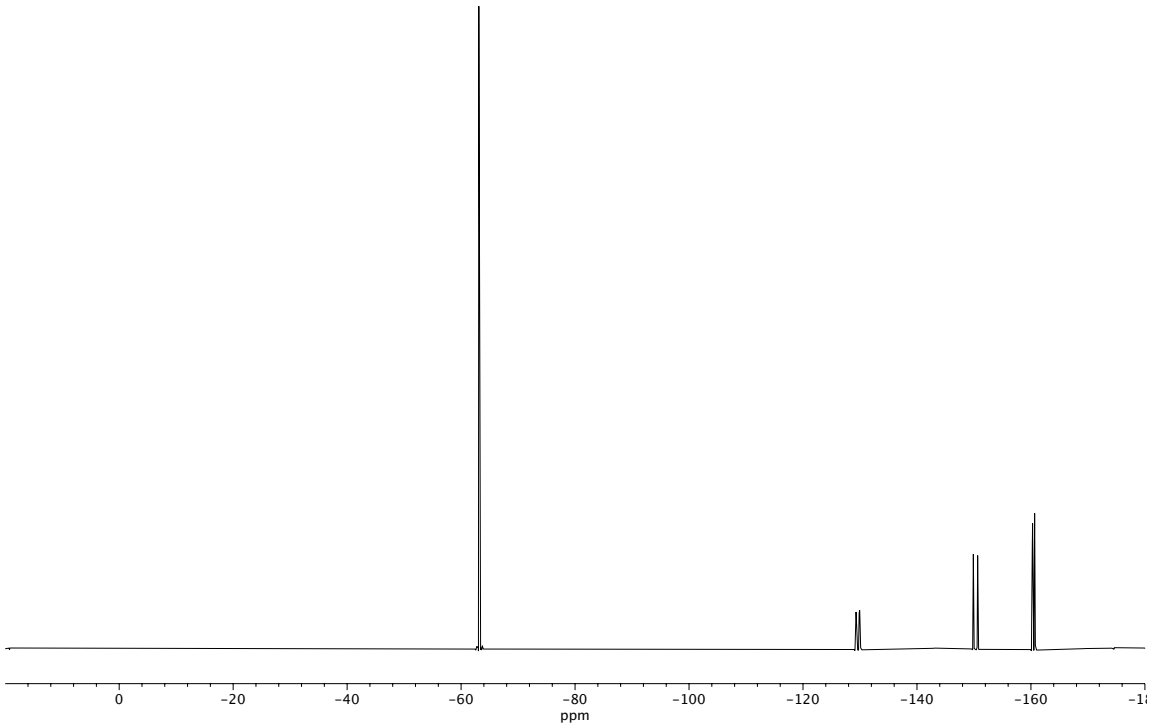

Figure A5.68 *^{19}F NMR (282 MHz, $CDCl_3$) of compound **L3**.*

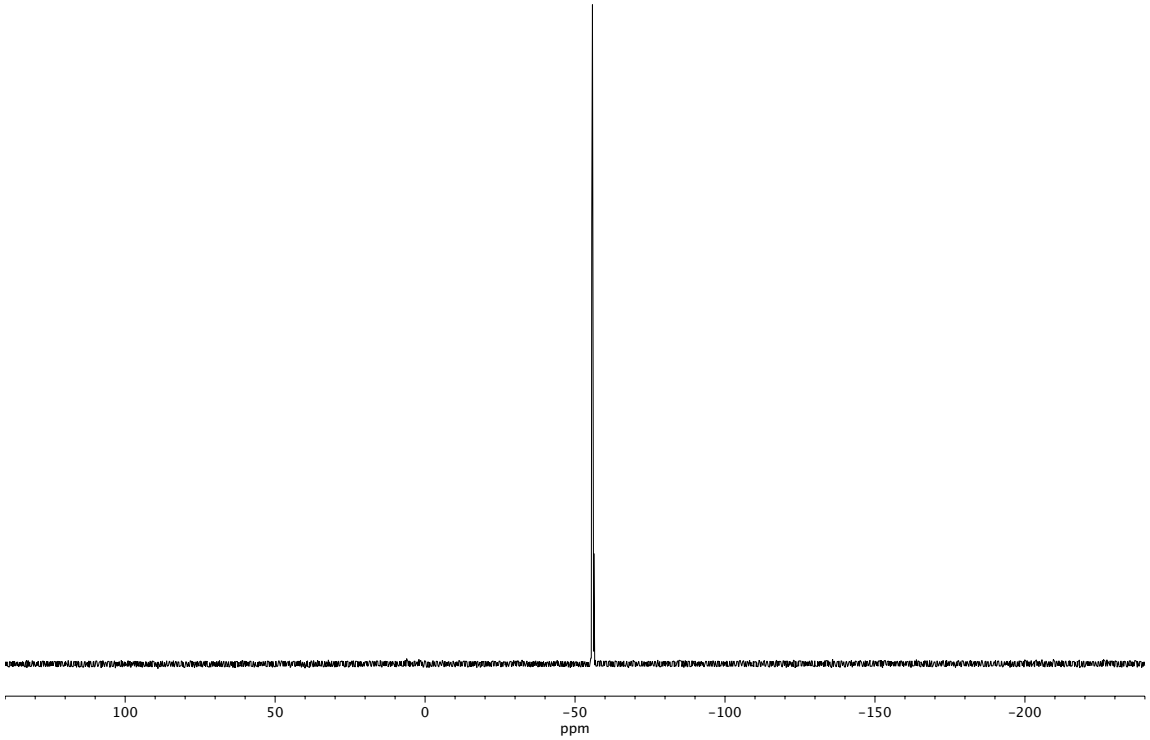

Figure A5.69 *^{31}P NMR (162 MHz, $CDCl_3$) of compound **L3**.*

CHAPTER 4

Global Diastereoconvergence in the Ireland–Claisen Rearrangement of Isomeric Enolates: Synthesis of Tetrasubstituted α-Amino Acids [†]

4.1 INTRODUCTION

For over forty years, the Ireland–Claisen rearrangement has been a mainstay for the construction of a diversity of carbon–carbon bonds in organic synthesis.[1] The ubiquity of the Ireland–Claisen rearrangement can be attributed to the relative ease of accessing the requisite allylic ester and the robust and predictable stereochemical outcome of the rearrangement. Consequently, the Ireland–Claisen rearrangement has been an indispensable tool for the construction of sterically encumbered vicinal stereogenic centers. Despite the utility of the Ireland–Claisen rearrangement, one longstanding challenge is the implementation of fully substituted acyclic allyl ester enolates derived from α,α-disubstituted esters. This is presumably a consequence of the difficulty in controlling the enolate geometry in tetrasubstituted ester-derived systems. The Ireland–Claisen rearrangement typically proceeds through a predictable and well-defined chair-like transition state, thus, *E*- and *Z*-enolate geometries lead to diastereomeric products, necessitating a highly selective enolization protocol for efficient diastereoselection.

[†]This research was performed in collaboration with Alex Cusumano, Eric J. Alexy, and Yun E. Du. Portions of this chapter have been reproduced with permission from Fulton, T. J.; Cusumano, A. Q.; Alexy, E. J.; Du, Y. E.; Zhang, H.; Stoltz, B. M. *J. Am. Chem. Soc.* **2020**, *142*, 21938–21947.

Few examples of fully substituted, acyclic enolates in highly diastereoselective Ireland–Claisen rearrangements have been reported to date.[2] Zakarian and coworkers established the first effective protocol for the selective enolization of chiral α,α-disubstituted esters utilizing chiral Koga-type[3] bases to impart *E*/*Z* enolization selectivity (Figure 4.1.1A).[4] Although this protocol enables the selective generation of either *E*- or *Z*-tetrasubstituted ester enolates under mild conditions to access both diastereomeric series of rearrangement products, the utilization of allylic esters with highly enantioenriched or enantiopure α-stereocenters is required and each substrate requires optimization of the chiral base. Crimmins and coworkers utilized a chiral auxiliary approach to prepare chiral, non-racemic α-methyl-β-hydroxy allylic esters toward the synthesis of briarane natural products (Scheme 4.1.1B).[5] In this approach, enolization selectivity is imparted by chelation and steric approach control to provide Ireland–Claisen rearrangement products with generally excellent diastereoselectivity.

More recently, Zakarian and coworkers investigated the diastereodivergent Ireland–Claisen rearrangement of tetrasubstituted α-alkoxy ester enolates toward the synthesis of α-alkoxy carboxylic acids (Scheme 4.1.1C).[6] While the chelation-controlled, kinetic *Z*-selective enolization of α-alkoxy esters has been well established,[7] Zakarian and coworkers found an *E*-selective enolization could be achieved with judicious choice of base and solvent based on prior research from Langlois and coworkers.[8] While a variety of α-alkoxy carboxylic acid products were obtained with good to excellent diastereoselectivity, the level of control over enolate geometry is highly substrate dependent, particularly for *E*-selective enolization.

Figure 4.1.1 *Stereoselective Ireland–Claisen Rearrangements of Fully Substituted Acyclic α,α-Disubstituted Esters.*

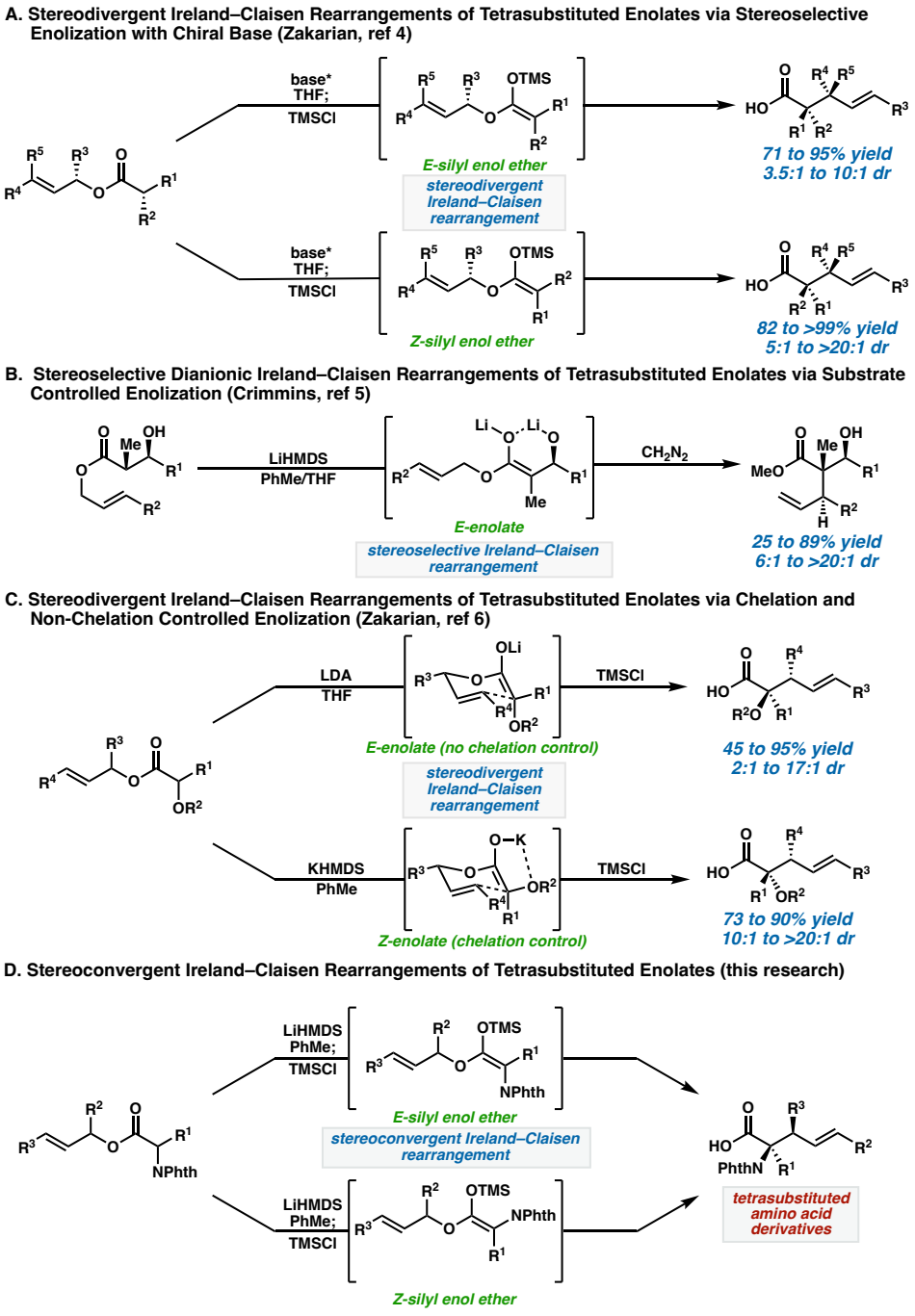

We addressed the limitations of enolate geometry control by developing a system wherein both enolate geometries converge to a single diastereomer of product, rendering

the enolization selectivity inconsequential (Figure 4.1.1D). This was accomplished in the context of tetrasubstituted amino acid synthesis wherein intramolecular interactions of an α-phthalimide group with an *E*-phenyl substituted allyl olefin serves to overturn the inherent preference for the chair-like transition state from the *E*-silyl enol ether ($\Delta\Delta G^{\ddagger}$ = –3.8 kcal/mol). In contrast, these interactions reinforce the energetic preference for the chair-like transition state from the *Z*-silyl enol ether ($\Delta\Delta G^{\ddagger}$ = 5.5 kcal/mol). Consequently, in the case of a *Z*-phenyl substituted allyl olefin, the *E*-silyl enol ether rearranges via a chair-like transition state, while from the *Z*-silyl enol ether a boat-like transition state is favored.

The ability to incorporate an enantioenriched allylic stereogenic center in the Ireland–Claisen rearrangement allows for the transfer of chirality with generally excellent stereochemical fidelity. We demonstrate that chirality transfer is conserved within the divergent transition state preference from *E*-and *Z*-silyl enol ethers. In this study, we detail the computational design and modeling and experimental investigation of the Ireland–Claisen rearrangement of tetrasubstituted α-phthalimido ester enolates toward the synthesis of non-natural tetrasubstituted α-amino acid derivatives bearing vicinal stereogenic centers (Figure 4.1.1D).

4.2 QUANTUM MECHANICAL EVALUATION OF THE DIASTEREOCONVERGENT IRELAND–CLAISEN REARRANGEMENT

Quantum Mechanics (QM) calculations were carried out to probe the energetic requirements for a diastereoconvergent transformation. A multi-level approach was employed in which geometries, thermodynamic corrections, and solvation free energies are obtained via density functional theory (DFT) with final electronic energies obtained from

calculations with domain based local pair natural orbital coupled-cluster theory (DLPNO-CCSD(T)). Reported energies are relative Gibbs free energies in kcal/mol calculated at 298.15 K with the DLPNO-CCSD(T)/cc-pVTZ/SMD(Toluene)//B3LYP-D3(BJ)/6-31G(d) level of theory. Throughout the text, signed $\Delta\Delta G^{\ddagger}$ defined as $\Delta G^{\ddagger}$(boat) – $\Delta G^{\ddagger}$(chair) are provided. All computations were carried out using the ORCA program.[9] Full computational details as well as comparisons between DFT and coupled-cluster methods are included in the Section 4.10 (vide infra).

In a fully simplified model system, i.e., the trimethylsilyl enol ether derived from allyl acetate (**1**), an energetic preference of 2.6 kcal/mol is observed for the chair-like (**TS1**) over the boat-like transition state (**TS2**) (Figure 4.2.1A, D entry 1). A diastereoconvergent rearrangement will occur in the case of *E/Z*-mixtures of tetrasubstituted enolates when the sum of the interactions between the substituents for one enolate geometry overcomes the intrinsic preference for a chair-like transition state to the extent that the boat-like transition state is significantly favored. The groups of Houk, Neier, and Aviyente described a preference for a boat-like transition state in the Ireland–Claisen rearrangement of cyclohexenyl esters which was attributed to steric interactions between the enolate and cyclohexenyl fragments.[10] In the case of acyclic, tetrasubstituted enol ethers, these interactions are diminished.

We examined stereoconvergence in the Ireland–Claisen rearrangement in the context of the synthesis of valuable tetrasubstituted α-amino acid building blocks. The α-phthalimido group was chosen as a stable, easily removed, bis-protected α-amine.[11] Introduction of the α-phthalimido group imparts a minimal effect on the chair/boat

selectivities, with a preference for the chair-like (**TS3/TS5**) over boat-like transition state (**TS4/TS6**) for both *E*- and *Z*-silyl enol ethers (***(E/Z)*-64**) of 3.4 and 2.4 kcal/mol, respectively (Figure 4.2.1B, D entry 2). While introduction of substitution in the form of a phenyl group at the terminus of the allylic olefin slightly increases the preference for the chair-like transition state from ***(Z)*-66** to 4.2 kcal/mol, the boat-like transition state is 1.0 kcal/mol lower in energy than the chair-like transition state from enol ether ***(E)*-66** (Figure 2B, D entry 3).[12] This reversal in preference for chair versus boat-like transition state for the α-phthalimido *E*-silyl enol ethers is further exacerbated with additional substitution of the silyl enol ether. In fact, the boat-like transition state (**TS14**) derived from the corresponding α-phenyl-α-phthalimido *E*-silyl enol ether (***(E)*-69**) is computed to be 3.8 kcal/mol lower in energy than its chair counterpart (**TS13**) (Figure 4.2.1B, D entry 4).

In contrast, high levels of selectivity for the chair-like transition state are anticipated for the fully substituted *Z*-silyl enol ether (***(Z)*-69**), with the chair-like transition state (**TS11**) favored over the boat-like transition state (**TS12**) by 5.5 kcal/mol (Figure 4.2.1B, D entry 4). As a result, for the fully substituted system, the diastereoselectivity of the ensuing Ireland–Claisen rearrangement is anticipated to be independent of the *E/Z*-selectivity in the enolization and trapping of the requisite tetrasubstituted silyl enol ether. Note the diastereoconvergent effect is significantly less pronounced when the α-phenyl group is substituted for an α-ethyl substituent (Figure 4.2.1C, D entry 5).[13]

Figure 4.2.1 *Quantum Mechanical Investigation of the Diastereoconvergent Ireland–Claisen Rearrangement.*[a]

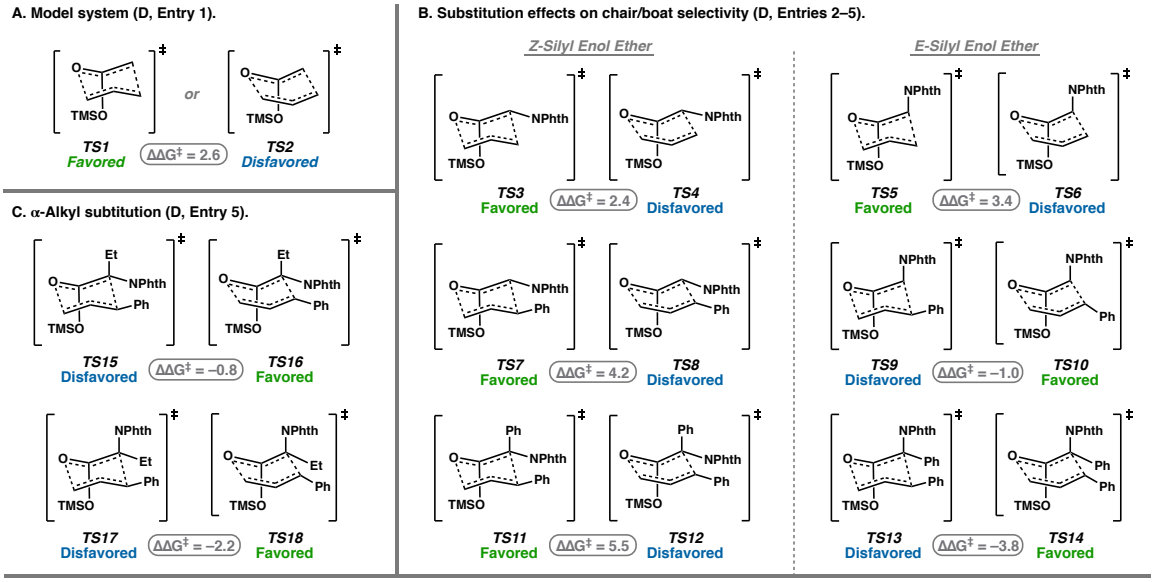

Entry	R^1	R^2	R^3	*TS-A*	*TS-B*	ΔΔG‡	*TS-C*	*TS-D*	ΔΔG‡	*A*	*B*	*C*	*D*
1	H	H	H	*TS1*	*TS2*	2.6	–	–	–	*62*	–	*63*	–
2	H	H	NPhth	*TS3*	*TS4*	2.4	*TS5*	*TS6*	3.4	*(Z)-64*	*(E)-64*	*65*	–
3	Ph	H	NPhth	*TS7*	*TS8*	4.2	*TS9*	*TS10*	–1.0	*(Z)-66*	*(E)-66*	*67*	*68*
4	Ph	Ph	NPhth	*TS11*	*TS12*	5.5	*TS13*	*TS14*	–3.8	*(Z)-69*	*(E)-69*	*70*	*71*
5	Ph	Et	NPhth	*TS15*	*TS16*	–0.8	*TS17*	*TS18*	–2.2	*(Z)-72*	*(E)-72*	*73*	*74*

[a] ΔΔG‡ (in kcal/mol) defined as ΔG‡ (boat) – ΔG‡ (chair) (A) Innate preference for chair-like TS. (B) Effect of substitution pattern on diastereoconvergence in the Ireland–Claisen rearrangement. (C) Probing α-alkyl substitution. (D) Diastereoconvergence, compound labels, and tabulated relative free energies [a]Absolute stereochemistry drawn arbitrarily – opposite enantiomeric series than TS-B/D.

4.3 EXPERIMENTAL INVESTIGATION OF DIASTEREOCONVERGENCE

Ireland–Claisen rearrangement of computationally modeled α-phthalimido cinnamyl ester **75** leads to >20:1 diastereoselection with under several different enolization

conditions (Table 4.3.1). Enolization conditions of 1:1 LiHMDS/Me_2NEt (entry 1) were originally developed by Gosselin, Zhang, and coworkers[14] for the highly selective enolization of α,α-disubstitued aryl ketones. Additionally, Stoltz and Zhang demonstrated these conditions can be applied to the selective enolization and trapping of a variety of acyclic α-aryl substituted carboxylic acid derivatives including α-ethyl-α-phenyl *t*-butyl, phenyl, and ethyl esters.[15] Enolization with LiHMDS (entry 2) and KHMDS (entry 3) without additives results in identical yields and diastereoselectivity. Notably, phthalimide protected amino acid **76a** is obtained without column chromatography and the relative stereochemistry was confirmed unambiguously by X-ray crystallography, matching the computationally predicted outcome.[16]

Table 4.3.1 *Investigation of the Ireland–Claisen Rearrangement Enolization Conditions.*[a]

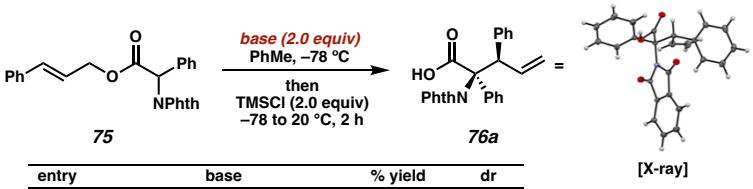

75 *76a*

entry	base	% yield	dr
1	LiHMDS, Me_2NEt (2.0 equiv)	92	>20:1
2	LiHMDS	90	>20:1
3	KHMDS	90	>20:1

[a] Reactions performed on a 1.00 mmol scale, yields of isolated products. Diastereomeric ratios were determined by ^1H NMR analysis.

Direct observation of and quantification of the ratio of enolate geometries formed in situ proved challenging due to the facile nature of the rearrangement at low temperature and heterogeneous reaction mixture. Thus, analogous di-hydro-α-phthalimide substituted ester **77** was examined as a surrogate to **75** that is incapable of undergoing the Ireland–Claisen rearrangement. A variety of kinetic enolate trapping reagents (e.g., TMSCl, TMSOTf, Ts_2O, Tf_2O) were studied employing the same enolization conditions (vide

supra). These trapping experiments failed due to the inability to form or isolate the resulting enol ethers; however, moderate yields of allyl enol carbonate isomers **A** and **B** were obtained with allyl chloroformate as an *O*-acylating reagent (Table 4.3.2). In each enolization and *O*-acylation control, a mixture of two isomeric enol carbonates was generated in varying *E*/*Z* ratios. Despite variable yields and selectivities, these results demonstrate that under each set of non-equilibrating enolization conditions, a mixture of enolates is generated. These yields do not necessarily reflect the true enolization selectivity due to the difficulty of *O*-acylation of the in situ-generated enolate. Although the reaction yield and diastereoselectivity of the Ireland–Claisen rearrangement of cinnamyl ester **75** is consistent for various enolization methods, our study proceeded with 1:1 LiHMDS/Me_2NEt as the standard enolization procedure as in practice this affords the cleanest reaction profile and most homogenous reaction mixture — necessitating only an acid/base extraction to afford the rearranged products in high purity in most cases.

Table 4.3.2 *Model Substrate Enolate Trapping Experiments.*[a]

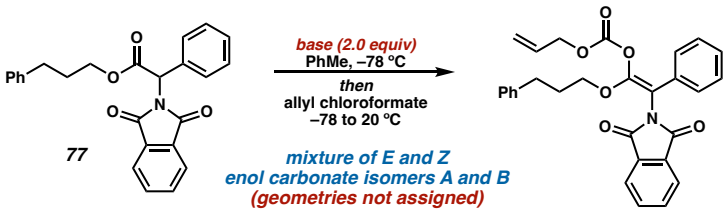

entry	base	% yield isomer A	% yield isomer B
1	LiHMDS, Me_2NEt (2.0 equiv)	16	23
2	LiHMDS	43	27
3	KHMDS	55	24

[a] Reactions performed on a 1.00 mmol scale, yields of isolated products.

4.4 ORIGINS OF DIASTEREOCONVERGENCE

The invariance of olefin geometry of the in situ-generated trimethylsilyl enol ethers in the diastereomeric selectivity of the subsequent Ireland–Claisen rearrangement to **76a**,

suggests a diastereoconvergent mechanism is indeed occurring. Kinetic enolization of **75** with LiHMDS/Me_2NEt and trapping with TMSCl affords a mixture of *E/Z* silyl enol ethers **(*Z*)-69** and **(*E*)-69**. Upon warming from –78 ºC, *Z*-enol ether **(*Z*)-69** undergoes the [3,3]-sigmatropic rearrangement preferentially through chair-like transition state **TS11** ($\Delta\Delta G^{\ddagger}$ = 5.5 kcal/mol), while *E*-enol ether **(*E*)-69** rearranges predominantly via boat-like transition state **TS14** ($\Delta\Delta G^{\ddagger}$ = –3.8 kcal/mol), yielding tetrasubstituted product **70** as a single diastereomer. With barrier heights of 19.6 and 19.9 kcal/mol for the rearrangement of **(*Z*)-69** and **(*E*)-69**, respectively, no appreciable resolution of the *E/Z*-silyl enol ether mixture is anticipated. Furthermore, these barrier heights are consistent with the experimentally observed reaction times considering gradual warming from –78 to 20 ºC.

Initial inspection of **TS11**–**TS14** reveals a commonality in which the planar phthalimide motif of the enolate fragment is rotated out of the plane defined by the olefin of the enolate (Figure 4.4.1). Examining the generality of this effect, the *E*- and *Z*-olefin isomers of both the simplified trisubstituted analog (**78**) and tetrasubstituted enolate (**79**), corresponding to the enolate fragments encountered in **TS11**–**TS14,** were optimized as the enolate anion (Figure 4.4.2). Indeed, a similar torsion around the N–C(olefin) bond is observed. The simplified trisubstituted enolates **(*E*)-78** and **(*Z*)-78**, present an optimal dihedral angle, defined between the planar enolate and phthalimide groups, of 55º and 53º, respectively. The rotation is further accentuated with introduction of an aryl substituent as in the case of α-phenyl tetrasubstituted enolates **(*E*)-79** and **(*Z*)-79** with dihedral angles of 85º and 66º, respectively (Figure 4.4.2). As is observed in **TS11–TS14**, the α-phenyl substituent remains nearly coplanar with the enolate fragment. This perturbation is likely

the result of the steric/electrostatic repulsion between the phthalimide oxygen and enolate oxygen atoms presenting a larger destabilizing force than the electronic stabilization gained through further conjugation with the enolate π-system as achieved with coplanarity.

Figure 4.4.1 *Origins of Diastereoconvergence in the Ireland–Claisen Rearrangement.*[a]

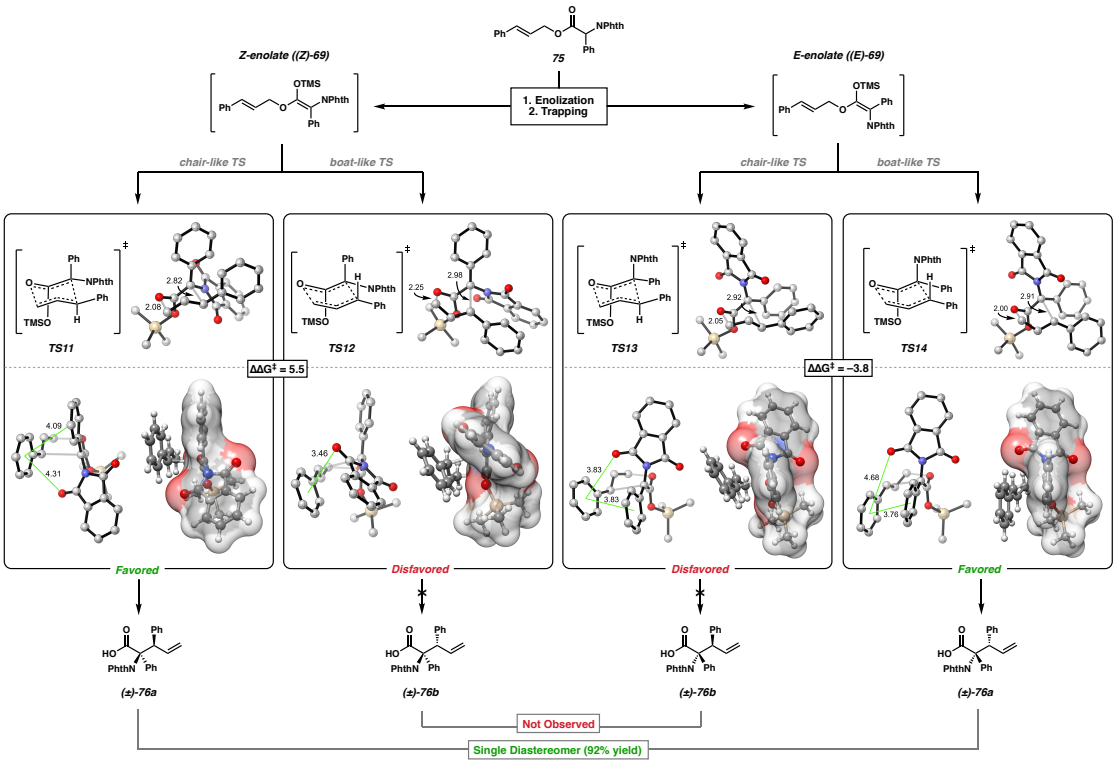

[a] Relative free energies given in kcal/mol. Surfaces depicted are solvent-excluded surfaces from Van der Waals radii with a probe radius of 1.4 Å.

Considering that the planar enolate and allyl fragments adopt a nearly parallel orientation in the transition state, the out-of-plane phthalimide substituent of the enolate scaffold is well poised to interact with substitution on the allyl fragment. Hence, the phthalimide group plays a key role in determining the stereochemical outcome of the reaction. Specifically, in the case of *Z*-silyl enol ether **(*Z*)-69**, eclipsing interactions between the equatorial, out-of-plane phthalimide group and phenyl ring of the cinnamyl

fragment are encountered in the boat-like transition state (**TS12**), resulting in a distortion of the transition state geometry. This adverse NPhth–Ph(cinnamyl) eclipsing interaction is largely relieved in the chair-like transition state (**TS11**). Hence, a substantial preference for the chair-like transition state (**TS11**) of 5.5 kcal/mol is afforded. In contrast, in the pericyclic transition states derived from *E*-silyl enol ether **(*E*)-69**, the phthalimide occupies an axial orientation. As a result, the chair-like transition state (**TS13**) bears the costly NPhth–Ph(cinnamyl) eclipsing interaction, which is greatly reduced in the boat-like transition state (**TS14**). The net interactions are substantial enough in magnitude to not only overcome the inherent preference for a chair-like transition state, but further favor the boat-like transition state by 3.8 kcal/mol.

To further highlight the role that the phthalimide moiety has in the stereocontrol of the rearrangement, control calculations were carried out in which the α-phthalimide of **(*E/Z*)-69** is replaced with an ethyl group (See Supporting Information for details). An analogous analysis to that of **TS11**–**TS14** revealed that the magnitude of $\Delta\Delta G^{\ddagger}$ of the chair/boat selectivity is reduced for both enolate geometries. Critically, with the α-phthalimide replaced with an α-ethyl substituent, the key diastereoconvergence of the transformation is lost as the chair-like transition state is favored for both *E*- and *Z*-silyl enol ethers by 1.5 and 1.2 kcal/mol, respectively.[17] Hence, in addition to being individually less selective (calculated maximum dr of 13:1 and 8:1), the overall diastereoselectivity is highly reliant on *E/Z*-selectivity of the initial enolization conditions.

Based on our working stereochemical model, if the NPhth–Ph(cinnamyl) eclipsing interaction is indeed the dominant element of stereocontrol, then inversion of the

axial/equatorial positioning of the phenyl group of the cinnamyl fragment, i.e., employing the *Z*-cinnamyl ester (**80**), leads to an inversion in the chair/boat transition state preference for *both* corresponding *E*- and *Z*-silyl enol ethers. In this case, the double-inversion in stereoselectivity affords the identical diastereomerof product **76a** as obtained from *E*-cinnamyl ester **75**.

Figure 4.4.2 *Geometric Perturbations Resulting from the Out-of-Plane Rotation of the Phthalimide Moiety.*[a]

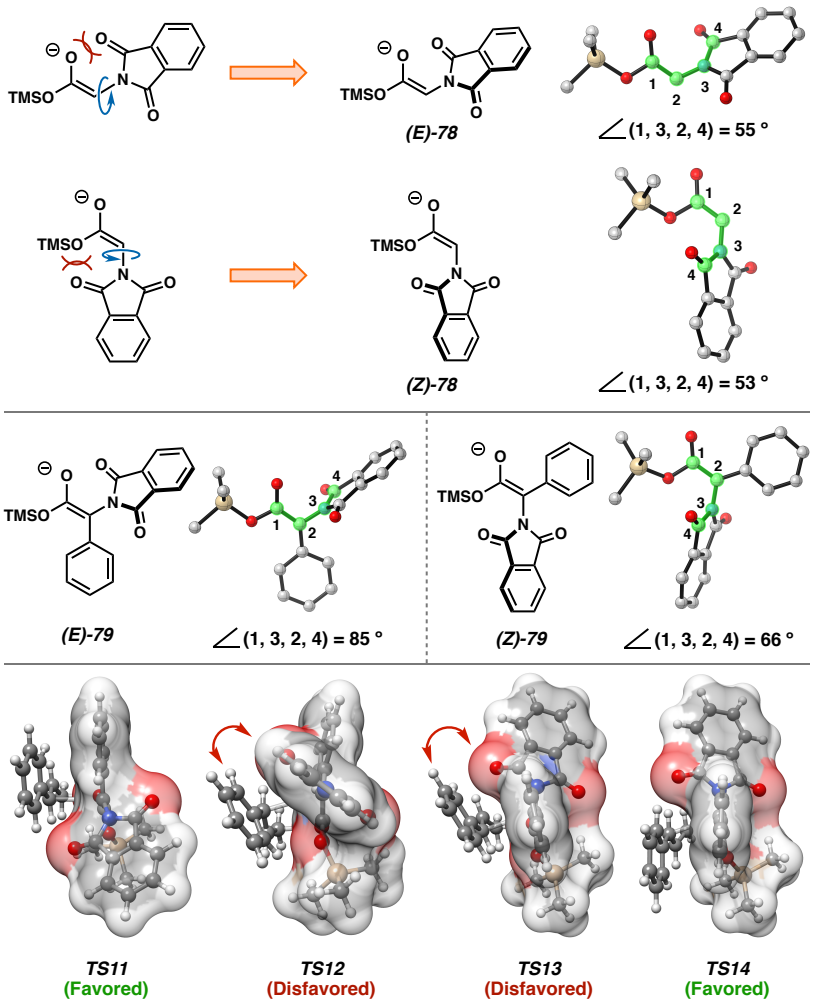

[a] Surfaces depicted are solvent-excluded surfaces from Van der Waals radii with a probe radius of 1.4 Å.

With respect to the *E*-cinnamyl system, a global inversion in the chair/boat transition state preference for both *E*/*Z*-silyl enol ethers is predicted (Figure 5). *Z*-silyl enol ether **(*Z*)-20** preferentially rearranges through a boat-like transition state (**TS19**) ($\Delta\Delta G^{\ddagger}$ = –1.0 kcal/mol), while for *E*-silyl enol ether **(*E*)-81**, the chair-like transition state (**TS20**) is preferred ($\Delta\Delta G^{\ddagger}$ = 5.2 kcal/mol). As anticipated, the Ireland–Claisen rearrangment of *Z*-cinnamyl ester **80** affords the same diastereomeric outcome as with *E*-cinnamyl ester **75**. In total, the diastereoselectivity of the transformation is invariant to any combination of the *E*/*Z*-geometry of both olefins of the in situ-generated silyl enol ether. We term this effect *global diastereoconvergence* — i.e., all possible stereoisomers derived from permutations of stereochemical elements of the reagent lead to formation of a single stereoisomer of product. To the best of our knowledge, this constitutes the first example of a globally diastereoconvergent Ireland–Claisen rearrangement of an acyclic, tetrasubstituted silyl enol ether.

Figure 4.4.3 *Global Stereoconvergence in the Ireland–Claisen Rearrangement of Z- and E-Cinnamyl Compounds* ***75*** *and* ***80****.*[a]

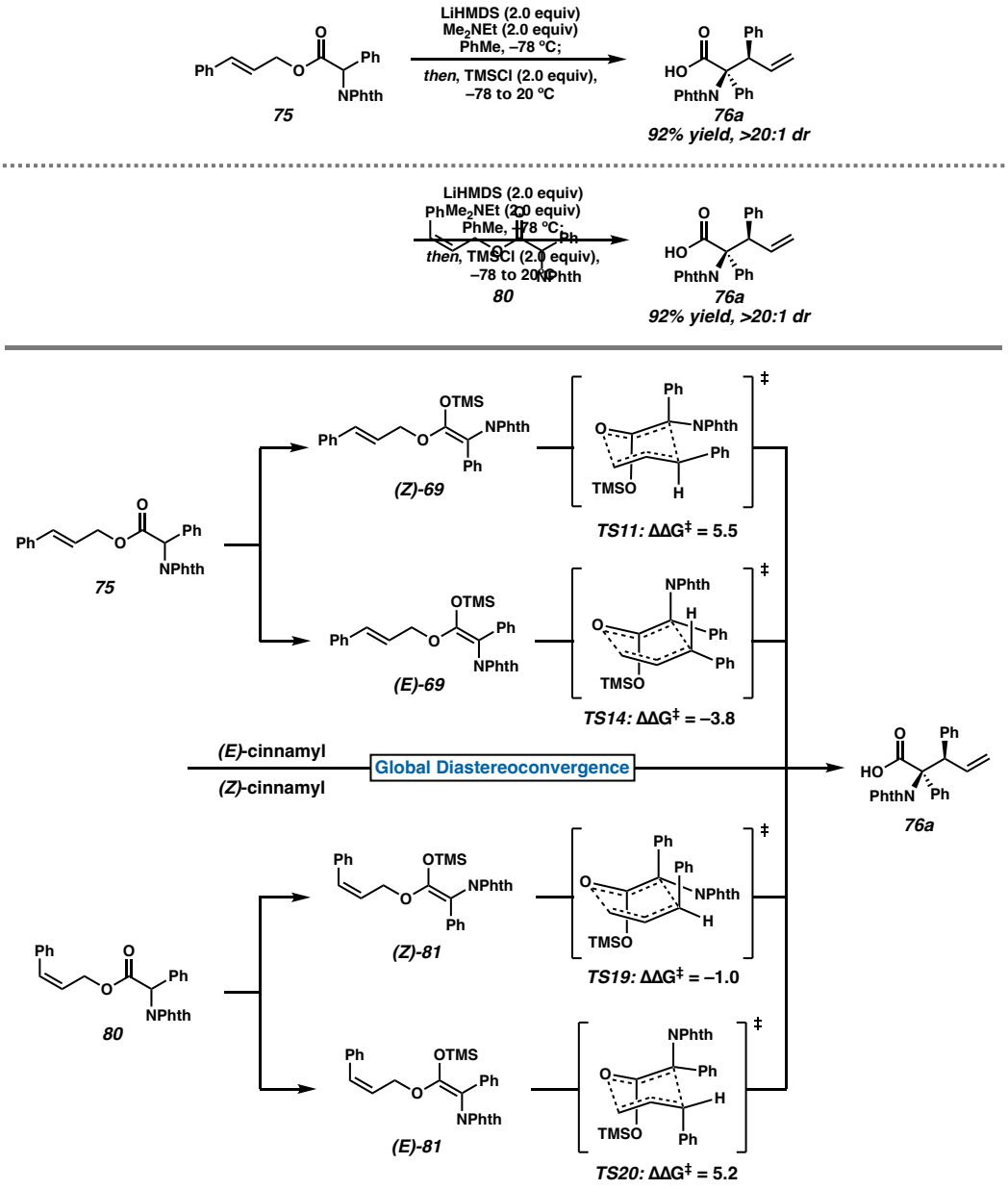

[a] Relative free energies given in kcal/mol.

4.5 INVESTIGATION OF CHIRALITY TRANSFER

A powerful feature of the Ireland–Claisen rearrangement is its ability to relay stereochemical information from a chiral center in the substrate to the absolute

stereochemistry of the rearranged product.[18] In contrast to previous achiral examples, the approach of a chiral cinnamyl fragment from either the *Re*- or *Si*-faces of the enol ether gives rise to diastereomeric transition states. For a mixture of *E/Z*-silyl enol ethers this gives rise to eight unique transition states which we modeled with regards to enantioenriched α-phthalimido ester **82** (Figure 4.5.1).

Analogous to our previous discussion, the *Z*- and *E*-silyl enol ethers derived from **82** preferentially rearrange via chair-like (**TS21**) and boat-like (**TS28**) transition states, respectively. While the NPhth–Ph(cinnamyl) eclipsing interaction drives the chair/boat selectivity in each silyl enol ether geometry, differentiation between the two diastereotopic chair-like (**TS21** and **TS23**) and boat-like (**TS26** and **TS28**) transition states must be achieved for effective chirality transfer. This component of the stereoselectivity arises in the energetic differences between axial and equatorial orientation of the methyl group (Figure 4.5.1). For the relevant chair-like transitions states (**TS21** and **TS23**) derived from the *Z*-enol ether of **82**, the 1,3-diaxial interactions imposed from the methyl group occupying an axial orientation carry an energetic penalty of 4.3 kcal/mol. Likewise, for the pair of boat-like transition states in the rearrangement of the *E*-enol ether (**TS26** and **TS28**) a preference of 1.4 kcal/mol is found for the equatorial orientation of the methyl group. As a result, the system exhibits diastereoconvergence with respect to chirality transfer. To experimentally demonstrate this, we synthesized the enantioenriched α-phthalimido ester from the requisite alcohol, in turn prepared via Corey–Bakshi–Shibata (CBS) reduction. Indeed, non-selective enolization, trapping as the TMS enol ether, and warming to 20 ºC affords the desired α,α-disubstituted acid. The crude acid was subsequently transformed

to methyl ester **83**, which was isolated in 86% yield over two steps, >20:1 dr, and with complete retention of enantiomeric excess (95% ee) (Figure 4.5.1).

Figure 4.5.1 *Chirality Transfer in the Diastereoconvergent Ireland–Claisen Rearrangement.*[a]

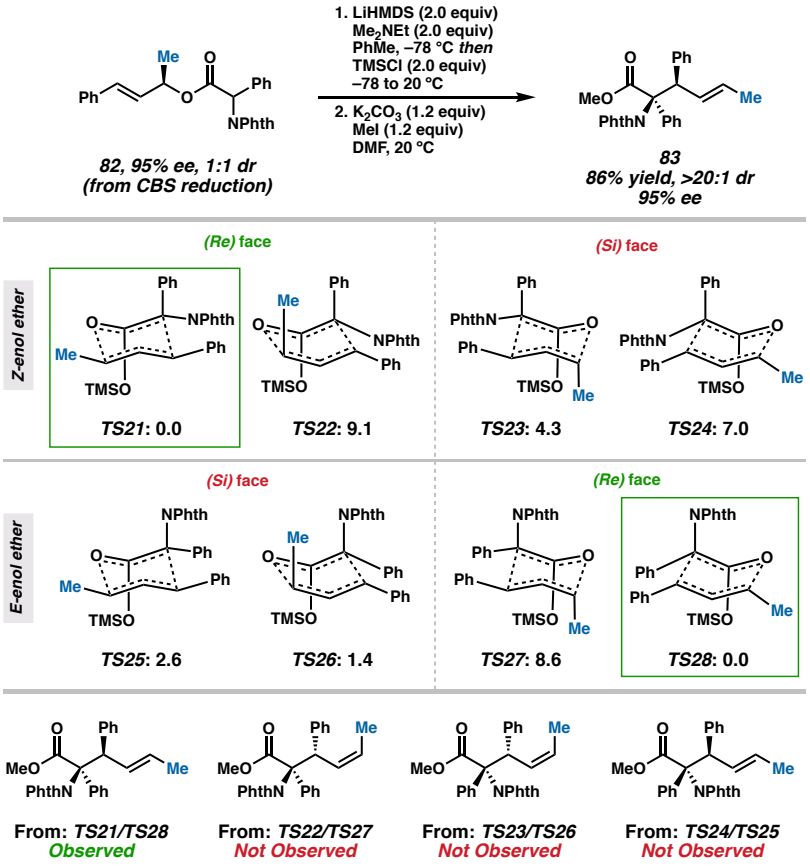

[a] Relative free energies (in kcal/mol) of the eight possible stereochemically distinct transition states for the rearrangement of the *E*- and *Z*-silyl enol ethers derived from **82**.

4.6 SCOPE OF THE DIASTEROCONVERGENT IRELAND–CLAISEN REARRANGEMENT

A variety of differentially substituted α-aryl, α-phthalimido esters were examined in the Ireland–Claisen rearrangement to explore the scope of this transformation (Table 4.6.1). The reaction was highly compatible with a broad scope of differentially substituted

esters, affording tetrasubstituted amino acid derivatives bearing an adjacent tertiary stereogenic center with generally >20:1 diastereoselectivity. Additionally, the rearrangement could be performed with standard substrate **75** on a 5.00 g (12.6 mmol) scale with identical yield and diastereoselectivity. In some cases, the carboxylic acid products were transformed into the corresponding methyl ester to circumvent challenges in substrate acid/base purification or decomposition of the parent carboxylic acid. With respect to the α-aryl group, a variety of both electron rich and electron deficient aryl rings were tolerated in excellent yields. Chloro and methoxy *ortho*-substitution was also well tolerated in the rearrangement, affording highly sterically encumbered amino acid derivatives **90** and **91** in excellent yields with >20:1 dr. Variation of the allylic olefin aryl group was also well tolerated, providing differentially substituted β-aryl groups in high yield and diastereoselection. Methyl *ortho*-substitution was also well tolerated, affording carboxylic acid **98** as a single diastereomer in 79% yield. In addition to these substrates, a variety of different heterocycles were incorporated, affording rearrangement products in generally >20:1 dr and moderate to excellent yield.

Table 4.6.1 *Scope of the Diastereoconvergent Ireland–Claisen Rearrangement.*[a]

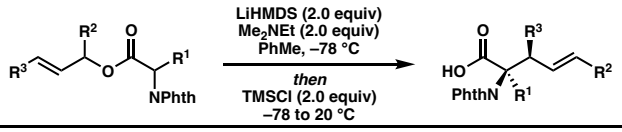

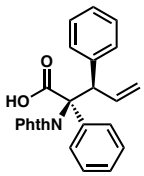

76a
92% yield, >20:1 dr
93% yield, >20:1 dr[b]

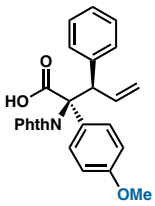

84
91% yield, >20:1 dr

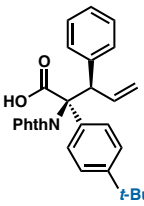

85
94% yield, >20:1 dr

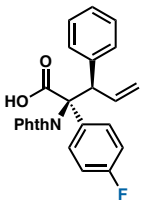

86
97% yield, >20:1 dr

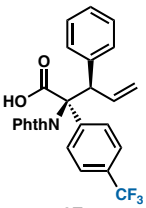

87
94% yield, >20:1 dr

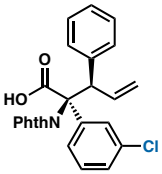

88
89% yield, >20:1 dr

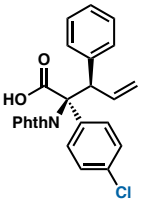

89
96% yield, >20:1 dr

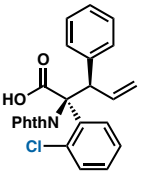

90[c]
95% yield, >20:1 dr

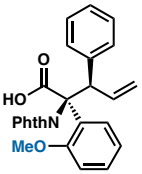

91[c]
87% yield, >20:1 dr

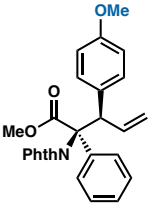

92
70% yield, >20:1 dr

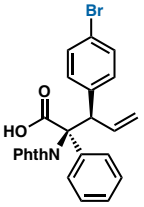

93
93% yield, >20:1 dr

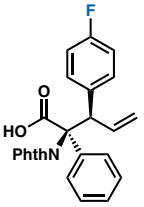

94
83% yield, >20:1 dr

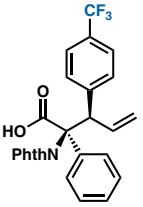

95
87% yield, >20:1 dr

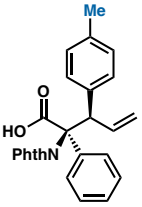

96
88% yield, >20:1 dr

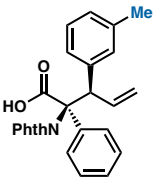

97
83% yield, >20:1 dr

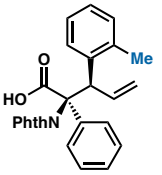

98
79% yield, >20:1 dr

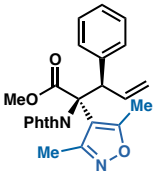

99
40% yield, >20:1 dr

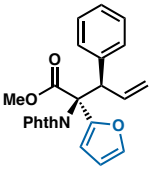

100
65% yield, >20:1 dr

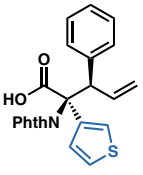

101
76% yield, >20:1 dr

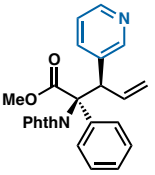

102
89% yield, >20:1 dr

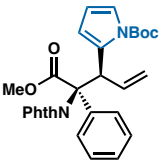

103
71% yield, 10:1 dr

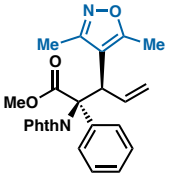

104
68% yield, >20:1 dr

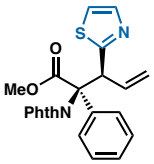

105
38% yield, >20:1 dr

[a] Reactions were performed on a 1.00 mmol scale, yields are of isolated products. Diastereomeric ratios were determined by ^{1}H NMR spectroscopy. In some cases, the crude products were converted to the corresponding methyl ester for isolation. Relative configuration was assigned by X-Ray diffraction of **76a**, all other relative configurations were assigned by analogy. [b] Reaction performed on a 5.00 g scale. [c] Rearrangement performed at 40 ºC.

While a broad scope of rearrangement products could be prepared utilizing this diastereoconvergent methodology, alkyl-substituted allylic esters proved to be challenging substrates (Scheme 4.6.2). *E*-hexenyl ester **106** afforded methyl ester **107** in 2.3:1 dr. A modest improvement in diastereoselectivity is observed with *Z*-pentenyl ester **108** which was isolated as methyl ester **109** in 3.7:1 dr. On the other hand, excellent diastereoselectivity and enantioretention (>99% ee) was observed with *(S)*-cyclohex-2-en-1-ol derived ester **110**. The relative and absolute stereochemistry of cyclohexene **111** was determined by single crystal X-ray diffraction.

Scheme 4.6.2 *Ireland–Claisen Rearrangement of Tetrasubstituted α-Phthalimido Esters with Alkyl Substituted Allyl Esters.*

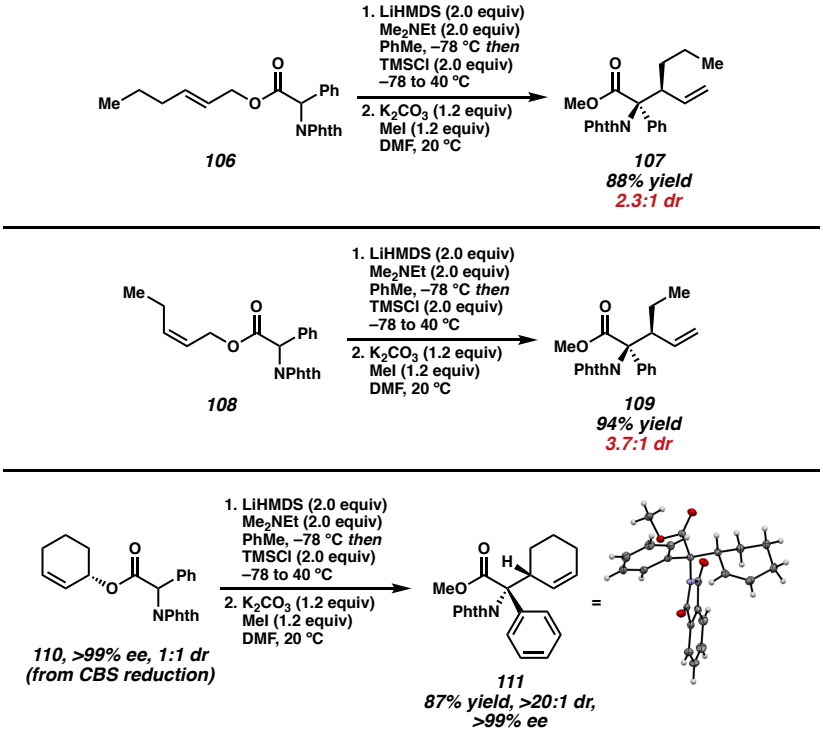

4.7 PRODUCT DERIVATIZATIONS

Derivatization of Ireland–Claisen rearrangement product **15a** afforded a range of densely functionalized small molecules (Scheme 4.7.1). Curtius rearrangement in *t*-BuOH provided bench-stable, differentially protected aminoacetal **112** in 82% yield. Iodolactonization afforded lactone **113** in an excellent 91% yield as a single diasteromer with the relative configuration confirmed by single crystal X-ray diffraction. Ozonolysis with reductive quenching provided cyclized product **114** in 11:1 dr and 86% yield. Methyl esterification with MeI/K_2CO_3 generated ester **115** in excellent 90% yield. Removal of the phthalimide proved challenging under standard hydrazine-mediated protocols due to competitive olefin reduction and slow phthalhydrazide removal. A modified Ganem protocol[19] reported by Davies[20] affected semi-reduction of the phthalimide. Methyl esterification followed by AcOH-mediated phthalide removal afforded α-amino acid methyl ester **116**.

Scheme 4.7.1 *Derivatizations of Ireland–Claisen Product* ***76a****.*

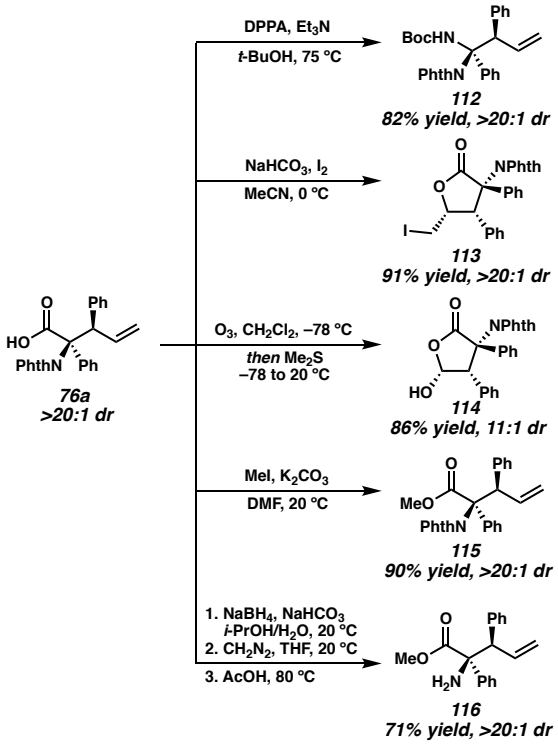

4.8 CONCLUSION

We have computationally modeled and experimentally developed a globally diastereoconvergent Ireland–Claisen rearrangement of α-phthalimido esters that is invariant to the geometry of the silyl enol ether and allylic ester olefin. A local coupled-cluster theory (DLPNO-CCSD(T)) and DFT multi-level approach was employed for the accurate determination of quantum mechanical energies. The scope of the rearrangement is broad with respect to aryl and heteroaryl substitution, and a variety of α-phthalimide-protected α-tetrasubstituted amino acids bearing a vicinal tertiary stereogenic center are isolated with generally excellent (>20:1) diastereoselection in good to excellent yields. Additionally, transfer of chirality with stereodefined α-phthalimido esters affords rearrangement products with excellent retention of chiral information. A range of densely

substituted small molecules can be readily prepared from representative rearrangement product **76a**.

4.9 EXPERIMENTAL SECTION

4.9.1 COMPUTATIONAL DETAILS

All quantum mechanical calculations were performed with ORCA version 4.1 and 4.2.[21] The resolution of identity (RI) and chain-of-spheres[22] (keyword = RIJCOSX) approximations were utilized for Coulomb and exchange integrals, respectively. Automatic generation of the auxiliary basis sets was employed (keyword = AutoAux).[23] The finest integration grid settings (Grid7, NoFinalGrid, GridX9) were utilized in all calculations. The values obtained from all quantum mechanical calculations are included in the supporting excel file.

4.9.1.1 Density Functional Theory (DFT) Calculations

Unless otherwise noted, geometry optimizations were carried out with the B3LYP global hybrid generalized gradient approximation (GGA) functional[24] with Becke–Johnson damped D3 dispersion corrections[25] (henceforth referred to as B3LYP-D3(BJ)) with the 6-31G(d) basis set on all atoms. Thermal corrections at 298.15 K were calculated from the unscaled vibrational frequencies at this level of theory. The Quasi-RRHO method was applied to correct for the breakdown of the harmonic oscillator approximation for low frequency vibrations.[26] All stationary points are characterized by the appropriate number of imaginary vibrational modes (zero for optimized geometries and one for transition states). Intrinsic reaction coordinate (IRC) analyses were carried out to ensure all transition states connect the appropriate starting materials and products.

Triple-ζ quality single point calculations were carried out on all stationary points with the B3LYP-D3(BJ) and M06-2X[27] density functionals with the def2-TZVPP basis set[28] on all atoms. The SMD implicit solvation model[29] for toluene (e = 2.374, r_{probe} = 1.300 Å, Refrac. = 1.330) was employed in these single point calculations. Thermal corrections obtained at the previous level of theory were then applied to these electronic energies to obtain the final DFT Gibbs free energies. Relative free energies are given in kcal/mol and are calculated for a 1 atm standard state at 298.15 K.

Conformer searching was carried out both manually and in Spartan Version 7. Conformers were subsequently optimized at the B3LYP-D3(BJ)/6-31G(d) level of theory. The lowest energy conformers [evaluated at B3LYP-D3(BJ)/def2-TZVPP/SMD(Toluene)//B3LYP-D3(BJ)/6-31G(d)] are reported. Note that for transition states, all conformers were considered in subsequent DFT and DLPNO-CCSD(T) calculations.

4.9.1.2 DLPNO-CCSD(T) Calculations

Additional single point calculations were performed on key optimized structured with the domain based local pair natural orbital coupled-cluster (DLPNO-CCSD(T)) method as described by Neese and coworkers and as implemented in ORCA.[30] The cc-pVTZ basis set,[31] with the corresponding cc-pVTZ/C and def2/J auxiliary basis sets,[32] are used on all atoms. Gaseous free energies are calculated by applying the thermodynamic corrections obtained at the optimization (DFT) level of theory to the gas phase electronic energies from DLPNO-CCSD(T) single point calculations. A free energy of solvation calculated from DFT (M06-2X/def2-TZVPP/SMD(Toluene)) is added to the gaseous

coupled-cluster free energies to afford the final reported coupled-cluster solvated Gibbs free energies as reported in the manuscript:

$$G^{CCSD(T)} = E(el)^{CCSD(T)} + ZPE + E(vib) + E(rot) + E(trans) + k_bT - TS + \Delta G(solv)^{DFT}$$

Similar results are obtained if the SMD for toluene is applied in the DLPNO-CCSD(T) calculations; however, we highlight that the solvent self-consistent reaction field (SCRF) is only optimized self-consistently with respect to the Hartree–Fock reference wavefunction and not with respect to the subsequent optimization of coupled-cluster amplitudes.

Notes:

- Similar results are obtained with the def2-TZVPP basis set in control experiments, although we elected to employ Dunning's cc-pVnZ family of basis sets for ease of basis set extrapolation with further calculations should the need arise.
- "TightPNO" settings were employed in all calculations.
- "TightPNO": $T_{CutPairs} = 10^{-5}$, $T_{CutDO} = 5x10^{-3}$, $T_{CutPNO} = 1.00x10^{-7}$, $T_{CutMKN} = 10^{-3}$.

4.9.1.3 Initial Benchmarking/Control Calculations

Given the importance of non-covalent interactions in controlling the stereochemical outcome of the stereoconvergent Ireland–Claisen reaction, final electronic energies were obtained at the DLPNO-CCSD(T) level of theory. For comparison, DFT single point calculations were carried out with the B3LYP-D3(BJ) and M06-2X functionals. Gratifyingly, the results from the DFT and coupled-cluster computations are in good agreement.

Table 4.9.3.1 *Comparison between DFT and DLPNO-CCSD(T) methods.*[a]

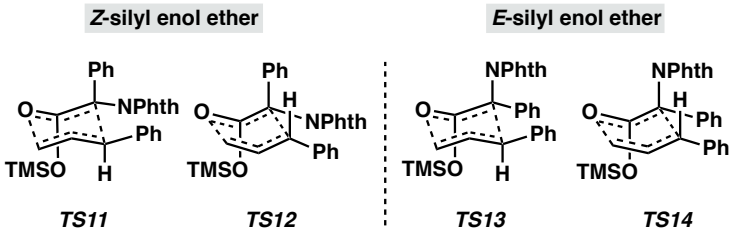

Method/Basis set	TS11	TS12	TS13	TS14
B3LYP-D3(BJ)/def2-TZVPP/SMD(PhMe)	0.0	4.3	3.8	0.0
M06-2X/def2-TZVPP/SMD(PhMe)	0.0	5.4	3.7	0.0
M06-2X/6-311++G(d,p)/SMD(PhMe)	0.0	5.4	3.7	0.0
DLPNO-CCSD(T)/cc-pVTZ	0.0	5.3	3.6	0.0
DLPNO-CCSD(T)/cc-pVTZ/SMD(PhMe)	0.0	5.5	3.8	0.0

[a] Single point calculations carried out on B3LYP-D3(BJ)/6-31G(d) optimized geometries

4.9.2 MATERIALS AND METHODS

Unless otherwise stated, reactions were performed in flame-dried glassware under an argon or nitrogen atmosphere using dry, deoxygenated solvents. Solvents were dried by passage through an activated alumina column under argon.33 Reaction progress was monitored by thin-layer chromatography (TLC) or Agilent 1290 UHPLC-MS. TLC was performed using E. Merck silica gel 60 F254 precoated glass plates (0.25 mm) and visualized by UV fluorescence quenching, *p*-anisaldehyde, or $KMnO_4$ staining. Silicycle Silia*Flash*® P60 Academic Silica gel (particle size 40–63 μm) was used for flash chromatography. ^{1}H NMR spectra were recorded on Varian Inova 500 MHz and Bruker 400 MHz spectrometers and are reported relative to residual $CHCl_3$ (δ 7.26 ppm). ^{13}C NMR spectra were recorded on a Varian Inova 500 MHz spectrometer (125 MHz) and Bruker

400 MHz spectrometers (100 MHz) and are reported relative to $CHCl_3$ (δ 77.16 ppm). Data for ^1H NMR are reported as follows: chemical shift (δ ppm) (multiplicity, coupling constant (Hz), integration). Multiplicities are reported as follows: s = singlet, d = doublet, t = triplet, q = quartet, p = pentet, sept = septuplet, m = multiplet, br s = broad singlet, br d = broad doublet. Data for ^{13}C NMR are reported in terms of chemical shifts (δ ppm). IR spectra were obtained by use of a Perkin Elmer Spectrum BXII spectrometer or Nicolet 6700 FTIR spectrometer using thin films deposited on NaCl plates and reported in frequency of absorption (cm^{-1}). Optical rotations were measured with a Jasco P-2000 polarimeter operating on the sodium D-line (589 nm), using a 100 mm path-length cell. High resolution mass spectra (HRMS) were obtained from Agilent 6200 Series TOF with an Agilent G1978A Multimode source in electrospray ionization (ESI+), atmospheric pressure chemical ionization (APCI+), or fast atom bombardment (FAB+). Reagents were purchased from commercial sources and used as received unless otherwise stated.

4.9.3 EXPERIMENTAL PROCEDURES

4.9.3.1 General Procedure for the Ireland–Claisen Rearrangement

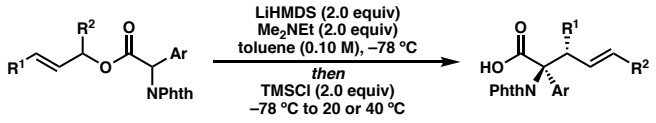

In a nitrogen-filled glovebox, an oven-dried 50 mL round bottom flask was charged with LiHMDS (335.0 mg, 2.00 mmol, 2.0 equiv) and a Teflon-coated stir bar. The flask was then sealed with a septum, removed from the glovebox, and placed under an atmosphere of nitrogen. To the flask was then added toluene (3.0 mL) and *N*,*N*-dimethylethylamine (213 μL, 2.00 mmol, 2.0 equiv). The resulting solution was stirred at

20 °C for 5 min, then the flask was immersed in a –78 °C dry ice/acetone bath. After stirring for 15 min, a solution of the α-phthalidomido ester (1.00 mmol, 1.0 equiv) dissolved in toluene (7.0 mL) was added dropwise over 5 min, resulting in the immediate formation of a dark red/purple opaque reaction mixture. The reaction was maintained at –78 °C for 2 h, after which time TMSCl (254 μL, 2.00 mmol, 2.0 equiv) was added dropwise over 1 min. The reaction flask was then removed from the cooling bath and allowed to warm to 20 °C, typically resulting in an opaque yellow/orange reaction mixture. After consumption of the α-phthalidomido ester was observed by TLC analysis (typically 2–4 h), the reaction was quenched with 1 N HCl (10 mL) and transferred to a separatory funnel with Et_2O (10 mL). As noted below, some compounds required heating to 40 °C for 24 h for full conversion. The layers were separated, and the aqueous layer was extracted with Et_2O (2 x 10 mL). The combined organic layers were dried over Na_2SO_4, filtered, and concentrated by rotary evaporation to afford the crude rearrangement product. Depending on the water solubility and/or stability of the product, the reaction was isolated using the following general procedures:

Isolation Procedure 1: The crude reaction mixture was transferred to a 50 mL round bottom flask containing a Teflon-coated stir bar with THF (5 mL) and 2 N HCl (1 mL). The resulting mixture was stirred vigorously at 20 °C for 30 min. THF was then removed via rotary evaporation and the reaction mixture was transferred to a separatory funnel with Et_2O (10 mL) and H_2O (10 mL). The pH of the aqueous layer was adjusted to 12 with sat. aq. Na_2CO_3 and the layers were mixed and separated. The aqueous layer was washed with an additional portion of Et_2O (10 mL), and the combined organic layers were washed with

H_2O basified to pH 12 with Na_2CO_3 (5 mL). The combined aqueous layers were then acidified to pH 3 with 4 N HCl and extracted with Et_2O (2 x 10 mL). The combined organic extracts were then dried over Na_2SO_4, filtered, and concentrated by rotary evaporation to afford the desired rearrangement product.

Isolation Procedure 2: The crude reaction mixture was transferred to a flame-dried 25 mL round bottom flask with DMF (3.3 mL). To the stirring solution was then added K_2CO_3 (165.8 mg, 1.20 mmol, 1.2 equiv) and MeI (75 μL, 1.2 mmol, 1.2 equiv). The resulting suspension was stirred rapidly at 20 °C. After consumption of the carboxylic acid rearrangement product was observed by TLC analysis, the reaction mixture was transferred to a separatory funnel with EtOAc (10 mL) and H_2O (10 mL). The layers were separated and the aqueous layer was extracted with EtOAc(2 x 10 mL). The combined organic layers were then washed with brine (10 mL), dried over Na_2SO_4, and concentrated via rotary evaporation. The crude product was then purified by flash column chromatography to afford the desired methyl ester.

Isolation Procedure 3: *Caution! Diazomethane is toxic and explosive; all operations should be carried out in a well-ventilated hood with adequate shielding.* The crude reaction mixture was transferred to a 50 mL round bottom flask with THF (5 mL). The flask was charged with a Teflon-coated stir bar and a blast shield was placed in front of the reaction flask. To the slowly stirring reaction mixture was then added freshly prepared CH_2N_2 (approx. 6 mL of a 0.2 M solution in Et_2O) drop-wise via a flame-polished pipette. After consumption of the carboxylic acid rearrangement product was observed by TLC analysis, acetic acid (2.0 mL) was added dropwise to quench residual CH_2N_2. The reaction mixture was stirred for 20 mins and then transferred to a separatory funnel with EtOAc (10 mL)

and sat. aq. $NaHCO_3$ (10 mL). The layers were separated and the aqueous was extracted with EtOAc (2 x 10 mL). The combined organics were dried over Na_2SO_4, filtered, and concentrated via rotary evaporation. The crude product was then purified by flash column chromatography to afford the desired methyl ester.

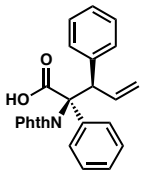

(2*S,3*R**)-2-(1,3-dioxoisoindolin-2-yl)-2,3-diphenylpent-4-enoic acid (76a)**

Prepared according to general procedure 1 with isolation procedure 1 and obtained as a white foam (364.5 mg, 0.917 mmol, 92% yield, >20:1 dr); ^{1}H NMR (500 MHz, Chloroform-*d*) δ 7.79 – 7.72 (m, 2H), 7.73 – 7.67 (m, 2H), 7.48 – 7.42 (m, 2H), 7.28 – 7.21 (m, 3H), 7.16 – 7.11 (m, 2H), 7.11 – 7.06 (m, 1H), 7.04 – 7.00 (m, 2H), 6.59 (ddd, *J* = 17.2, 10.4, 8.3 Hz, 1H), 5.50 (d, *J* = 8.2 Hz, 1H), 5.24 – 5.02 (m, 2H); ^{13}C NMR (100 MHz, Chloroform-*d*) δ 173.2, 167.9, 139.9, 138.3, 136.1, 134.4, 131.6, 130.6, 128.9, 128.1, 128.0, 127.7, 127.2, 123.6, 118.9, 71.5, 53.1. IR (Neat Film, NaCl) 3061 (br), 1778, 1722, 1497, 1470, 1448, 1369, 1348, 1320, 1265, 1200, 1161, 1110, 1087, 1034, 991, 961, 932, 841, 790, 725, 705, 682, 642 cm^{-1}; (MM:FAB+) *m/z* calc'd for $C_{25}H_{20}NO_4$ $[M+H]^+$: 398.1392, found 398.1394.

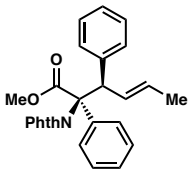

methyl (2*S*,3*R*,*E*)-2-(1,3-dioxoisoindolin-2-yl)-2,3-diphenylhex-4-enoate (83)

Prepared according to general procedure 1 with isolation procedure 2 with purification by silica gel chromatography (30% EtOAc in hexanes) to afford the desired product as a white solid (365.4 mg, 86% yield over 2 steps, >20:1 dr, 95% ee) $[\alpha]_D^{25}$ +49.5 (*c* 1.0, $CHCl_3$); ^1H NMR (400 MHz, Chloroform-*d*) δ 7.80 – 7.74 (m, 2H), 7.74 – 7.68 (m, 2H), 7.49 – 7.41 (m, 2H), 7.32 – 7.23 (m, 3H), 7.22 – 7.16 (m, 2H), 7.13 – 7.02 (m, 3H), 6.16 (ddd, *J* = 15.3, 8.8, 1.8 Hz, 1H), 5.57 (dq, *J* = 15.6, 6.5 Hz, 1H), 5.48 (d, *J* = 8.8 Hz, 1H), 3.60 (s, 3H), 1.59 (dd, *J* = 6.4, 1.7 Hz, 3H); ^{13}C NMR (100 MHz, Chloroform-*d*) δ 169.8, 168.0, 141.2, 136.5, 134.2, 131.7, 131.0, 130.5, 129.6, 128.9, 127.9, 127.7, 127.4, 126.9, 123.4, 71.7, 52.7, 52.3, 18.4; IR (Neat Film, NaCl) 1779, 1722, 1366, 1318, 1222, 1108, 1086, 972, 904, 734, 722; (MM:ESI-APCI+) *m/z* calc'd for $C_{27}H_{24}NO_4$ $[M+H]^+$: 426.1700, found 426.1694; SFC Conditions: 10% IPA, 2.5 mL/min, Chiralpak IC column, λ = 210 nm, t_R (min): minor = 5.79, major = 7.70.

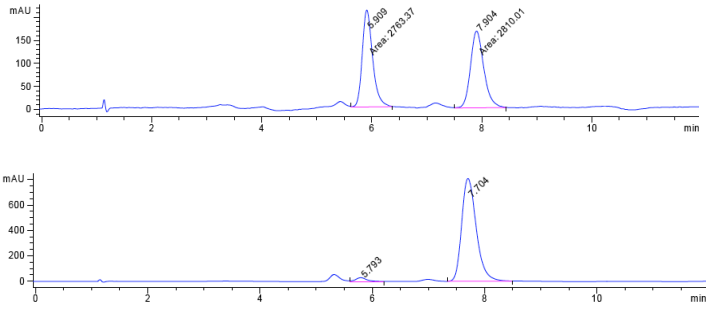

Peak #	RetTime [min]	Type	Width [min]	Area [mAU*s]	Height [mAU]	Area %
1	5.793	VB	0.2012	407.79361	30.26814	2.6956
2	7.704	VB	0.2818	1.47204e4	810.69513	97.3044

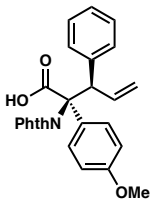

(2*S,3*R**)-2-(1,3-dioxoisoindolin-2-yl)-2-(4-methoxyphenyl)-3-phenylpent-4-enoic acid (84)**

Prepared according to general procedure 1 with isolation procedure 1 and obtained as a white foam (388.7 mg, 0.909 mmol, 91% yield, >20:1 dr); ^{1}H NMR (500 MHz, Chloroform-*d*) δ 7.79 – 7.74 (m, 2H), 7.74 – 7.70 (m, 2H), 7.43 – 7.37 (m, 2H), 7.21 – 7.15 (m, 2H), 7.14 – 7.09 (m, 1H), 7.08 – 7.04 (m, 2H), 6.83 – 6.79 (m, 2H), 6.61 (ddd, *J* = 17.1, 10.4, 8.3 Hz, 1H), 5.48 (d, *J* = 8.3 Hz, 1H), 5.21 – 5.09 (m, 2H), 3.79 (s, 3H); ^{13}C NMR (100 MHz, Chloroform-*d*) δ 173.0, 167.9, 159.2, 140.1, 138.4, 134.3, 131.6, 130.6, 130.2, 128.0, 127.9, 127.1, 123.5, 118.7, 113.1, 71.0, 55.3, 53.1; IR (Neat Film, NaCl) 3064 (br), 1776, 1722, 1608, 1512, 1462, 1369, 1347, 1321, 1256, 1180, 1120, 1086, 992, 962, 925, 828, 722, 703, 682 cm^{-1}; (MM:FAB+) *m/z* calc'd for $C_{26}H_{22}NO_5$ $[M+H]^+$: 428.1498, found 428.1489.

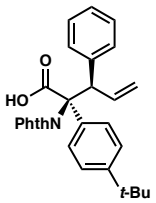

(2*S,3*R**)-2-(4-(*tert*-butyl)phenyl)-2-(1,3-dioxoisoindolin-2-yl)-3-phenylpent-4-enoic acid (85)**

Prepared according to general procedure 1 with purification by flash column chromatography (25% EtOAc in hexanes with 2% AcOH) and isolated as a tan amorphous solid (426.7 mg, 0.941 mmol, 94% yield, >20:1 dr); ^{1}H NMR (500 MHz, Chloroform-*d*) δ 7.79 – 7.73 (m, 2H), 7.72 – 7.68 (m, 2H), 7.39 – 7.31 (m, 2H), 7.28 – 7.21 (m, 2H), 7.17 – 7.12 (m, 2H), 7.12 – 7.06 (m, 1H), 7.05 – 6.99 (m, 2H), 6.61 (dt, *J* = 17.0, 9.9, 8.2 Hz, 1H), 5.49 (d, *J* = 8.2 Hz, 1H), 5.20 – 5.07 (m, 2H), 1.28 (s, 9H); ^{13}C NMR (100 MHz, Chloroform-*d*) δ 174.1, 167.9, 150.7, 140.0, 138.4, 134.3, 132.7, 131.5, 130.6, 128.5, 127.9, 127.0, 124.6, 123.4, 118.6, 71.3, 52.9, 34.5, 31.3; IR (Neat Film, NaCl) 3062 (br), 2963, 2361, 1778, 1722, 1715, 1652, 1506, 1470, 1506, 1470, 1368, 1348, 1319, 1267, 1204, 1122, 1087, 992, 931, 838, 773, 723, 704, 665 cm^{-1}; (MM:FAB+) *m/z* calc'd for $C_{29}H_{28}NO_4$ $[M+H]^+$: 454.2018, found 454.2022.

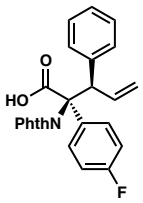

(2*S,3*R**)-2-(1,3-dioxoisoindolin-2-yl)-2-(4-fluorophenyl)-3-phenylpent-4-enoic acid (86)**

Prepared according to general procedure 1 with isolation procedure 1 and obtained as a white foam (404.6 mg, 0.974 mmol, 97% yield, >20:1 dr); ^{1}H NMR (500 MHz, Chloroform-*d*) δ 7.82 – 7.76 (m, 2H), 7.77 – 7.72 (m, 2H), 7.45 (t, *J* = 8.4, 5.1 Hz, 2H), 7.16 – 7.10 (m, 3H), 7.11 – 7.04 (m, 2H), 6.95 (t, *J* = 8.5 Hz, 2H), 6.60 (dt, *J* = 17.0, 9.9, 8.8 Hz, 1H), 5.49 (d, *J* = 8.2 Hz, 1H), 5.23 – 5.12 (m, 2H); ^{13}C NMR (100 MHz, Chloroform-*d*) δ 173.1, 167.9, 162.3 (d, $J_{C–F}$ = 247.9 Hz), 139.6, 138.0, 134.5, 131.9 (d, $J_{C–F}$ = 3.5 Hz), 131.5, 130.8 (d, $J_{C–F}$ = 8.1 Hz), 130.6, 128.1, 127.3, 123.6, 119.1, 114.6 (d, $J_{C–F}$ = 21.5 Hz), 71.0, 53.2; ^{19}F NMR (282 MHz, Chloroform-*d*) δ –62.69 – –62.73 (m); IR (Neat Film, NaCl) 3061, 1777, 1722, 1605, 1509, 1470, 1410, 1367, 1348, 1320, 1239, 1164, 1107, 1086, 990, 962, 929, 839, 723, 703 cm^{-1}; (MM:FAB+) *m/z* calc'd for $C_{25}H_{19}NO_4F$ $[M+H]^+$: 416.1298, found 416.1282.

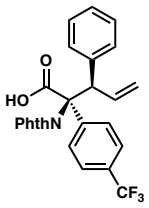

(2*S,3*R**)-2-(1,3-dioxoisoindolin-2-yl)-3-phenyl-2-(4-(trifluoromethyl)phenyl)pent-4-enoic acid (87)**

Prepared according to general procedure 1 with isolation procedure 1 with further purification by flash column chromatography (30% EtOAc in hexanes with 2% AcOH) and obtained as a white foam (438.6 mg, 0.942 mmol, 94% yield >20:1 dr); ^{1}H NMR (500 MHz, Chloroform-*d*) δ 7.81 – 7.77 (m, 2H), 7.77 – 7.73 (m, 2H), 7.60 (d, *J* = 8.5 Hz, 2H), 7.53 (d, *J* = 8.6 Hz, 2H), 7.19 – 7.10 (m, 3H), 7.09 – 7.03 (m, 2H), 6.57 (ddd, *J* = 17.1, 10.3, 8.5 Hz, 1H), 5.51 (d, *J* = 8.4 Hz, 1H), 5.24 – 5.15 (m, 2H); ^{13}C NMR (100 MHz, Chloroform-*d*) δ 173.3, 167.9, 140.1, 139.3, 137.7, 134.6, 131.4, 130.5, 130.1 (q, $J_{C–F}$ = 32.6 Hz), 129.4, 128.17, 127.4, 124.6 (q, $J_{C–F}$ = 3.7 Hz), 124.56 (q, $J_{C–F}$ = 272.8 Hz), 123.7, 119.4, 71.3, 53.1; ^{19}F NMR (282 MHz, Chloroform-*d*) δ –62.70; IR (Neat Film, NaCl) 3064 (br), 1778, 1722, 1617, 1470, 1454, 1413, 1370, 1327, 1267, 1170, 1124, 1072, 1017, 990, 963, 836, 724, 704, 656 cm^{-1}; (MM:FAB+) *m/z* calc'd for $C_{26}H_{19}NO_4F_3$ $[M+H]^+$: 466.1266, found 466.1287.

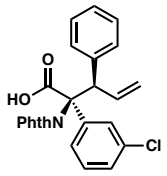

(2*S,3*R**)-2-(3-chlorophenyl)-2-(1,3-dioxoisoindolin-2-yl)-3-phenylpent-4-enoic acid (88)**

Prepared according to general procedure 1 with isolation procedure 1 and obtained as a white foam (385.0 mg, 0.891 mmol, 89% yield, >20:1 dr); ^{1}H NMR (500 MHz, Chloroform-*d*) δ 7.82 – 7.77 (m, 2H), 7.77 – 7.71 (m, 2H), 7.44 (t, *J* = 1.8 Hz, 1H), 7.38 – 7.35 (m, 1H), 7.25 (d, *J* = 1.8 Hz, 1H), 7.23 – 7.18 (m, 1H), 7.16 – 7.11 (m, 3H), 7.10 – 7.03 (m, 2H), 6.58 (ddd, *J* = 17.1, 10.4, 8.4 Hz, 1H), 5.47 (d, *J* = 8.4 Hz, 1H), 5.23 – 5.14 (m, 2H); ^{13}C NMR (100 MHz, Chloroform-*d*) δ 173.1, 167.8, 139.2, 138.1, 137.6, 134.4, 133.5, 131.3, 130.5, 129.3, 128.8, 128.2, 128.0, 127.3, 126.8, 123.6, 119.1, 71.0, 53.0; IR (Neat Film, NaCl) 3066 (br), 1777, 1720, 1470, 1454, 1430, 1370, 1319, 1266, 1121, 1074, 925, 721, 705 cm^{-1}; (MM:FAB+) *m/z* calc'd for $C_{25}H_{19}NO_4Cl$ $[M+H]^+$: 432.1003, found 432.1007.

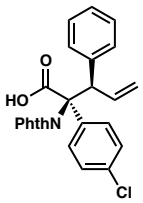

(2*S,3*R**)-2-(4-chlorophenyl)-2-(1,3-dioxoisoindolin-2-yl)-3-phenylpent-4-enoic acid (89)**

Prepared according to general procedure 1 with isolation procedure 1 and obtained as a white foam (416.7 mg, 0.964 mmol, 96% yield, >20:1 dr); ^{1}H NMR (500 MHz, Chloroform-*d*) δ 7.78 – 7.74 (m, 2H), 7.74 – 7.71 (m, 2H), 7.43 – 7.35 (m, 2H), 7.26 – 7.20 (m, 3H), 7.16 – 7.08 (m, 3H), 7.08 – 7.02 (m, 2H), 6.55 (ddd, *J* = 17.8, 10.1, 8.7 Hz, 1H), 5.45 (d, *J* = 8.3 Hz, 1H), 5.26 – 5.02 (m, 2H); ^{13}C NMR (100 MHz, $CDCl_3$) δ 172.9, 167.9, 139.6, 137.9, 134.8, 134.5, 134.1, 131.4, 130.5, 130.3, 128.1, 127.9, 127.3, 123.6, 119.1, 71.1, 53.0; IR (Neat Film, NaCl) 3062 (br), 1778, 1714, 1494, 1470, 1454, 1371, 1348, 1322, 1266, 1100, 1014, 992, 962, 856, 824, 723, 706, 682 cm^{-1}; (MM:FAB+) *m/z* calc'd for $C_{25}H_{19}NO_4Cl$ $[M+H]^+$: 432.1003, found 432.1005.

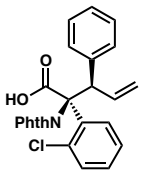

(2*S*,3*R*)-2-(2-chlorophenyl)-2-(1,3-dioxoisoindolin-2-yl)-3-phenylpent-4-enoic acid (90)

Prepared according to general procedure 1 with heating to 40 ºC with isolation procedure 1 and obtained as a white foam (409.2 mg, 0.948 mmol, 95% yield, >20:1 dr); ^{1}H NMR (500 MHz, Chloroform-*d*) δ 7.88 – 7.81 (m, 1H), 7.79 – 7.73 (m, 2H), 7.74 – 7.68 (m, 2H), 7.34 – 7.29 (m, 2H), 7.25 – 7.11 (m, 3H), 7.07 – 6.98 (m, 3H), 6.54 (ddd, *J* = 17.5, 10.4, 7.4 Hz, 1H), 5.96 (d, *J* = 7.4 Hz, 1H), 5.18 (d, *J* = 10.5 Hz, 1H), 5.09 (d, *J* = 17.1 Hz, 1H); ^{13}C NMR (100 MHz, Chloroform-*d*) δ 172.8, 168.0, 139.2, 138.1, 134.4, 134.3, 132.7, 131.9, 131.6, 131.4, 130.8, 129.1, 127.7, 127.0, 126.1, 123.5, 119.0, 72.4, 51.5; IR (Neat Film, NaCl) 3066 (br), 1777, 1720, 1470, 1454, 1430, 1370, 1319, 1266, 1121, 1074, 925, 721, 705 cm^{-1}; (MM:FAB+) *m/z* calc'd for $C_{25}H_{19}NO_4Cl$ $[M+H]^+$: 432.1003, found 432.1019.

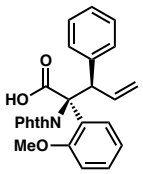

(2*S,3*R**)-2-(1,3-dioxoisoindolin-2-yl)-2-(2-methoxyphenyl)-3-phenylpent-4-enoic acid (91)**

Prepared according to general procedure 1 with heating to 40 ºC with isolation procedure 1 and obtained as a white foam (371.4 mg, 0.869 mmol, 87% yield, >20:1 dr); ^{1}H NMR (500 MHz, Chloroform-*d*) δ 7.80 – 7.73 (m, 2H), 7.76 – 7.68 (m, 2H), 7.69 – 7.62 (m, 1H), 7.36 – 7.29 (m, 3H), 7.12 – 7.02 (m, 3H), 7.04 – 6.94 (m, 1H), 6.91 – 6.83 (m, 1H), 6.59 (ddd, *J* = 17.0, 10.2, 8.0 Hz, 1H), 5.83 – 5.73 (m, 1H), 5.17 (d, *J* = 10.0 Hz, 1H), 5.16 – 5.10 (m, 1H), 3.70 (s, 3H); ^{13}C NMR (100 MHz, Chloroform-*d*) δ 172.1, 167.8, 156.7, 140.3, 138.9, 134.1, 131.6, 130.7, 130.7, 129.6, 127.6, 126.7, 124.7, 123.2, 120.3, 118.0, 111.5, 71.1, 55.6, 51.9; IR (Neat Film, NaCl) 3059 (br), 1776, 1716, 1490, 1463, 1435, 1370, 1319, 1249, 1024, 917, 725, 702 cm^{-1}; (MM:FAB+) *m/z* calc'd for $C_{26}H_{22}NO_5$ $[M+H]^+$: 428.1498, found 428.1515.

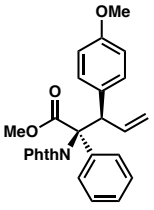

(2*S,3*R**)-2-(1,3-dioxoisoindolin-2-yl)-3-(4-methoxyphenyl)-2-phenylpent-4-enoic acid (92)**

Prepared according to general procedure 1 with isolation procedure 2 with purification by silica gel chromatography (30% EtOAc in hexanes) to afford the desired product as a light yellow oil (206.6 mg, 70% yield over 2 steps, >20:1 dr); ^{1}H NMR (400 MHz, Chloroform-*d*) δ 7.98 – 7.87 (m, 4H), 7.68 – 7.58 (m, 2H), 7.50 – 7.39 (m, 3H), 7.31 – 7.23 (m, 2H), 6.82 – 6.77 (m, 2H), 6.77 – 6.62 (m, 1H), 5.66 (dd, *J* = 8.2, 1.3 Hz, 1H), 5.35 – 5.26 (m, 2H), 3.88 (s, 3H), 3.79 (s, 3H); ^{13}C NMR (100 MHz, Chloroform-*d*) δ 169.8, 168.1, 158.5, 138.9, 136.5, 134.3, 132.3, 131.6, 131.5, 128.8, 127.7, 127.6, 123.5, 118.3, 113.3, 71.6, 55.2, 52.7, 52.5; IR (Neat Film, NaCl) 1778, 1716, 1610, 1512, 1468, 1367, 1319, 1228, 1180, 1115, 1035, 908, 846, 730; (MM:ESI-APCI+) *m/z* calc'd for $C_{27}H_{27}N_2O_5$ $[M+NH_4]^+$: 459.1914, found 459.1907.

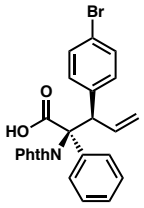

(2*S,3*R**)-3-(4-bromophenyl)-2-(1,3-dioxoisoindolin-2-yl)-2-phenylpent-4-enoic acid (93)**

Prepared according to general procedure 1 with isolation procedure 1 to afford the desired product as a light yellow solid (664.9 mg, 93% yield, >20:1 dr); ^{1}H NMR (400 MHz, DMSO-d_6) δ 7.92 – 7.83 (m, 2H), 7.88 – 7.80 (m, 2H), 7.45 (d, J = 7.1 Hz, 2H), 7.32 – 7.21 (m, 5H), 7.09 (d, J = 8.4 Hz, 2H), 6.42 (ddd, J = 17.2, 10.3, 8.7 Hz, 1H), 5.43 (d, J = 8.6 Hz, 1H), 5.15 – 5.06 (m, 2H); ^{13}C NMR (100 MHz, DMSO-d_6) δ 169.5, 167.5, 140.0, 138.5, 136.7, 135.0, 132.3, 130.7, 130.5, 128.7, 127.3, 127.2, 123.3, 119.9, 118.5, 70.5, 51.6; IR (Neat Film, NaCl) 1773, 1715, 1488, 1367, 1348, 1319, 1123, 1074, 1009, 719; (MM:ESI-APCI+) *m/z* calc'd for $C_{25}H_{22}BrN_2O_4$ $[M+NH_4]^+$: 493.0757, found 493.0792.

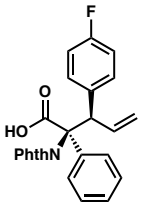

(2*S,3*R**)-2-(1,3-dioxoisoindolin-2-yl)-3-(4-fluorophenyl)-2-phenylpent-4-enoic acid (94)**

Prepared according to general procedure 1 with isolation procedure 1 to afford the desired product as a white solid (345.6 mg, 83% yield, >20:1 dr); ^{1}H NMR (400 MHz, Chloroform-*d*) δ 7.84 – 7.75 (m, 2H), 7.79 – 7.69 (m, 2H), 7.53 – 7.44 (m, 2H), 7.32 – 7.25 (m, 3H), 7.18 – 7.08 (m, 2H), 6.79 – 6.71 (m, 2H), 6.58 (ddd, *J* = 17.2, 10.5, 8.0 Hz, 1H), 5.52 (d, *J* = 8.0 Hz, 1H), 5.19 (dt, *J* = 10.4, 1.4 Hz, 1H), 5.12 (dt, *J* = 17.2, 1.5 Hz, 1H); ^{13}C NMR (100 MHz, Chloroform-*d*) δ 173.2, 168.0, 162.0 (d, $J_{C–F}$ = 245.9 Hz), 138.1, 135.6 (d, $J_{C–F}$ = 3.4 Hz), 134.5, 132.2 (d, $J_{C–F}$ = 8.0 Hz), 131.5, 128.8, 128.2, 127.8, 123.6, 119.0, 115.0, 114.8, 71.4, 52.2; ^{19}F NMR (282 MHz, Chloroform-*d*) δ –115.4 (dddd, *J* = 13.8, 8.5, 5.3, 1.6 Hz); IR (Neat Film, NaCl) 3070 (br), 1778, 1715, 1601, 1508, 1369, 1319, 1226, 910, 849, 720; (MM:ESI-APCI+) *m/z* calc'd for $C_{25}H_{22}FN_2O_4$ $[M+NH_4]^+$: 433.1558, found 433.1565.

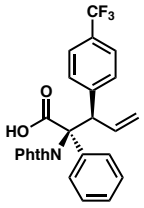

(2*S,3*R**)-2-(1,3-dioxoisoindolin-2-yl)-2-phenyl-3-(4-(trifluoromethyl)phenyl)pent-4-enoic acid (95)**

Prepared according to general procedure 1 with isolation procedure 1 to afford the desired product as a white solid (404.3 mg, 87% yield, >20:1 dr); ^{1}H NMR (400 MHz, Chloroform-*d*) δ 7.81 – 7.72 (m, 4H), 7.49 (dd, *J* = 6.3, 2.8 Hz, 2H), 7.29 (t, *J* = 4.1 Hz, 7H), 6.61 (ddd, *J* = 17.2, 10.4, 8.0 Hz, 1H), 5.60 (d, *J* = 8.0 Hz, 1H), 5.22 (dd, *J* = 10.5, 0.9 Hz, 1H), 5.14 (dd, *J* = 17.2, 1.0 Hz, 1H); ^{13}C NMR (100 MHz, Chloroform-*d*) δ ^{13}C NMR (101 MHz, Chloroform-*d*) δ 173.5, 167.9, 144.1, 137.5, 135.7, 134.6, 131.4, 131.0, 129.3 (q, *J* = 32.5 Hz), 128.7, 128.3, 127.9, 125.6, 124.8 (q, *J* = 3.8 Hz), 123.6, 122.9, 119.6, 71.3, 52.7; ^{19}F NMR (282 MHz, Chloroform-*d*) δ –62.6; IR (Neat Film, NaCl) 3077 (br), 1777, 1716, 1368, 1347, 1326, 1166, 1125, 1069, 908, 723 cm^{-1}; (MM:ESI-APCI+) *m/z* calc'd for $C_{26}H_{19}F_3NO_4$ $[M+H]^+$: 466.1261, found 466.1275.

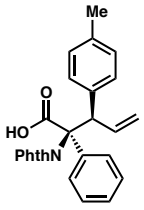

(2*S,3*R**)-2-(1,3-dioxoisoindolin-2-yl)-2-phenyl-3-(*p*-tolyl)pent-4-enoic acid (96)**

Prepared according to general procedure 1 with isolation procedure 1 to afford the desired product as a light yellow solid (364.1 mg, 88% yield, >20:1 dr); ^{1}H NMR (500 MHz, Chloroform-*d*) δ 7.81 – 7.76 (m, 2H), 7.75 – 7.68 (m, 2H), 7.51 – 7.46 (m, 2H), 7.26 (dd, *J* = 3.8, 2.7 Hz, 3H), 7.06 – 7.02 (m, 2H), 6.87 (d, *J* = 7.8 Hz, 2H), 6.61 (ddd, *J* = 16.9, 10.5, 8.2 Hz, 1H), 5.50 (d, *J* = 8.3 Hz, 1H), 5.22 – 5.07 (m, 2H), 2.23 (s, 3H); ^{13}C NMR (100 MHz, Chloroform-*d*) δ 173.1, 168.0, 138.4, 136.8, 136.7, 136.3, 134.3, 131.6, 130.4, 128.9, 128.7, 128.0, 127.7, 123.5, 118.6, 71.5, 52.7, 21.2; IR (Neat Film, NaCl) 3424 (br), 1778, 1714, 1514, 1367, 1318, 908, 722; (MM:ESI-APCI+) *m/z* calc'd for $C_{26}H_{25}N_2O_4$ $[M+NH_4]^+$: 429.1809, found 429.1817.

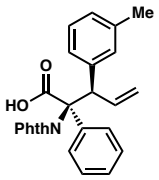

(2*S,3*R**)-2-(1,3-dioxoisoindolin-2-yl)-2-phenyl-3-(*m*-tolyl)pent-4-enoic acid (97)**

Prepared according to general procedure 1 with isolation procedure 1 to afford the desired product as a white solid (342.4 mg, 0.832 mmol, 83% yield, >20:1 dr); ^{1}H NMR (400 MHz, Chloroform-*d*) δ 7.80 – 7.70 (m, 4H), 7.52 – 7.44 (m, 2H), 7.31 – 7.27 (m, 3H), 7.07 (d, *J* = 7.7 Hz, 1H), 6.98 (t, *J* = 7.5 Hz, 1H), 6.93 – 6.88 (m, 1H), 6.85 (d, *J* = 1.8 Hz, 1H), 6.57 (ddd, *J* = 16.7, 10.8, 8.4 Hz, 1H), 5.53 – 5.39 (m, 1H), 5.19 – 5.10 (m, 2H), 1.95 (s, 3H); ^{13}C NMR (100 MHz, Chloroform-*d*) δ 172.1, 167.9, 140.1, 138.5, 137.4, 136.0, 134.3, 131.6, 131.2, 129.0, 128.0, 128.0, 127.8, 127.8, 127.7, 123.5, 118.7, 71.4, 53.1, 21.2; IR (Neat Film, NaCl) 1777, 1719, 1367, 1319, 908, 720, 698; (MM:ESI-APCI+) *m/z* calc'd for $C_{26}H_{22}NO_4$ $[M+H]^+$: 412.1549, found 412.1545.

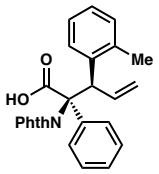

(2*S,3*R**)-2-(1,3-dioxoisoindolin-2-yl)-2-phenyl-3-(*o*-tolyl)pent-4-enoic acid (98)**

Prepared according to general procedure 1 with isolation procedure 1 to afford the desired product as a white foam (326.6 mg, 0.794 mmol, 79% yield, >20:1 dr); ^{1}H NMR (500 MHz, Chloroform-*d*) δ 7.96 – 7.88 (m, 2H), 7.87 – 7.74 (m, 2H), 7.41 (d, *J* = 7.7 Hz, 1H), 7.19 (q, *J* = 6.8 Hz, 2H), 7.14 (t, *J* = 7.4 Hz, 1H), 7.07 (t, *J* = 7.7 Hz, 2H), 7.01 (d, *J* = 7.5 Hz, 1H), 6.93 (d, *J* = 8.0 Hz, 2H), 6.72 (ddd, *J* = 17.4, 10.4, 7.3 Hz, 1H), 5.86 (d, *J* = 7.4 Hz, 1H), 5.11 (d, *J* = 10.4 Hz, 1H), 5.03 (d, *J* = 17.0 Hz, 1H), 1.70 (s, 3H); ^{13}C NMR (100 MHz, Chloroform-*d*) δ 174.0, 168.7, 139.1, 138.6, 137.2, 135.5, 134.6, 131.6, 130.4, 129.7, 128.1, 128.0, 127.4, 127.4, 126.2, 123.8, 117.9, 72.6, 48.3, 19.7; IR (Neat Film, NaCl) 3056 (br), 2366, 1774, 1716, 1489, 1418, 1369, 1345, 1318, 1244, 1124, 1086, 90, 909, 876, 794, 726, 698, 660; (MM:ESI-APCI+) *m/z* calc'd for $C_{26}H_{22}NO_4$ $[M+H]^+$: 412.1549, found 412.1534.

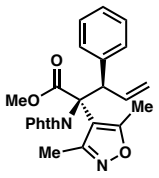

methyl (2*S,3*R**)-2-(3,5-dimethylisoxazol-4-yl)-2-(1,3-dioxoisoindolin-2-yl)-3-phenylpent-4-enoate (99)**

Prepared according to general procedure 1 with isolation procedure 2 and purification by flash column chromatography (20% EtOAc in hexanes) to afford the desired product as an amorphous white solid (171.9 mg, 0.399 mmol, 40% yield, >20:1 dr); ^{1}H NMR (500 MHz, Chloroform-*d*) δ 7.74 (s, 4H), 7.21 (d, *J* = 7.6 Hz, 2H), 7.09 (t, *J* = 7.3 Hz, 1H), 7.01 (t, *J* = 7.5 Hz, 2H), 6.82 (ddd, *J* = 17.3, 10.6, 6.5 Hz, 1H), 5.31 (d, *J* = 6.6 Hz, 1H), 5.23 (dt, *J* = 10.8, 1.6 Hz, 1H), 5.04 (dt, *J* = 17.4, 1.3 Hz, 1H), 3.60 (s, 3H), 2.47 (s, 3H), 2.26 (s, 3H); ^{13}C NMR (100 MHz, Chloroform-*d*) δ 168.6, 167.6, 159.0, 140.1, 138.7, 134.6, 131.2, 131.0, 127.9, 127.2, 123.6, 119.6, 111.9, 66.5, 52.9, 52.6, 14.3, 12.6; IR (Neat Film, NaCl) 3474, 3060, 3028, 2950, 2251, 1780, 1743, 1726, 1603, 1467, 1432, 1406, 1365, 1349, 1322, 1258, 1227, 1121, 1087, 1019, 1002, 964, 904, 858, 842, 792, 777, 760, 724, 704, 684, 626 cm^{-1}; (MM:ESI-APCI+) *m/z* calc'd for $C_{25}H_{23}N_2O_5$ $[M+H]^+$: 431.1607, found 431.1605.

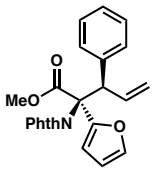

methyl (2*S,3*R**)-2-(1,3-dioxoisoindolin-2-yl)-2-(furan-2-yl)-3-phenylpent-4-enoate (100)**

Prepared according to general procedure 1 with isolation procedure 3 and purification by flash column chromatography (10–30% EtOAc in hexanes) to afford the desired product as a white foam (260.3 mg, 0.648 mmol, 65% yield, >20:1 dr); ^{1}H NMR (400 MHz, Chloroform-*d*) δ 7.79 – 7.70 (m, 2H), 7.71 – 7.62 (m, 2H), 7.49 – 7.38 (m, 1H), 7.15 (s, 5H), 6.69 – 6.53 (m, 1H), 6.43 (dt, *J* = 3.2, 0.5 Hz, 1H), 6.33 – 6.27 (m, 1H), 5.53 (d, *J* = 7.5 Hz, 1H), 5.24 – 5.10 (m, 2H), 3.81 (s, 3H); ^{13}C NMR (100 MHz, Chloroform-*d*) δ 167.7, 167.6, 148.3, 142.0, 138.7, 137.1, 134.2, 131.6, 130.2, 127.9, 127.3, 123.3, 118.4, 112.0, 110.7, 67.8, 52.9, 52.8; IR (Neat Film, NaCl) 3486, 3063, 3032, 2949, 2365, 1779, 1720, 1653, 1636, 1612, 1495, 1468, 1452, 1435, 1366, 1347, 1316, 1225, 1156, 1124, 1080, 1024, 928, 876, 784, 738, 716, 702, 684 cm^{-1}; (MM:FAB+) *m/z* calc'd for $C_{24}H_{20}NO_5$ $[M+H]^+$: 402.1341, found 402.1362.

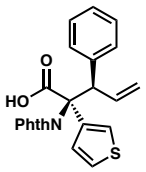

(2*S,3*R**)-2-(1,3-dioxoisoindolin-2-yl)-3-phenyl-2-(thiophen-3-yl)pent-4-enoic acid (101)**

Prepared according to general procedure 1 with isolation procedure 1 and obtained as a tan amorphous solid tan solid with a minor impurity (306.0 mg, 0.758 mmol, 76% yield, >20:1 dr); ^{1}H NMR (500 MHz, Chloroform-*d*) δ 7.90 – 7.83 (m, 2H), 7.77 – 7.69 (m, 2H), 7.51 – 7.47 (m, 1H), 7.36 – 7.32 (m, 3H), 7.32 – 7.28 (m, 3H), 7.28 – 7.23 (m, 1H), 6.59 (d, *J* = 15.9 Hz, 1H), 6.24 (dt, *J* = 15.9, 6.4 Hz, 1H), 6.16 (s, 1H), 4.93 – 4.82 (m, 2H); ^{13}C NMR (100 MHz, Chloroform-*d*) δ 172.4, 167.9, 138.8, 137.5, 137.2, 134.4, 131.6, 130.6, 128.3, 128.0, 127.4, 125.3, 124.2, 123.6, 118.9, 69.7, 53.9; ^{13}C NMR (100 MHz, Chloroform-*d*) δ 172.4, 167.9, 138.8, 137.5, 137.2, 134.4, 131.6, 130.6, 128.3, 128.0, 127.4, 125.3, 124.2, 123.6, 118.9, 69.7, 53.9; IR (Neat Film, NaCl) 2912 (br), 1774, 1714, 1366, 1343, 1319, 1227, 1169, 1122, 1058, 992, 771, 747, 721, 702, 674 cm^{-1}; (MM:FAB+) *m/z* calc'd for $C_{23}H_{18}NO_4S$ $[M+H]^+$: 404.0957, found 404.0944.

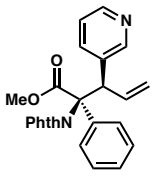

methyl (2*S,3*R**)-2-(1,3-dioxoisoindolin-2-yl)-2-phenyl-3-(pyridin-3-yl)pent-4-enoate (102)**

Prepared according to general procedure 1 with isolation procedure 3 and purification by flash column chromatography (10–60% EtOAc in hexanes) to afford the desired product as a white foam (365.5 mg, 0.891 mmol, 89% yield, >20:1 dr); ^{1}H NMR (500 MHz, Chloroform-*d*) δ 8.37 (d, *J* = 1.9 Hz, 1H), 8.36 (d, *J* = 1.5 Hz, 1H), 7.81 – 7.69 (m, 4H), 7.64 (dt, *J* = 8.1, 2.0 Hz, 1H), 7.52 – 7.43 (m, 2H), 7.35 – 7.26 (m, 3H), 7.08 (dd, *J* = 8.0, 4.8 Hz, 1H), 6.57 (ddd, *J* = 17.7, 10.5, 7.8 Hz, 1H), 5.56 (d, *J* = 7.8 Hz, 1H), 5.22 (d, *J* = 10.3 Hz, 1H), 5.13 (d, *J* = 17.2 Hz, 1H), 3.60 (s, 3H); ^{13}C NMR (100 MHz, Chloroform-*d*) δ 169.4, 168.0, 151.5, 148.1, 138.1, 137.5, 136.2, 135.8, 134.5, 131.3, 128.5, 128.0, 127.8, 123.6, 122.8, 119.5, 71.1, 52.8, 50.9; IR (Neat Film, NaCl) 3482, 3035, 2950, 1778, 1722, 1610, 1468, 1448, 1426, 1368, 1349, 1321, 1231, 1192, 1112, 1086, 1026, 970, 917, 902, 842, 794, 751, 716, 651 cm^{-1}; (MM:FAB+) *m/z* calc'd for $C_{25}H_{21}N_2O_4$ $[M+H]^+$: 413.1501, found 413.1505.

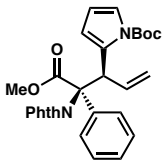

tert-butyl 2-((3*R,4*S**)-4-(1,3-dioxoisoindolin-2-yl)-5-methoxy-5-oxo-4-phenylpent-1-en-3-yl)-1*H*-pyrrole-1-carboxylate (103)**

Prepared according to general procedure 1 with isolation procedure 3 and purification by flash column chromatography (20% EtOAc in hexanes) to afford the desired product as a white foam (354.4 mg, 0.708 mmol, 71% yield, 10:1 dr measured by ratio of major δ 3.77 (s, 3H, integral = 2.71) to minor δ 3.73 (s, 3H, integral = 0.27)); ^{1}H NMR (500 MHz, Chloroform-*d*) δ Major: 7.89 – 7.83 (m, 2H), 7.78 – 7.73 (m, 2H), 6.78 (d, *J* = 7.7 Hz, 1H), 6.47 (ddd, *J* = 17.5, 10.3, 7.6 Hz, 1H), 6.09 (t, *J* = 3.4 Hz, 1H), 6.04 – 6.00 (m, 1H), 5.16 (d, *J* = 17.0 Hz, 1H), 3.77 (s, 3H), Minor: 7.70 – 7.66 (m, 0.2H), 7.60 – 7.56 (m, 0.2H), 7.31 – 7.28 (m, 0.4H), 6.81 (d, *J* = 7.5 Hz, 0.1H), 6.17 (ddd, *J* = 17.0, 10.3, 6.8 Hz, 0.1H), 5.92 (t, *J* = 3.5 Hz, 0.1H), 5.85 (d, *J* = 3.6 Hz, 0.1H), 5.04 – 4.99 (m, 0.1H), 3.73 (s, 0.3H), Overlapping: 7.23 – 7.14 (m, 4.4H), 7.06 – 7.00 (m, 2.1 H), 5.10 – 5.06 (m, 1.2H), 1.45 (s, 9.4H); ^{13}C NMR (100 MHz, $CDCl_3$) δ Major: 169.1, 168.2, 149.4, 137.7, 136.7, 134.4, 131.8, 131.6, 127.8, 127.6, 123.6, 121.9, 117.2, 114.6, 110.0, 84.0, 72.5, 52.5, 44.4, 28.0, Minor: 169.3, 168.1, 149.8, 137.4, 134.1, 131.9, 131.7, 128.2, 127.9, 127.5, 123.3, 121.6, 117.5, 114.8, 109.5, 83.7, 71.6, 52.8, 44.5, 28.1; IR (Neat Film, NaCl) 3484, 2950, 2981, 1778, 1732, 1613, 1470, 1416, 1395, 1369, 1324, 1239, 1165, 1128, 1067, 1000, 942, 924, 854, 817, 772, 725, 701, 665 cm^{-1}; (MM:FAB+) *m/z* calc'd for $C_{29}H_{29}N_2O_6$ $[M+H]^+$: 501.2026, found 501.2047.

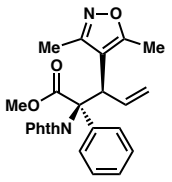

methyl (2*S,3*R**)-3-(3,5-dimethylisoxazol-4-yl)-2-(1,3-dioxoisoindolin-2-yl)-2-phenylpent-4-enoate (104)**

Prepared according to general procedure 1 with isolation procedure 3 and purification by flash column chromatography (30% EtOAc in hexanes) to afford the desired product as a white foam (291.7 mg, 0.678 mmol, 68% yield, >20:1 dr); ^{1}H NMR (500 MHz, Chloroform-*d*) δ 7.91 (dd, *J* = 5.4, 3.1 Hz, 2H), 7.83 (dd, *J* = 5.5, 3.1 Hz, 2H), 7.40 – 7.33 (m, 2H), 7.33 – 7.22 (m, 3H), 6.59 (ddd, *J* = 16.7, 10.5, 5.6 Hz, 1H), 5.33 (dt, *J* = 5.4, 1.9 Hz, 1H), 5.22 (dt, *J* = 10.4, 1.6 Hz, 1H), 5.03 (dt, *J* = 17.2, 1.3 Hz, 1H), 3.76 (s, 3H), 2.03 (s, 3H), 1.75 (s, 3H); ^{13}C NMR (100 MHz, Chloroform-*d*) δ 169.0, 168.6, 168.1, 160.7, 136.5, 135.5, 134.7, 131.5, 128.1, 128.1, 127.9, 123.8, 117.8, 111.3, 70.9, 52.8, 43.4, 12.4, 10.9; IR (Neat Film, NaCl) 3478, 3061, 2952, 1777, 1747, 1728, 1715, 1614, 1497, 1569, 1446, 1434, 1367, 1349, 1319, 1232, 1175, 1125, 1089, 1006, 967, 924, 794, 720, 701, 666 cm^{-1}; (MM:FAB+) *m/z* calc'd for $C_{25}H_{23}N_2O_5$ $[M+H]^+$: 431.1607, found 431.1594.

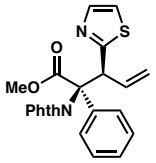

methyl (2*S,3*S**)-2-(1,3-dioxoisoindolin-2-yl)-2-phenyl-3-(thiazol-2-yl)pent-4-enoate (105)**

Prepared according to general procedure 1 with isolation procedure 3 and purification by flash column chromatography (30% EtOAc in hexanes) to afford the desired product as a tan amorphous solid (160.2 mg, 0.382 mmol, 38% yield, >20:1 dr); ^{1}H NMR (500 MHz, Chloroform-*d*) δ 7.80 – 7.76 (m, 2H), 7.75 – 7.70 (m, 2H), 7.53 – 7.48 (m, 2H), 7.41 (d, *J* = 3.3 Hz, 1H), 7.35 – 7.27 (m, 3H), 7.22 (d, *J* = 3.3 Hz, 1H), 6.55 – 6.47 (m, 1H), 5.80 (d, *J* = 9.1 Hz, 1H), 5.28 – 5.18 (m, 2H), 3.64 (s, 3H); ^{13}C NMR (100 MHz, Chloroform-*d*) δ 169.5, 168.5, 168.1, 142.2, 136.1, 135.5, 134.2, 131.7, 128.5, 128.0, 127.7, 123.4, 119.7, 119.5, 70.0, 53.1, 51.6; IR (Neat Film, NaCl) 2950, 2339, 1779, 1722, 1490, 1448, 1368, 1348, 1320, 1267, 1232, 1150, 1111, 1086, 1057, 988, 963, 899, 842, 758, 716, 695, 664 cm^{-1}; (MM:FAB+) *m/z* calc'd for $C_{23}H_{19}N_2O_4S$ $[M+H]^+$: 419.1066, found 419.1064.

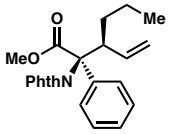

methyl (2*S,3*S**)-2-(1,3-dioxoisoindolin-2-yl)-2-phenyl-3-vinylhexanoate (107)**

Prepared according to general procedure 1 with isolation procedure 2 with purification by silica gel chromatography (0–30% EtOAc in hexanes) to afford the desired product as white foam (304.5 mg, 0.837 mmol, 84% yield, 2.3:1 dr measured by ratio of major δ 3.77 (s, 3H, integral = 2.98) to minor δ 3.73 (s, 3H, integral = 1.28)); ^{1}H NMR (500 MHz, Chloroform-*d*) δ Major: 7.76 – 7.68 (m, 2H), 7.67 – 7.61 (m, 2H), 5.86 (dt, *J* = 17.1, 9.8 Hz, 1H), 5.19 (dd, *J* = 17.1, 1.8 Hz, 1H), 5.12 (dd, *J* = 10.2, 1.9 Hz, 1H), 4.24 (t, *J* = 10.2 Hz, 1H), 3.77 (s, 3H), 1.55 (dt, *J* = 11.8, 5.9 Hz, 1H), 0.86 (t, *J* = 7.2 Hz, 3H); Minor: 7.79 – 7.73 (m, 0.8H), 7.71 – 7.64 (m, 1H), 5.55 (dt, *J* = 17.1, 9.8 Hz, 0.4H), 4.97 (dd, *J* = 10.3, 1.5 Hz, 0.4H), 4.90 (d, *J* = 17.1 Hz, 0.4H), 4.17 (t, *J* = 9.9 Hz, 0.5H), 3.73 (s, 1.3H), 1.77 (td, *J* = 12.1, 6.0 Hz, 0.4H), 1.09 – 1.00 (m, 0.5H), 0.89 (t, *J* = 7.3 Hz, 1.8H); Overlapping: 7.62 – 7.55 (m, 3H), 7.33 – 7.15 (m, 4.8H), 1.50 – 1.27 (m, 3H), 0.98 – 0.89 (m, 2H), ^{13}C NMR (100 MHz, Chloroform-*d*) δ 169.0, 167.9, 138.6, 137.9, 136.9, 136.3, 134.1, 134.1, 131.6, 131.6, 128.1, 127.9, 127.8, 127.6, 127.5, 123.3, 123.2, 119.2, 118.7, 71.7, 70.9, 52.3, 52.2, 48.2, 46.3, 32.6, 32.3, 20.8, 20.7, 14.2, 14.0; IR (Neat Film, NaCl) 2953, 1776, 1743, 1718, 1368, 1317, 1222, 994, 934, 718, 700 cm^{-1}; (MM:FAB+) *m/z* calc'd for $C_{23}H_{24}NO_4$ $[M+H]^+$: 378.1705 found 378.1690.

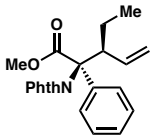

methyl (2*S,3*S**)-2-(1,3-dioxoisoindolin-2-yl)-3-ethyl-2-phenylpent-4-enoate (109)**

Prepared according to general procedure 1 with isolation procedure 2 with purification by silica gel chromatography (0–30% EtOAc in hexanes) to afford the desired product as white foam (293.9 mg, 0.841 mmol, 84% yield, 3.7:1 dr measured by ratio of major δ 3.78 (s, 3H, integral = 2.85) to minor δ 3.76 (s, 3H, integral = 0.78); ^{1}H NMR (400 MHz, Chloroform-*d*) Major: δ 7.78 – 7.74 (m, 2H), 7.70 – 7.66 (m, 2H), 7.62 – 7.58 (m, 2H), 7.34 – 7.27 (m, 3H), 5.87 (ddd, *J* = 17.1, 10.2, 9.4 Hz, 1H), 5.23 (ddd, *J* = 17.1, 2.1, 0.4 Hz, 1H), 5.18 (dd, *J* = 10.3, 2.1 Hz, 1H), 3.78 (s, 3H), 1.77 – 1.63 (m, 1H), 1.02 – 0.94 (m, 5H), Minor: δ 7.80 – 7.77 (m, 2H), 7.71 – 7.69 (m, 2H), 7.65 – 7.62 (m, 2H), 7.25 – 7.19 (m, 3H), 5.56 (ddd, *J* = 17.1, 10.3, 9.0 Hz, 1H), 5.02 (dd, *J* = 10.3, 1.8 Hz, 1H), 4.94 (ddd, *J* = 17.1, 1.8, 0.7 Hz, 1H), 3.76 (s, 3H), 1.90 (dqd, *J* = 12.8, 7.0, 1.3 Hz, 1H), 1.16 – 1.04 (m, 1H), 0.96 – 0.87 (m, 4H); ^{13}C NMR (100 MHz, Chloroform-*d*) Major: δ 169.2, 168.1, 138.0, 136.6, 134.2, 131.7, 128.1, 128.0, 127.9, 123.3, 119.6, 71.1, 52.5, 48.7, 23.6, 12.2, Minor δ 168.9, 168.5, 138.8, 135.9, 134.2, 131.8, 127.9, 127.7, 127.7, 123.4, 119.1, 71.8, 52.3, 50.1, 23.7, 12.2; IR (Neat Film, NaCl) 3476, 3064, 3030, 2967, 2935, 2875, 1777, 1746, 1714, 1722, 1638, 1613, 1498, 1468, 1448, 1456, 1434, 1384, 1367, 1351, 1320, 1267, 1227, 1145, 1111, 1084, 1004, 922, 894, 792, 775, 719, 699, 658 cm^{-1}; (MM:FAB+) *m/z* calc'd for $C_{22}H_{22}NO_4$ $[M+H]^+$: 364.1549 found 364.1535.

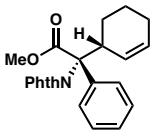

methyl (*S*)-2-((*S*)-cyclohex-2-en-1-yl)-2-(1,3-dioxoisoindolin-2-yl)-2-phenylacetate (111)

Prepared according to general procedure 1 with heating to 40 ºC with isolation procedure 2 and purification by flash column chromatography (0–30% EtOAc in hexanes) to afford the desired product as a white amorphous solid (327.0 mg, 0.871 mmol, 87% yield, >20:1 dr, >99% ee); $[\alpha]_D^{25}$ –48.8 (*c* 1.0, $CHCl_3$); ^1H NMR (400 MHz, Chloroform-*d*) δ 7.85 – 7.74 (m, 2H), 7.75 – 7.67 (m, 2H), 7.71 – 7.62 (m, 2H), 7.36 – 7.21 (m, 3H), 5.83 (dp, *J* = 10.4, 1.8 Hz, 1H), 5.76 – 5.66 (m, 1H), 4.46 – 4.34 (m, 1H), 3.69 (s, 3H), 2.06 – 1.56 (m, 5H), 1.28 (tdd, *J* = 12.4, 10.7, 2.9 Hz, 1H); ^{13}C NMR (100 MHz, $CDCl_3$) δ 168.9, 168.3, 134.1, 131.6, 128.8, 128.0, 127.8, 127.7, 127.7, 123.3, 71.4, 52.3, 40.2, 25.2, 25.1, 22.5; IR (Neat Film, NaCl) 3475, 3035, 2930, 2361, 1778, 1738, 1722, 1715, 1614, 1496, 1469, 1446, 1434, 1367, 1348, 1320, 1227, 1194, 1149, 1117, 1084, 1058, 1034, 1008, 940, 910, 792, 753, 719, 696, 682, 665 cm^{-1}; (MM:FAB+) *m/z* calc'd for $C_{23}H_{22}NO_4$ [M+H]+: 376.1549, found 376.1526. SFC Conditions: 10% IPA, 2.5 mL/min, Chiralpak OB-H column, λ = 210 nm, t_R (min): minor = 7.30, major = 9.80.

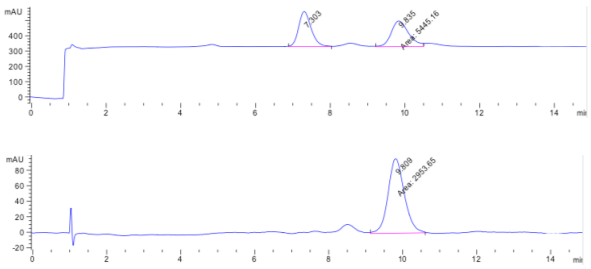

Peak #	RetTime [min]	Type	Width [min]	Area [mAU*s]	Height [mAU]	Area %
1	9.809	MM	0.5114	2953.65332	96.25382	100.0000

4.9.3.2 Ireland–Claisen Rearrangement of (*Z*)-3-phenylallyl 2-(1,3-dioxoisoindolin-2-yl)-2-phenylacetate (80)

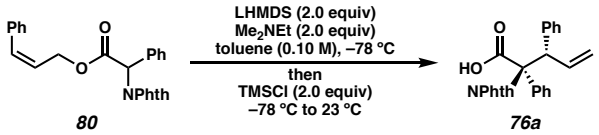

Ireland–Claisen rearrangement of (*Z*)-cinnamyl ester **80** was performed on a 1.00 mmol scale according to general procedure 1 with isolation procedure 1 and to afford product **76a** as a white foam (366.0 mg, 0.921 mmol, 92% yield, >20:1 dr); ^{1}H NMR (500 MHz, Chloroform-*d*) δ 7.79 – 7.72 (m, 2H), 7.73 – 7.67 (m, 2H), 7.48 – 7.42 (m, 2H), 7.28 – 7.21 (m, 3H), 7.16 – 7.11 (m, 2H) (d, *J* = 7.6 Hz, 1H), 7.11 – 7.06 (m, 1H), 7.04 – 7.00 (m, 2H), 6.59 (ddd, *J* = 17.2, 10.4, 8.3 Hz, 1H), 5.50 (d, *J* = 8.2 Hz, 1H), 5.24 – 5.02 (m, 2H); ^{13}C NMR (100 MHz, Chloroform-*d*) δ 173.2, 167.9, 139.9, 138.3, 136.1, 134.4, 131.6, 130.6, 128.9, 128.1, 128.0, 127.7, 127.2, 123.6, 118.9, 71.5, 53.1. IR (Neat Film, NaCl) 3061 (br), 1778, 1722, 1497, 1470, 1448, 1369, 1348, 1320, 1265, 1200, 1161, 1110, 1087, 1034, 991, 961, 932, 841, 790, 725, 705, 682, 642 cm^{-1}; (MM:FAB+) *m/z* calc'd for $C_{25}H_{20}NO_4$ $[M+H]^+$: 398.1392, found 398.1394.

4.9.3.3 Ireland–Claisen Rearrangements of Substrates Relevant to Figure 4.2.1

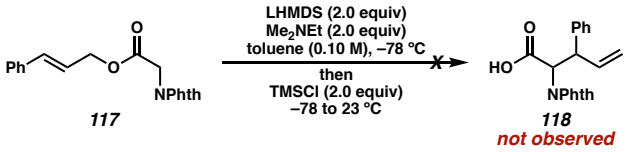

Ireland–Claisen rearrangement of ester **117** was performed on a 1.00 mmol scale according to general procedure 1. After consumption of α-phthalidomido ester **117** was observed by TLC analysis (ca. 30 min), the reaction was quenched with 1 N HCl (10 mL) and transferred to a separatory funnel with Et_2O (10 mL). The layers were separated and the aqueous layer was extracted with Et_2O (2 x 10 mL). The combined organic layers were dried over Na_2SO_4, filtered, and concentrated by rotary evaporation. ^1H, ^{13}C, and HRMS analysis indicated a complex mixture of products without evidence for the formation of desired product **118**.

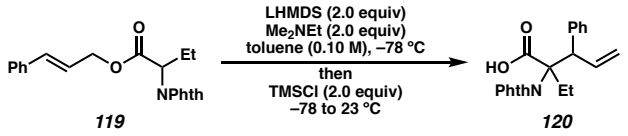

Ireland–Claisen rearrangement of ester **119** was performed on a 1.00 mmol scale according to general procedure 1. After consumption of the α-phthalidomido ester **119** was observed by TLC analysis (ca. 4 h), the reaction was quenched with 1 N HCl (10 mL) and transferred to a separatory funnel with Et_2O (10 mL). The layers were separated and the aqueous layer was extracted with Et_2O (2 x 10 mL). The combined organic layers were dried over Na_2SO_4, filtered, and concentrated by rotary evaporation to afford the crude rearrangement product. Purification by silica gel column chromatography (20 to 70% EtOAc in hexanes) afforded the desired product **120** as an amorphous white solid (241.9

mg, 0.692 mmol, 69% yield, 2.7:1 dr measured by ratio of major 4.87 (d, J = 9.1 Hz, 1H, integral = 1.00) to minor 4.32 (d, J = 9.2 Hz, 1H, integral = 0.37)); ^{1}H NMR (500 MHz, Chloroform-*d*) δ Major: 6.59 (dt, J = 16.8, 9.7 Hz, 1H), 5.17 – 5.10 (m, 2H), 4.87 (d, J = 9.1 Hz, 1H), 2.49 (dq, J = 14.7, 7.4 Hz, 1H), 0.96 (t, J = 7.3 Hz, 3H), Minor: 6.50 (dt, J = 16.7, 9.7 Hz, 0.4H), 5.05 – 4.99 (m, 0.8H), 4.32 (d, J = 9.2 Hz, 0.4H), 2.77 (dq, J = 14.6, 7.3 Hz, 0.4H), 1.00 (t, J = 7.3 Hz, 1.1H), Overlapping: 7.78 – 7.72 (m, 2.6H), 7.72 – 7.65 (m, 2.7H), 7.28 – 7.23 (m, 3.4H), 7.21 – 7.13 (m, 4H), 2.30 (dq, J = 14.6, 7.3 Hz, 1.4H); ^{13}C NMR (100 MHz, $CDCl_3$) δ Major: 175.1, 168.4, 139.3, 137.0, 134.2, 131.5, 129.9, 128.4, 127.3, 123.3, 118.3, 69.9, 53.3, 27.3, 9.2, Minor:175.5, 168.6, 139.3, 137.3, 134.2, 131.4, 130.2, 128.1, 127.2, 123.4, 117.8, 69.7, 55.7, 28.3, 9.8; IR (Neat Film, NaCl) 2943 (br), 2352, 1778, 1714, 1456, 1367, 1352, 1318, 1254, 1157, 1072, 995, 956, 912, 869, 760, 726, 630, 612 cm^{-1}; (MM:ESI-APCI+) *m/z* calc'd for $C_{21}H_{20}NO_4$ $[M+H]^+$: 350.1392, found 350.1366.

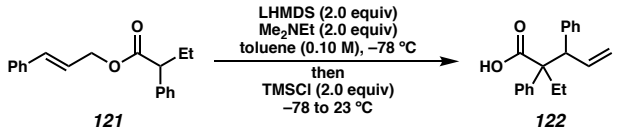

Ireland–Claisen rearrangement of ester **121** was performed on a 1.00 mmol scale according to general procedure 1. After consumption of the α-phenyl ester **121** was observed by TLC analysis (ca. 4 h), the reaction was quenched with 1 N HCl (10 mL) and transferred to a separatory funnel with Et_2O (10 mL). The layers were separated, and the aqueous layer was extracted with Et_2O (2 x 10 mL). The combined organic layers were dried over Na_2SO_4, filtered, and concentrated by rotary evaporation to afford the crude rearrangement product. Purification by silica gel column chromatography (10 to 50% EtOAc in hexanes) afforded the desired product **122** as a white foam (244.1 mg, 0.871 mmol, 87% yield, 2.9:1 dr measured by ratio of major 0.87 (t, J = 7.3 Hz, 3H, integral = 3.00) to minor 0.93 (t, J = 7.3 Hz, 3H, integral =1.05)); ^{1}H NMR (500 MHz, Chloroform-*d*) δ ^{1}H NMR (500 MHz, Chloroform-*d*) δ Major: 6.89 (d, J = 7.2 Hz, 2.0H), 5.12 – 5.05 (m, 2.1H), 2.21 – 2.08 (m, J = 6.9 Hz, 2H), 0.87 (t, J = 7.3 Hz, 3H) Minor: 6.56 (d, J = 7.4 Hz, 0.67H), 5.20 – 5.12 (m, 0.6H), Overlapping: 7.33 – 7.21 (m, 4.4H), 7.19 – 7.07 (m, 4.7H),7.07 – 7.01 (m, 2.0H), 6.10 – 5.95 (m, 1.3H), 4.18 – 4.11 (m, 1.3H), 2.01 – 1.94 (m, 0.7H), 0.93 (t, J = 7.3 Hz, 1.1H); ^{13}C NMR (100 MHz, Chloroform-*d*) δ Major:180.8, 140.7, 137.6, 137.6, 130.1, 129.7, 127.7, 127.4, 127.0, 126.8, 117.5, 60.4, 56.3, 30.3, 9.5, Minor: 181.0, 139.1, 138.6, 136.2, 130.5, 130.0, 127.7, 127.3, 127.2, 127.0, 117.5, 60.7, 57.0, 29.4, 9.5; (MM:FAB+) *m/z* calc'd for $C_{19}H_{21}O_2$ $[M+H]^+$: 281.1542, found 281.1541.

4.9.3.4 Derivatizations of Rearrangement Products

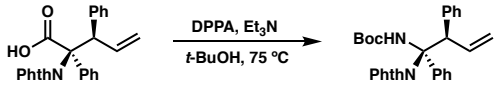

***tert*-butyl ((1*S**,2*R**)-1-(1,3-dioxoisoindolin-2-yl)-1,2-diphenylbut-3-en-1-yl)carbamate (112)**

To a flame-dried 10 mL round bottom flask with a Teflon-coated magnetic stir bar was added carboxylic acid **15a** (79.5 mg, 0.200 mmol, 1.0 equiv), *t*-BuOH (1.0 mL), Et_3N (39 μL, 0.28 mmol, 1.4 equiv), and DPPA (52 μL, 0.24 mmol, 1.2 equiv). The flask was then immersed in a metal heating block at 75 ºC and stirred rapidly. After 20 h, the reaction was complete by TLC analysis. The reaction was cooled to 20 ºC, concentrated by rotary evaporation, and directly purified by silica gel column chromatography (15% Et_2O in hexanes) to afford **51** as a viscous yellow oil (76.8 mg, 0.164 mmol, 82% yield); *Note: for ^{1}H and ^{13}C spectra some peak broadening and rotameric peaks are observed.* ^{1}H NMR (400 MHz, Chloroform-*d*) δ 7.82 – 7.65 (m, 4H), 7.48 – 7.43 (m, 2H), 7.42 – 7.36 (m, 1H), 7.30 – 7.20 (m, 4H), 7.13 – 7.00 (m, 3H), 6.67 – 6.52 (m, 1H), 5.50 (d, *J* = 8.4 Hz, 1H), 5.20 – 5.05 (m, 2H), 1.20 (s, 9H); ^{13}C NMR (100 MHz, Chloroform-*d*) δ 167.7, 167.4, 140.8, 139.0, 137.0, 134.0, 131.6, 130.5, 130.1, 128.8, 127.7, 127.3, 127.1, 126.8, 126.1, 123.2, 120.3, 120.2, 118.3, 82.4, 72.2, 52.5, 27.4; IR (Neat Film, NaCl) 2976, 2169, 1778, 1721, 1600, 1489 1467, 1367, 1320, 1244, 1157, 1087, 963, 914, 778, 750, 718, 700 cm^{-1};(MM:FAB+) *m/z* calc'd for $C_{28}H_{26}N_2O_4$ $[M–CH_2]^{+\bullet}$: 454.1893, found 454.1905.

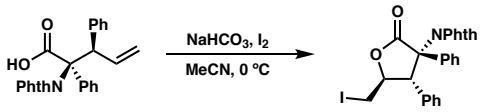

2-((3*S,4*S**,5*S**)-5-(iodomethyl)-2-oxo-3,4-diphenyltetrahydrofuran-3-yl)isoindoline-1,3-dione (113)**

To a flame-dried 1 dram vial with a Teflon-coated magnetic stirring bar was added carboxylic acid **15a** (79.5 mg, 0.200 mmol, 1.0 equiv) and MeCN (700 μL). The heterogeneous reaction mixture was then cooled in a 0 ºC ice bath for 10 min, then $NaHCO_3$ (168.0 mg, 2.00 mmol, 10.0 equiv) was added. After stirring for an additional 5 min, the reaction flask was charged with I_2 (152.3 mg, 0.600 mmol, 3.0 equiv). The resulting orange/black suspension was stirred vigorously at 20 ºC for 3 h, after which time TLC analysis showed full consumption of carboxylic acid **15a**. The reaction mixture was transferred to a separatory funnel with 10 mL Et_2O and 10 mL H_2O. The layers were separated and the aqueous layer was extracted with Et_2O (3 x 5 mL). The combined organic layers were washed with sat. aq. $Na_2S_2O_3$ (5 mL), dried over Na_2SO_4, filtered, and concentrated to afford a white solid. Purification by silica gel column chromatography (25% EtOAc in hexanes) afforded the desired product as an amorphous white solid (94.5 mg, 0.181 mmol, 91% yield, >20:1 dr); ^{1}H NMR (500 MHz, Chloroform-*d*) δ 7.89 – 7.84 (m, 2H), 7.79 (dd, *J* = 5.5, 3.1 Hz, 2H), 7.56 – 7.51 (m, 2H), 7.37 – 7.25 (m, 5H), 7.14 (d, *J* = 6.1 Hz, 3H), 5.29 (d, *J* = 4.0 Hz, 1H), 5.12 (ddd, *J* = 9.4, 5.6, 4.2 Hz, 1H), 3.23 (dd, *J* = 10.1, 5.7 Hz, 1H), 2.68 – 2.61 (m, 1H); ^{13}C NMR (100 MHz, Chloroform-*d*) δ 171.1, 167.3, 134.9, 134.0, 132.8, 131.2, 130.4, 130.0, 129.1, 128.6, 128.2, 127.5, 124.0, 80.2, 67.9, 53.8, 0.8; IR (Neat Film, NaCl) 3034, 1790, 1774, 1722, 1498, 1468, 1448, 1364,

1347, 1315, 1266, 1169, 1124, 1084, 1058, 1008, 959, 917, 872, 735, 718, 697 cm^{-1};

(MM:FAB+) *m/z* calc'd for $C_{25}H_{19}NO_4I$ $[M+H]^+$: 524.0359, found 524.0360.

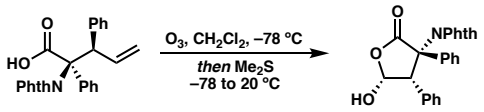

2-((3*S,4*S**,5*R**)-5-hydroxy-2-oxo-3,4-diphenyltetrahydrofuran-3-yl)isoindoline-1,3-dione (114)**

A 10 mL round bottom flask was charged with a Teflon-coated magnetic stir bar, carboxylic acid **15a** (79.5 mg, 0.200 mmol, 1.0 equiv) and CH_2Cl_2 (2 mL). The resulting solution was cooled in a –78 ºC dry ice/acetone bath for 10 min, after which time ozone was bubbled through the solution for 30 min, generating a pale blue solution with TLC analysis indicating full consumption of carboxylic acid **15a**. The reaction was then sparged with O_2 for 10 min, affording a colorless solution to which SMe_2 (44 μL, 0.60 mmol, 3.0 equiv) was then added. The colorless reaction mixture was warmed to 20 ºC and allowed to stir for 2 h, after which time it was loaded directly onto a silica gel column and eluted (0–5% MeOH/CH_2Cl_2) to afford the desired product as a white foam (68.1 mg, 0.171 mmol, 86% yield, 11:1 dr measured by ratio of major δ 5.61 (d, J = 7.0 Hz, 1H, integral = 1.00) to minor δ 5.40 (d, J = 4.5 Hz, 1H, integral = 0.09); ^{1}H NMR (500 MHz, Chloroform-*d*) Major: δ 7.90 – 7.83 (m, 2H), 7.81 – 7.73 (m, 2H), 7.37 – 7.17 (m, 6H), 7.04 (d, J = 7.5 Hz, 2H), 7.00 (d, J = 8.0 Hz, 2H), 6.06 (d, J = 6.9 Hz, 1H), 5.61 (d, J = 7.0 Hz, 1H), 4.23 – 4.16 (m, 1H), Minor: 6.27 (dd, J = 10.3, 4.6 Hz, 1H) 5.40 (d, J = 4.5 Hz, 1H); ^{13}C NMR (100 MHz, Chloroform-*d*) δ 170.9, 168.4, 134.7, 132.9, 131.9, 131.5, 129.5, 128.6, 128.2, 128.2, 128.0, 123.8, 99.4, 71.6, 54.5; IR (Neat Film, NaCl) 3456, 3064 (br), 1770, 1721, 1608, 1500, 1469, 1450, 1378, 1346, 1323, 1265, 1169, 1122, 1087, 1062, 969, 949, 891, 874, 852, 772, 719, 699, 670 cm^{-1}; (MM:FAB+) *m/z* calc'd for $C_{24}H_{18}NO_5$ $[M+H]^+$: 400.1185, found 400.1194.

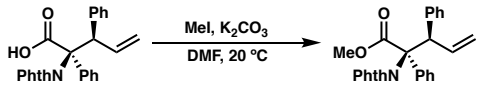

methyl (2*S,3*R**)-2-(1,3-dioxoisoindolin-2-yl)-2,3-diphenylpent-4-enoate (115)**

To a flame-dried 10 mL round bottom flask with a Teflon-coated magnetic stir bar was added carboxylic acid **15a** (397.4 mg, 1.00 mmol, 1.0 equiv) and DMF (3.3 mL). To the colorless solution was then added K_2CO_3 (276.4 mg, 2.00 mmol, 2.0 equiv) and MeI (106 μL, 1.70 mmol, 1.7 equiv). The resulting suspension was stirred rapidly at 20 ºC for 30 min, at which time TLC analysis indicated full conversion of carboxylic acid **15a**. The reaction mixture was then transferred to a separatory funnel with EtOAc (10 mL) and H_2O (10 mL). The layers were separated, and the aqueous layer was extracted with EtOAc (3 x 5 mL). The combined organics were washed with brine (5 mL), dried over Na_2SO_4, filtered, and concentrated to afford a yellow oil which was purified by silica gel chromatography (30% Et_2O in hexanes) to afford the desired methyl ester as a white foam (372.0 mg, 0.904 mmol, 90% yield); ^{1}H NMR (500 MHz, Chloroform-*d*) δ 7.80 – 7.69 (m, 4H), 7.48 – 7.43 (m, 2H), 7.31 – 7.24 (m, 3H), 7.22 – 7.18 (m, 2H), 7.14 – 7.03 (m, 3H), 6.58 (ddd, *J* = 17.1, 10.4, 8.3 Hz, 1H), 5.53 (d, *J* = 8.4 Hz, 1H), 5.21 – 5.08 (m, 2H), 3.60 (s, 3H); ^{13}C NMR (100 MHz, Chloroform-*d*) δ 169.7, 168.0, 140.5, 138.7, 136.3, 134.3, 131.6, 130.6, 128.8, 127.9, 127.8, 127.6, 127.0, 123.4, 118.7, 71.5, 53.2, 52.7; IR (Neat Film, NaCl) 3060, 3030, 2951, 1778, 1721, 1611, 1498, 1448, 1348, 1366, 1320, 1270, 1229, 1110, 1087, 1006, 968, 922, 901, 775, 758, 738, 720 cm^{-1}; (MM:FAB+) *m/z* calc'd for $C_{26}H_{22}NO_4$ $[M+H]^+$: 412.1549, found 412.1524.

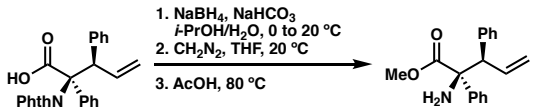

amino acid methyl ester 116

To a 100 mL round bottom flask with a Teflon-coated magnetic stirring bar was added carboxylic acid **15a** (397.4 mg, 1.00 mmol, 1.0 equiv), *i*-PrOH (16 mL), and saturated aqueous $NaHCO_3$ solution (1.4 mL). The resulting cloudy reaction mixture was cooled in an ice bath for 5 min. To the cooled reaction was then added $NaBH_4$ (227.0 mg, 6.00 mmol, 6.0 equiv) slowly with vigorous stirring. The ice bath was then removed, and the reaction allowed to stir at 20 ºC for 12 h, after which time full consumption of acid **15a** was observed by LC/MS analysis. The reaction mixture was concentrated to dryness, then passed through a 2x4 cm plug of silica gel with 10% MeOH in EtOAc (50 mL). The solution was then concentrated to a yellow foam which was used directly without further purification.

Caution! Diazomethane is toxic and explosive; all operations should be carried out in a well-ventilated hood with adequate shielding. To a 50 mL round bottom flask with a Teflon-coated stirring bar was added the crude product and THF (5 mL). The flask was placed behind a blast shield, and to the slowly stirring reaction mixture was then added freshly prepared CH_2N_2 (approx. 6 mL of a 0.2 M solution in Et_2O) drop-wise via a flame-polished pipette. Acetic acid (2.0 mL) was added dropwise to quench residual CH_2N_2. After stirring an additional 15 min, the reaction mixture was concentrated to a yellow foam.

The flask was sealed with a rubber septum, the purged and evacuated 3x with N_2. To the flask was then added AcOH (2.0 mL) was the reaction mixture was stirred at 80 ºC for 8 h in a heating well. The brown reaction solution was then cooled to 20 ºC and poured

into a separatory funnel containing 20 mL sat. aq. $NaHCO_3$ and 20 mL EtOAc. The separatory funnel was shaken, and the layers separated. The aqueous layer was extracted 2 x 10 mL EtOAc and the combined organics were dried over Na_2SO_4. Purification by column chromatography (0 to 10% MeOH in CH_2Cl_2) afforded the desired amino acid methyl ester as a white foam (163.5 mg, 0.707 mmol, 71% yield over 3 steps); ^{1}H NMR (400 MHz, Chloroform-*d*) δ 7.82 – 7.62 (m, 2H), 7.41 – 7.22 (m, 8H), 6.04 (ddd, *J* = 17.1, 10.3, 8.3 Hz, 1H), 4.96 (dq, *J* = 10.4, 1.3 Hz, 1H), 4.86 (dt, *J* = 17.2, 1.3 Hz, 1H), 4.46 (d, *J* = 8.3 Hz, 1H), 3.57 (s, 3H); ^{13}C NMR (100 MHz, Chloroform-*d*) δ 174.8, 140.6, 140.0, 136.3, 129.8, 128.5, 128.3, 127.7, 127.3, 126.6, 118.6, 67.4, 56.9, 52.6; IR (Neat Film, NaCl) 3370, 2919, 2360, 1719, 1597, 1490, 1446, 1227, 1032, 1008, 944, 920, 778, 752, 730, 714, 701, 668 cm^{-1}; (MM:ESI-APCI+) *m/z* calc'd for $C_{18}H_{20}NO_2$ $[M+H]^+$: 282.1494, found 282.1497.

4.9.3.5 Preparation of Ireland–Claisen Substrates

General Procedure 2

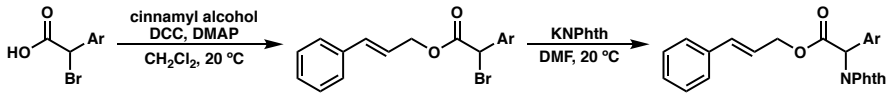

To a flame-dried 100 mL round bottom flask was added commercial or previously reported α-bromo carboxylic acid (10.0 mmol, 1.0 equiv), cinnamyl alcohol (1.74 g, 13.0 mmol, 1.3 equiv), DMAP (122.2 mg, 1.0 mmol, 0.10 equiv) and CH_2Cl_2 (50 mL). The resulting solution was then cooled in a 0 ºC ice/water bath for 10 minutes after which time DCC (2.68 g, 13.0 mmol, 1.3 equiv) was added in a single portion. The resulting solution was vigorously stirred at 20 ºC for 12 h, during which time a white solid precipitates. After the reaction was complete by TLC analysis (typically 12 h), the reaction mixture was

concentrated by rotary evaporation and the resulting solid cake was suspended in 30 mL of Et_2O. The mixture was then filtered through a 2 x 5 cm celite pad with 2 x 20 mL rinses of Et_2O. The resulting solution was concentrated by rotary evaporation and eluted through a 5 x 10 cm plug of silica gel, eluting with 15% Et_2O in hexanes. The crude ester was then used in the next step without further purification.

To a flame-dried 100 mL round bottom flask was added the crude α-bromo ester prepared above and DMF (33 mL). To the resulting solution was then added potassium phthalimide (3.70 g, 20.0 mmol, 2.0 equiv) in a single portion. The resulting slurry was then vigorously stirred at 20 ºC. After the reaction was complete by TLC analysis (typically 12 h), the reaction mixture was quenched with 20 mL of H_2O. The reaction mixture was then transferred with 30 mL of EtOAc to a separatory funnel containing 20 mL of brine. The layers were separated and the aqueous was extracted with EtOAc (2 x 20 mL). The combined organics were washed with brine (30 mL), dried over Na_2SO_4, and concentrated. The crude α-phthalimide ester was then purified by column chromatography.

General Procedure 3

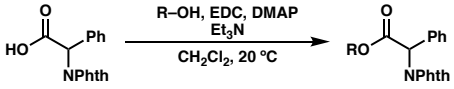

To a flame-dried round bottom flask was added the alcohol (2.0 equiv), DMAP (0.10 equiv), the α-phthalimide carboxylic acid (2.0 equiv), CH_2Cl_2 (0.10 M) and Et_3N (2.0 equiv). To the resulting solution was then added the EDC•HCl (2.0 equiv) in a single portion. The resulting solution was vigorously stirred at 20 ºC for 12 h. The reaction mixture was then diluted with CH_2Cl_2 (20 mL) and transferred to a separatory funnel. The organic layer was washed with 0.5 N HCl (20 mL), sat. aq. $NaHCO_3$ (10 mL), and brine

(10 mL). The organic layer was then dried over Na_2SO_4, filtered, and concentrated. The resulting crude mixture was then purified by column chromatography to afford the desired α-phthalidomido esters.

General Procedure 4

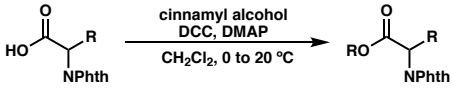

To a flame-dried round bottom flask was added cinnamyl alcohol (1.5 equiv), DMAP (0.20 equiv), α-phthalimido carboxylic acid (1.5 equiv), CH_2Cl_2 (0.20 M). The stirring solution was then cooled in an ice bath and to the resulting solution was then added the DCC (1.5 equiv) in a single portion. The resulting solution was vigorously stirred at 20 ºC for 12 h. To the reaction mixture was then added silica gel (10 g) and the resulting slurry was concentrated to a dry solid which was loaded directly onto a silica gel flash column for purification to afford the corresponding α-phthalimido cinnamyl ester.

General Procedure 5

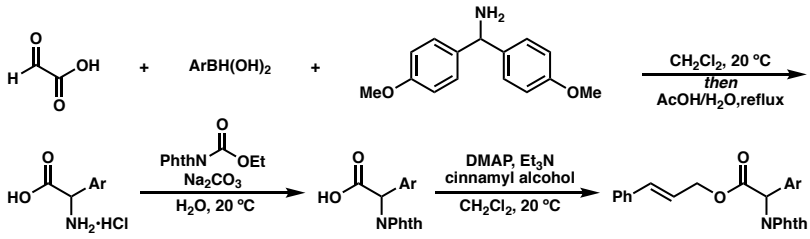

This general procedure was adapted from a procedure reported by Petasis and coworkers.34 To a 250 mL round bottom flask with a Teflon-coated magnetic stir bar was added glyoxylic acid hydrate (1.4253 g, 15.00 mmol, 1.0 equiv), CH_2Cl_2 (75 mL), and bis(4-methoxyphenyl)methanamine (3.65 g, 15.0 mmol, 1.0 equiv). The resulting heterogeneous reaction mixture was stirred rapidly for 5 min, after which time aryl boronic

acid (15.0 mmol, 1.0 equiv) was added in a single portion, causing the precipitation of a white solid. The reaction was stirred vigorously for 16 h, after which time the reaction mixture was concentrated by rotary evaporation. To the flask was then added 70% v/v AcOH/H_2O (75 mL), and the flask was affixed with a reflux condenser. The mixture was then heated to reflux in a metal heating block (preheated to 115 ºC) for 1 h, after which time the mixture became homogeneous. After cooling to 20 ºC, 3 N HCl (32 mL) was then added, the mixture was transferred to a separatory funnel with H_2O (5 mL), and washed with CH_2Cl_2 (3 x 20 mL). The aqueous layer was then partially concentrated to approximately 10 mL total volume, frozen in a dry ice/acetone bath, and lyophilized to afford the crude amino acid hydrochloride which was used without purification.

To a 250 mL round bottom flask with a Teflon-coated magnetic stir bar was added the crude amino acid hydrochloride, H_2O (75 mL), Na_2CO_3 (2.38 g, 22.5 mmol, 1.5 equiv), and *N*-ethoxycarbonylphthalimide (4.93 g, 22.5 mmol, 1.5 equiv). The reaction mixture was stirred vigorously for 3 h, after which time it was transferred to a separatory funnel with H_2O (10 mL). The pH of the aqueous layer was adjusted to 12 with sat. aq. Na_2CO_3 solution, then the aqueous layer was washed with Et_2O (3 x 50 mL). The aqueous layer was then acidified to pH 2 with 2 N HCl and extracted with EtOAc (3 x 50 mL), dried over Na_2SO_4, filtered, and concentrated to afford the desired carboxylic acid which was used without further purification.

To a 500 mL round bottom flask was added the carboxylic acid, CH_2Cl_2 (150 mL), Et_3N (4.2 mL, 30 mmol, 2.0 equiv), DMAP (366.5 mg, 3.00 mmol, 0.20 equiv), and cinnamyl alcohol (4.03 g, 30.0 mmol, 2.0 equiv). To the rapidly stirring solution was then added EDC•HCl (5.75 g, 30.0 mmol, 2.0 equiv) in a single portion. The reaction was

stirred until full consumption of the carboxylic acid by TLC analysis, after which time the reaction mixture was diluted with CH_2Cl_2 (100 mL) and transferred to a separatory funnel. The organic layer was washed with 0.5 N HCl (50 mL), sat. aq. $NaHCO_3$ (50 mL), and brine (50 mL). The organic layer was then dried over Na_2SO_4, filtered, and concentrated. The resulting crude mixture was then purified by column chromatography to afford the desired α-phthalidomido esters.

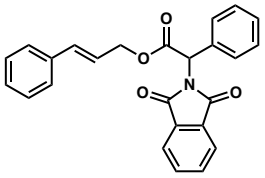

(*E*)-cinnamyl 2-(1,3-dioxoisoindolin-2-yl)-2-phenylacetate (75)

Performed on a 10.00 mmol scale according to general procedure 3 and purified by silica gel chromatography (50% CH_2Cl_2, 2% EtOAc in hexanes) to afford the desired product as an amorphous white solid (3.59 g, 9.03 mmol, 90% yield); ^{1}H NMR (500 MHz, Chloroform-*d*) δ 7.88 – 7.82 (m, 2H), 7.74 – 7.69 (m, 2H), 7.61 – 7.55 (m, 2H), 7.41 – 7.28 (m, 7H), 7.28 – 7.23 (m, 1H), 6.60 (d, *J* = 15.9 Hz, 1H), 6.25 (dt, *J* = 15.8, 6.4 Hz, 1H), 6.07 (s, 1H), 4.90 (qdd, *J* = 12.8, 6.4, 1.3 Hz, 2H); ^{13}C NMR (100 MHz, Chloroform-*d*) δ 167.9, 167.1, 136.1, 134.7, 134.5, 134.3, 131.8, 129.8, 128.7, 128.6, 128.2, 126.7, 123.7, 122.4, 66.7, 56.0; IR (Neat Film, NaCl) 3476, 3060, 3030, 2929, 1772, 1746, 1721, 1611, 1496, 1468, 1450, 1385, 1337, 1214, 1184, 1111, 1088, 1076, 1020, 968, 894, 842, 790, 777, 720, 697, 661 cm^{-1}; (MM:FAB+) *m/z* calc'd for $C_{25}H_{20}NO_4$ $[M+H]^+$: 398.1392, found 398.1368.

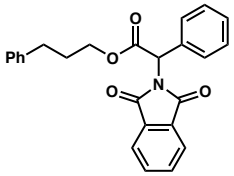

3-phenylpropyl 2-(1,3-dioxoisoindolin-2-yl)-2-phenylacetate (77)

Performed on a 5.00 mmol scale according to general procedure 3 and purified by silica gel chromatography (20% EtOAc in hexanes) to afford the desired product as a viscous, colorless oil (1.9659 g, 4.92 mmol, 98% yield); ^{1}H NMR (500 MHz, Chloroform-*d*) δ 7.91 – 7.85 (m, 2H), 7.77 – 7.70 (m, 2H), 7.60 (d, *J* = 7.3 Hz, 2H), 7.38 (dt, *J* = 12.0, 7.0 Hz, 3H), 7.27 (t, *J* = 7.6 Hz, 2H), 7.20 (t, *J* = 7.3 Hz, 1H), 7.11 (d, *J* = 7.5 Hz, 2H), 6.04 (s, 1H), 4.27 (t, *J* = 6.4 Hz, 2H), 2.61 (t, *J* = 7.7 Hz, 2H), 1.97 (p, *J* = 6.8 Hz, 2H); ^{13}C NMR (100 MHz, Chloroform-*d*) δ 168.0, 167.2, 141.0, 134.6, 134.3, 131.8, 129.9, 128.7, 128.6, 128.5, 126.1, 123.6, 65.5, 56.0, 32.0, 30.2; IR (Neat Film, NaCl) 3472, 3062, 3028, 2957, 1773, 1746, 1717, 1603, 1515, 1496, 1468, 1454, 1385, 1336, 1215, 1186, 1110, 1076, 1021, 958, 917, 897, 828, 746, 721, 698, 668, 660 cm^{-1}; (MM:FAB+) *m/z* calc'd for $C_{25}H_{22}NO_4$ $[M+H]^+$: 400.1549, found 400.1550.

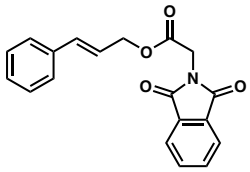

cinnamyl 2-(1,3-dioxoisoindolin-2-yl)acetate (117)

Performed on a 3.00 mmol scale according to general procedure 4 and purified by silica gel chromatography (50% CH_2Cl_2, 2% EtOAc in hexanes) to afford the desired product as an amorphous white solid (895.0 mg, 2.79 mmol, 93% yield); ^{1}H NMR (500 MHz, Chloroform-*d*) δ 7.94 – 7.83 (m, 2H), 7.79 – 7.71 (m, 2H), 7.40 – 7.35 (m, 2H), 7.34 – 7.29 (m, 2H), 7.28 – 7.22 (m, 1H), 6.64 (d, *J* = 15.8 Hz, 1H), 6.25 (dt, *J* = 15.9, 6.5 Hz, 1H), 4.82 (d, *J* = 6.4 Hz, 2H), 4.49 (s, 2H); ^{13}C NMR (100 MHz, Chloroform-*d*) δ 167.5, 167.2, 136.0, 135.0, 134.3, 132.1, 128.7, 128.3, 126.8, 123.7, 122.3, 66.5, 39.0; IR (Neat Film, NaCl) 2341, 2359, 1716, 1456, 1417, 1391, 1316, 1194, 1112, 956, 759, 734, 711 cm^{-1}; (MM:ESI-APCI+) *m/z* calc'd for $C_{19}H_{19}N_2O_4$ $[M+NH_4]^+$: 339.1345, found 339.1333.

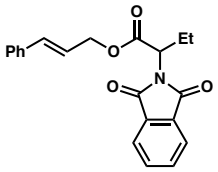

cinnamyl 2-(1,3-dioxoisoindolin-2-yl)butanoate (119)

Performed on a 4.00 mmol scale according to general procedure 3 and purified by silica gel chromatography (0 to 20% EtOAc in hexanes) to afford the desired product as a colorless, viscous oil (1.2869 g, 3.68 mmol, 92% yield); ^{1}H NMR (500 MHz, Chloroform-*d*) δ 7.93 – 7.85 (m, 2H), 7.81 – 7.73 (m, 2H), 7.40 – 7.31 (m, 4H), 7.30 – 7.24 (m, 1H), 6.63 (d, *J* = 15.9 Hz, 1H), 6.25 (dt, *J* = 15.9, 6.4 Hz, 1H), 4.88 – 4.79 (m, 3H), 2.42 – 2.25 (m, 2H), 0.99 (t, *J* = 7.5 Hz, 3H); ^{13}C NMR (100 MHz Chloroform-*d*) δ 169.2, 167.8, 136.1, 134.5, 134.3, 131.9, 128.7, 128.2, 126.7, 123.6, 122.6, 66.3, 53.9, 22.3, 11.1; IR (Neat Film, NaCl) 3476, 3028, 2971, 2879, 1775, 1744, 1716, 1612, 1495, 1467, 1449, 1388, 1290, 1265, 1215, 1149, 1112, 1073, 1041, 967, 898, 743, 720, 693 cm^{-1}; (MM:ESI-APCI+) *m/z* calc'd for $C_{21}H_{20}NO_4$ $[M+H]^+$: 350.1392, found 350.1404.

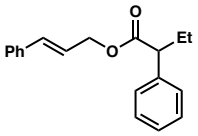

cinnamyl 2-phenylbutanoate (121)

Performed on a 4.00 mmol scale according to general procedure 3 and purified by silica gel chromatography (0 to 20% EtOAc in hexanes) to afford the desired product as a colorless, viscous oil (1.0340 g, 3.69 mmol, 92% yield); ^{1}H NMR (500 MHz, Chloroform-*d*) δ 7.41 – 7.16 (m, 10H), 6.53 (d, *J* = 15.9 Hz, 1H), 6.23 (dt, *J* = 15.8, 6.1 Hz, 1H), 4.73 (qd, *J* = 13.0, 6.1 Hz, 2H), 3.51 (t, *J* = 7.7 Hz, 1H), 2.14 (dq, *J* = 14.8, 7.4 Hz, 1H), 1.85 (dq, *J* = 14.1, 7.4 Hz, 1H), 0.92 (t, *J* = 7.3 Hz, 3H); ^{13}C NMR (100 MHz, $CDCl_3$) δ 173.9, 139.2, 139.1, 136.4, 136.3, 133.8, 128.7, 128.7, 128.2, 128.1, 128.1, 127.4, 127.3, 126.7, 126.7, 123.3, 123.3, 65.2, 53.6, 26.9, 26.8, 12.3, 12.3; IR (Neat Film, NaCl) 3028, 2965, 2933, 2875, 1733, 1600, 1495, 1453, 1381, 1346, 1266, 1221, 1198, 1164, 1119, 1072, 1028, 965, 731, 696 cm^{-1}; (MM:FAB+) *m/z* calc'd for $C_{19}H_{21}O_2$ $[M]^{+\bullet}$: 280.1483, found 280.1463.

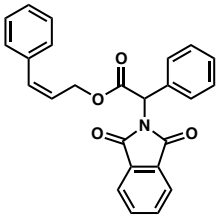

(*Z*)-3-phenylallyl 2-(1,3-dioxoisoindolin-2-yl)-2-phenylacetate (80)

Performed on a 3.00 mmol scale according to general procedure 3 and purified by silica gel chromatography (0–30% EtOAc in hexanes) to afford the desired product as an amorphous white solid (1.056 g, 2.66 mmol, 89% yield); ^{1}H NMR (400 MHz, Chloroform-*d*) δ 7.80 – 7.73 (m, 2H), 7.69 – 7.58 (m, 2H), 7.53 – 7.45 (m, 2H), 7.35 – 7.21 (m, 5H), 7.21 – 7.15 (m, 1H), 7.14 – 7.05 (m, 2H), 6.58 (dt, *J* = 11.8, 1.5 Hz, 1H), 5.97 (s, 1H), 5.70 (dt, *J* = 11.7, 6.7 Hz, 1H), 4.92 (dd, *J* = 6.7, 1.6 Hz, 2H); ^{13}C NMR (100 MHz, Chloroform-*d*) δ 168.0, 167.2, 135.9, 134.5, 134.3, 133.7, 131.9, 129.9, 128.8, 128.7, 128.7, 128.5, 127.7, 125.1, 123.7, 63.2, 56.0; IR (Neat Film, NaCl) 3045, 1746, 1715, 1682, 1558, 1496, 1468, 1451, 1384, 1337, 1301, 1217, 1109, 1076, 962, 829, 788, 771, 722, 700, 638 cm^{-1}; (MM:FAB+) *m/z* calc'd for $C_{25}H_{20}NO_4$ $[M+H]^+$: 398.1392, found 398.1412.

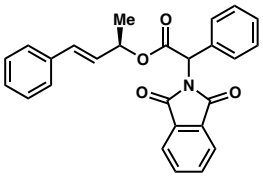

(*R*, *E*)-4-phenylbut-3-en-2-yl 2-(1,3-dioxoisoindolin-2-yl)-2-phenylacetate (82)

Performed on a 4.83 mmol scale according to general procedure 3 and purified by silica gel chromatography (20% EtOAc in hexanes) to afford a viscous oil (1.8586 g, 4.52 mmol, 94% yield, 1:1 dr); ^{1}H NMR (500 MHz, Chloroform-*d*) δ 7.85 (ddd, *J* = 9.8, 5.4, 3.0 Hz, 2H), 7.75 – 7.67 (m, 2H), 7.61 – 7.55 (m, 2H), 7.43 – 7.22 (m, 8H), 6.57 (ddd, *J* = 16.0, 2.9, 1.1 Hz, 1H), 6.15 (dt, *J* = 15.9, 6.7 Hz, 1H), 6.06 (d, *J* = 4.5 Hz, 1H), 5.71 (dpd, *J* = 9.7, 6.5, 1.2 Hz, 1H), 1.46 (d, *J* = 6.5 Hz, 1.5H), 1.43 (d, *J* = 6.5 Hz, 1.5H); ^{13}C NMR (100 MHz, Chloroform-*d*) δ 167.4, 167.4, 167.2, 167.2, 136.3, 136.3, 134.6, 134.3, 134.3, 132.2, 132.2, 131.9, 129.9, 129.9, 128.7, 128.6, 128.6, 128.6, 128.1, 128.1, 128.0, 126.7, 123.7, 123.7, 73.5, 73.4, 56.3, 56.2, 20.4, 20.3; IR (Neat Film, NaCl) 1717, 1384, 1213, 1108, 1076, 1037, 965, 722, 695; (MM:ESI-APCI+) *m/z* calc'd for $C_{26}H_{25}N_2O_4$ $[M+NH_4]^+$: 429.1809, found 429.1799.

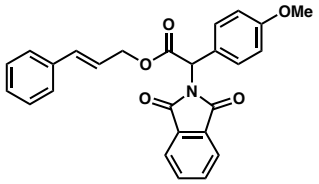

cinnamyl 2-(1,3-dioxoisoindolin-2-yl)-2-(4-methoxyphenyl)acetate (123)

Prepared on a 10.00 mmol scale according to general procedure 2 and purified by column chromatography (30–100% CH_2Cl_2 in hexanes) to provide a white foam (1.63g, 3.81 mmol, 38% yield); ^{1}H NMR (500 MHz, Chloroform-*d*) δ 7.87–7.82 (m, 2H), 7.75–7.67 (m, 2H), 7.53 – 7.47 (m, 2H), 7.36 – 7.28 (m, 4H), 7.23–7.27 (m, 1H), 6.92–6.83 (m, 2H), 6.60 (dd, *J* = 15.9, 1.4 Hz, 1H), 6.24 (dt, *J* = 15.8, 6.4 Hz, 1H), 6.01 (s, 1H), 4.88 (qdd, *J* = 12.8, 6.4, 1.4 Hz, 2H), 3.79 (s, 3H); ^{13}C NMR (100 MHz, Chloroform-*d*) δ 168.3, 167.3, 159.8, 136.2, 134.8, 134.3, 132.0, 131.3, 128.7, 128.3, 126.8, 126.8, 123.7, 122.5, 114.0, 66.8, 55.6, 55.4; IR (Neat Film, NaCl) 3027, 2935, 2838, 2364, 1772, 1746, 1716, 1612, 1515, 1467, 1384, 1336, 1306, 1252, 1214, 1180, 1105, 1032, 966, 910, 834, 793, 738, 716, 694, 645 cm^{-1}; HRMS (MM:ESI-APCI+) *m/z* calc'd for $C_{26}H_{22}NO_5$ $[M+H]^+$: 428.1492, found 428.1507.

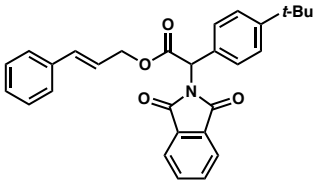

cinnamyl 2-(4-(*tert*-butyl)phenyl)-2-(1,3-dioxoisoindolin-2-yl)acetate (124)

Prepared on a 10.00 mmol scale according to general procedure 2 and purified by column chromatography (30–90% CH_2Cl_2 in hexanes) to provide a white foam (2.73 g, 6.02 mmol, 60% yield); ^{1}H NMR (500 MHz, Chloroform-*d*) δ 7.87–7.79 (m, 2H), 7.74–7.68 (m, 2H), 7.52 – 7.46 (m, 2H), 7.40–7.28 (m, 6H), 7.27–7.23 (m, 1H), 6.59 (dd, *J* = 15.9, 1.4 Hz, 1H), 6.25 (dt, *J* = 15.9, 6.4 Hz, 1H), 6.04 (s, 1H), 4.89 (qdd, *J* = 12.8, 6.4, 1.4 Hz, 2H), 1.30 (s, 9H); ^{13}C NMR (100 MHz, Chloroform-*d*) δ 168.2, 167.2, 151.6, 136.2, 134.7, 134.3, 132.0, 131.5, 129.6, 128.7, 128.2, 126.8, 125.7, 123.7, 122.6, 66.8, 55.8, 34.7, 31.4; IR (Neat Film, NaCl) 2960, 1773, 1748, 1717, 1508, 1466, 1384, 1219, 1186, 1108, 966, 910, 842, 721 cm^{-1}; HRMS (MM:ESI-APCI+) *m/z* calc'd for $C_{29}H_{28}NO_4$ $[M+H]^+$: 454.2013, found 454.2010.

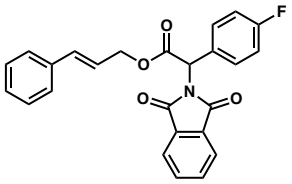

cinnamyl 2-(1,3-dioxoisoindolin-2-yl)-2-(4-fluorophenyl)acetate (125)

Prepared on a 10.00 mmol scale according to general procedure 2 and purified by column chromatography (35% CH_2Cl_2, 2% EtOAc in hexanes) to provide an amorphous white solid (2.48 g, 5.97 mmol, 60% yield); ^{1}H NMR (500 MHz, Chloroform-*d*) δ 7.98 – 7.84 (m, 2H), 7.82 – 7.75 (m, 2H), 7.65 – 7.59 (m, 2H), 7.43 – 7.34 (m, 4H), 7.34 – 7.27 (m, 1H), 7.13 – 7.05 (m, 2H), 6.66 (d, J = 15.9 Hz, 1H), 6.29 (dt, J = 15.8, 6.5 Hz, 1H), 6.08 (s, 1H), 4.94 (qdd, J = 12.7, 6.5, 1.4 Hz, 2H).; ^{13}C NMR (100 MHz, Chloroform-*d*) δ 167.9, 167.2, 162.8 (d, $J_{C–F}$ = 248.1 Hz), 136.1, 135.0, 134.5, 131.9, 131.9 (d, $J_{C–F}$ = 1.7 Hz), 130.5 (d, $J_{C–F}$ = 3.5 Hz), 128.7, 128.3, 126.8, 123.8, 122.3, 115.7 (d, $J_{C–F}$ = 21.7 Hz), 67.0, 55.3; ^{19}F NMR (282 MHz, Chloroform-*d*) δ –112.87 (tt, J = 8.5, 5.1 Hz); IR (Neat Film, NaCl) 3045, 2940, 1747, 1716, 1607, 1512, 1469, 1384, 1336, 1224, 1184, 1162, 1112, 1096, 968, 895, 848, 837, 742, 717, 694 cm^{-1}; (MM:FAB+) *m/z* calc'd for $C_{25}H_{19}NO_4F$ $[M+H]^+$: 416.1298, found 416.1275.

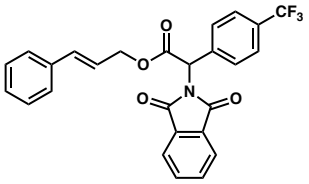

cinnamyl 2-(1,3-dioxoisoindolin-2-yl)-2-(4-(trifluoromethyl)phenyl)acetate (126)

Prepared on a 10.00 mmol scale according to general procedure 2 and purified by column chromatography (27% CH_2Cl_2, 3% EtOAc in hexanes) to provide an amorphous white solid (2.76 g, 6.30 mmol, 63% yield); ^{1}H NMR (500 MHz, Chloroform-*d*) δ 7.90 – 7.84 (m, 2H), 7.77 – 7.72 (m, 2H), 7.70 (d, J = 8.2 Hz, 2H), 7.62 (d, J = 8.2 Hz, 2H), 7.38 – 7.29 (m, 4H), 7.29 – 7.23 (m, 1H), 6.60 (d, J = 15.8 Hz, 1H), 6.24 (dt, J = 15.9, 6.5 Hz, 1H), 6.09 (s, 1H), 4.90 (dddd, J = 20.5, 12.8, 6.5, 1.2 Hz, 2H); ^{13}C NMR (100 MHz, Chloroform-*d*) δ 167.3, 167.1, 138.3, 136.0, 135.1, 134.5, 131.7, 130.8 (q, $J_{C–F}$ = 32.6 Hz), 130.3, 128.7, 128.3, 126.8, 125.6 (q, $J_{C–F}$ = 3.7 Hz), 124.0 (q, $J_{C–F}$ = 272.3 Hz), 123.9, 122.1, 67.1, 55.4; ^{19}F NMR (282 MHz, Chloroform-*d*) δ –62.7; IR (Neat Film, NaCl) 3486, 3044, 2938, 2116, 1774, 1747, 1720, 1620, 1495, 1469, 1449, 1422, 1385, 1326, 1385, 1326, 1216, 1170, 1125, 1105, 1069, 966, 909, 847, 745, 719 cm^{-1}; (MM:FAB+) *m/z* calc'd for $C_{26}H_{19}NO_4F_3$ $[M+H]^+$: 466.1266, found 466.1255.

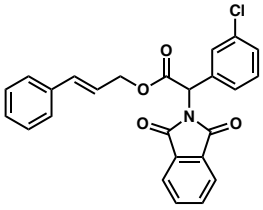

cinnamyl 2-(3-chlorophenyl)-2-(1,3-dioxoisoindolin-2-yl)acetate (127)

Prepared on a 10.00 mmol scale according to general procedure 2 and purified by column chromatography (35% CH_2Cl_2, 2% EtOAc in hexanes) to provide an amorphous white solid (2.66 g, 6.16 mmol, 62% yield); ^{1}H NMR (500 MHz, Chloroform-*d*) δ 7.89 – 7.83 (m, 2H), 7.76 – 7.70 (m, 2H), 7.59 – 7.54 (m, 1H), 7.46 (dt, *J* = 6.6, 2.0 Hz, 1H), 7.37 – 7.29 (m, 6H), 7.29 – 7.22 (m, 1H), 6.60 (d, *J* = 15.8 Hz, 1H), 6.23 (dt, *J* = 15.8, 6.4 Hz, 1H), 6.00 (s, 1H), 4.88 (tdd, *J* = 13.1, 6.4, 1.2 Hz, 2H); ^{13}C NMR (100 MHz, Chloroform-*d*) δ 167.4, 167.1, 136.3, 136.1, 135.0, 134.5, 134.5, 131.8, 130.0, 129.9, 129.0, 128.7, 128.3, 128.1, 126.8, 123.9, 122.2, 67.0, 55.4; IR (Neat Film, NaCl) 3044, 1775, 1746, 1721, 1610, 1469, 1447, 1382, 1312, 1256, 1216, 1188, 1104, 967, 912, 738, 722, 710 cm^{-1}; (MM:FAB+) *m/z* calc'd for $C_{25}H_{19}NO_4Cl$ $[M+H]^+$: 432.1003, found 432.1024.

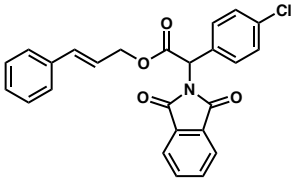

cinnamyl 2-(4-chlorophenyl)-2-(1,3-dioxoisoindolin-2-yl)acetate (128)

Prepared on a 10.00 mmol scale according to general procedure 2 and purified by column chromatography (35% CH_2Cl_2, 2% EtOAc in hexanes) to provide a white foam (2.60 g, 6.02 mmol, 60% yield); ^{1}H NMR (500 MHz, Chloroform-*d*) δ 7.88 – 7.82 (m, 2H), 7.76 – 7.70 (m, 2H), 7.53 – 7.48 (m, 2H), 7.37 – 7.29 (m, 6H), 7.28 – 7.22 (m, 1H), 6.60 (dd, *J* = 15.9, 1.5 Hz, 1H), 6.23 (dt, *J* = 15.8, 6.5 Hz, 1H), 6.02 (s, 1H), 4.94 – 4.80 (m, 2H); ^{13}C NMR (100 MHz Chloroform-*d*) δ 167.6, 167.1, 136.1, 135.1, 134.8, 134.5, 133.0, 131.8, 131.3, 128.9, 128.7, 128.3, 126.8, 123.84, 122.2, 67.0, 55.3; IR (Neat Film, NaCl) 3024, 1773, 1745, 1717, 1493, 1467, 1384, 1216, 1186, 1090, 963, 911, 737, 723, 7103 cm^{-1}; (MM:FAB+) *m/z* calc'd for $C_{25}H_{19}NO_4Cl$ $[M+H]^+$: 432.1003, found 432.1018.

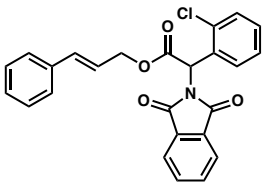

cinnamyl 2-(2-chlorophenyl)-2-(1,3-dioxoisoindolin-2-yl)acetate (129)

Prepared on a 10.00 mmol scale according to general procedure 2 and purified by column chromatography (10–90% CH_2Cl_2 in hexanes) to provide a white foam (2.72 g, 6.30 mmol, 63% yield); ^{1}H NMR (500 MHz, Chloroform-*d*) δ 7.89 – 7.84 (m, 2H), 7.77 – 7.71 (m, 2H), 7.69 – 7.63 (m, 1H), 7.44 – 7.37 (m, 1H), 7.37 – 7.23 (m, 7H), 6.60 (d, *J* = 15.9 Hz, 1H), 6.56 (d, *J* = 1.7 Hz, 1H), 6.24 (dt, *J* = 15.9, 6.4 Hz, 1H), 4.94 – 4.86 (m, 2H); ^{13}C NMR (100 MHz, Chloroform-*d*) δ 167.6, 167.2, 136.1, 134.9, 134.5, 134.4, 131.9, 131.8, 131.6, 130.1, 129.6, 128.7, 128.3, 126.8, 123.8, 122.2, 66.9, 53.5; IR (Neat Film, NaCl) 3024, 1773, 1746, 1717, 1493, 1384, 1216, 1186, 1090, 963, 737, 723, 710 cm^{-1}; HRMS (MM:ESI-APCI+) *m/z* calc'd for $C_{25}H_{19}ClNO_4$ $[M+H]^+$: 432.0997, found 432.0984.

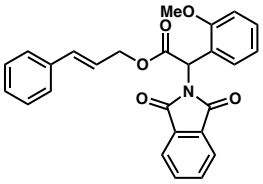

cinnamyl 2-(1,3-dioxoisoindolin-2-yl)-2-(2-methoxyphenyl)acetate (130)

Prepared on a 10.00 mmol scale according to general procedure 2 and purified by column chromatography (50% CH_2Cl_2, 2% EtOAc in hexanes) to provide a white amorphous solid (2.67 g, 6.25 mmol, 63% yield); ^{1}H NMR (500 MHz, Chloroform-*d*) δ 7.87 – 7.81 (m, 2H), 7.74 – 7.67 (m, 2H), 7.56 – 7.50 (m, 1H), 7.36 – 7.28 (m, 5H), 7.27 – 7.23 (m, 1H), 6.96 (t, *J* = 7.5 Hz, 1H), 6.89 (d, *J* = 8.2 Hz, 1H), 6.64 – 6.54 (m, 2H), 6.25 (dt, *J* = 15.9, 6.3 Hz, 1H), 4.88 (d, *J* = 6.2 Hz, 2H), 3.84 (s, 3H); ^{13}C NMR (100 MHz, Chloroform-*d*) δ 168.5, 167.3, 157.3, 136.2, 134.4, 134.2, 131.9, 130.6, 130.0, 128.6, 128.1, 126.7, 123.5, 122.6, 122.3, 120.3, 110.7, 66.5, 55.8, 50.3; IR (Neat Film, NaCl) 1841, 1720, 1602, 1494, 1466, 1384, 1251, 1216, 1097, 1026, 963, 902, 748, 718 cm^{-1}; (MM:FAB+) *m/z* calc'd for $C_{26}H_{22}NO_5$ $[M+H]^+$: 428.1498, found 428.1500.

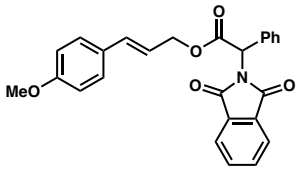

(*E*)-3-(4-methoxyphenyl)allyl 2-(1,3-dioxoisoindolin-2-yl)-2-phenylacetate (131)

Performed on a 2.72 mmol scale according to general procedure 3 and purified by silica gel chromatography (30% EtOAc in hexanes) to afford a viscous yellow oil (1.10 g, 2.57 mmol, 95% yield); ^{1}H NMR (500 MHz, Chloroform-*d*) δ 7.89 – 7.81 (m, 2H), 7.75 – 7.68 (m, 2H), 7.61 – 7.53 (m, 2H), 7.39 – 7.31 (m, 3H), 7.30 – 7.27 (m, 2H), 6.87 – 6.80 (m, 2H), 6.59 – 6.50 (m, 1H), 6.11 (dt, *J* = 15.8, 6.6 Hz, 1H), 6.06 (s, 1H), 4.87 (qdd, *J* = 12.6, 6.6, 1.3 Hz, 2H), 3.81 (d, *J* = 0.8 Hz, 3H); ^{13}C NMR (100 MHz, Chloroform-*d*) δ 168.0, 167.2, 159.7, 134.6, 134.5, 134.3, 131.9, 129.9, 128.9, 128.7, 128.6, 128.0, 123.7, 120.1, 114.1, 67.1, 56.1, 55.4; IR (Neat Film, NaCl) 1772, 1746, 1716, 1607, 1512, 1384, 1337, 1250, 1220, 1175, 1113, 1033, 966, 906, 895, 838, 721, 699; HRMS (MM:ESI-APCI+) *m/z* calc'd for $C_{26}H_{25}N_2O_5$ $[M+NH_4]^+$: 445.1758, found 445.1748.

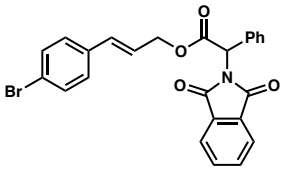

(*E*)-3-(4-bromophenyl)allyl 2-(1,3-dioxoisoindolin-2-yl)-2-phenylacetate (132)

Performed on a 2.00 mmol scale according to general procedure 3 and purified by silica gel chromatography (20% EtOAc, in hexanes) to afford a viscous colorless oil (897.1 mg, 1.88 mmol, 94% yield); ^{1}H NMR (500 MHz, Chloroform-*d*) δ 7.84 (dd, *J* = 5.4, 3.1 Hz, 2H), 7.74 – 7.67 (m, 2H), 7.63 – 7.54 (m, 2H), 7.46 – 7.31 (m, 5H), 7.23 – 7.16 (m, 2H), 6.55 – 6.47 (m, 1H), 6.23 (dt, *J* = 15.9, 6.3 Hz, 1H), 6.08 (s, 1H), 4.99 – 4.81 (m, 2H); ^{13}C NMR (100 MHz, Chloroform-*d*) δ 167.9, 167.1, 135.1, 134.5, 134.3, 133.4, 131.8, 131.8, 129.8, 128.8, 128.7, 128.2, 123.7, 123.3, 122.0, 66.5, 56.0; IR (Neat Film, NaCl) 1772, 1748, 1717, 1487, 1384, 1214, 1185, 1109, 1073, 1008, 965, 721, 699; HRMS (MM:ESI-APCI+) *m/z* calc'd for $C_{25}H_{22}BrN_2O_4$ $[M+NH_4]^+$: 493.0757, found 493.0748.

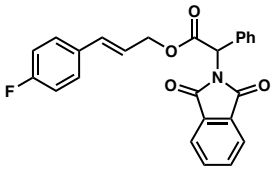

(*E*)-3-(4-fluorophenyl)allyl 2-(1,3-dioxoisoindolin-2-yl)-2-phenylacetate (133)

Performed on a 2.79 mmol scale according to general procedure 3 and purified by silica gel chromatography (20% EtOAc in hexanes) to afford a viscous yellow oil (1.0238 g, 2.46 mmol, 88% yield); ^{1}H NMR (300 MHz, Chloroform-*d*) δ 7.85 (dd, *J* = 5.5, 3.1 Hz, 2H), 7.72 (dd, *J* = 5.5, 3.1 Hz, 2H), 7.62 – 7.52 (m, 2H), 7.43 – 7.27 (m, 5H), 7.05 – 6.91 (m, 2H), 6.56 (dd, *J* = 15.9, 1.4 Hz, 1H), 6.16 (dt, *J* = 15.9, 6.4 Hz, 1H), 6.06 (s, 1H), 4.96 – 4.79 (m, 2H); ^{13}C NMR (100 MHz, Chloroform-*d*) δ 168.0, 167.1, 162.7 (d, *J* = 247.6 Hz), 134.5, 134.3, 133.6, 132.3 (d, *J* = 3.3 Hz), 131.8, 129.8, 128.7, 128.6, 128.3 (d, *J* = 8.1 Hz), 123.7, 122.2 (d, *J* = 2.2 Hz), 115.6 (d, *J* = 21.7 Hz), 66.6, 56.0; ^{19}F NMR (282 MHz, Chloroform-*d*) δ –113.5 (tt, *J* = 8.6, 5.4 Hz); IR (Neat Film, NaCl) 1773, 1748, 1716, 1601, 1508, 1385, 1227, 1185, 1112, 968, 908, 722, 700; HRMS (MM:ESI-APCI+) *m/z* calc'd for $C_{25}H_{22}FN_2O_4$ $[M+NH_4]^+$: 433.1558, found 433.1544.

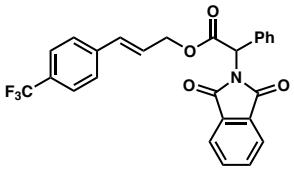

(*E*)-3-(4-(trifluoromethyl)phenyl)allyl 2-(1,3-dioxoisoindolin-2-yl)-2-phenylacetate (134)

Performed on a 2.00 mmol scale according to general procedure 3 and purified by silica gel chromatography (25% EtOAc in hexanes) to afford a viscous colorless oil (799.2 mg, 1.72 mmol, 86% yield); ^{1}H NMR (500 MHz, Chloroform-*d*) δ 7.90 – 7.81 (m, 2H), 7.77 – 7.68 (m, 2H), 7.64 – 7.53 (m, 4H), 7.46 – 7.31 (m, 5H), 6.66 – 6.57 (m, 1H), 6.34 (dt, *J* = 15.9, 6.0 Hz, 1H), 6.10 (s, 1H), 4.98 – 4.85 (m, 2H); ^{13}C NMR (100 MHz, Chloroform-*d*) δ 167.9, 167.2, 139.6 (d, *J* = 1.5 Hz), 134.5, 134.4, 132.8, 131.8, 129.9 (q, *J* = 32.5) 129.8, 128.8, 128.7, 126.9, 125.6 (q, *J* = 3.8 Hz), 125.2, 123.9 (q, *J* = 271.8) 123.7, 66.2, 56.0; ^{19}F NMR (282 MHz, Chloroform-*d*) δ –62.5; IR (Neat Film, NaCl) 1773, 1750, 1719, 1615, 1385, 1326, 1214, 1168, 1120, 1068, 720, 698; HRMS (MM:ESI-APCI+) *m/z* calc'd for $C_{26}H_{22}N_2O_4$ $[M+NH_4]^+$: 483.1526, found 483.1512.

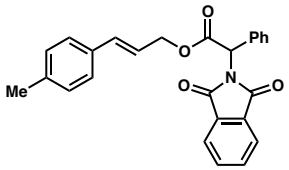

(*E*)-3-(*p*-tolyl)allyl 2-(1,3-dioxoisoindolin-2-yl)-2-phenylacetate (135)

Performed on a 2.72 mmol scale according to general procedure 3 and purified by silica gel chromatography (20% EtOAc in hexanes) to afford a viscous yellow oil (1.0574 g, 2.57 mmol, 94% yield); ^{1}H NMR (500 MHz, Chloroform-*d*) δ 7.91 – 7.82 (m, 2H), 7.72 (dd, *J* = 5.5, 3.0 Hz, 2H), 7.62 – 7.55 (m, 2H), 7.41 – 7.31 (m, 3H), 7.28 – 7.22 (m, 3H), 7.16 – 7.08 (m, 2H), 6.57 (dd, *J* = 15.9, 1.3 Hz, 1H), 6.19 (dt, *J* = 15.8, 6.5 Hz, 1H), 6.06 (s, 1H), 4.88 (qdd, *J* = 12.7, 6.5, 1.3 Hz, 2H), 2.34 (s, 2H); ^{13}C NMR (100 MHz, Chloroform-*d*) δ 168.0, 167.2, 138.2, 134.8, 134.5, 134.3, 133.3, 131.9, 129.9, 129.4, 128.7, 128.7, 126.7, 123.7, 121.3, 67.0, 56.1, 21.3; IR (Neat Film, NaCl) 1772, 1748, 1716, 1384, 1222, 1182, 1108, 1076, 966, 906, 719, 698 cm^{-1}; HRMS (MM:ESI-APCI+) *m/z* calc'd for $C_{26}H_{25}N_2O_4$ $[M+NH_4]^+$: 429.1809, found 429.1818.

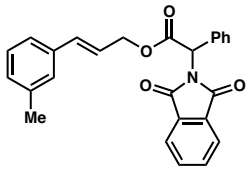

(*E*)-3-(*m*-tolyl)allyl 2-(1,3-dioxoisoindolin-2-yl)-2-phenylacetate (136)

Performed on a 2.00 mmol scale according to general procedure 3 and purified by silica gel chromatography (20% EtOAc in hexanes) to afford a viscous oil (779 mg, 1.89 mmol, 95% yield); ^{1}H NMR (500 MHz, Chloroform-*d*) δ 7.85 (dd, *J* = 5.4, 3.1 Hz, 2H), 7.71 (dd, *J* = 5.5, 3.0 Hz, 2H), 7.63 – 7.56 (m, 2H), 7.42 – 7.32 (m, 3H), 7.23 – 7.13 (m, 3H), 7.08 (d, *J* = 7.4 Hz, 1H), 6.62 – 6.54 (m, 1H), 6.25 (dt, *J* = 15.8, 6.4 Hz, 1H), 6.09 (s, 1H), 4.90 (qdd, *J* = 12.8, 6.4, 1.4 Hz, 2H), 2.35 (s, 3H); ^{13}C NMR (100 MHz, Chloroform-*d*) δ 168.0, 167.1, 138.2, 136.0, 134.9, 134.5, 134.3, 131.8, 129.9, 129.0, 128.7, 128.6, 128.5, 127.4, 123.9, 123.7, 122.2, 66.8, 56.0, 21.4; IR (Neat film, NaCl) 1772, 1747, 1715, 1605, 1468, 1456, 1385, 1214, 1186, 1111, 1076, 966, 908, 776, 721, 697; (MM:ESI-APCI+) *m/z* calc'd for $C_{26}H_{25}N_2O_4$ $[M+NH_4]^+$: 429.1809, found 429.1791.

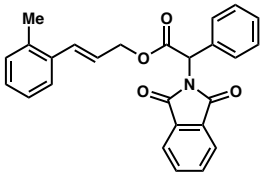

(*E*)-3-(*o*-tolyl)allyl 2-(1,3-dioxoisoindolin-2-yl)-2-phenylacetate (137)

Performed on a 3.00 mmol scale according to general procedure 3 and purified by silica gel chromatography (0–30% EtOAc in hexanes) to afford a viscous, colorless oil (716.0 mg, 1.74 mmol, 58% yield); ^{1}H NMR (500 MHz, Chloroform-*d*) δ 7.88 – 7.82 (m, 2H), 7.75 – 7.67 (m, 2H), 7.63 – 7.56 (m, 2H), 7.45 – 7.31 (m, 4H), 7.20 – 7.08 (m, 3H), 6.82 (d, *J* = 15.7 Hz, 1H), 6.14 (dt, *J* = 15.8, 6.3 Hz, 1H), 6.08 (s, 1H), 4.98 – 4.86 (m, 2H), 2.28 (s, 3H); ^{13}C NMR (100 MHz, Chloroform-*d*) δ 167.9, 167.1, 135.8, 135.3, 134.5, 134.3, 132.4, 131.9, 130.4, 129.9, 128.7, 128.7, 128.1, 126.2, 125.9, 123.7, 66.9, 56.1, 19.8; IR (Neat Film, NaCl) 3477, 3065, 3030, 2948, 2358, 2258, 1772, 1747, 1716, 1636, 1614, 1496, 1485, 1468, 1456, 1385, 1358, 1337, 1216, 1186, 1112, 1076, 966, 909, 720, 699 cm^{-1}; (MM:ESI-APCI+) *m/z* calc'd for $C_{26}H_{22}NO_4$ $[M+H]^+$: 412.1549, found 412.1549.

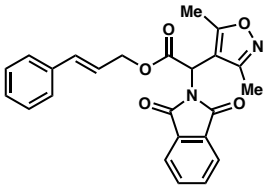

cinnamyl 2-(3,5-dimethylisoxazol-4-yl)-2-(1,3-dioxoisoindolin-2-yl)acetate (138)

Performed according to general procedure 5 and purified by column chromatography (0–30% EtOAc in hexanes) to afford an amorphous white solid (1.2173 g, 2.92 mmol, 19% yield over 4 steps); ^{1}H NMR (500 MHz, Chloroform-*d*) δ 7.90 – 7.83 (m, 2H), 7.78 – 7.72 (m, 2H), 7.38 – 7.25 (m, 5H), 6.65 (d, *J* = 15.8 Hz, 1H), 6.25 (dt, *J* = 15.8, 6.7 Hz, 1H), 5.98 (s, 1H), 4.89 (d, *J* = 6.6 Hz, 2H), 2.49 (s, 3H), 2.34 (s, 3H); ^{13}C NMR (100 MHz, Chloroform-*d*) δ 169.3, 166.9, 166.6, 159.5, 135.7, 135.6, 134.4, 131.5, 128.6, 128.3, 126.7, 123.7, 121.6, 108.2, 67.2, 45.7, 12.2, 10.5; IR (Neat Film, NaCl) 3509, 2935, 1726, 1677, 1430, 1364, 1340, 1299, 1240, 1175, 1114, 1050, 1002, 925, 839, 816, 754, 694 cm^{-1}; (MM:FAB+) *m/z* calc'd for $C_{24}H_{21}N_2O_5$ $[M+H]^+$: 417.1450, found 417.1469.

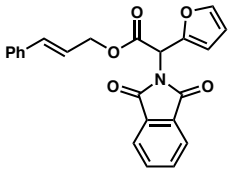

cinnamyl 2-(1,3-dioxoisoindolin-2-yl)-2-(furan-2-yl)acetate (139)

Performed according to general procedure 5 and purified by column chromatography (0–30% EtOAc in hexanes) to afford an amorphous white solid (1.7335 g, 4.47 mmol, 30% yield over 4 steps); ^{1}H NMR (500 MHz, Chloroform-*d*) δ 7.92 – 7.82 (m, 2H), 7.80 – 7.69 (m, 2H), 7.42 – 7.37 (m, 1H), 7.37 – 7.28 (m, 4H), 7.28 – 7.22 (m, 1H), 6.65 – 6.57 (m, 2H), 6.38 (dd, *J* = 3.1, 1.8 Hz, 1H), 6.24 (dt, *J* = 15.9, 6.4 Hz, 1H), 6.18 (s, 1H), 4.94 – 4.84 (m, 2H); ^{13}C NMR (100 MHz, Chloroform-*d*) δ 166.8, 166.2, 146.8, 142.7, 136.1, 134.9, 134.4, 131.9, 128.7, 128.3, 126.8, 123.8, 122.1, 110.9, 110.7, 67.1, 49.5; IR (Neat Film, NaCl) 3838, 3472, 3027, 1750, 1721, 1662, 1646, 1493, 1467, 1449, 1426, 1384, 1336, 1300, 1221, 1192, 1110, 1089, 1073, 1014, 964, 933, 906, 886, 833, 734, 715, 70, 692 cm^{-1}; (MM:FAB+) *m/z* calc'd for $C_{23}H_{18}NO_5$ $[M+H]^+$: 388.1185, found 388.1206.

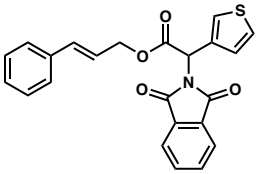

cinnamyl 2-(1,3-dioxoisoindolin-2-yl)-2-(thiophen-3-yl)acetate (140)

Performed according to general procedure 5 and purified by column chromatography (0–30% EtOAc in hexanes) to afford an amorphous white solid with a minor, inseparable impurity (1.7355 g, 4.30 mmol, 29% yield over 4 steps); ^{1}H NMR (500 MHz, Chloroform-*d*) δ 7.92 – 7.87 (m, 2H), 7.79 – 7.73 (m, 2H), 7.54 – 7.51 (m, 1H), 7.40 – 7.31 (m, 6H), 7.31 – 7.26 (m, 1H), 6.62 (d, *J* = 15.8 Hz, 1H), 6.27 (dt, *J* = 15.9, 6.4 Hz, 1H), 6.20 (s, 1H), 4.91 (qd, *J* = 12.8, 6.3 Hz, 2H); ^{13}C NMR (100 MHz, Chloroform-*d*) δ 167.7, 167.0, 136.1, 134.7, 134.3, 131.8, 128.7, 128.6, 128.2, 126.7, 126.0, 125.9, 123.7, 122.3, 66.8, 51.0; IR (Neat Film, NaCl) 3474, 3102, 3060, 3027, 2933, 2699, 2482, 2296, 2258, 1948, 1888, 1770, 1747, 1722, 1714, 1613, 1550, 1513, 1494, 1469 1456, 1449, 1384, 1337, 1298, 1220, 1179, 1108, 1088, 1020, 968, 910, 886, 838, 800, 732, 711, 693, 668 cm^{-1}; (MM:FAB+) *m/z* calc'd for $C_{23}H_{18}NO_4S$ $[M+H]^+$: 404.0957, found 404.0968.

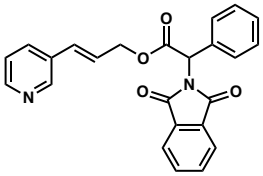

(*E*)-3-(pyridin-3-yl)allyl 2-(1,3-dioxoisoindolin-2-yl)-2-phenylacetate (141)

Performed on a 4.75 mmol scale according to general procedure 3 and purified by silica gel chromatography (30–100% EtOAc in hexanes) to afford the desired product as an amorphous white solid (1.5260 g, 3.83 mmol, 81% yield);^{1}H NMR (500 MHz, Chloroform-*d*) δ 8.53 (s, 1H), 8.51 – 8.44 (m, 1H), 7.94 – 7.81 (m, 2H), 7.77 – 7.67 (m, 2H), 7.72 – 7.66 (m, 1H), 7.62 – 7.54 (m, 2H), 7.45 – 7.32 (m, 3H), 7.31 – 7.21 (m, 1H), 6.56 (d, *J* = 16.0 Hz, 1H), 6.32 (dt, *J* = 15.9, 6.1 Hz, 1H), 6.07 (s, 1H), 5.00 – 4.82 (m, 2H); ^{13}C NMR (100 MHz, Chloroform-*d*) δ 167.8, 167.0, 148.8, 148.2, 134.3, 134.3, 133.2, 131.8, 131.7, 130.4, 129.7, 128.7, 128.6, 124.9, 123.6, 123.5, 66.0, 55.9; IR (Neat Film, NaCl) 3471, 3033, 2938, 1771, 1747, 1716, 1613, 1385, 1337, 1264, 1222, 1186, 1111, 1088, 1076, 970, 895, 721, 700 cm^{-1} ;(MM:FAB+) *m/z* calc'd for $C_{24}H_{19}N_2O_4$ $[M+H]^+$: 399.1345, found 399.1358.

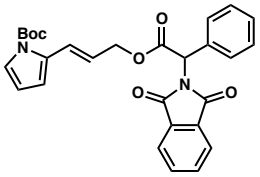

tert-butyl (_E_)-2-(3-(2-(1,3-dioxoisoindolin-2-yl)-2-phenylacetoxy)prop-1-en-1-yl)-1_H_-pyrrole-1-carboxylate (142)

Performed on a 4.48 mmol scale according to general procedure 3 and purified by silica gel chromatography (20% EtOAc in hexanes) to afford the desired product as an amorphous white solid (1.9915g, 4.09 mmol, 91% yield); ^{1}H NMR (500 MHz, Chloroform-*d*) δ 7.85 (dt, *J* = 7.5, 3.8 Hz, 2H), 7.71 (dq, *J* = 7.3, 4.0 Hz, 2H), 7.55 (d, *J* = 7.5 Hz, 2H), 7.34 (dq, *J* = 9.7, 6.9 Hz, 4H), 7.23 – 7.17 (m, 1H), 6.41 (d, *J* = 3.4 Hz, 1H), 6.13 (t, *J* = 3.4 Hz, 1H), 6.08 – 5.99 (m, 1H), 6.04 (s, 1H), 4.93 – 4.78 (m, 2H), 1.58 (s, 9H); ^{13}C NMR (100 MHz, Chloroform-*d*) δ 167.9, 167.1, 149.2, 134.5, 134.2, 132.5, 131.8, 129.8, 128.6, 128.6, 126.3, 123.6, 122.3, 121.8, 111.9, 110.9, 84.0, 67.0, 56.0, 28.0; IR (Neat Film, NaCl) 3476, 3064, 2982, 2940, 1738, 1722, 1716, 1613, 1496, 1469, 1456, 1385, 1372, 1323, 1247, 1214, 1183, 1172, 1165, 1128, 1069, 962, 892, 847, 721, 699 cm^{-1};(MM:FAB+) *m/z* calc'd for $C_{28}H_{26}N_2O_6$ $[M]^{+\bullet}$: 486.1791, found 486.1808.

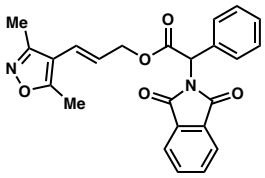

(*E*)-3-(3,5-dimethylisoxazol-4-yl)allyl 2-(1,3-dioxoisoindolin-2-yl)-2-phenylacetate (143)

Performed on a 6.20 mmol scale according to general procedure 3 and purified by silica gel chromatography (30% EtOAc in hexanes) to afford the desired product as an amorphous white solid (2.0168 g, 4.84 mmol, 78% yield);^{1}H NMR (500 MHz, Chloroform-*d*) δ 7.90 – 7.81 (m, 2H), 7.77 – 7.70 (m, 2H), 7.60 – 7.53 (m, 2H), 7.40 – 7.30 (m, 3H), 6.29 (d, *J* = 16.3 Hz, 1H), 6.05 (s, 1H), 5.92 (dt, *J* = 16.2, 6.2 Hz, 1H), 4.90 – 4.80 (m, 2H), 2.38 (s, 3H), 2.29 (s, 3H); ^{13}C NMR (100 MHz, Chloroform-*d*) δ 167.8, 167.0, 166.2, 158.2, 134.4, 134.3, 131.7, 129.7, 128.7, 128.6, 123.6, 123.5, 122.4, 111.8, 66.6, 55.9, 11.6, 11.4; IR (Neat Film, NaCl) 3044, 1747, 1716, 1676, 1610, 1430, 1385, 1337, 1213, 1110, 1076, 962, 893, 721, 699, 682 cm^{-1}; (MM:FAB+) *m/z* calc'd for $C_{24}H_{21}N_2O_5$ [M+H]+: 417.1450, found 417.1478.

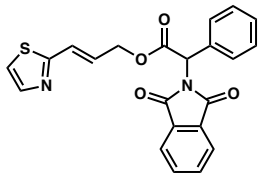

(*E*)-3-(thiazol-2-yl)allyl 2-(1,3-dioxoisoindolin-2-yl)-2-phenylacetate (144)

Performed on a 6.28 mmol scale according to general procedure 3 and purified by silica gel chromatography (30% EtOAc in hexanes) to afford the desired product as an viscous, colorless semisolid (1.32 g, 3.24 mmol, 52% yield); ^{1}H NMR (500 MHz, Chloroform-*d*) δ 7.89 – 7.84 (m, 2H), 7.77 (d, *J* = 3.2 Hz, 1H), 7.75 – 7.70 (m, 2H), 7.59 – 7.54 (m, 2H), 7.40 – 7.32 (m, 3H), 7.26 (d, *J* = 3.2 Hz, 1H), 6.78 (dt, *J* = 15.9, 1.4 Hz, 1H), 6.61 (dt, *J* = 15.9, 5.9 Hz, 1H), 6.07 (s, 1H), 4.99 – 4.86 (m, 2H); ^{13}C NMR (100 MHz, Chloroform-*d*) δ 167.9, 167.2, 165.5, 143.6, 134.4, 134.4, 131.9, 129.8, 128.9, 128.7, 128.6, 126.7, 123.8, 119.0, 65.5, 56.0; IR (Neat Film, NaCl) 3476. 3060, 1772, 1750, 1716, 1610, 1487, 1467, 1456, 1385, 1336, 1216, 1186, 1110, 1076, 960, 894, 787, 772, 760, 719, 699, 638 cm^{-1} ;(MM:FAB+) *m/z* calc'd for $C_{22}H_{17}N_2O_4S$ $[M+H]^+$: 405.0909, found 405.0899.

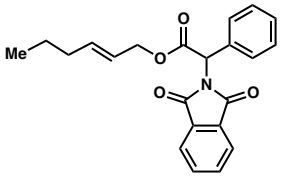

(*E*)-hex-2-en-1-yl 2-(1,3-dioxoisoindolin-2-yl)-2-phenylacetate (106)

Performed on a 3.00 mmol scale according to general procedure 3 and purified by silica gel chromatography (0–25% EtOAc in hexanes) to afford the desired product as a colorless oil (784.8 mg, 2.16 mmol, 72% yield); ^{1}H NMR (500 MHz, Chloroform-*d*) δ 7.90 – 7.80 (m, 2H), 7.75 – 7.68 (m, 2H), 7.58 – 7.51 (m, 2H), 7.41 – 7.28 (m, 3H), 6.02 (s, 1H), 5.73 (dt, *J* = 13.9, 6.8 Hz, 1H), 5.56 – 5.49 (m, 1H), 4.67 (qd, *J* = 12.2, 6.5 Hz, 2H), 2.00 (q, *J* = 7.1 Hz, 2H), 1.37 (h, *J* = 7.3 Hz, 2H), 0.87 (t, *J* = 7.4 Hz, 3H); ^{13}C NMR (100 MHz, Chloroform-*d*) δ 168.0, 167.2, 137.3, 134.6, 134.3, 131.9, 129.9, 128.7, 128.6, 123.7, 123.3, 67.0, 56.1, 34.3, 22.1, 13.7; IR (Neat Film, NaCl) 3838, 3472, 2956, 2932, 1773, 1745, 1719, 1610, 1498, 1467, 1457, 1426, 1384, 1338, 1302, 1216, 1186, 1116, 1089, 1076, 1016, 996, 970, 906, 894, 835, 776, 760, 768, 719, 699, 661, 645 cm^{-1}; (MM:ESI-APCI+) *m/z* calc'd for $C_{22}H_{22}NO_4$ $[M+H]^+$: 364.1549, found 364.1572.

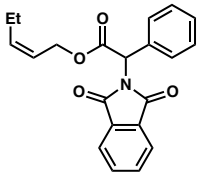

(*Z*)-pent-2-en-1-yl 2-(1,3-dioxoisoindolin-2-yl)-2-phenylacetate (108)

Performed on a 3.00 mmol scale according to general procedure 3 and purified by silica gel chromatography (0–25% EtOAc in hexanes) to afford the desired product as a colorless oil (903.9 mg, 2.59 mmol, 86% yield); ^{1}H NMR (500 MHz, Chloroform-*d*) δ 7.88 – 7.82 (m, 2H), 7.75 – 7.68 (m, 2H), 7.54 (d, *J* = 7.4 Hz, 2H), 7.41 – 7.28 (m, 3H), 6.02 (s, 1H), 5.63 (dt, *J* = 10.6, 7.5 Hz, 1H), 5.51 – 5.41 (m, 1H), 4.83 – 4.73 (m, 2H), 2.10 (p, *J* = 7.5 Hz, 2H), 0.95 (t, *J* = 7.5 Hz, 3H); ^{13}C NMR (100 MHz, Chloroform-*d*) δ 168.0, 167.2, 137.8, 134.6, 134.3, 131.9, 129.9, 128.7, 128.6, 123.7, 122.0, 62.0, 56.0, 21.0, 14.1; IR (Neat Film, NaCl 3473, 3025, 2964, 2935, 1772, 1747, 1718, 1649, 1498, 1467, 1458, 1384, 1266, 1214, 1186, 1108, 1088, 1076, 1020, 996, 976, 906, 893, 842, 719, 699 cm^{-1}; (MM:ESI-APCI+) *m/z* calc'd for $C_{21}H_{20}NO_4$ $[M+H]^+$: 350.1392, found 350.1422.

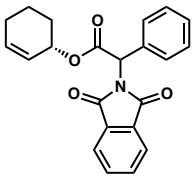

(*S*)-cyclohex-2-en-1-yl 2-(1,3-dioxoisoindolin-2-yl)-2-phenylacetate (110)

Performed on a 3.00 mmol scale and purified by silica gel chromatography (0–30% EtOAc in hexanes) to afford the desired product as an amorphous white solid (953.4 mg, 2.64 mmol, 66% yield, 1:1 dr); ^{1}H NMR (500 MHz, Chloroform-*d*) δ 7.84 (q, *J* = 5.5, 4.6 Hz, 2H), 7.71 (dt, *J* = 5.5, 2.6 Hz, 2H), 7.54 (dd, *J* = 7.8, 2.3 Hz, 2H), 7.38 – 7.29 (m, 3H), 6.01 (s, 0.5H), 6.00 (s, 0.5H), 5.93 (tt, *J* = 13.2, 3.8 Hz, 1H), 5.79 – 5.72 (m, 0.5H), 5.72 – 5.65 (m, 0.5H), 5.49 – 5.38 (m, 1H), 2.06 – 1.83 (m, 3H), 1.81 – 1.70 (m, 1H), 1.58 (dp, *J* = 13.1, 6.6 Hz, 2H); ^{13}C NMR (100 MHz, Chloroform-*d*) δ 167.7, 167.7, 167.2, 134.7, 134.3, 134.3, 133.4, 133.2, 131.9, 129.9, 129.8, 128.6, 128.5, 125.1, 125.1, 123.6, 70.4, 70.4, 56.2, 56.1, 28.2, 28.1, 24.9, 24.8, 18.8, 18.7; IR (Neat Film, NaCl) 3472, 3034, 2935, 2866, 2831, 1773, 1741, 1734, 1718, 1650, 1612, 1550, 1497, 1467, 1455, 1426, 1385, 1360, 1337, 1231, 1214, 1187, 1161, 1112, 1089, 1076, 1051, 1018, 1006, 961, 909, 855, 844, 834, 816, 785, 778, 760, 767, 719, 699, 682, 661 cm^{-1}; (MM:FAB+) *m/z* calc'd for $C_{22}H_{20}NO_4$ $[M+H]^+$: 362.1392, found 362.1408.

4.9.3.6 Investigation of Enolization Selectivity

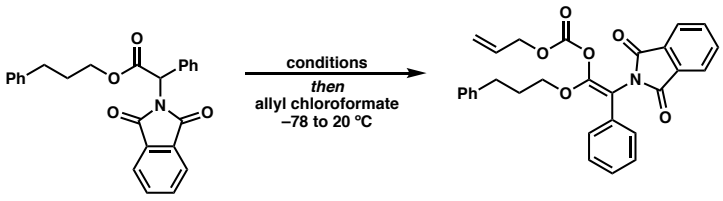

77

enol carbonates A and B geometries not assigned

entry	enolization conditions	% yield isomer A	% yield isomer B
1	LiHMDS (2.0 equiv), Me_2NEt (2.0 equiv), PhMe (0.10 M), – 78 °C, 2 h	16	23
2	LiHMDS (2.0 equiv), PhMe (0.10 M), – 78 °C, 2 h	43	27
3	KHMDS (2.0 equiv), PhMe (0.10 M), – 78 °C, 2 h	55	24

In a nitrogen-filled glovebox, an oven-dried 50 mL round bottom flask was charged with LiHMDS (335.0 mg, 2.00 mmol, 2.0 equiv) *or* KHMDS (399.0 mg, 2.00 mmol, 2.0 equiv) and a Teflon-coated stir bar. The flask was then sealed with a septum, removed from the glovebox, and placed under an atmosphere of nitrogen. To the flask was then added toluene (3.0 mL) and for entry 1, *N*,*N*-dimethylethylamine (213 μL, 2.00 mmol, 2.0 equiv). The resulting solution was stirred at 20 °C for 5 min, then the flask was immersed in a –78 °C dry ice/acetone bath. After stirring for 15 min, a solution of the α-phthalidomido ester **16** (1.00 mmol, 1.0 equiv) dissolved in toluene (7.0 mL) was added dropwise over 5 min, resulting in the immediate formation of a dark red/purple opaque reaction mixture. The reaction was maintained at –78 °C for 2 h, after which time allyl chloroformate (217 μL, 2.00 mmol, 2.0 equiv) was added dropwise over 1 min. The reaction flask was then removed from the cooling bath and allowed to warm to 20 °C. After 30 min, the reaction was quenched with 1 N HCl (10 mL) and transferred to a separatory funnel with Et_2O (10 mL). The layers were separated and the aqueous layer was extracted with Et_2O (2 x 10 mL). The combined organic layers were dried over

Na_2SO_4, filtered, and concentrated by rotary evaporation to afford the crude allyl enol carbonates. Due to substantial NMR overlap of enol carbonates A and B, the crude reaction mixtures were purified directly by silica gel chromatography (0–30% EtOAc in hexanes). Enol carbonate olefin geometries were not assigned unambiguously, therefore the higher R_f enol carbonate by TLC analysis (30% EtOAc) is designated enol carbonate A and the lower R_f enol carbonate by TLC analysis (30% EtOAc) is designated enol carbonate B.

Entry 1: 76.6 mg, 0.158 mmol, 16% yield of enol carbonate A; 112.2 mg, 0.232 mmol, 23% yield enol carbonate B

Entry 2: 209.3 mg, 0.433 mmol, 43% yield of enol carbonate A; 131.7 mg, 0.272 mmol, 27% yield enol carbonate B

Entry 3: 266.4 mg, 0.551 mmol, 55% yield of enol carbonate A; 116.3 mg, 0.241 mmol, 24% yield enol carbonate B

Enol carbonate A: colorless, viscous oil; ^{1}H NMR (400 MHz, Chloroform-*d*) δ 7.76 (dd, *J* = 5.5, 3.1 Hz, 2H), 7.61 (dd, *J* = 5.5, 3.1 Hz, 2H), 7.29 – 7.24 (m, 2H), 7.20 – 7.13 (m, 2H), 7.13 – 7.03 (m, 3H), 7.03 – 6.97 (m, 1H), 6.93 – 6.86 (m, 2H), 5.68 (ddt, *J* = 17.1, 10.5, 5.8 Hz, 1H), 5.17 (dq, *J* = 17.2, 1.3 Hz, 1H), 5.11 (dq, *J* = 10.5, 1.1 Hz, 1H), 4.49 (dt, *J* = 5.7, 1.2 Hz, 2H), 3.88 (t, *J* = 6.3 Hz, 2H), 2.41 (dd, *J* = 8.5, 7.0 Hz, 2H), 1.81 – 1.68 (m, 2H); ^{13}C NMR (100 MHz, Chloroform-*d*) δ 167.2, 150.8, 141.1, 134.3, 133.1, 132.2, 130.5, 128.6, 128.4, 127.9, 127.6, 126.0, 123.8, 119.9, 103.4, 69.9, 69.8, 31.8, 30.9; IR (Neat Film, NaCl) 3069, 3026, 2955, 1777, 1725, 1680, 1604, 1496, 1468, 1446, 1420, 1383, 1264, 1201, 1173, 1113, 1088, 1071, 1020, 975, 941, 913, 883, 766, 753, 721, 699 cm^{-1}; (MM:FAB+) *m/z* calc'd for $C_{29}H_{26}NO_6$ $[M+H]^+$: 484.1760, found 484.1739.

Enol carbonate B: colorless, viscous oil; ^{1}H NMR (400 MHz, Chloroform-*d*) δ 7.78 – 7.71 (m, 2H), 7.64 – 7.56 (m, 2H), 7.39 – 7.31 (m, 2H), 7.20 – 7.12 (m, 2H), 7.12 – 7.06 (m, 3H), 7.05 – 7.00 (m, 1H), 6.98 – 6.94 (m, 2H), 5.62 (ddt, *J* = 17.1, 10.4, 5.8 Hz, 1H), 5.09 (dq, *J* = 17.2, 1.4 Hz, 1H), 4.99 (dq, *J* = 10.5, 1.1 Hz, 1H), 4.45 (dt, *J* = 5.8, 1.3 Hz, 2H), 3.92 (t, *J* = 6.3 Hz, 2H), 2.50 (dd, *J* = 8.3, 7.0 Hz, 2H), 1.92 – 1.80 (m, 2H); ^{13}C NMR (100 MHz, Chloroform-*d*) δ 166.9, 151.3, 150.8, 141.1, 134.4, 132.7, 132.1, 130.6, 128.6, 128.5, 128.5, 127.9, 127.5, 126.1, 123.9, 119.8, 103.5, 71.2, 69.8, 31.9, 30.9; IR (Neat Film, NaCl) 3059, 3026, 2955, 1777, 1725, 1672, 1604, 1496, 1468, 1445, 1424, 1385, 1300, 1250, 1203, 1165, 1110, 1088, 1071, 996, 948, 882, 760, 748, 721, 700 cm^{-1}; (MM:FAB+) *m/z* calc'd for $C_{29}H_{26}NO_6$ $[M+H]^+$: 484.1760, found 484.1740.

4.9.4 DETERMINATION OF ENANTIOMERIC EXCESS

Table 4.9.4.1 *Determination of Enantiomeric Excess*

entry	compound	assay conditions	t_R of major isomer (min)	t_R of minor isomer (min)	% ee
1	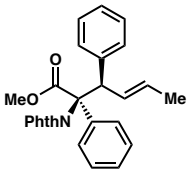 ***83***	10% *i*-PrOH, 2.5 mL/min Chiralpak IC column λ = 210 nm	5.79	7.70	95
2	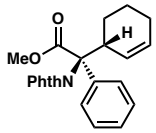 ***108***	10% *i*-PrOH, 2.5 mL/min Chiralpak IC column λ = 210 nm	5.79	7.70	>99

4.10 REFERENCES AND NOTES

(1) (a) Ireland, R. E.; Mueller, R. H. The Claisen Rearrangement of Allyl Esters. *J. Am. Chem. Soc.* **1972**, *94*, 5897–5898. (b) Ireland, R. E.; Mueller, R. H.; Willard, A. K. *J. Am. Chem. Soc.* **1976**, *98*, 2868–2877.

(2) For a recent review see: Pierrot, D.; Marek, I. Synthesis of Enantioenriched Vicinal Tertiary and Quaternary Carbon Stereogenic Centers within an Acyclic Chain. *Angew. Chem. Int. Ed.* **2020**, *59*, 36–49.

(3) For a review see: O'Brien, P. Recent Advances in Asymmetric Synthesis using Chiral Lithium Amide Bases. *J. Chem. Soc. Perkin Trans. 1.* **1998**, 1439–1457.

(4) (a) Qin, Y.-C.; Stivala, C. E.; Zakarian, A. Acyclic Stereocontrol in the Ireland–Claisen Rearrangement of α-Branched Esters *Angew. Chem. Int. Ed.* **2007**, *46*, 7466–7469. (b) Stivala, C. E.; Zakarian, A. Total Synthesis of (+)-Pinnatoxin A. *J. Am. Chem. Soc.* **2008**, *130*, 3774–3776. (c) Stivala, C. E.; Zakarian, A. Studies Toward the Synthesis of Spirolides: Assembly of the Elaborated E-Ring Fragment.

Org. Lett. **2009**, *11*, 839–842. (d) Gu, Z.; Hermann, A. T.; Stivala, C. E.; Zakarian, A. Stereoselective Construction of Adjacent Quaternary Chiral Centers by the Ireland-Claisen Rearrangement: Stereoselection with Esters of Cyclic Alcohols. *Synlett* **2010**, *11*, 1717–1722. (e) Araoz, R.; Servent, D.; Molgó, J.; Iorga, B. I.; Fruchart–Gaillard, C.; Benoit, E.; Gu, Z.; Stivala, C.; Zakarian, A. Total Synthesis of Pinnatoxins A and G and Revision of the Mode of Action of Pinnatoxin A. *J. Am. Chem. Soc.* **2011**, *133*, 10499–10511.

(5) (a) Crimmins, M. T.; Knight, J. D.; Williams, P. S.; Zhang, Y. Stereoselective Synthesis of Quaternary Carbons via the Dianionic Ireland–Claisen Rearrangement. *Org. Lett.* **2014**, *16*, 2458–2461. (b) Crimmins, M. T.; Zhang, Y.; Williams, P. S. Approach to the Synthesis of Briarane Diterpenes through a Dianionic Claisen Rearrangement and Ring-Closing Metathesis. *Org. Lett.* **2017**, *19*, 3907–3910.

(6) Podunavac, M.; Lacharity, J. J.; Jones, K. E.; Zakarian, A. Stereodivergence in the Ireland–Claisen Rearrangement of α-Alkoxy Esters. *Org. Lett.* **2018**, *20*, 4867–4870.

(7) (a) Moore, J. T.; Hanhan, N. V.; Mahoney, M. E.; Cramer, S. P.; Shaw, J. T. Enantioselective Synthesis of Isotopically Labeled Homocitric Acid Lactone. *Org. Lett.* **2013**, *15*, 5615–5617. (b) Whitesell, J. K.; Helbling, A. M. Preparation of β,γ-Unsaturated Methyl Esters from Allylic Alcohols. *J. Org. Chem.* **1980**. *45*, 4135–4139. (c) Sato, T.; Tajima, K.; Fujisawa, T. Diastereoselective Synthesis of Erythro- and Threo-2-hydroxy-3-methyl-4-pentenoic Acids by the Ester Enolate

Claisen Rearrangement of 2-Butenyl 2-Hydroxyacetate. *Tetrahedron Lett*. **1983**, *24*, 729–730. (d) Bartlett, P. A.; Tanzella, D. J.; Barstow, J. F. J. Ester-enolate Claisen Rearrangement of Lactic Acid Derivatives. *J. Org. Chem*. **1982**, *47*, 3941–3945. (e) Burke, S. D.; Fobare, W. F.; Pacofsky, G. J. J. Chelation Control of Enolate Geometry. Acyclic Diasteroselection via the Enolate Claisen Rearrangement. *J. Org. Chem*. **1983**, *48*, 5221–5228.

(8) Picoul, W.; Urchegui, R.; Haudrechy, A.; Langlois, Y. A Novel Stereoselective Route to a Fumagillin and Ovalicin Synthetic Intermediate. *Tetrahedron Lett*. **1999**, *40*, 4797−4800.

(9) (a) Neese, F. Software Update: The ORCA Program System, Version 4.0. *Wiley Interdisciplinary Reviews: Computational Molecular Science* **2018**, *8*, e1327. (b) Neese, F. The ORCA Program System. *Wiley Interdisciplinary Reviews: Computational Molecular Science* **2012**, *2*, 73–78.

(10) (a) Gül, Ş.; Schoenebeck, F.; Aviyente, V.; Houk, K. N. Computational Study of Factors Controlling the Boat and Chair Transition States of Ireland−Claisen Rearrangements. *J. Org. Chem.* **2010**, *75* (6), 2115–2118. (b) Khaledy, M. M.; Kalani, M. Y. S.; Khuong, K. S.; Houk, K. N.; Aviyente, V.; Neier, R.; Soldermann, N.; Velker, J. Origins of Boat or Chair Preferences in the Ireland−Claisen Rearrangements of Cyclohexenyl Esters: A Theoretical Study. *J. Org. Chem.* **2003**, *68* (2), 572–577.

(11) Tellam, J. P.; Kociok-Köhn, G.; Carbery, D. R. An Ireland−Claisen Approach to β-Alkoxy α-Amino Acids. *Org. Lett.* **2008**, *10* (22), 5199–5202.

(12) Experimentally, this reaction did not provide the desired product (see Supporting Information for details):

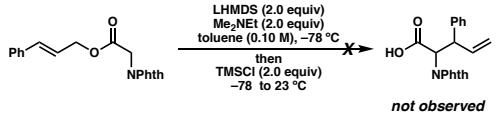

(13) Experimentally, a 2.7:1 dr is obtained (see Supporting Information for details):

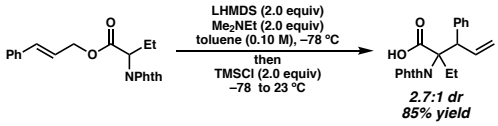

(14) Mack, K. A.; McClory, A.; Zhang, H.; Gosselin, F.; Collum, D. B. Lithium Hexamethyldisilazide-Mediated Enolization of Highly Substituted Aryl Ketones: Structural and Mechanistic Basis of the E/Z Selectivities. *J. Am. Chem. Soc.* **2017**, *139*, 12182−12189. (b) Li, B. X.; Le, D. N.; Mack, K. A.; McClory, A.; Lim, N. K.; Cravillion, T.; Savage, S.; Han, C.; Collum, D. B.; Zhang, H.; Gosselin, F. Highly Stereoselective Synthesis of Tetrasubstituted Acyclic All-Carbon Olefins via Enol Tosylation and Suzuki–Miyaura Coupling. *J. Am. Chem. Soc.* **2017**, *139*, 10777−10783.

(15) Alexy, E. J.; Fulton, T. J.; Zhang, H.; Stoltz, B. M. Palladium-catalyzed Enantioselective Decarboxylative Allylic Alkylation of Fully Substituted *N*-acyl Indole-Derived Enol Carbonates. *Chem. Sci.* **2019**, *10*, 5996−6000.

(16) Similar products in the opposite diasteromeric series have been prepared previously by iridium/phase transfer catalysis: Su, Y.-L.; Li, Y.-H.; Chen, Y.-G.; Han, Z.-Y. Ir/PTC Cooperatively Catalyzed Asymmetric Umpolung Allylation of α-imino

Ester Enabled Synthesis of α-quaternary Amino Acid Derivatives Bearing Two Vicinal Stereocenters. *Chem*. *Commun*. **2017**, *53*, 1985–1988.

(17) Experimentally, a 2.9:1 dr is obtained (see Supporting Information for details):

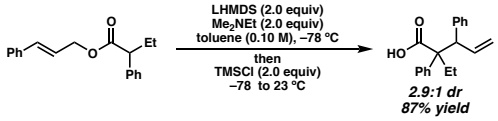

(18) For relevant reviews on the Ireland−Claisen rearrangement, see: (a) Chai, Y.; Hong, S.-P.; Lindsay, H. A.; McFarland, C.; McIntosh, M. C. New aspects of the Ireland and related Claisen rearrangements. Tetrahedron **2002**, *58*, 2905−2928. (b) McFarland, C. M.; McIntosh, M. C. The Ireland−Claisen Rearrangement (1972−2004). In The Claisen Rearrangement: Methods and Applications; Hiersemann, M., Nubbemeyer, U., Eds.; Wiley-VCH: Weinheim, **2007**; pp 117−210. (c) Ilardi, E. A.; Stivala, C. E.; Zakarian, A. [3,3]-Sigmatropic rearrangements: recent applications in the total synthesis of natural products. *Chem*. *Soc*. *Rev*. **2009**, *38*, 3133−3148.

(19) Osby, J. O.; Martin, M. G.; Ganem, B. An Exceptionally Mild Deprotection of Phthalimides. *Tetrahedron Lett*. **1984**, *25*, 2093–2096.

(20) Alford, J. S.; Davies, H. M. L. Expanding the Scope of Donor/Acceptor Carbenes to *N*-Phthalimido Donor Groups: Diastereoselective Synthesis of 1-Cyclopropane α-Amino Acids. *Org*. *Lett*. **2012**, *14*, 6020–6023.

(21) (a) Neese, F. The ORCA Program System. *Wiley Interdisciplinary Reviews: Computational Molecular Science* **2012**, *2*, 73–78. (b) Neese, F. Software Update:

The ORCA Program System, Version 4.0. *Wiley Interdisciplinary Reviews: Computational Molecular Science* **2018**, *8*, e1327.

(22) Neese, F.; Wennmohs, F.; Hansen, A.; Becker, U. Efficient, Approximate and Parallel Hartree–Fock and Hybrid DFT Calculations. A 'Chain-of-Spheres' Algorithm for the Hartree-Fock Exchange. *Chemical Physics* **2009**, *356*, 98–109.

(23) Stoychev, G. L.; Auer, A. A.; Neese, F. Automatic Generation of Auxiliary Basis Sets. *J. Chem. Theory Comput.* **2017**, *13*, 554–562.

(24) Stephens, P. J.; Devlin, F. J.; Chabalowski, C. F.; Frisch, M. J. Ab Initio Calculation of Vibrational Absorption and Circular Dichroism Spectra Using Density Functional Force Fields. *J. Phys. Chem.* **1994**, *98*, 11623–11627.

(25) (a) Grimme, S.; Antony, J.; Ehrlich, S.; Krieg, H. A consistent and accurate *ab initio* parametrization of density functional dispersion correction (DFT-D) for the 94 elements H-Pu *J. Chem. Phys.* **2010**, *132*, 154104. (b) Grimme, S.; Ehrlich, S.; Goerigk, L. *J. Comput. Chem.* **2011**, *32*, 1456–1465. (c) Becke, A. D.; Johnson, E. R. A density-functional model of the dispersion interaction. *J. Chem. Phys.* **2005**, *122*, 154101. (d) Johnson, E. R.; Becke, A. D. A post-Hartree–Fock model of intermolecular interactions. *J. Chem. Phys.* **2005**, *123*, 024101. (e) Johnson, E. R.; Becke, A. D. A post-Hartree-Fock model of intermolecular interactions: Inclusion of higher-order corrections. *J. Chem. Phys.* **2006**, *124*, 174104.

(26) Grimme, S. Supramolecular Binding Thermodynamics by Dispersion-Corrected Density Functional Theory. *Chemistry — A European Journal* **2012**, *18*, 9955–9964.

(27) Zhao, Y.; Truhlar, D. G. The M06 Suite of Density Functionals for Main Group Thermochemistry, Thermochemical Kinetics, Noncovalent Interactions, Excited States, and Transition Elements: Two New Functionals and Systematic Testing of Four M06-Class Functionals and 12 Other Functionals. *Theor Chem Account* **2008**, *120*, 215–241.

(28) Weigend, F.; Ahlrichs, R. Balanced Basis Sets of Split Valence, Triple Zeta Valence and Quadruple Zeta Valence Quality for H to Rn: Design and Assessment of Accuracy. *Phys. Chem. Chem. Phys.* **2005**, *7*, 3297–3305.

(29) Marenich, A. V.; Cramer, C. J.; Truhlar, D. G. Universal Solvation Model Based on Solute Electron Density and on a Continuum Model of the Solvent Defined by the Bulk Dielectric Constant and Atomic Surface Tensions. *J. Phys. Chem. B* **2009**, *113*, 6378–6396.

(30) (a) Riplinger, C.; Neese, F. An Efficient and near Linear Scaling Pair Natural Orbital Based Local Coupled Cluster Method. *J. Chem. Phys.* **2013**, *138*, 034106. (b) Riplinger, C.; Sandhoefer, B.; Hansen, A.; Neese, F. Natural Triple Excitations in Local Coupled Cluster Calculations with Pair Natural Orbitals. *J. Chem. Phys.* **2013**, *139*, 134101. (c) Riplinger, C.; Pinski, P.; Becker, U.; Valeev, E. F.; Neese, F. Sparse Maps—A Systematic Infrastructure for Reduced-Scaling Electronic Structure Methods. II. Linear Scaling Domain Based Pair Natural Orbital Coupled Cluster Theory. *J. Chem. Phys.* **2016**, *144*, 024109.

(31) Dunning, T. H. Gaussian Basis Sets for Use in Correlated Molecular Calculations. I. The Atoms Boron through Neon and Hydrogen. *J. Chem. Phys.* **1989**, *90*, 1007–1023.

(32) For def2/J, see: (a) Weigend, F. Accurate Coulomb-Fitting Basis Sets for H to Rn. *Phys. Chem. Chem. Phys.* **2006**, *8*, 1057–1065. For cc-pVTZ/C, see: (b) Weigend, F.; Köhn, A.; Hättig, C. Efficient Use of the Correlation Consistent Basis Sets in Resolution of the Identity MP2 Calculations. *J. Chem. Phys.* **2002**, *116*, 3175–3183.

(33) Pangborn, A. M.; Giardello, M. A.; Grubbs, R. H.; Rosen, R. K.; Timmers, F. J. Safe and Convenient Procedure for Solvent Purification. *Organometallics* **1996**, *15*, 1518–1520.

(34) Petasis, N. A.; Goodman, A.; Zavialov, I. A. A new synthesis of α-arylglycines from aryl boronic acids. *Tetrahedron* **1997**, *53*, 16463–16470.

APPENDIX 6

Spectra Relevant to Chapter 4:

Global Diastereoconvergence in the Ireland–Claisen Rearrangement of Isomeric Enolates: Synthesis of Tetrasubstituted α-Amino Acids

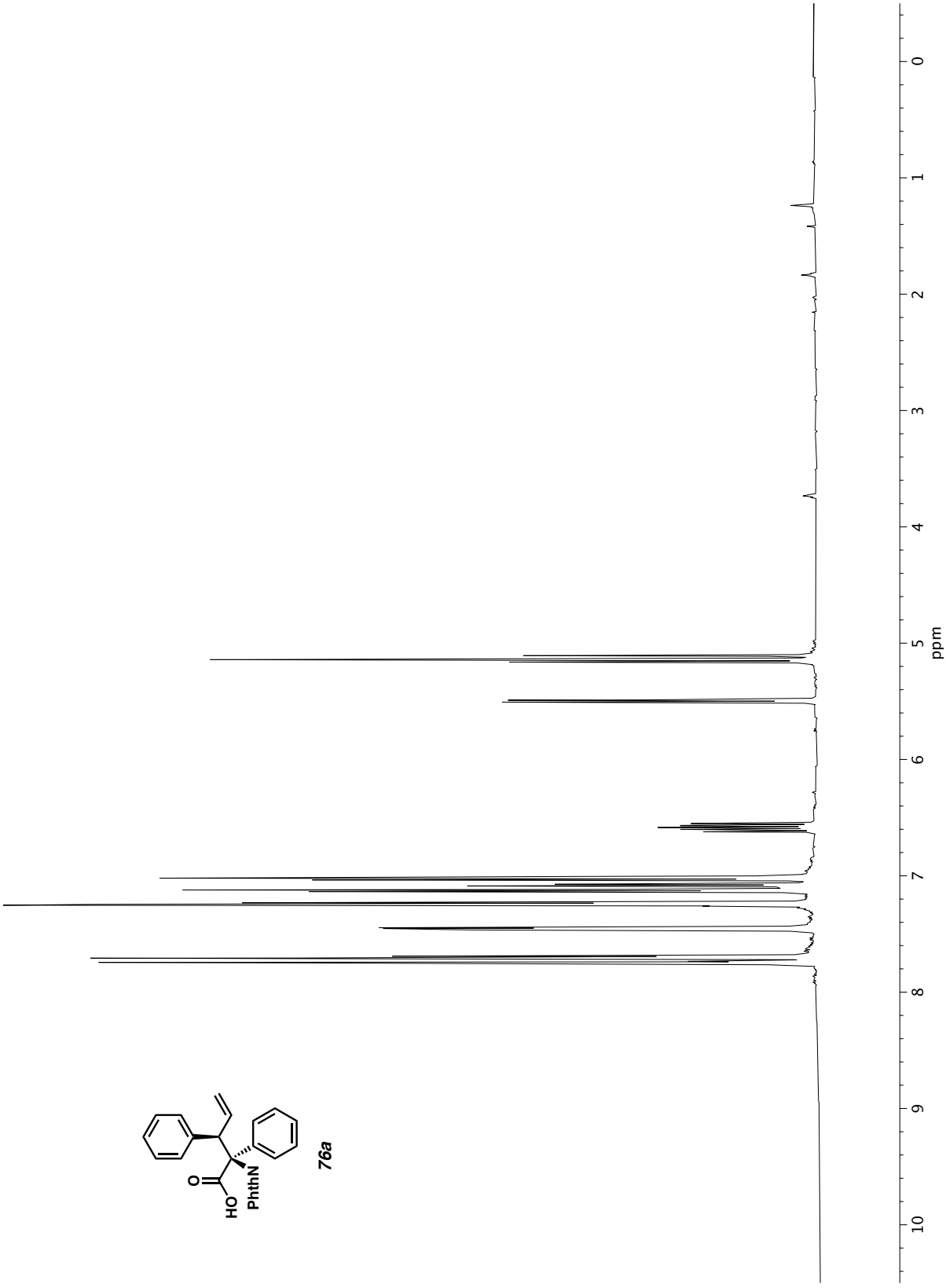

Figure A6.1 *^1H NMR (500 MHz, $CDCl_3$) of compound* ***76a****.*

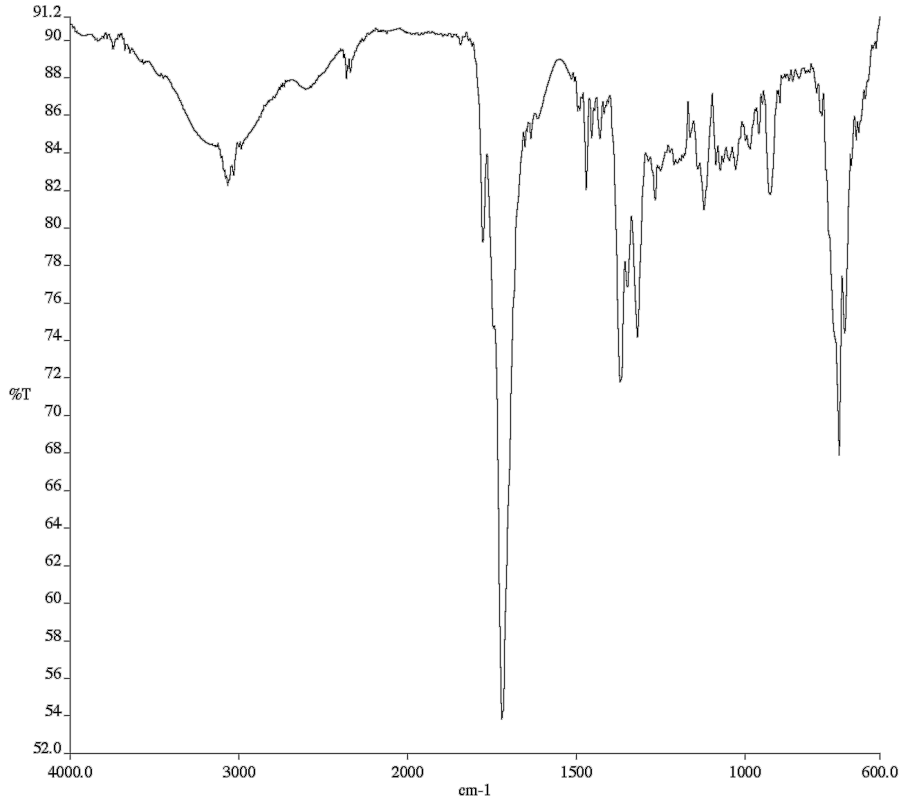

Figure A6.2 *Infrared spectrum (Thin Film, NaCl) of compound* ***76a***

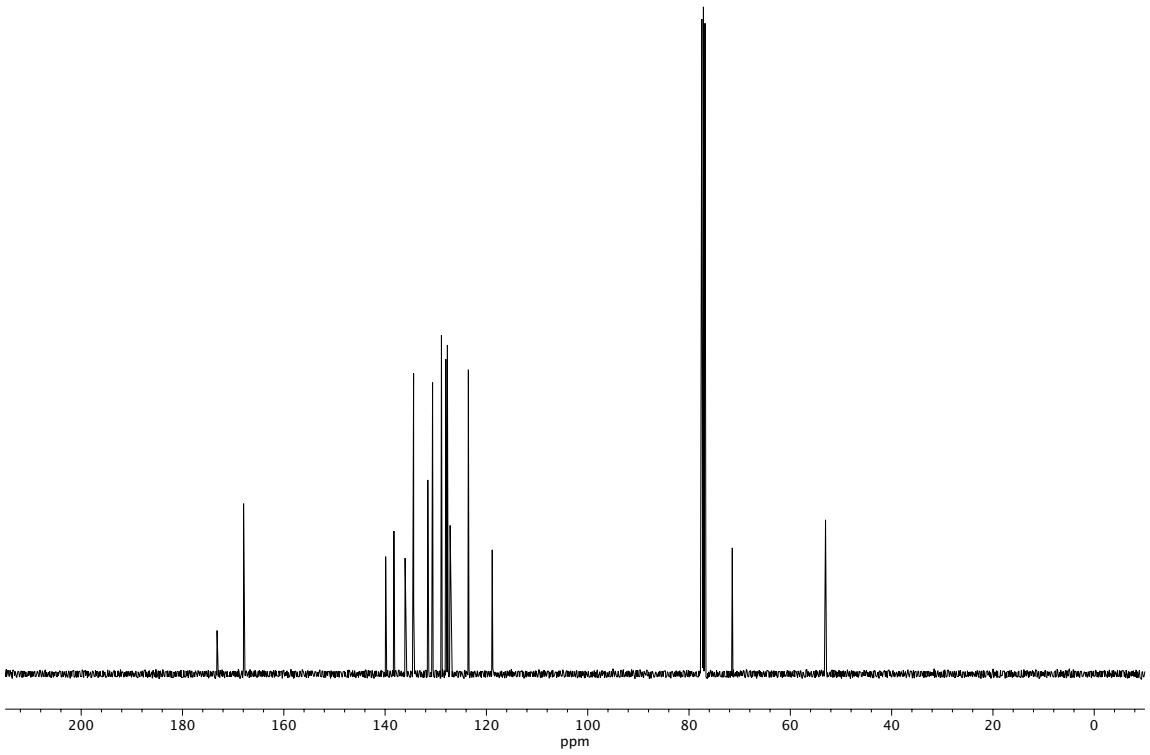

Figure A6.3 *^{13}C NMR (100 MHz, $CDCl_3$) of compound* ***76a****.*

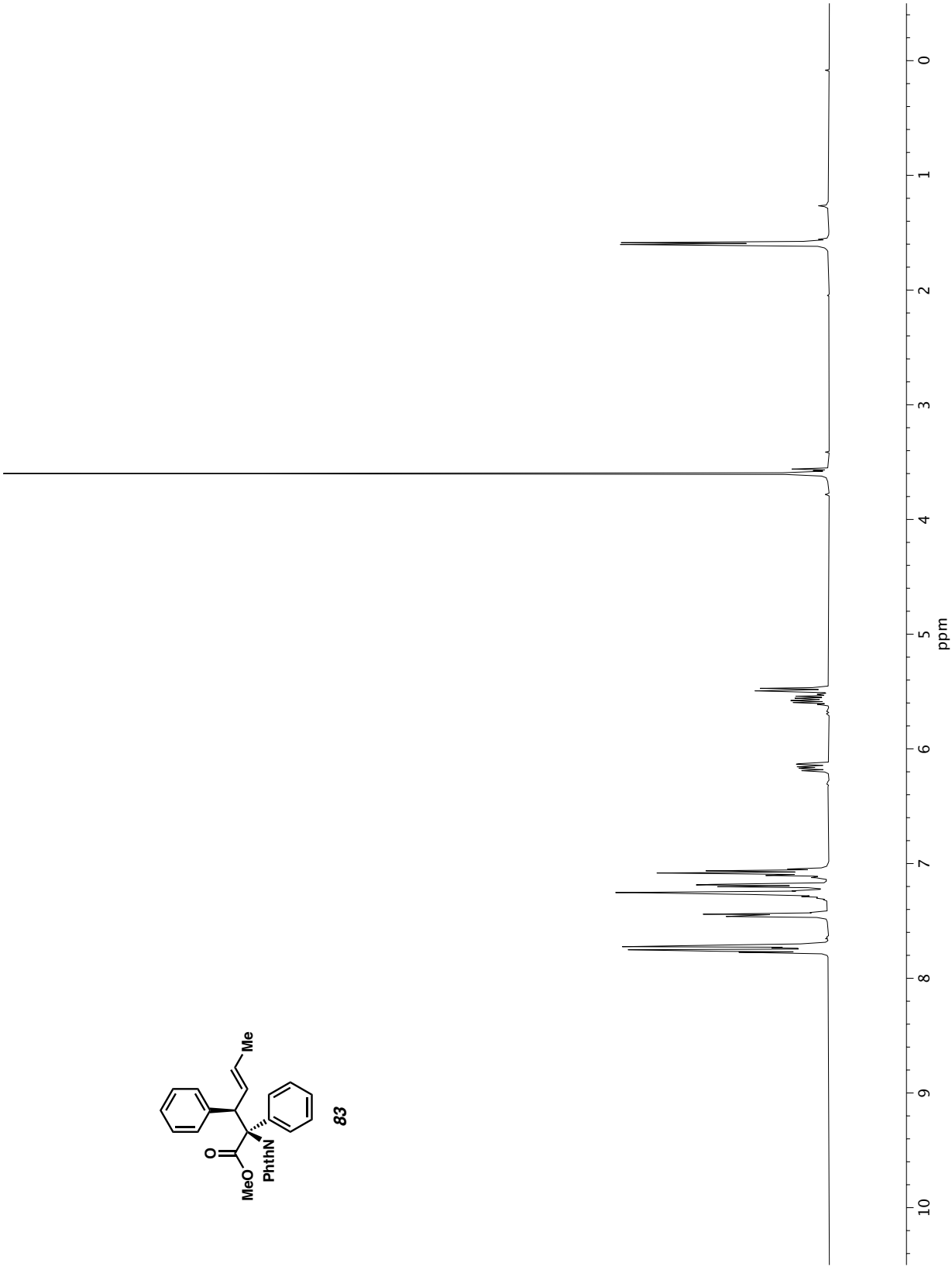

Figure A6.4 *^1H NMR (500 MHz, $CDCl_3$) of compound **83**.*

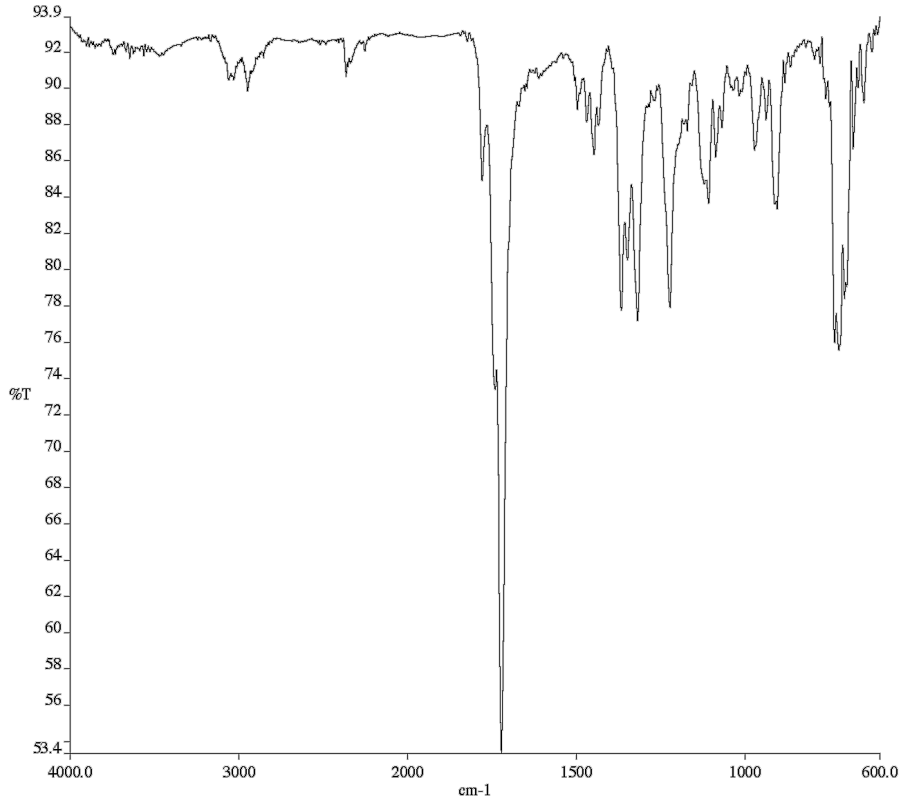

Figure A6.5 *Infrared spectrum (Thin Film, NaCl) of compound* ***83****.*

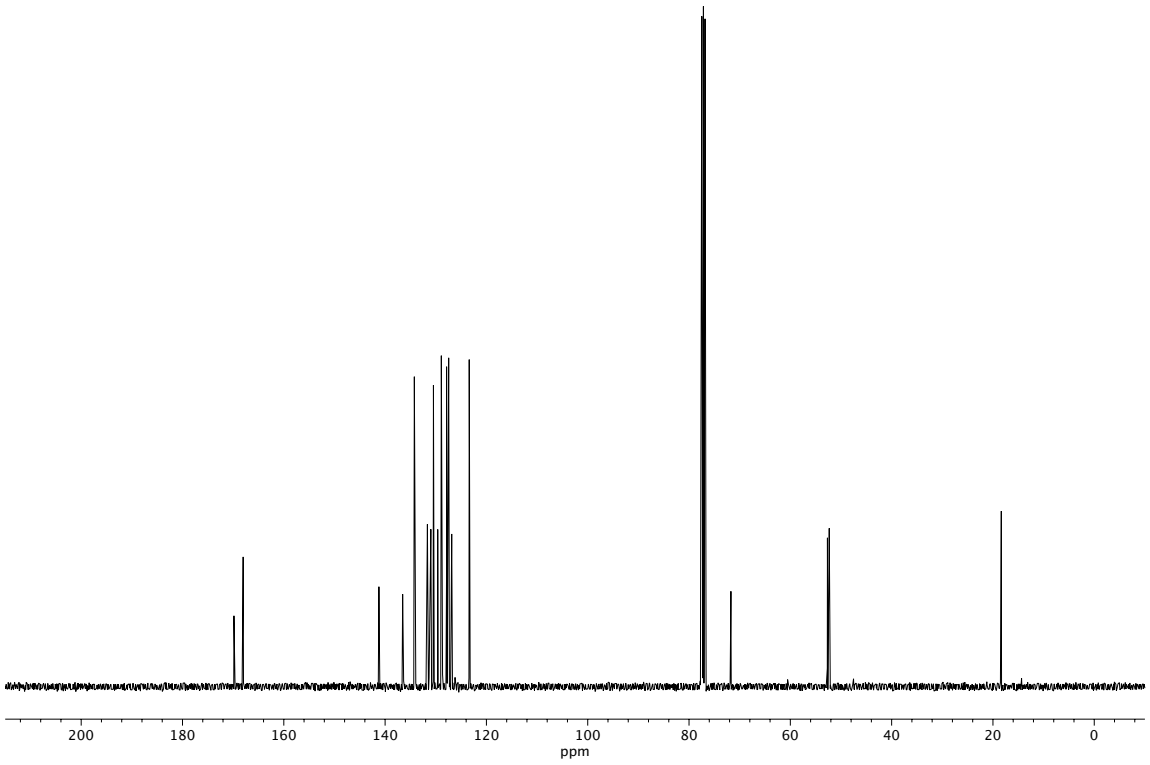

Figure A6.6 *^{13}C NMR (100 MHz, $CDCl_3$) of compound* ***83****.*

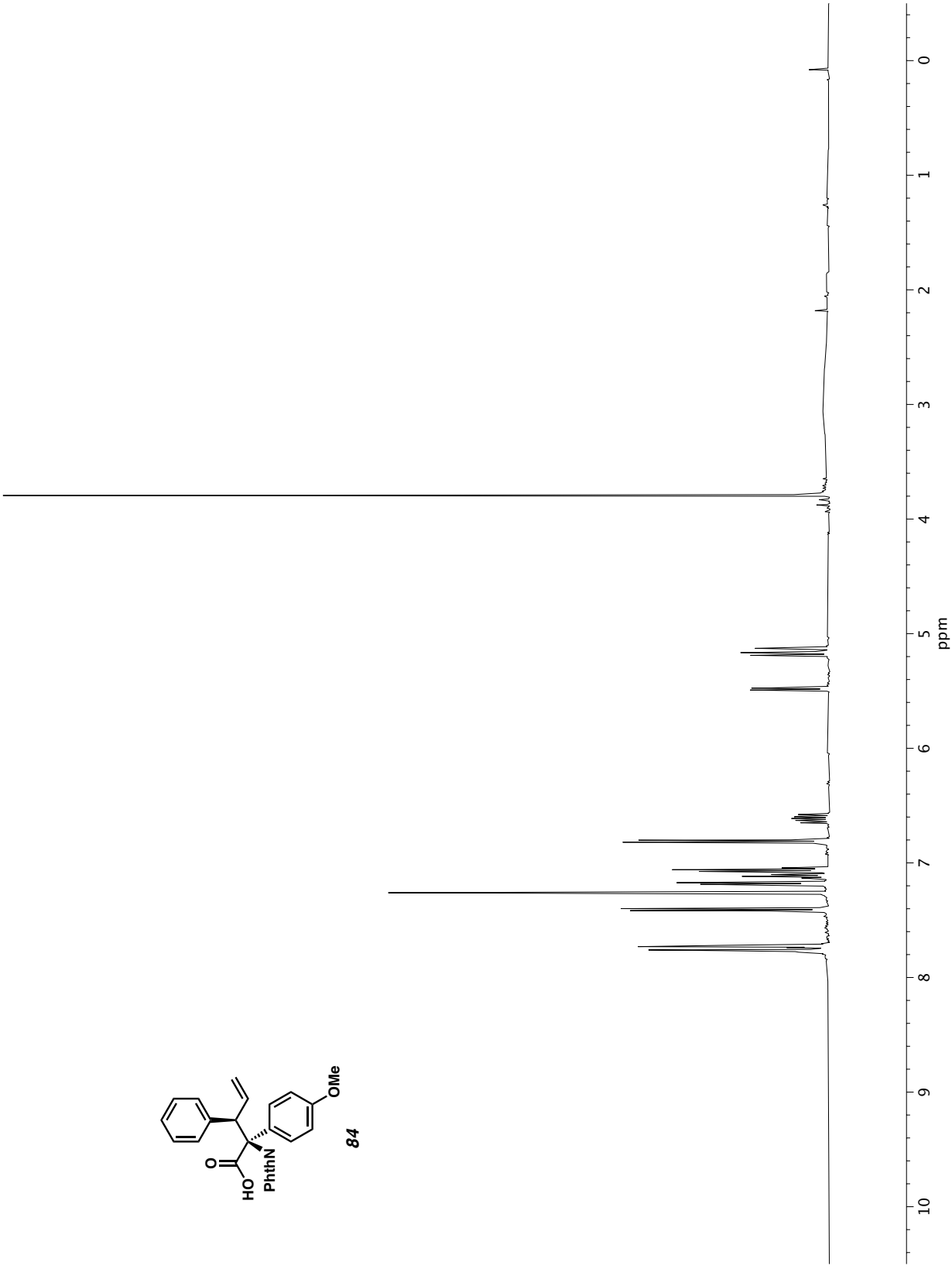

Figure A6.7 *^1H NMR (500 MHz, $CDCl_3$) of compound **84**.*

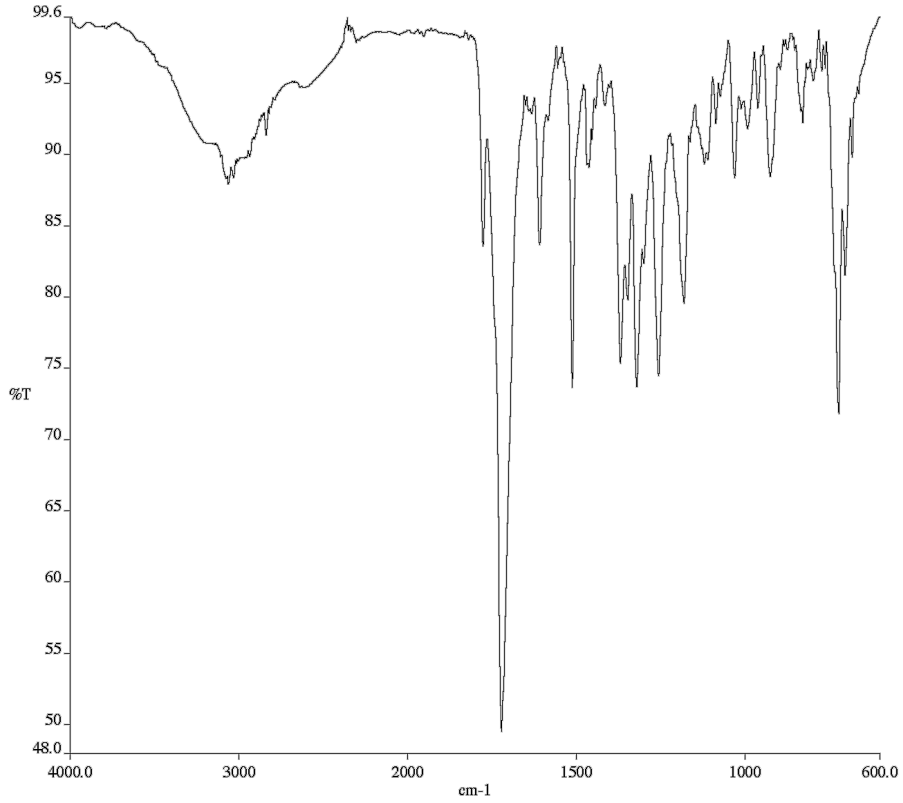

Figure A6.8 *Infrared spectrum (Thin Film, NaCl) of compound* ***84****.*

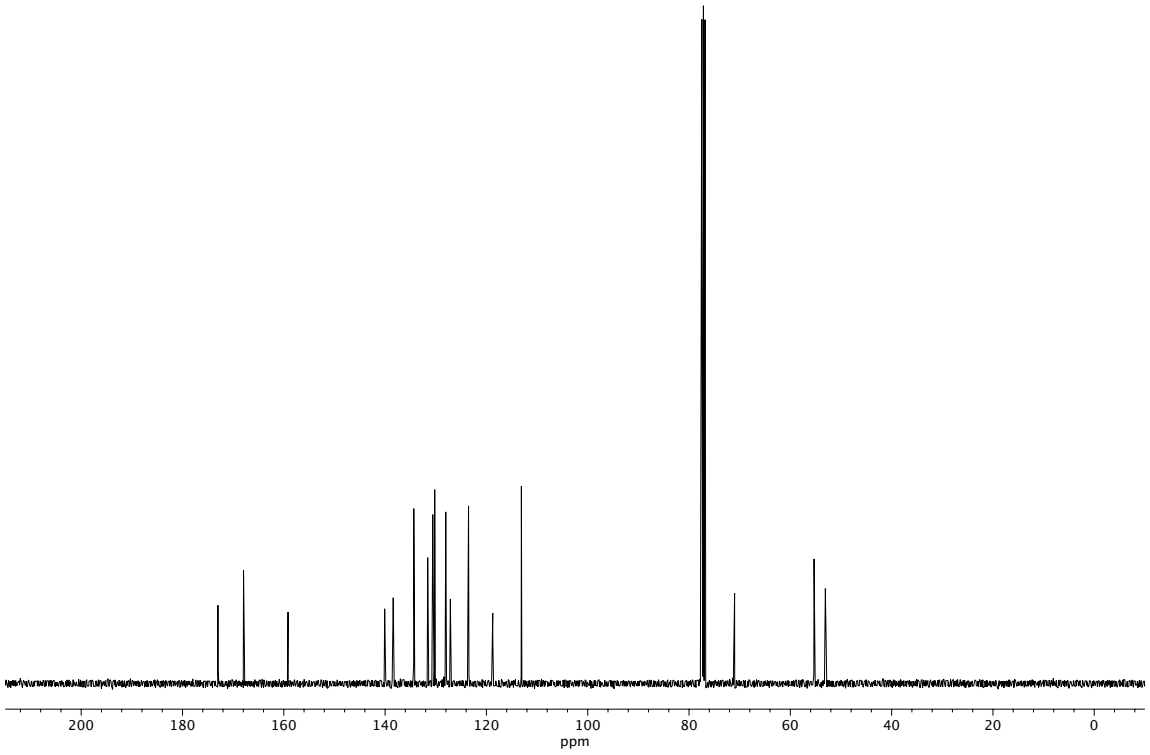

Figure A6.9 *^{13}C NMR (100 MHz, $CDCl_3$) of compound* ***84****.*

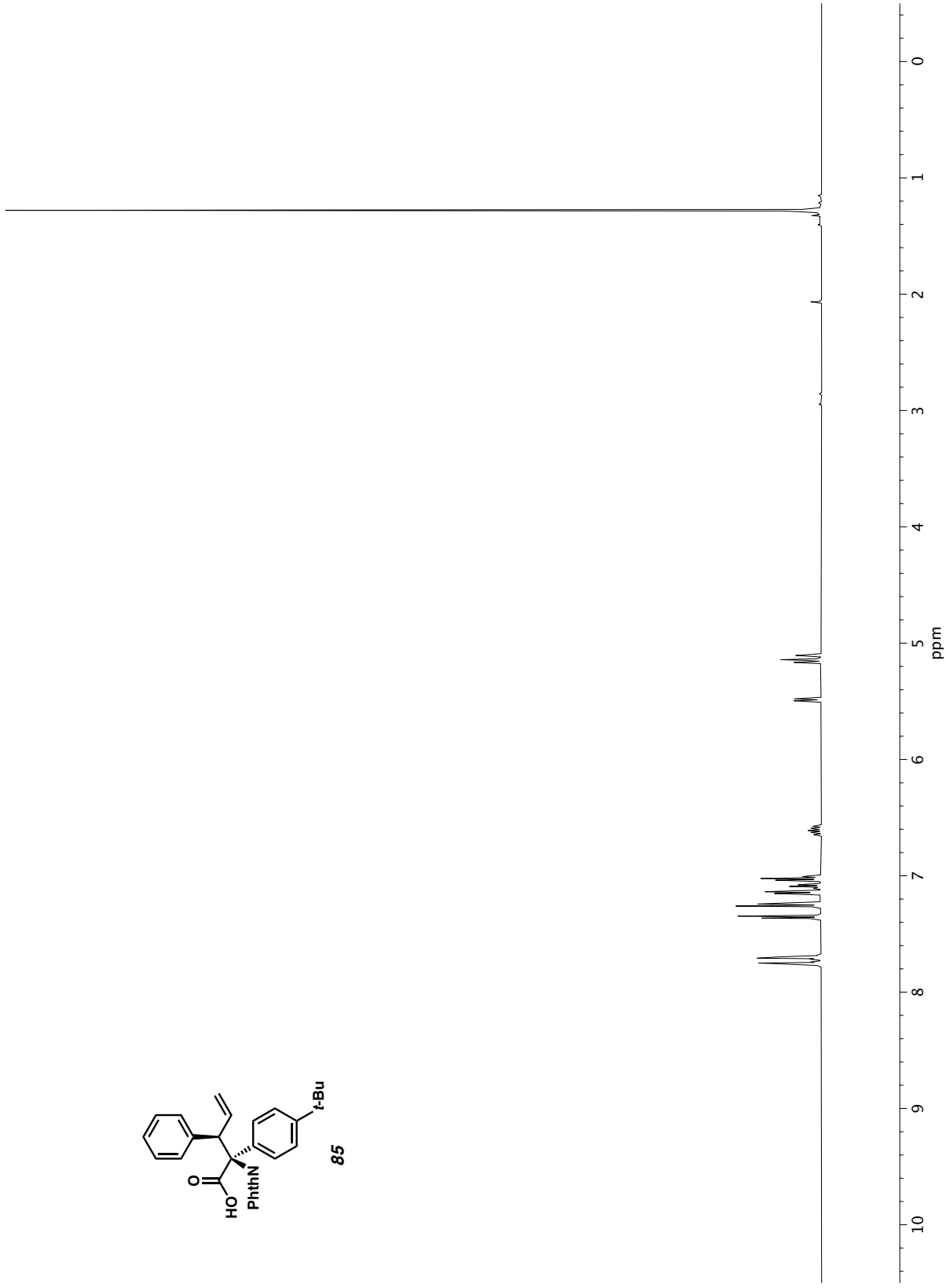

Figure A6.10 *^{1}H NMR (500 MHz, $CDCl_3$) of compound **85**.*

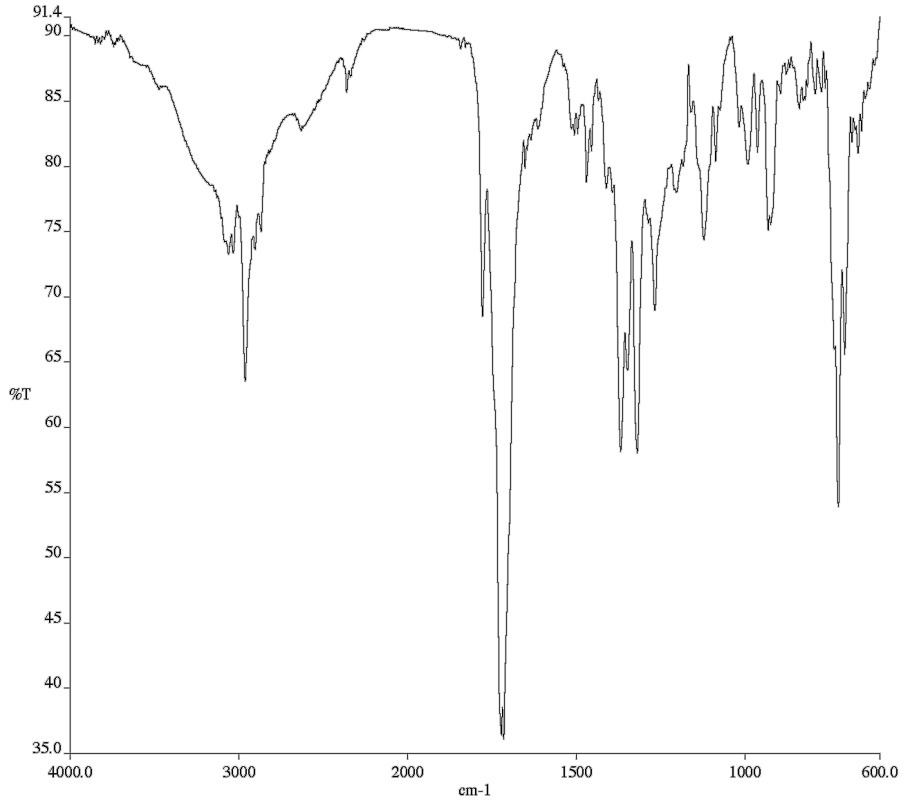

Figure A6.11 *Infrared spectrum (Thin Film, NaCl) of compound* ***85****.*

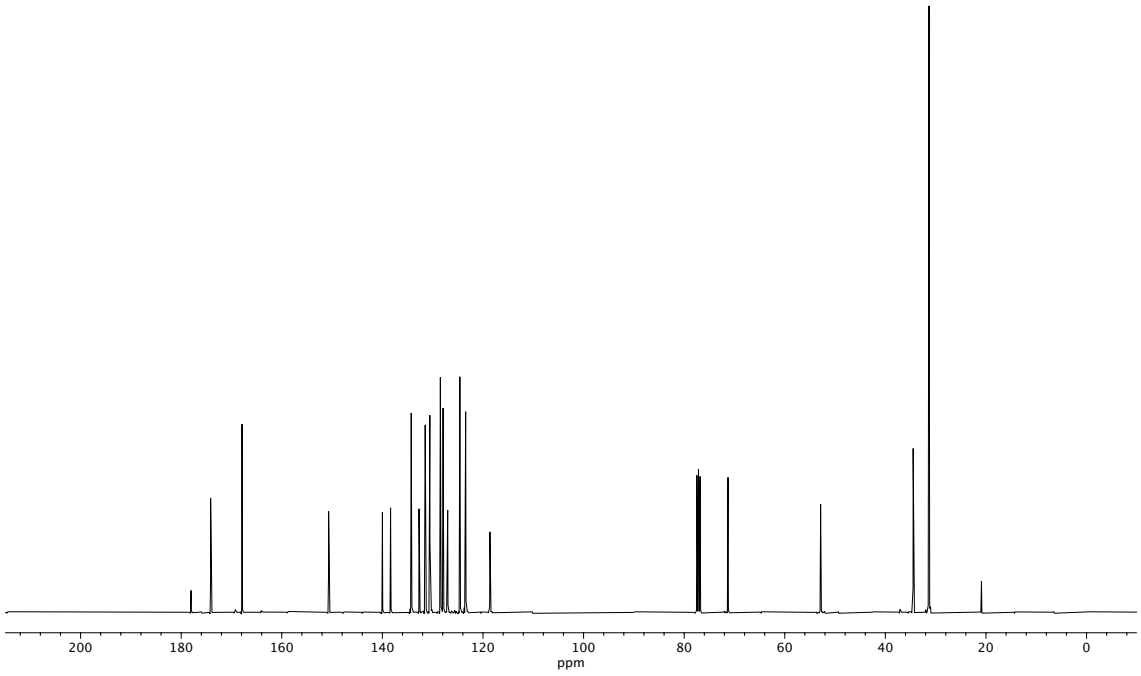

Figure A6.12 *^{13}C NMR (100 MHz, $CDCl_3$) of compound* ***85****.*

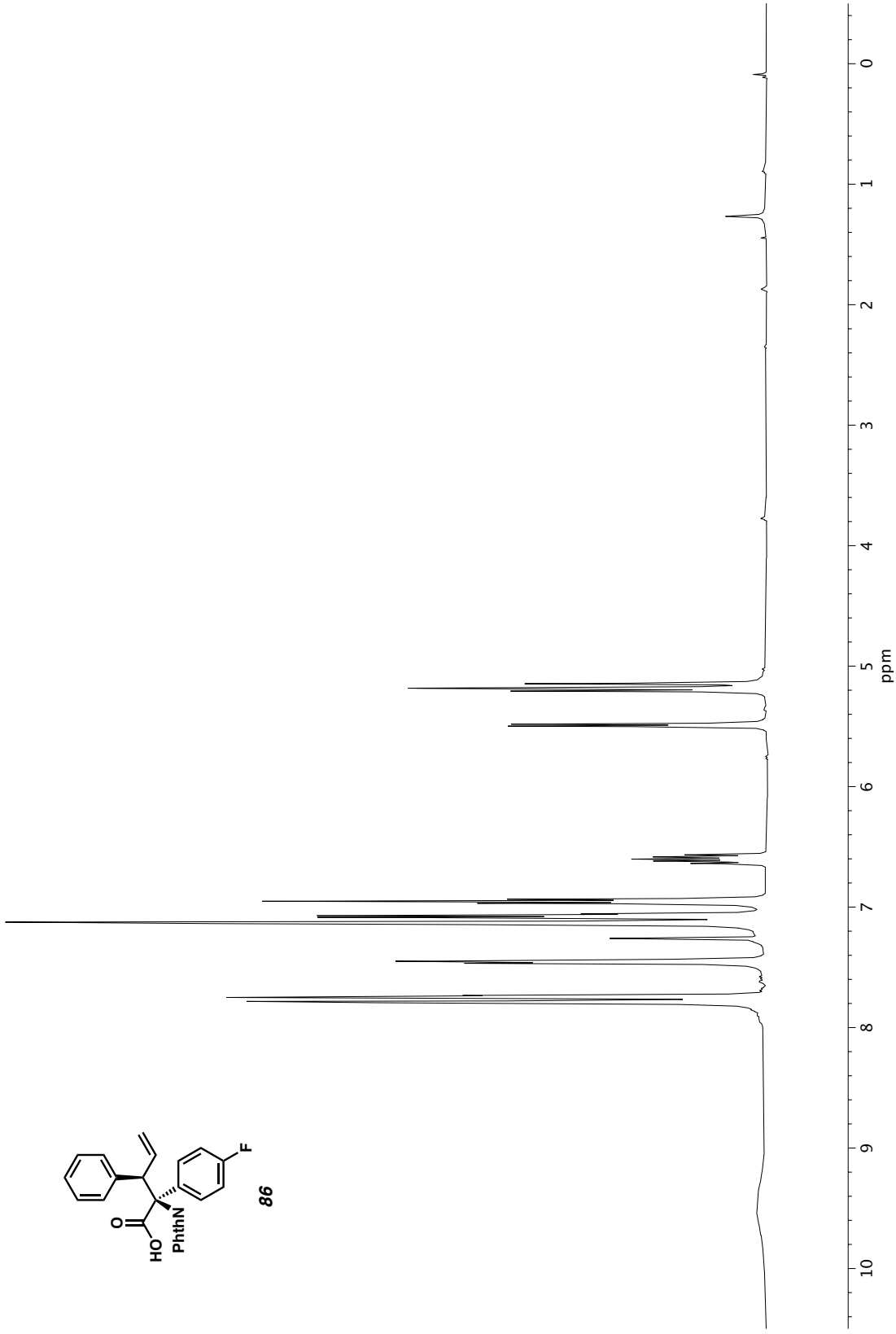

Figure A6.13 *^{1}H NMR (500 MHz, $CDCl_3$) of compound* ***86***.

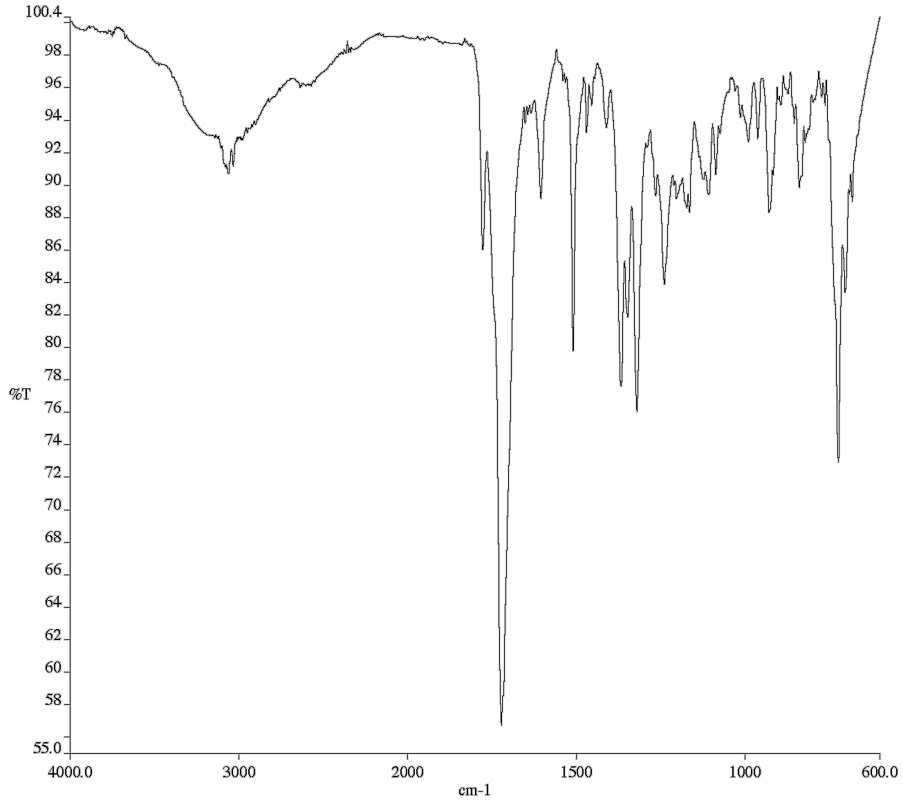

Figure A6.14 *Infrared spectrum (Thin Film, NaCl) of compound* ***86****.*

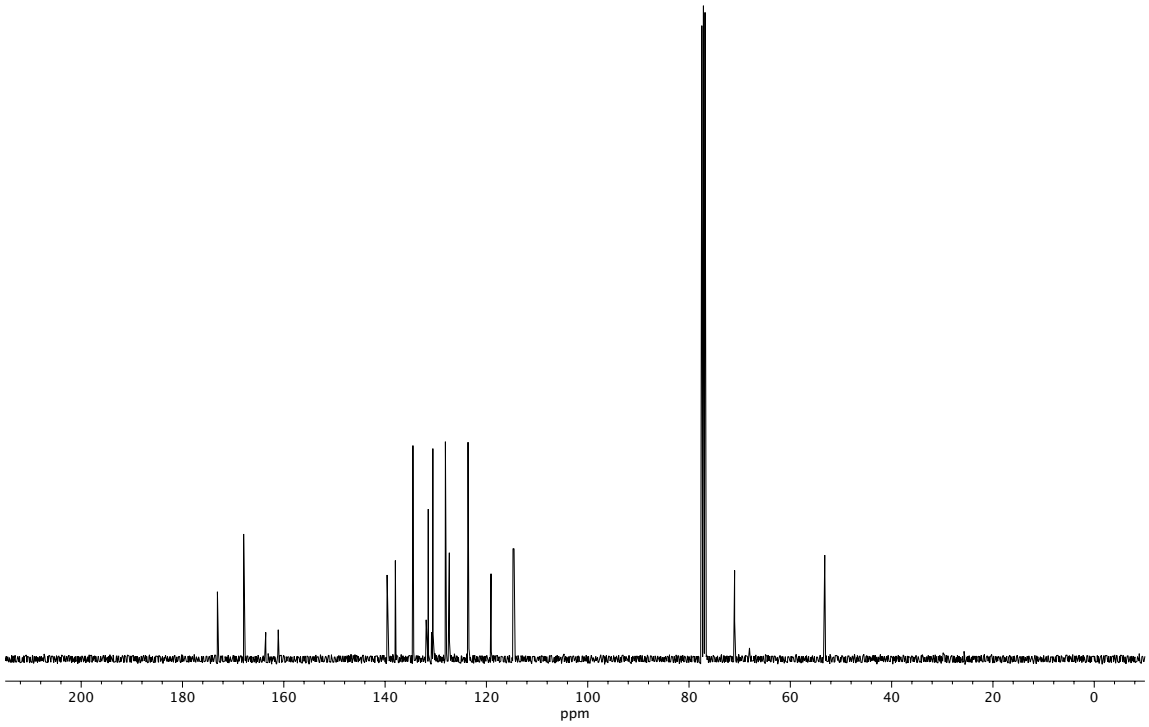

Figure A6.15 *^{13}C NMR (100 MHz, $CDCl_3$) of compound* ***86****.*

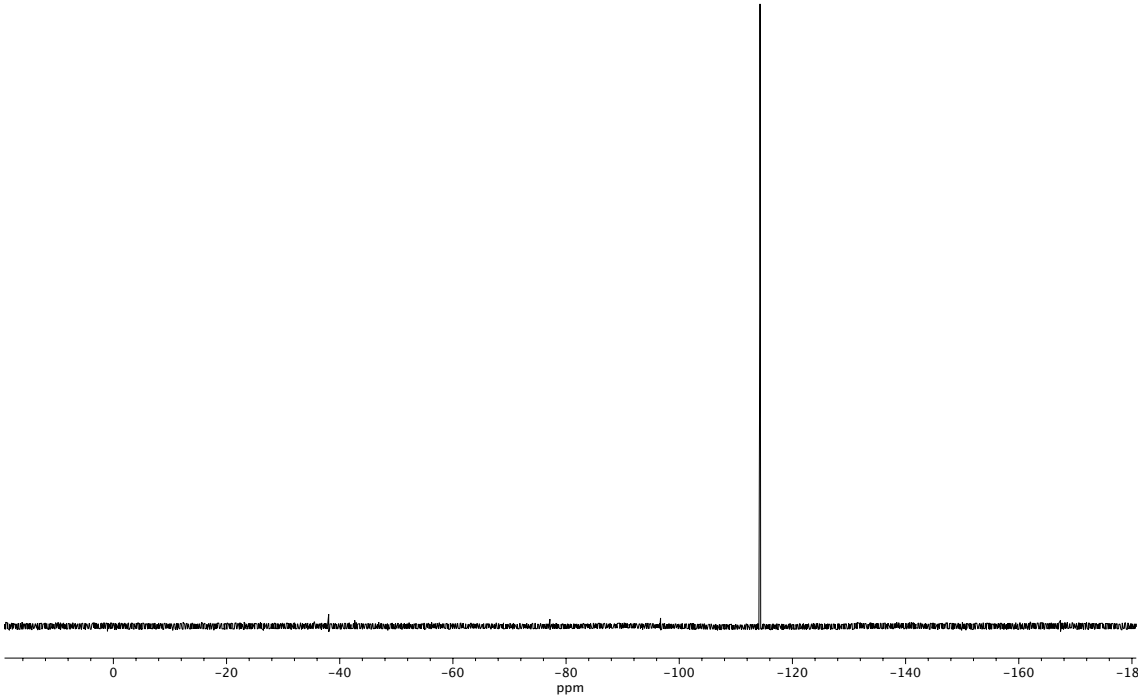

Figure A6.16 ^{19}F NMR (282 MHz, $CDCl_3$) of compound **86**.

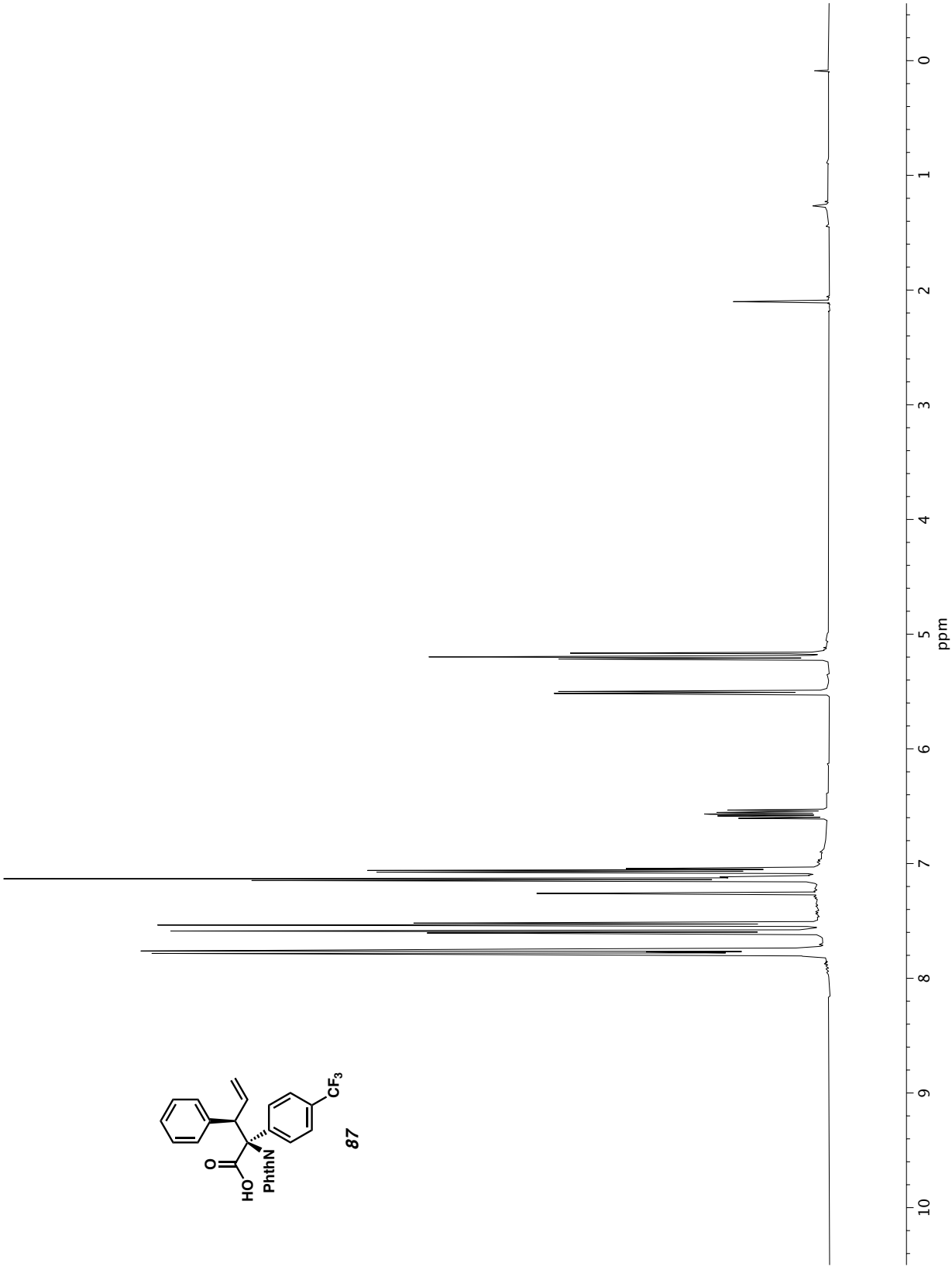

Figure A6.17 *^{1}H NMR (500 MHz, $CDCl_3$) of compound **87**.*

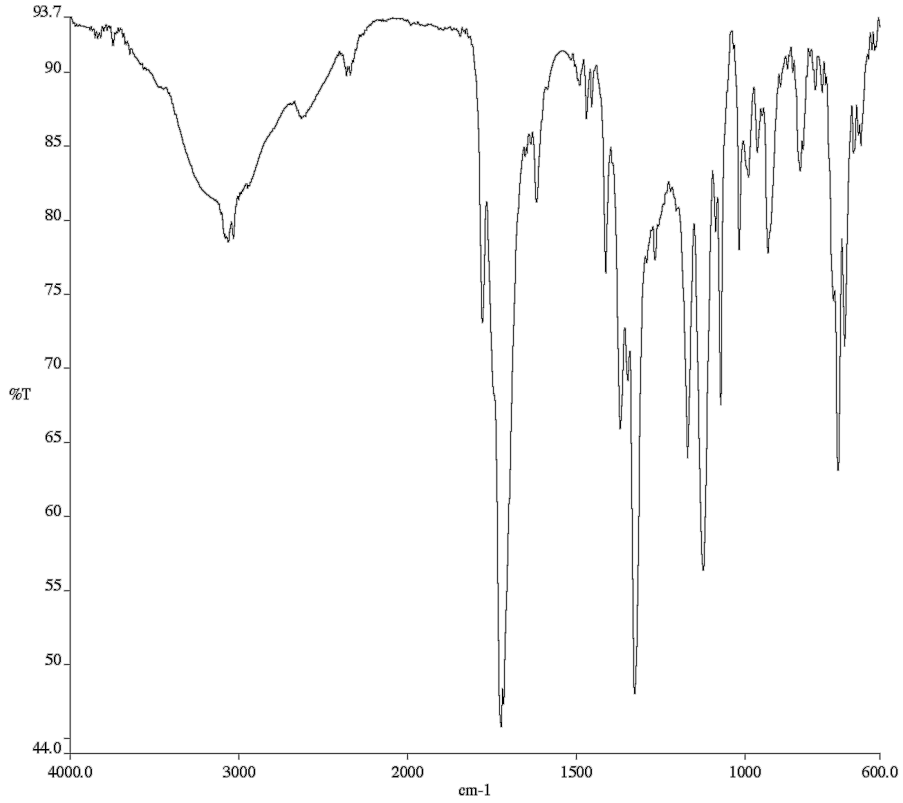

Figure A6.18 *Infrared spectrum (Thin Film, NaCl) of compound* ***87****.*

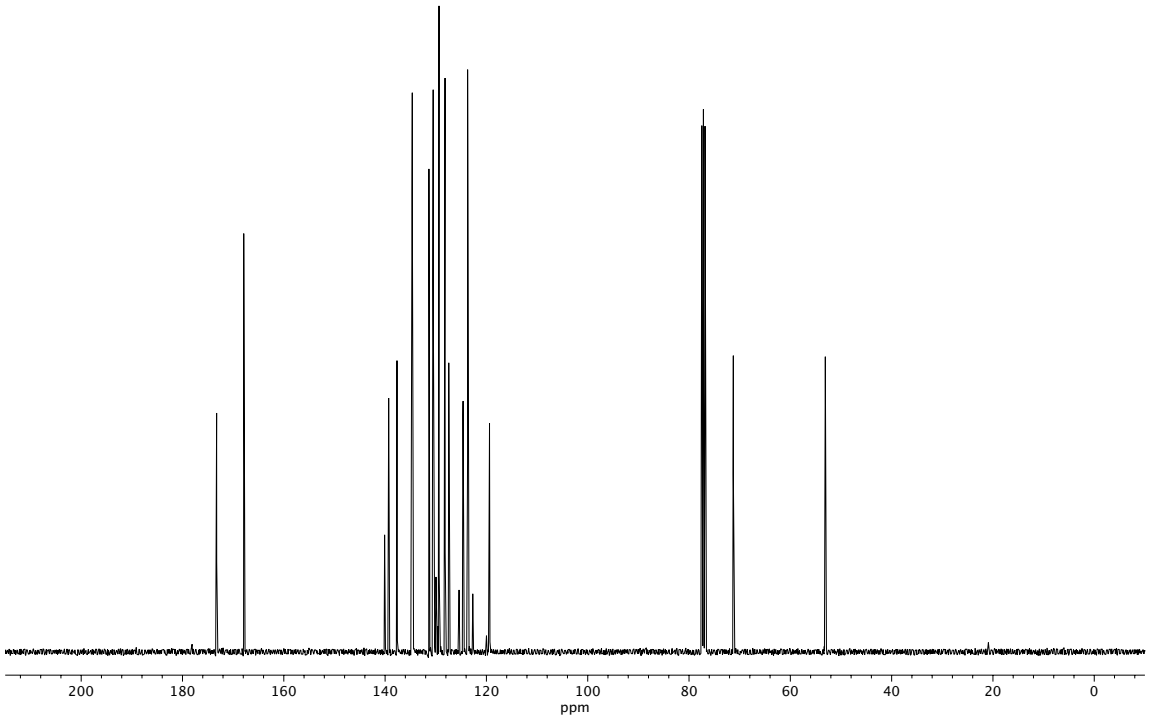

Figure A6.19 *^{13}C NMR (100 MHz, $CDCl_3$) of compound* ***87****.*

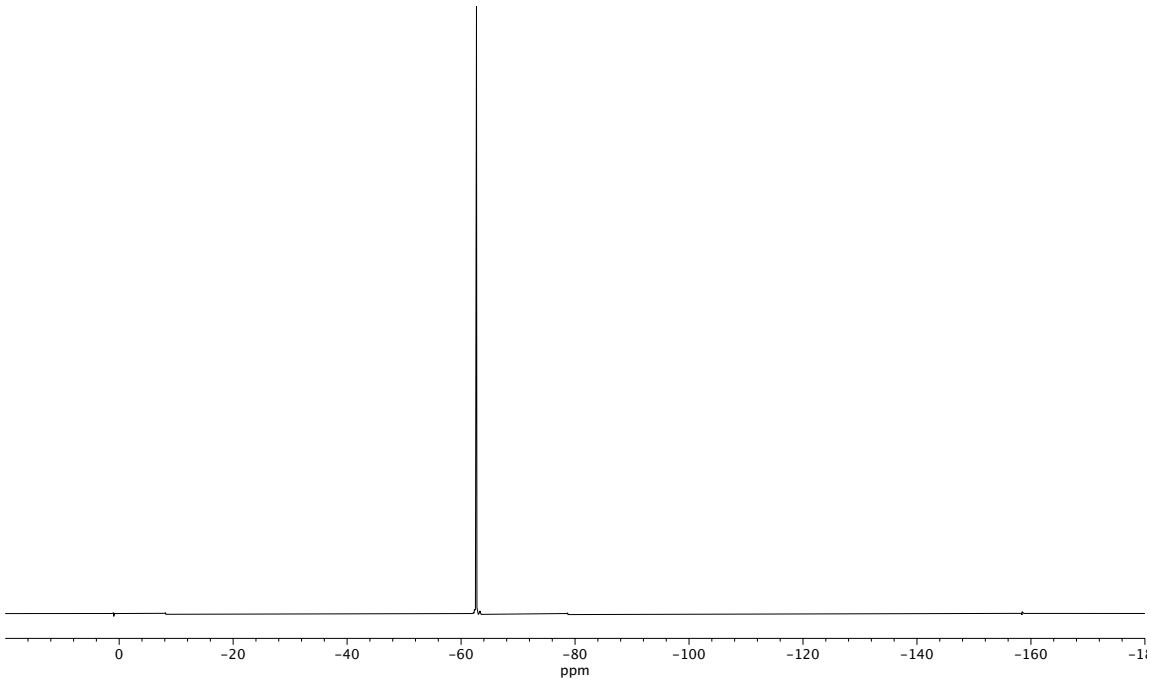

Figure A6.20 *^{19}F NMR (282 MHz, $CDCl_3$) of compound **87**.*

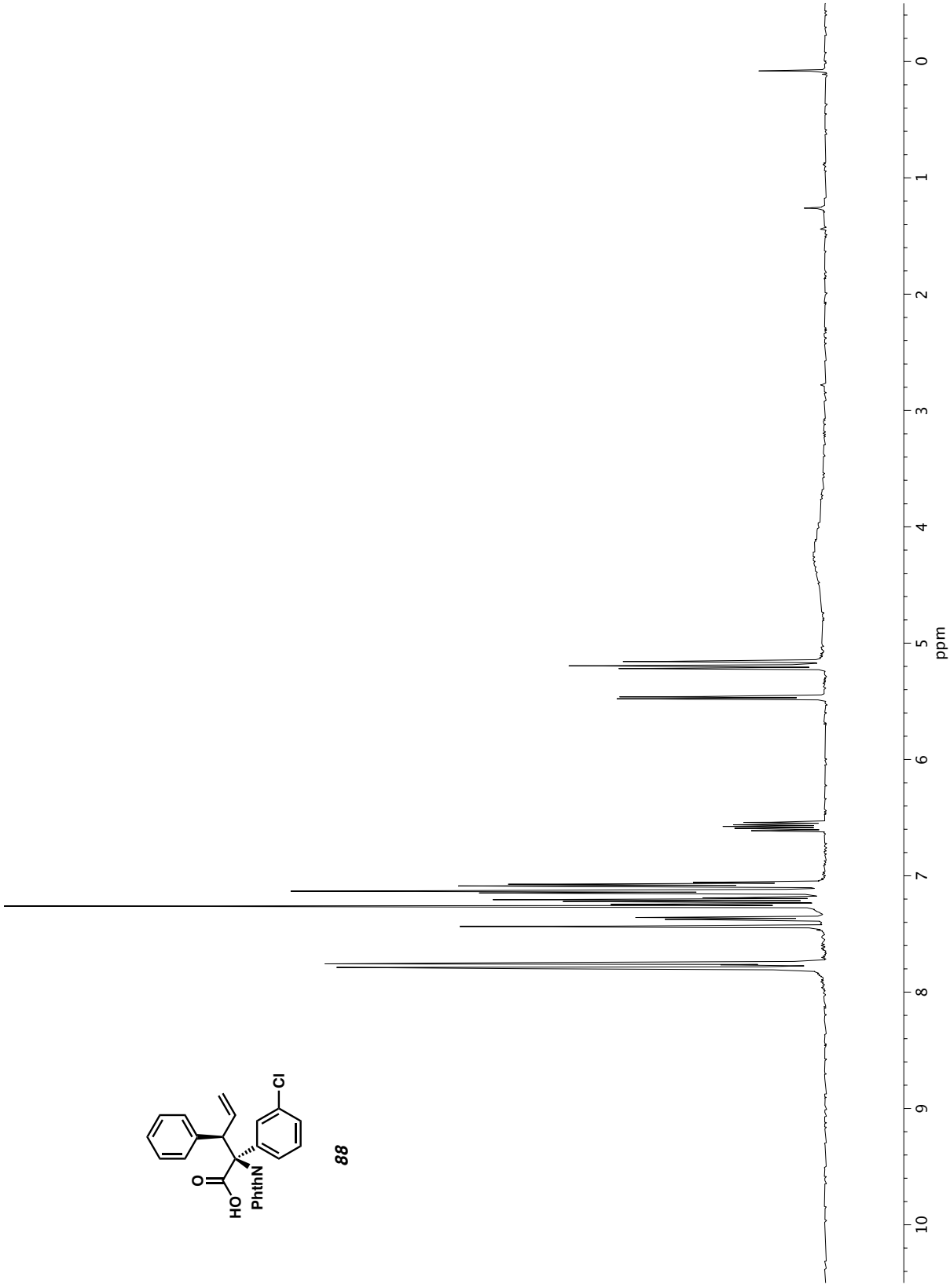

Figure A6.21 *^1H NMR (500 MHz, $CDCl_3$) of compound* ***88****.*

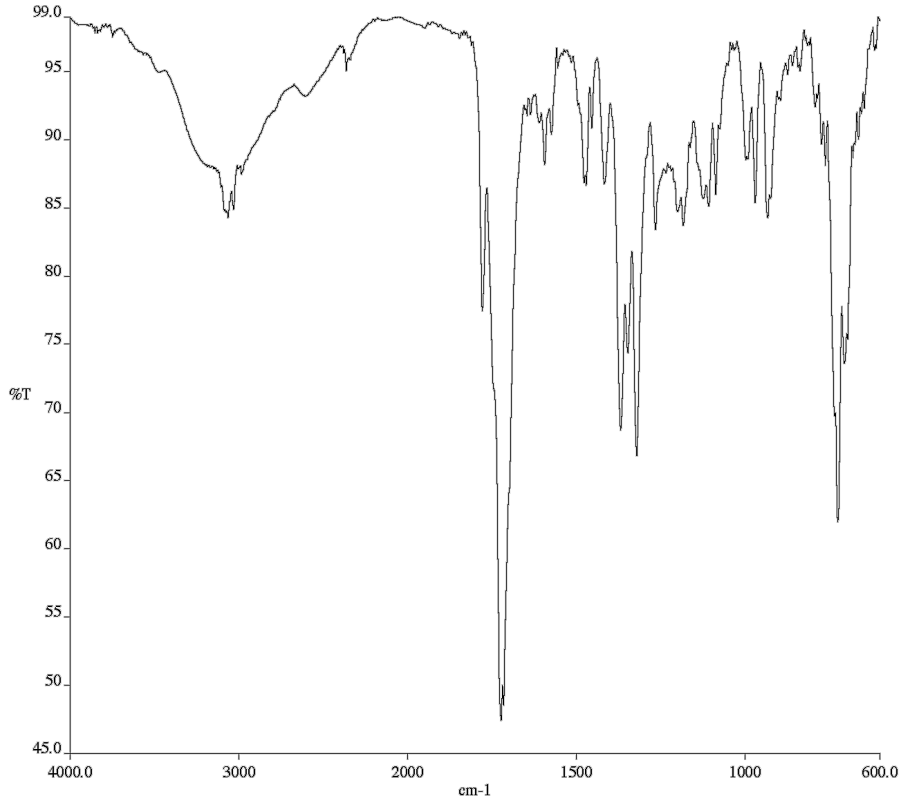

Figure A6.22 *Infrared spectrum (Thin Film, NaCl) of compound* ***88****.*

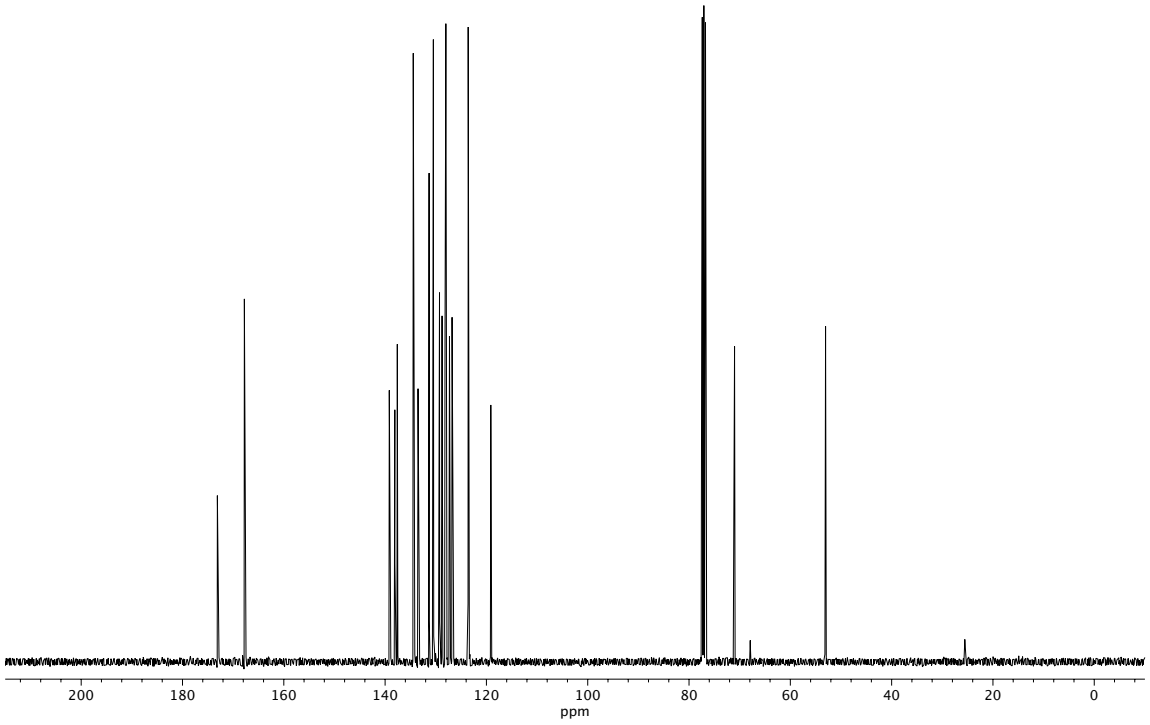

Figure A6.23 *^{13}C NMR (100 MHz, $CDCl_3$) of compound* ***88****.*

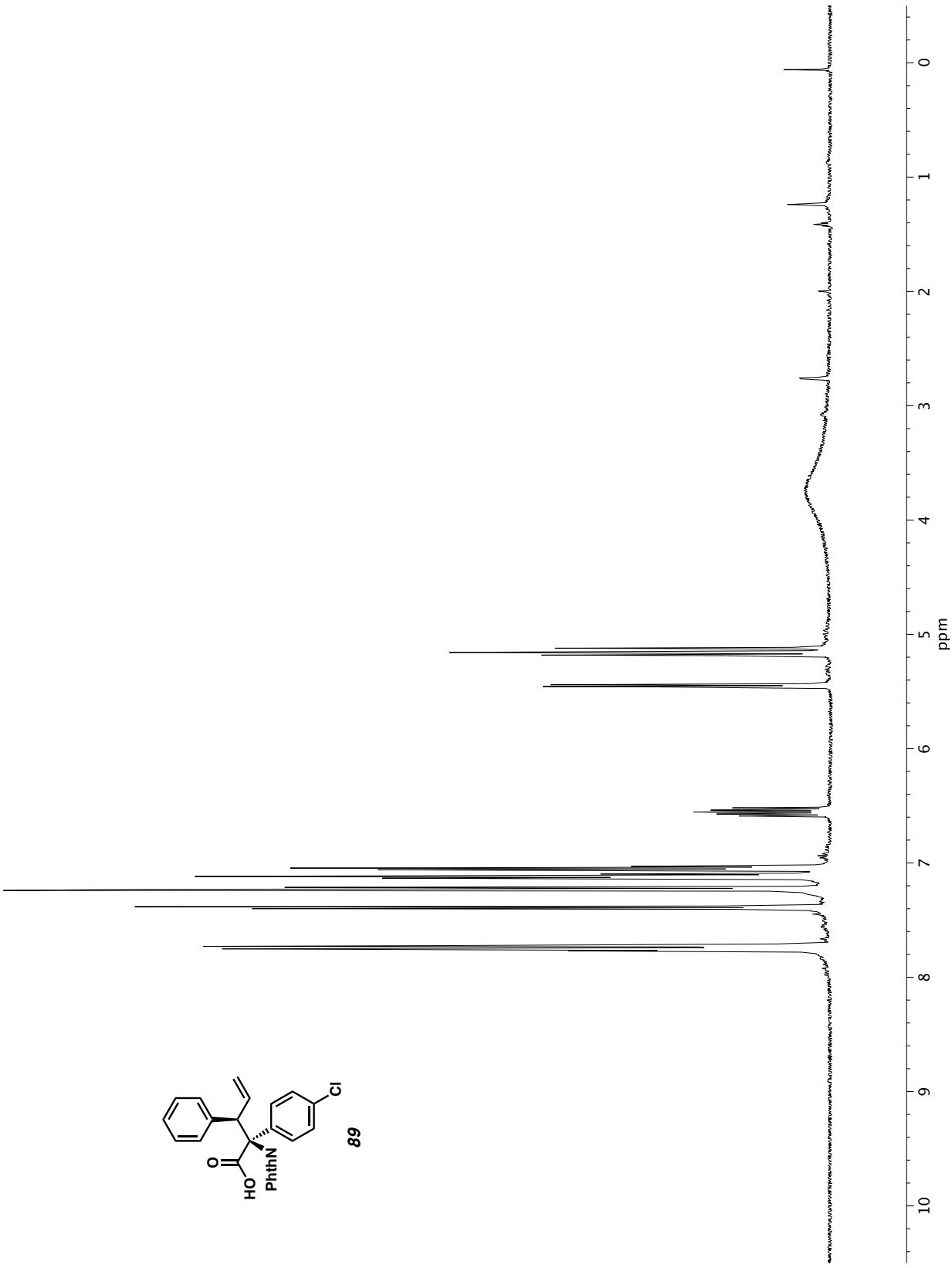

Figure A6.24 *^1H NMR (500 MHz, $CDCl_3$) of compound **89**.*

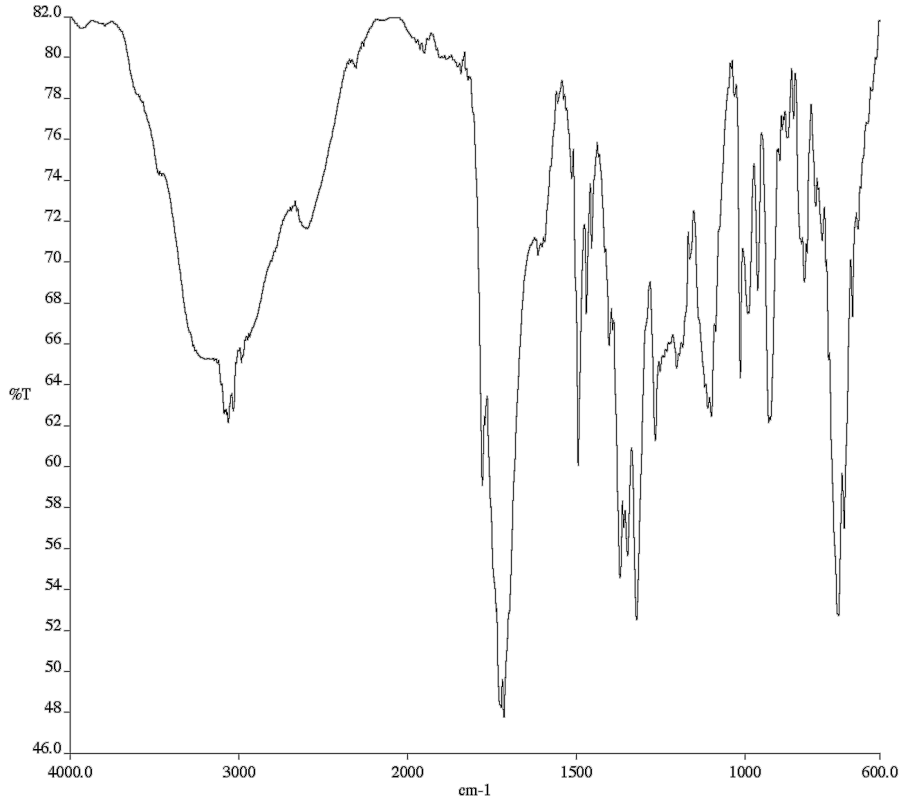

Figure A6.25 *Infrared spectrum (Thin Film, NaCl) of compound* ***89***.

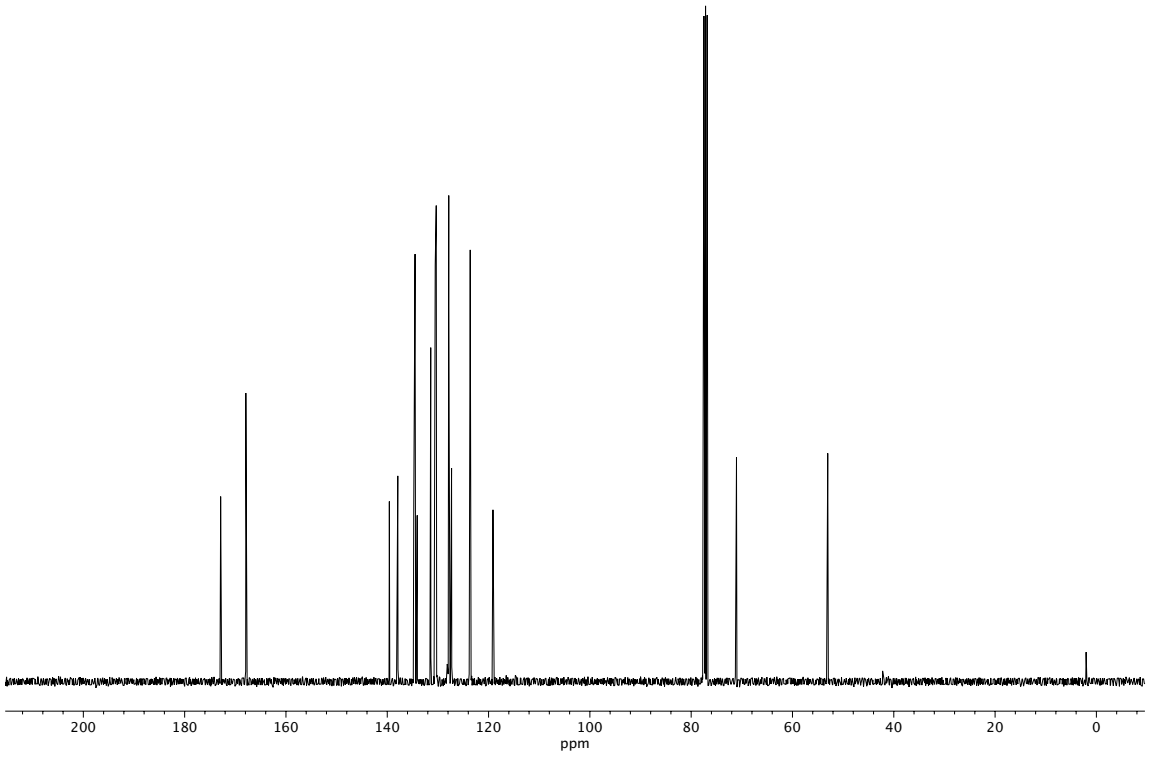

Figure A6.26 ^{13}C NMR (100 MHz, $CDCl_3$) of compound **89**.

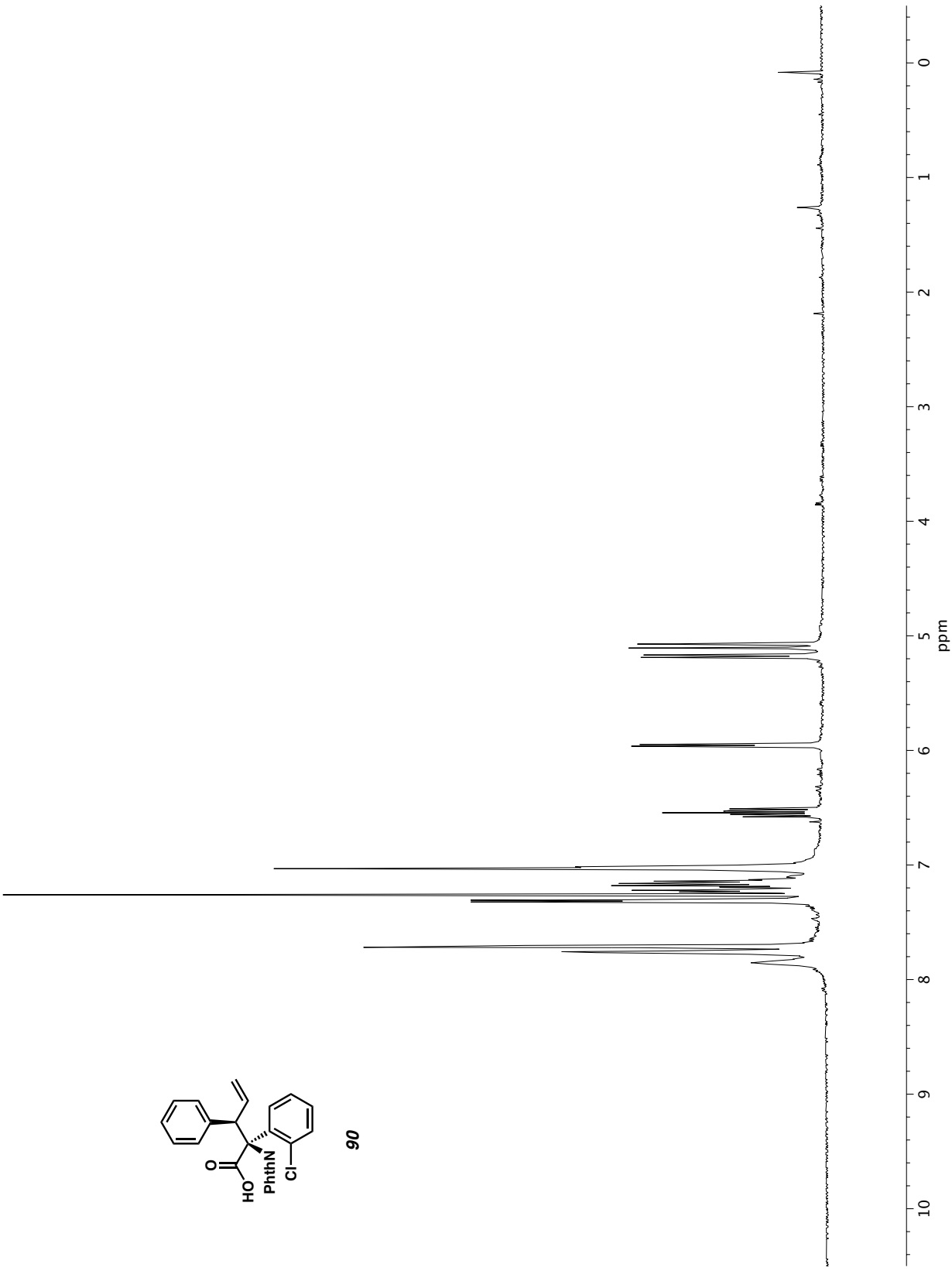

Figure A6.27 *^1H NMR (500 MHz, $CDCl_3$) of compound **90**.*

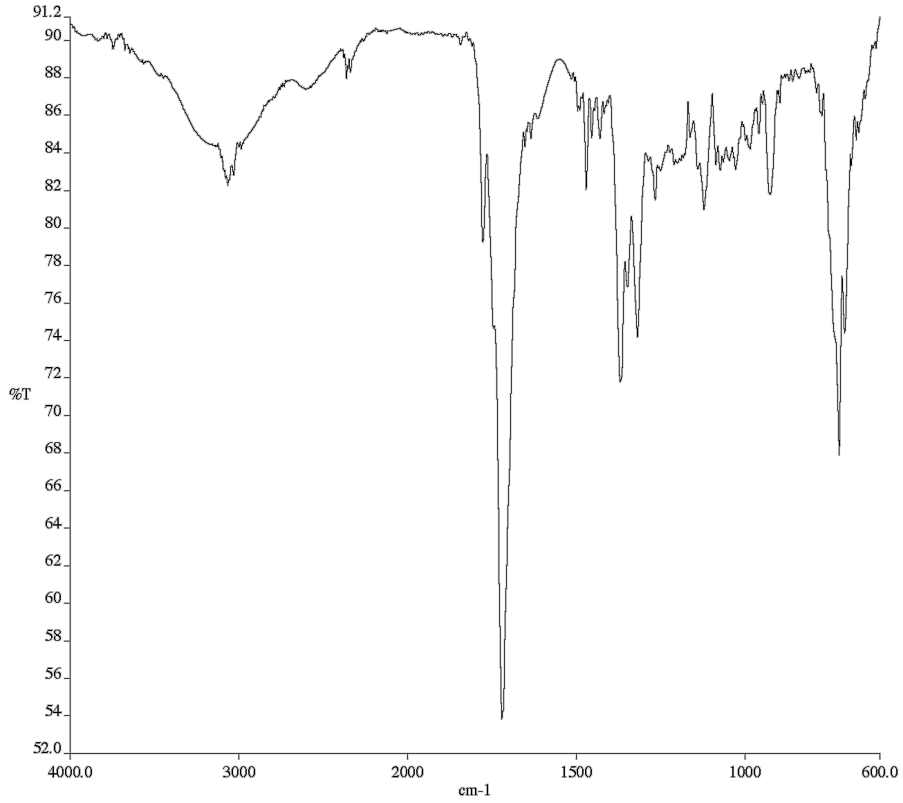

Figure A6.28 *Infrared spectrum (Thin Film, NaCl) of compound* ***90****.*

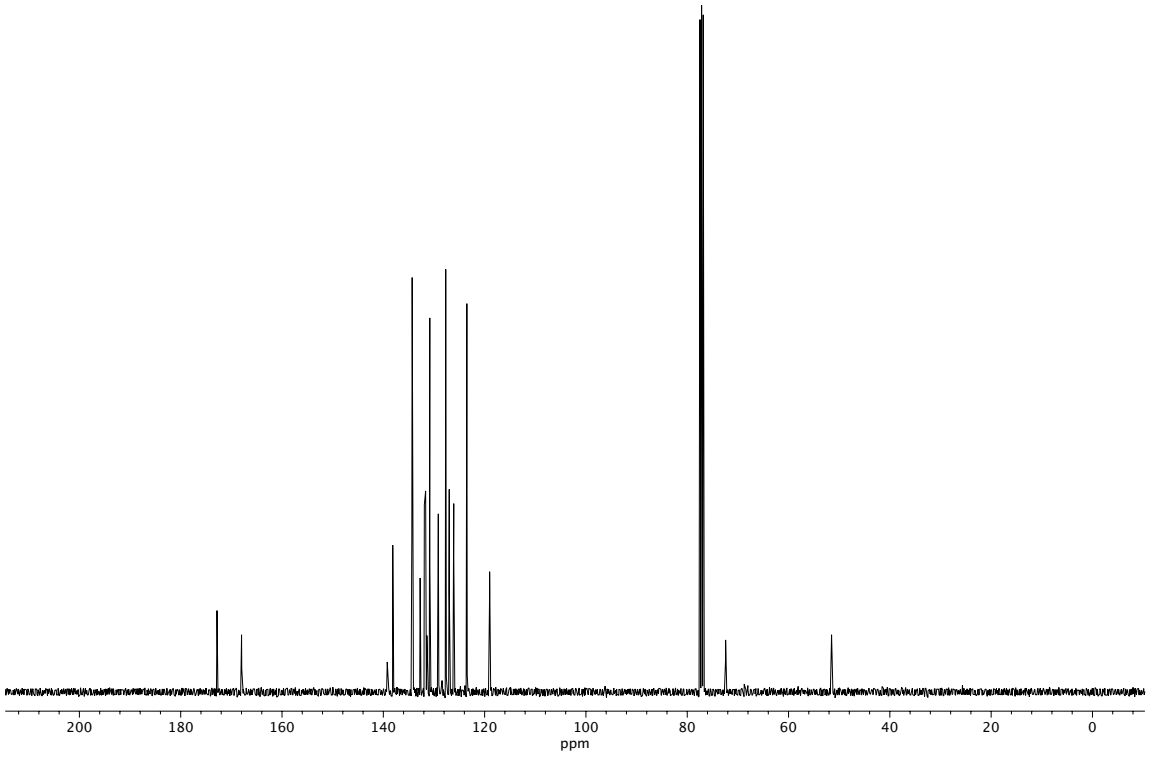

Figure A6.29 *^{13}C NMR (100 MHz, $CDCl_3$) of compound* ***90****.*

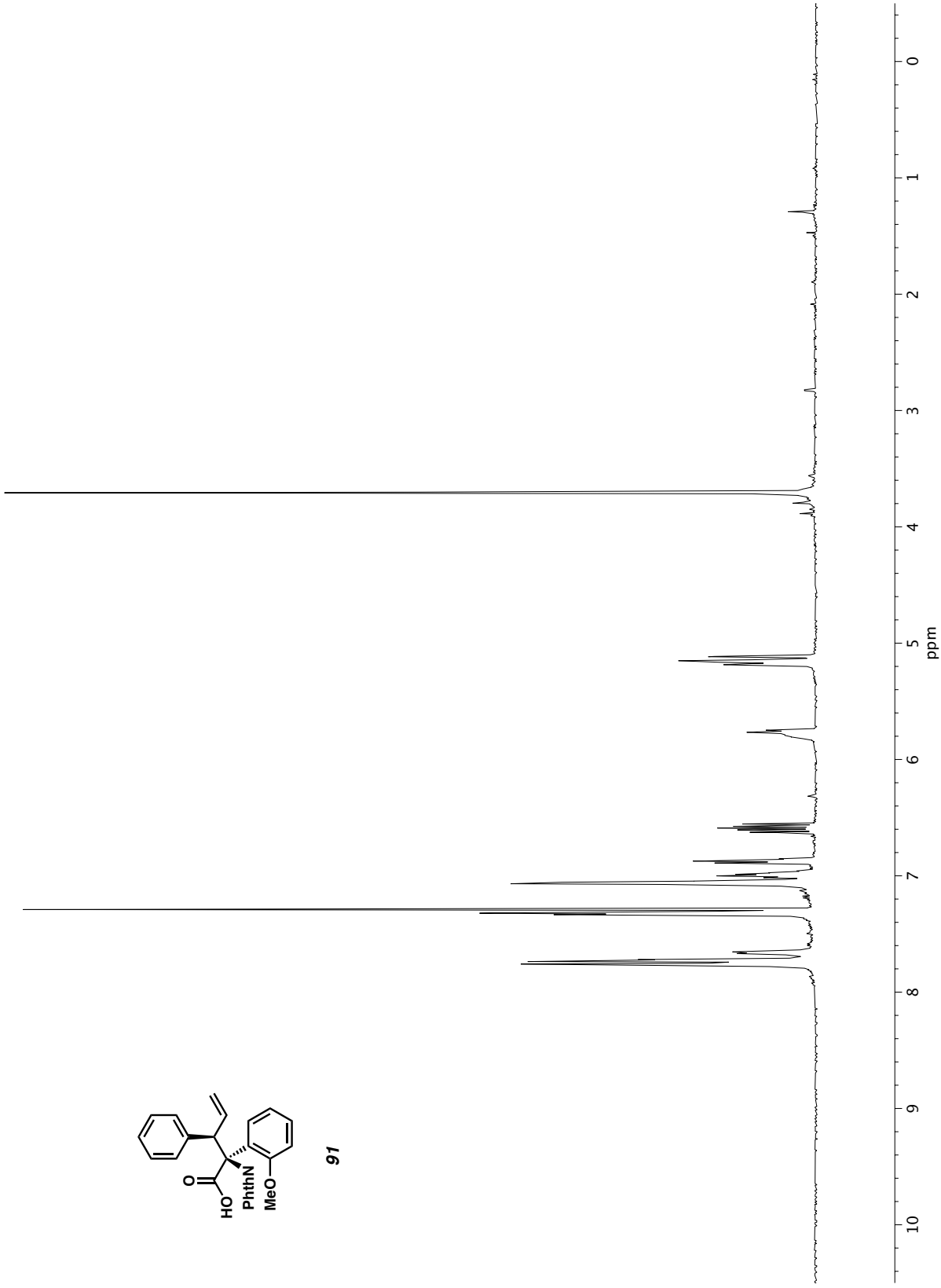

Figure A6.30 *^{1}H NMR (500 MHz, $CDCl_3$) of compound* ***91***.

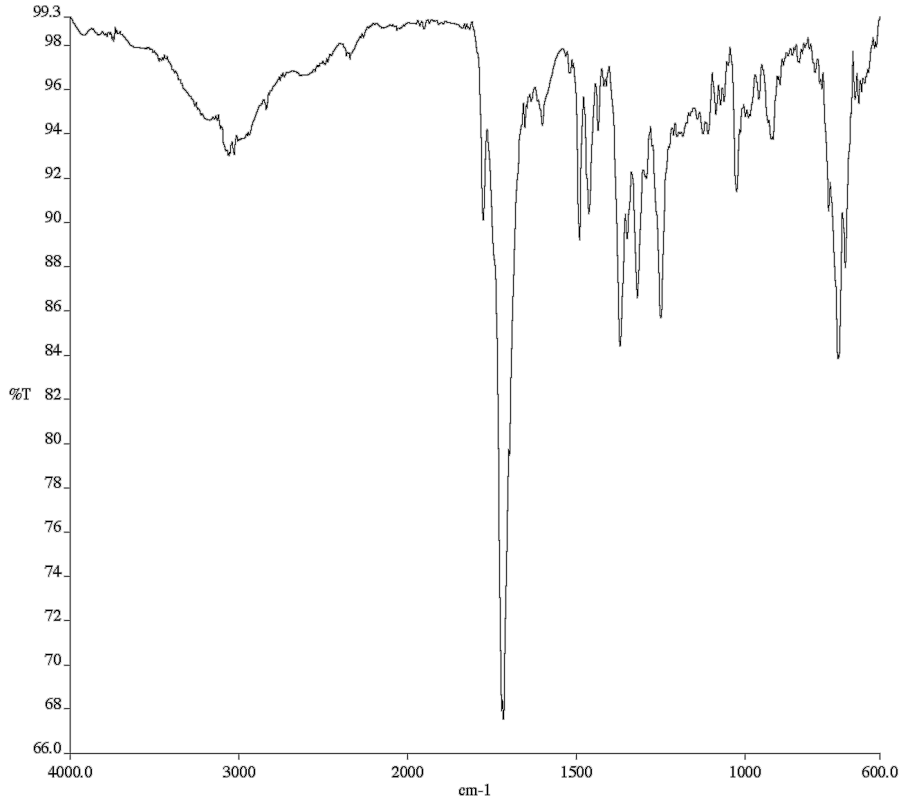

Figure A6.31 *Infrared spectrum (Thin Film, NaCl) of compound* ***91****.*

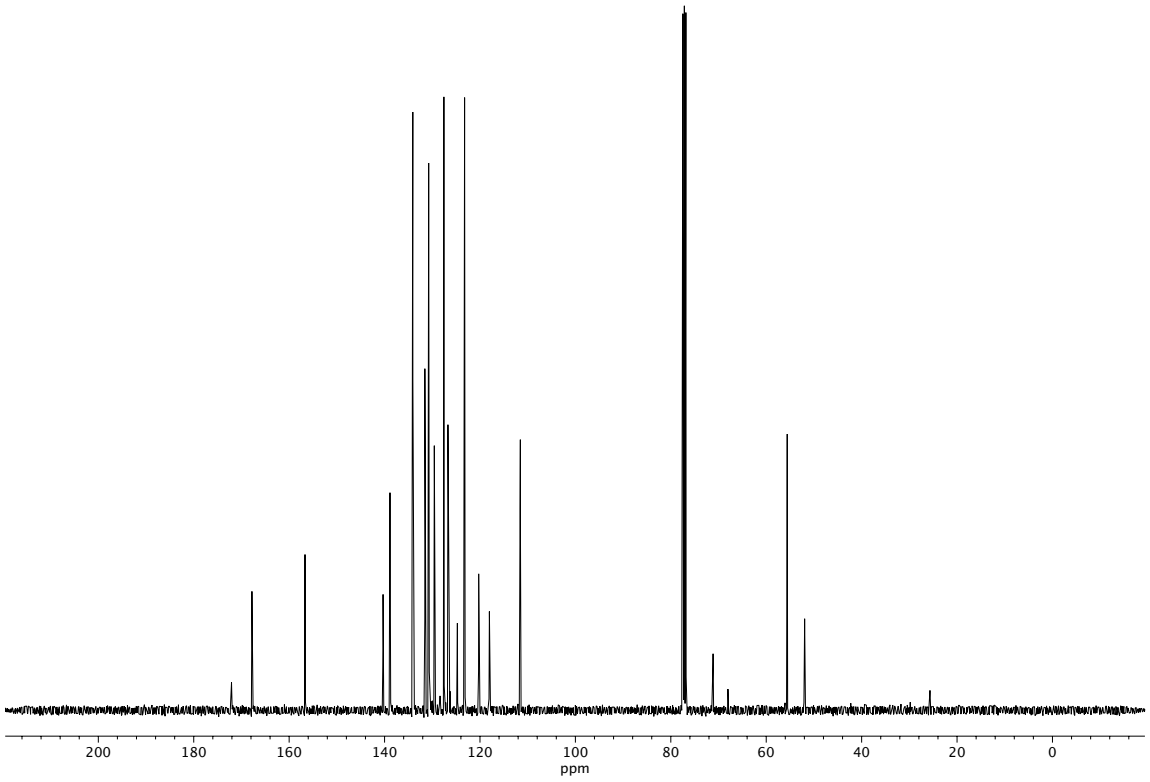

Figure A6.32 *^{13}C NMR (100 MHz, $CDCl_3$) of compound* ***91****.*

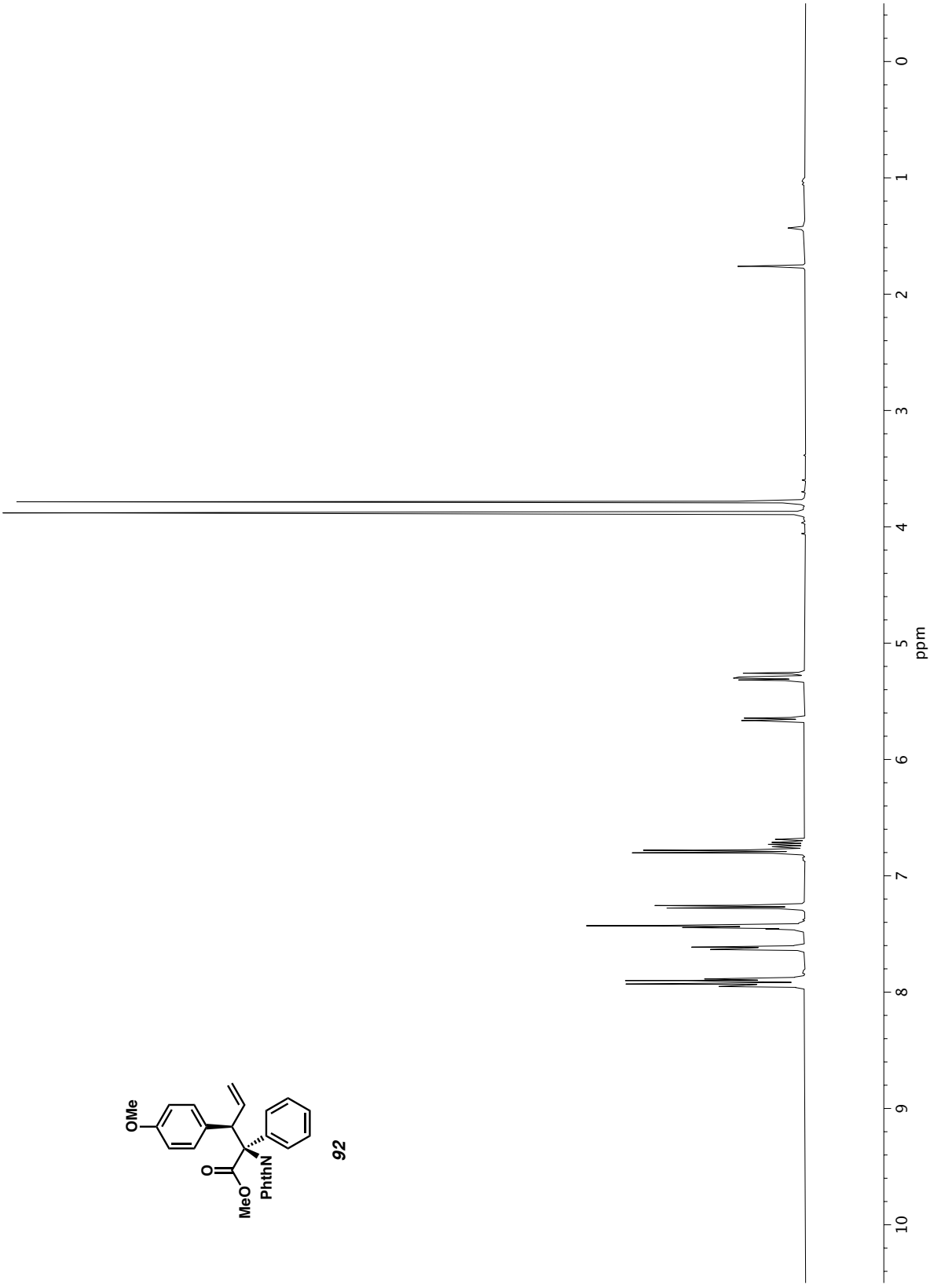

Figure A6.33 *^{1}H NMR (500 MHz, $CDCl_3$) of compound **92**.*

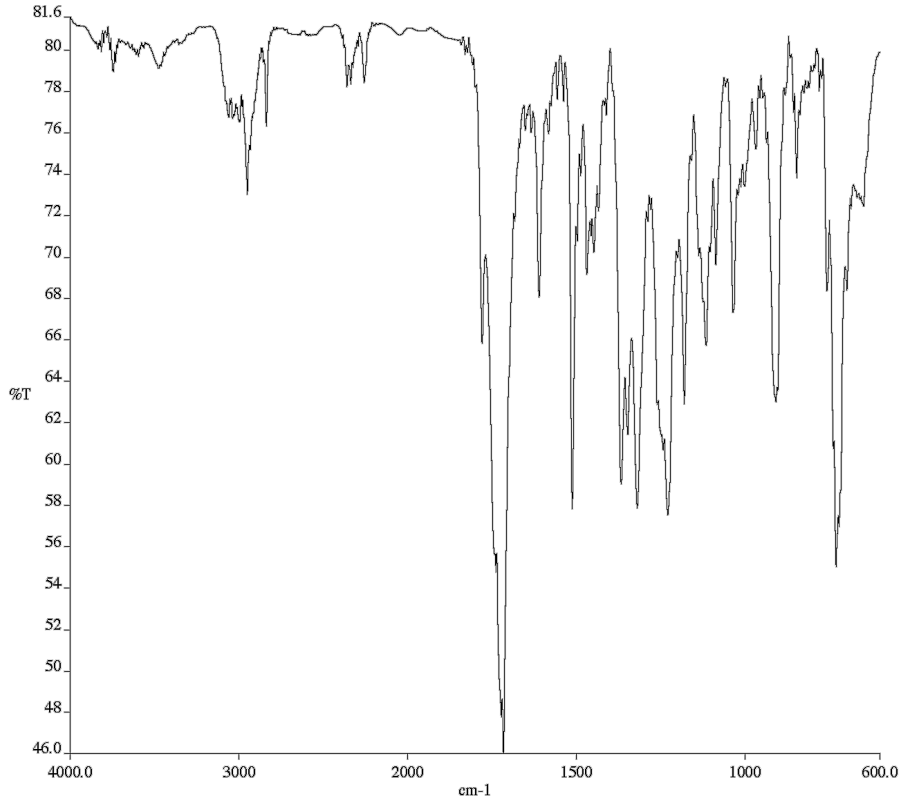

Figure A6.34 *Infrared spectrum (Thin Film, NaCl) of compound* ***92****.*

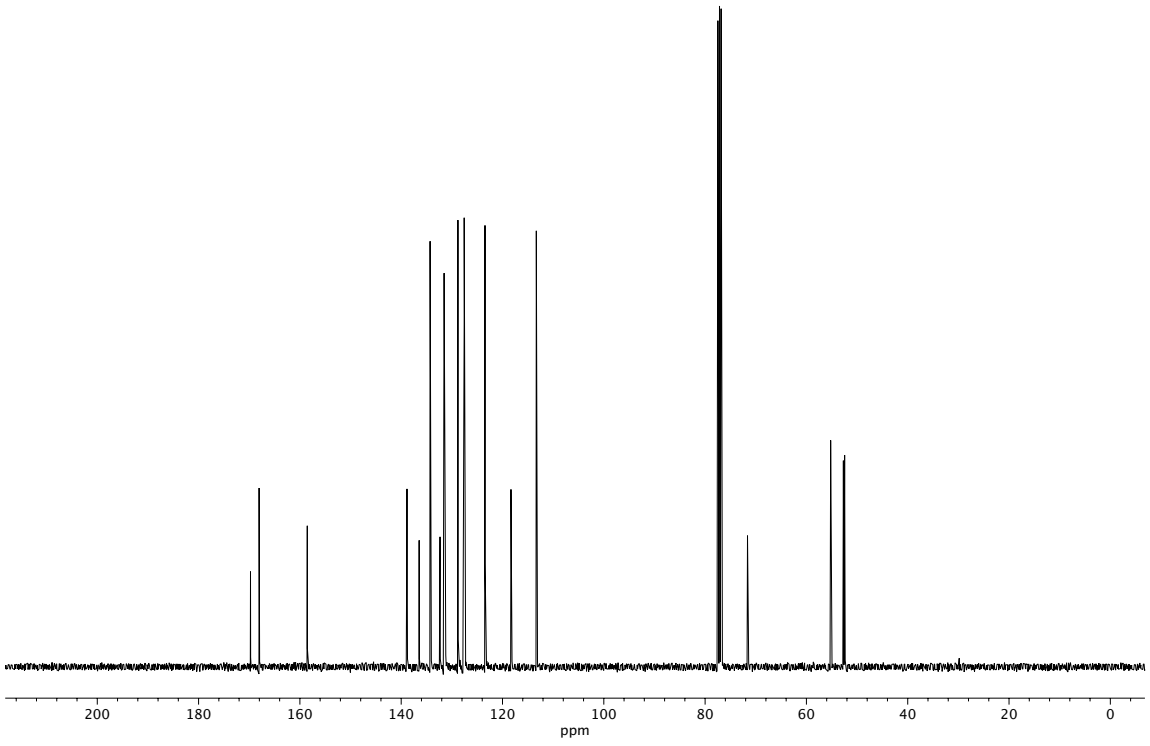

Figure A6.35 *^{13}C NMR (100 MHz, $CDCl_3$) of compound* ***92****.*

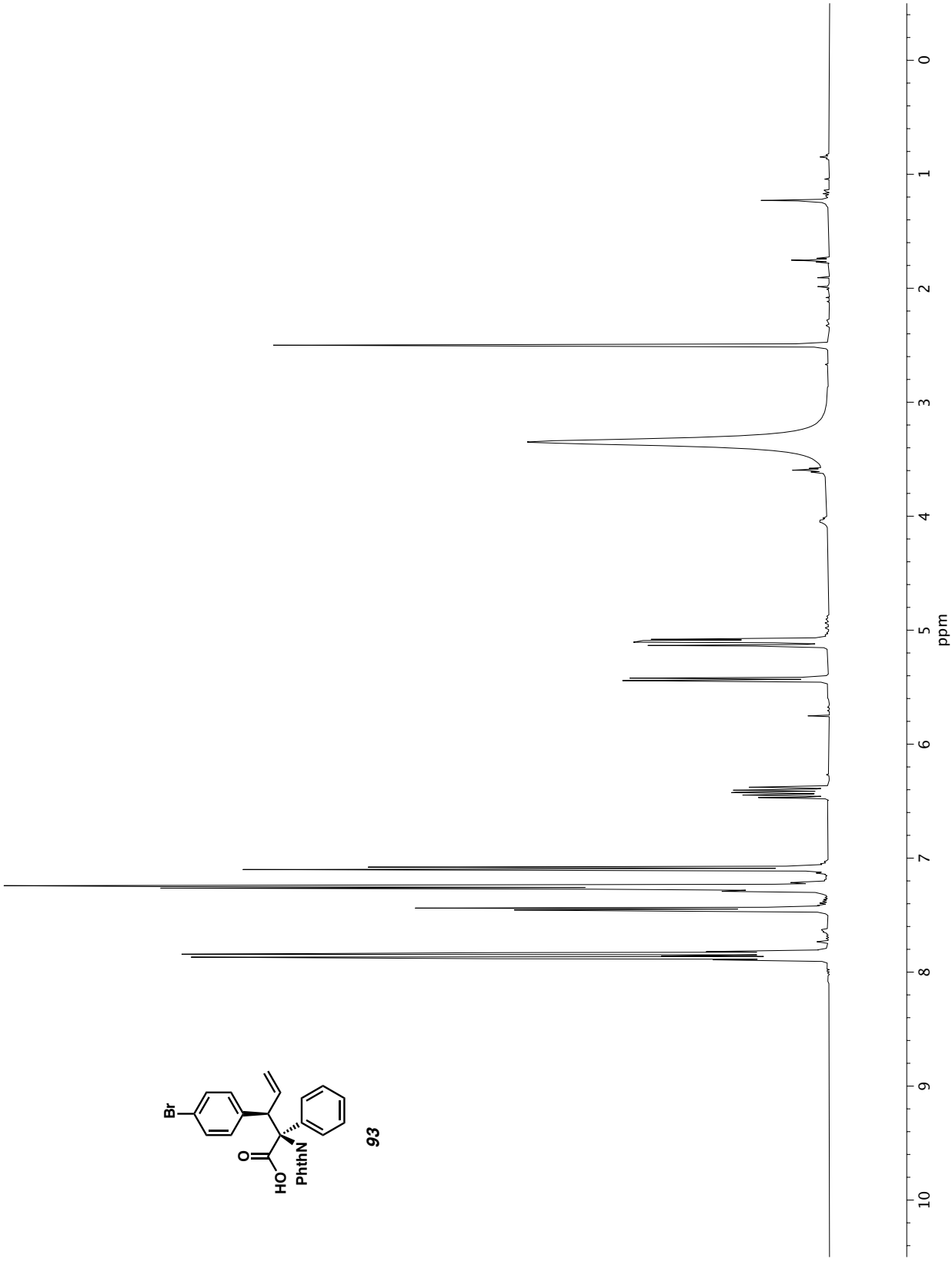

Figure A6.36 *^{1}H NMR (500 MHz, DMSO-d_6) of compound **93**.*

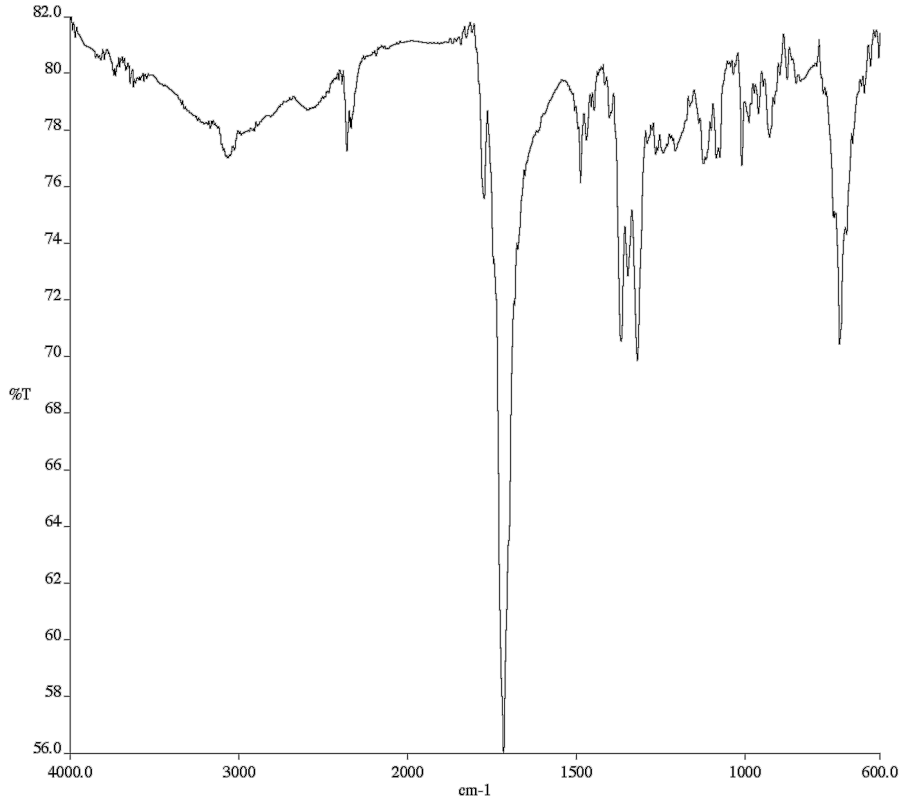

Figure A6.37 *Infrared spectrum (Thin Film, NaCl) of compound* ***93****.*

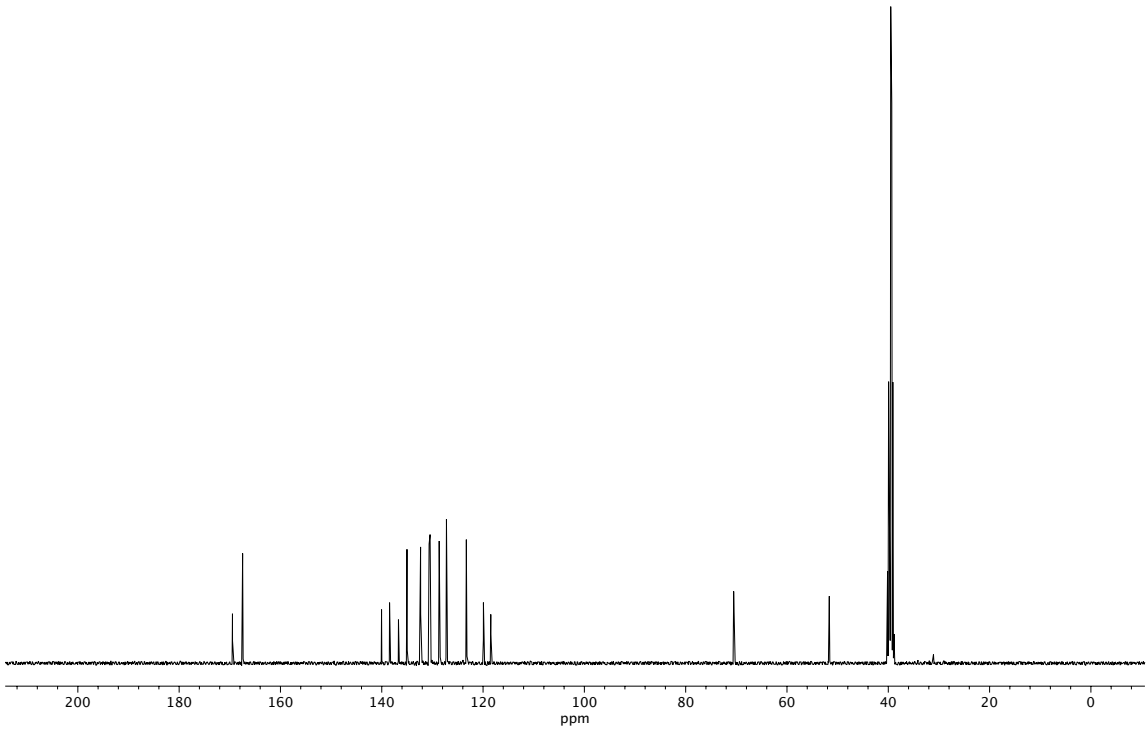

Figure A6.38 *^{13}C NMR (100 MHz, DMSO-d_6) of compound* ***93****.*

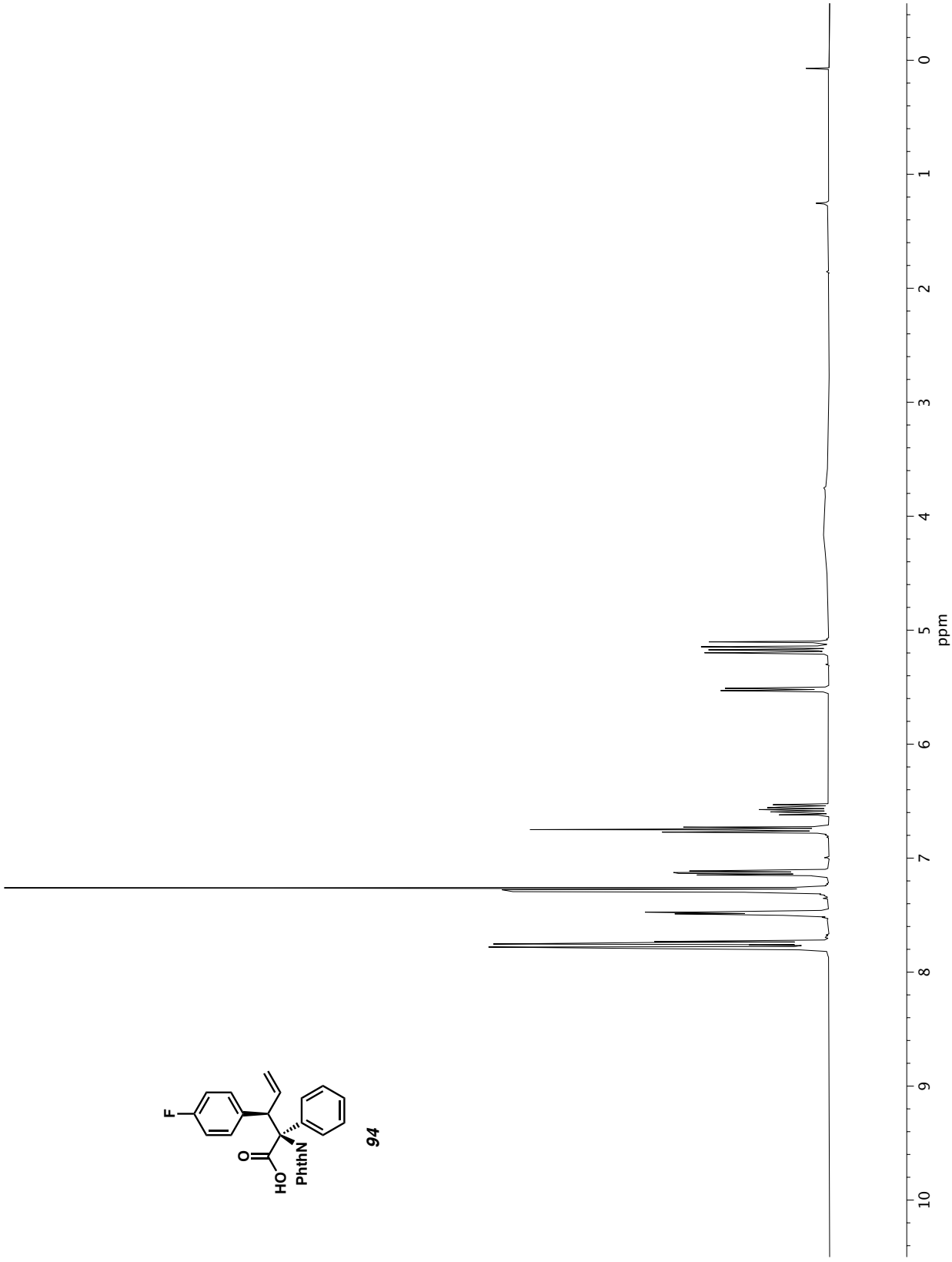

Figure A6.39 *^{1}H NMR (500 MHz, $CDCl_3$) of compound **94**.*

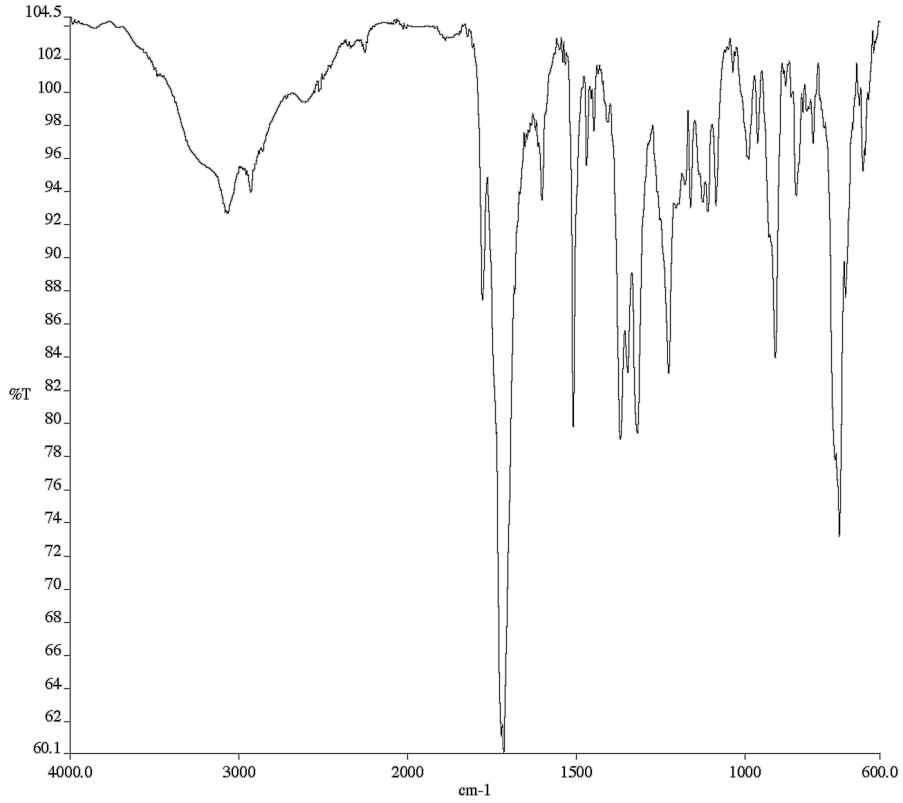

Figure A6.40 *Infrared spectrum (Thin Film, NaCl) of compound* ***94****.*

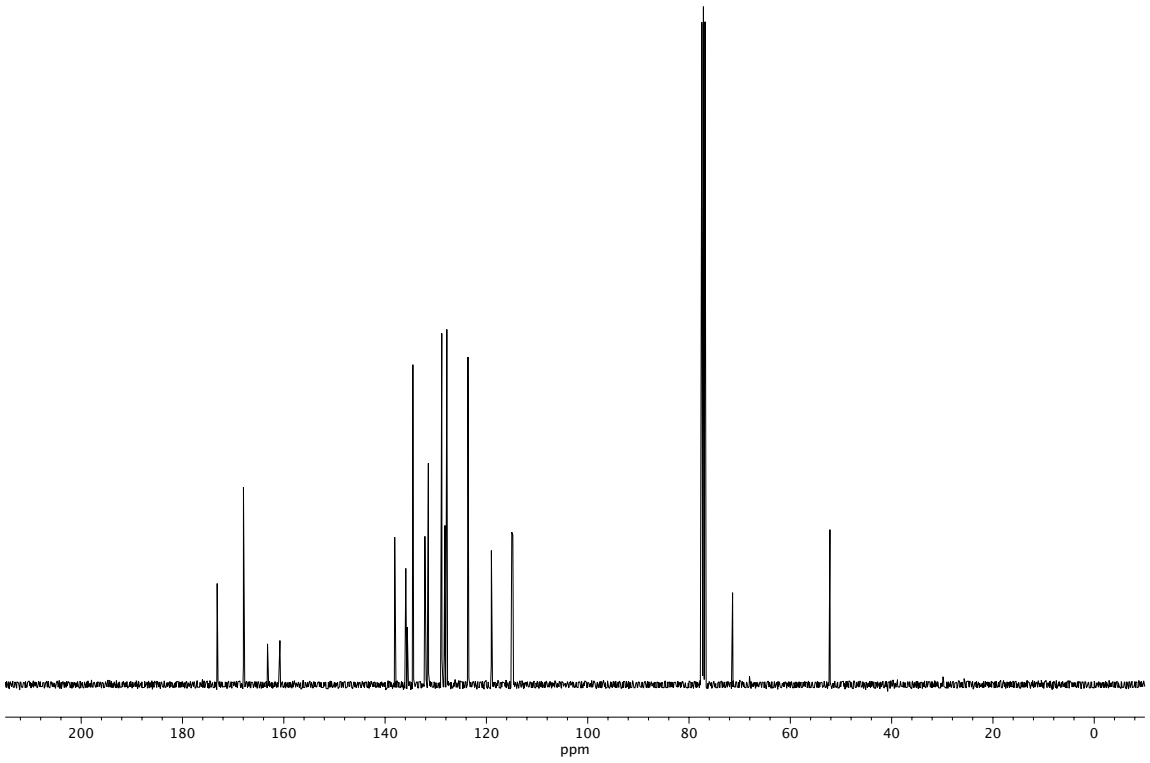

Figure A6.41 *^{13}C NMR (100 MHz, $CDCl_3$) of compound* ***94****.*

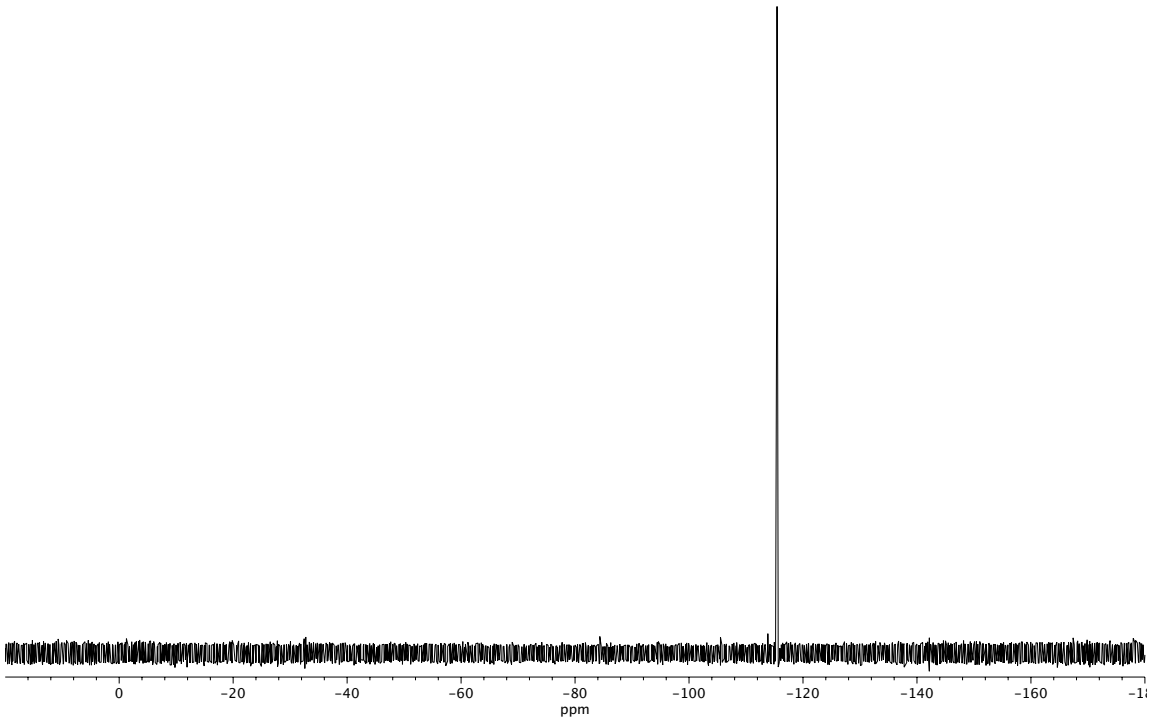

Figure A6.42 *^{19}F NMR (282 MHz, $CDCl_3$) of compound* ***94****.*

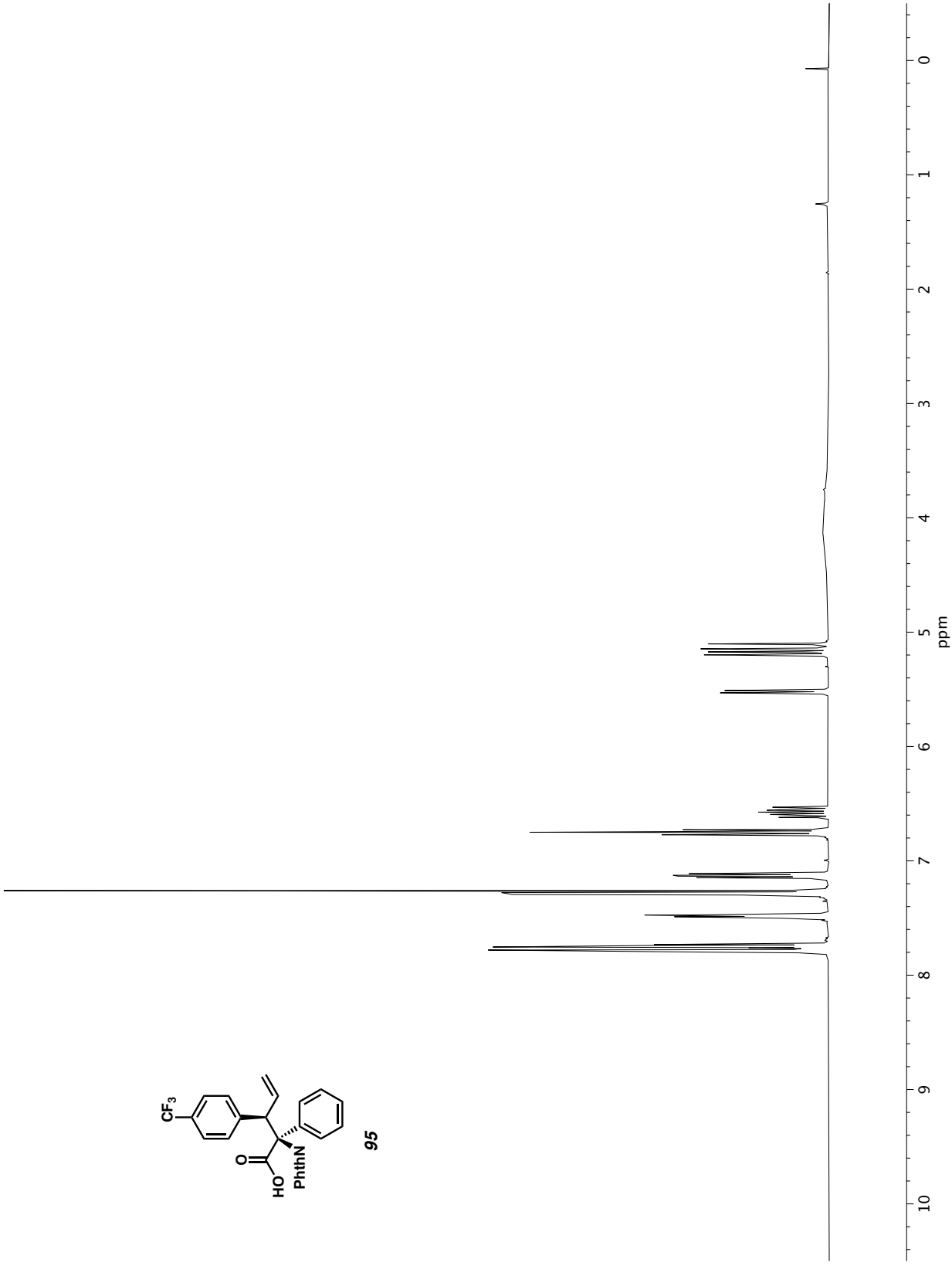

Figure A6.43 *^{1}H NMR (500 MHz, $CDCl_3$) of compound **95**.*

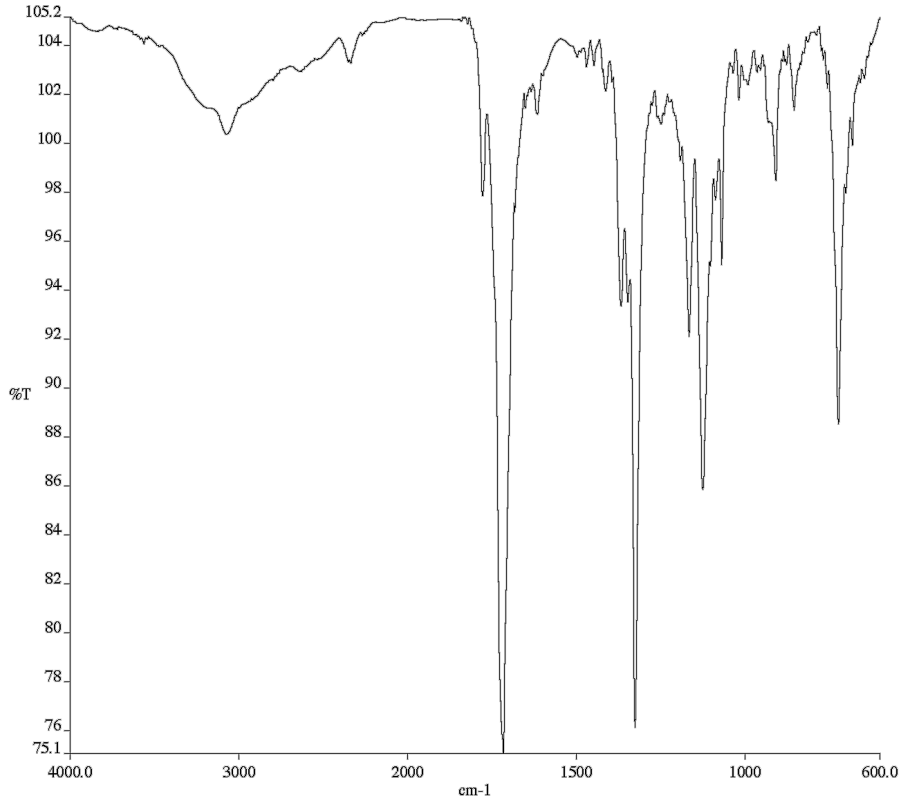

Figure A6.44 *Infrared spectrum (Thin Film, NaCl) of compound* ***95****.*

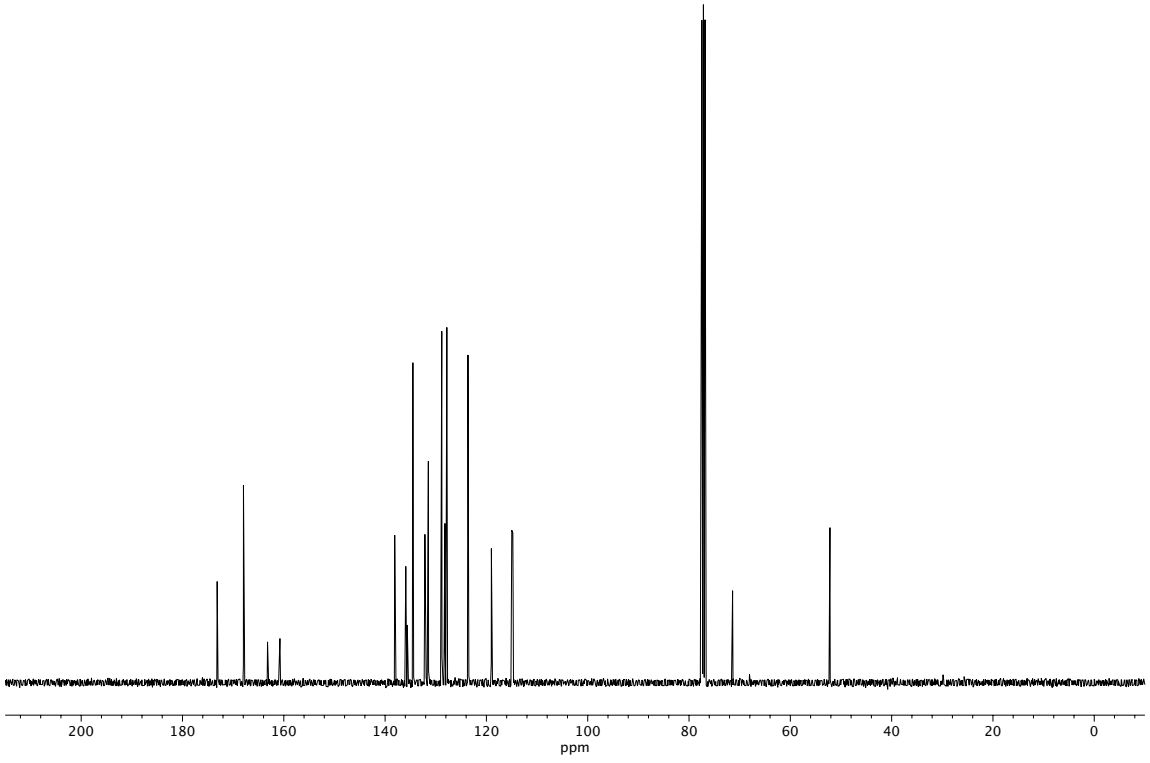

Figure A6.45 *^{13}C NMR (100 MHz, $CDCl_3$) of compound* ***95****.*

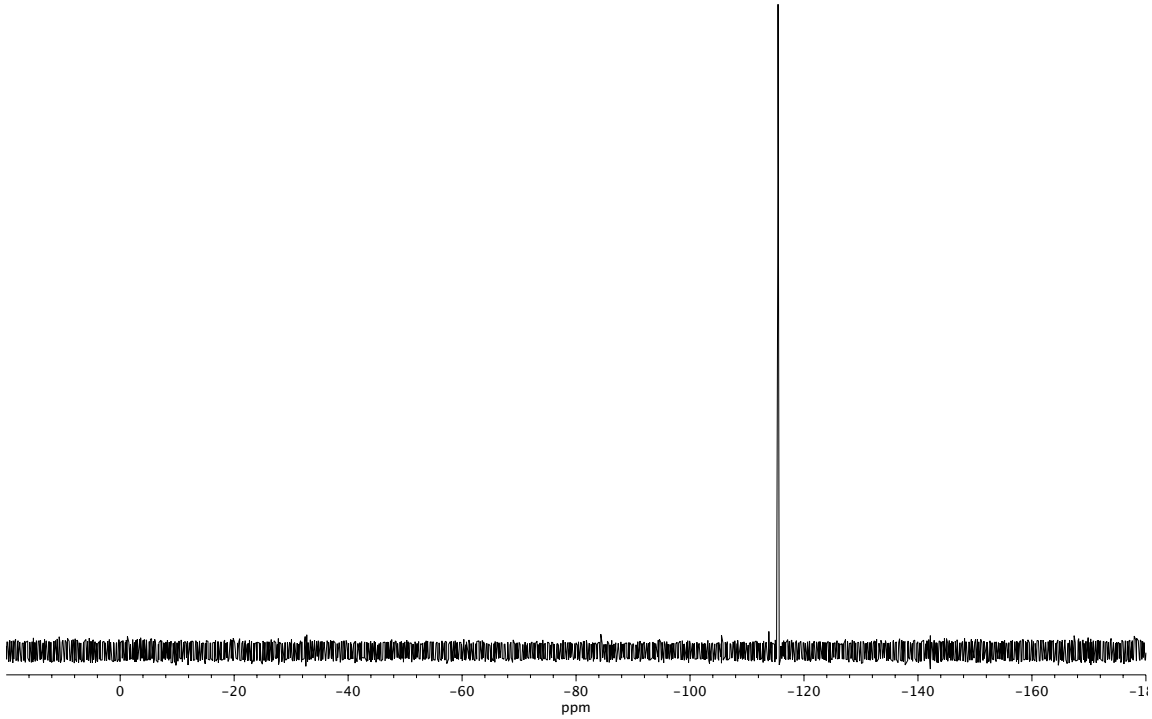

Figure A6.46 *^{19}F NMR (282 MHz, $CDCl_3$) of compound* ***95****.*

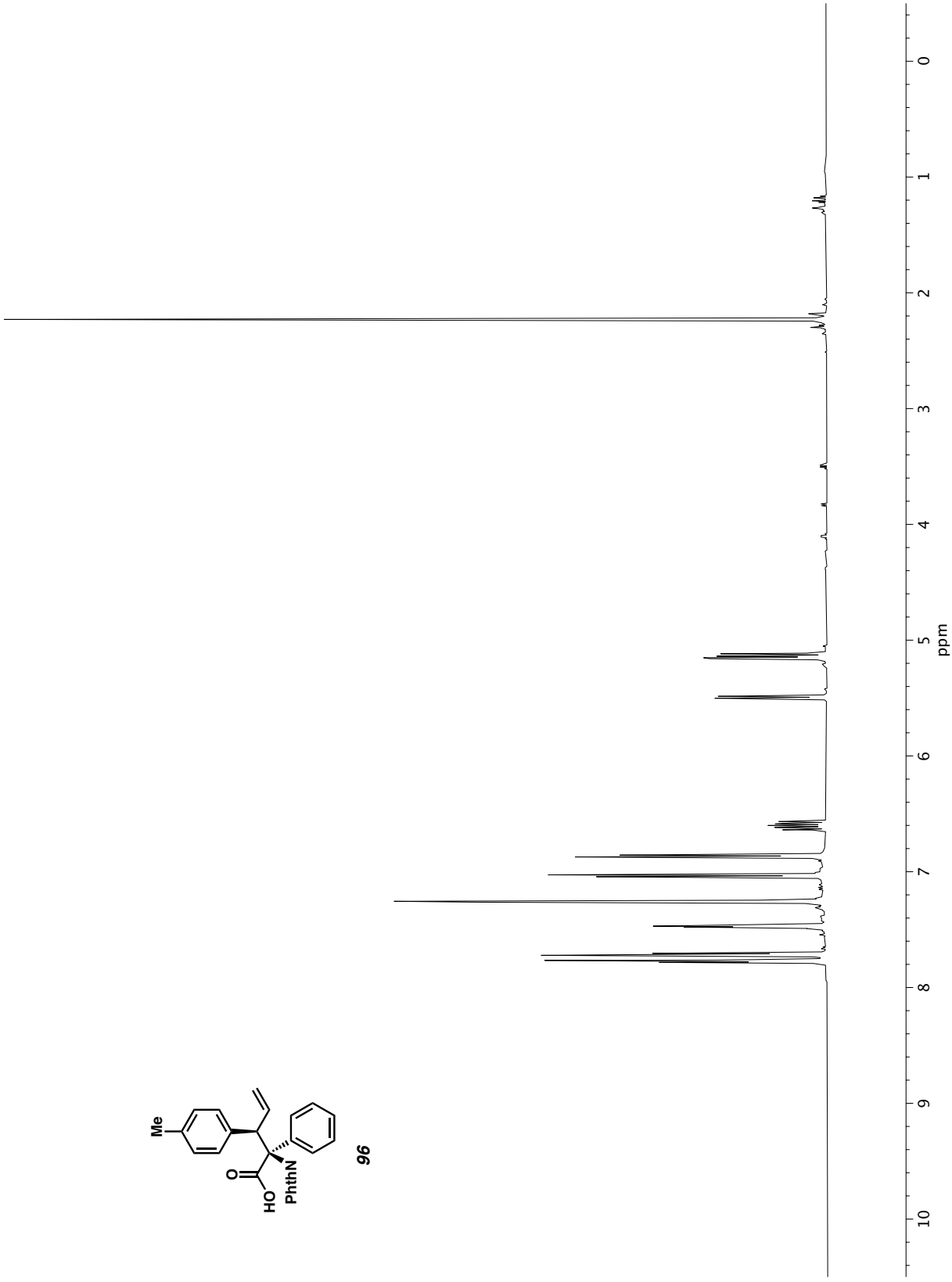

Figure A6.47 *^{1}H NMR (500 MHz, $CDCl_3$) of compound* ***96***.

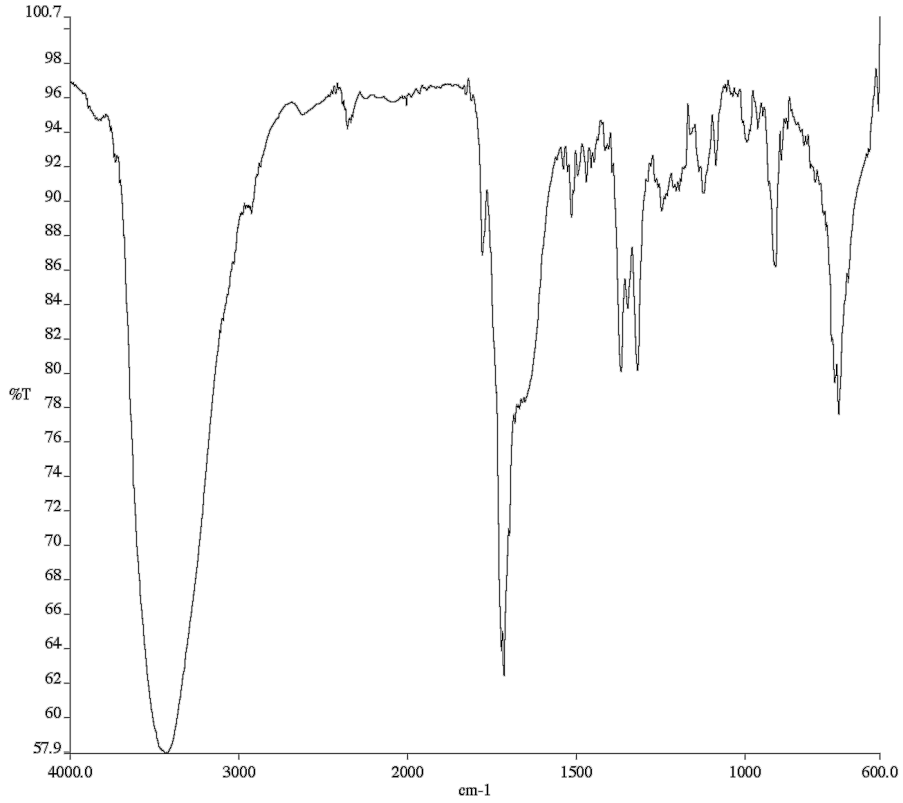

Figure A6.48 *Infrared spectrum (Thin Film, NaCl) of compound* ***96****.*

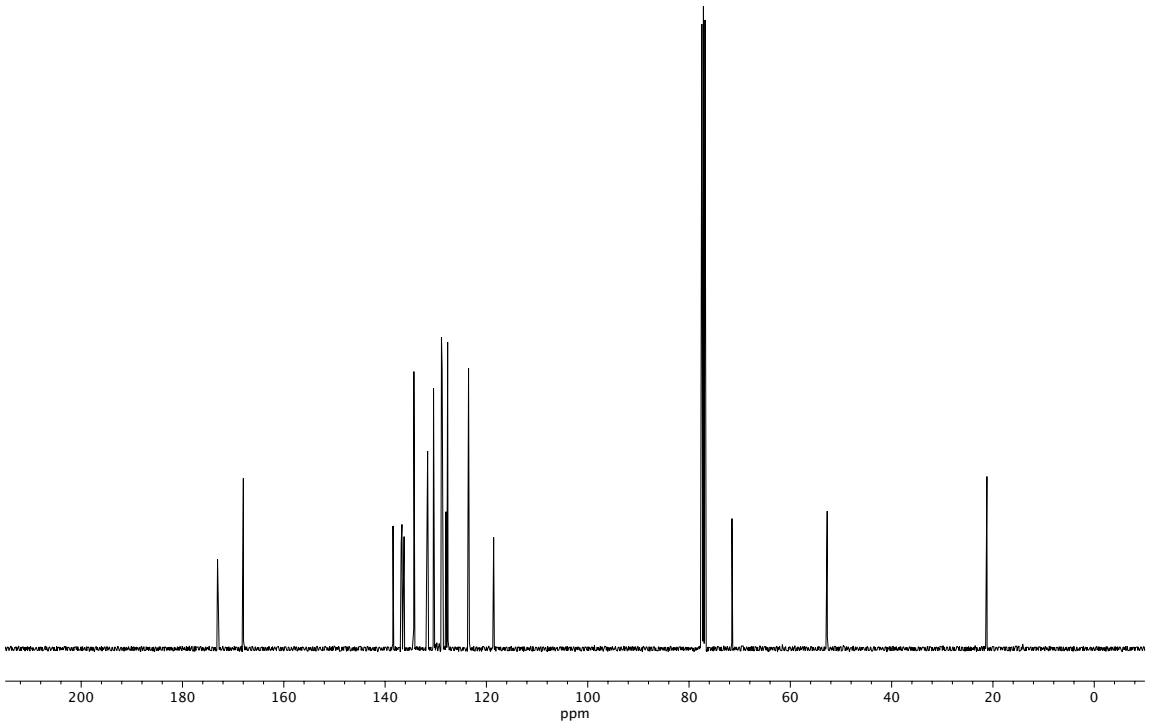

Figure A6.49 *^{13}C NMR (100 MHz, $CDCl_3$) of compound* ***96****.*

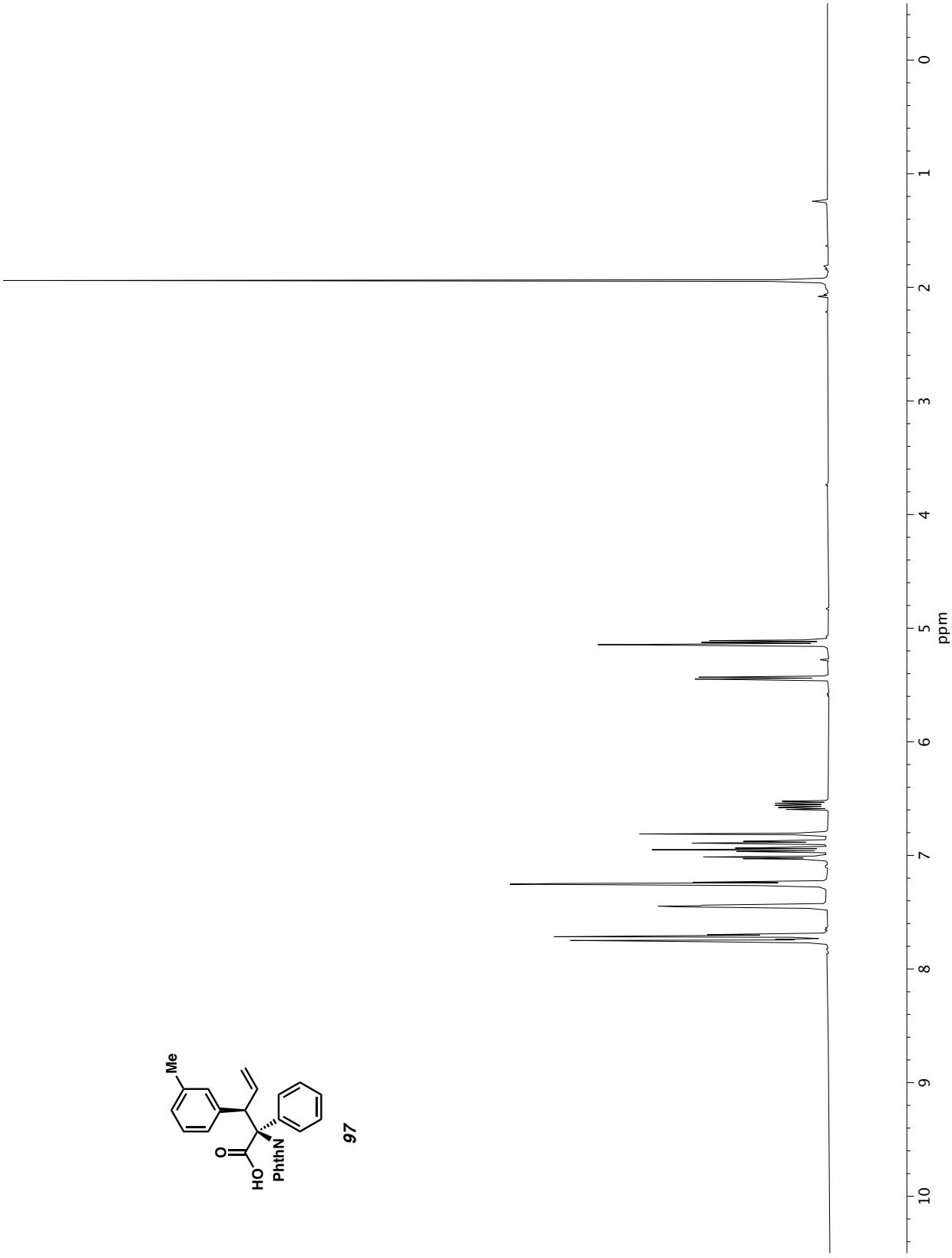

Figure A6.50 *^{1}H NMR (500 MHz, $CDCl_3$) of compound **97**.*

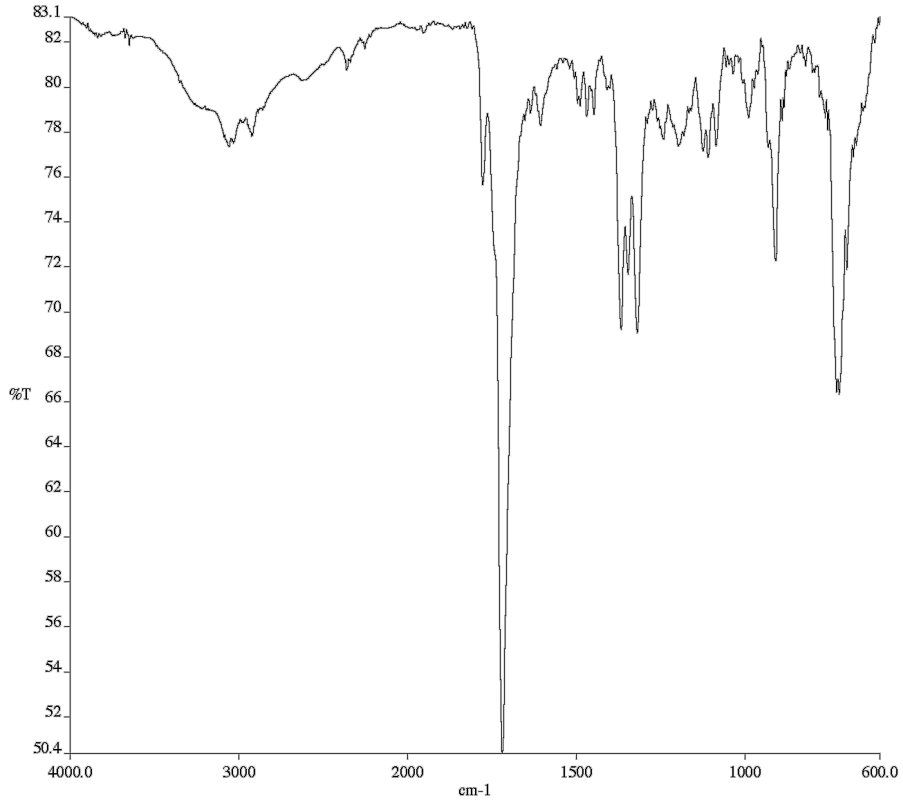

Figure A6.51 *Infrared spectrum (Thin Film, NaCl) of compound* ***97****.*

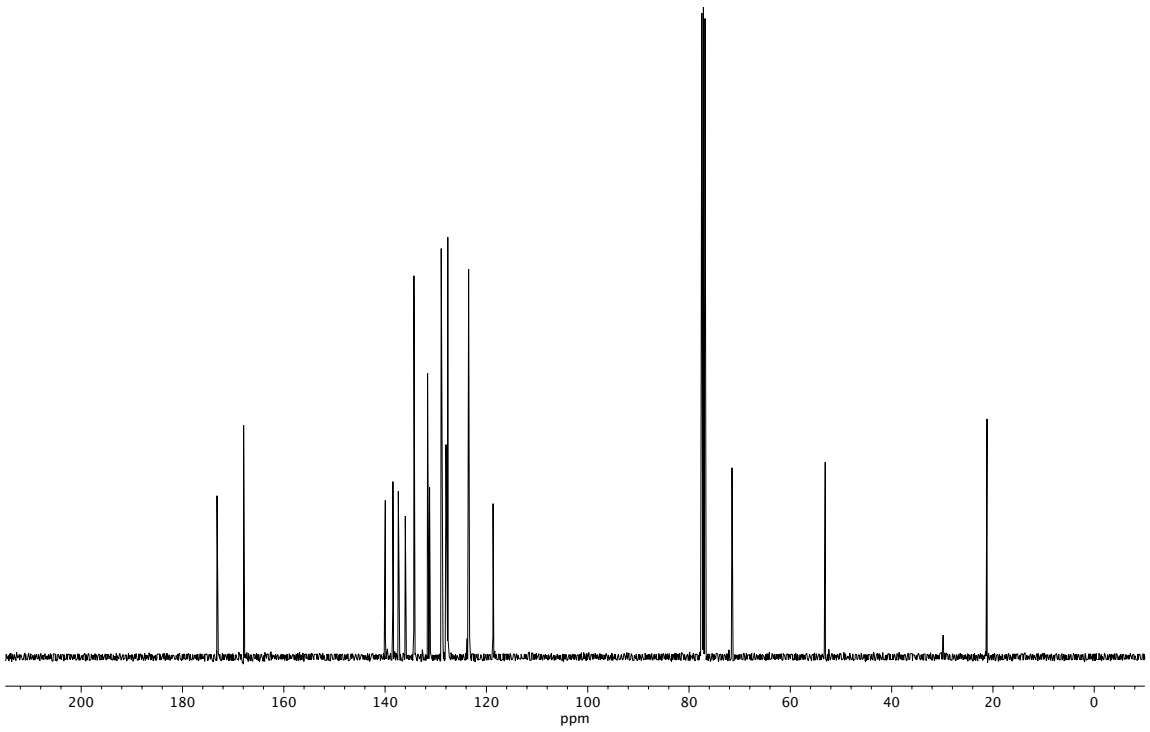

Figure A6.52 *^{13}C NMR (100 MHz, $CDCl_3$) of compound* ***97****.*

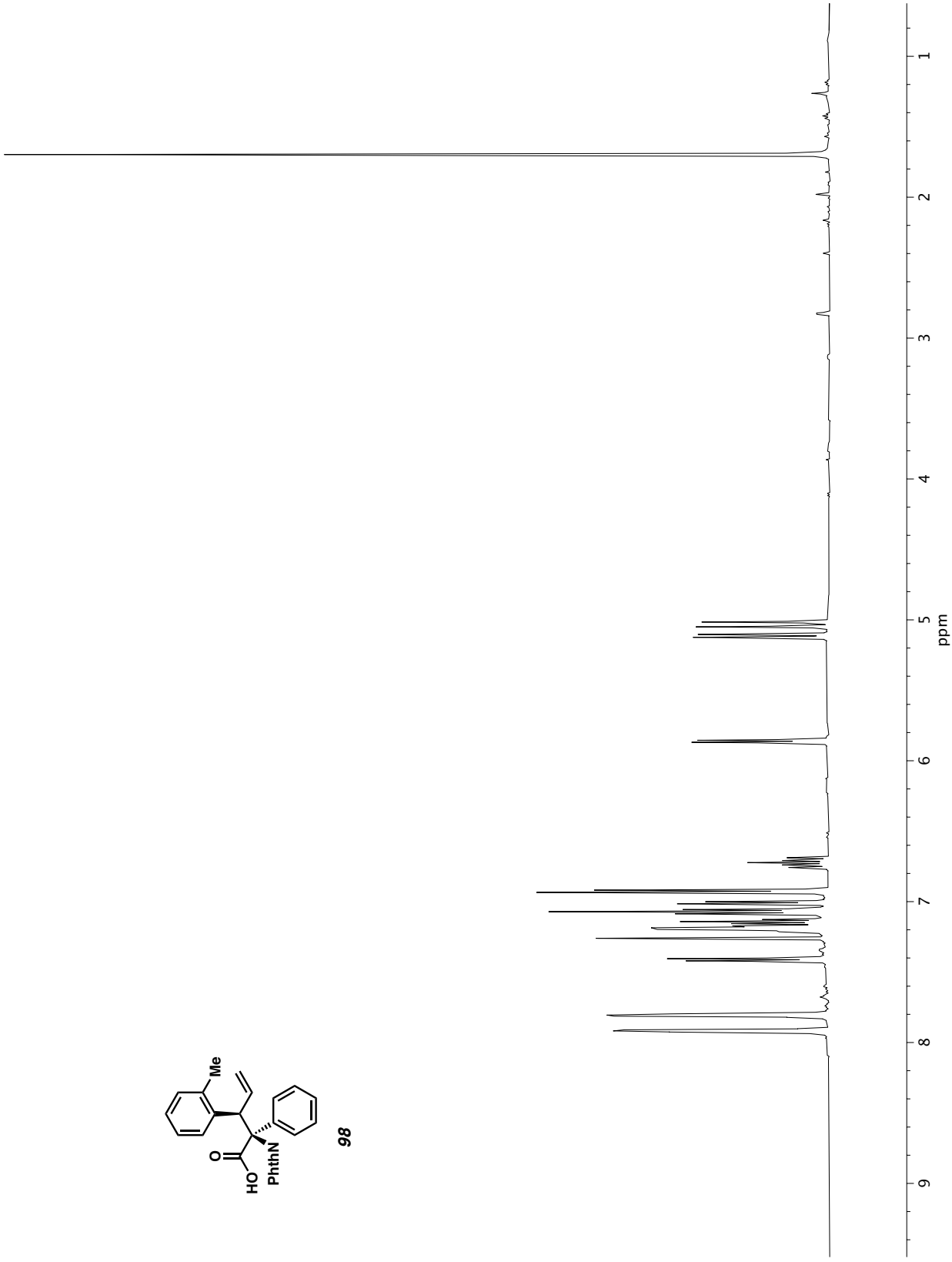

Figure A6.53 *^{1}H NMR (500 MHz, $CDCl_3$) of compound **98**.*

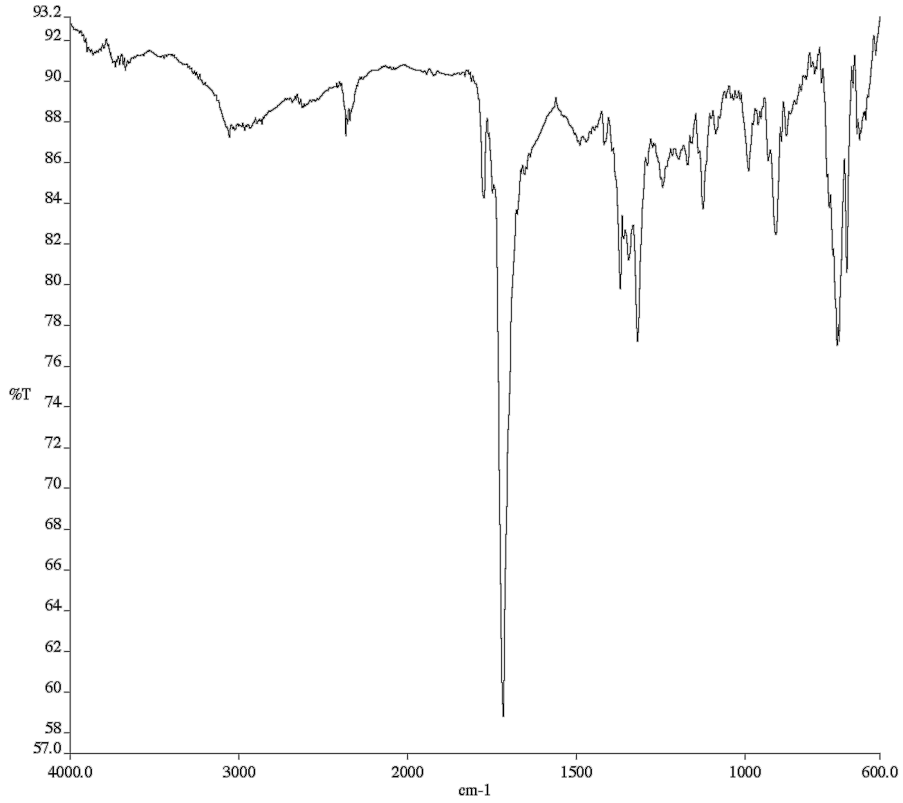

Figure A6.54 *Infrared spectrum (Thin Film, NaCl) of compound* ***98****.*

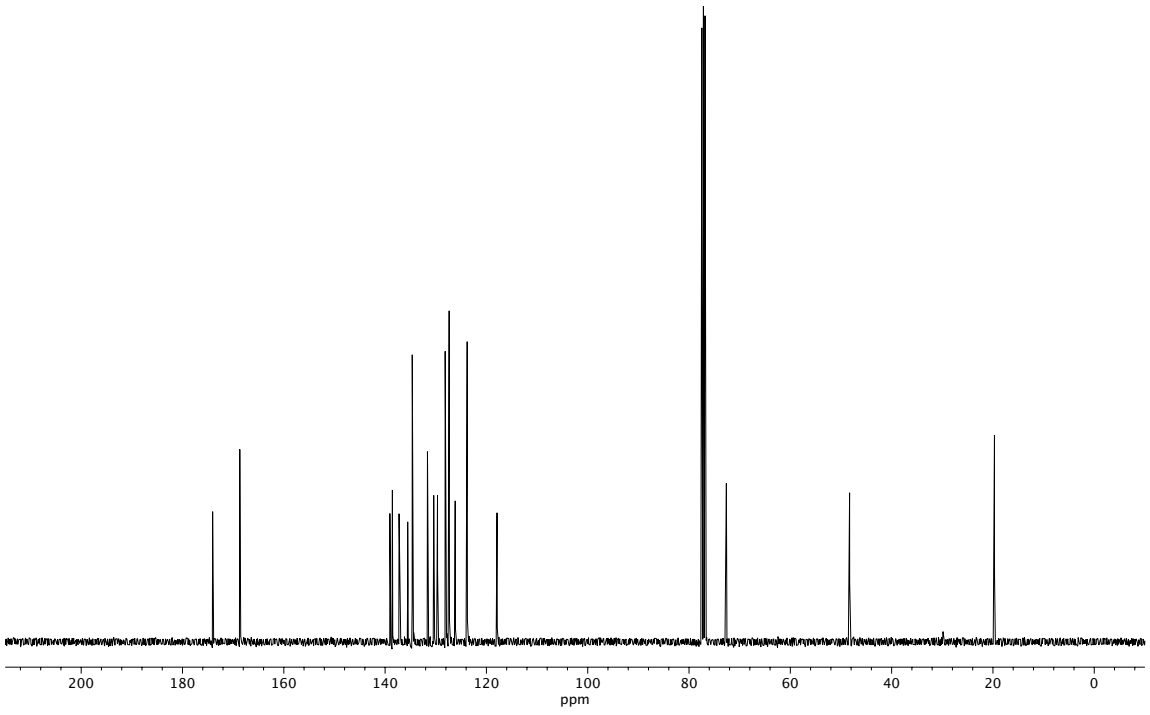

Figure A6.55 *^{13}C NMR (100 MHz, $CDCl_3$) of compound* ***98****.*

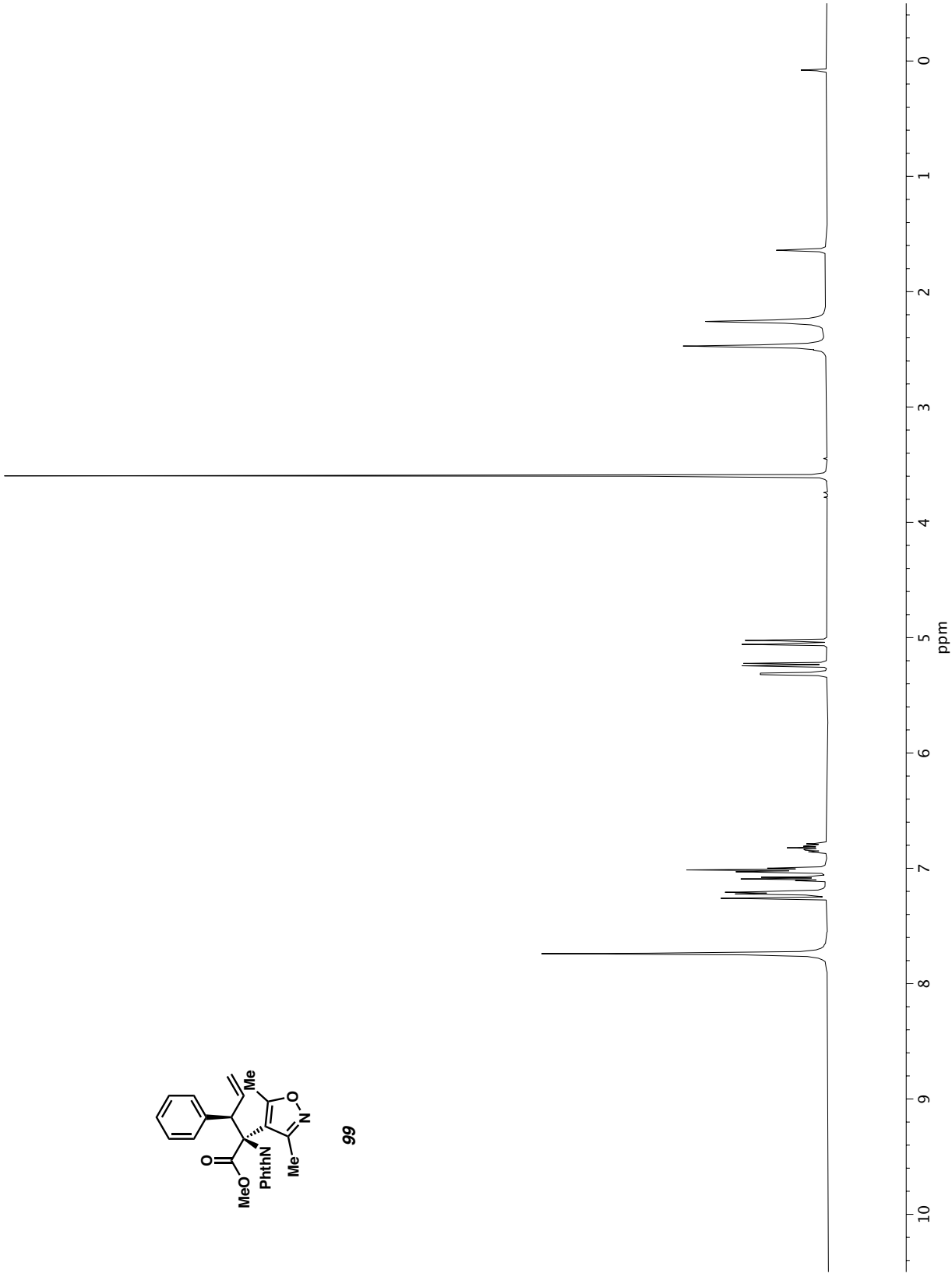

Figure A6.56 *^{1}H NMR (500 MHz, $CDCl_3$) of compound **99**.*

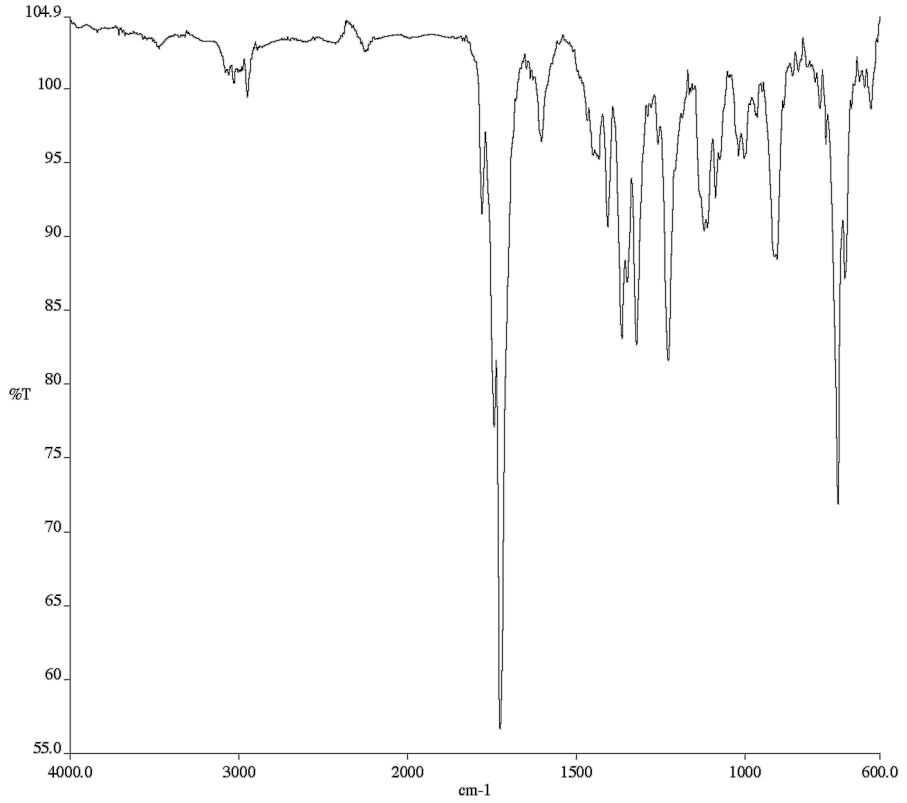

Figure A6.57 *Infrared spectrum (Thin Film, NaCl) of compound* ***99****.*

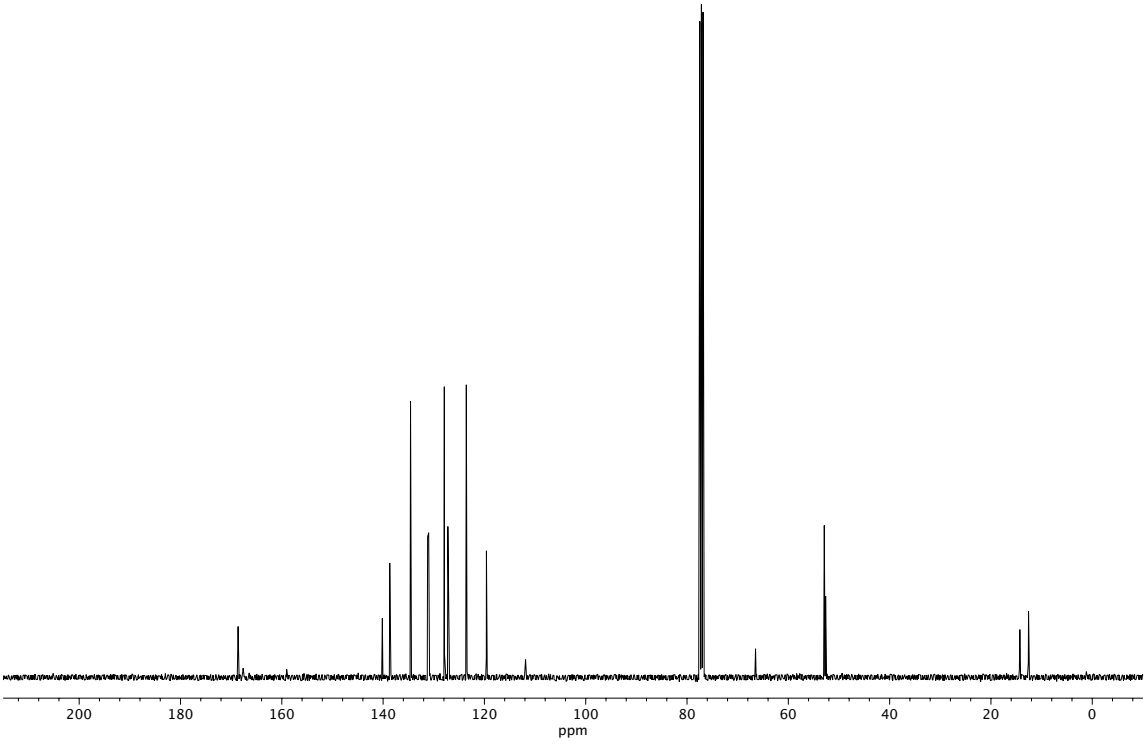

Figure A6.58 *^{13}C NMR (100 MHz, $CDCl_3$) of compound* ***99****.*

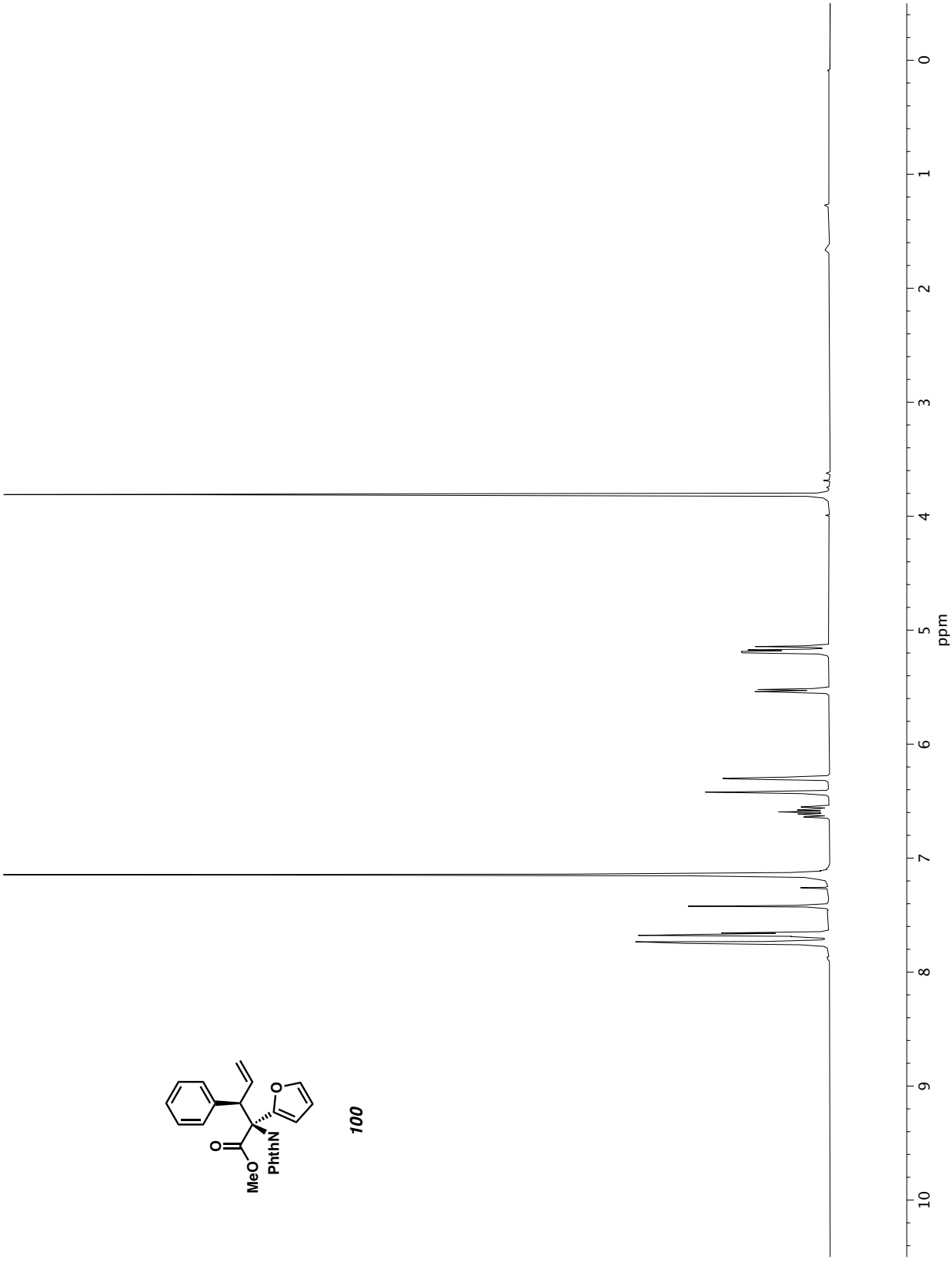

Figure A6.59 *^1H NMR (500 MHz, $CDCl_3$) of compound* ***100***.

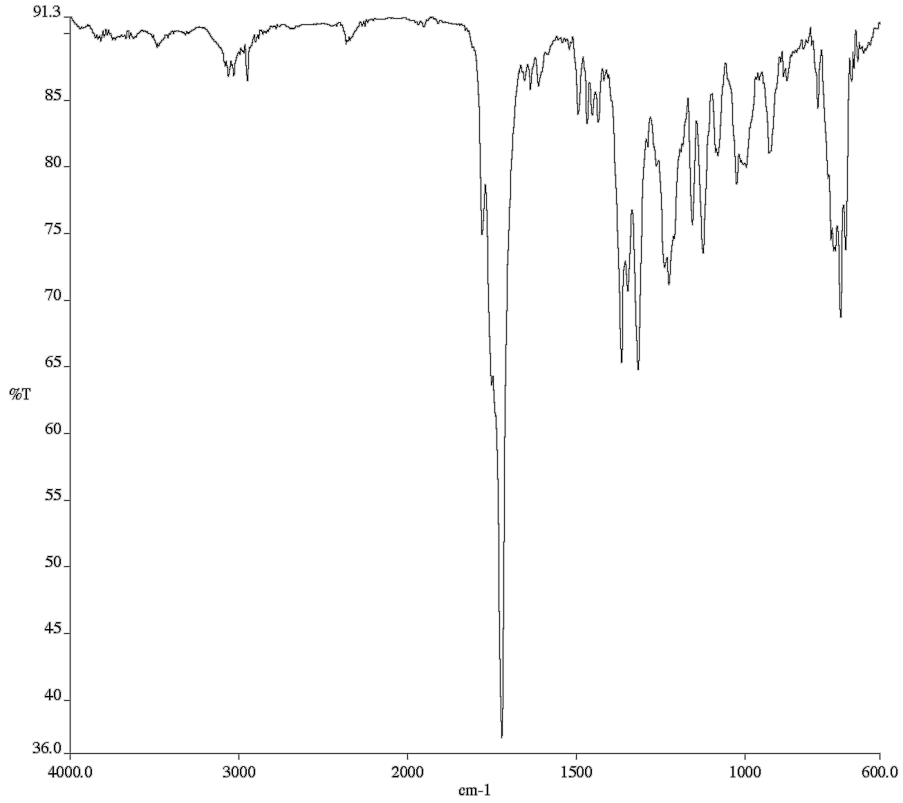

Figure A6.60 *Infrared spectrum (Thin Film, NaCl) of compound* ***100****.*

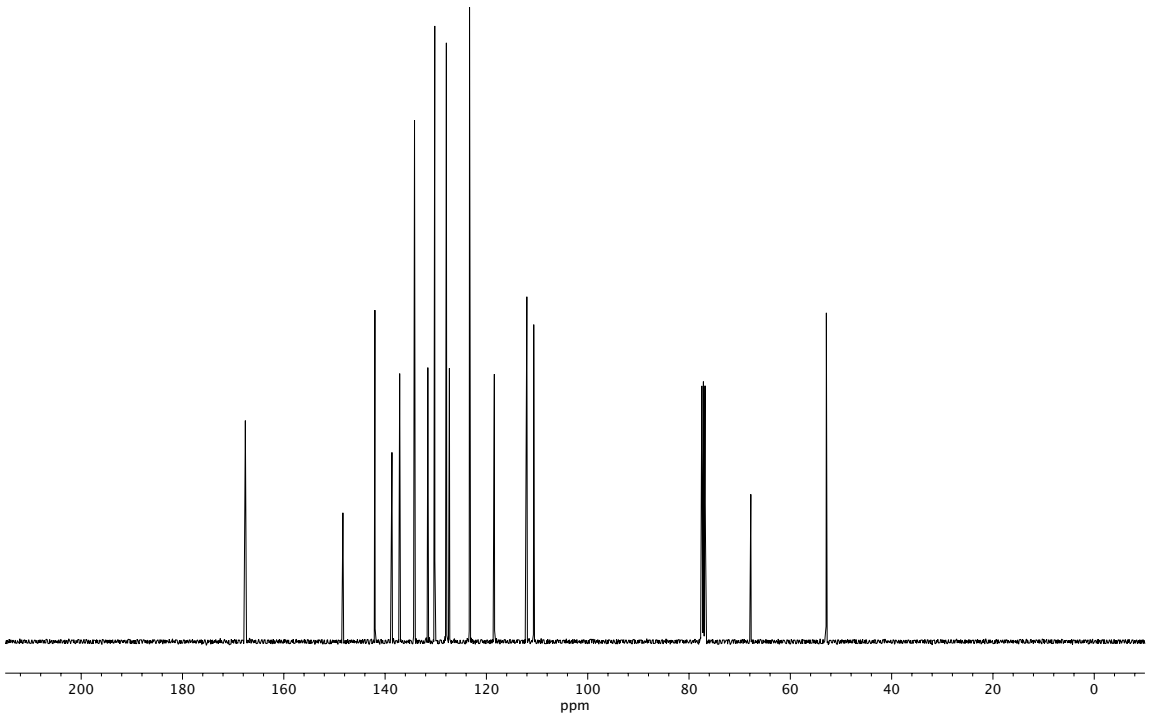

Figure A6.61 *^{13}C NMR (100 MHz, $CDCl_3$) of compound* ***100****.*

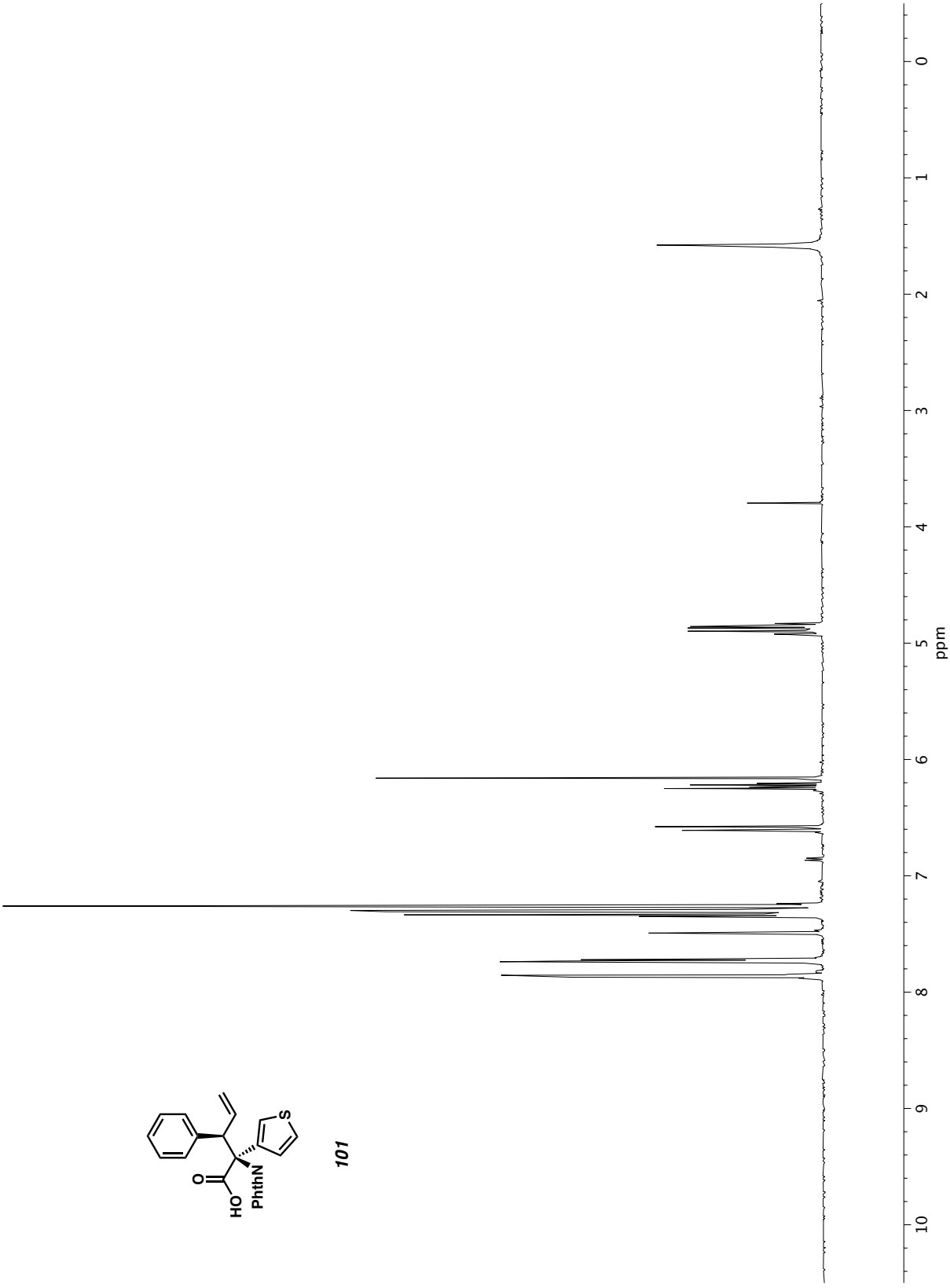

Figure A6.62 *^1H NMR (500 MHz, $CDCl_3$) of compound* ***101***.

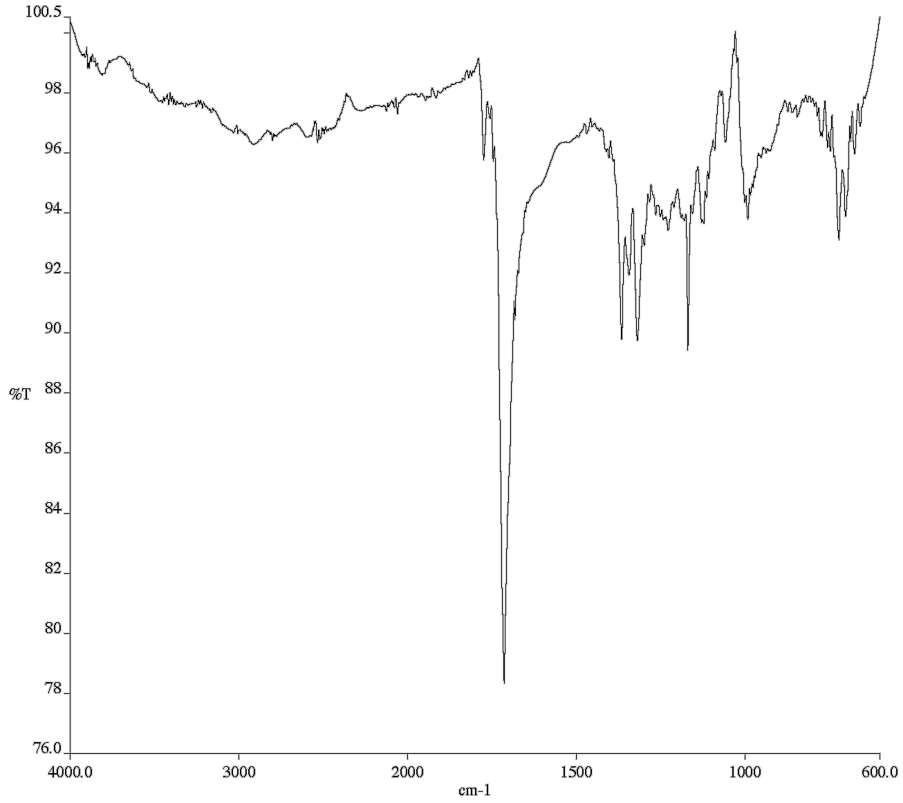

Figure A6.63 *Infrared spectrum (Thin Film, NaCl) of compound* ***101****.*

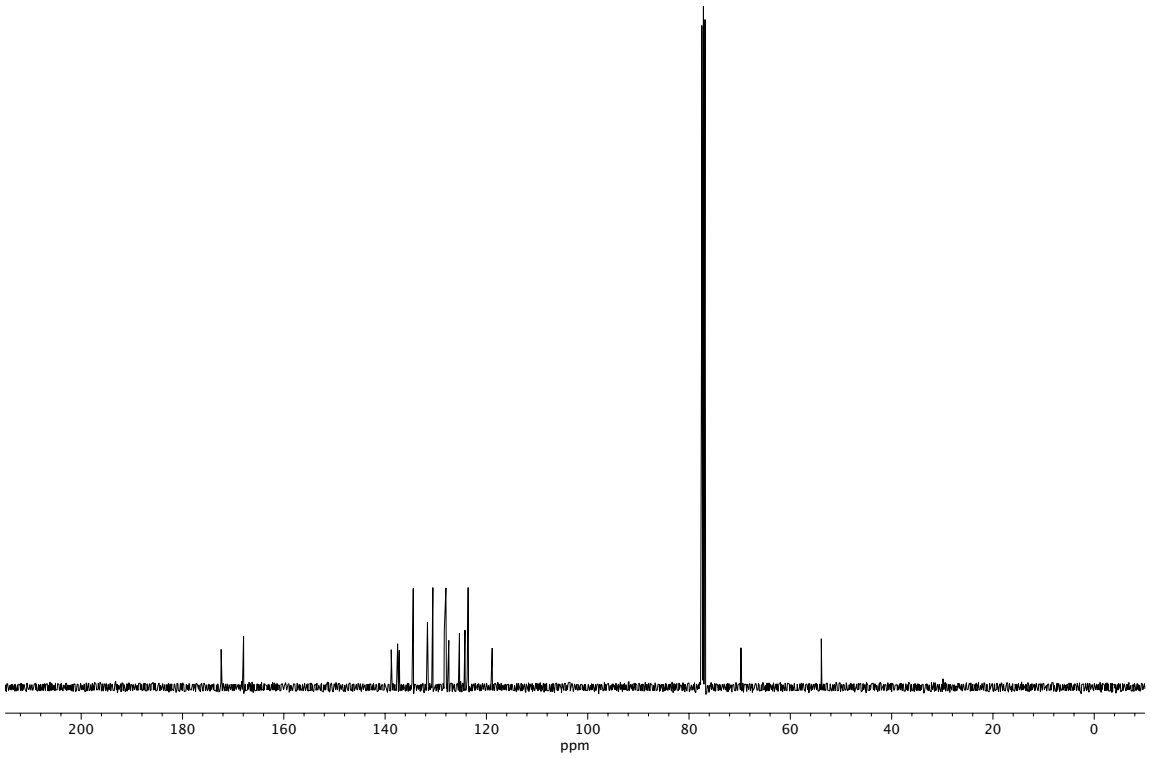

Figure A6.64 *^{13}C NMR (100 MHz, $CDCl_3$) of compound* ***101****.*

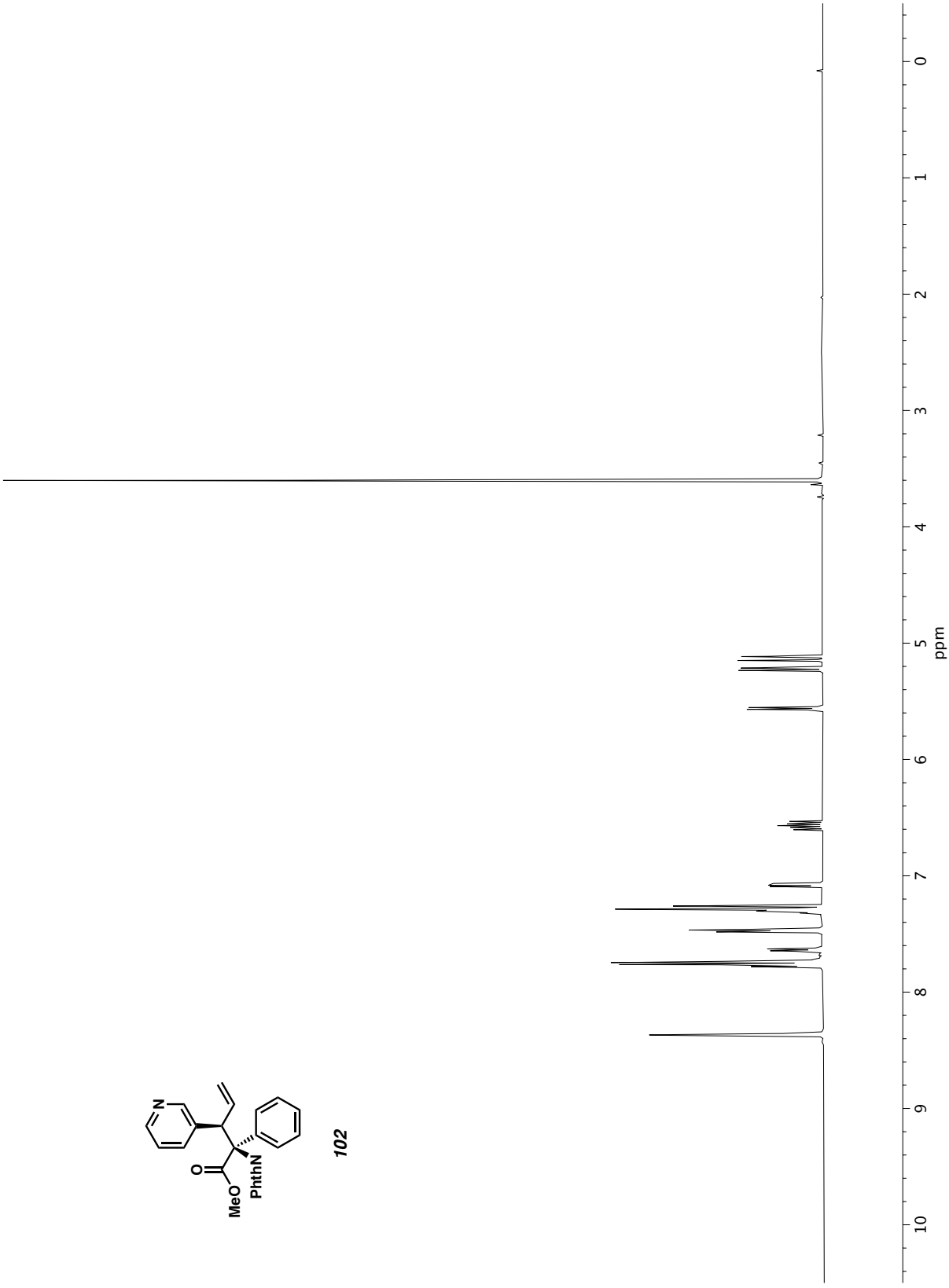

Figure A6.65 *^1H NMR (500 MHz, $CDCl_3$) of compound* ***102***.

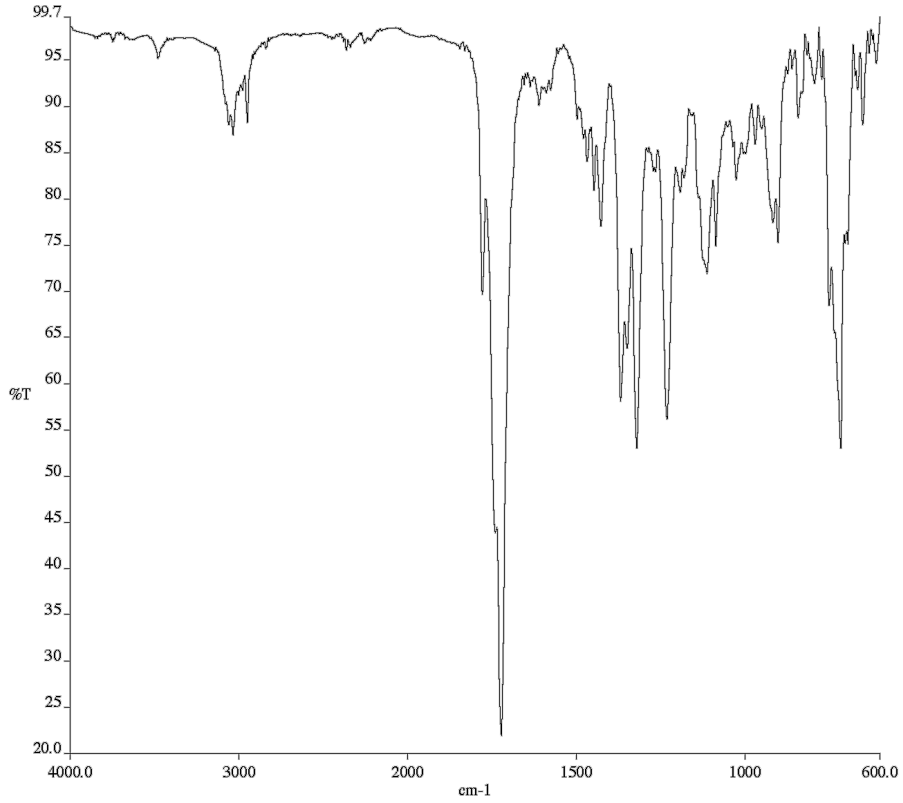

Figure A6.66 *Infrared spectrum (Thin Film, NaCl) of compound* ***102****.*

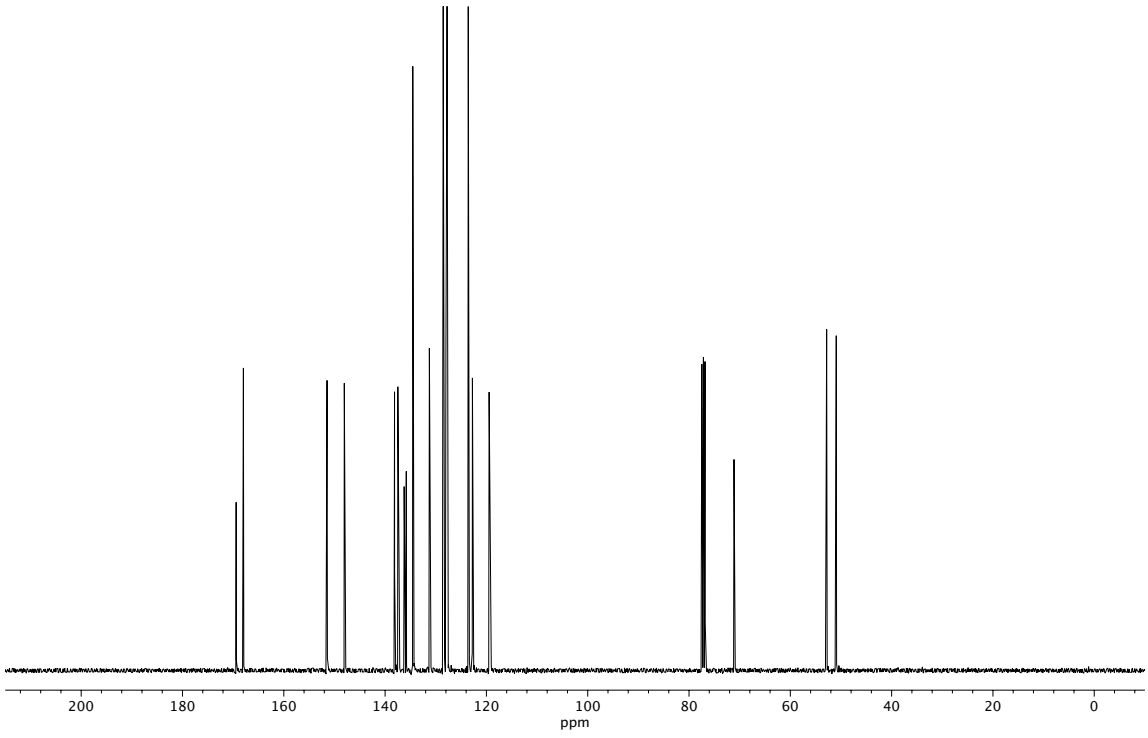

Figure A6.67 *^{13}C NMR (100 MHz, $CDCl_3$) of compound* ***102****.*

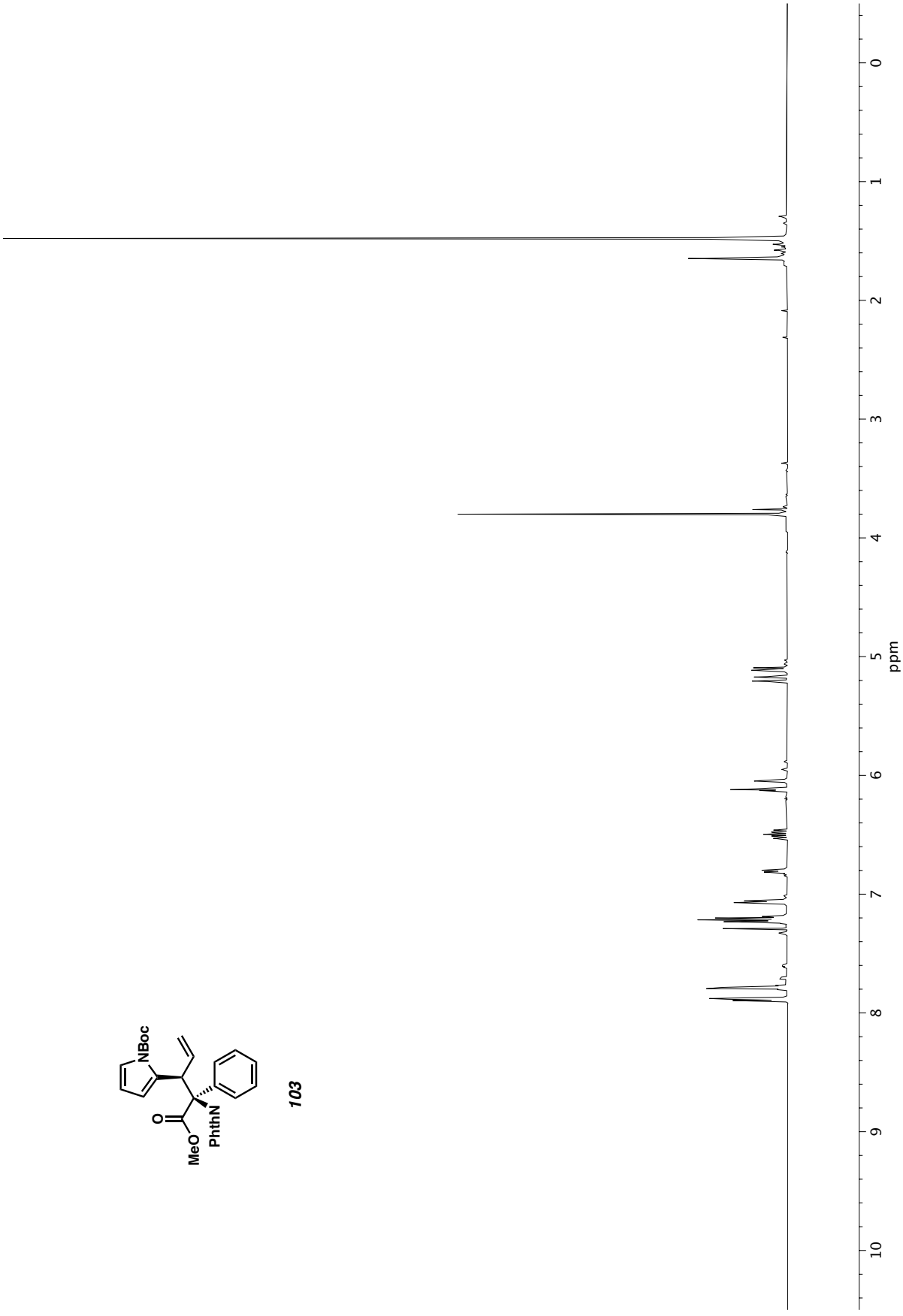

103

Figure A6.68 *^1H NMR (500 MHz, $CDCl_3$) of compound* ***103***.

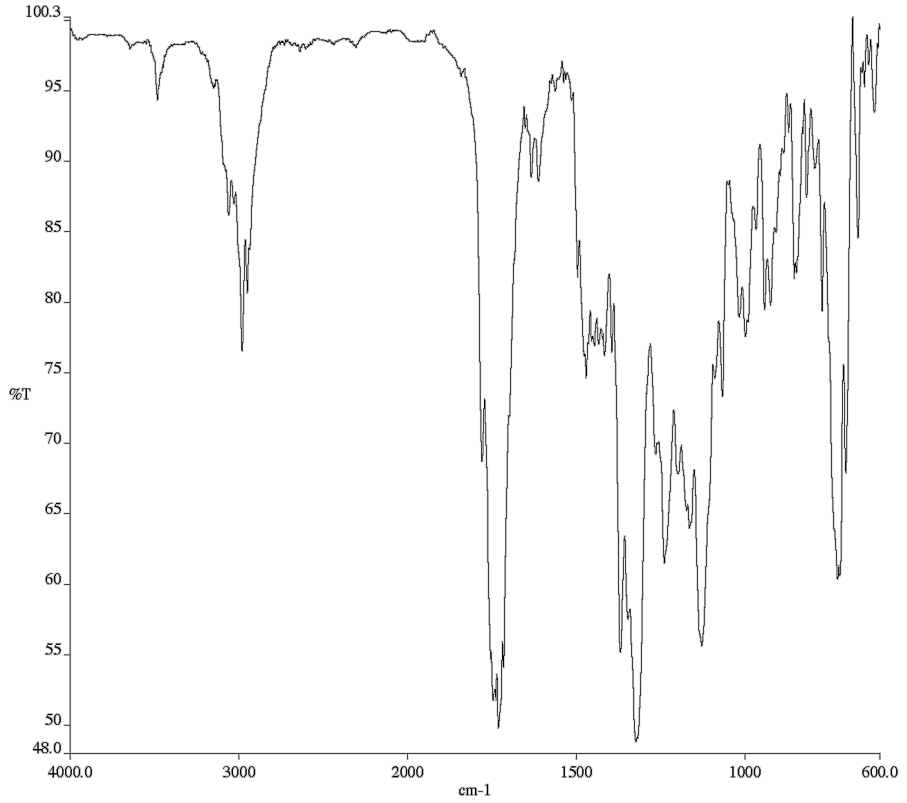

Figure A6.69 *Infrared spectrum (Thin Film, NaCl) of compound* ***103****.*

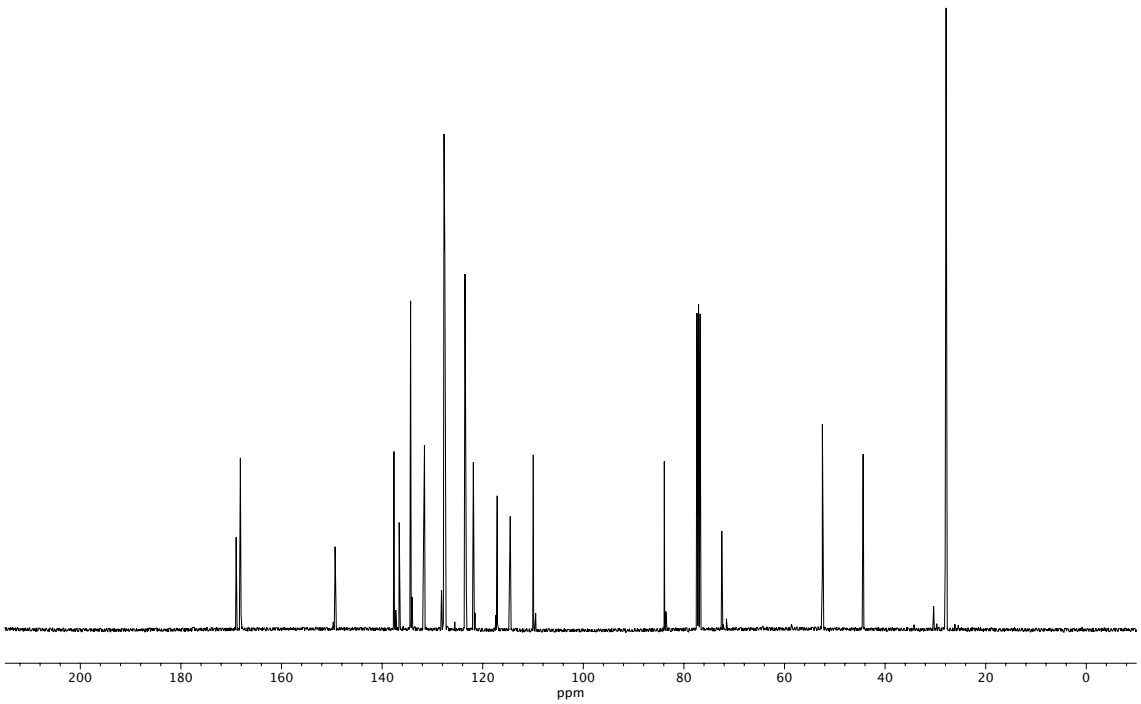

Figure A6.70 *^{13}C NMR (100 MHz, $CDCl_3$) of compound* ***103****.*

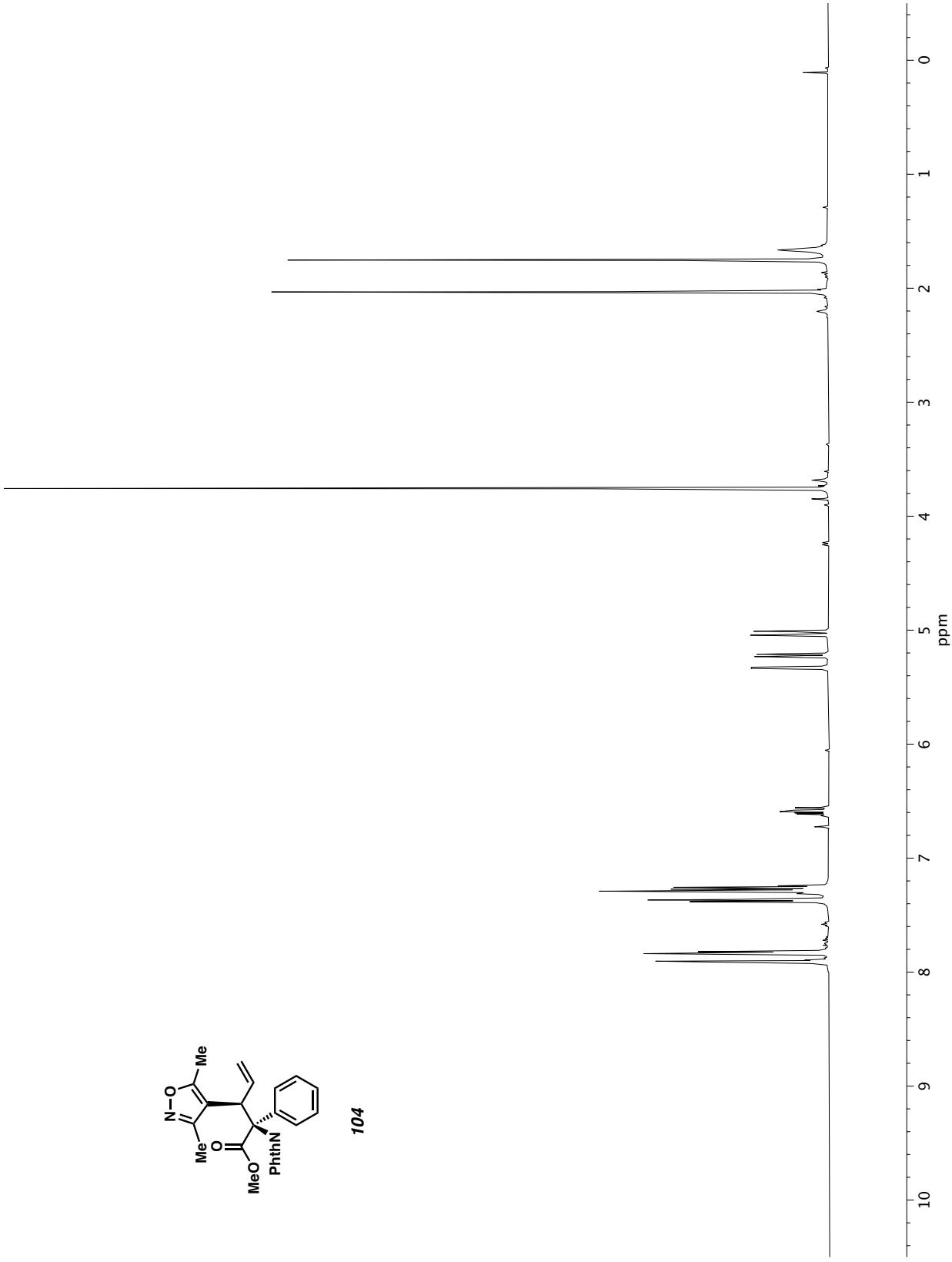

104

Figure A6.71 *^{1}H NMR (500 MHz, $CDCl_3$) of compound* ***104****.*

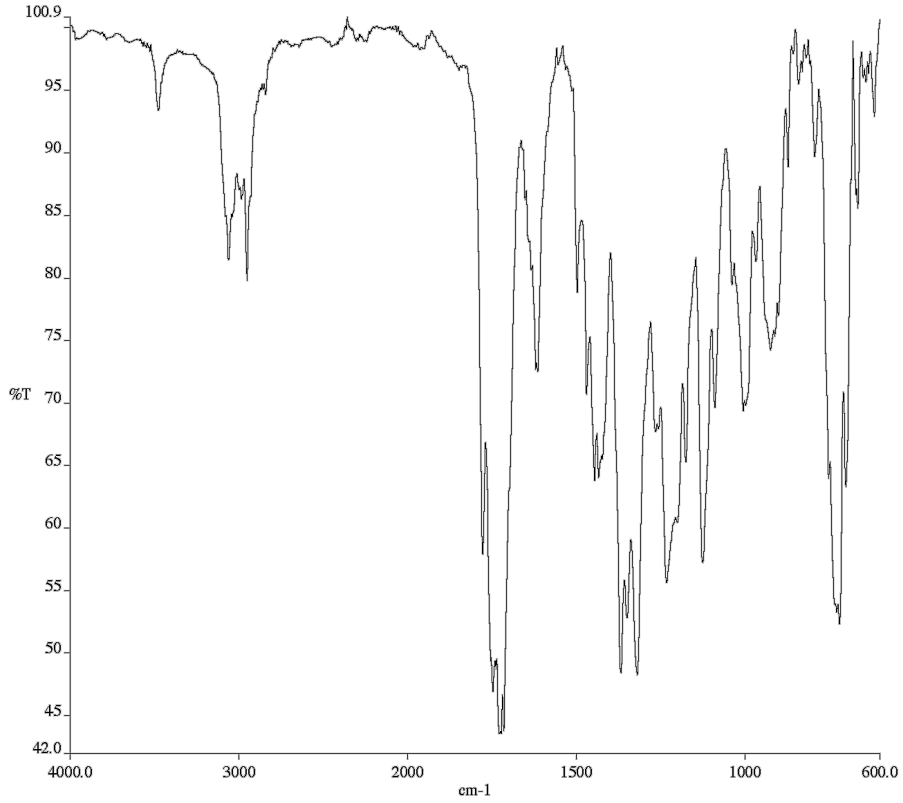

Figure A6.72 *Infrared spectrum (Thin Film, NaCl) of compound* ***104****.*

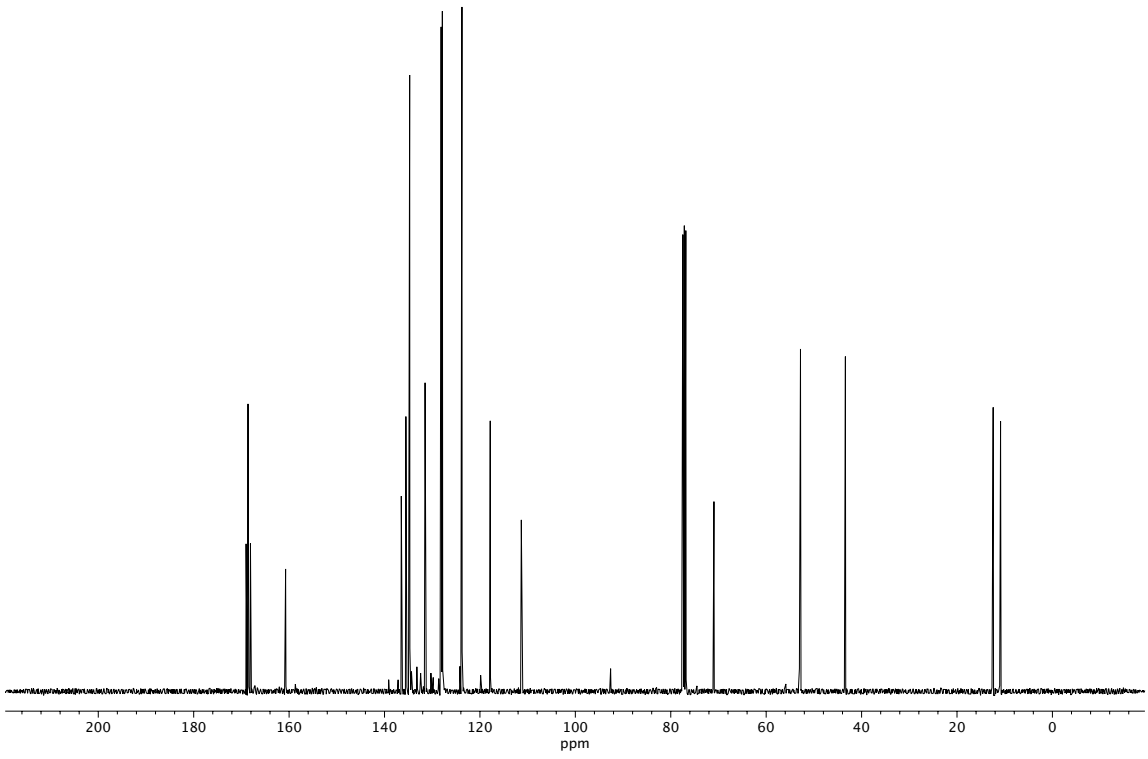

Figure A6.73 *^{13}C NMR (100 MHz, $CDCl_3$) of compound* ***104****.*

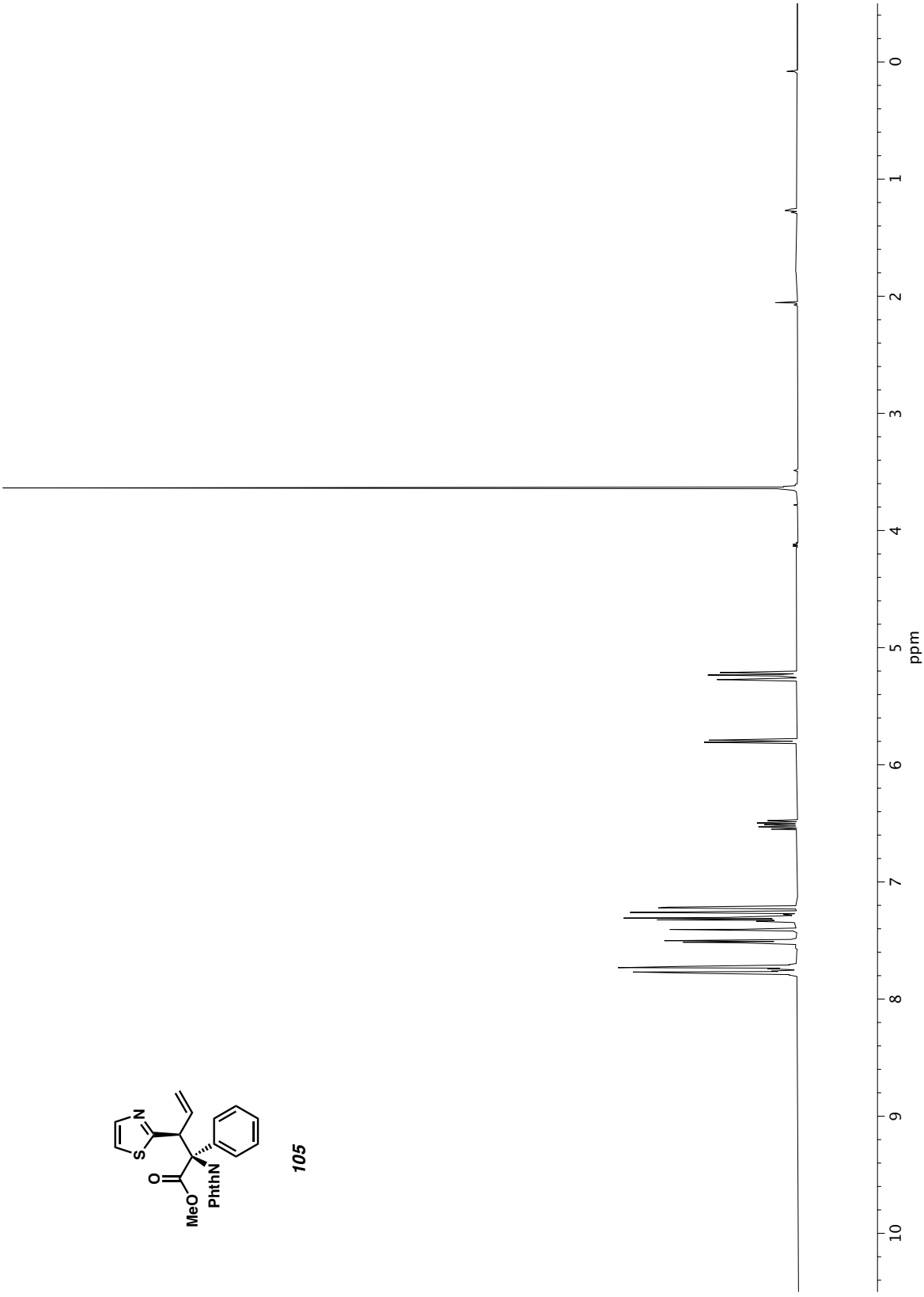

105

Figure A6.74 *^1H NMR (500 MHz, $CDCl_3$) of compound* ***105***.

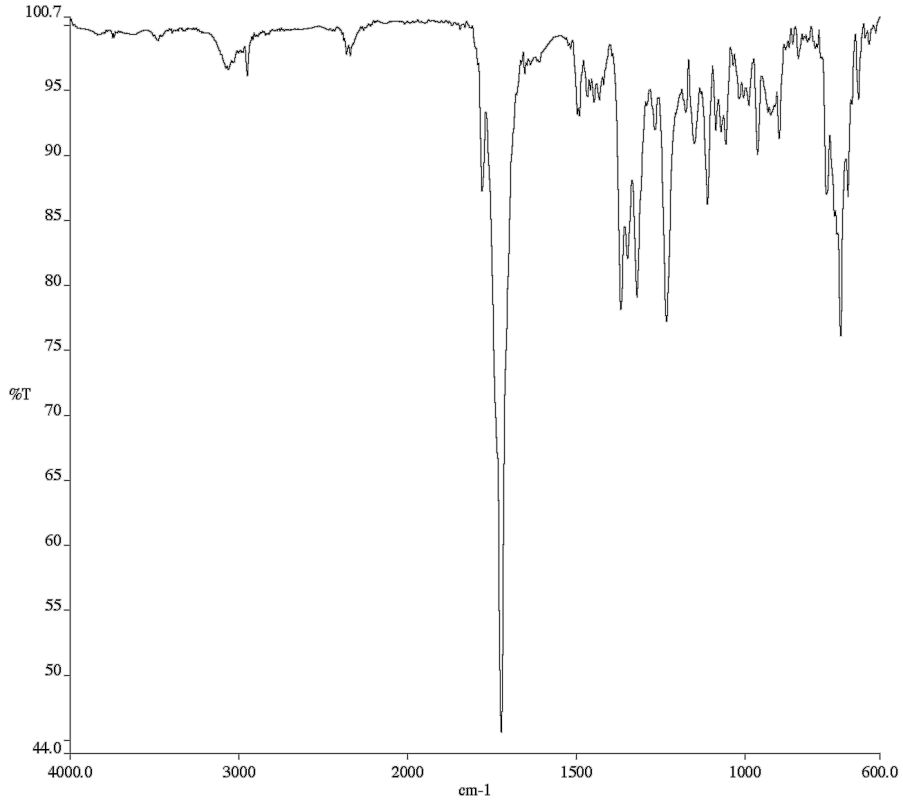

Figure A6.75 *Infrared spectrum (Thin Film, NaCl) of compound* ***105****.*

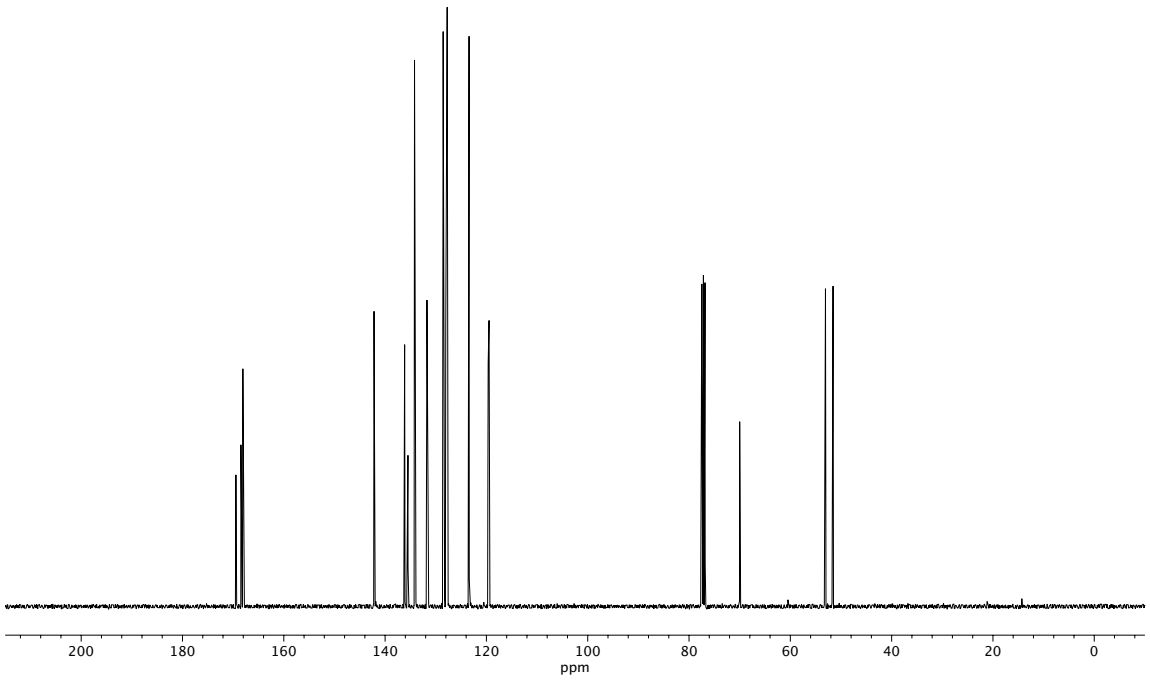

Figure A6.76 *^{13}C NMR (100 MHz, $CDCl_3$) of compound* ***105****.*

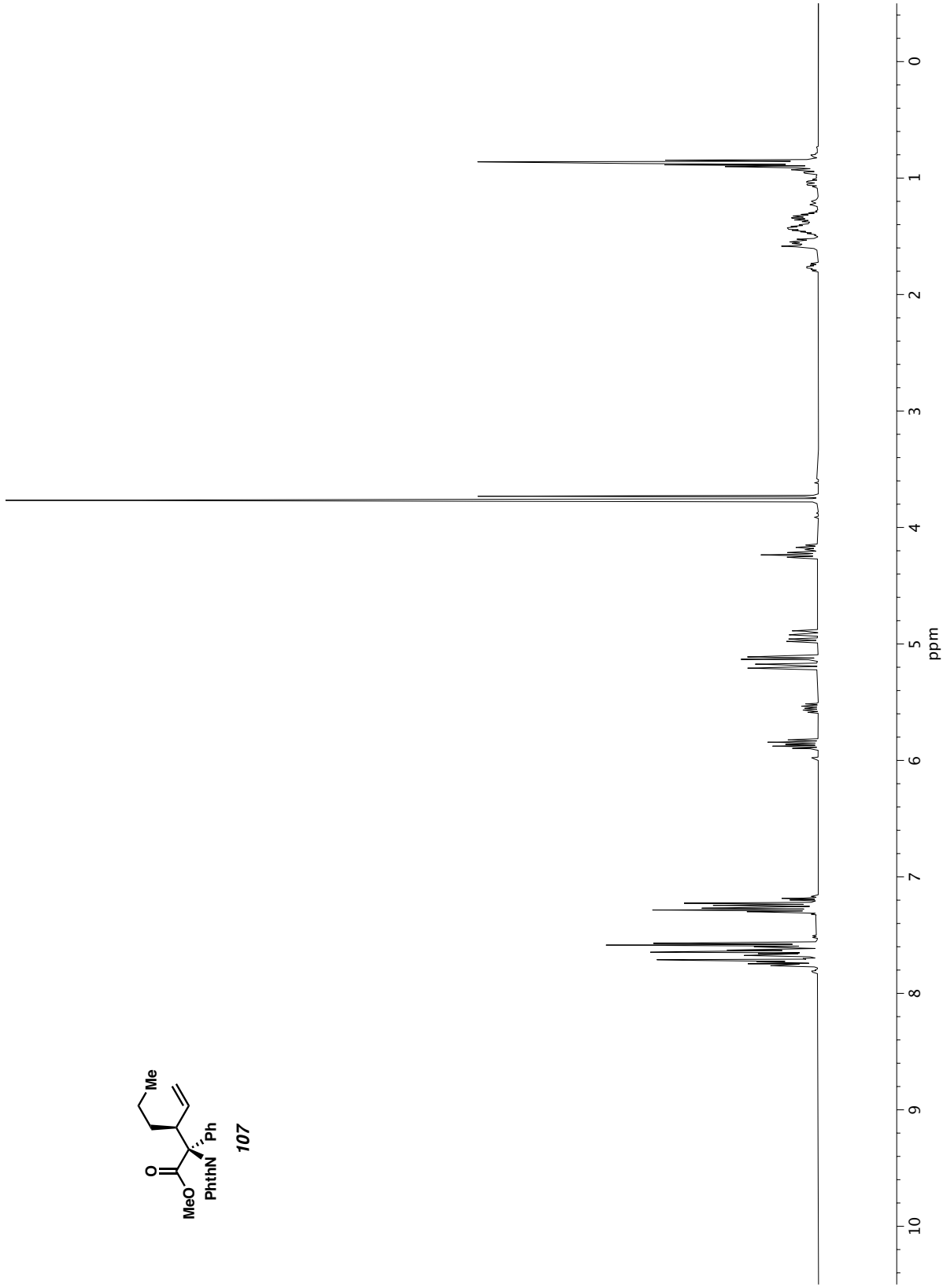

Figure A6.77 *^{1}H NMR (500 MHz, $CDCl_3$) of compound **107**.*

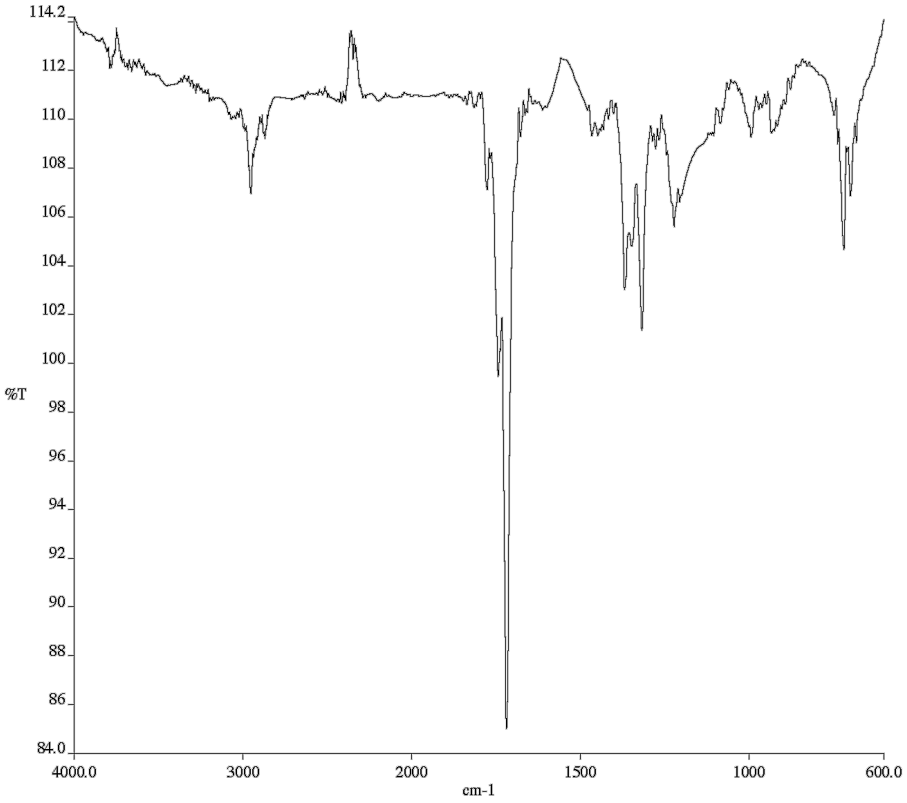

Figure A6.78 *Infrared spectrum (Thin Film, NaCl) of compound* ***107****.*

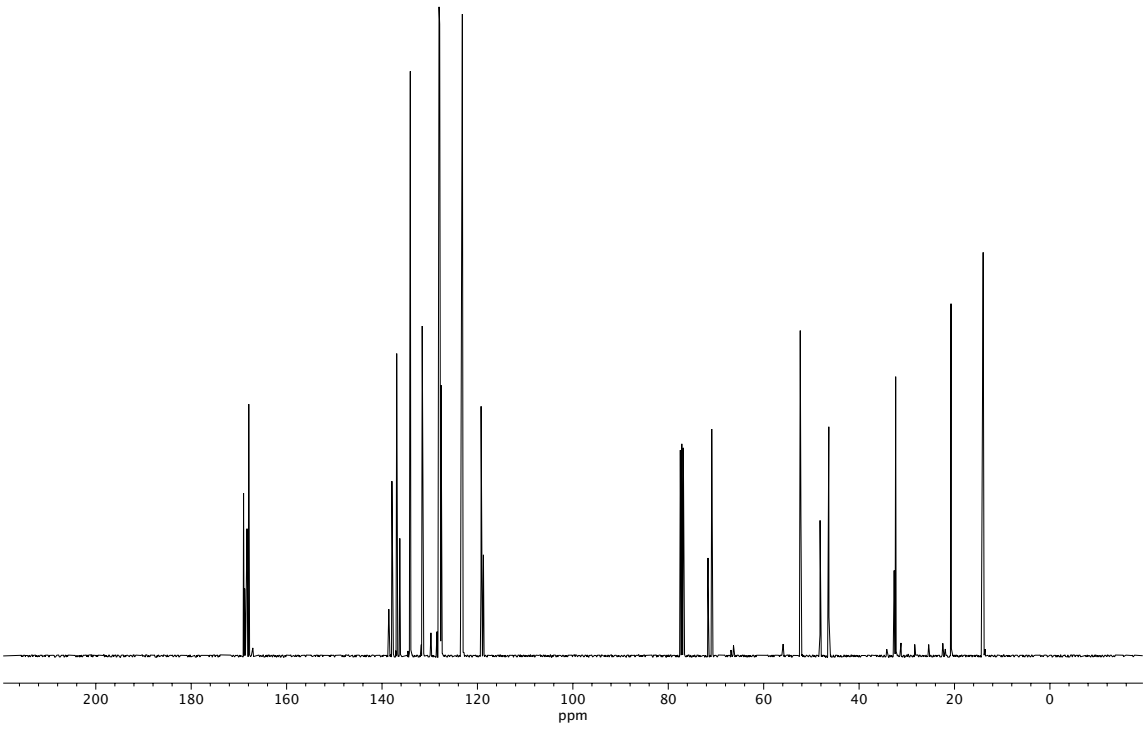

Figure A6.79 *^{13}C NMR (100 MHz, $CDCl_3$) of compound* ***107****.*

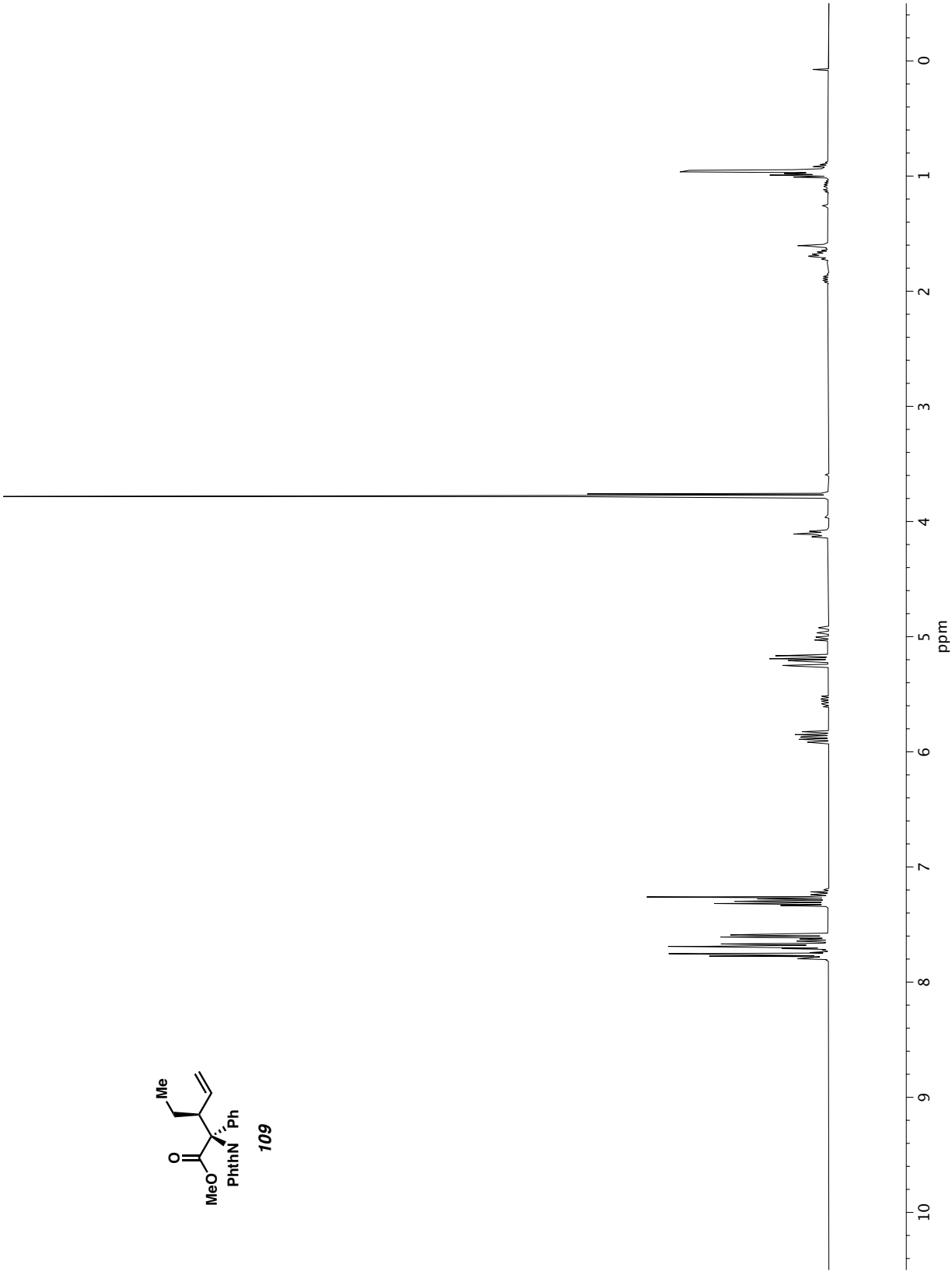

Figure A6.80 *^1H NMR (500 MHz, $CDCl_3$) of compound **109**.*

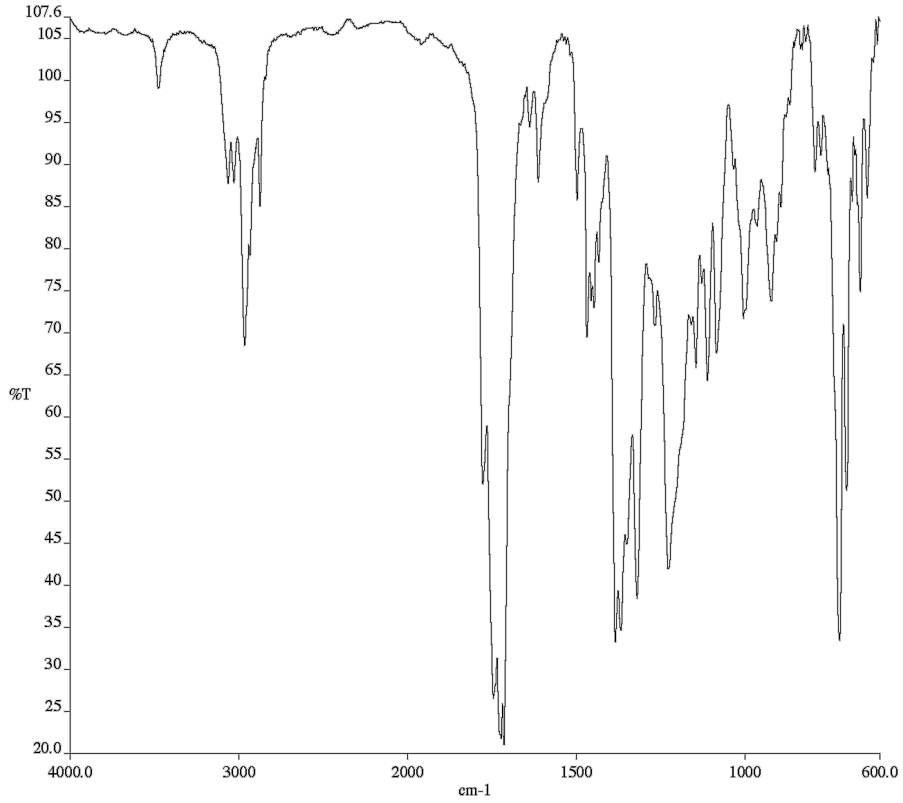

Figure A6.81 *Infrared spectrum (Thin Film, NaCl) of compound* ***109****.*

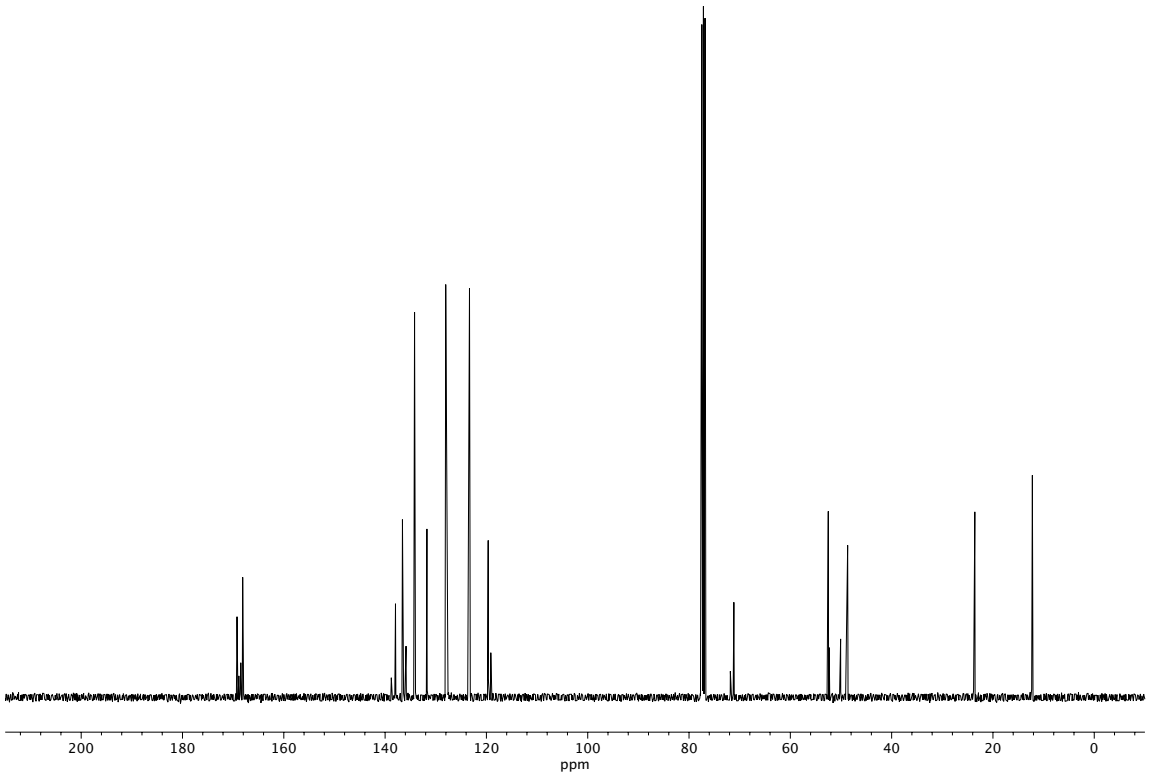

Figure A6.82 *^{13}C NMR (100 MHz, $CDCl_3$) of compound* ***109****.*

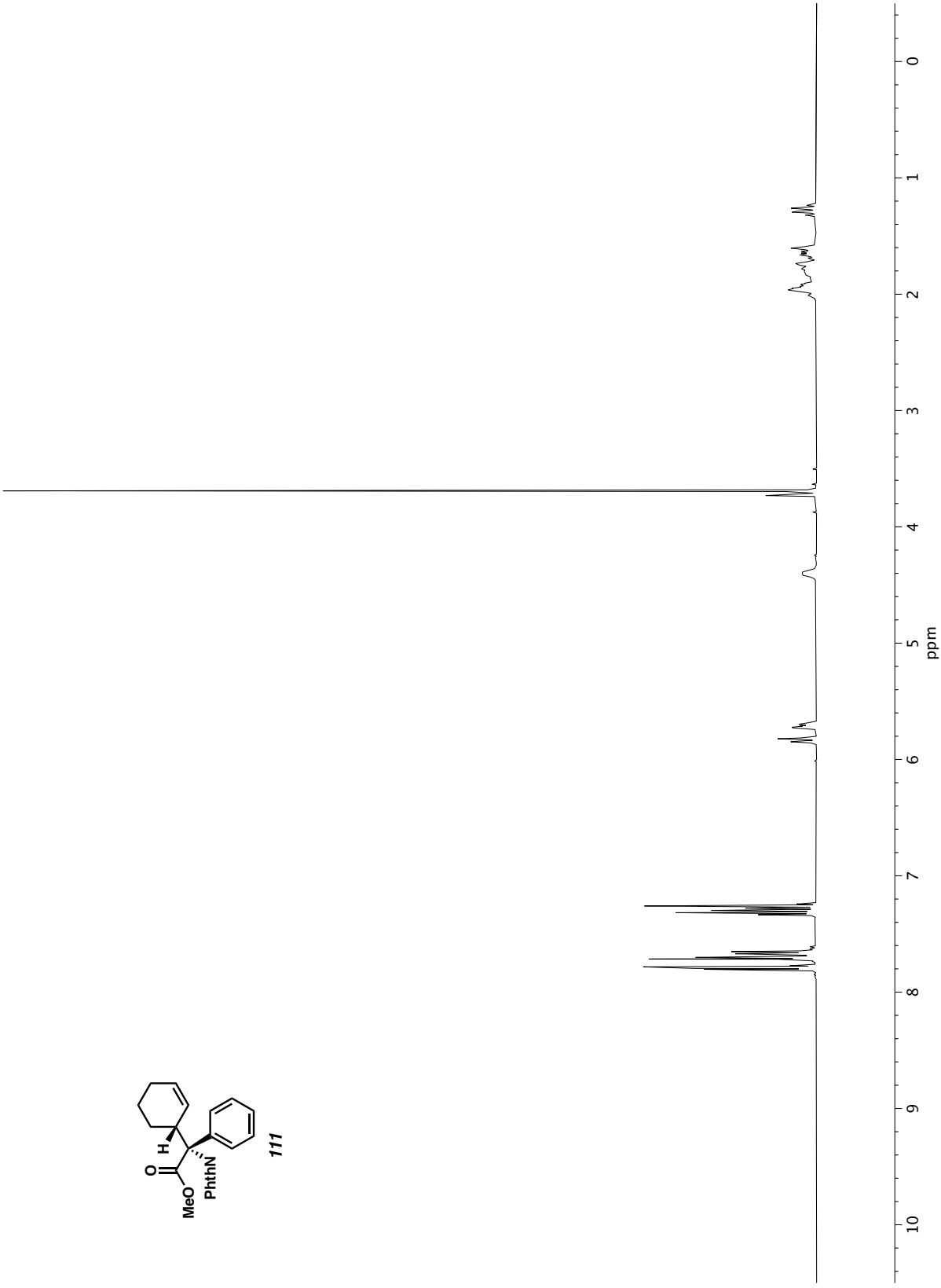

Figure A6.83 *^{1}H NMR (500 MHz, $CDCl_3$) of compound **111**.*

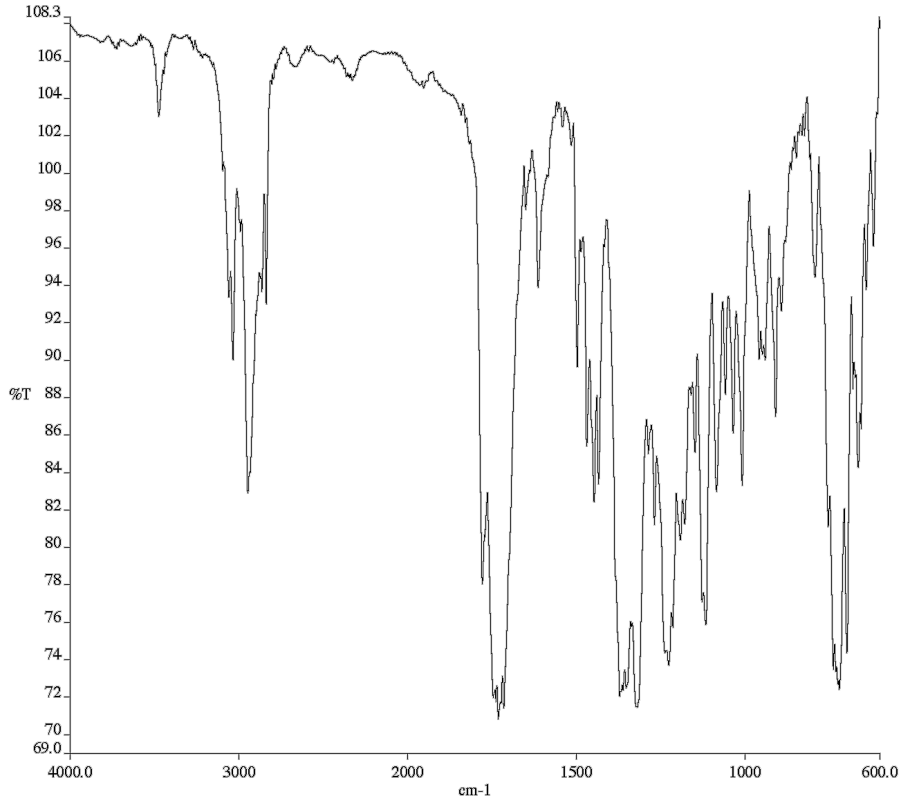

Figure A6.84 *Infrared spectrum (Thin Film, NaCl) of compound* ***111****.*

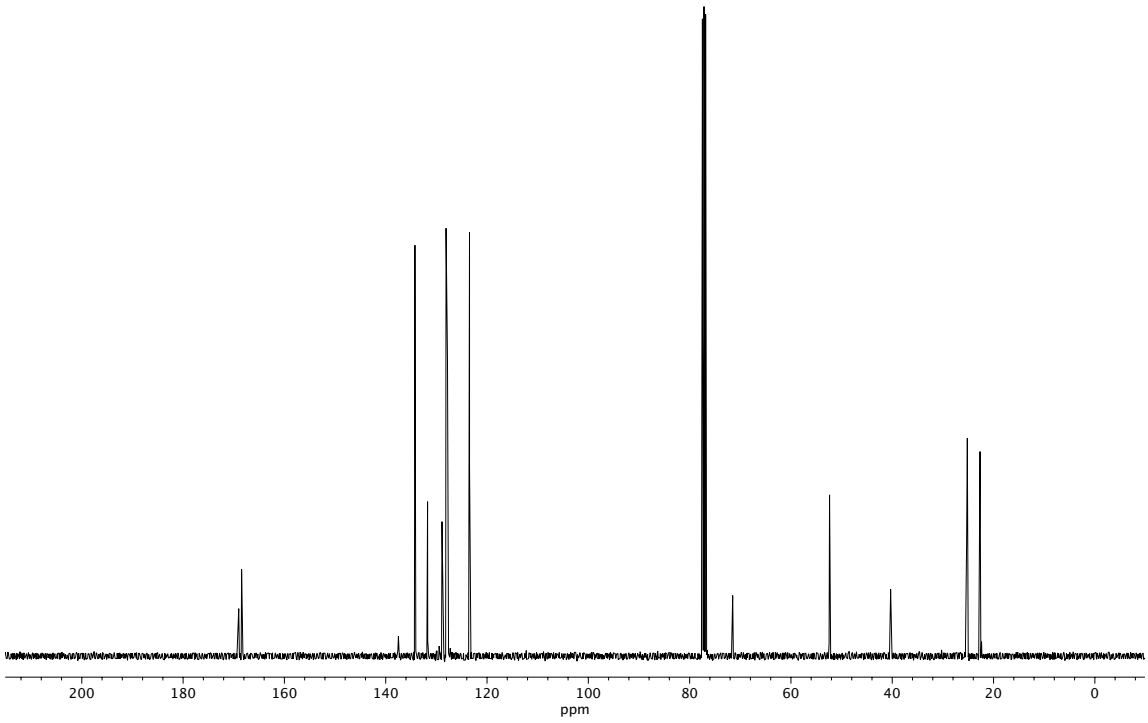

Figure A6.85 *^{13}C NMR (100 MHz, $CDCl_3$) of compound* ***111****.*

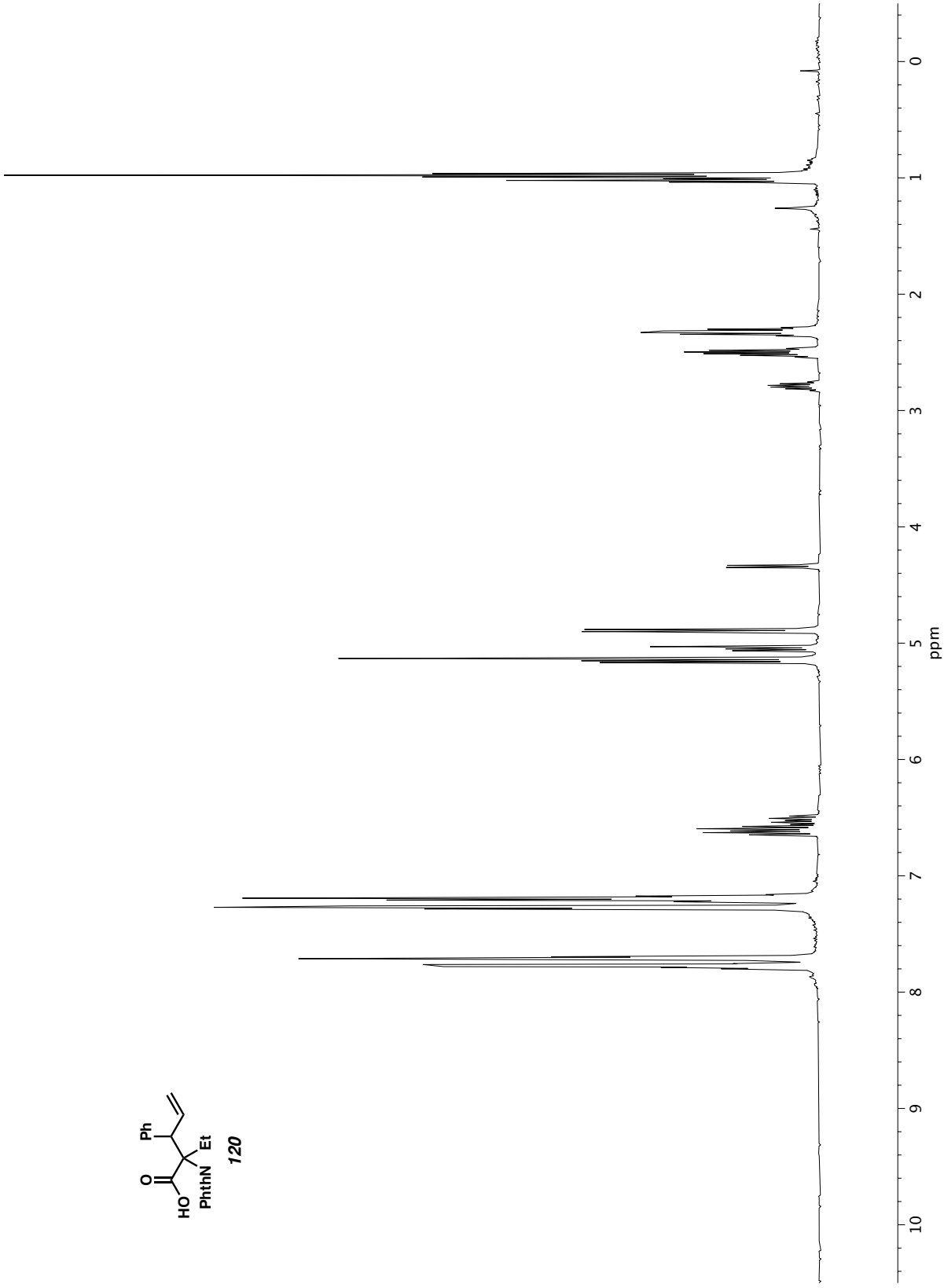

Figure A6.86 *^1H NMR (500 MHz, $CDCl_3$) of compound **120**.*

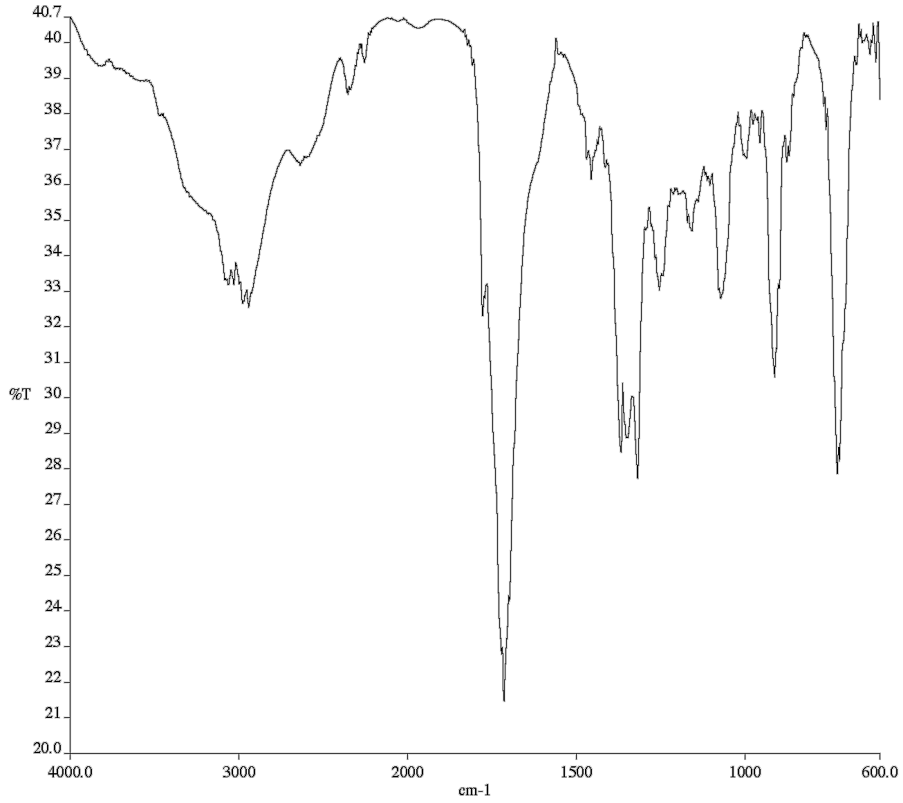

Figure A6.87 *Infrared spectrum (Thin Film, NaCl) of compound* ***120****.*

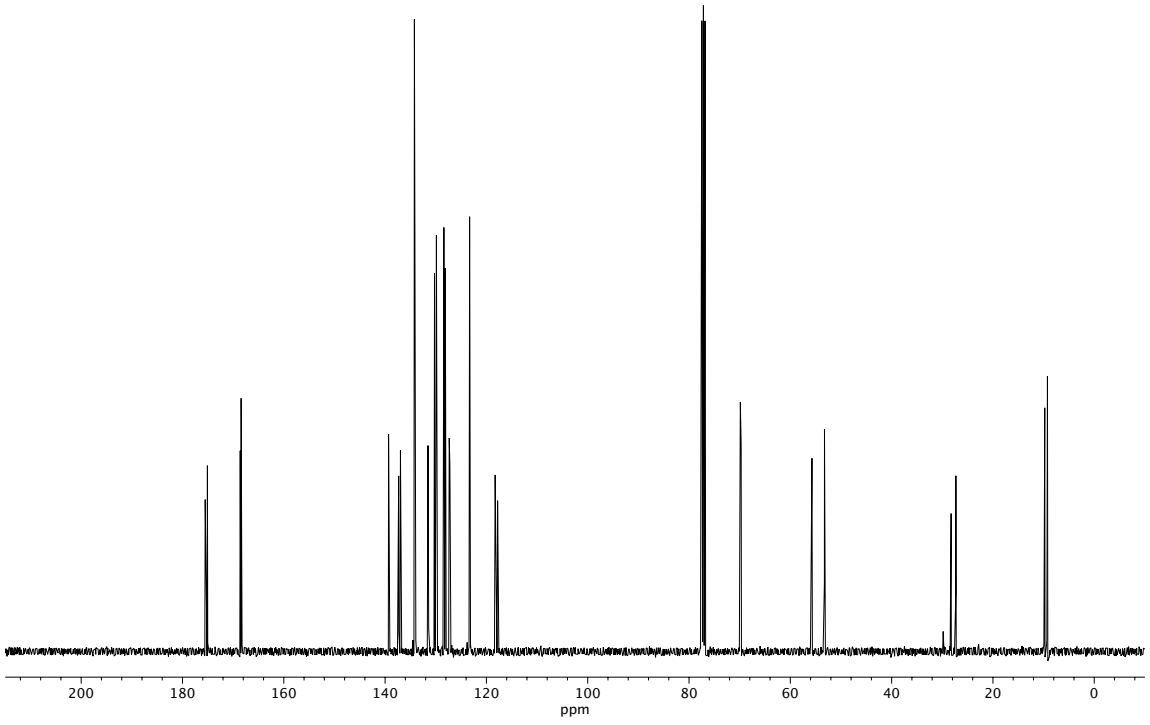

Figure A6.88 *^{13}C NMR (100 MHz, $CDCl_3$) of compound* ***120****.*

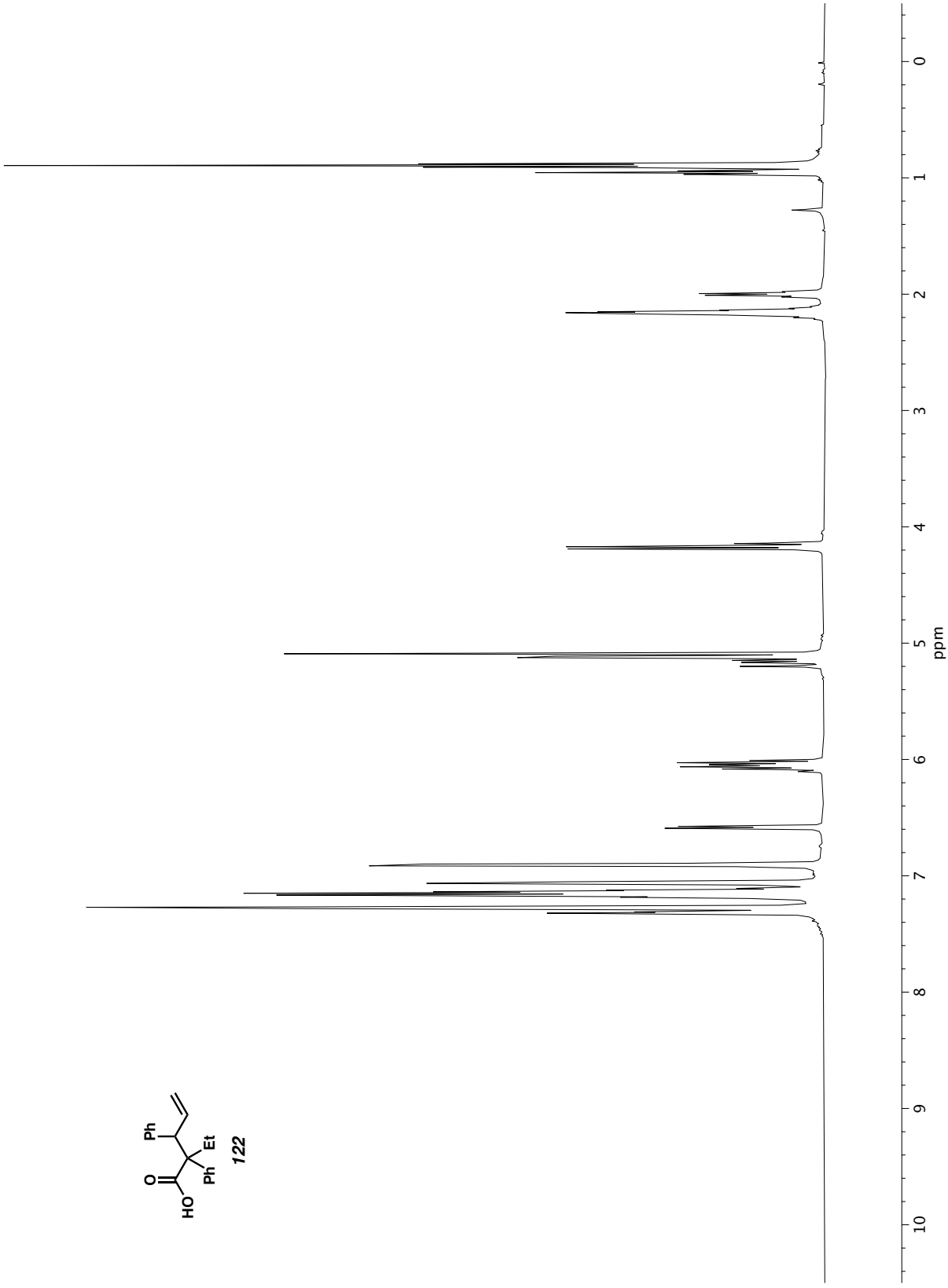

Figure A6.89 *^1H NMR (500 MHz, $CDCl_3$) of compound* ***122***.

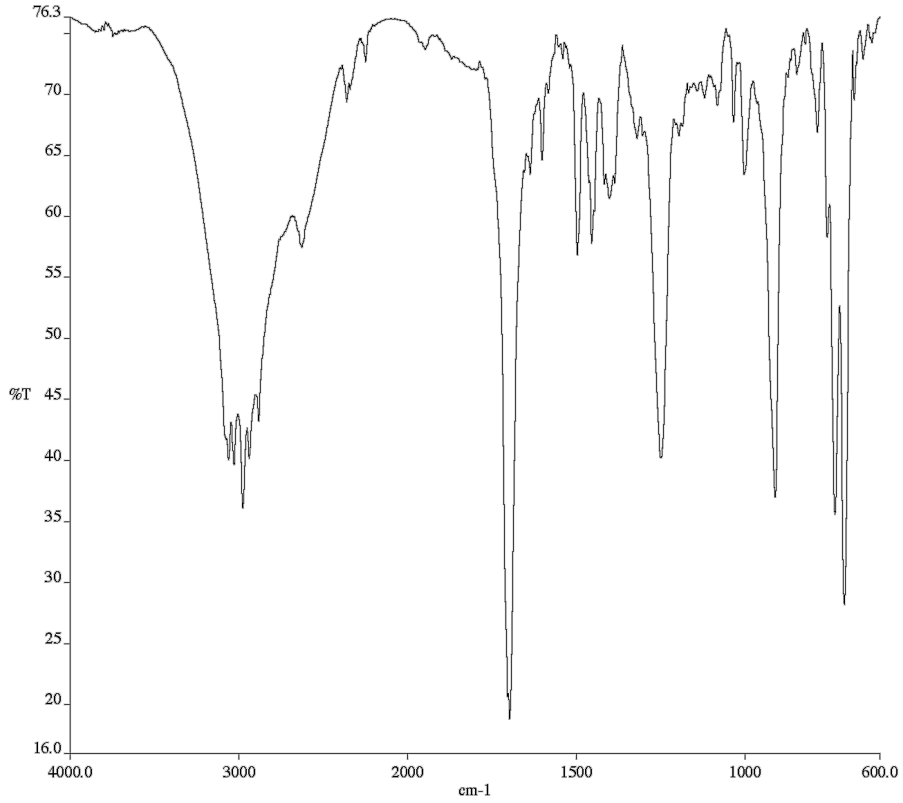

Figure A6.90 *Infrared spectrum (Thin Film, NaCl) of compound* ***122****.*

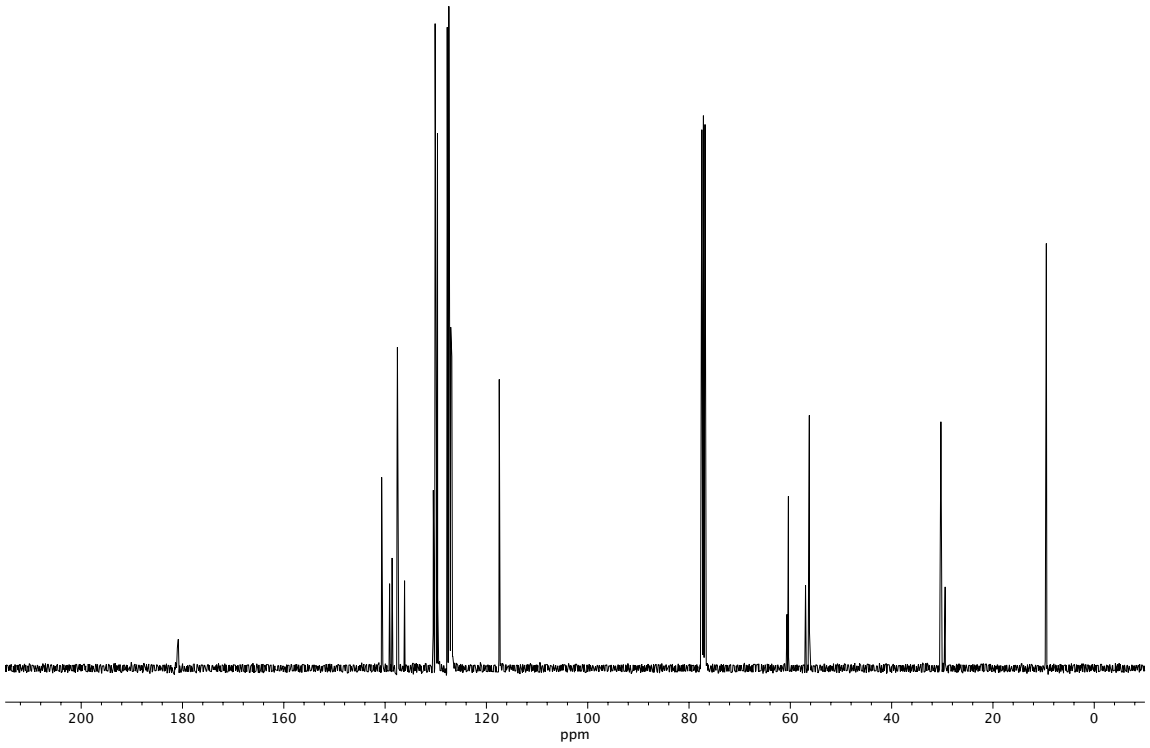

Figure A6.91 *^{13}C NMR (100 MHz, $CDCl_3$) of compound* ***122****.*

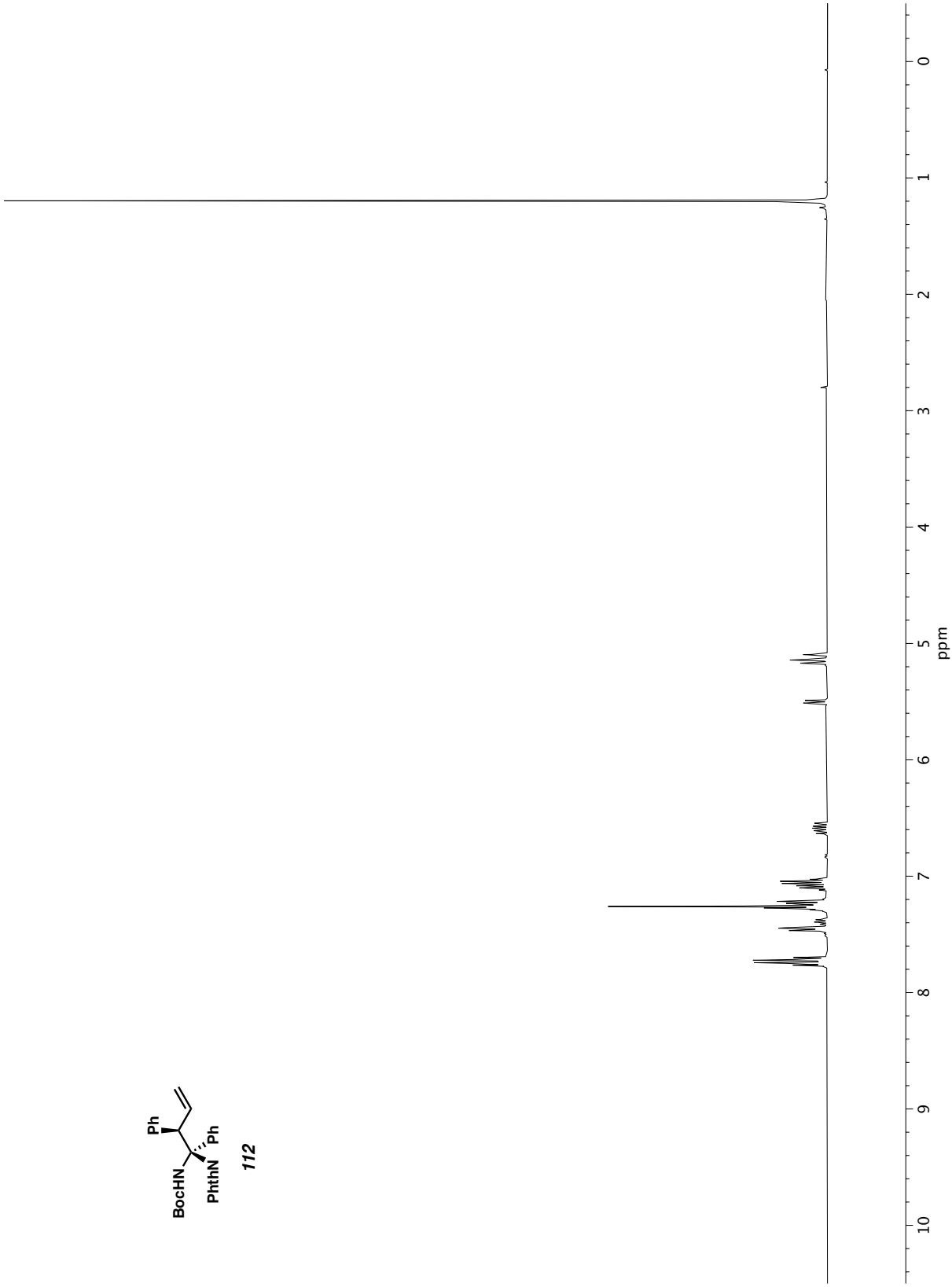

Figure A6.92 *^1H NMR (400 MHz, $CDCl_3$) of compound **112**.*

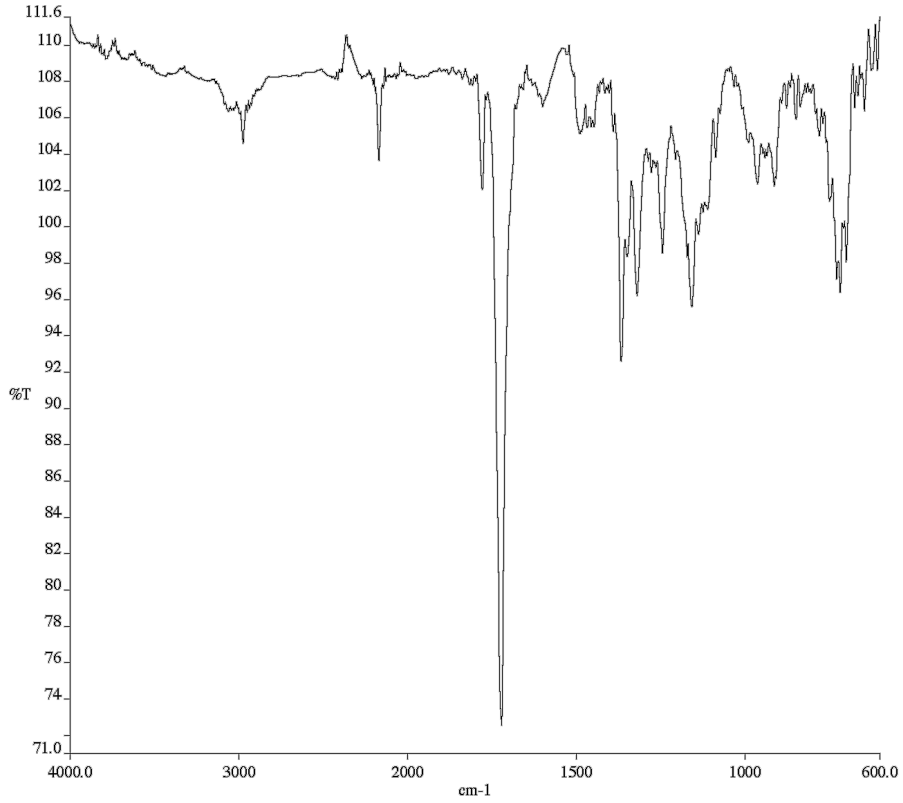

Figure A6.93 *Infrared spectrum (Thin Film, NaCl) of compound* ***112****.*

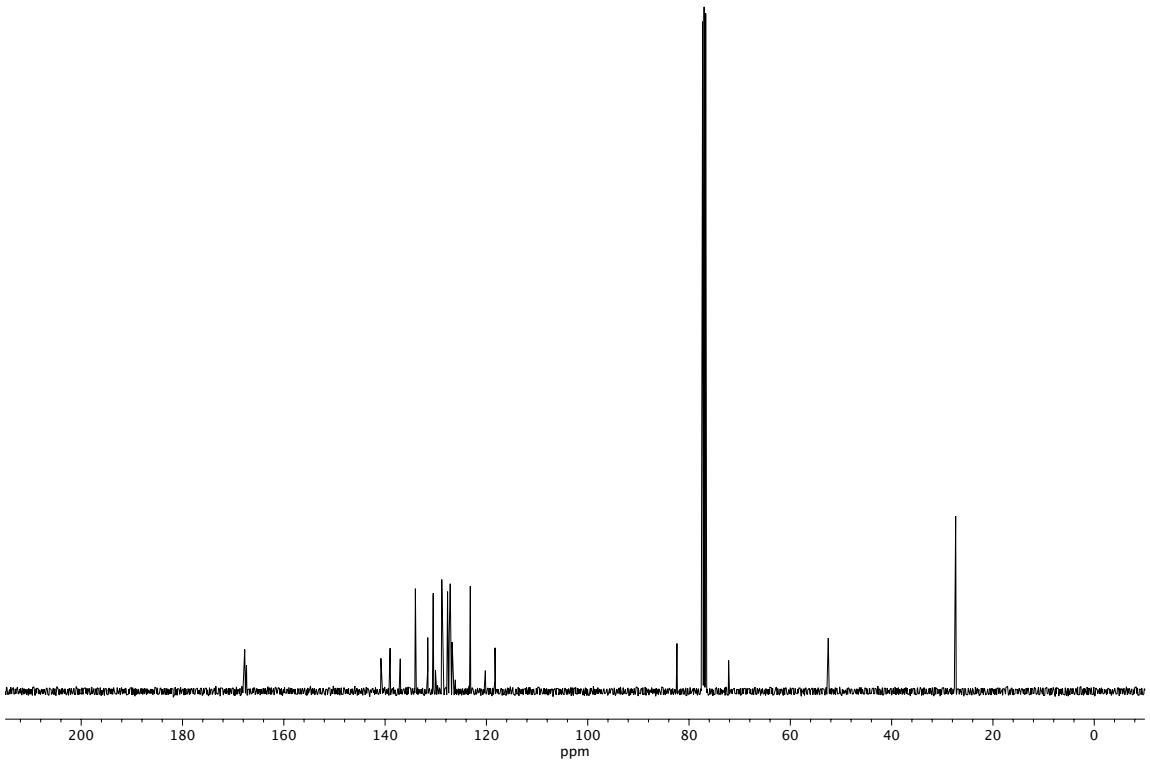

Figure A6.94 *^{13}C NMR (100 MHz, $CDCl_3$) of compound* ***112****.*

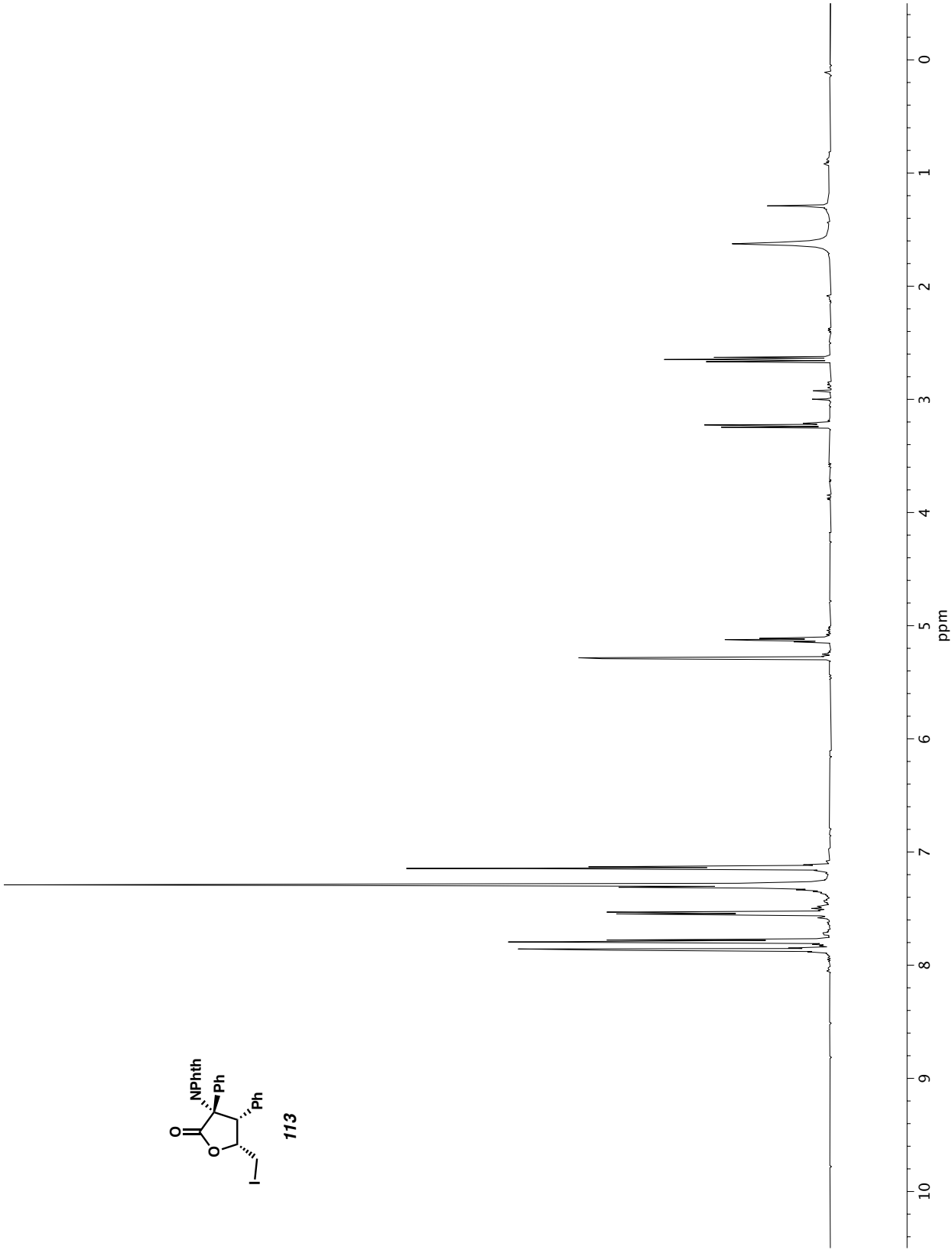

Figure A6.95 *^1H NMR (500 MHz, $CDCl_3$) of compound **113**.*

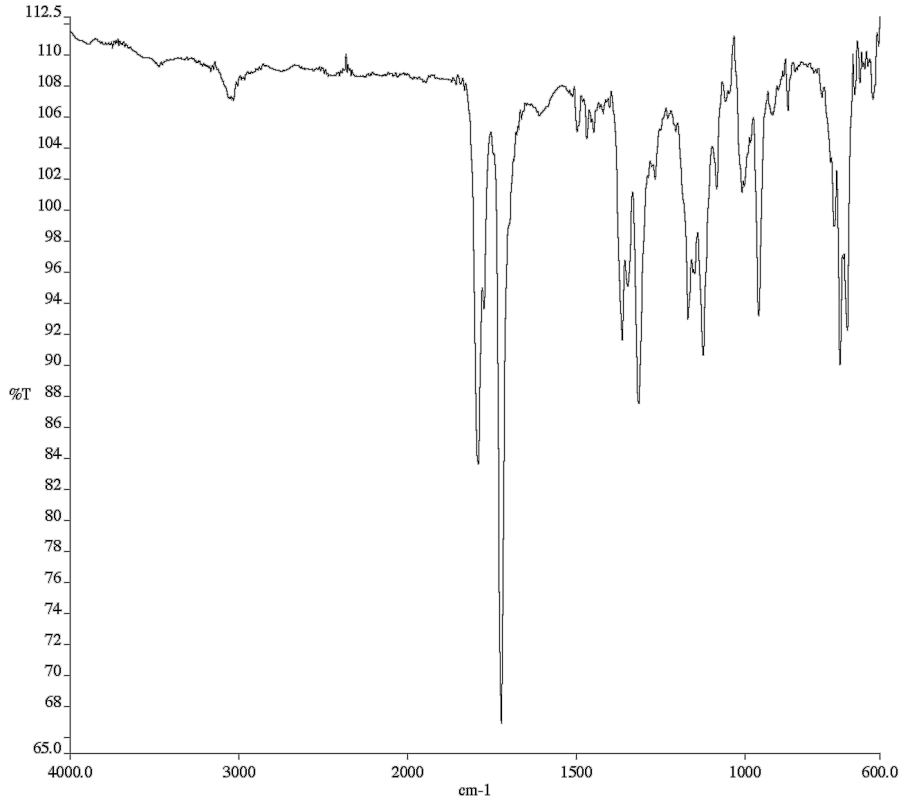

Figure A6.96 *Infrared spectrum (Thin Film, NaCl) of compound* ***113****.*

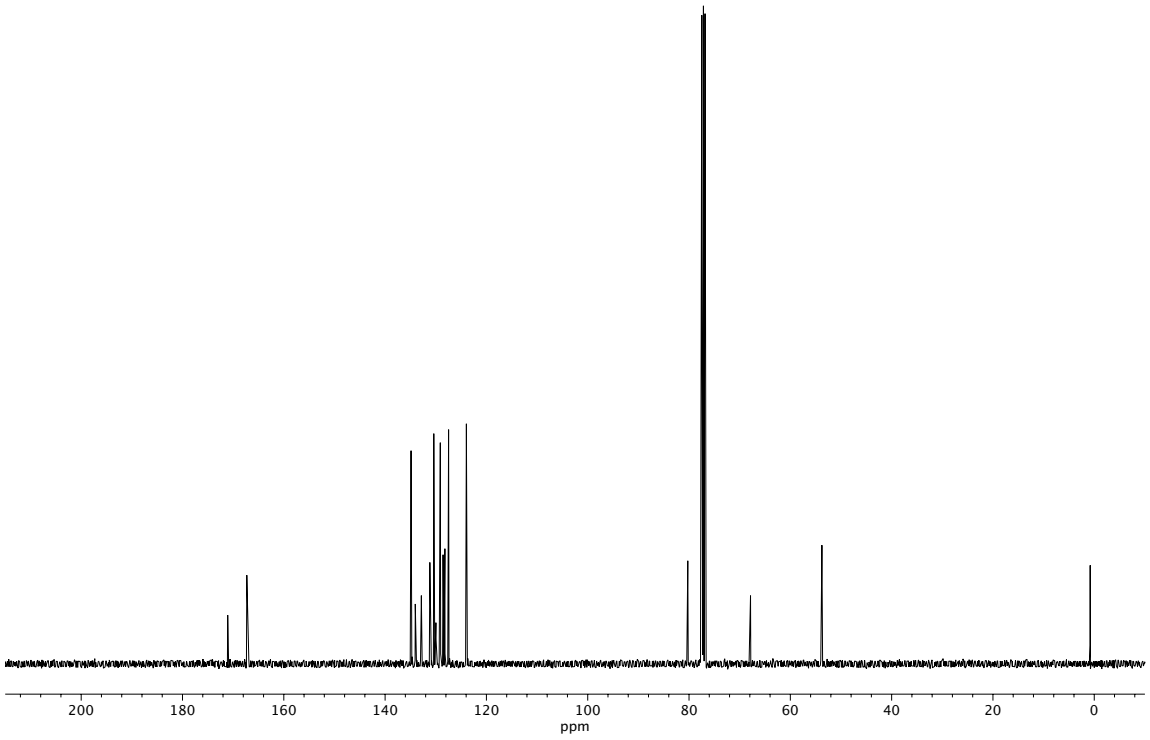

Figure A6.97 *^{13}C NMR (100 MHz, $CDCl_3$) of compound* ***113****.*

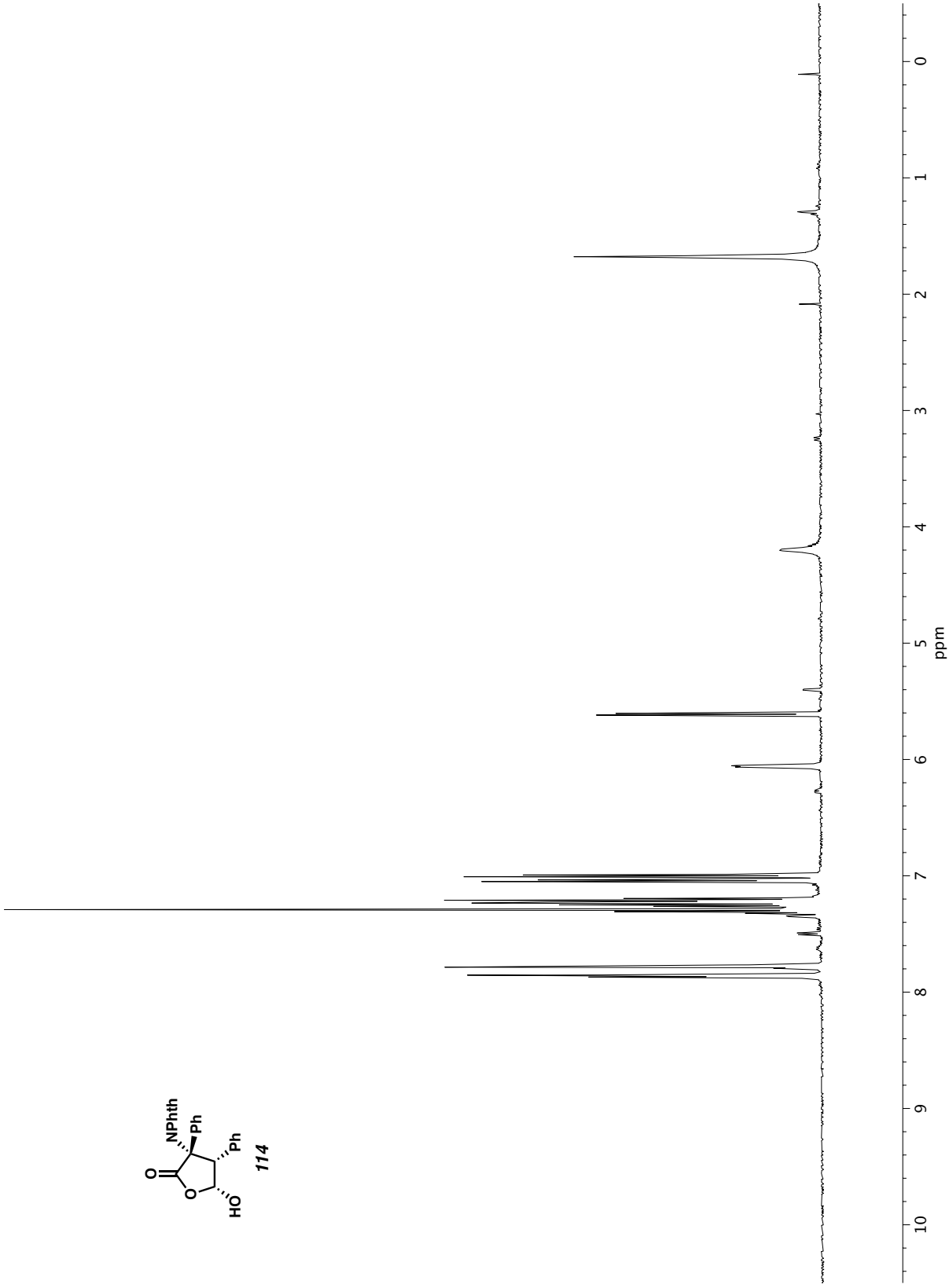

Figure A6.98 *^1H NMR (500 MHz, $CDCl_3$) of compound **114**.*

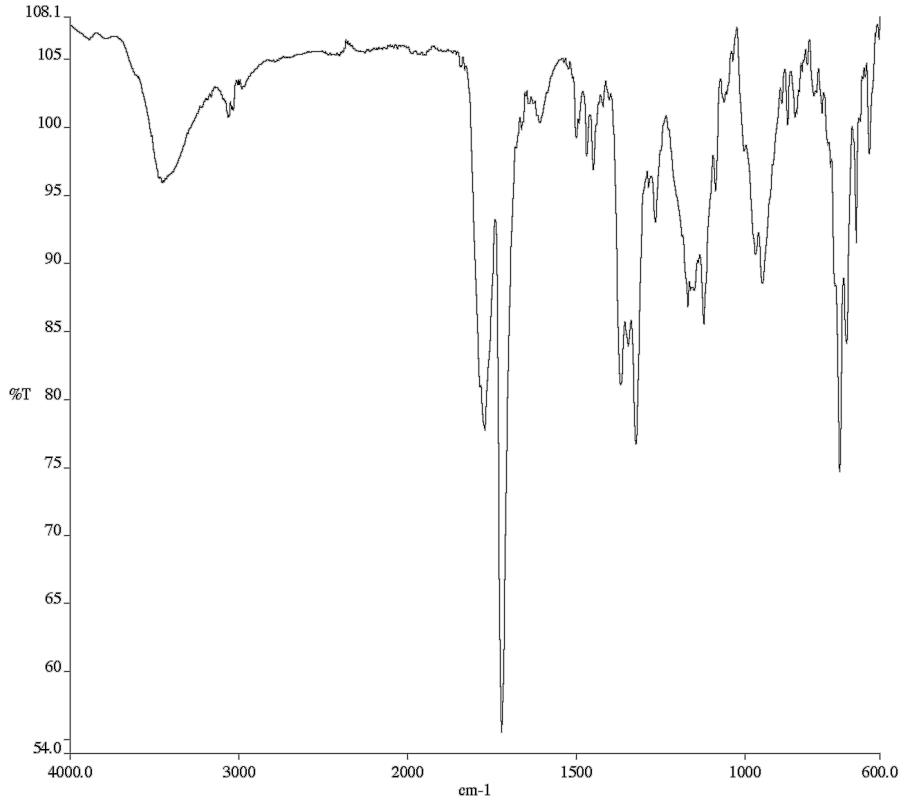

Figure A6.99 *Infrared spectrum (Thin Film, NaCl) of compound* ***114****.*

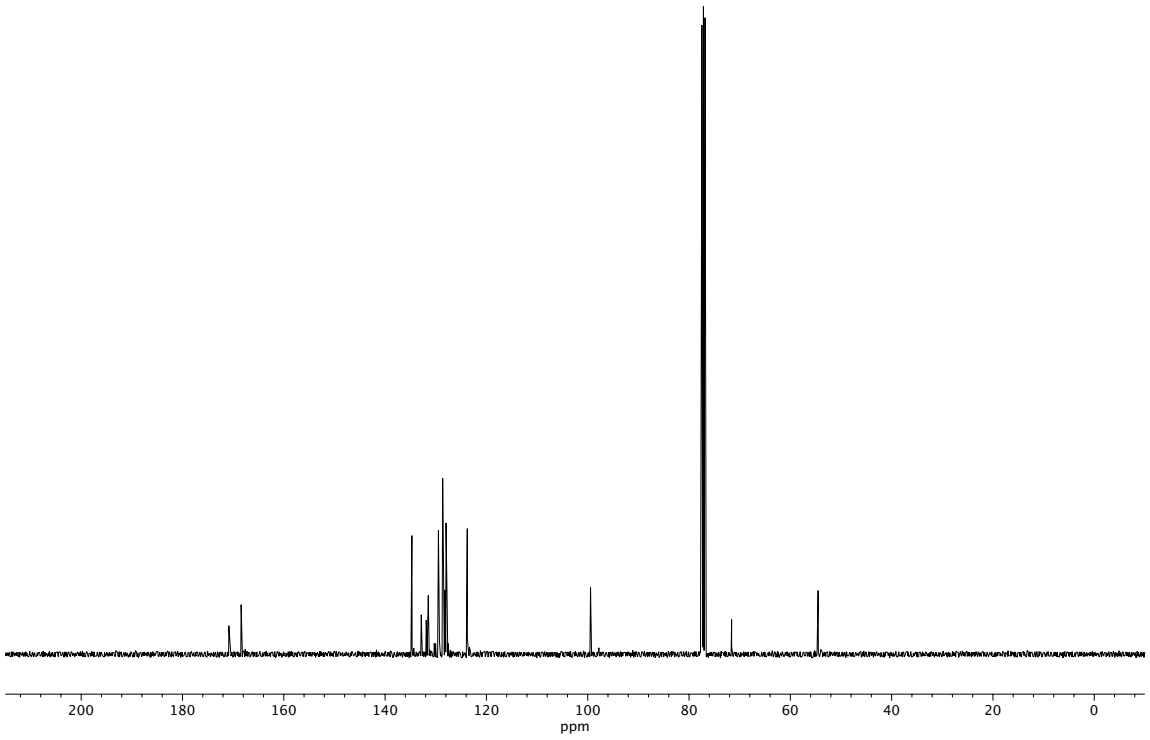

Figure A6.100 *^{13}C NMR (100 MHz, $CDCl_3$) of compound* ***114****.*

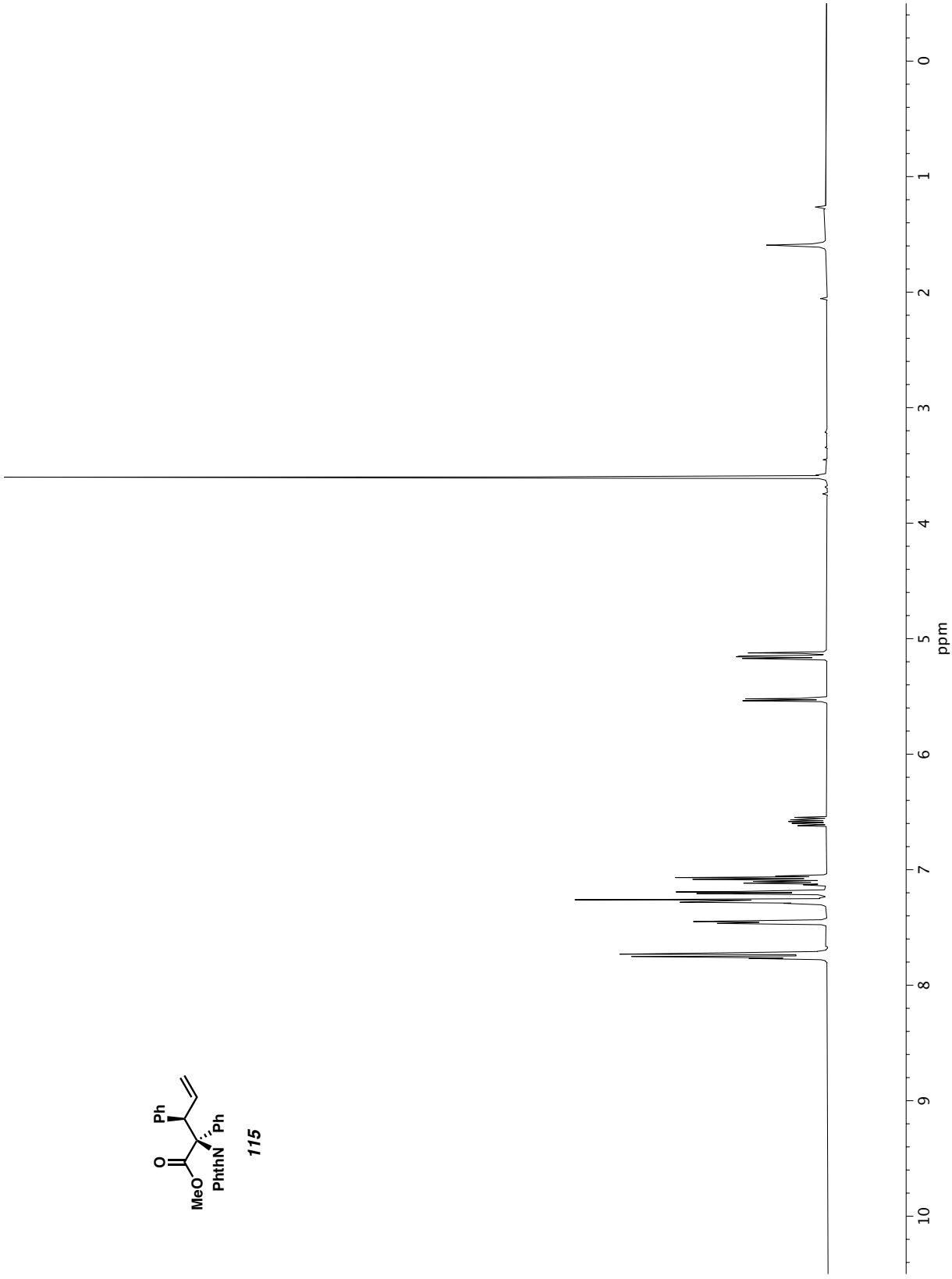

Figure A6.101 *^{1}H NMR (500 MHz, $CDCl_3$) of compound **115**.*

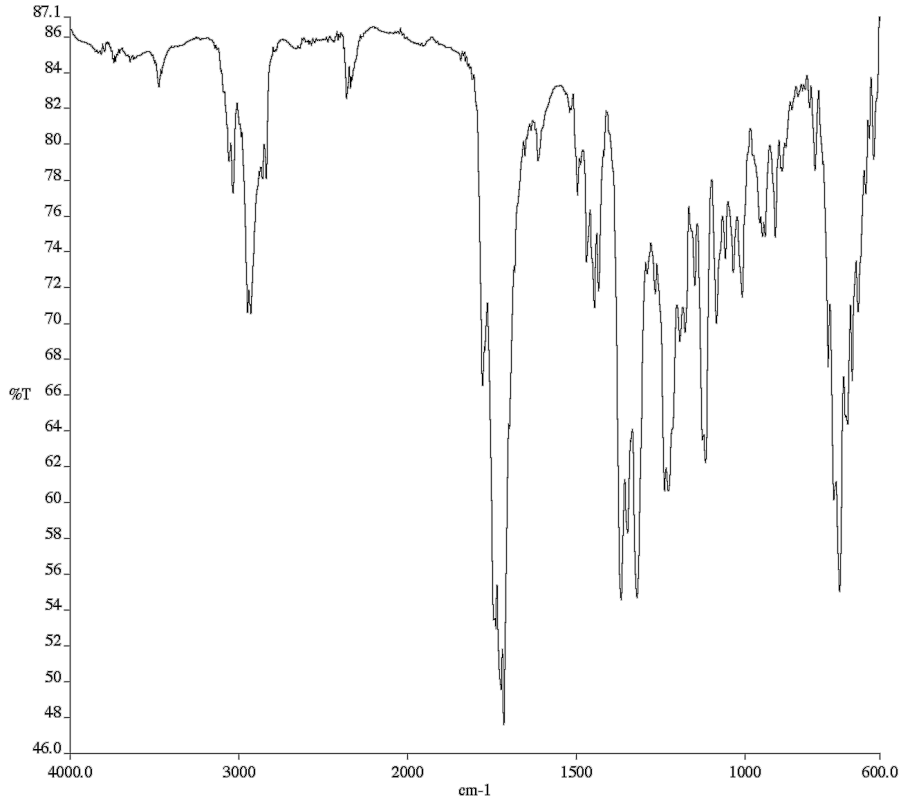

Figure A6.102 *Infrared spectrum (Thin Film, NaCl) of compound* ***115****.*

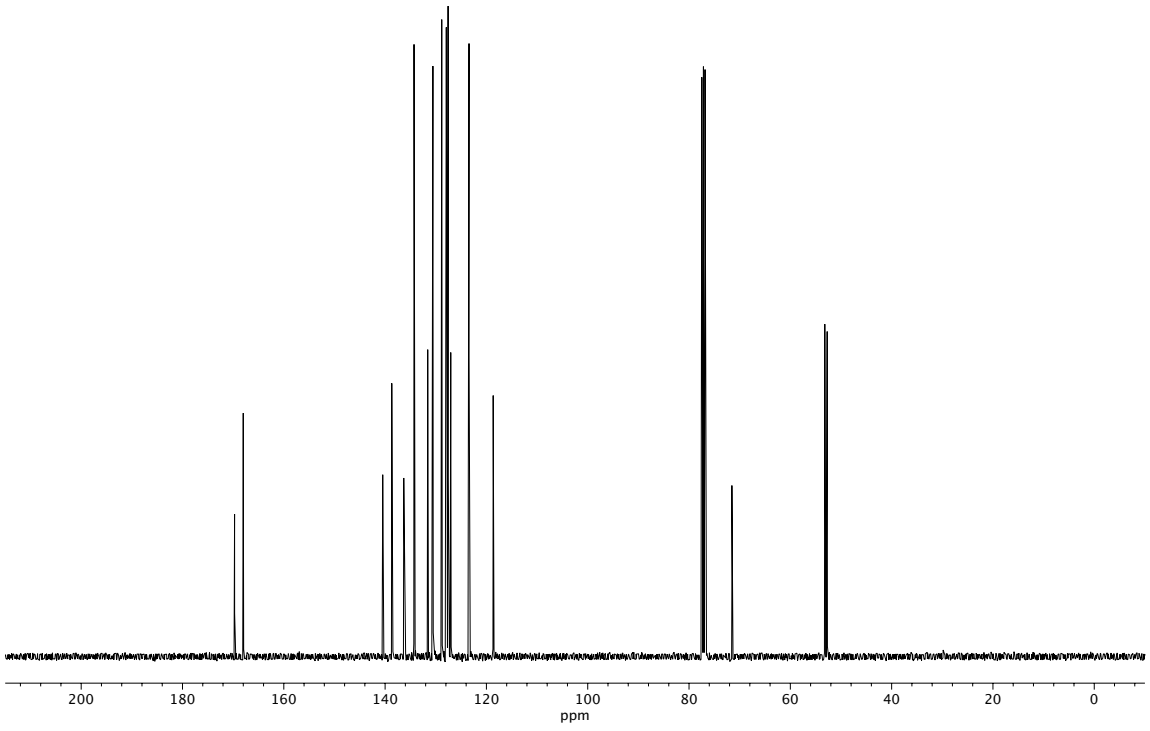

Figure A6.103 *^{13}C NMR (100 MHz, $CDCl_3$) of compound* ***115****.*

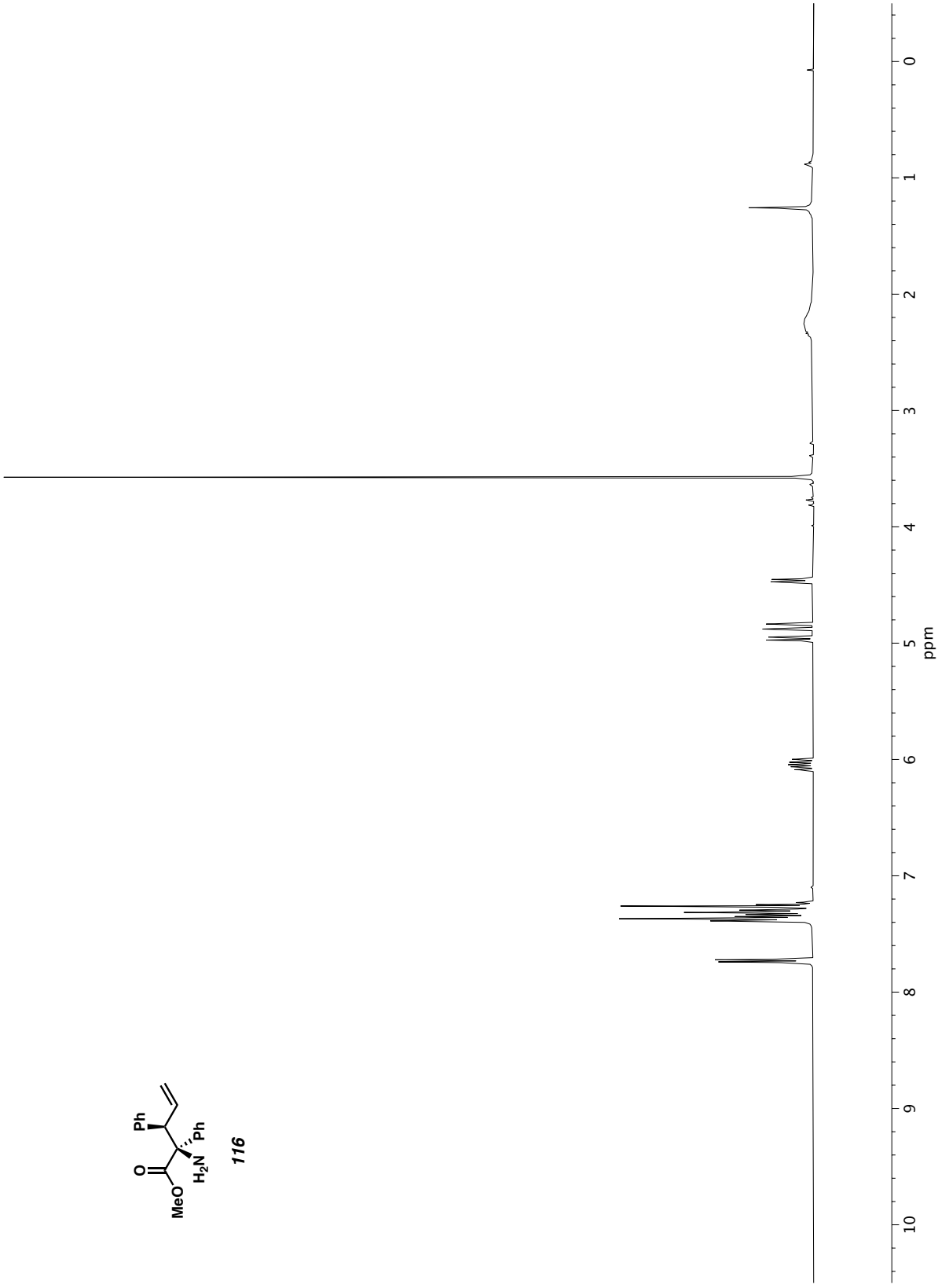

Figure A6.104 *^{1}H NMR (400 MHz, $CDCl_3$) of compound* ***116****.*

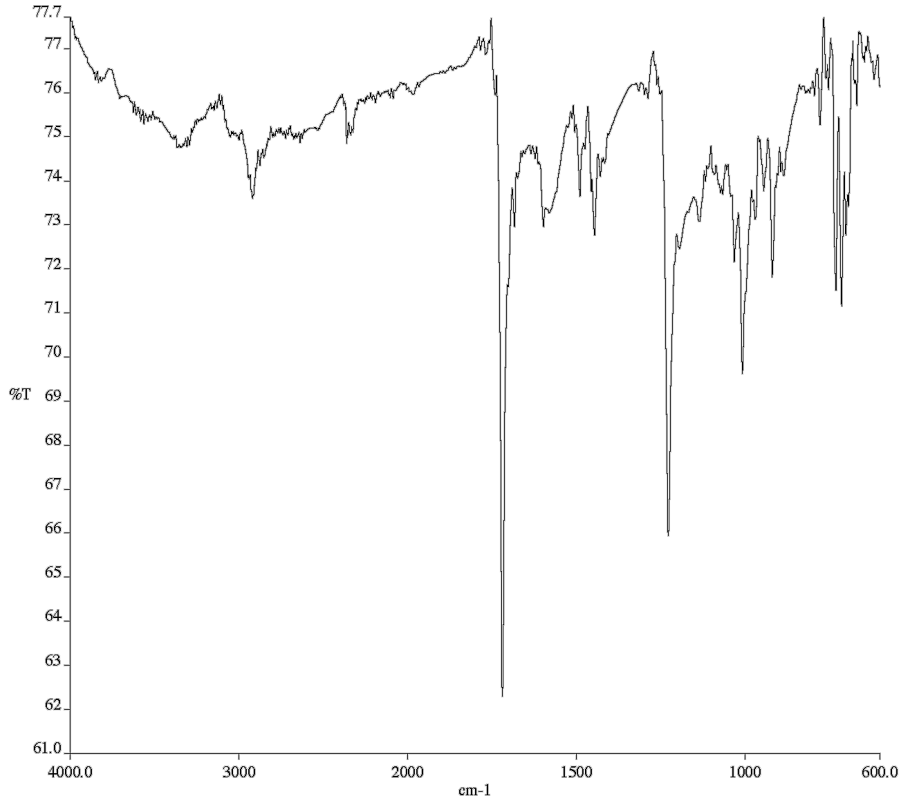

Figure A6.105 *Infrared spectrum (Thin Film, NaCl) of compound* ***116****.*

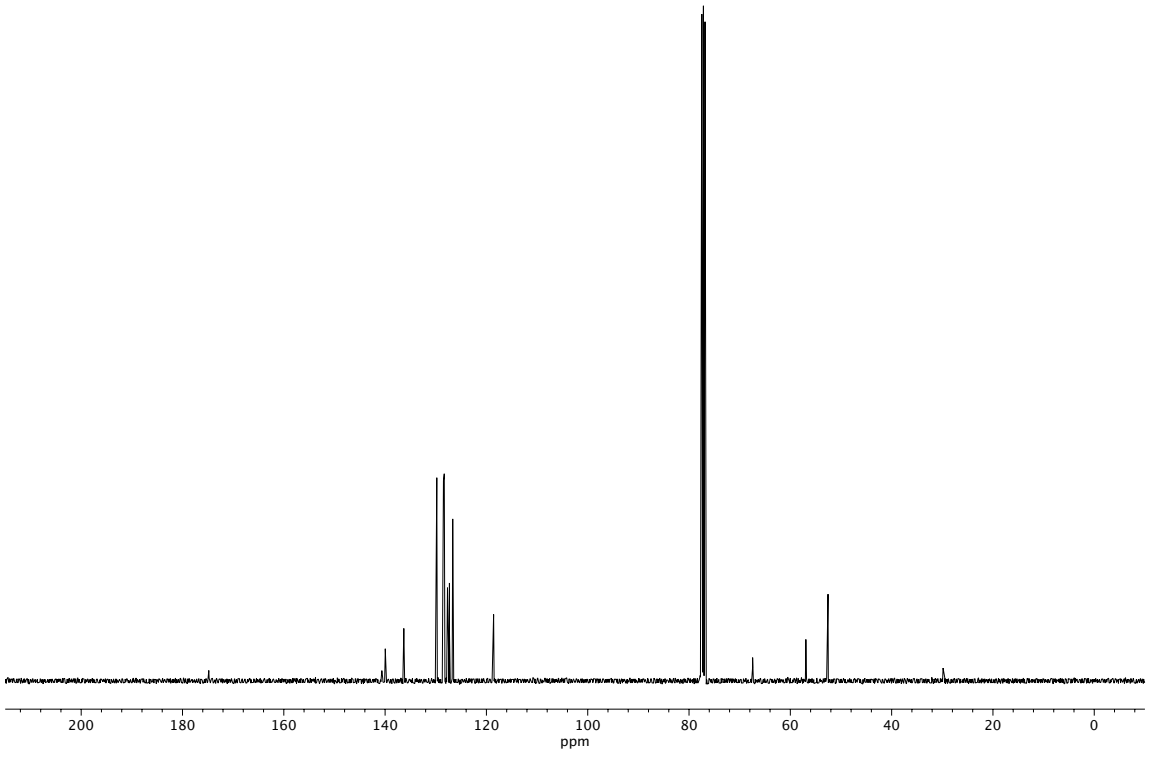

Figure A6.106 *^{13}C NMR (100 MHz, $CDCl_3$) of compound* ***116****.*

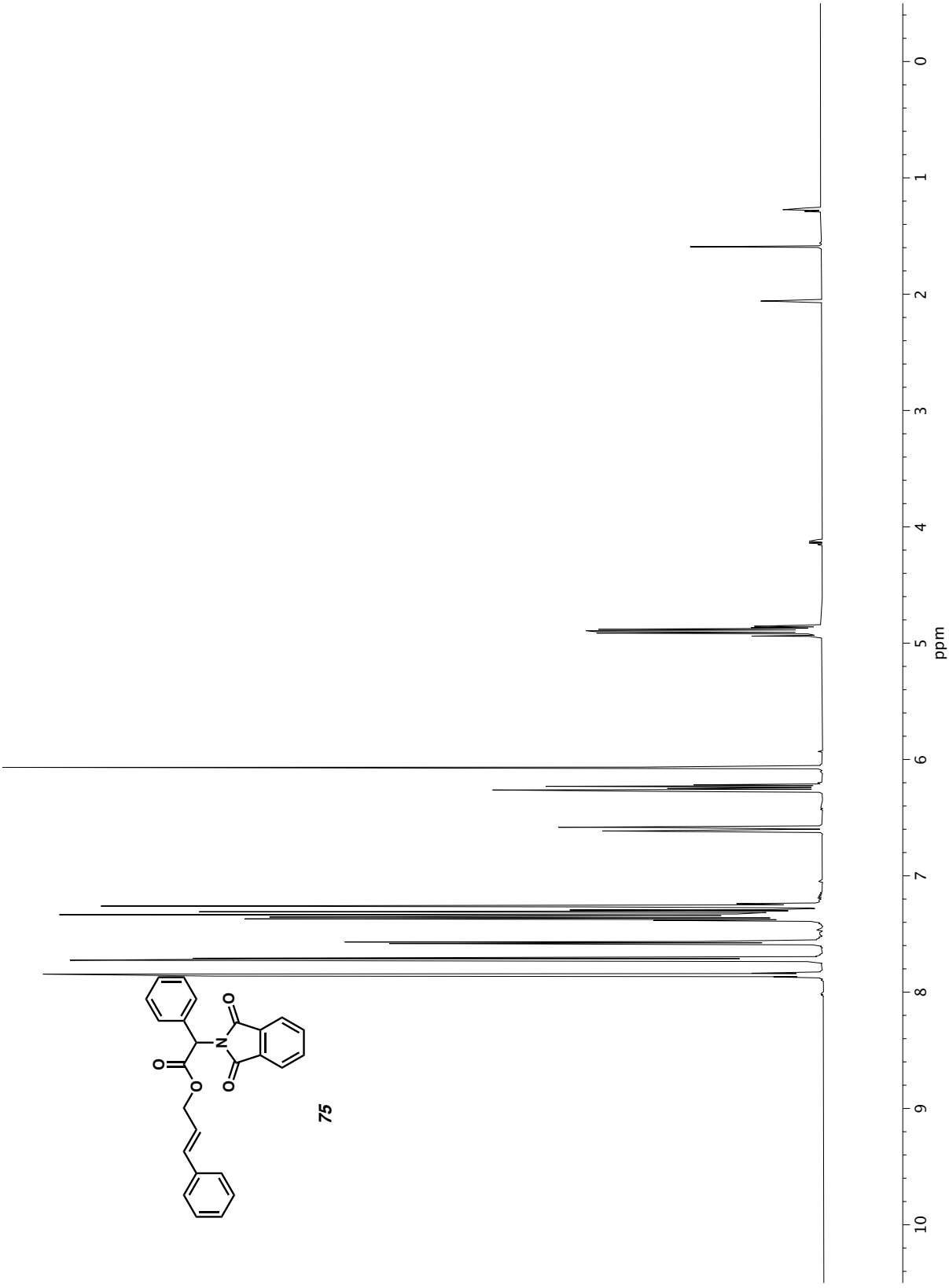

Figure A6.107 *^1H NMR (500 MHz, $CDCl_3$) of compound **75**.*

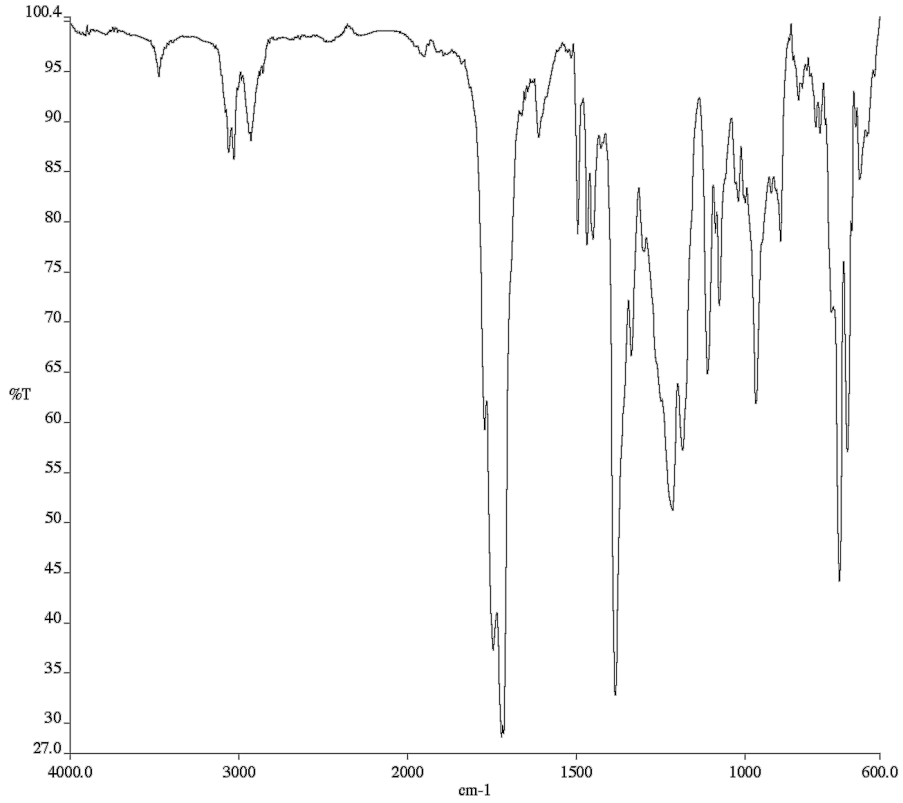

Figure A6.108 *Infrared spectrum (Thin Film, NaCl) of compound **75**.*

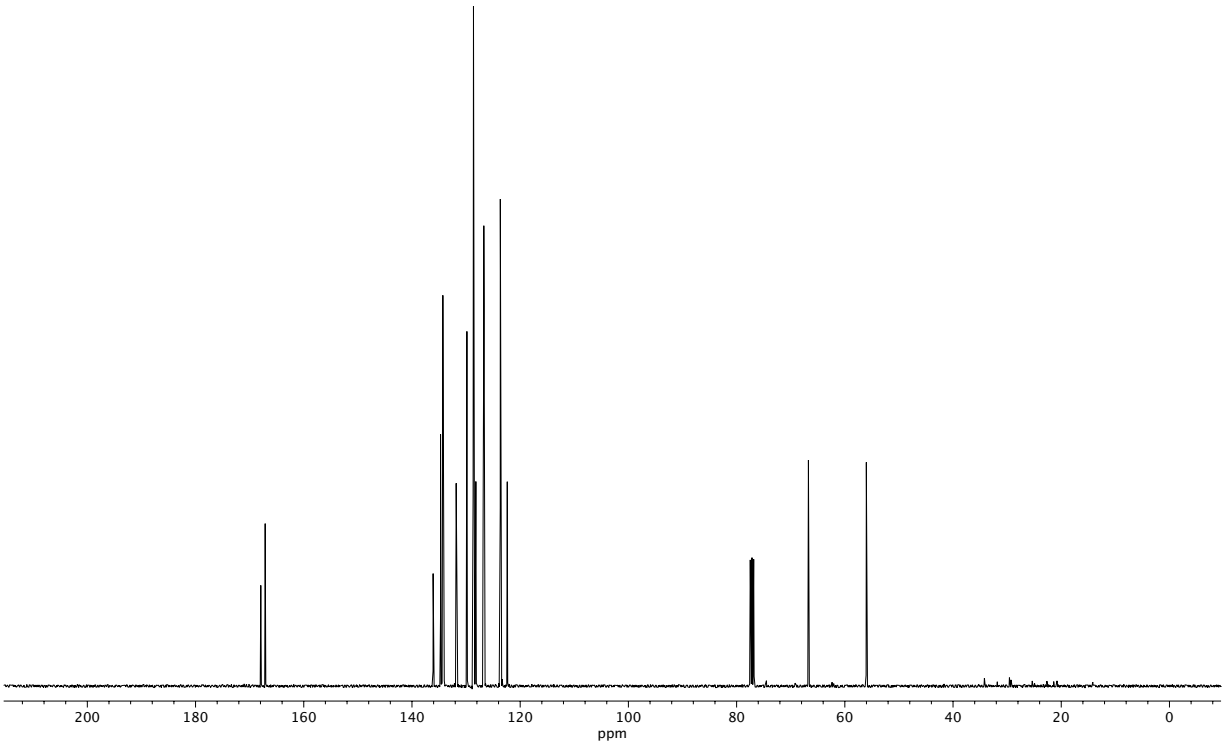

Figure A6.109 *^{13}C NMR (100 MHz, $CDCl_3$) of compound **75**.*

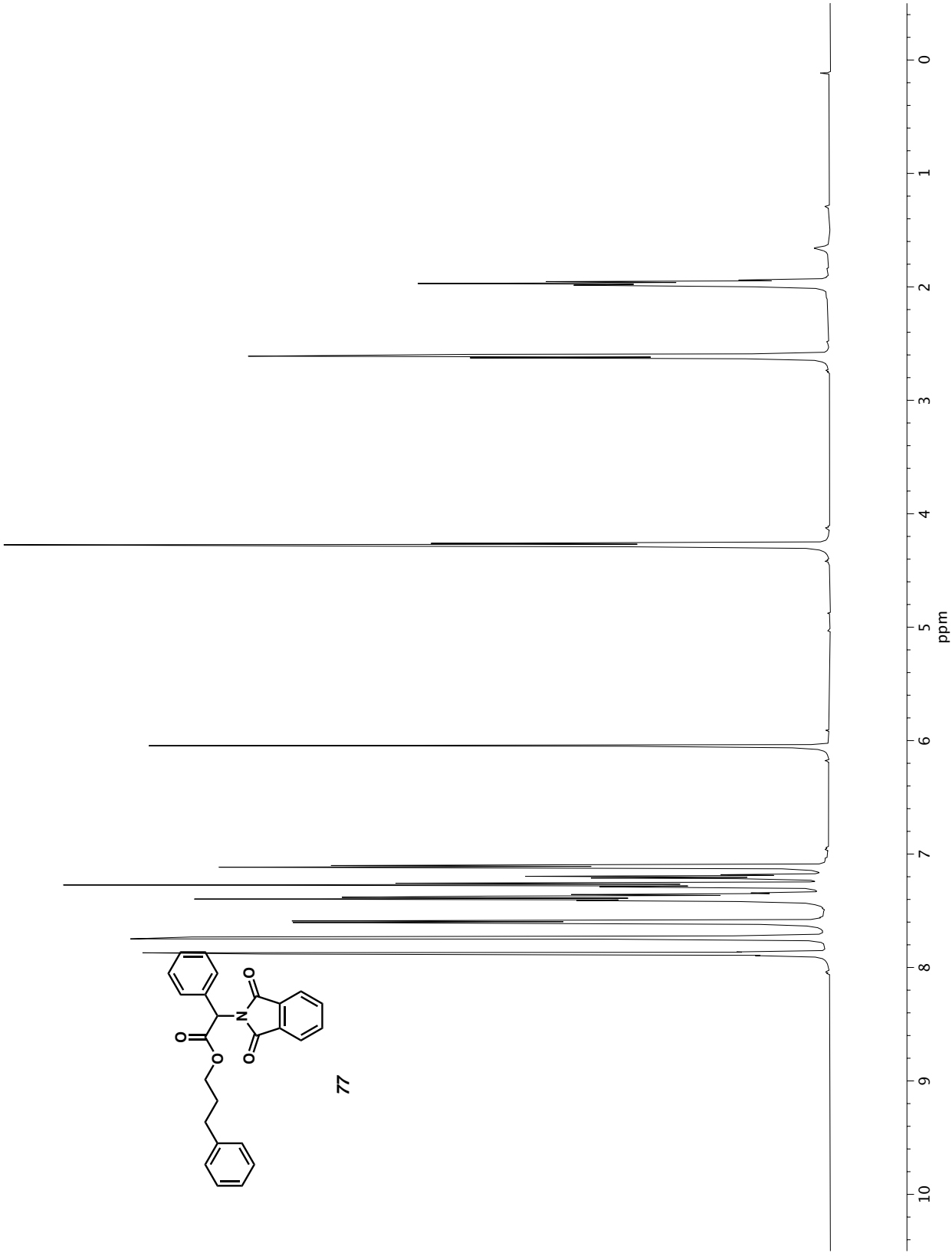

Figure A6.110 *^1H NMR (500 MHz, $CDCl_3$) of compound **77**.*

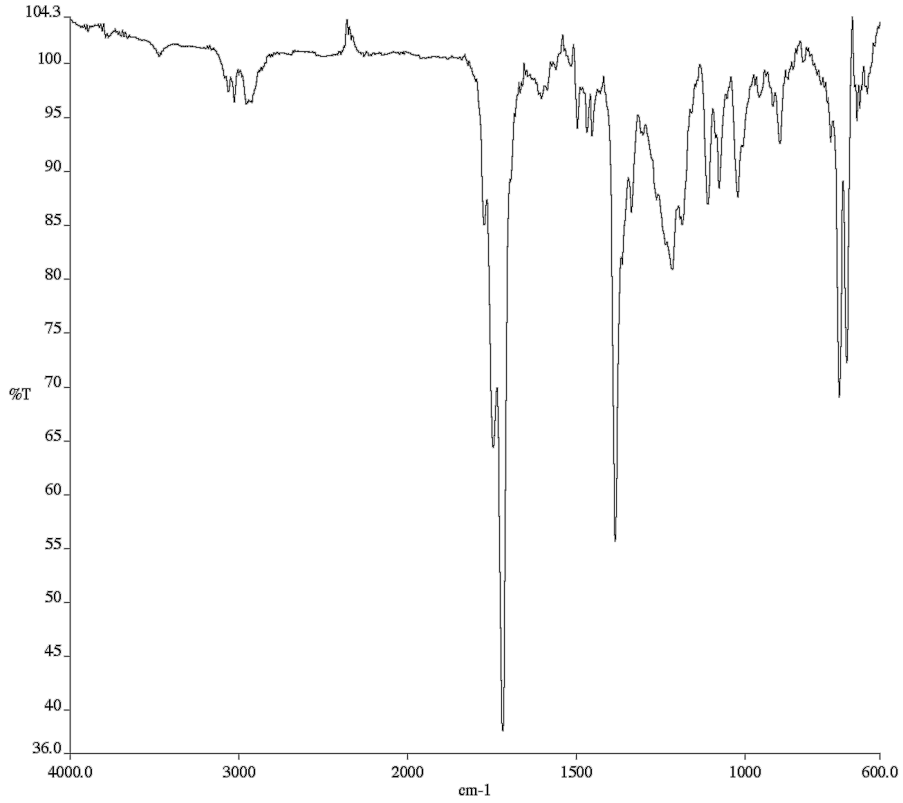

Figure A6.111 *Infrared spectrum (Thin Film, NaCl) of compound 77.*

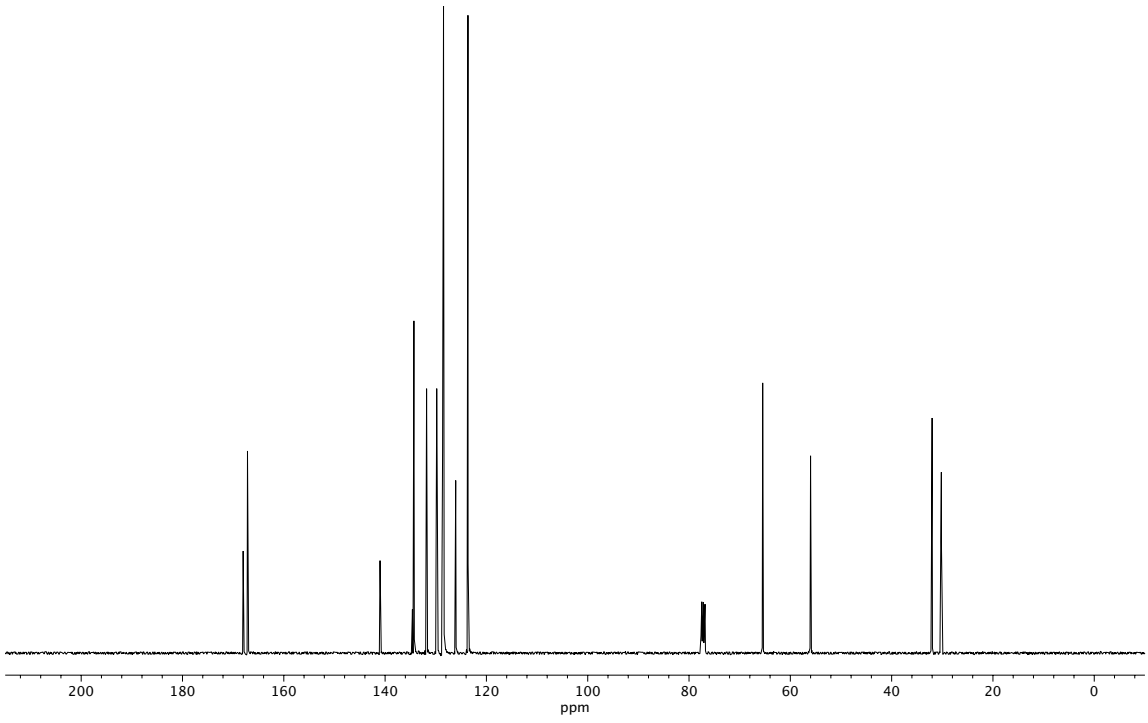

Figure A6.112 *^{13}C NMR (100 MHz, $CDCl_3$) of compound 77.*

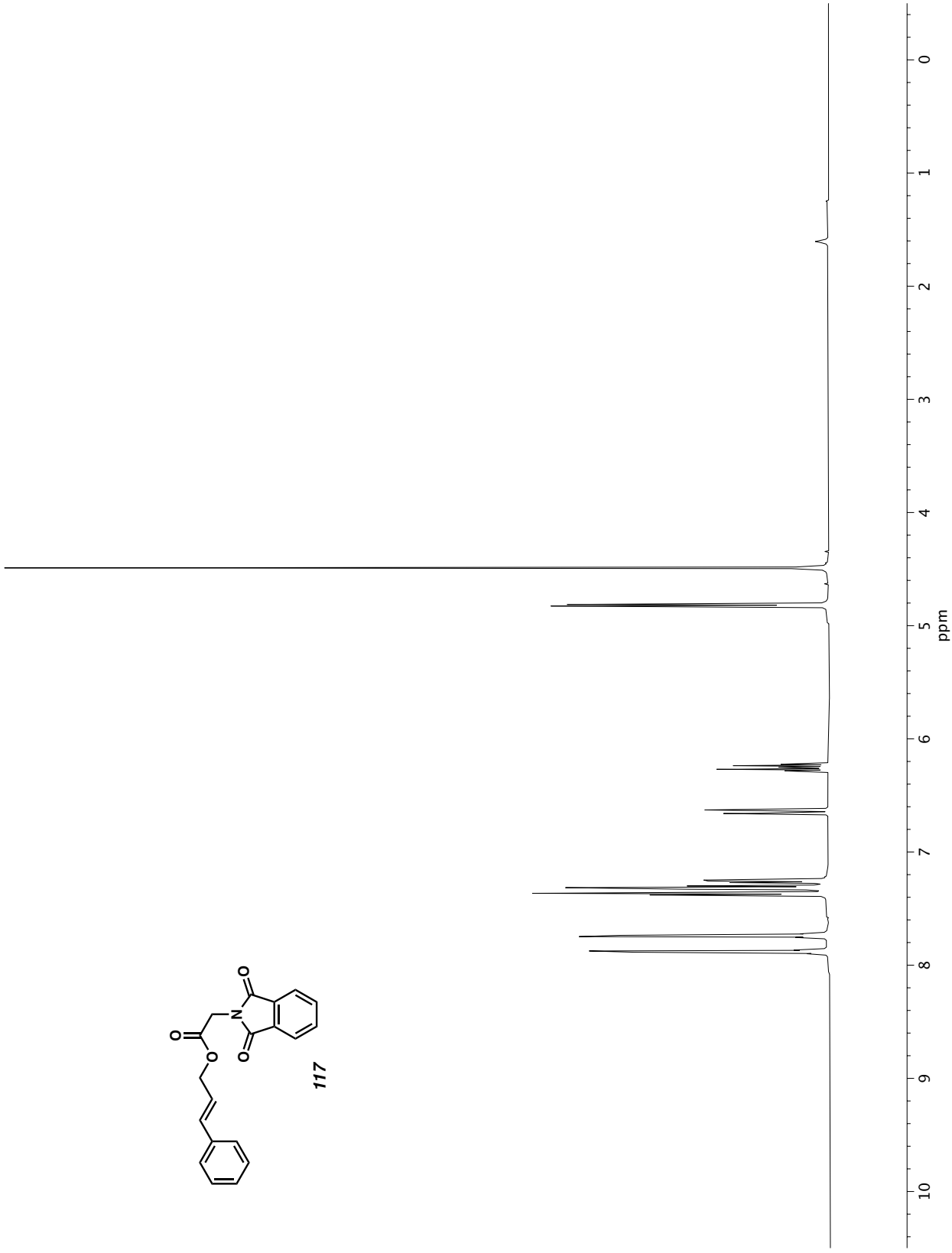

Figure A6.113 *^{1}H NMR (500 MHz, $CDCl_3$) of compound **117**.*

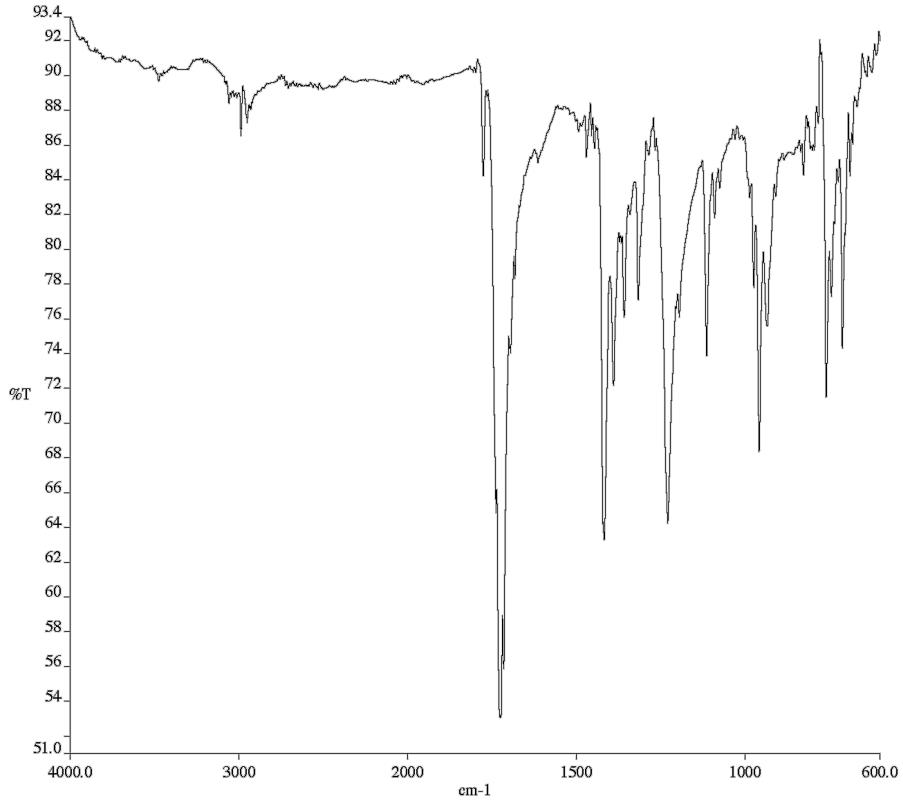

Figure A6.114 *Infrared spectrum (Thin Film, NaCl) of compound* ***117****.*

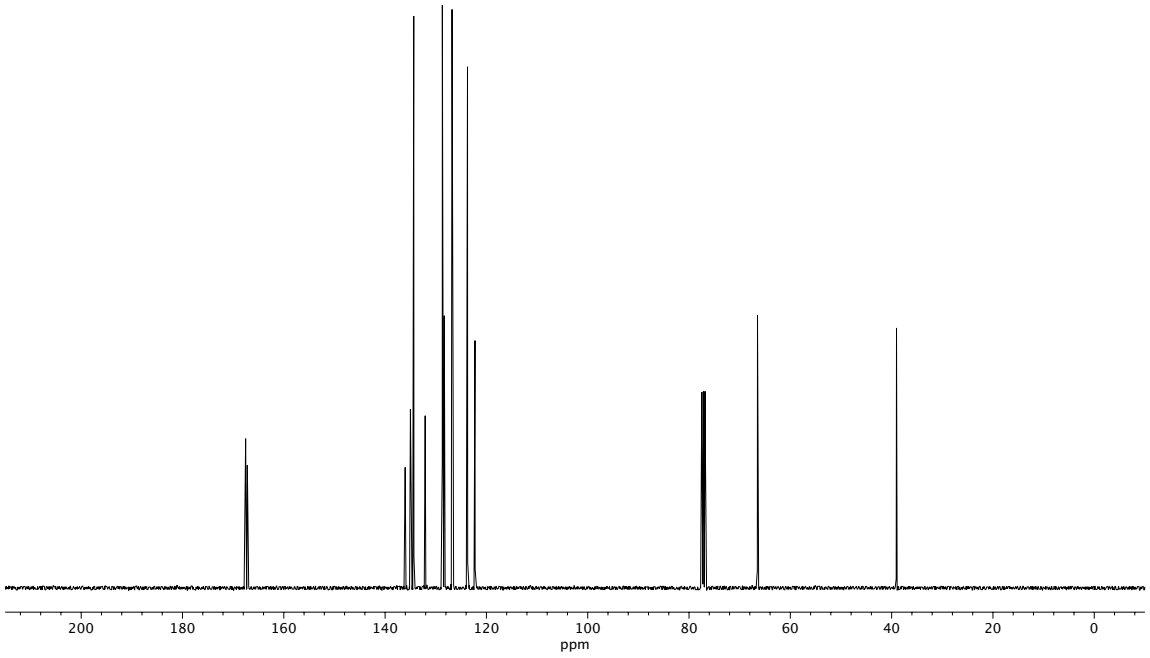

Figure A6.115 *^{13}C NMR (100 MHz, $CDCl_3$) of compound* ***117****.*

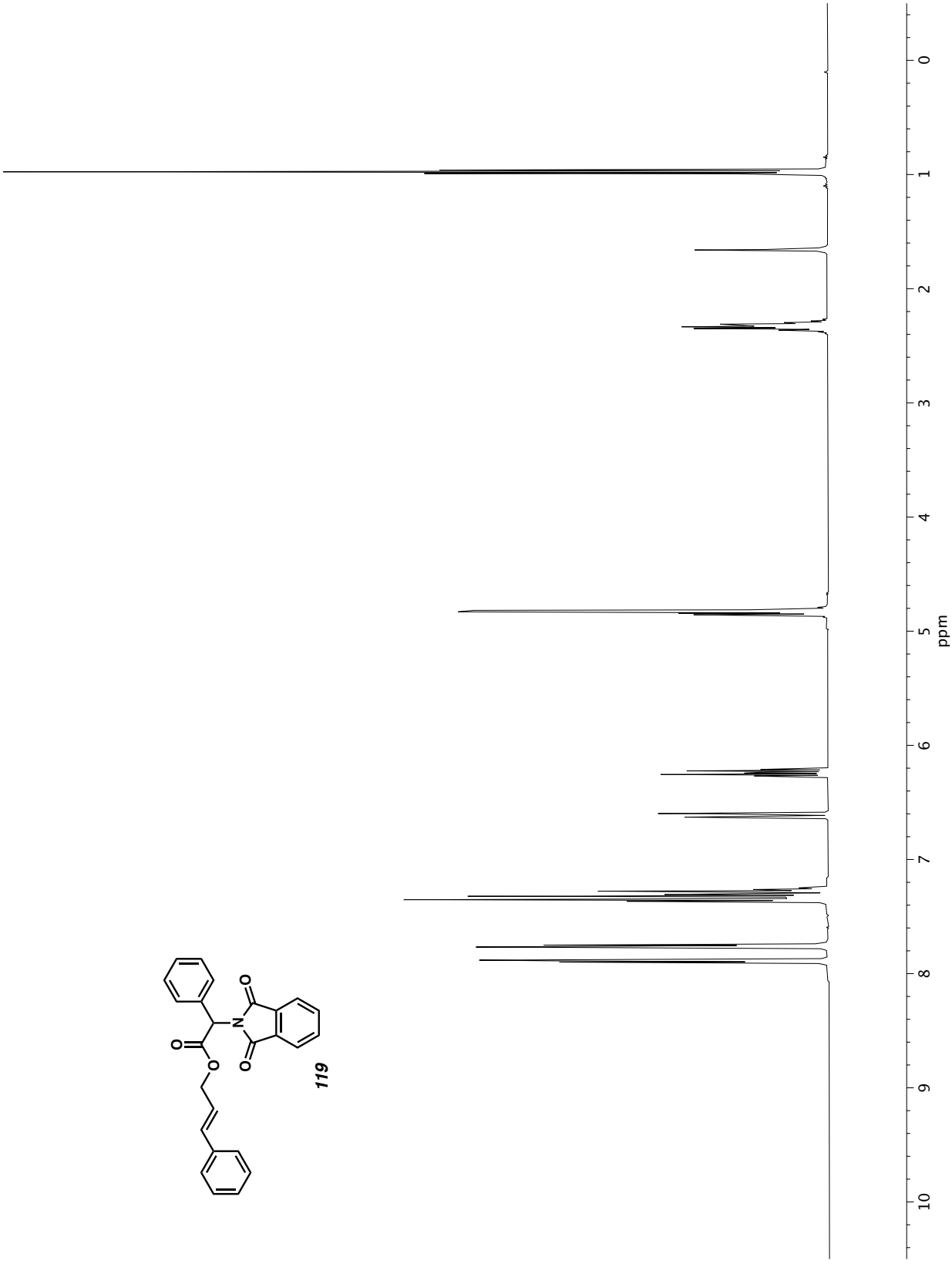

Figure A6.116 *^1H NMR (500 MHz, $CDCl_3$) of compound **119**.*

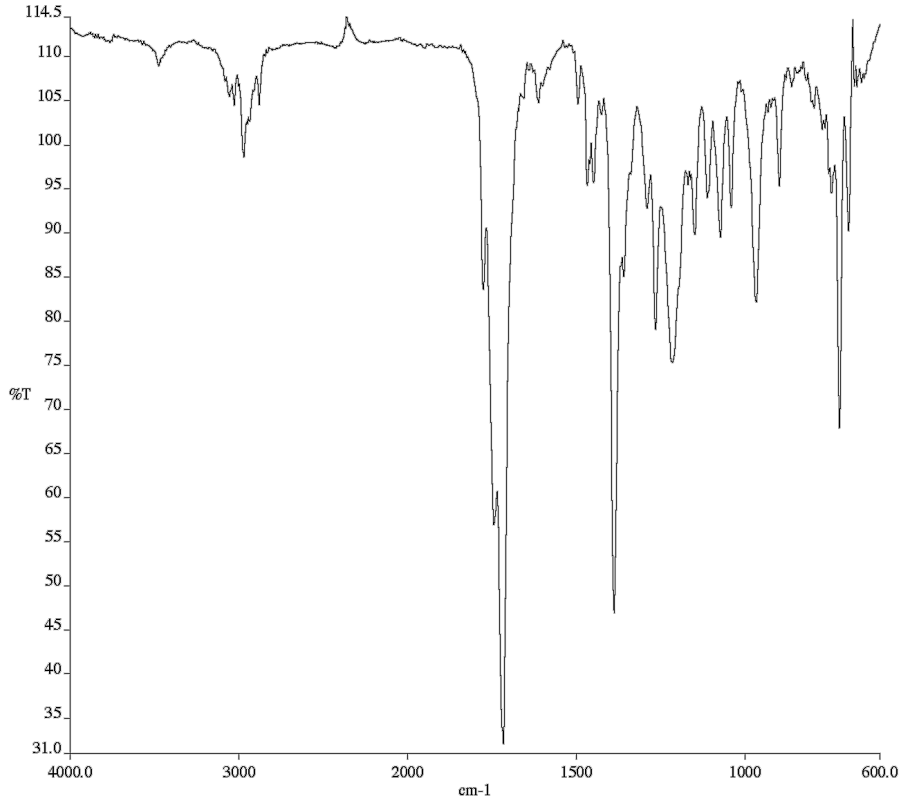

Figure A6.117 *Infrared spectrum (Thin Film, NaCl) of compound* ***119****.*

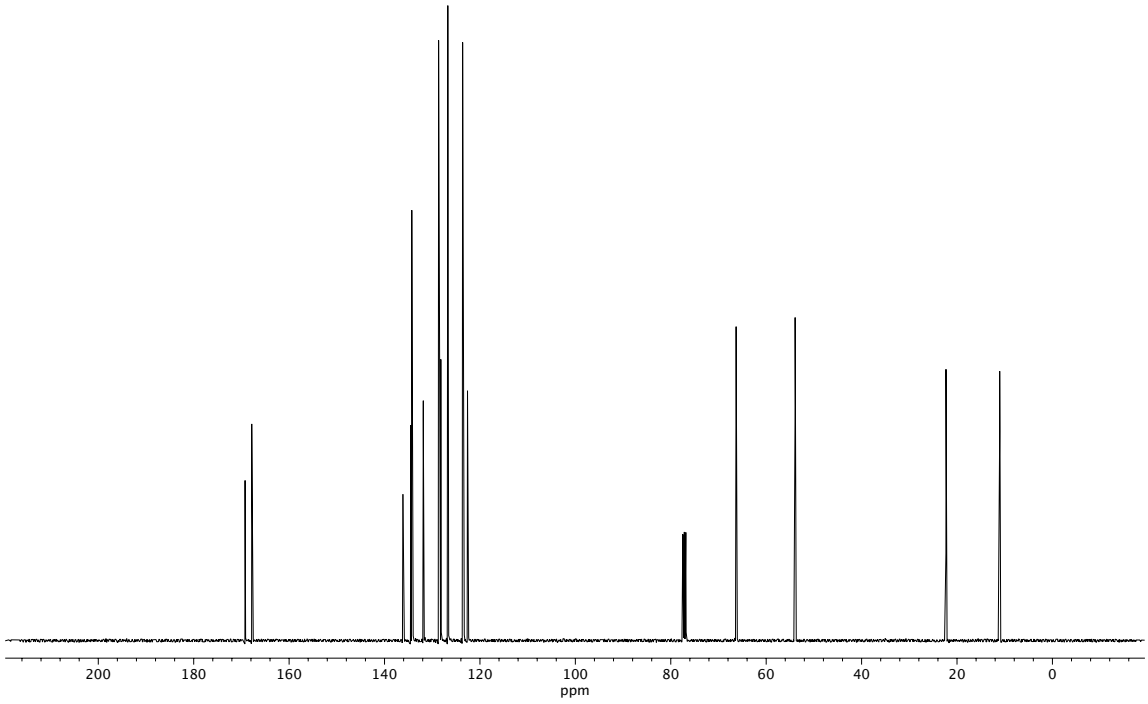

Figure A6.118 *^{13}C NMR (100 MHz, $CDCl_3$) of compound* ***119****.*

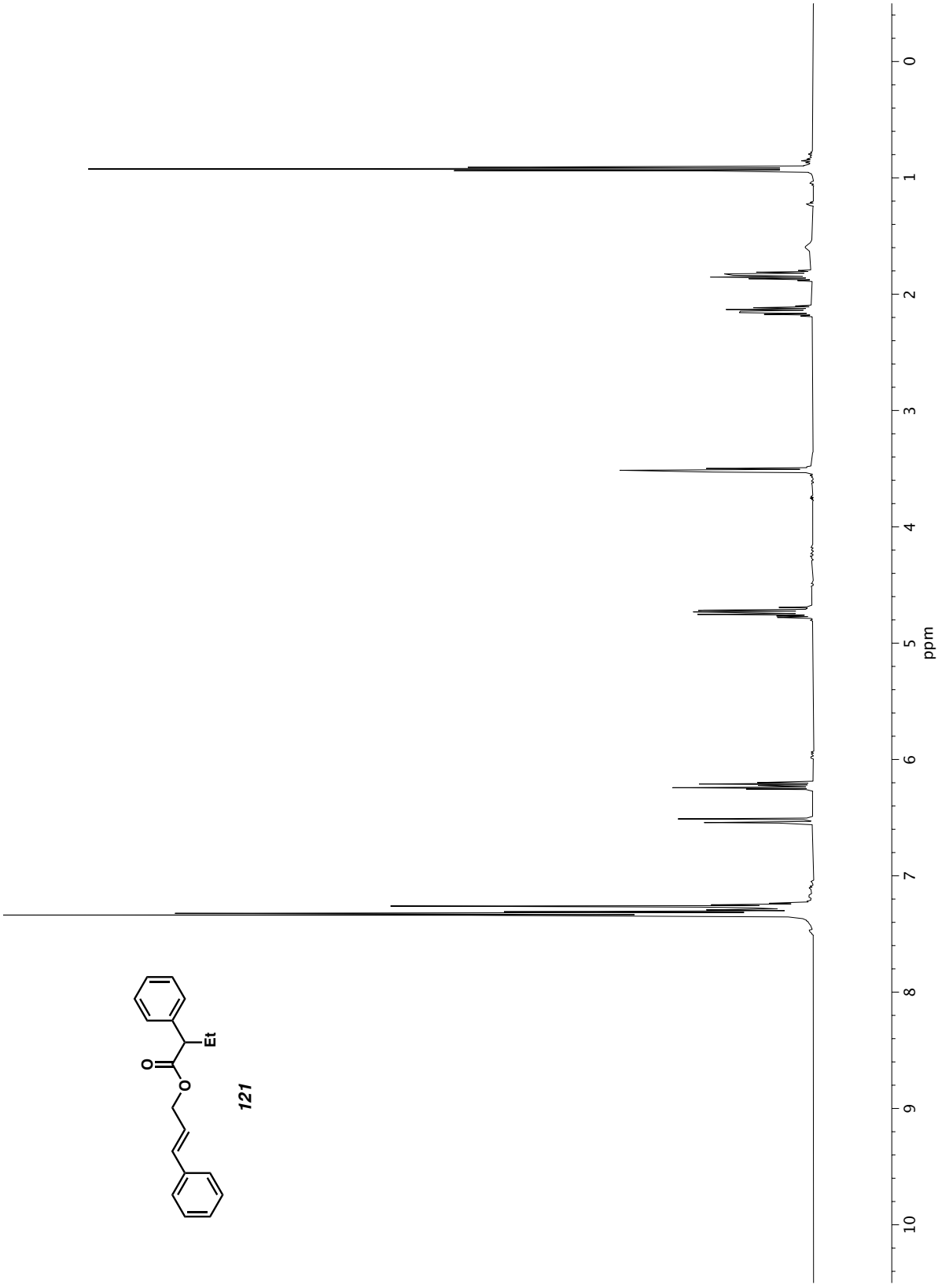

Figure A6.119 *^{1}H NMR (500 MHz, $CDCl_3$) of compound* ***121****.*

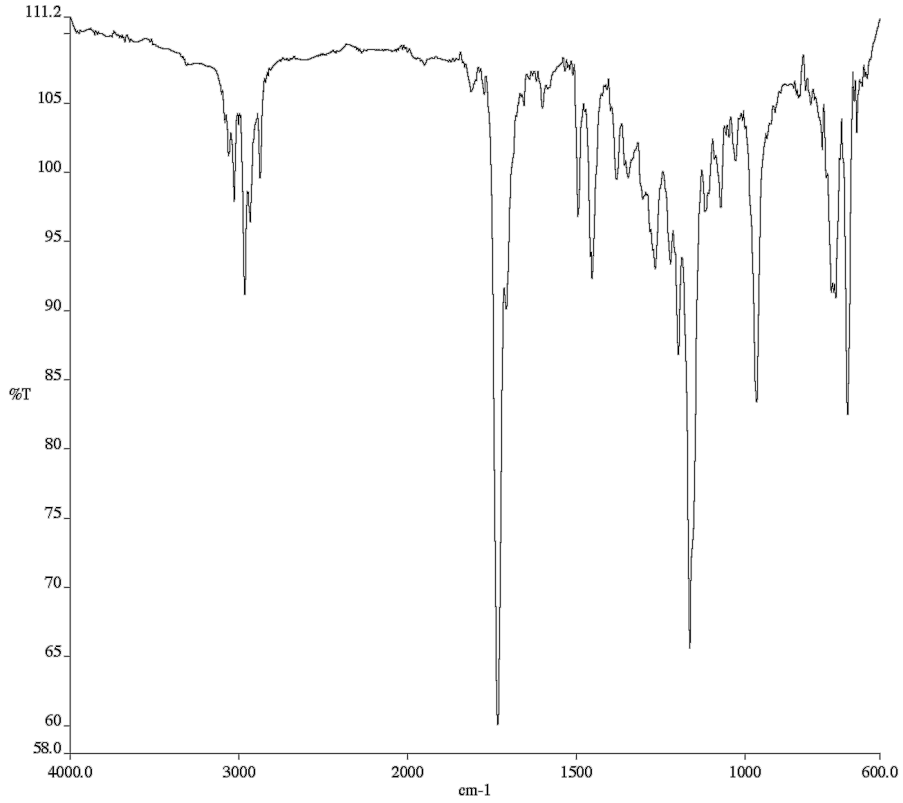

Figure A6.120 *Infrared spectrum (Thin Film, NaCl) of compound* ***121****.*

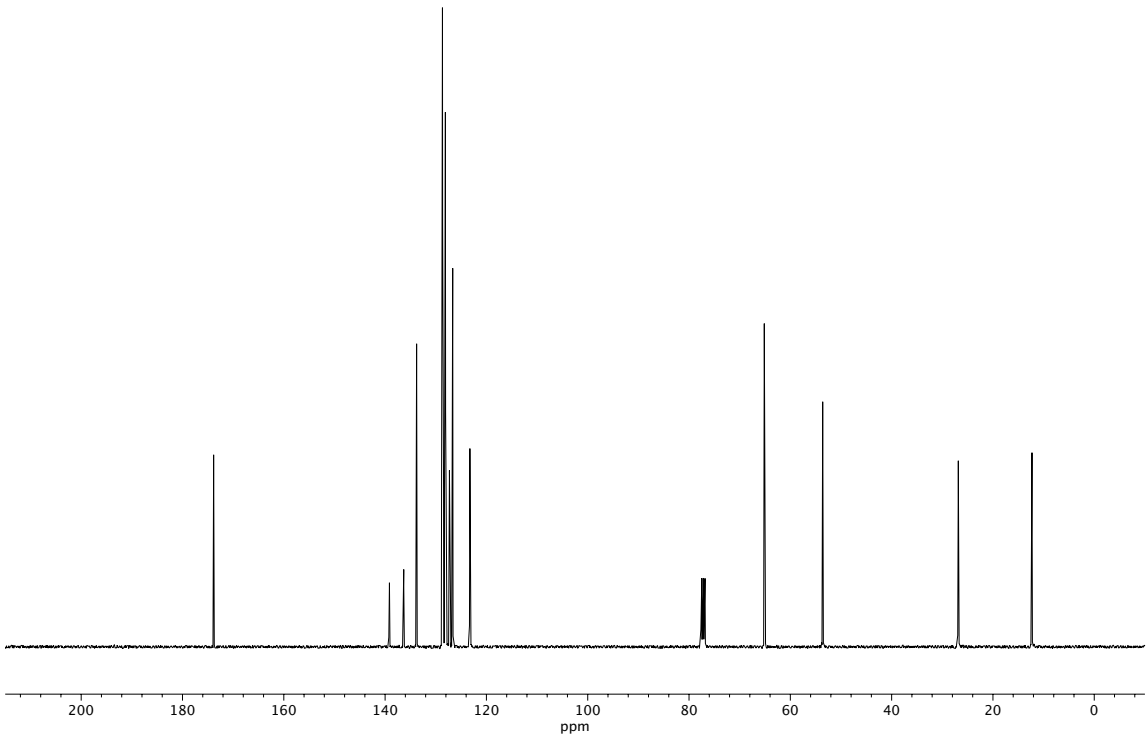

Figure A6.121 *^{13}C NMR (100 MHz, $CDCl_3$) of compound* ***121****.*

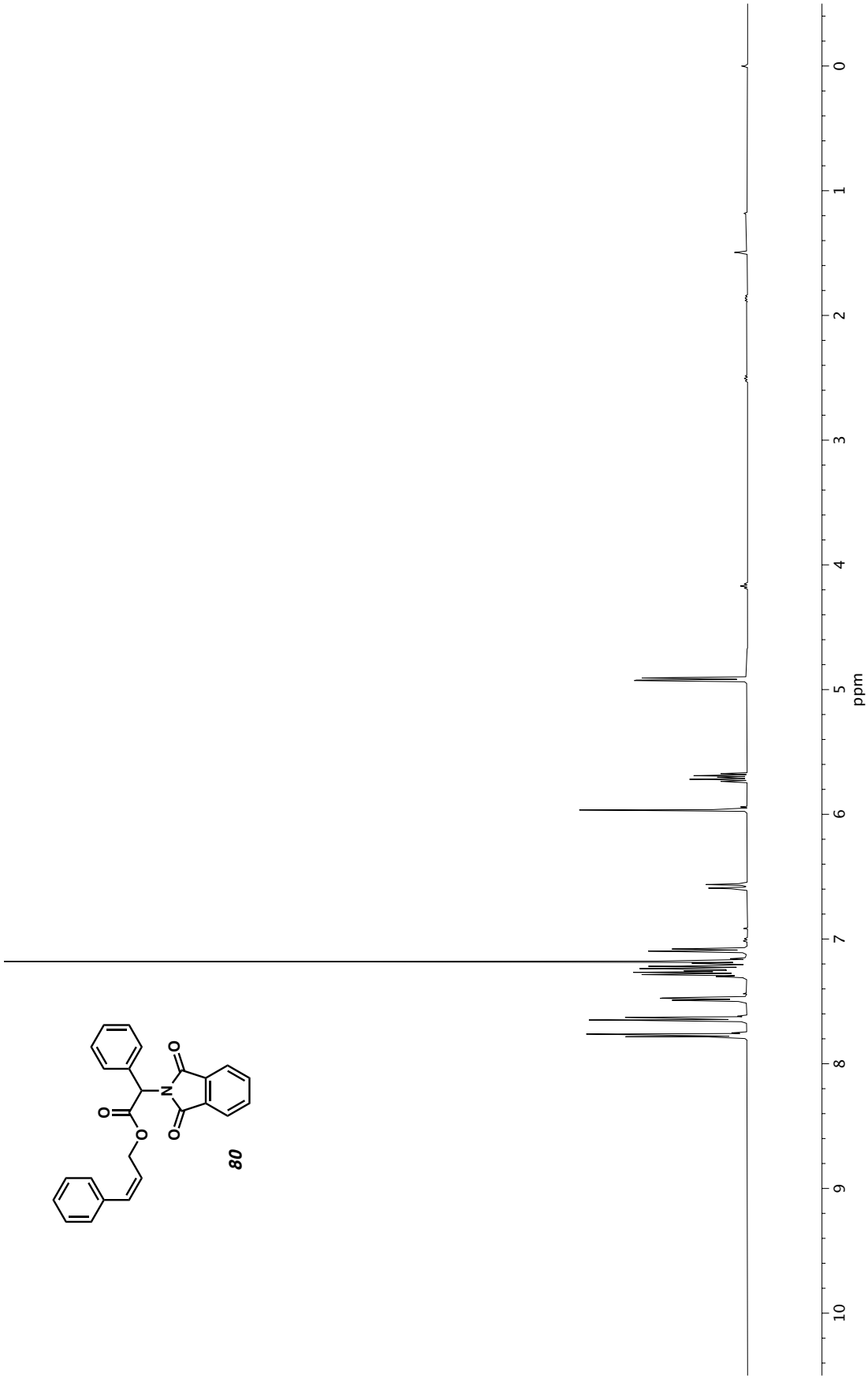

Figure A6.122 *^{1}H NMR (500 MHz, $CDCl_3$) of compound* ***80***.

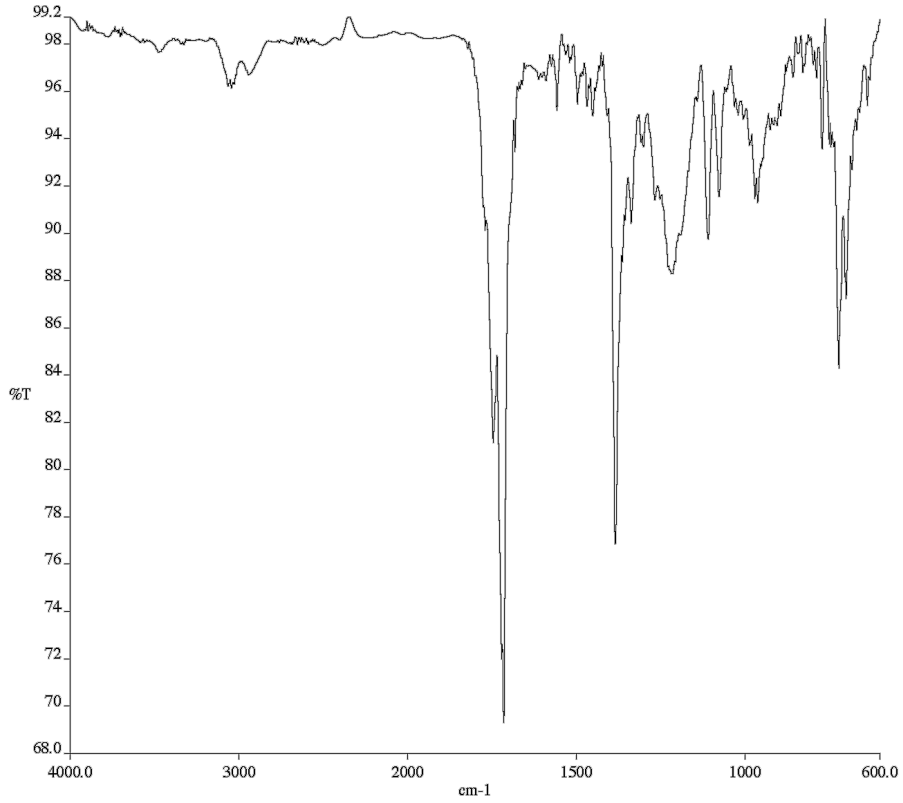

Figure A6.123 *Infrared spectrum (Thin Film, NaCl) of compound* ***80****.*

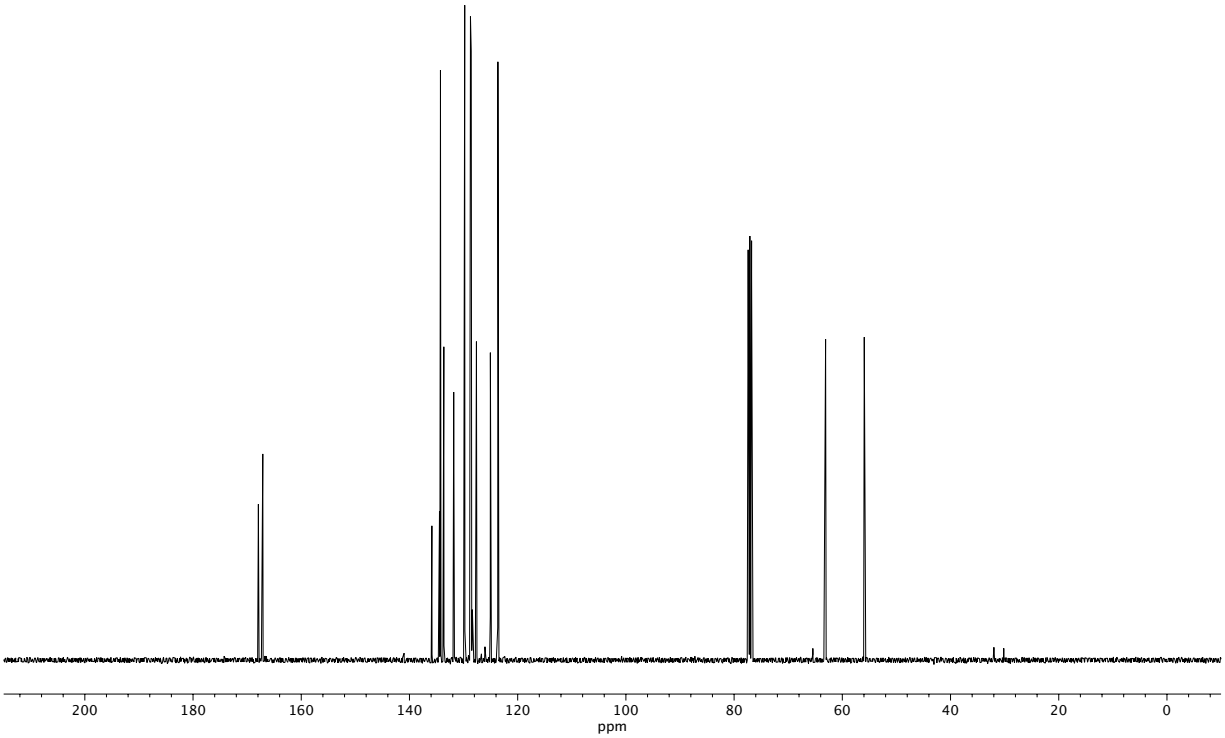

Figure A6.124 *^{13}C NMR (100 MHz, $CDCl_3$) of compound* ***80****.*

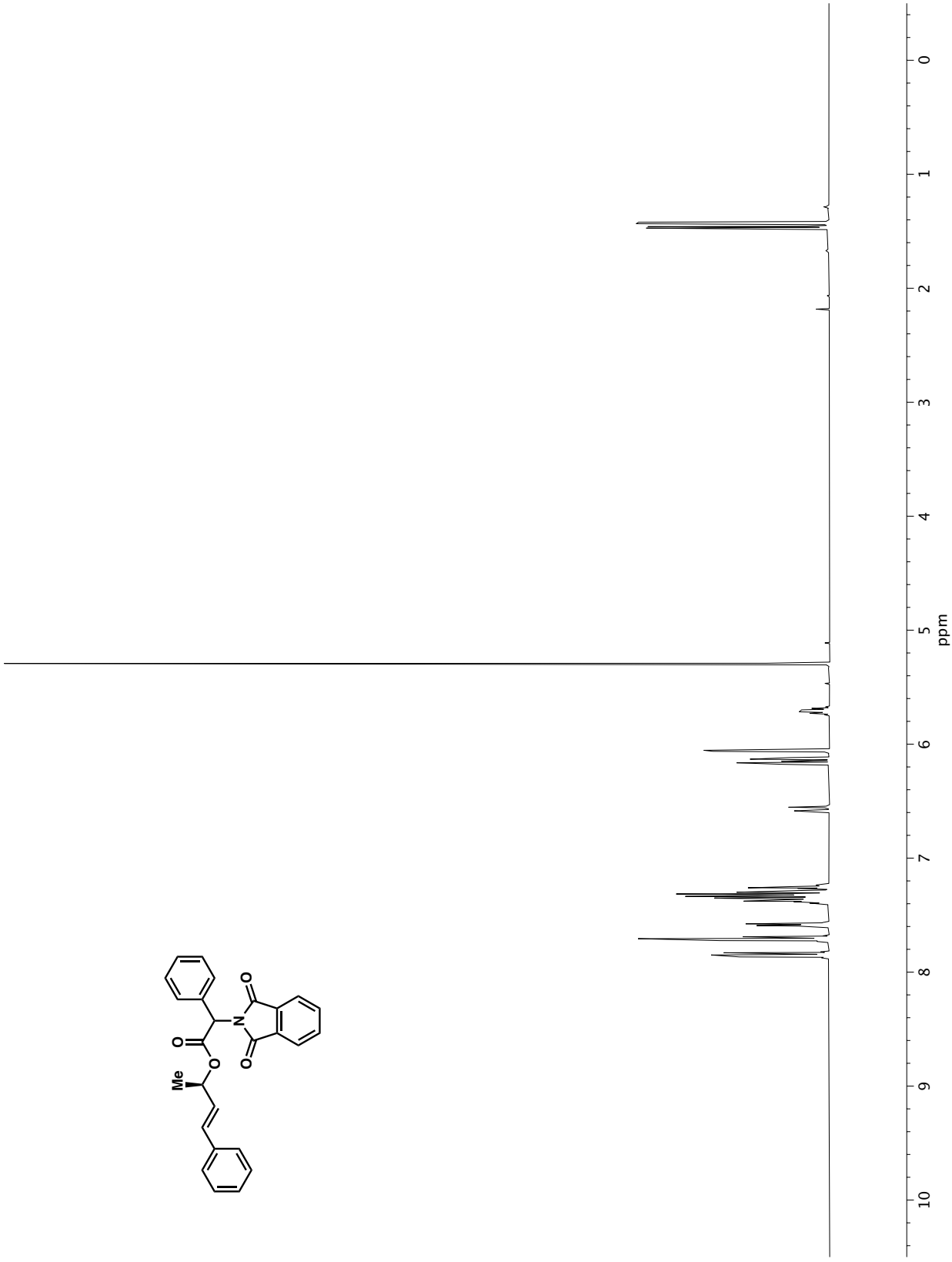

Figure A6.125 *^{1}H NMR (500 MHz, $CDCl_3$) of compound* ***82***.

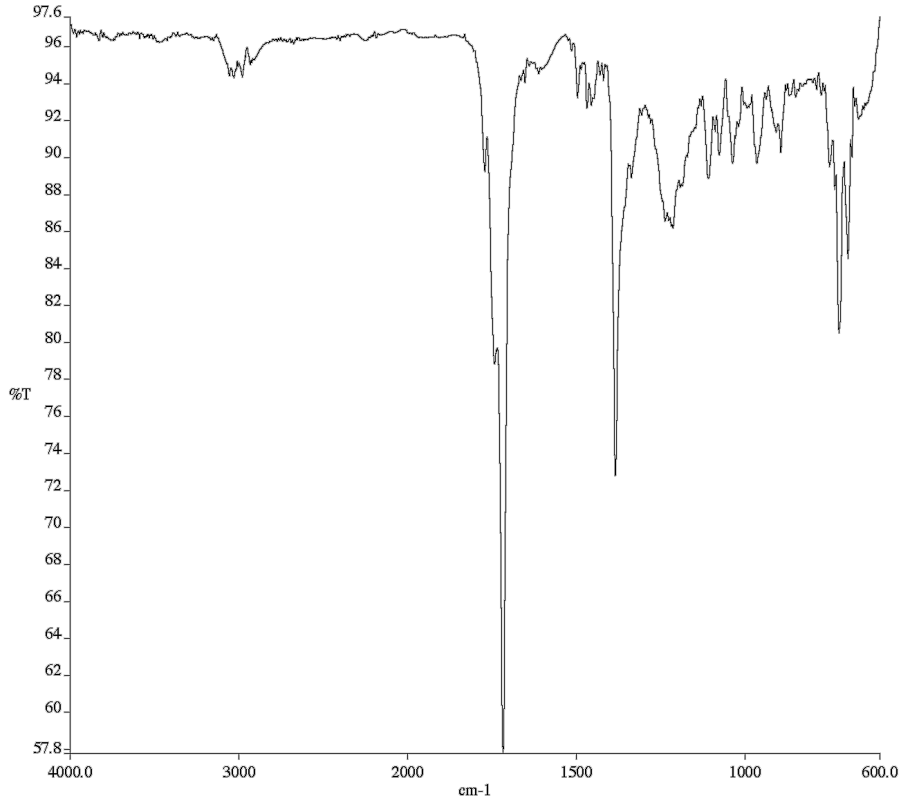

Figure A6.126 *Infrared spectrum (Thin Film, NaCl) of compound* ***82****.*

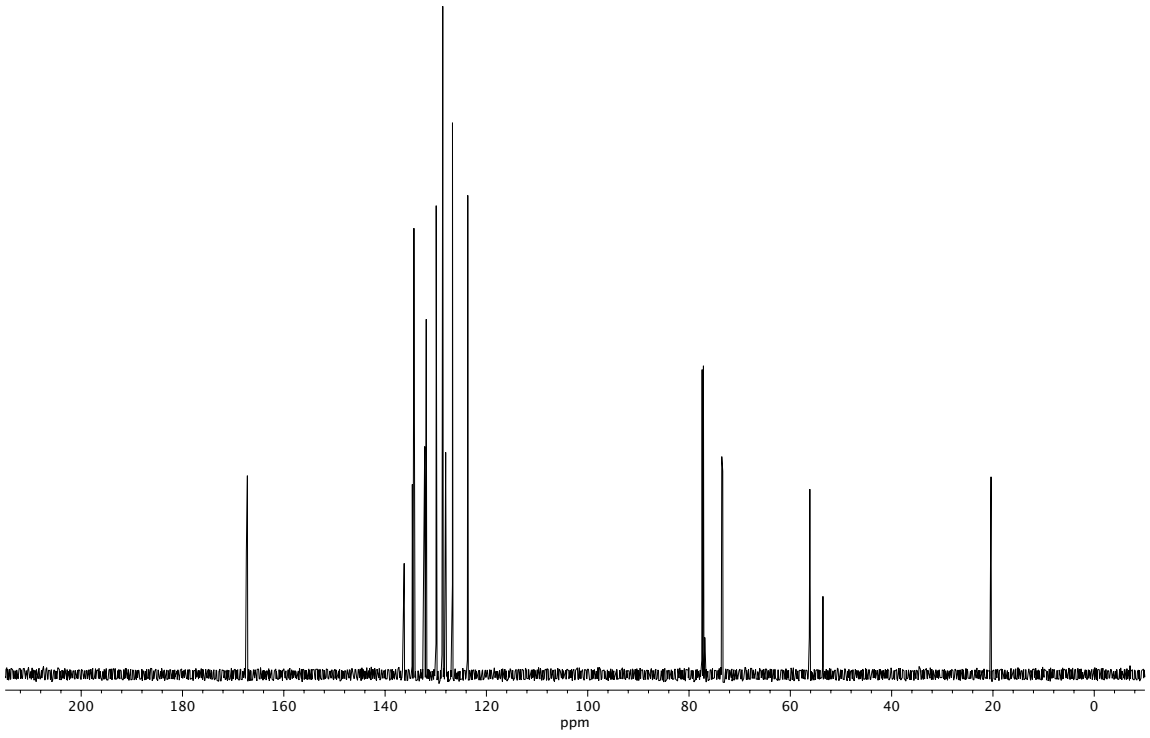

Figure A6.127 *^{13}C NMR (100 MHz, $CDCl_3$) of compound* ***82****.*

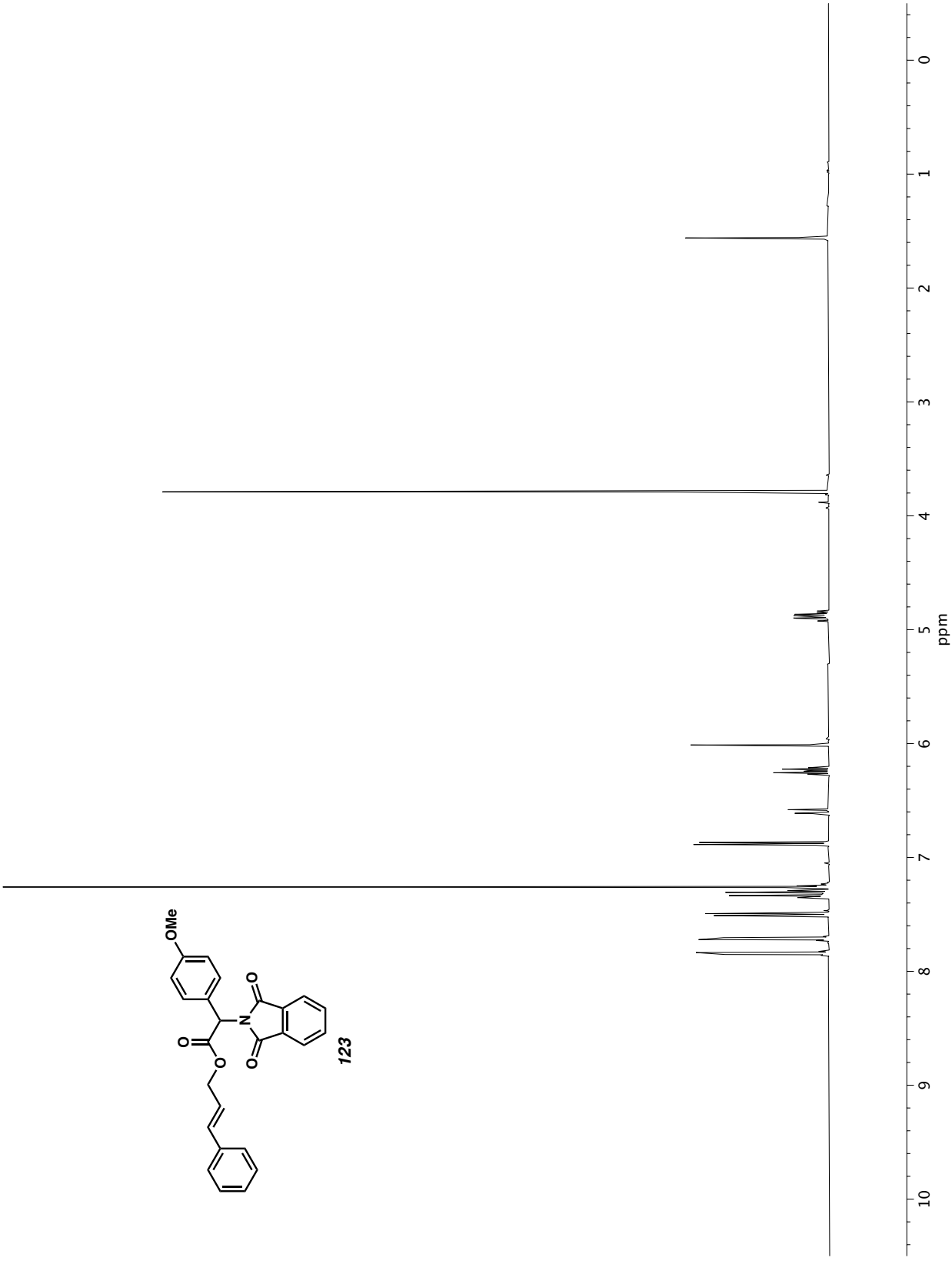

Figure A6.128 *^{1}H NMR (500 MHz, $CDCl_3$) of compound **123**.*

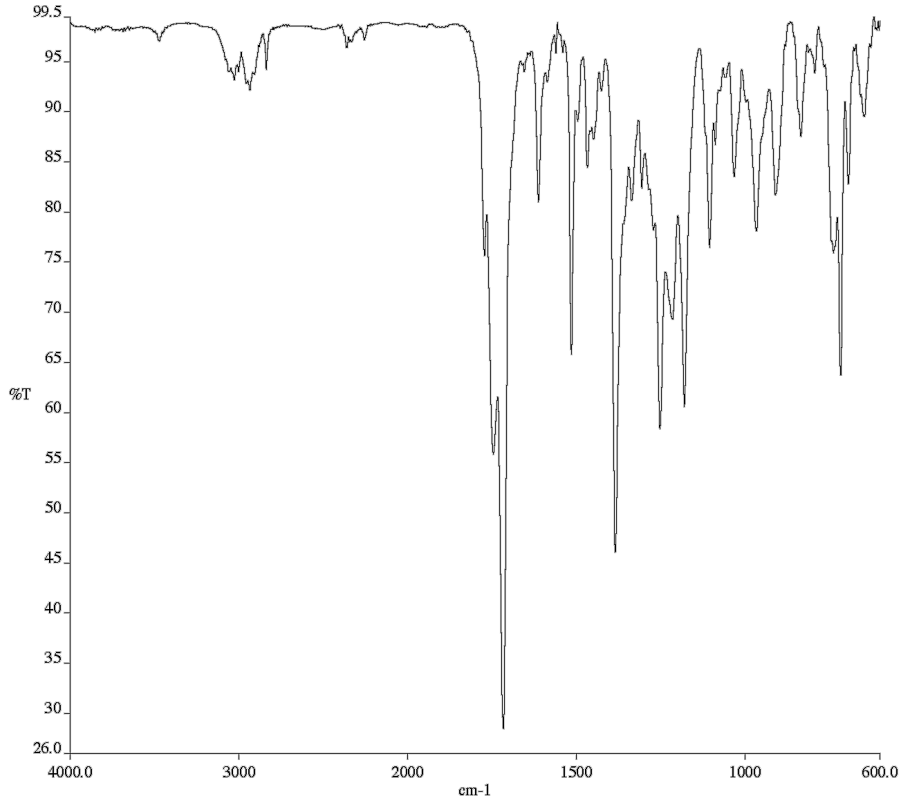

Figure A6.129 *Infrared spectrum (Thin Film, NaCl) of compound* ***123****.*

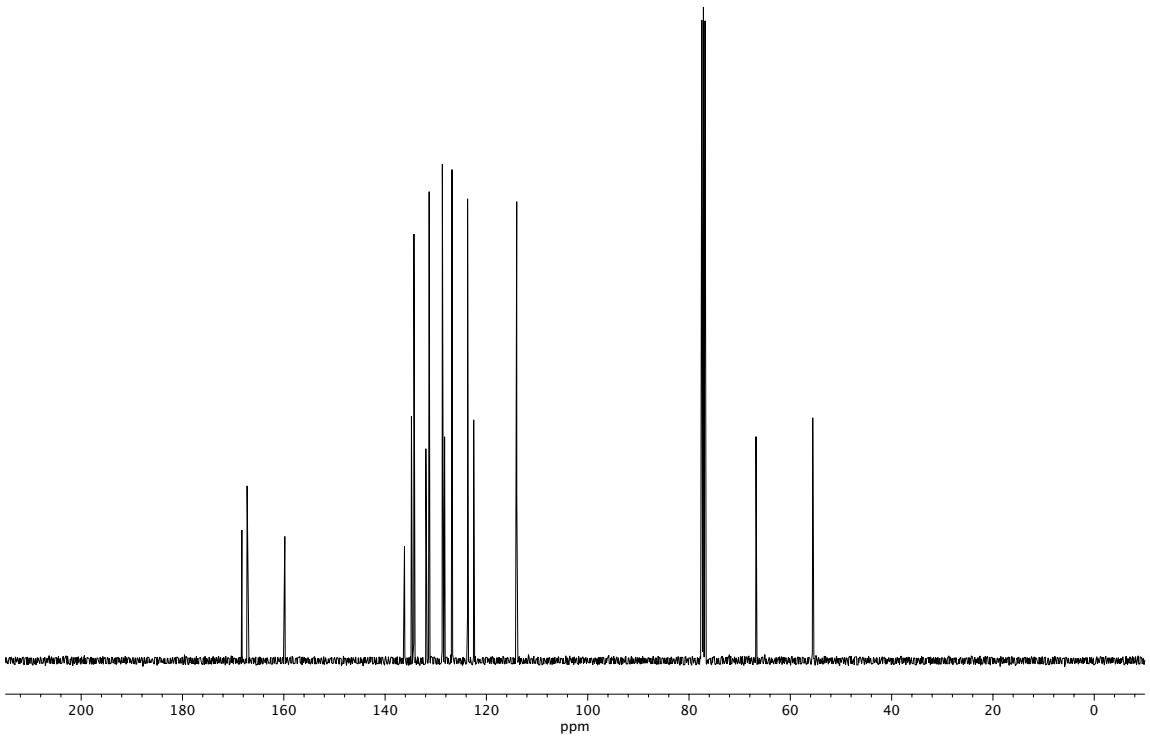

Figure A6.130 *^{13}C NMR (100 MHz, $CDCl_3$) of compound* ***123****.*

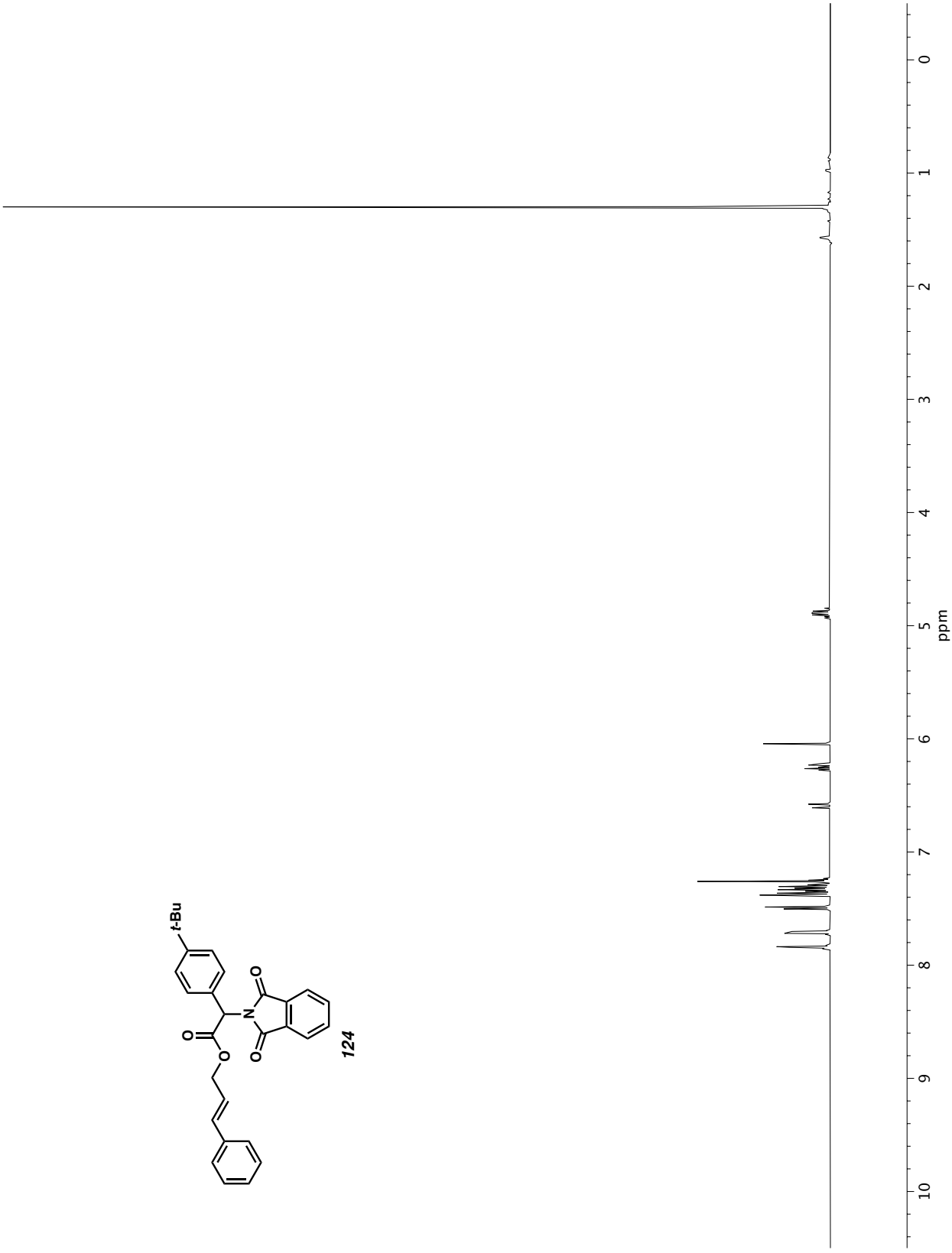

Figure A6.131 *^{1}H NMR (500 MHz, $CDCl_3$) of compound **124**.*

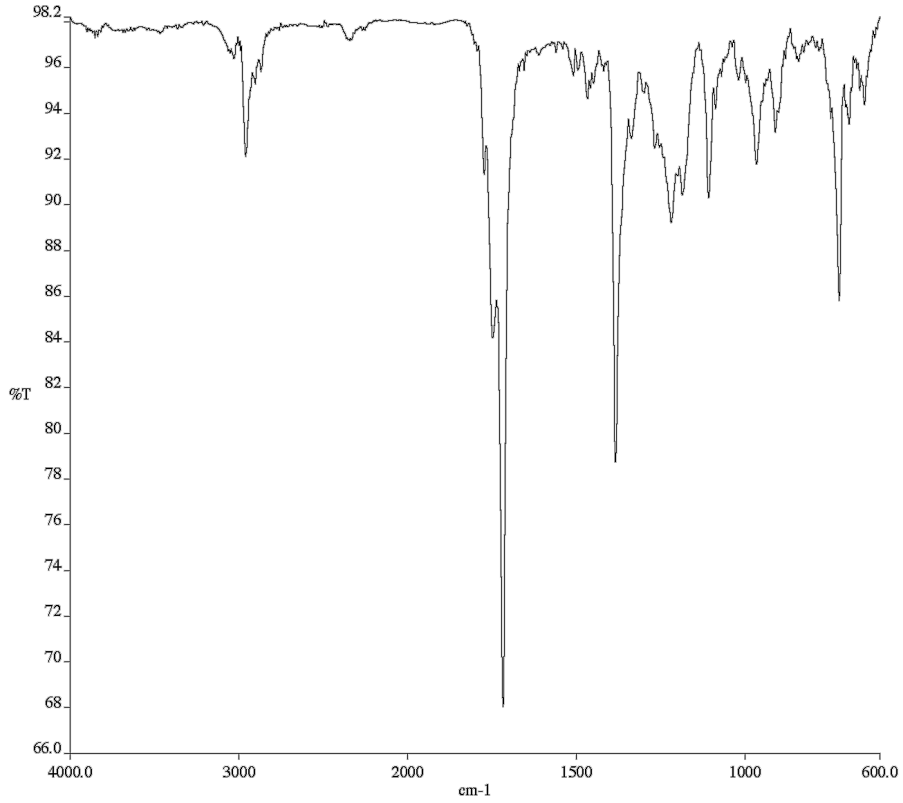

Figure A6.132 *Infrared spectrum (Thin Film, NaCl) of compound* ***124****.*

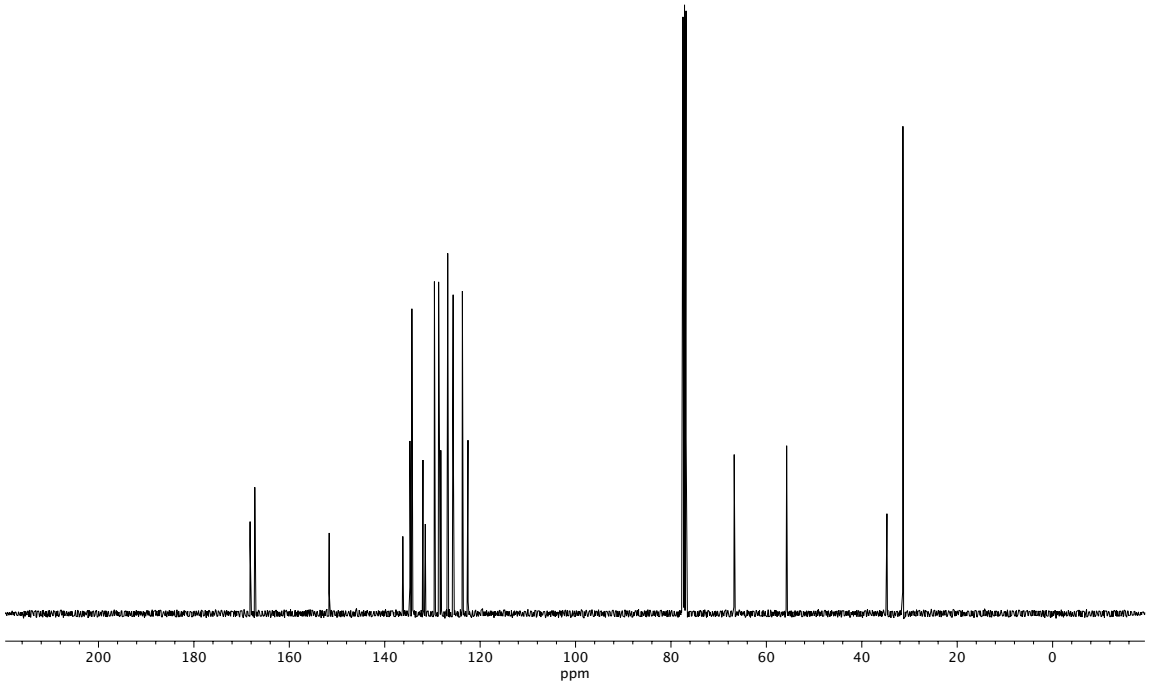

Figure A6.133 *^{13}C NMR (100 MHz, $CDCl_3$) of compound* ***124****.*

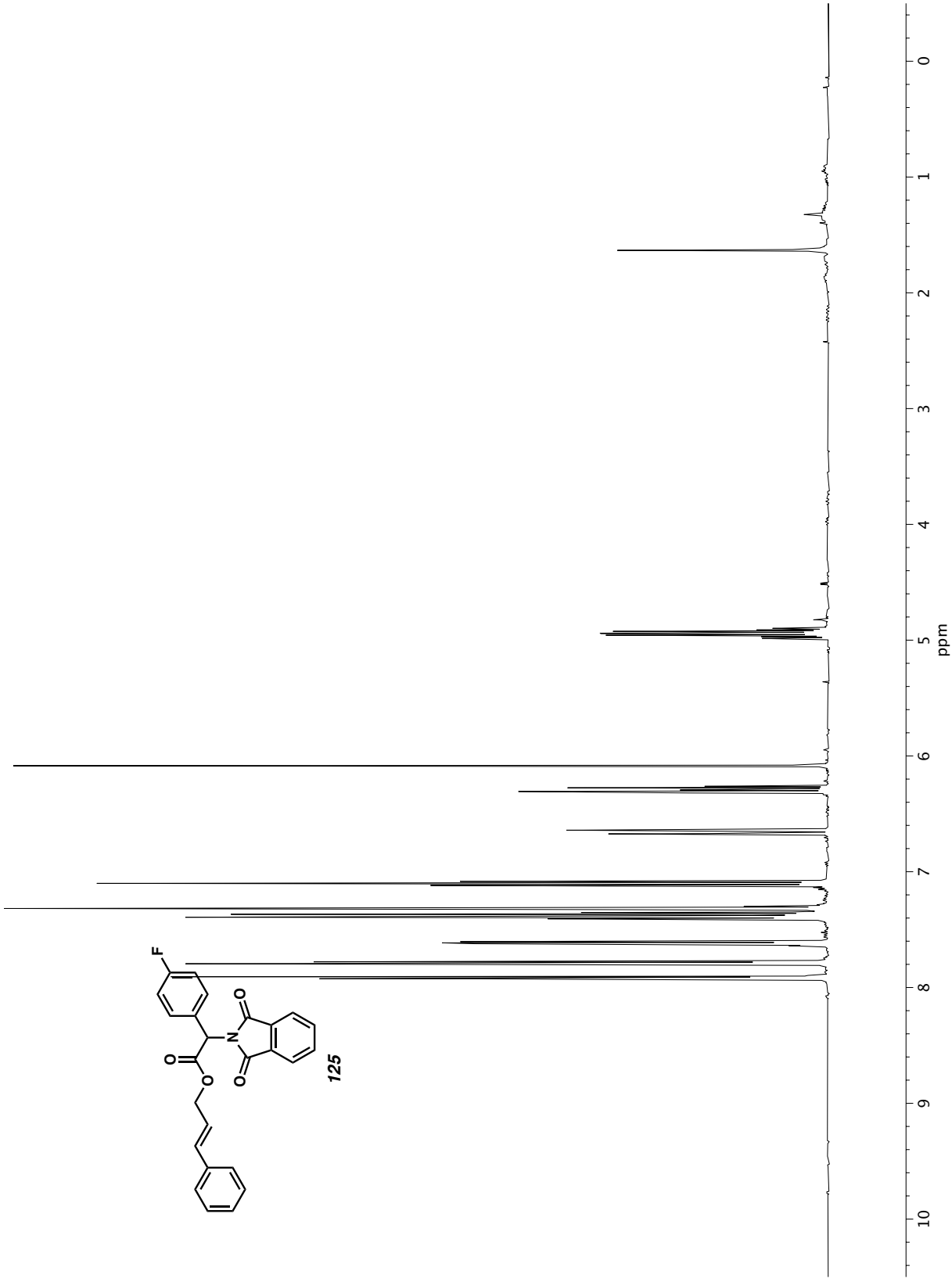

Figure A6.134 *^{1}H NMR (500 MHz, $CDCl_3$) of compound **125**.*

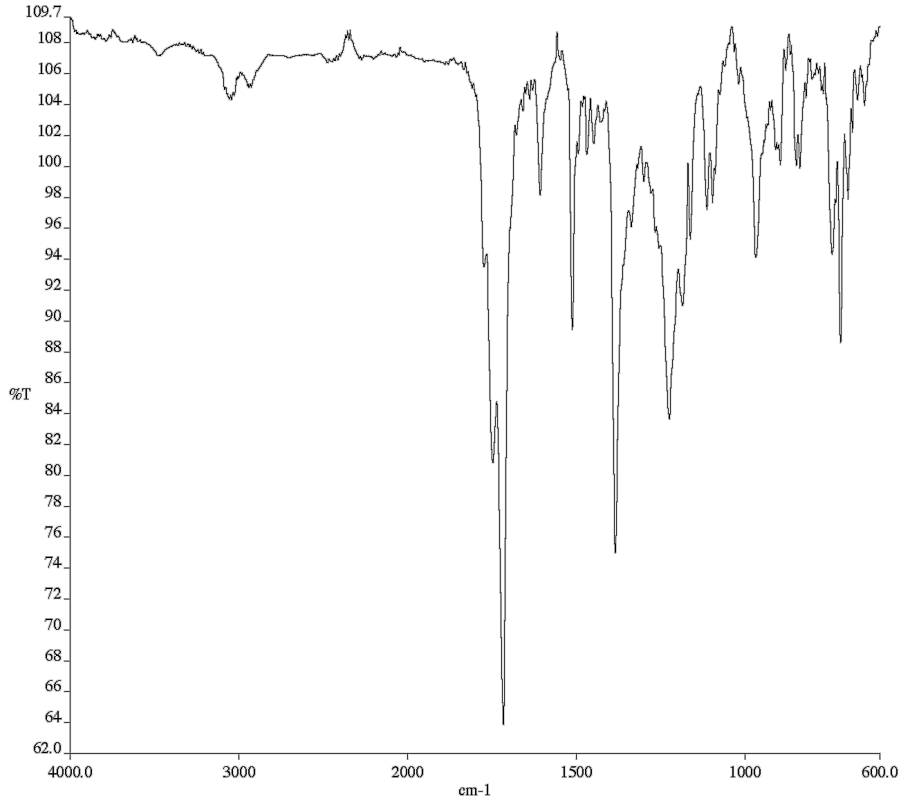

Figure A6.135 *Infrared spectrum (Thin Film, NaCl) of compound* ***125****.*

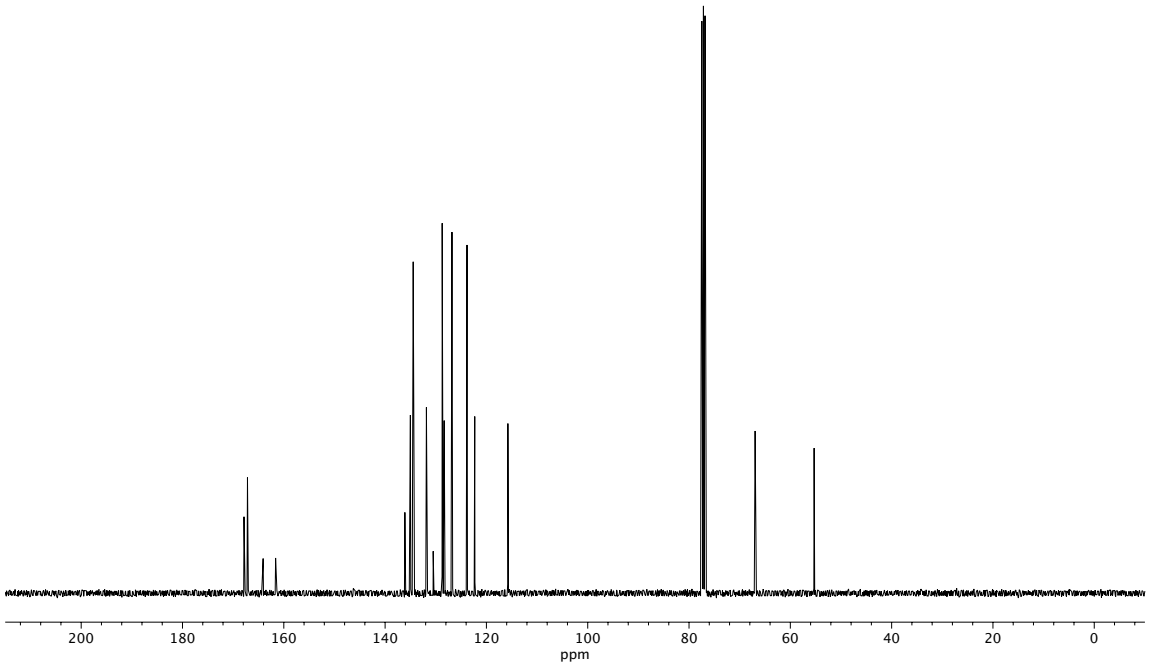

Figure A6.136 *^{13}C NMR (100 MHz, $CDCl_3$) of compound* ***125****.*

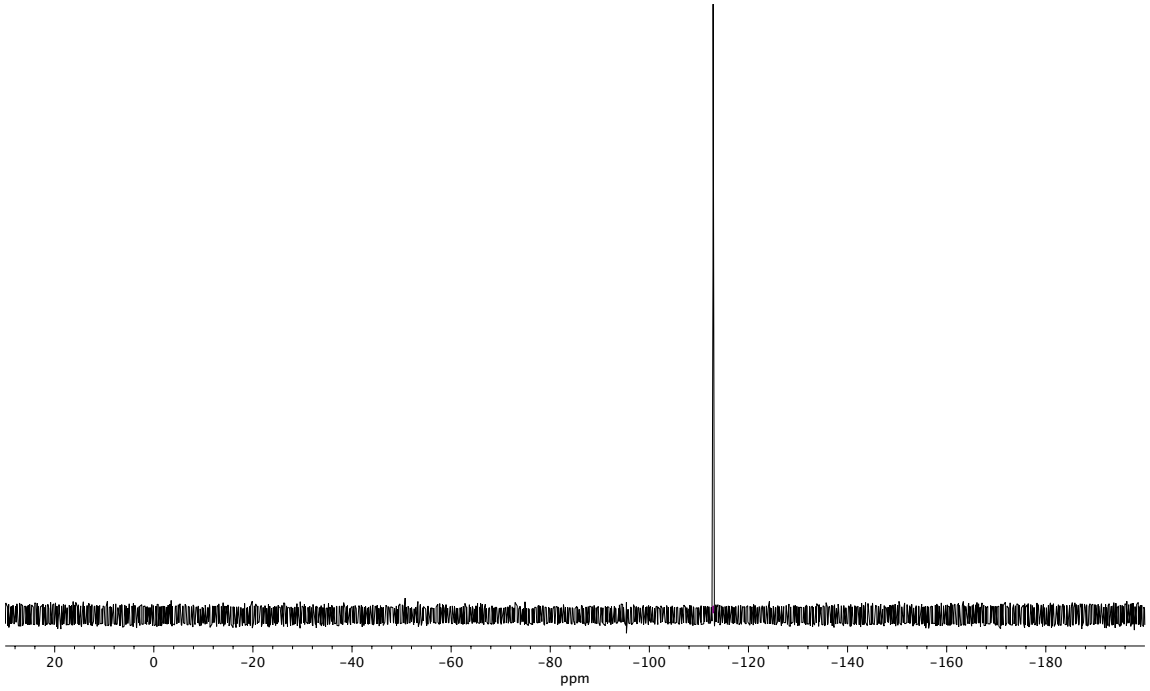

Figure A6.137 *^{19}F NMR (282 MHz, $CDCl_3$) of compound **125**.*

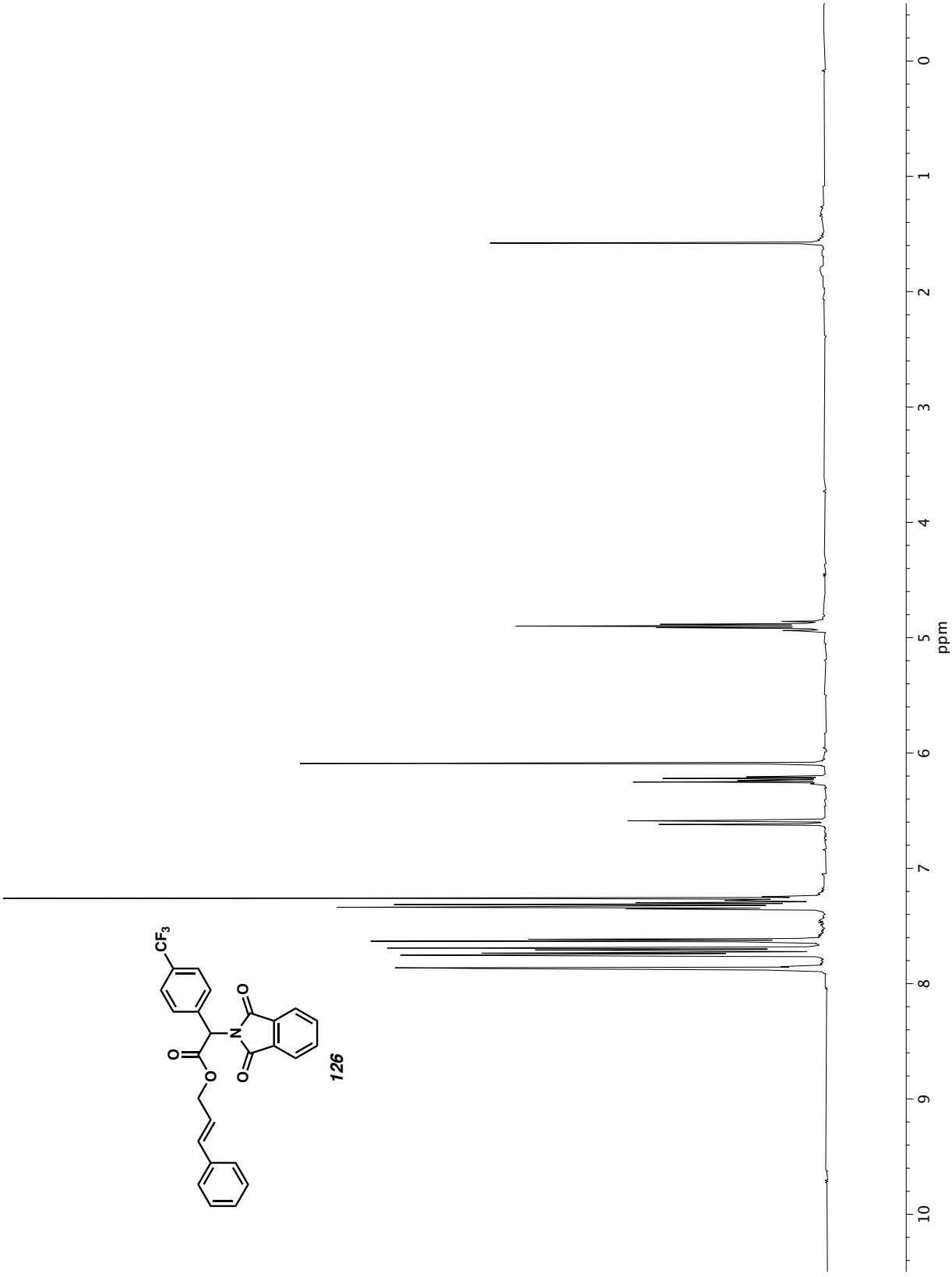

Figure A6.138 *^{1}H NMR (500 MHz, $CDCl_3$) of compound **126**.*

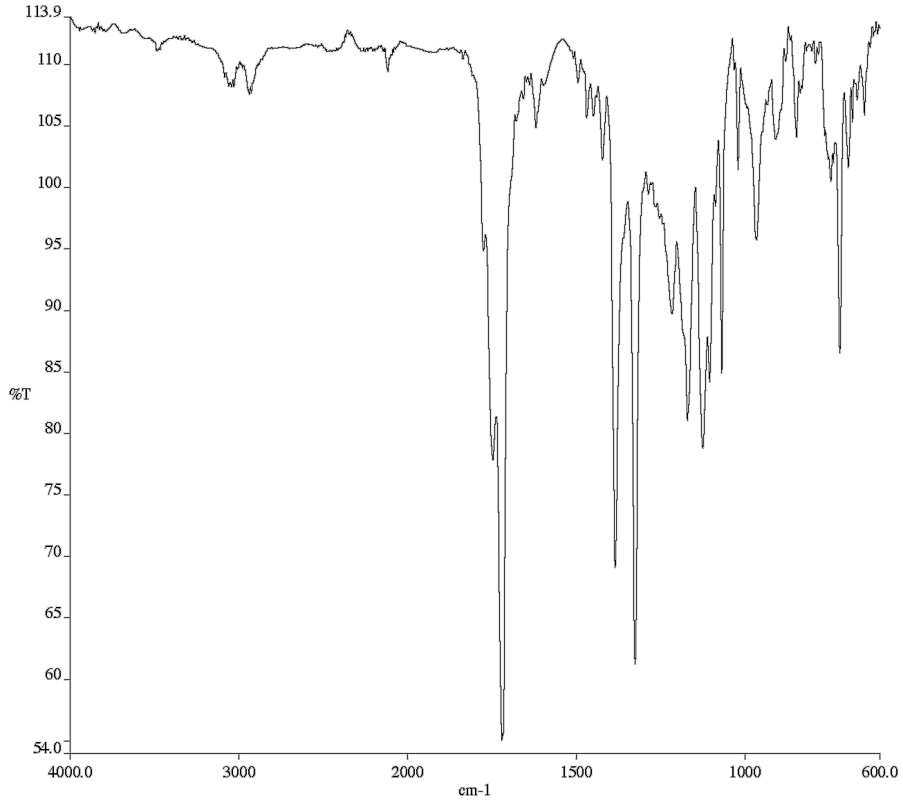

Figure A6.139 *Infrared spectrum (Thin Film, NaCl) of compound* ***126****.*

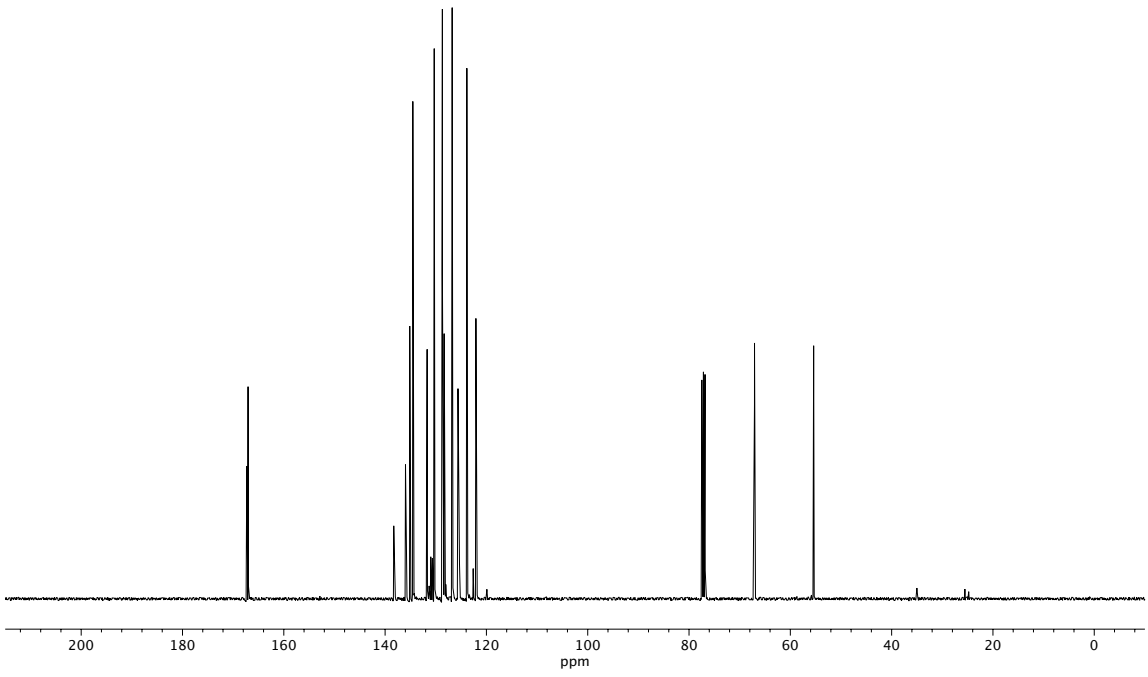

Figure A6.140 *^{13}C NMR (100 MHz, $CDCl_3$) of compound* ***126****.*

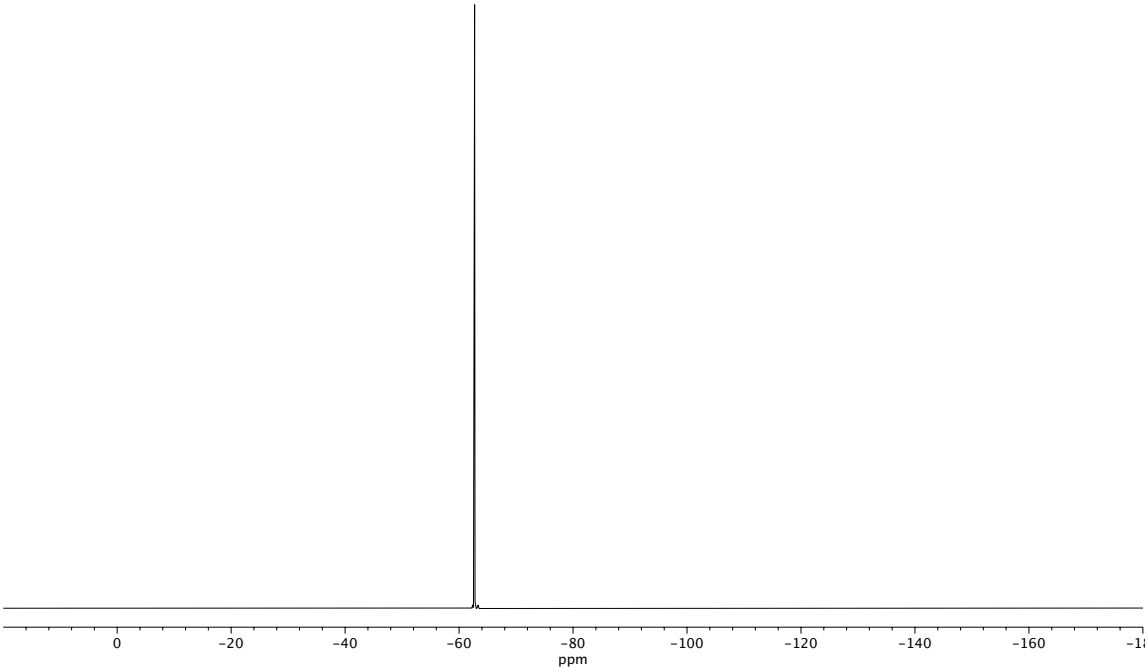

Figure A6.141 *^{19}F NMR (282 MHz, $CDCl_3$) of compound* ***126****.*

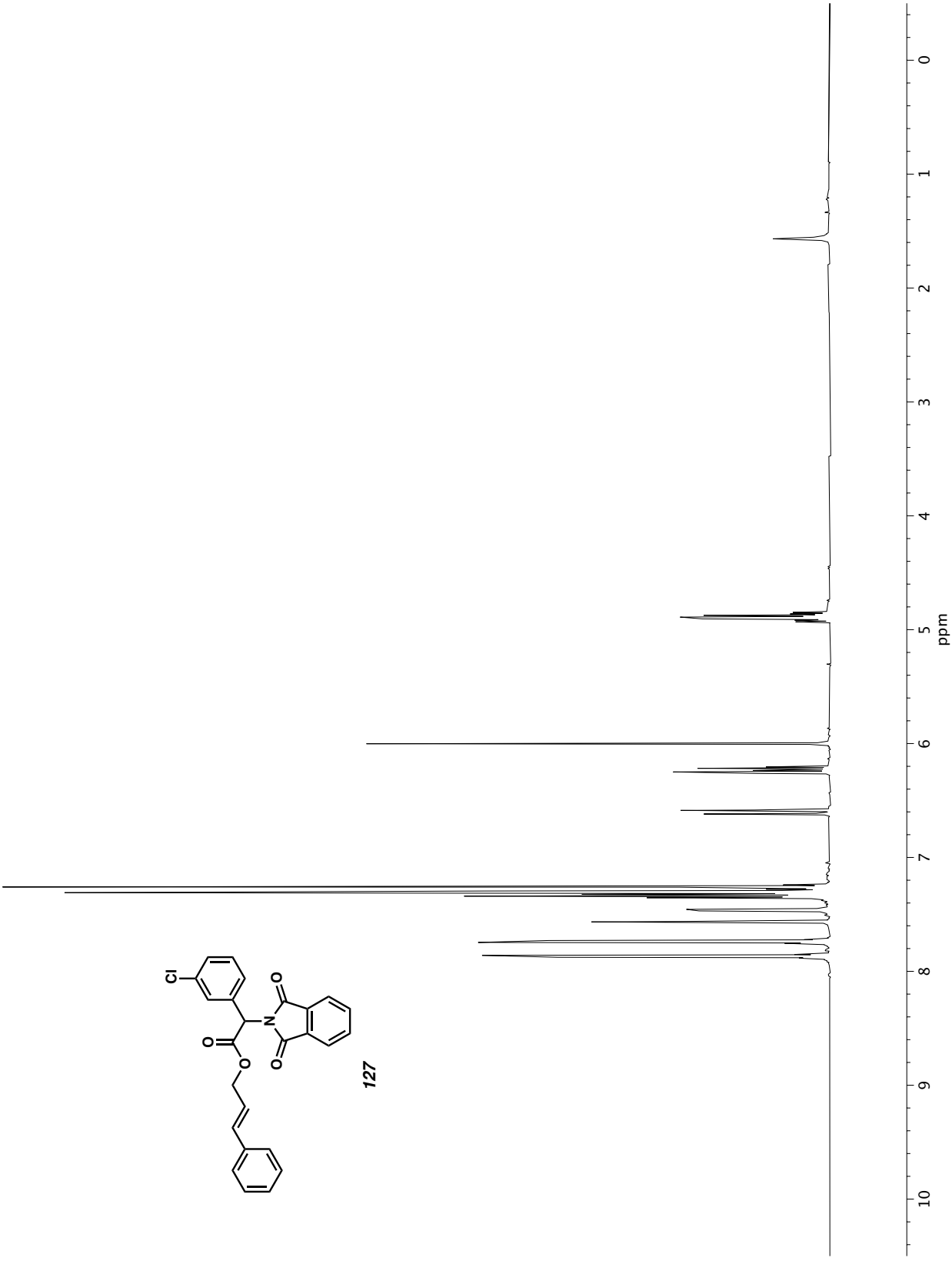

Figure A6.142 *^{1}H NMR (500 MHz, $CDCl_3$) of compound **127**.*

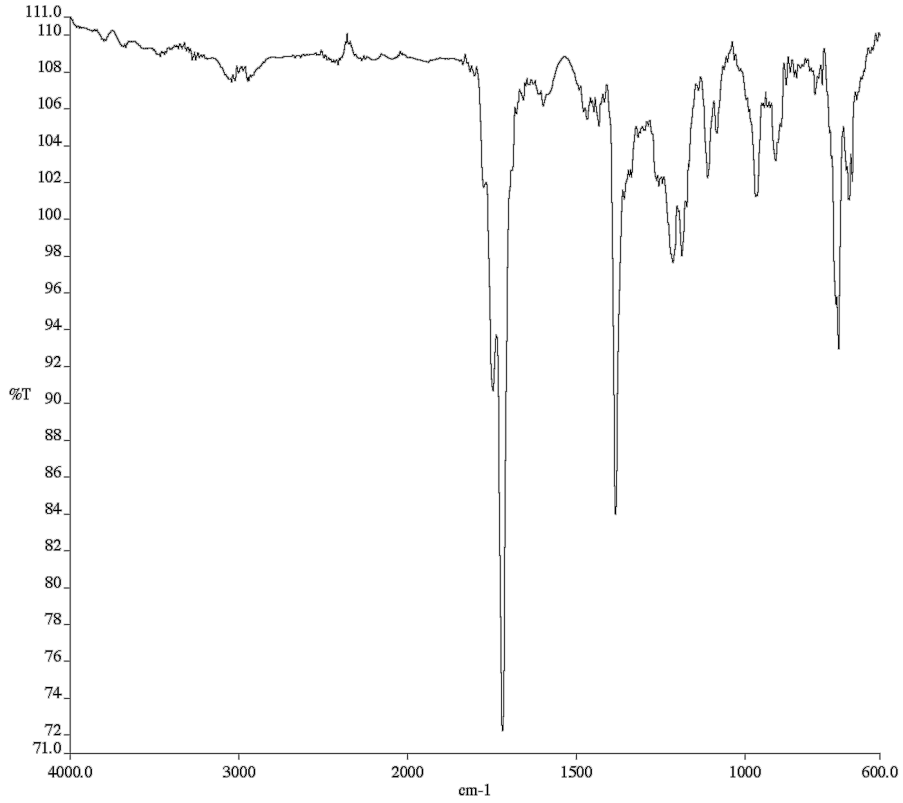

Figure A6.143 *Infrared spectrum (Thin Film, NaCl) of compound* ***127****.*

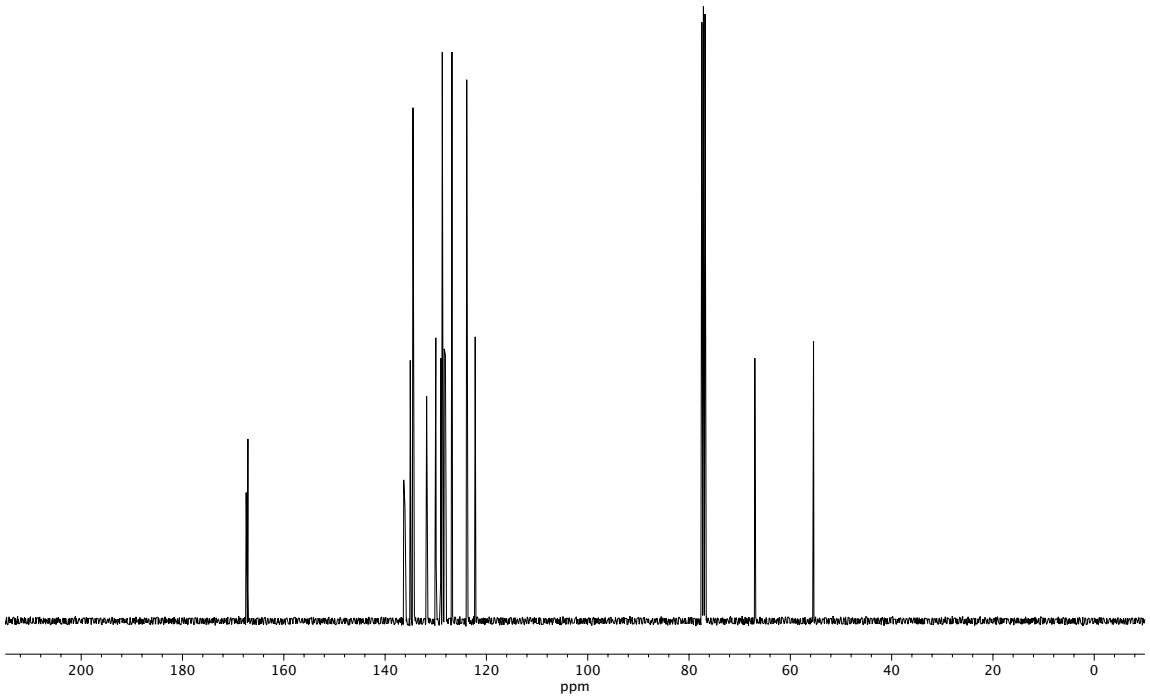

Figure A6.144 *^{13}C NMR (100 MHz, $CDCl_3$) of compound* ***127****.*

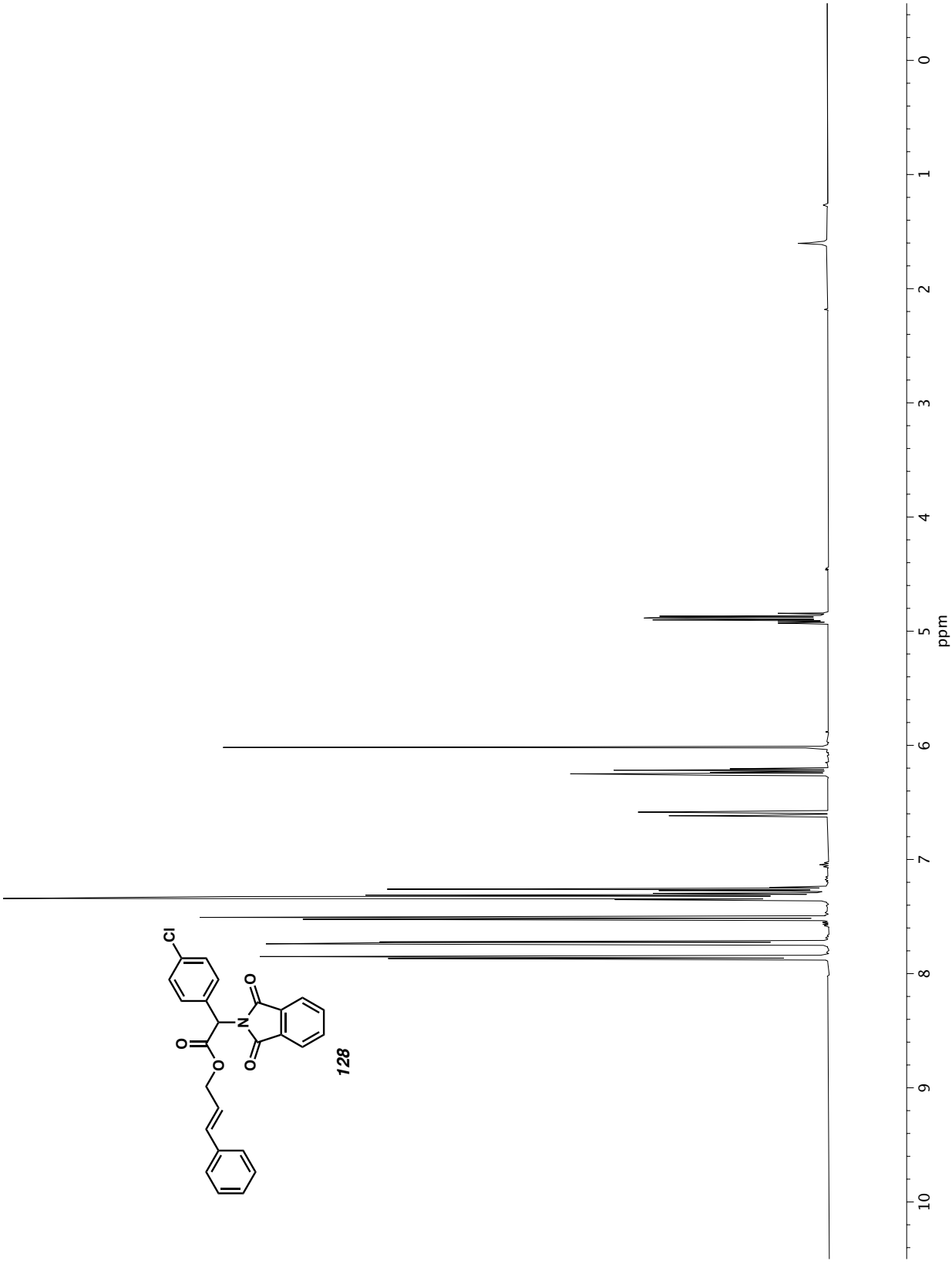

Figure A6.145 *^1H NMR (500 MHz, $CDCl_3$) of compound **128**.*

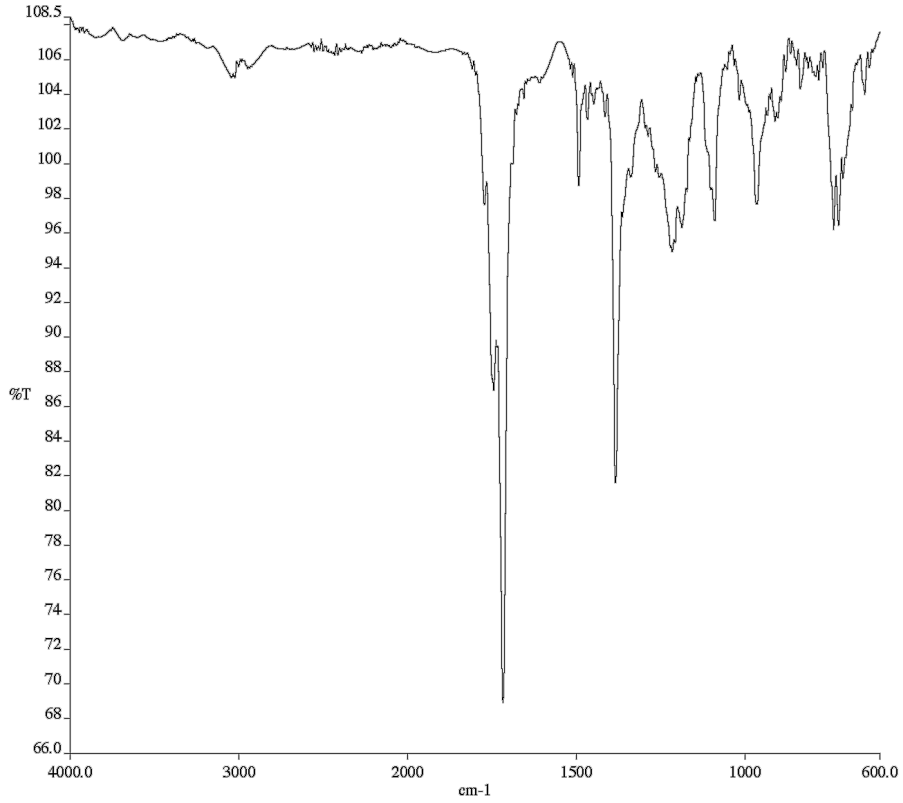

Figure A6.146 *Infrared spectrum (Thin Film, NaCl) of compound* ***128****.*

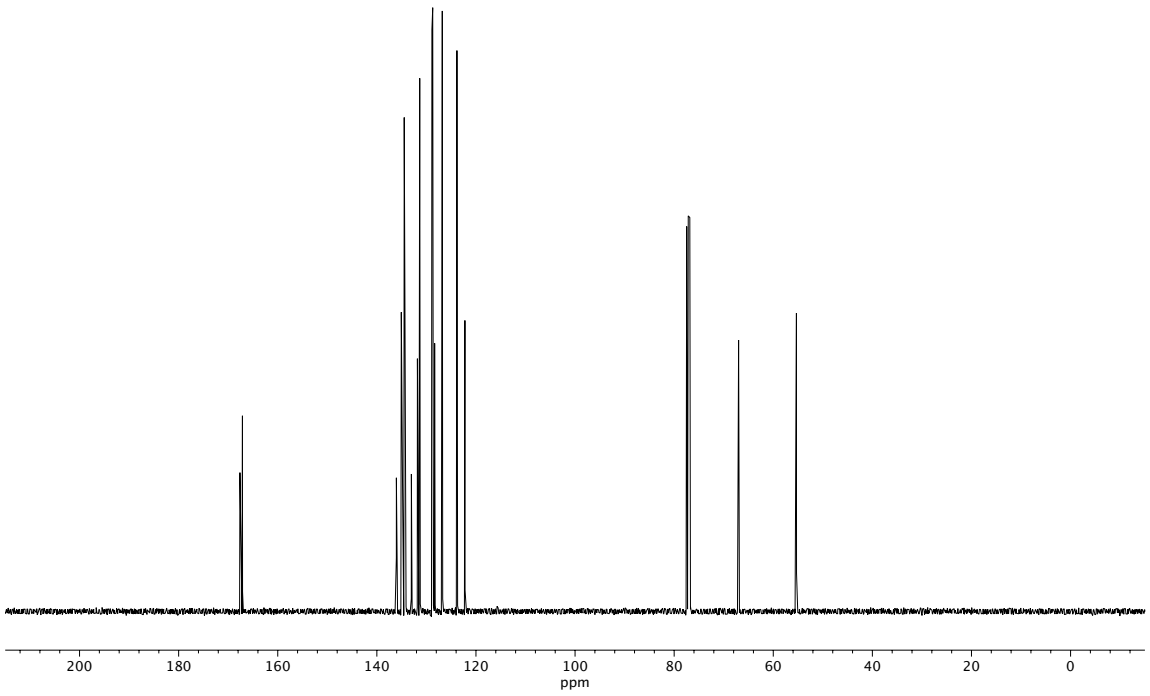

Figure A6.147 *^{13}C NMR (100 MHz, $CDCl_3$) of compound* ***128****.*

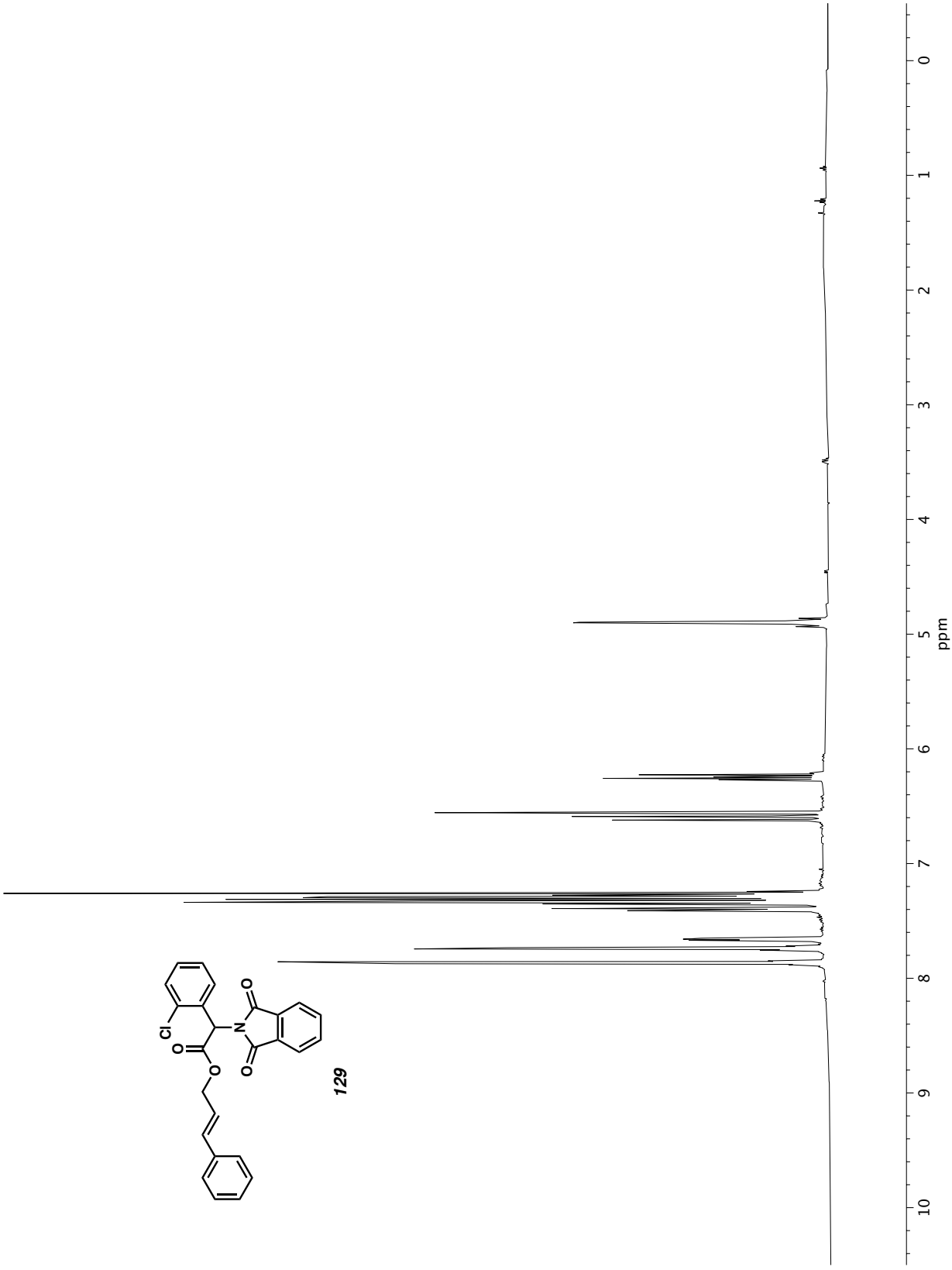

Figure A6.148 *^{1}H NMR (500 MHz, $CDCl_3$) of compound **129**.*

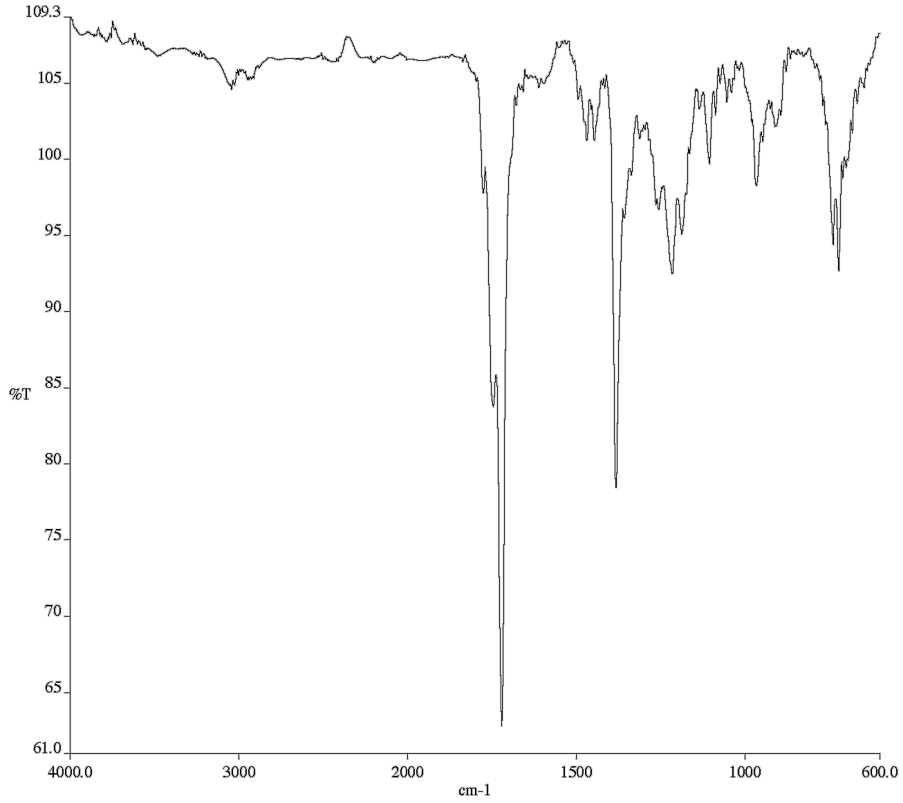

Figure A6.149 *Infrared spectrum (Thin Film, NaCl) of compound* ***129****.*

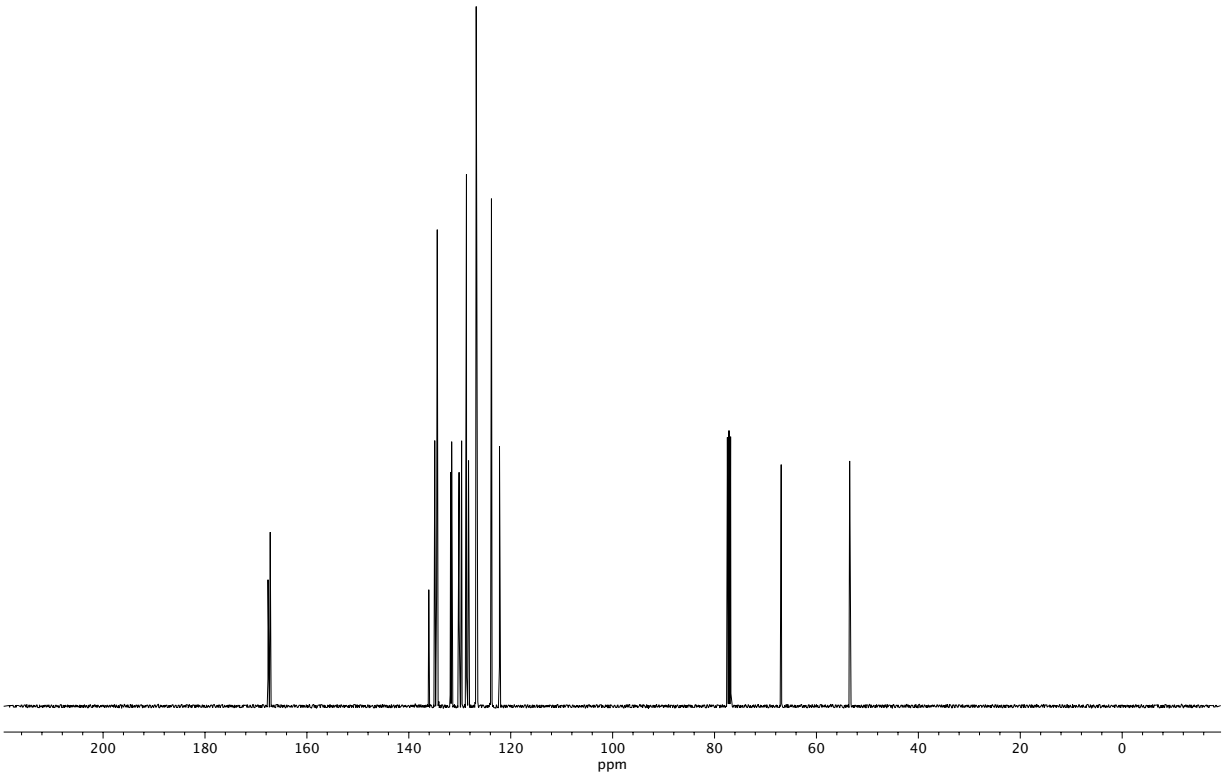

Figure A6.150 *^{13}C NMR (100 MHz, $CDCl_3$) of compound* ***129****.*

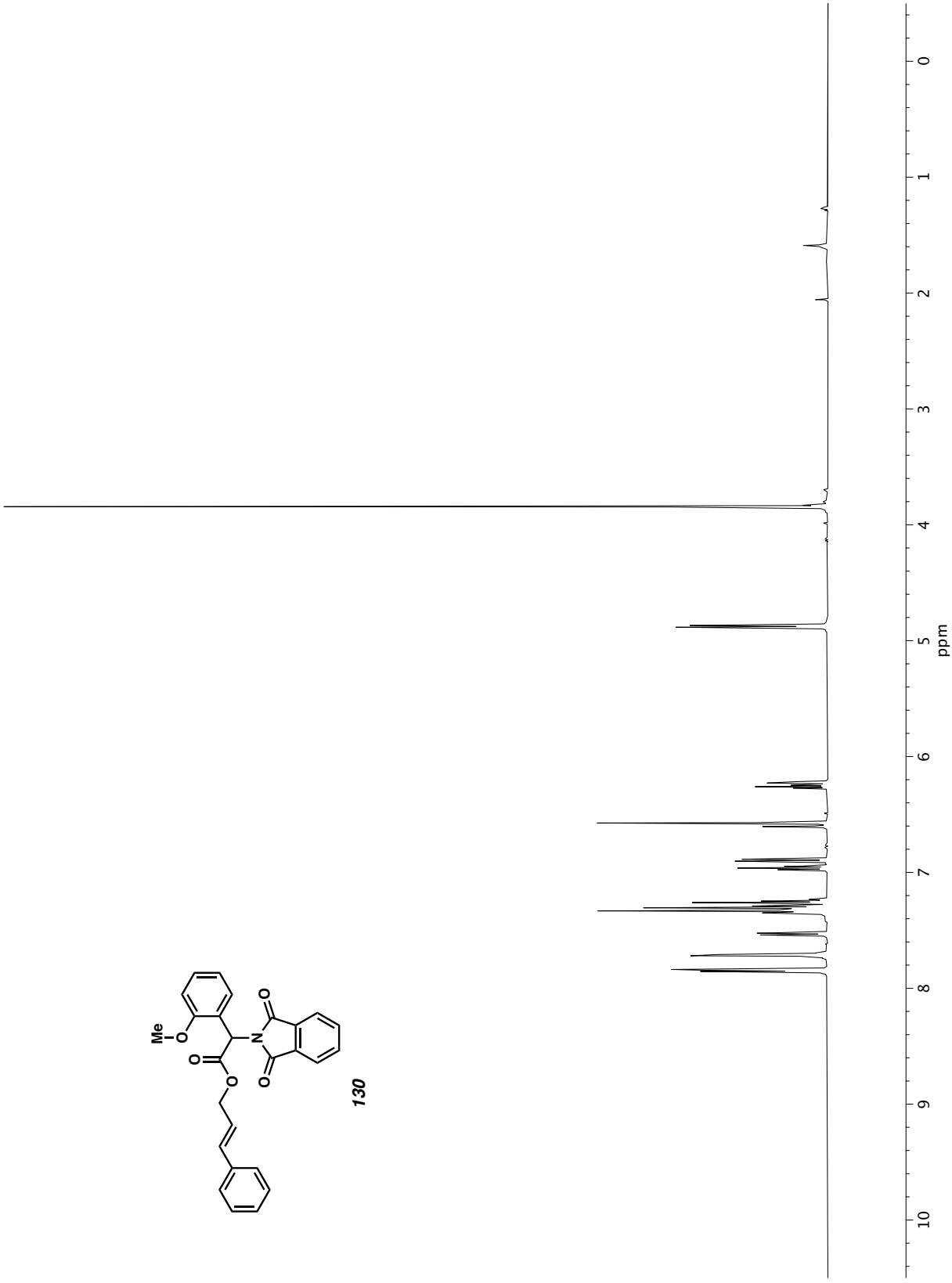

Figure A6.151 *^{1}H NMR (500 MHz, $CDCl_3$) of compound **130**.*

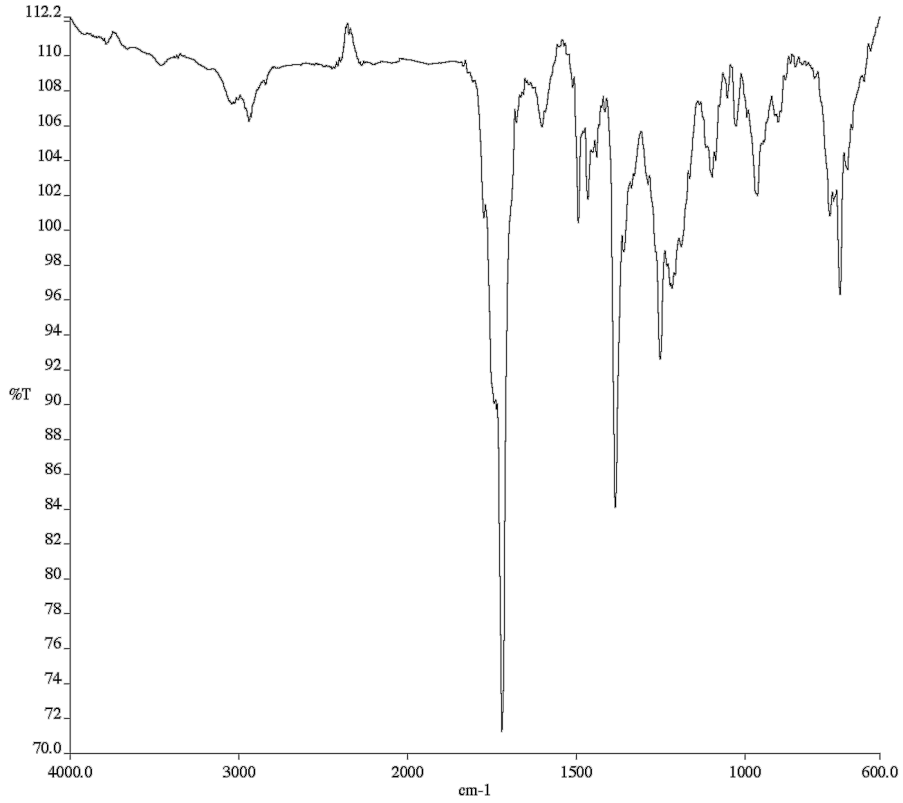

Figure A6.152 *Infrared spectrum (Thin Film, NaCl) of compound* ***130****.*

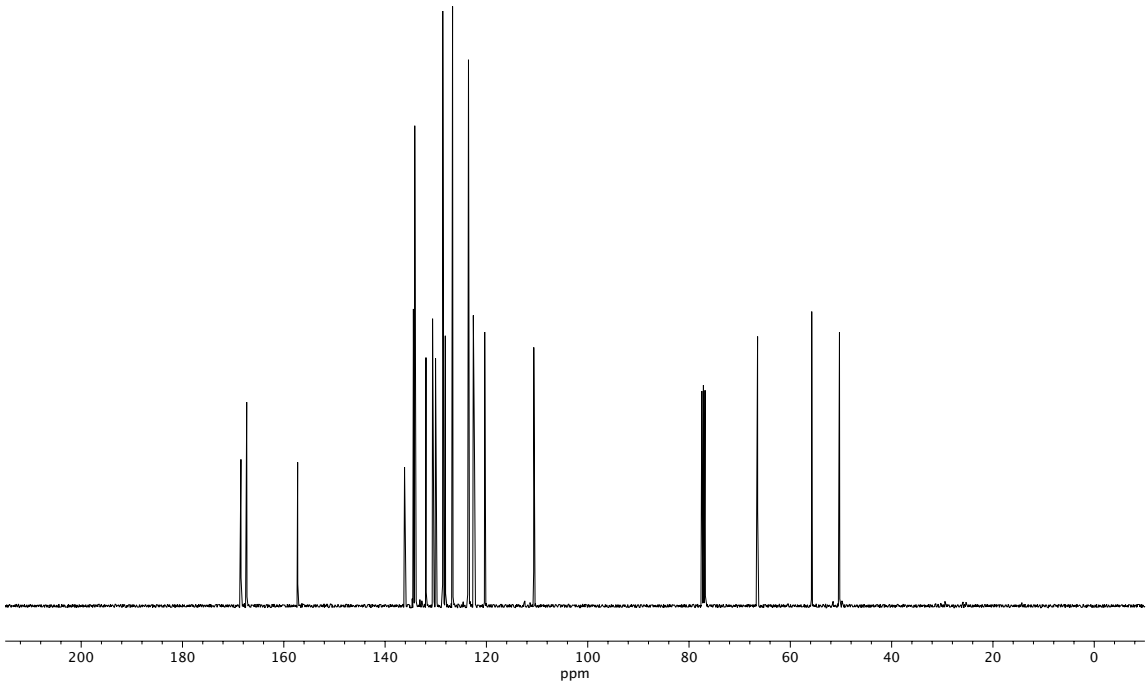

Figure A6.153 *^{13}C NMR (100 MHz, $CDCl_3$) of compound* ***130****.*

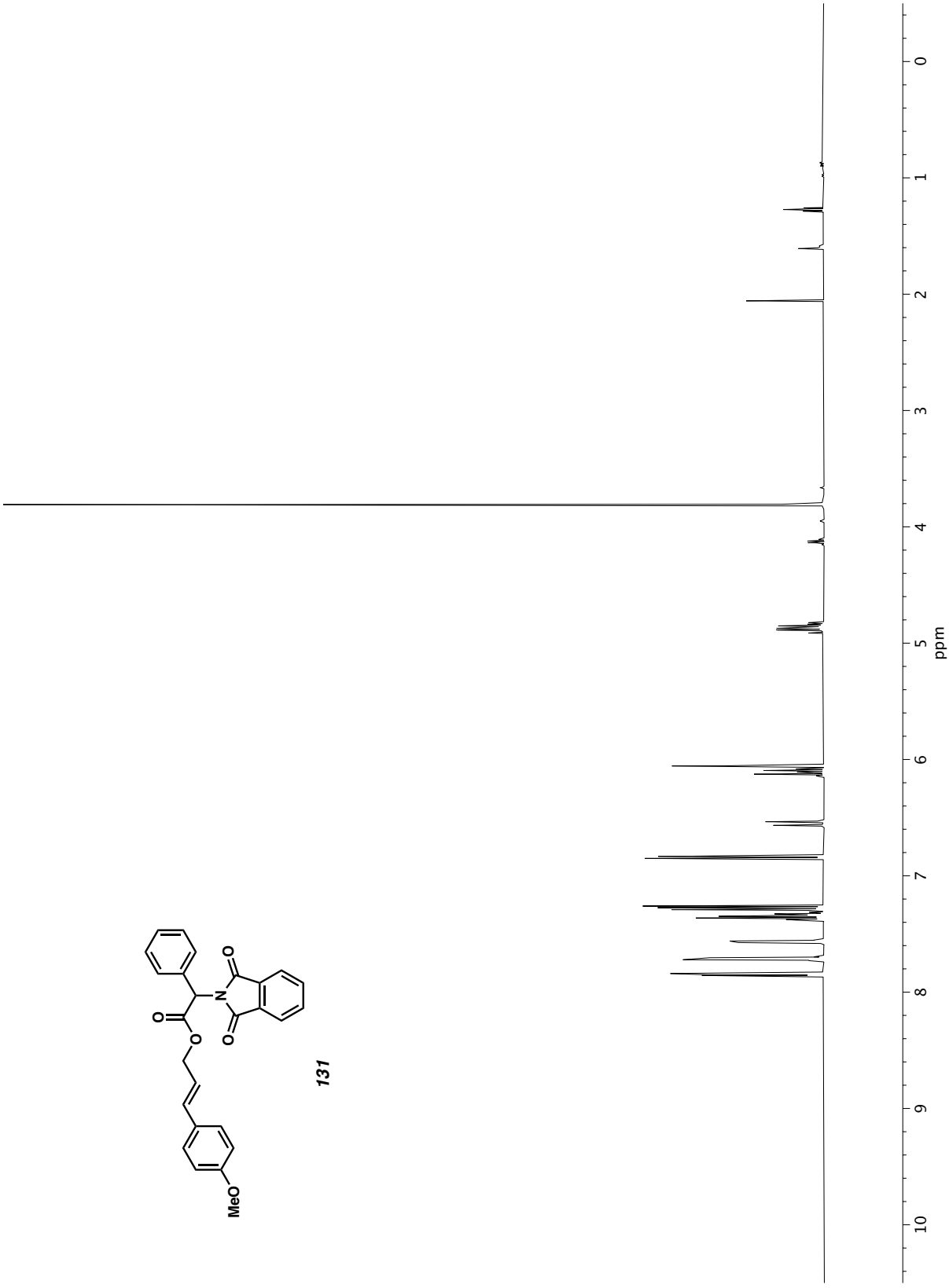

Figure A6.154 *^{1}H NMR (500 MHz, $CDCl_3$) of compound **131**.*

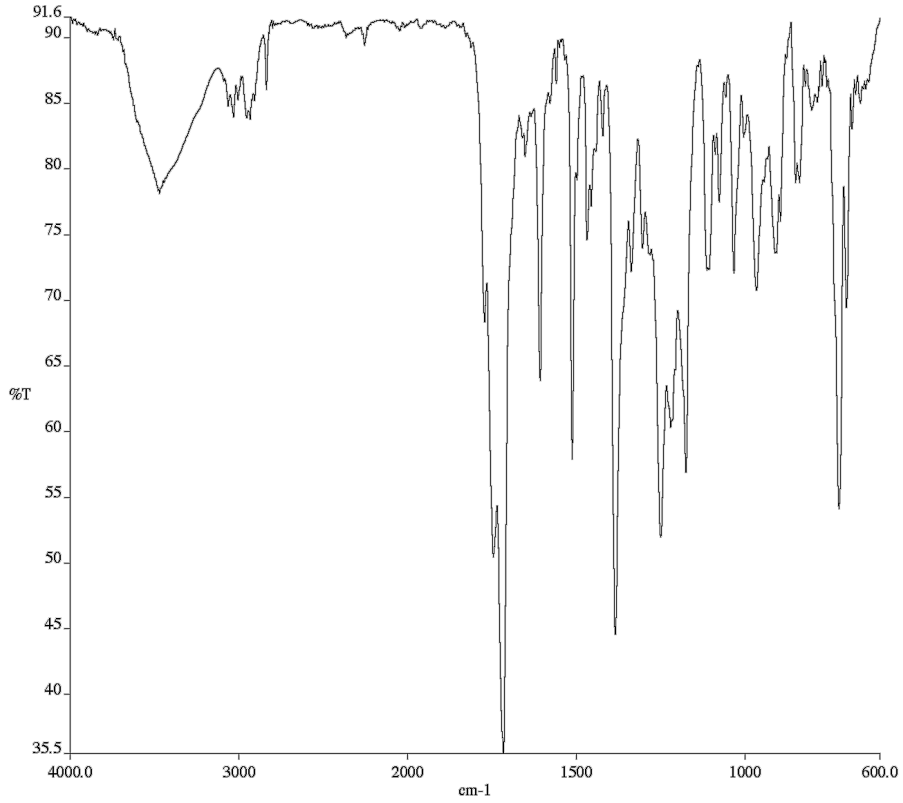

Figure A6.155 *Infrared spectrum (Thin Film, NaCl) of compound* ***131****.*

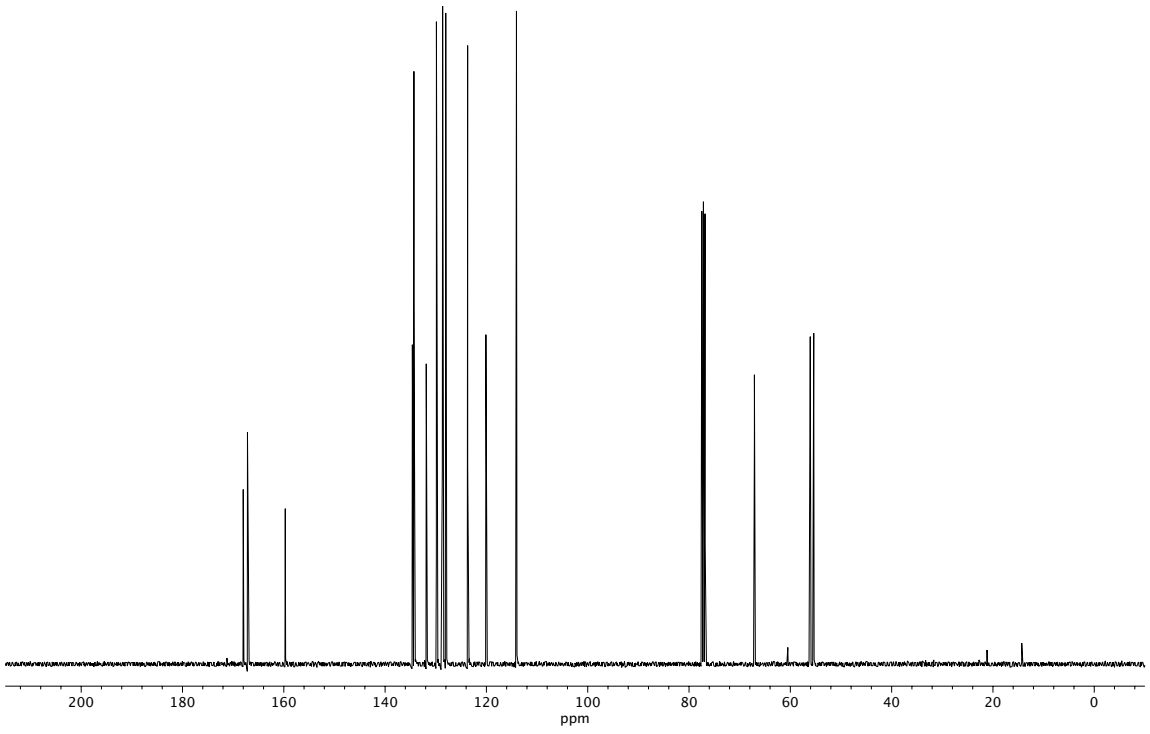

Figure A6.156 *^{13}C NMR (100 MHz, $CDCl_3$) of compound* ***131****.*

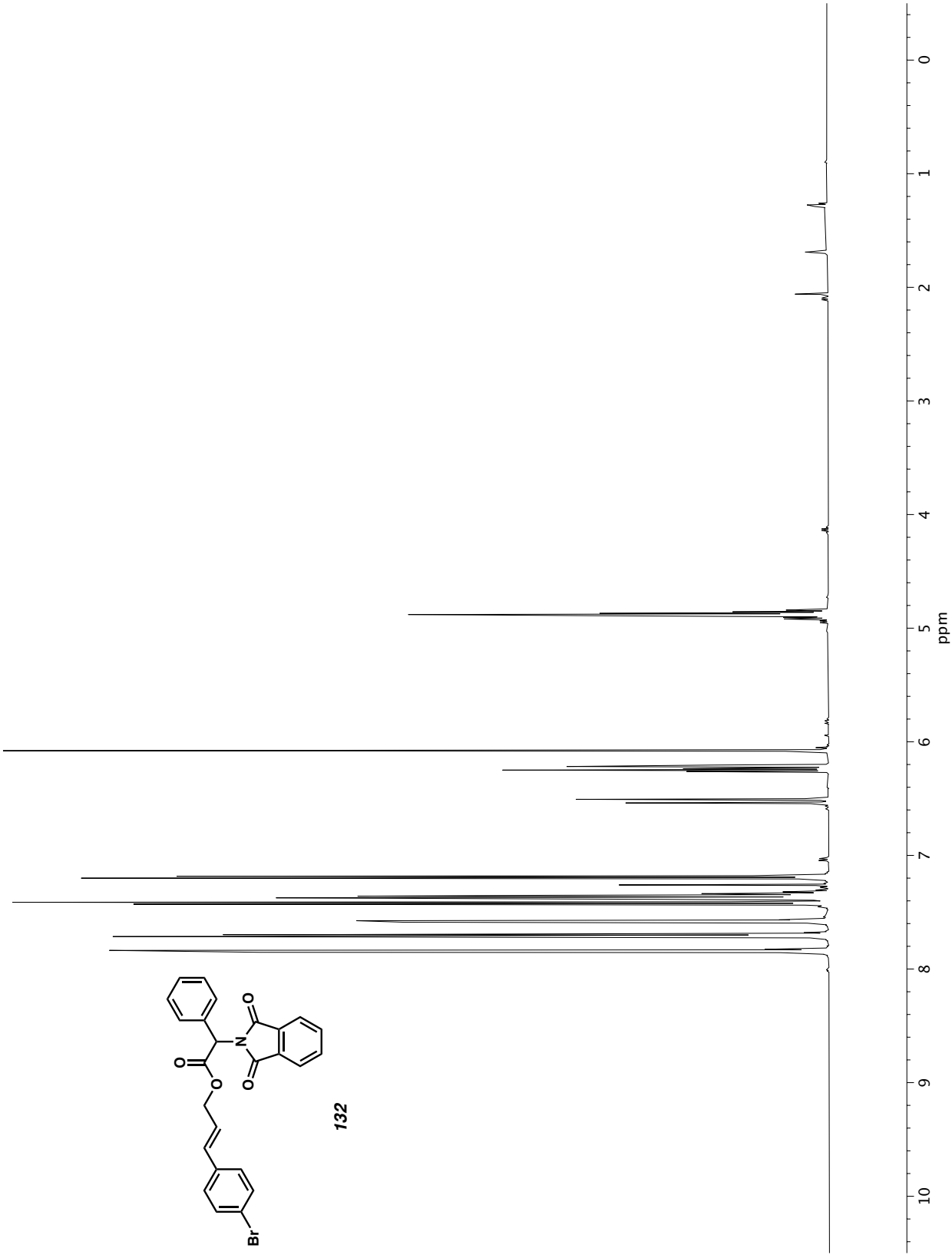

Figure A6.157 *^1H NMR (500 MHz, $CDCl_3$) of compound **132**.*

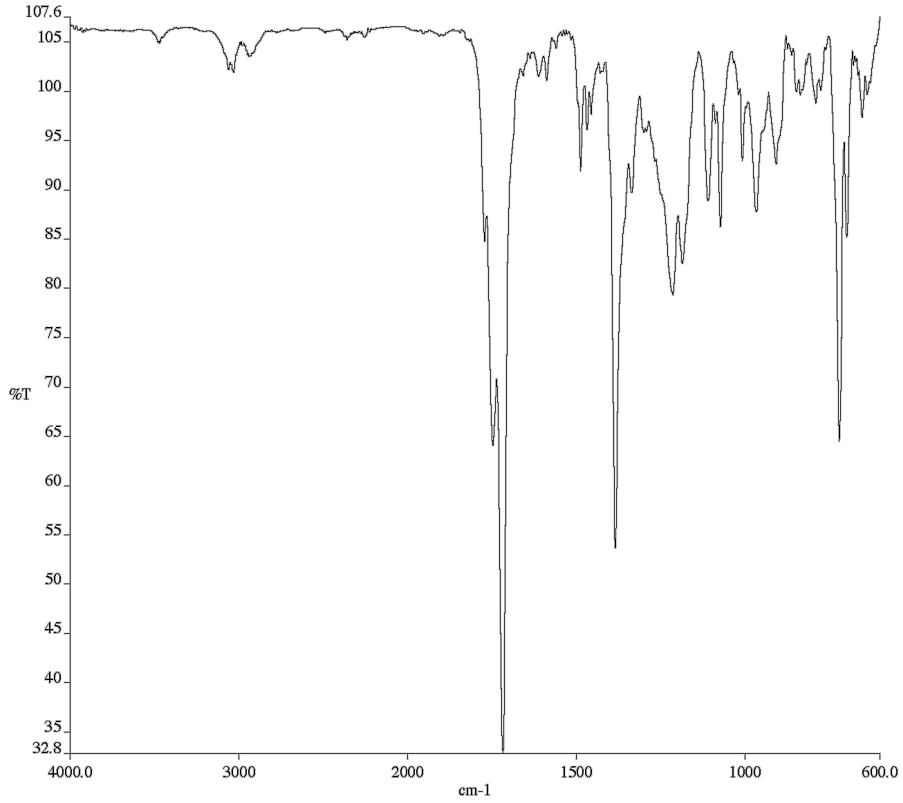

Figure A6.158 *Infrared spectrum (Thin Film, NaCl) of compound* ***132****.*

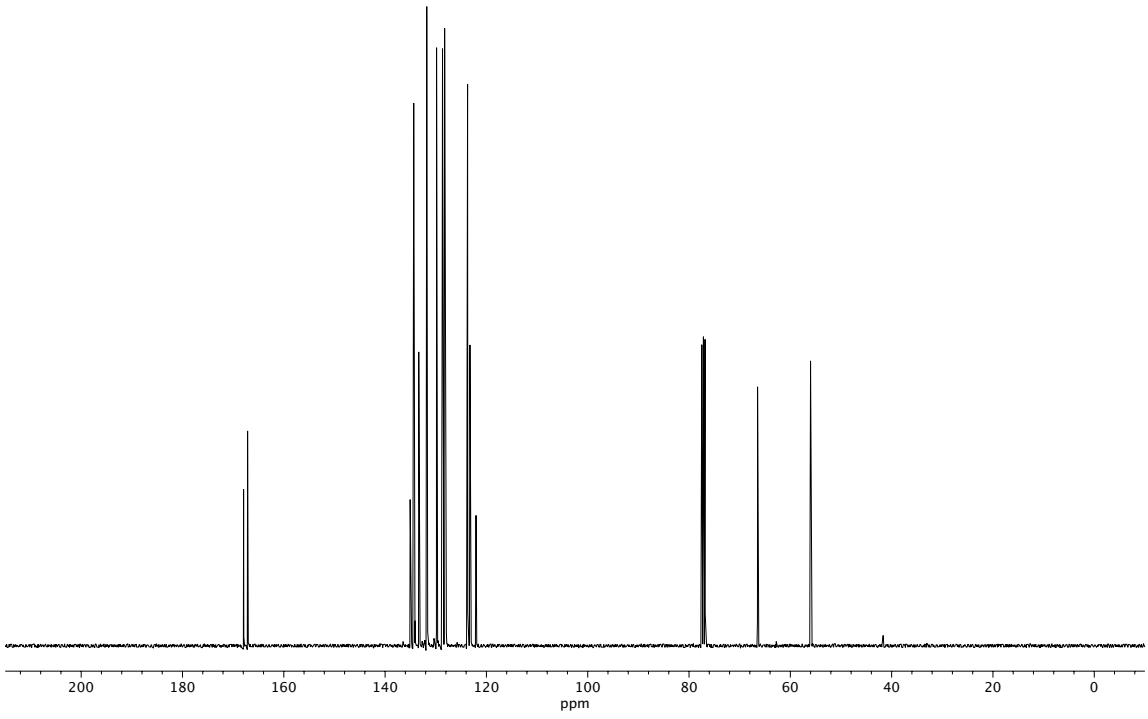

Figure A6.159 *^{13}C NMR (100 MHz, $CDCl_3$) of compound* ***132****.*

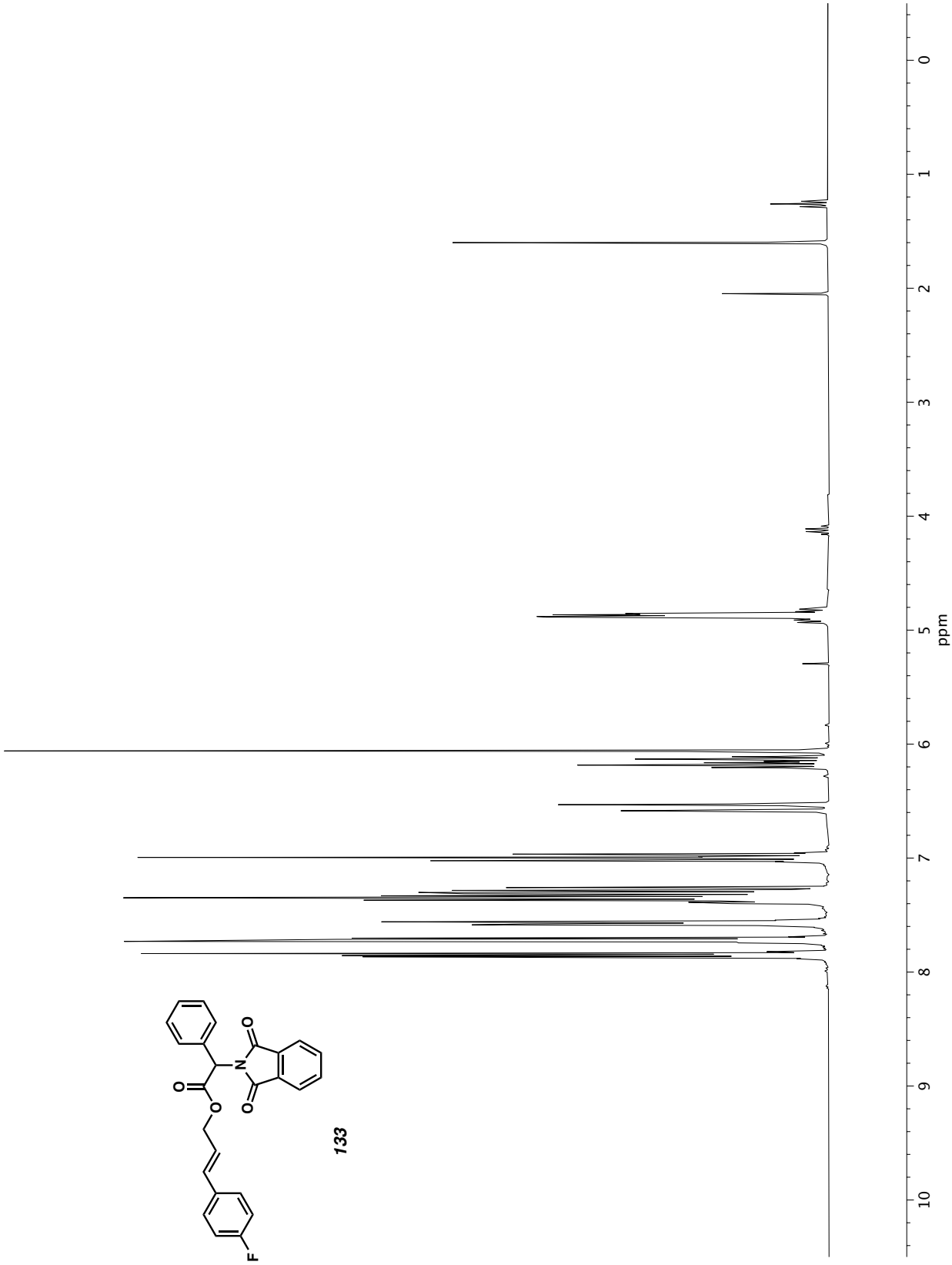

Figure A6.160 *^{1}H NMR (500 MHz, $CDCl_3$) of compound **133**.*

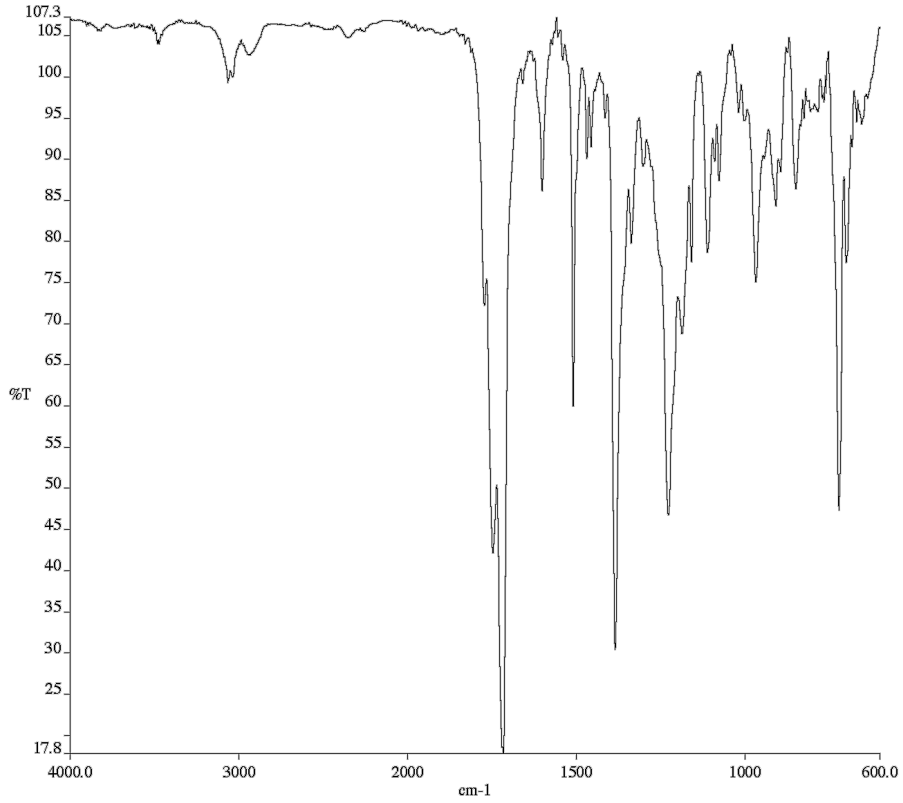

Figure A6.161 *Infrared spectrum (Thin Film, NaCl) of compound* ***133****.*

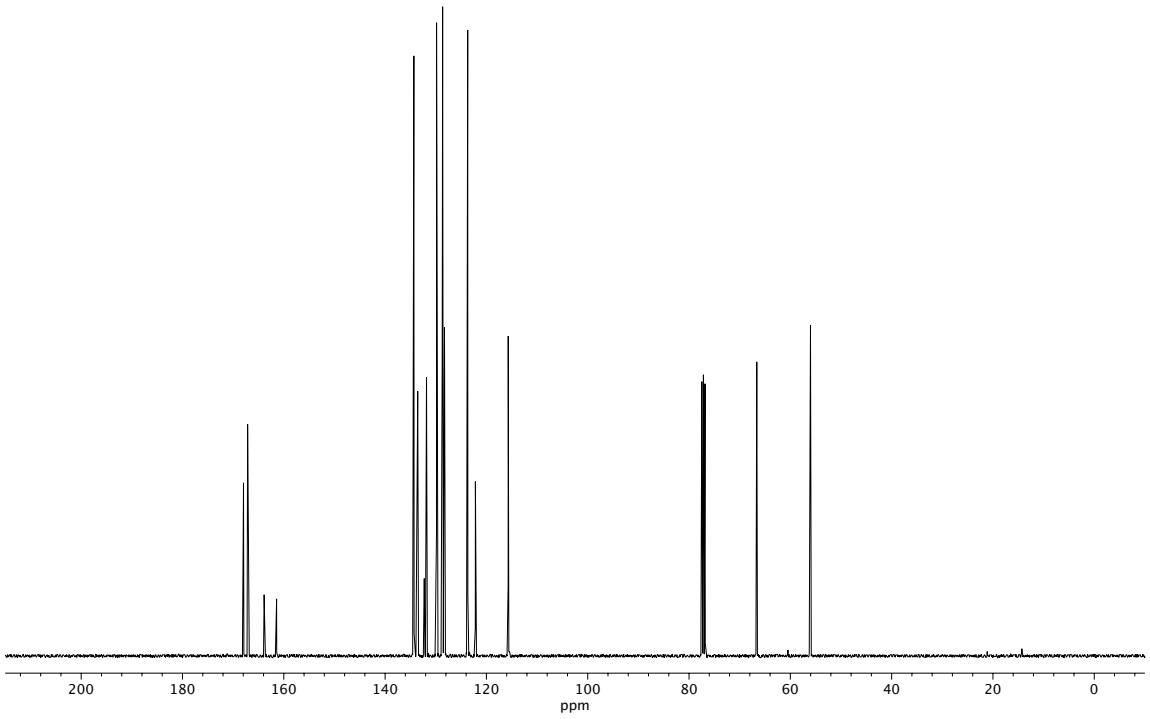

Figure A6.162 *^{13}C NMR (100 MHz, $CDCl_3$) of compound* ***133****.*

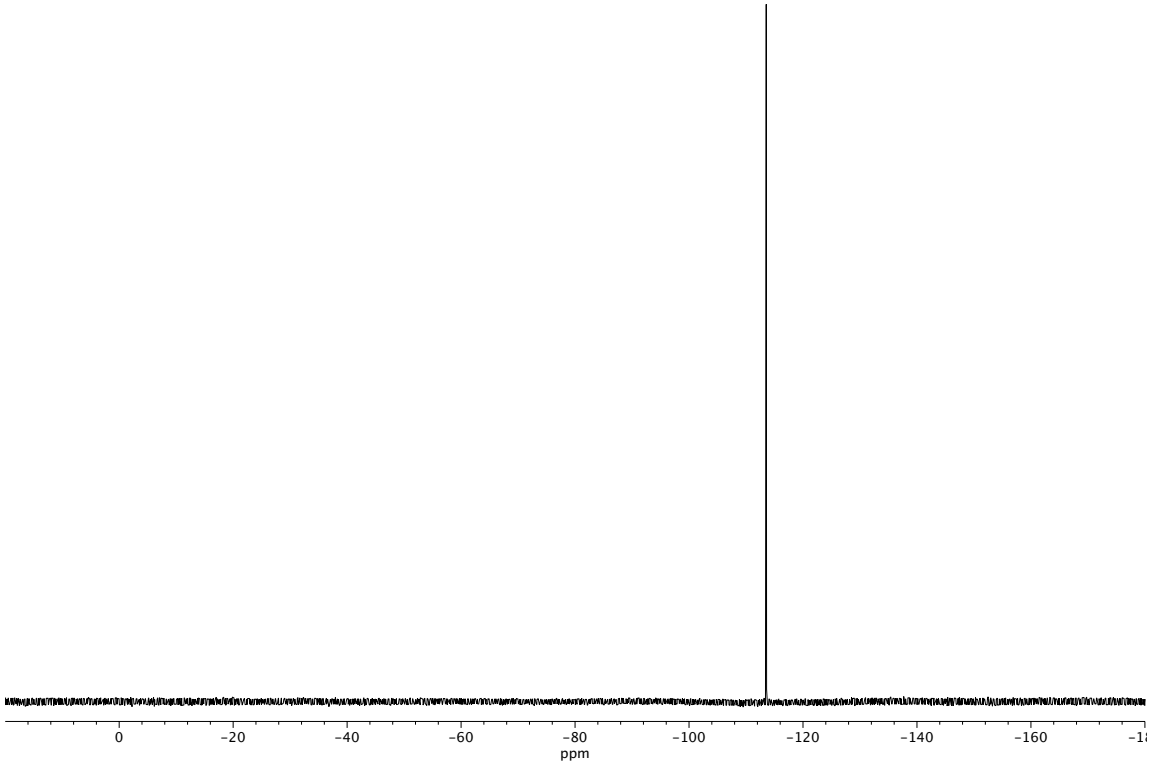

Figure A6.163 *^{19}F NMR (282 MHz, $CDCl_3$) of compound **133**.*

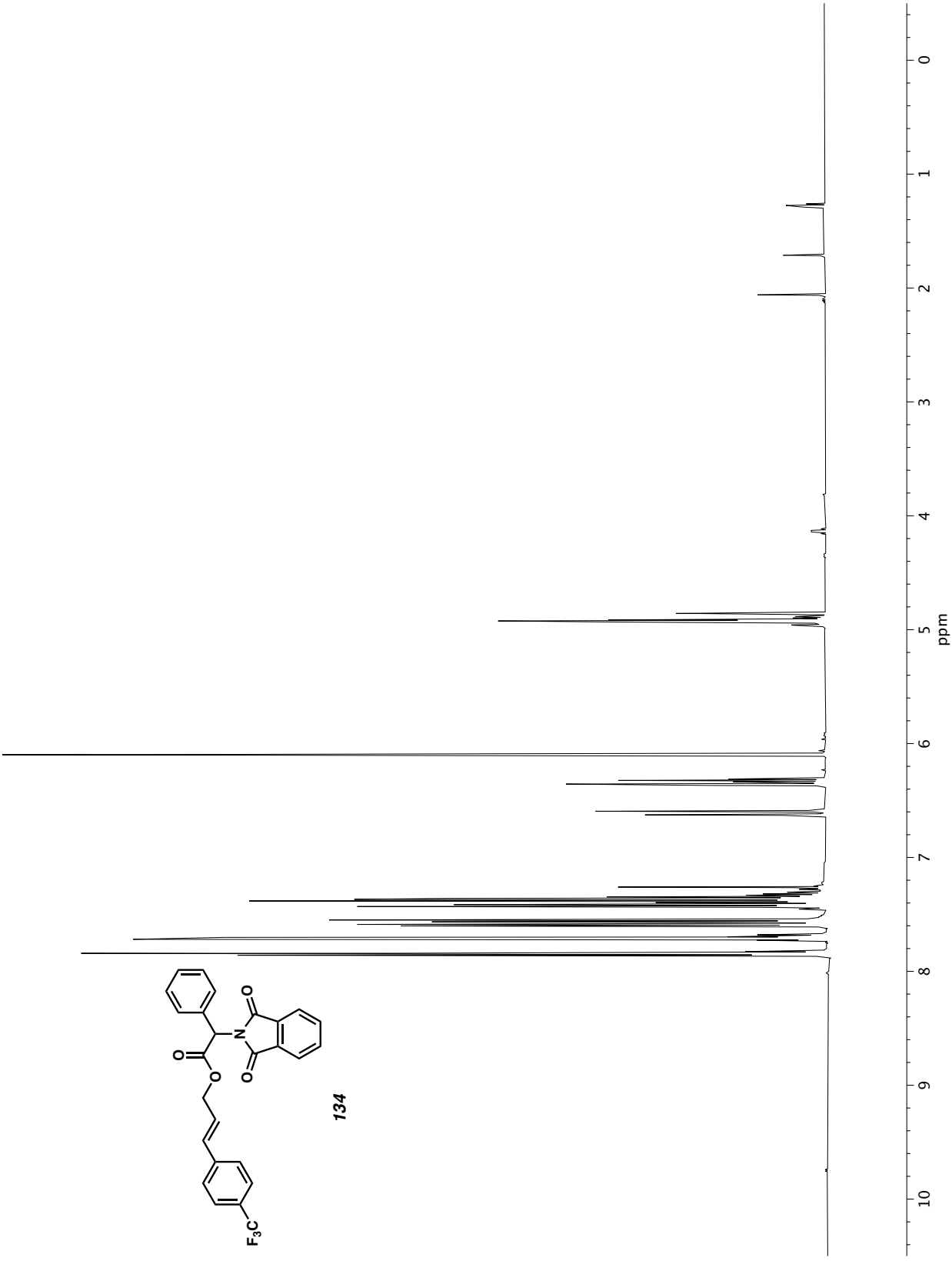

Figure A6.164 *^{1}H NMR (500 MHz, $CDCl_3$) of compound **134**.*

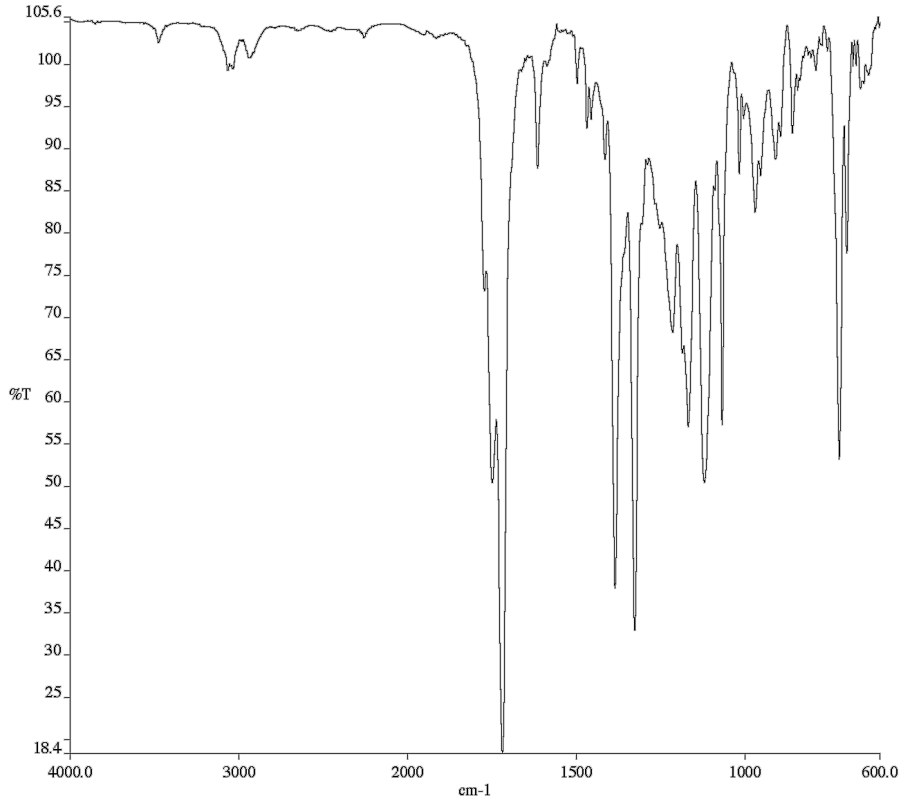

Figure A6.165 *Infrared spectrum (Thin Film, NaCl) of compound* ***134****.*

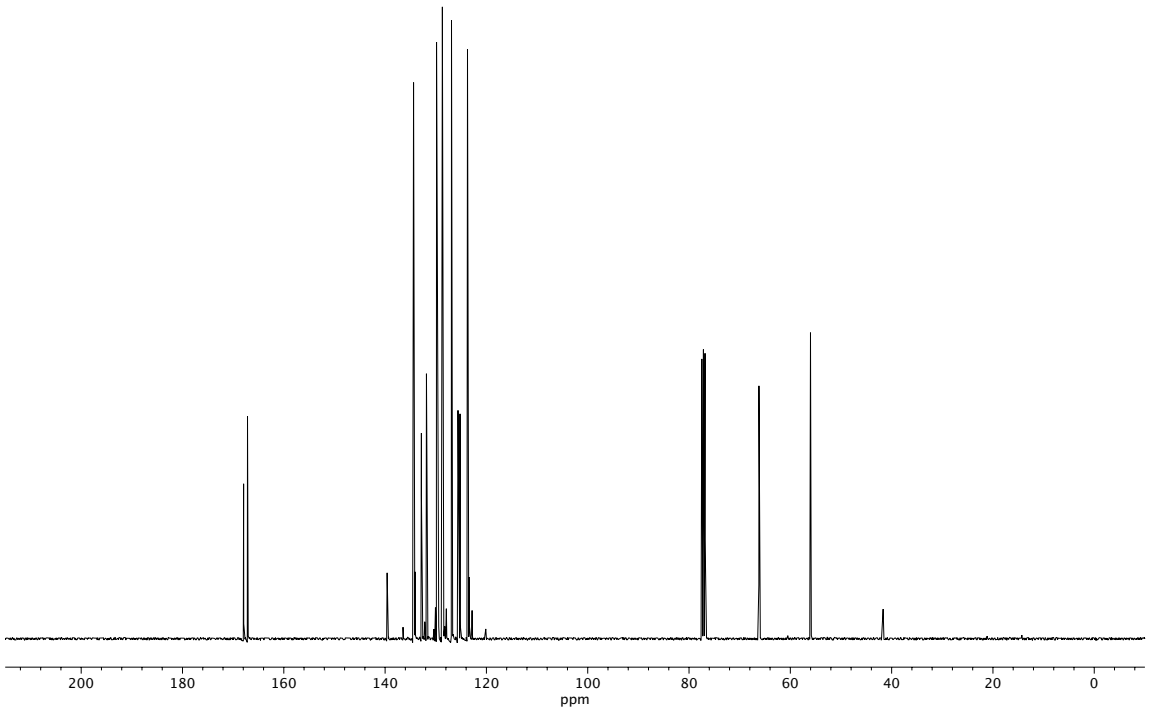

Figure A6.166 *^{13}C NMR (100 MHz, $CDCl_3$) of compound* ***134****.*

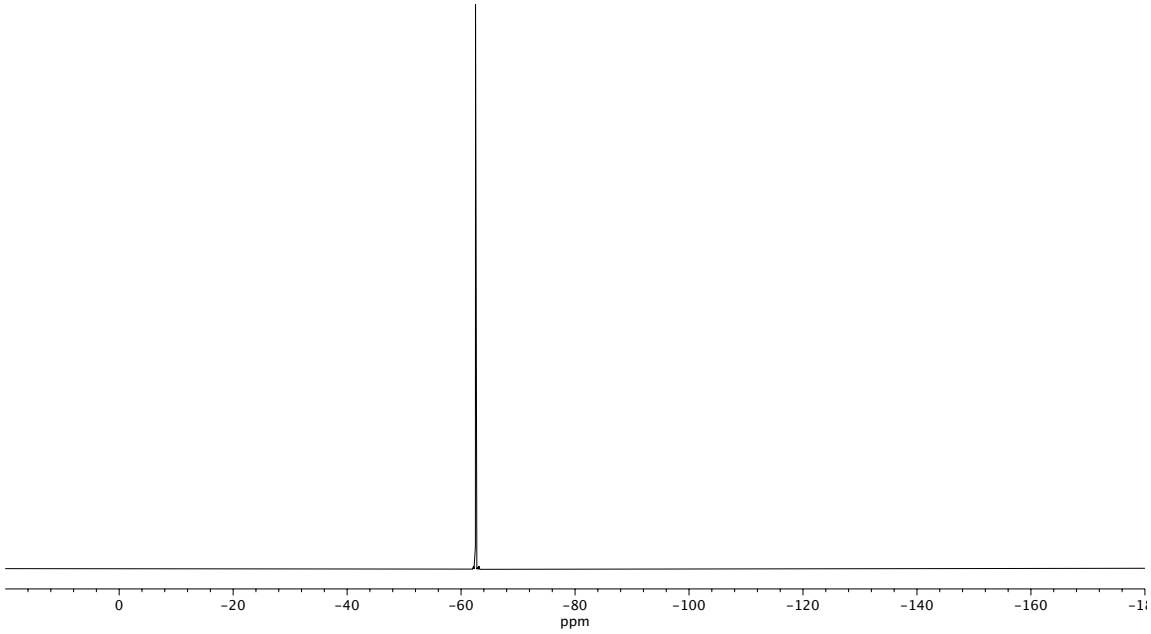

Figure A6.167 *^{19}F NMR (282 MHz, $CDCl_3$) of compound **134**.*

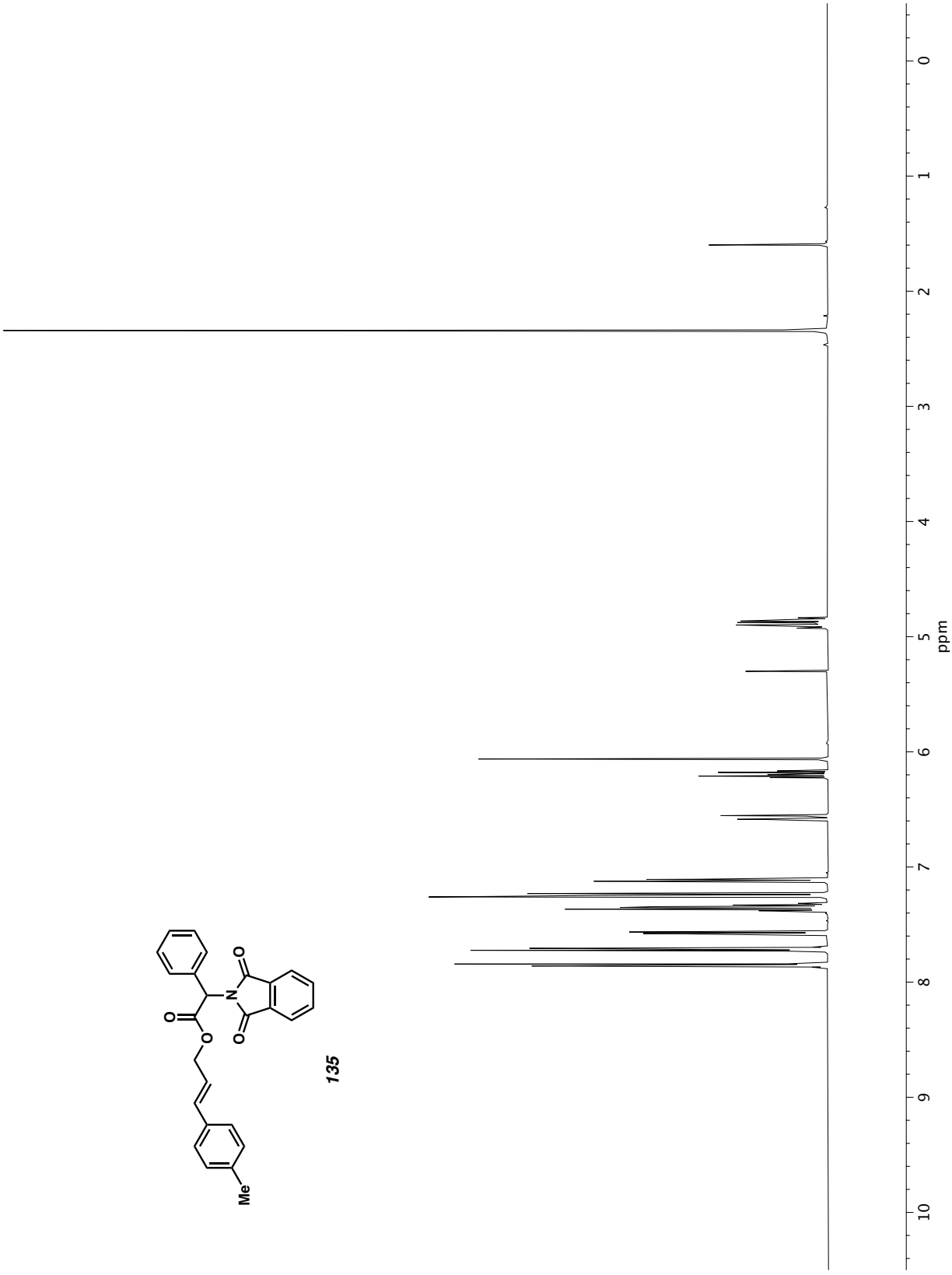

Figure A6.168 *^{1}H NMR (500 MHz, $CDCl_3$) of compound **135**.*

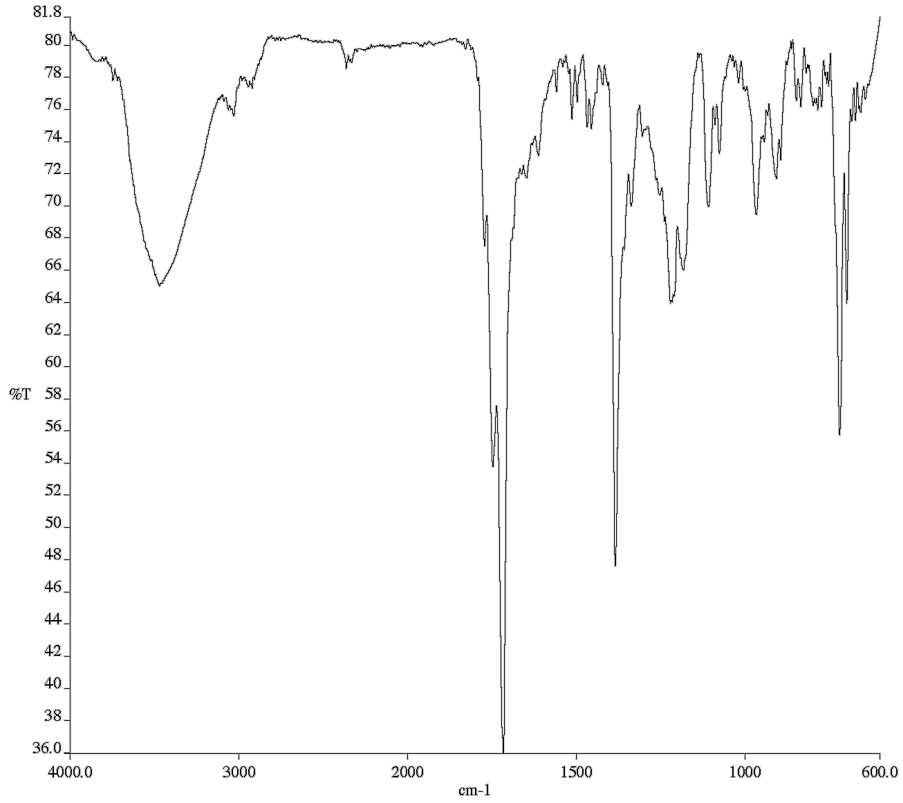

Figure A6.169 *Infrared spectrum (Thin Film, NaCl) of compound* ***135****.*

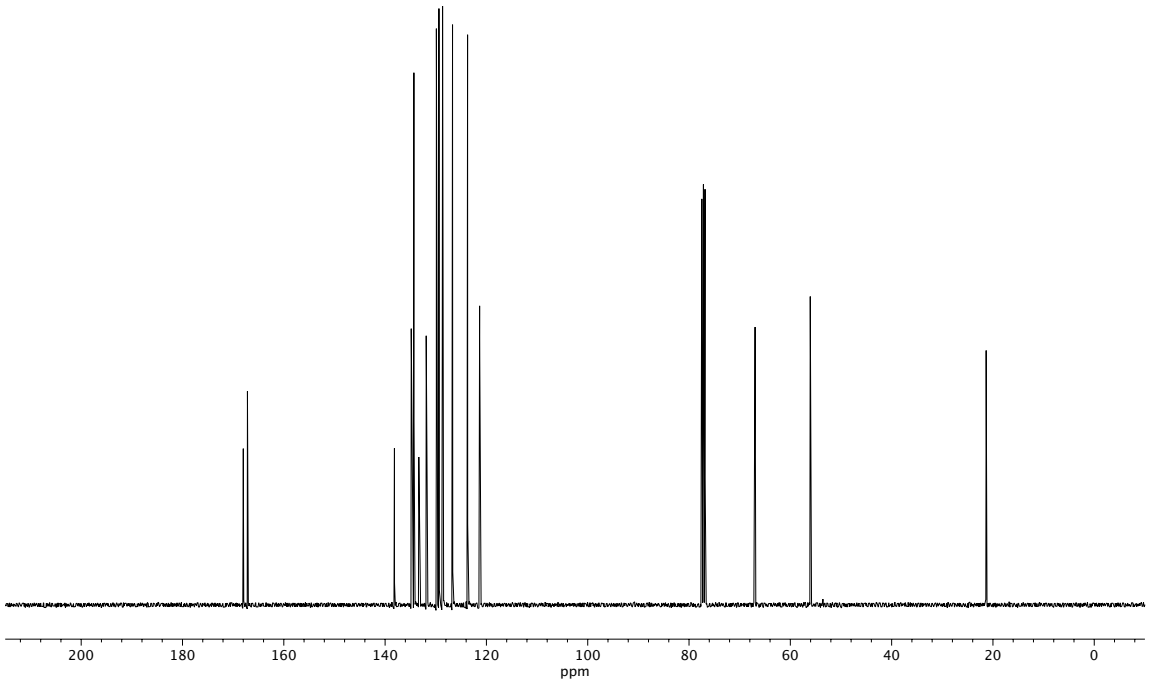

Figure A6.170 *^{13}C NMR (100 MHz, $CDCl_3$) of compound* ***135****.*

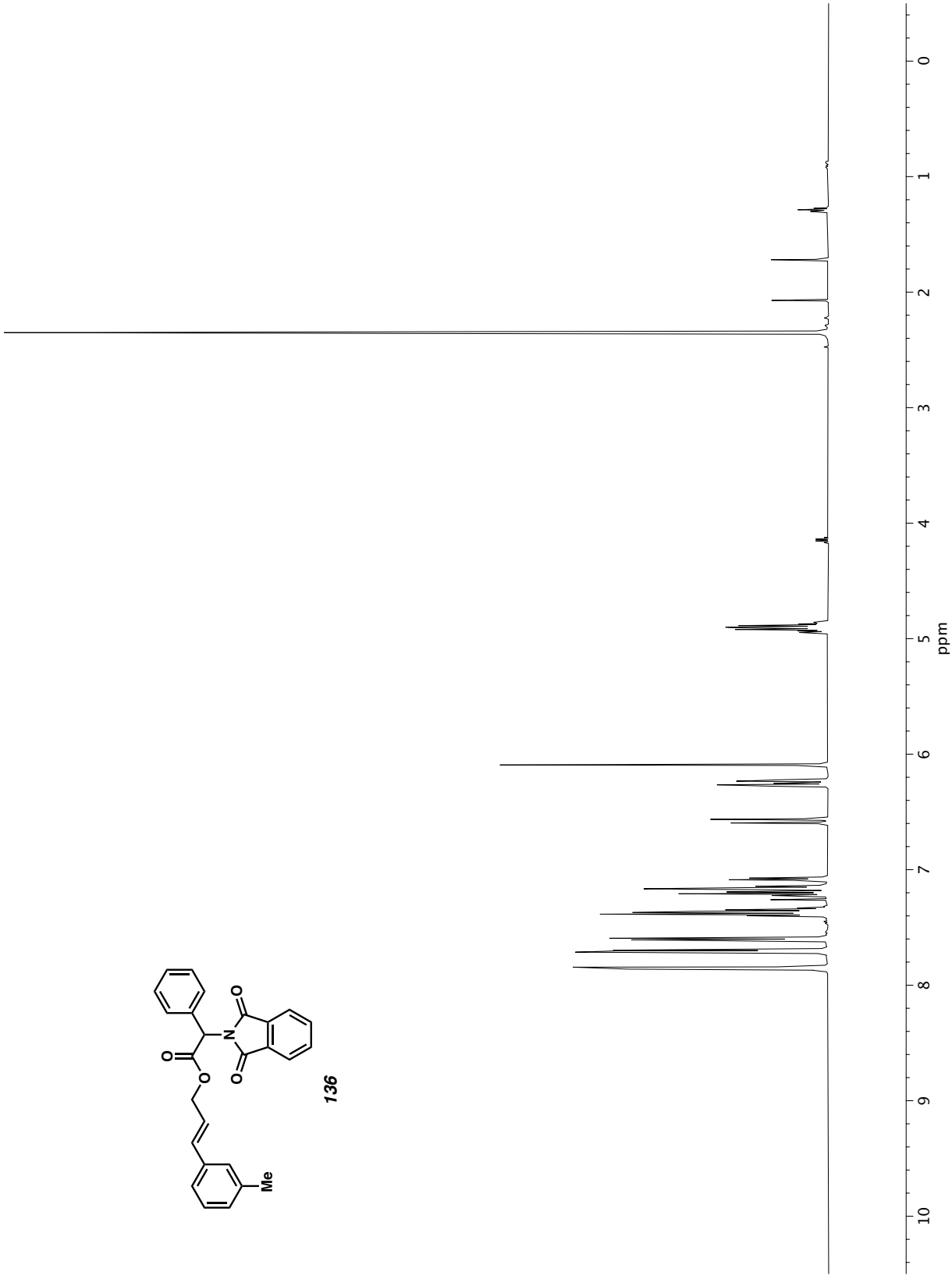

Figure A6.171 *^{1}H NMR (500 MHz, $CDCl_3$) of compound **136**.*

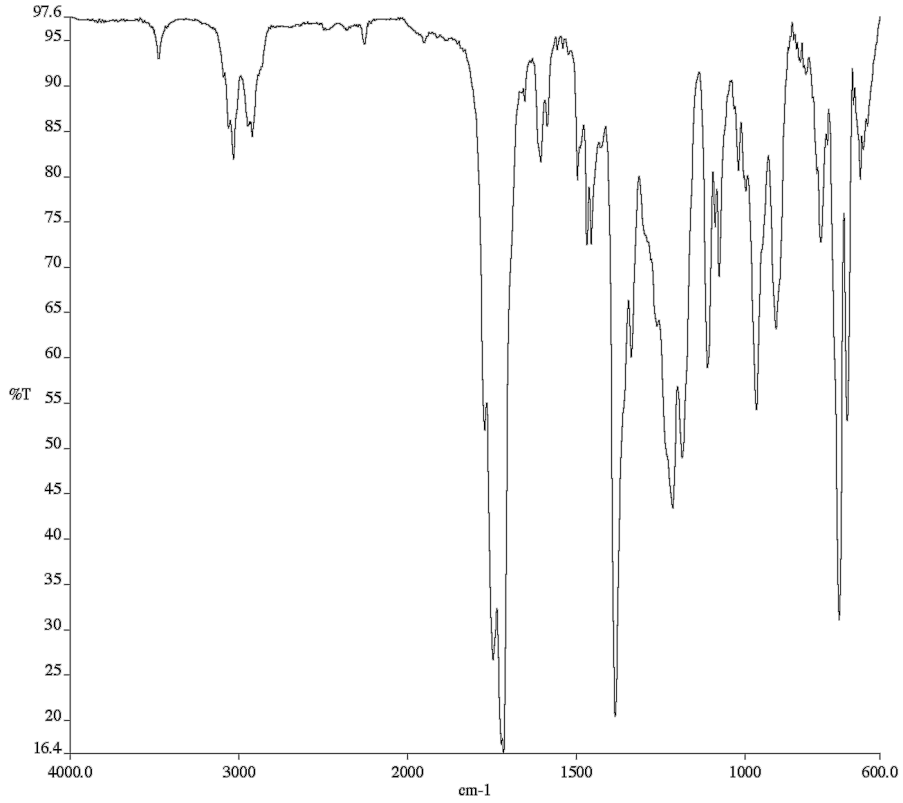

Figure A6.172 *Infrared spectrum (Thin Film, NaCl) of compound* ***136****.*

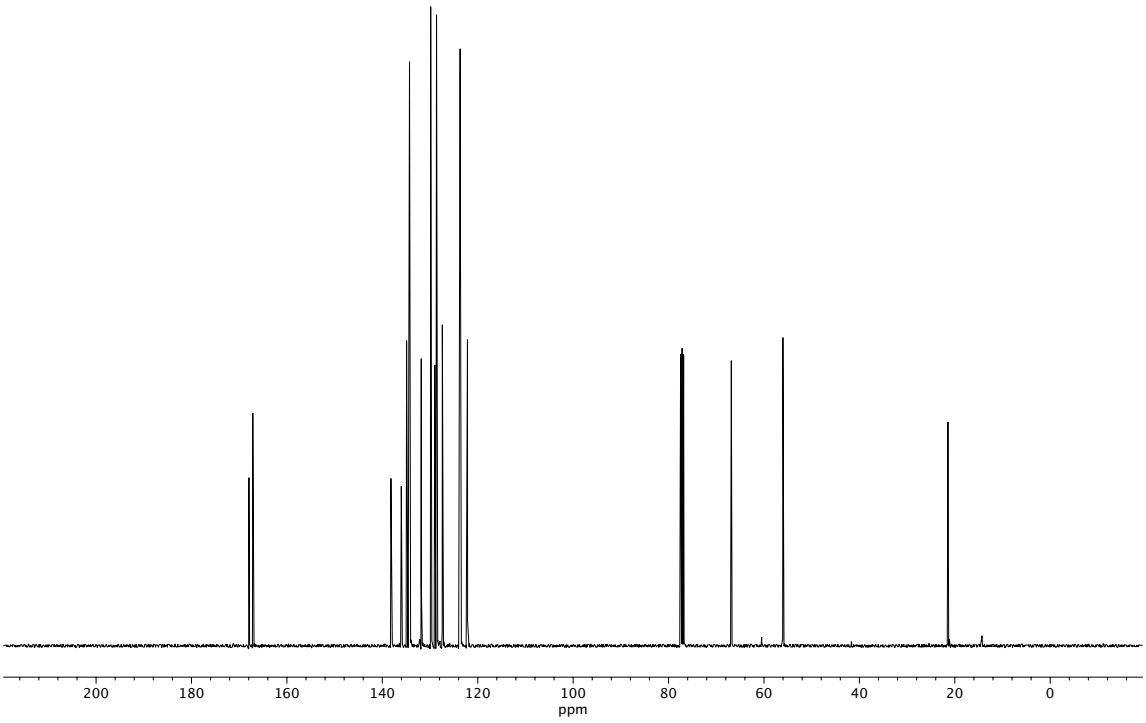

Figure A6.173 *^{13}C NMR (100 MHz, $CDCl_3$) of compound* ***136****.*

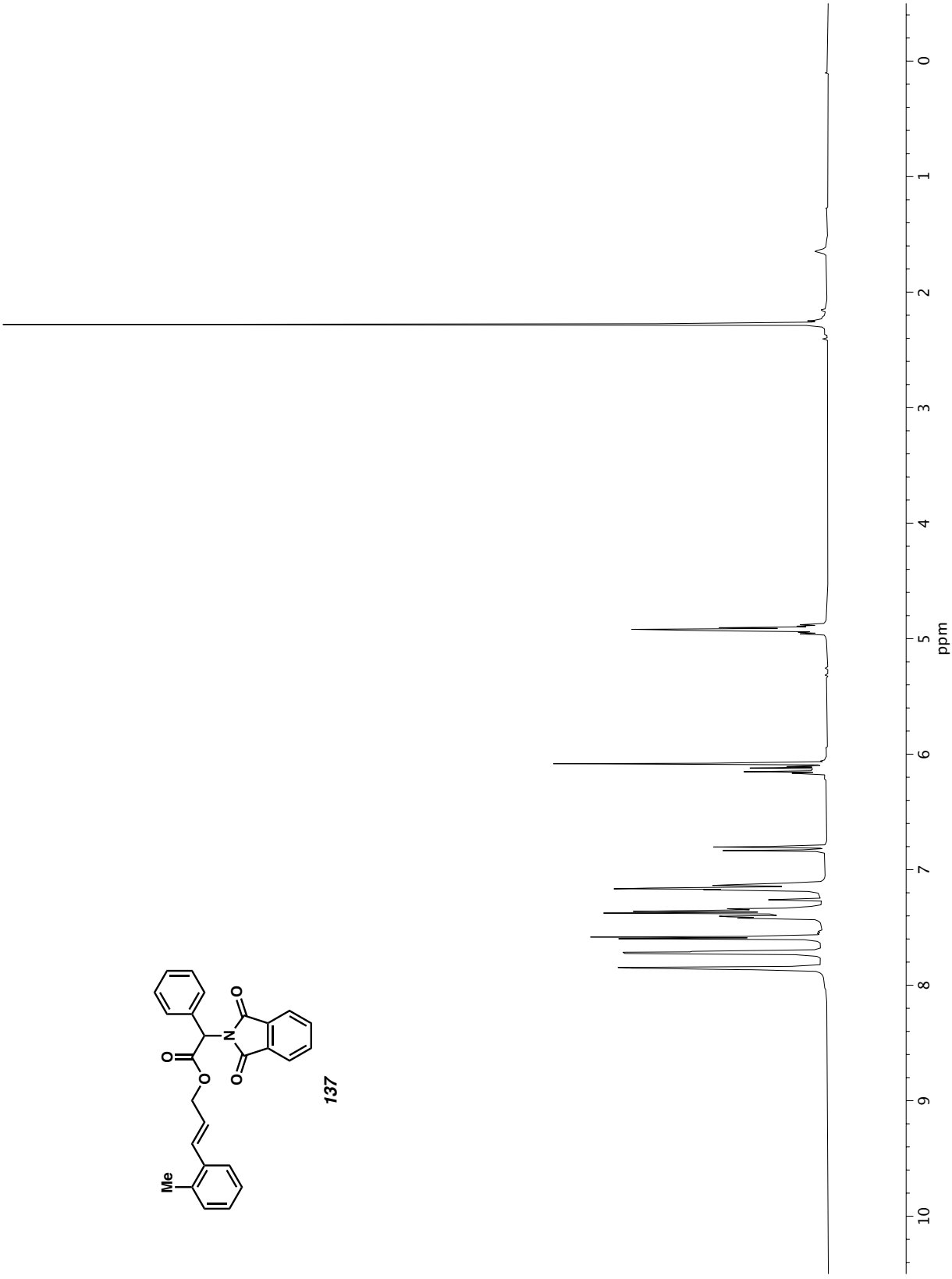

Figure A6.174 *^{1}H NMR (500 MHz, $CDCl_3$) of compound **137**.*

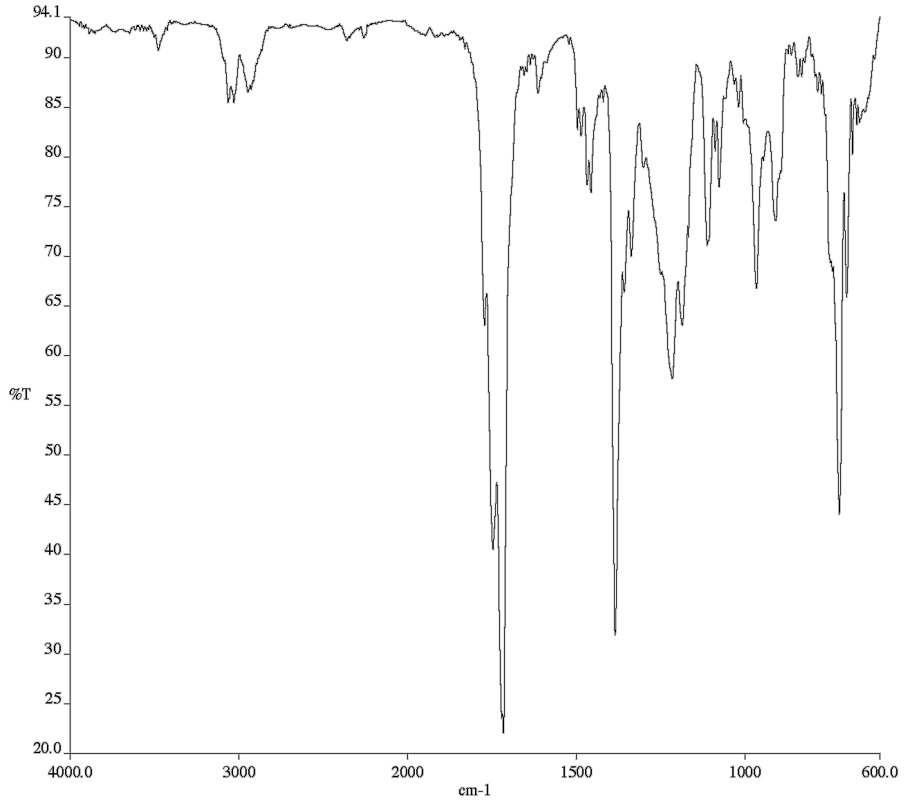

Figure A6.175 *Infrared spectrum (Thin Film, NaCl) of compound **137**.*

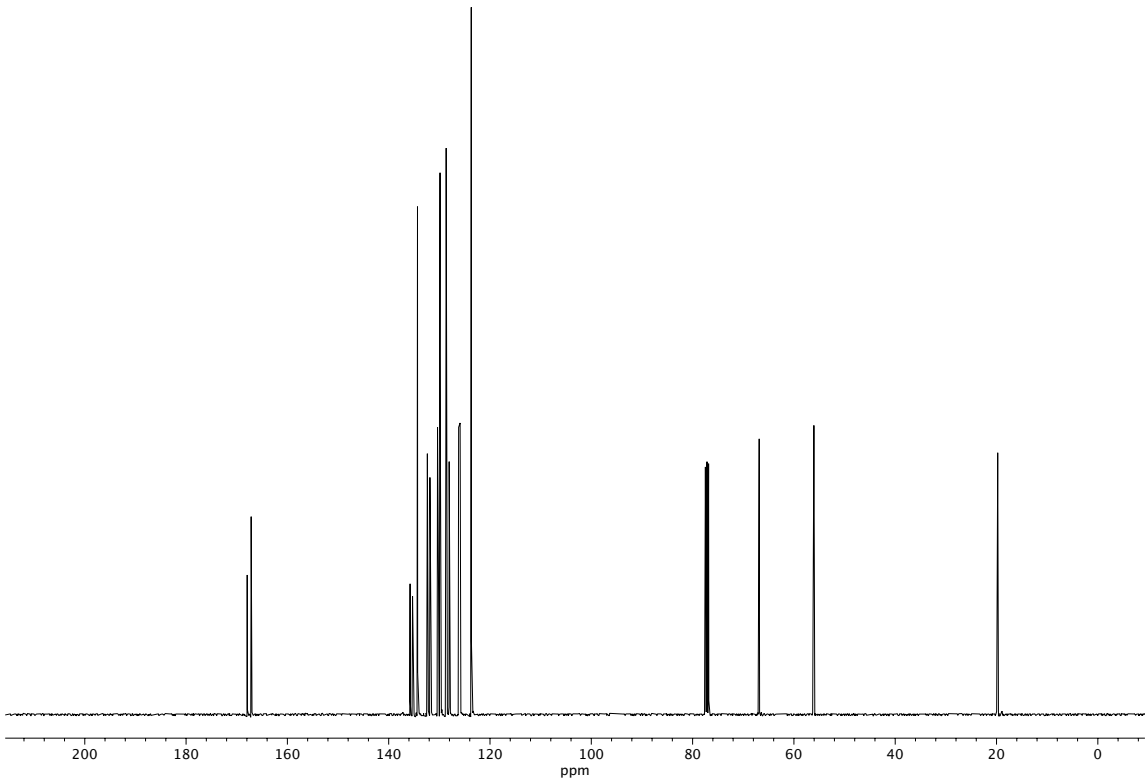

Figure A6.176 *^{13}C NMR (100 MHz, $CDCl_3$) of compound **137**.*

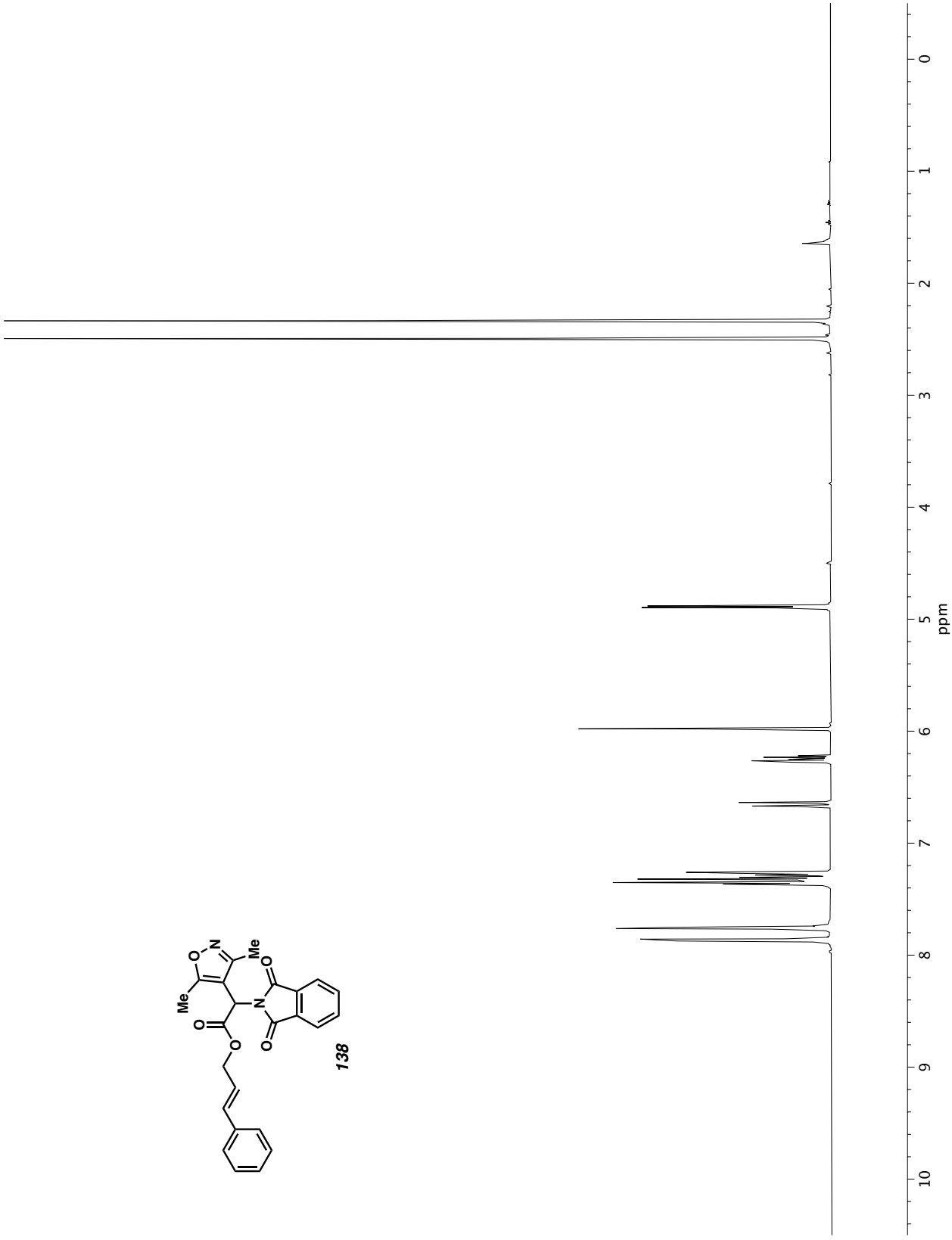

Figure A6.177 *^{1}H NMR (500 MHz, $CDCl_3$) of compound **138**.*

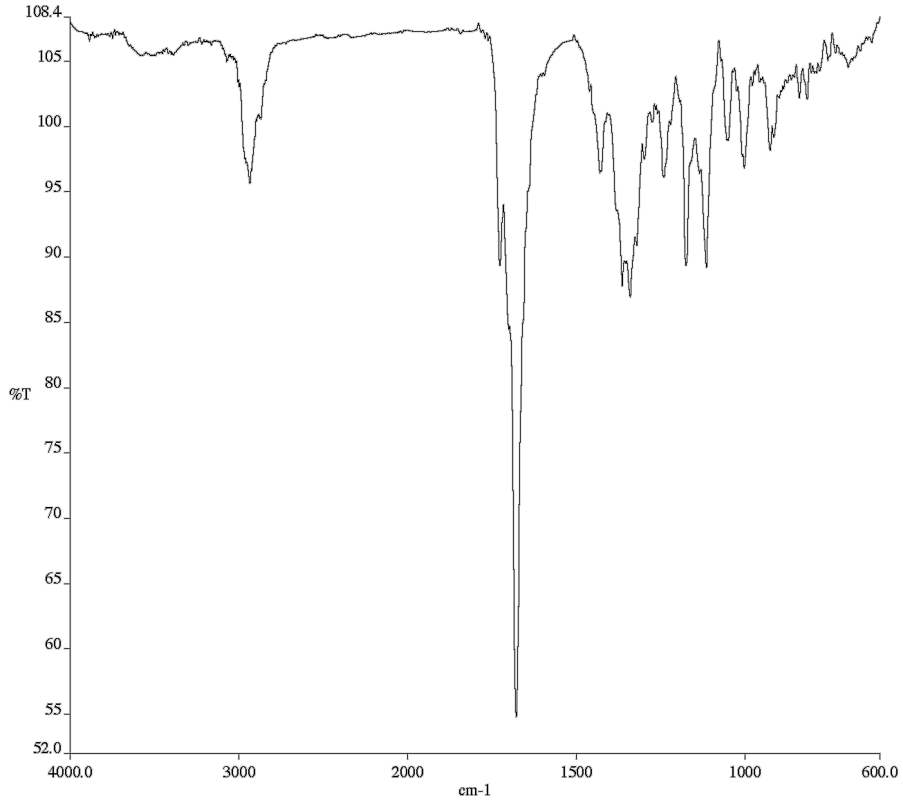

Figure A6.178 *Infrared spectrum (Thin Film, NaCl) of compound* ***138****.*

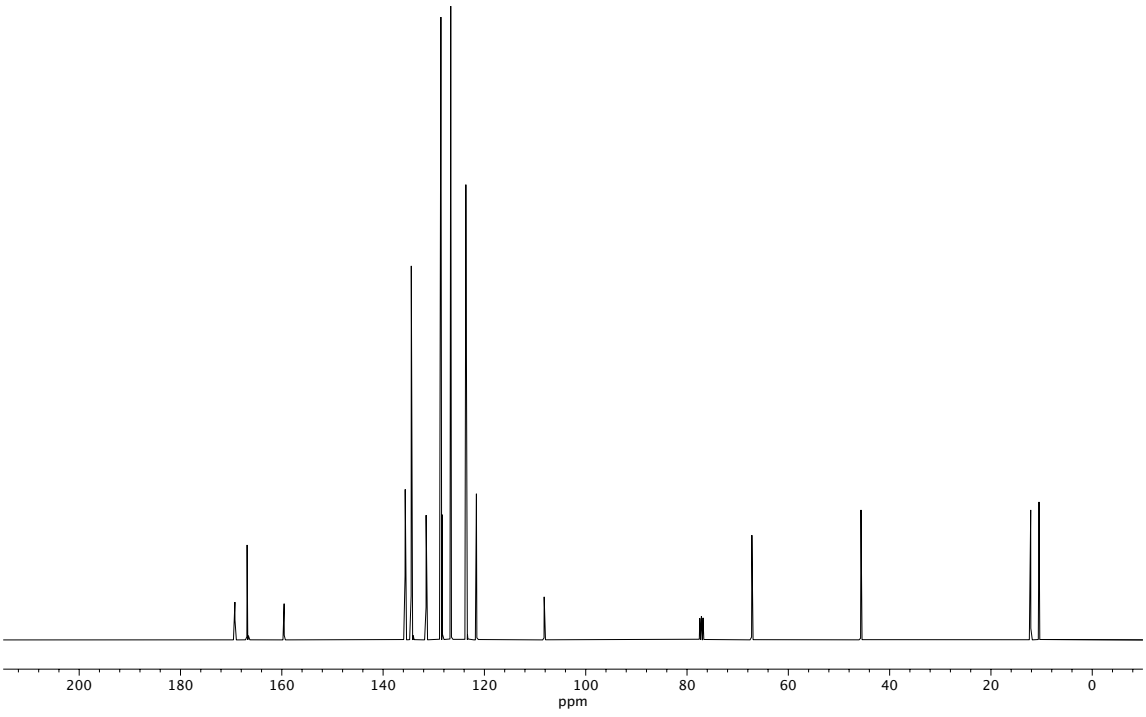

Figure A6.179 *^{13}C NMR (100 MHz, $CDCl_3$) of compound* ***138****.*

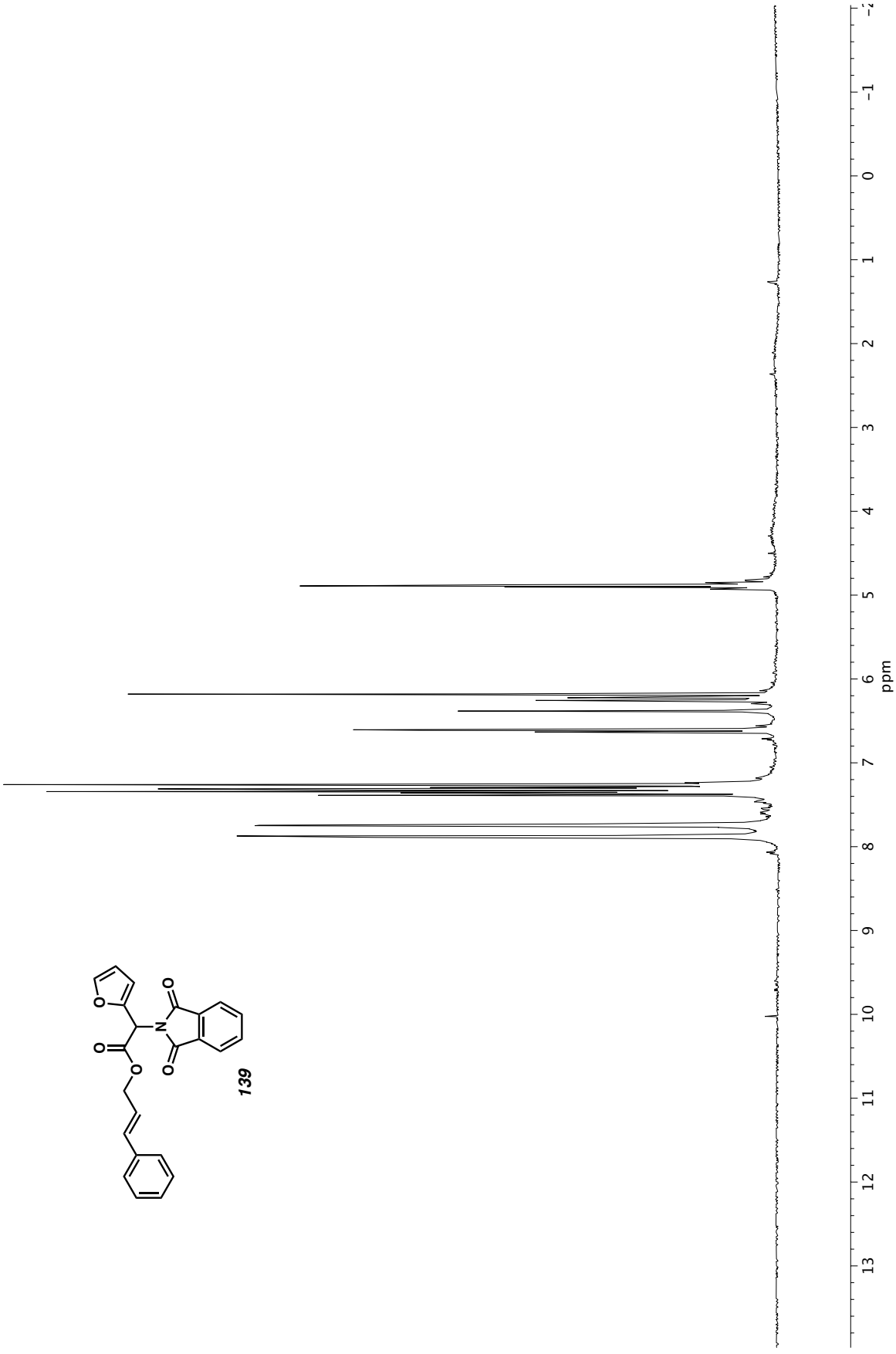

Figure A6.180 *^{1}H NMR (500 MHz, $CDCl_3$) of compound **139**.*

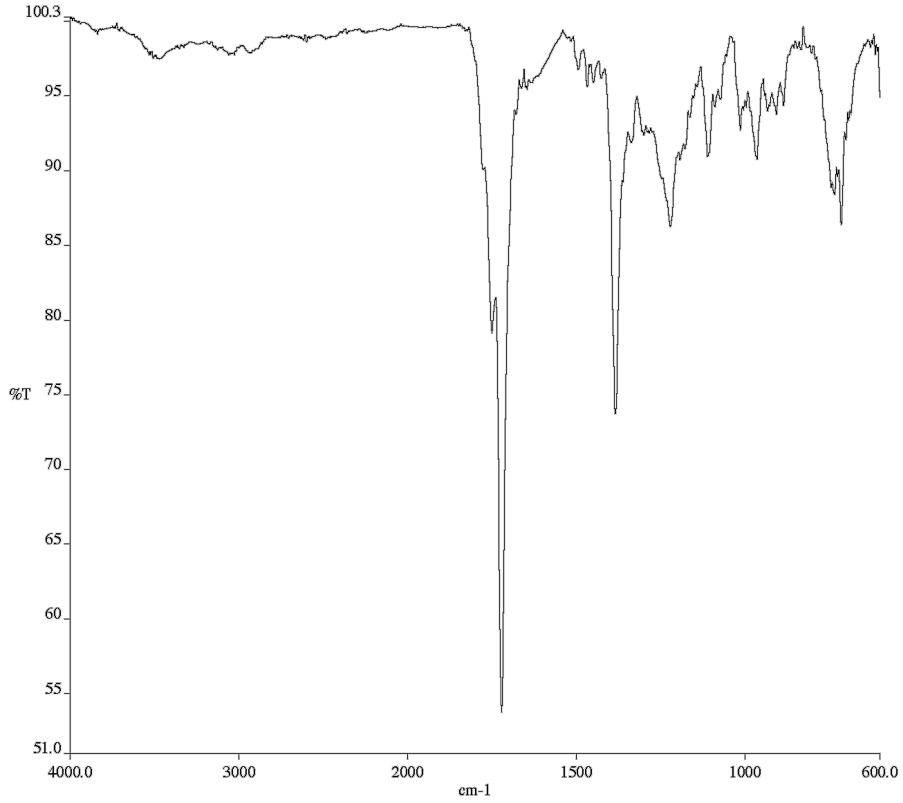

Figure A6.181 *Infrared spectrum (Thin Film, NaCl) of compound* ***139****.*

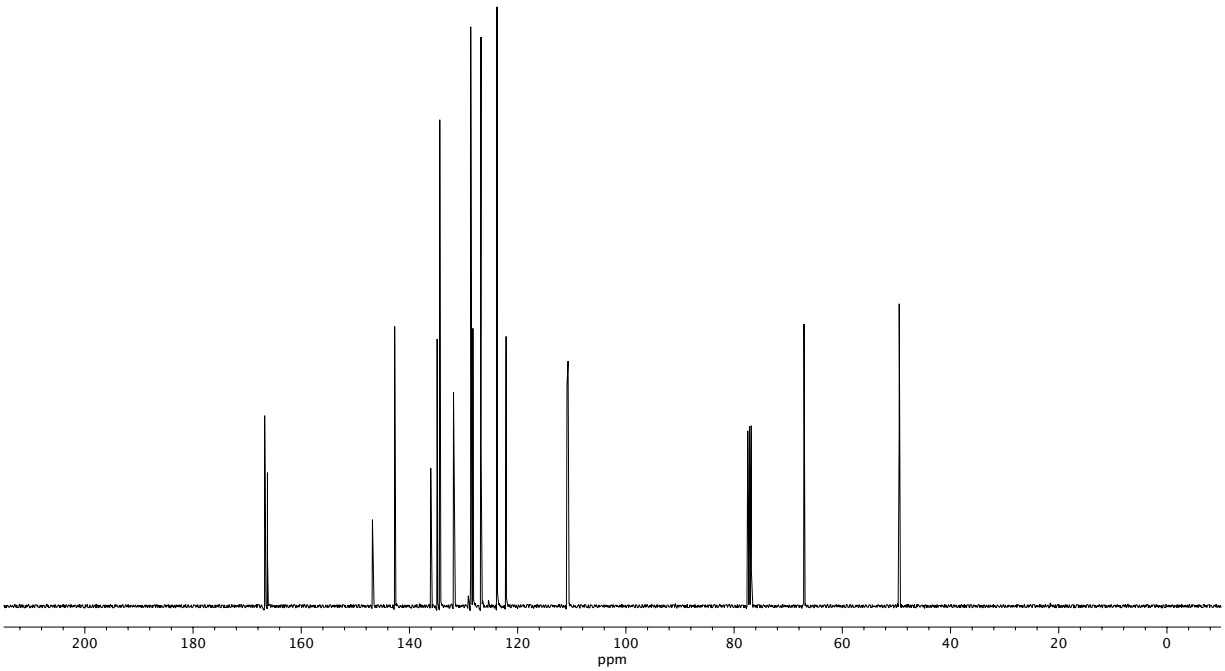

Figure A6.182 *^{13}C NMR (100 MHz, $CDCl_3$) of compound* ***139****.*

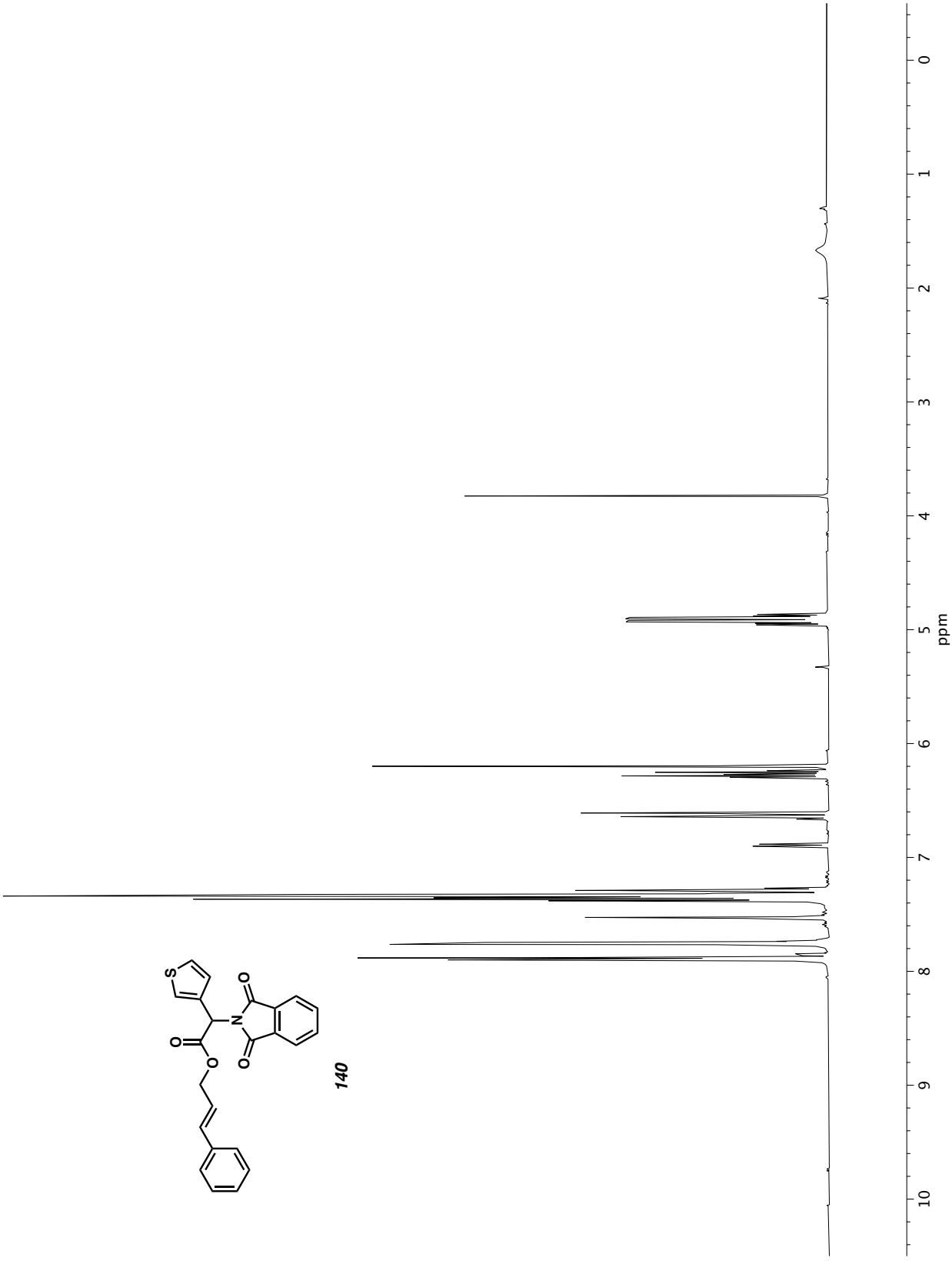

Figure A6.183 *^{1}H NMR (500 MHz, $CDCl_3$) of compound **140**.*

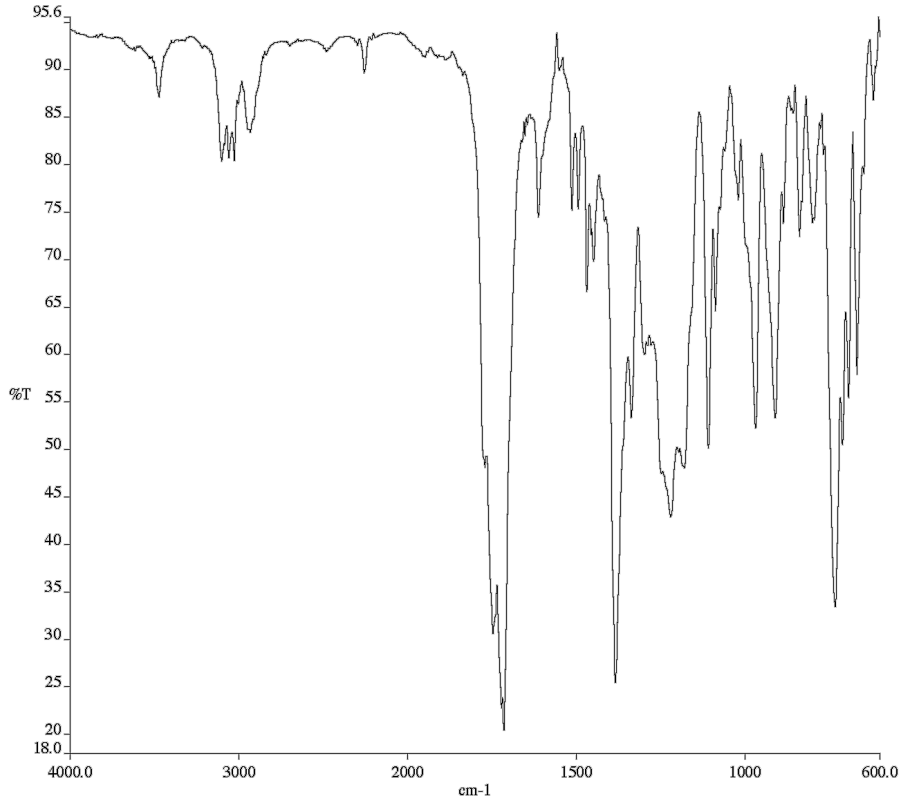

Figure A6.184 *Infrared spectrum (Thin Film, NaCl) of compound* ***140****.*

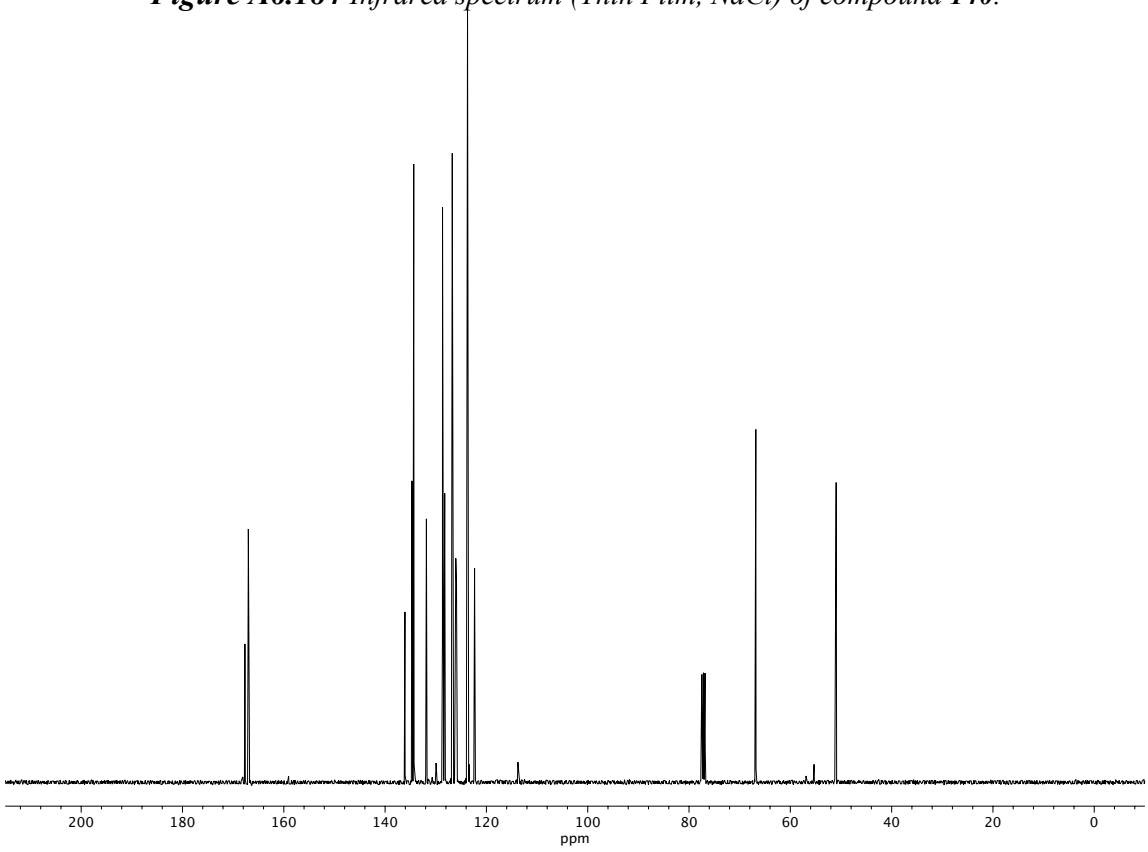

Figure A6.185 *^{13}C NMR (100 MHz, $CDCl_3$) of compound* ***140****.*

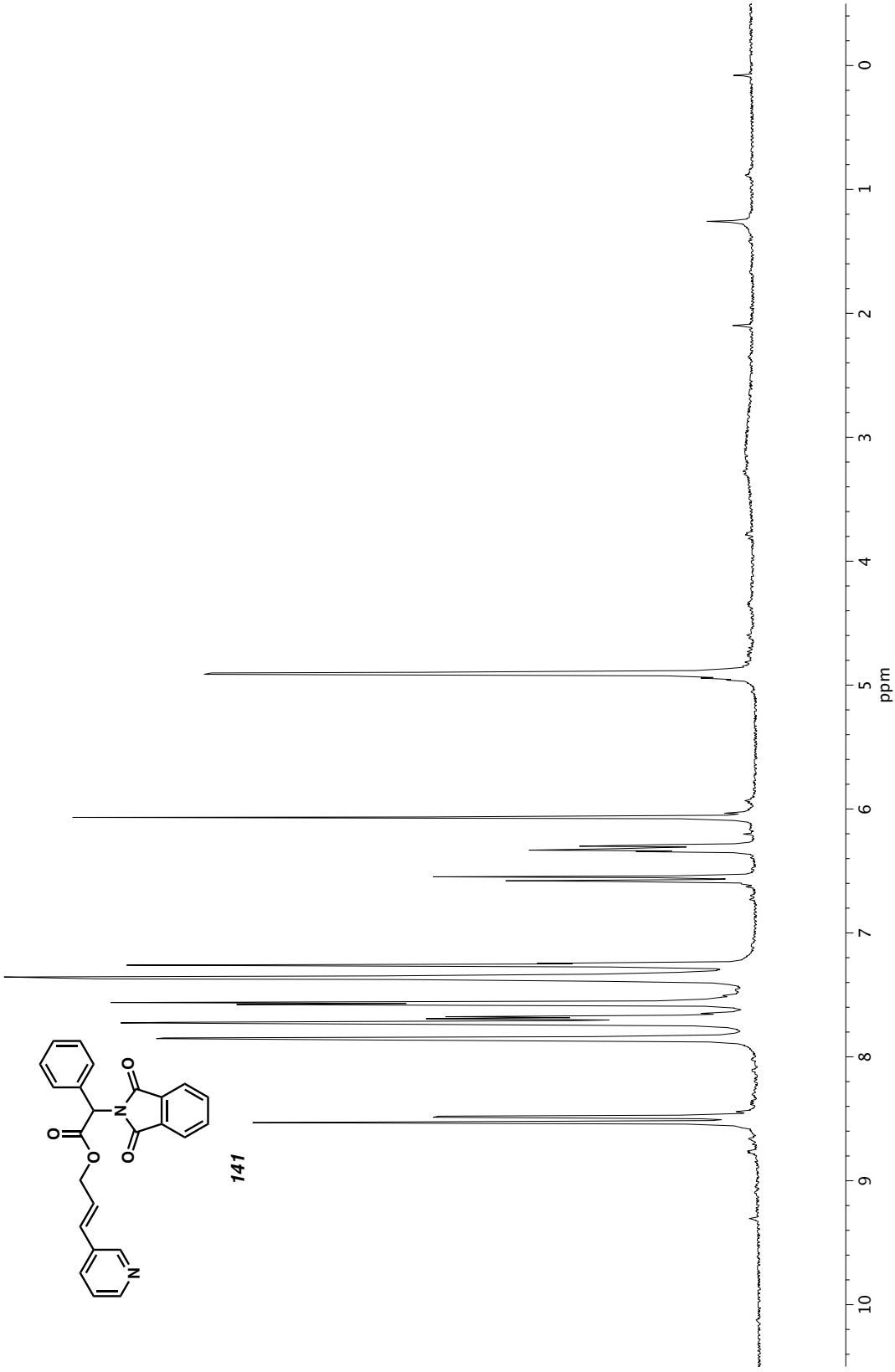

Figure A6.186 *^{1}H NMR (500 MHz, $CDCl_3$) of compound **141**.*

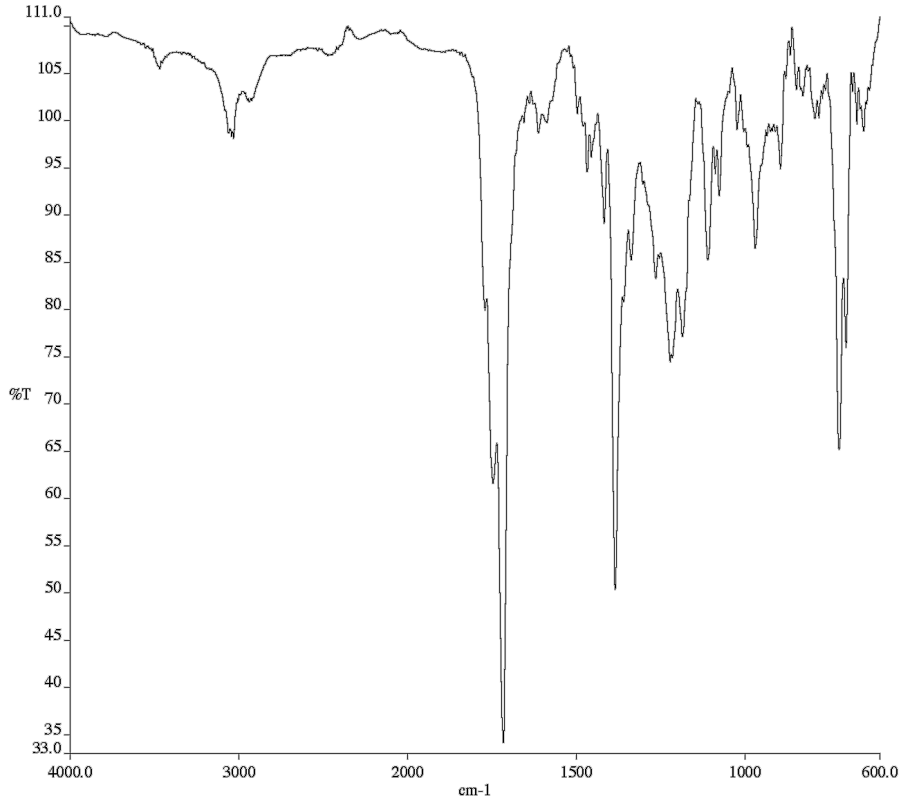

Figure A6.187 *Infrared spectrum (Thin Film, NaCl) of compound* ***141****.*

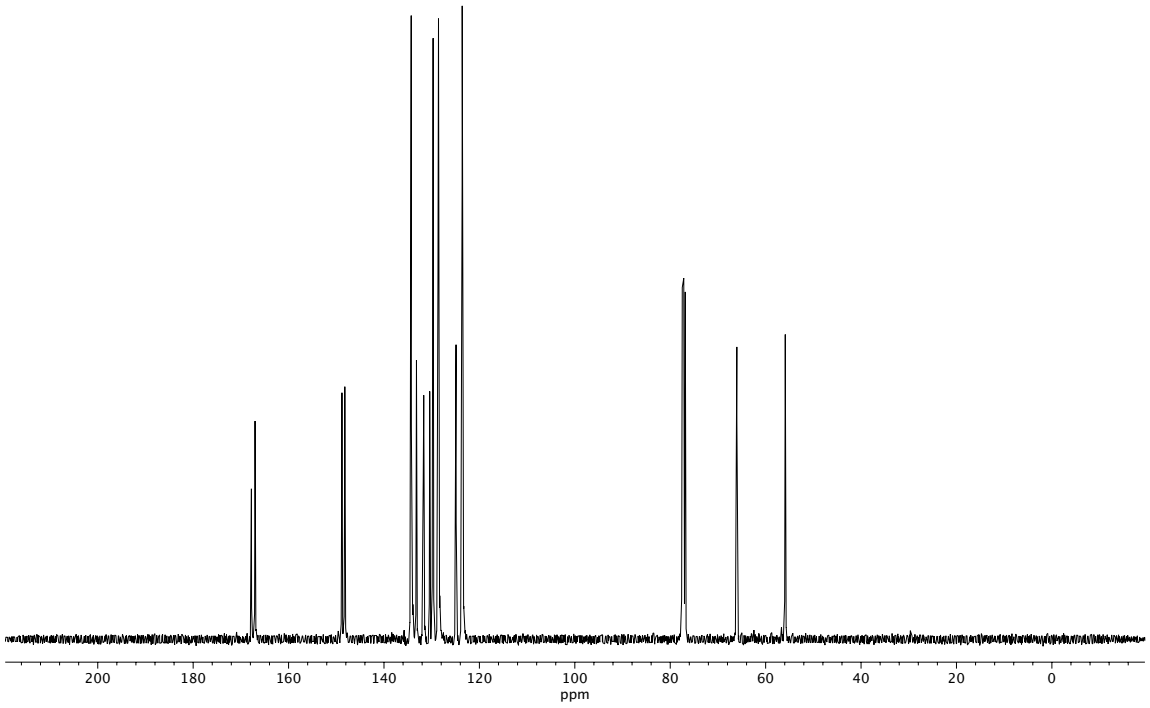

Figure A6.188 *^{13}C NMR (100 MHz, $CDCl_3$) of compound* ***141****.*

Figure A6.189 *^{1}H NMR (500 MHz, $CDCl_3$) of compound* ***142***.

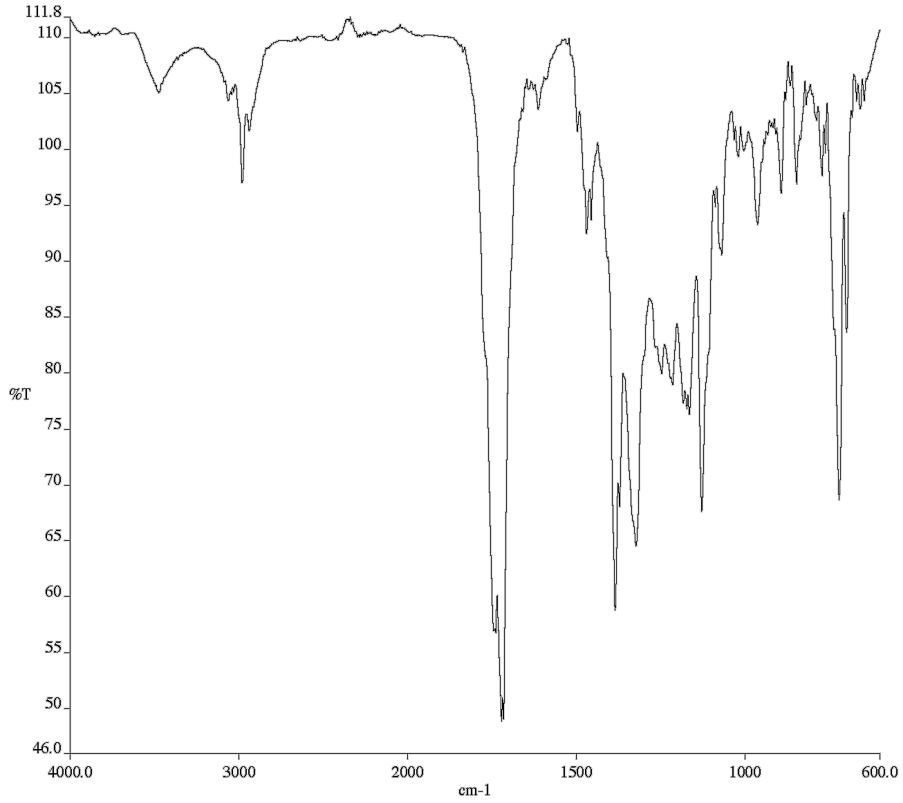

Figure A6.190 *Infrared spectrum (Thin Film, NaCl) of compound* ***142****.*

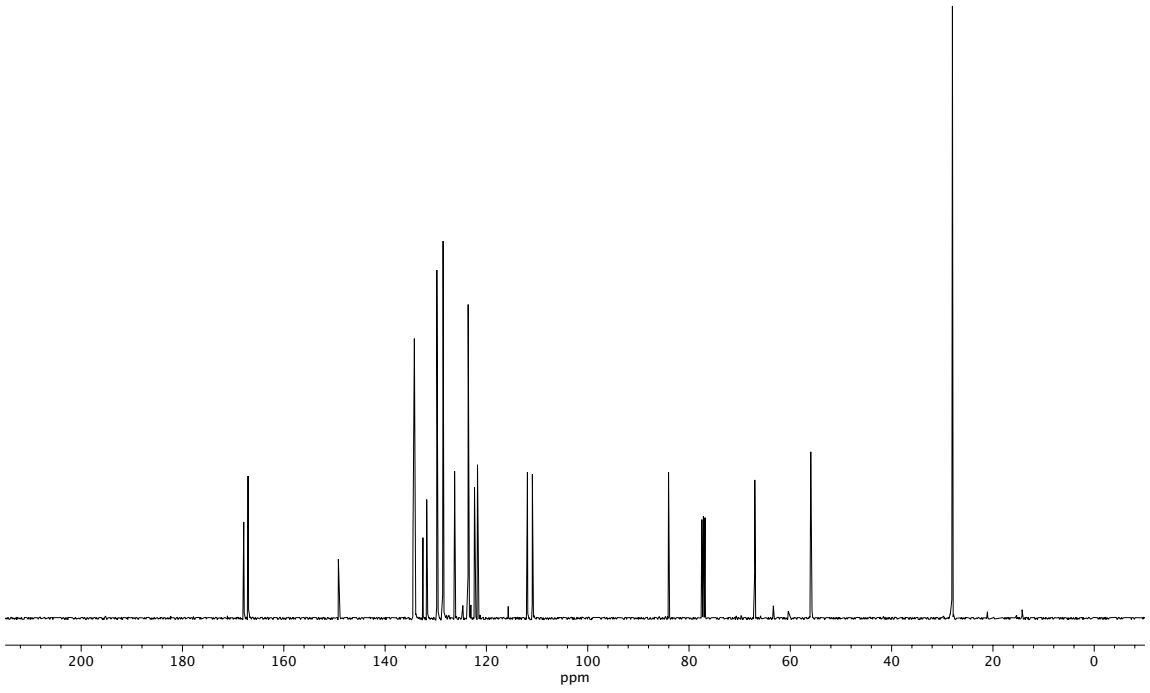

Figure A6.191 *^{13}C NMR (100 MHz, $CDCl_3$) of compound* ***142****.*

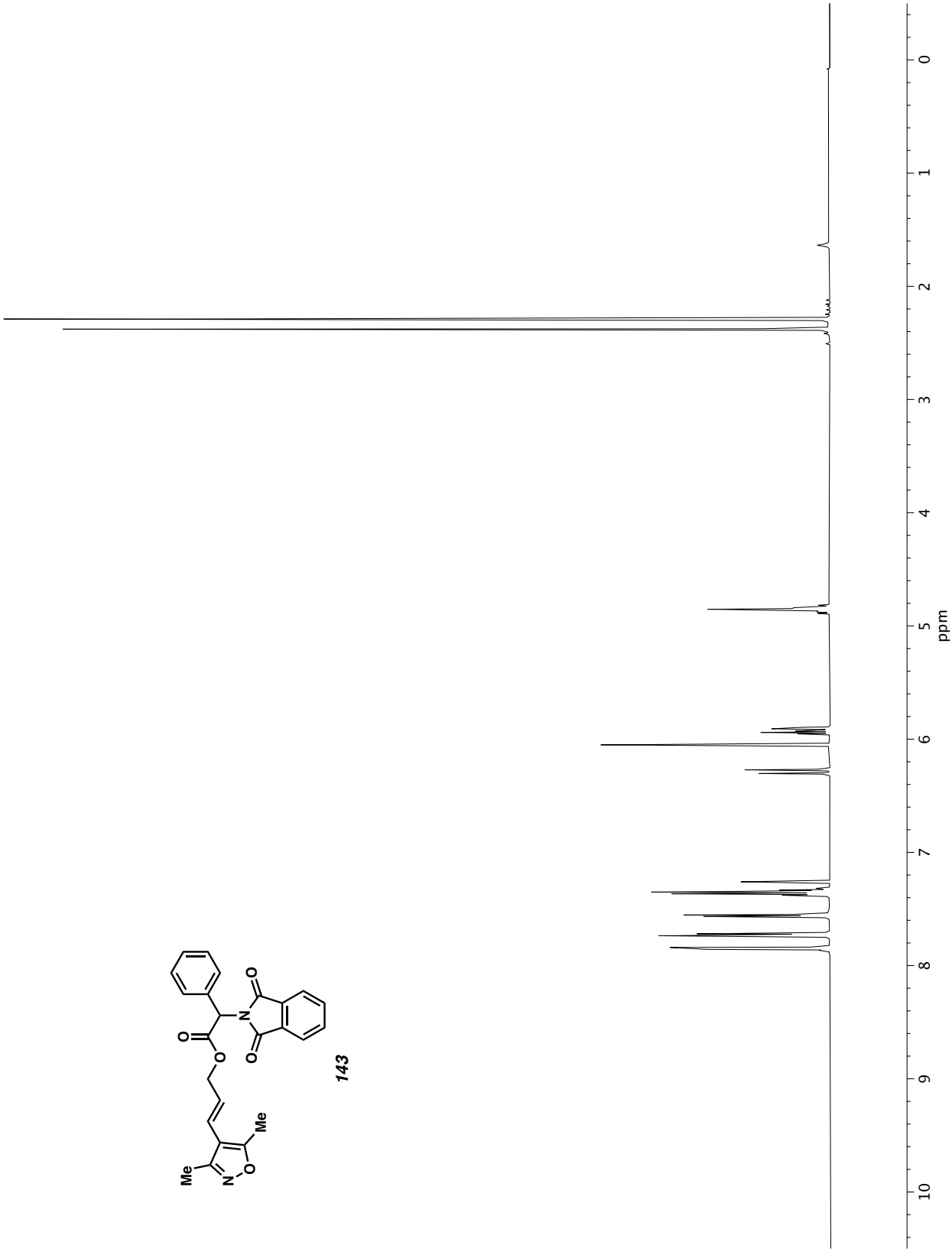

Figure A6.192 *^{1}H NMR (500 MHz, $CDCl_3$) of compound **143**.*

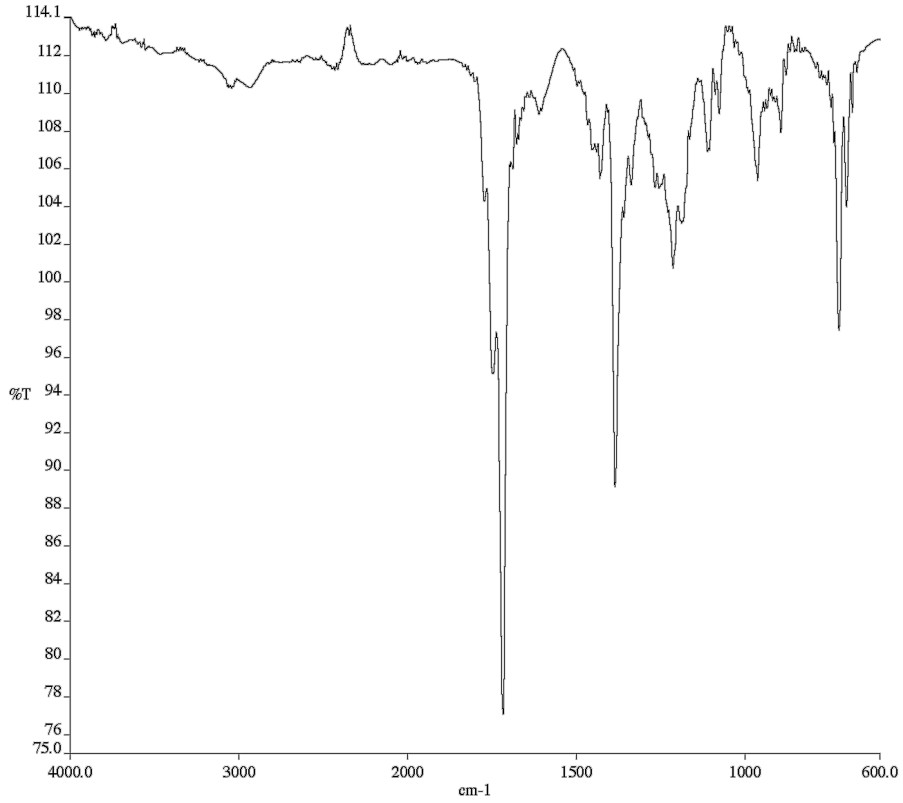

Figure A6.193 *Infrared spectrum (Thin Film, NaCl) of compound* ***143****.*

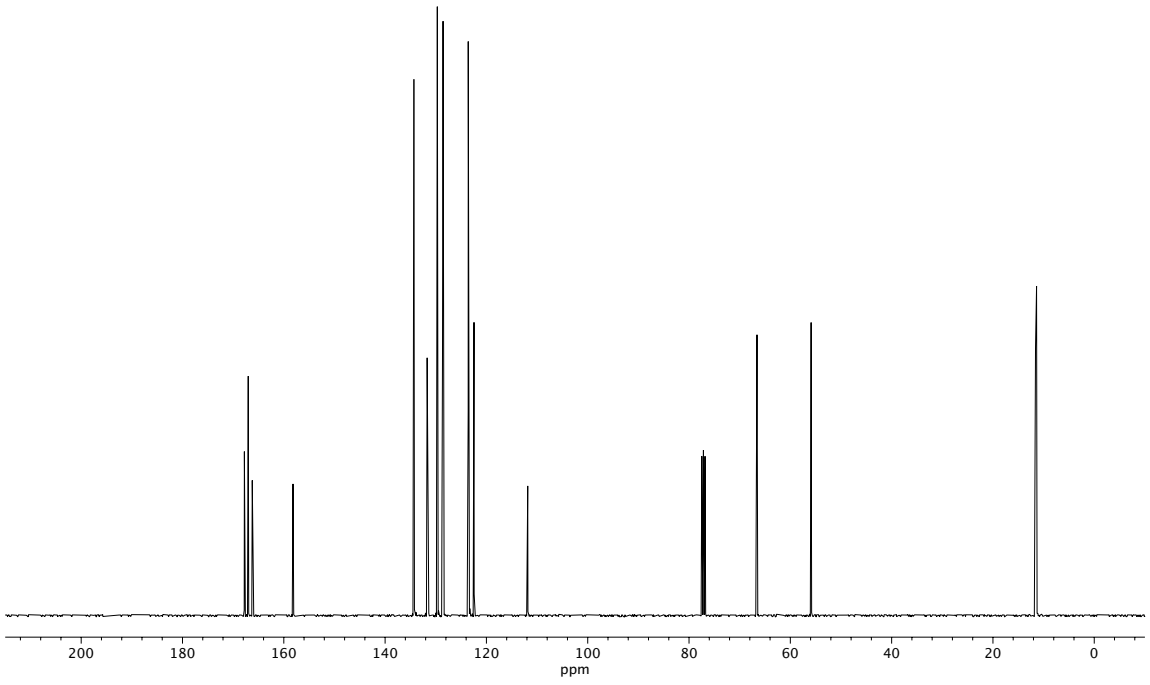

Figure A6.194 *^{13}C NMR (100 MHz, $CDCl_3$) of compound* ***143****.*

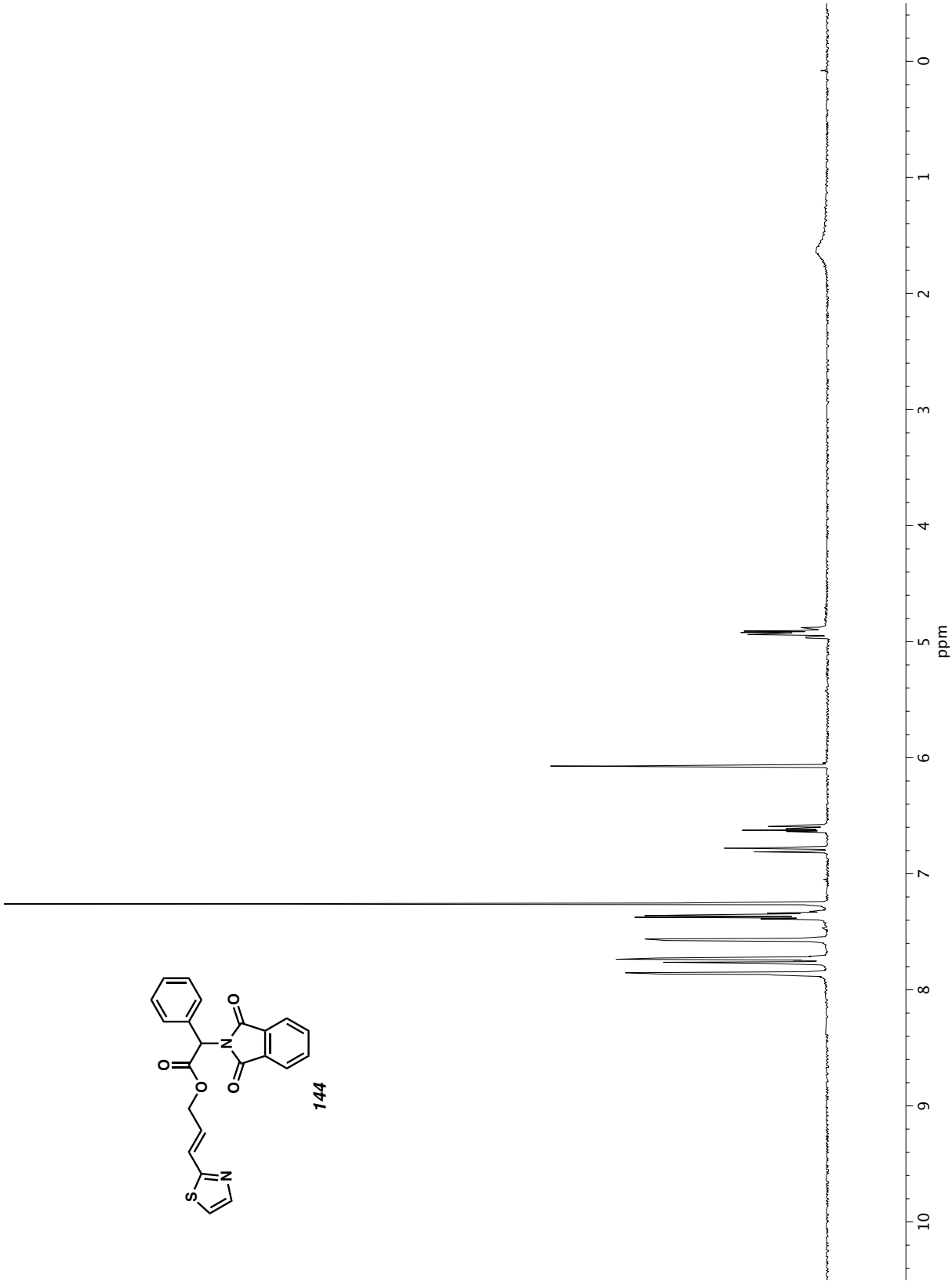

Figure A6.195 *^{1}H NMR (500 MHz, $CDCl_3$) of compound **144**.*

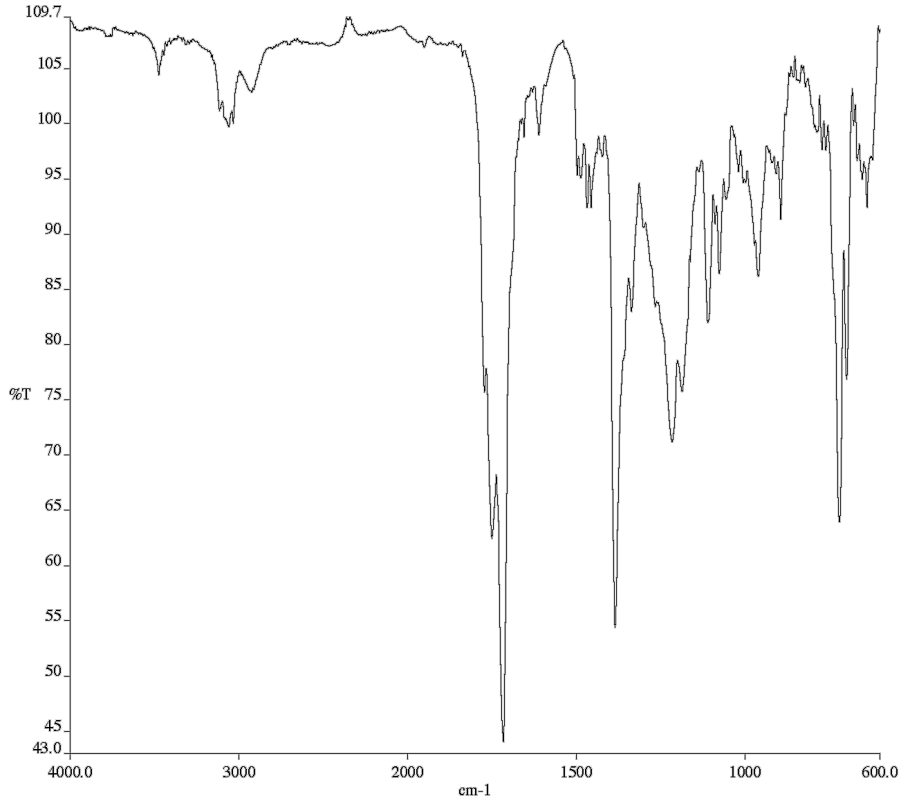

Figure A6.196 *Infrared spectrum (Thin Film, NaCl) of compound* ***144****.*

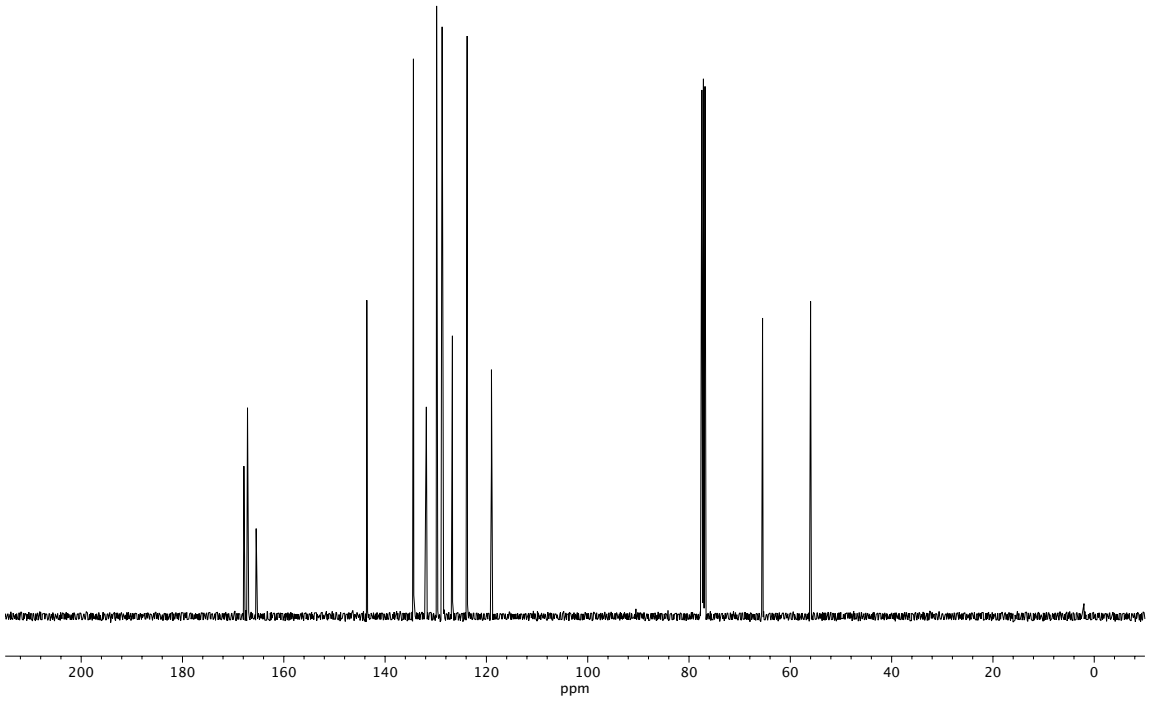

Figure A6.197 *^{13}C NMR (100 MHz, $CDCl_3$) of compound* ***144****.*

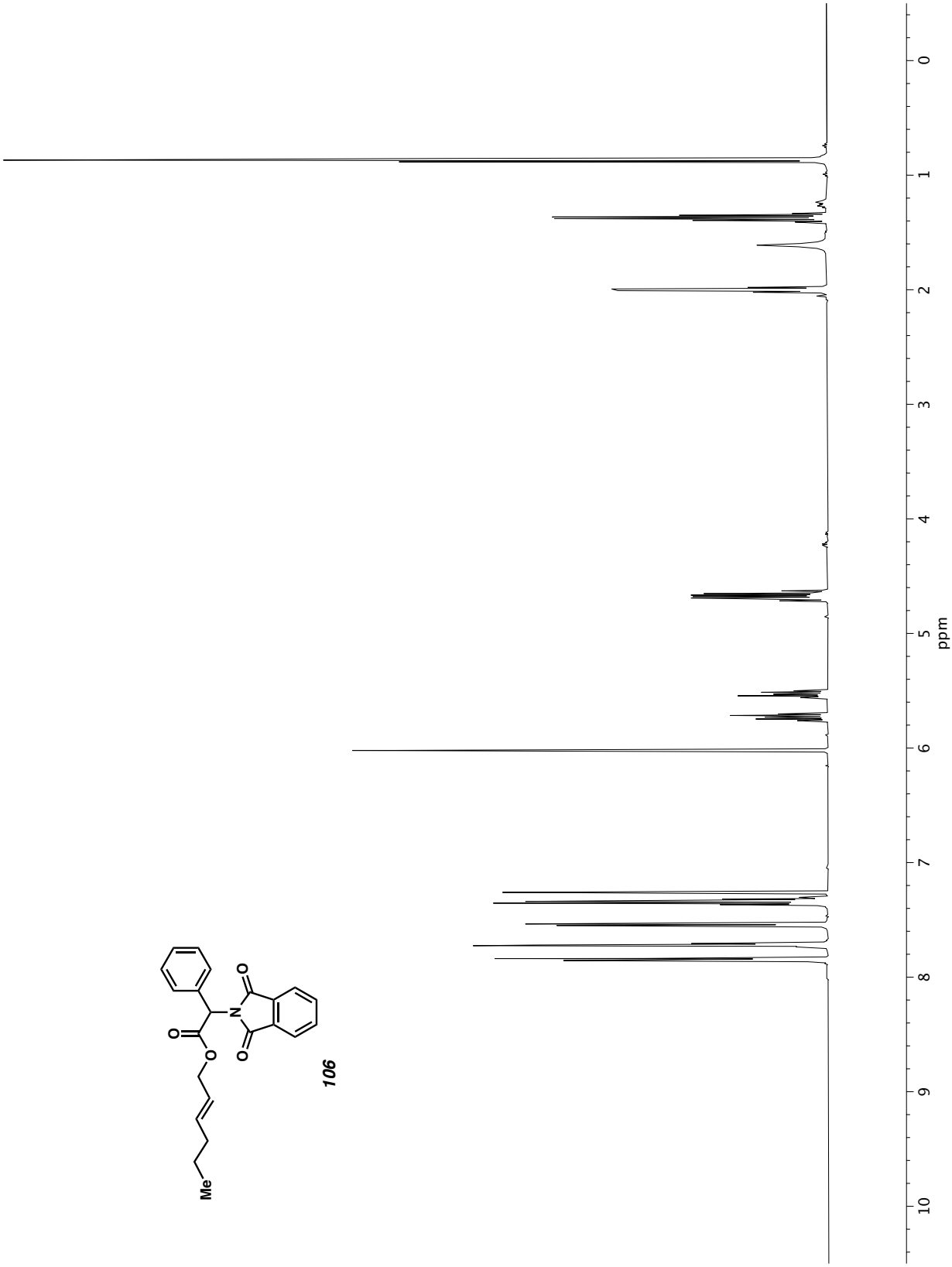

Figure A6.198 *^1H NMR (500 MHz, $CDCl_3$) of compound **106**.*

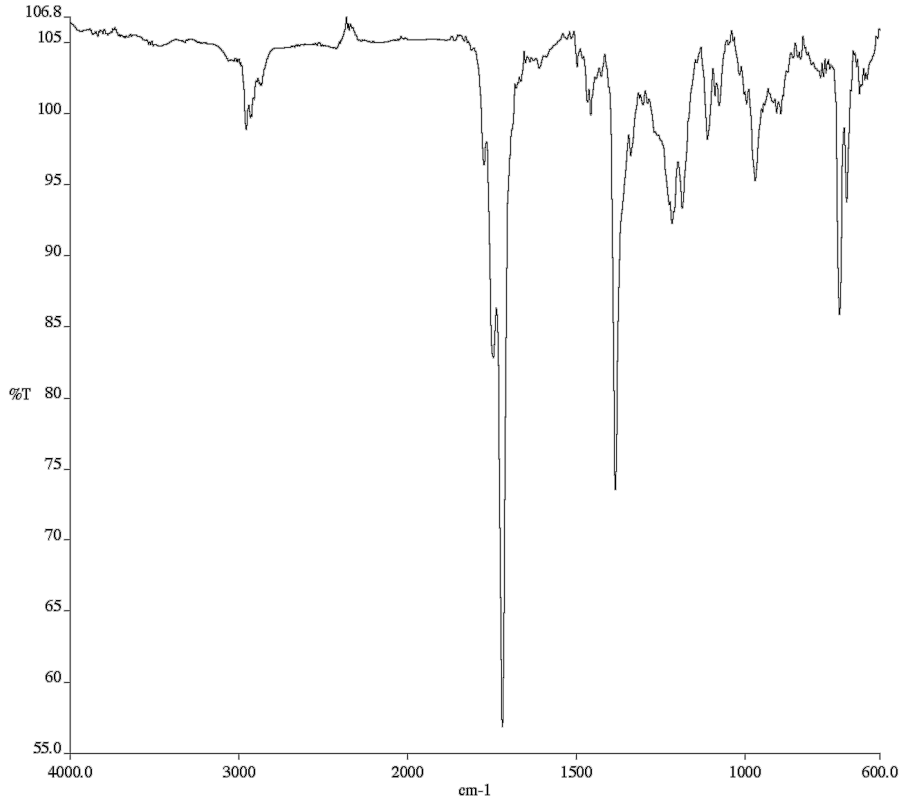

Figure A6.199 *Infrared spectrum (Thin Film, NaCl) of compound* ***106****.*

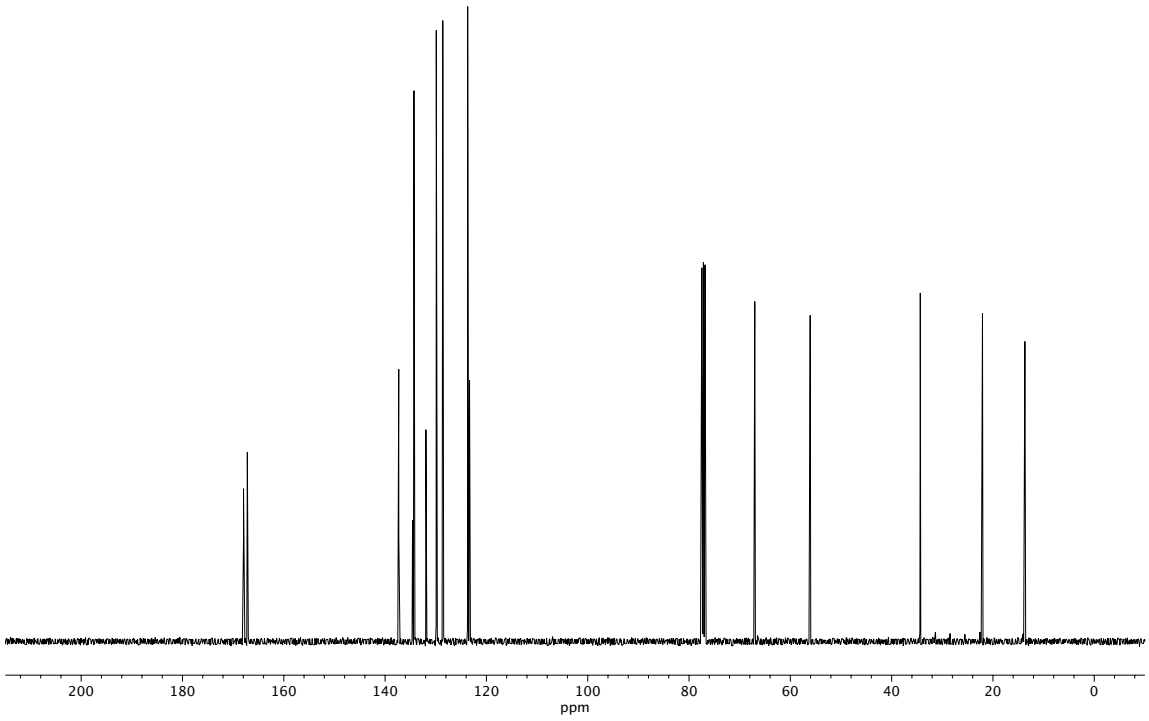

Figure A6.200 *^{13}C NMR (100 MHz, $CDCl_3$) of compound* ***106****.*

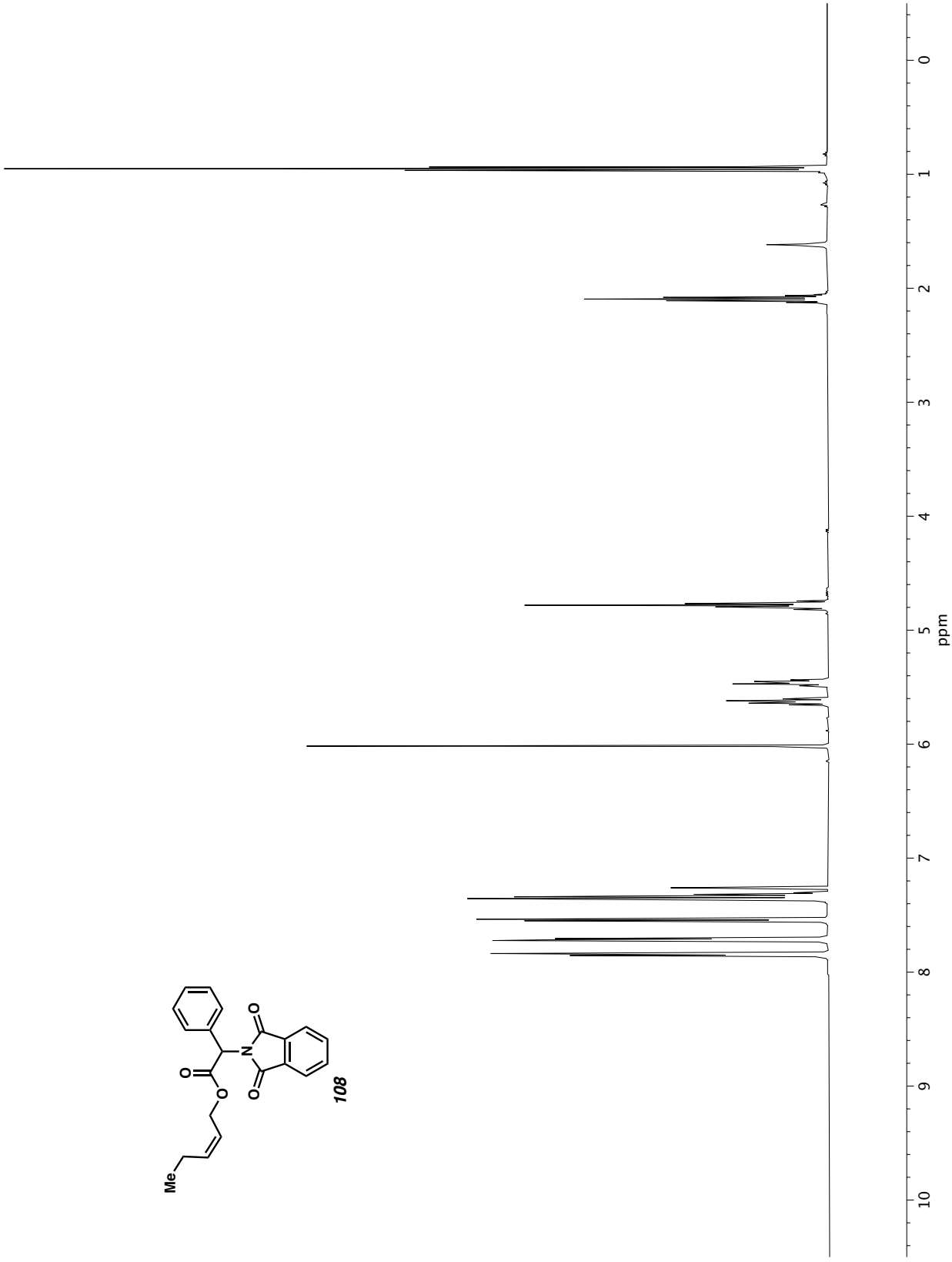

Figure A6.201 *^{1}H NMR (500 MHz, $CDCl_3$) of compound **108**.*

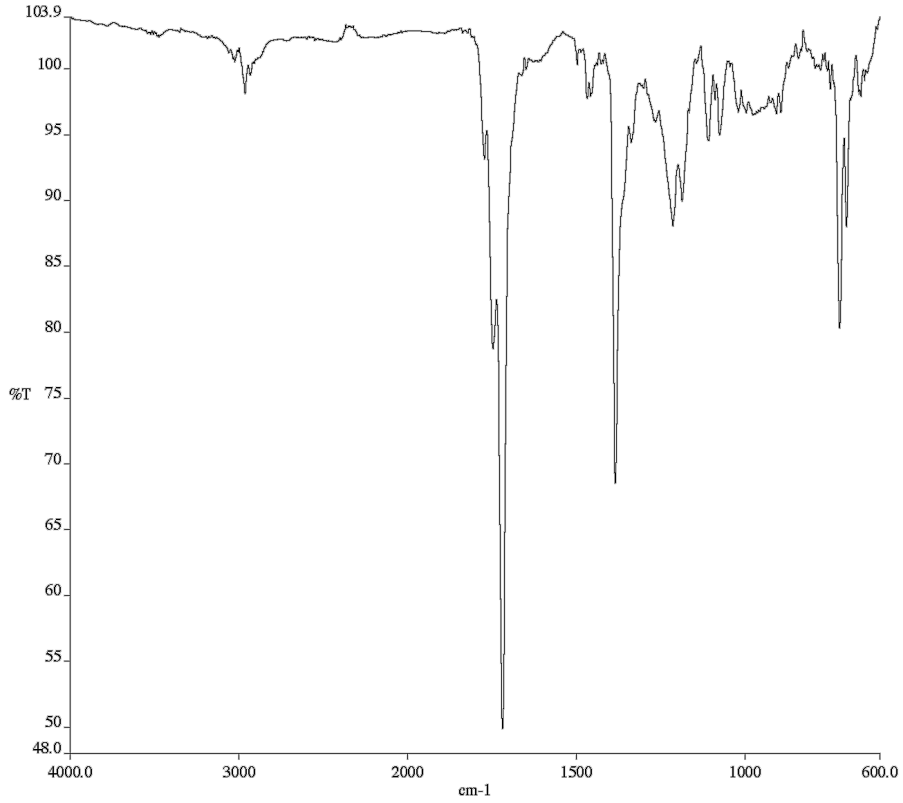

Figure A6.202 *Infrared spectrum (Thin Film, NaCl) of compound* ***108****.*

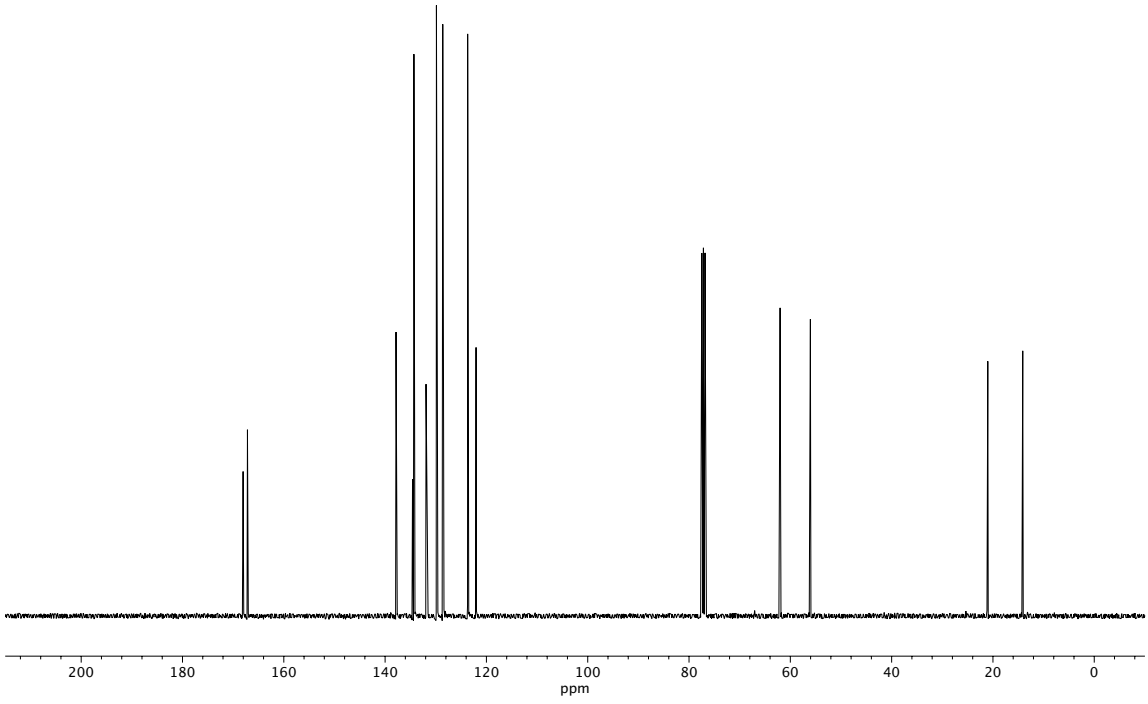

Figure A6.203 *^{13}C NMR (100 MHz, $CDCl_3$) of compound* ***108****.*

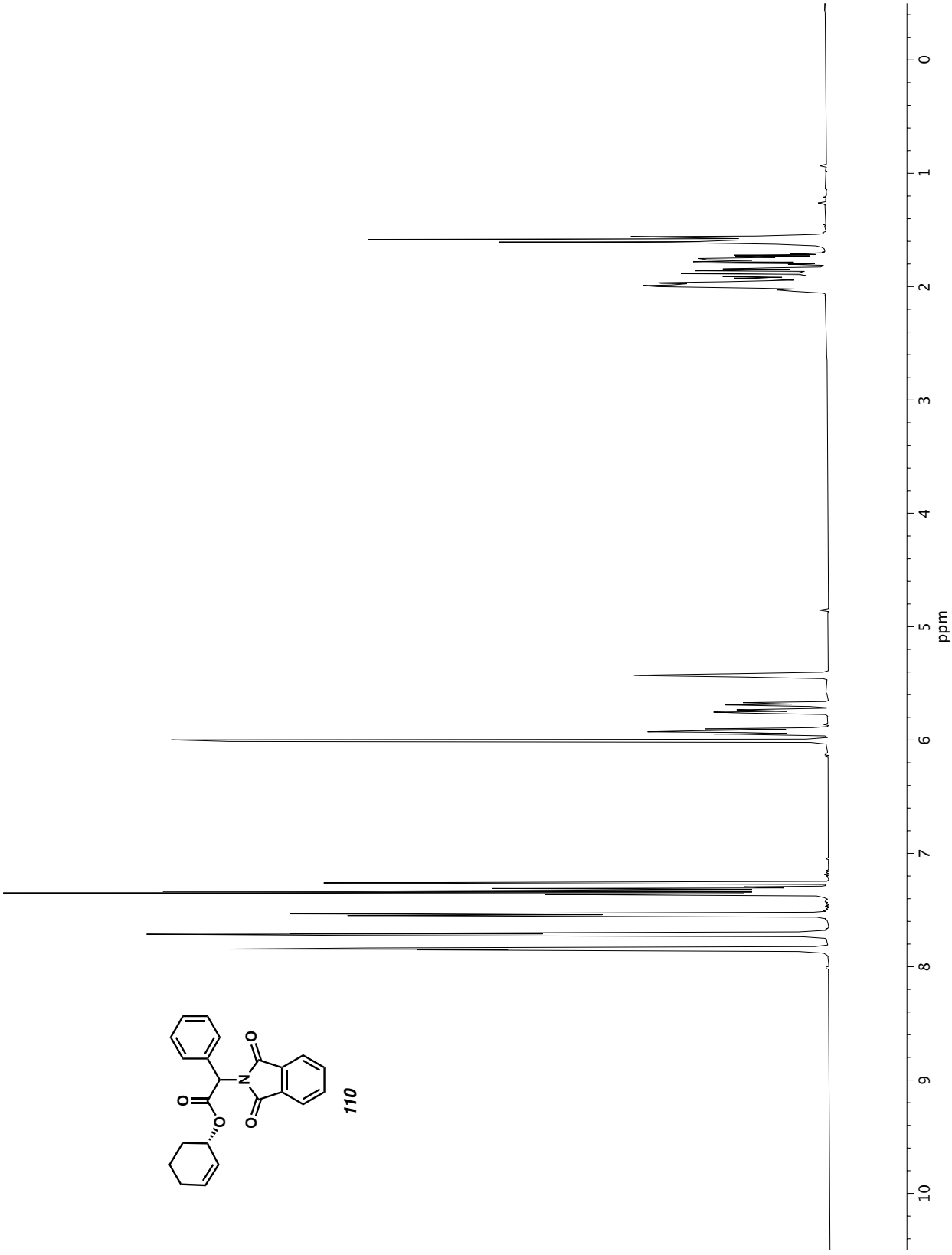

Figure A6.204 *^{1}H NMR (500 MHz, $CDCl_3$) of compound* ***110****.*

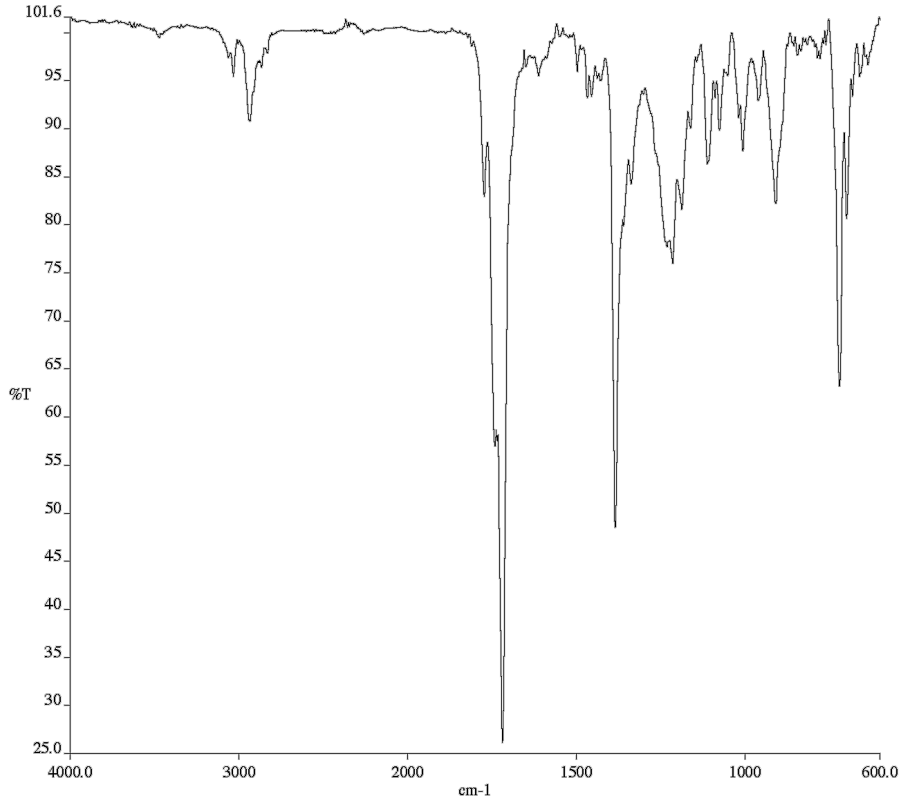

Figure A6.205 *Infrared spectrum (Thin Film, NaCl) of compound* ***110****.*

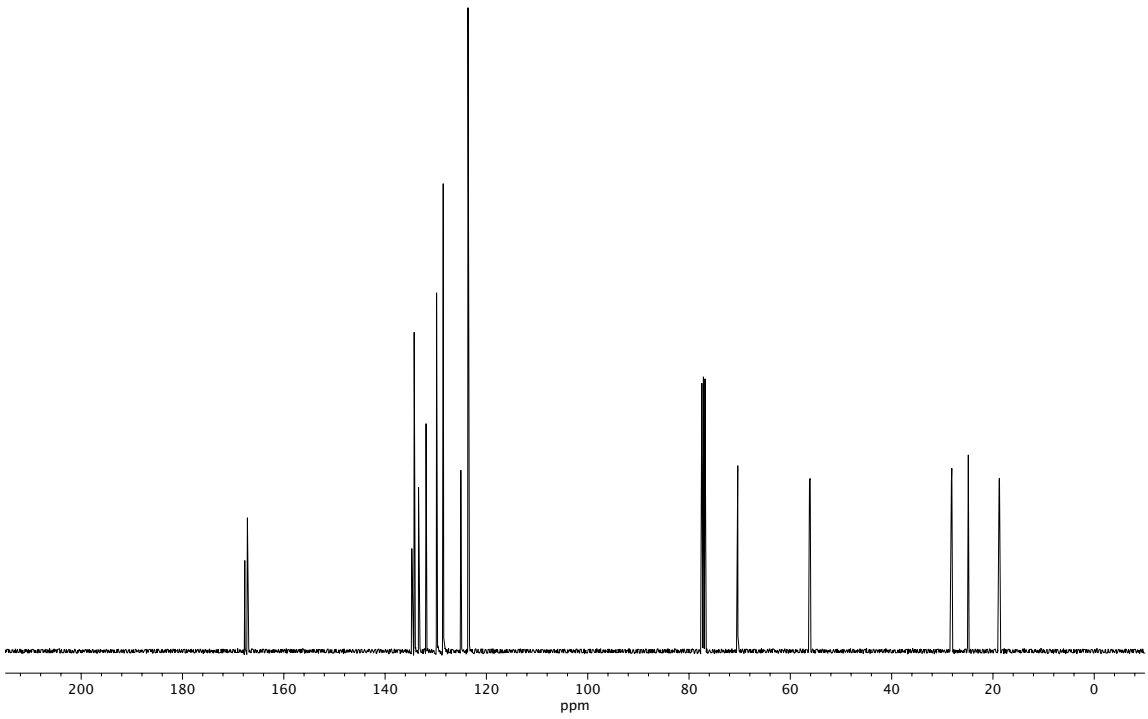

Figure A6.206 *^{13}C NMR (100 MHz, $CDCl_3$) of compound* ***110****.*

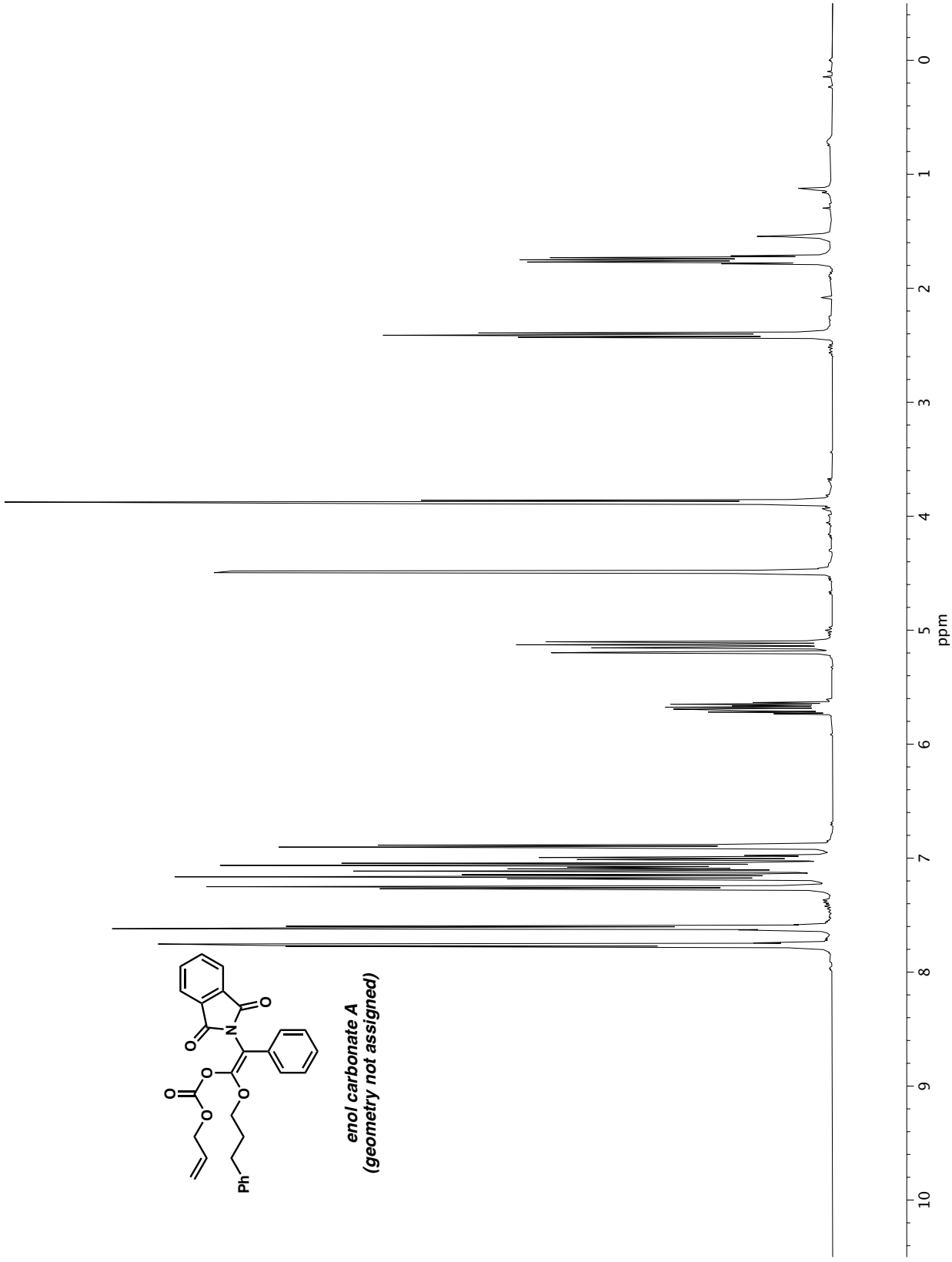

Figure A6.207 *^1H NMR (400 MHz, $CDCl_3$) of compound* ***enol carbonate A****.*

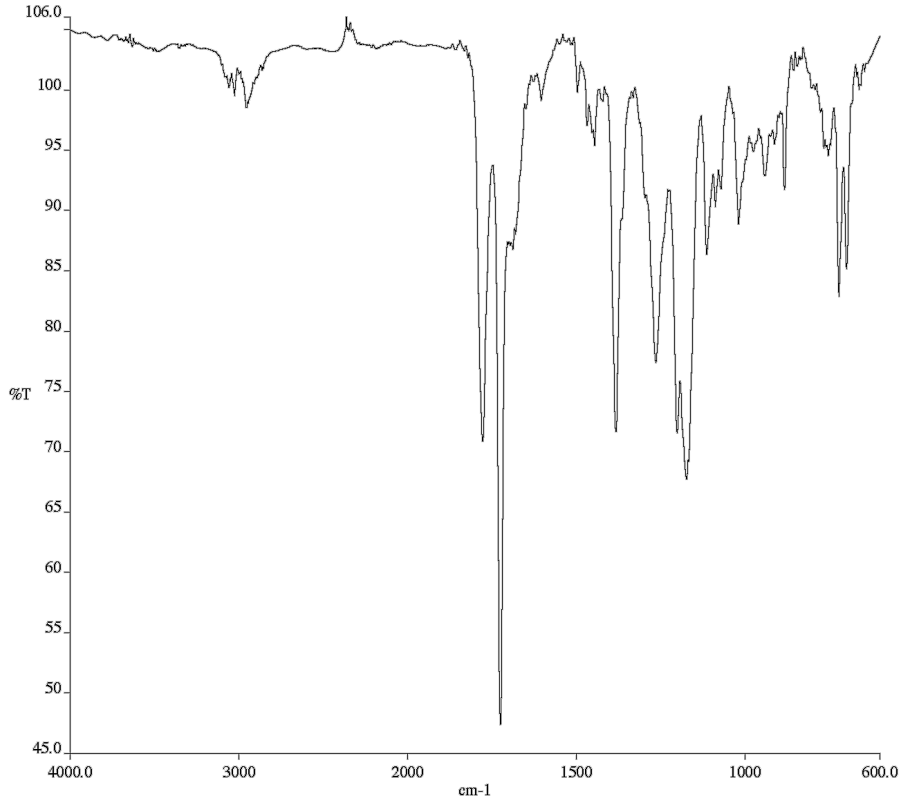

Figure A6.208 *Infrared spectrum (Thin Film, NaCl) of compound* ***enol carbonate A****.*

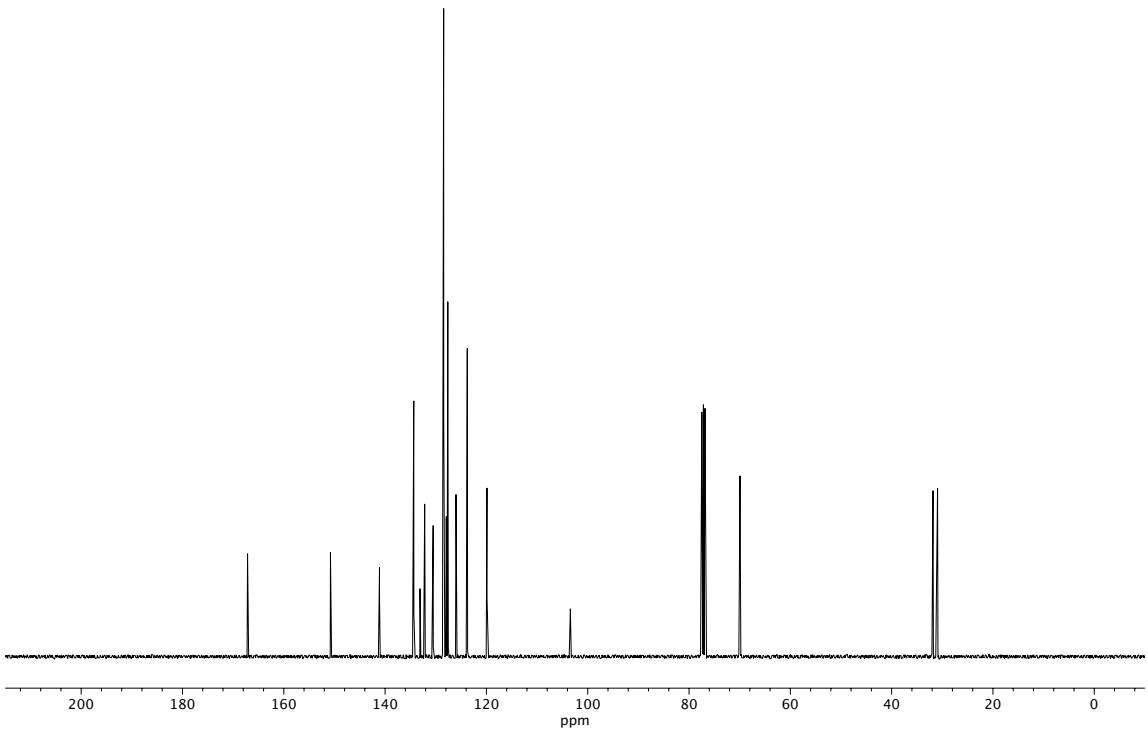

Figure A6.209 *^{13}C NMR (100 MHz, $CDCl_3$) of compound* ***enol carbonate A****.*

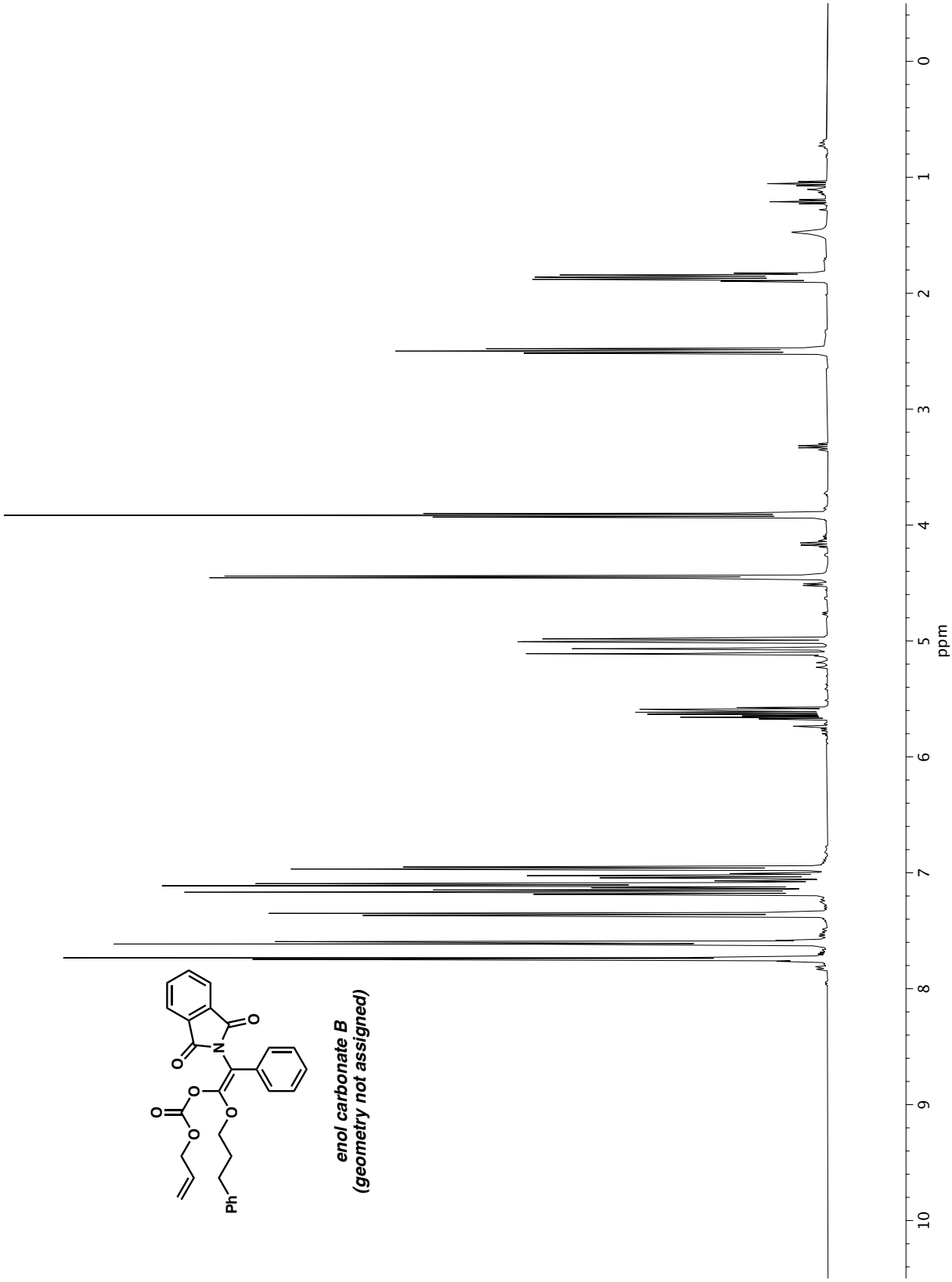

Figure A6.210 *^{1}H NMR (400 MHz, $CDCl_3$) of compound* ***enol carbonate B***.

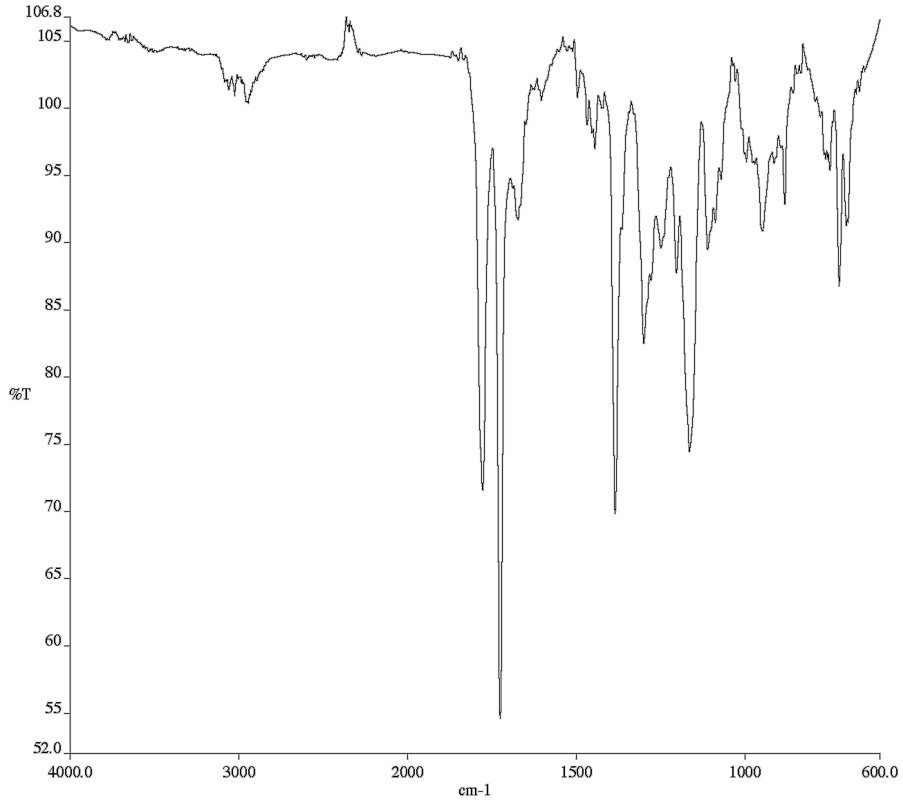

Figure A6.211 *Infrared spectrum (Thin Film, NaCl) of compound* ***enol carbonate B****.*

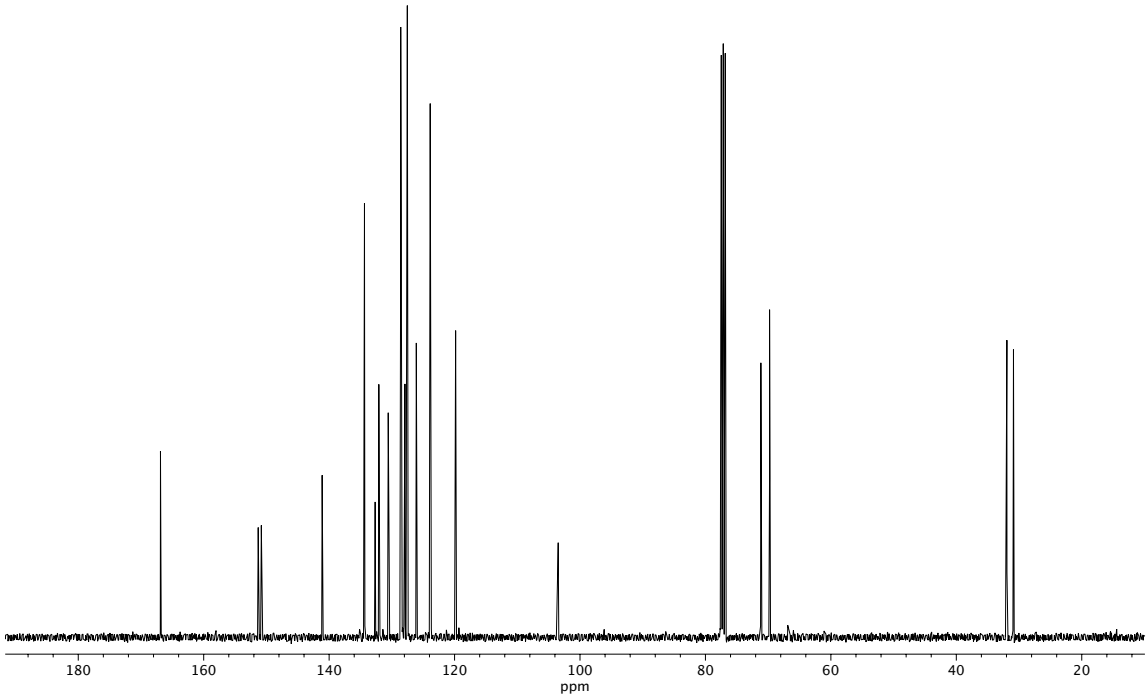

Figure A6.212 *^{13}C NMR (100 MHz, $CDCl_3$) of compound* ***enol carbonate B****.*

APPENDIX 7

X-Ray Crystallography Reports Relevant to Chapter 4:

Global Diastereoconvergence in the Ireland–Claisen

Rearrangement of Isomeric Enolates:

Synthesis of Tetrasubstituted α-Amino Acids

A7.1 GENERAL EXPERIMENTAL

X-Ray crystallographic analysis was obtained from the Caltech X-Ray Crystallography Facility using a Bruker D8 Venture Kappa Duo Photon 100 CMOS or a Bruker AXS KAPPA APEX II diffractometer.

A7.2 X-RAY CRYSTRAL STRUCTURE ANALYSIS OF IRELAND–CLAISEN REARRANGEMENT PRODUCT 76a (V19143)

An X-ray quality crystal of Ireland–Claisen rearrangement product **76a** (compound V18448) was grown by slow cooling of a solution in toluene (approx. 50 mg/600 μL). Low-temperature diffraction data (ϕ-and ω-scans) were collected on a Bruker AXS D8 VENTURE KAPPA diffractometer coupled to a PHOTON II CPAD detector with Mo K_α radiation ($\lambda = 0.71073$ Å) from an IμS micro-source for the structure of compound V19143. The structure was solved by direct methods using SHELXS[1] and refined against F^2 on all data by full-matrix least squares with SHELXL-2017[2] using established refinement techniques.[3] All non-hydrogen atoms were refined anisotropically. All hydrogen atoms were included into the model at geometrically calculated positions and refined using a riding model. The isotropic displacement parameters of all hydrogen atoms were fixed to 1.2 times the U value of the atoms they are linked to (1.5 times for methyl groups). Compound V19143 crystallizes in the triclinic space group P–1 with one molecule in the asymmetric unit. The coordinates for the hydrogen atom bound to O1 were located in the difference Fourier synthesis and refined semi-freely with the help of a restraint on the O–H distance (0.84(4) Å).

Figure A7.2.1 *X-Ray Coordinate of Ireland–Claisen Rearrangement Product* ***76a***

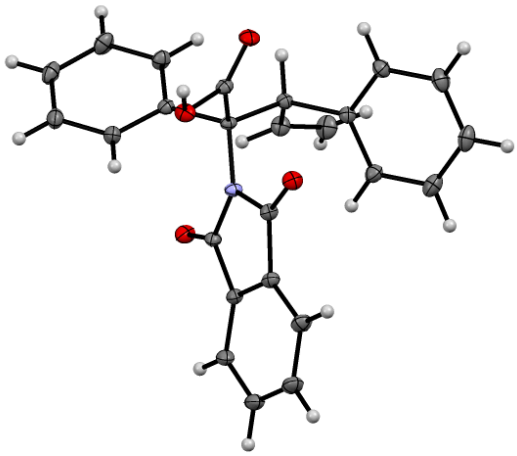

Table A7.2.1 *Crystal Data and Structure Refinement for* ***76a*** *(V19143)*

Identification code	V19143	
Empirical formula	C25 H19 N O4	
Formula weight	397.41	
Temperature	100(2) K	
Wavelength	0.71073 Å	
Crystal system	Triclinic	
Space group	P-1	
Unit cell dimensions	a = 8.645(2) Å	a= 93.927(13)°.
	b = 10.036(3) Å	b= 96.322(12)°.
	c = 12.230(3) Å	g = 113.900(15)°.
Volume	956.8(4) $Å^3$	
Z	2	
Density (calculated)	1.379 Mg/m^3	
Absorption coefficient	0.094 mm^{-1}	
F(000)	416	
Crystal size	0.450 x 0.250 x 0.150 mm^3	
Theta range for data collection	2.636 to 36.329°.	
Index ranges	-14<=h<=14, -16<=k<=16, -20<=l<=20	
Reflections collected	47728	
Independent reflections	9254 [R(int) = 0.0600]	

Completeness to theta = 25.242°	99.6 %
Absorption correction	Semi-empirical from equivalents
Max. and min. transmission	0.7389 and 0.6940
Refinement method	Full-matrix least-squares on F^2
Data / restraints / parameters	9254 / 1 / 274
Goodness-of-fit on F^2	1.035
Final R indices [I>2sigma(I)]	R1 = 0.0449, wR2 = 0.1207
R indices (all data)	R1 = 0.0555, wR2 = 0.1309
Extinction coefficient	n/a
Largest diff. peak and hole	0.586 and -0.297 e.$Å^{-3}$

Table A7.2.2 *Atomic Coordinates (x 10^4) and Equivalent Isotropic Displacement Parameters ($Å^2$x 10^3) for* ***76a*** *(V19143). U(eq) is Defined as One Third of the Trace of the Orthogonalized U^{ij} Tensor.*

	x	y	z	U(eq)
C(1)	5924(1)	5535(1)	1870(1)	13(1)
O(1)	6544(1)	6036(1)	955(1)	17(1)
O(2)	5608(1)	4314(1)	2102(1)	18(1)
C(2)	5878(1)	6774(1)	2682(1)	11(1)
N(1)	5163(1)	7649(1)	2043(1)	12(1)
C(6)	3796(1)	7005(1)	1165(1)	13(1)
O(3)	3204(1)	5730(1)	752(1)	16(1)
C(7)	3264(1)	8171(1)	849(1)	14(1)
C(8)	1938(1)	8087(1)	62(1)	18(1)
C(9)	1782(1)	9400(1)	-82(1)	21(1)
C(10)	2917(1)	10728(1)	539(1)	21(1)
C(11)	4220(1)	10785(1)	1356(1)	18(1)
C(12)	4354(1)	9476(1)	1498(1)	14(1)
C(13)	5526(1)	9155(1)	2317(1)	13(1)
O(4)	6555(1)	9979(1)	3080(1)	19(1)
C(21)	7800(1)	7664(1)	3141(1)	13(1)
C(22)	8882(1)	8605(1)	2491(1)	16(1)
C(23)	10631(1)	9341(1)	2856(1)	20(1)
C(24)	11337(1)	9147(1)	3877(1)	20(1)
C(25)	10286(1)	8199(1)	4523(1)	21(1)
C(26)	8526(1)	7451(1)	4155(1)	17(1)
C(3)	4787(1)	6121(1)	3610(1)	13(1)
C(31)	2887(1)	5214(1)	3199(1)	13(1)
C(32)	2197(1)	3682(1)	3091(1)	17(1)
C(33)	434(1)	2859(1)	2804(1)	22(1)
C(34)	-653(1)	3553(1)	2607(1)	23(1)
C(35)	26(1)	5073(1)	2685(1)	21(1)
C(36)	1777(1)	5896(1)	2992(1)	17(1)
C(4)	5062(1)	7322(1)	4541(1)	16(1)

C(5)	4064(1)	7193(1)	5313(1)	22(1)

Table A7.2.3 *Bond lengths [Å] and angles [°] for V19143*

C(1)-O(2)	1.2038(9)
C(1)-O(1)	1.3352(10)
C(1)-C(2)	1.5532(10)
O(1)-H(1O)	0.850(12)
C(2)-N(1)	1.4807(9)
C(2)-C(21)	1.5486(11)
C(2)-C(3)	1.5626(11)
N(1)-C(6)	1.4053(10)
N(1)-C(13)	1.4201(10)
C(6)-O(3)	1.2155(9)
C(6)-C(7)	1.4797(11)
C(7)-C(8)	1.3841(11)
C(7)-C(12)	1.3884(11)
C(8)-C(9)	1.3989(13)
C(8)-H(8)	0.9500
C(9)-C(10)	1.3971(14)
C(9)-H(9)	0.9500
C(10)-C(11)	1.4008(12)
C(10)-H(10)	0.9500
C(11)-C(12)	1.3857(11)
C(11)-H(11)	0.9500
C(12)-C(13)	1.4899(11)
C(13)-O(4)	1.2081(10)
C(21)-C(22)	1.3963(11)
C(21)-C(26)	1.3966(11)
C(22)-C(23)	1.3904(12)
C(22)-H(22)	0.9500
C(23)-C(24)	1.3902(14)
C(23)-H(23)	0.9500
C(24)-C(25)	1.3842(14)
C(24)-H(24)	0.9500
C(25)-C(26)	1.3988(12)
C(25)-H(25)	0.9500

C(26)-H(26)	0.9500
C(3)-C(31)	1.5244(11)
C(3)-C(4)	1.5249(11)
C(3)-H(3)	1.0000
C(31)-C(32)	1.3956(11)
C(31)-C(36)	1.3990(11)
C(32)-C(33)	1.3967(12)
C(32)-H(32)	0.9500
C(33)-C(34)	1.3894(14)
C(33)-H(33)	0.9500
C(34)-C(35)	1.3869(14)
C(34)-H(34)	0.9500
C(35)-C(36)	1.3908(12)
C(35)-H(35)	0.9500
C(36)-H(36)	0.9500
C(4)-C(5)	1.3264(12)
C(4)-H(4)	0.9500
C(5)-H(5A)	0.9500
C(5)-H(5B)	0.9500

O(2)-C(1)-O(1)	124.51(7)
O(2)-C(1)-C(2)	123.19(7)
O(1)-C(1)-C(2)	111.85(6)
C(1)-O(1)-H(1O)	109.9(9)
N(1)-C(2)-C(21)	111.86(6)
N(1)-C(2)-C(1)	108.70(6)
C(21)-C(2)-C(1)	101.80(6)
N(1)-C(2)-C(3)	110.60(6)
C(21)-C(2)-C(3)	112.53(6)
C(1)-C(2)-C(3)	111.00(6)
C(6)-N(1)-C(13)	110.41(6)
C(6)-N(1)-C(2)	122.40(6)
C(13)-N(1)-C(2)	126.44(6)
O(3)-C(6)-N(1)	125.27(7)
O(3)-C(6)-C(7)	127.79(7)

N(1)-C(6)-C(7)	106.94(6)
C(8)-C(7)-C(12)	122.17(7)
C(8)-C(7)-C(6)	129.64(7)
C(12)-C(7)-C(6)	108.19(7)
C(7)-C(8)-C(9)	116.69(8)
C(7)-C(8)-H(8)	121.7
C(9)-C(8)-H(8)	121.7
C(10)-C(9)-C(8)	121.37(8)
C(10)-C(9)-H(9)	119.3
C(8)-C(9)-H(9)	119.3
C(9)-C(10)-C(11)	121.18(8)
C(9)-C(10)-H(10)	119.4
C(11)-C(10)-H(10)	119.4
C(12)-C(11)-C(10)	116.97(8)
C(12)-C(11)-H(11)	121.5
C(10)-C(11)-H(11)	121.5
C(11)-C(12)-C(7)	121.54(7)
C(11)-C(12)-C(13)	130.16(7)
C(7)-C(12)-C(13)	108.27(6)
O(4)-C(13)-N(1)	126.09(7)
O(4)-C(13)-C(12)	127.95(7)
N(1)-C(13)-C(12)	105.94(6)
C(22)-C(21)-C(26)	118.31(7)
C(22)-C(21)-C(2)	119.86(7)
C(26)-C(21)-C(2)	121.55(7)
C(23)-C(22)-C(21)	120.88(8)
C(23)-C(22)-H(22)	119.6
C(21)-C(22)-H(22)	119.6
C(24)-C(23)-C(22)	120.38(8)
C(24)-C(23)-H(23)	119.8
C(22)-C(23)-H(23)	119.8
C(25)-C(24)-C(23)	119.40(8)
C(25)-C(24)-H(24)	120.3
C(23)-C(24)-H(24)	120.3
C(24)-C(25)-C(26)	120.31(8)

C(24)-C(25)-H(25)	119.8
C(26)-C(25)-H(25)	119.8
C(21)-C(26)-C(25)	120.68(8)
C(21)-C(26)-H(26)	119.7
C(25)-C(26)-H(26)	119.7
C(31)-C(3)-C(4)	111.16(6)
C(31)-C(3)-C(2)	114.66(6)
C(4)-C(3)-C(2)	110.84(6)
C(31)-C(3)-H(3)	106.6
C(4)-C(3)-H(3)	106.6
C(2)-C(3)-H(3)	106.6
C(32)-C(31)-C(36)	118.46(7)
C(32)-C(31)-C(3)	120.66(7)
C(36)-C(31)-C(3)	120.76(7)
C(31)-C(32)-C(33)	120.41(8)
C(31)-C(32)-H(32)	119.8
C(33)-C(32)-H(32)	119.8
C(34)-C(33)-C(32)	120.47(8)
C(34)-C(33)-H(33)	119.8
C(32)-C(33)-H(33)	119.8
C(35)-C(34)-C(33)	119.50(8)
C(35)-C(34)-H(34)	120.3
C(33)-C(34)-H(34)	120.3
C(34)-C(35)-C(36)	120.13(8)
C(34)-C(35)-H(35)	119.9
C(36)-C(35)-H(35)	119.9
C(35)-C(36)-C(31)	121.00(8)
C(35)-C(36)-H(36)	119.5
C(31)-C(36)-H(36)	119.5
C(5)-C(4)-C(3)	125.11(8)
C(5)-C(4)-H(4)	117.4
C(3)-C(4)-H(4)	117.4
C(4)-C(5)-H(5A)	120.0
C(4)-C(5)-H(5B)	120.0
H(5A)-C(5)-H(5B)	120.0

Symmetry transformations used to generate equivalent atoms:

Table A7.2.4 *Anisotropic displacement parameters ($Å^2 x\ 10^3$) for* ***76a*** *(V19143). The anisotropic displacement factor exponent takes the form: $-2p^2[\ h^2\ a^{*2}U^{11} + ... + 2\ h\ k\ a^*\ b^*\ U^{12}]$*

	U^{11}	U^{22}	U^{33}	U^{23}	U^{13}	U^{12}
C(1)	14(1)	12(1)	14(1)	-1(1)	1(1)	6(1)
O(1)	23(1)	16(1)	14(1)	-1(1)	5(1)	10(1)
O(2)	22(1)	12(1)	22(1)	1(1)	4(1)	9(1)
C(2)	12(1)	10(1)	12(1)	0(1)	1(1)	6(1)
N(1)	14(1)	10(1)	12(1)	0(1)	0(1)	6(1)
C(6)	14(1)	13(1)	11(1)	0(1)	1(1)	6(1)
O(3)	19(1)	14(1)	14(1)	-3(1)	0(1)	7(1)
C(7)	16(1)	15(1)	13(1)	2(1)	2(1)	8(1)
C(8)	19(1)	22(1)	16(1)	4(1)	0(1)	10(1)
C(9)	22(1)	27(1)	21(1)	9(1)	2(1)	14(1)
C(10)	22(1)	22(1)	25(1)	11(1)	7(1)	14(1)
C(11)	17(1)	14(1)	24(1)	6(1)	6(1)	9(1)
C(12)	14(1)	13(1)	16(1)	3(1)	3(1)	7(1)
C(13)	14(1)	10(1)	17(1)	1(1)	2(1)	6(1)
O(4)	18(1)	13(1)	23(1)	-4(1)	-2(1)	6(1)
C(21)	12(1)	12(1)	13(1)	0(1)	1(1)	5(1)
C(22)	14(1)	17(1)	18(1)	4(1)	3(1)	6(1)
C(23)	14(1)	18(1)	26(1)	2(1)	5(1)	5(1)
C(24)	13(1)	20(1)	26(1)	-5(1)	-1(1)	5(1)
C(25)	17(1)	26(1)	18(1)	-2(1)	-3(1)	9(1)
C(26)	15(1)	20(1)	14(1)	1(1)	-1(1)	7(1)
C(3)	13(1)	12(1)	13(1)	1(1)	2(1)	5(1)
C(31)	13(1)	13(1)	13(1)	1(1)	2(1)	5(1)
C(32)	17(1)	13(1)	18(1)	1(1)	2(1)	5(1)
C(33)	19(1)	16(1)	23(1)	-1(1)	3(1)	1(1)
C(34)	14(1)	26(1)	22(1)	-4(1)	1(1)	4(1)
C(35)	15(1)	26(1)	22(1)	-2(1)	1(1)	10(1)
C(36)	15(1)	17(1)	19(1)	1(1)	2(1)	9(1)
C(4)	18(1)	17(1)	14(1)	-2(1)	2(1)	7(1)

C(5)	24(1)	25(1)	17(1)	-1(1)	6(1)	10(1)

Table A7.2.5 *Hydrogen coordinates (x 10^4) and isotropic displacement parameters ($Å^2$x 10^3) for V19143.*

	x	y	z	U(eq)
H(1O)	6581(17)	5342(14)	536(11)	20
H(8)	1171	7182	-360	22
H(9)	886	9390	-612	26
H(10)	2803	11607	404	25
H(11)	4978	11681	1792	21
H(22)	8416	8744	1790	20
H(23)	11348	9980	2404	24
H(24)	12531	9660	4129	25
H(25)	10761	8055	5219	25
H(26)	7818	6792	4600	21
H(3)	5237	5440	3940	15
H(32)	2931	3197	3213	20
H(33)	-25	1818	2744	26
H(34)	-1853	2990	2420	28
H(35)	-707	5553	2529	25
H(36)	2226	6938	3063	20
H(4)	6025	8233	4570	20
H(5A)	3089	6298	5312	27
H(5B)	4323	7994	5867	27

Table A7.2.6 Torsion angles [°] for V19143.

O(2)-C(1)-C(2)-N(1)	-141.93(7)
O(1)-C(1)-C(2)-N(1)	45.42(8)
O(2)-C(1)-C(2)-C(21)	99.90(8)
O(1)-C(1)-C(2)-C(21)	-72.76(7)
O(2)-C(1)-C(2)-C(3)	-20.06(10)
O(1)-C(1)-C(2)-C(3)	167.28(6)
C(21)-C(2)-N(1)-C(6)	150.72(7)
C(1)-C(2)-N(1)-C(6)	39.11(9)
C(3)-C(2)-N(1)-C(6)	-82.99(8)
C(21)-C(2)-N(1)-C(13)	-40.15(9)
C(1)-C(2)-N(1)-C(13)	-151.76(7)
C(3)-C(2)-N(1)-C(13)	86.14(8)
C(13)-N(1)-C(6)-O(3)	179.89(7)
C(2)-N(1)-C(6)-O(3)	-9.42(12)
C(13)-N(1)-C(6)-C(7)	0.68(8)
C(2)-N(1)-C(6)-C(7)	171.37(6)
O(3)-C(6)-C(7)-C(8)	3.61(14)
N(1)-C(6)-C(7)-C(8)	-177.21(8)
O(3)-C(6)-C(7)-C(12)	-176.58(8)
N(1)-C(6)-C(7)-C(12)	2.61(8)
C(12)-C(7)-C(8)-C(9)	2.43(12)
C(6)-C(7)-C(8)-C(9)	-177.78(8)
C(7)-C(8)-C(9)-C(10)	0.21(13)
C(8)-C(9)-C(10)-C(11)	-2.21(14)
C(9)-C(10)-C(11)-C(12)	1.53(13)
C(10)-C(11)-C(12)-C(7)	1.08(12)
C(10)-C(11)-C(12)-C(13)	-176.79(8)
C(8)-C(7)-C(12)-C(11)	-3.16(12)
C(6)-C(7)-C(12)-C(11)	177.01(7)
C(8)-C(7)-C(12)-C(13)	175.13(7)
C(6)-C(7)-C(12)-C(13)	-4.71(8)
C(6)-N(1)-C(13)-O(4)	175.02(8)
C(2)-N(1)-C(13)-O(4)	4.80(12)

C(6)-N(1)-C(13)-C(12)	-3.45(8)
C(2)-N(1)-C(13)-C(12)	-173.67(6)
C(11)-C(12)-C(13)-O(4)	4.72(14)
C(7)-C(12)-C(13)-O(4)	-173.36(8)
C(11)-C(12)-C(13)-N(1)	-176.84(8)
C(7)-C(12)-C(13)-N(1)	5.07(8)
N(1)-C(2)-C(21)-C(22)	-39.46(9)
C(1)-C(2)-C(21)-C(22)	76.44(8)
C(3)-C(2)-C(21)-C(22)	-164.69(6)
N(1)-C(2)-C(21)-C(26)	146.64(7)
C(1)-C(2)-C(21)-C(26)	-97.46(8)
C(3)-C(2)-C(21)-C(26)	21.42(9)
C(26)-C(21)-C(22)-C(23)	-1.64(11)
C(2)-C(21)-C(22)-C(23)	-175.73(7)
C(21)-C(22)-C(23)-C(24)	0.28(12)
C(22)-C(23)-C(24)-C(25)	0.79(13)
C(23)-C(24)-C(25)-C(26)	-0.46(13)
C(22)-C(21)-C(26)-C(25)	1.96(12)
C(2)-C(21)-C(26)-C(25)	175.95(7)
C(24)-C(25)-C(26)-C(21)	-0.93(13)
N(1)-C(2)-C(3)-C(31)	54.99(8)
C(21)-C(2)-C(3)-C(31)	-179.10(6)
C(1)-C(2)-C(3)-C(31)	-65.76(8)
N(1)-C(2)-C(3)-C(4)	-71.86(7)
C(21)-C(2)-C(3)-C(4)	54.05(8)
C(1)-C(2)-C(3)-C(4)	167.39(6)
C(4)-C(3)-C(31)-C(32)	-130.31(8)
C(2)-C(3)-C(31)-C(32)	103.00(8)
C(4)-C(3)-C(31)-C(36)	45.45(9)
C(2)-C(3)-C(31)-C(36)	-81.24(9)
C(36)-C(31)-C(32)-C(33)	-1.27(12)
C(3)-C(31)-C(32)-C(33)	174.58(7)
C(31)-C(32)-C(33)-C(34)	0.99(13)
C(32)-C(33)-C(34)-C(35)	0.63(14)
C(33)-C(34)-C(35)-C(36)	-1.94(14)

C(34)-C(35)-C(36)-C(31)	1.67(13)
C(32)-C(31)-C(36)-C(35)	-0.05(12)
C(3)-C(31)-C(36)-C(35)	-175.90(7)
C(31)-C(3)-C(4)-C(5)	35.57(11)
C(2)-C(3)-C(4)-C(5)	164.33(8)

Symmetry transformations used to generate equivalent atoms:

D-H...A	d(D-H)	d(H...A)	d(D...A)	<(DHA)
O(1)-H(1O)...O(3)#1	0.850(12)	1.915(12)	2.7303(10)	160.5(13)

Symmetry transformations used to generate equivalent atoms:
#1 -x+1,-y+1,-z

A7.3 X-RAY CRYSTRAL STRUCTURE ANALYSIS OF IRELAND–CLAISEN REARRANGEMENT PRODUCT 111 (V20078)

An X-ray quality crystal of Ireland–Claisen Rearrangement Product **111** (compound V20078) was grown by slow cooling of a solution in *i*-PrOH (approx. 20 mg/300 μL). Low-temperature diffraction data (ϕ-and ω-scans) were collected on a Bruker AXS D8 VENTURE KAPPA diffractometer coupled to a PHOTON II CPAD detector with Cu K_α radiation (λ = 1.54178 Å) from an IμS micro-source for the structure of compound V20078. The structure was solved by direct methods using SHELXS[1] and refined against F^2 on all data by full-matrix least squares with SHELXL-2018[2] using established refinement techniques.[3] All non-hydrogen atoms were refined anisotropically. All hydrogen atoms were included into the model at geometrically calculated positions and refined using a riding model. The isotropic displacement parameters of all hydrogen atoms were fixed to 1.2 times the *U* value of the atoms they are linked to (1.5 times for methyl groups). All disordered atoms were refined with the help of similarity restraints on the 1,2- and 1,3-distances and displacement parameters as well as rigid bond restraints for anisotropic displacement parameters. Compound V20078 crystallizes in the triclinic space group *P*1 with two molecules in the asymmetric unit.

Figure A7.3.1 *X-Ray Coordinate of Ireland–Claisen Rearrangement Product* ***111*** *(V20078)*

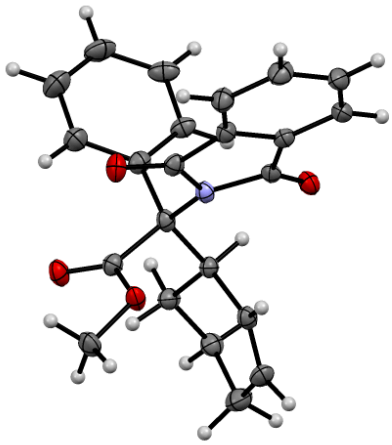

Table A7.3.1 *Crystal Data and Structure Refinement for* ***111*** *(V20078)*

Identification code	V20078	
Empirical formula	C23 H21 N O4	
Formula weight	375.41	
Temperature	100(2) K	
Wavelength	1.54178 Å	
Crystal system	Triclinic	
Space group	P1	
Unit cell dimensions	a = 8.7657(4) Å	a= 79.3918(12)°.
	b = 9.6615(5) Å	b= 89.6083(13)°.
	c = 11.4746(6) Å	g = 82.2116(12)°.
Volume	946.20(8) $Å^3$	
Z	2	
Density (calculated)	1.318 Mg/m^3	
Absorption coefficient	0.734 mm^{-1}	
F(000)	396	
Crystal size	0.200 x 0.150 x 0.100 mm^3	
Theta range for data collection	3.920 to 74.662°.	
Index ranges	-10<=h<=10, -10<=k<=12, -14<=l<=14	
Reflections collected	43609	

Independent reflections	7033 [R(int) = 0.0302]
Completeness to theta = 67.679°	99.0 %
Absorption correction	Semi-empirical from equivalents
Max. and min. transmission	0.7538 and 0.6661
Refinement method	Full-matrix least-squares on F^2
Data / restraints / parameters	7033 / 3 / 507
Goodness-of-fit on F^2	1.048
Final R indices [I>2sigma(I)]	R1 = 0.0387, wR2 = 0.1032
R indices (all data)	R1 = 0.0391, wR2 = 0.1041
Absolute structure parameter	-0.22(12)
Extinction coefficient	n/a
Largest diff. peak and hole	0.241 and -0.220 e.$Å^{-3}$

Table A7.3.2 Atomic Coordinates (x 10^4) and Equivalent Isotropic Displacement Parameters ($Å^2$x 10^3) for **111** (V20078). U(eq) is Defined as One Third of the Trace of the Orthogonalized U^{ij} tensor.

	x	y	z	U(eq)
C(1)	6288(3)	4066(3)	7505(2)	15(1)
N(1)	7046(2)	3211(2)	8607(2)	16(1)
C(11)	6637(3)	1885(3)	9145(2)	17(1)
O(1)	5602(2)	1330(2)	8815(2)	22(1)
C(12)	7725(3)	1332(3)	10165(2)	19(1)
C(13)	7807(4)	85(3)	10991(3)	26(1)
C(14)	8981(4)	-143(3)	11854(3)	31(1)
C(15)	9998(4)	828(3)	11880(3)	30(1)
C(16)	9900(3)	2087(3)	11050(3)	24(1)
C(17)	8741(3)	2309(3)	10190(2)	19(1)
C(18)	8348(3)	3509(3)	9178(2)	17(1)
O(2)	8995(2)	4543(2)	8885(2)	20(1)
C(21)	4566(3)	3871(3)	7493(2)	17(1)
O(3)	3880(2)	3729(2)	6632(2)	24(1)
O(4)	3906(2)	4037(2)	8520(2)	19(1)
C(22)	2246(3)	4092(3)	8512(3)	22(1)
C(31)	6200(3)	5679(3)	7504(2)	16(1)
C(32)	5942(3)	6199(3)	8557(3)	19(1)
C(33)	5778(3)	7649(3)	8550(3)	23(1)
C(34)	5824(3)	8606(3)	7485(3)	26(1)
C(35)	6048(4)	8095(3)	6443(3)	25(1)
C(36)	6243(3)	6644(3)	6444(3)	20(1)
C(41)	7091(3)	3625(3)	6391(2)	16(1)
C(42)	8729(3)	3958(3)	6304(2)	18(1)
C(43)	9846(3)	3209(3)	5799(3)	22(1)
C(44)	9616(3)	1979(3)	5221(3)	25(1)
C(45)	7929(3)	1766(3)	5176(3)	24(1)
C(46)	7076(3)	2066(3)	6297(2)	19(1)
C(101)	3411(3)	5804(3)	2643(2)	19(1)

N(101)	2805(3)	6625(2)	1479(2)	18(1)
C(111)	3232(3)	7972(3)	1031(2)	20(1)
O(101)	4204(3)	8496(2)	1477(2)	27(1)
C(112)	2251(3)	8578(3)	-41(3)	21(1)
C(113)	2232(4)	9844(3)	-827(3)	26(1)
C(114)	1131(4)	10127(3)	-1740(3)	29(1)
C(115)	118(4)	9166(3)	-1858(3)	28(1)
C(116)	152(3)	7890(3)	-1066(3)	23(1)
C(117)	1233(3)	7624(3)	-154(3)	20(1)
C(118)	1513(3)	6402(3)	845(2)	18(1)
O(102)	777(2)	5420(2)	1086(2)	24(1)
C(121)	5160(3)	5846(3)	2700(2)	20(1)
O(103)	5883(2)	5842(2)	3591(2)	26(1)
O(104)	5815(2)	5729(2)	1656(2)	23(1)
C(122)	7473(3)	5659(4)	1663(3)	28(1)
C(131)	2488(3)	6488(3)	3593(3)	22(1)
C(132)	3062(4)	7422(4)	4217(3)	31(1)
C(133)	2126(5)	8068(4)	5001(4)	43(1)
C(134)	623(4)	7830(4)	5161(3)	35(1)
C(135)	22(4)	6929(3)	4534(3)	29(1)
C(136)	957(3)	6266(3)	3755(3)	23(1)
C(141)	3225(3)	4186(3)	2761(2)	19(1)
C(142)	3830(3)	3512(3)	1735(3)	22(1)
C(143)	4396(4)	2147(3)	1864(3)	27(1)
C(144)	4603(4)	1142(3)	3034(3)	32(1)
C(145)	3726(4)	1755(3)	4008(3)	25(1)
C(146)	3895(4)	3318(3)	3935(3)	24(1)

Table A7.3.3 *Bond Lengths [Å] and Angles [°] for* ***111*** *(V20078)*

C(1)-N(1)	1.484(3)
C(1)-C(21)	1.547(4)
C(1)-C(31)	1.550(4)
C(1)-C(41)	1.555(4)
N(1)-C(11)	1.408(3)
N(1)-C(18)	1.409(3)
C(11)-O(1)	1.210(3)
C(11)-C(12)	1.487(4)
C(12)-C(13)	1.383(4)
C(12)-C(17)	1.387(4)
C(13)-C(14)	1.400(5)
C(13)-H(13)	0.9500
C(14)-C(15)	1.383(5)
C(14)-H(14)	0.9500
C(15)-C(16)	1.393(4)
C(15)-H(15)	0.9500
C(16)-C(17)	1.389(4)
C(16)-H(16)	0.9500
C(17)-C(18)	1.487(4)
C(18)-O(2)	1.208(3)
C(21)-O(3)	1.199(3)
C(21)-O(4)	1.335(3)
O(4)-C(22)	1.449(3)
C(22)-H(22A)	0.9800
C(22)-H(22B)	0.9800
C(22)-H(22C)	0.9800
C(31)-C(36)	1.393(4)
C(31)-C(32)	1.397(4)
C(32)-C(33)	1.387(4)
C(32)-H(32)	0.9500
C(33)-C(34)	1.394(4)
C(33)-H(33)	0.9500
C(34)-C(35)	1.378(5)

C(34)-H(34)	0.9500
C(35)-C(36)	1.389(4)
C(35)-H(35)	0.9500
C(36)-H(36)	0.9500
C(41)-C(42)	1.512(4)
C(41)-C(46)	1.532(4)
C(41)-H(41)	1.0000
C(42)-C(43)	1.331(4)
C(42)-H(42)	0.9500
C(43)-C(44)	1.500(4)
C(43)-H(43)	0.9500
C(44)-C(45)	1.523(4)
C(44)-H(44A)	0.9900
C(44)-H(44B)	0.9900
C(45)-C(46)	1.537(4)
C(45)-H(45A)	0.9900
C(45)-H(45B)	0.9900
C(46)-H(46A)	0.9900
C(46)-H(46B)	0.9900
C(101)-N(101)	1.483(4)
C(101)-C(121)	1.541(4)
C(101)-C(131)	1.545(4)
C(101)-C(141)	1.575(4)
N(101)-C(111)	1.408(4)
N(101)-C(118)	1.412(4)
C(111)-O(101)	1.209(4)
C(111)-C(112)	1.486(4)
C(112)-C(113)	1.378(4)
C(112)-C(117)	1.390(4)
C(113)-C(114)	1.394(4)
C(113)-H(113)	0.9500
C(114)-C(115)	1.393(5)
C(114)-H(114)	0.9500
C(115)-C(116)	1.387(5)
C(115)-H(115)	0.9500

C(116)-C(117)	1.381(4)
C(116)-H(116)	0.9500
C(117)-C(118)	1.481(4)
C(118)-O(102)	1.209(3)
C(121)-O(103)	1.206(4)
C(121)-O(104)	1.342(4)
O(104)-C(122)	1.446(4)
C(122)-H(12A)	0.9800
C(122)-H(12B)	0.9800
C(122)-H(12C)	0.9800
C(131)-C(136)	1.394(4)
C(131)-C(132)	1.396(4)
C(132)-C(133)	1.389(5)
C(132)-H(132)	0.9500
C(133)-C(134)	1.373(6)
C(133)-H(133)	0.9500
C(134)-C(135)	1.383(5)
C(134)-H(134)	0.9500
C(135)-C(136)	1.392(4)
C(135)-H(135)	0.9500
C(136)-H(136)	0.9500
C(141)-C(142)	1.507(4)
C(141)-C(146)	1.524(4)
C(141)-H(141)	1.0000
C(142)-C(143)	1.327(4)
C(142)-H(142)	0.9500
C(143)-C(144)	1.502(5)
C(143)-H(143)	0.9500
C(144)-C(145)	1.516(4)
C(144)-H(14A)	0.9900
C(144)-H(14B)	0.9900
C(145)-C(146)	1.524(4)
C(145)-H(14C)	0.9900
C(145)-H(14D)	0.9900
C(146)-H(14E)	0.9900

C(146)-H(14F)	0.9900
N(1)-C(1)-C(21)	109.5(2)
N(1)-C(1)-C(31)	111.1(2)
C(21)-C(1)-C(31)	101.9(2)
N(1)-C(1)-C(41)	110.8(2)
C(21)-C(1)-C(41)	110.4(2)
C(31)-C(1)-C(41)	112.7(2)
C(11)-N(1)-C(18)	110.8(2)
C(11)-N(1)-C(1)	122.8(2)
C(18)-N(1)-C(1)	126.0(2)
O(1)-C(11)-N(1)	125.4(3)
O(1)-C(11)-C(12)	128.2(3)
N(1)-C(11)-C(12)	106.4(2)
C(13)-C(12)-C(17)	122.0(3)
C(13)-C(12)-C(11)	129.7(3)
C(17)-C(12)-C(11)	108.2(2)
C(12)-C(13)-C(14)	116.3(3)
C(12)-C(13)-H(13)	121.9
C(14)-C(13)-H(13)	121.9
C(15)-C(14)-C(13)	121.8(3)
C(15)-C(14)-H(14)	119.1
C(13)-C(14)-H(14)	119.1
C(14)-C(15)-C(16)	121.6(3)
C(14)-C(15)-H(15)	119.2
C(16)-C(15)-H(15)	119.2
C(17)-C(16)-C(15)	116.6(3)
C(17)-C(16)-H(16)	121.7
C(15)-C(16)-H(16)	121.7
C(12)-C(17)-C(16)	121.7(3)
C(12)-C(17)-C(18)	108.3(2)
C(16)-C(17)-C(18)	130.0(3)
O(2)-C(18)-N(1)	125.7(3)
O(2)-C(18)-C(17)	128.0(3)
N(1)-C(18)-C(17)	106.3(2)
O(3)-C(21)-O(4)	124.2(2)

O(3)-C(21)-C(1)	123.9(2)
O(4)-C(21)-C(1)	111.5(2)
C(21)-O(4)-C(22)	114.6(2)
O(4)-C(22)-H(22A)	109.5
O(4)-C(22)-H(22B)	109.5
H(22A)-C(22)-H(22B)	109.5
O(4)-C(22)-H(22C)	109.5
H(22A)-C(22)-H(22C)	109.5
H(22B)-C(22)-H(22C)	109.5
C(36)-C(31)-C(32)	118.8(3)
C(36)-C(31)-C(1)	120.6(2)
C(32)-C(31)-C(1)	120.3(2)
C(33)-C(32)-C(31)	120.5(3)
C(33)-C(32)-H(32)	119.7
C(31)-C(32)-H(32)	119.7
C(32)-C(33)-C(34)	120.3(3)
C(32)-C(33)-H(33)	119.9
C(34)-C(33)-H(33)	119.9
C(35)-C(34)-C(33)	119.3(3)
C(35)-C(34)-H(34)	120.4
C(33)-C(34)-H(34)	120.4
C(34)-C(35)-C(36)	120.9(3)
C(34)-C(35)-H(35)	119.6
C(36)-C(35)-H(35)	119.6
C(35)-C(36)-C(31)	120.3(3)
C(35)-C(36)-H(36)	119.9
C(31)-C(36)-H(36)	119.9
C(42)-C(41)-C(46)	109.3(2)
C(42)-C(41)-C(1)	111.7(2)
C(46)-C(41)-C(1)	114.6(2)
C(42)-C(41)-H(41)	107.0
C(46)-C(41)-H(41)	107.0
C(1)-C(41)-H(41)	107.0
C(43)-C(42)-C(41)	123.3(3)
C(43)-C(42)-H(42)	118.3

C(41)-C(42)-H(42)	118.3
C(42)-C(43)-C(44)	124.1(3)
C(42)-C(43)-H(43)	117.9
C(44)-C(43)-H(43)	117.9
C(43)-C(44)-C(45)	112.2(2)
C(43)-C(44)-H(44A)	109.2
C(45)-C(44)-H(44A)	109.2
C(43)-C(44)-H(44B)	109.2
C(45)-C(44)-H(44B)	109.2
H(44A)-C(44)-H(44B)	107.9
C(44)-C(45)-C(46)	112.0(2)
C(44)-C(45)-H(45A)	109.2
C(46)-C(45)-H(45A)	109.2
C(44)-C(45)-H(45B)	109.2
C(46)-C(45)-H(45B)	109.2
H(45A)-C(45)-H(45B)	107.9
C(41)-C(46)-C(45)	109.2(2)
C(41)-C(46)-H(46A)	109.8
C(45)-C(46)-H(46A)	109.8
C(41)-C(46)-H(46B)	109.8
C(45)-C(46)-H(46B)	109.8
H(46A)-C(46)-H(46B)	108.3
N(101)-C(101)-C(121)	108.4(2)
N(101)-C(101)-C(131)	106.1(2)
C(121)-C(101)-C(131)	114.3(2)
N(101)-C(101)-C(141)	110.9(2)
C(121)-C(101)-C(141)	105.5(2)
C(131)-C(101)-C(141)	111.6(2)
C(111)-N(101)-C(118)	110.4(2)
C(111)-N(101)-C(101)	120.8(2)
C(118)-N(101)-C(101)	126.9(2)
O(101)-C(111)-N(101)	124.5(3)
O(101)-C(111)-C(112)	128.9(3)
N(101)-C(111)-C(112)	106.7(2)
C(113)-C(112)-C(117)	121.9(3)

C(113)-C(112)-C(111)	130.4(3)
C(117)-C(112)-C(111)	107.7(3)
C(112)-C(113)-C(114)	116.6(3)
C(112)-C(113)-H(113)	121.7
C(114)-C(113)-H(113)	121.7
C(115)-C(114)-C(113)	121.5(3)
C(115)-C(114)-H(114)	119.3
C(113)-C(114)-H(114)	119.3
C(116)-C(115)-C(114)	121.5(3)
C(116)-C(115)-H(115)	119.2
C(114)-C(115)-H(115)	119.2
C(117)-C(116)-C(115)	116.8(3)
C(117)-C(116)-H(116)	121.6
C(115)-C(116)-H(116)	121.6
C(116)-C(117)-C(112)	121.8(3)
C(116)-C(117)-C(118)	129.6(3)
C(112)-C(117)-C(118)	108.7(2)
O(102)-C(118)-N(101)	126.5(3)
O(102)-C(118)-C(117)	127.3(3)
N(101)-C(118)-C(117)	106.1(2)
O(103)-C(121)-O(104)	123.4(3)
O(103)-C(121)-C(101)	124.8(3)
O(104)-C(121)-C(101)	111.4(2)
C(121)-O(104)-C(122)	114.6(2)
O(104)-C(122)-H(12A)	109.5
O(104)-C(122)-H(12B)	109.5
H(12A)-C(122)-H(12B)	109.5
O(104)-C(122)-H(12C)	109.5
H(12A)-C(122)-H(12C)	109.5
H(12B)-C(122)-H(12C)	109.5
C(136)-C(131)-C(132)	118.1(3)
C(136)-C(131)-C(101)	118.3(3)
C(132)-C(131)-C(101)	123.3(3)
C(133)-C(132)-C(131)	120.0(3)
C(133)-C(132)-H(132)	120.0

C(131)-C(132)-H(132)	120.0
C(134)-C(133)-C(132)	121.3(3)
C(134)-C(133)-H(133)	119.4
C(132)-C(133)-H(133)	119.4
C(133)-C(134)-C(135)	119.7(3)
C(133)-C(134)-H(134)	120.2
C(135)-C(134)-H(134)	120.2
C(134)-C(135)-C(136)	119.4(3)
C(134)-C(135)-H(135)	120.3
C(136)-C(135)-H(135)	120.3
C(135)-C(136)-C(131)	121.5(3)
C(135)-C(136)-H(136)	119.2
C(131)-C(136)-H(136)	119.2
C(142)-C(141)-C(146)	110.9(2)
C(142)-C(141)-C(101)	114.9(2)
C(146)-C(141)-C(101)	111.6(2)
C(142)-C(141)-H(141)	106.3
C(146)-C(141)-H(141)	106.3
C(101)-C(141)-H(141)	106.3
C(143)-C(142)-C(141)	122.5(3)
C(143)-C(142)-H(142)	118.8
C(141)-C(142)-H(142)	118.8
C(142)-C(143)-C(144)	124.4(3)
C(142)-C(143)-H(143)	117.8
C(144)-C(143)-H(143)	117.8
C(143)-C(144)-C(145)	111.7(3)
C(143)-C(144)-H(14A)	109.3
C(145)-C(144)-H(14A)	109.3
C(143)-C(144)-H(14B)	109.3
C(145)-C(144)-H(14B)	109.3
H(14A)-C(144)-H(14B)	107.9
C(144)-C(145)-C(146)	111.4(3)
C(144)-C(145)-H(14C)	109.3
C(146)-C(145)-H(14C)	109.3
C(144)-C(145)-H(14D)	109.3

C(146)-C(145)-H(14D)	109.3
H(14C)-C(145)-H(14D)	108.0
C(145)-C(146)-C(141)	110.2(2)
C(145)-C(146)-H(14E)	109.6
C(141)-C(146)-H(14E)	109.6
C(145)-C(146)-H(14F)	109.6
C(141)-C(146)-H(14F)	109.6
H(14E)-C(146)-H(14F)	108.1

Symmetry transformations used to generate equivalent atoms:

Table A7.3.4 *Anisotropic Displacement Parameters ($Å^2$x 10^3) for* ***111*** *(V20078). The Anisotropic Displacement Factor Exponent Takes the Form: $-2p^2[h^2 a^{*2}U^{11} + ... + 2 h k a^* b^* U^{12}]$.*

	U^{11}	U^{22}	U^{33}	U^{23}	U^{13}	U^{12}
C(1)	16(1)	15(1)	13(1)	-2(1)	0(1)	-2(1)
N(1)	13(1)	18(1)	16(1)	-1(1)	0(1)	-3(1)
C(11)	19(1)	18(1)	15(1)	-2(1)	4(1)	-3(1)
O(1)	24(1)	22(1)	21(1)	-4(1)	-2(1)	-7(1)
C(12)	21(1)	21(1)	15(1)	-4(1)	2(1)	0(1)
C(13)	32(2)	20(1)	22(2)	-1(1)	0(1)	-2(1)
C(14)	41(2)	25(2)	20(2)	3(1)	-5(1)	7(1)
C(15)	30(2)	31(2)	25(2)	-5(1)	-11(1)	8(1)
C(16)	22(1)	28(2)	23(2)	-7(1)	-4(1)	2(1)
C(17)	17(1)	22(1)	18(1)	-6(1)	0(1)	2(1)
C(18)	14(1)	23(1)	15(1)	-6(1)	1(1)	1(1)
O(2)	16(1)	24(1)	22(1)	-4(1)	0(1)	-6(1)
C(21)	17(1)	17(1)	16(1)	-3(1)	0(1)	-2(1)
O(3)	19(1)	36(1)	19(1)	-9(1)	-1(1)	-5(1)
O(4)	13(1)	29(1)	18(1)	-8(1)	1(1)	-3(1)
C(22)	13(1)	31(2)	23(2)	-8(1)	2(1)	-4(1)
C(31)	12(1)	18(1)	19(1)	-4(1)	0(1)	-2(1)
C(32)	15(1)	22(1)	21(1)	-6(1)	1(1)	-2(1)
C(33)	21(1)	25(1)	27(2)	-12(1)	1(1)	-2(1)
C(34)	26(2)	18(1)	36(2)	-8(1)	0(1)	-3(1)
C(35)	28(2)	19(1)	27(2)	1(1)	-1(1)	-4(1)
C(36)	20(1)	22(1)	19(1)	-5(1)	1(1)	-2(1)
C(41)	18(1)	18(1)	13(1)	-3(1)	2(1)	-1(1)
C(42)	20(1)	18(1)	16(1)	-2(1)	1(1)	-2(1)
C(43)	18(1)	26(1)	21(1)	-1(1)	3(1)	-3(1)
C(44)	21(2)	29(2)	24(2)	-7(1)	5(1)	5(1)
C(45)	22(2)	27(2)	24(2)	-11(1)	2(1)	0(1)
C(46)	20(1)	18(1)	21(1)	-5(1)	2(1)	-2(1)
C(101)	19(1)	25(1)	15(1)	-4(1)	-1(1)	-3(1)

N(101)	17(1)	23(1)	16(1)	-4(1)	0(1)	-4(1)
C(111)	21(1)	22(1)	18(1)	-7(1)	3(1)	-5(1)
O(101)	30(1)	29(1)	23(1)	-6(1)	-4(1)	-11(1)
C(112)	21(1)	24(2)	19(1)	-8(1)	-1(1)	-2(1)
C(113)	30(2)	24(2)	24(2)	-5(1)	-3(1)	-4(1)
C(114)	38(2)	22(2)	24(2)	-3(1)	-4(1)	0(1)
C(115)	30(2)	28(2)	25(2)	-9(1)	-9(1)	5(1)
C(116)	19(1)	25(2)	27(2)	-10(1)	-3(1)	1(1)
C(117)	20(1)	21(1)	20(1)	-8(1)	1(1)	0(1)
C(118)	13(1)	23(1)	19(1)	-8(1)	2(1)	-2(1)
O(102)	18(1)	26(1)	27(1)	-4(1)	-2(1)	-5(1)
C(121)	23(1)	22(1)	17(1)	-4(1)	1(1)	-4(1)
O(103)	24(1)	35(1)	18(1)	-5(1)	-4(1)	-5(1)
O(104)	17(1)	36(1)	19(1)	-10(1)	1(1)	-6(1)
C(122)	16(1)	39(2)	31(2)	-10(1)	1(1)	-5(1)
C(131)	26(2)	22(1)	17(1)	-3(1)	1(1)	-2(1)
C(132)	28(2)	36(2)	31(2)	-15(1)	-1(1)	-1(1)
C(133)	44(2)	44(2)	46(2)	-28(2)	1(2)	-2(2)
C(134)	41(2)	34(2)	30(2)	-14(1)	9(1)	6(1)
C(135)	29(2)	24(2)	30(2)	-2(1)	10(1)	2(1)
C(136)	26(2)	21(1)	22(1)	-5(1)	6(1)	-2(1)
C(141)	20(1)	20(1)	16(1)	-5(1)	-2(1)	-2(1)
C(142)	19(1)	28(2)	18(1)	-6(1)	0(1)	-3(1)
C(143)	26(2)	31(2)	26(2)	-14(1)	3(1)	-1(1)
C(144)	37(2)	25(2)	35(2)	-10(1)	0(1)	1(1)
C(145)	28(2)	25(2)	20(2)	-2(1)	-3(1)	0(1)
C(146)	27(2)	25(2)	18(1)	-6(1)	-3(1)	4(1)

Table A7.3.5 *Hydrogen Coordinates (x 10^4) and Isotropic Displacement Parameters ($Å^2$x 10^3) for* ***111*** *(V20078).*

	x	y	z	U(eq)
H(13)	7106	-580	10974	31
H(14)	9082	-988	12438	37
H(15)	10783	632	12477	36
H(16)	10590	2761	11072	29
H(22A)	1972	3208	8321	33
H(22B)	1788	4899	7915	33
H(22C)	1854	4206	9296	33
H(32)	5878	5555	9283	23
H(33)	5635	7991	9273	28
H(34)	5702	9600	7477	31
H(35)	6068	8744	5714	30
H(36)	6408	6308	5720	24
H(41)	6513	4214	5682	19
H(42)	8973	4741	6625	22
H(43)	10852	3471	5804	26
H(44A)	10218	1103	5667	30
H(44B)	10011	2144	4404	30
H(45A)	7863	775	5088	29
H(45B)	7420	2407	4473	29
H(46A)	6000	1869	6256	23
H(46B)	7586	1438	7007	23
H(113)	2934	10492	-749	31
H(114)	1070	10995	-2295	35
H(115)	-612	9388	-2496	34
H(116)	-535	7232	-1146	28
H(12A)	7927	4817	2227	42
H(12B)	7760	6515	1900	42
H(12C)	7856	5597	867	42
H(132)	4092	7617	4106	37

H(133)	2533	8686	5435	51
H(134)	-1	8281	5700	42
H(135)	-1019	6765	4633	34
H(136)	541	5649	3325	28
H(141)	2093	4137	2781	23
H(142)	3804	4087	967	26
H(143)	4690	1781	1169	32
H(14A)	5712	934	3253	39
H(14B)	4238	236	2958	39
H(14C)	4117	1212	4790	30
H(14D)	2622	1657	3939	30
H(14E)	4997	3421	4002	28
H(14F)	3350	3677	4601	28

Table A7.3.6 *Torsion Angles [°] for* ***111*** *(V20078).*

C(21)-C(1)-N(1)-C(11)	34.9(3)
C(31)-C(1)-N(1)-C(11)	146.7(2)
C(41)-C(1)-N(1)-C(11)	-87.2(3)
C(21)-C(1)-N(1)-C(18)	-152.7(2)
C(31)-C(1)-N(1)-C(18)	-40.9(3)
C(41)-C(1)-N(1)-C(18)	85.3(3)
C(18)-N(1)-C(11)-O(1)	-177.1(3)
C(1)-N(1)-C(11)-O(1)	-3.6(4)
C(18)-N(1)-C(11)-C(12)	2.5(3)
C(1)-N(1)-C(11)-C(12)	176.0(2)
O(1)-C(11)-C(12)-C(13)	-1.5(5)
N(1)-C(11)-C(12)-C(13)	178.9(3)
O(1)-C(11)-C(12)-C(17)	178.5(3)
N(1)-C(11)-C(12)-C(17)	-1.1(3)
C(17)-C(12)-C(13)-C(14)	-0.3(4)
C(11)-C(12)-C(13)-C(14)	179.7(3)
C(12)-C(13)-C(14)-C(15)	0.2(5)
C(13)-C(14)-C(15)-C(16)	0.3(5)
C(14)-C(15)-C(16)-C(17)	-0.7(5)
C(13)-C(12)-C(17)-C(16)	-0.1(4)
C(11)-C(12)-C(17)-C(16)	179.9(3)
C(13)-C(12)-C(17)-C(18)	179.3(3)
C(11)-C(12)-C(17)-C(18)	-0.7(3)
C(15)-C(16)-C(17)-C(12)	0.6(4)
C(15)-C(16)-C(17)-C(18)	-178.7(3)
C(11)-N(1)-C(18)-O(2)	177.0(3)
C(1)-N(1)-C(18)-O(2)	3.8(4)
C(11)-N(1)-C(18)-C(17)	-2.9(3)
C(1)-N(1)-C(18)-C(17)	-176.1(2)
C(12)-C(17)-C(18)-O(2)	-177.8(3)
C(16)-C(17)-C(18)-O(2)	1.6(5)
C(12)-C(17)-C(18)-N(1)	2.2(3)
C(16)-C(17)-C(18)-N(1)	-178.5(3)

N(1)-C(1)-C(21)-O(3)	-138.4(3)
C(31)-C(1)-C(21)-O(3)	103.8(3)
C(41)-C(1)-C(21)-O(3)	-16.2(4)
N(1)-C(1)-C(21)-O(4)	48.3(3)
C(31)-C(1)-C(21)-O(4)	-69.4(3)
C(41)-C(1)-C(21)-O(4)	170.6(2)
O(3)-C(21)-O(4)-C(22)	-2.4(4)
C(1)-C(21)-O(4)-C(22)	170.8(2)
N(1)-C(1)-C(31)-C(36)	149.3(2)
C(21)-C(1)-C(31)-C(36)	-94.1(3)
C(41)-C(1)-C(31)-C(36)	24.3(3)
N(1)-C(1)-C(31)-C(32)	-36.2(3)
C(21)-C(1)-C(31)-C(32)	80.4(3)
C(41)-C(1)-C(31)-C(32)	-161.3(2)
C(36)-C(31)-C(32)-C(33)	-1.9(4)
C(1)-C(31)-C(32)-C(33)	-176.5(2)
C(31)-C(32)-C(33)-C(34)	1.9(4)
C(32)-C(33)-C(34)-C(35)	-0.6(4)
C(33)-C(34)-C(35)-C(36)	-0.7(5)
C(34)-C(35)-C(36)-C(31)	0.7(5)
C(32)-C(31)-C(36)-C(35)	0.6(4)
C(1)-C(31)-C(36)-C(35)	175.2(3)
N(1)-C(1)-C(41)-C(42)	-64.9(3)
C(21)-C(1)-C(41)-C(42)	173.6(2)
C(31)-C(1)-C(41)-C(42)	60.3(3)
N(1)-C(1)-C(41)-C(46)	60.0(3)
C(21)-C(1)-C(41)-C(46)	-61.5(3)
C(31)-C(1)-C(41)-C(46)	-174.7(2)
C(46)-C(41)-C(42)-C(43)	22.5(4)
C(1)-C(41)-C(42)-C(43)	150.3(3)
C(41)-C(42)-C(43)-C(44)	2.0(4)
C(42)-C(43)-C(44)-C(45)	5.3(4)
C(43)-C(44)-C(45)-C(46)	-37.2(4)
C(42)-C(41)-C(46)-C(45)	-52.7(3)
C(1)-C(41)-C(46)-C(45)	-178.9(2)

C(44)-C(45)-C(46)-C(41)	62.4(3)
C(121)-C(101)-N(101)-C(111)	-46.2(3)
C(131)-C(101)-N(101)-C(111)	77.1(3)
C(141)-C(101)-N(101)-C(111)	-161.5(2)
C(121)-C(101)-N(101)-C(118)	151.2(3)
C(131)-C(101)-N(101)-C(118)	-85.6(3)
C(141)-C(101)-N(101)-C(118)	35.8(4)
C(118)-N(101)-C(111)-O(101)	172.7(3)
C(101)-N(101)-C(111)-O(101)	7.4(4)
C(118)-N(101)-C(111)-C(112)	-6.4(3)
C(101)-N(101)-C(111)-C(112)	-171.7(2)
O(101)-C(111)-C(112)-C(113)	3.1(5)
N(101)-C(111)-C(112)-C(113)	-177.9(3)
O(101)-C(111)-C(112)-C(117)	-175.7(3)
N(101)-C(111)-C(112)-C(117)	3.3(3)
C(117)-C(112)-C(113)-C(114)	0.4(4)
C(111)-C(112)-C(113)-C(114)	-178.4(3)
C(112)-C(113)-C(114)-C(115)	-0.9(5)
C(113)-C(114)-C(115)-C(116)	0.6(5)
C(114)-C(115)-C(116)-C(117)	0.2(5)
C(115)-C(116)-C(117)-C(112)	-0.7(4)
C(115)-C(116)-C(117)-C(118)	177.4(3)
C(113)-C(112)-C(117)-C(116)	0.4(4)
C(111)-C(112)-C(117)-C(116)	179.4(3)
C(113)-C(112)-C(117)-C(118)	-178.1(3)
C(111)-C(112)-C(117)-C(118)	0.9(3)
C(111)-N(101)-C(118)-O(102)	-172.1(3)
C(101)-N(101)-C(118)-O(102)	-7.9(5)
C(111)-N(101)-C(118)-C(117)	6.9(3)
C(101)-N(101)-C(118)-C(117)	171.1(2)
C(116)-C(117)-C(118)-O(102)	-4.1(5)
C(112)-C(117)-C(118)-O(102)	174.2(3)
C(116)-C(117)-C(118)-N(101)	176.9(3)
C(112)-C(117)-C(118)-N(101)	-4.7(3)
N(101)-C(101)-C(121)-O(103)	147.3(3)

C(131)-C(101)-C(121)-O(103)	29.2(4)
C(141)-C(101)-C(121)-O(103)	-93.8(3)
N(101)-C(101)-C(121)-O(104)	-39.5(3)
C(131)-C(101)-C(121)-O(104)	-157.7(2)
C(141)-C(101)-C(121)-O(104)	79.4(3)
O(103)-C(121)-O(104)-C(122)	-2.6(4)
C(101)-C(121)-O(104)-C(122)	-175.8(2)
N(101)-C(101)-C(131)-C(136)	72.4(3)
C(121)-C(101)-C(131)-C(136)	-168.1(3)
C(141)-C(101)-C(131)-C(136)	-48.5(3)
N(101)-C(101)-C(131)-C(132)	-101.4(3)
C(121)-C(101)-C(131)-C(132)	18.1(4)
C(141)-C(101)-C(131)-C(132)	137.7(3)
C(136)-C(131)-C(132)-C(133)	1.9(5)
C(101)-C(131)-C(132)-C(133)	175.7(3)
C(131)-C(132)-C(133)-C(134)	-1.4(6)
C(132)-C(133)-C(134)-C(135)	0.1(6)
C(133)-C(134)-C(135)-C(136)	0.6(5)
C(134)-C(135)-C(136)-C(131)	0.0(5)
C(132)-C(131)-C(136)-C(135)	-1.3(5)
C(101)-C(131)-C(136)-C(135)	-175.4(3)
N(101)-C(101)-C(141)-C(142)	50.6(3)
C(121)-C(101)-C(141)-C(142)	-66.6(3)
C(131)-C(101)-C(141)-C(142)	168.7(2)
N(101)-C(101)-C(141)-C(146)	178.0(2)
C(121)-C(101)-C(141)-C(146)	60.8(3)
C(131)-C(101)-C(141)-C(146)	-63.9(3)
C(146)-C(141)-C(142)-C(143)	21.9(4)
C(101)-C(141)-C(142)-C(143)	149.6(3)
C(141)-C(142)-C(143)-C(144)	-4.3(5)
C(142)-C(143)-C(144)-C(145)	14.7(4)
C(143)-C(144)-C(145)-C(146)	-42.7(4)
C(144)-C(145)-C(146)-C(141)	61.8(3)
C(142)-C(141)-C(146)-C(145)	-49.4(3)
C(101)-C(141)-C(146)-C(145)	-178.8(2)

Symmetry transformations used to generate equivalent atoms:

A7.4 X-RAY CRYSTRAL STRUCTURE ANALYSIS OF IRELAND–CLAISEN REARRANGEMENT PRODUCT 113 (d19152)

An X-ray quality crystal of Iodolactonization product **113** (compound d19152) was grown by slow cooling of a solution in toluene (approx. 50 mg/600 μL). Low temperature (100K) X-ray data were collected with a Bruker AXS KAPPA APEX II diffractometer running at 50 kV and 30 mA (Mo K_α = 0.71073 Å; PHOTON 100 CMOS detector with TRIUMPH graphite monochromator). All diffractometer manipulations, including data collection, integration, and scaling were carried out using the Bruker APEX3 software. An absorption correction was applied using SADABS. The space group was determined, and the structure solved by intrinsic phasing using XT. Refinement was full-matrix least squares on F^2 using XL. All non-hydrogen atoms were refined using anisotropic displacement parameters. Hydrogen atoms were placed in idealized positions and the coordinates refined. The isotropic displacement parameters of all hydrogen atoms were fixed at 1.2 times the U_{eq} value of the bonded atom. Compound D19152 crystallizes in the monoclinic space group $P2_1/n$ (#14) with one molecule in the asymmetric unit.

Figure A7.4.1 *X-Ray Coordinate of Iodolactonization Product* ***113*** *(d19152)*

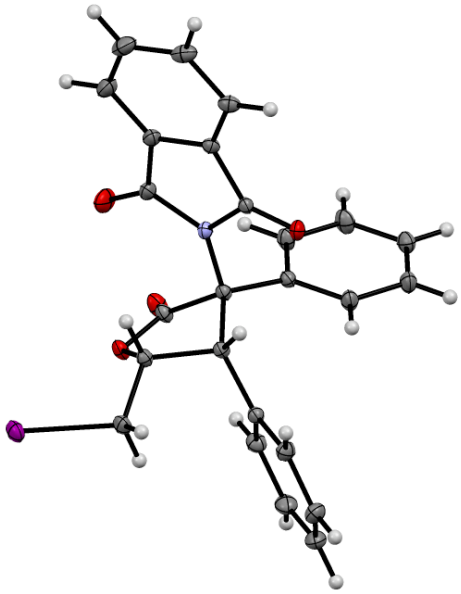

A7.4.1 *Crystal Data and Structure Refinement for d19152*

Identification code	d19152	
Empirical formula	C25 H18 I N O4	
Formula weight	523.30	
Temperature	100 K	
Wavelength	0.71073 Å	
Crystal system	Monoclinic	
Space group	P 1 21/n 1	
Unit cell dimensions	a = 10.564(3) Å	a= 90°
	b = 11.245(3) Å	b= 99.605(14)°
	c = 18.024(4) Å	g = 90°
Volume	2111.0(9) $Å^3$	
Z	4	
Density (calculated)	1.647 g/cm^3	
Absorption coefficient	1.550 mm^{-1}	
F(000)	1040	
Crystal size	0.38 x 0.28 x 0.23 mm^3	
Theta range for data collection	2.095 to 39.457°.	
Index ranges	-18 £ h £ 18, -19 £ k £ 19, -32 £ l £ 31	
Reflections collected	116544	

Independent reflections	12393 [R(int) = 0.0317]
Completeness to theta = 25.242°	100.0 %
Absorption correction	Semi-empirical from equivalents
Max. and min. transmission	1.0000 and 0.9003
Refinement method	Full-matrix least-squares on F^2
Data / restraints / parameters	12393 / 0 / 280
Goodness-of-fit on F^2	1.045
Final R indices [I>2sigma(I)]	R1 = 0.0235, wR2 = 0.0543
R indices (all data)	R1 = 0.0321, wR2 = 0.0572
Extinction coefficient	n/a
Largest diff. peak and hole	0.582 and -1.257 e.$Å^{-3}$

A7.4.2 *Atomic Coordinates (x 10^4) and Equivalent Isotropic Displacement Parameters ($Å^2$x 10^3) for* ***113*** *(d19152). U(eq) is Defined as one Third of the Trace of the Orthogonalized U^{ij} Tensor*

	x	y	z	U(eq)	pop
I(1)	69462(2)	42397(2)	2320(2)	183(1)	1
O(1)	91487(8)	27284(8)	29620(5)	262(2)	1
O(2)	70094(6)	57024(6)	39843(4)	153(1)	1
O(3)	66878(7)	29559(6)	18651(3)	146(1)	1
O(4)	66269(8)	14619(6)	26660(4)	197(1)	1
N(1)	77648(7)	40606(7)	34013(4)	123(1)	1
C(1)	64824(8)	35589(7)	31003(4)	116(1)	1
C(2)	58040(8)	44885(7)	25247(4)	117(1)	1
C(3)	65422(8)	42399(8)	18656(5)	126(1)	1
C(4)	66452(9)	25118(8)	25523(5)	139(1)	1
C(5)	89720(8)	36292(9)	32989(5)	159(1)	1
C(6)	99316(8)	44973(9)	36764(5)	153(1)	1
C(7)	112555(9)	45394(11)	37153(6)	212(2)	1
C(8)	118931(9)	55061(11)	40936(6)	232(2)	1
C(9)	112402(9)	63773(10)	44307(6)	204(2)	1
C(10)	99104(9)	63219(9)	43919(5)	164(1)	1
C(11)	92837(8)	53747(8)	40017(4)	128(1)	1
C(12)	78907(8)	51282(8)	38246(4)	119(1)	1
C(13)	58413(8)	31854(8)	37607(4)	125(1)	1
C(14)	62680(10)	21628(9)	41678(5)	174(2)	1
C(15)	57814(10)	18590(9)	48140(5)	204(2)	1
C(16)	48741(9)	25774(10)	50691(5)	188(2)	1
C(17)	44428(10)	35903(10)	46649(5)	199(2)	1
C(18)	49211(9)	38934(9)	40158(5)	176(2)	1
C(19)	43592(8)	43835(8)	22863(5)	129(1)	1
C(20)	36645(9)	54402(9)	21319(5)	165(1)	1
C(21)	23455(9)	54181(10)	18704(6)	206(2)	1

C(22)	17004(9)	43390(10)	17649(6)	215(2)	1
C(23)	23815(10)	32842(10)	19149(6)	207(2)	1
C(24)	37016(9)	33017(9)	21724(5)	169(1)	1
C(25)	58542(9)	46312(9)	11081(5)	164(1)	1

A7.4.3 *Bond Lengths [Å] and Angles [°] for* ***113*** *(d19152)*

I(1)-C(25)	2.1507(10)
O(1)-C(5)	1.2114(12)
O(2)-C(12)	1.2066(10)
O(3)-C(3)	1.4520(11)
O(3)-C(4)	1.3433(11)
O(4)-C(4)	1.1989(11)
N(1)-C(1)	1.4841(12)
N(1)-C(5)	1.4051(12)
N(1)-C(12)	1.4167(11)
C(1)-C(2)	1.5603(12)
C(1)-C(4)	1.5646(12)
C(1)-C(13)	1.5234(12)
C(2)-H(2)	1.0000
C(2)-C(3)	1.5512(12)
C(2)-C(19)	1.5196(13)
C(3)-H(3)	1.0000
C(3)-C(25)	1.5015(12)
C(5)-C(6)	1.4878(14)
C(6)-C(7)	1.3894(14)
C(6)-C(11)	1.3854(13)
C(7)-H(7)	0.9500
C(7)-C(8)	1.3953(17)
C(8)-H(8)	0.9500
C(8)-C(9)	1.3944(17)
C(9)-H(9)	0.9500
C(9)-C(10)	1.3962(14)
C(10)-H(10)	0.9500
C(10)-C(11)	1.3828(13)
C(11)-C(12)	1.4790(12)
C(13)-C(14)	1.3977(13)
C(13)-C(18)	1.3926(13)
C(14)-H(14)	0.9500
C(14)-C(15)	1.3918(13)

C(15)-H(15)	0.9500
C(15)-C(16)	1.3891(14)
C(16)-H(16)	0.9500
C(16)-C(17)	1.3874(15)
C(17)-H(17)	0.9500
C(17)-C(18)	1.3919(13)
C(18)-H(18)	0.9500
C(19)-C(20)	1.3999(13)
C(19)-C(24)	1.3990(13)
C(20)-H(20)	0.9500
C(20)-C(21)	1.3945(14)
C(21)-H(21)	0.9500
C(21)-C(22)	1.3892(16)
C(22)-H(22)	0.9500
C(22)-C(23)	1.3902(16)
C(23)-H(23)	0.9500
C(23)-C(24)	1.3944(14)
C(24)-H(24)	0.9500
C(25)-H(25A)	0.9900
C(25)-H(25B)	0.9900

C(4)-O(3)-C(3)	110.44(6)
C(5)-N(1)-C(1)	127.87(7)
C(5)-N(1)-C(12)	110.96(7)
C(12)-N(1)-C(1)	121.12(7)
N(1)-C(1)-C(2)	106.16(7)
N(1)-C(1)-C(4)	109.09(7)
N(1)-C(1)-C(13)	108.47(7)
C(2)-C(1)-C(4)	99.85(6)
C(13)-C(1)-C(2)	119.31(7)
C(13)-C(1)-C(4)	113.31(7)
C(1)-C(2)-H(2)	109.2
C(3)-C(2)-C(1)	98.90(6)
C(3)-C(2)-H(2)	109.2
C(19)-C(2)-C(1)	117.65(7)

C(19)-C(2)-H(2)	109.2
C(19)-C(2)-C(3)	112.27(7)
O(3)-C(3)-C(2)	104.27(6)
O(3)-C(3)-H(3)	109.6
O(3)-C(3)-C(25)	109.03(7)
C(2)-C(3)-H(3)	109.6
C(25)-C(3)-C(2)	114.49(7)
C(25)-C(3)-H(3)	109.6
O(3)-C(4)-C(1)	109.05(7)
O(4)-C(4)-O(3)	121.84(8)
O(4)-C(4)-C(1)	128.80(8)
O(1)-C(5)-N(1)	125.01(9)
O(1)-C(5)-C(6)	128.89(9)
N(1)-C(5)-C(6)	106.10(8)
C(7)-C(6)-C(5)	130.44(9)
C(11)-C(6)-C(5)	108.29(8)
C(11)-C(6)-C(7)	121.24(9)
C(6)-C(7)-H(7)	121.6
C(6)-C(7)-C(8)	116.80(10)
C(8)-C(7)-H(7)	121.6
C(7)-C(8)-H(8)	119.1
C(9)-C(8)-C(7)	121.79(9)
C(9)-C(8)-H(8)	119.1
C(8)-C(9)-H(9)	119.6
C(8)-C(9)-C(10)	120.90(10)
C(10)-C(9)-H(9)	119.6
C(9)-C(10)-H(10)	121.6
C(11)-C(10)-C(9)	116.88(9)
C(11)-C(10)-H(10)	121.6
C(6)-C(11)-C(12)	108.61(8)
C(10)-C(11)-C(6)	122.37(8)
C(10)-C(11)-C(12)	128.96(8)
O(2)-C(12)-N(1)	125.11(8)
O(2)-C(12)-C(11)	128.88(8)
N(1)-C(12)-C(11)	106.00(7)

C(14)-C(13)-C(1)	119.38(7)
C(18)-C(13)-C(1)	121.75(8)
C(18)-C(13)-C(14)	118.60(8)
C(13)-C(14)-H(14)	119.7
C(15)-C(14)-C(13)	120.63(9)
C(15)-C(14)-H(14)	119.7
C(14)-C(15)-H(15)	119.8
C(16)-C(15)-C(14)	120.38(9)
C(16)-C(15)-H(15)	119.8
C(15)-C(16)-H(16)	120.4
C(17)-C(16)-C(15)	119.20(8)
C(17)-C(16)-H(16)	120.4
C(16)-C(17)-H(17)	119.7
C(16)-C(17)-C(18)	120.60(9)
C(18)-C(17)-H(17)	119.7
C(13)-C(18)-H(18)	119.7
C(17)-C(18)-C(13)	120.58(9)
C(17)-C(18)-H(18)	119.7
C(20)-C(19)-C(2)	117.30(8)
C(24)-C(19)-C(2)	124.04(8)
C(24)-C(19)-C(20)	118.55(8)
C(19)-C(20)-H(20)	119.6
C(21)-C(20)-C(19)	120.87(9)
C(21)-C(20)-H(20)	119.6
C(20)-C(21)-H(21)	120.0
C(22)-C(21)-C(20)	120.09(10)
C(22)-C(21)-H(21)	120.0
C(21)-C(22)-H(22)	120.2
C(21)-C(22)-C(23)	119.51(9)
C(23)-C(22)-H(22)	120.2
C(22)-C(23)-H(23)	119.7
C(22)-C(23)-C(24)	120.60(10)
C(24)-C(23)-H(23)	119.7
C(19)-C(24)-H(24)	119.8
C(23)-C(24)-C(19)	120.37(9)

C(23)-C(24)-H(24)	119.8
I(1)-C(25)-H(25A)	109.3
I(1)-C(25)-H(25B)	109.3
C(3)-C(25)-I(1)	111.72(6)
C(3)-C(25)-H(25A)	109.3
C(3)-C(25)-H(25B)	109.3
H(25A)-C(25)-H(25B)	107.9

Symmetry transformations used to generate equivalent atoms:

A7.4.4 *Anisotropic Displacement Parameters ($Å^2$x 10^3) for 113 (d19152). The Anisotropic Displacement Factor Exponent Takes the Form: $-2p^2[h^2 a^{*2}U^{11} + ... + 2 h k a^* b^* U^{12}]$._

	U^{11}	U^{22}	U^{33}	U^{23}	U^{13}	U^{12}
I(1)	216(1)	219(1)	125(1)	11(1)	63(1)	-14(1)
O(1)	219(3)	257(4)	304(4)	-124(3)	27(3)	92(3)
O(2)	148(2)	167(3)	153(3)	-29(2)	49(2)	28(2)
O(3)	213(3)	127(3)	102(2)	-8(2)	39(2)	22(2)
O(4)	326(4)	114(3)	154(3)	-5(2)	45(2)	30(2)
N(1)	127(3)	132(3)	114(2)	-17(2)	27(2)	25(2)
C(1)	140(3)	111(3)	99(3)	-3(2)	22(2)	14(2)
C(2)	138(3)	108(3)	106(3)	2(2)	22(2)	11(2)
C(3)	149(3)	121(3)	109(3)	5(2)	26(2)	11(2)
C(4)	186(3)	125(3)	107(3)	-12(2)	24(2)	21(3)
C(5)	149(3)	182(4)	144(3)	-12(3)	21(2)	57(3)
C(6)	133(3)	189(4)	135(3)	17(3)	19(2)	40(3)
C(7)	142(3)	276(5)	218(4)	26(3)	34(3)	56(3)
C(8)	128(3)	295(5)	264(4)	75(4)	7(3)	13(3)
C(9)	163(4)	218(4)	212(4)	57(3)	-27(3)	-22(3)
C(10)	169(3)	160(4)	150(3)	22(3)	-9(3)	1(3)
C(11)	127(3)	147(3)	108(3)	24(2)	11(2)	19(2)
C(12)	136(3)	129(3)	95(3)	0(2)	27(2)	17(2)
C(13)	141(3)	133(3)	102(3)	0(2)	23(2)	4(2)
C(14)	223(4)	165(4)	143(3)	31(3)	61(3)	43(3)
C(15)	273(4)	192(4)	161(3)	52(3)	78(3)	25(3)
C(16)	189(4)	243(4)	143(3)	24(3)	57(3)	-16(3)
C(17)	190(4)	271(5)	151(3)	21(3)	71(3)	53(3)
C(18)	198(4)	199(4)	140(3)	22(3)	59(3)	57(3)
C(19)	141(3)	135(3)	110(3)	-5(2)	22(2)	7(2)
C(20)	156(3)	158(3)	179(3)	-9(3)	25(3)	23(3)
C(21)	160(4)	240(4)	212(4)	-13(3)	16(3)	53(3)
C(22)	145(3)	304(5)	191(4)	-46(3)	11(3)	-5(3)
C(23)	182(4)	236(4)	198(4)	-39(3)	19(3)	-46(3)

C(24)	178(3)	161(4)	167(3)	-14(3)	23(3)	-18(3)
C(25)	182(3)	197(4)	115(3)	26(3)	33(2)	25(3)

A7.4.5 *Hydrogen Coordinates (x 10^4) and Isotropic Displacement Parameters ($Å^2$x 10^3) for* ***113*** *(d19152)*

	x	y	z	U(eq)
H(2)	6017	5308	2723	14
H(3)	7407	4624	1972	15
H(7)	11705	3939	3495	25
H(8)	12796	5573	4122	28
H(9)	11707	7017	4690	25
H(10)	9457	6908	4623	20
H(14)	6896	1670	4002	21
H(15)	6071	1156	5082	24
H(16)	4553	2378	5515	23
H(17)	3815	4081	4833	24
H(18)	4617	4589	3744	21
H(20)	4097	6182	2206	20
H(21)	1888	6142	1764	25
H(22)	801	4322	1592	26
H(23)	1944	2545	1841	25
H(24)	4157	2575	2271	20
H(25A)	5693	5498	1118	20
H(25B)	5013	4224	997	20

A7.4.6 *Torsion Angles [°] for* ***113*** *(d19152)*

O(1)-C(5)-C(6)-C(7)	3.25(18)
O(1)-C(5)-C(6)-C(11)	-178.70(10)
O(3)-C(3)-C(25)-I(1)	-63.31(8)
N(1)-C(1)-C(2)-C(3)	75.39(7)
N(1)-C(1)-C(2)-C(19)	-163.61(7)
N(1)-C(1)-C(4)-O(3)	-84.86(8)
N(1)-C(1)-C(4)-O(4)	101.48(11)
N(1)-C(1)-C(13)-C(14)	-73.89(10)
N(1)-C(1)-C(13)-C(18)	100.01(9)
N(1)-C(5)-C(6)-C(7)	-176.34(10)
N(1)-C(5)-C(6)-C(11)	1.71(10)
C(1)-N(1)-C(5)-O(1)	-3.07(15)
C(1)-N(1)-C(5)-C(6)	176.54(8)
C(1)-N(1)-C(12)-O(2)	1.01(13)
C(1)-N(1)-C(12)-C(11)	-177.87(7)
C(1)-C(2)-C(3)-O(3)	39.31(8)
C(1)-C(2)-C(3)-C(25)	158.36(7)
C(1)-C(2)-C(19)-C(20)	146.36(8)
C(1)-C(2)-C(19)-C(24)	-37.39(11)
C(1)-C(13)-C(14)-C(15)	174.16(9)
C(1)-C(13)-C(18)-C(17)	-173.61(9)
C(2)-C(1)-C(4)-O(3)	26.18(9)
C(2)-C(1)-C(4)-O(4)	-147.47(10)
C(2)-C(1)-C(13)-C(14)	164.51(8)
C(2)-C(1)-C(13)-C(18)	-21.60(12)
C(2)-C(3)-C(25)-I(1)	-179.65(6)
C(2)-C(19)-C(20)-C(21)	176.48(8)
C(2)-C(19)-C(24)-C(23)	-176.58(8)
C(3)-O(3)-C(4)-O(4)	172.99(9)
C(3)-O(3)-C(4)-C(1)	-1.18(9)
C(3)-C(2)-C(19)-C(20)	-99.86(9)
C(3)-C(2)-C(19)-C(24)	76.39(10)
C(4)-O(3)-C(3)-C(2)	-24.90(9)

C(4)-O(3)-C(3)-C(25)	-147.60(7)
C(4)-C(1)-C(2)-C(3)	-37.94(7)
C(4)-C(1)-C(2)-C(19)	83.06(8)
C(4)-C(1)-C(13)-C(14)	47.40(11)
C(4)-C(1)-C(13)-C(18)	-138.70(9)
C(5)-N(1)-C(1)-C(2)	-113.25(9)
C(5)-N(1)-C(1)-C(4)	-6.46(11)
C(5)-N(1)-C(1)-C(13)	117.40(9)
C(5)-N(1)-C(12)-O(2)	178.57(8)
C(5)-N(1)-C(12)-C(11)	-0.31(9)
C(5)-C(6)-C(7)-C(8)	177.59(10)
C(5)-C(6)-C(11)-C(10)	-179.47(8)
C(5)-C(6)-C(11)-C(12)	-1.92(10)
C(6)-C(7)-C(8)-C(9)	1.29(16)
C(6)-C(11)-C(12)-O(2)	-177.41(9)
C(6)-C(11)-C(12)-N(1)	1.42(9)
C(7)-C(6)-C(11)-C(10)	-1.20(14)
C(7)-C(6)-C(11)-C(12)	176.35(8)
C(7)-C(8)-C(9)-C(10)	-0.95(16)
C(8)-C(9)-C(10)-C(11)	-0.47(14)
C(9)-C(10)-C(11)-C(6)	1.54(13)
C(9)-C(10)-C(11)-C(12)	-175.48(8)
C(10)-C(11)-C(12)-O(2)	-0.07(15)
C(10)-C(11)-C(12)-N(1)	178.75(8)
C(11)-C(6)-C(7)-C(8)	-0.24(14)
C(12)-N(1)-C(1)-C(2)	63.87(9)
C(12)-N(1)-C(1)-C(4)	170.66(7)
C(12)-N(1)-C(1)-C(13)	-65.49(9)
C(12)-N(1)-C(5)-O(1)	179.57(10)
C(12)-N(1)-C(5)-C(6)	-0.82(9)
C(13)-C(1)-C(2)-C(3)	-161.86(7)
C(13)-C(1)-C(2)-C(19)	-40.86(10)
C(13)-C(1)-C(4)-O(3)	154.19(7)
C(13)-C(1)-C(4)-O(4)	-19.46(13)
C(13)-C(14)-C(15)-C(16)	-0.79(16)

C(14)-C(13)-C(18)-C(17)	0.33(14)
C(14)-C(15)-C(16)-C(17)	1.09(16)
C(15)-C(16)-C(17)-C(18)	-0.70(16)
C(16)-C(17)-C(18)-C(13)	-0.01(16)
C(18)-C(13)-C(14)-C(15)	0.07(14)
C(19)-C(2)-C(3)-O(3)	-85.56(8)
C(19)-C(2)-C(3)-C(25)	33.49(10)
C(19)-C(20)-C(21)-C(22)	0.48(15)
C(20)-C(19)-C(24)-C(23)	-0.38(13)
C(20)-C(21)-C(22)-C(23)	-0.61(16)
C(21)-C(22)-C(23)-C(24)	0.25(16)
C(22)-C(23)-C(24)-C(19)	0.25(15)
C(24)-C(19)-C(20)-C(21)	0.02(13)

Symmetry transformations used to generate equivalent atoms:

A7.5 REFERENCES AND NOTES

(1) Sheldrick, G. M. Phase annealing in *SHELX*-90: direct methods for larger structures. *Acta Cryst.* **1990**, A46, 467–473.

(2) Sheldrick, G. M. Crystal structure refinement with *SHELXL*. *Acta Cryst.* **2015**, C71, 3–8.

(3) Müller, P. Practical suggestions for better crystal structures. *Crystallography Reviews* **2009**, *15*, 57–83.

APPENDIX 8

Diastereodivergent Ireland–Claisen Rearrangements of Isomeric Enolates[†]

A8.1 INTRODUCTION

The Ireland–Claisen rearrangement is one of the most enabling tactics for the stereoselective construction of carbon–carbon bonds available to chemists.[1] The ability to reliably predict and control stereochemical outcomes in Ireland–Claisen rearrangements has led to its extensive implementation in organic synthesis. In the context of fully substituted acyclic ester enolates, however, the Ireland–Claisen rearrangement remains highly limited in scope.[2,3] This is ostensibly due to the lack of procedures that enable control over the enolate geometry in acyclic α,α-disubstituted esters.[4] New methods that address this selective enolization challenge are therefore highly desirable for enabling stereoselective carbon–carbon bond formation to generate vicinal stereogenic centers in acyclic motifs. Toward this end, we previously developed and computationally modeled a class of globally diastereoconvergent Ireland–Claisen rearrangements of α-phthalimido,α-aryl-cinnamyl ester-derived enolates to prepare tetrasubstituted α-amino acids bearing a vicinal tertiary stereogenic center in excellent diastereoselectivity (Figure A8.1.1A, also see Chapter 4).[5] The geometry of both the enolate and cinnamyl olefin were

[†]This research was performed in collaboration with Joel Monroy, Maximillian Kaiser, Alex Cusumano, and Eric J. Alexy.

inconsequential to the diastereoselectivity in these systems, thus obviating the requirement for selective enolization, albeit at the expense of accessing only a single diasteromeric series of product. To further expand the scope of acyclic Ireland–Claisen rearrangements, we have investigated the diastereodivergent[3c] synthesis of a series of α-alkyl,α-aryl carboxylic acids bearing vicinal tertiary or quaternary stereogenic centers by harnessing a selective enolization protocol[6] in concert with substrate design (Figure A8.1.1B).

Figure A8.1.1 *Stereoconvergent and Stereodivergent Approaches to the Ireland–Claisen Rearrangement of Fully Substituted Acyclic Enolates.*

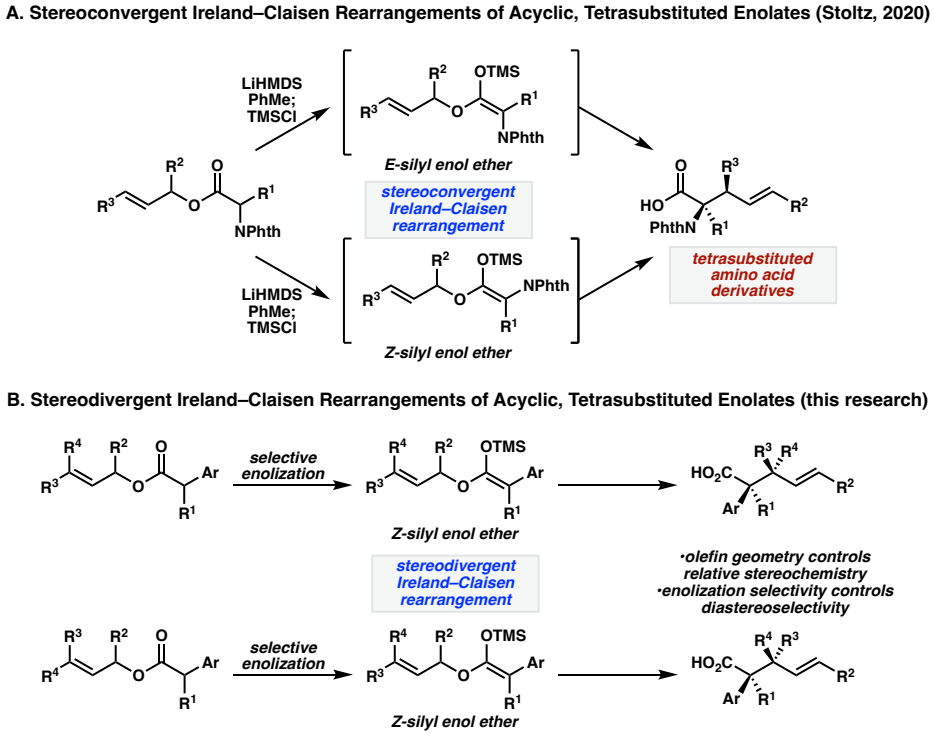

A8.2 DEVELOPMENT OF THE DIASTEREODIVERGENT IRELAND–CLAISEN REARRANGEMENT

In our previous investigation,[5] we found enolization with a selective enolization protocol[6] and Ireland–Claisen rearrangement of α-phenyl,α-ethyl ester **121** led to the

formation of carboxylic acid **122** in 87% yield in 2.9:1 diastereoselection (Scheme 5.2.1). Computational modeling of this system predicts a 1.5 and 1.2 kcal/mol preference for a chair-like transition states for both the *Z*- and *E*-silyl enol ethers (calculated maximum dr of 13:1 and 8:1, respectively).[5] We hypothesized that the low diastereoselectivity in this Ireland–Claisen rearrangement is the result of poor enolization geometry control given that the predicted chair-like transition states would lead to the formation of diastereomeric products with higher diastereoselectivities. We reasoned that incorporation of substitution geminal to the ester sp^3 oxygen atom might impact the enolization selectivity while also enabling transfer of chirality in enantioenriched substrates. We subsequently examined a series of substrates incorporating such substitution using α-methyl, α-phenyl substitution as a model system (Table A8.2.1). Increasing the steric size of the R group from H to Me or Et led to higher diastereoselectivities of 4.0:1 and 5.2:1, respectively (entries 1–3). Further increasing the steric size of this substituent to *i*-Pr led to a lower diastereoselectivity of 3.2:1, however, *t*-Bu substitution provided the highest observed diastereoselectivity of 10.6:1 (entries 4–5).

Scheme A8.2.1 *Initial Investigation of an α-Aryl,α-Alkyl Acyclic Cinnamyl Ester.*[5]

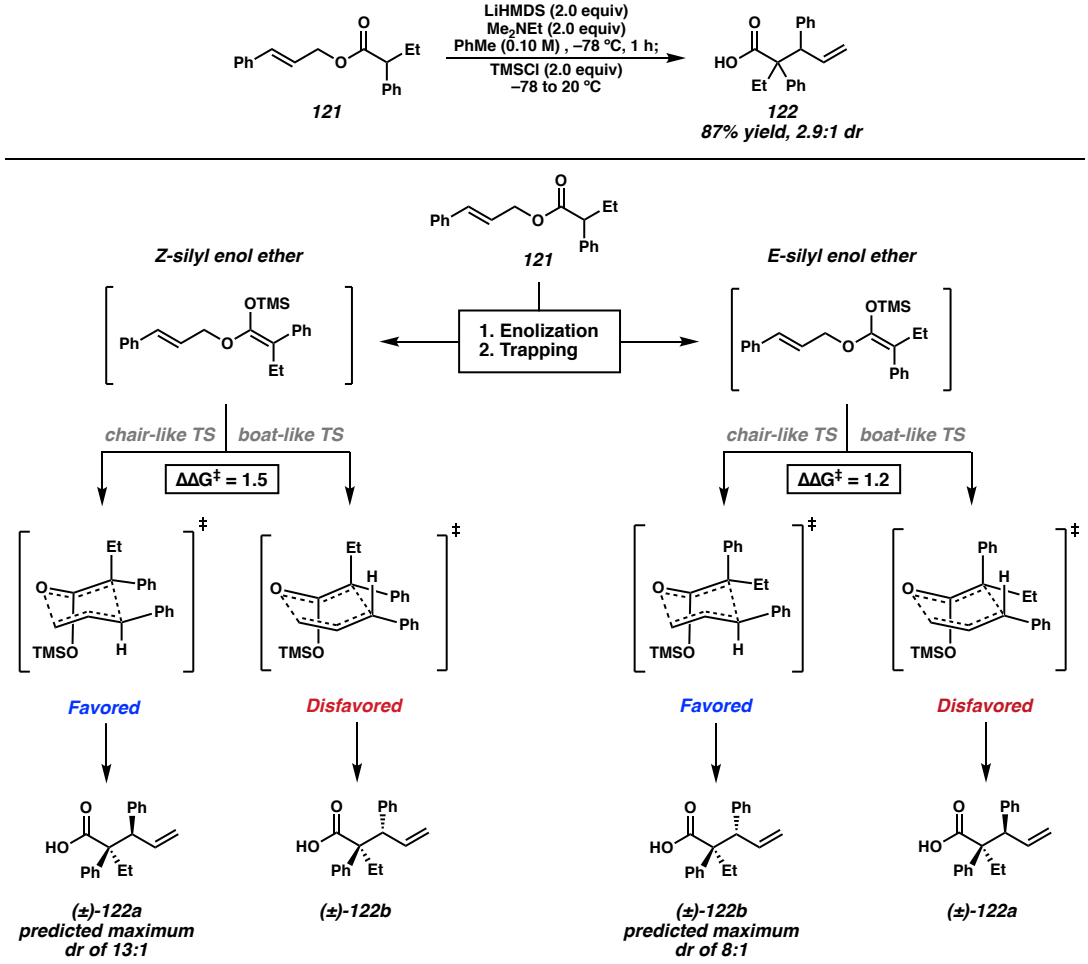

Table A8.2.1 *Effect of Substitution on the Diastereoselectivity of the Ireland–Claisen Rearrangement.*

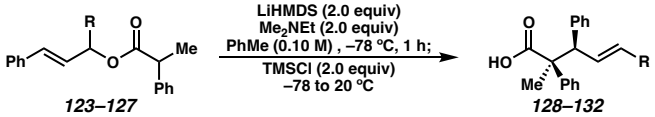

entry	R	dr	% yield
1	H	2.0:1	91
2	Me	4.0:1	92
3	Et	5.2:1	87
4	*i*-Pr	3.2:1	85
5	*t*-Bu	11.2:1	78

Several enolate trapping experiments were then performed with saturated ester model **133** to ascertain the degree of enolate geometry control, however, we were unable to isolate any products in these experiments. At this juncture, we were curious as to how the steric size of the α-alkyl substituent impacted the diastereoselectivity in the Ireland–Claisen rearrangement. Prior research with this selective enolization protocol demonstrated a precipitous drop in enolization selectivity in α-Me substituted systems compared with α-Et substitution.[6,7] In these new systems (i.e. **123** and **134**), both α-Me and α-Et substitution lead to similar levels of diastereoselectivity (10.6:1 and 11.0:1, respectively) favoring the same diastereomeric series of product, as confirmed by X-Ray crystallographic analysis (Scheme A8.2.3). If these esters undergo the Ireland–Claisen via chair-like transition states as predicted in substrate **121** (Figure A8.1.1), the relative *syn*-Ph stereochemistry indicates that the enolization is *Z*-selective. This is in contrast to α-aryl,α-alkyl aryl ketone-derived systems which undergo *E*-selective enolization with a slightly modified protocol.[6,7a] These results are also at odds with related ester systems investigated in Chapter 2 (see Scheme 2.2.1). As a control, we performed the enolization with ester **123** in absence of the Me_2NEt additive and observed a significant drop in diastereoselectivity from 10.6:1 to 1.5:1 (Table A8.2.2, entries 1–2). Utilizing KHMDS as a base also led to a significant drop in diastereoselectivity from 10.6:1 to 4.8:1 (entries 1 and 3). Interestingly, each of these enolization protocols favors the same diastereomeric series of products whereas in prior research, enolization with LiHMDS/Me_2NEt favors the opposite enolate geometry as that formed with other enolization conditions.[7,8]

Scheme A8.2.2 *Failed Enolate Trapping Experiments.*

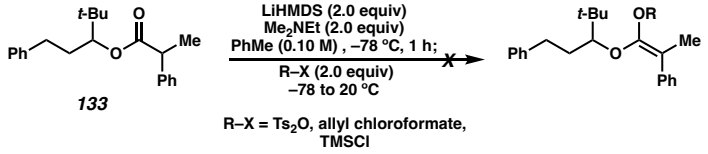

Scheme A8.2.3 *Comparison of α-Me and α-Et Substituents.*

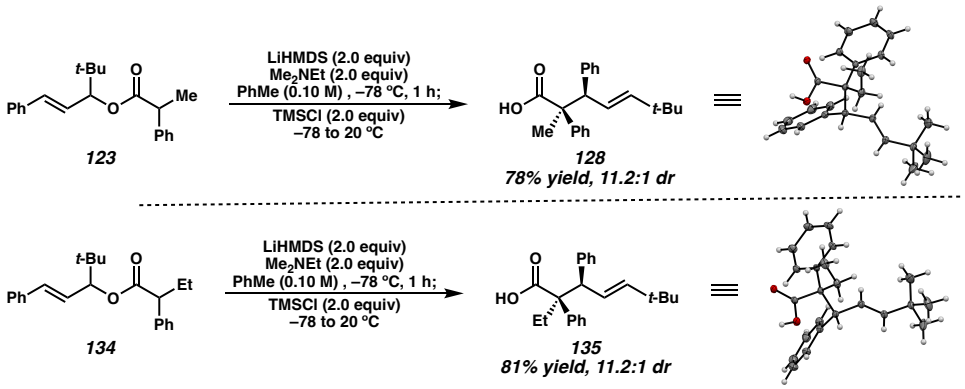

Table A8.2.2 *Enolization Control Experiments.*

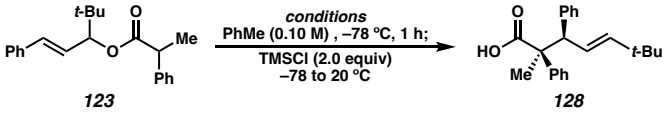

entry	enolization conditions	dr	% yield
1	LiHMDS (2.0 equiv), Me_2NEt (2.0 equiv)	10.6:1	72
2	LiHMDS (2.0 equiv)	1.5:1	79
3	KHMDS (2.0 equiv)	4.8:1	69

If chair-like transition states are favored in *both* enolate geometries, then utilizing a *Z*-cinnamyl olefin would enable selective access to the *anti*-Ph diastereomeric series. Accordingly, *Z*-olefin **136** was prepared and subjected to the Ireland–Claisen rearrangement protocol to generate carboxylic acid **137** in 55% yield and 17.4:1 dr favoring the *anti*-Ph diastereomer, which was unambiguously characterized by X-Ray crystallographic analysis. This result provides further evidence for a *Z*-selective enolization

in these α-aryl,α-alkyl systems and demonstrates diastereodivergence with respect to the relative stereochemistry which is dictated by the geometry of the cinnamyl olefin.

Scheme A8.2.4 *Diastereodivergence of the Ireland–Claisen Rearrangement.*

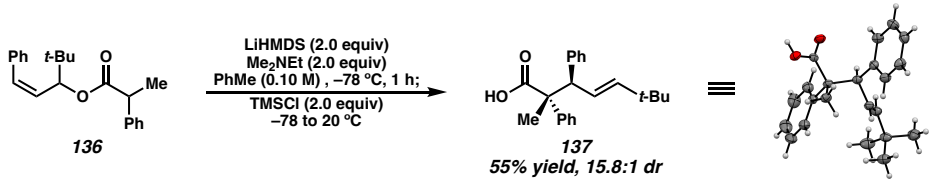

A8.3 INVESTIGATION OF CHIRALITY TRANSFER

A powerful feature of the Ireland–Claisen rearrangement is its ability to relay stereochemical information during the [3,3]-rearrangement with excellent stereochemical fidelity. Noyori asymmetric hydrogenation enabled access to *(S)*-***123*** in an excellent 92% ee. Ireland–Claisen rearrangement of *(S)*-**23** then provided enantioenriched acid *(S,R)*-**128** in 81% yield and 13.2:1 dr with complete enantioretention.

Scheme A8.3.1 *Transfer of Chirality with an Enantioenriched Ester.*

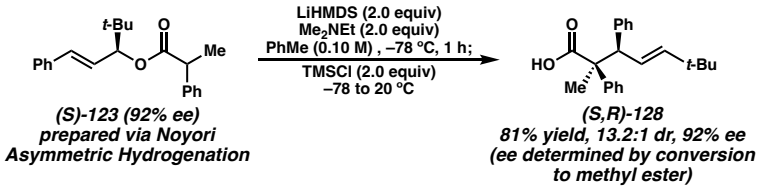

A8.4 INVESTIGATION OF VICINAL QUATERNARY CENTER FORMATION

The formation of vicinal quaternary stereogenic centers with high selectivity is a formidable challenge in organic synthesis,[9] particularly within the context of acyclic vicinal quaternary stereogenic centers.[2,10] We hypothesized that our selective enolization/Ireland–Claisen rearrangement protocol could also be leveraged in the stereodivergent synthesis of vicinal quaternary stereogenic centers by utilizing substrates

bearing geometrically defined 1,1,2-trisubstituted olefins. Toward this end, we examined the series of trisubstituted olefins **138**–**142** in vicinal quaternary center formation (Table A8.4.1). As a point of reference, for ester **138** where R = H, desired rearrangement product **143** is formed in 90% yield and 3.3:1 dr (entry 1). Increasing the steric bulk of the R group to R = Me (**139**) or R = Et (**140**) increases the diastereoselectivity to 6.1:1 and 8.4:1, respectively (entries 2 and 3). Further increasing the size of R to R = *i*-Pr provides the optimal diastereoselectivity of 10.0:1 whereas a bulkier *t*-Bu group (**142**) decreases the selectivity to A8.3:1 in this system (entries 4 and 5).

Table A8.4.1 *Optimization of Substrates for Vicinal Quaternary Center Formation.*

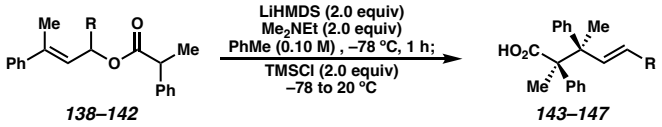

138–142 *143–147*

entry	R	dr	% yield
1	H	3.3:1	90
2	Me	6.1:1	94
3	Et	8.4:1	88
4	*i*-Pr	10.0:1	80
5	*t*-Bu	5.3:1	80

To access the opposite diastereomeric series, we investigated *Z*-olefin substrates **148**–**150** (Table A8.4.2). It should be noted that a substrate where R = *t*-Bu could not be prepared in a geometrically pure form and was therefore not investigated. For R = Me (**148**), Et (**149**), and *i*-Pr (**150**), diastereoselectivities of 4.6:1, 5.0:1, and 6.4:1 were measured, respectively, favoring the *anti*-bis-aryl diasteromer (entries 1–3). While products derived from the *Z*-olefin series **148**–**150** were isolated in lower levels of selectivity compared to the *E*-olefin series **138**–**142**, this stereodivergence represents a substantial step forward in acyclic stereocontrol in vicinal quaternary stereogenic center formation.

Table A8.4.2 *Diastereodivergence in Vicinal Quaternary Center Formation.*

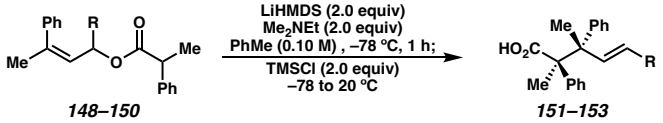

148–150 *151–153*

entry	R	dr	% yield
1	Me	4.6:1	98
2	Et	5.0:1	85
3	*i*-Pr	6.4:1	88

Scheme A8.4.1 *Chirality Transfer in the Formation of Vicinal Quaternary Centers.*

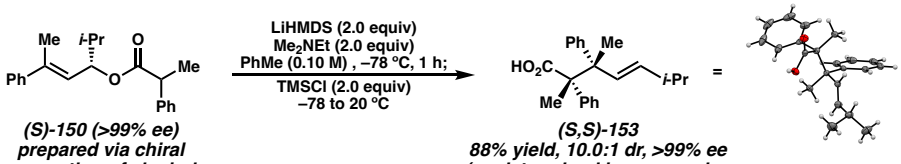

(S)-150 (>99% ee) prepared via chiral separation of alcohol

(S,S)-153 88% yield, 10.0:1 dr, >99% ee (ee determined by conversion to methyl ester)

A8.5 SCOPE OF THE DIASTEREODIVERGENT IRELAND–CLAISEN REARRANGEMENT

With diastereoselective access to products bearing vicinal tertiary/quaternary and quaternary/quaternary stereogenic centers, we examined the scope of this transformation. In all cases, the yield and diastereoselectivity reported are of isolated product diastereomeric mixtures as crude reaction mixtures did not allow for accurate determination of diastereoselectivity. To the best of our abilities, product diastereomers *were not* separated chromatographically and therefore the diastereoselectivities reported reflect our most accurate assessment of the reaction diastereoselectivity. With respect to vicinal quaternary/tertiary stereogenic centers, α-alkyl substituted products including *i*-Bu (**154**, 14.3:1 dr), *n*-pentyl (**155**, 9.2:1 dr), and allyl (**157**, 14.4:1 dr) groups were well tolerated whereas benzyl substituted product **156** was isolated with in a diminished 5.2:1 dr (Table A8.5.1). Electron-rich β-aryl substituted products were generally isolated in high

dr whereas more electron-poor β-aryl groups such as 4-CF_3-phenyl (**168**, 7.7:1 dr) and 4-F-phenyl (**169**, 9.3:1 dr) were isolated with lower diastereoselectivity. Notably, 4-MeO-phenyl products **162** (27:1 dr) and **163** (32:1 dr) were isolated in excellent dr in both diastereomeric series. Carboxylic acid **164** bearing a sterically encumbered *o*-tolyl substituent was isolated in an excellent 10.5:1 dr. Heterocyclic furan and pyridine containing products **170** and **171** were also isolated in excellent dr (10.4:1 and 42.6:1, respectively). Carboxylic acid product **172** containing a 2-Me-phenyl group at the α-position was isolated in a low 1.8:1 dr, ostensiably due to poor enolization geometry control with a highly sterically encumbered α-aryl group. Substitution with 4-MeO-phenyl at the α-position also led to a diminished dr of 5.5:1 in carboxylic acid **173** whereas 4-Br-phenyl product **174** was isolated in an excellent 21.7:1 dr.

Generally high diasteroeselectivities were also observed in vicinal quaternary/quaternary Ireland–Claisen rearrangements (Table A8.5.2). Carboxylic acid **175** containing a β-ethyl group was isolated in a slightly lower dr of 8.8:1 compared with β-methyl model substrate **143** which was isolated in 10.0:1 dr. Highly sterically encumbered chromane **176** and 2-Chloro-phenyl product **177** were isolated with excellent diastereoselectivities of 15.1:1 and 13.4:1, respectively. Additionally, β-aryl substituted products containing 4-MeO-phenyl (**178**, 10.9:1 dr), 4-CF_3-Ph (**179**, 8.2:1 dr), and 2-napthyl (**180**, 8.6:1 dr) groups were isolated in high dr. Finally, geraniol-derived product **181** and nerol-derived product **182** were isolated in good diastereoselectivities of 5.9:1 and 7.3:1 dr, respectively.

Table A8.5.1 *Scope of Vicinal Quaternary/Tertiary Carboxylic Acid Products.*

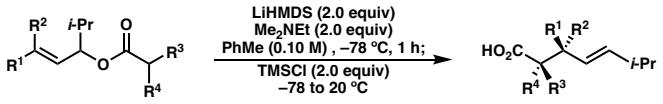

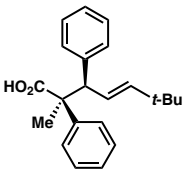

128
72% yield, 10.6:1 dr

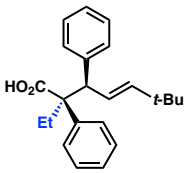

135
85% yield, 11.3:1 dr

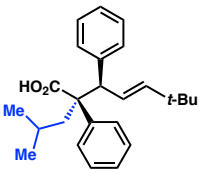

154
82% yield, 14.3:1 dr

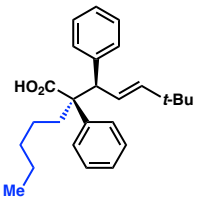

155
81% yield, 9.2:1 dr

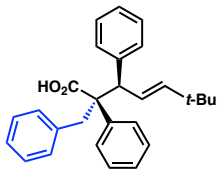

156
82% yield, 5.2:1 dr

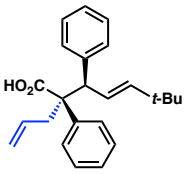

157
74% yield, 14.4:1 dr

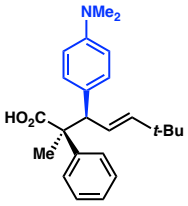

158
82% yield, 9.5:1 dr

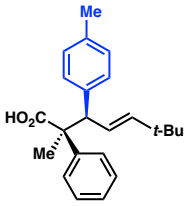

159
59% yield, 18.8:1 dr

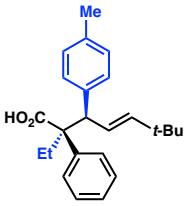

160
85% yield, 11.6:1 dr

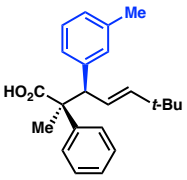

161
84% yield, 16.1:1 dr

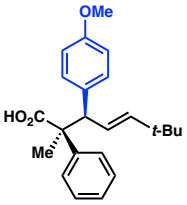

162
93% yield, 27.0:1 dr

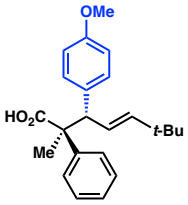

163
60% yield, 32.0:1 dr

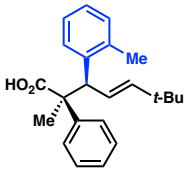

164
79% yield, 10.5:1 dr

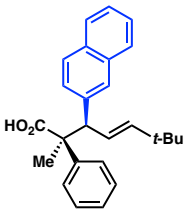

165
80% yield, 11.5:1 dr

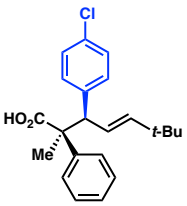

166
86% yield, 14.1:1 dr

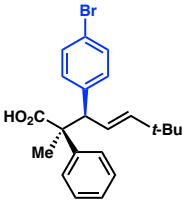

167
84% yield, 14.1:1 dr

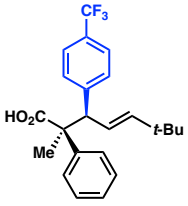

168
70% yield, 7.7:1 dr

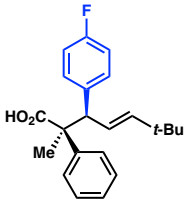

169
83% yield, 9.3:1 dr

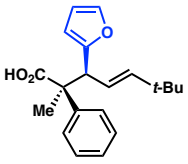

170
90% yield, 10.4:1 dr

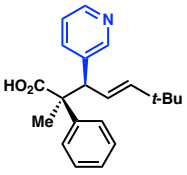

171
83% yield, 42.6:1 dr

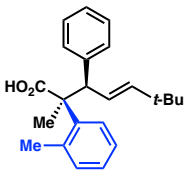

172
54% yield, 1.8:1 dr

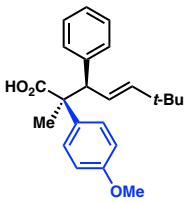

173
84% yield, 5.5:1 dr

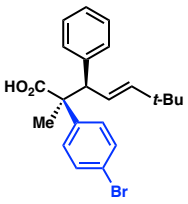

174
80% yield, 21.7:1 dr

Table A8.5.2 *Scope of Vicinal Quaternary/Quaternary Carboxylic Acid Products.*

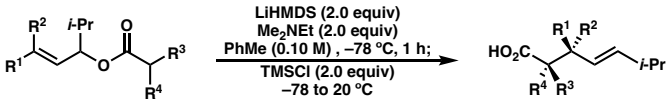

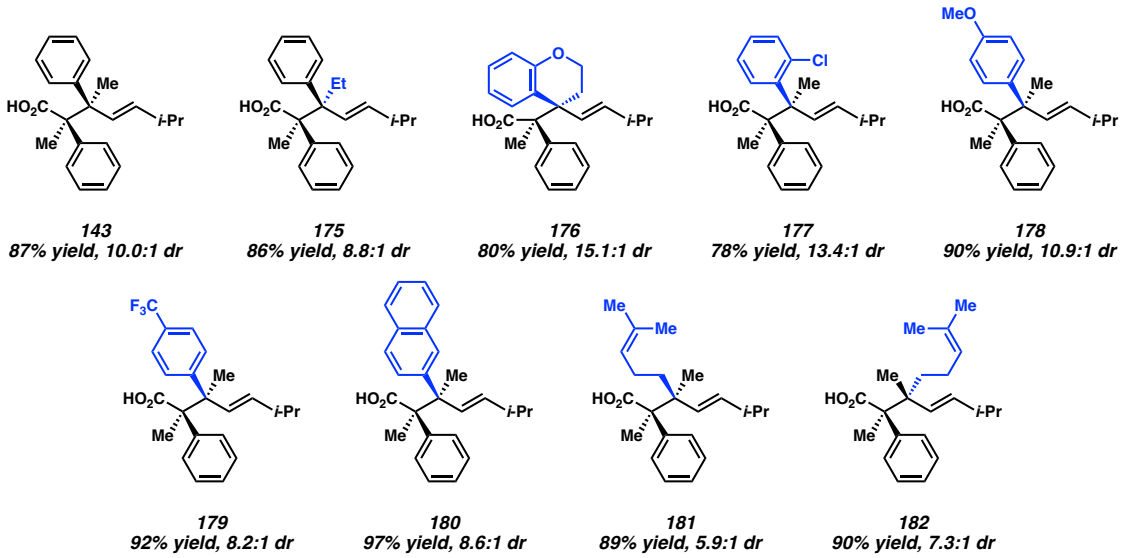

143
87% yield, 10.0:1 dr

175
86% yield, 8.8:1 dr

176
80% yield, 15.1:1 dr

177
78% yield, 13.4:1 dr

178
90% yield, 10.9:1 dr

179
92% yield, 8.2:1 dr

180
97% yield, 8.6:1 dr

181
89% yield, 5.9:1 dr

182
90% yield, 7.3:1 dr

A8.6 PRODUCT DERIVATIZATIONS

Derivatizations of Ireland–Claisen product **150** containing vicinal quaternary stereogenic centers were performed to demonstrate the synthetic utility of these Ireland–Claisen rearrangements. Carboxylic acid reduction with $LiAlH_4$ was utilized to prepare alcohol **183**. Ozonolysis with PPh_3 reductive workup resulted in the formation of *O*-acyl lactol **184** in a 2:1 ratio of hydroxy epimers. Derivative **184** served as an interesting point of divergence for other derivatization reactions. Treatment of ozonolysis product **184** with DAST results in the formation of fluoride **185** as a single fluoride epimer. Wittig methylenation produced carboxylic acid **186**, constituting a two-step exchange of olefin substitution from rearrangement product **150**. Finally, treatment of ozonolysis product **185** with Jones reagent provides C_2-symmetric compound **187**.

Scheme A8.6.1 *Derivatizations of Ireland–Claisen Product* ***150****.*

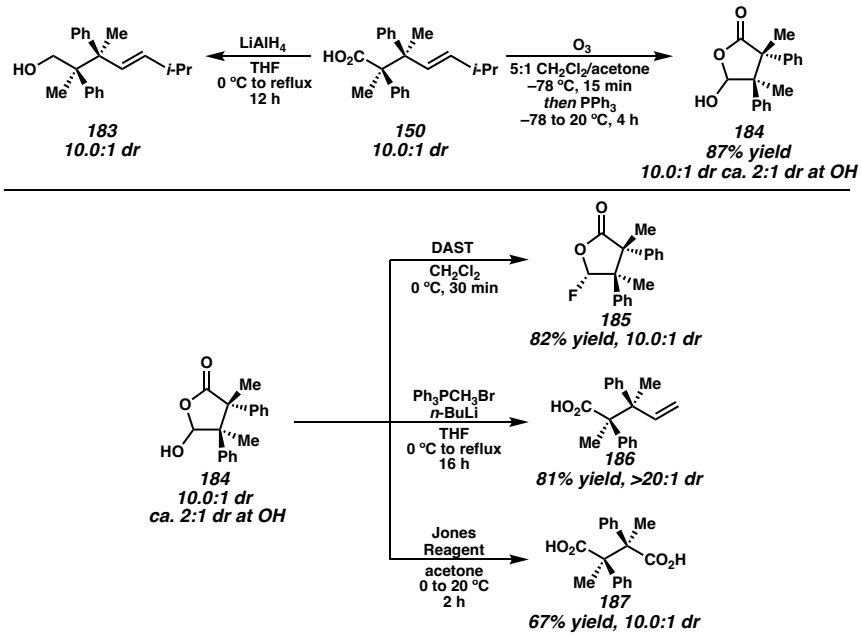

A8.7 CONCLUSION

We have developed a series of Ireland–Claisen rearrangements for the diastereoselective synthesis of extremely congested vicinal tertiary/quaternary and quaternary/quaternary stereogenic centers. Our protocol harnesses a substrate-derived selective enolization selective enolization procedure that enables the diastereoselective Ireland–Claisen rearrangements. Both diastereomeric series of products are accessible via this approach and the reaction scope and limitations are discussed. Derivatization reactions of vicinal quaternary center containing product **150** are presented to demonstrate the synthetic utility of these extremely sterically encumbered acyclic products.

A8.8 REFERENCES AND NOTES

(1) (a) Ireland, R. E.; Mueller, R. H. The Claisen Rearrangement of Allyl Esters. *J. Am. Chem. Soc.* **1972**, *94*, 5897–5898. (b) Ireland, R. E.; Mueller, R. H.; Willard, A. K. *J. Am. Chem. Soc.* **1976**, *98*, 2868–2877.

(2) For a recent review see: Pierrot, D.; Marek, I. Synthesis of Enantioenriched Vicinal Tertiary and Quaternary Carbon Stereogenic Centers within an Acyclic Chain. *Angew. Chem. Int. Ed.* **2020**, *59*, 36–49.

(3) For examples of strategies to achieve stereoselective acyclic Ireland–Claisen rearrangements, see: (a) Crimmins, M. T.; Knight, J. D.; Williams, P. S.; Zhang, Y. Stereoselective Synthesis of Quaternary Carbons via the Dianionic Ireland–Claisen Rearrangement. *Org. Lett.* **2014**, *16*, 2458–2461. (b) Crimmins, M. T.; Zhang, Y.; Williams, P. S. Approach to the Synthesis of Briarane Diterpenes through a Dianionic Claisen Rearrangement and Ring-Closing Metathesis. *Org. Lett.* **2017**, *19*, 3907–3910. (c) Podunavac, M.; Lacharity, J. J.; Jones, K. E.; Zakarian, A. Stereodivergence in the Ireland–Claisen Rearrangement of α-Alkoxy Esters. *Org. Lett.* **2018**, *20*, 4867–4870.

(4) For examples employing selective enolizations, see: (a) Qin, Y.-C.; Stivala, C. E.; Zakarian, A. Acyclic Stereocontrol in the Ireland–Claisen Rearrangement of α-Branched Esters *Angew. Chem. Int. Ed.* **2007**, *46*, 7466–7469. (b) Stivala, C. E.; Zakarian, A. Total Synthesis of (+)-Pinnatoxin A. *J. Am. Chem. Soc.* **2008**, *130*, 3774–3776. (c) Stivala, C. E.; Zakarian, A. Studies Toward the Synthesis of Spirolides: Assembly of the Elaborated E-Ring Fragment. *Org. Lett.* **2009**, *11*, 839–

842. (d) Gu, Z.; Hermann, A. T.; Stivala, C. E.; Zakarian, A. Stereoselective Construction of Adjacent Quaternary Chiral Centers by the Ireland-Claisen Rearrangement: Stereoselection with Esters of Cyclic Alcohols. *Synlett* **2010**, *11*, 1717–1722. (e) Araoz, R.; Servent, D.; Molgó, J.; Iorga, B. I.; Fruchart–Gaillard, C.; Benoit, E.; Gu, Z.; Stivala, C.; Zakarian, A. Total Synthesis of Pinnatoxins A and G and Revision of the Mode of Action of Pinnatoxin A. *J. Am. Chem. Soc.* **2011**, *133*, 10499–10511.

(5) Fulton, T. J.; Cusumano, A. Q.; Alexy, E. J.; Du, Y. E.; Zhang, H.; Houk, K. N.; Stoltz, B. M. Global Diastereoconvergence in the Ireland–Claisen Rearrangement of Isomeric Enolates: Synthesis of Tetrasubstituted α-Amino Acids. *J. Am. Chem. Soc.* **2020**, *142*, 21938–21947.

(6) Mack, K. A.; McClory, A.; Zhang, H.; Gosselin, F.; Collum, D. B. Lithium Hexamethyldisilazide-Mediated Enolization of Highly Substituted Aryl Ketones: Structural and Mechanistic Basis of the E/Z Selectivities. *J. Am. Chem. Soc.* **2017**, *139*, 12182−12189. (b) Li, B. X.; Le, D. N.; Mack, K. A.; McClory, A.; Lim, N. K.; Cravillion, T.; Savage, S.; Han, C.; Collum, D. B.; Zhang, H.; Gosselin, F. Highly Stereoselective Synthesis of Tetrasubstituted Acyclic All-Carbon Olefins via Enol Tosylation and Suzuki–Miyaura Coupling. *J. Am. Chem. Soc.* **2017**, *139*, 10777−10783.

(7) (a) Alexy, E. J.; Zhang, H.; Stoltz, B. M. Palladium-Catalyzed Decarboxylative Allylic Alkylation of Fully Substituted Acyclic Enol Carbonates. *J. Am. Chem. Soc.* **2018**, *140*, 10109–10112. (b) Alexy, E. J.; Fulton, T. J.; Zhang, H.; Stoltz, B. M. Palladium-catalyzed Enantioselective Decarboxylative Allylic Alkylation of Fully

Substituted *N*-acyl Indole-Derived Enol Carbonates. *Chem*. *Sci*. **2019**, *10*, 5996−6000. (c) Lavernhe, R.; Alexy, E. J.; Zhang, H.; Stoltz, B. M. Palladium-Catalyzed Enantioselective Decarboxylative Allylic Alkylation of Acyclic α-*N*-Pyrrolyl/Indolyl Ketones. *Org*. *Lett*. **2020**, *22*, 4272–4275.

(8) Fulton, T. J.; Wu, B.; Alexy, E. J.; Zhang, H.; Stoltz, B. M. Palladium-catalyzed α,β-dehydrogenation of acyclic ester equivalents by a novel electron deficient phosphinooxazoline ligand. *Tetrahedron* **2019**, *75*, 4104–4109.

(9) (a) Peterson, E. A.; Overman, L. E.; Contiguous Stereogenic Quaternary Carbons: A Daunting Challenge in Natural Products Synthesis. *Proc*. *Natl*. *Acad*. *Sci*. *U.S.A.* **2004**, *101*, 11943–11948. (b) Long, R.; Huang, J.; Gong, J.; Yang, Z.; Direct Construction of Vicinal All-Carbon Quaternary Stereocenters in Natural Product Synthesis. *Nat*. *Prod*. *Rep*. **2015**, *32*, 1584–1601. (c) Zhou, F.; Zhu, L.; Pan, B.; Shi, Y.; Liu, Y.; Zhou, J. Catalytic Enantioselective Construction of Vicinal Quaternary Carbon Stereocenters. *Chem*. *Sci*. **2020**, *11*, 9341–9365.

(10) (a) Feng, J.; Holmes, M.; Krische, M. J. Acyclic Quaternary Carbon Stereocenters via Enantioselective Transition Metal Catalysis. *Chem*. *Rev*. **2017**, *117*, 12564–12580. (b) Das, J. P.; Marek, I.; Enantioselective Synthesis of All-Carbon Stereogenic Centers in Acyclic Systems. *Chem*. *Commun*. **2011**, *47*, 4593–4623.

APPENDIX 9

The Total Synthesis of Havellockate[†]

A9.1 INTRODUCTION

Marine organisms produce a vast array of complex natural products that have enthralled chemists for decades. The polycyclic furanobutenolide-derived cembrenoid and norcembrenoid natural products isolated from soft corals of the *Sinularia* genus are a synthetically challenging class of such marine natural products, with only two members of this natural product family succumbing to total synthesis efforts to date.[1] Our laboratory has long been fascinated with the structural complexity of these targets and has engaged in efforts toward several members of this family of natural products, including bielschowskysin[2] (**188**) and ineleganolide[3] (**189**), with our most recent efforts culminating in the first total synthesis of norcembranoid diterpenoid (–)-scabrolide A (**190**) (Figure A9.1.1A).[4] Havellockate (**191**) is a C_{20} cembranoid isolated from *Sinularia granosa* in 1998 and is characterized by a highly oxygenated *cis*-fused tricyclic core reminiscent of yonarane-type norcembranoids (blue) and a unique spiro-fused β-hydroxybutanolide ring not observed in other congeners of this class (Figure A9.1.1B).[5,6] In addition to these structural features, havellockate possesses eight stereogenic centers, seven of which are contiguous.

[†]This research was performed in collaboration with Nicholas J. Hafeman, Melinda Chan, Eric J. Alexy, and Steven A. Loskot.

Figure A9.1.1 *Furanobutenolide-derived Cembranoid and Norcembranoid Diterpenoids.*

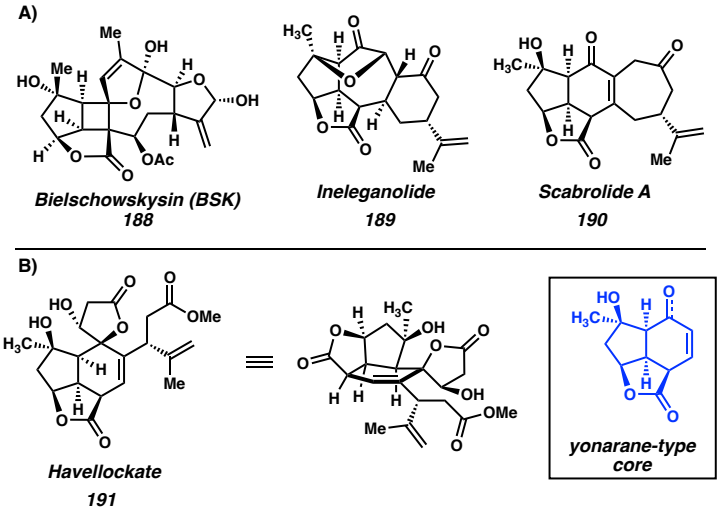

A9.2 RETROSYNTHETIC ANALYSIS

No completed total syntheses of havellockate have been disclosed, however, synthetic efforts by Mehta[7] and Barriault[8] highlight the synthetic challenge of this natural product. Retrosynthetically, we first turned our attention to the potentially sensitive spirolactone moiety, which we envisaged installing at a late stage from enone **192** (Scheme A9.2.1). From enone **192**, an intramolecular Diels–Alder disconnection and redox manipulations simplified our target to propiolic ester **193**, a sequence previously utilized in our group's synthesis of (–)-scarbolide A. Finally, propiolic ester **193** could arise from aldehyde **194** and sulfone **195** via a convergent Julia–Kocienski olefination.[9]

Scheme A9.2.1 *Retrosynthetic Analysis of Havellockate.*

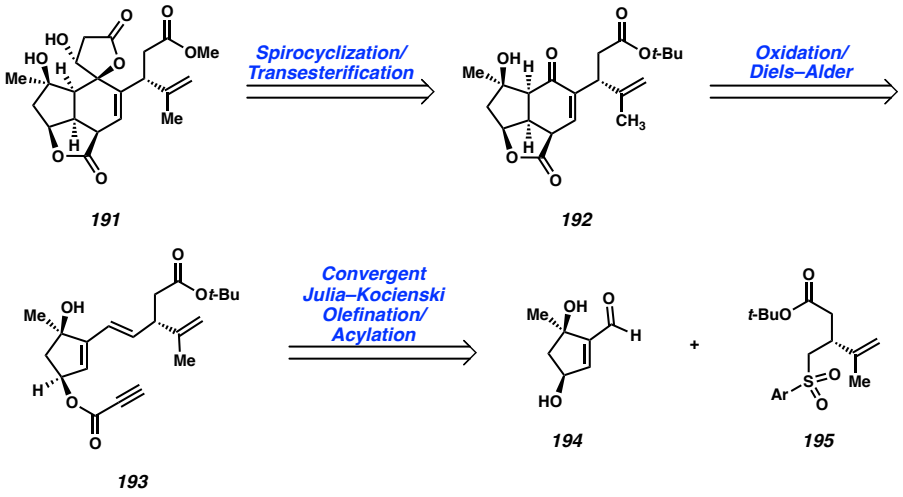

A9.3 THE TOTAL SYNTHESIS OF HAVELLOCKATE

Our efforts commenced with the synthesis of aldehyde **194** from previously reported (–)-linalool-derived enone **196** (Scheme A9.3.1).[10] Bromination of enone **196** followed by cyanide conjugate addition/elimination provided vinylogous acyl nitrile **197**. Diastereoselective Leuche reduction and alcohol protection affords nitrile **199**, which is subsequently reduced to aldehyde **194** with DIBAL. The sulfone fragment was prepared from known acyl oxazolidinone **199** (Scheme A9.3.2). Following δ-deprotonation, α-alkylation with *t*-Bu bromoacetate and reductive auxiliary removal yielded alcohol **201** in >99% ee. A Mitsunobu reaction with 1-phenyltetrazole thiol (PTSH) and sulfide oxidation was then used to prepare sulfone **195**.

Scheme A9.3.1 *Synthesis of the Aldehyde Coupling Partner.*

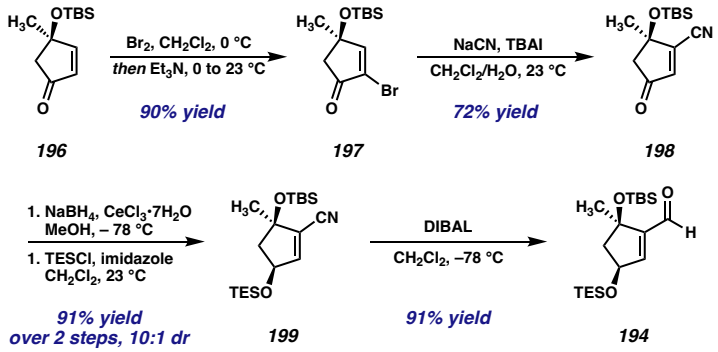

Scheme A9.3.2 *Synthesis of the Sulfone Coupling Partner.*

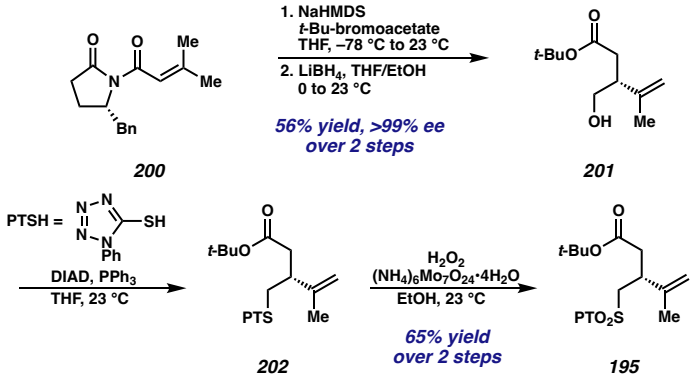

With both coupling partners in hand, we turned our attention to the convergent olefination. Addition of KHMDS to a mixture of sulfone **195** and aldehyde **194** at –78 ºC forged the required C=C bond with >20:1 *E*-selectivity. Deprotection of the 2º and 3º alcohols with TBAF provided diol **203**, setting the stage for 2º alcohol acylation and intramolecular Diels–Alder cycloaddition, which would serve to complete the carbocyclic core. Based on our group's prior efforts with similar esterification reactions,[3,4] we did not anticipate difficulty in the preparation of propiolic ester **193**. Upon treatment of diol **203** with propiolic acid with diisopropylcarbodiimide (DIC) and dimethyl aminopyridine (DMAP), relatively facile conversion to ester **193** occurs, however, our attempts to isolate and purify this intermediate were met with frustration (Scheme A9.3.3). We observed ester

193 spontaneously decomposes after prolonged exposure to silica gel or upon concentration to a neat compound after purification. Consequently, the esterification reaction mixture was quickly passed through a plug of silica gel and the partially purified fractions were added directly into the xylenes solvent for the Diels–Alder reaction. After removal of the residual lower-boiling solvents, the xylenes solution was degassed and heated to 120 ºC to accomplish the Diels–Alder cycloaddition which proceeds in a modest 44% yield. Despite significant efforts to optimize this sequence, including the examination of a variety of propiolic acid surrogates, we were unable to realize a higher-yielding alternative. Fortunately, this convergent sequence still enabled sufficient material throughput to explore our late-stage chemistry.

With access to Diels–Alder product **202**, a three-step oxidation protocol involving alcohol-directed olefin epoxidation, reductive epoxide opening, and oxidation with concomitant olefin migration generated key enone **192**. We initially investigated the diastereoselective 1,2-addition of Grignard reagents to enone **192**, however, these efforts were met with no productive C–C bond formation. Specifically, addition of vinyl magnesium bromide (as a model nucleophile) to a solution of enone **192** in THF led to only recovered enone. We attribute this to the basicity of the Grignard reagent, which, in this case, deprotonates the vinylogous β-ketoester (acidic proton highlighted in red) before 1,2-addition can occur.

Scheme A9.3.3 *Convergent Synthesis of the Core and Failed 1,2-Addition of Grignard Reagents.*

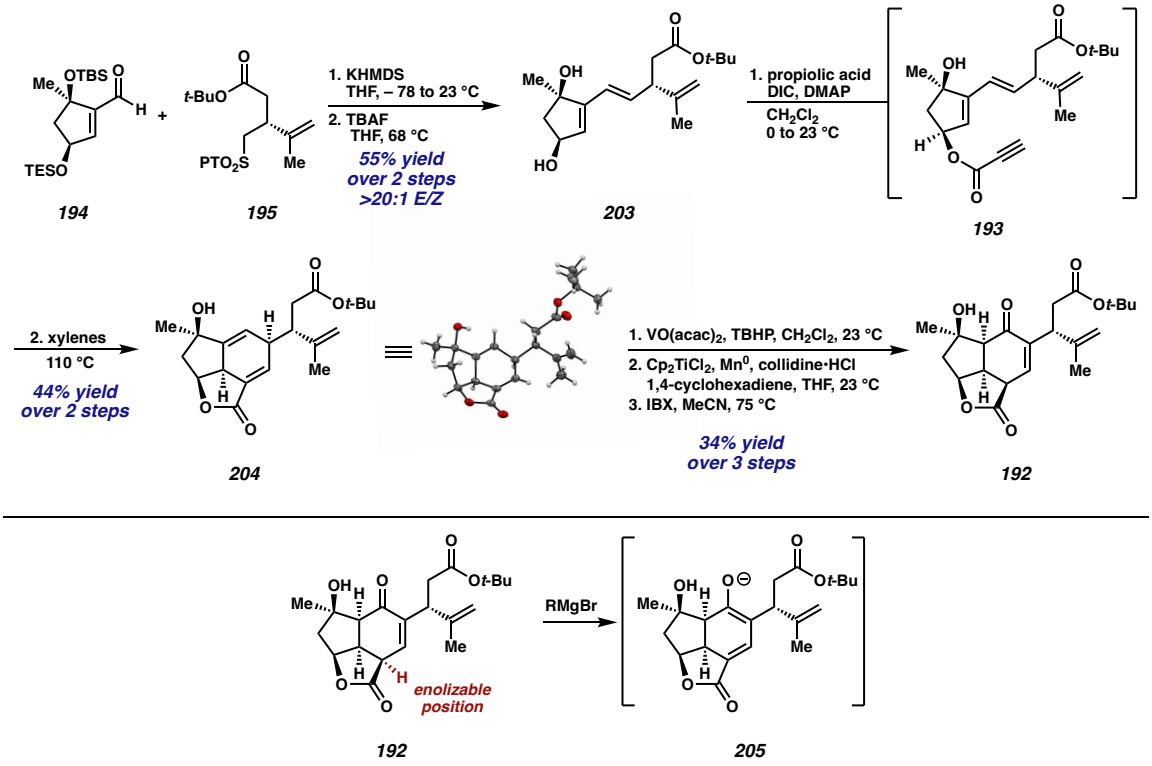

We were pleased to find the required carbon atoms for the spirocyclic lactone could be installed via the Barbier addition of a less basic allyl zinc reagent derived from 3-bromopropenyl acetate (Scheme A9.3.4).[11] Following deacetylation, triol **206** was isolated in 22% yield in >20:1 dr. Unfortunately, we were unable to affect the necessary conversion of the *t*-Bu ester in triol **206** to the methyl ester required for completion of havellockate.

Scheme A9.3.4 *Successful Barbier Addition of an Organozinc Reagent and Failed Conversion to a Methyl Ester.*

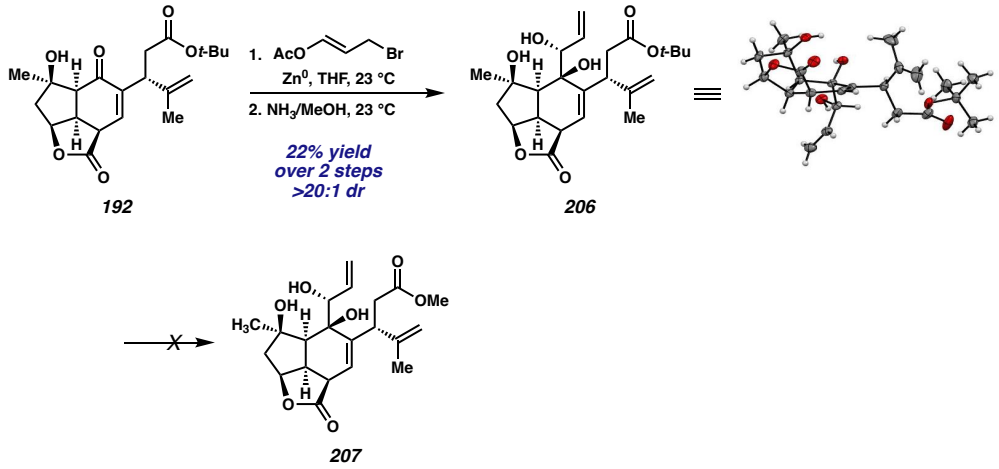

Returning to enone **192**, we found the *t*-Bu ester could be smoothly converted to the required methyl ester in a two-step sequence utilizing formic acid to chemoselectively form the corresponding carboxylic acid which was treated with diazomethane to affect methyl ester formation (Scheme A9.3.5). Methyl ester enone **208** was then subjected to Barbier allylation and deacetylation to afford triol **208** in 20% yield. At this stage in our efforts, the diastereoselectivity and byproducts of this reaction are currently under investigation. Elaboration of the terminal olefin was accomplished via a hydrosilylation/Tamao–Fleming sequence which delivered tetraol **209** in 27% yield. Catalytic Stahl oxidation with concomitant lactonization then afforded havellockate (**191**) which was unambiguously identified via X-Ray crystallographic analysis.

Scheme A9.3.5 *Completion of the Total Synthesis of Havellockate*

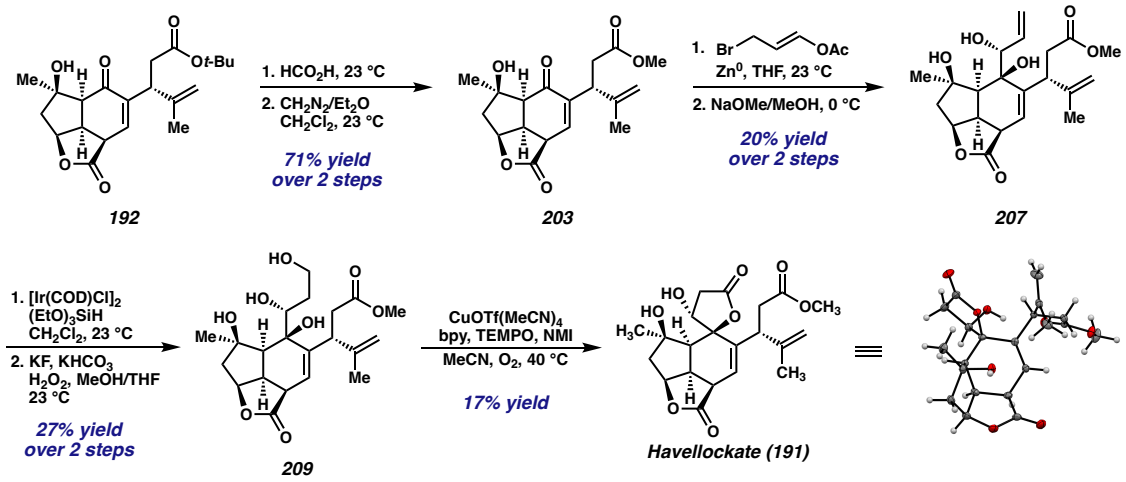

A9.4 CONCLUSION

We have developed the first successful total synthesis of C_{20} cembranoid havellockate. The core was rapidly assembled via a convergent Julia–Kocienski olefination and a subsequent intramolecular Diels–Alder/oxidation sequence previously utilized in our group's total synthesis of (–)-scabrolide A. Following conversion of the *t*-Bu ester to a methyl ester, late-stage installation of the spirocyclic lactone moiety was accomplished via Barbier of the enone core with a functionalized allyl zinc reagent. Finally, a hydrosilylation/Tamao–Fleming oxidation and Stahl oxidation delivered havellockate which was unambiguously identified via X-Ray crystallography. Ongoing efforts are focused on optimizing the synthetic route.

A9.5 REFERENCES AND NOTES

(1) Craig, R. A.; Stoltz, B. M. Polycyclic Furanobutenolide-Derived Cembranoid and Norcembranoid Natural Products: Biosynthetic Connections and Synthetic Efforts. *Chem*. *Rev*. **2017**, *117*, 7878–7909.

(2) Meyer, M. E.; Phillips, J. H.; Ferreira, E. M.; Stoltz, B. M. Use of a palladium(II)-catalyzed oxidative kinetic resolution in synthetic efforts toward bielschowskysin. *Tetrahedron*. **2013**, *69*, 7627–7635.

(3) (a) Craig, R. A.; Roizen, J. L.; Smith, R. C.; Jones, A. C.; Virgil, S. C.; Stoltz, B. M. Enantioselective, convergent synthesis of the ineleganolide core by a tandem annulation cascade. *Chem*. *Sci*. **2017**, *8*, 507–514. (b) Craig, R. A.; Roizen, J. L.; Smith, R. C.; Jones, A. C.; Virgil, S. C.; Stoltz, B. M. Unified Enantioselective, Convergent Synthetic Approach toward the Furanobutenolide-Derived Polycyclic Norcembranoid Diterpenes: Synthesis of a Series of Ineleganoloids by Oxidation State Manipulation of the Carbocyclic Core. *J*. *Org*. *Chem*. **2019**, *84*, 7722–7746. (c) Roizen, J. L.; Jones, A. C.; Smith, R. C.; Virgil, S. C.; Stoltz, B. M. Model Studies to Access the [6,7,5,5]-Core of Ineleganolide Using Tandem Translactonization–Cope or Cyclopropanation–Cope Rearrangements as Key Steps. *J*. *Org*. *Chem* **2017**, *82*, 13051–13067.

(4) Hafeman, N. J.; Loskot, S. A.; Reimann, C. E.; Pritchett, B. P.; Virgil, S. C.; Stoltz, B. M. The Total Synthesis of (–)-Scabrolide A. *J*. *Am*. *Chem*. *Soc*. **2020**, *142*, 8585–8590.

(5) Ammanamanchi, S. R. A; Mukku, J. R. V.; Sarada, P.; Clardy, J.; Lobkovsky, E. Havellockate, A Novel Seco and Spiro Lactone Diterpenoid from the Indian Ocean Soft Coral *Sinularia granosa*. *Tetrahedron Lett*. **1998**, *39*, 139–142.

(6) Tseng, Y.-J.; Ahmed, A. F.; Dai, C.-F.; Chiang, M. Y.; Sheu, J.-H. Sinulochmodins A–C, Three Novel Terpenoids from the Soft Coral *Sinularia lochmodes*. *Org. Lett.* **2005**, *7*, 3813–3816.

(7) Mehta, G.; Kumaran, R. S. Studies towards the total synthesis of novel marine diterpene havellockate. Construction of the tetracyclic core. *Tetrahedron Lett*. **2001**, *42*, 8097–8100.

(8) Beingesser, R. L.; Farand, J. A.; Barriault, L. Progress toward the Total Synthesis of (±)-Havellockate. *J. Org. Chem*. **2010**, *75*, 6337–6346.

(9) Blakemore, P. R.; Milicevic-Sephton, S.; Ciganek, E. The Julia–Kocienski Olefination. *Org. React*. **2018**, *95*, 1–261.

(10) Brill, Z. G.; Grover, H. K.; Maimone, T. J. Enantioselective synthesis of an ophiobolin sesterterpene via a programmed radical cascade. *Science* **2016**, *352*, 1078–1082.

(11) Lombardo, M.; Morganti, S.; Trombini, C. 3-Bromopropenyl Esters in Organic Synthesis: Indium- and Zinc-Mediated Entries to Alk-1-ene-3,4-diols. *J. Org. Chem*. **2003**, *68*, 997–1006.

APPENDIX 10

Synthetic Summary for Appendix 9:

The Total Synthesis of Havellockate

Scheme A10.1 *Synthesis of Aldehyde Fragment* ***194***

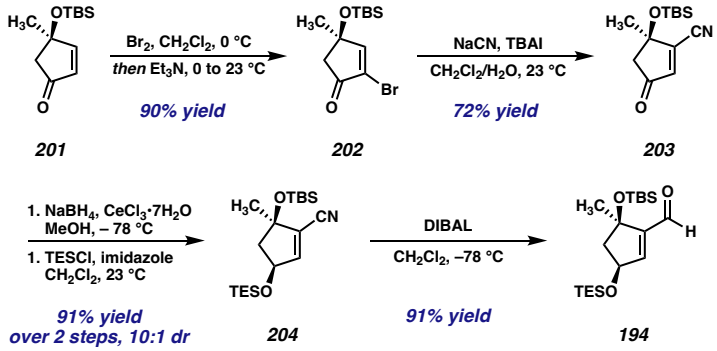

Scheme A10.2 *Synthesis of Sulfone Fragment* ***195***

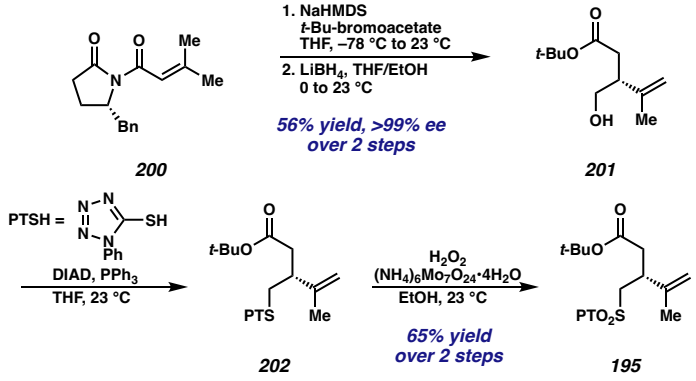

Scheme A10.3 *Convergent Julia–Kocienski Olefination and Total Synthesis of Havellockate*

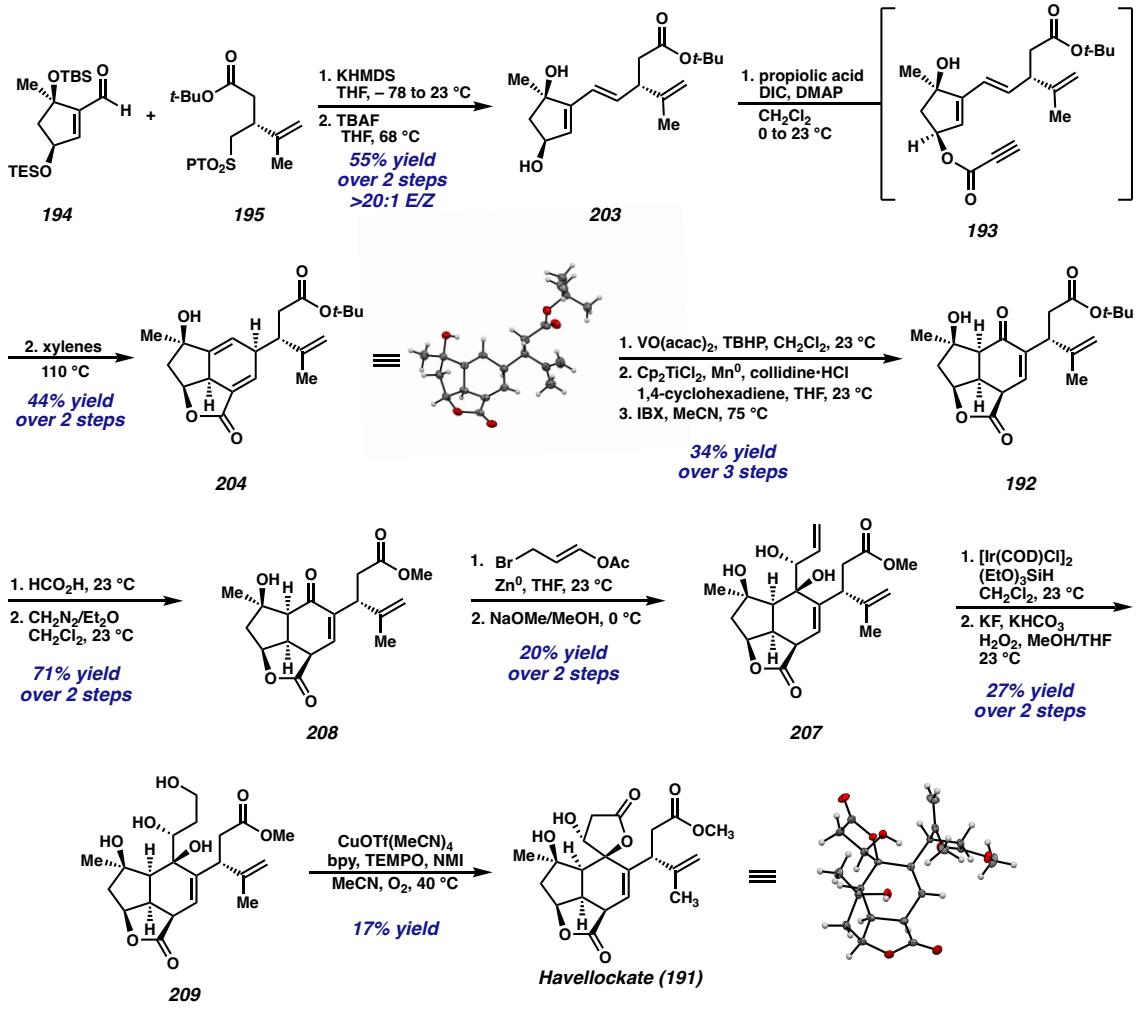

APPENDIX 11

The CryoEM Method MicroED as a Powerful Tool for Small Molecule Structure Determination[†]

A11.1 INTRODUCTION

The history of organic chemistry closely parallels the development of new methods for structural characterization. The earliest studies were driven by melting point determination, and over the past 175 years more complex methods for interrogation of structure have been developed. Techniques such as polarimetry,[1] UV-vis,[2] and infrared spectroscopy,[3] coupled with electron paramagnetic resonance,[4] vibrational circular dichroism,[5] circular dichroism,[6] and mass spectrometry[7] have been commonly employed over the years, dramatically expanding our ability to assign structures. In the past 50 years, however, the explosion of NMR spectroscopy[8] and the accompanying abundance of individual NMR experiments have produced a wealth of detailed structural information for organic chemists. Indeed, NMR is a mainstay in chemistry and the most predominant method employed in both routine synthetic experiments and in advanced structural elucidation of complex small molecules. In the current state-of-the-art, only single crystal X-ray diffraction holds a higher place in terms of precision, producing unequivocal

[†]This research was performed in collaboration with Christopher G. Jones, Michael W. Martynowycz, and Johan Hattne. Portions of this chapter have been reproduced with permission from Jones, C. G.; Martynowycz, M. W.; Hattne, J.; Fulton, T. J.; Stoltz, B. M.; Rodriguez, J. A.; Nelson, H. M.; Gonen, T. *ACS Cent. Sci.* **2018**, *11*, 1587–1592.

structural information about the position, orientation, connectivity, and placement of individual atoms and bonds within a given molecule.

For decades, small molecule X-ray analysis has been the definitive tool for structural analysis.[9] This technique, however, is not within limitations. The process is considered by many an *art*, where the production of high-quality crystals suitable for X-ray diffraction requires uncodified "tricks of the trade" as well as a certain amount of luck! Additionally, even after a substance has been crystallized, there is no guarantee that the particular crystal form will be amenable to X-ray diffraction. Since crystal growth is both a slow and arduous process, X-ray diffraction has not been an effective tool for rapid, on-the-fly structural determination of small molecules. For this reason, X-ray diffraction is generally not implemented as a routine analytical tool for the practicing organic chemist, despite the fact that the structural data provided are far superior to any other characterization method to date.

In this study, we employed the recently developed electron cryo-microscopy (cryoEM) method microcrystal electron diffraction (MicroED)[10] to address the long standing need for fast and reliable structure determination in organic chemistry. Recently, electron diffraction was used to solve the structure of a methylene blue derivative, although no scope studies were undertaken to allow the reader to assess the applicability of the of the methodology.[11] Moreover, a specialized detector was used for their experiments, limiting the broad adaptability of their approach to the wider synthetic community.[11] We demonstrate that with minimal sample preparation and experiment time, simple powders and seemingly amorphous materials (in some cases, solids isolated *via* silica gel chromatography and rotary evaporation) could be directly used in MicroED studies,

leading to rapid, high quality structural elucidation of several classes of complex molecules with atomic resolution, in many cases below 1 Å. Moreover, we utilize a commercially available microscope that is already in use at universities around the world. MicroED has the potential to dramatically accelerate and impact the fields of synthetic chemistry, natural product chemistry, drug discovery, and many others by delivering rapid, high resolution atomic structures of complex, small molecules with minimal sample preparation or formal crystallization procedures.

A11.2 RESULTS AND DISCUSSION

The applicability of MicroED was initially tested on the naturally occurring steroid progesterone (**1**) as a model system (Figure A11.2.1). The sample was obtained as a powder from chemical supplier Preparations Laboratories Inc. (we estimate the bottle to be more than 20 years old). Small quantities of the seemingly amorphous solid were transferred directly from the bottle on to a glass cover slides and ground between another slide to produce a fine powder. The powder was then deposited on a holey carbon-copper grid, cooled to liquid nitrogen temperatures, and transferred to a cryo electron microscope operating at an acceleration voltage of 200 kV (Thermo Fisher Talos Arctica). An overview of the preparation is shown in Figure A11.2.1. Upon imaging, thousands of nano crystals were easily discernable on the grid surface providing ample nanocrystals to investigate for diffraction. Typically, for samples such as these, the vast majority of nano crystals diffracted to ~1 Å resolution or better. Through continuous rotation of the sample stage, 140 degrees of diffraction data could be collected from a single nano crystal[12] while the improved autoloader and piezo stage of the Talos Arctica allowed us to travel through the zero degree point without introducing errors in crystal position. Typically, the stage was

rotated at 0.5 degrees per second and an entire data set was collected in less than 3 minutes as a movie using a bottom mount CetaD CMOS detector fitted with a thick scintillator for diffraction studies. Software developed from previous studies was used to convert the initially diffraction movie frames into SMV format for expeditious processing in the readily available XDS software package commonly used for X-ray crystallography.[13] By collecting data from just a single nanocrystal, the structure of steroid **210** was resolved to an impressive 1 Å resolution. The entire process, from bottle to structure, was easily accomplished in less than 30 minutes.

Figure A11.2.1 *The Process of Applying MicroED to Small Molecule Structural Analysis.*

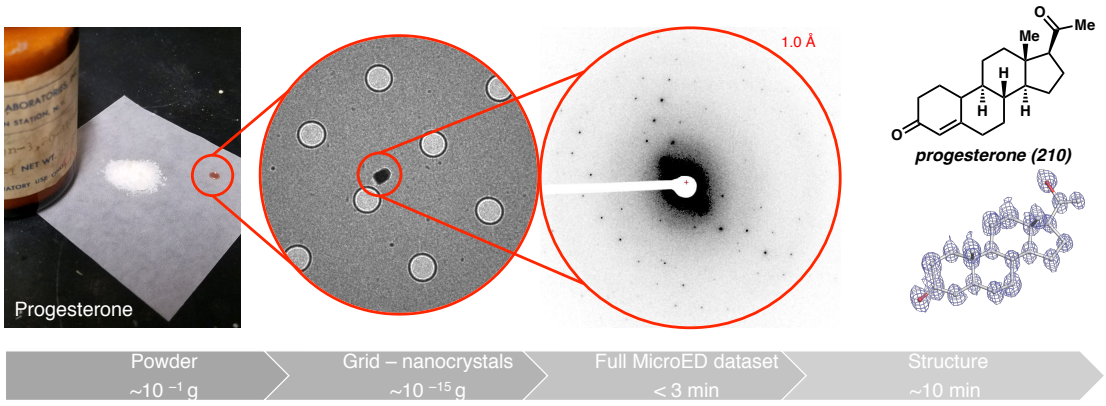

Encouraged by these results, we wanted to investigate a wide range of natural products to fully explore the scope and applicability of this powerful structural determination method for small molecules (Figure A11.2.2A). The Talos Arctica was particularly amenable to our studies as it is capable of storing up to 12 different samples at once, providing effortless swapping of sample grids for rapid investigation of multiple compounds. Once a reliable sample prep routine had been established, over-the-counter medications were purchased from local pharmacies for investigation. Tablets of CVS-

branded acetaminophen and Kroger-branded ibuprofen were crushed using a mortar and pestle and the ground powder was placed on EM grids as described above. Despite the heterogeneity of such pharmaceuticals, which typically include a multitude of coatings, binders, and other formulation agents, we were astonished to obtain such clearly resolved atomic resolution structures of both acetaminophen (**211**) and ibuprofen (**212**) in rapid succession. Just as impressively, structures of the sodium channel blocker carbamazepine (**213**) and the macrocyclic polypetide antibiotic thiostrepton (**220**) were also determined from seemingly amorphous powders used as received from Sigma-Aldrich. We went on to further study several commercially available natural products and derivatives. Once again, compounds were used as received, without any crystallization, to yield atomic resolution structures of biotin (**214**), ethisterone (**215**), cinchonine (**216**), and brucine (**217**). Of the eleven different commercial bioactives examined, all eleven yielded processable MicroED data. Of those eleven compounds, ten were amenable to rapid structure determination by direct methods,[14] while one was determined by molecular replacement.[15] As mentioned previously, all structures were obtained without any crystallization attempts or chemical modifications to compounds examined. While these pharmaceutical and commercial natural products were likely recrystallized for purification purposes by the manufacturer, the powders examined by MicroED possessed nano crystals a billionth the size (~100 nm) of crystals typically needed for X-ray crystallography. This was powder to structure.

Next, we decided to investigate compounds that were never crystallized, but instead were purified by flash column chromatography. Since silica gel chromatography is the most common method of purification in early-stage research for complex molecules in drug discovery, natural product isolation efforts, and synthesis efforts in general, we were interested to see whether solid samples prepared in such a way would be amenable to analysis by MicroED. Four compounds, purified by chromatographic methods, were collected from our laboratories and samples of these seemingly amorphous solids were analyzed. Here, two of four compounds diffracted, yielding atomic resolution structures at or below 1 Å (**218** and **213**, Figure A11.2.2A and B). While the success rate for these compounds was 50%, it is worthy to note that no crystallization procedures were employed in the isolation of these materials. Notably, (+)-limaspermadine (**218**), an alkaloid natural product synthesized by our labs,[16] was resolved from a residue of only milligram quantities of material following flash chromatography and rotary evaporation from a scintillation vial (Figure A11.2.2B). Furthermore, while it is extremely challenging to observe protons in X-ray structures, electrons interact with matter more strongly than X-rays and are affected by charge making them relatively common to observe in MicroED data.[17] For all structures resolved from our samples, at least some, if not most protons could be observed on the molecule In particular, the density maps obtained for limaspermidine (**218**) and carbamazepine (**213**) after refinement showed protons associated with almost all atoms in these molecules (Figure A11.2.2C).

Figure A11.2.2 *Different Types of Small Molecule Structures Solved by MicroED. A) Several Pharmaceuticals, Vitamins, Commercial Natural Products and Synthetic Samples Resolved through MicroED. B) Example of an Amorphous Film Utilized in this Study Leading to 1 Å Resolution Data. C) Protons Could be Observed for Several Compounds through MicroED. Green Spheres are Fo-Fc maps Showing Positive Density Belonging to Hydrogen Atoms of the Molecule.*

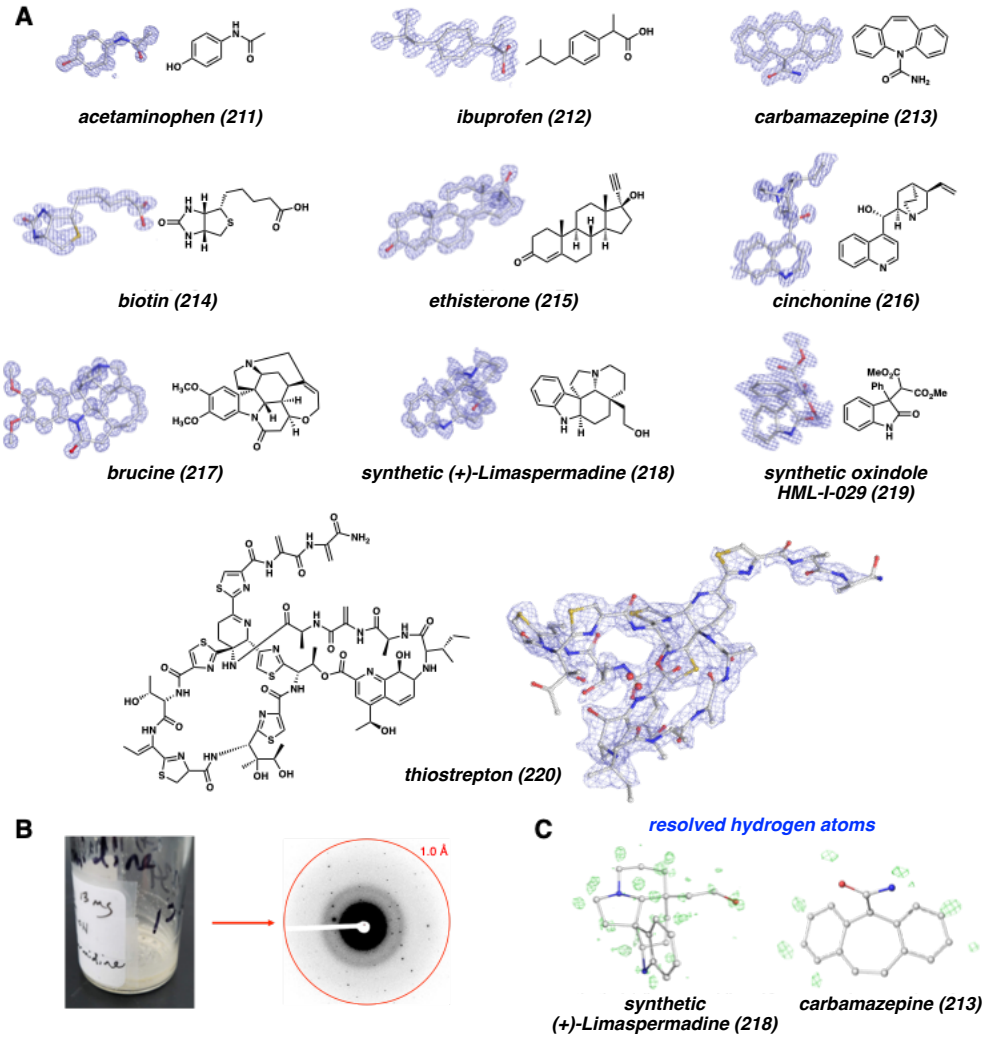

Astounded by the ease with which such high-quality data was obtained and the apparent generality of MicroED to small molecules, we undertook studies to examine heterogeneous samples (mixtures of compounds). In the case of heterogeneous samples, single crystal X-ray diffraction precludes the study of mixtures and NMR is poorly suited for this task. For this experiment, mixtures of four compounds (**213**, **214**, **216** and **217**, *cf.* Figure A11.2.3) were crushed together and deposited on a holey carbon grid. Several crystal forms belonging to the different compounds in the mixture were visually identified on the grids (Fig. 3). MicroED data was collected from several nano crystals and the identity of each species was resolved within minutes by confirmation of unit cell parameters as determined through XDS. After compound identification, atomic resolution structures could be rapidly determined for all small molecules present in the mixture (Figure A11.2.3).

Figure A11.2.3 *Identification of Compounds from Heterogeneous Mixtures.*

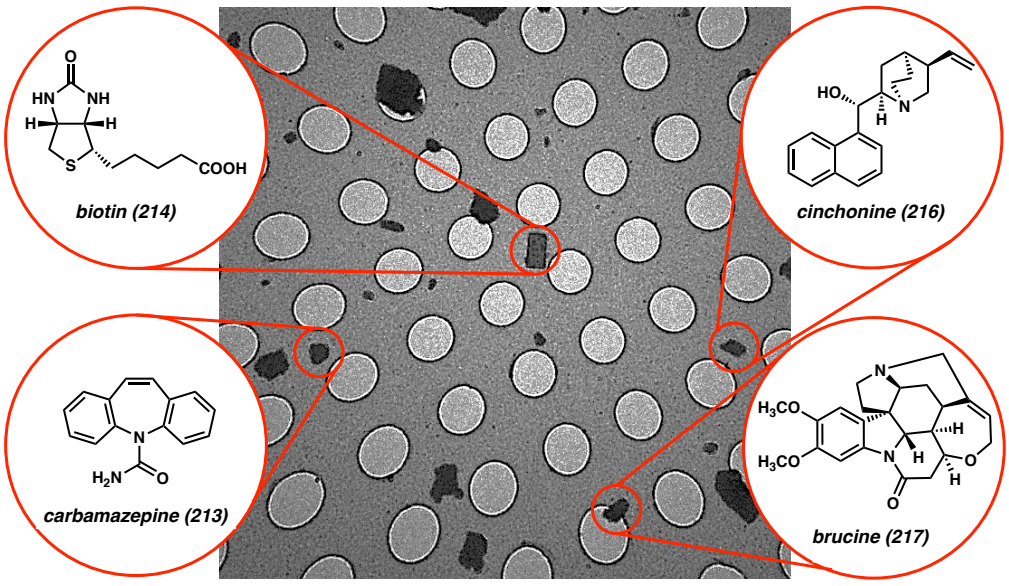

A11.3 CONCLUSION

The results described here introduce a powerful new characterization tool into the organic chemist's toolbox. While MicroED was initially developed for structure determination of biological material such as proteins in a frozen, hydrated state[18] we demonstrate that cross pollination of macromolecular structural methods of cryoEM are powerful tools for chemical synthesis, drug characterization, and drug discovery. Prior to this work, MicroED has allowed for the structural charaterizarion of several proteins from crystals which had generally been unsuitable for X-ray crystallography due to their small size or morphologies**Error! Bookmark not defined.**,[19]. Despite this success, the MicroED method has largely gone unnoticed in the small molecule communities. Based on our findings, we anticipate that MicroED will be enthusiastically received by many types of small molecule chemists in both academia and industry. Here we have shown that a variety of seemingly amorphous solid materials can lead to rapid atomic resolution structure determination by MicroED with little or no additional sample preparation or crystallization. The fact that a solid film in a flask, following solvent removal from a flash chromatography purification, can lead to an atomic resolution molecular structure, is evidence that MicroED will likely have a profound effect on the structural characterization work-flow of organic chemists. Although the past 50 years have seen huge advances in the state-of-the-art, no completely new techniques have been introduced that alter the routine structural interrogation of organic substances. NMR[8], IR[3], UV-Vis[2], and X-ray diffraction[9] have been routinely in place since the 1960's and are still utilized today as the most common methods for structure determination in chemistry. We believe that electron diffraction is potentially the next big

advance in the field and are enthusiastic about the prospects of expanding its utility as a routine analytical technique for chemists.[20,21]

A11.4 REFERENCES AND NOTES

(1) Schreier, P.; Bernreuther, A.; Huffer, M.; *Analysis of Chiral Organic Molecules: Methodology and Applications*; Walter de Gruyter" Berlin, 2011.

(2) Scott, A. I. *Interpretation of the Ultraviolet Spectra of Natural Products: International Series of Monographs on Organic Chemistry*; Elsevier: Amsterdam, 2013; Vol. 7.

(3) Coates, J. Interpretation of infrared spectra, a practical approach. In *Encyclopedia of Analytical Chemistry: Applications, Theory, and Instrumentation*; Meyers, R. A., Ed.; Wiley: New York, 2000; Vol. *12*, pp 10815–10837.

(4) Dougherty, D. A. Spin control in organic molecules. *Acc*. *Chem*. *Res*. **1991**, *24*, 88–94.

(5) Stephens, P. J.; Devlin, F. J.; Pan, J. J. The determination of the absolute configurations of chiral molecules using vibrational circular dichroism (VCD) spectroscopy. *Chirality* **2008**, *20*, 643–663.

(6) Berova, N.; Bari, L. D.; Pescitelli, G. Application of electronic circular dichroism in configurational and conformational analysis of organic compounds. *Chem. Soc. Rev*. **2007**, *36*, 914−931.

(7) De Hoffmann, E. Mass spectrometry. In *Kirk Othmer Encyclopedia of Chemical Technology*; John Wiley & Sons: New York, 2000.

(8) Günther, H. *NMR Spectroscopy: Basic Principles, Concepts and Applications in Chemistry*; John Wiley & Sons: New York, 2013.

(9) Dunitz, J. D. *X-ray Analysis and the Structure of Organic Molecules;* Verlag Helvetica Chimica Acta: Zürich, 1995.

(10) Shi, D.; Nannenga, B. L.; Iadanza, M. G.; Gonen, T. Three-dimensional electron crystallography of protein microcrystals. *eLife* **2013**, *2*, e01345.

(11) Gruene, T.; Wennmacher, J. T. C.; Zaubitzer, C.; Holstein, J. J.; Heidler, J.; Fecteau-Lefebvre, A.; De Carlo, S.; Müller, E.; Goldie, K. N.; Regeni, I.; Li, T.; Santiso-Quinones, G.; Steinfeld, G.; Handschin, S.; van Genderen, E.; van Bokhoven, J. A.; Clever, G. H.; Pantelic, R. Rapid structure determination of microcrystalline molecular com- pounds using electron diffraction. *Angew. Chem. Int. Ed.* **2018**, *57*, 16313–16317.

(12) Nannenga, B. L.; Shi, D.; Leslie, A. G. W.; Gonen, T. High-resolution structure determination by continuous-rotation data collection in MicroED. *Nat. Methods* **2014**, *11*, 927−930.

(13) Hattne, J.; Reyes, F. E.; Nannenga, B. L.; Shi, D.; de la Cruz, M. J.; Leslie, A. G. W.; Gonen, T. MicroED data collection and processing. *Acta Crystallogr., Sect. A: Found. Adv*. **2015**, *71*, 353−360.

(14) Sheldrick, G. SHELXT - Integrated space-group and crystal-structure determination. *Acta Crystallogr., Sect. A: Found. Adv*. **2015**, *71*, 3−8.

(15) Vagin, A.; Teplyakov, A. MOLREP: an Automated Program for Molecular Replacement. *J. Appl. Crystallogr*. **1997**, *30*, 1022−1025.

(16) Pritchett, B. P.; Donckele, E. J.; Stoltz, B. M. Enantioselective Catalysis Coupled with Stereodivergent Cyclization Strategies Enables Rapid Syntheses of (+)-Limaspermidine and (+)-Kopsihainanine A. *Angew. Chem., Int. Ed.* **2017**, *56*, 12624−12627.

(17) (a) Henderson, R. The potential and limitations of neutrons, electrons and X-rays for atomic resolution microscopy of unstained biological molecules. *Q. Rev. Biophys.* **1995**, *28*, 171−193. (b) Vergara, S.; Lukes, D. A.; Martynowycz, M. W.; Santiago, U.; Plascencia-Villa, G.; Weiss, S. C.; de la Cruz, M. J.; Black, D. M.; Alvarez,M.M.;Lopẹz-Lozano,X.;Barnes,C.O.;Lin,G.;Weissker, H.-C.; Whetten, R. L.; Gonen, T.; Yacaman, M. J.; Calero, G. MicroED Structure of Au146(p-MBA)57 at Subatomic Resolution Reveals a Twinned FCC Cluster. *J. Phys. Chem. Lett.* **2017**, *8*, 5523− 5530. (c) Rodriguez, J. A.; Ivanova, M. I.; Sawaya, M. R.; Cascio, D.; Reyes, F. E.; Shi, D.; Sangwan, S.; Guenther, E. L.; Johnson, L. M.; Zhang, M.; Jiang, L.; Arbing, M. A.; Nannenga, B. L.; Hattne, J.; Whitelegge, J.; Brewster, A. S.; Messerschmidt, M.; Boutet, S.; Sauter, N. K.; Gonen, T.; Eisenberg, D. S. Structure of the toxic core of alpha-synuclein from invisible crystals. *Nature* **2015**, *525*, 486−490. (d) Sawaya, M. R.; Rodriguez, J.; Cascio, D.; Collazo, M. J.; Shi, D.; Reyes, F. E.; Hattne, J.; Gonen, T.; Eisenberg, D. S. Ab initio structure determination from prion nanocrystals at atomic resolution by MicroED. *Proc. Natl. Acad. Sci. U. S. A.* **2016**, *113*, 11232−11236. (e) Hattne, J.; Shi, D.; Glynn, C.; Zee, C.-T.; Gallagher-Jones, M.; Martynowycz, M. W.; Rodriguez, J. A.; Gonen, T. Analysis of Global and Site-Specific Radiation Damage in Cryo-EM. *Structure* **2018**, *26*, 759−766.

(18) (a) de la Cruz, M. J.; Hattne, J.; Shi, D.; Seidler, P.; Rodriguez, J.; Reyes, F. E.; Sawaya, M. R.; Cascio, D.; Weiss, S. C.; Kim, S. K.; Hinck, C. S.; Hinck, A. P.; Calero, G.; Eisenberg, D.; Gonen, T. Atomic resolution structures from fragmented protein crystals by the cryoEM method MicroED. *Nat. Methods* **2017**, *14*, 399−402. (b) Nannenga, B. L.; Shi, D.; Hattne, J.; Reyes, F. E.; Gonen, T. Structure of catalase determined by MicroED. *eLife* **2014**, *3*, e03600.

(19) Gallagher-Jones, M.; Glynn, C.; Boyer, D. R.; Martynowycz, M. W.; Hernandez, E.; Miao, J.; Zee, C.-T.; Novikova, I. V.; Goldschmidt, L.; McFarlane, H. T.; Helguera, G. F.; Evans, J. E.; Sawaya, M. R.; Cascio, D.; Eisenberg, D. S.; Gonen, T.; Rodriguez, J. A. Sub-ångstrom cryo-EM structrure of a prion protofibril reveals a polar clasp. *Nat. Struct. Mol. Biol*. **2018**, *25*, 131−134.

(20) Martynowycz, M. W.; Gonen, T. From electron crystallography of 2D crystals to MicroED of 3D crystals. *Curr. Opin. Colloid Interface Sci*. **2018**, *34*, 9−16.

(21) Nannenga, B. L.; Gonen, T. Protein structure determination by MicroED. *Curr. Opin. Struct. Biol.* **2014**, *27*, 24−31.

APPENDIX 12

Characterization of Reactive Organometallic Species via MicroED[†]

A11.1 INTRODUCTION

For over a century, crystallography has fueled developments in modern chemistry. Within the chemical enterprise, crystallography has played a particularly special role in organometallic chemistry. Here, NMR-silent nuclei, paramagnetic spin, diversity of bonding and coordination environments, and poor reactivity profiles hinder the application of many solution-state characterization techniques. However, the need for carefully prepared single crystals with dimensions on the order of 0.1 mm^3 can also limit the application of X-ray crystallography. Moreover, neutron diffraction can be limited by the requirement of even larger crystals (~0.5 mm^3) and incompatibility with boron-containing compounds, as a result of destructive nuclear reactions.[1] Electron diffraction, as opposed to X-ray diffraction, offers several benefits, primarily the ability to circumvent the need for such large crystals for successful structural analysis of molecular compounds. Since earlier work by Kolb et al.[2] and Mugnaioli et al.[3] to adapt 3D electron diffraction techniques for structural analysis, several studies using a variety of electron diffraction techniques have been employed to structurally characterize inorganic and organic−inorganic hybrid

[†]This research was performed in collaboration with Christopher G. Jones, Matthew Asay, Lee Joon Kim, Jack F. Kleinsasser, Ambarneil Saha, Kevin R. Berkley, Dulio Cascio, Andrey G. Malyutin, and Matthew, P. Conley. Portions of this chapter have been reproduced with permission from Jones, C. G.; Asay, M.; Kim, L. J.; Kleinsasser, J. F.; Saha, A.; Fulton, T. J.; Berkley, K. R.; Cascio, D.; Malyutin, A. G.; Conley, M. P.; Stoltz, B. M.; Lavallao, V.; Rodríguez, J. A.; Nelson, H. M. *ACS Cent. Sci*. **2019**, *5*, 1507–1513.

materials such as metal organic frameworks.[4–10] Although these studies demonstrate power of such techniques, we aim to adapt this method as a routine structural characterization tool for inorganic and organometallic chemists who often rely on traditional X-ray analysis as their primary means of characterization for highly reactive and unstable compounds. Here we employ the electron diffraction technique MicroED under ambient temperature using a 300 keV TEM to structurally characterize several organometallic compounds, reactive intermediates, and transition-metal coordination complexes, which are of interest to the practicing chemist and are often employed as catalytic reagents for a variety of important synthetic transformations. Despite there being several different methods for the collection of electron diffraction data, we found that the continuous rotation technique used for MicroED is readily implemented on currently available instruments, and data obtained from this method is easily processed using standard, freely available, crystallographic software.[11] The MicroED method itself, which has typically been employed for large macromolecular structure analysis, is often performed under cryogenic conditions to preserve the hydration state of such biomolecules. However, prior studies have shown that by leveraging sensitive detectors, it is possible to use low electron doses to collect diffraction for small molecule structure determination under ambient temperatures, even for compounds that are particularly beam sensitive.[12–15] Using ambient temperature MicroED, we successfully resolved the first crystal structure of the privileged hydrozirconation reagent chloridobis(η^5cyclopentadienyl)hydridozirconium, colloquially known as Schwartz's reagent, which was obtained from bulk powder utilized as purchased and determined by direct methods. We also report the ab initio structure of a Pd(II) 1,2-dipallidated alkyl species, obtained as a precipitant from the reaction mixture of ethylene

with a pseudo-low-coordinate Pd(I) dimer. As a demonstration of the broad applicability of MicroED, we also determine the structures of five other transition-metal complexes.

A12.2 RESULTS AND DISCUSSION

Having recently reported the application of the CryoEM method MicroED to determine structures of several complex organic molecules,[16] we now evaluated the facility with which MicroED could interrogate complex organometallic species. We were particularly interested in chemical entities that failed to yield structures by conventional structural elucidation methods—crystallography or solution-state characterization. We first interrogated the structure of chloridobis(η5cyclopentadienyl)hydridozirconium **221** (Figure A12.2.1A),[17] a well known industrial catalyst colloquially referred to as Schwartz's reagent. Schwartz's reagent sees widespread use in modern organic synthesis and is useful for a number of unique transformations mediated via hydrozirconation intermediates.[18–20] However, despite its synthetic relevance and the countervailing fact that half a century has transpired since Wailes and Weigold first discovered this species,[21,22] no single crystal structure of this canonical zirconocene complex has been obtained. This gap in crystallographic data has been attributed to the low solubility of the complex in hydrocarbon and ethereal solvents and its reactivity with polar chlorinated solvents,[23] precluding its crystallization and hindering NMR studies. As such, the currently accepted structure of Schwartz's reagent, a centrosymmetric dimer doubly linked by two bridging hydride ligands, represents a reconstruction from a combination of FTIR spectroscopy,[21,22] solid-state ^{35}Cl NMR studies,[24] and X-ray diffraction of related complexes.[25] To confirm this inferred structure, we subjected commercially acquired Schwartz's reagent to ambient temperature MicroED. Continuous-rotation data was collected from three crystals at

ambient temperature (ca. 23 °C), using a low flux 300 keV electron beam (e.g., below 0.01 $e^{-}/Å^2$ per second) and a TVIPS XF-416 camera in rolling shutter mode (Figure A12.2.3B). The resulting diffraction was reduced and merged to obtain a high-completeness (90.6%) data set resolved at 1.15 Å. The room temperature Schwartz's structure was then determined ab initio by direct methods and refined to reveal the expected centrosymmetric dimer. Importantly, refinement proceeded smoothly and required no ex post facto corrections, calculations, or molecular replacement procedures.[26] The structure with riding hydrogens on the cyclopentadienyl ligands refined with anisotropic displacement parameters to an R1 value of 14.9%. Critically, we had already observed suggestive regions of electron density consistent with bridging hydrides in the initial difference Fourier map (Figure A12.2.1B). To trace this more explicitly, we tracked peaks in the screened Coulomb potential within the unit cell, representing atomic locations. A sampling of consecutive two-dimensional slices in real space along the a-axis at the central mirror plane, which runs orthogonal to the cyclopentadienyl rings but bisects the zirconium, chlorine, and hydrogen atoms (Figure A12.2.1C) shows two hydrides emerging from the void space of the noise floor, thus corroborating the hydride positions observed during structural refinement (Figure A12.2.1D).

Figure A12.2.1 *Determination of the Structure of Schwartz's Reagent via MicroED.*

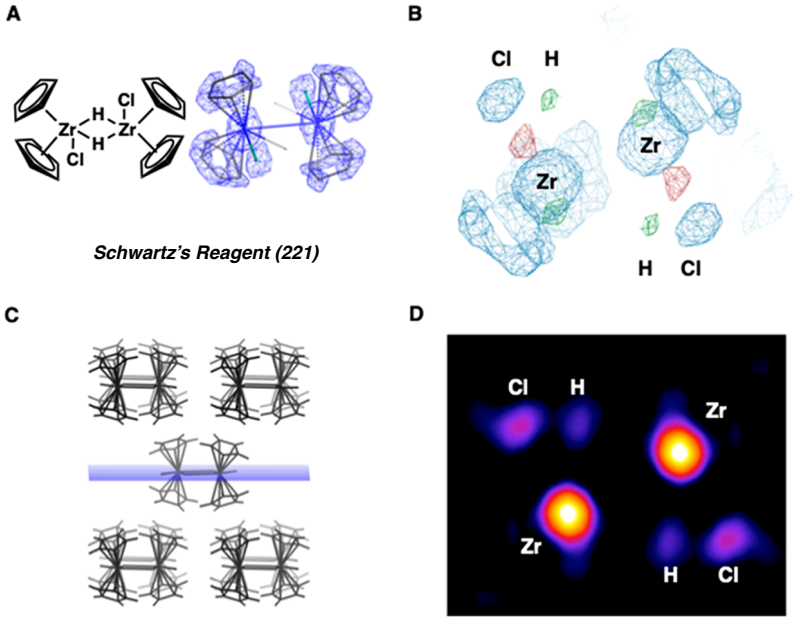

Concurrent to our study of the application of MicroED to organometallic species, we sought to apply this powerful technique to active research problems in our groups including the reactivity of dimeric Pd(I) complexes. Dimeric palladium(I) species featuring Pd−Pd bonds have been previously reported to react with a variety of small molecules to give homolytic cleavage[27] or insertion products.[28] Pd(I) dimer **222** (Figure A12.2.2), synthesized by thermolysis or UV irradiation of the methyl palladium phosphine precursor,[29] was fully characterized by single crystal XRD (Figure A12.2.2B) and multinuclear NMR. To study the reactivity of this species (2), a THF solution was treated with ethylene gas, which interestingly led to a dramatic color change and precipitation of a yellow solid (Figure A12.2.2A). Efforts to characterize this solid, however, were frustrated by the lack of solubility and fragile nature of the putative ethylene adduct, as treatment of the precipitant with a variety of crystallization and/or NMR solvents led to rapid gas release and reformation of starting material **222**. Typically, such physical

properties of a reactive intermediate would preclude definitive structural characterization. The yellow precipitate was instead taken directly from the reaction mix and deposited on an EM grid for characterization by MicroED. Remarkably, under high magnification, the apparently amorphous solid proved to have nanocrystalline domains. Diffraction movies were reduced to yield a high-completeness data set that produced an ab initio solution, which during refinement led to the definitive structural assignment of the species as the unexpected oxidative insertion product **223**. Such ethylene insertion products have been reported but remain rare.[30–32] This structure features two Pd(II) phosphine moieties linked by the reduced ethylene linker (Figure A12.2.2C, D). The extended linker precludes ipso-π-arene interactions of the phosphines, and therefore, one equivalent of THF completes the coordination sphere of each palladium center. The solid-state $^{13}C\{^{1}H\}$ cross-polarization magic angle spinning (CPMAS) NMR spectrum of **223** contains a signal at 37 ppm assigned to the reduced ethylene fragment. The $^{11}B\{^{1}H\}$ and $^{31}P\{^{1}H\}$ CPMAS NMR spectroscopy are also consistent with the structure of **223** obtained from microED measurements. These NMR spectra also demonstrate the homogeneity of the sample.

Figure A12.2.2 *MicroED and X-Ray Crystallographic Structures of Pd-species* ***222*** *and* ***223****.*

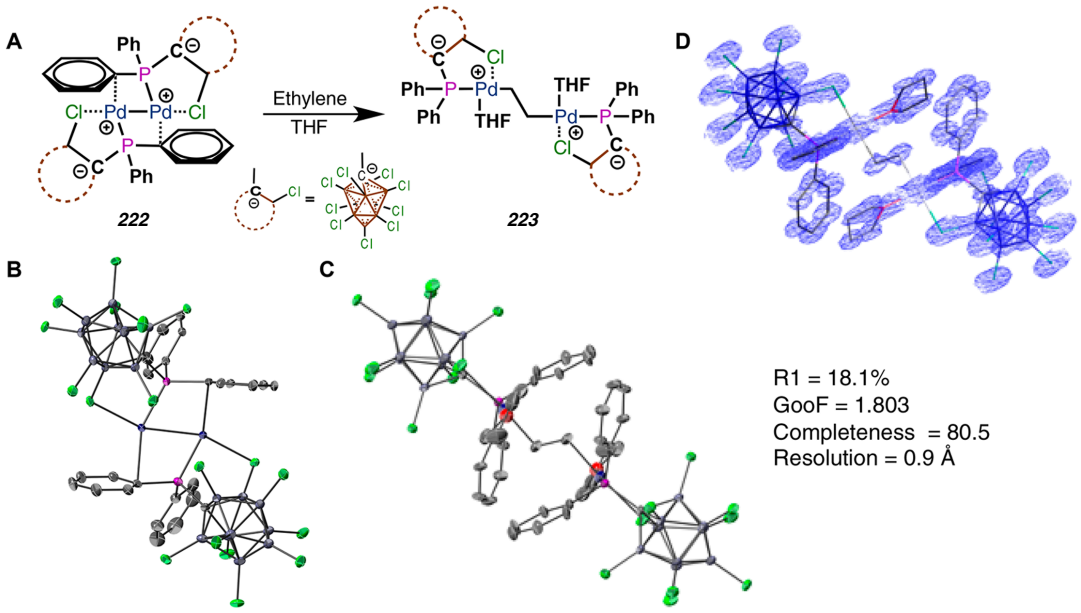

To establish the generality of our approach we went on to determine structures of five additional commonly used organometallic compounds and transition-metal coordination complexes (Figure A12.2.3). The structures of tris(acetylacetonato)iron(III) [$Fe(acac)_3$](**224**), benzylidene-bis(tricyclohexylphosphino)-dichlororuthenium (Grubbs' first generation catalyst) (**225**), [1,1-bis(diphenylphosphino)ferrocene]dichloronickel(II) (**226**), Pd(dibenzylideneacetone)((S)-4-tert-butyl-2-[2-(diphenylphosphino)phenyl]-2-oxazoline) (Pd(dba)(PHOX)) (**226**), and carbonyl(hydrido)tris (triphenylphosphane)rhodium(I) [$HRh(CO)(PPh_3)_3$] (**227**), (Figure A12.2.3A), were all determined using direct methods from data collected at noncryogenic temperatures. Together, this set of molecular structures demonstrates the utility of ambient temperature electron diffraction for the study of transition metal complexes. Bulk powders of these compounds were analyzed by MicroED as described above, and data collected from one or

more crystals were merged resulting in the assignment of space group and unit cell parameters that closely matched published values for XRD structures of these compounds, with the exception of compounds **226** and **227**, which are new polymorphs.[33,36] For a direct comparison, electron diffraction structures of compounds **224**, **225**, and **228** were overlaid with previously reported X-ray structures.[37,39] Rootmean-square (RMS) values were calculated based on the deviation of atomic position resulting in RMS values of 0.0514, 0.1311, 0.1733 Å and a maximum deviation of 0.1140, 0.2270, and 0.3289 Å for compounds 4, 5, and 8, respectively (Figure A12.2.4). On the basis of the overlaid structures, the position of the observed hydride in the case of the Rh−H complex (**225**) is both geometrically and symmetrically consistent with the published X-ray crystallographic data with a deviation of 0.164 Å.[40] Although the published structures of these compounds are associated with lower statistical errors in general, our ambient temperature MicroED structures were determined from bulk powders (i.e., no formal recrystallization) and maintain sufficiently accurate statistical parameters (Figure A12.2.3C) to unambiguously characterize the connectivity of these compounds. These considerations render electron diffraction a powerful alternative for structural determination of transition metal hydride structures. Several previous studies use electron diffraction data for the determination of hydrogen atom positions[41−44] in metal hydrides, which are capable of exhibiting different chemical, electronic, and bonding properties in comparison to typical hydrogen atoms, and thus, the current quality of electron diffraction data obtained in this study does not allow for their unambiguous placement with high-enough precision to facilitate accurate discussion of bond lengths and angles. Although collecting data in continuous-rotation mode helps reduce dynamical scattering, residual dynamical scattering present in the data

limits the accuracy of refinements based on a kinematical scattering approximation, and therefore, bond distances derived in this way can potentially be chemically inconsistent.[45] This problem has been well-analyzed by several other groups including Palatinus et al., who have used dynamical refinement on electron diffraction data collected in precession mode to help reduce statistical errors in atomic placement and bonding.[43,45,46,47] It is expected that such statistics of hydride localization as well as bond lengths and angles for all atomic constituents will improve with subsequent amelioration of microscopes and detectors. Furthermore, improvements in refinement software such as Jana, which has previously been used for processing of precession data, may now allow the possibility of applying dynamical refinements to continuous-rotation data, further reducing statistical error.[42,43]

Figure A12.2.3 *Structures Determined by Ambient Temperature MicroED.*

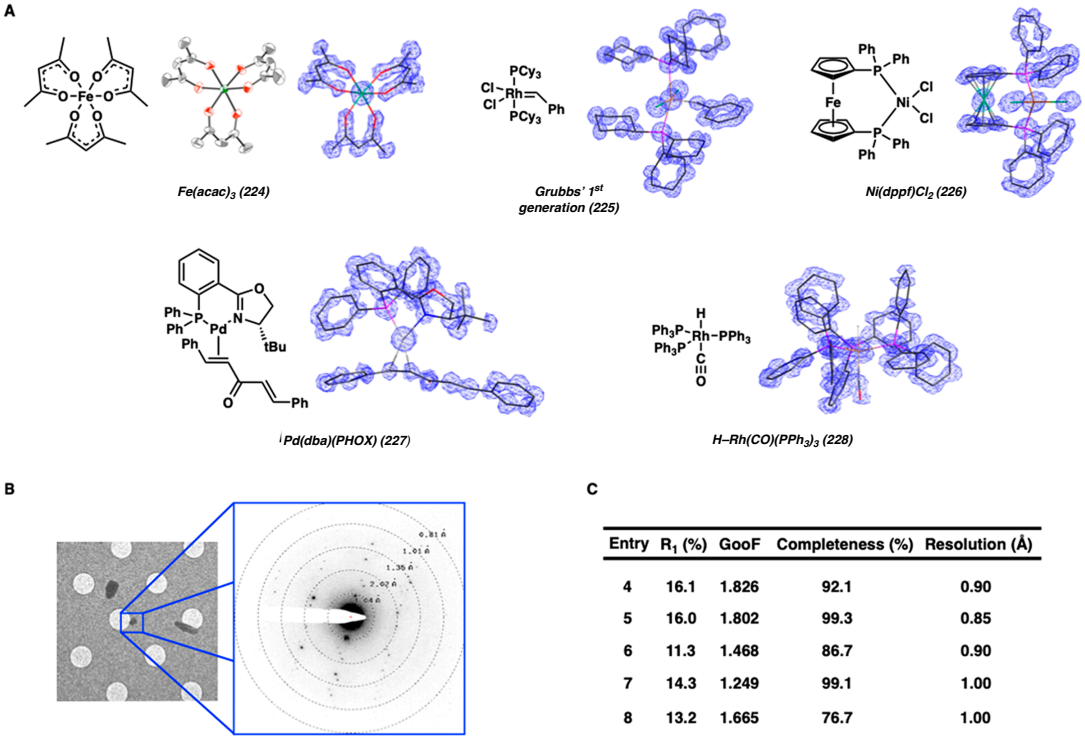

Entry	R_1 (%)	GooF	Completeness (%)	Resolution (Å)
4	16.1	1.826	92.1	0.90
5	16.0	1.802	99.3	0.85
6	11.3	1.468	86.7	0.90
7	14.3	1.249	99.1	1.00
8	13.2	1.665	76.7	1.00

Figure A12.2.4 *Overlay of Ambient Temperature ED (red) and Previously Reported X-Ray Diffraction (blue) Structures.*

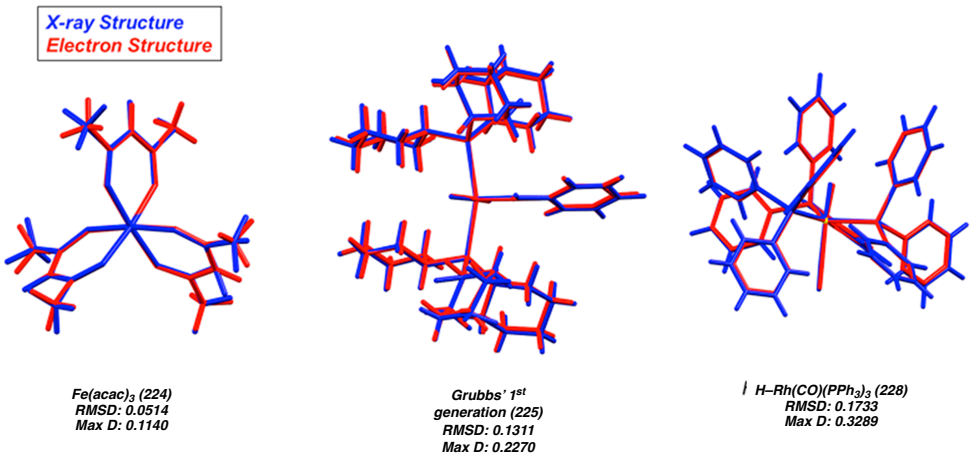

A12.3 CONCLUSION

Ambient temperature electron diffraction is an advantageous step toward the routine determination of organometallic species and potentially applicable to a wide array of small molecule organometallic and inorganic solids. The ability to routinely solve structures from nanocrystalline material and unambiguously determine the position of all atoms, including historically challenging hydrides attached to heavy atoms, presents chemists with a potent tool for the broad identification and characterization of elusive, but relevant, complexes. Armed with this method, we have determined structures of a diverse series of organometallic compounds and transition-metal coordination complexes, including those obtained from both commercial and laboratory synthesis. Importantly, each of these structures was determined ab initio by direct methods and refined using methods common to XRD. Our application of ambient temperature MicroED to the structure determination of Schwartz's reagent, obtained directly from the commercial seemingly

amorphous powder, highlights the power of this new approach. Despite the importance of this molecule in synthetic chemistry, no previous high-resolution crystal structures have been obtained, as a result of the seemingly amorphous nature of the white powder obtained by precipitation during its preparation. Our ambient temperature MicroED structure not only confirms the dimeric nature of the reagent but more remarkably identifies the likely locations of bridging hydrides that are visible in electrostatic potential maps and can be refined freely. This method also allows for the determination of an unusual Pd(II) intermediate that was not amenable to structure determination by solution-state NMR or single crystal X-ray diffraction. Moreover, neutron diffraction would be incompatible with this compound because of destructive boron neutron capture nuclear reactions. Importantly, although several protein structures have been determined by MicroED using molecular replacement, and structures of small molecules and polypeptides of known connectivity have been determined from MicroED data via direct methods, the reported Pd(II) complex (**223**) is a rare example of a novel complex small molecule identified by MicroED without prior knowledge of the structure or other corroborating solution-state spectroscopic methods. Although our data does not facilitate extensive discussions of bond lengths or angles because of higher-thanexpected statistical errors in refinement compared to traditional XRD, the fact that cryogenic temperatures are not required to obtain structural information from reactive metal complexes is ground-breaking, as many research institutions can make rapid use of readily available TEM facilities. Moreover, utilization of a more sensitive and faster detector, with shorter dead-time,[11] reduces peak overlap between frames as well. Ambient temperature measurements also dramatically simplify sample preparation and loading, eliminating issues typically associated with cryogenic

cooling that often complicate crystal screening and data collection (e.g., ice deposition). We envision that microelectron diffraction will continue to improve and find new applications in the molecular sciences. Efforts directed toward a multitude of new frontiers in small molecule electron diffraction are already underway. These efforts are expected to bring new horizons for small molecule structure determination over the coming months and years.

A12.4 REFERENCES AND NOTES

(1) Nedunchezhian, K.; Aswath, N.; Thiruppathy, M.; Thirugnanamurthy, S. Boron neutron capture therapy- A literature review. *J. Clin. Diagn. Res*. **2016**, *10*, ZE01−ZE04.

(2) Kolb, U.; Gorelik, T.; Kubel, C.; Otten, M. T.; Hubert, D. Towards automated diffraction tomography: Part I — Data acquisition. *Ultramicroscopy* **2007**, *107*, 507−513.

(3) Mugnaioli, E.; Gorelik, T.; Kolb, U. “Ab initio” structure solution from electron diffraction data obtained by a combination of automated diffraction tomography and precession technique. *Ultramicroscopy* **2009**, *109*, 758−765.

(4) Portoles-Gil, N.; Lanza, A.; Aliaga-Alcalde, N.; Ayllon, J. A.; Gemmi, M.; Mugnaioli, E.; Lopez-Periago, A. M.; Domingo, C. Crystalline curcumin bioMOF obtained by precipitation in supercritical CO_2 and structural determination by electron diffraction tomography. *ACS Sustainable Chem. Eng.* **2018**, *6*, 12309−12319.

(5) Yuan, S.; Qin, J.-S.; Xu, H.-Q.; Su, J.; Rossi, D.; Chen, Y.; Zhang, L.; Lollar, C.; Wang, Q.; Jiang, H.-L.; Son, D. H.; Xu, H.; Huang, Z.; Zou, X.; Zhou, H.-C. $[Ti_8Zr_2O_{12}(COO)_{16}]$ cluster: An ideal inorganic building unit for photoactive metal−organic frameworks. *ACS Cent. Sci*. **2018**, *4*, 105−111.

(6) Denysenko, D.; Grzywa, M.; Tonigold, M.; Streppel, B.; Krkljus, I.; Hirscher, M.; Mugnaioli, E.; Kolb, U.; Hanss, J.; Volkmer, D. Elucidating gating effects for hydrogen sorption in MFU-4-type triazolate-based metal−organic frameworks featuring different pore sizes. *Chem.- Eur. J.* **2011**, *17*, 1837−1848.

(7) Feyand, M.; Mugnaioli, E.; Vermoortele, F.; Bueken, B.; Dieterich, J. M.; Reimer, T.; Kolb, U.; de Vos, D.; Stock, N. Automated diffraction tomography for the structure elucidation of twinned, sub-micrometer crystals of a highly porous, catalytically active bismuth metal−organic framework. *Angew. Chem. Int. Ed.* **2012**, *51*, 10373−10376.

(8) Wang, B.; Rhauderwiek, T.; Inge, A. K.; Xu, H.; Yang, T.; Huang, Z.; Stock, N.; Zou, X. A porous cobalt tetraphosphonate metal− organic framework: Accurate structure and guest molecule location determined by continuous-rotation electron diffraction. *Chem.- Eur. J.* **2018**, *24*, 17429−17433.

(9) Bellussi, G.; Montanari, E.; Di Paola, E.; Millini, R.; Carati, A.; Rizzo, C.; O'Neil Parker, W., Jr.; Gemmi, M.; Mugnaioli, E.; Kolb, U.; Zanardi, S. ECS-3: A crystalline hybrid organic−inorganic aluminosilicate with open porosity. *Angew. Chem. Int. Ed.* **2012**, *51*, 666−669.

(10) Yun, Y.; Zou, X.; Hovmoller, S.; Wan, W. Three-dimensional electron diffraction as a complementary technique to powder X-ray diffraction for phase identification and structure solution of powders. *IUCrJ* **2015**, *2*, 267−282.

(11) Gemmi, M.; La Placa, M. G. I.; Galanis, A. S.; Rauch, E. F.; Nicolopoulos, S. Fast electron diffraction tomography. *J. Appl. Crystallogr.* **2015**, *48*, 718−727.

(12) Gorelik, T. E.; van de Streek, J.; Kilbinger, A. F. M.; Brunklaus, G.; Kolb, U. Ab-initio crystal structure analysis and refinement approaches of oligo p-benzamides based on electron diffraction data. *Acta Crystallogr., Sect. B: Struct. Sci*. **2012**, *68*, 171−181.

(13) van Genderen, E.; Clabbers, M. T. B.; Das, P. P.; Stewart, A.; Nederlof, I.; Barentsen, K. C.; Portillo, Q.; Pannu, N. S.; Nicolopoulos, S.; Gruene, T.; Abrahams, J. P. Ab initio structure determination of nanocrystals of organic pharmaceutical compounds by electron diffraction at room temperature using a Timepix quantum area direct electron detector. *Acta Crystallogr., Sect. A: Found. Adv*. **2016**, *72*, 236−242.

(14) Das, P. P.; Mugnaioli, E.; Nicolopoulos, S.; Tossi, C.; Gemmi, M.; Galanis, A.; Borodi, G.; Pop, M. M. Crystal structures of two important pharmaceuticals solved by 3D precession electron diffraction tomography. *Org. Process Res. Dev.* **2018**, *22*, 1365−1372.

(15) Das, P. P.; Mugnaioli, E.; Nicolopoulos, S.; Tossi, C.; Gemmi, M.; Galanis, A.; Borodi, G.; Pop, M. M. Crystal structures of two important pharmaceuticals solved by 3D precession electron diffraction tomography. *Org. Process Res. Dev*. **2018**, *22*, 1365−1372. (16) Jones, C. G.; Martynowycz, M. W.; Hattne, J.; Fulton, T. J.;

Stoltz, B. M.; Rodriguez, J. A.; Nelson, H. M.; Gonen, T. The cryoEM method microED as a powerful tool for small molecule structure determination. *ACS Cent. Sci*. **2018**, *4*, 1587−1592.

(17) Hart, D. W.; Schwartz, J. Hydrozirconation. Organic synthesis via organozirconium intermediates. Synthesis and rearrangement of alkylzirconium(IV) complexes and their reaction with electrophiles. *J. Am. Chem. Soc.* **1974**, *96*, 8115−8116.

(18) Schwartz, J.; Labinger, J. A. Hydrozirconation: A new transition metal reagent for organic synthesis. *Angew. Chem., Int. Ed.* **1976**, *15*, 333−340.

(19) Wieclaw, M. M.; Stecko, S. Hydrozirconation of C = X functionalities with Schwartz's reagent. *Eur. J. Org. Chem*. **2018**, *2018*, 6601−6623.

(20) Pinheiro, D. L. J.; de Castro, P. P.; Amarante, G. W. Recent developments and synthetic applications of nucleophilic zirconocene complexes from Schwartz's reagent. *Eur. J. Org. Chem.* **2018**, *2018*, 4828−4844.

(21) Kautzner, B.; Wailes, P. C.; Weigold, H. Hydrides of bis(cyclopentadienyl)zirconium. *J. Chem. Soc. D* **1969**, 1105a.

(22) Wailes, P. C.; Weigold, H. Hydrido complexes of zirconium I. Preparation. *J. Organomet. Chem.* **1970**, *24*, 405−411.

(23) Takahashi, T.; Suzuki, N.; Jayasuriya, N.; Wipf, P. Chlorobis(cyclopentadienyl)hydridozirconium. *Encyclopedia of Reagents for Organic Synthesis* **2006**.

(24) Rossini, A. J.; Mills, R. W.; Briscoe, G. A.; Norton, E. L.; Geier, S. J.; Hung, I.; Zheng, S.; Autschbach, J.; Schurko, R. W. Solid-state chlorine NMR of group IV

transition metal organometallic complexes. *J. Am. Chem. Soc.* **2009**, *131*, 3317−3330.

(25) Harlan, C. J.; Bott, S. G.; Barron, A. R. Methyl−hydride metathesis between [Zr(cp)2Me2] and [HAl(μ3-NBut)]4: molecular structures of [Me1-xHxAl(μ3-NBut)]4 (x = 0, 0.78 or 1) and [(cp)2ZrMe(μ-H)]2 (cp = η5-C5H5). *J. Chem. Soc., Dalton Trans.* **1997**, 637−642.

(26) The appropriate electron scattering factors were used; see: Peng, L. M. Electron atomic scattering factors and scattering potentials of crystals. *Micron* **1999**, *30*, 625−648.

(27) Fafard, C. M.; Adhikari, D.; Foxman, B. M.; Mindiola, D. J.; Ozerov, O. V. Addition of ammonia, water, and dihydrogen across a single Pd−Pd bond. *J. Am. Chem. Soc.* **2007**, *129*, 10318−10319.

(28) Huacuja, R.; Graham, D. J.; Fafard, C. M.; Chen, C.-H.; Foxman, B. M.; Herbert, D. E.; Alliger, G.; Thomas, C. M.; Ozerov, O. V. Reactivity of a Pd(I)−Pd(I) dimer with O_2: monohapto Pd superoxide and dipalladiumperoxide in equilibrium. *J. Am. Chem. Soc.* **2011**, *133*, 3820−3823.

(29) Kleinsasser, J. F.; Reinhart, E. D.; Estrada, J.; Jordan, R. F.; Lavallo, V. Ethylene oligomerization and polymerization by palladium(II) methyl complexes supported by phosphines bearing a perchlorinated 10-vertex closo-carborane anion substituent. *Organometallics* **2018**, *37*, 4773−4783.

(30) Hetterscheid, D. G. H.; Kaiser, J.; Reijerse, E.; Peters, T. P. J.; Thewissen, S.; Blok, A. N. J.; Smits, J. M. M.; de Gelder, R.; de Bruin, B. Ir^{II}(ethene): Metal or carbon radical? *J. Am. Chem. Soc.* **2005**, *127*, 1895−1905.

(31) Van Voorhees, S. L.; Wayland, B. B. Formation of metallo hydride, formyl, and alkyl complexes of Rh(TMTAA). *Organometallics* **1987**, *6*, 204−206.

(32) Huacuja, R. Synthesis and reactivity of unusual palladium (II) complexes supported by a diarylamido/BIS(phosphine) PNP pincer ligand. Ph.D. Dissertation, Texas A&M University, 2014; available electronically from http://hdl.handle.net/1969.1/152457.

(33) Weng, S.-S.; Ke, C.-S.; Chen, F.-K.; Lyu, Y.-F.; Lin, G.-Y. Transesterification catalyzed by iron(III) β-diketonate species. *Tetrahedron* **2011**, *67*, 1640−1648.

(34) Torker, S.; Muller, A.; Sigrist, R.; Chen, P. Tuning the steric properties of a metathesis catalyst for copolymerization of norbornene and cyclooctene toward complete alternation. *Organometallics* **2010**, *29*, 2735−2751.

(35) Casellato, U.; Ajo, D.; Valle, G.; Corain, B.; Longato, B.; Graziani, R. Heteropolymetallic complexes of 1,1'-bis(diphenylphosphino) ferrocene (dppf). II. Crystal structure of dppf and NiCl2(dppf). *J. Crystallogr. Spectrosc. Res*. **1988**, *18*, 583−590.

(36) Sherden, N. H.; Behenna, D. C.; Virgil, S. C.; Stoltz, B. M. Unusual allylpalladium carboxylate complexes: identification of the resting state of catalytic enantioselective decarboxylative allylic alkylation reactions of ketones. *Angew. Chem. Int. Ed*. **2009**, *48*, 6840−6843.

(37) Trnka, T. M. Catalyst for olefin metathesis: ruthenium alkylidene complexes with phosphine and N-heterocyclic ligands. Ph.D. Dissertation, California Institute of Technology, Pasadena, CA, 2002.

(38) Iball, J.; Morgan, C. H. A refinement of the crystal structure of ferric acetylacetonate. *Acta Crystallogr.* **1967**, *23*, 239−244.

(39) La Placa, S. J.; Ibers, J. A. Crystal and molecular structure of tritriphenylphosphine rhodium carbonyl hydride. *Acta Crystallogr.* **1965**, *18*, 511−519.

(40) Babra, I. S.; Morley, L. S.; Nyburg, S. C.; Parkins, A. W. The crystal and molecular structure of a new polymorph of carbonylhydridotris(triphenylphosphine)rhodium(I) having a Rh–H stretching absorption at 2013 cm^{-1}. *J. Crystallogr. Spectrosc. Res.* **1993**, *23*, 997−1000.

(41) Mugnaioli, E.; Gemmi, M. Single-crystal analysis of nanodomains by electron diffraction tomography: mineralogy at the orderdisorder borderline. Z. *Kristallogr.-Cryst. Mater*. **2018**, *233*, 163−178.

(42) Hynek, J.; Brazda, P.; Rohlícek, J.; Londesborough, M. G. S.; Demel, J. Phosphinic acid based linkers: Building blocks in metal− organic framework chemistry. *Angew. Chem. Int. Ed.* **2018**, *57*, 5016–5019.

(43) Palatinus, L.; Brazda, P.; Boullay, P.; Perez, O.; Klementova, M.; Petit, S.; Eigner, V.; Zaarour, M.; Mintova, S. Hydrogen positions in single nanocrystals revealed by electron diffraction. *Science* **2017**, *355*, 166−169.

(44) Clabbers, M. T. B.; Gruene, T.; van Genderen, E.; Abrahams, J. P. Reducing dynamical electron scattering reveals hydrogen atoms. *Acta Crystallogr., Sect. A: Found. Adv*. **2019**, *75*, 82−93.

(45) Palatinus, L.; Jacob, D.; Cuvillier, P.; Klementova, M.; Sinkler, W.; Marks, L. D. Structure refinement from precession electron diffraction data. *Acta Crystallogr., Sect. A: Found. Crystallogr.* **2013**, *69*, 171−188.

(46) Palatinus, L.; Petricek, V.; Correa, C. A. Structure refinement using precession electron diffraction tomography and dynamical diffraction: theory and implementation. *Acta Crystallogr., Sect. A: Found. Adv.* **2015**, *71*, 235−244.

(47) Palatinus, L.; Correa, C. A.; Steciuk, G.; Jacob, D.; Roussel, P.; Boullay, P.; Klementova, M.; Gemmi, M.; Kopecek, J.; Domeneghetti, M. C.; Camara, F.; Petricek, V. Structure refinement using precession electron diffraction tomography and dynamical diffraction: tests on experimental data. *Acta Crystallogr., Sect. B: Struct. Sci., Cryst. Eng. Mater.* **2015**, *71*, 740−751.

APPENDIX 13

Notebook Cross-Reference for New Compounds

Table A13.1 *Notebook Cross-Reference for Chapter 1*

Compound	^{1}H NMR (instrument)	^{13}C NMR (instrument)	Yield/Procedure
4	TJF-IX-263A file: TJF-IX-myrifabralA (FID)	TJF-IX-263A file: TJF-IX-myrifabralA (Florence)	TJF-IX-263
5	TJF-IX-271A (FID)	TJF-IX-271A (Florence)	TJF-IX-271A
6	TJF-III-065A (Indy)	TJF-III-065A (Florence)	TJF-III-065A
7	TJF-V-147 (Indy)	TJF-V-147 (Florence)	TJF-V-147
8	TJF-III-229 (Indy)	TJF-III-229 (Florence)	TJF-V-239
11	TJF-IV-259A (Indy)	TJF-IV-259A (Florence)	TJF-IV-259A
14	TJF-IX-183A (Indy)	TJF-IX-183A (Florence)	TJF-IX-183,185
16	TJF-III-155A (Indy)	TJF-III-155 (Florence)	TJF-III-195

Figure A13.2 *Notebook Cross-Reference for Chapter 2*

Compound	^{1}H NMR (instrument)	^{13}C NMR (instrument)	Yield/Procedure
19a	EJA-VIII-205-sm (Indy)	EJA-VIII-205-sm (florence)	XX
19b	TJF-V-033A_proton2 (Indy)	TJF-V-033A_carbon (florence)	TJF-V-033
19c	TJF-V-031A_proton (Indy)	TJF-V-031A_carbon (florence)	TJF-V-031
19d	TJF-V-029A_proton_2 (Indy)	TJF-V-029A_carbon2 (florence)	TJF-V-029
19e	EJA-VIII-057 (Indy)	EJA-VIII-057 (florence)	EJA-VIII-057
19f	EJA-VIII-059 (Indy)	EJA-VIII-059 (florence)	EJA-VIII-059
19g	EJA-VIII-067 (Indy)	EJA-VIII-067 (florence)	EJA-VIII-067
19h	EJA-VIII-073 (Indy)	EJA-VIII-073 (florence)	EJA-VIII-073
19i	TJF-IV-177A_proton (Indy)	TJF-IV-177A_carbon (florence)	TJF-IV-177
19j	TJF-IV-199A_proton2 (Indy)	TJF-IV-199A_carbon (florence)	TJF-IV-199
19k	EJA-VIII-065-2 (Indy)	EJA-VIII-065 (florence)	EJA-VIII-065
19l	TJF-IV-191A_proton (Indy)	TJF-IV-191A_carbon (florence)	TJF-IV-191
19m	TJF-IV-197A_proton (Indy)	TJF-IV-197A_carbon (florence)	TJF-IV-197
19n	EJA-VIII-121 (Indy)	EJA-VIII-121 (florence)	.
19o	EJA-VIII-147 (Indy)	EJA-VIII-147 (florence)	EJA-VIII-147
20a	TJF-IV-153A_proton (Indy)	TJF-IV-153A_carbon (Indy)	EJA-VIII-205
20b	TJF-V-035A_proton (Indy)	TJF-V-035A_carbon (florence)	TJF-V-035A
20c	TJF-V-035C_proton (Indy)	TJF-V-035C_carbon (florence)	TJF-V-035C
20d	TJF-V-035B (Indy)	TJF-V-035B (florence)	TJF-V-035B
20e	TJF-IV-217D_proton (Indy)	TJF-IV-217D_carbon (florence)	TJF-IV-217D
20f	TJF-IV-227A(217E) proton (Indy)	TJF-IV-227A_carbon (florence)	TJF-IV-227A
20g	TJF-IV-227B_proton (Indy)	TJF-IV-227B_carbon (florence)	TJF-IV-227B
20h	TJF-IV-217B_proton2 (Indy)	TJF-IV-217B_carbon (florence)	TJF-IV-217B
20i	TJF-IV-217G_proton (Indy)	TJF-IV-217G_carbon (florence)	TJF-IV-217G
20j	TJF-IV-217A_proton (Indy)	TJF-IV-217A_carbon (florence)	TJF-IV-217A
20k	TJF-IV-217C_proton (Indy)	TJF-IV-217C_carbon (florence)	TJF-IV-217C
20l	TJF-IV-217I_proton (Indy)	TJF-IV-217I_carbon (florence)	TJF-IV-217I
20m	TJF-IV-217H_proton (Indy)	TJF-IV-217H_carbon (florence)	TJF-IV-217H
20n	TJF-V-035D_proton (Indy)	TJF-V-035D_carbon (verona)	TJF-V-035D
20o	TJF-V-035E_proton (Indy)	TJF-V-035E_carbon (verona)	TJF-V-035E

Figure A13.3 *Notebook Cross-Reference for Chapter 2 (continued)*

Compound	^{1}H NMR (instrument)	^{13}C NMR (instrument)	Yield/Procedure
21	EJA-VIII-213-2 (HG3)	EJA-VIII-213-2 (florence)	EJA-VIII-213
22	EJA-VIII-215 (florence)	EJA-VIII-215 (florence)	EJA-VIII-215
23	TJF-V-123cr (Indy)	TJF-V-123A_carbon (florence)	TJF-V-123
24	TJF-V-121A (florence)	TJF-V-121A (florence)	TJF-V-121
25	EJA-VII-285 (Indy)	EJA-VII-285 (florence)	EJA-VII-285
26	EJA-VIII-047-col (Indy)	EJA-VIII-047 (florence)	EJA-VIII-047
27	EJA-VIII-051 (Indy)	EJA-VIII-051 (florence)	EJA-VIII-051
28	EJA-VIII-055 (Indy)	EJA-VIII-055 (florence)	EJA-VIII-055
29	TJF-IV-071A_proton_hv3 (Indy)	TJF-IV-071A_carbon (florence)	TJF-IV-071A
30	EJA-VIII-119 (Indy)	EJA-VIII-119 (florence)	EJA-VIII-119
31	EJA-VIII-137 (Indy)	EJA-VIII-137 (florence)	EJA-VIII-137
32	EJA-VIII-069 (Indy)	EJA-VIII-069 (florence)	EJA-VIII-069
33	TJF-IV-169A_proton (Indy)	TJF-IV-196A (misnamed) (florence)	TJF-IV-169
34	TJF-IV-187A_proton (Indy)	TJF-IV-187A_carbon (florence)	TJF-IV-187
35	EJA-VIII-043 (Indy)	EJA-VIII-043 (florence)	EJA-VIII-061,043
36	TJF-IV-293A (Indy)	TJF-IV-295_carbon (florence)	TJF-IV-295
37	TJF-V-025A (Indy)	TJF-V-025_carbon (florence)	TJF-V-025
38	TJF-IV-293A_proton (Indy)	TJF-V-293_carbon (misnamed) (florence)	TJF-IV-293
39	TJF-IV-069crystal	TJF-IV-069crystal	TJF-IV-069
40	TJF-IV-185_char (Indy)	TJF-IV-185_char (florence)	TJF-IV-185
41	TJF-IV-189A_proton (Indy)	TJF-IV-189A_carbon (florence)	TJF-IV-189
L2	TJF-IV-195A_proton3 (Indy)	TJF-IV-195A_carbon (florence)	TJF-IV-195

Figure A13.4 *Notebook Cross-Reference for Chapter 3*

Compound	^{1}H NMR (instrument)	^{13}C NMR (instrument)	Yield/Procedure
42a	TJF-VI-253A	TJF-VI-253A	TJF-VI-253
42b	TJF-VI-253B	TJF-VI-253B	TJF-VI-253
42c	TJF-VI-253D	TJF-VI-253D	TJF-VI-253
42d	TJF-VI-253E	TJF-VI-253E	TJF-VI-253
42e	TJF-VI-253C	TJF-VI-253C	TJF-VI-253
42f	TJF-VI-253J	TJF-VI-253J	TJF-VI-253
42g	TJF-VI-253H	TJF-VI-253H	TJF-VI-253
42h	TJF-VI-253F	TJF-VI-253F	TJF-VI-253
42i	TJF-VI-253G	TJF-VI-253G	TJF-VI-253
(Z)-19a	BW-II-023A (florence)	BW-II-023A (florence)	BW-II-023
53	TJF-VI-217A (florence)	TJF-VI-217A (florence)	TJF-VI-217
54	TJF-VI-235A (florence)	TJF-VI-235A (florence)	TJF-VI-235
55	TJF-VI-213A (florence)	TJF-VI-213A (florence)	TJF-VI-213
56	TJF-VI-215A (florence)	TJF-VI-215A (florence)	TJF-VI-215
57	TJF-VI-219	TJF-VI-219	TJF-VI-219
58	BW-II-027 (florence)	BW-II-027 (florence)	BW-II-027
59	TJF-VI-237A	TJF-VI-237A	TJF-VI-237
60	TJF-VI-227	TJF-VI-227	TJF-VI-227
61	TJF-VI-171A (florence)	TJF-VI-171A (florence)	TJF-VI-171A
L4	TJF-VI-179A(florence) (misnamed)	TJF-VI-179A(florence) (misnamed)	TJF-VI-177
L3	TJF-VI-187A (florence)	TJF-VI-187A (florence)	TJF-VI-187

Figure A13.5 *Notebook Cross-Reference for Chapter 4*

Compound	^{1}H NMR (instrument)	^{13}C NMR (instrument)	Procedure
75	EJA-X-245-2 (Indy)	TJF-VIII-163A (florence)	TJF-VIII-163
76a	TJF-VI-279B (from *E*-cinnamyl) (Indy)	TJF-VI-279B (from *E*-cinnamyl) (florence)	–
76a	TJF-X-055 (from *Z*-cinnamyl) (Indy)	TJF-X-055 (from *Z*-cinnamyl) (florence)	TJF-X-055
77	TJF-VII-169A_proton (Indy)	TJF-VII-169A_carbon (florence)	TJF-IX-269
80	TJF-X-Zcinnamyl (Indy)	TJF-X-Zcinnamyl (florence)	TJF-X-049
82	EJA-X-217	EJA-X-217	EJA-X-233
83	EJA-X-243_proton (Indy)	EJA-X-243A-me (florence)	EJA-X-243
84	TJF-VII-215 (Indy)	TJF-VII-215 (florence)	TJF-VII-215
85	TJF-VIII-227 (misnamed) (Indy)	TJF-VII-227 (misnamed) (florence)	TJF-VII-229
86	TJF-VII-231 (Indy)	TJF-VII-231 (florence)	TJF-VII-231
87	TJF-VII-247 (Indy)	TJF-VII-247 (florence)	TJF-VII-247
88	TJF-VII-233A_proton (Indy)	TJF-VII-233A (florence)	TJF-VII-233
89	TJF-VII-249A_proton (Indy)	TJF-VII-249A_carbon (florence)	TJF-VII-249
90	TJF-VIII-199A (misnamed) (Indy)	TJF-III-199 (misnamed) (florence)	TJF-VII-199
91	TJF-VII-241 (Indy)	TJF-VII-241 (florence)	TJF-VII-241
92	EJA-X-263-ester-2 (Indy)	EJA-X-263-ester-2 (florence)	EJA-X-263
93	EJA-X-203 (Indy)	EJA-X-203 (florence)	EJA-X-203
94	EJA-X-267_proton (Indy)	EJA-X-267_carbon (florence)	EJA-X-267
95	EJA-X-179A_proton (Indy)	EJA-X-179A_proton (florence)	EJA-X-179A
96	EJA-X-265-3 (Indy)	EJA-X-265-3 (florence)	EJA-X-265
97	EJA-X-197 (Indy)	EJA-X-197 (florence)	EJA-X-197
98	TJF-X-083 (Indy)	TJF-X-083 (florence)	TJF-X-083
99	TJF-IX-181_proton (Indy)	TJF-IX-181_carbon (florence)	TJF-IX-181
100	TJF-X-159A (Indy)	TJF-X-159A (florence)	TJF-X-159
101	TJF-IX-169_proton (Indy)	TJF-IX-169-CARBON (florence)	TJF-IX-169
102	TJF-VIII-273_proton (Indy)	TJF-VIII-273_carbon (florence)	TJF-VIII-273
103	TJF-VIII-275_2 (Indy)	TJF-VIII-275 (florence)	TJF-VIII-275
104	TJF-VIII-269A_proton (Indy)	TJF-VIII-269A_carbon (florence)	TJF-VIII-269
105	TJF-VIII-277A_proton (Indy)	TJF-VIII-277A_carbon (florence)	TJF-VIII-277
106	TJF-X-041A (Indy)	TJF-X-041A_carbon (florence)	TJF-X-041
107	TJF-X-053_proton (Indy)	TJF-X-053_carbon (florence)	TJF-X-053
108	TJF-X-039A (Indy)	TJF-X-039A_carbon (florence)	TJF-X-039

Figure A13.6 *Notebook Cross-Reference for Chapter 4 (continued)*

Compound	^{1}H NMR (instrument)	^{13}C NMR (instrument)	Procedure
109	TJF-X-057A (Indy)	TJF-X-057A (florence)	TJF-X-057
110	TJF-VIII-219A_proton (Indy)	TJF-VIII-219A (florence)	TJF-VII-223, VIII-219
111	TJF-X-051A (Indy)	TJF-X-051A (florence)	TJF-X-051
112	TJF-VIII-027A (florence)	TJF-VIII-027A (florence)	TJF-VIII-027
113	TJF-IX-017 (misnamed) (florence)	TJF-IX-017 (misnamed) (florence)	TJF-VII-275
114	TJF-VIII-051A_carbon (florence)	TJF-VIII-051A_carbon (florence)	TJF-VIII-051
115	TJF-VIII-271A_proton (Indy)	TJF-VIII-271A_carbon (florence)	TJF-VIII-271A
116	TJF-X-199A_char (florence)	TJF-X-199A_char (florence)	TJF-X-199
117	TJF-X-115A (Indy)	TJF-X-115A (florence)	TJF-X-115
119	TJF-X-095A (Indy)	TJF-X-095A (florence)	TJF-X-095
120	TJF-X-155_2 (Indy)	TJF-X-155_carbon2 (Indy)	TJF-X-155
121	TJF-X-133A_2 (Indy)	TJF-X-133A (florence)	TJF-X-133
122	TJF-X-157A_2 (Indy)	TJF-X-157A_2 (florence)	TJF-X-157
123	TJF-VII-165A (Indy)	TJF-VII-165A (florence)	TJF-VII-165
124	TJF-VII-185A (Indy)	TJF-VII-185A_carbon (florence)	TJF-VII-185
125	TJF-VII-191A (Indy)	TJF-VII-191A_carbon (florence)	TJF-VII-191
126	TJF-VII-167A (Indy)	TJF-VII-167A_carbon (florence)	TJF-VII-167
127	TJF-VII-195A (Indy)	TJF-VII-195A_carbon (florence)	TJF-VII-195
128	TJF-VII-193A (Indy)	TJF-VII-193A_carbon (florence)	TJF-VII-193
129	TJF-VII-163A (misnamed) (Indy)	TJF-VII-163A_carbon (misnamed) (florence)	TJF-VII-153
130	TJF-VII-187A (Indy)	TJF-VII-187A_carbon (florence)	TJF-VII-187
131	EJA-X-257 (Indy)	EJA-X-257 (florence)	EJA-X-257
132	EJA-X-173 (Indy)	EJA-X-173 (florence)	EJA-X-173
133	EJA-X-261 (Indy)	EJA-X-261 (florence)	EJA-X-261
134	EJA-X-171 (Indy)	EJA-X-171 (florence)	EJA-X-171
135	EJA-X-259 (Indy)	EJA-X-259 (florence)	EJA-X-259
136	EJA-X-187 (Indy)	EJA-X-187 (florence)	EJA-X-187

Figure A13.7 *Notebook Cross-Reference for Chapter 4 (continued)*

Compound	^{1}H NMR (instrument)	^{13}C NMR (instrument)	Procedure
137	TJF-X-073A (Indy)	TJF-X-075A (misnamed) (florence)	TJF-X-073
138	TJF-IX-155A (Indy)	TJF-IX-155A_carbon (florence)	TJF-IX-155
139	TJF-IX-139A_proton (Indy)	TJF-IX-139A_carbon (florence)	TJF-IX-139
140	TJF-IX-157A_proton (Indy)	TJF-IX-157-carbon (florence)	TJF-IX-157
141	TJF-VIII-129A_proton (Indy)	TJF-VIII-129A_carbon (florence)	TJF-VIII-129
142	TJF-VIII-251A_proton (Indy)	TJF-VIII-251A_carbon (florence)	TJF-VIII-251
143	TJF-VIII-243 (Indy)	TJF-VIII-243 (florence)	TJF-VIII-243
144	TJF-IX-thiazoleester (Indy)	TJF-IX-thiazoleester (florence)	TJF-VIII-245
enol carbonate A	TJF-IX-275_spotA (florence)	TJF-IX-275_spotA (florence)	TJF-IX-275
enol carbonate B	TJF-IX-275_spotB (florence)	TJF-IX-275_spotB (florence)	TJF-IX-275

ABOUT THE AUTHOR

Tyler James Fulton was born in Hazelton, Pennsylvania on March 21, 1994 to Rachel Kuchar and John Fulton. Tyler primarily grew up in Drums and Freeland, Pennsylvania. His interest in chemistry began in high school in Ms. Laura Petro's chemistry class. Tyler started his undergraduate studies as a pre-med biochemistry major at Bucknell University in 2012, but quickly changed to a chemistry major after taking freshman organic chemistry with Professor Mike Krout. In the spring of 2013, Tyler began research in Dr. Krout's lab, studying the copper-catalyzed conjugate addition of functionalized organozinc reagents to generate quaternary centers. Tyler pursued a dual B.S./M.S. degree under Professor Krout's supervision. Tyler completed his B.S. degree in spring 2016 and his M.S. degree in summer 2016.

Upon completion of his B.S./M.S. degrees, Tyler moved to Pasadena, California, to pursue a doctoral degree at the California Institute of Technology under the Direction of Professor Brian M. Stoltz. His research interests focused on the development of methods for acyclic stereocontrol and complex molecule total synthesis. Following completion of his graduate studies in April 2020, Tyler will begin a postdoctoral appointment in the lab of Professor Frances H. Arnold at Caltech.